

JOURNAL OF

CHROMATOGRAPHY

INCLUDING ELECTROPHORESIS AND OTHER SEPARATION METHODS

EDITORS

U. A. Th. Brinkman (Amsterdam)
 R. W. Giese (Boston, MA)
 J. K. Haken (Kensington, N.S.W.)
 K. Macek (Prague)
 L. R. Snyder (Orinda, CA)

EDITORS, SYMPOSIUM VOLUMES

E. Heftmann (Orinda, CA), Z. Deyl (Prague)

EDITORIAL BOARD

D. W. Armstrong (Rolla, MO)
 W. A. Aue (Halifax)
 P. Boček (Brno)
 A. A. Boulton (Saskatoon)
 P. W. Carr (Minneapolis, MN)
 N. H. C. Cooke (San Ramon, CA)
 V. A. Davankov (Moscow)
 Z. Deyl (Prague)
 S. Dilli (Kensington, N.S.W.)
 H. Engelhardt (Saarbrücken)
 F. Erni (Basle)
 M. B. Evans (Hatfield)
 J. L. Glajch (N. Ellersica, MA)
 G. A. Guiochon (Knoxville, TN)
 P. R. Haddad (Hobart, Tasmania)
 I. M. Hais (Hradec Králové)
 W. S. Hancock (San Francisco, CA)
 S. Hjertén (Uppsala)
 Cs. Horváth (New Haven, CT)
 J. F. K. Huber (Vienna)
 K.-P. Hupé (Waldbronn)
 T. W. Hutchens (Houston, TX)
 J. Janák (Brno)
 P. Jandera (Pardubice)
 B. L. Karger (Boston, MA)
 J. J. Kiskand (Newport, DE)
 E. sz. Kováts (Lausanne)
 A. J. P. Martin (Cambridge)
 L. W. McLaughlin (Chestnut Hill, MA)
 E. D. Morgan (Keele)
 J. D. Pearson (Kalamazoo, MI)
 H. Poppe (Amsterdam)
 F. E. Regnier (West Lafayette, IN)
 P. G. Righetti (Milan)
 P. Schoenmakers (Eindhoven)
 R. Schwarzenbach (Dübendorf)
 R. E. Shoup (West Lafayette, IN)
 A. M. Siouffi (Marseille)
 D. J. Strydom (Boston, MA)
 N. Tanaka (Kyoto)
 S. Terabe (Hyogo)
 K. K. Unger (Mainz)
 R. Verpoorte (Leiden)
 Gy. Vigh (College Station, TX)
 J. T. Watson (East Lansing, MI)
 B. D. Westerglund (Uppsala)

EDITORS, BIBLIOGRAPHY SECTION

Z. Deyl (Prague), J. Janák (Brno), V. Schwarz (Prague)

JOURNAL OF CHROMATOGRAPHY

INCLUDING ELECTROPHORESIS AND OTHER SEPARATION METHODS

Scope. The *Journal of Chromatography* publishes papers on all aspects of **chromatography, electrophoresis** and related methods. Contributions consist mainly of research papers dealing with chromatographic theory, instrumental developments and their applications. The section *Biomedical Applications*, which is under separate editorship, deals with the following aspects: developments in and applications of chromatographic and electrophoretic techniques related to clinical diagnosis or alterations during medical treatment; screening and profiling of body fluids or tissues related to the analysis of active substances and to metabolic disorders; drug level monitoring and pharmacokinetic studies; clinical toxicology; forensic medicine; veterinary medicine; occupational medicine; results from basic medical research with direct consequences in clinical practice. In *Symposium volumes*, which are under separate editorship, proceedings of symposia on chromatography, electrophoresis and related methods are published.

Submission of Papers. The preferred medium of submission is on disk with accompanying manuscript (see *Electronic manuscripts* in the Instructions to Authors, which can be obtained from the publisher, Elsevier Science Publishers B.V., P.O. Box 330, 1000 AH Amsterdam, Netherlands). Manuscripts (in English; *four* copies are required) should be submitted to: Editorial Office of *Journal of Chromatography*, P.O. Box 681, 1000 AR Amsterdam, Netherlands, Telefax (+31-20) 5862 304, or to: The Editor of *Journal of Chromatography, Biomedical Applications*, P.O. Box 681, 1000 AR Amsterdam, Netherlands. Review articles are invited or proposed in writing to the Editors who welcome suggestions for subjects. An outline of the proposed review should first be forwarded to the Editors for preliminary discussion prior to preparation. Submission of an article is understood to imply that the article is original and unpublished and is not being considered for publication elsewhere. For copyright regulations, see below.

Publication. The *Journal of Chromatography* (incl. *Biomedical Applications*) has 40 volumes in 1993. The subscription prices for 1993 are:

J. Chromatogr. (incl. *Cum. Indexes, Vols. 601-650*) + *Biomed. Appl.* (Vols. 612-651):

Dfl. 8520.00 plus Dfl. 1320.00 (p.p.h.) (total ca. US\$ 5927.75)

J. Chromatogr. (incl. *Cum. Indexes, Vols. 601-650*) only (Vols. 623-651):

Dfl. 7047.00 plus Dfl. 957.00 (p.p.h.) (total ca. US\$ 4821.75)

Biomed. Appl. only (Vols. 612-622):

Dfl. 2783.00 plus Dfl. 363.00 (p.p.h.) (total ca. US\$ 1895.25).

Subscription Orders. The Dutch guilder price is definitive. The US\$ price is subject to exchange-rate fluctuations and is given as a guide. Subscriptions are accepted on a prepaid basis only, unless different terms have been previously agreed upon. Subscriptions orders can be entered only by calendar year (Jan.-Dec.) and should be sent to Elsevier Science Publishers, Journal Department, P.O. Box 211, 1000 AE Amsterdam, Netherlands, Tel. (+31-20) 5803 642, Telefax (+31-20) 5803 598, or to your usual subscription agent. Postage and handling charges include surface delivery except to the following countries where air delivery via SAL (Surface Air Lift) mail is ensured: Argentina, Australia, Brazil, Canada, China, Hong Kong, India, Israel, Japan*, Malaysia, Mexico, New Zealand, Pakistan, Singapore, South Africa, South Korea, Taiwan, Thailand, USA. *For Japan air delivery (SAL) requires 25% additional charge of the normal postage and handling charge. For all other countries airmail rates are available upon request. Claims for missing issues must be made within six months of our publication (mailing) date, otherwise such claims cannot be honoured free of charge. Back volumes of the *Journal of Chromatography* (Vols. 1-611) are available at Dfl. 230.00 (plus postage). Customers in the USA and Canada wishing information on this and other Elsevier journals, please contact Journal Information Center, Elsevier Science Publishing Co. Inc., 655 Avenue of the Americas, New York, NY 10010, USA, Tel. (+1-212) 633 3750, Telefax (+1-212) 633 3764.

Abstracts/Contents Lists published in Analytical Abstracts, Biochemical Abstracts, Biological Abstracts, Chemical Abstracts, Chemical Titles, Chromatography Abstracts, Clinical Chemistry Abstracts, Current Awareness in Biological Sciences (CABS), Current Contents/Life Sciences, Current Contents/Physical, Chemical & Earth Sciences, Deep-Sea Research/Part B: Oceanographic Literature Review, Excerpta Medica, Index Medicus, Mass Spectrometry Bulletin, PASCAL-CNRS, Pharmaceutical Abstracts, Referativnyi Zhurnal, Research Alert, Science Citation Index and Trends in Biotechnology.

US Mailing Notice. *Journal of Chromatography* (ISSN 0021-9673) is published weekly (total 58 issues) by Elsevier Science Publishers (Sara Burgerhartstraat 25, P.O. Box 211, 1000 AE Amsterdam, Netherlands). Annual subscription price in the USA US\$ 5927.75 (subject to change), including air speed delivery. Application to mail at second class postage rate is pending at Jamaica, NY 11431. **USA POSTMASTERS:** Send address changes to *Journal of Chromatography*, Publications Expediting, Inc., 200 Meacham Avenue, Elmont, NY 11003. Airfreight and mailing in the USA by Publication Expediting.

See inside back cover for Publication Schedule, Information for Authors and information on Advertisements.

© 1993 ELSEVIER SCIENCE PUBLISHERS B.V. All rights reserved.

0021-9673/93/\$06.00

No part of this publication may be reproduced, stored in a retrieval system or transmitted in any form or by any means, electronic, mechanical, photocopying, recording or otherwise, without the prior written permission of the publisher, Elsevier Science Publishers B.V., Copyright and Permissions Department, P.O. Box 521, 1000 AM Amsterdam, Netherlands.

Upon acceptance of an article by the journal, the author(s) will be asked to transfer copyright of the article to the publisher. The transfer will ensure the widest possible dissemination of information.

Special regulations for readers in the USA. This journal has been registered with the Copyright Clearance Center, Inc. Consent is given for copying of articles for personal or internal use, or for the personal use of specific clients. This consent is given on the condition that the copier pays through the Center the per-copy fee stated in the code on the first page of each article for copying beyond that permitted by Sections 107 or 108 of the US Copyright Law. The appropriate fee should be forwarded with a copy of the first page of the article to the Copyright Clearance Center, Inc., 27 Congress Street, Salem, MA 01970, USA. If no code appears in an article, the author has not given broad consent to copy and permission to copy must be obtained directly from the author. All articles published prior to 1980 may be copied for a per-copy fee of US\$ 2.25, also payable through the Center. This consent does not extend to other kinds of copying, such as for general distribution, resale, advertising and promotion purposes, or for creating new collective works. Special written permission must be obtained from the publisher for such copying.

No responsibility is assumed by the Publisher for any injury and/or damage to persons or property as a matter of products liability, negligence or otherwise, or from any use or operation of any methods, products, instructions or ideas contained in the materials herein. Because of rapid advances in the medical sciences, the Publisher recommends that independent verification of diagnoses and drug dosages should be made.

Although all advertising material is expected to conform to ethical (medical) standards, inclusion in this publication does not constitute a guarantee or endorsement of the quality or value of such product or of the claims made of it by its manufacturer.

This issue is printed on acid-free paper.

Printed in the Netherlands

CONTENTS

(Abstracts/Contents Lists published in Analytical Abstracts, Biochemical Abstracts, Biological Abstracts, Chemical Abstracts, Chemical Titles, Chromatography Abstracts, Current Awareness in Biological Sciences (CABS), Current Contents/Life Sciences, Current Contents/Physical, Chemical & Earth Sciences, Deep-Sea Research/Part B: Oceanographic Literature Review, Excerpta Medica, Index Medicus, Mass Spectrometry Bulletin, PASCAL-CNRS, Referativnyi Zhurnal, Research Alert and Science Citation Index)

REGULAR PAPERS

Column Liquid Chromatography

- Retention on non-polar adsorbents in liquid-solid chromatography. Effect of grafted alkyl chains
by G. Fóti, M. L. Belvito, A. Alvarez-Zepeda and E. sz. Kováts (Lausanne, Switzerland) (Received October 26th, 1992) 1
- Modeling of the adsorption behavior and the chromatographic band profiles of enantiomers. Behavior of methyl mandelate on immobilized cellulose
by F. Charton, S. C. Jacobson and G. Guiochon (Knoxville, TN and Oak Ridge, TN, USA) (Received October 27th, 1992) 21
- Characterization of non-linear adsorption properties of dextran-based polyelectrolyte displacers in ion-exchange systems
by S. D. Graham, G. Jayaraman and S. M. Cramer (Troy, NY, USA) (Received October 1st, 1992) 37
- Ion-exchange displacement chromatography of proteins. Dextran-based polyelectrolytes as high affinity displacers
by G. Jayaraman, S. D. Graham and S. M. Cramer (Troy, NY, USA) (Received October 1st, 1992) 53
- Improved computer algorithm for characterizing skewed chromatographic band broadening. II. Results and comparisons
by W. W. Yau, S. W. Rementer, J. M. Boyajian, J. J. DeStefano, J. F. Graff, K. B. Lim and J. J. Kirkland (Wilmington, DE, USA) (Received October 14th, 1992) 69
- Functionalized polymer particles for chiral separation
by T. Hargitai, P. Reinholdsson and B. Törnell (Lund, Sweden) and R. Isaksson (Uppsala, Sweden) (Received October 21st, 1992) 79
- New alumina-based stationary phases for high-performance liquid chromatography. Synthesis by olefin hydrosilation on a silicon hydride-modified alumina intermediate
by J. J. Pesek, J. E. Sandoval and M. Su (San Jose, CA, USA) (Received October 16th, 1992) 95
- Examination of some reversed-phase high-performance liquid chromatography systems for the determination of lipophilicity
by D. P. Nowotnik, T. Feld and A. D. Nunn (New Brunswick, NJ, USA) (Received September 29th, 1992) 105
- Evaluation of silanol-deactivated silica-based reversed phases for liquid chromatography of erythromycin
by J. Paesen, P. Claeys, E. Roets and J. Hoogmartens (Leuven, Belgium) (Received October 12th, 1992) 117
- Selective complex formation of saccharides with europium(III) and iron(III) ions at alkaline pH studied by ligand-exchange chromatography
by M. Stefansson (Uppsala, Sweden) (Received October 20th, 1992) 123
- Separation of glucooligosaccharides and polysaccharide hydrolysates by gradient elution hydrophilic interaction chromatography with pulsed amperometric detection
by A. S. Feste and I. Khan (Houston, TX, USA) (Received October 23rd, 1992) 129
- Determination of hyaluronic acid by high-performance liquid chromatography of the oligosaccharides derived therefrom as 1-(4-methoxy)phenyl-3-methyl-5-pyrazolone derivatives
by K. Kakehi, M. Ueda, S. Suzuki and S. Honda (Osaka, Japan) (Received September 23rd, 1992) 141
- Separation and isolation of trace impurities in L-tryptophan by high-performance liquid chromatography
by M. W. Trucksess (Washington, DC, USA) (Received October 10th, 1992) 147
- Sequence-specific DNA affinity chromatography: application of a group-specific adsorbent for the isolation of restriction endonucleases
by C. Pozidis, G. Vlatakis and V. Bouriotis (Heraklion, Greece) (Received October 9th, 1992) 151
- Quantitative analysis of tylosin by column liquid chromatography
by E. Roets, P. Beirinckx, I. Quintens and J. Hoogmartens (Leuven, Belgium) (Received September 29th, 1992) 159
- Analysis of the explosive 2,4,6-trinitrophenylmethylnitramine (tetryl) in bush bean plants
by S. D. Harvey, R. J. Fellows, D. A. Cataldo and R. M. Bean (Richland, WA, USA) (Received September 29th, 1992) 167

(Continued overleaf)

ห้องสมุดกรมวิทยาศาสตร์บริการ

10 ส.ค. 2536

Contents (continued)

Liquid-gel partitioning using Lipidex in the determination of polychlorinated biphenyls in cod liver oil by C. Weistrand and K. Norén (Stockholm, Sweden) (Received October 19th, 1992)	179
High-performance liquid chromatographic determination of methanesulphinic acid as a method for the determination of hydroxyl radicals by S. Fukui, Y. Hanasaki and S. Ogawa (Kyoto, Japan) (Received September 24th, 1992)	187
Ion chromatography of nitrite and carbonate in inorganic matrices on an octadecyl-poly(vinyl alcohol) gel column using acidic eluents by S. Rokushika, F. M. Yamamoto and K. Kihara (Kyoto, Japan) (Received October 13th, 1992)	195

Column Liquid Chromatography-Gas Chromatography

Use of an open-tubular trapping column as phase-switching interface in on-line coupled reversed-phase liquid chromatography-capillary gas chromatography by H. G. J. Mol, J. Staniewski, H.-G. Janssen and C. A. Cramers (Eindhoven, Netherlands) and R. T. Ghijsen and U. A. Th. Brinkman (Amsterdam, Netherlands) (Received October 12th, 1992)	201
Comparative study of the determination of triacylglycerol in vegetable oils using chromatographic techniques by A. A. Carelli and A. Cert (Seville, Spain) (Received October 20th, 1992)	213

Gas Chromatography

Structure-gas chromatographic retention time models of tetra- <i>n</i> -alkylsilanes and tetra- <i>n</i> -alkylgermanes using topological indexes by E. J. Kupchik (Jamaica, NY, USA) (Received October 27th, 1992)	223
Effect of variations in gas chromatographic conditions on the linear retention indices of selected chemical warfare agents by M. Kokko (Helsinki, Finland) (Received September 23rd, 1992)	231
Relationship between Kováts retention indices and molecular connectivity indices of tetralones, coumarins and structurally related compounds by A. C. Arruda, V. E. F. Heinzen and R. A. Yunes (Florianópolis, Brazil) (Received August 18th, 1992)	251
Ambient temperature gas purifier suitable for the trace analysis of carbon monoxide and hydrogen and the preparation of low-level carbon monoxide calibration standards in the field by B. E. Foulger and P. G. Simmonds (Poole, UK) (Received August 7th, 1992)	257
Evaluation of Carboxen carbon molecular sieves for trapping replacement chlorofluorocarbons by S. J. O'Doherty, P. G. Simmonds and G. Nickless (Bristol, UK) and W. R. Betz (Bellefonte, PA, USA) (Received October 29th, 1992)	265
Application of dithiocarbamate resin-metal complexes as stationary phases in gas chromatography by C.-F. Yeh, S.-D. Chyueh, W.-S. Chen, J.-D. Fang and C.-Y. Liu (Taipei, Taiwan) (Received October 20th, 1992)	275
Gas chromatographic analysis of high-molecular-mass polycyclic aromatic hydrocarbons. II. Polycyclic aromatic hydrocarbons with relative molecular masses exceeding 328 by A. Bemgård, A. Colmsjö and B.-O. Lundmark (Solna, Sweden) (Received October 15th, 1992)	287
Simultaneous determination of planar chlorobiphenyls and polychlorinated dibenzo- <i>p</i> -dioxins and -furans in Dutch milk using isotope dilution and gas chromatography-high-resolution mass spectrometry by J. A. van Rhijn, W. A. Traag, P. F. van de Spreng and L. G. M. Th. Tuinstra (Wageningen, Netherlands) (Received August 19th, 1992)	297

Supercritical Fluid Chromatography

Injection of large volumes of aqueous solutions in capillary supercritical fluid chromatography and sample preconcentration by multiple injections by S. Bouissel, F. Erni and R. Link (Basle, Switzerland) (Received September 28th, 1992)	307
--	-----

Electrophoresis

pH gradient simulator for electrophoretic techniques in a Windows environment by E. Giaffreda, C. Tonani and P. G. Righetti (Milan, Italy) (Received October 19th, 1992)	313
Protein and peptide mobility in capillary zone electrophoresis. A comparison of existing models and further analysis by V. J. Hilser, Jr. and G. D. Worosila (Suffern, NY, USA) and S. E. Rudnick (Riverdale, NY, USA) (Received November 2nd, 1992)	329

Capillary electrophoretic protein separations in polyacrylamide-coated silica capillaries and buffers containing ionic surfactants by M. A. Strege and A. L. Lagu (Indianapolis, IL, USA) (Received October 30th, 1992)	337
Determination of the number and relative molecular mass of subunits in an oligomeric protein by two-dimensional electrophoresis. Application to the subunit structure analysis of rat liver amidophosphoribosyltransferase by T. Yamaoka and K. Yamashita (Ibaraki, Japan) and M. Itakura (Tokushima City, Japan) (Received October 6th, 1992)	345
Separation of drug stereoisomers by capillary electrophoresis with cyclodextrins by T. E. Peterson (Fort Worth, TX, USA) (Received October 21st, 1992)	353
Separation and simultaneous determination of the active ingredients in theophylline tablets by micellar electrokinetic capillary chromatography by Q.-x. Dang and L.-x. Yan (Xian, China) and Z.-p. Sun and D.-k. Ling (Beijing, China) (Received October 20th, 1992)	363
Determination of alkylphosphonic acids by capillary zone electrophoresis using indirect UV detection by G. A. Pianetti, M. Taverna, A. Baillet, G. Mahuzier and D. Baylocq-Ferrier (Chatenay-Malabry, France) (Received October 23rd, 1992)	371
Metal ion capillary zone electrophoresis with direct UV detection: determination of transition metals using an 8-hydroxyquinoline-5-sulphonic acid chelating system by A. R. Timerbaev, W. Buchberger, O. P. Semenova and G. K. Bonn (Linz, Austria) (Received August 11th, 1992)	379
SHORT COMMUNICATIONS	
<i>Column Liquid Chromatography</i>	
Glycosaminoglycans and proteins: different behaviours in high-performance size-exclusion chromatography by N. Volpi and L. Bolognani (Modena, Italy) (Received October 28th, 1992)	390
Adsorption losses during extraction and derivatization efficiency by benzylation of plant putrescine for high-performance liquid chromatographic analysis by M. Z. Hauschild (Lyngby, Denmark) (Received November 2nd, 1992)	397
High-performance liquid chromatographic determination of cardenolides in <i>Digitalis</i> leaves after solid-phase extraction by H. Wiegreb and M. Wichtl (Marburg/Lahn, Germany) (Received October 27th, 1992)	402
Determination of acidic saponins in crude drugs by high-performance liquid chromatography on octadecylsilyl porous glass by H. Kanazawa, Y. Nagata, Y. Matsushima, M. Tomoda and N. Takai (Tokyo, Japan) (Received November 3rd, 1992)	408
Determination of Lovastatin (mevinolin) and mevinolinic acid in fermentation liquids by R. Kysilka and V. Křen (Prague, Czechoslovakia) (Received October 23rd, 1992)	415
Simultaneous high-performance liquid chromatographic determination of alterosolanol A, B, C, D, E and F by N. Okamura, A. Yagi, H. Haraguchi and K. Hashimoto (Hiroshima, Japan) (Received November 10th, 1992)	418
Isolation and determination of alizarin in cell cultures of <i>Rubia tinctorum</i> and emodin in <i>Dermocybe sanguinea</i> using solid-phase extraction and high-performance liquid chromatography by Z. A. Tóth (Budapest, Hungary) and O. Raatikainen, T. Naaranlahti and S. Auriola (Kuopio, Finland) (Received October 28th, 1992)	423
<i>Gas Chromatography</i>	
Improved procedure for the derivatization and gas chromatographic determination of hydroxycarboxylic acids treated with chloroformates by P. Hušek (Prague, Czechoslovakia) (Received October 9th, 1992)	429
Preparation of methyl esters of fatty acids with trimethylsulphonium hydroxide —an appraisal by A. H. El-Hamdy and W. W. Christie (Ayr, UK) (Received November 12th, 1992)	438
<i>Electrophoresis</i>	
Capillary electrophoretic separation of recombinant granulocyte-colony-stimulating factor glycoforms by E. Watson and F. Yao (Thousand Oaks, CA, USA) (Received November 23rd, 1992)	442
BOOK REVIEW	
Advances in lipid methodology I (edited by W. W. Christie), by A. Kuksis (Toronto, Canada)	447
AUTHOR INDEX	449

JOURNAL OF CHROMATOGRAPHY

VOL. 630 (1993)

JOURNAL of CHROMATOGRAPHY

INCLUDING ELECTROPHORESIS AND OTHER SEPARATION METHODS

EDITORS

U. A. Th. BRINKMAN (Amsterdam), R. W. GIESE (Boston, MA), J. K. HAKEN (Kensington, N.S.W.), K. MACEK (Prague),
L. R. SNYDER (Orinda, CA)

EDITORS, SYMPOSIUM VOLUMES

E. HEFTMANN (Orinda, CA), Z. DEYL (Prague)

EDITORIAL BOARD

D. W. Armstrong (Rolla, MO), W. A. Aue (Halifax), P. Boček (Brno), A. A. Boulton (Saskatoon), P. W. Carr (Minneapolis, MN),
N. H. C. Cooke (San Ramon, CA), V. A. Davankov (Moscow), Z. Deyl (Prague), S. Dilli (Kensington, N.S.W.), H. Engelhardt
(Saarbrücken), F. Erni (Basle), M. B. Evans (Hatfield), J. L. Glajch (N. Billerica, MA), G. A. Guiochon (Knoxville, TN), P. R.
Haddad (Hobart, Tasmania), I. M. Hais (Hradec Králové), W. S. Hancock (San Francisco, CA), S. Hjertén (Uppsala), Cs. Horváth
(New Haven, CT), J. F. K. Huber (Vienna), K.-P. Hupe (Waldbronn), T. W. Hutchens (Houston, TX), J. Janák (Brno), P. Jandera
(Pardubice), B. L. Karger (Boston, MA), J. J. Kirkland (Wilmington, DE), E. sz. Kováts (Lausanne), A. J. P. Martin (Cambridge),
L. W. McLaughlin (Chestnut Hill, MA), E. D. Morgan (Keele), J. D. Pearson (Kalamazoo, MI), H. Poppe (Amsterdam), F. E.
Regnier (West Lafayette, IN), P. G. Righetti (Milan), P. Schoenmakers (Eindhoven), R. Schwarzenbach (Dübendorf), R. E.
Shoup (West Lafayette, IN), A. M. Siouffi (Marseille), D. J. Strydom (Boston, MA), N. Tanaka (Kyoto), S. Terabe (Hyogo), K. K.
Unger (Mainz), R. Verpoorte (Leiden), Gy. Vigh (College Station, TX), J. T. Watson (East Lansing, MI), B. D. Westerlund
(Uppsala)

EDITORS, BIBLIOGRAPHY SECTION

Z. Deyl (Prague), J. Janák (Brno), V. Schwarz (Prague)



ELSEVIER
AMSTERDAM — LONDON — NEW YORK — TOKYO

J. Chromatogr., Vol. 630 (1993)

ห้องสมุดที่พิมพ์ และ เผยแพร่ บริการ

© 1993 ELSEVIER SCIENCE PUBLISHERS B.V. All rights reserved.

0021-9673/93/\$06.00

No part of this publication may be reproduced, stored in a retrieval system or transmitted in any form or by any means, electronic, mechanical, photocopying, recording or otherwise, without the prior written permission of the publisher, Elsevier Science Publishers B.V., Copyright and Permissions Department, P.O. Box 521, 1000 AM Amsterdam, Netherlands.

Upon acceptance of an article by the journal, the author(s) will be asked to transfer copyright of the article to the publisher. The transfer will ensure the widest possible dissemination of information.

Submission of an article for publication entails the authors' irrevocable and exclusive authorization of the publisher to collect any sums or considerations for copying or reproduction payable by third parties (as mentioned in article 17 paragraph 2 of the Dutch Copyright Act of 1912 and the Royal Decree of June 20, 1974 (S. 351) pursuant to article 16 b of the Dutch Copyright Act of 1912) and/or to act in or out of Court in connection therewith.

Special regulations for readers in the USA. This journal has been registered with the Copyright Clearance Center, Inc. Consent is given for copying of articles for personal or internal use, or for the personal use of specific clients. This consent is given on the condition that the copier pays through the Center the per-copy fee stated in the code on the first page of each article for copying beyond that permitted by Sections 107 or 108 of the US Copyright Law. The appropriate fee should be forwarded with a copy of the first page of the article to the Copyright Clearance Center, Inc., 27 Congress Street, Salem, MA 01970, USA. If no code appears in an article, the author has not given broad consent to copy and permission to copy must be obtained directly from the author. All articles published prior to 1980 may be copied for a per-copy fee of US\$ 2.25, also payable through the Center. This consent does not extend to other kinds of copying, such as for general distribution, resale, advertising and promotion purposes, or for creating new collective works. Special written permission must be obtained from the publisher for such copying.

No responsibility is assumed by the Publisher for any injury and/or damage to persons or property as a matter of products liability, negligence or otherwise, or from any use or operation of any methods, products, instructions or ideas contained in the materials herein. Because of rapid advances in the medical sciences, the Publisher recommends that independent verification of diagnoses and drug dosages should be made.

Although all advertising material is expected to conform to ethical (medical) standards, inclusion in this publication does not constitute a guarantee or endorsement of the quality or value of such product or of the claims made of it by its manufacturer.

This issue is printed on acid-free paper.

Printed in the Netherlands

Retention on non-polar adsorbents in liquid–solid chromatography

Effect of grafted alkyl chains

György Fóti, Mary Lisa Belvito, Aurelio Alvarez-Zepeda and Ervin sz. Kováts

Laboratoire de Chimie Technique, École Polytechnique Fédérale de Lausanne, CH-1015 Lausanne (Switzerland)

(First received August 4th, 1992; revised manuscript received October 26th, 1992)

ABSTRACT

The retention of 39 molecular probes was measured on chemically bonded dense layers of (3,3-dimethylbutyl)dimethylsiloxy (DMB) and tetradecyldimethylsiloxy (C_{14}) substituents on silica as a function of the composition of the binary acetonitrile–water eluent. The sign of the “associated system peak” was also noted. The composition dependence of retention, measured as areal retention volume, could be described on both non-polar stationary phases by the two-parameter Snyder–Soczewinski equation and by the three parameter Schoenmakers equation in a broad but restricted composition range. The areal retention volume on the surface with grafted alkyl chains was equal to or higher than that on the non-swelling, smooth, non-polar DMB surface. Additional retention on the C_{14} surface increased with increasing adsorption force (retention) on the DMB surface and it was a function of the composition of the eluent. A possible interpretation of the sign of the “associated system peak” generated by the injection of a pure solute is also given in terms of solvation of the solute in the mobile phase and in terms of the modification of the non-polar adsorbent by the adsorbed solute.

INTRODUCTION

The problem of the effect of surface-bonded alkyl chains on retention will be addressed by comparing retention data measured on a tetradecyldimethylsiloxy (C_{14})-covered silica with those measured on a surface covered with a dense layer of (3,3-dimethylbutyl)dimethylsiloxy (DMB) substituents, depicted in Fig. 1. Several arguments speak in favour of the use of this special pair of adsorbents together with acetonitrile–water (AN–W) as a binary eluent for the study of this problem. First, with the corresponding dimethylaminosilanes as silylating agents, reproducible, dense layers of C_{14} and DMB can be

grafted on widely differing silicon dioxide preparations [1]. Second, the excess adsorption isotherm from acetonitrile–water mixtures is nearly the same at the liquid– C_{14} and the liquid–DMB interface, as shown in Fig. 1 [2]. Third, the suitability of the DMB-covered surface as a smooth, non-swelling, non-polar standard has already been demonstrated by wetting experiments [3,4]. In fact, the DMB layer doubly shields the underlying matrix. The first dense layer formed by the methylenedimethylsiloxy base of the substituent implies a second dense layer formed by the *tert.*-butyl umbrella of the 3,3-dimethylbutyl group. Fourth, tetradecyldimethylsiloxy graft was preferred in this study to the widely used octadecyldimethylsiloxy (C_{18}) graft because latter shows a quasi-liquid–solid transition around 20°C. The corresponding transition of the C_{14} phase is around 0°C.

On the basis of these premises, differences in

Correspondence to: E. sz. Kováts, Laboratoire de Chimie Technique, École Polytechnique Fédérale de Lausanne, CH-1015 Lausanne, Switzerland.

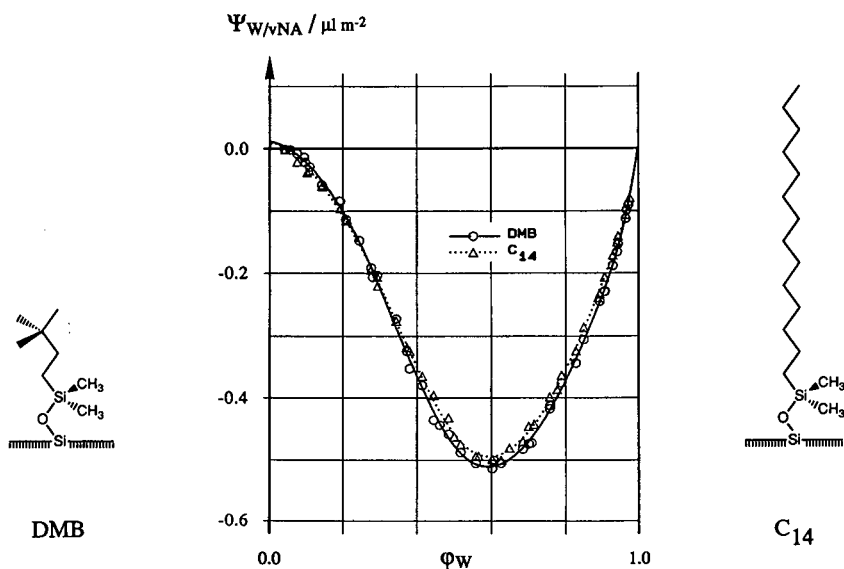


Fig. 1. Excess adsorption isotherms of water at the liquid–solid interface between acetonitrile–water as binary eluent and a dense layer of (○) (3,3-dimethylbutyl)dimethylsiloxy (DMB)- and (Δ) tetradecyldimethylsiloxy (C_{14})-covered silica as solid adsorbent as a function of the volume fraction of water, ϕ_W . Adsorption isotherms are given in terms of volume adsorbed per unit surface area with reference to the vNA Gibbs convention, *i.e.*, nothing is adsorbed in terms of volume ($\Sigma\Psi_{i/vNA} = 0$).

retention on the C_{14} phase compared with those on the DMB standard at the same AN–W eluent composition can be clearly attributed to the presence of the C_{14} chains at the surface if retention is expressed using a column-independent intensive quantity. Consequently, following the proposal of Kiselev and Yashin [5], retention data will be given as areal retention volumes, V_s ($\mu\text{l/m}^2 \equiv \text{nm}$), derived from a net retention volume which is in accordance with Gibbs' description of excess adsorption at the liquid–solid interface [6,7]. Arguments in favour of the areal retention volume and the unsuitability of the widely applied capacity factor, k' , are expressed hereafter (see below).

Successful application of adsorbents with grafted n -alkyl chains in liquid–solid chromatography has largely stimulated the study of their adsorption properties. Primitively, they have been considered as solids covered with a chemically immobilized liquid monolayer at their surface. Early investigations have demonstrated that retention increases with increasing “carbon loading”, *i.e.*, on grafts with longer chain length and/or increasing density (ligand surface concentration) of the surface layer [8–21]. Unger and co-workers [22,23] were the first to point

out that retention must also depend on the available surface area of the stationary phase in the column, S , and proposed to examine the dependence of $\log(\text{retention}/S)$ as a function of the chain length of the graft. It has been shown that this normalized logarithmic retention is a linear function of the chain length and/or the carbon content per unit surface area. The drawback of these and subsequent studies had been the use of ill-defined or incompletely surface-substituted adsorbents. Scott and Kucera [11] demonstrated the lack of correlation between retention and surface coverage or chain length for commercial adsorbents. In several studies, laboratory-made silica-based alkyl dimethylsiloxy-covered adsorbents have been applied, but surface treatment was made with inefficient silylating agents such as chloro- or methoxyalkyl dimethylsilanes. With such agents, the ligand surface concentration decreases with increasing chain length of the alkyl substituent. It has been shown that retention increases with increasing chain length of the graft up to about ten carbons, then retention levels off for longer alkyl chain grafts [24]. This type of dependence may be due to the combined effect of increasing chain length and, parallel to that, a decreasing surface coverage.

Lork [25] confirmed this dependence on a series of stationary phases with constant but very low ($\Gamma_{\text{sox}} = 2.1 \mu\text{mol/m}^2$) areal concentration of the alkyl-dimethylsiloxy graft. In fact, the surface concentration amounted to about 60% of that obtained with alkyl-dimethyl(dimethylamino)silane as silylating agent [1]. This general picture is even more confusing considering the observation of several workers that the nature of the function describing the dependence of retention on chain length or on areal concentration of the graft is different for different types of solutes [26,27].

In summary, despite numerous efforts to measure and understand the influence of the chain length and areal concentration of the grafted chains, interpretation of the results of these studies is difficult. Experiments have always been conducted either on incompletely silylated surfaces or on surfaces where the areal concentration of the alkyl graft depended on the chain length. Even on surfaces with the densest layers, silanol groups contribute to adsorption. In Fig. 1 the slight positive water adsorption at low water concentrations has been shown to be due to specific adsorption of water on silanols “visible” across the graft by the small water molecule [2]. Therefore, incompletely silylated silica is certainly a heterogeneous adsorbent, hence it is not surprising that the areal concentration of the graft influences retention. Also, it is unfortunate that retention has generally been reported in terms of the capacity factor, k' , which is essentially the relative retention of the solute referred to that of a solute believed to be unretained. Considering the multitude of “unretained” solutes proposed and applied in these studies, one has to conclude that the capacity factor only allows comparison of retention data obtained in one study by a given worker on a given column at a given eluent composition. It is important to note that capacity factor is not an intensive quantity even if the zero retention is determined relative to a hold-up volume defined by a given Gibbs convention.

The aim of this paper is to report retention data of a series of solutes of differing polarity on two silica-based adsorbents covered with a dense, chemically bonded, non-polar monolayer, one with and the other without grafted C_{14} alkyl chains. Retention will be given as areal retention volume referred to the BET surface area of the stationary phase in the column.

THEORETICAL BACKGROUND

The relationship between adsorption and retention in liquid–solid chromatography with binary eluents has been treated extensively [6,7,28]. In this section will be summarized the underlying principles and the necessary equations for the evaluation and interpretation of the experimental data.

The Gibbs convention

Mixtures of non-electrolytes are nearly ideal concerning the additivity of the volume of the components, *i.e.*, the partial volumes can be equated to those of the pure components with sufficient precision. Therefore, the mass balance of a component, *i*, in the column at equilibrium with a multi-component mixture can be replaced by the volume balance

$$V_{\kappa,i} = \varphi_i V_{\mu/\text{CX}} + S \Psi_{i/\text{CX}} \quad (1)$$

where $V_{\kappa,i}$ is the total material content of component, *i*, in terms of volume at adsorption equilibrium under isocratic conditions (the isocratic capacity, x , of *i*), φ_i is the volume fraction of *i* in the bulk liquid (eluent), $V_{\mu/\text{CX}}$ is the volume of the eluent in the column (μ : mobile phase), S is the surface area of the adsorbent and $\Psi_{i/\text{CX}}$ is the adsorbed volume of component *i* per unit surface area. The bulk liquid volume and the adsorbed volume are defined quantities only if a “convention” is agreed upon (CX: Convention X). For a system consisting of a binary eluent of components A and B and a solute (su), eqn. 1 represents three independent relationships with four unknowns, $V_{\mu/\text{CX}}$, $\Psi_{\text{A}/\text{CX}}$, $\Psi_{\text{B}/\text{CX}}$ and $\Psi_{\text{su}/\text{CX}}$. Following Gibbs’ proposal, a convention has to be stated in order to obtain the fourth equation. For several reasons the convention expressed in eqn. 2 is particularly attractive:

$$\sum \Psi_{i/v\text{NA}} = 0 \quad (2)$$

i.e., the sum of the adsorbed amount in terms of volume is zero. This convention is named the vNA-convention; *Nothing is Adsorbed* in terms of volume. Obviously, with this convention the total liquid in the column is considered as the mobile phase and eqn. 3 holds:

$$V_{\kappa/\text{tot}} = V_{\mu/v\text{NA}} \quad (3)$$

where $V_{\mu/v\text{NA}}$ is the hold-up volume. This hold-up

volume is independent of the eluent composition if the partial molar volumes of all components in the mixture as well as in the adsorbed state are equal to the molar volume of the pure components.

Retention

With a binary eluent, A/B, the retention volume, $V_{R,i}$, of a component, i ($=$ su, A, B), is given by [2,6]

$$V_{R,i} = \left(\frac{\partial V_{\kappa,i}}{\partial \varphi_i} \right)_{\varphi_A^0} - \varphi_i^0 \left(\frac{\partial V_{\kappa,\text{tot}}}{\partial \varphi_i} \right)_{\varphi_A^0} \quad (4)$$

where the superscript zero refers to concentrations at equilibrium in the column before injection. Combination of eqns. 1, 3 and 4 gives the retention volume of a solute, su:

$$V_{R,\text{su}} = V_{\mu/\nu\text{NA}} + S \left(\frac{\partial \Psi_{\text{su}/\nu\text{NA}}}{\partial \varphi_{\text{su}}} \right)_{\varphi_A^0}; \quad \varphi_{\text{su}} \rightarrow 0 \quad (5)$$

and the retention volume of the injection of component A or B of the binary eluent:

$$V_{R,A} = V_{R,B} = V_{\mu/\nu\text{NA}} + S \left(\frac{\partial \Psi_{A/\nu\text{NA}}}{\partial \varphi_A} \right)_{\varphi_A^0} \quad (6)$$

called the system peak (SP) or concentration peak. Application of eqn. 4 to labelled components of the eluent, A* and B*, and combination of the results give the necessary relationship for the experimental determination of the hold-up volume:

$$V_{\mu/\nu\text{NA}} = \varphi_A V_{R,A^*} + \varphi_B V_{R,B^*} \quad (7)$$

The hold-up volume, $V_{\mu/\nu\text{NA}}$, has been shown to be independent of eluent composition [2,29]. Its knowledge allows the calculation of the net retention volume:

$$V_{N,\text{su}/\nu\text{NA}} = V_{R,\text{su}} - V_{\mu/\nu\text{NA}} \quad (8)$$

The areal retention volume is defined as

$$V_{S,\text{su}/\nu\text{NA}} = \frac{1}{S} \cdot V_{N,\text{su}/\nu\text{NA}} = \left(\frac{\partial \Psi_{\text{su}/\nu\text{NA}}}{\partial \varphi_{\text{su}}} \right)_{\varphi_A^0} \quad (9)$$

The areal retention volume, $V_{S,\text{su}/\nu\text{NA}}$, can be identified as the slope of the areal excess isotherm of the solute at the eluent composition. It is an intensive, model-independent characteristic of solute retention. It is related to the solute adsorption equilibrium at the eluent composition, φ_A^0 , and as such it can be a positive or a negative quantity. This representation of solute retention does not suppose

the existence of any autonomous liquid stationary phase, and implies that solute retention in liquid–solid chromatography is an interfacial phenomenon necessarily proportional to the extent of the adsorbent surface area in the column, S . Obviously, the determination of S requires the use of a non-chromatographic technique. Nevertheless, using this representation, areal retention volumes are independent of column construction and adsorbent morphology. Hence they allow comparison of retention data between different laboratories.

Capacity factor

The widely used capacity factor of a solute, k'_{su} , is the ratio of a reduced retention volume, $V_{N,\text{su}}$, and the retention of a substance believed to traverse the column with the same velocity as that of the mobile phase, V_0 :

$$k'_{\text{su}} = \frac{V_{R,\text{su}} - V_0}{V_0} = \frac{V_{N,\text{su}}}{V_0} \quad (10)$$

Obviously, the capacity factor is not suitable to report system-independent retention data, for several reasons. When using eqn. 10, it is believed that V_0 is a correct hold-up volume equal to the volume of a mobile bulk liquid in the column. However, in a liquid–solid adsorption system there is no possibility of identifying a liquid of bulk composition and a distinct layer at the interface having a different composition. Therefore, the proposal to determine the hold-up volume by injection of a “non-adsorbed” component leads to a wide variety of hold-up volume definitions. Hold-up volume differences of up to 100% can be found following different methods proposed for its determination [6,7,11,23, 30–35]. Moreover, this hold-up volume also includes column tubing contributions making it dependent on the actual measuring system. Even if everyone agreed to report capacity factors using a hold-up volume belonging only to the column and referring to a given Gibbs convention (e.g., $V_0 = V_{\mu/\nu\text{NA}}$), the resulting $k'_{\text{su}/\nu\text{NA}}$ would still not be an intensive property of the solute. In fact, the net retention volume, $V_{N,\text{su}/\nu\text{NA}}$, is proportional to the surface area of the adsorbent but the hold-up volume, $V_{\mu/\nu\text{NA}}$, is not. As an example, in two columns of similar volume packed with two adsorbents having surface areas of S and $2S$, the net retention will differ by a factor of 2 whereas the hold-up volume may be

about the same. For reasons outlined above, it is proposed that liquid chromatographic data be reported in terms of areal retention volumes instead of the capacity factor.

The capacity factor or “mass distribution coefficient” is defined as the ratio of the amounts of solute in the stationary phase and in the mobile phase. Based on this definition, the capacity factor related to the vNA convention, $k'_{su/vNA}$, can be interpreted as follows. The relationship of eqn. 9 between the adsorption isotherm of the solute, $\Psi_{su/vNA}$, at the eluent composition φ_A^0 and its concentration in the eluent can be written as

$$V_{N,su/vNA}/S = \Psi_{su/vNA}/\varphi_{su}; \quad \varphi_{su} \rightarrow 0 \quad (11)$$

In fact, the value of the derivative of the solute isotherm, $\Psi_{su/vNA}(\varphi_{su})$, with respect to the volume fraction of the solute is equal to the ratio given in eqn. 11 at $\varphi_{su} \rightarrow 0$. Use of the experimental definition of the capacity factor given in eqn. 10 with $V_0 = V_{\mu/vNA}$ and eqns. 1, 8 and 11 gives

$$k'_{su/vNA} = \frac{V_{N,su/vNA}}{V_{\mu/vNA}} = \frac{S\Psi_{su/vNA}}{\varphi_{su}V_{\mu/vNA}} = \frac{S\Psi_{su/vNA}}{V_{\kappa,su} - S\Psi_{su/vNA}} \quad (12)$$

Eqn. 12 shows that this capacity factor is the ratio of the excess adsorbed amount of the solute (expressed as volume) and of the non-adsorbed part contained in the total liquid volume [36]. The excess adsorbed amount of the solute, and hence also the capacity factor related to the vNA convention, $k'_{su/vNA}$, can be positive or negative.

Areal retention volume, capacity factor and distribution coefficient

The relationship between the capacity factor and the areal retention volume referring to the vNA convention is obtained from eqns. 9 and 10 to give

$$SV_{S,su/vNA} = k'_{su/vNA}V_{\mu/vNA} \quad (13)$$

the link being given by the adsorbent surface area and the hold-up volume. With the necessary changes, eqn. 13 is of general validity for any hold-up definition.

Unlike the capacity factor, the distribution coefficient of the solute, $K_{D,su}$, defined as the ratio of the solute concentration near the interface and that in

the bulk liquid, would be a correct intensive quantity to characterize solute retention. However, with convention vNA it is meaningless. In fact, Gibbs' interpretation of adsorption by defining excess quantities is not a model, it does not locate anywhere the adsorbed excess of the solute and it does not define any liquid stationary phase. Application of the vNA (or any other) Gibbs convention does not allow the calculation of a distribution coefficient, $K_{D,su/vNA}$, because only knowledge of an adsorption excess isotherm does not permit the calculation of a local concentration near the interface.

In order to compare our data with literature values, a retention volume is needed that permits the calculation of a distribution coefficient. This can be found by introducing an unusual Gibbs convention as follows. As has been shown, if the partial molar volumes of eluent components in both the bulk liquid and the adsorbed state are the same as their molar volume in the pure state, the hold-up volume, $V_{\mu/vNA}$, is equal to the volume of the total liquid phase in the column. Let us now define a film of thickness τ parallel to the surface of the adsorbent as stationary phase, designated by \mathfrak{S} , and attribute all adsorption to this film of uniform composition. Applying this τ convention, derived from the vNA convention, the volume of the stationary liquid, $V_{\mathfrak{S}/\tau}$, is equal to τS . The remaining volume of the total liquid is now considered as the mobile phase, and consequently the hold-up volume is given by

$$V_{\mu/\tau} = V_{\mu/vNA} - \tau S \quad (14)$$

i.e., it is defined with reference to the hold-up volume, $V_{\mu/vNA}$. The necessary relationships for the calculation of the corresponding areal retention volume, $V_{S,su/\tau}$, the related capacity factor, $k'_{su/\tau}$, and the distribution coefficient, $K_{D,su/\tau}$, are as follows:

$$V_{S,su/\tau} = V_{S,su/vNA} + \tau \quad (15)$$

$$k'_{su/\tau} = \frac{V_{S,su/vNA} + \tau}{(V_{\mu/vNA}/S) - \tau} \quad (16)$$

$$K_{D,su/\tau} = k'_{su/\tau}V_{\mu/\tau}/V_{\mathfrak{S}/\tau} = 1 + V_{S,su/vNA}/\tau \quad (17)$$

On the areal retention volume scale, transformation of the vNA convention to the τ convention represents a simple shift by the arbitrarily chosen layer thickness, τ . On the capacity factor scale, however, not only the zero point but also the units change owing to such a transformation, as illus-

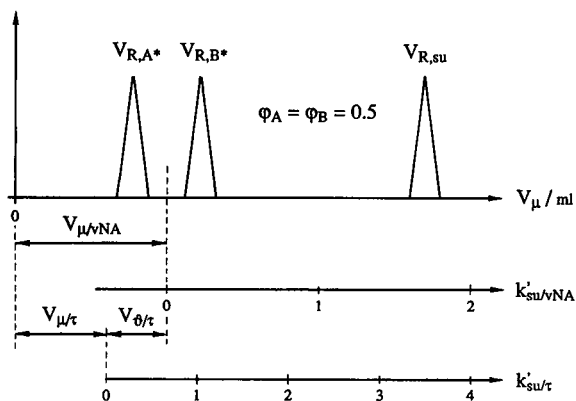


Fig. 2. Illustration of eqns. 14–17 on a hypothetical example where $\varphi_A = \varphi_B = 0.5$. In this case the hold-up volume, $V_{\mu/vNA}$, is exactly mid-way between the retention volumes of the labelled components of the binary eluent, V_{R,A^*} and V_{R,B^*} . The scale of the capacity factor, $k'_{su/vNA}$, is related to this hold-up volume. The volume of the hypothetical stationary phase, $V_{g/t} = \tau S$, is deduced from the total mobile phase volume, $V_{\mu/vNA}$, to give a new hypothetical mobile phase volume, $V_{\mu/\tau}$, which is the unit of the second capacity factor scale, $k'_{su/\tau}$.

trated in Fig. 2. For a solute having zero excess adsorption, $V_{S,su/vNA}$ is equal to zero. Such a solute has a uniform concentration in the whole liquid phase ("mobile, μ " and "stationary, ϑ ") and eqn. 16 gives $k'_{su/\tau} = V_{g/t}/V_{\mu/\tau}$, the phase ratio, and eqn. 17 gives $K_{D,su/\tau} = 1$.

Choice of the stationary layer thickness, τ

For the columns applied in this study a column hold-up volume corrected for the extra-column volumes of tubings and connections was measured and reported in ref. 2 to give $V_{\mu/vNA} = 2.1$ – 2.3 ml. The surface area of the adsorbent in the column was around $S = 340$ m², giving a liquid volume per unit surface area of $V_{\mu/vNA}/S \approx 6.5$ $\mu\text{l}/\text{m}^2 \equiv 65$ Å. Obviously, to avoid negative mobile phase volumes, the value of the thickness, τ , must be less than 65 Å. On the other hand, there is also a lower limit of the layer thickness to ensure that surface concentrations are always positive and monotonously increasing functions of bulk concentrations, which is a thermodynamic necessity [7]. This minimum thickness is about 15 Å in AN–W mixtures on both surfaces (C_{14} and DMB) as shown by the corresponding excess adsorption isotherms [2]. In conclusion, a value of 15 Å is proposed for τ . With this layer thickness, the

volume of the stationary phase in our columns is $V_{g/t}/S = 1.5$ $\mu\text{l}/\text{m}^2$ and that of the mobile phase $V_{\mu/\tau}/S \approx 6.5 - 1.5 = 5.0$ $\mu\text{l}/\text{m}^2$, both referred to unit surface area, to give a phase ratio of $V_{g/t}/V_{\mu/\tau} \approx 0.30$. As an example, for a solute retained with $V_{S,su/vNA} = 2.0$ $\mu\text{l}/\text{m}^2$, the fraction in the τ interfacial layer is 41% of the total.

Obviously, the choice of the thickness $\tau = 15$ Å is only valid for the actual working system, *i.e.*, AN–W binary eluent mixtures on DMB and C_{14} surfaces. In other systems the choice of a different thickness may be necessary.

Concluding remarks

It should be emphasized that the introduction of the τ convention was simply a device to enable literature proposals to be applied for the description of the composition dependence of retention. In fact, these proposals are based on models assuming the existence of a stationary phase of given volume. Such a model implies that negative net retention volumes do not exist and leads to equations relating the logarithm of net retention to the eluent composition. It was therefore necessary to transform the areal retention volumes related to the vNA convention (which permits negative values) to areal retention volumes referred to an appropriate τ convention which excludes negative values. Actually, the minimum of such a layer thickness identified as the minimum slope of the binary excess isotherm, and this choice implies that areal retention volumes of any solute calculated with the corresponding hold-up volume are never negative. This statement remains valid as long as the binary adsorption equilibrium is not considerably altered by the solute, which is always supposed to be present in infinite dilution. All solutes used in this study fulfilled this requirement, and consequently eqn. 17 for the calculation of a distribution coefficient will always be applicable.

EXPERIMENTAL

Materials

The precipitated silica for the preparation of the stationary phases was LiChrosorb Si 100 from Merck (Darmstadt, Germany) with a nominal particle diameter of 10 μm and a pore diameter of 100 Å. Nitrogen adsorption isotherms were measured at

77 K. BET evaluation of the isotherm in the relative pressure range $0.05 < P_e/P_0 < 0.23$ gave a specific surface area of $s = 298 \pm 3 \text{ m}^2/\text{g}$ (average of three determinations). Nitrogen for adsorption experiments (99.999%) and liquid nitrogen for thermostating (99.8%) were obtained from Carbagas (Lausanne, Switzerland). The silylating agents (purity >98%) N-[(3,3-dimethylbutyl)dimethylsilyl]-N,N-dimethylamine and N-(tetradecyldimethylsilyl)-N,N-dimethylamine were synthesized in our laboratory [37]. Acetonitrile (AN) for HPLC from Ammann Technik (Kölliken, Switzerland) was used as received. Doubly distilled water (W) was prepared by distilling deionized water over potassium permanganate in a Fontavapor-285 Pyrex glass still from Büchi (Flawil, Switzerland). The solutes, research-grade deuterated compounds (isotope purity >99.5%) $\text{D}^2\text{H}_2\text{O}$ and $\text{CD}^2\text{H}_3\text{CN}$ (W* and AN*) from Chemie Uetikon (Uetikon, Switzerland) and research-grade 1-alkanols, 2-alkanols, 2-alkanones, 1-alkyl acetates, *n*-alkanes and 2,2-dimethylalkanes from Fluka (Buchs, Switzerland), were used as received.

Chromatographic columns

Column materials were prepared by reaction of vacuum-dried (10^{-3} Torr at 120°C for 10 h) LiChrosorb Si 100 with R-dimethyl(dimethylamino)silane (ca. $15 \mu\text{mol}/\text{m}^2$) at 180°C for 100 h, following the reported procedure [1]. Surface concentrations of the siloxy substituents, Γ_{siox} , listed in Table I were calculated with the carbon content of the silylated products measured by elemental analysis and with the BET specific surface area of the unreacted silica, using the equation given previously [38]. The columns used and the procedure for column packing were described in detail previously [39]. Columns were dried at 120°C in a stream of argon and the mass of the stationary phase in the column, m_g , was determined by weighing (see Table I). This operation was repeated after having finished all chromatographic experiments. After 2 years of use no significant loss of the stationary phase mass was observed [39]. The surface area of the adsorbent in the columns was assumed to be equal to that of the unmodified silica [40], given by

$$S = sm_g \{1 + 10^{-6} \Gamma_{\text{siox}} s [M(\text{R}) - \text{corr}]\}^{-1} \quad (18)$$

where s (m^2/g) is the specific surface area of the

TABLE I
CHARACTERISTICS OF THE STATIONARY PHASES AND COLUMNS USED

Γ_{siox} is the surface concentration of the alkyl dimethylsilyloxy substituent, m_g is the mass of the adsorbent and S is the surface area of the adsorbent, assumed to be equal to the surface area of the silicon dioxide in the column. Standard deviations are given in the bottom row.

Stationary phase	Column		
	Γ_{siox} ($\mu\text{mol}/\text{m}^2$)	m_g (g)	S (m^2)
Graft			
DMB	3.85	1.302	334
C ₁₄	4.09	1.547	352
S.D.	± 0.02	± 0.002	± 4

unmodified silica, Γ_{siox} ($\mu\text{mol}/\text{m}^2$) is the surface concentration of the graft, $M(\text{R})$ is the molar mass of the trialkylsilyl substituent and corr (= 2.5) is a correction for proton substituted and water desorbed during silylation [38]. Column characteristics are listed in Table I.

Apparatus

Nitrogen adsorption isotherms were measured with a modified Sorptomatic 1800 apparatus from Carlo Erba (Milan, Italy) [38]. The carbon contents of the column materials were determined with a Model 240B elemental analyser (Perkin-Elmer, Norwalk, CT, USA).

The chromatographic apparatus was described in detail previously [41]. It was an assembly of a Model 510 solvent-delivery pump, a Model U6K injector (loop volume 1 ml) and a Model 410 differential refractometer detector (cell volume $10 \mu\text{l}$), all from Waters (Milford, MA, USA). Columns were mounted in parallel in a thermostated bath at $20.0 \pm 0.1^\circ\text{C}$. Retention times (t_R) were measured with a Model SP4290 integrator (Spectra-Physics, Santa Clara, CA, USA). The flow-rate of the eluent, \dot{V}_R , was measured at $20.0 \pm 0.1^\circ\text{C}$ with a reproducibility of $0.005 \text{ ml}/\text{min}$; it had a long-term stability of $\pm 0.2\%$. The nominal flow-rate was $2.0 \text{ ml}/\text{min}$ throughout. Retention volumes (V_R) were calculated from retention times and the actual flow-rate. The mean column pressure (P_c) was approximately half of the inlet pressure (typical values $P_c = 20\text{--}50 \text{ bar}$).

Experiments

General. The binary AN–W eluent mixture of the appropriate composition, prepared by weighing an amount sufficient for all experiments on both columns, was degassed by bubbling helium through the mixture and kept under a slight helium overpressure (0.07 bar) during the experiments. The columns were equilibrated with the eluent of a given composition for 10 min.

Hold-up volume. First, pure W and AN were injected in order to identify the binary concentration peak (system peak), followed by mixtures of AN–W* and AN*–W of the same composition (mol/mol) as that of the eluent to give the retention volumes V_{R,W^*} and V_{R,AN^*} (W* and AN* represent deuterated water and acetonitrile, respectively). The system hold-up volume, $V_{\mu/NA}$, was calculated with eqn. 7.

Solutes. Members of different homologous series (1-alkanols, 2-alkanols, 2-alkanones, 1-alkyl acetates, *n*-alkanes and 2,2-dimethylalkanes) were injected and their retention times were measured. Weakly retained solutes were dissolved in the binary eluent in a ratio of up to 1:20 (v/v); solid solutes were injected in ethanol solution. Typical volumes injected were 0.5–1.5 μl , always aiming at the smallest possible reproducible signal. Measurements were made on both surfaces at eluent compositions listed in Table II and repeated at least seven times at each eluent composition. The reproducibility of the retention volume of the deuterated eluent components was $\sigma_{\text{rel}} = \pm 0.4\%$ and that of the solutes was $\sigma_{\text{rel}} \leq \pm 0.8\%$. Each solute, except solids, was also injected as a pure substance for the determination of the sign of the associated system peak.

Evaluation of asymmetric peaks

In Fig. 3 are shown chromatograms of *n*-heptane on the DMB surface at the eluent composition $\varphi_W = 0.293$. It was observed that the chromatograms obtained with different amounts injected followed the same trace at the fronting side. In order to determine the retention time at zero sample volume, it was assumed that the peak broadening in the column could be estimated from the narrow rear side of the peak. If this side corresponded to half of a Gaussian distribution, the standard deviation of the peak broadening can be determined from the distance between the mode and the intercept of the tangent of the rear side of the peak with the baseline,

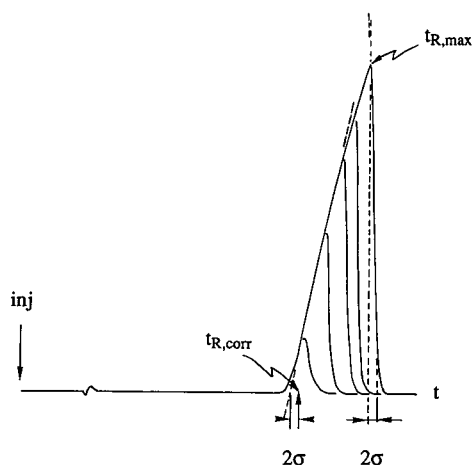


Fig. 3. Evaluation of the retention time of a solute eluting with asymmetric peaks. It shows the superposition of a series of fronting peaks obtained by injecting different volumes of *n*-heptane (2.0–0.1 μl) at $\varphi_W = 0.293$ onto the DMB-covered surface. It was assumed that the contribution to the standard deviation of the peak dispersion on the fronting side can be estimated from the dispersion of the (non-tailing) rear side of the peak. With this hypothesis, the retention time of an infinitesimal sample, $t_{R,corr}$, could be constructed.

equalling 2σ (see Fig. 3). Admitting that the same peak broadening is valid for the front side, the correct peak position should be at a distance of 2σ from the intercept of the tangent of the front side with the baseline. This evaluation was applied to all *n*-alkanes and 2,2-dimethylalkanes.

In several instances the opposite situation was found, with tailing peaks. Injection of different amounts of 1-butyl acetate onto the C_{14} surface at the eluent composition $\varphi_W = 0.602$ gave the mirror image of Fig. 3. For the determination of the peak position at zero amount injected, the analogous evaluation was applied. Tailing peaks were observed on both columns for 1-alkanols and 2-alkanols at $V_{S,su/vNA} > 12\text{--}15 \mu\text{l}/\text{m}^2$, for 2-alkanones at $V_{S,su/vNA} > 3\text{--}4 \mu\text{l}/\text{m}^2$ and for 1-alkyl acetates at $V_{S,su/vNA} > 7\text{--}8 \mu\text{l}/\text{m}^2$.

Retention data

In Table II are listed the experimental areal retention volumes of solutes at different eluent compositions, φ_W , referring to the vNA convention on the DMB-covered surface, $V_{S,su/vNA}^{\text{DMB}}$, and on the C_{14} -covered surface, $V_{S,su/vNA}^{C_{14}}$, calculated with eqn. 9.

TABLE II

AREAL RETENTION VOLUMES, $V_{S, \text{su}/V_{NA}}$ ($\mu\text{l}/\text{m}^2$), ON DMB- AND C_{14} -COVERED STATIONARY PHASES AT DIFFERENT VOLUME FRACTIONS OF WATER, φ_w , IN THE ACETONITRILE–WATER BINARY ELUENT

The column temperature was $20.0 \pm 0.1^\circ\text{C}$. Data on the C_{14} -covered adsorbent are in the second rows *in italics*. The sign of the associated system peak (+ if it is rich in AN) given as superscript.

Solute	φ_w														
	0.028	0.057	0.095	0.193	0.293	0.373	0.445	0.518	0.602	0.685	0.757	0.829	0.908	0.946	0.973
1-Alkanols															
Methanol	0.34 ⁻	0.14 ⁻	0.05 ⁻	-0.36 ⁺	-0.43 ⁺	-0.46 ⁺	-0.50 ⁺	-0.39 ⁺	-0.48 ⁻	-0.20 ⁻	-0.19 ⁻	0.14 ⁻	0.44 ⁻	0.79 ⁻	1.24 ⁻
	<i>0.20⁻</i>	<i>0.05⁻</i>	<i>-0.05⁻</i>	<i>-0.33⁺</i>	<i>-0.45⁺</i>	<i>-0.46⁺</i>	<i>-0.51⁺</i>	<i>-0.47⁺</i>	<i>-0.40⁻</i>	<i>-0.18⁻</i>	<i>-0.17⁻</i>	<i>0.09⁻</i>	<i>0.32⁻</i>	<i>0.70⁻</i>	<i>1.08⁻</i>
Ethanol	0.16 ⁻	0.10 ⁺	0.09 ⁺	-0.18 ⁺	-0.26 ⁺	-0.24 ⁺	-0.22 ⁺	-0.13 ⁺	0.12 ⁺	0.19 ⁺	0.34 ⁻	0.76 ⁻	1.32 ⁻	2.53 ⁻	3.66 ⁻
	<i>0.25⁻</i>	<i>0.08⁺</i>	<i>0.03⁺</i>	<i>-0.17⁺</i>	<i>-0.23⁺</i>	<i>-0.25⁺</i>	<i>-0.20⁺</i>	<i>-0.15⁺</i>	<i>0.20⁺</i>	<i>0.18⁺</i>	<i>0.30⁻</i>	<i>0.68⁻</i>	<i>1.21⁻</i>	<i>2.65⁻</i>	<i>3.80⁻</i>
1-Propanol	0.22 ⁺	0.17 ⁺	0.16 ⁺	0.00 ⁺	0.10 ⁺	0.23 ⁺	0.57 ⁺	0.58 ⁺	0.99 ⁺	1.39 ⁺	2.04 ⁺	3.04 ⁺	6.03 ⁺	9.25 ⁺	12.1 ⁺
	<i>0.42⁺</i>	<i>0.24⁺</i>	<i>0.20⁺</i>	<i>0.06⁺</i>	<i>0.17⁺</i>	<i>0.29⁺</i>	<i>0.55⁺</i>	<i>0.61⁺</i>	<i>1.13⁺</i>	<i>1.36⁺</i>	<i>1.96⁺</i>	<i>2.58⁺</i>	<i>6.05⁺</i>	<i>9.72⁺</i>	<i>14.8⁺</i>
1-Butanol	0.34 ⁺	0.31 ⁺	0.31 ⁺	0.30 ⁺	0.51 ⁺	0.90 ⁺	1.41 ⁺	2.10 ⁺	2.93 ⁺	4.28 ⁺	6.38 ⁺	10.0 ⁺	19.4 ⁺	28.9 ⁺	40.4 ⁺
	<i>0.58⁺</i>	<i>0.45⁺</i>	<i>0.38⁺</i>	<i>0.39⁺</i>	<i>0.56⁺</i>	<i>1.01⁺</i>	<i>1.52⁺</i>	<i>2.08⁺</i>	<i>3.13⁺</i>	<i>4.52⁺</i>	<i>6.59⁺</i>	<i>10.0⁺</i>	<i>22.0⁺</i>	<i>35.7⁺</i>	<i>57.3⁺</i>
1-Pentanol	0.51 ⁺	0.48 ⁺	0.49 ⁺	0.59 ⁺	1.04 ⁺	1.74 ⁺	2.67 ⁺	3.73 ⁺	5.88 ⁺	9.28 ⁺	16.1 ⁺	26.7 ⁺	60.8 ⁺	94.3 ⁺	143 ⁺
	<i>0.86⁺</i>	<i>0.74⁺</i>	<i>0.70⁺</i>	<i>0.95⁺</i>	<i>1.29⁺</i>	<i>2.10⁺</i>	<i>3.01⁺</i>	<i>4.18⁺</i>	<i>6.77⁺</i>	<i>10.7⁺</i>	<i>17.7⁺</i>	<i>31.6⁺</i>	<i>80.9⁺</i>	<i>143⁺</i>	<i>231⁺</i>
1-Hexanol	0.63 ⁺	0.67 ⁺	0.75 ⁺	1.01 ⁺	1.76 ⁺	2.84 ⁺	4.33 ⁺	6.47 ⁺	11.2 ⁺	18.3 ⁺	36.7 ⁺	73.1 ⁺	-	-	-
	<i>1.20⁺</i>	<i>1.16⁺</i>	<i>1.19⁺</i>	<i>1.62⁺</i>	<i>2.41⁺</i>	<i>3.68⁺</i>	<i>5.32⁺</i>	<i>7.71⁺</i>	<i>13.9⁺</i>	<i>23.4⁺</i>	<i>48.6⁺</i>	<i>101⁺</i>	-	-	-
1-Heptanol	0.87 ⁺	0.91 ⁺	1.02 ⁺	1.54 ⁺	2.52 ⁺	3.96 ⁺	6.14 ⁺	10.4 ⁺	17.0 ⁺	36.4 ⁺	-	-	-	-	-
	<i>1.53⁺</i>	<i>1.54⁺</i>	<i>1.84⁺</i>	<i>2.35⁺</i>	<i>3.53⁺</i>	<i>5.19⁺</i>	<i>7.61⁺</i>	<i>14.3⁺</i>	<i>21.6⁺</i>	<i>54.3⁺</i>	-	-	-	-	-
1-Nonanol	1.40 ⁺	1.58 ⁺	1.79 ⁺	3.26 ⁺	5.48 ⁺	9.50 ⁺	14.8 ⁺	23.2 ⁺	-	-	-	-	-	-	-
	<i>3.14⁺</i>	<i>3.54⁺</i>	<i>4.03⁺</i>	<i>6.26⁺</i>	<i>10.4⁺</i>	<i>15.8⁺</i>	<i>27.6⁺</i>	<i>44.5⁺</i>	-	-	-	-	-	-	-
1-Undecanol	2.11 ⁺	2.61 ⁺	2.98 ⁺	6.11 ⁺	10.4 ⁺	17.0 ⁺	36.6 ⁺	54.2 ⁺	-	-	-	-	-	-	-
	<i>5.81⁺</i>	<i>6.92⁺</i>	<i>8.43⁺</i>	<i>15.1⁺</i>	<i>26.1⁺</i>	<i>42.9⁺</i>	-	-	-	-	-	-	-	-	-
1-Tridecanol	2.82	3.81	4.39	9.37	17.5	30.9	-	-	-	-	-	-	-	-	-
	<i>10.4</i>	<i>13.3</i>	<i>17.1</i>	<i>32.0</i>	<i>61.1</i>	<i>108</i>	-	-	-	-	-	-	-	-	-
1-Tetradecanol	3.36	4.59	5.74	-	-	-	-	-	-	-	-	-	-	-	-
	<i>13.9</i>	<i>18.2</i>	<i>24.0</i>	-	-	-	-	-	-	-	-	-	-	-	-
1-Hexadecanol	4.78	7.02	10.4	-	-	-	-	-	-	-	-	-	-	-	-
	<i>23.1</i>	<i>33.7</i>	<i>44.0</i>	-	-	-	-	-	-	-	-	-	-	-	-
1-Octadecanol	6.79	9.59	-	-	-	-	-	-	-	-	-	-	-	-	-
	<i>38.1</i>	<i>57.0</i>	-	-	-	-	-	-	-	-	-	-	-	-	-
1-Eicosanol	9.57	14.1	-	-	-	-	-	-	-	-	-	-	-	-	-
	<i>61.3</i>	<i>99.4</i>	-	-	-	-	-	-	-	-	-	-	-	-	-
2-Alkanols															
2-Propanol	0.28 ⁺	0.18 ⁺	0.17 ⁺	0.00 ⁺	-0.02 ⁺	0.05 ⁺	0.14 ⁺	0.31 ⁺	0.56 ⁺	1.04 ⁺	1.37 ⁺	2.28 ⁺	4.62 ⁺	7.17 ⁺	10.0 ⁺
	<i>0.42⁺</i>	<i>0.18⁺</i>	<i>0.17⁺</i>	<i>0.06⁺</i>	<i>0.00⁺</i>	<i>0.06⁺</i>	<i>0.15⁺</i>	<i>0.31⁺</i>	<i>0.71⁺</i>	<i>0.90⁺</i>	<i>1.32⁺</i>	<i>2.04⁺</i>	<i>4.49⁺</i>	<i>7.72⁺</i>	<i>11.5⁺</i>
2-Butanol	0.34 ⁺	0.31 ⁺	0.23 ⁺	0.24 ⁺	0.40 ⁺	0.73 ⁺	1.09 ⁺	1.64 ⁺	2.14 ⁺	3.20 ⁺	4.48 ⁺	7.20 ⁺	14.3 ⁺	20.9 ⁺	30.6 ⁺
	<i>0.58⁺</i>	<i>0.40⁺</i>	<i>0.37⁺</i>	<i>0.34⁺</i>	<i>0.45⁺</i>	<i>0.77⁺</i>	<i>1.12⁺</i>	<i>1.68⁺</i>	<i>2.39⁺</i>	<i>3.20⁺</i>	<i>4.52⁺</i>	<i>6.93⁺</i>	<i>15.2⁺</i>	<i>24.6⁺</i>	<i>40.5⁺</i>
2-Pentanol	0.51 ⁺	0.49 ⁺	0.44 ⁺	0.59 ⁺	0.93 ⁺	1.50 ⁺	2.25 ⁺	3.12 ⁺	4.72 ⁺	7.05 ⁺	11.3 ⁺	19.9 ⁺	43.4 ⁺	67.7 ⁺	109 ⁺
	<i>0.86⁺</i>	<i>0.64⁺</i>	<i>0.67⁺</i>	<i>0.79⁺</i>	<i>1.12⁺</i>	<i>1.75⁺</i>	<i>2.46⁺</i>	<i>3.48⁺</i>	<i>5.20⁺</i>	<i>7.53⁺</i>	<i>11.9⁺</i>	<i>21.2⁺</i>	<i>53.1⁺</i>	<i>92.0⁺</i>	<i>161⁺</i>
2-Hexanol	0.63 ⁺	0.67 ⁺	0.66 ⁺	1.01 ⁺	1.64 ⁺	2.56 ⁺	3.84 ⁺	5.47 ⁺	9.05 ⁺	15.0 ⁺	27.5 ⁺	53.7 ⁺	-	-	-
	<i>1.14⁺</i>	<i>1.05⁺</i>	<i>1.09⁺</i>	<i>1.45⁺</i>	<i>2.07⁺</i>	<i>3.22⁺</i>	<i>4.94⁺</i>	<i>6.15⁺</i>	<i>11.1⁺</i>	<i>17.6⁺</i>	<i>32.0⁺</i>	<i>64.9⁺</i>	-	-	-

(Continued on p. 10)

TABLE II (continued)

Solute	φ_w														
	0.028	0.057	0.095	0.193	0.293	0.373	0.445	0.518	0.602	0.685	0.757	0.829	0.908	0.946	0.973
2,2-Dimethylalkanes															
2,2-Dimethyl- butane	1.94 ⁻	2.77 ⁻	3.38 ⁻	6.16 ⁻	11.6 ⁻	18.8 ⁻	-	-	-	-	-	-	-	-	-
	4.86 ⁰	6.50 ⁰	7.97 ⁰	15.4 ⁰	27.9 ⁰	45.5 ⁰	-	-	-	-	-	-	-	-	-
2,2-Dimethyl pentane	2.47 ⁻	3.59 ⁻	4.45 ⁻	8.12 ⁻	15.6 ⁻	26.8 ⁻	-	-	-	-	-	-	-	-	-
	6.64 ⁰	9.09 ⁰	11.3 ⁰	19.7 ⁰	43.8 ⁰	72.9 ⁰	-	-	-	-	-	-	-	-	-
2,2-Dimethyl- hexane	3.18 ⁻	3.82 ⁻	4.92 ⁻	10.8 ⁻	21.6 ⁻	-	-	-	-	-	-	-	-	-	-
	8.64 ⁰	12.3 ⁰	15.5 ⁰	31.8 ⁰	65.2 ⁰	-	-	-	-	-	-	-	-	-	-

The standard deviation of the areal retention volumes was calculated to be $\sigma_{V_{S,su/vNA}} = \pm(0.08 + 0.012 V_{S,su/vNA}) \mu\text{l}/\text{m}^2$. The sign of the associated system peak is given as a superscript (+ and - for a system peak rich and poor in AN, respectively).

RESULTS AND DISCUSSION

As indicated in the Introduction, adsorption isotherms from AN–W mixtures are almost congruent on the two chemically modified (DMB and C_{14}) surfaces. Hence, the “hard” DMB surface can be considered as a reference, and a difference in areal retention volume on the C_{14} surface at the same eluent composition can unequivocally be attributed to the presence of the bonded alkyl chains. In the following, first the dependence of areal retention on composition on the DMB surface will be discussed, then the additional retention on the C_{14} surface. The system peak accompanying the injection of a pure solute can be positive or negative, *i.e.*, rich or poor in AN. An interpretation of the sign of this system peak will also be given.

Solute retention as a function of eluent composition

The dependence of the areal retention volume, $V_{S,su/vNA}$, on eluent composition shows the often reported general trend of increasing retention with increasing water content and also with increasing carbon number of the homologues. In Fig. 4 are plotted, as an illustration, areal retention volumes on the DMB surface, $V_{S,su/vNA}^{\text{DMB}}$, for homologous 1-alkanols as a function of the volume fraction of

water in the eluent, φ_w . This example is particularly interesting because several homologues could be measured in the whole or in a broad concentration range. This general trend is the same for other homologous series and is also observed for data on the C_{14} surface. The plot suggests that the composition dependence of the retention of all solutes follows a similar law when choosing an individual starting point for each solute on the composition scale.

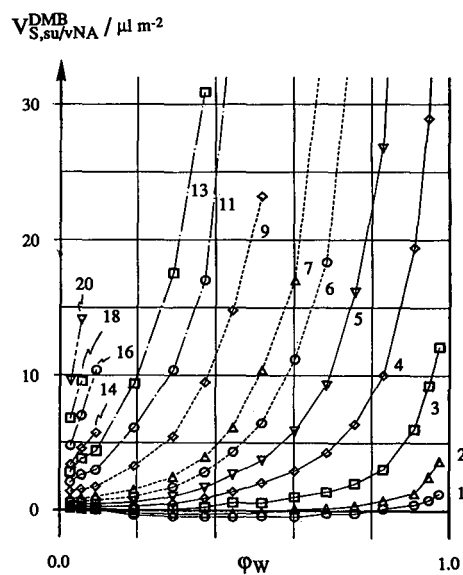


Fig. 4. Areal retention volumes, $V_{S,su/vNA}^{\text{DMB}}$, of 1-alkanols, $C_zH_{2z+1}OH$ with $z = 1-20$ as indicated, on the DMB-covered surface as a function of the volume fraction of water, φ_w , in the binary AN–W eluent.

Two equations are widely used to describe retention as a function of eluent composition. The most often used, due to Snyder [42] and Soczewinski [43], proposes that the logarithm of retention is a linear function of the logarithm of the volume fraction of the organic component. The second equation, due to Schoenmakers *et al.* [44], proposes a quadratic expression for the dependence of the logarithm of retention on the eluent composition. Neither equation is applicable to areal retention volumes in the vNA convention, $V_{S,su/vNA}$, because this retention characteristic can be negative (*e.g.*, methanol and ethanol; see Fig. 4).

Areal retention volumes determined with reference to the vNA convention, $V_{S,su/vNA}$, differ from those referring to a hold-up volume with a stationary layer of $\tau = 15 \text{ \AA}$, $V_{S,su/15}$, by a constant of 1.5 \mu l/m^2 , as explained under Theoretical Background (see eqn. 15). This areal retention is never negative because it corresponds to the minimum layer thickness determined by the minimum slope of the excess adsorption isotherm of the eluent components [7]. Further, the areal τ retention volume with

$\tau = 15 \text{ \AA}$, $V_{S,su/15}$, is roughly proportional to capacity factors reported in the literature where the hold-up volume has been determined with a solute which at all compositions has been believed to be less adsorbed than either component of the eluent. Consequently, this areal retention volume and/or the related distribution coefficient, $K_{D,su/15}$, is suitable for examining the validity of the Snyder–Soczewinski and the Schoenmakers equations:

$$\ln K_{D,su/15} = A + B \ln \phi_{AN} \quad (19)$$

$$\ln K_{D,su/15} = a + b\phi_W + c(\phi_W)^2 \quad (20)$$

Eqns. 19 and 20 were originally formulated for the logarithm of the capacity factor. The distribution coefficient, $K_{D,su/15}$, is proportional to the areal retention volume, hence it is also roughly proportional to literature capacity factors. Consequently, the original equations differ from eqns. 19 and 20 by a common constant for all solutes.

At first sight, it is obvious that neither equation can describe retention in the whole composition range. Fig. 5 shows the plot of the logarithm of the

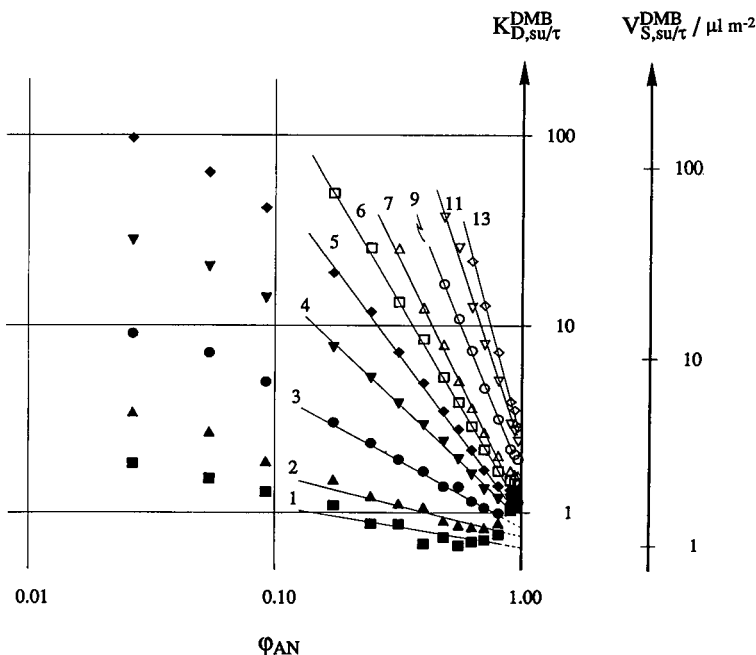


Fig. 5. Illustration of the use of eqn. 19 for the description of the composition dependence of the logarithm of the distribution coefficient, $\ln K_{D,su/15}^{DMB}$, with a stationary phase thickness of $\tau = 15 \text{ \AA}$ on the example of 1-alkanols, $C_zH_{2z+1}OH$ with $z = 1-13$ as indicated, on the DMB-covered surface. Solid lines are traces of the linear regression of $\ln K_{D,su/15}^{DMB}$ fitted to experimental points in the composition range $\phi_{AN} = 0.1-0.9$. The scale of the areal τ retention volumes is also shown.

distribution coefficient on the DMB surface, $\ln K_{D,su/15}^{DMB}$, of the 1-alkanols as a function of the logarithm of the volume fraction of acetonitrile in the eluent, $\ln \varphi_{AN}$. For comparison, the logarithmic areal τ retention volume scale, $\ln V_{S,su/15}^{DMB}$, is also shown in Fig. 5. It is seen that the plot is fairly linear in the composition range $0.1 < \varphi_{AN} < 0.9$, with the exception of weakly retained homologues. The Snyder–Soczewinski plot for other solutes confirms these qualitative conclusions. Based on the underlying model the slope, B , of eqn. 19 should be proportional to the molar volume of the solutes. Fig. 6 shows the plot of the constant B of all solutes on the DMB surface as a function of the molar volume. The plot is strongly curved for weakly retained solutes, and further, the constant B seems to depend also on the polarity of the solutes.

The applicability of eqn. 20 is illustrated in Fig. 7, where solid lines represent quadratic regressions in the composition range $0.0 < \varphi_w < 0.9$, where the representation of experimental points by eqn. 20 is very satisfactory as was pointed out by Schoenmakers *et al.* [45]. The dotted lines show the quadratic regressions if all points are included in the

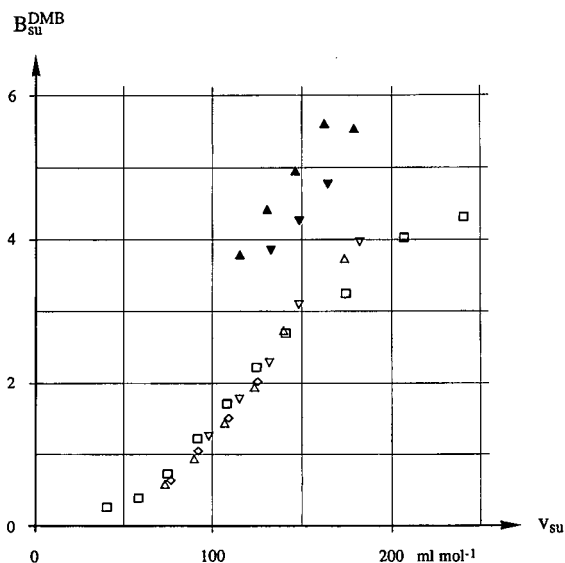


Fig. 6. Value of the constant B_{su}^{DMB} (slope) in the linear regression eqn. 19 (the logarithm of the distribution coefficient, $\ln K_{D,su/\tau}^{DMB}$, with $\tau = 15 \text{ \AA}$ vs. the logarithm of the volume fraction of AN in the eluent, $\ln \varphi_{AN}$) as a function of the molar volume of the solutes, v_{su} . Experimental points outside the composition range $\varphi_{AN} = 0.1\text{--}0.9$ were not considered for the regression (see text and Fig. 5). \blacktriangle = *n*-Alkanes; \blacktriangledown = 2,2-dimethylalkanes; \square = 1-alkanols; \diamond = 2-alkanols; \triangle = 2-alkanones; ∇ = 1-alkyl acetates.

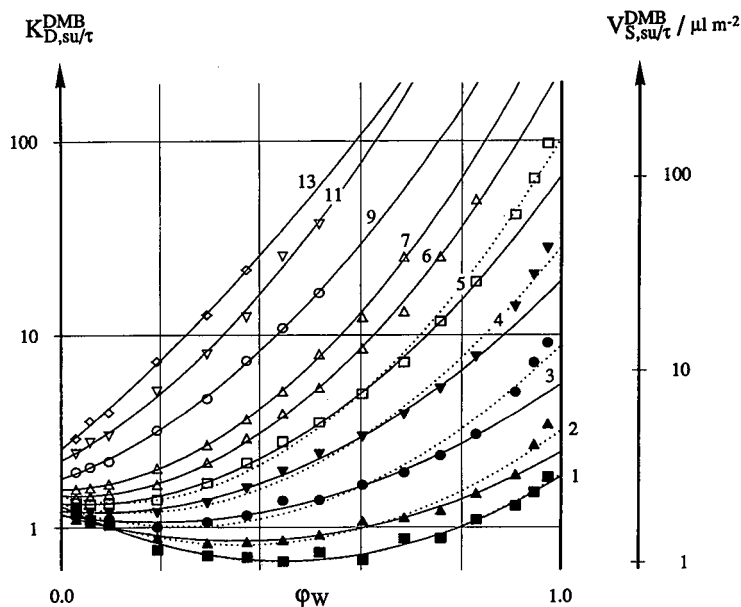


Fig. 7. Illustration of the description of the composition dependence of the logarithm of the distribution coefficients, $\ln K_{D,su/\tau}^{DMB}$, calculated with $\tau = 15 \text{ \AA}$, by eqn. 20 as a function of the volume fraction of water, φ_w , in the binary AN–W eluent on the example of 1-alkanols, $C_zH_{2z+1}OH$ with $z = 1\text{--}13$ as indicated, on the DMB-covered surface. Solid lines are traces of the quadratic eqn. 20 fitted to points in the range $\varphi_w = 0.0\text{--}0.9$; dotted lines are traces of eqn. 20 fitted to all experimental points including those in the water-rich region. The scale of the areal τ retention volumes is also shown.

whole composition domain. It is interesting that this regression is suitable for extrapolation to pure acetonitrile as eluent but gives erroneous results for pure water. Based on the underlying model [44], the value of the volume fraction of water at the minimum retention, $\varphi_{W,\min}$, either real or hypothetical, calculated from the quadratic regression for moderately retained solutes, should be related to the Hildebrand solubility parameter of the eluent components, δ_{AN} and δ_W , and that of the solute, δ_{su} , according to

$$\varphi_{W,\min} = -b/2c = (\delta_{su} - \delta_{AN})/(\delta_W - \delta_{AN}) \quad (21)$$

In Fig. 8 the experimental value of the volume fraction of water at minimum retention, $\varphi_{W,\min}(\text{exp})$, is plotted as a function of the value predicted by eqn. 21 for weakly retained solutes. The correlation is poor.

In summary, the two-parameter eqn. 19 describes solute retention as a function of eluent composition in the domain $\varphi_W = 0.1\text{--}0.9$, whereas the three-parameter eqn. 20 is applicable in the range $\varphi_W = 0.0\text{--}0.9$. With these restrictions in mind, both equations are well suited for interpolation but are poorly related to their respective underlying models.

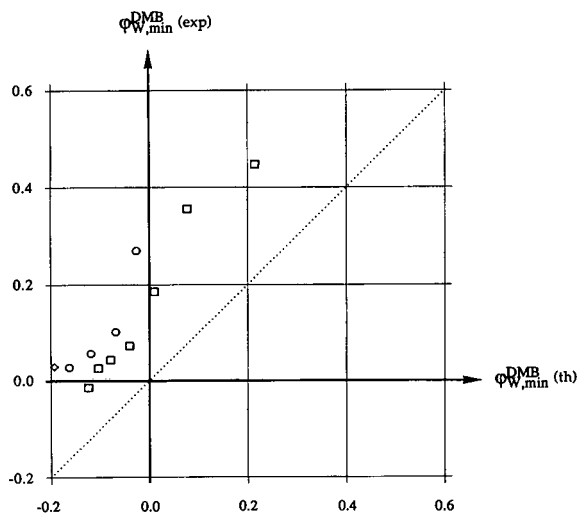


Fig. 8. Composition of the binary AN–W mixture at which retention is minimum on the DMB-covered surface, $\varphi_{W,\min}^{\text{DMB}}$, as a function of its theoretical value. Experimental minima are calculated from eqn. 20 fitted to experimental points in the range $\varphi_W = 0.0\text{--}0.9$; theoretical composition of the binary eluent at minimum retention is calculated with eqn. 21. \square = 1-Alkanols; \circ = 2-Alkanols; \diamond = 2-Alkanones.

Additional retention on the C_{14} surface

Areal retention volumes as a function of eluent composition show similar trends on the C_{14} and DMB surfaces. For a first comparison, regression coefficient of the Snyder–Soczewinski equation were calculated in the range $\varphi_W = 0.1\text{--}0.9$ on both adsorbents by using distribution coefficients, $K_{D,su/15}$. In Fig. 9 is shown the plot of the intercept, A , of eqn. 19 on the C_{14} surface as a function of the intercept, A , obtained on the reference surface, DMB. Fig. 10 shows the analogous plot of the constant B in eqn. 19, showing that the value of the constant is about the same on both surfaces. The value of the intercept A is also the same on both surfaces for weakly retained solutes, whereas for more strongly adsorbed solutes the intercept A on the C_{14} surface is about twice that on the DMB reference. Intercept A is interpreted as the logarithm of the distribution coefficient in a hypothetical pure acetonitrile (recall that eqn. 19 is only valid up to $\varphi_{AN} = 0.9$). In summary, the distribution coefficient at $\varphi_{AN} = 1$ of weakly retained solutes is the same on both surfaces, whereas for strongly retained solutes they are related by

$$K_{D,su/15}^{C_{14}} = (K_{D,su/15}^{\text{DMB}})^2 \quad (\varphi_{AN} = 1) \quad (22)$$

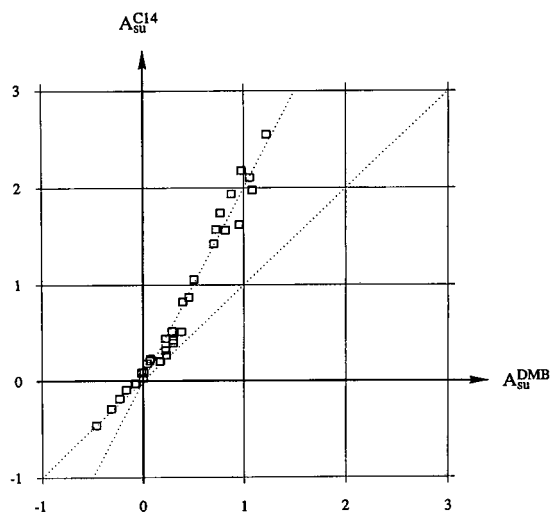


Fig. 9. Plot of coefficients A of the Snyder–Soczewinski equation (eqn. 19) fitted to experimental points determined on the C_{14} graft as a function of those found on the DMB reference surface.

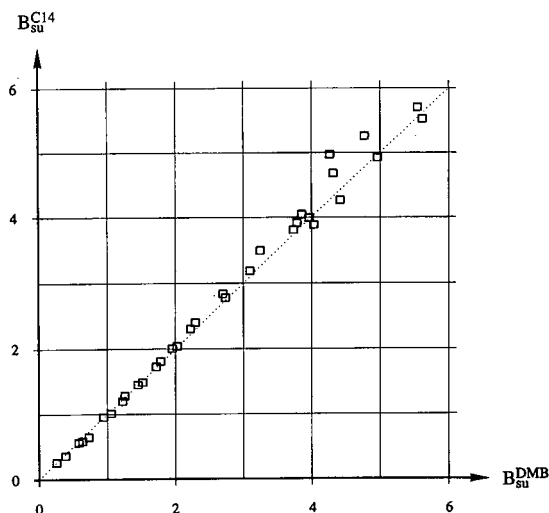


Fig. 10. Plot of the slope B of the Snyder–Soczewinski equation (eqn. 19) fitted to experimental points determined on the C_{14} graft as a function of those found on the DMB reference surface.

The change in correlation laws suggests different retention mechanisms for weakly and strongly retained (adsorbed) solutes.

In order to examine differences in retention in the whole composition range, let us examine the behaviour of the function $\Delta V_{S,su}^{C_{14}}$ defined as

$$\Delta V_{S,su}^{C_{14}} = V_{S,su/vNA}^{C_{14}} - V_{S,su/vNA}^{DMB} \equiv V_{S,su/\tau}^{C_{14}} - V_{S,su/\tau}^{DMB} \quad (\varphi_w = \text{constant}) \quad (23)$$

i.e., the additional areal retention volume on the C_{14} surface at the same eluent composition. This additional retention is independent of the hold-up volume definition. As examples, in Figs. 11 and 12 additional retention volumes are plotted as a function of the areal retention volumes on the reference surface, $V_{S,su/vNA}^{DMB}$, at two different eluent compositions. The latter retention measures the adsorption strength of the solute on a “hard” non-polar surface. It is seen that the additional retention is independent of the nature of the solute. As a main effect, the additional retention is proportional to retention on the reference surface, DMB, where its dependence

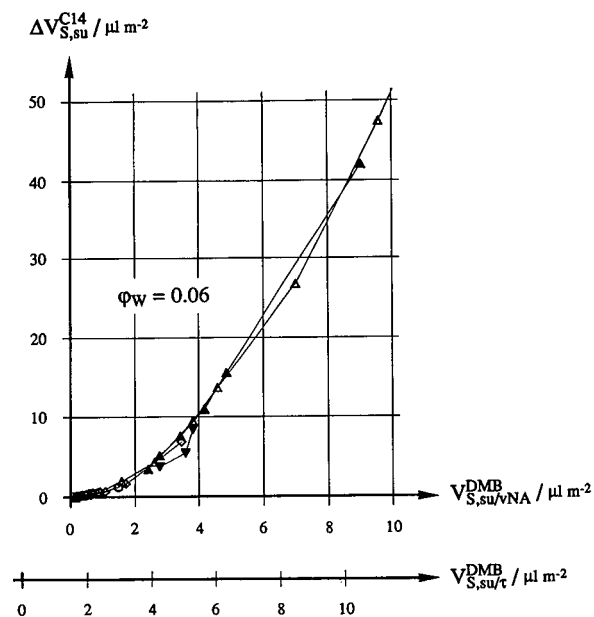


Fig. 11. Additional areal retention volumes on the C_{14} -covered surface, $\Delta V_{S,su}^{C_{14}}$, plotted as a function of areal retention volumes measured on the DMB reference surface, $V_{S,su/vNA}^{DMB}$, at the composition $\varphi_w = 6\%$ of the AN–W binary eluent. The scale of the areal τ retention volumes, with $\tau = 15 \text{ \AA}$, is also shown. \blacktriangle = n -Alkanes; \blacktriangledown = 2,2-dimethylalkanes; \triangle = 1-alkanols; ∇ = 2-alkanols; \circ = 2-alkanones; \diamond = 1-alkyl acetates.

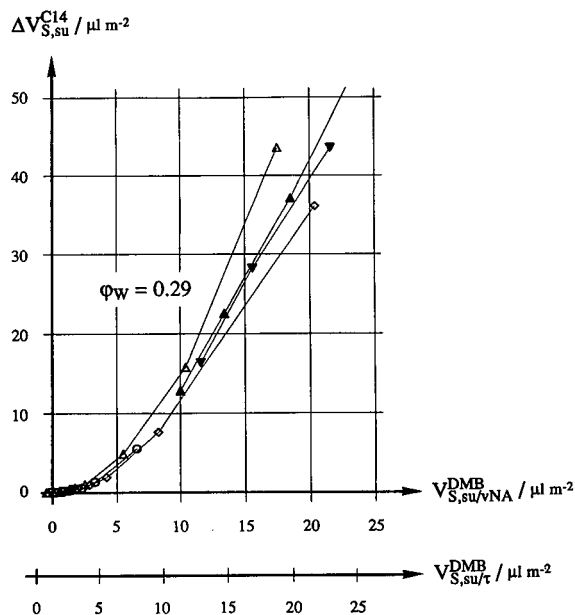


Fig. 12. Additional areal retention volumes on the C_{14} -covered surface, $\Delta V_{S,su}^{C_{14}}$, plotted as a function of areal retention volumes measured on the DMB reference surface, $V_{S,su/vNA}^{DMB}$, at the composition $\varphi_w = 29\%$ of the AN–W binary eluent. The scale of the areal τ retention volumes, with $\tau = 15 \text{ \AA}$, is also shown. Symbols as in Fig. 11.

can be approximated by the following one-parameter equation:

$$\Delta V_{S,su}^{C_{14}} = C(\varphi_w)(V_{S,su/vNA}^{DMB})^2 \quad (24)$$

In Fig. 13 the coefficient $C(\varphi_w)$ is plotted as a function of the composition of the eluent, φ_w . It is seen that the dependence of the additional retention on adsorption strength decreases with increasing water content in the eluent. In Fig. 14 the additional retention is plotted as a function of composition, φ_w , and areal retention volume on the reference surface, $V_{S,su/vNA}^{DMB}$, as a three-dimensional graph. As a general rule the retention increasing effect of the C_{14} graft is zero for slightly retained solutes and is less and less pronounced with increasing water concentration in the AN–W mixture.

The sign of the system peak

The slight perturbation of the composition of an m -component eluent gives rise to a set of $m - 1$ system peaks (also called concentration peaks [6] or eigenpeaks [46]). Injection of a small amount of an n -component solute mixture also perturbs the composition and will result in $m + n - 1$ peaks, of which n are called solute peaks and the remaining $m - 1$ are

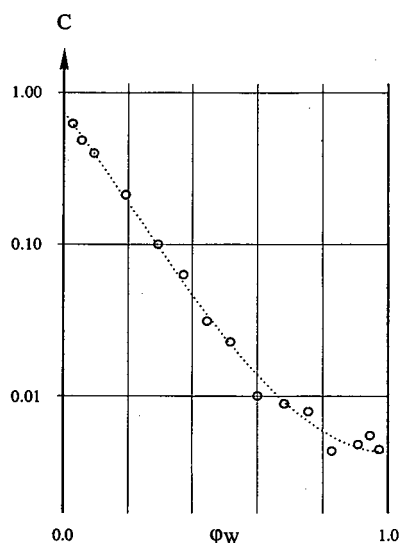


Fig. 13. Plot of coefficient C in eqn. 24 (logarithmic scale) relating additional retention on the C_{14} surface to the square of areal retention on the DMB surface as a function of the volume fraction of water in the binary AN–W eluent. The dotted line is the trace of the cubic polynomial regression of the logarithm of C on the volume fraction of water.

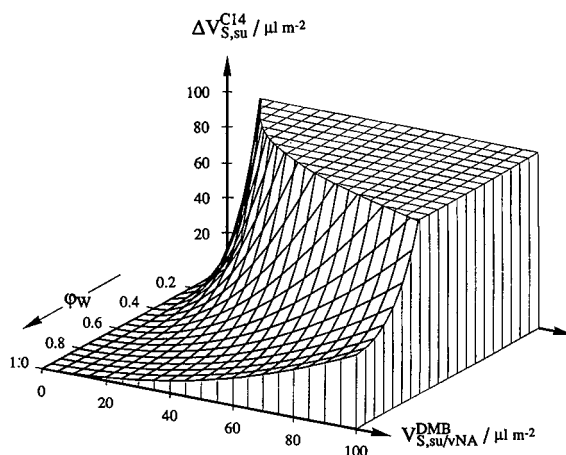


Fig. 14. Additional retention volume on the C_{14} surface, $\Delta V_{S,su}^{C_{14}}$, as a function of the areal retention volume of solutes on the DMB reference surface, $V_{S,su/vNA}^{DMB}$, and of the volume fraction of water in the binary AN–W eluent, φ_w . The surface is calculated with eqn. 24 using coefficients $C(\varphi_w)$ obtained by the regression shown in Fig. 13.

the associated system peaks. A solute peak will comprise one of the solutes contained in the solute mixture together with the m components of the eluent but, as a general rule, the concentration ratio of the eluent components will be different from that of the eluent mixture. The $m - 1$ associated system peaks, each having a different composition, contain only the n components of the eluent. The mathematical treatment of such a general case leads to the DeVault matrix [47]. An eigenvalue of the matrix corresponds to the retention characteristics of a peak [6,35,46,48] whereas the associated eigenvector is the composition in the column section where the peak is located [47,49,50]. Although the mathematical solution is known, "... it remains difficult to develop an intuitive direct understanding of the phenomena", as pointed out by Poppe [50]. Nevertheless, several attempts have been made to relate concentration changes under the peak to solvent displacement by the solute at the liquid–adsorbent interface [51,52] or to its preferential solvation in the eluent [53] or to a combination of both [46].

In a binary eluent mixture the phenomenon is greatly simplified as there will be only one system peak with invariant retention. Its retention volume is proportional to the slope of the excess adsorption isotherm of the binary eluent (see eqn. 6). In the

binary organic solvent–water mixture, a slight perturbation may be induced either by injection of the organic component or by injection of water, both provoking a system peak of the same retention and magnitude but of the opposite sign. In the following we shall designate a system peak as positive if it originates from injection of the organic component, and consequently the composition under the peak is richer in the organic component compared with the eluent, and as a negative system peak in the opposite case. As a general rule, the system peak also appears when a pure solute or a mixture of solutes is injected. As already noted by Melander *et al.* [46], the amplitude of the system peak which accompanies the peak of a pure solute, its “associated system peak”, gives valuable additional information on the adsorption mechanism of the solute in question.

Let us put forward the question of the sign and amplitude of the associated system peak. In Fig. 15 is illustrated the origin of the system peak for two extreme situations. In the first case, for a non-retained solute, there will be a concentration change in the binary eluent by preferential solvation. The corresponding excess solvation isotherm (see Fig. 15a) can be deduced by analogy with excess isotherms observed on adsorbents. A non-polar solute (N in Fig. 15) will have a (+)U-type solvation isotherm, where the sign (+) designates an organic-rich solvate layer. An amphiphilic molecule (A in Fig. 15) should have, as a general rule, a (-/+)S-type isotherm, *i.e.*, it will be preferentially solvated by water at low water concentrations (strong interaction of water with the hydrophilic head) and by the organic component at high water contents. Finally, solvation of a polar-type molecule (P in Fig. 15) must have a (-)U-type excess isotherm. In the column section where the solute is dissolved there will be a perturbation of the eluent composition of the opposite sign. Consequently, non- or weakly retained non-polar solutes will provoke a negative system peak, a non-retained polar solute will give rise to a positive system peak and the sign of the system peak associated with a non-retained amphiphilic molecule will change the sign from positive to negative with increasing water concentration. It is obvious that the sign of the system peak of a non-retained solute is independent of the nature of the adsorbent.

For the second extreme case of a strongly retained

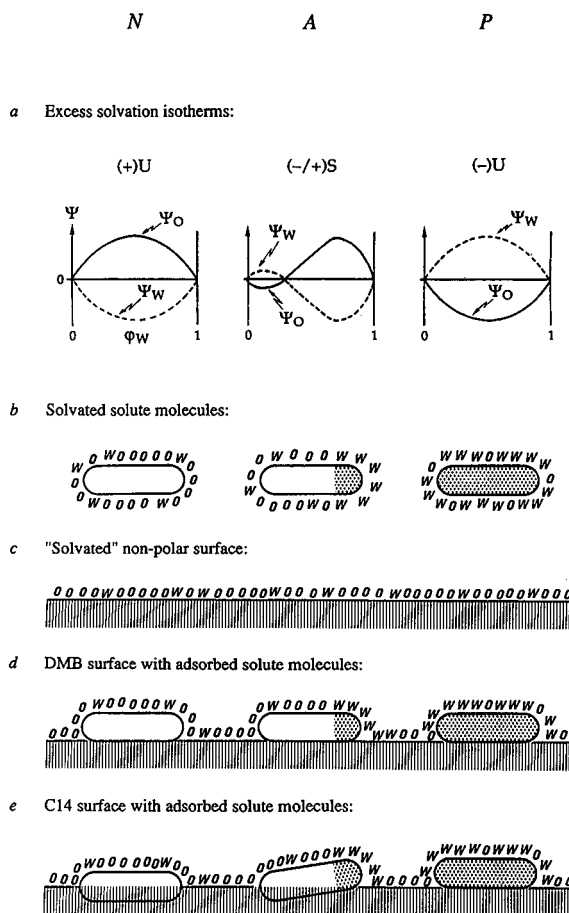


Fig. 15. Illustration of preferential (excess) adsorption on the surface of a non-polar adsorbent and of the preferential solvation of N = non-polar, A = amphiphilic and P = polar solutes in contact with an organic liquid–water (O–W) binary mixture. (a) Solvation excess isotherms of solutes of different polarity as a function of the water content in the O–W mixture: (+)U-type isotherm of non-polar solutes (N), (-/+)S-type isotherm of amphiphilic solutes (A) and (-)U-type isotherm due to preferential solvation by water of polar solutes (P). (b, c) Solvation/adsorption layers from the O–W mixture at some intermediate composition; (b) preferential solvation of solutes and (c) organic-rich adsorption layer near the non-polar surface in the absence of solutes. (d, e) Change of the adsorption layer in the presence of different types of adsorbed solutes on the hard DMB and the penetrable C₁₄ graft, respectively.

solute, the effect of preferential solvation can be neglected. In fact, such a molecule will most of the time be adsorbed and constitute part of the surface of the adsorbent. In Fig. 15c is illustrated the preferential adsorption of the organic component of

the eluent on a non-polar surface, such as DMB and C₁₄, following a (+)U-type excess isotherm. This isotherm will be only slightly perturbed by an adsorbed non-polar molecule on a hard-type non-polar DMB surface (see Fig. 15d) and even less on a soft-type (C₁₄) surface where the molecule can even penetrate the surface layer (see Fig. 15e). Consequently, there will be no or negligible perturbation of the isotherm and no or negligible system peak. Adsorption of polar-type and amphiphilic molecules will provoke throughout the whole composition range a positive system peak as the surface will become more hydrophilic with the adsorbed molecule.

This qualitative discussion concerning the sign of the associated system peak can be summarized as follows:

solute:	non-polar		amphiphilic		polar	
φ_w :	low	high	low	high	low	high
retention:						
weak:	–	+	–	–	+	+
strong:	0	+	+	+	(+)	

Based on similar arguments, Melander *et al.* [46] arrived at essentially the same conclusions. Let us emphasize that all solutes have stronger retention at higher water concentrations, φ_w . Consequently, at low water content the sign of the system peak should be discussed following the rules of a weakly retained solute, whereas at high water contents the rules of strongly retained solutes should be considered. The observed sign of the associated system peak, listed in Table II, is in accordance with this qualitative discussion with the exception of methanol and ethanol. In fact, the solvation isotherm was discussed by assuming that the molecule in solution is an adsorbing “colloidal” particle having a surface on which the small molecules of the eluent are adsorbed. Solvation of small molecules such as methanol and ethanol, comparable in size to the eluent components, probably follows a different rule. In Table II the superscript \pm is used to indicate composition where the sign of the system peak was not significant due to change of sign. This behaviour was observed for some of the 2-alkanones and 1-alkyl acetates as amphiphilic solutes on both surfaces at decreasing water concentrations for higher homologues. The change of sign takes place at about the same value of retention for a homolo-

gous series and corresponds to a compensation of solvation and adsorption effects. On the DMB surface, alkanes as non-polar solutes show a negative system peak which becomes zero at higher retentions where the fraction of solute molecules further away from the surface is negligible. The absence of the system peak in such cases is indicated in Table II with the superscript zero. No system peak was observed for alkanes and isoalkanes on the C₁₄ surface where non-polar solutes might penetrate into the liquid-like bulk of the C₁₄ chains.

CONCLUSIONS

It has been shown that retention of a solute on a non-polar adsorbent having grafted C₁₄ chains can be given as a function of its retention on the hard non-polar standard DMB surface. Combination of eqns. 23 and 24 gives

$$V_{S,su/vNA}^{Alkyl} = V_{S,su/vNA}^{DMB} (1 + C^{Alkyl} V_{S,su/vNA}^{DMB}) \quad (25)$$

The dependence of the areal retention volume on the DMB surface, $V_{S,su/vNA}^{DMB}$, as a function of the eluent composition can be described by eqns. 19 and 20 in their respective validity domains. Also, the coefficient C^{Alkyl} in eqn. 25 is a function of the composition but, to a first approximation, independent of the nature (polarity) of the solute, hence the function $C^{Alkyl}(\varphi_w)$ seems to be a characteristic of the (non-polar) stationary phase in question and of the organic component in the O–W binary eluent. On the C₁₄ surface, it decreases from its highest value in pure acetonitrile to very low values in the water-rich region following an exponential law as a function of the volume fraction of water, φ_w . Its amplitude being a measure of the additional retention on the surface with alkyl grafts, we conclude that the latter surface becomes increasingly similar to the hard DMB adsorbent with increasing water content.

In eqn. 25, the symbol of the areal retention on the surface with alkyl graft is designated by the superscript Alkyl instead of C₁₄, indicating that we believe that this equation is of general validity for non-polar adsorbents with grafted chains. The validity of this generalization remains to be proved, but its possibility is strongly suggested by findings on such stationary phases reported in the literature (see Introduction). In fact, the similar behaviour of such

stationary phases has been repeatedly demonstrated and it is generally admitted that additional retention is positive and increases with increasing chain length and increasing density of the graft. Obviously, differences between such adsorbents will be accounted for by the function $C^{\text{Alkyl}}(\varphi_{\text{W}})$.

The excess adsorption isotherms at the interface between the AN–W mixtures and the DMB and C₁₄ adsorbents are nearly congruent, as shown in Fig. 1. This result implies that acetonitrile does not penetrate the C₁₄ surface, *i.e.*, both surfaces are very similar in contact with this eluent. On the other hand, the additional retention of the solutes on the C₁₄ graft can only be explained if possible penetration of the solutes into the C₁₄ surface is admitted. With respect to solute behaviour, the similarity of the surfaces is given by the amplitude of the function $C^{\text{Alkyl}}(\varphi_{\text{W}})$, and consequently the adsorbents resemble each other most in contact with a water-rich eluent. Indeed, it seems to be logical that the C₁₄ graft is “softer” in contact with the organic component and becomes harder and harder in contact with water-rich eluents, where the C₁₄ chains are increasingly strongly excluded from the liquid by a similar law that is valid for non-polar solutes such as alkanes. Solid-state ²H-NMR studies by Zeigler and Maciel [54] of silicas covered by deuterated C₁₈ chains in contact with liquids of different polarity seem to confirm these conclusions.

ACKNOWLEDGEMENTS

This paper reports on part of a project financed by the “Fonds National Suisse de la Recherche Scientifique”. Technical help from Y. Bessard and Ph. Jacquemet is gratefully acknowledged. Deuterated solvents were a gift from Chemie Uetikon (Switzerland). Thanks are due to François Riedo of the “École d’Ingénieurs de Fribourg”, Switzerland, for discussions and to Professor H. Poppe for his criticism and suggestions.

REFERENCES

- 1 K. Szabó, N. L. Ha, Ph. Schneider, P. Zeltner and E. sz. Kováts, *Helv. Chim. Acta*, 67 (1984) 2128.
- 2 G. Fóti, Ch. de Reyff and E. sz. Kováts, *Langmuir*, 6 (1990) 759.
- 3 G. Körösi and E. sz. Kováts, *Colloids Surfaces*, 2 (1981) 315.
- 4 E. sz. Kováts, *Pure Appl. Chem.*, 61 (1989) 1937.
- 5 A. V. Kiselev and Ya. I. Yashin, *La Chromatographie Gaz–Solide*, Masson, Paris, 1969, p. 24.
- 6 F. Riedo and E. sz. Kováts, *J. Chromatogr.*, 239 (1982) 1.
- 7 N. L. Ha, J. Ungvárai and E. sz. Kováts, *Anal. Chem.*, 54 (1982) 2410.
- 8 R. E. Majors and M. J. Hopper, *J. Chromatogr. Sci.*, 12 (1974) 767.
- 9 R. K. Gilpin, J. A. Korpi and C. A. Janicki, *Anal. Chem.*, 47 (1975) 1498.
- 10 E. J. Kikta and E. Grushka, *Anal. Chem.*, 48 (1976) 1098.
- 11 R. P. W. Scott and P. Kucera, *J. Chromatogr.*, 142 (1977) 213.
- 12 K. Karch, I. Sebastian and I. Halász, *J. Chromatogr.*, 122 (1976) 3.
- 13 C. J. Little, A. D. Dale and M. B. Evans, *J. Chromatogr.*, 153 (1978) 381.
- 14 C. J. Little, A. D. Dale and M. B. Evans, *J. Chromatogr.*, 153 (1978) 543.
- 15 H. Hemetsberger, W. Maasfeld and H. Ricken, *Chromatographia*, 9 (1976) 303.
- 16 H. Hemetsberger, M. Kellermann and H. Ricken, *Chromatographia*, 10 (1977) 726.
- 17 P. Spacek, M. Kubin, S. Vozka and B. Porsch, *J. Liq. Chromatogr.*, 3 (1980) 1465.
- 18 B. Shaikh and J. E. Tomaszewski, *Chromatographia*, 17 (1983) 675.
- 19 H. Hemetsberger, P. Behrensmeier, J. Henning and H. Ricken, *Chromatographia*, 12 (1979) 71.
- 20 H. Engelhardt and G. Ahr, *Chromatographia*, 14 (1981) 227.
- 21 C. H. Lochmüller and D. R. Wilder, *J. Chromatogr. Sci.*, 17 (1979) 574.
- 22 K. K. Unger, N. Becker and P. Roumeliotis, *J. Chromatogr.*, 125 (1976) 115.
- 23 P. Roumeliotis and K. K. Unger, *J. Chromatogr.*, 149 (1978) 211.
- 24 G. E. Berendsen and L. de Galan, *J. Chromatogr.*, 196 (1980) 21.
- 25 K. D. Lork, *Doctoral Thesis*, Johannes Gutenberg-Universität, Mainz, 1988.
- 26 M. C. Hennion, C. Picard and M. Claude, *J. Chromatogr.*, 166 (1978) 21.
- 27 M. L. Miller, R. W. Linton, S. G. Bush and J. W. Jorgenson, *Anal. Chem.*, 56 (1984) 2204.
- 28 E. sz. Kováts, in F. Bruner (Editor), *The Science of Chromatography (Journal of Chromatography Library, Vol. 32)*, Elsevier, Amsterdam, 1985, p. 205.
- 29 A. Alvarez-Zepeda and D. E. Martire, *J. Chromatogr.*, 550 (1991) 285.
- 30 Cs. Horváth and H. J. Lin, *J. Chromatogr.*, 126 (1976) 401.
- 31 H. Colin, N. Ward and G. Guiochon, *J. Chromatogr.*, 149 (1978) 169.
- 32 R. M. McCormick and B. L. Karger, *Anal. Chem.*, 52 (1980) 2249.
- 33 E. H. Slaats, W. Markovski, J. Fekete and H. Poppe, *J. Chromatogr.*, 207 (1981) 299.
- 34 H. A. H. Billiet, J. P. J. van Dalen, P. J. Schoenmakers and L. de Galan, *Anal. Chem.*, 55 (1983) 847.
- 35 J. H. Knox and R. Kaliszan, *J. Chromatogr.*, 349 (1985) 211.
- 36 G. H. Findenegg and F. Köster, *J. Chem. Soc., Faraday Trans. 1*, 82 (1986) 2691.

- 37 Ph. Schneider, R. Cloux, K. Fóti and E. sz. Kováts, *Synthesis*, (1990) 1027.
- 38 J. Gobet and E. sz. Kováts, *Adsorpt. Sci. Technol.*, 1 (1984) 77.
- 39 G. Fóti, M. L. Belvito and E. sz. Kováts, *J. Chromatogr.*, 440 (1988) 315.
- 40 J. Gobet and E. sz. Kováts, *Adsorpt. Sci. Technol.*, 1 (1984) 285.
- 41 G. Fóti and E. sz. Kováts, *Langmuir*, 5 (1989) 232.
- 42 L. R. Snyder, *Principles in Adsorption Chromatography*, Marcel Dekker, New York, 1968, p. 185.
- 43 E. Soczewinski, *Anal. Chem.*, 41 (1969) 179.
- 44 P. J. Schoenmakers, H. A. H. Billiet, R. Tijssen and L. de Galan, *J. Chromatogr.*, 149 (1978) 519.
- 45 P. J. Schoenmakers, H. A. H. Billiet and L. de Galan, *J. Chromatogr.*, 282 (1983) 107.
- 46 W. R. Melander, J.-F. Erard and Cs. Horváth, *J. Chromatogr.*, 282 (1983) 229.
- 47 D. DeVault, *J. Am. Chem. Soc.*, 65 (1943) 532.
- 48 S. Golshan-Shirazi and G. Guiochon, *Anal. Chem.*, 62 (1990) 923.
- 49 F. Helfferich and G. Klein, *Multicomponent Chromatography, a Theory of Interferences*, Marcel Dekker, New York, 1970.
- 50 H. Poppe, *J. Chromatogr.*, 506 (1990) 45.
- 51 S. Levin and E. Grushka, *Anal. Chem.*, 58 (1986) 1602.
- 52 J. Crommen, G. Schill and P. Herné, *Chromatographia*, 25 (1988) 397.
- 53 D. Berek, T. Bleha and Z. Pevná, *J. Chromatogr. Sci.*, 14 (1976) 560.
- 54 R. C. Zeigler and G. E. Maciel, *J. Am. Chem. Soc.*, 113 (1991) 6349.

Modeling of the adsorption behavior and the chromatographic band profiles of enantiomers

Behavior of methyl mandelate on immobilized cellulose

Frederic Charton[☆], Stephen C. Jacobson and Georges Guiochon

Department of Chemistry, University of Tennessee, Knoxville, TN 37996-1501 (USA) and Division of Analytical Chemistry, Oak Ridge National Laboratory, Oak Ridge, TN 67831-6120 (USA)

(First received August 25th, 1992; revised manuscript received October 27th, 1992)

ABSTRACT

The adsorption isotherms of (–)- and (+)-methyl mandelate from a hexane–isopropanol (90:10) solution were measured on a chromatographic column packed with 4-methylcellulose tribenzoate coated on silica. These isotherms are accounted for by a bi-Langmuir isotherm model, the two Langmuir terms having widely different initial slopes and saturation capacities, but each term having the same saturation capacity for the two enantiomers. The competitive isotherms were also measured. They are in excellent agreement with the prediction of a competitive bi-Langmuir model based on the single-component isotherms. The individual band profiles are in agreement with the profiles calculated from these isotherms. Thus, a simplified competitive isotherm can be used to model a separation on a chiral stationary phase the recognition mechanism of which is not well identified and the adsorption behavior of which is certainly not ideal.

INTRODUCTION

It has been proved [1,2] that the enantiomers of pharmaceuticals often differ in their pharmacological and side-effects. They can even have opposite biological activities. Thus, drug manufacturers are now required to study the physiological properties of each enantiomer, and can be compelled to produce one of them pure [3]. Different methods are available for the separation of enantiomers [4]. In connection with the investigation of the differential pharmacological properties of enantiomeric drugs, the direct chromatographic resolution of racemic mixtures on chiral stationary phases (CSPs) has

been extensively studied in the recent past, but essentially for analytical purposes [5].

For preparative purposes, stereoselective synthesis and purification by crystallization are the preferred approaches. If these methods cannot be implemented, industrial-scale preparative chromatography on CSPs becomes an attractive separation process for enantiomers. This process is expensive, however, and to reduce its contribution to the total production costs it must be optimized, which is difficult to do correctly with a purely empirical approach because of the number of parameters involved and the intricacy of their interactions. Although it has been suggested that displacement chromatography could hold some advantages over elution for the separation of enantiomers [6], the optimization of the experimental conditions is even more complex in displacement than in elution chromatography. Furthermore, the current trend in

Correspondence to: G. Guiochon, Department of Chemistry, University of Tennessee, Knoxville, TN 37996-1501, USA.

[☆] On leave from the Laboratoire des Sciences du Genie Chimique, ENSIC, Nancy, France.

preparative chromatography is towards the use of new operating schemes, such as simulated moving bed, as alternatives to the classical elution chromatography [7,8]. In this event an empirical optimization cannot succeed, and a more rigorous approach is necessary.

The fundamentals of the optimization of overloaded chromatography have been studied using the analytical solution of the ideal model [9,10] and numerical calculations based on the equilibrium–dispersive model [11]. Excellent agreement has been reported in several instances between experimental and calculated results regarding optimization [12, 13]. The main practical difficulty is in the modeling of the competitive equilibrium isotherms. More experimental data are needed in this area.

The modeling of enantioseparations on immobilized bovine serum albumin (BSA) [13–15] and on microcrystalline cellulose triacetate [16] has already been undertaken successfully. The choice of a suitable isotherm model depends considerably, however, on the retention mechanism. There are numerous CSPs, which differ in the nature of their chiral discriminator, and hence in their chiral recognition mechanism. A number of them must be investigated in order to compare their properties and to attempt the derivation of general rules. The main object of this work is the study of enantiomeric resolution on a cellulose-based stationary phase different from microcrystalline cellulose triacetate.

There are a large number of CSPs prepared by adsorption of cellulose derivatives on a macroporous silica support [17]. As CSPs, these phases are characterized by high loading capacities and fast mass transfers, *i.e.*, good efficiencies [18], and are considered as good choices for preparative applications [19]. On the other hand, the choice of solvents which can be used as mobile phase is narrowly limited [20]. In this work, we modeled the separation of the enantiomers of methyl mandelate, using 4-methylcellulose tribenzoate coated on silica as a CSP [21]. We determined the single-component adsorption isotherms of both enantiomers and their competitive isotherms. We used the equilibrium–dispersive model of chromatography [22] to calculate the response of the column to injections of each enantiomer and their mixtures. The validation of the model comes from the successful matching between experimental and calculated individual band profiles.

THEORY

The prediction of individual elution band profiles in chromatography requires first the experimental determination of the primary data of thermodynamic and kinetic nature, and second the use of a suitable numerical method for the integration of a system of partial differential equations derived from the mass balance equations of the components involved.

Calculation of band profiles

In this work, we used the equilibrium–dispersive model of chromatography [22]. This model assumes constant and instantaneous equilibrium between mobile and stationary phases. The contributions to band broadening due to axial dispersion and to the finite rate of the mass transfer kinetics are accounted for by a lumped apparent dispersion coefficient, D_{ap} . The mass balance equation for one component, in an infinitesimal column slice, can be written as

$$\frac{\partial C}{\partial t} + \frac{1 - \varepsilon_T}{\varepsilon_T} \cdot \frac{\partial q}{\partial t} + u_0 \cdot \frac{\partial C}{\partial x} = D_{ap} \cdot \frac{\partial^2 C}{\partial x^2} \quad (1)$$

where C is the concentration in the mobile phase, q is the amount adsorbed at the surface of the solid phase in equilibrium with C , u_0 is the mobile phase flow velocity and ε_T is the total porosity of the bed, taking into account the void between the beads and the intraparticle porosity; ε_T is derived from the retention time t_0 of a non-retained component whose propagation velocity is u_0 . In this model, q is related to C by the equilibrium isotherm.

We also assume that D_{ap} is constant, and equal to its value under linear conditions. D_{ap} is related to the column length, L , and to the number of theoretical plates, N , by the equation

$$D_{ap} = \frac{u_0 L}{2N} \quad (2)$$

This simplification is acceptable because, at high concentrations, the thermodynamic effects, *i.e.*, the non-linear behavior of the equilibrium isotherm, influences the band profile much more strongly than the kinetic effects. Under the experimental conditions prevailing in preparative chromatography, the latter effects appear to be a correction to the band profile predicted by the equilibrium (ideal) model, and hence are properly accounted for by a lumped kinetic coefficient.

For a multi-component system, we write as many eqns. 1 as there are components. In this case, however, the different components of the mixture compete for access to the adsorption sites on the stationary phase. Thus, the amount of component i adsorbed at equilibrium depends not only on C_i , but also on the concentrations of all the other components in the mobile phase, through a competitive adsorption isotherm:

$$q_i = q_i(C_1, C_2, \dots) \quad (3)$$

Finally, we need initial and boundary conditions to solve the problem. In elution chromatography, the column is initially empty:

$$C_i(x, t = 0) = 0 \quad (4)$$

The boundary conditions express the continuity of the flux at the column inlet and outlet. At the column inlet, the boundary condition corresponds to the injection of a rectangular pulse of the feed solution, of composition C_F and width t_F . As the column efficiency is high in HPLC, the boundary conditions can be simplified by neglecting the dispersion effect. These conditions are reduced to

$$C_i(x = 0, t) = C_{Fi} \quad 0 \leq t \leq t_F \quad (5)$$

$$C_i(x = 0, t) = 0 \quad t < 0, \quad t > t_F \quad (6)$$

Only numerical solutions are available for the equilibrium–dispersive model. The algorithms proposed have recently been reviewed [22]. For most practical applications, the finite difference method proposed by Rouchon *et al.* [23] is the fastest and most efficient algorithm, but its accuracy can be lacking in some instances, when the concentration of the second component relative to that of the first is low [24]. In this method, the dispersion term is accounted for by the numerical dispersion, through the proper choice of the size of the integration grid in the time and space domains. This numerical scheme is rigorous for a single-component system in linear chromatography [24]. In other instances, errors occur but they remain small, especially for systems such as ours, when the column has a very high efficiency (4000 theoretical plates for the most retained compound at 0.8 ml/min).

Excellent results, in agreement with experimental data, were reported previously when using the equilibrium–dispersive model and the calculation

method just described for the modeling of several separations performed by liquid chromatography [12–16,24–26].

Equilibrium isotherm

The proper representation of the competitive isotherms is the keystone of our modeling effort. Our purpose is to determine the competitive isotherms which relate the compositions of the liquid and adsorbed phases at equilibrium for enantiomer mixtures. In practice, the easiest approach by far is the direct estimation of the competitive isotherms from the individual isotherms of the pure components.

Several models and equations are available to fit experimental isotherm data for single components. The classical model used in non-linear chromatography is the Langmuir adsorption isotherm [27]:

$$q = \frac{aC}{1 + bC} \quad (7)$$

where a and b are numerical coefficients. Even though this model, which assumes ideal behavior for both the solution and the adsorbed phase, is an approximation in the best of cases, it has been used successfully in many instances [25,28].

This model does not apply to our data, however (see below). An alternative which was successful for modeling the adsorption data of pure enantiomers is the bi-Langmuir model [29–31]

$$q = \frac{aC}{1 + bC} + \frac{AC}{1 + BC} \quad (8)$$

which can be considered as the extension of the Langmuir model to the case of a surface covered with patches of two different kinds.

In a second step, we need to model the competitive adsorption of binary mixtures. The competitive Langmuir isotherm model [32] is the competitive extension of the single-component Langmuir isotherms. Its parameters are those of the single-component isotherm. For a bi-Langmuir isotherm, the competitive Langmuir model can be applied separately to the two terms, assuming non-cooperative adsorption on the two types of sites [14,15,30]. The competitive isotherm is then

$$q_i = \frac{a_i C_i}{1 + b_1 C_1 + b_2 C_2} + \frac{A_i C_i}{1 + B_1 C_1 + B_2 C_2} \quad (9)$$

The Langmuir competitive isotherm model satisfies the Gibbs adsorption equation and, consequently, is thermodynamically consistent only if the column saturation capacities $q_{s_i} = a_i/b_i$ of the two components are equal [33]. To correct for this discrepancy when they are not, Levan and Vermeulen [34] developed a binary isotherm, based on the IAS theory [35], which is valid for mixtures of gases and vapors whose individual isotherms are of the Langmuir or Freundlich types. This isotherm is written as a Taylor series. Its straightforward extension to solutions has been used previously [36]. For binary mixtures of components which have individual isotherms following the Langmuir model, the two-term expansion of the Levan–Vermeulen isotherm can be written as

$$q_1 = \frac{q_s b_1 C_1}{1 + b_1 C_1 + b_2 C_2} + \Delta_{12} \quad (10)$$

$$q_2 = \frac{q_s b_2 C_2}{1 + b_1 C_1 + b_2 C_2} - \Delta_{12} \quad (11)$$

with

$$q_s = \frac{a_1 C_1 + a_2 C_2}{b_1 C_1 + b_2 C_2} \quad (12)$$

$$\Delta_{12} = (q_{s_1} - q_{s_2}) \frac{b_1 b_2 C_1 C_2}{(b_1 C_1 + b_2 C_2)^2} \ln(1 + b_1 C_1 + b_2 C_2) \quad (13)$$

Although it may look complex, this isotherm is explicit and requires only the parameters of the single-component isotherms.

EXPERIMENTAL

Equipment

The chromatographic experiments were performed with an HP1090 liquid chromatograph (Hewlett-Packard, Palo Alto, CA, USA), equipped with a multi-solvent delivery system, an automatic sample injector with a 250- μ l loop, a diode-array UV detector and a computer data acquisition system. Acquired data were downloaded to one of the VAX computers at the University of Tennessee Computer Center. Also, a Gilson (Middleton, WI, USA) Model 203 fraction collector was used to complement the HP system.

Materials

Column. A 25 cm \times 0.46 cm I.D. Chiralcel OJ column (Daicel, Tokyo, Japan) was used (average particle size 10 μ m). The total column porosity ($\epsilon_T = 0.70$) was determined by injecting 1,3,5-tri-*tert.*-butylbenzene, a substance which can be considered to be non-retained on this stationary phase. This value of the porosity was in a very good agreement with that derived from the retention of the solvent peak.

Mobile phase and chemicals. For all chromatographic experiments, the mobile phase was hexane–2-propanol (90:10, v/v). Hexane and 2-propanol were purchased from Burdick and Jackson (Muskegon, MI, USA). L-Methyl mandelate and D-methyl mandelate (both of purity >99%), the racemic mixture (purity >98%) and 1,3,5-tri-*tert.*-butylbenzene were purchased from Fluka (Ronkonkoma, NY, USA). All compounds were used as received.

Procedures

All the experiments reported were performed at 30°C.

Determination of equilibrium isotherm data. Different chromatographic methods are available to measure the adsorption data for a pure compound [37]. In the present instance, the column efficiency was high enough to use ECP (elution by characteristic point) with good accuracy. The isotherm is derived from the diffuse rear boundary of the profile obtained when injecting a large-volume plug of a high-concentration solution.

Assuming that the rear diffuse boundary is very close to that which would be obtained for an infinitely efficient column, we can derive the concentration of the solute adsorbed on the solid phase, q , in equilibrium with the concentration, C , in the mobile phase from the retention volume of the latter through the classical equation [37]

$$q = \int_0^c \frac{V_R - V_0}{V_S} \cdot dC \quad (14)$$

where V_R , V_0 and V_S are the retention volume, the column hold-up volume and the solid-phase volume, respectively.

The equilibrium data were determined at a flow-rate of 0.8 ml/min. The average width of the injected plug was ca. 5 min and its concentration was ca.

4 g/l. Because the HP1090 system is not equipped with a large enough sample loop, the injections were made by programming the multi-solvent delivery system. The diode-array detector signal was recorded with a 640-ms period, at a wavelength of 270 nm. The response signal was converted into concentrations through a calibration graph. The slightly non-linear detector response was fitted to a third-order polynomial. Following conversion into concentration units, the equilibrium data were calculated individually for each enantiomer. About 50 experimental points, evenly spaced over the concentration range, were used to determine the equilibrium isotherm.

Competitive adsorption data were measured using a binary frontal analysis method [38]. In all experiments, the initial concentration of the enantiomers in the column was zero. Thus, the concentration of the more retained component in the intermediate plateau [38] was also zero and there was no need to analyze the corresponding eluate. The concentration of the less retained component in this intermediate plateau was derived from the calibration graph at 250 nm, at which wavelength the detector response was linear over the whole concentration range studied. The retention volumes and the corresponding concentrations were inserted into the equation given by Jacobson *et al.* [38] to determine the amount adsorbed. The measurements of adsorbed amounts could not be made for values of the total concentration higher than *ca.* 1.2 g/l. At higher concentrations, the intermediate plateau [38] disappeared.

Determination of elution profiles. The elution profiles of the pure enantiomers were obtained by injecting increasingly large volumes of a given solution. The detector signal was converted into a concentration profile through the calibration graph, linear over the concentration range used. This graph is the same for both enantiomers. Mixtures prepared by mixing the two pure enantiomers in 1:3 and 4:1 ratios were also injected. All injections were performed at a flow-rate of 0.8 ml/min, corresponding to an approximate value of 8 for the Peclet number ($d_p = 10 \mu\text{m}$, $D_m = 1 \cdot 10^{-5} \text{ cm}^2/\text{s}$).

For mixtures, the individual elution profiles were determined in the mixed-band region by collecting fractions of the eluent and reinjecting them onto the same column, but under analytical conditions. Frac-

tions were collected at 9-s intervals, from the start of the elution of the first component through the estimated end of the mixed zone. The relative concentration of the two enantiomers in a fraction is equal to the peak-area ratio. Combined with the recorded total signal of the detector, this allows the determination of the individual concentration profiles.

RESULTS AND DISCUSSION

Modeling of single-component equilibrium isotherms

The Scatchard plot of the single-component data (Fig. 1) is not linear, which shows that the classical Langmuir model cannot account for the isotherms. A two-site adsorption model, including enantioselective and non-selective sites, appears to be plausible in the present instance. This justifies the use of a bi-Langmuir isotherm, a model already used successfully for the modeling of other enantiomeric separations [12,13].

For all compounds, there are a variety of molecular interactions with a stationary phase, the combination of which accounts for the retention. Both enantiomers have complex interactions with the chiral stationary phase (CSP), some of which are

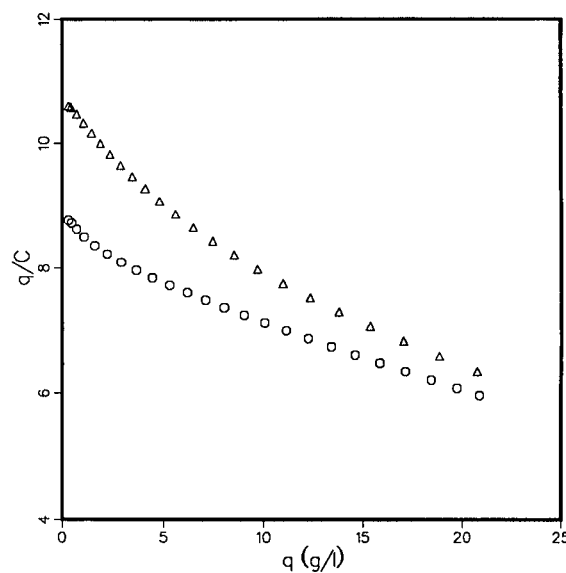


Fig. 1. Scatchard plots (*i.e.*, q/C versus q) of the experimental adsorption data for (○) (–)-methyl-D-mandelate [(–)-MM] and (△) (+)-methyl-L-mandelate [(+)-MM].

achiral (hence identical for both enantiomers), while others involve the stereochemistry of the enantiomers and the CSP, causing the formation of a transient diastereomeric solute–CSP complex. If the stability of the complex is different for the two enantiomers, they will be separated. For the more strongly retained enantiomer, at least, the formation energy of this complex is higher than the energy of conventional intermolecular interactions [5,19,20]. Thus, a bi-Langmuir isotherm is likely; the first term would represent the retention linked with the chiral recognition mechanism, while the second term would include all the non-enantioselective interactions. Previous investigations of the chiral recognition process on cellulose-band CSP have disclosed the existence of two types of retention mechanisms [39,40].

If this assumption is correct, no chiral selectivity should be involved in the second term of a bi-Langmuir isotherm model. The coefficients A and B (eqns. 8 and 9) should be the same for both enantiomers, in which event the total number of parameters of the model is reduced to 6. Thus, we fitted together the two sets of experimental data, one for each enantiomer. We used a program based on a simplex algorithm to minimize the following objective function:

$$\delta = \delta_D + \delta_L = \sqrt{\frac{1}{N_D} \sum_1^{N_D} \left(\frac{q_{\text{exp}_i} - q_{\text{cal}_i}}{q_{\text{exp}_i}} \right)^2} + \sqrt{\frac{1}{N_L} \sum_1^{N_L} \left(\frac{q_{\text{exp}_j} - q_{\text{cal}_j}}{q_{\text{exp}_j}} \right)^2} \quad (15)$$

TABLE I
ISOTHERM PARAMETERS

Model of competitive isotherm:

$$q_{(x)} = LV_{(x)}[C_{(-)}, C_{(+)}] + \frac{Q_s BC_{(x)}}{1 + B[C_{(-)} + C_{(+)}]}$$

where $x = -, +$; LV refers to the Levan–Vermeulen isotherm calculated with the coefficients of the individual isotherms on the selective sites.

Number of parameters	Type of sites	Isomer	a	b (l/g)	q_s (g/l)
6 (Model 1)	Selective	(-)-	1.83	0.786	2.33
	Selective	(+)-	3.86	1.11	3.48
	Non-selective	(-)- and (+)-	6.91	0.076	91.2

where the subscripts D and L refer to the (-)-methyl-D-mandelate and the (+)-methyl-L-mandelate, respectively, while N_D and N_L are the numbers of data points for the D - and L -enantiomers, respectively. The use of a weighted function (eqn. 15) permits a good accuracy of the fit at both low and high concentrations. The use of an alternate objective function, $\delta_D + \delta_L + |\delta_D - \delta_L|$, was abandoned because local optima appeared.

The values derived for the isotherm parameters are summarized in Table I. The experimental (symbols) and calculated (dotted lines) isotherm data are compared in Fig. 2. They are in excellent agreement. The (+)-enantiomer is the more retained on this stationary phase. It can be seen in Table I that, as reported previously [12], the adsorption energy on the non-enantioselective sites is lower than that on the enantioselective sites (*i.e.*, B is lower than b), but that the saturation capacity of these non-selective sites is much higher.

Modeling of competitive equilibrium isotherm

The competitive isotherm contains two terms, one for the enantioselective and the other for the non-selective sites. The latter term is obviously the Langmuir term corresponding to the sum of the concentrations of the two enantiomers.

The extrapolated values of the saturation capacity for the enantioselective sites are not the same for the two enantiomers (Table I). Therefore, we cannot use for them a competitive Langmuir isotherm which would not be thermodynamically consistent

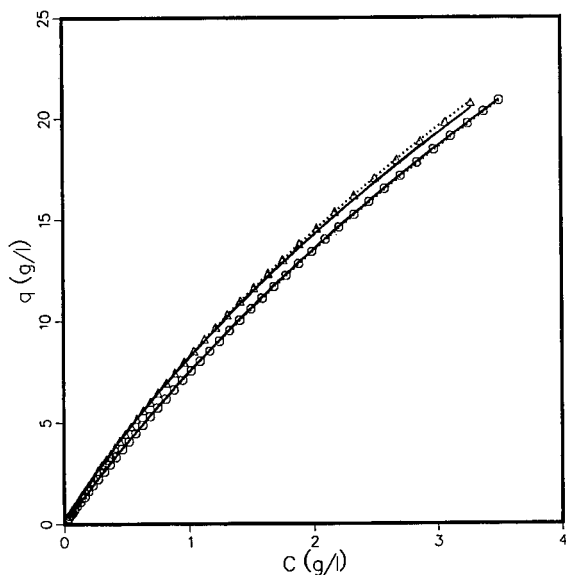


Fig. 2. Experimental adsorption data for (O) (-)-MM and (Δ) (+)-MM on a Chiralcel OJ phase at 30°C. The lines correspond to the isotherm equations derived from Models 1 (dotted lines) and 2 (solid lines).

[34,35]. In such a case, the Levan–Vermeulen isotherm [34] is the simplest competitive isotherm model that can be used and we adopted it for the enantioselective sites (Table I).

However, the adsorption data were measured in a range of concentrations which, although high enough to encompass the range covered by chromatographic bands at the time of their elution, was

limited to *ca.* 3.5 g/l. The amount adsorbed at this concentration corresponds to only 20% of the estimated saturation capacity, which, accordingly, was determined by extrapolation. Such values are inaccurate and must be considered with caution. Further, although large in relative terms (30%), the difference between the extrapolated values of the saturation capacities of the enantioselective sites for the two enantiomers is small compared with the total saturation capacities, which increases the inaccuracy of the estimate.

Not knowing the nature of the chiral retention mechanism, we used a second approach, previously developed in the study of the separation of racemic mixtures of amino acids on immobilized BSA [12,13]. We assumed that the saturation capacities of the two enantiomers were equal for the enantioselective sites, $a_{(-)}/b_{(-)} = a_{(+)}/b_{(+)}$, and we fitted our data to a five-parameter isotherm model (Table II). We could not derive these parameters in a straightforward way, however. Actually, when we fitted our data with a five-parameter model, we obtained parameter values different from the previous values (in Table I), including a saturation capacity for the non-enantioselective sites which was twice as large as that obtained in the first approach. These parameters did not provide a satisfactory calculation of the elution profiles. This result can be understood if we consider that the objective function being the same for both models, the optimization procedure for the five-parameter model is limited to the sub-domain of the six-parameter space where we have the relation $qs_{(-)} = qs_{(+)}$. Hence, the optimum

TABLE II
ISOTHERM PARAMETERS

Model of competitive isotherm:

$$q_{(x)} = \frac{q_s B_{(x)} C_{(x)}}{1 + b_{(-)} C_{(-)} + b_{(+)} C_{(+)}} + \frac{Q_s B C_{(x)}}{1 + B[C_{(-)} + C_{(+)}]}$$

where $x = -, +$.

Number of parameters	Type of sites	Isomer	a	b (l/g)	q_s (g/l)
5 (Model 2)	Selective	(-)-	2.14	0.506	4.22
	Selective	(+)-	4.31	1.022	4.22
	Non-Selective	(-)- and (+)-	6.50	0.071	91.2

of the objective function in this sub-domain can be far from the real optimum.

Because of its flexibility, we can expect the six-parameter model to give a relatively good approximation of the saturation capacity on the non-stereselective sites. Then, in order to obtain more realistic values of the isotherm parameters, we assumed the value of this saturation capacity to be correct, and determined the remaining four parameters of the five-parameter model (Table II). Indeed, the two models give almost identical individual isotherms (Fig. 2, second isotherm in solid lines), except for a slight difference in the high concentration range, for the (+)-enantiomer. As the saturation capacities are now equal, however, we can derive a competitive bi-Langmuir isotherm from the second model.

These two models, referred to below as Models 1 (Table I) and 2 (Table II), were used to predict the competitive isotherms. In Fig. 3, we compare the experimental data on competitive adsorption obtained by binary frontal analysis (symbols) and the isotherms calculated with the two models (solid lines). The comparison is made for different values of the relative composition of the mobile phase. The two models gave identical results, which are also in very good agreement with experimental data. In most instances, the difference was less than 2%. The structures of the two competitive isotherm models are different, and they give different amounts adsorbed on the two types of sites for a given concentration. However, because of a fortuitous compensation, the two models give virtually identical values for the total amount adsorbed, in the concentration range investigated. A significant difference would arise only at concentrations much higher than those at which accurate measurements could be carried out.

Single-component band profiles

Fig. 4 shows a chromatogram obtained under linear conditions, with a very small amount injected (2 μg). The retention times derived from it are in excellent agreement with the initial slopes of the enantiomer isotherms. The selectivity is low ($\alpha = 1.22$), but the efficiency is high for both components and the resolution complete ($R_s = 2.5$). The plate numbers determined with the conventional method are $N_{(-)} = 4500$ and $N_{(+)} = 4000$ at a velocity of 0.08 cm/s ($F_v = 0.8$ ml/min), giving reduced plate

heights of 5.6 and 6.2, respectively, for a Peclet number close to 8.

As the single-component isotherm data were de-

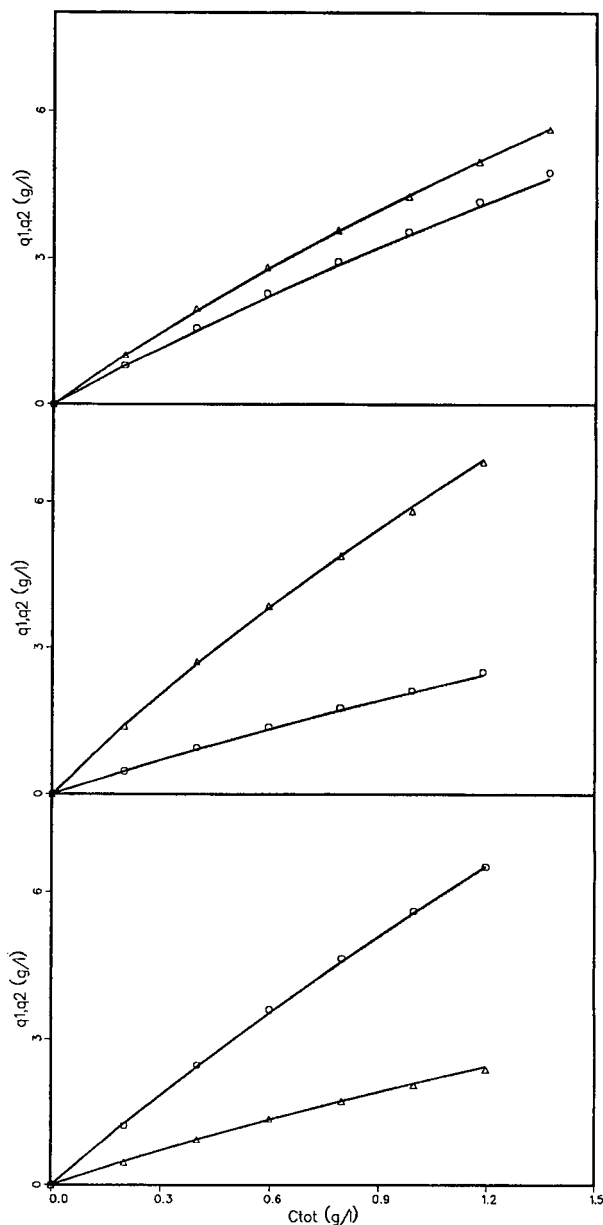


Fig. 3. Experimental competitive adsorption data (○) (–)-MM and (Δ) (+)-MM and calculated isotherms (dotted lines for Model 1, solid lines for Model 2), for different mixtures of constant compositions. Ratios $C(+)/C(-)$: top = 1.05; middle = 2.43; bottom = 0.32.

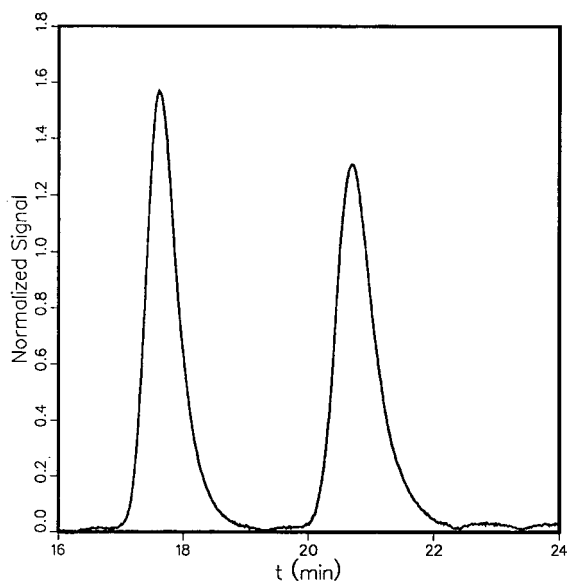


Fig. 4. Normalized chromatogram under linear conditions for the racemic mixture. Volume injected, 50 μ l; total concentration, 40 mg/l; total amount, 2 μ g.

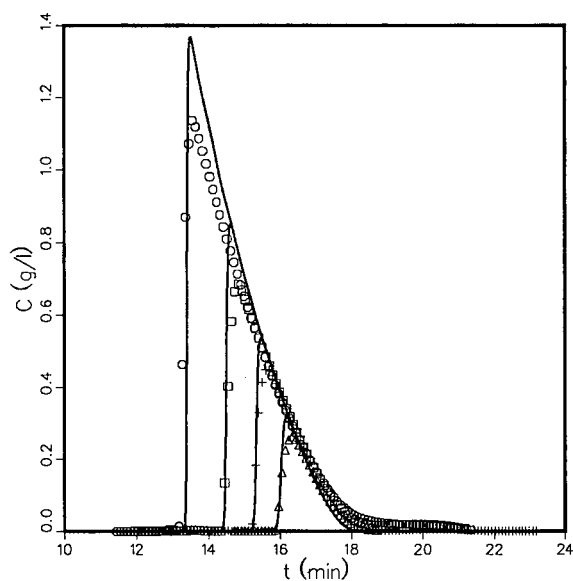


Fig. 5. Experimental (symbols) and calculated (solid lines) elution profiles for injections of samples of different volumes of a 2.6 g/l (-)-MM solution. Model 2 (Table II) was used for the calculations. Volumes injected: 100, 200, 400 and 800 μ l.

rived by ECP, a method based on the ideal model, comparing recorded band profiles obtained on injection of large-sized samples with the results of calculations based on the equilibrium-dispersive model, is a circular argument. We can, however, compare the band profiles calculated from the isotherm data with the profiles recorded 2 months later, using the same column but another instrument, in a different location. This illustrates the kind of reproducibility achieved for chromatographic data and the modeling accuracy that can be expected in attempts at designing separation units.

Figs. 5 and 6 compare recorded (symbols) and calculated (lines) chromatograms for four consecutive injections of increasing volumes of given solutions (*ca.* 2.5 g/l) of the pure (-) and (+)-enantiomers, respectively. In order to achieve overlay of the diffuse boundaries of the four profiles, the time scale is corrected of the width of the injected plug. The elution profiles were calculated with the second isotherm model. They agree well with the experimental data and confirm the validity of the individual isotherms measured. They also show the good stability of the cellulose column, if used under

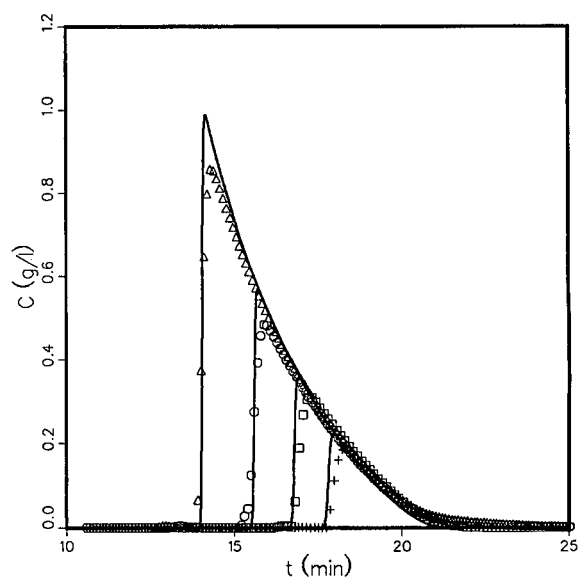


Fig. 6. Experimental (symbols) and calculated (solid lines) elution profiles for injections of samples of different volumes of a 2.6 g/l (+)-MM solution. Model 2 was used for the calculations. Volumes injected: 100, 200, 400 and 800 μ l.

regular and smooth conditions. The baseline bump behind the (–)-enantiomer profile in Fig. 5 is due to a small amount of (+)-isomer (1.5%). The individual band profiles of the two enantiomers calculated with the two isotherm models are compared in Fig. 7. These results reflect the agreement observed between the single-component isotherms (Fig. 2): the profiles differ by the thickness of the line in the case of the less retained enantiomer, and hardly more for the other enantiomer.

Individual band profiles in binary mixtures

There are two important separation problems for enantiomers, the separation of the racemic mixture and the purification of one enantiomer from moderate or low concentrations of the other. Our purpose was to model either type of separation for large sample sizes, *i.e.*, under overloaded conditions. Separations of the racemic mixture are presented in the Figs. 8 and 9. Figs. 8 and 9 show the chromatograms (symbols) obtained for increasingly large amounts of the racemic mixture, going from nearly “touching band” separation [41] to an important degree of band overlapping. The lines show the pro-

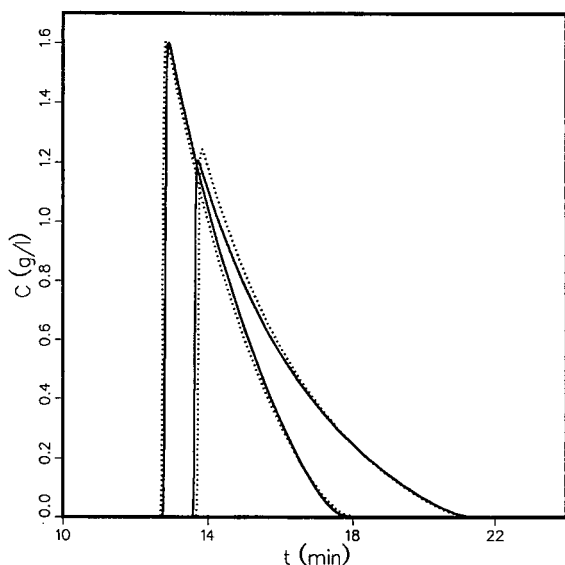


Fig. 7. Comparison of the individual elution profiles calculated with the isotherms derived from Models 1 (dotted lines) and 2 (solid lines) for the two enantiomers [(–)-MM is the less retained]. Concentration of injected solution, 2.50 g/l; volume injected, 1.0 ml.

files calculated using the competitive isotherm derived from Model 2.

There is general agreement between the experimental and simulated profiles, although a systematic deviation is observed for the chromatograms in Fig. 8, as the less retained (–)-enantiomer elutes too early. This anomaly does not appear in Fig. 9. The difference between calculated and experimental chromatograms is a mere retention time shift of *ca.* 1.5%. It can be simply explained by the difficulty encountered in resetting exactly the flow-rate and the dead volumes. For the two largest amounts in Fig. 8, and to a lesser extent in Fig. 9, the shapes of the experimental and calculated rear diffuse boundaries are also different in the high concentration range.

We see that the inflection point is slightly higher on the calculated profiles than on the experimental ones. The inflection point on this rear boundary corresponds to the intermediate plateau of the more retained component predicted by the ideal model but which cannot be observed for this mixture composition, because the column efficiency is too low. The concentration of this plateau, and hence of the inflection point, depend only on the competitive equilibrium isotherm. The divergence observed is due to a small error in the competitive isotherm.

To check further the validity of band profiles calculations, we determined experimentally, by analysis of collected fractions, the individual band profiles of the two enantiomers for 2-mg samples of three different binary mixtures, having relative compositions 1:1 (Fig. 10), 4:1 (Fig. 11) and 1:3 (Fig. 12). The total injection concentration was 8 g/l and the maximum concentration of the eluted bands was of the order of 1 g/l, which corresponds to a high degree of column overload. The injection concentration exceeds the range within which were determined single-component (0–3.5 g/l, Fig. 1) and competitive isotherms (0–1.2 g/l, Fig. 3). Dilution occurs quickly, however, and during most of the band migration its concentration is within the range studied.

In Figs. 10–12, we compare the experimental profiles with those calculated with Models 1 (dotted lines) and 2 (solid lines). The two models give slightly different calculated profiles, which suggests that the two isotherm models are less similar than observed in Fig. 3 at high concentrations. The general

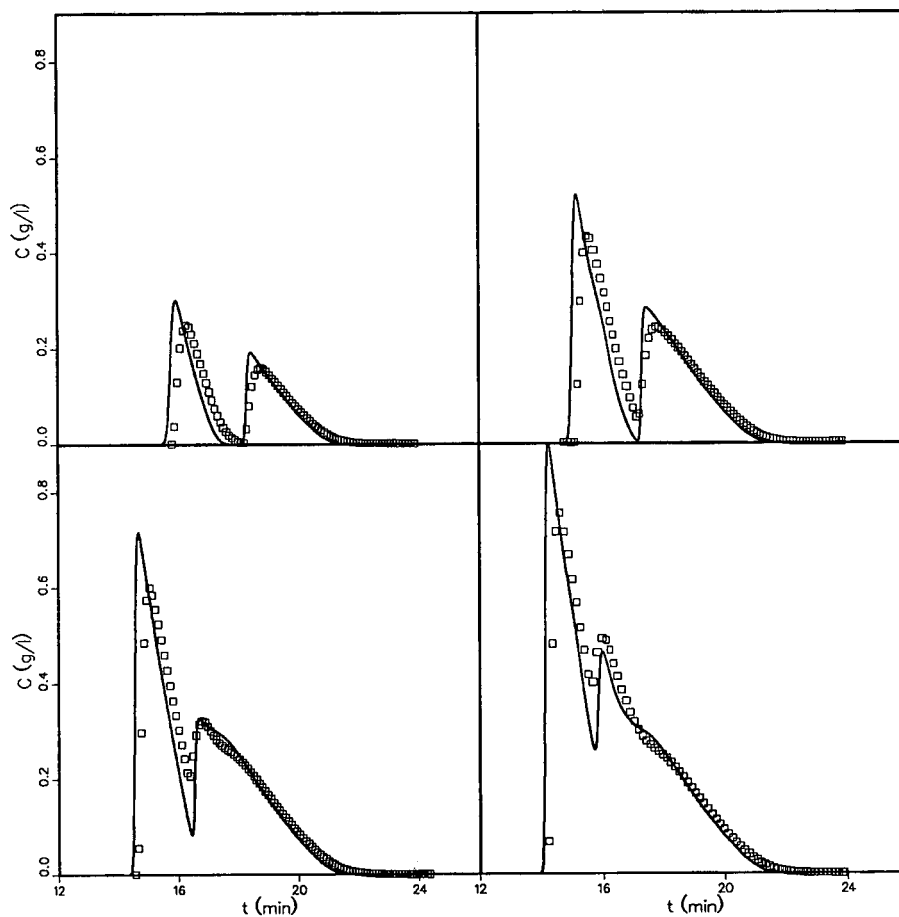


Fig. 8. Experimental (symbols) and calculated (lines) chromatograms (total concentration of the two enantiomers) for different volumes injected of a racemic mixture of methyl (-) and (+)-mandelate. $C(-) = C(+)$ = 4.1 g/l. Volumes injected: 50, 100, 150 and 200 μ l. The solid lines were calculated using the competitive isotherm Model 2 (Table II).

agreement is better with the profile calculated with Model 2 than Model 1. Both models give an excellent prediction of the individual profiles for the 4:1 mixture (Fig. 11), possibly because the concentration of the second component is much lower in this instance than in the other two (Figs. 10 and 12). On the other hand, the agreement between calculated and experimental profiles for the 1:3 mixture (Fig. 12), for which the second component concentration is much higher, is less satisfactory.

Differences are noted at the end of the rear diffuse boundary of the (+)-enantiomer, whereas excellent agreement was observed in Figs. 10 and 11. Indeed, this part of the band profile depends only on the

isotherm of the more retained solute. Fig. 9 shows the global signal observed for the experiment reported in Fig. 10. In Fig. 10, we see clearly that the inflection point on the diffuse boundary of the (+)-enantiomer is higher for the calculated than for the recorded profile, regardless of the model chosen for calculations. This points to an error in the competitive isotherms, causing in turn an error in the concentrations of the two components in the mixed zone of the chromatogram: we observe in Figs. 10 and 12 that the calculated concentrations of the (-)-enantiomer in the mixed zone between the bands of pure enantiomers are too low whereas those of the (+)-enantiomer are too high. This

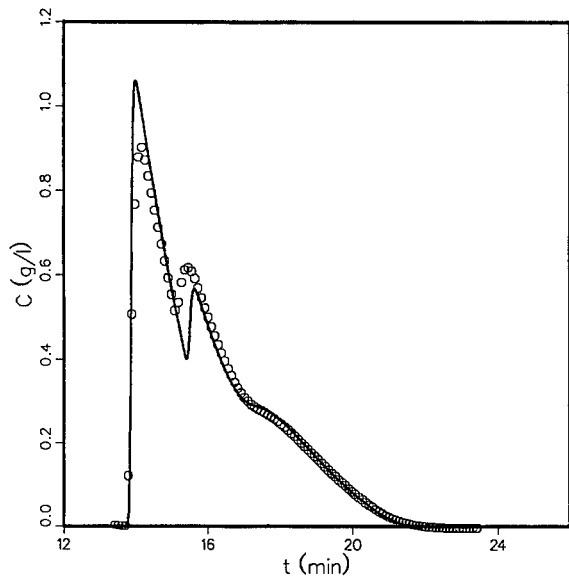


Fig. 9. Same as Fig. 8, but $C(-) = 4.2$ g/l and $C(+) = 3.8$ g/l; volume injected, 250 μ l.

means that our competitive isotherm induces too much displacement effect. This is especially true for Model 1-

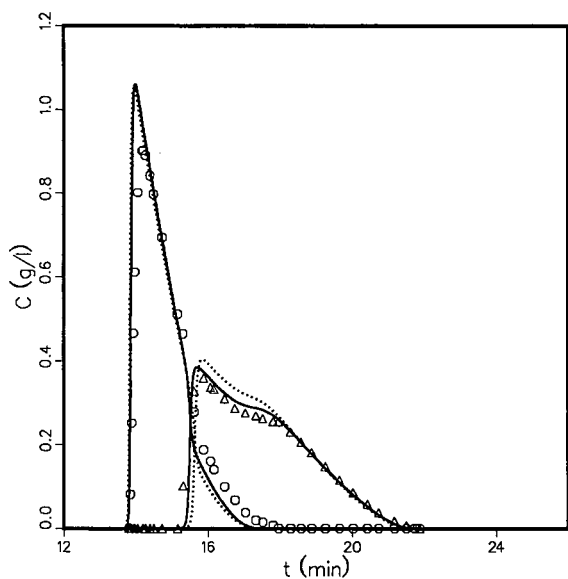


Fig. 10. Comparison between experimental [$\circ = (-)$ -MM; $\triangle = (+)$ -MM] and calculated (dotted lines for Model 1, solid lines for Model 2) individual elution profiles for an injection of a binary mixture. Sample composition, $C(-) = 4.2$ g/l and $C(+) = 3.8$ g/l; sample volume, 250 μ l.

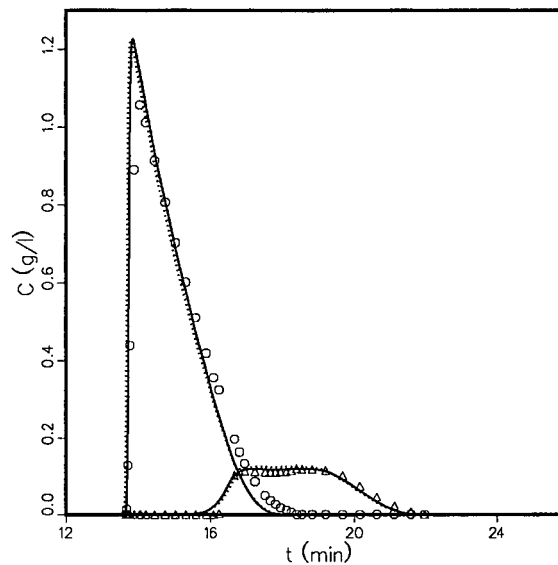


Fig. 11. Same as Fig. 10, but $C(-) = 6.2$ g/l and $C(+) = 1.5$ g/l.

In Fig. 3, the agreement between predicted and experimental data for the adsorption of mixtures is very good, and we expected a still better agreement between experimental and calculated profiles than observed in Figs. 8-12, even though experimental parameters other than the isotherms are involved.

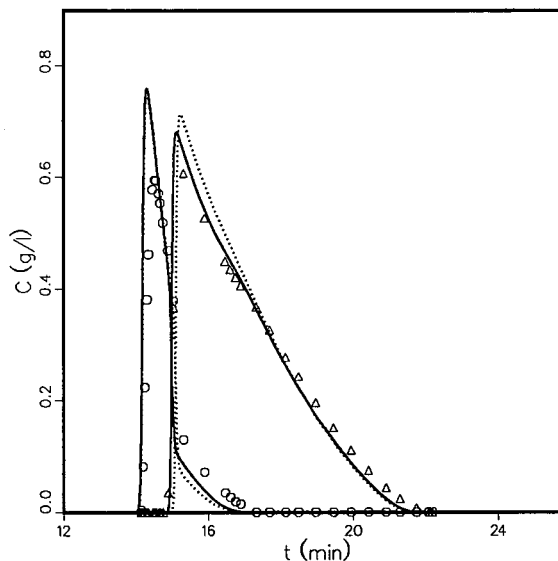


Fig. 12. Same as Fig. 10, but $C(-) = 1.8$ g/l and $C(+) = 5.9$ g/l.

TABLE III
ISOTHERM PARAMETERS

Model of competitive isotherm:

$$q_{(x)} = \frac{q_s B_{(x)} C_{(x)}}{1 + b_{(-)} C_{(-)} + b_{(+)} C_{(+)}} + \frac{Q_s B C_{(x)}}{1 + B[C_{(-)} + C_{(+)}]}$$

where $x = -, +$.

Number of parameters	Type of sites	Isomer	a	b (l/g)	q_s (g/l)
5	Selective	(-)-	2.05	0.741	2.76
	Selective	(+)-	3.90	1.414	2.76
	Non-Selective	(-)- and (+)-	7.12	0.079	89.9

For these experiments, we used small volumes of highly concentrated samples. To confirm the validity of our competitive isotherms in the concentration range where binary adsorption data could be determined more accurately (Fig. 3), we injected a large volume of a dilute sample of the racemic mixture (Fig. 13). The amount injected is almost the same as for Fig. 10, but the concentration is about seven times lower.

To check the degree of stability of the column

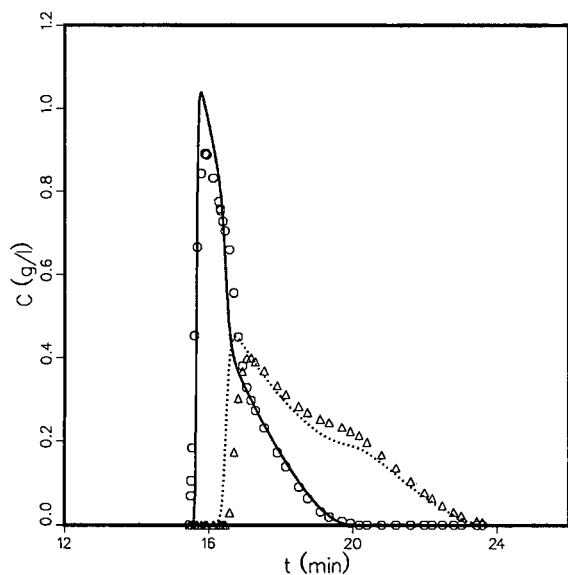


Fig. 13. Comparison between experimental [○ = (-)-MM; △ = (+)-MM] and calculated (Table III) individual profiles for an injection of a binary mixture. Sample composition, $C(-) = 0.66$ g/l and $C(+) = 0.68$ g/l; sample volume, 1.60 ml.

performance during the few months that elapsed between the two experiments, we measured again the adsorption equilibrium data for each enantiomer at the time of the second experiment, for concentrations up to 1.3 g/l. The new values of the parameters were calculated for the isotherm, following the procedure described above for Model 2 (see Table III). These values are very close to the former values (Table II) but not close enough to avoid the use of the old parameter values resulting in significant differences in the calculated elution profiles. With the new parameter values, the agreement observed in Fig. 13 is only slightly better than that in Fig. 10.

All these results prove that the competitive isotherm model chosen (Model 2) gives a very good approximation of the adsorption behavior of the enantiomers, and permits a calculation of adsorption data for mixtures that is precise enough for the modeling of preparative chromatography.

CONCLUSIONS

As previously reported in a number of instances [41], there is generally very good agreement between experimental and calculated individual band profiles for large-sized injections of binary mixtures in the whole range of relative compositions. The extent of this agreement is limited by the accuracy of the modeling of the competitive isotherms. This has several important consequences, as follows.

The accuracy of the equilibrium-dispersive model is more than adequate. At least for low relative

molecular mass compounds, there is no need for a more exact kinetic model. This simplifies considerably the collection of the data required for modeling, as only the plot of the column height equivalent to a theoretical plate *versus* the flow velocity is needed.

The modeling of the competitive isotherm is critical. Unless a simple, clearly identifiable, selective retention mechanism is used, simple models may lack accuracy, and it may be impossible to predict the competitive adsorption behavior merely from the single-component isotherms.

At this stage, accurate experimental data are needed, as reliable isotherm models are lacking. These data must encompass the entire range of concentrations experienced in a band during its migration, *i.e.*, must go from zero to the injection concentration.

Although imperfect, current models permit the calculation of band profiles which are in sufficient agreement with experimental data to warrant their use in optimization procedures.

The difficulty in selecting an adsorption isotherm model that is accurate for enantiomeric separations on cellulose is related to our present ignorance regarding the origin of its enantioselectivity. With five carbon atoms out of six exhibiting chirality, cellulose provides a highly chiral environment, and it is difficult at this stage to suggest any particular mechanism to explain its enantioselectivity. In the light of that lack of understanding, it is most interesting to observe that there seems to be no enantioselective component in the low-energy molecular interaction term, while the high-energy interaction term accounts for all the enantioselectivity. Whether there are also some high-energy, non-selective molecular interactions involved remains an unanswered question. We note, however, that the enantioselective retention mechanism, although described by the same empirical isotherm as for mandelic acid on immobilized BSA, is profoundly different. With BSA, the enantioselective retention mechanism involves strong interactions between the enantiomers and a hydrophobic pouch in the protein molecule [42], thus validating the basic assumptions of the Langmuir model for the enantioselective sites [43]. Also noteworthy is the considerable difference observed between the adsorption behavior of the enantiomers of methyl mandelate on Chiralcel OJ

and of those of Tröger's base on microcrystalline cellulose triacetate [8].

ACKNOWLEDGEMENTS

This work was supported in part by Grant CHE-9201663 of the National Science Foundation and by the cooperative agreement between the University of Tennessee and the Oak Ridge National Laboratory. F.C. thanks Rhône-Poulenc for financial support of this work. We are grateful to Hewlett-Packard for the gift of a Model 1090A liquid chromatograph with its data system and to ADA for the software that permits the transfer of the data files recorded by the liquid chromatograph to the computer center. We acknowledge continuous support of our computational efforts by the University of Tennessee Computing Center.

REFERENCES

- 1 M. Simonyi, *Med. Res. Rev.*, 4 (1984) 359.
- 2 E. J. Ariens, *Med. Res. Rev.*, 6 (1986) 451.
- 3 W. H. De Camp, *Chirality*, 1 (1989) 2.
- 4 M. Lienne, M. Caude, A. Tambute and R. Rosset, *Analisis*, 15 (1987) 431.
- 5 I. W. Wainer and C. Alembik, in M. Zief and L. J. Crane (Editors), *Chromatographic Chiral Separations*, Marcel Dekker, New York, 1988, p. 355.
- 6 G. Vigh, G. Quintero and G. Farkas, *ACS Symp. Ser.*, 434, (1990) 181.
- 7 R. M. Nicoud and M. Bailly, in M. Perrut (Editor), *Proceedings PREP'92, Nancy, France, April 1992*, Société Française de Chimie, Paris, p. 205.
- 8 A. Seidel-Morgenstern and G. Guiochon, to be published.
- 9 S. Golshan-Shirazi and G. Guiochon, *J. Chromatogr.*, 517 (1990) 229.
- 10 S. Golshan-Shirazi and G. Guiochon, *J. Chromatogr.*, 536 (1991) 57.
- 11 A. Felinger and G. Guiochon, *J. Chromatogr.*, 591 (1992) 31.
- 12 S. Jacobson, A. Felinger and G. Guiochon, *Biotech. Bioeng.*, 40 (1992) 1210.
- 13 S. Jacobson, A. Felinger and G. Guiochon, *Biotech. Prog.*, in press.
- 14 S. Jacobson, S. Golshan-Shirazi and G. Guiochon, *AIChE J.*, 37 (1991) 836.
- 15 S. Jacobson, S. Golshan-Shirazi and G. Guiochon, *J. Am. Chem. Soc.*, 112 (1990) 6493.
- 16 A. Seidel-Morgenstern and G. Guiochon, to be published.
- 17 Y. Okamoto, M. Kawashima and K. Hatada, *J. Am. Chem. Soc.*, 106 (1984) 5357.
- 18 Y. Okamoto, M. Kawashima, R. Aburatani, K. Hatada, T. Nishiyama and M. Masuda, *Chem. Lett.*, (1986) 1237.
- 19 E. Francotte and A. Junker-Buchheit, *J. Chromatogr.*, 576 (1992) 1.

- 20 D. M. Johns, in W. J. Lough (Editor), *Chiral Liquid Chromatography*, Rutledge, Chapman & Hall, London, 1989, p. 166.
- 21 Y. Okamoto, R. Aburatani and K. Hatada, *J. Chromatogr.*, 389 (1987) 95.
- 22 S. Golshan-Shirazi and G. Guiochon, in F. Dondi and G. Guiochon (Editors), *Theoretical Advancement in Chromatography and Related Separation Techniques, NATO ASI, No. C. 383*, Kluwer, Delft, 1992, p. 35.
- 23 P. Rouchon, M. Schonauer, P. Valentin and G. Guiochon, *Sep. Sci. Technol.*, 22 (1987) 1793.
- 24 M. Czok and G. Guiochon, *Comput. Chem. Eng.*, 14 (1990) 1435.
- 25 A. M. Katti, M. Czok and G. Guiochon, *J. Chromatogr.*, 556 (1991) 205.
- 26 M. Diack and G. Guiochon, *Anal. Chem.*, 63 (1988) 2634.
- 27 I. Langmuir, *J. Am. Chem. Soc.*, 38 (1916) 2221.
- 28 S. Golshan-Shirazi and G. Guiochon, *Anal. Chem.*, 60 (1988), 2634.
- 29 D. Graham, *J. Phys. Chem.*, 57 (1953) 665.
- 30 J. D. Andrade, *Surface and Interfacial Aspects of Biomedical Polymers*, Plenum Press, New York, 1985, Ch. I.
- 31 R. J. Laub, *ACS Symp. Ser.*, 297 (1986) 1.
- 32 G. M. Schwab, *Ergebnisse des Exacten Naturwissenschaften*, Vol. 7, Springer, Berlin, 1928, p. 276.
- 33 C. Kembell, E. K. Rideal and E. A. Guggenheim, *Trans. Faraday Soc.*, 44 (1984) 948.
- 34 M. D. Levan and Vermeulen, *J. Phys. Chem.*, 85 (1981) 3247.
- 35 A. L. Meyers and J. M. Prausnitz, *AIChE J.*, 11 (1965) 121.
- 36 S. Golshan-Shirazi, J.-X. Huang and G. Guiochon, *Anal. Chem.*, 63 (1991) 1147.
- 37 A. M. Katti and G. Guiochon, *Adv. Chromatogr.*, 32 (1991) 1.
- 38 J. Jacobson, J. M. Frenz and C. Horváth, *Ind. Eng. Chem. Res.*, 26 (1987) 43.
- 39 I. W. Wainer, R. M. Stiffin and T. Shibata, *J. Chromatogr.*, 411 (1987) 139.
- 40 Y. Fukui, A. Ichida, T. Shibata and K. Mori, *J. Chromatogr.*, 515 (1990) 85.
- 41 G. Guiochon, A. M. Katti, M. Diack, M. Z. El Fallah, S. Golshan-Shirazi, S. C. Jacobson and A. Seidel-Morgenstern, *Acc. Chem. Res.*, 25 (1992) 366.
- 42 S. Allenmark and S. Andersson, *Chirality*, 4 (1992) 24.
- 43 S. C. Jacobson, S. Andersson, S. Allenmark and G. Guiochon, in preparation.

Characterization of non-linear adsorption properties of dextran-based polyelectrolyte displacers in ion-exchange systems

Shishir D. Gadam, Guhan Jayaraman and Steven M. Cramer

Howard P. Isermann Department of Chemical Engineering, Rensselaer Polytechnic Institute, Troy, NY 12180-3590 (USA)

(First received June 11th, 1992; revised manuscript received October 1st, 1992)

ABSTRACT

Experimental studies were carried out on the non-linear adsorption properties of dextran-based polyelectrolytes in anion- and cation-exchange chromatographic systems. By monitoring both the induced salt gradients and sequential breakthrough fronts, parameters were determined for use in a Steric Mass Action (SMA) model of non-linear ion-exchange chromatography. These parameters include: total ion capacity of the columns, characteristic charge, steric factor, equilibrium constant, and maximum adsorptive capacity for each of the polyelectrolytes. In addition the number of functional groups were determined by elemental analysis. The values of the SMA parameters were found to be independent of salt and polyelectrolyte bulk phase compositions. Parameters were also determined for a variety of proteins. Experimental isotherms for the polyelectrolytes and proteins were compared with those simulated by the SMA model. Finally, the implications of polyelectrolyte adsorption properties with respect to their ability to act as efficient displacers in ion-exchange displacement systems are discussed.

INTRODUCTION

The adsorption of polyelectrolytes at interfaces plays an important role in numerous industrial processes (*e.g.*, colloid stabilization, emulsification, flocculation, drug delivery systems, chromatographic separations). Clearly, a fundamental understanding of polyelectrolyte adsorption behavior is critical for enhancing its successful application in these technologies.

The adsorption of charged macromolecules at interfaces depends on many variables (*e.g.*, molecular mass, polyelectrolyte charge, surface charge, ionic strength and segment–segment interaction). Several theories of polyelectrolyte adsorption have been proposed in the literature [1–3]. These funda-

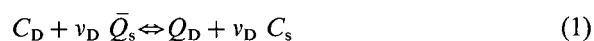
mental approaches are based on the lattice theory for adsorption of uncharged polymers developed by Roe [4] and Scheutjens and Fleer [5,6]. Adsorption of linear polyelectrolytes on highly charged surfaces are characterized by high-affinity isotherms, flat adsorbed layers and weak dependence upon molecular mass and salt concentration [2].

To date, relatively few studies have been carried out on the adsorption properties of polyelectrolyte displacers in chromatographic systems. Peterson and Torres [7,8] have employed frontal chromatography to determine the “number of bonds formed” between carboxymethyl dextrans and anionic chromatographic surfaces. Jen and Pinto [9] have examined the linear elution behavior of low-molecular-mass dextran sulphate. For relatively high-molecular-mass polyelectrolyte displacers ($M_r > 10\,000$) it is not feasible to determine the adsorption properties by linear elution techniques due to their high binding affinity and low desorption rates. Furthermore, measurement of steric effects in polyelectrolyte

Correspondence to: S. M. Cramer, Howard P. Isermann Department of Chemical Engineering, Rensselaer Polytechnic Institute, Troy, NY 12180-3590, USA.

adsorption has not been reported in the chromatographic literature to date.

The steric mass action ion-exchange model (SMA) developed by Brooks and Cramer [10] explicitly accounts for steric effects in multicomponent protein equilibria and is able to predict complex behavior in ion-exchange displacement systems. Assuming that ion exchange is the only mechanism involved during adsorption, the stoichiometric exchange of the polyelectrolyte displacer and the exchangeable salt counter-ions can be represented by,



where C and Q are the mobile and stationary phase concentrations, ν_D is the characteristic charge of the displacer, and subscripts D and s refer to the displacer and salt, respectively. The equilibrium constant is defined as,

$$K_D = \left(\frac{Q_D}{C_D} \right) \left(\frac{C_s}{\bar{Q}_s} \right)^{\nu_D} \quad (2)$$

Electroneutrality on the stationary phase requires

$$A \equiv Q_s + (\nu_D + \sigma_D) Q_D \quad (3)$$

where σ_D is the steric factor of the displacer.

The required model parameters for each component are: characteristic charge ν , steric factor σ and equilibrium constant K . The characteristic charge represents the number of interactions between the adsorbent surface and a single macromolecule. The steric factor of a macromolecule represents the number of sterically hindered salt counter-ions on the adsorbent surface which are unavailable for exchange with other macromolecules in solution. The equilibrium constant is a measure of the affinity of the molecule. Earlier treatments of mass action ion-exchange equilibria assume that the binding of a macromolecule to the adsorbent surface only effects a number of adsorbent sites equal to its characteristic charge. As will be seen in this work, the steric shielding of the stationary phase sites plays an important role in the behavior of non-linear ion-exchange systems.

In order to employ this model for predicting the displacement behavior, it is critical that appropriate experimental protocols be developed for determining model parameters for the proteins and high-affinity polyelectrolyte displacers. In this manuscript, we will present experimental protocols for

measuring SMA parameters of a variety of dextran-based polyelectrolyte displacers. The techniques presented here enable the determination of steric effects in polyelectrolyte adsorption along with the characteristic charge, equilibrium constant, and saturation binding capacity of the molecule in two sequential frontal experiments. In fact, this work has utility for characterizing any non-linear ion-exchange adsorptive system. The parameters obtained in this manuscript are employed in the subsequent paper for simulating complex displacement behavior and investigating the effect of induced salt gradients in ion-exchange systems.

EXPERIMENTAL

Materials

Strong anion-exchange (SAX) (quaternary methyl amine, 8 μm , 50 \times 5 mm I.D.) and cation-exchange (SCX) (sulphopropyl, 8 μm , 50 \times 5 mm I.D.) columns were donated by Millipore (Waters Chromatography Division, Millipore, Milford, MA, USA). Tris-HCl and Tris buffer were purchased from Fisher Scientific (Springfield, NJ, USA). Sodium chloride, sodium nitrate, sodium monobasic phosphate, sodium dibasic phosphate and all proteins were purchased from Sigma (St. Louis, MO, USA). All dextran-based polyelectrolyte displacers were donated by Pharmacia-LKB Biotechnology (Uppsala, Sweden). Cellulose triacetate membranes (5000 and 10 000 molecular mass cut off) were obtained from Sartorius (Göttingen, Germany). Reagent grade potassium chromate, silver nitrate and cesium chloride were obtained from Aldrich (Milwaukee, WI, USA). Polyvinylsulphuric acid potassium salt (PVSK), polydiallyl dimethyl ammonium chloride (polyDADMAC) and *o*-toluidine blue indicator were obtained from Nalco (Naperville, IL, USA).

Apparatus

Ultrafiltration of polyelectrolytes was carried out using an Amicon 8050 stirred cell (Amicon, Danvers, MA, USA). All frontal and elution chromatographic experiments were carried out with a modular chromatographic system consisting of a Model LC 2150 pump (LKB, Bromma, Sweden), a spectro-

flow 757 UV–Vis detector (Applied Biosystems, Foster City, CA, USA) and a Waters R401 differential refractometer. Data acquisition from the frontal experiments was carried out using Kipp and Zonen BD40 strip-chart recorder (Delft, Holland), and Waters Maxima 820 chromatographic workstation. Fractions of the column effluent were collected using an LKB 2212 Helirac fraction collector. Sodium ion analysis was performed using a Perkin-Elmer, Model 3030 (Perkin-Elmer, Norwalk, CT, USA) atomic absorption spectrophotometer. A 10-port valve Model C10W injector (Valco, Houston, TX, USA) with multiple loops was used to conduct all the frontal experiments. Lyophilization was carried out using a Model Lyph Lock 4.5 Freeze Dry System (Labconco, Kansas City, MO, USA).

Procedures

Purification of polyelectrolytes

All the polyelectrolyte displacers were ultrafiltered as well as diafiltered to remove salts and other low-molecular-mass impurities. 5000 and 10 000 molecular mass cut off membranes were employed to purify the M_r 10 000 and 20 000–50 000 displacers, respectively. After ultrafiltration, the retentate was lyophilized.

Polyelectrolyte analysis

All polyelectrolytes were analyzed using a colloidal titration assay provided by Nalco Chemical Company. For analysis of dextran sulphates, a known volume of polyDADMAC reagent was added to the aqueous displacer solutions. Subsequent addition of *o*-toluidine indicator produced a colorimetric change. The excess polyDADMAC reagent was titrated against PVSK in presence of a *o*-toluidine indicator. For the analysis of DEAE–dextran the solution was titrated against PVSK without addition of the polyDADMAC reagent. Linear calibrations were obtained with both of these titrations.

Analyses for counter-ions

Chloride ion analysis. Chloride ion analysis was carried out using the ASTM assay [11]. For calibration, a known amount of chloride ion in 50 ml deionized water was titrated against 0.01 *M* silver nitrate using potassium chromate indicator solu-

tion. This technique was able to accurately monitor down to 10 μmol of chloride ion. A blank titration was performed to account for the chloride in water. The technique was able to selectively detect chloride ions in the presence of other salts, proteins, and displacers.

Sodium ion analysis. For the cation-exchange experiments, sodium was analyzed using atomic absorption spectrometry. Effluent fractions were diluted 3000-fold in plastic tubes containing 5 g/l cesium chloride solution (to minimize background noise) and their amounts quantitated against known Na^+ ion standards (10–50 μM).

Bed capacity measurements

Anion-exchange column. The capacity of the anion exchanger was measured in two different ways. The column was first perfused with 10 column volumes of 50 mM Tris–HCl buffer, pH 7.5. A front of 100 mM nitrate was then introduced and the column effluent was monitored at 310 nm. In addition, the column effluent was collected for subsequent chloride analysis. The bed capacity was then determined from both the nitrate breakthrough front as well as the total amount of displaced chloride. The nitrate breakthrough technique is similar to that reported by Bentreop and Engelhardt [12].

Cation-exchange column. The cation exchanger was first equilibrated with 100 mM sodium phosphate buffer, pH 7.5, for approximately 10 column volumes followed by a front of 1 *M* ammonium sulphate. The column effluent was collected for subsequent sodium analysis. The bed capacity was then determined by measuring the amount of sodium ions displaced by the ammonium front.

Elemental analyses of dextran-based displacers

For each polyelectrolyte, the number of functional groups per molecule (*e.g.*, sulphate and DEAE) were determined from sulphur and nitrogen elemental analysis. The elemental analyses were carried out by Galbraith Laboratories (Knoxville, TN, USA).

Determination of SMA parameters and induced salt gradients for polyelectrolyte displacers

Dextran sulphate in anion-exchange system. The following experimental protocol was employed for the chromatographic characterization of dextran sulphates:

(1) *Stationary phase concentration*: stationary phase concentrations of the dextran sulphate displacers were determined using frontal chromatography [13]. A 50 × 5 mm I.D. column was equilibrated with Tris buffer, pH 7.5, for approximately 10 column volumes. A front of dextran sulphate solution in the carrier was then introduced into the column at 0.2 ml/min and the column effluent was monitored at 252 nm to determine the breakthrough volume. The stationary phase concentration of the displacer, Q_D , was determined from the breakthrough volume, V_B , by

$$Q_D = C_D (V_B - V_0)/V_{sp} \quad (4a)$$

where C_D is the mobile phase concentration of polyelectrolyte displacer, V_0 is the dead volume of the column and V_{sp} is the column stationary phase volume. The number of moles of displacer adsorbed on the stationary phase, n_D , was calculated by

$$n_D = C_D (V_B - V_0) = Q_D V_{sp} \quad (4b)$$

(2) *Induced salt gradient*: during the frontal experiment, the column effluent was collected for subsequent chloride analysis. The induced salt gradient was then determined by measuring the total amount of chloride displaced, n_1 , during the frontal experiment:

$$\Delta C_s = n_1/(V_B - V_0) \quad (5)$$

where ΔC_s is the step increase in the mobile phase counter-ion concentration upon displacer adsorption (Fig. 1).

(3) *Characteristic charge*: the characteristic charge

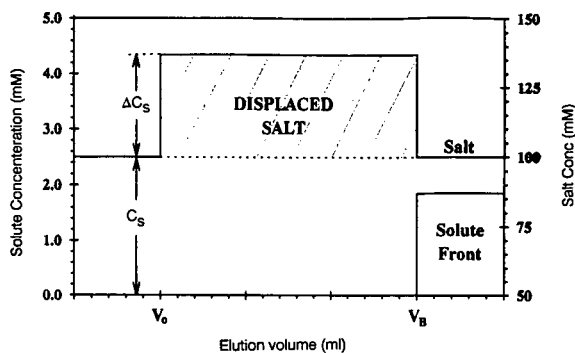


Fig. 1. Schematic of the induced salt gradient frontal chromatographic technique for determination of characteristic charge of polyelectrolytes.

of the displacer, v_D , was determined from the induced salt gradient using the following expression:

$$v_{D, \text{chloride}} = n_1/n_D = \Delta C_s/C_D \quad (6)$$

This approach for determining the characteristic charge from the induced salt gradient is depicted in Fig. 1.

(4) *Steric factor*: at sufficiently low mobile phase salt concentration the displacer completely saturates the stationary phase material. Frontal experiment under these conditions can be employed to determine the steric factor, σ_D , from the following expression [10]:

$$\sigma_D = (A/Q_D^{\text{max}}) - v_D \quad (7)$$

where A is the ion bed capacity and Q_D^{max} is the maximum stationary phase capacity of the polyelectrolyte displacer.

An independent direct measurement of steric factor can be carried out using a nitrate frontal experiment. A front of 100 mM sodium nitrate was perfused into a column saturated with the displacer. The column effluent was monitored at 310 nm to determine the nitrate breakthrough volume. Since the nitrate ions are small, they are able to access the sterically hindered chloride ions present on the surface and undergo ion exchange. The steric factor for the adsorbed displacer can then be determined from the nitrate breakthrough volume, $V_{B, \text{nitrate}}$, by

$$\sigma_{D, \text{nitrate}} = C_{\text{nitrate}} (V_{B, \text{nitrate}} - V_0)/n_D \quad (8)$$

where C_{nitrate} is the concentration of the nitrate front. In addition, the steric factor can be determined by measuring the chloride ion displaced by the nitrate front, n_2 , as given by

$$\sigma_{D, \text{chloride}} = n_2/n_D \quad (9)$$

In order to check the internal consistency of these methods, the characteristic charge of dextran sulphate can be independently calculated using the expression:

$$v_{D, \text{nitrate}} = (A/Q_D^{\text{max}}) - \sigma_{D, \text{nitrate}} \quad (10)$$

where, Q_D^{max} is determined by eqn. 4 under saturation conditions and $\sigma_{D, \text{nitrate}}$ is determined by eqn. 8.

An example of this sequential chromatographic method for the 10 000 dextran sulphate displacer is presented in Fig. 2.

(5) *Equilibrium adsorption constant*: the equilibri-

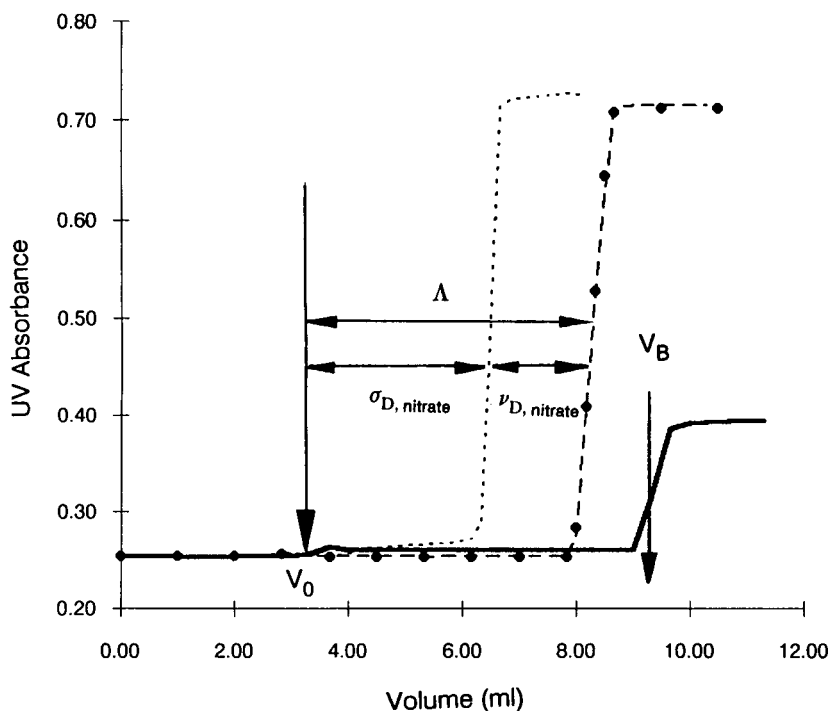


Fig. 2. Sequential frontal chromatographic protocol for determination of SMA parameters for dextran sulphate. Chromatographic conditions: nitrate fronts, 100 mM sodium nitrate; dextran sulphate front, 10 mg/ml in 50 mM Tris-HCl, pH 7.5. The horizontal arrows represent the elution volumes used to determine the corresponding model parameters. --- = Nitrate front (initial); ● = nitrate front (after regeneration); — = M_r 10 000 dextran sulphate; - - - = nitrate front (saturated column).

um constant for the ion-exchange process is defined in eqn. 3. Once the characteristic charge and steric factor are measured independently as described above, a frontal experiment was employed for the determination of the equilibrium constant K_D . This experiment was performed under elevated mobile phase salt conditions where the solute does not completely saturate the bed. The equilibrium constant was directly calculated from the breakthrough volume using the independently determined values of the characteristic charge (ν_D) and steric factor (σ_D) by the expression [10]:

$$K_D = \frac{1}{\beta} \left(\frac{V_B}{V_0} - 1 \right) \left(\frac{C_s}{A - (\nu_D + \sigma_D) \frac{C_D}{\beta} \left(\frac{V_B}{V_0} - 1 \right)} \right)^{\nu_D} \quad (11)$$

where β is the column phase ratio and C_s is the initial salt concentration in the carrier.

At the end of these experimental procedures, the column was regenerated by passing five column volumes of 1.5 M NaCl solution in 100 mM phosphate buffer, pH 2.1, as the regenerant. The total ion bed capacity was then re-determined to ensure complete regeneration of the column.

DEAE-dextran in cation-exchange system. The experimental protocols for measuring the SMA parameters of DEAE-dextran displacers in the cation-exchange system were similar to those described above for the anion-exchange displacers. Mobile phases consisted of various concentrations of sodium phosphate buffer, pH 6.0. Column effluents were monitored using refractive index (RI) detection. Sodium ion content was determined using atomic absorption spectroscopy. The regenerant solution was 1 M NaCl in 100 mM phosphate buffer, pH 11.0.

Determination of SMA parameters for proteins

The SMA parameters for several proteins were

obtained according to the protocol described by Brooks and Cramer [10]. Briefly, linear elution experiments were carried out at various mobile phase salt concentrations in order to determine the characteristic charge (v_p) and equilibrium constant (K_p) by the following equations:

$$\log k' = \log (\beta K_p A^{v_p}) - v_p \log C_s \quad (12)$$

where a plot of a $\log k'$ vs. $\log C_s$ yields a straight line with a slope of $-v_p$, and intercept of $\log (\beta K_p A^{v_p})$. Linear elution data for β -lactoglobulin A and B were obtained on the SAX column using Tris chloride mobile phase. In the cation-exchange system, linear elution data were obtained for α -chymotrypsinogen A, cytochrome *c*, and lysozyme using sodium phosphate buffer. The steric factor for the proteins was obtained from a single non-linear frontal chromatographic experiment according to the expression:

$$\sigma_p = \frac{\beta}{C_p \Pi} \left[A - C_s \left(\frac{\Pi}{\beta K_p} \right)^{1/v_p} \right] - v_p \quad (13a)$$

where,

$$\Pi = \left(\frac{V_B}{V_0} - 1 \right) \quad (13b)$$

In order to verify the model simulations, experimental isotherms of the proteins were also measured at several mobile phase salt conditions by frontal chromatography [13].

RESULTS AND DISCUSSION

In this paper, we present a simple experimental protocol for obtaining the SMA parameters required for simulating a wide range of displacement behavior. As described in the experimental section, a set of linear elution experiments along with one non-linear frontal experiment for the proteins, and two frontal experiments for the displacer, will yield sufficient information to determine all SMA parameters. In this paper, a rigorous evaluation of this parameter estimation protocol is carried out by comparing results from different techniques. Furthermore, the dependence of these parameters on mobile phase conditions and their relationship to the functional group density of the polyelectrolyte is investigated.

Bed capacity of ion exchangers

The total ion bed capacity for the anion-exchange column was determined *in situ* by a frontal experiment using sodium nitrate. These results were compared to capacities obtained by measuring the total amount of chloride ion displaced during the nitrate frontal experiment. As seen in Fig. 3A, there is excellent agreement between the values obtained from both methods. The bed capacities for the cation-exchange system were also determined at different salt concentrations (Fig. 3B). As seen in the figures, the bed capacities for both the anion- and cation-exchange systems were independent of the salt concentrations employed in the frontal experiments. Thus, a single frontal experiment is sufficient for the determination of total ion bed capacity. The ability to measure total ion bed capacity *in situ* facilitates SMA parameter estimation and enables a rapid test of column regeneration. As seen in Fig. 2, the superimposed initial and final nitrate breakthrough fronts confirm complete regeneration of the column from the adsorption of dextran sulphate molecules.

The bed capacity is reported here in molar units rather than equivalents. For a univalent ion the numerical value of bed capacity is the same in both units, since each ion binds to one site on the surface. The bed capacity of the cation exchanger for the divalent ions calcium and magnesium was independently measured, using the same frontal technique, to be 390 mM for each ion. Thus bed capacity for these divalent ions was not half of that for the sodium ion (561 mM) for the same adsorbent. This indicates that each divalent ion does not bind to exactly two sites on the surface due to morphological constraints. Clearly, a bed capacity expressed in mequiv. would be misleading in this case. In general, the use of mM units along with a specification of "characteristic charge" of the counter-ion is a more useful way of expressing bed capacity. In fact, mM units are required in order to develop a solute movement analysis of this model, as described in the subsequent paper.

Functional group density and characteristic charge of polyelectrolytes

While the determination of the characteristic charge and equilibrium constant from linear elution

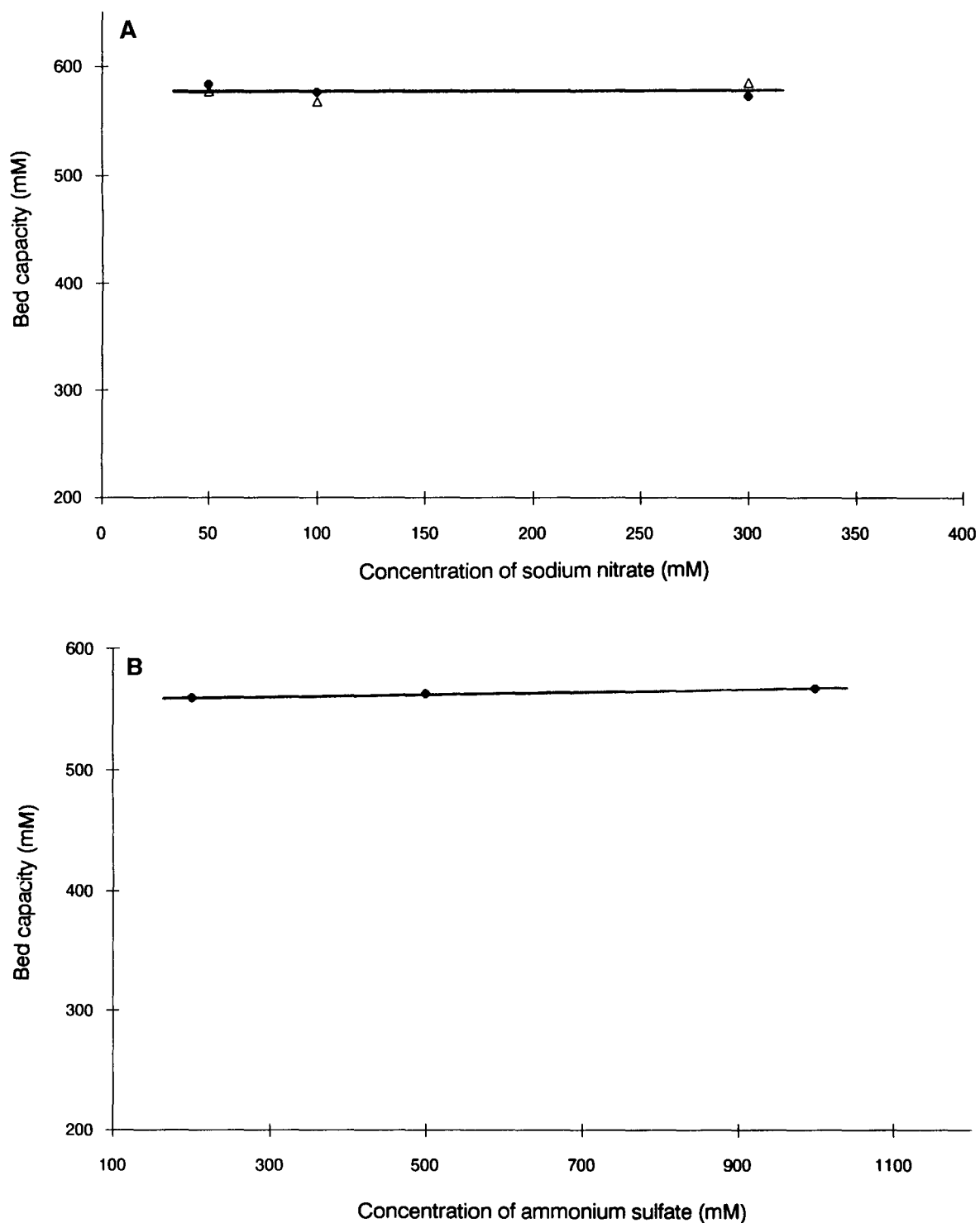


Fig. 3. Bed capacities of ion-exchange columns. (A) Anion-exchange column using the (Δ) nitrate and (\bullet) chloride techniques; flow-rate: 0.25 ml/min; UV wavelength: 310 nm. (B) Cation-exchange column using ammonium sulphate; flow-rate: 0.5 ml/min.

data works well for moderately retained proteins, it is quite difficult to characterize high-molecular-mass polyelectrolyte displacers in this fashion due to their high affinity. Frontal chromatography, on the other hand, is well suited for parameter estimations for these high-affinity compounds.

Several frontal chromatographic methods were employed to determine both the characteristic charge and steric factor of the displacers as described in the experimental section. Table I presents SMA parameters for dextran sulphate obtained with both the chloride- and nitrate-based techniques. As seen in the table, both techniques yielded essentially the same values. These results confirm the hypothesis that a front of nitrate ions, passed through a column saturated with the displacer, is able to access all the sterically hindered ion-exchange sites on the surface. Since these two methods are internally consistent, all future parameter estimations for anion-exchange systems can be carried out using the more convenient nitrate-based methods.

Parameter measurements for M_r 10 000 and 50 000 dextran sulphate displacers were carried out at various salt and polyelectrolyte concentrations to examine the effects of these operating conditions on

the SMA parameters. These studies employed moderate mobile phase salt concentrations, typically used for the displacement experiments. As seen in Table I, both the characteristic charge and the steric factors were essentially independent of mobile phase salt and displacer concentration. The characteristic charge of these polyelectrolytes was invariant even when the mobile phase salt concentration was increased 5 to 10 fold. Similarly, the steric factor was observed to be independent of the mobile phase salt and displacer concentration. These results are significant in that they indicate, for these high affinity displacers, that the measurement of these parameters under a single set of mobile phase conditions is sufficient to predict their adsorption behavior for a range of mobile phase conditions. The characteristic charge and steric factor of DEAE-dextran displacers in the cation-exchange system were also found to be insensitive to the mobile phase salt and displacer concentrations.

Fig. 4a and b shows the induced salt gradient produced by the adsorption of the displacers at various salt and solute concentrations. As seen in the figure, the induced salt gradient for each displacer increased linearly with the displacer concentration.

TABLE I

CHARACTERISTIC CHARGE AND STERIC FACTOR OF DEXTRAN SULPHATES: COMPARISON OF TECHNIQUES

Chromatographic conditions: SAX column; buffer; tris chloride, pH 7.5; ion bed capacity = 567 mM.

M_r	Salt concentration (mM)	Dextran sulphate concentration (mM)	$v_{D, \text{chloride}}^a$	$v_{D, \text{nitrate}}^b$	$\sigma_{D, \text{chloride}}^c$	$\sigma_{D, \text{nitrate}}^d$
10 000	50	0.5	33.8	32.3	33.12	34.8
10 000	50	1	31.3	29.2	34.5	33.6
10 000	100	0.5	30.2	32.4	32.2	34.2
10 000	100	1	32.1	31.0	32.2	32.1
10 000	100	2	32.3	32.5	34.0	33.2
10 000	250	1	N.D.	31.1	N.D.	33.4
50 000	50	0.2	152.3	145.7	160.0	166.7
50 000	50	0.4	144	145.1	169.7	165.3
50 000	100	0.2	140.9	141.6	160.1	161.8
50 000	100	0.4	137.4	137.2	161.3	165.1
50 000	500	0.4	N.D.	135.9	N.D.	167.1

^a Defined in eqn. 3.

^b Defined in eqn. 7.

^c Defined in eqn. 6.

^d Defined in eqn. 5.

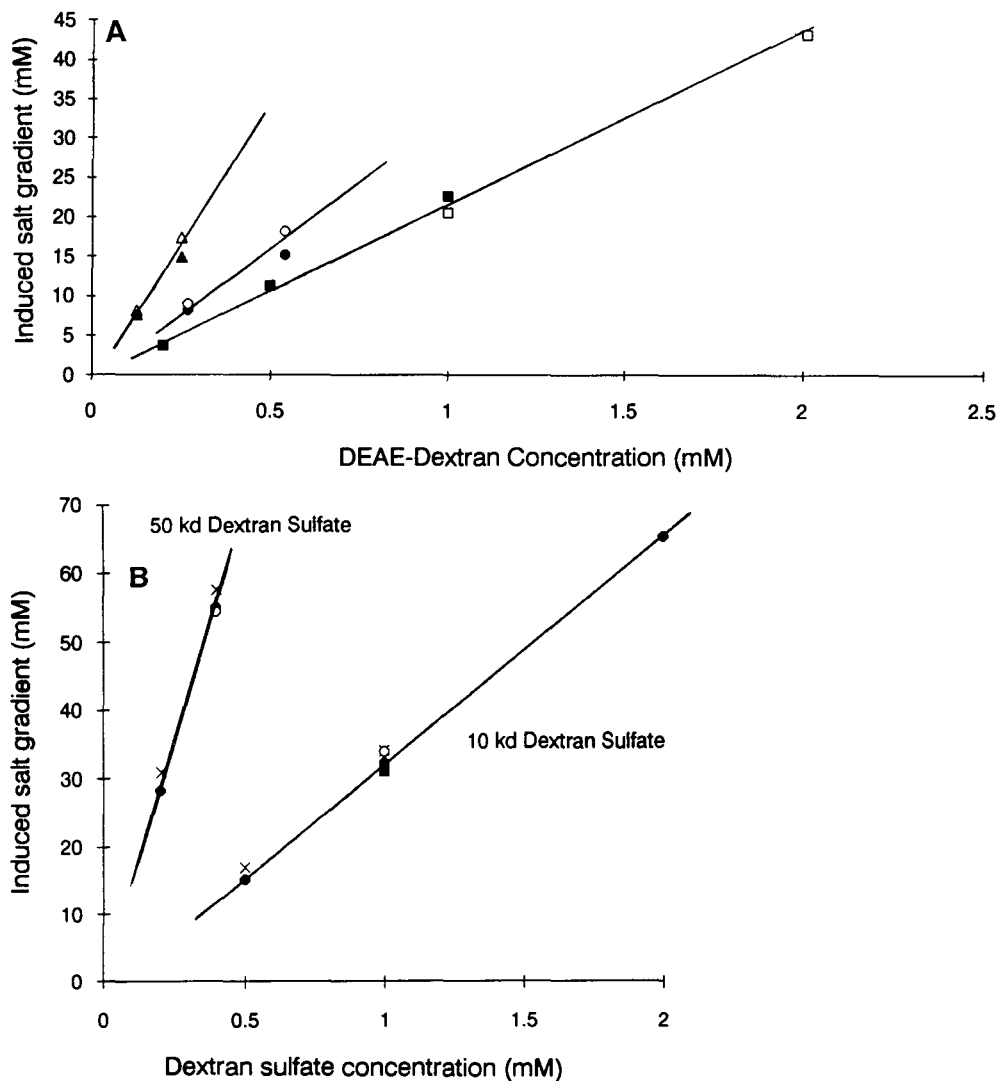


Fig. 4. Induced salt gradients as a function of inlet displacer concentration in ion-exchange systems. (A) *M*, 10 000 (□, ■), 20 000 (○, ●) and 40 000 (△, ▲) DEAE-dextran in cation-exchange system; closed symbols at 20 mM Na⁺; open symbols at 75 mM Na⁺, pH 6.0; flow-rate: 0.2 ml/min; detection: RI. (B) Dextran sulphate (10 000 and 50 000) in anion-exchange system at (×) 50, (●) 100, (■) 250 and (○) 500 mM Cl⁻, pH 7.5; flow-rate: 0.2 ml/min; detection: UV 252 nm. kd = kilodalton.

The average characteristic charge of the polyelectrolyte displacers can be obtained directly from the slope of these lines and are presented in Table II.

Data obtained from the elemental analyses was employed to calculate the functional group density and the number of functional groups in each polyelectrolyte. As expected, higher-molecular-mass displacers possess correspondingly higher numbers of

functional groups and characteristic charges. The dextran sulphates have a greater degree of functionalization than the DEAE-dextran materials. The characteristic charge and functional group results are also presented in normalized form (*i.e.*, per repeating unit of the polymer). The repeating unit employed in these calculations was the disaccharide [14]. While the functional group density of

TABLE II
CHARACTERISTIC CHARGE AND FUNCTIONAL GROUP DENSITY OF DEXTRAN POLYELECTROLYTES

Displacer	Elemental analyses (% w/w)	Functional group density ^a	Number of functional groups (<i>f</i>)	Characteristic charge (ν_D)	Normalized characteristic charge ^b	Fraction of groups bound (ν_D/f)
10 000 Dextran sulphate	16.0% S	2.67	59	31	1.65	0.62
50 000 Dextran sulphate	16.3% S	2.77	255	140	1.52	0.55
10 000 DEAE-dextran	3.7% N	1.15	26	21	0.91	0.81
20 000 DEAE-dextran	2.8% N	0.81	40	31	0.62	0.78
40 000 DEAE-dextran	3.5% N	1.08	100	64	0.69	0.64

^a Functional group density is defined as the average number of functional groups per repeating unit of the polyelectrolyte.

^b Normalized characteristic charge is defined as the characteristic charge per repeating unit of the polyelectrolyte.

each class of dextran-based polyelectrolytes was essentially constant (with the exception of the M_r 20 000 DEAE-dextran), the normalized characteristic charge decreased with molecular mass. In other words, a relatively smaller fraction of the total number of functional groups is bound for higher-molecular-mass polyelectrolytes. This effect is the most striking for the DEAE-dextran materials. In fact, this change in normalized characteristic charge with molecular mass is a reflection of different conformations of these polyelectrolytes in the adsorbed state. It is likely that, an increase in molecular mass is associated with an increase in the relative amounts of loops and tails in the adsorbed polyelectrolyte.

Steric factor of polyelectrolytes

Table III presents the average values of the steric factors for dextran sulphates and DEAE dextrans of various molecular masses. For all polyelectrolytes, the values of the steric factors were comparable to

the characteristic charges. These results indicate that a significant portion of the adsorption sites on the chromatographic surface are sterically blocked by the polyelectrolytes and are not available for exchange with unbound polyelectrolytes solutes. The characteristic charge and the steric factor of these linear polyelectrolytes depends on the number of functional groups on the polyelectrolyte and their positioning relative to the exchange sites on the adsorption surface. Table III also indicates that the ratio of steric factor to characteristic charge increased with molecular mass. This effect is more pronounced for the DEAE-dextrans. This is due to a combination of lower normalized characteristic charge and relatively less dense surface coverage for higher-molecular-mass polyelectrolytes.

It is important to note that the steric factor reported in this manuscript represents the salt counter-ions which are "unavailable" for exchange with other macromolecules. In practice, this parameter may also include size-exclusion effects. How-

TABLE III
AVERAGE VALUES OF SMA PARAMETERS FOR DEXTRAN DISPLACERS

Displacer	Characteristic charge (ν_D)	Steric factor (σ_D)	(σ_D/ν_D)	Q_D^{\max} (mM)	$Q_D^{\max} \cdot \nu_D$ (mequiv.)
10 000 Dextran sulphate	31	33	1.06	9.11	282
50 000 Dextran sulphate	140	162	1.16	1.87	260
10 000 DEAE-dextran	21	32	1.52	10.66	223
40 000 DEAE-dextran	64	130	2.03	3.08	196

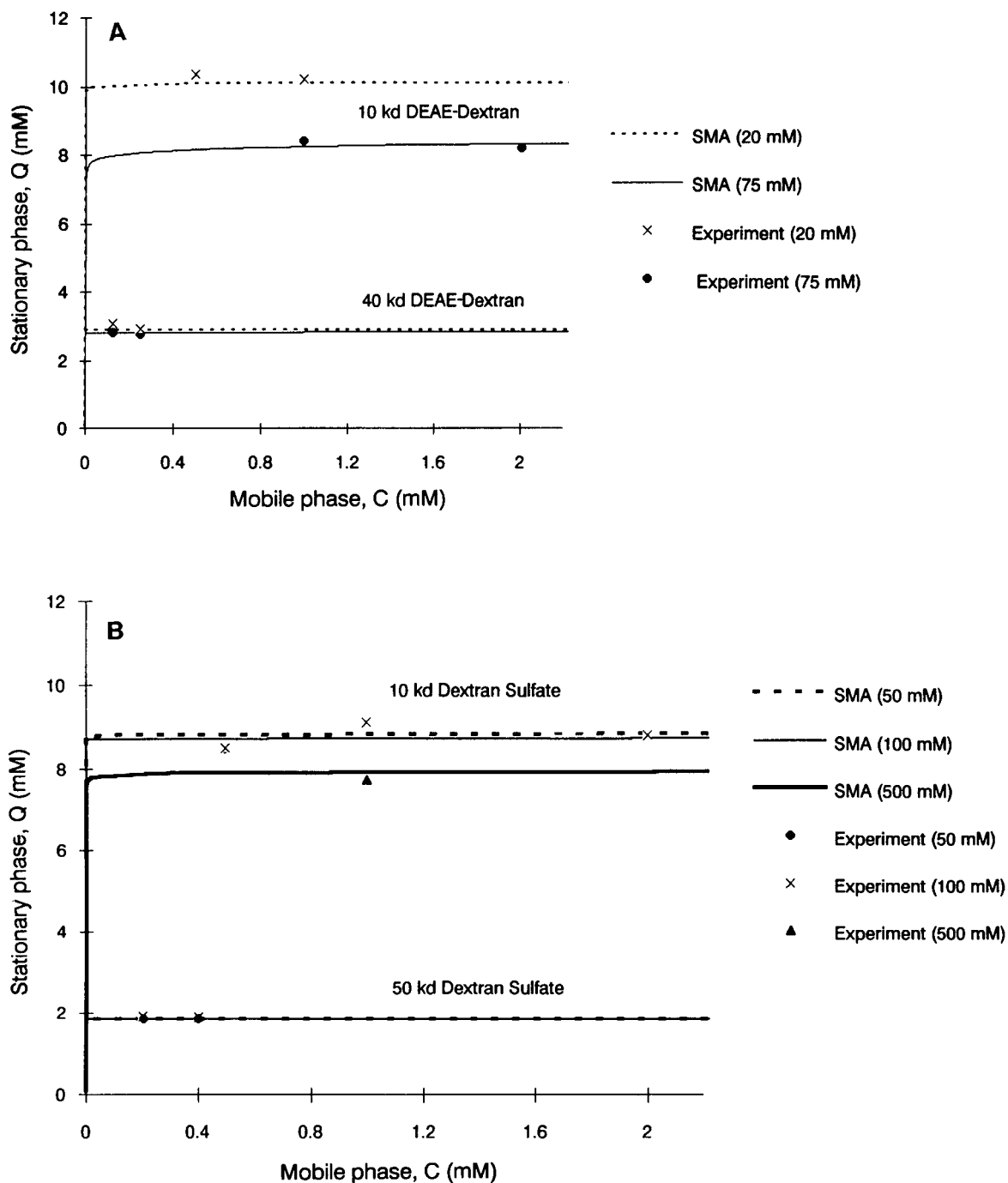


Fig. 5. Experimental and SMA isotherms of (A) DEAE-dextran; mobile phase: sodium phosphate, pH 6.0; detection: RI and (B) dextran sulphate; mobile phase: Tris-HCl, pH 7.5; flow-rate: 0.2 ml/min; detection: UV 252 nm.

ever, chromatographic analysis of the macromolecules under unretained conditions indicated no measurable size-exclusion effects in these columns.

The affinity of binding of a polyelectrolyte increased with molecular mass due to a corresponding increase in its characteristic charge. Conversely, the maximum molar binding capacity (Q^{\max}) decreased with increase in molecular mass as shown in Table III. The product of the stationary phase concentration of the polyelectrolyte and its characteristic charge ($Q^{\max} \cdot v$) is a measure of the total number of interactions between the adsorbed polyelectrolyte and the adsorbent surface under the saturation conditions. For higher-molecular-mass polyelectrolytes, a correspondingly smaller number of total bonds are formed with the surface, due to their greater steric factor.

Equilibrium adsorption constant of polyelectrolytes

Once the characteristic charge and steric factor are measured independently, the equilibrium adsorption constant can be calculated from a frontal experiment under non-saturating conditions using eqn. 11. However, the value of K can only be determined for molecules which demonstrate salt-dependent adsorption behavior. In practice, this is quite difficult for the higher-molecular-mass displacers since their Q values exhibit very little or no dependence on the mobile phase salt concentration. M_r 50 000 dextran sulphate exhibited maximum saturation at all salt concentrations used in the experiments. Accordingly, a sufficiently high value of K was employed in the isotherm simulations. While a K value was obtained for the M_r 40 000 DEAE-dextran ($K = 5.45 \cdot 10^{44}$), this value is only approximate due to the weak salt dependence of the polyelectrolyte. On the other hand, the smaller displacers (M_r 10 000 dextran sulphate, 10 000 DEAE-dextran) exhibited significant salt-dependent adsorption behavior. The K values for the M_r 10 000 dextran sulphate and DEAE-dextran displacers were determined to be $3.6 \cdot 10^{28}$ and 0.0063, respectively. It is important to note that the equilibrium constant in the SMA formalism is defined differently from the conventional Henry's law constant. This wide range of values is due to the exponential dependence of K on characteristic charge (eqn. 3) and the fact that the equilibrium constant K is unique for each ion-exchange equilibria.

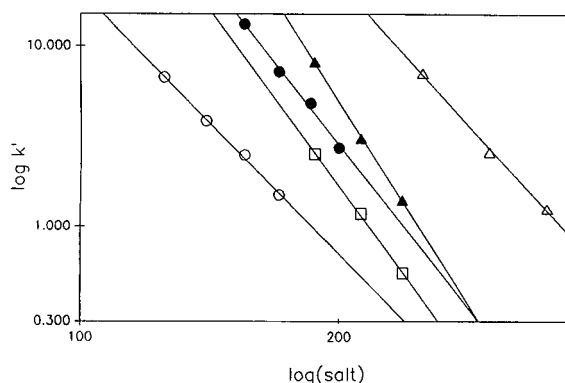


Fig. 6. Linear elution data for the determination of protein characteristic charge and equilibrium adsorption constant. Chromatographic conditions: for anion-exchange proteins [(▲) β -lactoglobulin A and B, (□) β -lactoglobulin B]; mobile phase: Tris-HCl, pH 7.5; for cation-exchange proteins [(○) α -chymotrypsinogen, (●) cytochrome c and (△) lysozyme]; mobile phase: sodium phosphate, pH 6.0.

Isotherms of polyelectrolytes

Once the characteristic charge, steric factor and equilibrium constants are determined, the isotherms of the polyelectrolytes can be simulated using the SMA formalism of Brooks and Cramer [10]. The experimentally measured isotherms of the polyelectrolytes were compared with the simulated isotherms in Fig. 5.

These results confirm the square nature of the polyelectrolyte equilibrium isotherms under different mobile phase salt concentrations [2,3,15]. Since these polyelectrolytes approach square isotherms,

TABLE IV

SMA PARAMETERS FOR PROTEINS

Chromatographic conditions: β -lactoglobulin A and B: SAX column, Tris buffer, pH 7.5; other proteins: SCX column, sodium phosphate buffer, pH 6.0.

Protein	Characteristic charge (v_p)	Steric factor (σ_p)	Equilibrium constant (K_p)
α -Chymotrypsinogen	4.8	49.2	$9.22 \cdot 10^{-3}$
Cytochrome c	6.0	53.6	$1.06 \cdot 10^{-2}$
Lysozyme	5.3	34.0	$1.84 \cdot 10^{-1}$
β -Lactoglobulin A	7.5	38.2	$5.44 \cdot 10^{-3}$
β -Lactoglobulin B	6.3	47.5	$6.42 \cdot 10^{-3}$

measurements need only be carried out at one or two polyelectrolyte mobile phase concentrations. As seen in the figures, the equilibrium binding capacity (Q) of higher-molecular-mass polyelectrolytes is essentially independent of the mobile phase salt concentration. On the other hand, the lower-molec-

ular-mass polyelectrolytes (10 000) display some variance in their binding capacities with mobile phase salt concentration. Salt counter-ions compete more effectively for adsorption sites with lower-molecular-mass polyelectrolytes having a relatively smaller number of bonds with the surface. The

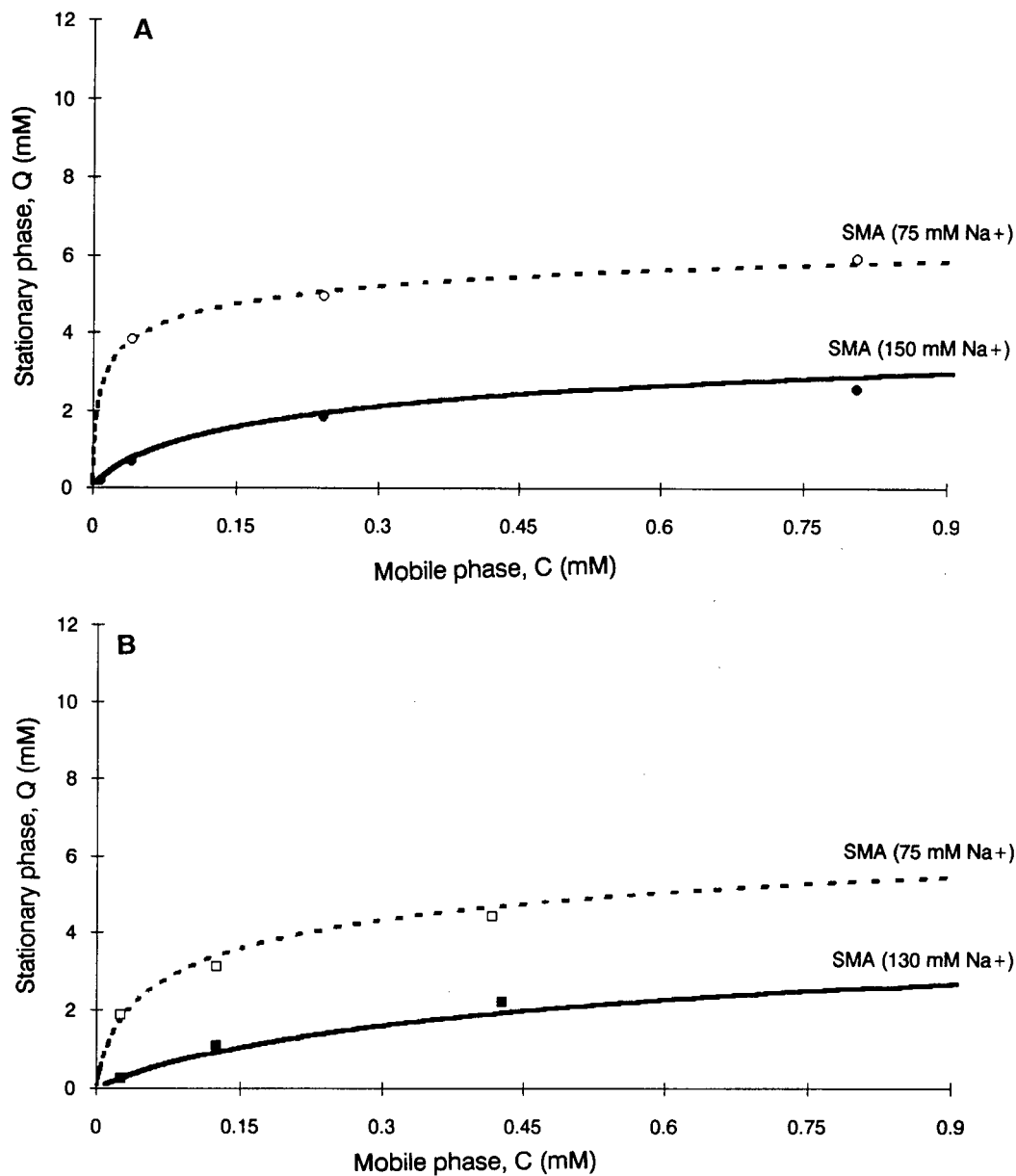


Fig. 7. Experimental and SMA isotherms of (A) cytochrome *c* at (○) 75 mM and (●) 150 mM sodium phosphate, pH 6.0; (B) α -chymotrypsinogen at (□) 75 mM and (■) 130 mM sodium phosphate, pH 6.0.

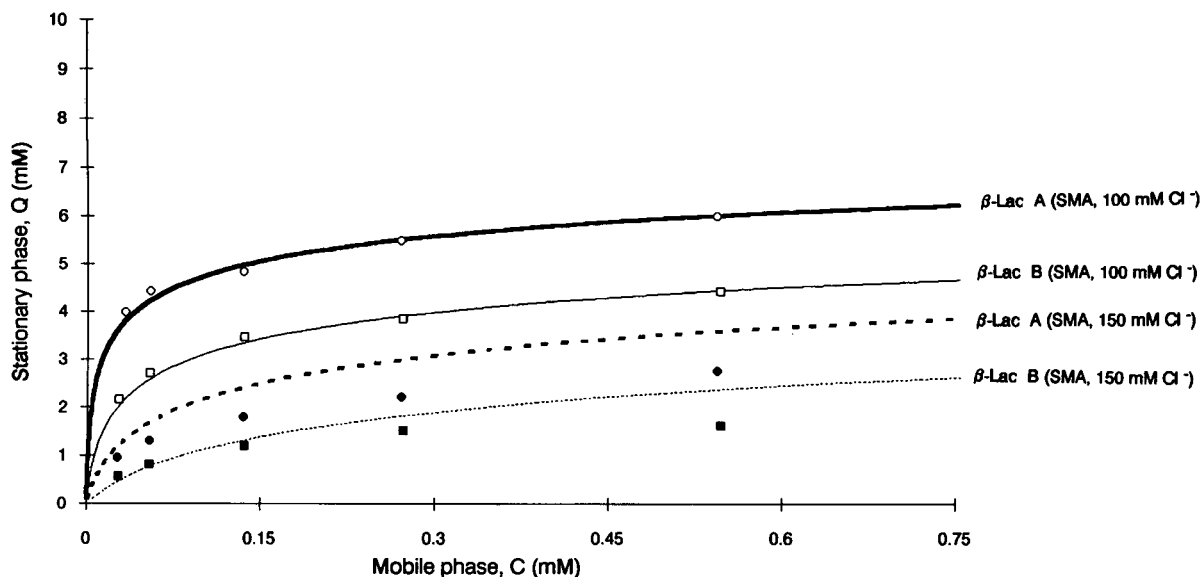


Fig. 8. Experimental and SMA isotherms of β -lactoglobulin A and B at 100 mM (open symbols) and 150 mM (closed symbols); mobile phase: Tris-HCl, pH 7.5.

weaker salt dependence of the polyelectrolyte isotherms as compared to the protein isotherms lends significant flexibility for design of displacement chromatographic separation of proteins.

SMA parameters of proteins

The characteristic charge and equilibrium constant for several model proteins were obtained using the linear elution method described in the experimental section. As seen in Fig. 6, all measured proteins exhibited linear $\ln k'$ plots. The steric factors of the proteins were determined using the non-linear frontal chromatographic technique in concert with eqn. 13. The resulting SMA parameters for these proteins are presented in Table IV. In contrast to the results described above for the dextran-based displacers, the proteins exhibited significantly higher steric factors relative to their characteristic charge. This is not surprising in light of the conformational constraints in the protein molecules.

Once the SMA parameters are obtained for a given protein, the model can then be used to generate adsorption isotherms at any salt concentration. Clearly, an important test of the SMA formalism is a comparison between theoretical and experimentally

determined isotherms. Adsorption isotherms of the proteins cytochrome *c* and α -chymotrypsinogen A are presented in Fig. 7. These results confirm that the SMA formalism is well suited for describing protein adsorption behavior at various salt conditions. In contrast, the isotherms for β -lactoglobulin A and B (Fig. 8) are not as well described by the SMA formalism. There are several possible explanations for this deviation from "ideal" SMA behavior. These include: aggregation [16–18], as well as salt-dependent changes in the adsorbed protein conformation. These phenomena are currently under active investigation in our laboratory.

CONCLUSIONS

Frontal chromatography offers a useful technique for characterizing the adsorption behavior of high-affinity polyelectrolytes. The experimental techniques presented in this paper not only enable us to measure the SMA parameters but also provide a powerful tool to evaluate the efficacy of polyelectrolytes as displacers for ion-exchange protein separations.

The physico-chemical properties (*e.g.*, functional group density and molecular mass) of the polyelec-

trolytes will have a profound effect on their efficacy as a displacer for ion-exchange protein separations. For a given functional group density of the polyelectrolyte and ligand distribution of the adsorbent surface, adsorption of higher-molecular-mass polyelectrolyte is associated with a decrease in normalized characteristic charge and a corresponding increase in the steric factor. For a given molecular mass, a higher density of functional groups on the polyelectrolyte will result in a higher characteristic charge and lower steric factor with a concomitant increase in the induced salt gradient. Thus, by manipulating the functional group density and molecular mass of the polyelectrolyte, one can control the affinity of the molecule as well as the induced salt gradients. Furthermore, the density of ion-exchange sites on the chromatographic surface will directly influence the characteristic charge and steric factor of the polyelectrolyte. In the subsequent manuscript we will examine these effects with respect to the ion-exchange displacement separation of proteins.

These parameter estimation protocols in concert with the SMA formalism establish a powerful framework for rational design of efficient displacers for ion-exchange systems. Extension of these studies to a variety of polyelectrolyte compounds will lead to a formulation of generalized rules of thumb relating the polyelectrolyte structure to their adsorption behavior.

SYMBOLS

All mobile phase concentrations are defined per unit volume of mobile phase. All stationary phase concentrations and the bed capacities are defined per unit volume of stationary phase.

C_D	Concentration of polyelectrolyte in the mobile phase (mM)
C_{nitrate}	Concentration of the nitrate front in the mobile phase (mM)
C_P	Concentration of protein in the mobile phase (mM)
C_s	Salt concentration in the carrier (mM)
ΔC_s	Step increase in the mobile phase salt concentration upon displacer adsorption (mM)
k'	Dimensionless retention time of proteins
K_D	Equilibrium constant of polyelectrolyte displacers

K_P	Equilibrium constant of proteins
n_1	Salt displaced by displacer front (mmol)
n_2	Salt displaced by nitrate front (mmol)
n_D	Displacer adsorbed on the stationary phase (mmol)
Q_D	Stationary phase concentration of the displacer (mM)
Q_D^{max}	Maximum binding capacity of the polyelectrolyte on the stationary phase (mM)
\bar{Q}_s	Stationary phase concentration of sterically unhindered salt (mM)
V_0	Dead volume of the column (ml)
V_B	Breakthrough volume of displacer front (ml)
$V_{B\text{-nitrate}}$	Breakthrough volume of nitrate front (ml)
V_{sp}	Column stationary phase volume (ml)

Greek letters

β	Column phase ratio
A	Ion bed capacity (mM)
v_p	Characteristic charge of proteins
$v_{D,\text{chloride}}$	Characteristic charge of the displacer based on chloride method defined in eqn. 6
$v_{D,\text{nitrate}}$	Characteristic charge of the displacer based on nitrate method defined in eqn. 10
σ_P	Steric factor of proteins
$\sigma_{D,\text{chloride}}$	Steric factor of the displacer based on chloride method defined in eqn. 9
$\sigma_{D,\text{nitrate}}$	Steric factor of the displacer based on nitrate method defined in eqn. 8

ACKNOWLEDGEMENTS

This research was funded by Millipore Corporation and grants BCS-9112481 and CTS-8957746 (a Presidential Young Investigator Award to S. M. Cramer) from the National Science Foundation. Chromatographic materials and equipment were donated by Millipore Corporation (Waters Chromatography Division, Millipore, Milford, MA, USA). The dextran derivatives were donated by Pharmacia-LKB Biotechnology. The authors acknowledge Professor Joyce Diwan (Department of Biology, Rensselaer Polytechnic Institute) for use of the atomic absorption spectrophotometer.

REFERENCES

- 1 H. A. van der Schee and J. Lyklema, *J. Phys. Chem.*, 88 (1984) 6661.
- 2 J. Papenhuyzen, H. A. van der Schee and G. J. Fleer, *J. Colloid Interface Sci.*, 104 (1985) 553.
- 3 O. A. Evers, G. J. Fleer, J. M. H. M. Scheutjens and J. Lyklema, *J. Colloid Interface Sci.*, 111 (1986) 446.
- 4 R. J. Roe, *J. Chem. Phys.*, 60 (1974) 4192.
- 5 J. M. H. M. Scheutjens and G. J. Fleer, *J. Phys. Chem.*, 83 (1979) 1619.
- 6 J. M. H. M. Scheutjens and G. J. Fleer, *J. Phys. Chem.*, 84 (1980) 178.
- 7 E. A. Peterson, *Anal. Biochem.*, 90 (1978) 767.
- 8 E. A. Peterson and A. R. Torres, *Anal. Biochem.*, 130 (1983) 271.
- 9 S. C. D. Jen and N. G. Pinto, *J. Chromatogr. Sci.*, 29 (1991) 1.
- 10 C. A. Brooks and S. M. Cramer, *AIChE J.*, 38 (12) (1992) 1969.
- 11 *Standard Test Methods for Chloride Ion in Water, Annual Book of ASTM Standards*, Vol. 11.01, ASTM, Philadelphia, PA, 1991.
- 12 D. Bentrop and H. Engelhardt, *J. Chromatogr.*, 556 (1991) 363.
- 13 J. Jacobson, J. Frenz and Cs. Horváth, *J. Chromatogr.*, 316 (1988) 53.
- 14 K. G. Ludwig-Baxter, R. N. Rej, A. S. Perlin and G. A. Neville, *J. Pharm. Sci.*, 80 (7) 1991.
- 15 J. Blaakmeer, M. R. Bohmer, M. A. Cohen Stuart and G. J. Fleer, *Macromolecules*, 23 (1990) 2301.
- 16 H. A. McKenzie, in H. A. McKenzie (Editor), *Milk Proteins: Chemistry and Molecular Biology*, Vol. 2, Academic Press, New York, 1971, Ch. 14.
- 17 R. D. Whitley, K. E. Cott, J. A. Berninger and N.-H. L. Wang, *AIChE J.*, 37 (4) (1991) 555.
- 18 N. Grinberg, R. Blanco, D. M. Yarmush and B. L. Karger, *Anal. Chem.*, 61 (6) (1989) 515.

Ion-exchange displacement chromatography of proteins

Dextran-based polyelectrolytes as high affinity displacers

Guhan Jayaraman, Shishir D. Gadam and Steven M. Cramer

Howard P. Isermann Department of Chemical Engineering, Rensselaer Polytechnic Institute, Troy, NY 12180-3590 (USA)

(First received June 11th, 1992; revised manuscript received October 1st, 1992)

ABSTRACT

Dextran-based polyelectrolyte displacers were successfully employed for the displacement purification of proteins in ion-exchange displacement systems. The effect of molecular mass was investigated by examining the efficacy of DEAE-dextran and dextran sulfate displacers of various molecular masses in cation- and anion-exchange systems, respectively. Induced salt gradients produced during these displacement experiments were measured in order to study their effect on the protein separations. The unique characteristics of these displacements were well predicted by simulations obtained from a steric mass action (SMA) ion-exchange model. These displacements differ from the traditional vision of displacement chromatography in several important ways: the isotherm of the displacer does not necessarily lie above the feed component isotherms; the concentration of the displaced proteins can sometimes exceed that of the displacer; higher-molecular-mass displacers are not necessarily more efficacious than lower-molecular-mass compounds; and the salt gradients induced by the adsorption of the displacer produce different salt micro-environments for each displaced protein.

INTRODUCTION

Ion-exchange chromatography is ubiquitous in the downstream processing of biopharmaceuticals. Conventional overloaded elution modes used for preparative chromatography are often associated with significant peak tailing and dilution of the product [1]. Gradient operation, while overcoming dilution effects, requires sufficiently high separation factors in order to achieve the desired resolution. Displacement chromatography offers a promising alternative for preparative separations by overcoming disadvantages prevalent in both of the conventional operational modes [2–4]. The displacement process is based on the competition of solutes for adsorption sites on the stationary phase according to their relative binding affinities and mobile phase

concentrations. It takes advantage of the non-linearity of the solute isotherms such that relatively large feeds can be separated on a given column. Furthermore, the tailing observed in overloaded elution chromatography is greatly reduced in the displacement mode due to self-sharpening boundaries formed in the process resulting in the recovery of the purified components at significantly higher concentrations. In fact, displacement chromatography is often able to improve upon the inherent resolving power of linear elution chromatography while maintaining the high throughput and concentration effects present in gradient elution. These advantages of displacement chromatography make it well suited for the downstream processing of biopharmaceuticals.

Anion-exchange displacement chromatography of proteins has been studied by several investigators. Peterson and co-workers have used carboxymethyl-dextrans as displacers for various protein mixtures [5–10]. Horváth and co-workers have em-

Correspondence to: S. M. Cramer, Howard P. Isermann Department of Chemical Engineering, Rensselaer Polytechnic Institute, Troy, NY 12180-3590, USA.

ployed chondroitin sulfate to displace β -galactosidase [11] and β -lactoglobulins [12,13]. Jen and Pinto have performed protein displacements using relatively low-molecular-mass dextran sulfate [14] and poly(vinylsulfonic acid) [15] as displacers. Ghose and Mattiasson [16] have examined the purification of lactate dehydrogenase using a carboxymethyl-starch displacer. Cramer and co-workers [17–19] have examined a variety of cation-exchange displacement systems. Recent work in our laboratory [20,21] has examined the efficacy of natural biopolymeric displacers (*viz.* protamine and heparin) for protein purification in ion-exchange systems.

Despite these encouraging results, the widespread implementation of displacement chromatography for industrial bioseparations continues to be constrained by several crucial problems. One of the major constraints is the lack of suitable non-toxic displacers for the displacement purification of pharmaceutical products. The optimal design and synthesis of potentially non-toxic displacers for application in various chromatographic systems (ion-exchange, hydrophobic interaction, metal affinity, etc.) is one of the major challenges in this field.

For ion-exchange chromatographic systems, polyelectrolytes derived from naturally occurring biopolymers are promising candidates for potentially non-toxic displacers in pharmaceutical purification processes. In this paper, we investigate the efficacy of various molecular mass dextran-based polyelectrolytes as displacers of proteins in ion-exchange chromatographic systems. Parameters obtained from the previous paper [22] are used in a steric mass action (SMA) model, described elsewhere [23], to simulate the displacement profiles and the theoretical predictions are compared with experimental results.

EXPERIMENTAL

Materials

Strong anion-exchange (SAX) (quaternary methyl amine, 8 μ m, 100 \times 5 mm I.D.) and cation-exchange (SCX) (sulfopropyl, 8 μ m, 100 \times 5 mm I.D.) columns were donated by Millipore (Waters Chromatography Division, Millipore, Milford, MA, USA). Tris-HCl and Tris buffer were pur-

chased from Fisher Scientific (Springfield, NJ, USA). Sodium chloride, sodium nitrate, sodium monobasic phosphate, sodium dibasic phosphate, and all proteins were purchased from Sigma (St. Louis, MO, USA). All dextran-based polyelectrolyte displacers were donated by Pharmacia-LKB Biotechnology (Uppsala, Sweden). Cellulose triacetate membranes (5000 and 10 000 molecular mass cut off) were obtained from Sartorius (Goettingen, Germany). Reagent grade potassium chromate, silver nitrate and cesium chloride were obtained from Aldrich (Milwaukee, WI, USA). Polyvinylsulfuric acid potassium salt (PVSK), polydiallyl dimethyl ammonium chloride (polyDADMAC) and indicator *o*-toluidine blue, were obtained from Nalco (Naperville, IL, USA).

Apparatus

Diafiltration of displacer compounds was carried out in an Amicon 8050 stirred cell (Amicon, Danvers, MA, USA) using the cellulose triacetate UF membranes. All displacement experiments were carried out using a Model LC 2150 pump (LKB, Bromma, Sweden) connected to the chromatographic columns via a Model C10W 10-port valve (Valco, Houston, TX, USA). Fractions of the column effluent were collected using LKB 2212 Helirac fraction collector (LKB).

Protein analysis of the collected fractions was carried out using a Model Waters 590 HPLC pump, a Model 7125 sampling valve (Rheodyne, Cotati, CA, USA), a spectroflow 757 UV-Vis absorbance detector (Applied Biosystems, Foster City, CA, USA) and a Model C-R3A Chromatopac integrator (Shimadzu, Kyoto, Japan). Sodium analysis was done using a Perkin-Elmer, Model 3030 (Perkin-Elmer, Norwalk, CT, USA) atomic absorption spectrophotometer. Lyophilization was carried out using a Model Lyph Lock 4.5 Freeze Dry System (Labconco, Kansas City, MO, USA).

Procedures

Purification of polyelectrolytes

All polyelectrolyte displacers were diafiltered to remove salts and other low-molecular-mass impurities. 5000 and 10 000 molecular mass cut off membranes were employed to purify the M_r 10 000 and

20 000–50 000 displacers, respectively. After diafiltration, the retentate was lyophilized.

Operation of the displacement chromatograph

In all displacement experiments, the columns were initially equilibrated with the carrier and then sequentially perfused with feed, displacer and regenerant solutions. The feed and the displacer solutions were prepared in the same buffer as the carrier. Fractions of the column effluent were collected directly from the column outlet to avoid extra-column dispersion of the purified components.

Displacement chromatography of proteins in cation-exchange systems

Two-component separations. Feed mixtures of α -chymotrypsinogen and cytochrome *c* were separated by displacement chromatography using DEAE–dextran displacers in a SCX column. The feed load, displacer molecular mass and concentrations employed for each separation are given in the figure legends of the corresponding displacement chromatograms (Figs. 1 and 4). All displacement experiments were carried out at room temperature at a flow-rate of 0.1 ml/min using 75 mM sodium phosphate buffer, pH 6.0, as the carrier. Fractions of 100 μ l were collected for subsequent analysis of protein, displacer and sodium ion concentrations in the effluent.

Three-component separations. Feed mixtures of α -chymotrypsinogen, cytochrome *c* and lysozyme were separated by displacement chromatography using a M_r 40 000 DEAE–dextran displacer under the same operating conditions specified above. The feed load and displacer concentration employed in this separation are given in the legend of Fig. 5.

Displacement chromatography of proteins in anion-exchange systems

Two-component crude mixtures of β -lactoglobulin A and B were purified by displacement chromatography using dextran-sulfate displacers in a SAX column. The feed load, displacer molecular mass and concentrations employed for each separation are given in the legends of Figs. 7 and 9. All displacement experiments were carried out at room temperature at a flow-rate of 0.1 ml/min using 75 mM Tris–HCl buffer, pH 7.5, as the carrier. Fractions of 100 μ l were collected for subsequent analy-

sis of protein, displacer and chloride ion concentrations in the effluent.

Regeneration

The cation-exchange column was regenerated after each displacement experiment by passing ten column volumes of a 1 M NaCl solution in 100 mM phosphate buffer, pH 11.0. The anion exchange column was regenerated by passing five column volumes of 1.5 M NaCl solution in 100 mM phosphate buffer, pH 2.1. The total ion bed capacity was then redetermined to ensure complete regeneration of the column.

Protein analysis by HPLC

Protein analyses of the fractions collected during the displacement experiments were performed by ion-exchange HPLC under isocratic elution conditions. Mobile phases were: 175 mM sodium phosphate, pH 6.0, and 165 mM NaCl solution in 25 mM Tris–HCl buffer, pH 7.5, for the cation-exchange and anion exchange protein analyses, respectively. Displacement fractions were diluted 10–400 fold with the eluent and 20- μ l samples were injected at a flow-rate of 0.5 ml/min. The column effluent was monitored at 280 nm.

Displacer analysis

All polyelectrolyte displacers were analyzed using the colloidal titration assay provided by Nalco. For analysis of dextran sulfates, a known volume of polyDADMAC reagent was added to the aqueous displacer solutions. Subsequent addition of *o*-toluidine indicator produced a colorimetric change. The excess polyDADMAC reagent was titrated against PVSK in presence of a *o*-toluidine indicator. For the analysis of DEAE–dextran, the solution was titrated against PVSK without addition of the polyDADMAC reagent. Linear calibrations were obtained with both of these titrations.

Analyses for counter-ions

Chloride ion analysis. Chloride ion analysis was conducted using the ASTM assay [24]. Known amount of chloride ion in a 50 ml deionized water background was titrated against 0.01 M silver nitrate using potassium chromate indicator solution. This technique was able to accurately monitor down to 10 μ mol of chloride ion. A blank titration

was performed to account for the chloride in water. The technique was able to selectively detect chloride ions in the presence of other salts, proteins and displacers.

Sodium ion analysis. For the cation-exchange experiments, sodium was analyzed using atomic absorption spectroscopy. Effluent fractions were diluted 3000 fold in plastic tubes in 5 g/l cesium chloride solution (to minimize background noise) and their amounts quantitated against known Na^+ ion standards (10–50 μM).

RESULTS AND DISCUSSION

Although several investigators have examined the utility of ion-exchange displacement chromatography for the purification of proteins, no controlled study has been reported to date on the effect of displacer molecular mass. In addition, there is a paucity of potentially non-toxic displacers, currently available for the purification of therapeutic proteins. The effects of induced salt gradients on protein ion-exchange displacement chromatography have also not been studied in depth. In this manuscript we investigate the efficacy of dextran-based polyelectrolyte displacers for protein purification in both cation- and anion-exchange systems. The effect of displacer molecular mass and induced salt gradients on displacement behavior were examined in the context of the SMA formalism [23].

The SMA formalism of Brooks and Cramer [23] can be employed to calculate the isotachic displacement profile under induced salt gradient conditions. The velocity of the displacer front was determined from a solute movement analysis to be:

$$u_D = \frac{u_0}{1 + \beta \frac{Q_D}{C_D}} \quad (1)$$

where u_D is the linear velocity of the displacer front, u_0 is the chromatographic velocity, β is the column phase ratio and C_D and Q_D are the isotachic concentrations of displacer in the mobile and stationary phases, respectively. The slope of the displacement operating line (Δ) can be given by:

$$\Delta = \frac{Q_D}{C_D} = K_D \left[\frac{\Delta - (v_D + \sigma_D)Q_D}{C_S} \right]^{v_D} \quad (2)$$

where C_S is the carrier salt concentration; K_D is the equilibrium constant for displacer; Δ is the ion bed capacity of the salt counter-ion; v_D is the characteristic charge and σ_D is the steric factor of displacer. Once the slope of the displacer operating line is determined (eqn. 2), the breakthrough volume can be calculated from eqn. 1. Under isotachic conditions, the induced salt gradient results in the following elevated salt concentrations in each purified protein zone:

$$(C_S)_P = \frac{\Delta - (C_S + v_D C_D) \Delta \left(1 + \frac{\sigma_P}{v_P} \right)}{\left\{ \left(\frac{\Delta}{K_P} \right)^{1/v_P} - \Delta \left[1 + \left(\frac{\sigma_P}{v_P} \right) \right] \right\}} \quad (3)$$

where $(C_S)_P$ is the salt concentration in isotachic zone corresponding to purified protein component P; K_P , v_P and σ_P are the equilibrium constant, characteristic charge and steric factor for the protein, respectively. The isotachic concentration of the displaced protein component, C_P , can then be calculated directly from the expression:

$$C_P = \frac{\Delta - (C_S)_P \left(\frac{\Delta}{K_P} \right)^{1/v_P}}{(v_P + \sigma_P) \Delta} \quad (4)$$

Finally, the width of the isotachic displacement zone, V_P , is determined from a simple mass balance:

$$V_P = V_F \frac{(C_P)_F}{C_P} \quad (5)$$

where V_F is the feed volume and $(C_P)_F$ is the feed concentration of protein component, P.

Simulations based on the SMA model [23] were employed to establish appropriate conditions for the displacement experiments and to predict the displacement profiles, induced salt gradients, and appropriate adsorption isotherms. Simulation parameters for the proteins and displacers are presented in Table I.

Displacement chromatography in cation-exchange columns

Previous work in our laboratory on cation-exchange displacement chromatography [17–19] was extended to DEAE-dextran polyelectrolyte displacers.

Initial work with these macromolecules had indicated that the displacement of surface-bound

TABLE I

SMA MODEL PARAMETERS FOR PROTEINS AND DISPLACERS [22]

Monovalent ion capacity of the columns, λ : SCX = 561 mM ; SAX = 567 mM.

Component	Characteristic charge (v_D)	Steric factor (σ_D)	Q_D^{\max} (mM)	Equilibrium constant (K_p)
α -Chymotrypsinogen A	4.8	49.2	10.4	$9.22 \cdot 10^{-3}$
Cytochrome <i>c</i>	6.0	53.6	9.4	$1.06 \cdot 10^{-2}$
Lysozyme	5.3	34.0	13.0	$1.84 \cdot 10^{-1}$
β -Lactoglobulin A	7.5	38.2	12.0	$5.44 \cdot 10^{-3}$
β -Lactoglobulin B	6.3	47.5	10.2	$6.42 \cdot 10^{-3}$
40 000 DEAE-dextran	64	130	3.08	$5.45 \cdot 10^{44}$
10 000 Dextran sulfate	31	33	9.11	$3.61 \cdot 10^{28}$

counter-ions by the adsorbing displacer resulted in an induced salt gradient which facilitated desorption of protein molecules from the stationary phase. In addition, the presence of low-molecular-mass ionic impurities within the displacer solutions were shown to have deleterious effects on the effluent profile of the separands. In order to carry out a controlled study on the effects of induced salt gra-

dients, the dextran based displacers were subjected to ultrafiltration to remove all low-molecular-mass ionic impurities. Displacement chromatographic separations of protein mixtures containing α -chymotrypsinogen A, cytochrome *c* and lysozyme were carried out in strong cation-exchange columns using M_r 10 000 and 40 000 DEAE-dextran polyelectrolytes as displacers.

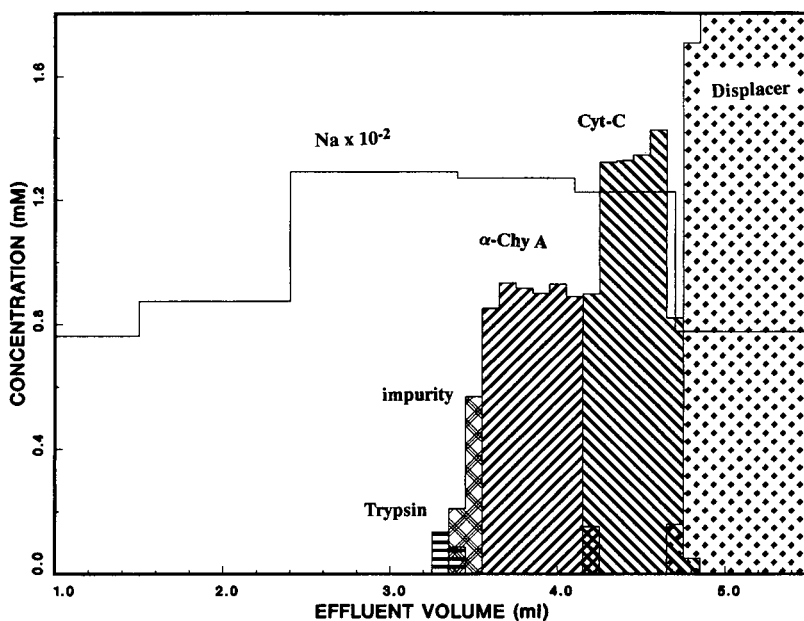


Fig. 1. Displacement chromatogram of a two-component protein separation using M_r 10 000 DEAE-dextran as displacer. Column: 100×5 mm I.D. strong cation-exchanger ($8 \mu\text{m}$); carrier: 75 mM sodium phosphate buffer, pH 6.0; displacer, 2.36 mM DEAE-dextran (M_r 10 000) in carrier; feed, 0.9 ml of 0.74 mM each of α -chymotrypsinogen A and cytochrome *c* in carrier; flow-rate, 0.1 ml/min; fraction size, 100 μl each.

The displacement purification of a two-protein mixture of α -chymotrypsinogen A and cytochrome *c* by the M_r 10 000 DEAE-dextran displacer is shown in Fig. 1. This separation resulted in concentrated adjacent zones of α -chymotrypsinogen A and cytochrome *c* with sharp boundaries between the displacement zones. In addition, the process resulted in the purification of two trace impurities. Analytical chromatograms of adjacent fractions 5–10 (corresponding to elution volume 3.3–3.8 ml in the displacement chromatogram shown in Fig. 1) are presented in Fig. 2a and the protein standards trypsin, α -chymotrypsinogen A, and α -chymotrypsin are shown in Fig. 2b. As seen in Fig. 2a, fractions

8–10 consisted of essentially pure α -chymotrypsinogen A while fraction 5 contained pure trypsin. According to Sigma [25], α -chymotrypsinogen A (Type II from bovine pancreas) typically has associated trace quantities of trypsin which can be seen in the standard chromatogram (Fig. 2b). Although Sigma [25] also indicated that α -chymotrypsin may be present in trace amounts, no α -chymotrypsin was observed in the chromatograms of pure α -chymotrypsinogen A or the displacement fractions. Rather, fraction 7 contained a trace component which had a slightly different retention time than α -chymotrypsinogen A (Fig. 2a). This trace component could be a cleavage product or an impurity

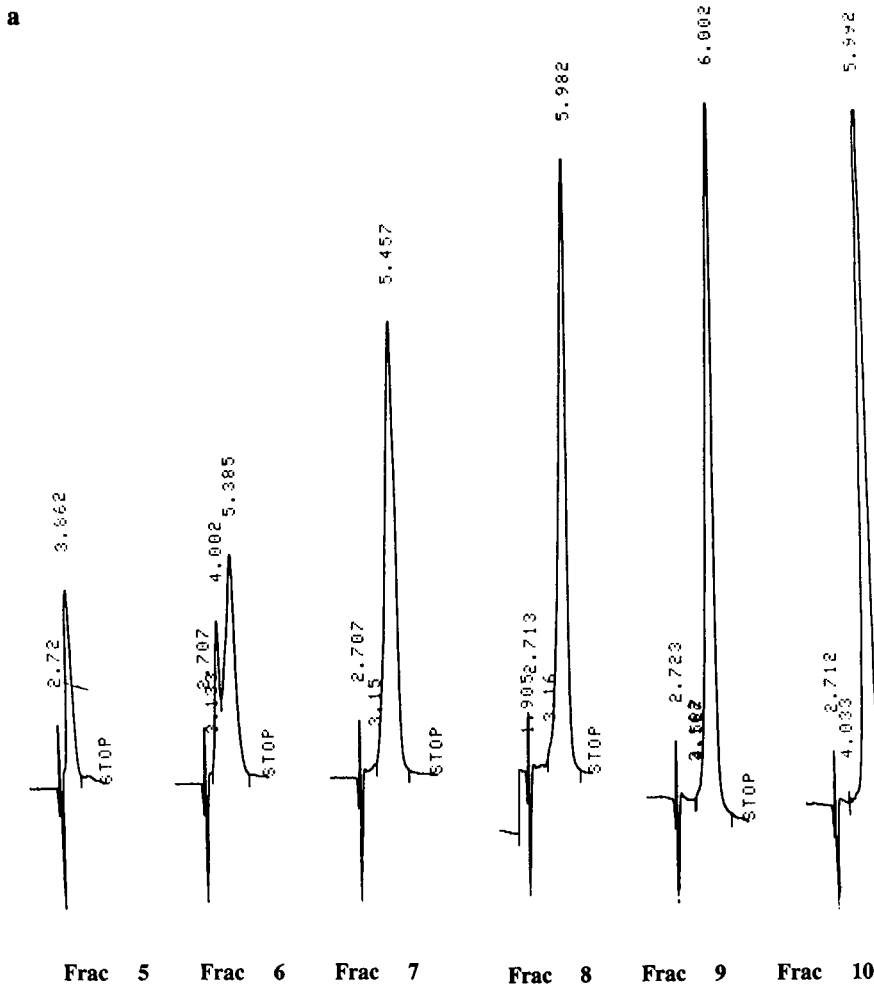


Fig. 2.

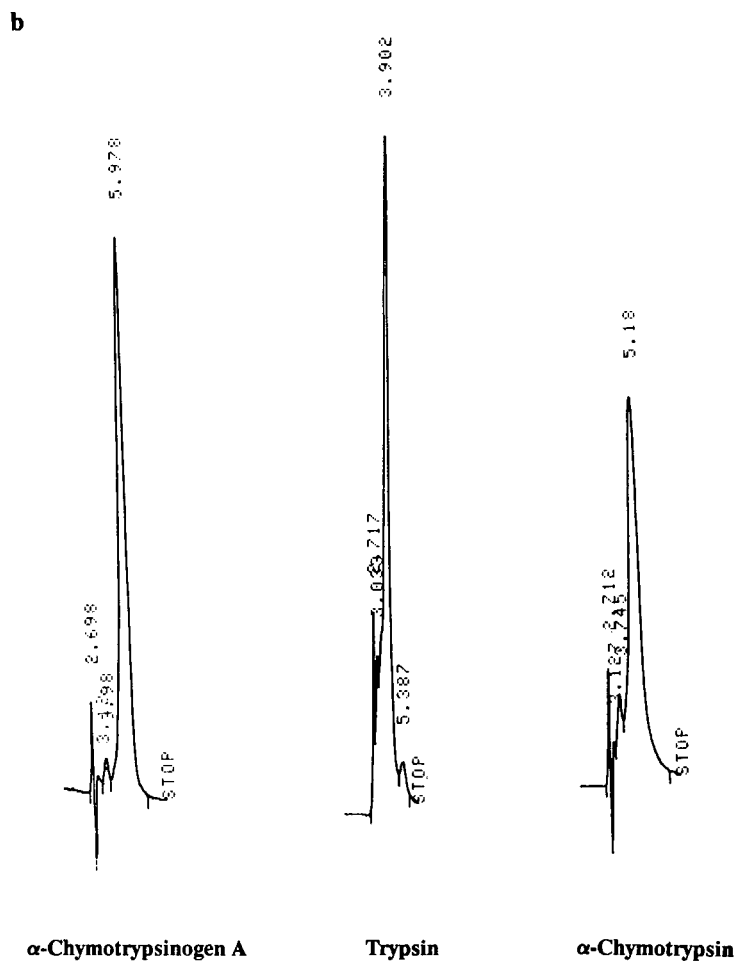


Fig. 2. Analytical chromatograms of (a) adjacent displacement fractions (Frac) 5–10 corresponding to elution volume 3.3–3.8 ml in Fig. 1; (b) protein standards α -chymotrypsinogen A, trypsin and α -chymotrypsin (0.1 mg/ml each). Column: 100×5 mm I.D. strong cation-exchanger ($8 \mu\text{m}$); elution buffer: 175 mM sodium phosphate, pH 6.0; flow-rate, 0.5 ml/min; dilutions: fraction 5, 100-fold; fractions 6–10, 200-fold. The values in the figure indicate t_r in min.

from the original feed mixture, as yet unidentified. Nevertheless, this separation illustrates the inherent high resolving power of the technique.

The counter-ion gradient induced by the adsorption of the displacer was also measured in this experiment. As seen in Fig. 1, this displacement resulted in a 45 mM increase in salt concentration in the purified protein zones. This induced salt gradient results in a depression of the salt sensitive protein isotherms from the initial carrier conditions, which can have a significant impact on the effluent displacement profile. In fact, recent work in our lab-

oratory [20] has demonstrated that induced salt gradients can sometimes result in elution of the proteins ahead of the displacement train.

The effect of induced salt gradient on these protein displacements was studied in the context of the SMA formalism [23]. Parameters for these simulations were obtained as described in the previous paper [22]. The model was employed to simulate the adsorption isotherms under both the initial carrier and induced salt gradient conditions as well as the isotachic effluent displacement profiles. The SMA model was also employed to facilitate methods de-

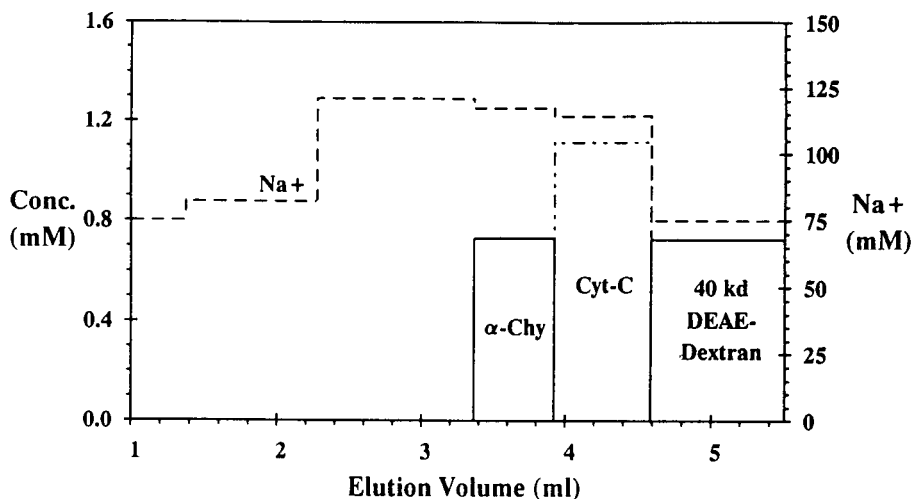


Fig. 3. SMA simulation of a two-component protein displacement using M_r 40 000 DEAE-dextran as displacer. Conditions as described in Fig. 1 with the exception of: displacer, 0.75 mM DEAE-dextran (40 000) in carrier; feed, 0.9 ml of 0.74 mM α -chymotrypsinogen A (α -Chy) and 0.88 mM cytochrome *c* (Cyt-C) in carrier. Model parameters for this simulation are given in Table I. kd = kilodalton.

velopment for all subsequent displacement experiments. SMA parameters are presented in Table I and simulation conditions (*e.g.*, column conditions, displacer concentration, feed load, etc.) are given in the figure legends.

Fig. 3 illustrates an SMA simulation of the isotachic displacement profile for the separation of α -chymotrypsinogen A and cytochrome *c* using M_r 40 000 DEAE-dextran as the displacer. As seen in the figure, the model predicts the displacement of the proteins along with an induced salt gradient. Furthermore, this simulation indicates that the concentration of the displaced proteins will exceed that of the displacer. The adsorption isotherms under both the initial carrier and induced salt gradient conditions are presented in Fig. 4. As expected, the induction of a salt (counter-ion) gradient results in the depression of the protein isotherms from their initial equilibrium conditions. Clearly, the use of a solute movement analysis with the initial carrier isotherms would result in an incorrect prediction of the concentrations of the proteins in the displacement train.

A displacement experiment was carried out under the same conditions employed in the simulation and the effluent profile is presented in Fig. 5. The experimentally measured induced salt gradient and the

displacement profiles in Fig. 5 match extremely well with the SMA simulation shown in Fig. 3. Effluent protein concentrations are in good agreement with the values obtained from the intersection of the operating line with the protein isotherms under induced salt gradient conditions (Fig. 4b). In addition, this separation resulted in the purification of the trace components associated with α -chymotrypsinogen A. These results indicate that dextran-based cationic displacers can produce efficient protein displacements and that the SMA formalism is well suited to describe these polyelectrolyte systems. This displacement differs from the traditional vision of displacement chromatography in several important ways: the isotherm of the displacer lies below and crosses the feed component isotherms; the concentration of the displaced proteins exceed that of the displacer; and the salt gradients induced by the adsorption of the displacer produce different salt environments for each displaced protein.

The inlet displacer concentrations employed in these cation-exchange experiments were chosen so that the displacer breakthrough time in the column effluent remained the same. This enabled a more direct examination of the effect of displacer molecular weight. As seen from Figs. 1 and 5, the resulting displacement profiles with the M_r 10 000 and

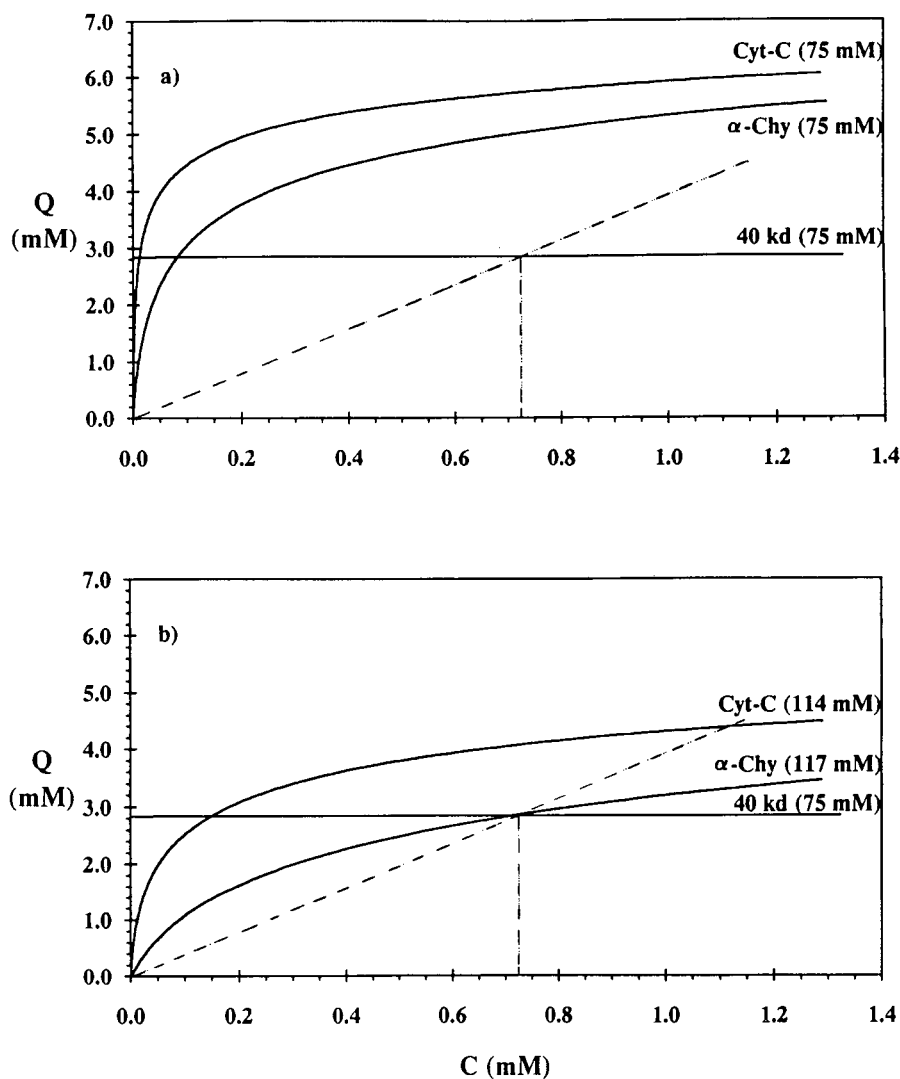


Fig. 4. SMA simulations of protein (α -chymotrypsinogen A, cytochrome c) and displacer (M_r 40 000 DEAE-dextran) adsorption isotherms at: (a) initial carrier and (b) induced salt gradient conditions in a strong cation-exchange column. Model parameters for these isotherms are reported in Table I.

40 000 DEAE-dextran displacers are quite similar. The inlet concentrations required to achieve the same breakthrough volume were 2.36 and 0.75 mM for the 10 000 and 40 000 DEAE-dextran displacers, respectively. As described in the previous paper [22], the fraction of functional groups bound for the M_r 10 000 DEAE-dextran is greater than that of the 40 000 DEAE-dextran. Accordingly, a higher concentration of disaccharide repeating units is

required for the 40 000 DEAE-dextran in order to achieve the same displacement chromatographic effect. The implications of this for displacer design will be addressed in the concluding section.

To further illustrate the efficacy of displacement chromatography using polyelectrolyte displacers, a three component protein mixture of α -chymotrypsinogen A, cytochrome c and lysozyme was subjected to displacement purification by the M_r

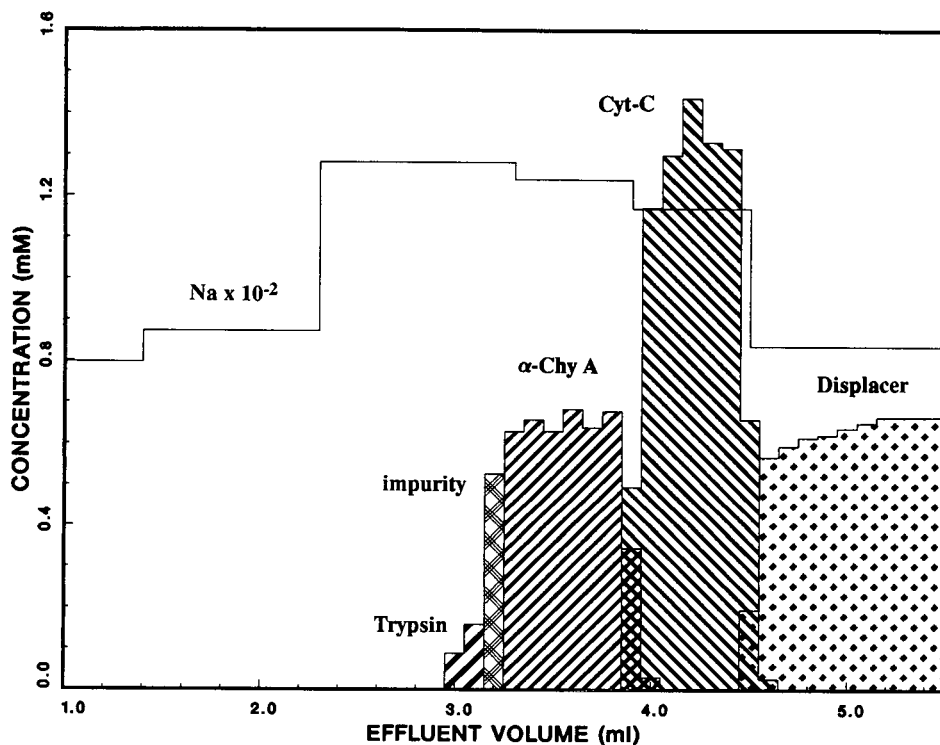


Fig. 5. Displacement chromatogram of a two-component protein separation using M_r 40 000 DEAE-dextran as displacer. Conditions as described in Fig. 3.

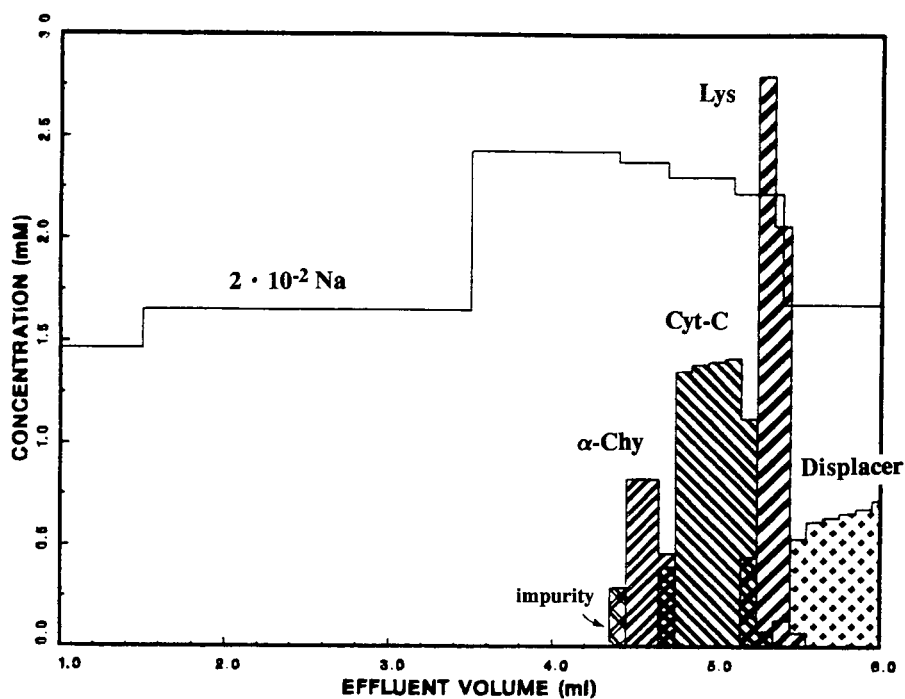


Fig. 6. Displacement chromatogram of a three-component protein separation using M_r 40 000 DEAE-dextran polyelectrolyte as displacer. Conditions as described in Fig. 3 with the exception of: feed, 2.0 ml of 0.15 mM α -chymotrypsinogen A, 0.4 mM cytochrome c, and 0.3 mM lysozyme in the carrier.

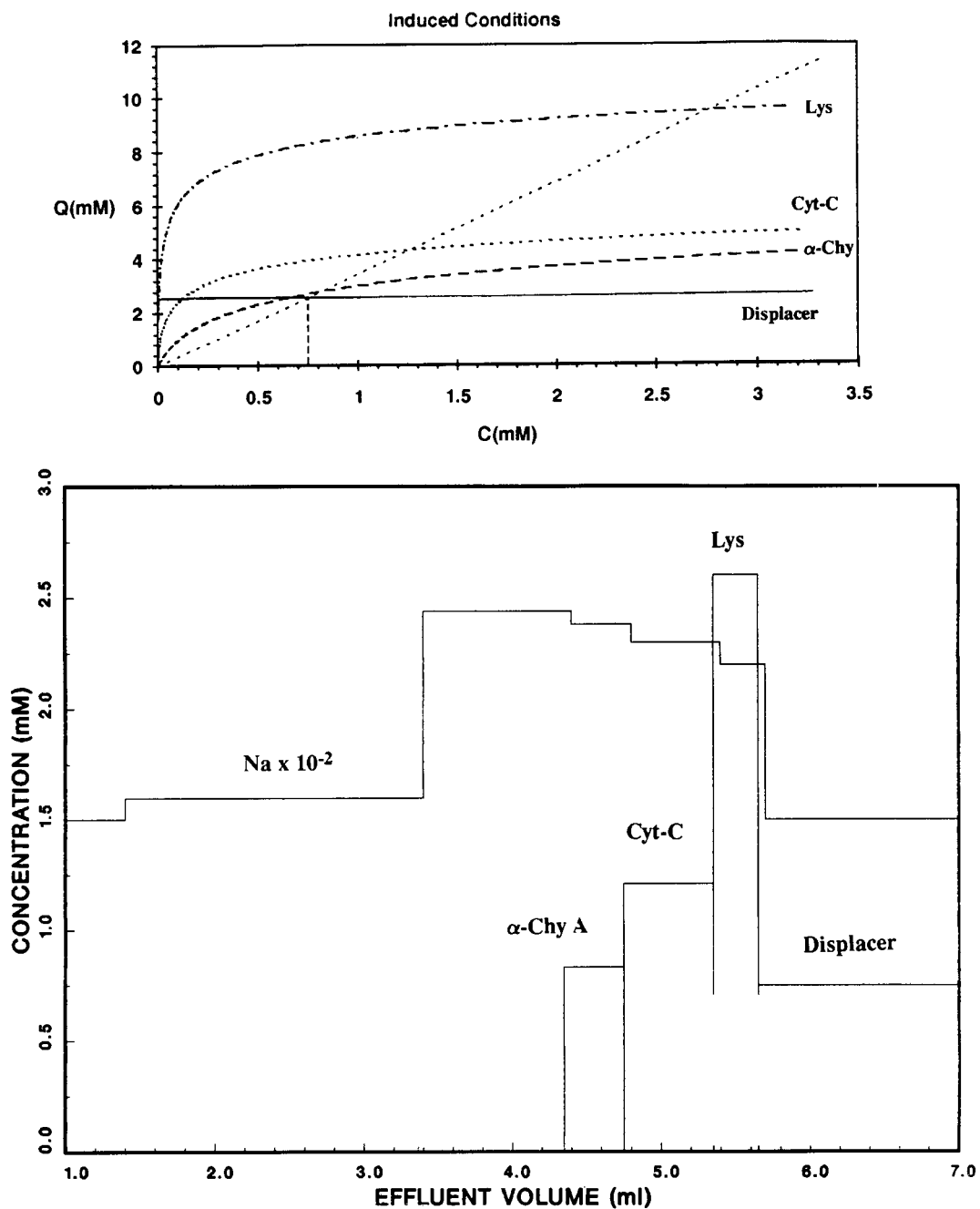


Fig. 7. SMA simulation of a three-component protein displacement using M_r 40 000 DEAE-dextran as displacer and the corresponding protein isotherms under induced salt gradient conditions. Conditions as described in Fig. 6. Simulation parameters are given in Table I.

40 000 DEAE–dextran displacer (Fig. 6). This separation resulted in the purification of more than 25 mg of the three component protein mixture on the analytical column with minimal amounts of mixing. Again, this displacement profile under induced salt gradient conditions is well predicted by the corresponding SMA isotherms and simulations (Fig. 7).

Displacement chromatography in anion-exchange columns

Displacement chromatographic separations of β -lactoglobulins A and B were carried out in strong anion exchange columns using M_r 10 000 and 50 000 dextran sulfate displacers. Although displacement separations with dextran sulfate have been reported previously [14], the objective of the present study was to verify the SMA formalism for anion-exchange displacement systems and to determine the effects of displacer molecular mass and

induced salt gradients on the displacement profiles. The anion exchange displacement simulations were performed using the experimentally measured parameters (Table I), obtained in the previous paper [22].

The displacement purification of β -lactoglobulins A and B by a M_r 10 000 dextran sulfate displacer and the corresponding SMA simulation are shown in Figs. 8 and 9, respectively. This separation was characterized by concentrated, adjacent zones of purified β -lactoglobulin A and B with minimal amounts of dispersion. The salt gradient induced by the adsorption of the displacer resulted in a depression of the protein isotherms from the initial equilibrium conditions as shown in Fig. 10. The concentration of β -lactoglobulin B obtained in the displacement experiment is slightly higher than predicted by the model. Since β -lactoglobulins A and B are prone to aggregation [26], the SMA model in the

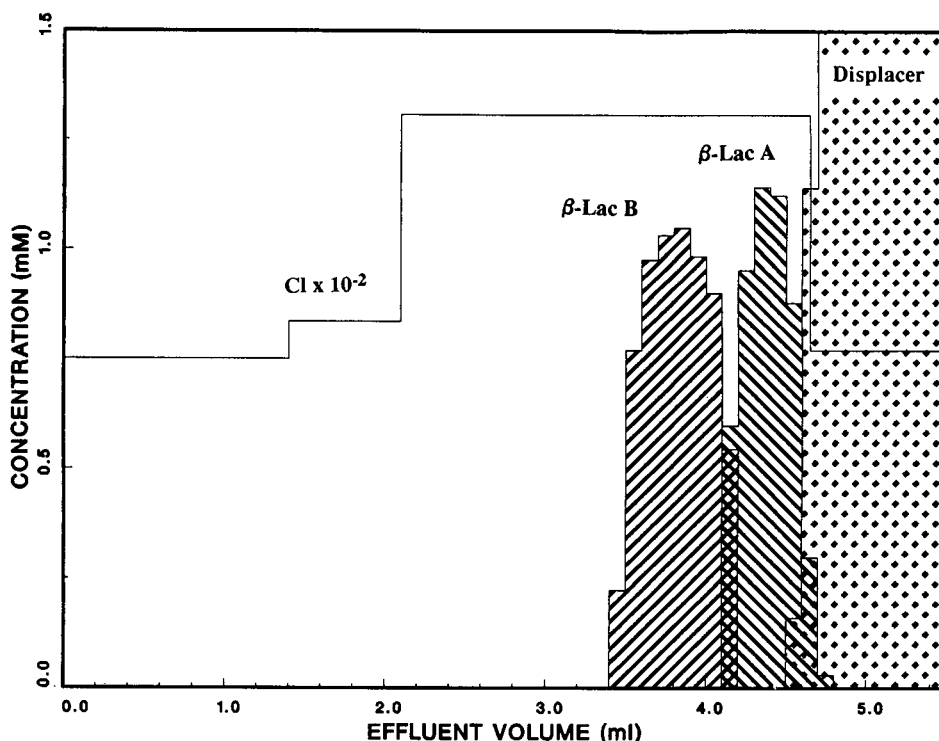


Fig. 8. Displacement chromatogram of a two-component protein displacement separation using M_r 10 000 dextran sulfate as displacer. Column: 100×5 mm I.D. strong anion exchanger ($8 \mu\text{m}$); carrier: 75 mM Tris–HCl buffer, pH 7.5; displacer, 2.0 mM dextran sulfate (10 000) in carrier; feed, 1.0 ml of 19 mg total crude protein mixture in the carrier; flow-rate, 0.1 ml/min ; fraction size, $100 \mu\text{l}$ each. β -Lac = β -Lactoglobulin.

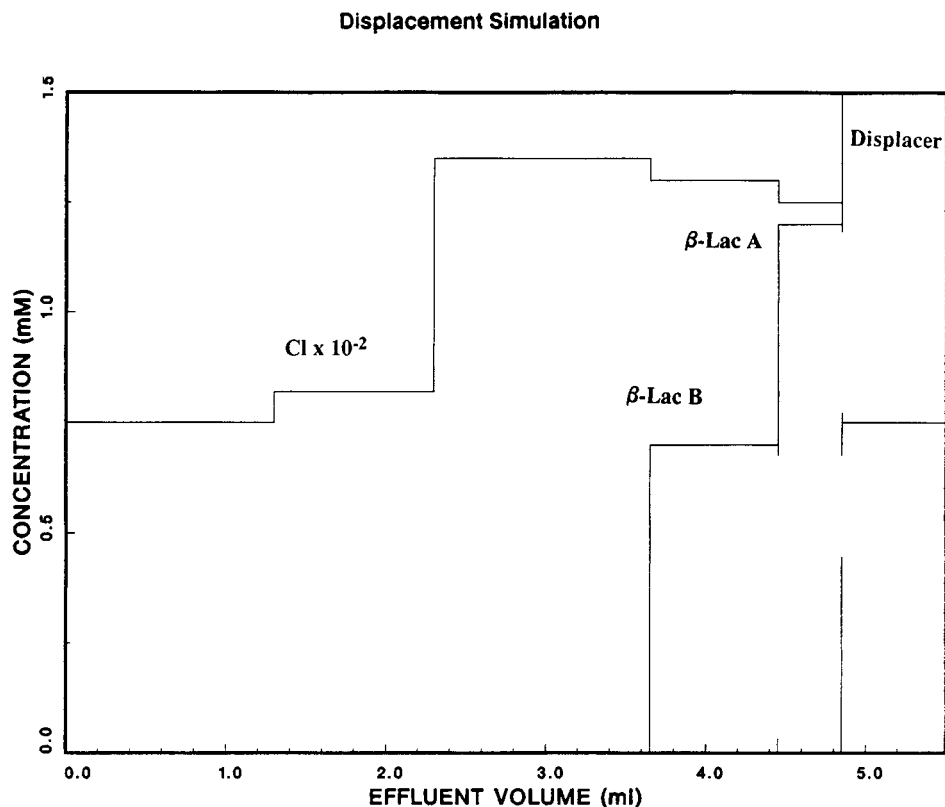


Fig. 9. SMA simulation of a two-component protein displacement using dextran sulfate (10 000) as displacer. Conditions as described in Fig. 8. Simulation parameters are given in Table I.

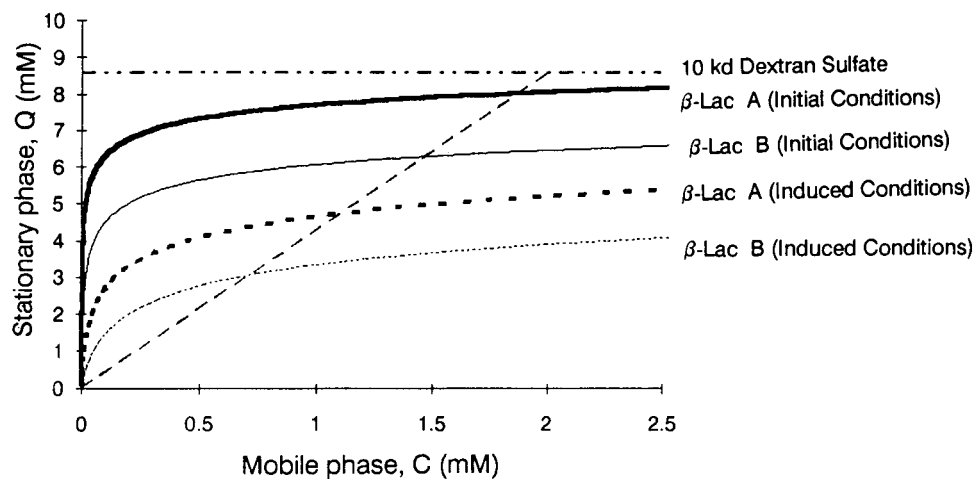


Fig. 10. Simulation of protein (β -lactoglobulin A & B) and displacer (M_r 10 000 dextran sulfate) isotherms based on SMA model at initial carrier and induced salt gradient conditions in a strong anion-exchange column. Model parameters for isotherm simulation are reported in Table I.

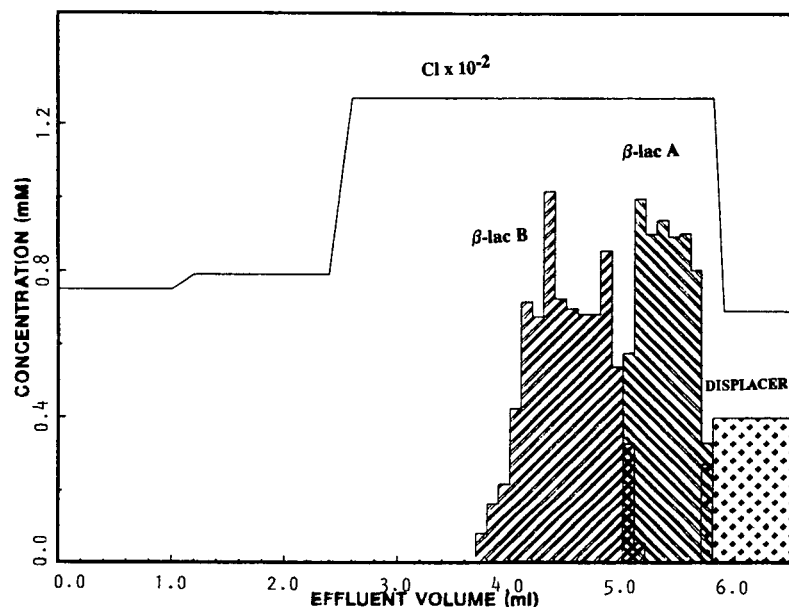


Fig. 11. Displacement chromatogram of a two-component protein separation using M_r 50 000 dextran sulfate as displacer. Conditions as described in Fig. 8 with the exception of: displacer, 0.4 mM dextran sulfate (50 000); feed, 1.1 ml of 22 mg total crude protein mixture in carrier.

current form is not able to completely describe the protein adsorption isotherms [22]. Nevertheless, the model still provides a reasonable prediction of the displacement profiles under induced salt gradient conditions.

A similar displacement experiment was carried out using the dextran sulfate (50 000) displacer to examine the effect of molecular weight on displacer efficacy (Fig. 11). In contrast to the DEAE–dextran experiments described above, these anion-exchange

experiments were carried out at the same “normalized concentration” (*i.e.*, concentration of disaccharide repeating units) with all other conditions remaining the same. As seen in Figs. 9 and 11, under these conditions the breakthrough times of the two displacers are quite different. The longer breakthrough time associated with the higher-molecular-mass (50 000) displacer is due to relatively lower fraction of functional groups bound for dextran sulfate (50 000) as compared to the M_r 10 000 mole-

TABLE II
YIELDS OF PURIFIED PROTEIN IN DISPLACEMENT EXPERIMENTS

Displacer	Feed components	Yield (99% purity) (%)
10 000 DEAE–dextran	α -chymotrypsinogen A	97.6
	Cytochrome <i>c</i>	87.4
40 000 DEAE–dextran	α -chymotrypsinogen A	93.1
	Cytochrome <i>c</i>	84.8
40 000 DEAE–dextran	α -chymotrypsinogen A	80.9
	Cytochrome <i>c</i>	78.5
	Lysozyme	52.1
50 000 dextran sulfate	β -lactoglobulin B	95.1
	β -lactoglobulin A	85.7

cule. For a detailed discussion of these effects the reader is referred to the previous manuscript [22].

Table II presents the yields of purified protein at 99% purity for the displacement experiments presented in this paper. As seen in the Table, high yields of very pure protein were obtained in all of these displacements. As expected, higher yields were obtained for the proteins emerging first in the displacement train. Furthermore, zone overlap had a more significant impact on highly concentrated protein zones (e.g., the lysozyme zone in the three-component protein displacement) due to the smaller widths of these bands. The displacement experiments presented in this manuscript clearly illustrate the ability of this technique for high-resolution/high-throughput preparative protein purifications.

CONCLUSIONS

This research has focused on displacement chromatographic separation of proteins in ion-exchange systems using high-affinity, dextran-based polyelectrolytes as displacers. High-yield displacement separations were obtained and good agreement was observed between the displacement experiments and theoretical predictions obtained with the Steric Mass Action (SMA) ion-exchange model. The inherent power of this technique was aptly demonstrated by the simultaneous concentration and purification of trace components present in the feed mixtures.

Displacement experiments were carried out with various molecular mass displacers in order to gain further insight into the non-linear binding properties of these dextran-based compounds. For a given functional group density, it was seen that smaller-molecular-mass displacers bind more efficiently due to relatively higher surface coverage and lower steric factors involved. Thus, lower-molecular-mass displacers require relatively lower mass loadings to achieve the same breakthrough as analogous higher-molecular-mass displacers. These displacements differ from the traditional vision of displacement chromatography in several important ways: the isotherm of the displacer does not necessarily lie above the feed component isotherms; the concentration of the displaced proteins can sometimes exceed that of the displacer; higher-molecular-mass displacers are not necessarily more efficacious than lower-molec-

ular-mass polyelectrolytes; and salt gradients induced by the adsorption of the displacer produces different salt environments for each displaced protein. The work presented in these two manuscripts provides a framework for evaluating the efficacy of future displacers for ion-exchange systems.

SYMBOLS

C_D	Displacer concentration in the bulk phase/carrier (mM)
C_P	Isotachic concentration of displaced protein, P, in the effluent (mM)
$(C_P)_F$	Feed concentration of protein component, P (mM)
C_S	Carrier salt concentration (mM)
$(C_S)_P$	Bulk phase salt concentration in isotachic zone corresponding to purified protein component, P (mM)
K_D	Equilibrium constant for displacer (dimensionless)
K_P	Equilibrium constant for protein P (dimensionless)
Q_D	Isotachic stationary phase concentration of displacer (mM)
Q_D^{\max}	Maximum binding capacity of the displacer (mM)
u_D	Linear velocity of the displacer front (cm/s)
u_o	Chromatographic velocity
V_F	Feed volume (ml)
V_P	Volume (width) of isotachic zone containing purified protein component, P (ml)
β	Column phase ratio (dimensionless)
Δ	Slope of the displacer operating line (dimensionless)
Λ	Ion bed capacity of monovalent salt counter-ion (mM)
ν_D	Characteristic charge of displacer (dimensionless)
σ_D	Steric factor for displacer (dimensionless)
ν_P	Characteristic charge of protein, P (dimensionless)
σ_P	Steric factor for protein, P (dimensionless)

ACKNOWLEDGEMENTS

This research was funded by Millipore Corporation and grants BCS-9112481 and CTS-8957746 (a

Presidential Young Investigator Award to S. M. Cramer) from the National Science Foundation. Chromatographic materials and equipment were donated by Millipore Corporation (Waters Chromatography Division, Millipore, Milford, MA). The dextran derivatives were donated by Pharmacia-LKB Biotechnology. The authors acknowledge Professor Joyce Diwan (Department of Biology, Rensselaer Polytechnic Institute) for use of the atomic absorption spectrophotometer.

REFERENCES

- 1 J. H. Knox and H. M. Pyper, *J. Chromatogr.*, 363 (1986) 1.
- 2 Cs. Horváth, in F. Bruner (Editor), *The Science of Chromatography*, Elsevier, Amsterdam, 1985, p.179.
- 3 J. Frenz and Cs. Horváth, in Cs. Horváth (Editor), *High Performance Liquid Chromatography — Advances and Perspectives*, Vol. 8, Academic Press, Orlando, FL, 1988, p. 211.
- 4 S. M. Cramer and G. Subramanian, *Sep. Purif. Methods*, 19(1) (1990) 31.
- 5 E. A. Peterson, *Anal. Biochem.*, 90 (1978) 767.
- 6 A. R. Torres and E. A. Peterson, *Anal. Biochem.*, 98 (1979) 353.
- 7 E. A. Peterson and A. R. Torres, *Anal. Biochem.*, 130 (1983) 271.
- 8 A. R. Torres, B. E. Dunn, S. C. Edberg and E. A. Peterson, *J. Chromatogr.*, 316 (1984) 125.
- 9 A. R. Torres, S. C. Edberg and E. A. Peterson, *J. Chromatogr.*, 389 (1987) 177.
- 10 B. E. Dunn, S. C. Edberg and A. R. Torres, *Anal. Biochem.*, 168 (1988) 25.
- 11 A. W. Liao and Cs. Horváth, *Ann. N.Y. Acad. Sci.*, 589 (1990) 182.
- 12 A. W. Liao, Z. El Rassi, D. M. LeMaster and Cs. Horváth, *Chromatographia*, 24 (1987) 881.
- 13 A. L. Lee, A. W. Liao and Cs. Horváth, *J. Chromatogr.*, 443 (1988) 31.
- 14 S.-C. D. Jen and N. G. Pinto, *J. Chromatogr. Sci.*, 29 (1991) 478.
- 15 S.-C. D. Jen and N. G. Pinto, *J. Chromatogr.*, 519 (1990) 87.
- 16 S. Ghose and B. J. Mattiasson, *J. Chromatogr.*, 547 (1991) 145.
- 17 G. Subramanian, M. W. Phillips and S. M. Cramer, *J. Chromatogr.*, 439 (1988) 341.
- 18 G. Subramanian and S. M. Cramer, *Biotechnol. Progress*, 5 (1989) 92.
- 19 G. Subramanian, M. W. Phillips, G. Jayaraman and S. M. Cramer, *J. Chromatogr.*, 484 (1989) 225.
- 20 J. A. Gerstner and S. M. Cramer, *Biotechnol. Progress*, in press.
- 21 J. A. Gerstner and S. M. Cramer, *BioPharm*, 5 (9) (1992) 42.
- 22 S. Gadam, G. Jayaraman and S. M. Cramer, *J. Chromatogr.*, 630 (1993) 37.
- 23 C. A. Brooks and S. M. Cramer, *AIChE J.*, 38 (12) (1992) 1969.
- 24 *Standard test methods for chloride ion in water*, ASTM, D512, December 1989.
- 25 Sigma Chemical Company, personal communication, 1992.
- 26 R. D. Whitley, K. E. Vancott, J. A. Berninger and N.-H. L. Wang, *AIChE J.*, 37(4) (1991) 555.

Improved computer algorithm for characterizing skewed chromatographic band broadening

II. Results and comparisons

W. W. Yau, S. W. Rementer, J. M. Boyajian, J. J. DeStefano^{*}, J. F. Graff^{**}, K. B. Lim^{***} and J. J. Kirkland^{*}

E. I. DuPont de Nemours & Company, Central Research and Development, Experimental Station, P.O. Box 80228, Wilmington, DE 19880-0228 (USA)

(First received August 20th, 1992; revised manuscript received October 14th, 1992)

ABSTRACT

A newly developed method using an exponentially modified Gaussian peak shape model produces results that are more precise and less subject to baseline noise than previous methods for characterizing chromatographic band broadening. The method requires only precisely measurable experimental peak parameters: peak retention time, peak height, peak area, and peak centroid (first moment). Accuracy and precision of the new method were compared with other digital approaches by using computer-synthesized peaks and experimental chromatographic data from many HPLC columns. The proposed method offers a reasonable compromise between accuracy, precision, and convenience. A rapid visual estimate of peak skew can be made by inspecting peak shape and referring to a calibration plot involving peak parameters. Peak variance and skew data from this method are also useful for finding column dispersion corrections in size-exclusion chromatography calibrations.

INTRODUCTION

Accurate and precise information from real peaks is needed for many analytical applications in gas and liquid chromatography, and other separation methods. This is often a challenging task that requires sophisticated computational methods involving computers. Since the simple Gaussian model can produce serious errors in finding plate number,

peak asymmetry factor, and resolution [1], various other approaches have been proposed. The most accepted and used of these is based on the exponentially modified Gaussian (EMG) model [2–6]. Reviews of EMG uses have been given [7,8]. Empirical equations using EMG models have been proposed for calculating chromatographic figures of merit [9], and the effect of random noise on measurements by the EMG model has been addressed [10].

A new method of extracting band-broadening parameters from noisy and skewed chromatographic peaks recently was proposed [11]. This method also is based on the EMG model, but is more accurate and less susceptible to baseline noise than previously used methods. In this new procedure (the “DuPont method”), only four easily and precisely-determinable peak parameters are measured on an experimental chromatographic peak: (1) peak reten-

Correspondence to: W. W. Yau, Henkel Corp., 300 Brookside Avenue, Ambler, PA 19002, USA (present address).

^{*} Present address: Rockland Technologies Inc., 538 First State Boulevard, Newport, DE 19804, USA.

^{**} Present address: Medical Products, Glasgow Site, Building 606, Wilmington, DE 19898, USA.

^{***} Present address: Chemistry Department, Purdue University, W. Lafayette, IN 47907, USA.

tion time, (2) peak height, (3) peak area, and (4) peak centroid.

To evaluate efficacy, we compared the DuPont method with true moment calculations, the James–Martin method [12], and the Dorsey–Foley method (sometimes called the Foley–Dorsey method) [6]. These different methods provide distinctive features and offer different levels of compromise between accuracy and precision. In the present study, critical comparisons established the limitations, applicabilities, and performance of these methods. In one part, we used computer-synthesized chromatographic peaks containing built-in noise and baseline drift. Peaks created with the EMG model permitted a careful study of peak skew measurements. Other investigated parameters included the effects of random *versus* cyclic baseline noise, and various degrees of baseline drifts. Only results with random baseline noise are given in this paper. Results obtained with cyclic noise and baseline drift did not significantly change results or the conclusions regarding the proposed new DuPont method. An advantage of a computer-simulation study of this type is the complete objectivity that is possible. Also, computer simulation permits the study of a wider range of peak shape differences than is conveniently available from experimental approaches. Identical computer-synthesized data sets were used to test the different peak characterization methods.

The second part of this study involved the use of “real” chromatographic peaks experimentally developed using seventeen columns with a wide range of types and characteristics. With data from these columns, we developed a quantitative comparison of the various peak characterization methods.

THEORY

The new digital DuPont method of characterizing chromatographic peaks [11] requires only precisely measurable peak parameters for the calculation. These consist of peak retention time, t_p ; peak height, h_p ; peak area, M_0 ; and, the peak centroid (first moment), M_1 . Fig. 1 illustrates the needed parameters. A chromatographic peak can be described as a time distribution of the peak height $h(t)$ at any retention time, t . A real chromatographic peak usually can be reliably described by a Gaussian distribution modified with an exponential function,

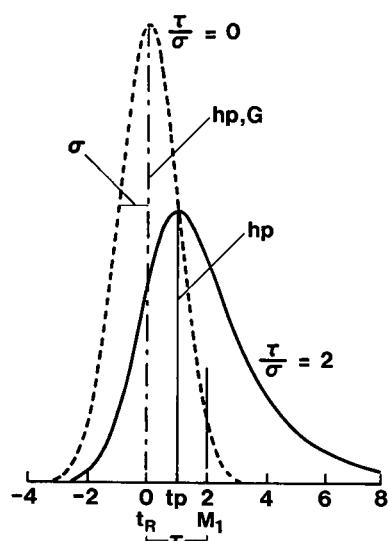


Fig. 1. Peak shape model for exponentially modified Gaussian (EMG). From ref. 10.

where σ is the standard deviation or width at 60.7% of the height of the Gaussian component, τ is the exponential time decay constant, and t_G is the retention time for the Gaussian component of the peak. The EMG peak model can be described as:

$$h(t) = \frac{M_0}{\tau\sigma\sqrt{2\pi}} \int_0^{\infty} \exp\left[-\left(\frac{t-t_G-t'}{\sqrt{2}\sigma}\right)^2 - \frac{t'}{\tau}\right] dt' \quad (1)$$

where t' = the integration retention time variable. The statistical moments of the peak can be mathematically defined, and these statistical moments can be related to the peak shape parameters, as summarized in Table I.

Moment method

For the peak moment method, calculation of plate number, N , skew, and peak variance σ^2 is determined by a point-by-point summation of terms within the integral from the beginning to the end of the peak (eqns. 2–7, Table I). This method assumes no peak shape and can produce the most accurate results. However, it is well-known that moments are quite sensitive to baseline noise. Precision often is too poor for the practical characterization of typical chromatographic peaks.

TABLE I
CHARACTERISTICS OF CHROMATOGRAPHIC PEAKS

Characteristic	Gaussian calculation	Eqn. No.	EMG calculation	Eqn. No.
m_0 (area)	$\int_0^{\infty} h(t) dt$	2		
m_1 (centroid)	$\int_0^{\infty} \frac{th(t) dt}{m_0}$	3	$t_R + \tau$	
m_2 (variance)	$\int_0^{\infty} \frac{(t - m_1)^2 h(t) dt}{m_0}$	4	$\sigma^2 + \tau^2$	9
m_3	$\int_0^{\infty} \frac{(t - m_1)^3}{m_0} h(t) dt$	5	$2\tau^3$	10
Peak skew	$m_3/m_2^{3/2}$	6	$2(\tau/\sigma)^3/(1 + \tau^2/\sigma^2)^{3/2}$	11
Plate number	m_1^2/m_2	7	$(t_R + \tau)^2/(\tau^2 + \sigma^2)$	12

James–Martin method

The James–Martin (J–M) method [12] assumes a strict Gaussian peak shape. Plate number is calculated as

$$N = (t_p/\sigma)^2 \quad (13)$$

or,

$$N = 2\pi (h_p t_p / M_0)^2 \quad (14)$$

Since a Gaussian peak shape is presumed, no information on peak skew can be obtained with this method.

Dorsey–Foley method

This method (DF–NA) uses the EMG model [6] that was available on the original Nelson Analytical PC software package. The expression for calculating plate number is:

$$N_{\text{SYS}} = [41.7(t_p/W_{0.1})^2]/[(B/A) + 1.25] \quad (15)$$

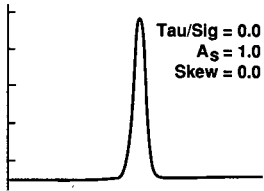
where N_{SYS} = plate number of a given (asymmetric) chromatographic system; $W_{0.1}$ = peak width at 10% of the peak height; B/A is the peak asymmetry factor at $W_{0.1}$. An upgrade version of this method (DF) was later available with improved peak detection and baseline logic.

DuPont method

The relationships for the DuPont method also utilize the EMG model. The theory and background for this method is detailed in a companion publication [11] and will not be repeated here. In this previous publication, a fully digital method is described, as well as a simplified computer algorithm with a graphical illustration.

EXPERIMENTAL

Computer-simulated peaks were generated with a VAX 3100 computer (Digital Equipment Corporation, Maynard, MA, USA) using in-house developed software. Fig. 2 illustrates the conformation of simulated peaks with various levels of imposed noise. Synthesized peaks of this type with various level of plate number and peak skew (with and without noise) were analyzed with the various peak characterization methods described above. For the simulation studies, moment, James–Martin, and DuPont calculations were made with in-house-developed software on a VAX Model 3100 computer. Dorsey–Foley calculations for the simulation study were carried out with commercial software



(Nelson Analytical, Cupertino, CA, USA) installed on the same computer. Dorsey–Foley measurements on columns were made with two versions of PC-based software (Nelson Analytical). Baseline “white” noise was produced with a random-noise generator for all methods. A two-points per second sampling rate

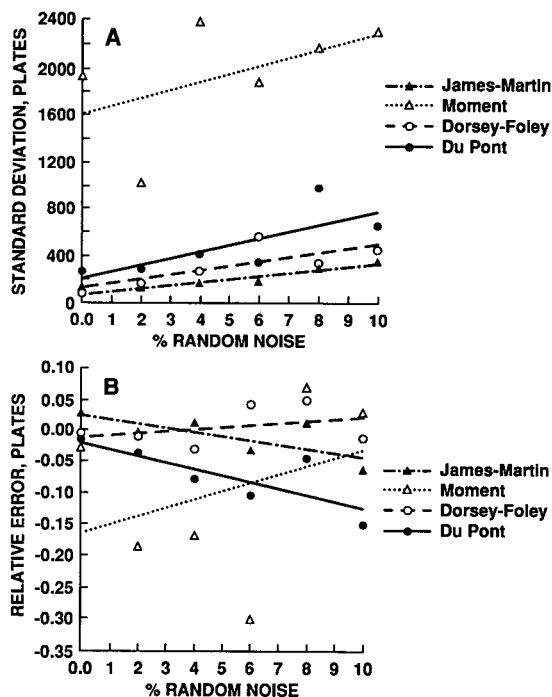


Fig. 5. Effect of noise on plate number measurements. $\tau/\sigma = 0.5$. (A) Precision measurements; (B) accuracy measurements.

noise imposed on the simulated chromatogram. These measured values are compared with the actual or true values used in the simulation. The J–M method provides precise measurements, but is increasingly inaccurate as increased peak tailing (increasing τ/σ ratio) occurs. This method shows *ca.* 15% error at a τ/σ ratio of 1.0, and a 60% error at a τ/σ ratio of 2.0. Similar results were obtained in a previous study [1]. The moment method shows poor precision and even poorer accuracy with small τ/σ values, because of a problem with the usual baseline bias presented by the computer algorithm. The percent error is about the same for increasing τ/σ values. For the same simulated peaks with 2% noise, the DF and DuPont methods both showed good precision and accuracy with increasing peak tailing.

Increasing the baseline random noise to 6% did not seriously change results from the J–M method from that seen at 2% noise—serious errors occur with increased peak tailing. However, the moment method shows much poorer precision with increased noise. The accuracy of measurements again appears

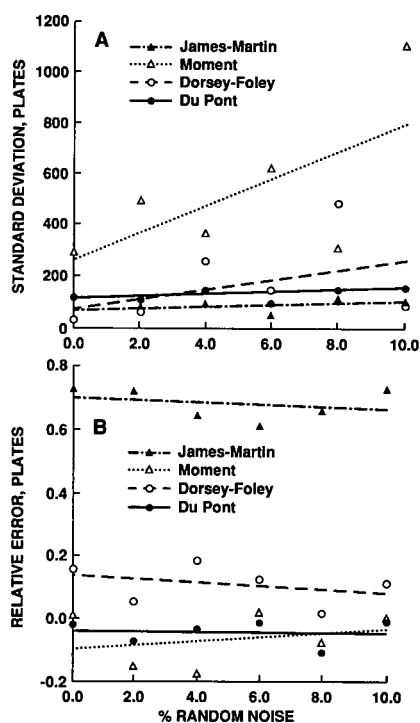


Fig. 6. Effect of noise on plate number measurements. $\tau/\sigma = 2.0$. (A) Precision measurements; (B) accuracy measurements.

similar for the DF and DuPont methods. But, precision of measurements of the DF method is degraded at higher baseline noise levels.

Fig. 5 compares the precision (Fig. 5A) and the accuracy (Fig. 5B) of plate number measurements made on tailing peaks with values of $\tau/\sigma = 0.5$ with random baseline noise varying from 0–1%. Precision of measurements (Fig. 5A) are best for the J–M method, and about the same for the DF and DuPont methods throughout the range of noise studied. The precision of moment measurements is quite poor, particularly with more symmetrical peaks, presumably because of problems in establishing accurate baseline start and stop points for the peaks. With tailing peak shapes, the accuracy of plate number measurements (Fig. 5B) is best for the J–M method, with the DF and DuPont method slightly poorer. The moment method provides the most inaccurate results because of bias in the baseline-cutting algorithm.

Fig. 6 compares the accuracy and precision of plate number measurements made on tailing peaks

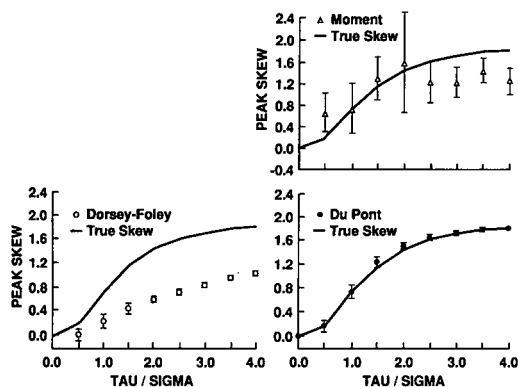


Fig. 7. Precision and accuracy of peak skew measurements. 2% Random noise.

with values of $\tau/\sigma = 2.0$ and random baseline noise from 0–10%. These data show that the J–M method is the most precise (Fig. 6A) and by far the most inaccurate (Fig. 6B). The moment method is both inaccurate and imprecise with badly tailing peaks. The DF method and the DuPont methods have about the same precision, but the commercially-available DF method is less accurate with badly tailing peaks.

Fig. 7 illustrates the ability of methods to measure peak skew (directly related to τ/σ and peak symmetry values) precisely and accurately for simulated peaks with 2% random noise. (The J–M method is incapable of peak skew information because of the

Gaussian-peak assumption.) The moment method is accurate but less precise at smaller τ/σ values; very poor precision and accuracy occur at large τ/σ ratios. The DF method is precise, but quite inaccurate with tailing peaks. The DuPont method shows both good accuracy and precision as peak tailing increases.

Increasing the random noise to 6% causes no significant change in the accuracy of the moment method, as shown in Fig. 8. However, method precision is further degraded. The precision of the DF method is about the same as with lower baseline noise, but accuracy is poorer. Increased noise does not perceptibly change the precision of the DuPont measurements, and accuracy is only slightly degraded.

It is important to note that Figs. 7 and 8 suggest that the DF method is inaccurate for peak skew measurements (errors exceeding 60% for $\tau/\sigma > 2$). These results contradict those from other studies regarding the level of accuracy with the DF method [6]. Since other investigators have not reported the DF equation to be inaccurate for peak skew [8], we suspect that the source of inconsistency is the commercial software available for this study.

Chromatographic peak study

Table II summarizes the experimental data obtained with the four peak characterization methods on seventeen different columns having widely varying plate numbers and peak tailing or peak skew values. The \pm values in this table represent the data spread (standard deviation) obtained with ten replicate sample separations.

Fig. 9 shows the plate number calculations from these column tests arbitrarily plotted against measured moment values. (True values are unknown and the moment method probably is the most accurate.) The intercept of these plots illustrate the accuracy of the measurements, while the spread of the values provides information on precision. The J–M method shows accuracy problems, since the plot does not intercept the origin. The DF and the DuPont methods show about the same accuracy and precision for plate number throughout the range of column studied. These results check well with results obtained by computer simulation.

Data in Fig. 10 compare peak skew calculations from the column tests. These results show that the

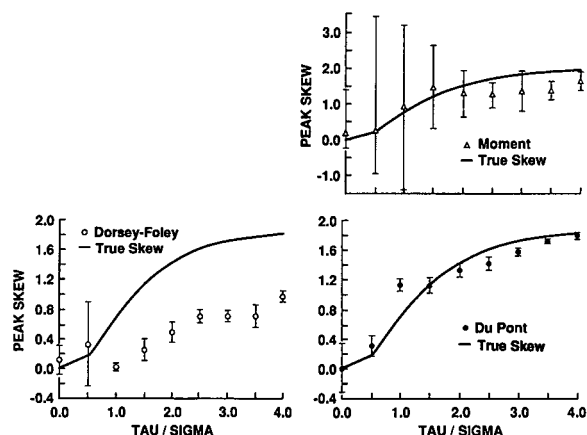


Fig. 8. Precision and accuracy of peak skew measurements. 6% Random noise.

TABLE II
TEST RESULTS: SUMMARY

σ_{av} = Average of individual σ values, an index that reflects the susceptibility of each method to baseline noise; r = correlation coefficient between an individual method referenced against the moment calculation; $\sigma_{yy'}$ = standard deviation from the best-fit linear-regression line between each method versus the moment calculation; a, b = intercept and slope of the best-fit line, $y = a + bx$.

LC	Plates ($N_{av} \pm \sigma$)				Skew ($Sk_{av} \pm \sigma$)			
	J-M	DF	DuPont	Moment	DF-NA	DF	DuPont	Moment
<i>Column-peak</i>								
A-1	6470 ± 260	5360 ± 230	6290 ± 220	5440 ± 190	0.54 ± 0.22	0.34 ± 0.14	0.14 ± 0.06	-0.01 ± 0.04
2	7310 ± 320	6600 ± 210	7330 ± 174	6340 ± 210	0.43 ± 0.18	0.17 ± 0.10	0.06 ± 0.04	-0.01 ± 0.04
3	7830 ± 320	7690 ± 140	7690 ± 400	6263 ± 110	0.10 ± 0.06	0.01 ± 0.04	-0.07 ± 0.10	0.04 ± 0.11
4	9180 ± 140	8832 ± 170	8720 ± 290	7460 ± 710	0.02 ± 0.05	-0.05 ± 0.04	-0.21 ± 0.10	-0.17 ± 0.06
B-1	10 750 ± 160	7490 ± 510	8490 ± 240	8650 ± 190	1.07 ± 0.47	0.77 ± 0.28	0.80 ± 0.05	0.76 ± 0.03
2	15 110 ± 130	11 360 ± 550	12 180 ± 400	12 570 ± 810	1.34 ± 0.35	0.72 ± 0.19	0.74 ± 0.08	0.72 ± 0.23
3	19 110 ± 1010	16 990 ± 1400	16 920 ± 310	16 160 ± 340	0.58 ± 0.22	0.38 ± 0.10	0.52 ± 0.04	0.68 ± 0.07
4	22 280 ± 170	19 408 ± 610	20 930 ± 240	19 450 ± 430	0.56 ± 0.21	0.23 ± 0.05	0.27 ± 0.03	0.51 ± 0.07
C-1	10 810 ± 190	6890 ± 230	7020 ± 250	6880 ± 340	1.49 ± 0.17	1.12 ± 0.04	1.22 ± 0.04	1.24 ± 0.04
2	14 210 ± 290	9750 ± 210	10 220 ± 300	10 070 ± 380	1.34 ± 0.22	0.92 ± 0.08	1.02 ± 0.04	1.06 ± 0.04
3	20 050 ± 230	15 330 ± 140	16 480 ± 420	15 600 ± 730	0.95 ± 0.23	0.50 ± 0.15	0.69 ± 0.05	0.79 ± 0.05
4	23 330 ± 170	19 180 ± 170	20 210 ± 540	19 280 ± 188	0.61 ± 0.15	0.50 ± 0.10	0.53 ± 0.06	0.67 ± 0.10
D-1	3660 ± 130	1870 ± 80	2040 ± 80	1950 ± 70	1.57 ± 0.07	1.53 ± 0.05	1.48 ± 0.05	1.49 ± 0.06
2	5302 ± 160	2460 ± 120	2820 ± 140	2700 ± 140	1.63 ± 0.05	1.58 ± 0.03	1.53 ± 0.02	1.44 ± 0.03
3	8520 ± 290	4200 ± 210	4700 ± 410	4130 ± 720	1.57 ± 0.09	1.47 ± 0.06	1.48 ± 0.08	1.49 ± 0.37
4 ^a	9940 ± 300	5220 ± 280	4900 ± 380	3130 ± 380	1.52 ± 0.05	1.41 ± 0.06	1.61 ± 0.05	2.24 ± 0.10
E-1 ^a	19 910 ± 280	8320 ± 230	8440 ± 360	5070 ± 270	1.57 ± 0.08	1.54 ± 0.05	1.74 ± 0.02	1.94 ± 0.01
<i>Statistics</i>								
σ_{av}	270	400	300	370	0.170	0.090	0.053	0.085
r	0.985	0.992	0.996	1	0.932	0.944	0.984	1
$\sigma_{yy'}$	1070	710	540	0	0.194	0.173	0.100	0
a	1888	163	312	0	0.272	0.032	-0.039	0
b	1.088	0.986	1.031	1	0.910	0.908	1.008	1

^a Unusual peak shape, not included in statistics; data plotted as cross (x) in summary plots.

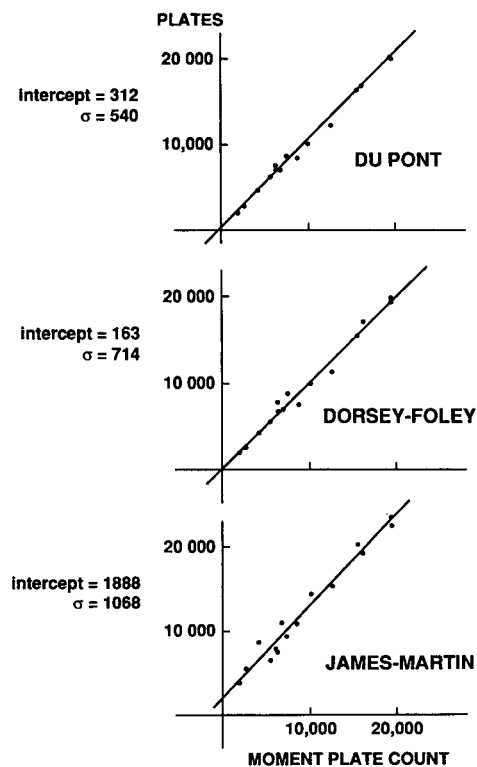


Fig. 9. Plate number calculations from column test experiments.

DF method has a positive bias; the plot intercepts the ordinate above the origin. The accuracy and precision of the DF method is about two-fold poorer

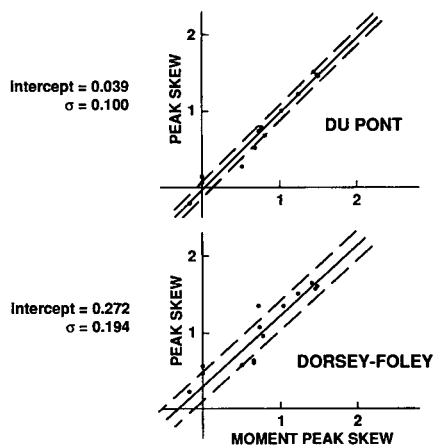


Fig. 10. Peak skew calculations from column test experiments.

than the DuPont method, as suggested by data in the Fig. 10B plots.

Table III ranks the peak characterizing methods based on the experimental separations. These results are based on replicate columns of five different types, using ten replicate runs with four solutes. Ranking numbers show that for plate number calculations, precision is best for J–M, closely followed by the DuPont method. The DF and the moment methods are 25–30% less precise. Both the DF and DuPont methods show good correlation with the moment values. Accuracy rankings show DF best, closely followed by DuPont; J–M is by far the least accurate for these “real” chromatographic peaks.

TABLE III

PEAK ANALYSIS RESULTS ON EXPERIMENTAL SEPARATIONS

Data from 5 columns, 4 solutes, 10 replicate runs each.

Computer analysis method	Plate number (rank ^a)		Peak skew (rank ^a)		Final ranking
	Precision, σ	Accuracy, ΔN	Precision, σ	Accuracy, ΔS	
James–Martin	270 (1)	1888 (4)	— (4)	— (4)	4
Moment	370 (3)	^b (3)	0.09 (2)	^b (3)	3
Dorsey–Foley	400 (4)	161 (1)	0.17 (3)	0.027 (2)	2
DuPont	300 (2)	312 (2)	0.05 (1)	–0.04 (1)	1

^a 1 = Most favorable; 4 = least favorable.

^b Moment analysis used as reference value on completely separated peaks; moment analysis may not be accurate as a reference at low signal-to-noise (S/N) ratios.

TABLE IV
CONCLUSIONS ON COMPUTER MEASUREMENT METHODS FOR EXPERIMENTAL PEAKS

Criteria		James–Martin	Moment	Dorsey–Foley	DuPont
Plates ^a	Precision	+++	0	+++	++
	Accuracy	--	+	+++	+++
Skew ^a	Precision	---	--	+++	+++
	Accuracy	---	++	---	+++
Overall rating		--	0	++	+++

^a $\tau/\sigma \leq 1$.

For measuring peak skew, the σ_{av} data in Table II show that the DuPont method is about 70% more precise than either the DF or moment method; J–M ranks last because of its inability to measure peak skew. The data in Table II further show that the DuPont method is more accurate in peak skew measurements. The correlation plots show $\sigma_{yy'}$ values about half that of the DF method measured by the commercial software. The slope of the linear regression line for the DuPont method shows only a 1% error from the ideal value of 1.0. The slope of the data for the DF method shows a 9% error from ideal. Poorest results are for the DF–NA method; the linear regression plot does not pass through the origin, resulting in skew accuracy bias.

CONCLUSIONS

A final ranking of the various computer methods for measuring plate number and peak skew or peak tailing depends on the level of background noise and the amount of peak tailing. Table IV summarizes our conclusions regarding the four methods studied, arbitrarily assuming peaks with $\tau/\sigma \leq 1$ (peak skew ≤ 0.71). The moment method is generally impractical in most real separations because of potential peak overlap problems, and difficulties in establishing accurate baseline “cut-points”. The J–M method is most precise for measuring plate number, but should be used only with highly symmetrical

peaks. The J–M method is incapable of measuring peak skew. Both the DF and the DuPont methods are competent for measuring the plate number and skew of peaks with good symmetry and low background noise. With increased baseline noise or more peak tailing, the DuPont method appears most satisfactory. The DuPont method has been used successfully in our laboratories for about four years in a variety of separations, including HPLC, GC, size-exclusion chromatography and field flow fractionation.

REFERENCES

- 1 J. J. Kirkland; W. W. Yau, H. J. Stoklosa and C. H. Dilks, Jr., *J. Chromatogr. Sci.*, 15 (1977) 303.
- 2 E. Grushka, *Anal. Chem.*, 44 (1972) 1733.
- 3 W. W. Yau, *Anal. Chem.*, 49 (1977) 395.
- 4 R. E. Pauls and L. B. Rogers, *Anal. Chem.*, 49 (1977) 625.
- 5 R. E. Pauls and L. B. Rogers, *Sep. Sci. Technol.*, 12 (1977) 395.
- 6 J. P. Foley and J. G. Dorsey, *Anal. Chem.*, 55 (1983) 730.
- 7 J. P. Foley and J. G. Dorsey, *J. Chromatogr. Sci.*, 22 (1984) 40.
- 8 M. S. Jeansonne and J. P. Foley, *J. Chromatogr. Sci.*, 29 (1991) 258.
- 9 M. S. Jeansonne and J. P. Foley, *J. Chromatogr.*, 461 (1989) 149.
- 10 J. V. H. Schudel and G. Guiochon, *J. Chromatogr.*, 457 (1988) 457.
- 11 W. W. Yau and J. J. Kirkland, *J. Chromatogr.*, 556 (1991) 111.
- 12 A. T. James and A. J. P. Martin, *Analyst*, 77 (1952) 915.

Functionalized polymer particles for chiral separation

Tihamér Hargitai, Per Reinholdsson and Bertil Törnell

Department of Chemical Engineering 2, University of Lund, P.O. Box 124, S-221 00 Lund (Sweden)

Roland Isaksson

Department of Pharmaceutical Chemistry, Analytical Pharmaceutical Chemistry, Biomedical Centre, Uppsala University, P.O. Box 574, S-751 23 Uppsala (Sweden)

(First received April 10th, 1992; revised manuscript received October 21st, 1992)

ABSTRACT

The synthetic chiral polymer poly(N-acryloyl-S-phenylalanine ethyl ester) was immobilized by grafting to macroporous polymer particles of various composition and structure in a process involving copolymerization of the chiral monomer with residual double bonds present in the macroporous support particles. The support particles were prepared by suspension or micro-suspension polymerization of trimethylolpropane trimethacrylate (TRIM), divinylbenzene or by copolymerization of styrene and TRIM. The maximum amount of immobilized chiral polymer and the mechanical properties of the resulting materials varied with the swelling capacity of the parent support particles. Up to 60% (w/w) of chiral polymer could be immobilized to the pore system of highly cross-linked TRIM particles. The enantioselectivity of the chiral stationary phases increased with increase in the amount of immobilized chiral polymer. The results of studies of porosity and particle size variation during grafting form the basis for a discussion of the structure of the final materials.

INTRODUCTION

Recently we reported [1] the preparation of and enantiomer separation on a new kind of chiral stationary phase (CSP) based on a chiral polymer, poly(N-acryloyl-S-phenylalanine ethyl ester), anchored in the pore system of macroporous polymer support particles composed of poly(trimethylolpropane trimethacrylate) (TRIM). Our preliminary results of enantiomer separations on these CSPs were very encouraging and prompted further studies. We now report on the preparation, characterization and chromatographic evaluation of CSPs based on the principles outlined above. The chiral polymer poly(N-acryloyl-S-phenylalanine ethyl ester) was immobilized to macroporous support particles pre-

pared by suspension or micro-suspension polymerization of TRIM, divinylbenzene (DVB) or by copolymerization of styrene (S) and TRIM. An extensive study was made to characterize the support particles and the CSPs, especially for the TRIM-based materials, in order to understand the functionalization process and the chromatographic performance of the materials. The materials were characterized with respect to their swelling capacity, porosity and compressibility, which are important determinants of the chromatographic performance of the CSPs. The variation of enantioselectivity, with chiral polymer loading, and the localization of the chiral polymer in the porous carrier particles are discussed.

EXPERIMENTAL

Chemicals

N-Acryloyl-S-phenylalanine ethyl ester (chiral

Correspondence to: R. Isaksson, Department of Pharmaceutical Chemistry, Analytical Pharmaceutical Chemistry, Biomedical Centre, Uppsala University, P.O. Box 574, S-751 23 Uppsala, Sweden.

monomer) was prepared according to the method described by Backmann [2]. The initiator α,α' -azoisobutyronitrile (AIBN) and ethylene glycol dimethacrylate (EDMA) were purchased from Merck. Poly(vinyl acetate) (PVAc) with a relative molecular mass (M_r) of 500 000 was obtained from BDH. 1,3,5-Tri-*tert.*-butylbenzene (TTB), *p*-nitrotoluene, acetanilide and hydroquinone were obtained from Fluka. Chlorthalidone was purchased from Sigma, and the racemates 7-methoxycoumarin dimer and coumarin dimer were a gift from Jan Sandström (Lund, Sweden) and Kailasam Venkatesan (Bangalore, India), respectively. Ammonium laurate was prepared by mixing 1.0 g of lauric acid (BHD) and ammonia to a pH of 9.6–9.8.

Two suspension stabilizers of poly(vinyl alcohol) (PVAI) were used: Rhodoviol (Rhone-Poulenc) with M_r 72 000 and a degree of hydrolysis of 71.5 mol%, and PVAI (Fluka) with M_r = 72 000 and a degree of hydrolysis of 97.5–99.5 mol%. All other chemicals were of analytical-reagent grade or better, and used as received.

The structures of the racemates chlorthalidone, 7-methoxycoumarin dimer and coumarin dimer are given in Fig. 1, together with the structures of the

chiral monomer N-acryloyl-S-phenylalanine ethyl ester and the monomer trimethylolpropane trimethacrylate (TRIM).

Support particles

The support materials TRIM particles, poly(divinylbenzene) (DVB) particles and poly(styrene-TRIM) (S/TRIM) particles were prepared in cooperation with Casco Nobel (Sundsvall, Sweden), by suspension or micro-suspension polymerization. The silica particles, LiChrosorb (diol phase, 10 μm , 300 Å), were a gift from Perstorp Biolytica (Lund, Sweden). Experimental details concerning the preparation of support particles are presented in Table I.

Preparation of chiral stationary phases based on porous carrier particles

The support particles, materials A–E in Table I, were functionalized according to the following procedure.

Porous polymer particles were first dispersed in water in a 200-ml reactor described elsewhere [1]. The monomer solution, containing the chiral monomer, initiator (AIBN) and solvent (toluene),

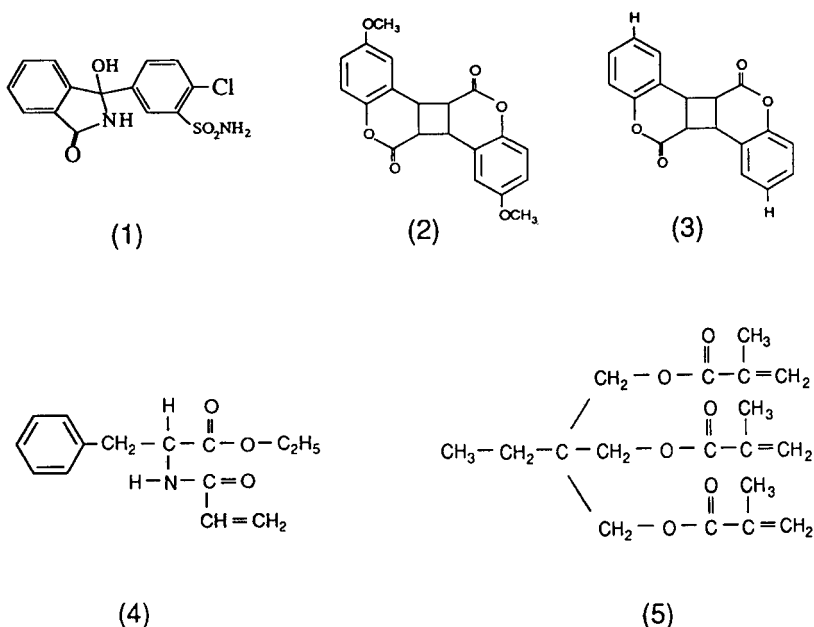


Fig. 1. Structure of the analytes and monomers: 1 = chlorthalidone; 2 = 7-methoxycoumarin dimer; 3 = coumarin dimer; 4 = N-acryloyl-S-phenylalanine ethyl ester; 5 = trimethylolpropane trimethacrylate (TRIM).

TABLE I
EXPERIMENTAL DATA FOR THE PREPARATION OF DIFFERENT SUPPORT PARTICLES

Material	Monomer (v/v)	Porogenic solvent (v/v)	Solvent-to-monomer ratio (v/v)	Polymerization		Particle size (μm)	
				Temperature ($^{\circ}\text{C}$)	Time (h)		
A	TRIM	Toluene	4:1	70	12	7.2	
B	TRIM	Toluene–isooctane (1:1)	1:1	(1)	65	6	8.3
				(2)	85	10	
				(3)	120	4	
C	DVB	Toluene	3:1	70	12	9.4	
D	DVB	Toluene	1:1	70	12	25	
E(50/50)	S/TRIM (50:50)	Toluene	4:1	(1)	60	12	5–20
				(2)	75	3	
E(40/60)	S/TRIM (40:60)	Toluene	4:1		60	12	5–20
					60	12	
E(20/80)	S/TRIM (20:80)	Toluene	4:1	60	12	5–20	

was then added to the particle dispersion. This solution was spontaneously drawn into the pore system of the particles by capillary pressure. The volume of the monomer solution used in the experiments was equal to the total swelling capacity of the particles with toluene, as determined experimentally. The concentration of the initiator was between 1 and 2.5 mol% of the chiral monomer. Prior to polymerization, the support particles containing the monomer solution were allowed to swell for about 2 h at 30–40 $^{\circ}\text{C}$. The polymerization was performed at 80 $^{\circ}\text{C}$ for about 4 h. The product was filtered off (sintered-glass filter) and washed, first with an excess of toluene to rid it of non-immobilized chiral polymer and monomer, then with dioxane, acetone and diethyl ether. The washed particles were dried overnight at 60 $^{\circ}\text{C}$.

Preparation of soft unreinforced chiral gels

Soft unreinforced gels, material F in Table I were prepared by means of suspension polymerization in the following way. A toluene solution of the chiral monomer, 1 mol% of the initiator and 10 mol% of the cross-linker (EDMA) with respect to chiral monomer, was suspended in water (stirrer rate 600 rpm) containing various suspension stabilizer. The polymerization experiments were performed in a nitrogen atmosphere in a stirred reaction vessel kept at 80 $^{\circ}\text{C}$ for 4–6 h. The gel particles formed were

filtered off (sintered-glass filter) and washed, first with hot water to rid them of suspension stabilizer, then with ethanol, acetone and toluene to eliminate monomers and uncross-linked polymers. No further preparation of the materials was done before the chromatographic evaluations.

Elemental analysis of CSPs

The amount of immobilized chiral polymer in the particles was calculated from the nitrogen content of the samples as determined by elemental analyses. The results of these analyses were in good agreement with those of gravimetric analyses, *i.e.*, from the mass difference of dry particles before and after functionalization.

Chromatographic evaluations

The chromatographic set-up used for chiral separations consisted of a Beckman Model 110 B pump, an LKB Model 2158 Uvicord SD UV detector and a BBC SE 120 dual-channel potentiometric recorder. The specific rotation was monitored with a Perkin-Elmer Model 141 M polarimeter equipped with an 80- μl (1 dm long) flow cell to establish the elution order between the enantiomers. The samples were injected by means of a Rheodyne Model 7120 loop injector.

Analytical columns were prepared by packing the CSPs (A–E) into stainless-steel columns (100 or 250

× 4.6 mm I.D.) with a descending slurry-packing technique. Prior to packing the CSPs were allowed to swell in the packing solvent for 2–4 h. Unreinforced, soft chiral gels (material F), used for the purpose of comparison, were packed into 500 × 10 mm I.D. glass columns by pouring a swollen, homogeneous and fairly thick gel suspension into the column. Before the chromatographic experiments, two or three column volumes of the eluent were pumped through the bed to equilibrate it. All CSPs were evaluated with an organic mobile phase, usually *n*-hexane–dioxane (55:45, v/v).

Swelling

The swelling of the particles in various solvents was measured using a method described previously [3]. About 0.2 g of dry particles was weighed into a tube, containing a 17–40- μm , sintered-glass filter disc at the bottom. The sample in its tube was immersed in the swelling agent at 25°C for 24 h. The amount of swelling agent taken up by the particles was determined by weighing the glass filter tube after removing excess of solvent by centrifugation for 15 min at 600 g. Some of the experiments were repeated with a reduced swelling time (1 h).

Size-exclusion chromatography (SEC)

The SEC experiments were performed with the same equipment as used for the chromatographic experiments described above. The solutes were TTB and polystyrene (PS) standards with M_r ranging from 600 to 2 700 000 and with a polydispersity ratio (M_w/M_n , where M_w = mass-average molecular mass and M_n = number-average molecular mass) of less than 1.1. Hexane–dioxane (55:45, v/v) was used as the eluent. The apparent radius (r) of the PS standards were calculated with the use of the following equation, due to Knox and Scott [4]:

$$r (\text{\AA}) = 0.0123 M_r^{0.588} \quad (1)$$

where M_r is the relative molecular mass of the PS standard.

Pressure stability

Analytical columns (100 × 4.6 mm I.D.) in standard chromatographic equipment (Varian VISTA 5500) were used to determine the relationship between flow-rate and back-pressure for the CSPs and the original support particles. Four different mate-

rials, three based on TRIM and one on silica particles, were tested. The swollen materials had similar particle sizes, 9–11 μm . The flow-rate was continuously increased to a maximum of 1.0 or 10.0 ml/min over 10 min, and then continuously decreased to zero also over 10 min. The pressure drop over the column was recorded continuously as the flow-rate changed.

Characterization of support particles and CSPs

The pore size distribution and pore volume of small pores (20–60 \AA in diameter) were measured by nitrogen adsorption and desorption according to the method of Emig and Hofmann [5], whereas the pore size distribution and pore volume of large pores (> 60 \AA in diameter) were measured by mercury porosimetry on a Micromeritics Model 9310 pore sizer. Specific surface area was measured with a Micromeritics Flowsorber 2500.

The particle size distribution of dry particles was determined from scanning electron microscopy (SEM) micrographs on an ISI 100 U instrument, and of swollen particles from light micrographs. The number-average particle size (D_n) was calculated from measurements on 1000 particles.

The amount of unreacted double bonds in the materials was measured by the bromine addition method, as reported previously [6].

RESULTS AND DISCUSSION

Chiral stationary phases (CSPs) were prepared by polymerization of the chiral monomer, N-acryloyl-S-phenylalanine ethyl ester, in the pore system of pre-made macroporous support particles. Immobilization of the chiral polymer to the support particles affects the prepared CSPs particle size and porosity (Table II). To clarify the properties of the support particles and the observed changes in the properties of the CSPs, a brief description of particle structure and of the proposed mechanism of particle formation [7] will be given. In the present discussion, the main emphasis is on experiments with the TRIM-based support particles A and B (Table I).

Particle structure formation of TRIM particles

Polymerization of TRIM monomer is thought to result initially in the formation of linear TRIM

TABLE II
CHARACTERIZATION OF TRIM-BASED MATERIALS

Material	Chiral polymer (%, w/w)	Particle size (μm)	Toluene swelling (g/g)	Surface area (m^2g)	Pore volume (cm^3/g)	
					20–60 Å	> 60 Å
A	0	7.2	4.0	494	0.22	0.50
A	24	9.1	2.5	342	0.13	1.20
A	37	9.2	1.9	181	0.06	0.88
A	50	–	1.7	40	0.01	0.20
B	0	8.3	1.5	490	0.21	0.88
B	6	–	1.2	514	0.19	0.83
B	11	8.3	1.1	461	0.17	0.76
B	21	8.4	1.1	321	0.12	0.58

polymer molecules, as methacrylic groups on adjacent TRIM residues in a linear TRIM oligomer molecule cannot add to each other owing to steric restrictions [8]. In media of good solvency, as with toluene, the linear TRIM polymer would be soluble. Such linear TRIM polymer molecules will copolymerize with growing chains, giving rise to branched molecules. Particle formation probably occurred via a phase separation process that first involved intermolecular cross-linking of branched molecules, leading to the formation of small swollen microgel particles (200–500 Å). Larger structural units, referred to as grains, having a size in the range 1000–1500 Å, were then formed by successive agglomeration of microgel particles. The interstices between the microgel particles and other packing defects in the grains may account for the presence of a fairly open network of fine pores (< 60 Å in diameter) in the final particles. The interstices between the grains form a continuous macroporous network (> 60 Å in diameter). This type of particle formation mechanism [7] would be relevant for material A particles, which were prepared using toluene as the porogenic agent. As will be discussed more fully below, the toluene swelling of A particles was about five times the total pore volume of the dry particles (Table II). This behaviour can be explained by re-expansion of micropore domains that collapsed during drying.

Polymerization of TRIM in the presence of a porogenic agent of poor solvency, toluene–isooctane (1:1), resulted in material B particles (Table I). These had a low swelling capacity, which was only

slightly (about 30%) larger than the total pore volume of the dry particles. In this instance, phase separation was probably predominantly due to a precipitation mechanism resulting in the formation of bundles of tightly packed linear polymers of TRIM [7]. Further agglomeration resulted in the formation of fine microsphere particles. The final particles consisted of coagulated microspheres. Owing to packing defects, the latter particles contained small pores (Table II). However, these small diameter pores did not shrink noticeably during drying or expand on immersion in toluene.

Swelling of TRIM particles

As support materials A and B both contain highly cross-linked material, their difference in swelling capacity (Table II), can largely be explained by the difference in the way their structural elements are joined together, rather than by a difference in the degree of cross-linking.

The toluene swelling of material A (Table II) corresponded fairly well with the toluene to TRIM ratio used in its preparation (Table I). This means that the swelling resulted in a reversal of the particle contraction that occurred during drying. The presence of bundles of flexible, crosslink-deficient molecules in the contact zones between intraparticle substructures is probably responsible for the reversible contraction and expansion of the particles during drying and swelling. Interestingly, support material A showed almost the same swelling capacity, 4.0–4.5 ml of swelling agent per gram of dry particles, in all organic solvents tested (Fig. 2), irrespective of

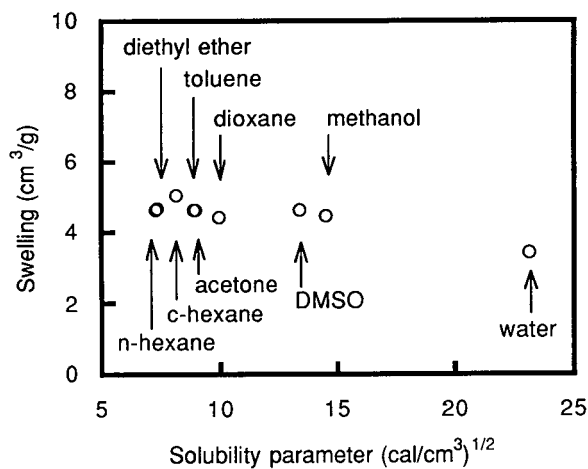


Fig. 2. Solvent uptake (swelling capacity) of support material A for different solvents.

their polarity. This suggests that the internal compression stress, built up during the drying process, relaxed as a solvent was introduced into the pore system. Similar swelling results have been reported for other highly cross-linked polymer particles [9]. Except with water, only a minor increase in particle swelling was observed as the swelling time was increased from 1 h to 24 h, whereas the water swelling doubled, approaching that of organic solvents after 24 h. This probably reflects the low plasticizing ability of water towards the TRIM polymer.

For B particles, the total pore volume of the dry particles corresponded fairly well with the volume of porogenic solvent used in their preparation (Table I). As discussed above, the toluene swelling was poor. These observations suggest that, in this instance, collapse and re-expansion of the small pores did not occur, or occurred to only a very limited extent. This supports the suggestion that the phase separation mechanism differed between porogenic media of high *versus* low solvency towards TRIM polymers.

TRIM-based chiral stationary phases

The functionalization process. Functionalization of TRIM particles involved polymerization of the chiral monomer in the pore system of the support particles. This was done in the presence of a solvent for the functional polymer and its monomer. Immobilization probably occurred by copolymeriza-

tion of the chiral monomer with residual double bonds present in the support particles. Continuous overnight extraction of the CSPs with organic solvents and their long-term stability in the chromatographic experiments strongly indicate that the chiral polymer was bound to the support matrix by covalent bonds. The consumption of residual double bonds during the grafting process to material A was verified by analysis based on bromine addition (Fig. 3) and by ¹³C cross-polarization magic angle spinning NMR analysis [6].

The maximum amount of chiral polymer that could be bound to the particles was found to vary with their swelling capacity and with the amount of residual double bonds. Up to 60% (w/w) chiral polymer could be immobilized to the highly swelling support material A, whereas a maximum of 21% (w/w) of chiral polymer could be immobilized to the poorer swelling support material B. A similar relationship between support swelling and the amount of grafted polymer has been reported previously with other kinds of polymeric support particles [10,11]. The higher grafting capacity of A particles compared with B particles can probably be explained as follows. The average number of unreacted double bonds in A and B particles was 9 and 6 mol%, respectively, of the initial amount of double bonds of TRIM monomer. For both materials, on maximum grafting, the amount of unreacted double bonds decreased to about 3 mol%. The remaining unreacted double bonds were obviously inaccessible to further grafting reactions. As a result, material A contained about twice as many accessible double bonds as did material B, or about 0.5 mmol/g TRIM particle. The difference in structure and its effect on swelling can explain the higher relative accessibility of the double bonds on material A.

The high yield of grafting and the simplicity of the functionalization method represent great advantages of the present support particles. As outlined under Experimental, the functionalization technique involved first the preparation of a suspension of porous support particles in water. To this suspension was then added a monomer–toluene solution containing a thermal initiator, which was sucked into the porous particles by capillary forces. The volume of the monomer solution added corresponded to the swelling capacity of the particles as determined in experiments with toluene. As the

polymerization and grafting reactions are almost complete, predetermined amounts of grafted functional polymer can be introduced in the particles simply by changing the concentration of the functional monomer in the added monomer solution. The functionalization method described is thus very suitable for work with expensive monomers. The concentration of chiral monomer in the monomer solution during preparation of CSPs was between 0.3 and 5.0 mol/l.

Chain length of grafted chiral polymer. The grafted chiral polymer may be attached to the support by one or several bonds, resulting in the formation of polymer loops. If the distribution of unreacted double bonds over the pore surface is assumed to be uniform, the amount of unreacted double bonds per unit volume of pores is much higher in the micropores than the macropores. Hence smaller loops would be formed in the micropores than the macropores.

An estimation of the loop size or chain length of the grafted chiral polymer, based on the consumption of double bonds (Fig. 3), predicts a very small average loop size, only about 2–4 monomer units. Such a small loop size would seriously restrict the conformational freedom of the chiral polymer and result in a low enantioselectivity [1]. In all likeli-

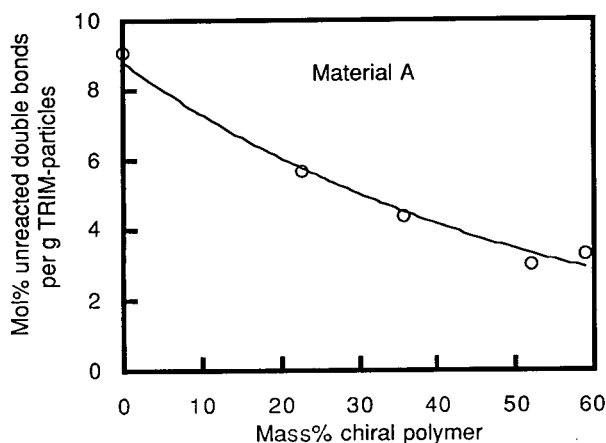


Fig. 3. Amount of unreacted residual double bonds of material A as a function of the amount of immobilized chiral polymer. The amount of unreacted double bonds is expressed in mol% of the initial amount of unreacted double bonds per unit mass of TRIM monomer. The bromine addition method was used for the determination of the unreacted double bonds.

hood, the distribution of loop size was broad. In the micropores, where the concentration of residual double bonds would be high, probably very small loops are formed, whereas in the macropores the loops might be long. This may be understood as follows. Assume functionalization of support particles A with 0.25 g (1 mmol) of chiral monomer/g TRIM. This would result in a decrease in the amount of unreacted double bonds in the TRIM particles by 3 mol% (0.26 mmol)/g TRIM (Fig. 3). If two thirds of the consumed double bonds in the TRIM particles react with only one monomer unit each, the remaining amount of chiral monomer (84% of the added amount) would form a grafted chiral polymer with an average chain length of ten monomer units ($M_r = 2500$). This loop size corresponds to the distance between cross-links in material F and should, as will be discussed further below, give the same enantioselectivity as the latter material.

Particle size and volume expansion

The number-average particle size (D_n) of unmodified support material A, A(0%), and material A immobilized with 37% (w/w) of chiral polymer, A(37%), was determined in both the dry and swollen states. On immersion in toluene, the particle size of material A(0%) increased from 7.2 μm (dry material) to 10.5 μm , whereas that of material A(37%) increased from 9.2 μm (dry material) to 10.7 μm . Introduction of the chiral polymer in the pore system of the highly swelling particles thus resulted in an irreversible increase in particle diameter (Table II). This confirms the assumption that a fraction of the chiral polymer becomes grafted in the swollen micropores, which would prevent them from contracting to their original size during drying.

The volume expansion factor on grafting was 2.1, as calculated from particle size data on dry material A(0%) and A(37%) (Table II). An alternative volume expansion factor for dry particles was calculated by comparing the total volume of modified material A, per unit mass of TRIM (*i.e.*, volume of 1 g of TRIM matrix plus volume of chiral polymer per gram of TRIM and the total pore volume per gram of TRIM), with that of the original support material A, assuming that both TRIM and the chiral polymer have unit density. This calculation gives a particle volume expansion factor of 1.8. The discrep-

ancy between these results is probably due to minor errors in the particle size determinations. The swelling of the particles was not isotropic, however, This is obvious from the observation that per gram of TRIM, the pore volume of pores with a diameter exceeding 60 Å increased by a factor of 3.2 on going from material A(0%) to A(24%). The pores thus expanded much more than the highly cross-linked part of the TRIM matrix. With material B, measurements indicated the particle volume expansion factor and the expansion factor for macropores (>60 Å in diameter) to be close to unity, *i.e.*, no significant matrix expansion was observed.

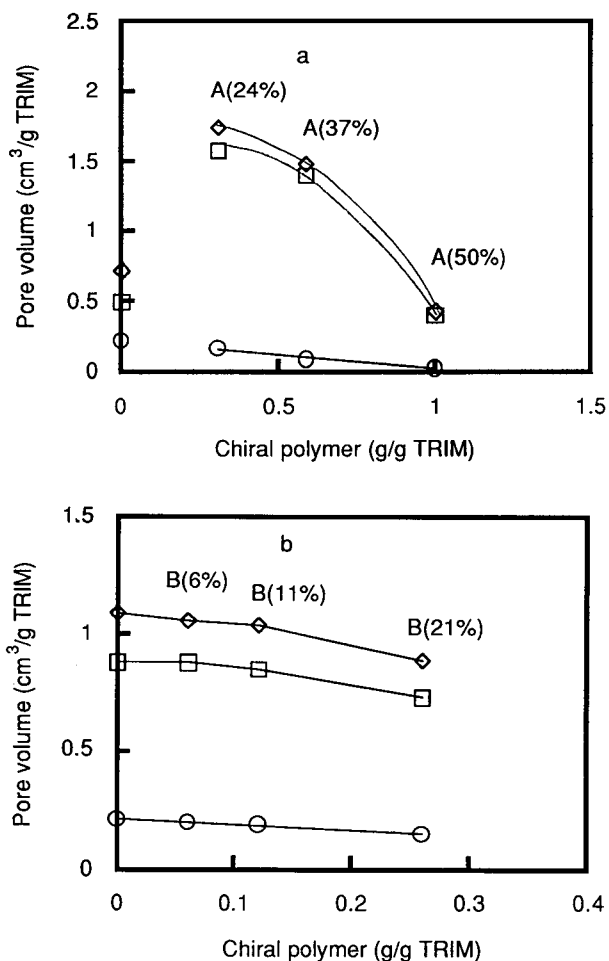


Fig. 4. Effect of the amount of immobilized chiral polymer on the specific pore volume of (a) material A and (b) material B. \diamond = Total pore volume; \square = pore volume of pores larger than 60 Å in diameter; \circ = pore volume of pores between 20 and 60 Å in diameter.

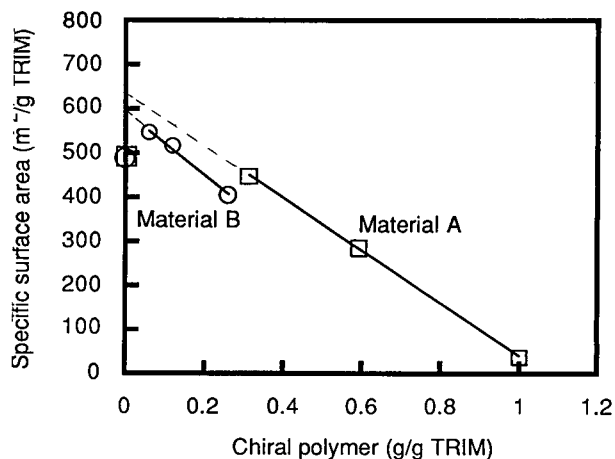


Fig. 5. Relationship between amount of immobilized chiral polymer and the specific surface area of materials A and B.

Porosity

Results from pore volume and specific surface area measurements for materials A and B before and after functionalization are presented in Table II. As shown in Fig. 4a for material A(0%) and A(24%), and suggested by particle size measurements, the total pore volume is increased after the grafting. The increase in pore volume depends on the previously discussed irreversible volume expansion of the particles due to deposition of polymer in the small pores. For the poorly swelling material B, a decrease in the total pore volume was observed at a comparable loading of chiral polymer (Fig. 4b).

The specific surface area of chiral stationary phases, based on materials A and B, decreases linearly with increasing amount of immobilized chiral polymer (Fig. 5). The decrease in surface area with increasing amounts of immobilized chiral polymer shows that grafting results in filling of the small pores which account for most of the specific surface area of the material. Extrapolation of the lines in Fig. 5 back to zero concentration of grafted polymer suggest that the specific surface area of the hypothetically unfunctionalized but expanded particles A and B would be 636 and 596 m²/g TRIM, respectively.

The cumulative pore volume curves for pores larger than 60 Å in diameter changed, as shown in Fig. 6. Comparison of the two support materials A and B shows that material B contains a higher vol-

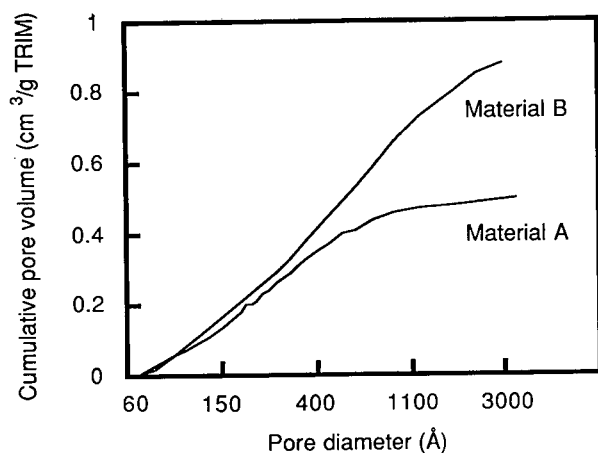


Fig. 6. Cumulative pore volume distribution curves of support materials A and B.

ume fraction of volume of material B (Table II). The cumulative pore volume curves for CSPs of material A and B are shown in Fig. 7. The irreversible volume expansion of material A (24%) is clearly observed in Fig. 7a.

Accessibility of the pore system in CSPs

A problem that arises from the introduction of the chiral polymer into the pore system of the support is whether the analytes can penetrate into the

pores after this functionalization. In separate study published elsewhere [12], another batch of support material A was functionalized by polymerizing acryloyl or methacryloyl chloride in the particle pore system. It was found that, even though a large fraction of the acid chloride polymers was localized in the micropores, these groups could be reacted with amines or alcohols to yield amides and esters in almost quantitative yields.

The amount of TRIM matrix of support particles A and B per unit length of packed column was constant, 0.25 and 0.53 g per column, respectively, and independent of the amount of immobilized chiral polymer (Fig. 8). The lower amount of support material A per unit length of column, as compared with support material B, is due to the greater volume swelling of material A. A linear decrease of the elution volume of TTB with an increase in the amount of immobilized chiral polymer was observed for the CSPs. From this decrease, the excluded volume was calculated to be 1.5 cm³ per gram of chiral polymer.

Pore accessibility was examined by inverse size-exclusion chromatography (SEC) using commercially available polystyrene (PS) standards having relative molecular masses ranging from 600 to 2 700 000. The diameters, d (Å), of the PS standards were calculated according to the equation given by Van Kreveland and Van den Hoed [13]. The maximum elution volume in the chromatographic sys-

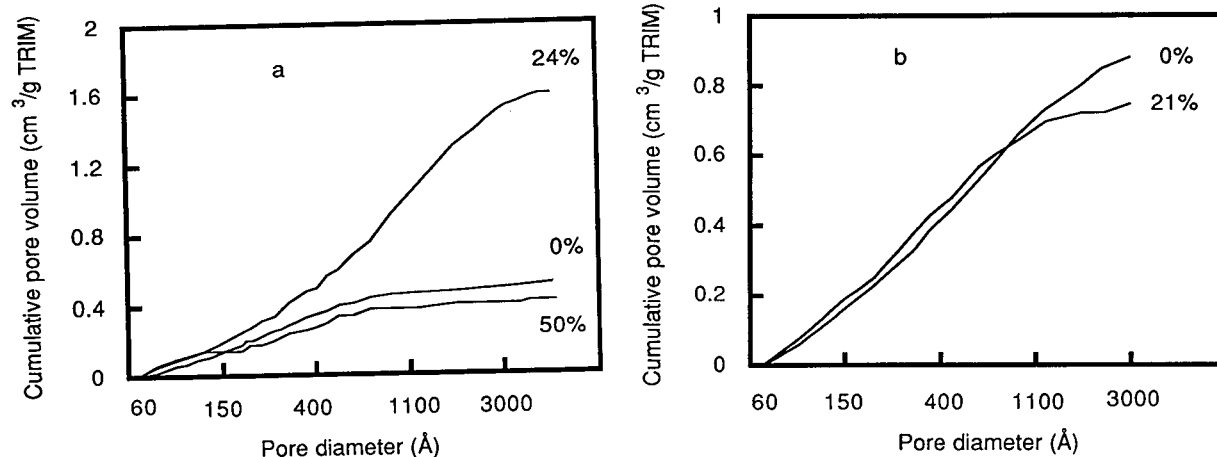


Fig. 7. Cumulative pore volume distribution curves for CSPs based on (a) support material A and (b) support material B.

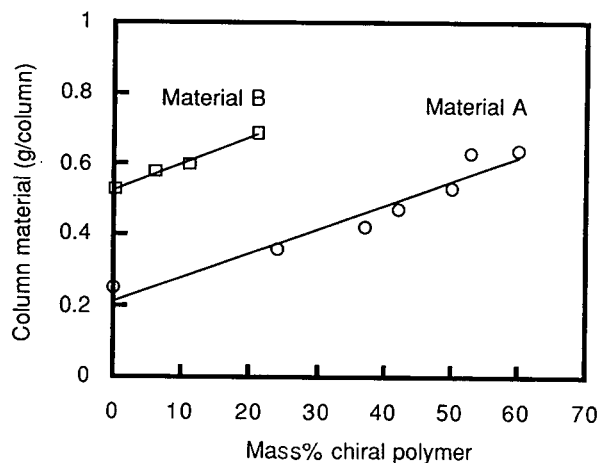


Fig. 8. Amount of dry column material as a function of the amount of immobilized chiral polymer for materials A and B. Columns, 100×4.6 mm I.D.

tem was measured with TTB, which is assumed to be non-retained by the support particles and the CSPs. The degree of permeation of the test molecules into the pore system of the polymer particles depends on both the amount of immobilized chiral polymer and the size of the test molecule. The results from the SEC experiments, presented in Fig. 9, show the decreased accessibility of the pore system due to the presence of the chiral polymer. These results confirm the presence of swollen chiral polymers in the macropores of the materials, especially for material A (50%). The porosity and separation range of TRIM particles have recently been determined from SEC experiments in toluene by injections of PS standards [14]: the total separation range for one type of TRIM particles was reported to range between M_r 250 and 2 700 000 of the PS standards, *i.e.*, about the same separation range as for support particles A and B in the present study.

Mechanical stability

The relationship between flow-rate and pressure drop of columns containing different support particles (A, B and silica particles) is presented in Fig. 10. As expected, the pressure drop of the column packed with the highly swelling material A increased very rapidly with increased in flow-rate. The poorly swelling material B yielded a pressure drop curve similar to that of the silica material at

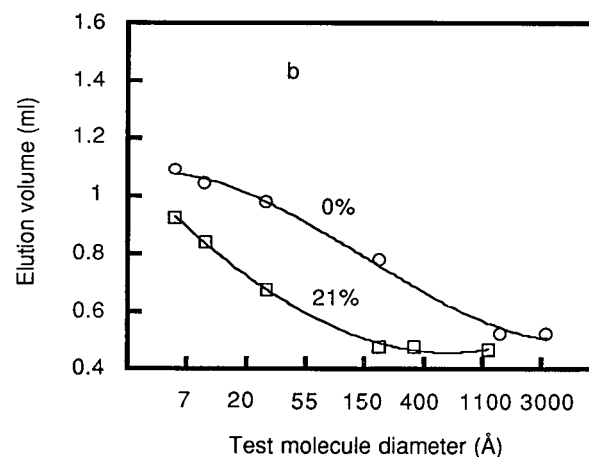
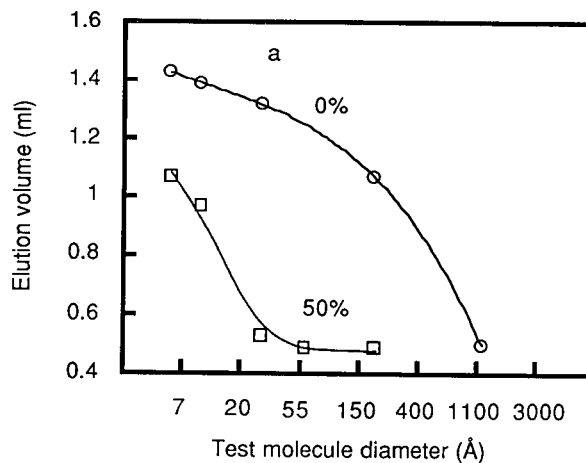


Fig. 9. Elution volume curves of (a) support material A and material A(50% chiral polymer) and (b) support material B and material B(21% chiral polymer) for TTB and different PS standards.

flow-rates up to 5 ml/min, *i.e.*, a range that is useful for chromatographic experiments. No permanent increase in flow-resistance was observed for material B or the silica material by decreasing the flow-rate continuously to zero, as is demonstrated by the symmetry of the curves showing the increase and the decrease of the flow (Fig. 10). An identical result of the pressure drop curve for material B was obtained by repeating the experiment after a pause of 5 min to allow the material to subside. The high pressure drop over the column at high flow-rates

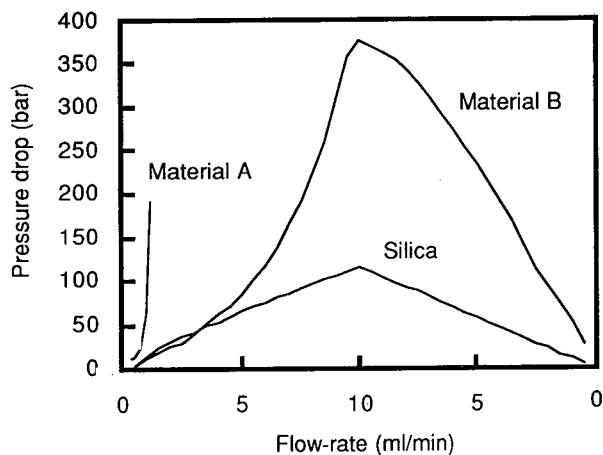


Fig. 10. Mechanical stability of different support particles, measured as the effect of the flow-rate on the column pressure drop. The linear increase and decrease in the flow-rate was 1 ml/min. Columns, 100×4.6 mm I.D.; mobile phase, toluene.

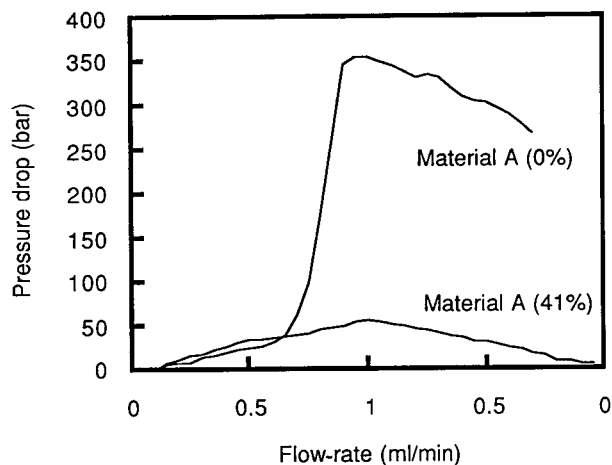


Fig. 11. Effect of the flow-rate on the column pressure drop of support material A and material A immobilized with 41% (w/w) of the chiral polymer. The linear increase and decrease in the flow-rate was 0.1 ml/min. Column, 100×4.6 mm I.D.; mobile phase, toluene.

(over 5 ml/min) thus seems to depend on reversible deformation (compression) of the particles. A significant increase in pressure stability was observed for material A as chiral polymer was immobilized to the particles. The column packed with material A(41%) manifests good chromatographic performance at flow-rates up to 1 ml/min, as compared with the column containing unmodified support material A (Fig. 11).

Characterization of DVB and styrene-TRIM-based materials

Other support particles that have been used for immobilization of the chiral polymer are support particles C and D, prepared with DVB, and support particles E(50/50), E(40/60) and E(20/80), prepared by copolymerization of styrene (S) with TRIM in different ratios (S/TRIM) (Tables I and III).

The DVB-based support particles, C and D, are

TABLE III

CHARACTERIZATION OF DVB- AND S/TRIM-BASED MATERIALS

Material	Chiral polymer (%, w/w)	Particle size (μm)	Toluene swelling (g/g)	Surface area (m^2/g)	Pore volume (cm^3/g)	
					20–60 Å	>60 Å
C	0	9.4	2.6	736	0.38	0.94
C	14			649		
C	44			118		0.26
D	0	25	1.0	543	0.25	0.51
D	5			483		
D	18			245	0.22	0.31
E(50/50)	0	5–20	3.3	3	0.00	0.05
E(50/50)	9		3.6	2		
E(40/60)	0	5–20	3.1	2	0.00	
E(40/60)	16		3.5	3		
E(20/80)	0	5–20	3.4	132	0.10	0.17
E(20/80)	23		3.9	4	0.00	0.14

similar to the TRIM-based support particles, A and B, both in properties and behaviour. Consequently, as with the TRIM based particles, higher amounts of chiral polymer could be immobilized to the highly swelling support material C than to the poorly swelling support material D (Table III). The surface areas of the CSPs show a linear decrease with increased amounts of immobilized chiral polymer. As with the TRIM-based materials, a linear decrease of the elution volume of TTB with an increased amount of immobilized chiral polymer was observed. The excluded volume for TTB on material D was $1.5 \text{ cm}^3/\text{g}$ chiral polymer, *i.e.*, comparable to that obtained on CSPs of material A and B.

The S/TRIM-based E(S/TRIM) particles (Tables I and III) differ in properties from the other support particles, A–D. The specific surface area and the total pore volumes of E particles are both very low, *i.e.*, homogeneous particles without any porosity in the dry state are obtained if a relatively large amount of styrene is copolymerized with TRIM (Table III). The swelling capacities of the three different E materials are similar and fairly high, about 3.3 g of toluene per unit mass of dry material. This indicates the presence of a pore system that collapses during drying of the material. The maximum amount of immobilized chiral polymer increases as the amount of TRIM in the support particles increases; the highest amount of immobilized chiral polymer, 23% (w/w), was obtained with the E(20/80) particles, whereas only 9% (w/w) of chiral polymer could be immobilized to E(50/50) particles (Table III). This may depend on larger amounts of available and accessible unreacted double bonds in the support particles with high amounts of TRIM, as for material E(20/80).

Chiral separations

The focus of this work has been on the characterization of the CSP, and not on screening enantiomer separations. Comparison of the materials has been based on the separation factor (α values) obtained for chlorthalidone as a model substance. A typical chromatogram of the separation of chlorthalidone has been reported previously [1].

Enantioselectivity versus amount of chiral polymer and kind of support. All CSPs manifested an increase in enantioselectivity with increase in the amount of immobilized chiral polymer (Fig. 12).

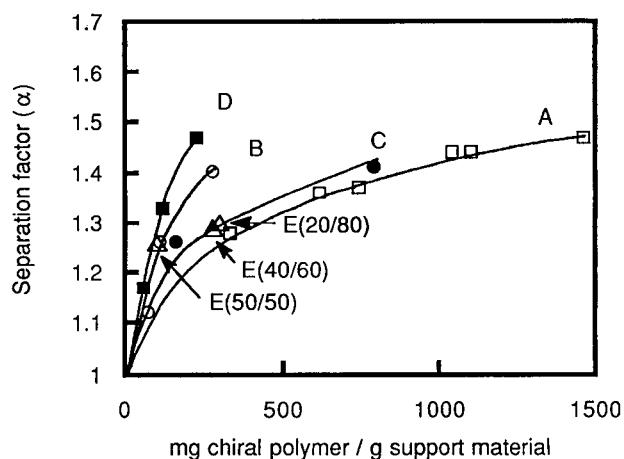


Fig. 12. Relationship between the amount of immobilized chiral polymer and the separation factor of chlorthalidone for CSPs A–E.

The highest separation factors per gram of immobilized chiral polymer were obtained for CSPs derived from the poorly swelling support particles of types B and D. However, as large amounts of chiral polymer are grafted to the highly swelling particles A and C, similar separation factors are obtained for these materials as for the poorly swelling materials B and D.

The observed difference in enantioselectivity of the TRIM-based CSPs may be explained by the chain length, or loop size, of the grafted chiral polymer. As mentioned before, the amount of polymerizable residual double bonds in support particle A is estimated to be twice that in support particle B. Owing to the large amount of unreacted double bonds in A particles and the high local concentration of double bonds in the small pores, a substantial fraction of the added chiral monomer forms only very short chains or loops (probably shorter than 2–4 monomer units), mainly located in the micropores. The results indicate that chains of such small size have little or no enantioselectivity. This is probably due to their poor capacity to form favourable enantioselective conformations. As larger amounts of chiral monomer are used in the functionalization process, the amount of grafted chiral polymer with a large loop size increases. Owing to the more compact structure of B particles, which seem to contain micropores with low swelling capacity, a larger

fraction of the added chiral monomer forms sufficiently long enantioselective chiral loops than in grafting to A particles.

The proposed explanation of the effect of chiral polymer chain length on CSP enantioselectivity is in accord with previously reported results on the effect of the degree of cross-linking on the enantioselectivity of soft chiral gels, namely that an increase in the degree of cross-linking gives a decrease in enantioselectivity [15]. The enantioselectivity of unsupported chiral gels is reported to be completely lost if as much as 50% of cross-linker is used in their preparation [15]. The soft unreinforced chiral gel used in this work, material F, was made in the presence of 10 mol% of cross-linker. This would result in an average chain length of the chiral polymer of ten chiral monomer units. As discussed above, loops of this length may well be present in the CSPs based on TRIM particles.

Surprisingly, high separation factors for chlorthalidone were obtained on CSPs prepared from the different support particles E (Fig. 12). Despite the materials having little or no porosity in the dry state, the grafted chiral polymer obviously has sufficient flexibility to create enantioselective conformations. The enantioselectivity of these CSPs and their physical properties, such as their low porosities and high swelling capacity, support the presence of a pore system in the materials that collapses during drying, and re-emerges in a good polymer solvent.

Although no effect of the functionality of the different polymer particle matrices (TRIM or DVB) on enantioselectivity is observed for chlorthalidone, such an effect could probably be observed for other racemates. The highest enantioselectivity obtained for chlorthalidone, on CSPs A–D ($\alpha \approx 1.5$), is similar to that obtained on unreinforced soft chiral gels, such as material F (to be discussed below), and significantly higher than that obtained on a silica-based (commercial) CSP (HIBAR Prepacked Column RT 250-4; Merck, Darmstadt, Germany) ($\alpha = 1.25$) containing 16% of the chiral polymer [1].

Chromatographic properties

Irrespective of whether TRIM- or DVB-based particles were used as supports, the capacity factors for the analytes studied, both chiral and achiral, increase non-linearly with an increase in the amount of immobilized chiral polymer (Fig. 13).

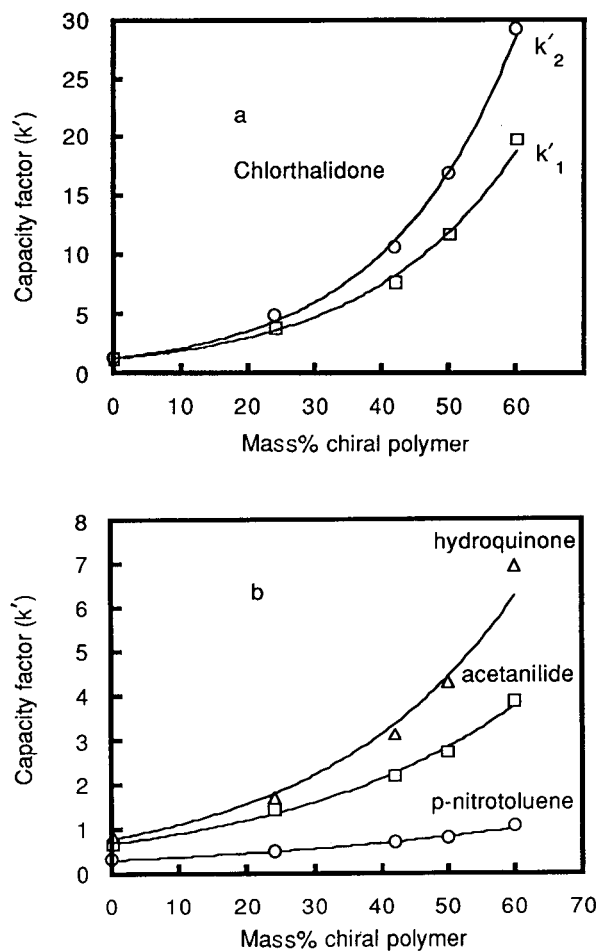


Fig. 13. Exponential dependence between the capacity factors (k') of (a) chlorthalidone and (b) three achiral analytes on the amount of immobilized chiral polymer on CSPs based on material A. Column, 100×4.6 mm I.D.; mobile phase, *n*-hexane-dioxane (55:45, v/v); flow-rate, 0.5 ml/min; detection, UV (254 nm).

The effects of temperature on separation factors, capacity factors and column efficiency are shown in Figs. 14–16. The capacity and selectivity factors are reduced by an increase in temperature, whereas the efficiency of the columns is improved. These results are typical of most chromatographic systems and can be explained by a reduced viscosity of the mobile phase which increases the diffusion and mass transfer rates, thus improving column efficiency. The highest column efficiency, presented in Fig. 17 as the height equivalent to a theoretical plate

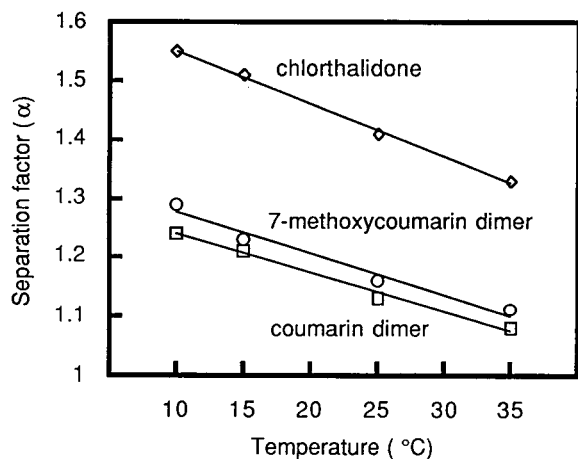


Fig. 14. Effect of column temperature on the separation factor (α) for three different racemates. CSP, material B (21% chiral polymer); column, 100×4.6 mm I.D.; mobile phase, *n*-hexane-dioxane (55:45, v/v); flow-rate, 0.7 ml/min; detection, UV (254 nm).

(HETP), was obtained for achiral compounds at very low flow-rates. No increase in peak widths with an increase of the amount immobilized chiral polymer could be observed.

Long-term stability and loadability of the columns

The CSPs A–E show very good long-term stability.

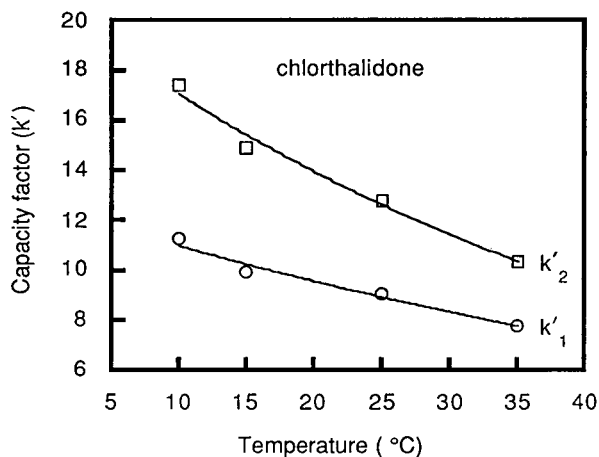


Fig. 15. Effect of column temperature on the capacity factors (k') of chlorthalidone. CSP, material B (21% chiral polymer); column, 100×4.6 mm I.D.; mobile phase, *n*-hexane-dioxane (55:45, v/v); flow-rate, 0.7 ml/min; detection, UV (254 nm).

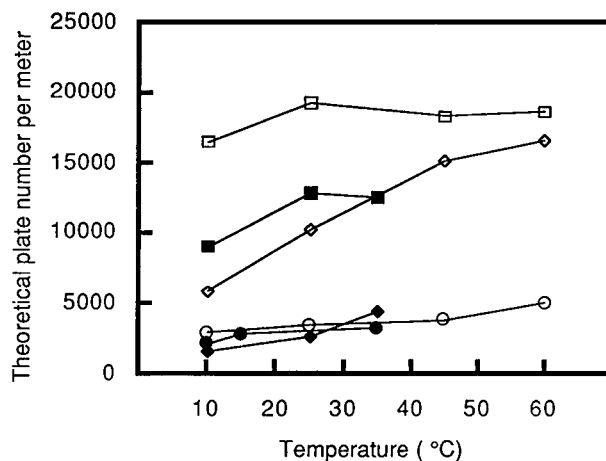


Fig. 16. Relationship between column temperature and the theoretical plate number (N) for three different analytes. Filled symbols denote results obtained on material B (21% chiral polymer) and unfilled symbols those on support material B. Detection, UV (254 nm); flow-rate, 0.7 ml/min; columns, 100×4.6 mm I.D.; mobile phase, *n*-hexane-dioxane (55:45, v/v). Analytes: \circ = chlorthalidone; \diamond = *p*-nitrotoluene; \square = TTB.

No change was observed in either selectivity or retention after continuous elution of more than 1000 column volumes of mobile phase (Fig. 16). Nor could any change in selectivity be observed after repacking CSPs that had been dried and stored for several months at ambient temperature. The loadability of the materials containing large

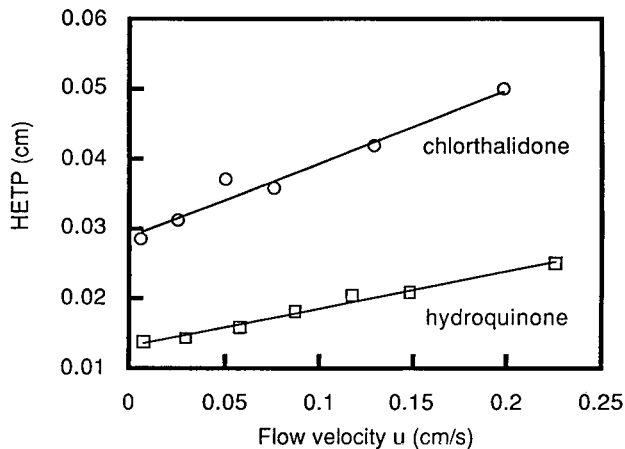


Fig. 17. Effect of flow-rate on the height equivalent to a theoretical plate (HETP) on support material B. Column, 100×4.6 mm I.D.; mobile phase, *n*-hexane-dioxane (55:45, v/v); detection, UV (254 nm).

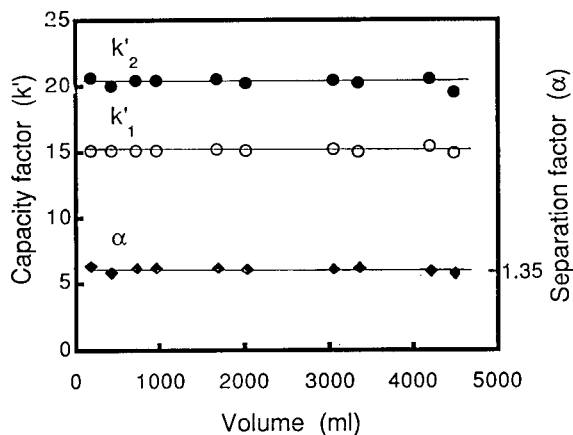


Fig. 18. Long-term stability of material A (33% chiral polymer). Analyte: chlorthalidone. Column, 250 × 4.6 mm I.D.; mobile phase, *n*-hexane–dioxane (50:50, v/v); flow-rate, 0.8 ml/min; detection, UV (254 nm).

amounts of chiral polymer seems to be fairly good. On an analytical column (250 × 4.6 mm I.D.), material A (55%), 1.2 mg of 7-methoxycoumarin dimer [16] or 5 mg of chlorthalidone could be completely separated in one run. The CSPs should therefore be of interest for preparative or semi-preparative applications.

TABLE IV

EFFECT OF SUSPENSION AND CO-STABILIZERS ON ENANTIOSELECTIVITY OF SOFT CHIRAL GELS

Between 9 and 10 mol% of the cross-linker EDMA, calculated on the amount of added chiral monomer, were used in the preparation of the CSPs

CSP	Suspension stabilizer		Separation factor (α)
	Type	Content (% w/w) ^a	
F1	PVAI	5.00	1.5
F2	PVAI	0.06	1.5
F3	without PVAI		1.5
F4	Rhodoviol	0.1	1.6
	Ammonium laurate	5.0	
F5	Rhodoviol	0.1	1.5
	PVAc ^b	0.25	

^a Amount (g) of suspension stabilizer per 100 g of water.

^b Added to the organic phase.

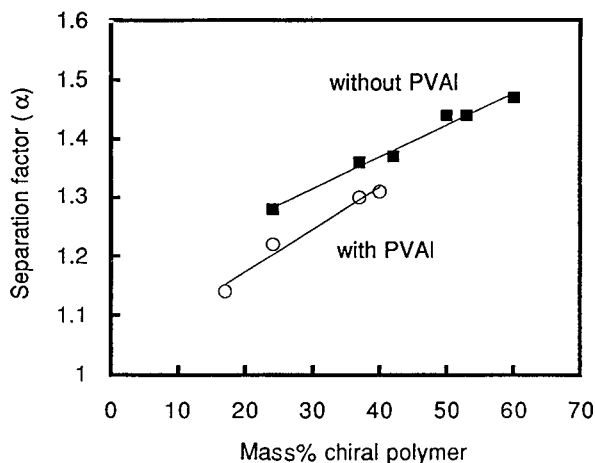


Fig. 19. Effect of the suspension stabilizer PVAI on CSP enantioselectivity for chlorthalidone. The CSPs are based on support material A. Columns, 100 × 4.6 mm I.D.; mobile phase, *n*-hexane–dioxane (55:45, v/v); flow-rate, 0.7 ml/min; detection, UV (254 nm).

Effect of suspension stabilizer on enantioselectivity

Blaschke and co-workers [15,17] found the enantioselectivity of soft chiral gels to depend not only on the structure of the chiral monomer and the degree of cross-linking, but also on the amount and kind of the suspension stabilizer used in the preparation of the CSPs. An increase in enantioselectivity with respect to mandelic acid was obtained when the amount of suspension stabilizer poly(vinyl alcohol) (PVAI) in water was increased from 0.25 to 2.5% (w/w), whereas enantioselectivity was completely lost on changing the suspension stabilizer to polyvinylpyrrolidone (PVP).

The role of the suspension stabilizer was taken into consideration in the present study, where the preparation of soft unreinforced chiral gels, material F, using various kinds and amounts of suspension stabilizers, was included with a view to comparing the effect of suspension stabilizer on enantioselectivity (Table IV). In our work, the amount and type of suspension stabilizers were found to have only a minor effect on the enantioselectivity of the soft giral gels (F). These findings are inconsistent with those reported by Blaschke and Donow [15].

Preparation of CSPs based on support material A in the presence of the suspension stabilizer PVAI [5% (w/w) in the water phase] did, however, affect the CSP enantioselectivity with respect to chlorthal-

idone. On comparable CSPs, the selectivity factors were significantly smaller for materials prepared in the presence of the suspension stabilizer (Fig. 19). The formation of non-enantioselective aggregates between the chiral polymer and PVAI would seem to be the reason for the lower enantioselectivity observed. The aggregate formation was confirmed in an experiment in which the chiral monomer was polymerized from a hot (80°C) homogeneous, aqueous solution containing 5% (w/w) of PVAI. A colloidal dispersion was obtained. The isolated product (a slimy mass) was insoluble in water, 6 M urea and all commonly used organic solvents, and no swelling of the material was observed in any of these solvents. According to elemental analyses, the material consisted of about equal amounts of chiral polymer and suspension stabilizer (PVAI). Attempts were made to use this material as a CSP, but without success. In another experiment, it was found that a solid aggregate was formed at the interface between a 5% (w/w) aqueous PVAI solution and a toluene solution of the chiral polymer. This interface aggregate manifested the same properties (of solubility, swelling and enantioselectivity) as the above-mentioned material obtained on polymerization. These observations clearly show the presence of fairly strong interactions between PVAI and the chiral polymer used, probably ascribable to a multiplicity of acid–base interactions. Further studies of the role of these interactions in the present context have not been made.

CONCLUSIONS

Large amounts of chiral polymer can be irreversibly immobilized to support particles by using residual double bonds in macroporous support particles as “handles” for the grafted polymer. The amount of immobilized chiral polymer can easily be varied, up to a maximum, by simply changing the monomer concentration in the added monomer solution, as the conversion of polymerization and grafting reactions are complete. The swelling capacity of the support particles and their content of residual double bonds are determinants of the maximum amount of immobilized chiral polymer. The enantioselectivity of the CSPs is comparable to that of

unreinforced soft chiral gels and higher than that of a comparable commercial CSP based on silica particles. The simple and straightforward method of introducing flexible chiral polymers to porous polymer particles presented in this paper should be useful for the preparation of stationary phases for analytical and preparative chiral separations, and possibly also for other kinds of chromatographic applications.

ACKNOWLEDGEMENTS

This work was supported by grants from the Swedish National Board for Technical Development. The kind cooperation of the late Mr. S. Porrvik, Casco Nobel, is gratefully acknowledged. Mr. S. Kiuru and Mrs. B. Svensson are gratefully thanked for their help with measuring pore volumes and specific surface areas.

REFERENCES

- 1 T. Hargitai, P. Reinholdsson, B. Törnell and R. Isaksson, *J. Chromatogr.*, 540 (1991) 145.
- 2 W. Backmann, *Thesis*, Rheinische Friedrich-Wilhelms Universität, Bonn, 1978, p. 23.
- 3 K. W. Pepper, D. Reichenberg and D. K. Hale, *J. Chem. Soc.*, (1952) 3129.
- 4 J. Knox and H. P. Scott, *J. Chromatogr.*, 316 (1989) 311.
- 5 G. Emig and H. Hofmann, *J. Catal.*, 8 (1967) 303.
- 6 T. Hjertberg, T. Hargitai and P. Reinholdsson, *Macromolecules*, 23 (1990) 3080.
- 7 P. Reinholdsson, T. Hargitai, R. Isaksson and B. Törnell, *Angew. Makromol. Chem.*, 192 (1991) 113.
- 8 J.-E. Rosenberg and P. Flodin, *Macromolecules*, 19 (1986) 1543.
- 9 M. Negre, M. Bartholin and A. Guyot, *Angew. Makromol. Chem.*, 106 (1982) 67.
- 10 A. Guyot and M. Bartholin, *Polym. Sci.*, 8 (1982) 277.
- 11 A. Guyot, A. Revillon and Q. Yuan, *Polym. Bull.*, 21 (1989) 577.
- 12 P. Reinholdsson, T. Hargitai, A. Nikitidis, R. Isaksson and C.-A. Andersson, *React. Polym.*, 17 (1992) 175–186.
- 13 M. E. van Kreveld and N. van den Hoed, *J. Chromatogr.*, 83 (1973) 111.
- 14 A. Schmid, L.-I. Kulin and P. Flodin, *Makromol. Chem.*, 192 (1991) 1223.
- 15 G. Blaschke and F. Donow, *Chem. Ber.*, 108 (1975) 1188.
- 16 T. Hargitai, P. Reinholdsson and J. Sandström, *Acta Chem. Scand.*, 45 (1991) 1076.
- 17 G. Blaschke and A.-D. Schwanghart, *Chem. Ber.*, 109 (1976) 1967.

New alumina-based stationary phases for high-performance liquid chromatography

Synthesis by olefin hydrosilation on a silicon hydride-modified alumina intermediate

Joseph J. Pesek, Junior E. Sandoval and Minggong Su

Department of Chemistry, San Jose State University, 1 Washington Square, San Jose, CA 95192 (USA)

(First received August 11th, 1992; revised manuscript received October 16th, 1992)

ABSTRACT

A silanization procedure is used to form a layer of silicon hydride on the surface of alumina. IR and NMR data confirm the presence of the hydride on the surface. Modification of the hydride intermediate is accomplished by reaction with a terminal olefin in the presence of a transition metal catalyst to form an alkyl-bonded material. Both IR and NMR confirm the bonding of the alkyl ligand to the hydride surface. Chromatographic tests indicate reversed-phase behavior. Exposure to high concentrations of phosphate solution for an extended period resulted in no significant deterioration of the bonded phase.

INTRODUCTION

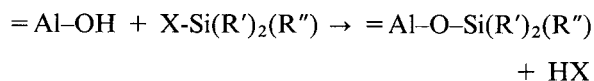
Silica-based stationary phases for HPLC have dominated HPLC applications for three decades. Their main advantages include availability in a variety of particle and pore sizes, high mechanical strength and reproducible separations with the same column under controlled experimental conditions. However, there are some disadvantages which preclude silica from being a universal support for HPLC and/or limit the scope and type of separations possible. For example, there are many manufacturers of silica, each using its own process for production, which has resulted in a wide substrate variation. In addition, even from a single source there are significant batch to batch variations which often make comparisons between dif-

ferent columns of the same stationary phase difficult. Probably the most serious drawback of silica and derivatized silica involve its limited pH stability, generally in the range of 2 to 8 [1,2]. This has led to the development of novel modification schemes for silica [3], the incorporation of other compounds such as zirconia into the silica matrix [4], or the use of alternate materials such as polymers [5–7].

Alumina offers still another alternative to silica because of its inherent higher pH stability. However, in contrast to its extensive use as a medium in column chromatography for purification purposes or for separations in the normal-phase mode, there are still relatively few reports involving alumina-based materials in the reversed-phase (RP) mode. Considering that RP methods represent the majority of HPLC applications, it will be necessary to develop modified aluminas similar to those that exist for silica. Only then will it be possible to identify any advantages that alumina may possess over silica because of its fundamentally higher pH stability.

Correspondence to: J. J. Pesek, Department of Chemistry, San Jose State University, 1 Washington Square, San Jose, CA 95192, USA.

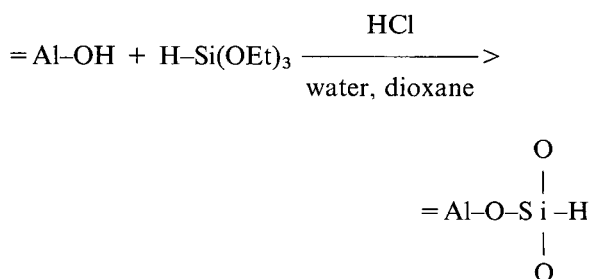
Knox and Pryde [8] were among the first to describe modifications to alumina which could be used in RP-HPLC. These phases were synthesized using standard organosilane chemistry which can be described by the following reaction:



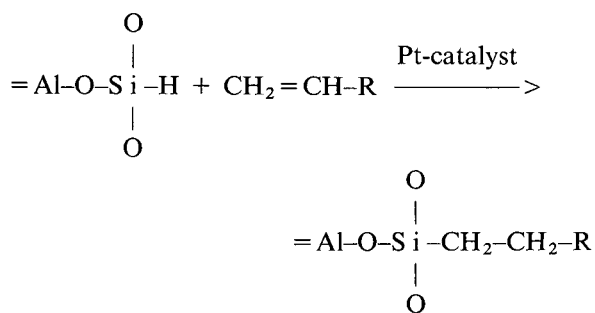
R' is generally a methyl group for typical monomeric and methoxy or ethoxy for polymeric stationary phases. However, no further work followed these initial reports. Another possibility involves physically coating alumina with a polystyrene-divinylbenzene copolymer, polybutadiene or polyoctadecylsilane [9]. These materials have excellent pH stability but often display strong retention, high column backpressures due to swelling in certain solvents and/or poorer chromatographic efficiency when compared to normal chemically bonded stationary phases [9]. Another approach for monomeric bonding can be accomplished by reacting organic phosphonic acids with alumina. This method leads to an =Al-O-P-R linkage at the surface. An octadecyl phase prepared by this approach was used in basic solvents (at pH values > 10) and with basic solutes [10]. However, no stability studies were done in order to determine the long-term reproducibility of these results. It was also noted that these linkages were unstable in phosphate buffer solutions. In another study, a variety of modification schemes involving Grignard reagents as well as organolithium and organoaluminum compounds were evaluated [11]. The results were not totally satisfactory but they certainly indicated that other methods of modification should be explored.

Recently it has been demonstrated that hydride intermediates on silica are a viable alternative to organosilane chemistry for producing bonded phases [12–14]. The final material contains a silicon-carbon bond at the surface which has been shown to have superior hydrolytic stability in comparison to the silicon-oxygen-silicon-carbon linkage that results when an organosilane reagent is used. The method involves forming a monolayer of silicon hydride on the surface which can then be reacted with a terminal olefin compound in the presence of a suitable catalyst to yield the final product. On silica, the hydride can be formed from either chlorination

of the surface followed by reduction with a species such as lithium aluminum hydride [12] or by reacting silica with triethoxysilane (TES) in an acidic medium [15]. Since the latter procedure is both faster and more efficient, it is the method of choice for producing the hydride intermediate. A similar approach for the synthesis of monomeric alumina-based stationary phases is reported here. The silicon hydride-modified alumina is prepared by silanization with TES in the presence of water, HCl as a catalyst and dioxane as the solvent:



Bonding of the organic moiety then follows by hydrosilylation of a terminal olefin on the hydride intermediate in the presence of a platinum catalyst:



From a practical point, the above method does involve a two-step process in contrast to the single silanization reaction utilized in the preparation of commercial chromatographic materials. Therefore, reproducibility in the synthetic process will be an ultimate concern when considering the usefulness of the proposed method. This first report presents the synthetic protocol for the proposed method as well as spectroscopic and preliminary chromatographic evaluation of the new material. Subsequent reports will give involve more rigorous chromatographic testing.

EXPERIMENTAL

Materials

Alumina (Biotage) with a mean particle size of 8 μm , a mean pore size of 334 \AA and a BET surface area of 49.0 m^2/g was dried overnight at 110°C under vacuum before use. In the synthetic procedures, TES (Huls America), 1-octene and 1-octadecene (Sigma) were used as received. The solutes used in the chromatographic testing were purchased (Aldrich) in the highest purity available. Water was purified on a Millipore filter system. All other mobile phases were of HPLC quality and synthetic materials were purchased in reagent grade. A commercial sample of C_{18} phosphonate alumina (Biotage) was used for comparison studies.

Synthetic procedures

Preparation of silanized alumina. Dried alumina (5 g) was placed in a 250-ml three-neck round-bottom flask with 110 ml of dioxane. The flask was placed in an oil bath at 80°C and then 5 ml of 3.1 M HCl was added while stirring. After several min 35 ml of TES (0.2 M in dry dioxane) in a self-equalizing funnel was added dropwise. This corresponds to a 10% excess of TES with respect to hydroxides on the alumina surface as determined by thermogravimetric analysis (TGA). The mixture was then refluxed for 5 h to ensure complete reaction of the available hydroxide groups [15]. After this period the TES alumina was washed successively twice with 100-ml portions of dioxane–water (80:20), dioxane and ether. The solid was then dried at room temperature for 4 h at atmospheric pressure followed by 1 h at 110°C under vacuum.

Preparation of C_8 and C_{18} alumina. The olefin (150 ml) and 1.00 ml of 50 mM dicyclopentadienyl platinum (II) in dry chloroform were placed in a three-neck round-bottom flask equipped with a condenser and a magnetic stirrer. The mixture was heated up to 70°C and maintained at this temperature until the solution became clear (at least 1 h). Then 5.0 g of hydride alumina (predried overnight) was added slowly by means of an addition funnel. After all the hydride alumina was in the flask, the solution temperature was raised to 85°C and maintained at this temperature for 96 h. The product was washed consecutively with 100-ml portions of toluene (4 times), dichloromethane (2 times) and diethyl

ether (2 times). The final product was first dried in air at room temperature for 12 h and then under vacuum at 110°C for 12 h.

Product evaluation and characterization

Spectroscopic and elemental analysis. All samples were analyzed by diffuse reflectance infrared Fourier transform (DRIFT) on a Perkin-Elmer Model 1800 spectrometer. Elemental analysis was performed on a Perkin-Elmer Model 240C Elemental Analyzer. TGA was done on a Perkin-Elmer Model 2 instrument. Differential scanning calorimetric (DSC) was done on a Perkin-Elmer Model 7 system. ^{13}C , ^{29}Si and ^{27}Al cross-polarization magic-angle spinning (CP-MAS) NMR spectra were obtained on a Bruker MSL 300 spectrometer. For ^{13}C and ^{29}Si , parameters similar to those reported in the literature were used [16]. For ^{27}Al , a recycle time of 5 s and a contact time of 5 ms required about 2000 scans to obtain the typical spectrum. Spectral simulation was done using the LINESIM program provided with the instrument. Analysis of silicon by atomic spectroscopy was done on a Beckman SMI Model III d.c. plasma spectrometer.

Stability studies. A methanol–water (0.1 M pH 7 phosphate buffer) (50:50) was used as the mobile phase. A test mixture (theophylline, *p*-nitroaniline, methylbenzoate, phenetol and *o*-xylene) was injected after each 100 column volumes of mobile phase.

Chromatographic studies. The bonded aluminas were packed into a 150 \times 4.6 mm I.D. stainless-steel column using a pneumatic amplification pump (Haskel) with methanol as the driving solvent. The instrumentation consisted of a Hewlett-Packard Model 1050 HPLC equipped with quaternary solvent delivery, an autosampler, a variable wavelength detector and a Chemstation for data analysis.

RESULTS AND DISCUSSION

In order for efficient silanization to occur on the alumina surface, it is necessary to know reasonably well the number of hydroxides per unit area. This can be determined by TGA analysis which gives a value of about 40 $\mu\text{mol}/\text{m}^2$. This value is certainly high when compared to most common chromatographic silicas which have about 8 $\mu\text{mol}/\text{m}^2$. However, it has been shown [15] that certain silicas (Vy-

dac TP, The Separations Group) sometimes give values in excess of $40 \mu\text{mol}/\text{m}^2$ for hydroxide determination by TGA and this has been attributed to either a large number of micropores and/or some tightly held water that is not easily removed during the initial heating to 110°C although the latter is unlikely under the drying condition used [17]. Since it is not known whether all hydroxyls measured by TGA will react during the silanization process, the nominal 10% excess of reagent used in the reaction may actually represent a considerably greater value.

The success of the silanization process can most easily be evaluated by DRIFT analysis. Fig. 1A is the spectrum of bare alumina which can be compared to Fig. 1B of the hydride-modified alumina

showing the strong Si-H stretching band near 2260 cm^{-1} . However, the position and width of the band are constant even as the extent of silanization is varied. The total amount of silane on the surface is determined by placing the material in strong base (0.1 M NaOH), heating and stirring for several h in order to strip off the silicon layer(s). Analysis by plasma emission spectroscopy results in a value of $15.1 \mu\text{mol}/\text{m}^2$ of Si on the surface. Only 38% of the total hydroxides as determined by TGA apparently reacted. Therefore, the unreacted OH groups probably represent hydroxides which are inaccessible to the TES because of steric considerations [17].

A much better indication concerning the nature of the hydride-modified material can be obtained

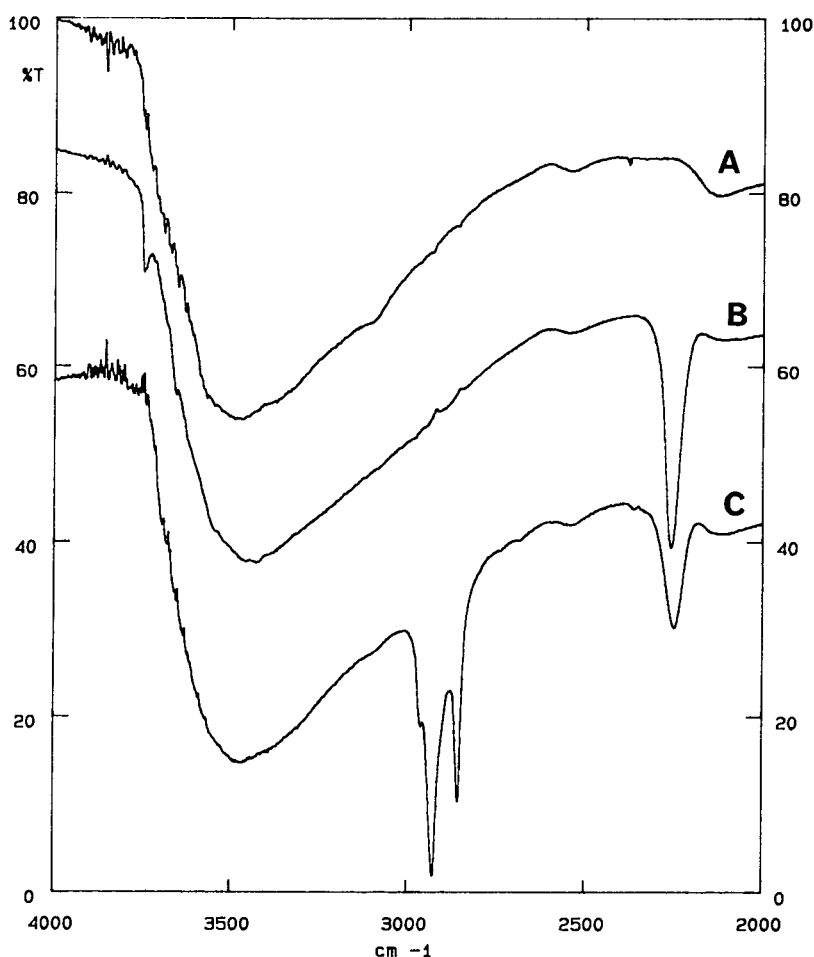


Fig. 1. DRIFT spectra of alumina materials: (A) bare alumina, (B) hydride alumina and (C) reaction product of hydride alumina with 1-octadecene.

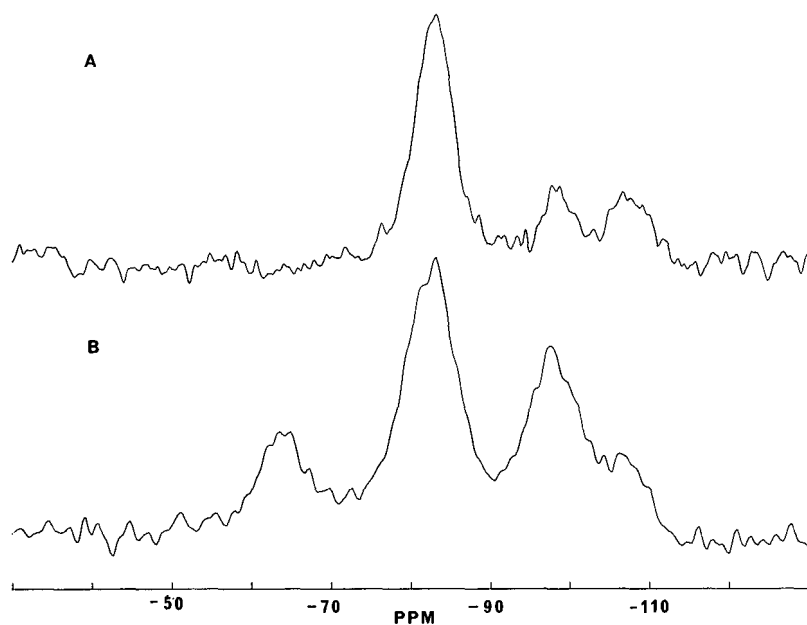


Fig. 2. ^{29}Si CP-MAS-NMR spectra of alumina materials: (A) hydride alumina and (B) reaction product of hydride alumina with 1-octadecene.

from the ^{29}Si CP-MAS-NMR spectrum. Fig. 2A shows a typical spectrum of an alumina following reaction with TES. The major peak at -85 ppm can be readily assigned to the Si–H group. However, two other minor peaks are also present in the spectrum. By analogy to spectra taken on silica, the peak at -110 ppm (Q_4) can be assigned to a silicon with four siloxane bonds while the peak at -100 ppm (Q_3) can be assigned to a silicon that has three siloxane bonds and one hydroxide group. These resonances are not part of any expected monolayer or multilayer structure since each silicon atom must have a hydride attached to it. Therefore the presence of Q_4 and Q_3 resonances must be due to either impurities in the starting reagent or some subsequent decomposition of the hydride-modified surface. Additional experiments are currently underway to study this problem. Despite these unknown aspects of the hydride surface, it was decided to try the olefin additions and test the product phases.

Both 1-octene and 1-octadecene were catalytically bonded to the hydride-modified material. Elemental analysis of the two products gave coverages of 5.5 and $4.4 \mu\text{mol}/\text{m}^2$ for the C_8 and C_{18} bonded phases, respectively. This represents reaction of

36% and 29% of the available hydrides for the two materials. Fig. 1C is a typical infrared spectrum of a product phase from the reaction of 1-octadecene with the hydride alumina. The strong bands between 2800 and 3000 cm^{-1} are the expected C–H stretching vibrations for the bonded alkyl moiety. The appearance of the C–H bands is accompanied by a diminishing of the Si–H band at 2260 cm^{-1} , which is expected when the hydride reacts with the olefin.

The success of the bonding reaction can also be confirmed by CP-MAS-NMR spectroscopy. Fig. 2B shows the ^{29}Si spectrum of the C_{18} bonded phase. In comparison to the hydride material, an additional peak at about -65 ppm is observed which can be attributed to the Si–C linkage formed in the bonding process. As expected a decrease in the signal intensity of the Si–H peak near -85 ppm occurs. The presence of the siloxane species (Q_4 and Q_3), as evidenced by the peaks at -110 and -100 ppm, are even more prominent in this spectrum. It is unclear whether there is an actual increase in intensity of these peaks, or as is more likely, their relative intensity compared to the other peaks in the spectrum has increased. When compared to the

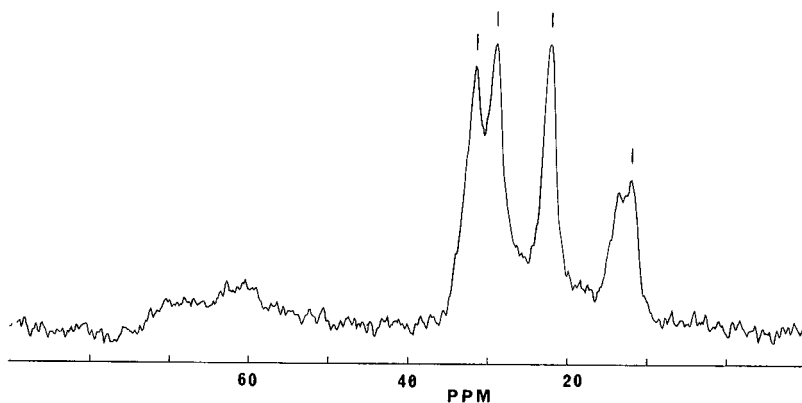


Fig. 3. ^{13}C CP-MAS-NMR spectrum of product from the reaction of hydride alumina with 1-octene.

spectrum of hydride material, the Q_3 peak has apparently increased relative to the Q_4 peak. Fig. 3 shows the ^{13}C CP-MAS spectrum of the octyl material which also verifies the bonding of the alkyl via olefinic addition. The peak positions in this spectrum as well as that of the C_{18} are identical to those obtained for bonding similar species to silica surfaces [16].

Finally, the ^{27}Al CP-MAS-NMR spectrum provides additional evidence to characterize the modification of the surface. Fig. 4A is the ^{27}Al spectrum of the C_{18} modified alumina. Similar to other reports in the literature on aluminas [18,19], the spec-

trum consists of two major peaks: the smaller peak at about 60 ppm represents tetrahedrally (T_d) coordinated aluminum ions and the peak at 1 ppm represents octahedrally (O_h) coordinated aluminum ions. The T_d resonance is about 18% of the total peak area which is in good agreement with the 15–20% tetrahedrally coordinated Al^{3+} found in most hydrated aluminas. Fig. 4B is the simulated spectrum while Fig. 4C represents the individual components in the simulated spectrum. Whether the three peaks in the simulated O_h portion of the spectrum are due to three different Al^{3+} environments or whether this just represents an increased distortion of octahedral symmetry by modification that results in enhanced quadrupolar effects (for ^{27}Al , $I = 5/2$) due to a non-symmetric electric field gradient is not clear. However, in the absence of effective cross-polarization (CP) the distortion in the octahedral peaks is much less indicating that species being observed in the CP spectrum are close to the surface where all of the available hydrogens are located. Table I is a comparison of the various peak areas for the bare, hydride, C_{18} and commercial aluminas. The areas of peaks 1 (T_d) and 2 remain relatively constant within experimental error except for the C_{18} sample which appears to decrease slightly while peak 3 decreases. Peak 4 is not present for the bare alumina, is small for the hydride alumina species and increases further for the C_{18} alumina. The appearance of peak 4 can be interpreted as the formation of new species (hydride or alkyl bonded moiety) or by an increased distortion of the O_h symmetry during the modification process.

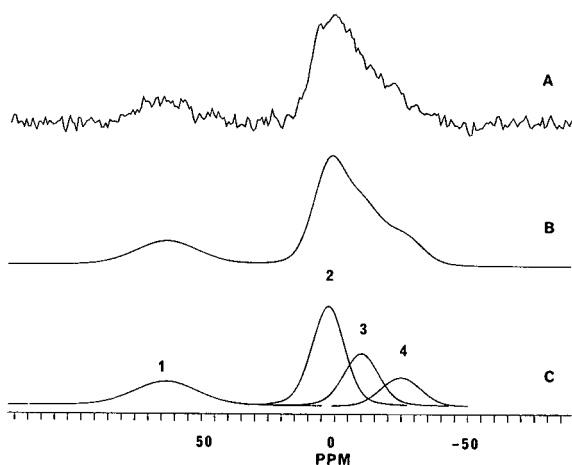


Fig. 4. ^{27}Al CP-MAS-NMR spectra of product from the reaction of hydride alumina with 1-octadecene: (A) experimental spectrum, (B) simulated spectrum and (C) simulated spectrum with individual components.

TABLE I

RELATIVE PEAK AREAS FOR SIMULATED COMPONENTS IN ^{27}Al CP-MAS-NMR SPECTRA OF VARIOUS ALUMINAS

Sample	Peak number ^a			
	T _d		O _h	
	1	2	3	4
Bare alumina	0.18	0.48	0.33	-
Hydride alumina	0.16	0.52	0.28	0.05
C ₁₈ alumina	0.20	0.43	0.24	0.14
Biotage C ₁₈ (phosphonate ester)	0.17	0.51	0.24	0.08

^a Refer to Fig. 4 for peak labeling. Error in relative peak areas, ± 0.03 .

Fig. 5 shows the DSC/air curve of the hydride modified alumina. There is a single distinct peak for the thermooxidative process which has a maximum between 520–530°C. This can be compared to similar peaks for the polyhydrosiloxane (polymerization product of TES in the absence of alumina) which occurs at 365°C and the peak for hydride sil-

ica which occurs at 430–450°C [15]. Two conclusions can be drawn from this result. First, it is clear from the large shift in the peak for the thermooxidative process that the hydride surface is chemically bonded to the alumina surface as opposed to being a physically adsorbed layer of polymerized material. Second, the shift to an even higher temperature for alumina when compared to silica indicates a greater thermal stability for the hydride-modified silica. This may be useful when comparing the relative chemical stabilities under aggressive mobile phase conditions.

Since the spectroscopic studies indicated both successful formation of a hydride surface and subsequent hydrosilation with an olefin, some preliminary chromatographic experiments were undertaken in order to determine the retention properties of these materials. A test mixture consisting of theophylline, *p*-nitroaniline, methylbenzoate, phenetol and *o*-xylene was run on both the C₁₈ alumina synthesized from the hydride intermediate and a commercial C₁₈ alumina. The chromatograms are shown in Fig. 6A and B, respectively. In general separation is good by both materials with slightly more asymmetry, except for theophylline, in the peaks for the phosphonate column. Table II sum-

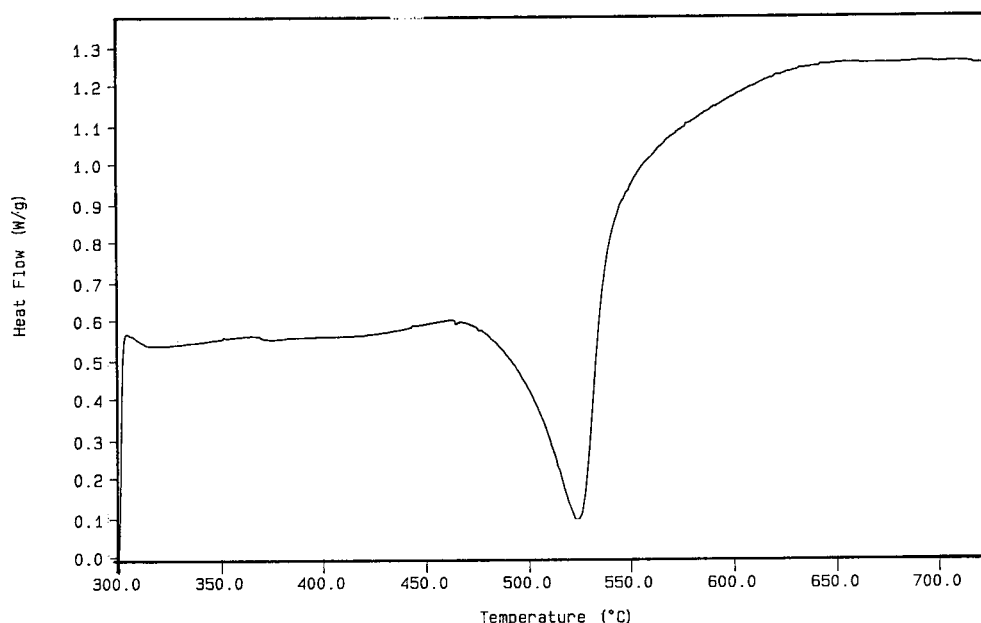


Fig. 5. DSC curve for the thermooxidation of hydride-modified alumina.

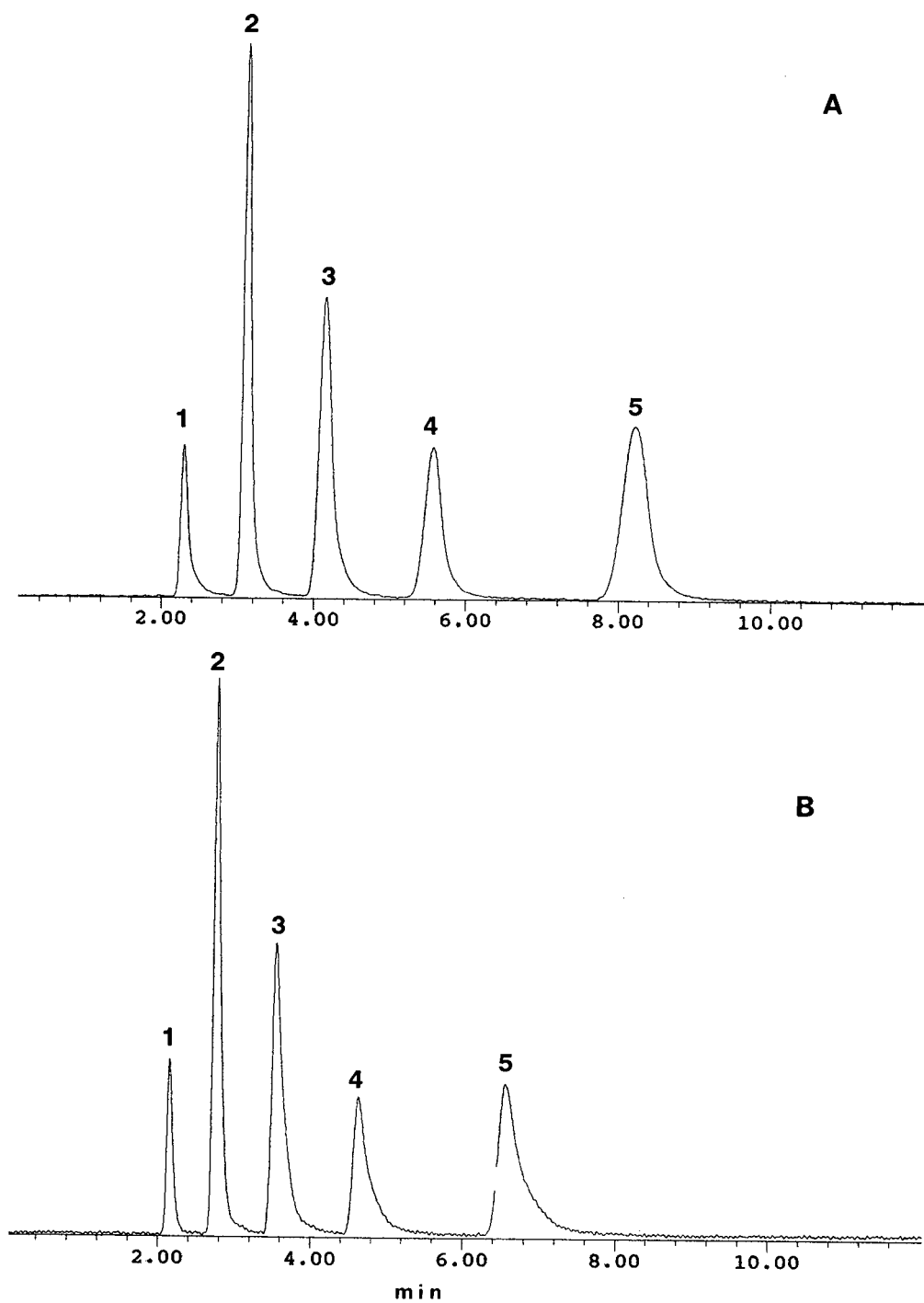


Fig. 6. Chromatogram of test mixture for reversed-phase behavior: (A) C_{18} from hydride and (B) phosphonate C_{18} . Mobile phase: acetonitrile-water (50:50). Peaks: 1 = theophylline; 2 = *p*-nitroaniline; 3 = methylbenzoate; 4 = phenetol; 5 = *o*-xylene.

TABLE II

EFFICIENCIES AND PEAK SYMMETRIES FOR HYDROSILATION AND PHOSPHONATE ALUMINA C₁₈ COLUMNS

Peak ^a	Efficiency	Asymmetry factor
<i>Hydrosilation C₁₈ column</i>		
1	860	2.15
2	3070	1.40
3	1500	1.60
4	1930	1.35
5	2000	1.25
<i>Phosphonate C₁₈ Column</i>		
1	1880	2.10
2	1890	2.50
3	1150	2.70
4	1030	2.85
5	950	3.10

^a Refer to Fig. 6 for peak identification.

marizes the efficiency (calculated with a base at 10% of the peak height) for both types of columns. Data for the C₈ column from the hydride intermediate gave similar results to the C₁₈ but with lower capacity factors. Both the C₈ and C₁₈ phases synthesized in this study were exposed to phosphate containing mobile phases at neutral pH with no evidence of deterioration in chromatographic performance or loss of bonded material as measured by elemental analysis.

In conclusion, it appears that the silanization/olefin addition procedure is a viable approach to the synthesis of various alkyl-bonded stationary phases on alumina. The product shows no evidence of decomposition in the presence of phosphate, as is reported for the commercial material. Preliminary chromatographic results indicate satisfactory separation under reversed-phase conditions where peak symmetry is good. Future studies will involve the nature of the hydride layer and its effect on chromatographic properties as well as the stability of the

bonded material under more severe mobile phase conditions.

ACKNOWLEDGEMENTS

Acknowledgement is made to the Donors of The Petroleum Research Fund, administered by the American Chemical Society, for partial support of this research as well as the Camille and Henry Dreyfus Scholar (JJP)/Fellow Program for Undergraduate Institutions. Biotage, Inc. generously donated the phosphonate-based C₁₈ material as well as the bare alumina used for the syntheses described in this publication.

REFERENCES

- 1 K. K. Unger, *Porous Silica - Its Properties and Use as Support in Column Liquid Chromatography (Journal of Chromatography Library, Vol. 16)*, Elsevier, Amsterdam, 1979.
- 2 R. K. Iler, *The Chemistry of Silica-Solubility, Polymerization, Colloid and Surface Properties, and Biochemistry*, Wiley, New York, 1979.
- 3 J. J. Kirkland, J. L. Glach and R. D. Farlee, *Anal. Chem.*, 61 (1989) 2.
- 4 R. D. Stout and J. J. DeStafano, *J. Chromatogr.*, 326 (1985) 63.
- 5 Y. B. Yang and M. Verzele, *J. Chromatogr.*, 387 (1987) 197.
- 6 J. Kohler, *Chromatographia*, 21 (1986) 573.
- 7 R. Abuelafiya and J. J. Pesek, *J. Liq. Chromatogr.*, 12 (1989) 1571.
- 8 J. H. Knox and A. Pryde, *J. Chromatogr.*, 112 (1975) 171.
- 9 U. Bien-Vogelsang, A. Deege, H. Figge, J. Kohler and G. Schomberg, *Chromatographia*, 19 (1984) 170.
- 10 J. E. Haky, S. Vemulapalli and L. F. Wieserman, *J. Chromatogr.*, 505 (1990) 307.
- 11 J. J. Pesek and H. D. Lin, *Chromatographia*, 28 (1989) 565.
- 12 J. E. Sandoval and J. J. Pesek, *Anal. Chem.*, 61 (1989) 2067.
- 13 J. E. Sandoval and J. J. Pesek, *Anal. Chem.*, 63 (1991) 2634.
- 14 J. E. Sandoval and J. J. Pesek, *US Pat.* 5 017 540 (1991).
- 15 C. H. Chu, E. Jonsson, M. Auvinen, J. J. Pesek and J. E. Sandoval, *Anal. Chem.*, in press.
- 16 B. Buszewski, *Chromatographia*, 28 (1989) 574.
- 17 J. Kohler, D. B. Chase, R. D. Farlee, A. J. Vega and J. J. Kirkland, *J. Chromatogr.*, 352 (1986) 275.
- 18 V. M. Mastikhin, O. P. Krivoruchko, B. P. Zolotovskii and R. A. Buyanov, *React. Kinet. Catal. Lett.*, 18 (1981) 117.
- 19 C. S. John, N. C. M. Alma and G. R. Hays, *Appl. Catal.*, 6 (1983) 341.

Examination of some reversed-phase high-performance liquid chromatography systems for the determination of lipophilicity

D. P. Nowotnik, T. Feld and A. D. Nunn

Bristol-Myers Squibb Pharmaceutical Research Institute, 1 Squibb Drive, P.O. Box 191, New Brunswick, NJ 08903-0191 (USA)

(First received March 23rd, 1992; revised manuscript received September 29th, 1992)

ABSTRACT

Three reversed-phase systems [based on the divinylbenzene–styrene copolymer (PRP-1), the C₁₈-derivatized divinylbenzene–styrene copolymer (ACT-1), and the Nucleosil C₈ columns] were studied for their suitability in lipophilicity determination. Acetonitrile–water was selected as the mobile phase. Correlation between log *k'* and log *P*_{eye} for both the PRP-1 and Nucleosil C₈ systems was superior to the correlation between log *k'* and either log *P*_{oct} or log *P*_{cyc} (oct = octanol; cyc = cyclohexane) on the ACT-1 column. On the PRP-1 and Nucleosil columns, correlation between log *k'* and log *P*_{oct} was much improved when test compounds were grouped into classifications of non-H bonding, single amphiprotics (alcohols, phenols, amides) or double amphiprotics. Although the PRP-1 system gave broad peaks with lipophilic substrates, there was good correlation between log *k'* values on the Nucleosil silica-based reversed-phase system and the polymer PRP-1 system, indicating that either is suitable for the determination of lipophilicity.

INTRODUCTION

While the lipophilicity index based on octanol–water partitioning (log *P*_{oct}) is well established in studies of quantitative structure–activity relationships [1,2], the lack of convenience and reliability of the traditional “shake-flask” method for log *P*_{oct} determination [3,4] has encouraged investigations into alternative methods. Since the mid-1970s, reversed-phase HPLC has been investigated for this purpose, and there have been several reviews of this area of research [5–11]. Generally, studies have evaluated the correlation between measured (or determined) lipophilicity and the logarithm of the capacity factor (*k'*).

The goal for many has been the development of a single HPLC system which will provide a direct measure of reliable log *P*_{oct} values for any given test

compound. A wide variety of reversed-phase HPLC systems have been examined for this purpose. For one HPLC system to mimic partitioning in octanol–water it is necessary for the hydrophobic and hydrophilic interactions in the stationary and mobile phases to be similar to those interactions in (respectively) the octanol and aqueous bulk phases. Retention in reversed-phase packing materials is primarily attributed to hydrophobic interaction, whereas partitioning into the octanol is effected by both hydrophobic and hydrogen bonding interactions.

Methanol appears to be the preferred organic modifier for the determination of lipophilicity by reversed-phase HPLC [7]. It has been suggested that ODS systems eluted with methanol–water provide good log *k'*–log *P*_{oct} correlations as methanol coats the reversed phase, giving it the necessary hydrogen-bonding properties to act as an octanol mimic (for example refs. 12 and 13). A high proportion of methanol in the eluent seems to be required to obtain a good correlation between log *k'* and log *P*_{oct} [13,14], although this is not always the case (for ex-

Correspondence to: D. P. Nowotnik, Bristol-Myers Squibb Pharmaceutical Research Institute, 1 Squibb Drive, P.O. Box 191, New Brunswick, NJ 08903-0191, USA.

ample, ref. 15). Using either methanol or acetonitrile as the organic modifier, there have been many reports where $\log k'$ in reversed-phase HPLC correlates well with the $\log P_{\text{oct}}$ values of a set of congeners (for example, refs. 16–20). However, correlation can be poor when test compounds are non-congeners (for example, refs. 21–25). Thus, it would appear that good correlation between $\log k'$ and $\log P_{\text{oct}}$ (when non-congeners are examined) may be restricted to certain combinations of stationary phase–mobile phase.

In those cases where it is necessary to group congeners to achieve good correlation between $\log k'$ and $\log P_{\text{oct}}$ the classifications were typically non-H bonders, H-bond acceptors, and amphiprotics. Taking non-H bonders as the reference, then H-bond acceptors can show greater binding to ODS columns than might be expected from their $\log P$ values [26–29] although amine additives can, in part, correct this deviation by blocking free silanol groups [30–32]. Amphiprotics generally display $\log k'$ values which are lower than predicted from their $\log P_{\text{oct}}$ values [27,33–35], presumably resulting from the lower contribution of H-bonding to partitioning into the lipophilic stationary phase compared to that found in the octanol bulk phase.

Kaliszan [10] and Braumann [7] have suggested that the search for the perfect HPLC system for determining $\log P_{\text{oct}}$ values might be a futile exercise. For quantitative structure–activity relationships (QSARs), reversed-phase HPLC $\log k'$ values could be used directly, particularly as the interactions in “dynamic” reversed-phase HPLC might provide a better model of solute interactions with biomembranes than “static” liquid–liquid partitioning [5,36,37]. There are now many examples of QSAR correlations which use $\log k'$ as the measure of lipophilicity [7,10,38], and correlations can be at least as good or better than provided by use of $\log P_{\text{oct}}$ values [39].

One potential problem to the use of $\log k'$ lipophilicity values is that, unlike $\log P_{\text{oct}}$, the scale is not universal; *i.e.* any given $\log k'$ value is specific to one HPLC system, which cannot readily be reproduced elsewhere with certainty. Braumann [7] examined six ODS columns, and found that $\log k'_w$ values for any given test substrate were similar on all systems, indicating that $\log k'_w$ might be used as a universal indicator of lipophilicity. However, other

studies have shown that $\log k'_w$ is not universal [40], which is not surprising given the diverse characteristics of ODS columns from different commercial sources [41]. Therefore, while $\log k'$ values may be used directly for QSARs studies, in reporting these data, it is still necessary to provide some data on the calibration of HPLC systems used in lipophilicity determination so that the $\log k'$ values and conclusions from the QSARs may be utilized by other researchers.

Our interest in lipophilicity determination stems from the necessity of developing structure–distribution relationships (SDRs) for the discovery of new $^{99\text{m}}\text{Tc}$ radiopharmaceuticals [42]. Problems of stability and purity with many $^{99\text{m}}\text{Tc}$ compounds indicate that an HPLC method for lipophilicity determination is preferable over the “shake-flask” method. In developing an HPLC method for the determination of lipophilicity of $^{99\text{m}}\text{Tc}$ radiopharmaceuticals, two groups independently selected the Hamilton PRP-1 column [43,44] calibrated to provide $\log P$ values. More recently, $\log k'$ values were used directly [45]. This column contained one of the first commercially available polymer-based reversed-phase packing materials. As it does not contain any uncapped silanol groups, the PRP-1 resin should not display any selective binding of basic compounds, as seen with most silica-based reversed-phase columns.

During the initial evaluation of the PRP-1 column with highly lipophilic compounds, Feld and Nunn [44] determined that use of aqueous methanol as mobile phase resulted in unacceptably broad peaks and long retention times. Feld and Nunn found that acetonitrile was a superior organic modifier for use with this column, and selected a mobile phase of acetonitrile–ammonium acetate buffer (65:35) [44]. This system was calibrated using standard organic compounds and $\log P$ data from the MedChem database [46]. However, there are some reported disadvantages of the PRP-1 packing material (low plate number and excessive resin swelling) [47], and π – π interactions with solutes may provide an additional retention mechanism [11]. As a result, we decided to investigate the potential of a other reversed-phase stationary phases (retaining the acetonitrile–ammonium acetate buffer mobile phase) for the determination of lipophilicity. We report here the results of studies using the divinylbenzene–

styrene copolymer (PRP-1), the C18-derivatized divinylbenzene–styrene copolymer (ACT-1), and the Nucleosil C8 columns for this purpose. Log k' values of test compounds obtained on these systems are compared to log P_{oct} and log P_{cyc} values for these compounds, obtained from the MedChem database.

EXPERIMENTAL

The following column–solvent combinations were examined (all systems tested used isocratic eluents):

(a) Interaction ACT-1 150×4.6 mm, $10 \mu\text{m}$ resin, eluted with acetonitrile–pH 4.6 0.1 M ammonium acetate buffer (70:30), at 0.75 ml/min.

(b) Nucleosil C₈ 150×4.6 mm, $5 \mu\text{m}$ resin, eluted with acetonitrile–pH 4.6 0.1 M ammonium acetate buffer (60:40), at 1.5 ml/min.

(c) Hamilton PRP-1 150×4.1 mm, $10 \mu\text{m}$ resin, eluted with acetonitrile–pH 4.6 0.1 M ammonium acetate buffer (65:35), at 2.0 ml/min.

The HPLC system used consisted of two Rainin Rabbit HPX pumps, controlled by a personal computer operating Gilson 712 software. The system was fitted with a Kratos UV detector, operating at 210, 230 or 254 nm (as appropriate for the analyte). The system allowed the moment of sample injection to be detected by the software, and sample retention times were provided automatically by the software on data analysis. The retention time of sodium nitrate (detected at 210 nm) was used as the column dead-time. All retention times were determined in triplicate, and the mean used to determine log k' .

HPLC columns were obtained from Alltech. HPLC-grade acetonitrile was obtained from J.T. Baker. Water was obtained from a Milli-Q purification system. All solvents were filtered and degassed prior to use.

Ammonia solution and glacial acetic acid were obtained from Mallinckrodt. pH 4.6 0.1 M Ammonium acetate buffer was prepared by dissolving 6.75 ml of concentrated ammonium hydroxide solution and 11.5 ml of glacial acetic acid in 500 ml of water, and diluting to 2 l.

All test compounds were obtained from Aldrich.

Measured octanol–water partition coefficients were obtained from the MedChem database [46], as log P^* (the most reliable determined value of log

P_{oct}) values. For three compounds (N,N-diethyl-*m*-toluamide, triphenylmethane and 2,6-diphenylphenol) log P^* values were unavailable, so cLog P (the value of log P_{oct} calculated by MedChem software) values were used instead. The values are listed in Table I.

Measured cyclohexane–water partition ratios were also obtained from the MedChem database, and are listed as log P_{cyc} . If several log P_{cyc} values were given in the MedChem database, the mean value was used (excluding any values which deviated substantially from the others). In some cases, log P_{cyc} values were calculated from given C₆–C₈ or C₁₈ *n*-alkane–water partition ratios, using the conversions derived by Seiler [48].

RESULTS AND DISCUSSION

Determination of lipophilicity with the PRP-1 column

As indicated earlier, our original decision to use the PRP-1 column for lipophilicity determination was based upon a preference to have a packing material devoid of free silanol groups (which can provide mechanisms for the retention of amines in addition to partitioning). A polymer-based column appeared to be suitable for these studies [16,49], even though low plate number and resin swelling problems were reported for the PRP-1 packing material. Good resolution between peaks was not a requirement of the study, and, provided that a single isocratic eluent was used, resin swelling would not be an issue (*i.e.* the void volume would remain constant). However, for the examination of lipophilic compounds (log $P_{\text{oct}} > 2$), a high proportion of an organic modifier was required, to elute such compounds in a reasonably short time. Feld and Nunn [44] elected to use acetonitrile–aqueous ammonium acetate (65:35) after evaluating a number of solvent combinations. This percentage of organic modifier is within the recommended guidelines (>25% water) which followed a multi-center European study on the determination of log P_{oct} by HPLC [50], and appeared to provide reliable log P_{oct} values based on calibration curves containing relatively few example compounds [44]. Feld and Nunn [44] observed two calibration curves; one for compounds without hydroxyl groups, and one for compounds which contained an hydroxyl group.

TABLE I

LOG P_{oct} AND LOG P_{cyc} VALUES OF TEST COMPOUNDS USED IN THIS STUDYn/a = Log P value not available

Compound	log P_{oct}	log P_{cyc}	Compound	log P_{oct}	log P_{cyc}
Acetanilide	1.16	-1.51	Ethyl acetate	0.73	0.34
<i>p</i> -Anisidine	0.95	-0.40	Ethylbenzene	3.15	2.76
Anisole	2.11	2.10	4-Ethylphenol	2.58	0.38
Benzaldehyde	1.48	1.24	Formamide	-1.51	-5.06
Benzamide	0.64	-1.28	4-Hydroxybenzamide	0.33	n/a
Benzene	2.13	2.38	2-Hydroxybenzyl alcohol	0.73	n/a
Benzophenone	3.18	3.29	2,6-Lutidine	1.68	0.67
Benzyl alcohol	1.10	-0.70	Methylene chloride	1.25	n/a
4-Chloro-3-methylphenol	3.10	0.15	1-Naphthol	2.84	0.54
4-Chloroaniline	1.83	0.64	2-Naphthol	2.70	0.09
<i>o</i> -Dichlorobenzene	3.38	3.47	Naphthalene	3.30	3.49
N,N-Diethyl- <i>m</i> -toluamide	2.31	n/a	Phenol	1.46	-0.81
1,5-Dihydroxynaphthalene	1.82	-2.23	N-Phenyl benzylamine	3.13	n/a
N,N-Dimethylbenzamide	0.62	n/a	2-Phenylphenol	3.09	1.71
1,2-Dichloroethane	1.48	1.67	Pyridine	0.65	-0.41
5,5-Diphenylhydantoin	2.47	-2.34	Quinoline	2.03	1.26
Diphenylmethane	4.14	n/a	Resorcinol	0.80	-3.79
Diphenylmethanol	2.67	n/a	Toluene	2.73	3.15
2,6-Diphenylphenol	5.25	n/a	Triphenylmethane	5.80	n/a
β -Estradiol	4.01	-0.02	Uracil	-1.07	n/a

We have extended the calibration of the PRP-1 system by measuring the log k' of more compounds, particularly compounds containing single hydroxyl and amide groups, and compounds with two amphiprotic substituents. The log k' values obtained are listed in Table II.

Linear regression analysis of the data was performed in plotting all log k' values against log P_{oct} , log P_{cyc} and log k' values of compounds separated into classes of non-H bonders, single amphiprotics (compounds with one hydroxyl or amide substituent), and double amphiprotics. Compounds with

TABLE II

LOG k' VALUES DETERMINED ON THE PRP-1 COLUMN

Compound	log k'	Compound	log k'
Acetanilide	-0.24	2,6-Diphenylphenol	1.30
Anisole	0.63	β -Estradiol	0.14
Benzamide	-0.49	Ethyl acetate	-0.05
Benzophenone	0.96	4-Ethylphenol	0.13
Benzyl alcohol	-0.15	Formamide	-1.11
4-Chloroaniline	0.33	4-Hydroxybenzamide	-0.94
<i>o</i> -Dichlorobenzene	0.94	Methylene chloride	0.27
1,2-Dichloroethane	0.32	Naphthalene	1.15
1,5-Dihydroxynaphthalene	-0.24	1-Naphthol	0.38
5,5-Diphenylhydantoin	-0.18	Phenol	-0.06
Diphenylmethane	1.13	Toluene	0.76
Diphenylmethanol	0.37	Uracil	-1.35

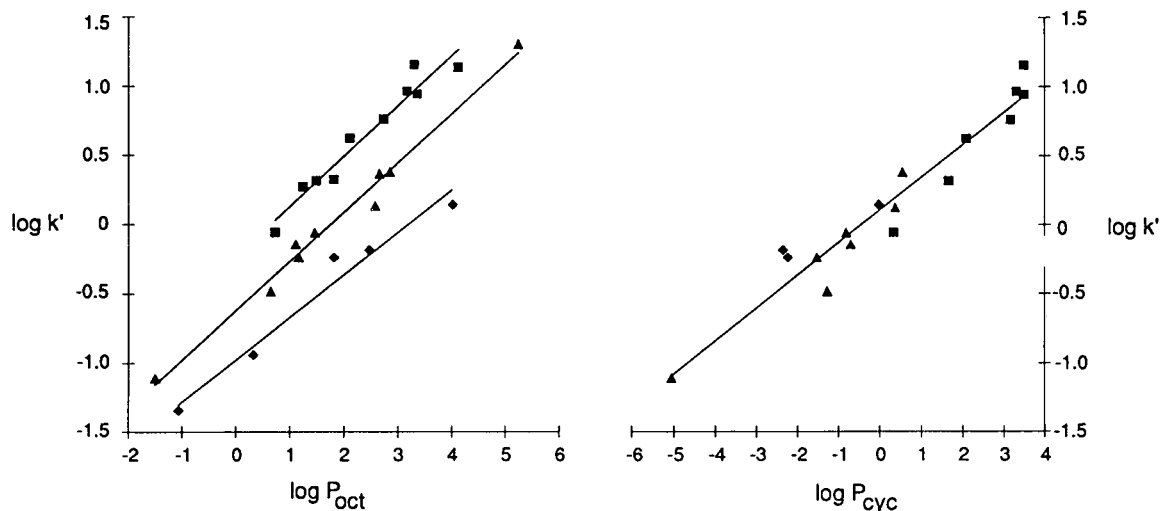


Fig. 1. Graphs of $\log k'$ vs. $\log P$ from data obtained on the PRP-1 column. ■ = Non-hydrogen bonders; ▲ = single amphiprotics; ◆ = double amphiprotics.

two amphiprotic substituents were selected such that minimal intramolecular H-bonding could occur. The results are as follows:

$$\begin{aligned} \log k' \text{ vs. } \log P_{\text{oct}} \text{ (all compounds)} \\ \log k' = 0.392 \log P_{\text{oct}} - 0.616; R = 0.879; \\ n = 24 \end{aligned} \quad (1)$$

$$\begin{aligned} \log k' \text{ vs. } \log P_{\text{cyc}} \text{ (all compounds)} \\ \log k' = 0.236 \log P_{\text{cyc}} + 0.106; R = 0.966; \\ n = 17 \end{aligned} \quad (2)$$

$$\begin{aligned} \log k' \text{ vs. } \log P_{\text{oct}} \text{ (matched set}^a) \\ \log k' = 0.352 \log P_{\text{oct}} + 0.525; R = 0.801; \\ n = 17 \end{aligned} \quad (3)$$

$$\begin{aligned} \log k' \text{ vs. } \log P_{\text{oct}} \text{ (non-H bonders)} \\ \log k' = 0.364 \log P_{\text{oct}} - 0.236; R = 0.971; \\ n = 10 \end{aligned} \quad (4)$$

$$\begin{aligned} \log k' \text{ vs. } \log P_{\text{oct}} \text{ (all amphiprotics)} \\ \log k' = 0.347 \log P_{\text{oct}} - 0.764; R = 0.937; \\ n = 14 \end{aligned} \quad (5)$$

$$\begin{aligned} \log k' \text{ vs. } \log P_{\text{oct}} \text{ (single amphiprotics)} \\ \log k' = 0.356 \log P_{\text{oct}} - 0.625; R = 0.993; \\ n = 9 \end{aligned} \quad (6)$$

$$\begin{aligned} \log k' \text{ vs. } \log P_{\text{oct}} \text{ (double amphiprotics)} \\ \log k' = 0.306 \log P_{\text{oct}} - 0.977; R = 0.966; \\ n = 5 \end{aligned} \quad (7)$$

The overall correlation between $\log k'$ vs. $\log P_{\text{cyc}}$ is far better than the correlation for $\log k'$ vs. $\log P_{\text{oct}}$ (eqns. 2 and 3). This is to be expected since hydrophobicity is the predominant factor influencing partitioning into both the stationary phase of this HPLC system, and the cyclohexane bulk phase, whereas partitioning into octanol, as described earlier, is influenced by both hydrophobic and H-bonding interactions between solute and solvent. When separated into amphiprotic (hydroxyl or primary–secondary amide) and non-H-bonding compounds, correlations between $\log k'$ and $\log P$ were improved, but it was clear that compounds containing two amphiprotic groups fell into a separate class to those containing a single amphiprotic substituent. Fig. 1 shows the $\log k'$ – $\log P$ data graphed, with the separate linear regression lines for the three classes of compounds examined, using $\log P_{\text{oct}}$ as the independent variable.

Determination of lipophilicity with the ACT-1 column

ACT-1 packing material is a C_{18} derivatised divinylbenzene–styrene copolymer which is claimed by the manufacturers to provide better resolution and

^a This set contains only those compounds which appear in the $\log k'$ vs. $\log P_{\text{cyc}}$ (all) set. The matched set was separated so that the linear regression analyses between $\log P_{\text{oct}}$ and $\log P_{\text{cyc}}$ can be compared directly.

TABLE III
LOG k' VALUES DETERMINED ON THE ACT-1 COLUMN

Compound	log k'	Compound	log k'
Acetanilide	-0.45	Ethyl acetate	-0.35
Anisole	0.21	4-Ethylphenol	-0.05
Benzamide	-0.68	Formamide	-1.15
Benzene	0.29	2-Hydroxybenzyl alcohol	-0.52
Benzophenone	0.48	2,6-Lutidine	-0.38
Benzyl alcohol	-0.41	Phenol	-0.27
4-Chloro-3-methylphenol	0.11	2-Phenylphenol	0.27
4-Chloroaniline	-0.04	Quinoline	0.27
<i>o</i> -Dichlorobenzene	0.63	Resorcinol	-0.52
N,N-Dimethylbenzamide	-0.48	Toluene	0.43
Diphenylmethanol	0.04	Uracil	-1.24

peak shapes than underivatized divinylbenzene–styrene copolymer (e.g. PRP-1). Lambert and co-workers [51,52] have studied the use of this packing for lipophilicity determinations in a 5-cm column (which is not commercially available), and found that, with a methanol–water eluent, log k' values were highly correlated to the log P_{alkane} coefficients of a diverse set of test samples. Our results using the ACT-1 column are shown in Table III.

A disadvantage of the ACT-1 column is the flow-rate restriction for acetonitrile–water mixtures of 0.75 ml/min. At this flow-rate, sample retention times are generally much longer on the 15-cm ACT-1 column than on the 15-cm PRP-1 column running at 2 ml/min. Therefore, while the claims for ACT-1 (better peak shape than PRP-1 columns) may be justified at equivalent flow-rates, the low flow restriction is undesirable when dealing with highly lipophilic compounds. The results of linear regression analysis were as follows:

$$\begin{aligned} &\log k' \text{ vs. } \log P_{\text{oct}} \text{ (all compounds)} \\ &\log k' = 0.361 \log P_{\text{oct}} - 0.750; R = 0.942; \\ & \quad \quad \quad n = 22 \quad (8) \end{aligned}$$

$$\begin{aligned} &\log k' \text{ vs. } \log P_{\text{cyc}} \text{ (all compounds)} \\ &\log k' = 0.187 \log P_{\text{cyc}} - 0.155; R = 0.925; \\ & \quad \quad \quad n = 19 \quad (9) \end{aligned}$$

$$\begin{aligned} &\log k' \text{ vs. } \log P_{\text{oct}} \text{ (matched set)} \\ &\log k' = 0.357 \log P_{\text{oct}} - 0.728; R = 0.925; \\ & \quad \quad \quad n = 19 \quad (10) \end{aligned}$$

$$\begin{aligned} &\log k' \text{ vs. } \log P_{\text{oct}} \text{ (non-H bonders)} \\ &\log k' = 0.379 \log P_{\text{oct}} - 0.633; R = 0.986; \\ & \quad \quad \quad n = 7 \quad (11) \end{aligned}$$

$$\begin{aligned} &\log k' \text{ vs. } \log P_{\text{oct}} \text{ (non-H bonders + H-bond} \\ &\text{acceptors)} \\ &\log k' = 0.401 \log P_{\text{oct}} - 0.712; R = 0.929; \\ & \quad \quad \quad n = 10 \quad (12) \end{aligned}$$

$$\begin{aligned} &\log k' \text{ vs. } \log P_{\text{oct}} \text{ (all amphiprotics)} \\ &\log k' = 0.310 \log P_{\text{oct}} - 0.786; R = 0.988; \\ & \quad \quad \quad n = 12 \quad (13) \end{aligned}$$

$$\begin{aligned} &\log k' \text{ vs. } \log P_{\text{oct}} \text{ (single amphiprotics)} \\ &\log k' = 0.295 \log P_{\text{oct}} - 0.756; R = 0.988; \\ & \quad \quad \quad n = 9 \quad (14) \end{aligned}$$

$$\begin{aligned} &\log k' \text{ vs. } \log P_{\text{oct}} \text{ (double amphiprotics)} \\ &\log k' = 0.395 \log P_{\text{oct}} - 0.817; R = 0.999; \\ & \quad \quad \quad n = 3 \quad (15) \end{aligned}$$

Graphs of log k' vs. log P_{oct} of individual compound classes are shown in Fig. 2. Two distinct classes can be seen, non-H bonders (a group which includes H-bond acceptors such as ethers and esters) and amphiprotics. There appears to be no distinction between compounds having either one or two amphiprotic groups.

Including all compounds for which log P_{oct} or log P_{cyc} data are available, correlation between log k' and either of these parameters is poor. Considering that an excellent correlation between log k' and log P_{alkane} was reported by Lambert and co-workers for the ACT-1 packing using a mobile phase of aqueous methanol [51,52], acetonitrile is clearly inferior to methanol as mobile phase modifier in conjunction with this packing material for the measurement of lipophilicity.

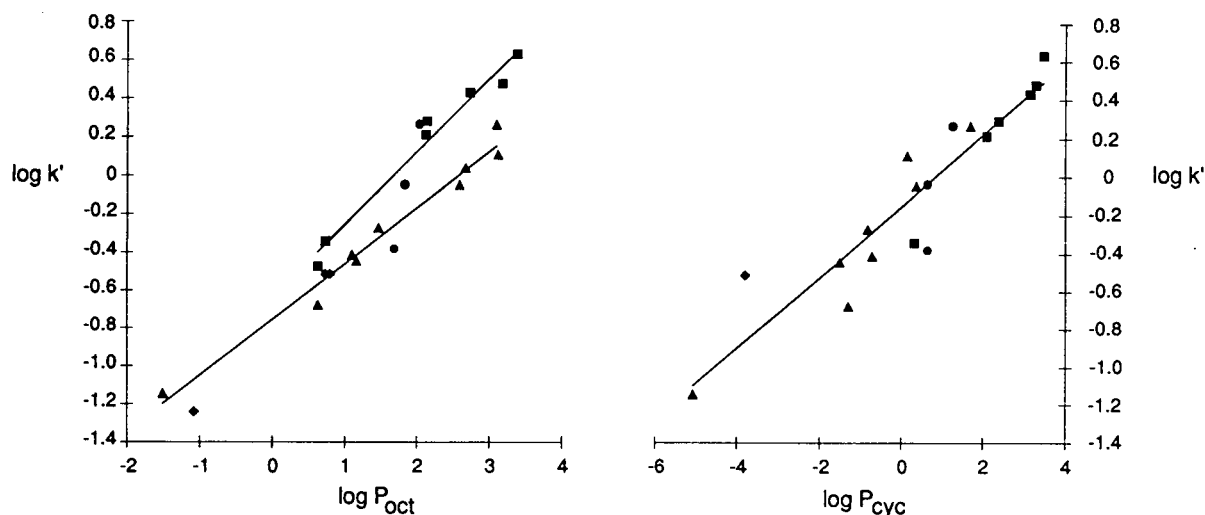


Fig. 2. Graphs of $\log k'$ vs. $\log P$ from data obtained on the ACT-1 column. ■ = Non-hydrogen bonders; ▲ = single amphiprotics; ◆ = double amphiprotics; ● = H-bond acceptors.

Determination of lipophilicity with the Nucleosil C8 column

The silica-based Nucleosil C8 column was included in this study for comparison with the polymer-based columns. We have used this column previously [53] and found no evidence that interaction with free silanols played an appreciable part in the retention of solutes. By comparison with the PRP-1 col-

umn, the higher plate number and lower lipophilicity of the stationary phase lead to sharper peaks and shorter retention times. After investigating several possible acetonitrile–buffer solvent ratios (not reported), an eluent containing acetonitrile–ammonium acetate buffer (60:40) was selected such that test compounds with a wide range of lipophilicities could be studied using a single solvent ratio. The

TABLE IV

LOG k' VALUES DETERMINED ON THE NUCLEOSIL C₈ COLUMN

Compound	$\log k'$	Compound	$\log k'$
Acetanilide	-0.12	β -Estradiol	0.17
<i>p</i> -Anisidine	-0.12	Ethyl acetate	-0.09
Anisole	0.17	Ethylbenzene	0.36
Benzamide	-0.28	Formamide	-0.63
Benzophenone	0.33	4-Hydroxybenzamide	-0.52
Benzyl alcohol	-0.15	2,6-Lutidine	0.25
4-Chloro-3-methylphenol	0.07	Naphthalene	0.36
4-Chloroaniline	0.08	2-Naphthol	0.06
<i>o</i> -Dichlorobenzene	0.38	1-Naphthol	0.10
1,5-Dihydroxynaphthlene	-0.19	Phenol	-0.12
N,N-Dimethyl- <i>m</i> -toluamide	0.16	N-Phenyl benzylamine	0.32
N,N-Dimethylbenzamide	-0.10	Pyridine	0.07
5,5-Diphenylhydantoin	-0.13	Quinoline	0.23
Diphenylmethanol	0.13	Toluene	0.27
2,6-Diphenylphenol	0.52	Triphenylmethane	0.71
		Uracil	-0.74

retention times of solutes using this system are listed in Table IV. Results of linear regression analyses on $\log k'$ - $\log P$ sets are given below:

$$\begin{aligned} \log k' \text{ vs. } \log P_{\text{oct}} \text{ (all compounds)} \\ \log k' = 0.180 \log P_{\text{oct}} - 0.325; R = 0.892; \\ n = 31 \end{aligned} \quad (16)$$

$$\begin{aligned} \log k' \text{ vs. } \log P_{\text{cyc}} \text{ (all compounds)} \\ \log k' = 0.111 \log P_{\text{cyc}} + 0.006; R = 0.955; \\ n = 22 \end{aligned} \quad (17)$$

$$\begin{aligned} \log k' \text{ vs. } \log P_{\text{oct}} \text{ (matched set)} \\ \log k' = 0.164 \log P_{\text{oct}} + 0.267; R = 0.840; \\ n = 22 \end{aligned} \quad (18)$$

$$\begin{aligned} \log k' \text{ vs. } \log P_{\text{oct}} \text{ (non-H bonders)} \\ \log k' = 0.161 \log P_{\text{oct}} - 0.186; R = 0.995; \\ n = 10 \end{aligned} \quad (19)$$

$$\begin{aligned} \log k' \text{ vs. } \log P_{\text{oct}} \text{ (all amphiprotics)} \\ \log k' = 0.175 \log P_{\text{oct}} - 0.437; R = 0.962; \\ n = 15 \end{aligned} \quad (20)$$

$$\begin{aligned} \log k' \text{ vs. } \log P_{\text{oct}} \text{ (single amphiprotics)} \\ \log k' = 0.164 \log P_{\text{oct}} - 0.360; R = 0.992; \\ n = 10 \end{aligned} \quad (21)$$

$$\begin{aligned} \log k' \text{ vs. } \log P_{\text{oct}} \text{ (double amphiprotics)} \\ \log k' = 0.180 \log P_{\text{oct}} - 0.556; R = 0.997; \\ n = 5 \end{aligned} \quad (22)$$

The results were similar to those found on the PRP-1 system. The overall correlation between $\log k'$ and $\log P_{\text{cyc}}$ was better than that between $\log k'$ and $\log P_{\text{oct}}$ (eqns. 17 and 18). Correlations between $\log k'$ and $\log P_{\text{oct}}$ were much improved when test substances were separated into individual classes (non-H bonders and amphiprotics), and, as was the case with the PRP-1 system, the correlation between $\log k'$ and $\log P_{\text{oct}}$ of amphiprotics could be improved further by separating these compounds into two classes; those containing a single amphiprotic substituent, and those containing two amphiprotic substituents. Several compounds with H-bond acceptor functional groups were also included in this study, but little correlation was found between $\log k'$ and $\log P_{\text{oct}}$ or $\log P_{\text{cyc}}$. Those with non-ionisable functional groups fell on (or close to) the non-H-bonder trend line. The remainder of the H-bond acceptors were bases; although weak bases were selected for study, the pH of the buffer used (pH 4.6) was probably inappropriate to ensure minimal ionization.

Comparison of the PRP-1 and Nucleosil C₈ columns

One purpose for this study was to examine alternative systems to the PRP-1 HPLC method for the determination of lipophilicity because of the concerns about resolution and peak shape (highly

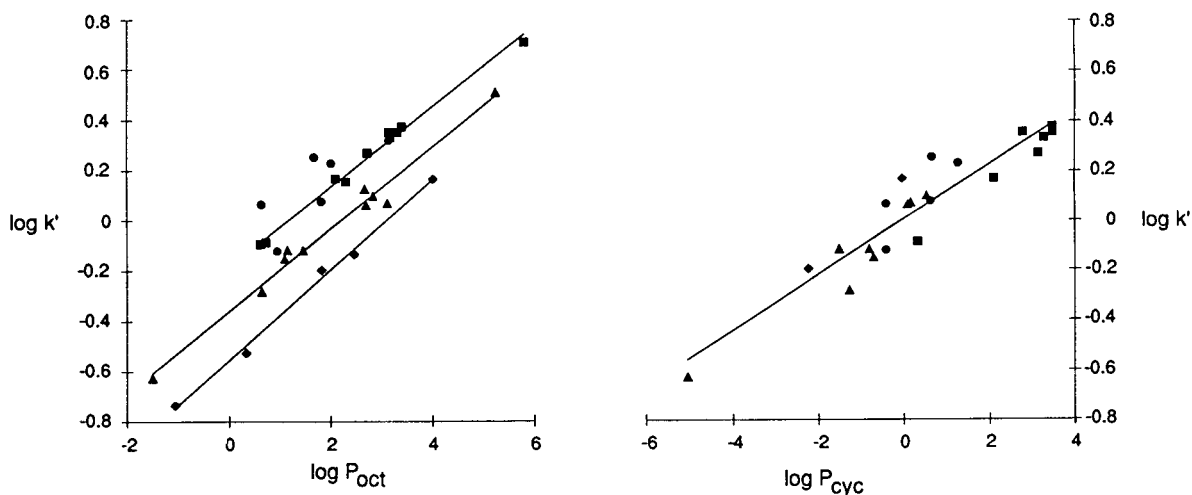


Fig. 3. Graphs of $\log k'$ vs. $\log P$ from data obtained on the Nucleosil C₈ column. ■ = Non-hydrogen bonders; ▲ = single amphiprotics; ◆ = double amphiprotics; ● = H-bond acceptors.

lipophilic compounds gave broad peaks) on the PRP-1 system. While the Nucleosil C8 system provided sharper peaks and shorter retention times than were observed on the PRP-1 system, the graphs shown in Figs. 1 and 3 suggest that both systems provided similar data. To confirm this, log k' values obtained on the PRP-1 system were compared with those on the Nucleosil C8 system.

A total of 20 compounds were examined on both PRP-1 (PRP) and Nucleosil (Nuc) C₈ systems. Linear regression analysis of log k' values obtained on both systems gave the following result:

$$\log k'_{\text{Nuc}} = 0.454 \log k'_{\text{PRP}} - 0.082. R = 0.995; \\ n = 19 \quad (23)$$

One compound was excluded from this comparison. β -Estradiol had a shorter retention time on the PRP-1 system than might be expected from its log P_{oct} , although its log k' on the Nucleosil C₈ system is close to the trend line for compounds with two amphiprotic groups. The remaining compounds represent a mixture of non-H bonders, and compounds with one or two amphiprotic substituents. As there is a highly correlated linear relationship between the log k' values obtained on either system, and both show good correlation between either log P_{cyc} or log P_{oct} (for congeners), either system appears to be suitable for the determination of lipophilicity. As the silica-based column may present anomalies with certain classes of compounds due to silanol interaction, the PRP-1 system might be superior, despite giving broad peaks with highly lipophilic compounds.

The influence of hydrogen bonding on log k'

In several previous studies, it was noted that compounds with amphiprotic substituents formed a separate group from compounds with no hydrogen bonding substituents when correlating log k' and log P_{oct} [for example 27,28,33–35]. This is not unreasonable when partitioning into the stationary phase has a high hydrophobic and low H-bonding components, such that log k' is more closely related to log P_{alkane} than log P_{oct} . Seiler [48] and others [54–56] have noted that interconversion of log P_{oct} and log P_{alkane} for any compound involves a term which sums all intermolecular hydrogen-bonding interactions experienced by that molecule. Thus, all amphiprotic compounds should not appear in a single

series (one highly correlated log k' –log P_{oct} plot) in HPLC systems which show good correlation between log k' and log P_{alkane} . Instead, the deviation of any compound from the log k' –log P_{oct} regression line should be a function of its intermolecular H-bonding capacity.

As the log k' values on the PRP-1 and Nucleosil C₈ systems used in this study demonstrated better correlation with log P_{cyc} than log P_{oct} we decided to evaluate whether there was an additive H-bonding effect on log k' . A series of compounds having two amphiprotic substituents were selected for evaluation. Compounds were selected on the basis that little or no intramolecular hydrogen bonding was possible. When examined on the PRP-1 and Nucleosil C₈ systems, these compounds clearly formed a separate group from compounds with only one amphiprotic substituent. As expected, the log k' –log P_{oct} regression line of the double amphiprotics deviated further from the regression line of non-H bonders than did the single amphiprotics, as would be expected from the known relationship between log P_{oct} and log P_{alkane} .

The validity of dividing the compounds into the groups non-hydrogen bonders, single amphiprotics and double amphiprotics in log k' vs. log P_{oct} plots was tested by two statistical methods. Using analysis of covariance, the slopes of the three sets of data for each column (PRP-1 and Nucleosil C₈) were found not to be different, whereas the intercepts were significantly different at $p < 0.05$. The Bonferroni multiple comparison procedure was used to ascertain the pairwise relationship between sets of data for each column. These were found to be different at $p < 0.001$.

CONCLUSIONS

The specific interactions experienced by test substrates in shake-flask determinations of lipophilicity are unlikely to be duplicated exactly in the HPLC experiment. It is therefore doubtful that any HPLC system can provide a scale of lipophilicity values which correlates perfectly with those obtained in the shake-flask experiment. Instead, HPLC can provide a scale of lipophilicity which is dependent upon the column–solvent combination, and which, as shown by others, can be equally valid in structure–activity correlations as the log P lipophilicity

scale. However, HPLC systems do need to be calibrated with substances of known (shake-flask) lipophilicity, so that lipophilicities ($\log k'$ values) obtained on one HPLC system can be compared to those obtained on another system.

In this study, the polymer-based PRP-1 and ACT-1 columns, and the silica-based C_8 systems were compared. The highly retentive nature of the PRP-1 column towards lipophilic compounds necessitated the use of acetonitrile as the organic modifier for this column, and all three columns were eluted with isocratic acetonitrile–aqueous ammonium acetate. The results from this study indicate that an acetonitrile–buffer mixture is unsuitable as an eluent for lipophilicity determination on the ACT-1 column. On the PRP-1 and Nucleosil C_8 columns with acetonitrile–buffer as eluent, there was far better correlation between $\log k'$ and $\log P_{\text{cyc}}$ than $\log k'$ and $\log P_{\text{oct}}$ ($R = 0.966$ and 0.801 , respectively, on the PRP-1 column; 0.955 and 0.840 , respectively, on the Nucleosil C_8 , from data using matched sets of compounds). However, when test substrates were divided into individual classes of non-H bonders, and compounds with either one or two amphiprotic substituents, correlation between $\log k'$ and $\log P_{\text{oct}}$ was notably improved. In plotting $\log k'$ vs. $\log P_{\text{oct}}$, compounds with either one or two amphiprotic substituents formed two distinct groups.

There was high correlation between $\log k'$ values obtained on the PRP-1 and Nucleosil C_8 systems. The lipophilicity scale provided by these systems should place series of compounds in a similar rank order to that obtained with $\log P_{\text{cyc}}$ measurement, but the rank order of lipophilicity will only be comparable to $\log P_{\text{oct}}$ in series of compounds with similar hydrogen-bonding properties.

ACKNOWLEDGEMENT

The authors wish to thank Dr. R.K. Narra for conducting the statistical analysis of the data.

REFERENCES

- C. Hansch and T. Fujita, *J. Am. Chem. Soc.*, 86 (1964) 1616.
- M. Cory, *Ann. Rep. Med. Chem.*, 17 (1982) 281.
- D. A. Brent, J. J. Sabatka, D. J. Minick and D. W. Henry, *J. Med. Chem.*, 26 (1983) 1014.
- J. C. Dearden and G. M. Bresnen, *Quant. Struct.–Act. Relat.*, 7 (1988) 133.
- E. Tomlinson, *J. Chromatogr.*, 113 (1975) 1.
- R. Kaliszan, *J. Chromatogr.*, 220 (1981) 71.
- T. J. Braumann, *J. Chromatogr.*, 373 (1986) 191.
- T. L. Hafkenschied and E. Tomlinson, *Adv. Chromatogr.*, 25 (1986) 1.
- H. Terada, *Quant. Struct.–Act. Relat.*, 5 (1986) 81.
- P. Kaliszan, *Quantitative Structure–Chromatographic Retention Relationships*, Wiley, New York, 1987.
- T. Hanai, *J. Chromatogr.*, 550 (1991) 313.
- R. P. W. Scott and C. F. Simpson, *J. Chromatogr.*, 197 (1980) 11.
- T. L. Hafkenschied and E. Tomlinson, *Int. J. Pharm.*, 16 (1983) 225.
- N. El Tayar, H. Van de Waterbeemd and B. Testa, *J. Chromatogr.*, 320 (1985) 293.
- C. Yamagami and N. Takao, *Chem. Pharm. Bull.*, 40 (1992) 925.
- V. De Biasi, W. J. Lough and M. B. Evans, *J. Chromatogr.*, 353 (1986) 279.
- S. E. Krikorian, T. A. Chorn and J. W. King, *Quant. Struct.–Act. Relat.*, 6 (1987) 65.
- A. Opperhuizen, T. L. Sinnige, J. van de Steen and O. Hutzinger, *J. Chromatogr.*, 388 (1987) 51.
- D. Reymond, G. N. Chung, J. M. Mayer and B. Testa, *J. Chromatogr.*, 391 (1987) 97.
- G. L. Biagi, M. C. Guerra, A. M. Barbaro, S. Barbieri, M. Recanatini and P. A. Borea, *J. Liq. Chromatogr.*, 13 (1990) 913.
- K. Valko, *J. Liq. Chromatogr.*, 7 (1984) 1014.
- F. Gaspari and M. Bonati, *J. Pharm. Pharmacol.*, 39 (1987) 252.
- N. El Tayar, A. Kakoulidou, T. Rothlisberger, B. Testa and J. Gal, *J. Chromatogr.*, 439 (1988) 237.
- R. M. Smith and C. M. Burr, *J. Chromatogr.*, 475 (1989) 57.
- A. Roda, A. Minutello, M. A. Angellotti and A. Fini, *J. Lipid Res.*, 31 (1990) 1433.
- W. E. Hammers, G. J. Meurs and C. L. de Ligny, *J. Chromatogr.*, 247 (1982) 1.
- C. V. Eadsforth, *Pest. Sci.*, 17 (1986) 311.
- K. Miyake, N. Mizuno and H. Terada, *Chem. Pharm. Bull.*, 34 (1986) 4787.
- J. J. Sabatka, D. J. Minick, T. K. Shumaker, G. L. Hodgson and D. A. Brent, *J. Chromatogr.*, 384 (1987) 349.
- S. H. Unger and G. H. Chiang, *J. Med. Chem.*, 24 (1981) 262.
- D. J. Minick, J. H. Frenz, M. A. Patrick and D. A. Brent, *J. Med. Chem.*, 31 (1988) 1923.
- A. Belchalanay, T. Rothlisberger, N. El Tayar and B. Testa, *J. Chromatogr.*, 473 (1989) 115.
- T. Braumann, G. Weber and L. H. Grimme, *J. Chromatogr.*, 261 (1983) 329.
- J. E. Haky and A. M. Young, *J. Liq. Chromatogr.*, 7 (1984) 675.
- T. Yamagami, H. Takami, K. Yamamoto, K. Miyoshi and N. Takao, *Chem. Pharm. Bull.*, 32 (1984) 4994.
- T. Braumann and L. H. Grimme, *J. Chromatogr.*, 206 (1981) 7.
- S. V. Galushko, I. P. Shishkina and I. V. Alekseeva, *J. Chromatogr.*, 547 (1991) 161.
- D. J. Minick, J. J. Sabatka and D. A. Brent, *J. Liq. Chromatogr.*, 10 (1987) 2565.

- 39 J. E. Garst, *J. Pharm. Sci.*, 73 (1984) 1623.
- 40 P. M. Sherblom and R. P. Eganhouse, *J. Chromatogr.*, 454 (1988) 37.
- 41 P. T. Ying and J. G. Dorsey, *Talanta*, 38 (1991) 237.
- 42 D. P. Nowotnik, in A. E. Theobald (Editor), *Radiopharmaceuticals: Using Radioactive Compounds in Pharmaceutics and Medicine*, Ellis Horwood, Chichester, 1989, Ch. 3, p. 28.
- 43 R. D. Neirinckx, D. P. Nowotnik, R. D. Pickett, R. C. Harrison and P. J. Eil, in H. Biersack and C. Winkler (Editors), *Amphetamines and pH Shift Agents: Basic Research and Clinical Results*, Walter de Gruyter, Bonn, 1986, p. 59.
- 44 T. Feld and A. D. Nunn, *J. Label. Compd. Radiopharm.*, 26 (1989) 274.
- 45 A. D. Nunn, T. Feld and R. K. Narra, in M. Nicolini, G. Bandoli and U. Mazzi (Editors), *Technetium and Rhenium in Chemistry and Nuclear Medicine 3*, Cortina International, Verona, 1990, p. 399.
- 46 *MedChem cLogP Program*, v 3.4.2, Day Light Chemical Information Systems, Irvin, CA.
- 47 B. Gawdzik, *J. Chromatogr.*, 600 (1992) 115.
- 48 P. Seiler, *Eur. J. Med. Chem.*, 9 (1974) 473.
- 49 K. Miyake, F. Kitaura, N. Mizuno and H. Terada, *Chem. Pharm. Bull.*, 35 (1987) 377.
- 50 W. Klein, W. Kordel, M. Weiss and H.J. Poremski, *Chemosphere*, 17 (1988) 361.
- 51 W. J. Lambert and L. A. Wright, *J. Chromatogr.*, 464 (1989) 400.
- 52 W. J. Lambert, L. A. Wright and J. K. Stevens, *Pharmaceut. Res.*, 7 (1990) 577.
- 53 S. Jurisson, W. Hirth, K. Linder, R. J. Di Rocco, R. K. Narra, D. P. Nowotnik and A. D. Nunn, *Nucl. Med. Biol.*, 18 (1991) 735.
- 54 N. El Tayar, R.-S. Tsai, B. Testa, P.-A. Carrupt and A. Leo, *J. Pharm. Sci.*, 80 (1991) 590.
- 55 M. H. Abraham, W. R. Lieb and N. P. Franks, *J. Pharm. Sci.*, 80 (1991) 719.
- 56 C. Altomare, R. S. Tsai, N. Eltayar, B. Testa, A. Carotti, S. Cellamare and P. G. Debenedetti, *J. Pharm. Pharmacol.*, 43 (1991) 191.

Evaluation of silanol-deactivated silica-based reversed phases for liquid chromatography of erythromycin

J. Paesen, P. Claeys, E. Roets and J. Hoogmartens

Laboratorium voor Farmaceutische Chemie, Instituut voor Farmaceutische Wetenschappen, Katholieke Universiteit Leuven, Van Evenstraat 4, B-3000 Leuven (Belgium)

(First received September 8th, 1992; revised manuscript received October 12th, 1992)

ABSTRACT

The suitability of eleven silanol-deactivated reversed phases for the liquid chromatography of erythromycin was investigated. The selectivity and efficiency of each stationary phase were examined. The performance was compared to that of a non-deactivated C_{18} silica-based reversed-phase material, Hypersil C_{18} ($5\ \mu\text{m}$). Two types of mobile phases were used, one containing no tetrabutylammonium (TBA) and the other containing TBA. Addition of TBA as a silanol-blocking agent improved the theoretical plate number and symmetry factor of the peaks corresponding to erythromycin A (EA) and erythromycin A enol ether for all the deactivated reversed phases. These results are an indication of the presence of some residual silanol activity in these phases. Separation of erythromycin E and EA was achieved on only two of the eleven phases. The selectivity was always poorer than that obtained in a previously described method using a poly(styrene-divinylbenzene) stationary phase.

INTRODUCTION

A disadvantage of liquid chromatography (LC) of basic substances on silica-based reversed-phases is peak tailing due to interaction with residual silanols on the silica backbone. In the LC of the macrolide antibiotic erythromycin, which is a mixture of several related substances all of which are bases, similar disadvantages were observed. The separation was improved by adding tetraalkylammonium compounds to the mobile phase, such as tetramethylammonium phosphate (TMA) or tetrabutylammonium hydrogensulphate (TBA) [1,2], TMA and TBA can act as silanol-blocking agents, so that interaction between erythromycin and the silanols is weakened. It was also observed that older columns performed better [1]. Ageing of C_8 - and C_{18} -derivatised silica-based reversed phases improved

the chromatography. It is believed that heating a packing material, conditioned with a mobile phase containing phosphoric acid, removes metal impurities from the silica backbone and hence influences the silanol activity. Nevertheless, large differences in selectivity were seen between different brands of reversed-phase materials [2,3].

In recent years, several silica-based reversed phases have been developed that are especially suitable for the chromatography of basic substances. These "silanol-deactivated" materials are claimed to have strongly reduced residual silanol activity and to produce better peak symmetry and efficiency. As a consequence, addition of triethylamine or tetraalkylammonium compounds would become superfluous. The suitability of several silanol-deactivated stationary phases for the LC of erythromycin was investigated. A non-deactivated silica-based reversed-phase material, Hypersil C_{18} ($5\ \mu\text{m}$), was used as a reference. The selectivity and efficiency of each stationary phase were determined, first with a mobile phase containing no TBA and then with a mobile phase containing 5% (v/v) of 0.2 M TBA. In

Correspondence to: J. Hoogmartens, Laboratorium voor Farmaceutische Chemie, Instituut voor Farmaceutische Wetenschappen, Katholieke Universiteit Leuven, Van Evenstraat 4, B-3000 Leuven (Belgium)

a previous study, the composition of the latter mobile phase was shown to be suitable for the chromatography of erythromycin on silica-based reversed phases [4]. It was the intention in this study to examine the performance of silanol-deactivated stationary phases compared with classical silica gel derivatized reversed phases.

EXPERIMENTAL

Samples

Pure erythromycin A (EA) was obtained by crystallization of a commercial sample as described previously [5]. Anhydroerythromycin A (AEA) [6], erythromycin A enol ether (EAEN) [7] and N-demethylerythromycin A (dMeEA) [8] were prepared from EA according to the described methods. A commercial sample was available containing EA, erythromycin B, C, F, E, (EB, EC, EF, EE), dMeEA, AEA and pseudoerythromycin A enol ether (psEAEN). Structures of these substances have been shown elsewhere [9].

Instrumentation

The chromatographic system consisted of a Model 6200 pump (Merck–Hitachi, Darmstadt, Germany), a Model CV-6-UHPa N60 injection valve (Valco, Houston, TX, USA) with a 20- μ l loop, a Model 441 UV detector set at 215 nm (Waters, Milford,

MA, USA) and an HP 3396 integrator (Hewlett-Packard, Avondale, PA, USA). The columns were maintained at 35°C using an immersion water-bath.

Stationary phases

The columns examined are listed in Table I. Columns I–VIII were packed by the manufacturer. Columns IX to XII were packed in the laboratory following a classical slurry-packing procedure [10]. Column characteristics are reported in Table I. Stationary phase manufacturers were as follows: A, Supelco (Bellefonte, PA, USA); B, Rockland Technologies (Newport, DE, USA); C, Shandon (Runcorn, UK); D, Merck (Darmstadt, Germany); E, Phase Separations (Queensferry, UK); F, Chrompack (Middelburg, Netherlands); G, J. T. Baker (Phillipsburg, NY, USA); and H, Dr. Buszewski (Lublin, Poland) [11].

Reagents, solvents and mobile phases

Ammonium dihydrogenphosphate and diammonium hydrogen phosphate of analytical-reagent grade (Merck) were used to prepare a 0.2 M phosphate buffer (pH 6.0). Tetrabutylammonium (TBA) hydrogensulphate (Janssen Chimica, Beerse, Belgium) was used to prepare a 0.2 M TBA solution, adjusted to pH 6.0 with 40% (w/v) sodium hydroxide, before the solution was made up to the final volume. LC-grade acetonitrile (grade S) and metha-

TABLE I
COLUMNS EXAMINED

Column No.	Stationary phase	Manufacturer	Particle size (μ m)	Column ^a length (cm)	Laboratory packed (L) or prepacked (P)
I	Supelcosil LC-ABZ	A	5	25	P
II	Zorbax R _x -C ₁₈	B	5	25	P
III	Zorbax SB-C ₈	B	5	15	P
IV	Hypersil BDS C ₁₈	C	5	25	P
V	LiChrospher 60 RP-Select B	D	5	25	P
VI	Spherisorb ODS-B	E	5	25	P
VII	Polyspher RP-18	D	10	15	P
VIII	Chromspher B	F	5	25	P
IX	Bakerbond BDC	G	5	25	L
X	Mono PB	H	5	10	L
XI	Mono-C ₁₈	H	7	10	L
XII	Hypersil C ₁₈	C	5	25	L

^a All 4.6 mm I.D.

TABLE II
COLUMN PARAMETERS

N_{EA} , S_{EA} , N_{EAEN} , S_{EAEN} = theoretical plate number (N) and symmetry factor (S) for EA and EAEN. – TBA = results obtained with mobile phase acetonitrile–0.2 M phosphate buffer (pH 6.0)–water [x :5:(95 – x)]; + TBA = results obtained with mobile phase acetonitrile–0.2 M phosphate buffer (pH 6.0)–0.2 M TBA (pH 6.0)–water [x :5:5:(90 – x)].

Column No.	Acetonitrile content, x (%)		N_{EA}/m		S_{EA}		N_{EAEN}/m		S_{EAEN}	
	– TBA	+ TBA	– TBA	+ TBA	– TBA	+ TBA	– TBA	+ TBA	– TBA	+ TBA
I	23	20	890	3600	2.2	0.9	25000	45000	1.4	1.1
II	28	25	440	2900	1.4	0.85	8600	23000	2.2	2.2
III	28	21	920	4830	10	1.5	7900	12400	2.0	1.6
IV	28	23	1080	3200	2.5	1.0	8200	41200	2.6	2.2
V	38	28	900	3320	6.3	1.2	460	7000	6.1	4.0
VI	28	22	1420	10400	5.3	1.1	8800	20100	6.2	4.9
VII	40	21	ND ^a	1180	ND	1.1	ND	470	ND	1.7
VIII	40	20	820	3700	3.3	1.8	2130	13600	3.3	1.9
IX	30	25	240	2640	3.2	1.1	ND	2140	> 10	2.9
X	27	24	3740	6180	0.9	0.7	17650	19000	2.9	1.5
XI	40	30	770	4650	2.8	1.5	1760	3260	3.0	2.3
XII	38	23	740	2140	2.8	1.4	2540	2920	2.4	2.0

^a ND = not determined.

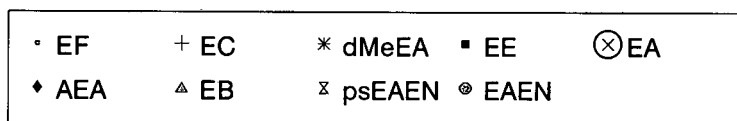
nol were from Rathburn Chemicals (Walkerburn, UK). Water was distilled twice from glass apparatus. Samples were dissolved in methanol–water (1:1). Mobile phase were prepared by adding the organic modifier (x ml) to 0.2 M phosphate buffer (pH 6.0)–0.2 M TBA (pH 6.0)–water [x :5:5:(90 – x)] or [x :5:0:(95 – x)]. No correction was made for volume contraction. Mobile phases were degassed by ultrasonication. The concentration of acetonitrile in the mobile phase was adjusted for each stationary phase in order to obtain comparable capacity factors for EA (Table II). The flow-rate was 1.5 ml/min for all columns except VII, X and XI (0.6 ml/min). In mobile phases containing TBA the amount of acetonitrile had to be decreased. The components of the mobile phases were the same as described previously for the analysis of erythromycin on C₁₈ silica-based reversed phases [4].

RESULTS AND DISCUSSION

The stationary phases I–XI (Table I), except VII, are silanol-deactivated silica-based reversed-phase materials, which are claimed to be suitable for the chromatography of basic compounds. Column VII contains a polymer-based C₁₈ reversed phase. Most columns had a length of 25 cm. The commercial

columns III and VII were available only in a 15-cm length. Laboratory-packed columns X and XI were packed in a 10-cm length owing to the limited amount of stationary phase available. The residual silanol activity of these packings should be strongly reduced or absent. If so, the presence of a quaternary ammonium compound such as TBA in the mobile phase should have no effect on the peak shape of the basic substances, as TBA is used to block interactions with residual silanols. The chromatography of the antibiotic erythromycin ($pK_a = 8.8$) using silica-based reversed phases is influenced by the residual silanol activity. It was seen previously that the chromatography could be improved by adding TMA [1] or TBA [4] to the mobile phase and by using aged stationary phases [1–3]. Ageing was said to eliminate metal impurities from the silica backbone, hence influencing the silanol activity. Loss of bonded phase and the consequent increase in silanol activity observed with some of the reversed-phase materials was merely seen as a secondary effect of the ageing procedure [3].

In the present study the performance of the silanol-deactivated materials in the LC of erythromycin was examined. As a reference a non-deactivated C₁₈ reversed-phase material, Hypersil C₁₈ (5 μ m) was used (column XII). This column was not condi-



column

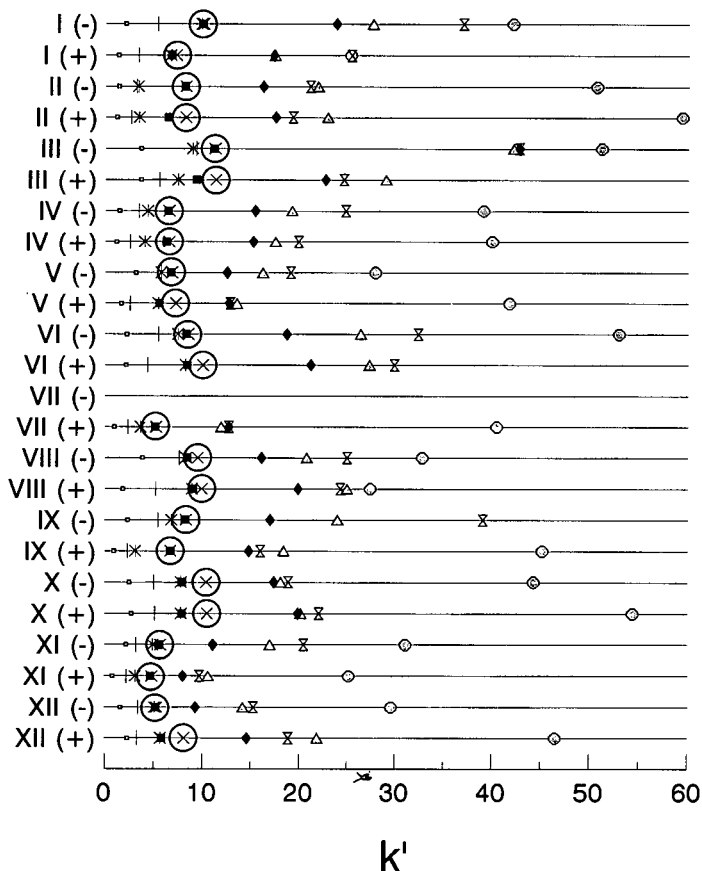


Fig. 1. Capacity factors. EA, EB, EC, EE and EF = erythromycin A, B, C, E and F, respectively; dMeEA = N-demethylerythromycin A; AEA = anhydroerythromycin A; EAEN = erythromycin A enol ether; psEAEN = pseudoerythromycin A enol ether. Mobile phase: (-) = acetonitrile-0.2 M phosphate buffer (pH 6.0)-water [x:5:(95 - x)]; (+) = acetonitrile-0.2 M phosphate buffer (pH 6.0)-0.2 M TBA (pH 6.0)-water [x:5:5:(90 - x)]. Flow rate: 1.5 ml/min except for columns X and XI (0.6 ml/min). Temperature: 35°C. Detection: UV at 215 nm.

tioned by ageing. In previous experiments it was observed that the chromatography of erythromycin was not affected much by ageing of Hypersil C₁₈ [3]. The mobile phase used in this study was that previously shown to ensure separation of EE from EA on silica-based reversed phases [4]. Therefore, the type of organic modifier, the buffer and the pH of

the mobile phase were not further adapted in these experiments. Indeed, it was the intention of this study to compare the performance of silanol-deactivated stationary phases with that of classical silica gel derivatized reversed phases. Capacity factors for EF, EC, dMeEA, EE, EA, AEA, psEAEN, EB and EAEN were determined on the twelve stationary

phases. First a mobile phase without TBA was used (Fig. 1). The amount (x) of acetonitrile was adjusted for each stationary phase to obtain similar capacity factors for EA and to optimize the separation of EA (see Table II).

The sequence of elution of the compounds eluted before the main peak EA was the same on all the columns as on the Hypersil C₁₈ columns *viz.*, EF, EC, dMeEA, except for column III (a C₈ material), where EC was eluted after dMeEA. Results for column VII were not included because the selectivity and peak shapes were very poor, so that capacity factors, symmetry factors and theoretical plate numbers could not be determined. It should be emphasized that this column contained a polymer-based stationary phase. The separation of dMeEA and EE from EA is most difficult to achieve. Satisfactory separation between dMeEA and EA was obtained on columns II, III, IV, V, VI, IX and X, while partial separation was obtained on columns I and VIII. On columns XI and XII dMeEA was not separated from the main peak. Separation between EE and EA was obtained only on columns I and VIII (partial separation of the pair EE + dMeEA as a shoulder on the main peak) and on column X (satisfactory separation between the pair EE + dMeEA and EA).

The order of elution for AEA, EB, psEAEN and EAEN was not the same on all the columns. On columns II and XI, EB was eluted after psEAEN. AEA was eluted close to EB and psEAEN on column III. EAEN was always retained strongly ($k' > 30$). On several columns k' for EAEN exceeded 60.

Fig. 1 also shows the results obtained with mobile phases containing TBA. Addition of TBA to the mobile phase caused the retention times to decrease, so the amount of organic modifier had to be adjusted in order to maintain similar capacity factors. Separation between EE, dMeEA and EA was improved on columns II, III, V, VI and XII. Overall, the pair EE + dMeEA was separated completely from EA on columns VI and X. Columns I, III, VIII and XII gave a partial separation. The order of elution EB–psEAEN was reversed on columns III and V compared with the results obtained with the TBA-free mobile phase.

Of course, the separation is governed not only by the selectivity but also by the theoretical plate number (N) per metre and the symmetry factor (S),

which were calculated for EA and for the strongly retained EAEN according to the prescriptions of the European Pharmacopoeia [12]. EAEN was shown previously to be very sensitive to changes in silanol activity, caused by ageing of the stationary phase [3]. In Table II it can be seen that the symmetry factor for EA and EAEN always decreased on adding TBA to the mobile phase. On columns III, V, VI and IX an important improvement in the symmetry was observed. Compared with the non-deactivated column XII, S_{EA} + TBA was better on all the columns, except on columns VIII and XI. The theoretical plate number for EA (N_{EA}) always increased using a mobile phase containing TBA. The highest N_{EA} values were found for the columns that gave the best separation between EE and EA (columns VI and X). N_{EAEN} + TBA was higher on all the deactivated phases than on the non-deactivated Hypersil C₁₈ column, except for column IX. Column VII, the polymer-based C₁₈ stationary phase, which does not have residual silanols, showed a poor efficiency. The reason for this is not clear.

Fig. 2 shows typical chromatograms obtained on columns XII and VI. For comparison, the separation obtained on a wide-pore poly(styrene–divinylbenzene) stationary phase (PLRP-S, 8 μ m, 1000 Å) using a previously described method is shown [9]. A special mobile phase was developed for this column. A major advantage of this polymer phase is that an alkaline mobile phase, in this instance of pH 9, can be used with no effect on the stability. Alkaline mobile phases allow a better separation of erythromycin.

The addition of TBA to the mobile phase clearly improved the quality of the separation. It was stated previously that erythromycin and related substances are very sensitive to small changes in the sorbent surface, especially to changes in the content of residual silanols [2]. TBA can act as a shielding agent for these silanols. At the same time a positively charged TBA layer can be formed on the stationary phase surface, causing repulsion of the positively charged erythromycin molecules. In order to avoid ionization of silanols it is better to use mobile phases of low pH. However, the major concern in this study was to compare the performance of these phases with that of a non-deactivated silica-based reversed phase for the chromatography of erythro-

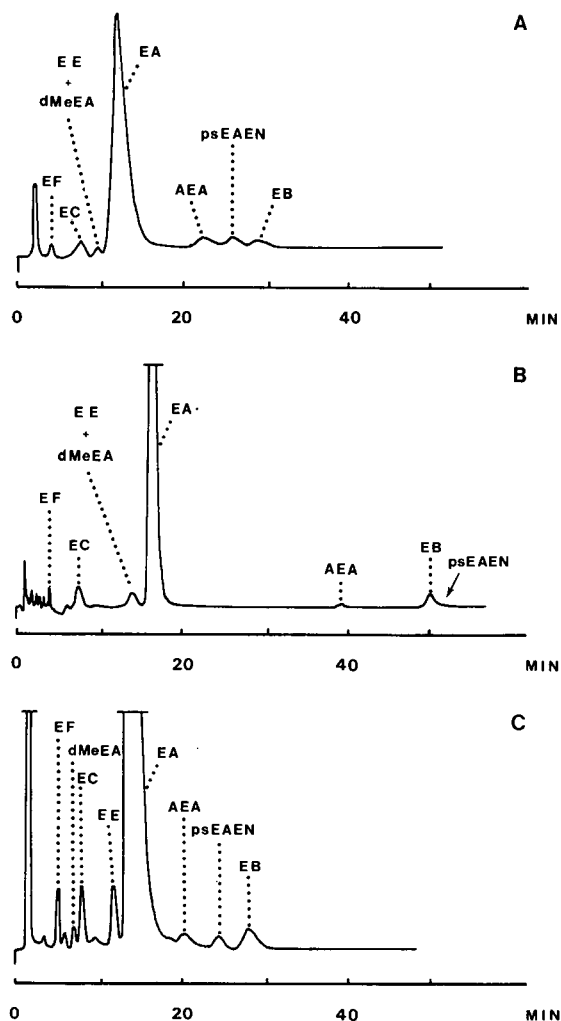


Fig. 2. Typical chromatograms. (A) Hypersil C_{18} , $5 \mu\text{m}$ (column XII); (B) Spherisorb ODS-B, $5 \mu\text{m}$ (column VI); (C) PLRP-S, $8 \mu\text{m}$, 1000 \AA [8].

mycin. Therefore, it was necessary to use a mobile phase comparable to that developed for the non-deactivated phases. On these phases, satisfactory separation of erythromycin could not be achieved using an acidic mobile phase. The results obtained in this study show that residual silanol activity still exists with these silanol-deactivated stationary phases when used with a mobile phase of neutral pH.

CONCLUSION

The different deactivated silica-based reversed phases examined showed variable performance in the chromatography of erythromycin A and related substances. Addition of TBA improved the peak symmetry and the efficiency, although this was not expected when using silanol-deactivated reversed phases. Compared with a non-deactivated reversed phase, only two columns (VI and X) out of eleven gave a better separation of EA when using a similar mobile phase. A method involving a wide-pore poly(styrene-divinylbenzene) stationary phase (PLRP-S, $8 \mu\text{m}$, 1000 \AA) and a specially developed mobile phase has been shown to be a better alternative for the LC of erythromycin. This method has been discussed elsewhere [9]. The fact that some stationary phases did not perform well in these experiments does not mean that they cannot be very suitable for solving other chromatographic problems.

ACKNOWLEDGEMENTS

The National Fund for Scientific Research (Belgium) is acknowledged for financial support. The authors thank the manufacturers for supplying the supports. A. Decoux is thanked for secretarial assistance.

REFERENCES

- 1 Th. Cachet, I. O. Kibwage, E. Roets, J. Hoogmartens and H. Vanderhaeghe, *J. Chromatogr.*, 409 (1987) 91.
- 2 Th. Cachet, I. Quintens, E. Roets and J. Hoogmartens, *J. Liq. Chromatogr.*, 12 (1989) 2171.
- 3 Th. Cachet, I. Quintens, J. Paesen, E. Roets and J. Hoogmartens, *J. Liq. Chromatogr.*, 14 (1991) 1203.
- 4 Th. Cachet, K. De Turck, E. Roets and J. Hoogmartens, *J. Pharm. Biomed. Anal.*, 9 (1991) 547.
- 5 I. O. Kibwage, E. Roets, J. Hoogmartens and H. Vanderhaeghe, *J. Chromatogr.*, 330 (1985) 275.
- 6 P. F. Wiley, K. Gerzon, E. H. Flynn, M. V. Sigal, O. Weaver, U. C. Quarck, R. R. Chauvette and R. Monahan, *J. Am. Chem. Soc.*, 79 (1957) 6062.
- 7 P. Kurath, P. H. Jones, R. S. Egan and T. J. Perun, *Experientia*, 27 (1971) 362.
- 8 E. H. Flynn, H. W. Murphy and R. E. McMahon, *J. Am. Chem. Soc.*, 77 (1955) 3104.
- 9 J. Paesen, E. Roets and J. Hoogmartens, *Chromatographia*, 32 (1991) 162.
- 10 J. Hoogmartens, E. Roets, G. Janssen and H. Vanderhaeghe, *J. Chromatogr.*, 244 (1982) 299.
- 11 B. Buszewski, J. Schmid, K. Albert and E. Bayer, *J. Chromatogr.*, 552 (1991) 415.
- 12 *European Pharmacopoeia*, Maisonneuve, Sainte Ruffine, France, 2nd ed., 1987, V.6.20.4.

Selective complex formation of saccharides with europium(III) and iron(III) ions at alkaline pH studied by ligand-exchange chromatography

Morgan Stefansson

Department of Analytical Pharmaceutical Chemistry, Biomedical Center, Uppsala University, Box 574, S-751 23 Uppsala (Sweden)

(First received July 31st, 1992; revised manuscript received October 20th, 1992)

ABSTRACT

At high pH, saccharides become negatively charged by deprotonation of one or several hydroxylic groups and they are highly and selectively retained by ligand-exchange chromatography. The systems consist of a sulphonated polystyrene strong cation exchanger in europium(III) or iron(III) form and sodium hydroxide as mobile phase. The degree of complex formation is dependent on solute character and concentration, metal ion and pH, the reaction being of second order as confirmed by breakthrough studies. Rapid desorption of the solutes is performed by the introduction of an acidic mobile phase. Monosaccharides, and especially sugar alcohols, are selectively retained by a column in Fe(III) form whereas all saccharides are strongly retained as Eu(III) complexes, *e.g.*, the capacity factor for the breakthrough of 10 μ M glucose, in 0.1 M NaOH as mobile phase, was *ca.* 3500. The systems are proposed to be highly selective for the analysis of sugars.

INTRODUCTION

Carbohydrates are polar compounds and difficult to retain in reversed-phase LC systems (for a review, see ref. 1) and the low capacity factors limit the number of compounds to be separated. The development of gas-liquid chromatographic (GLC) methods included the conversion of the sugars into volatile derivatives such as acetates [2] or trimethylsilyl ethers [3] and borohydride reduction [4]. The introduction of capillary columns with highly polar solid phases coupled with mass spectrometry [5] considerably improved the resolution and the confirmation of identification. Normal-phase partition chromatography has been used with polar solid phases, *e.g.*, silica or diol, amine, amide or cyano-functionalized silica, and a high content of acetonitrile in the mobile phase [6]. Refractive index or

UV absorption around 200 nm is usually employed, resulting in low sensitivity and limitations for mobile phase additives.

Most saccharides have pK_a values in the range 12–14 [7] and they can be separated by ion chromatography using strongly alkaline solutions. This separation mode, in combination with pulsed electrochemical detection, has been shown to offer high selectivity and sensitivity in the analysis of sugars, polyols and related compounds [8]. Sugars have also been separated by ligand-exchange chromatography using ion exchangers in different metal forms, calcium being the most commonly used [9]. Recently, carbohydrates [10] have been found to form strong complexes at alkaline pH with rare earths, yttrium and uranyl metal ions loaded on to a sulphonated polystyrene cation exchanger. The effects of mobile phase additives and temperature were studied [11] and the methodology was utilized for the bioanalysis of the diastereomeric glucuronides of almokalant from human urine [12].

In this study, saccharides were used as solutes in

Correspondence to: M. Stefansson, Department of Analytical Pharmaceutical Chemistry, Biomedical Center, Uppsala University, Box 574, S-751 23 Uppsala, Sweden.

order to investigate the influence of the anomeric hydroxylic group on complex formation compared with glycosides [10]. The retention mechanism is described as a ligand-exchange reaction and retention and isotherm studies were performed by frontal analysis using pulsed electrochemical detection.

EXPERIMENTAL

Instrumental

The LC instrumentation consisted of an LKB (Bromma, Sweden) Model 2150 HPLC pump, a Rheodyne Model 7125 injector with a 20- μ l loop, a Rheodyne Model 7000 switching valve (the valves were equipped with Tefzel alkali-resistant rotor seals), a pulsed electrochemical detection (PED) system with a gold working electrode and pH reference electrode (Dionex, Sunnyvale, CA, USA), a Kipp & Zonen BD 40 recorder and a Haake (Berlin-Steglitz, Germany) Fe water-bath for thermostating the chromatographic systems. The program for PED detection was $E_1 = 0.40$ V, $t_1 = 0$ –500 ms and integration for 300–500 ms, $E_2 = 0.90$ V, $t_2 = 510$ –590 ms and $E_3 = -0.30$ V, $t_3 = 600$ –650 ms. E_2 and E_3 are used to remove adsorbed compounds oxidatively and to reduce the gold oxide formed, respectively, in order to minimize fouling of the working electrode.

Chemicals and column packing

All test solutes, except for the metal chloride salts (Janssen Chimica, Beerse, Belgium) were obtained from Sigma (St. Louis, MO, USA) and used as received. Sodium hydroxide solutions were prepared from 1 M Titrisol solution (Merck, Darmstadt, Germany) and kept in a plastic bottle. The column packing was Hitachi-Gel 3011-S, 10–12 μ m, a spherical and macroporous sulphonated polystyrene resin in H⁺ form, kindly provided by Hitachi (Tokyo, Japan).

Column preparation

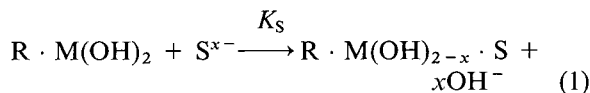
The ion exchanger was packed with water as slurry medium in a polished stainless-steel column (21 \times 4.6 mm I.D.). It was converted into the metal form by a 500- μ l injection of the metal salt (2 M). The excess of metal ions was rinsed off the column by washing with 0.3 M morpholinoethansulphonic acid (MES) buffer (pH 5.0) for 20 min. The metal

ions were held firmly by the resin and not eluted during the separation process. MES does not form complexes with the metal ions [10] and was used to elute the solutes rapidly from the resin after the breakthrough. The column was equilibrated with 10 ml of 0.1 M NaOH solution prior to each run.

RESULTS AND DISCUSSION

Principle and retention model

Saccharides are weak acids with pK_a values between 12 and 14 [7] and the negatively charged saccharides, S⁻, form complexes with the electrostatically immobilized metal ions, R · M(OH)₂, at pH > 11 [10]. Hydroxide ions compete for complex formation with the metal ions according to a ligand-exchange reaction and assuming one solute molecule and one metal ion in the complex [10]:



The capacity factor is

$$k' = q K_S^* [R \cdot M(OH)_2] / [OH^-]^x \quad (2)$$

where q is the phase ratio in the column and K_S^* is the apparent thermodynamic exchange constant; $K_S^* = K_S [1 / (1 + 10^{pK_a - pH})]$. C_s , the concentration of solute on the solid phase, is calculated accordingly and a linear relationship *versus* hydroxide concentration is obtained:

$$\ln C_s = \ln(K_S^* [R \cdot M(OH)_2] [S^{x-}]) - x \ln [OH^-] \quad (3)$$

The concentration of the metal ions on the cation exchanger was about 200 μ mol per column and the mass of the dry packing material in the H⁺ form, m , was 0.16 g, *i.e.*, 1.25 mmol of metal ions bound per gram of exchanger.

Breakthrough curves

Retention and isotherm studies were performed by the breakthrough (BT) technique. The BT curve (Fig. 1) is characterized by pronounced tailing, which was assumed to be caused by slow distribution kinetics. The complexation on the solid phase for chelating resins is often a slow process and, occasionally, such reactions have been shown [13] to be of approximately second order. The BT curve was normalized, by setting $BT_{1/2} = 0.5$, with respect to

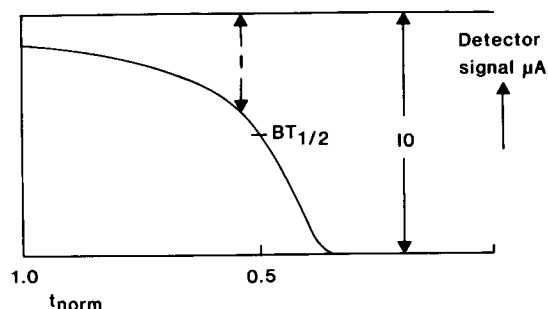


Fig. 1. Typical breakthrough curve. Mobile phase: 0.1 mM glucose in 0.1 M NaOH.

the time axis. $BT_{1/2}$ is defined as the time necessary for the detector signal to reach half of its maximum value. The effluent was monitored by PED. The equation for a simple second-order kinetic reaction:

$$-dI/I^2 = kdt \quad (4)$$

yields after integration and rearrangement

$$I_0/I = I_0kt + \text{intercept} \quad (5)$$

where I_0 is the concentration at $t = 0$ and I that at time t , k is the rate constant and the intercept is obtained when $BT_{1/2}$ is chosen as the starting point for calculation. A plot of I_0/I versus t (i.e., the value for normalization) was linear (Fig. 2). As a consequence, the distribution to the solid phase was concentration and time dependent. C_s was calculated from the BT curve according to

$$C_s = V_{BT} C_m/m \quad (6)$$

where V_{BT} is the BT volume minus the void volume, C_m the mobile phase concentration and m the

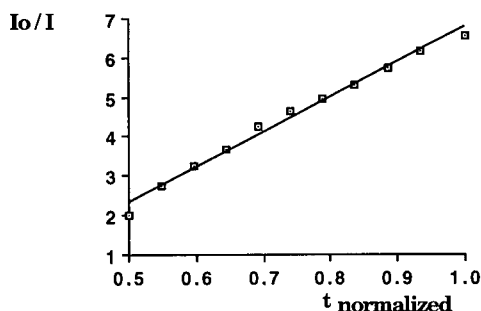


Fig. 2. Plot of the breakthrough curve kinetics according to a second-order reaction (eqn. 5).

amount of dry resin in H^+ form in the column (g/l). After BT, the solutes were desorbed by introduction of 0.3 M MES buffer (pH 5.0) for 10 min, followed by sodium hydroxide solution as the mobile phase until the eluent from the column was alkaline, i.e., the metal ions were converted into the corresponding hydroxides.

Carbon dioxide is taken up by the alkaline mobile phase, forming carbonate, which complexes with the metal ions and, hence, the mobile phase was prepared on a daily basis and protected by soda-lime tubes.

Influence of hydroxide concentration

The effect on solute distribution to the solid phase, C_s in $\mu\text{mol/g}$, versus the hydroxide concentration was investigated using glucose and sorbitol as solutes for the Eu(III) and the Fe(III) systems, respectively (Fig. 3). The initial increase in C_s is caused by the increasing degree of ionization of the sugars and subsequent complex formation with the metal ions. The decrease in C_s at high hydroxide concentrations is caused by the competition from hydroxide for complex formation and the maxima in C_s will be dependent on the pK_a values (glucose = 12.35 and sorbitol = 13.5 [7]). According to eqn. 3, $\ln C_s$ was plotted versus $\ln [OH^-]$ for sorbitol, glucuronic acid and glucose using the column in the Eu(III) form (Fig. 4). The slopes were -0.42 , -0.42 and -1.13 , respectively.

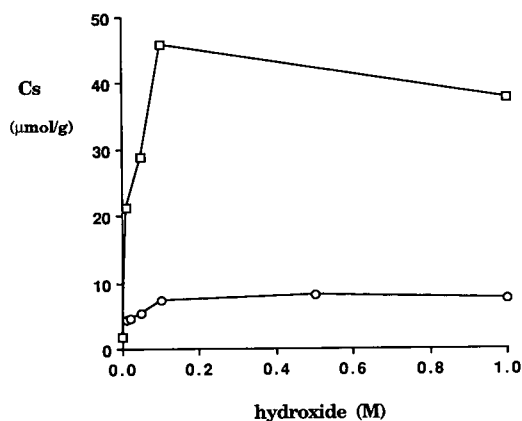


Fig. 3. pH dependence of C_s for (□) 1.0 mM glucose and (○) 1.0 mM sorbitol using the cation exchanger in europium(III) and iron(III) form, respectively, and sodium hydroxide as mobile phase.

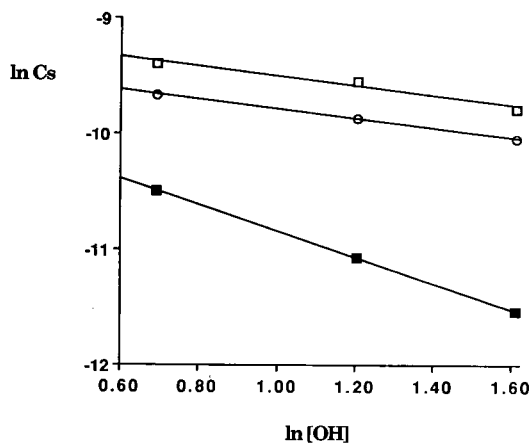


Fig. 4. Hydroxide competition on complex formation for (□) sorbitol, (○) glucuronic acid and (■) glucose on the europium (III)-loaded column plotted according to the retention model (eqn. 3).

Solute structure

The influence of solute structure on complex stability was studied by the BT technique and the results are given in Table I. All solutes were highly retained on the Eu(III) column. Di-, tri- and tetrasaccharides were retained to about the same extent (but less than the monosaccharides), possibly indicating the importance of steric effects on complex formation.

Substitution for a carboxylic acid at C-6 (sugar acids) increased the complex stability whereas an amino group (amino sugars) at C-2 gave an 80% reduction, probably owing to a decrease in the acid dissociation constants.

The sugar alcohols showed a different order in complex stability compared with their related monosaccharides (*e.g.*, xylitol–xylose, sorbitol–glucose). There was no relationship between the number of hydroxylic groups and the complex stability. As shown previously, the pK_a values is of fundamental importance (the sugar alcohols are approximately 1–10% as acidic as the corresponding monosaccharides [7]) and, most likely, the configuration of the solutes and the ability to orient the hydroxyl groups toward the metal ion are of major significance. In spite of the pK_a differences, they were retained to a similar extent as the monosaccharides, which might to be due to the more flexible and open-chain structure of the sugar alcohols, thus facilitating the complexation.

TABLE I

INFLUENCE OF STRUCTURE ON RETENTION IN THE Eu(III) SYSTEM

Column: Hitachi 3011-S, 21 × 4.6 mm I.D. in Eu(III)-form. Mobile phase: 0.1 M NaOH and 1.0 mM saccharide. C_s was measured at the inflection point with the baseline using frontal analysis.

No.	Solute	C_s ($\mu\text{mol/g}$)
<i>Monosaccharides</i>		
1	Ribose	158
2	Tagatose	119
3	Fructose	99.8
4	Sorbose	79.4
5	Lyxose	78.9
6	Galactose	74.2
7	Mannose	66.4
8	Xylose	55.2
9	Arabinose	46.9
10	Glucose	45.8
11	Fucose	40.8
<i>Disaccharides</i>		
12	Sucrose	38.4
13	Gentiobiose	37.4
14	Maltose	30.4
15	Melibiose	30.4
16	Lactose	28.9
17	Cellobiose	23.8
<i>Trisaccharide</i>		
18	Raffinose	30.2
<i>Tetrasaccharide</i>		
19	Stachyose	30.2
<i>Sugar acids</i>		
20	Galacturonic acid	77.7
21	Glucuronic acid	70.4
<i>Amino sugars</i>		
22	Galactosamine	18.9
23	Glucosamine	7.9
<i>Sugar alcohols</i>		
24	Xylitol	110
25	Sorbitol (glucitol)	104
26	Galactitol	94.8
27	Arabitol	80.2
28	Mannitol	74.8
29	Ribitol (adonitol)	41.1
<i>Micellaneous</i>		
30	myo-Inositol	43.9
31	β -Cyclodextrin	15.6

The results on the Fe(III)-loaded column are displayed in Table II. The complex stabilities were one to two orders of magnitude lower compared with

TABLE II
INFLUENCE OF STRUCTURE ON RETENTION IN THE
Fe(III) SYSTEM

Column: Hitachi 3011-S, 21 × 4.6 mm I.D. in Fe(III)-form.
Mobile phase: 0.1 M NaOH and 1.0 mM saccharide. C_s was
measured at the inflection point with the baseline using frontal
analysis.

No.	Solute	C_s ($\mu\text{mol/g}$)
<i>Monosaccharides</i>		
1	Tagatose	5.47
2	Ribose	5.20
3	Sorbose	1.98
4	Glucose	0.31
<i>Disaccharide</i>		
5	Sucrose	0.10
<i>Sugar acid</i>		
6	Glucuronic acid	0.00
<i>Sugar alcohols</i>		
7	Sorbitol (glucitol)	7.28
8	Xylitol	4.06
9	Galactitol	3.23
10	Mannitol	1.98
11	Arabitol	1.88
12	Ribitol (adonitol)	1.09

the Eu(III) column. This is certainly caused by the strong complex formation of hydroxide with the Fe(III) ion, *i.e.*, competition. Changes in selectivity

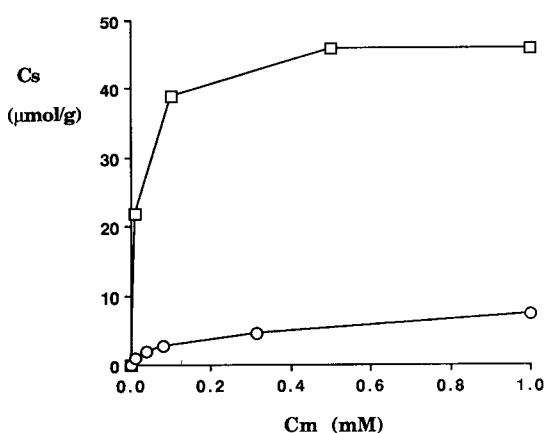


Fig. 5. Distribution isotherms for (□) glucose and (○) sorbitol on the Eu(III) and Fe(III) columns, respectively. Solute in 0.1 M NaOH as mobile phase.

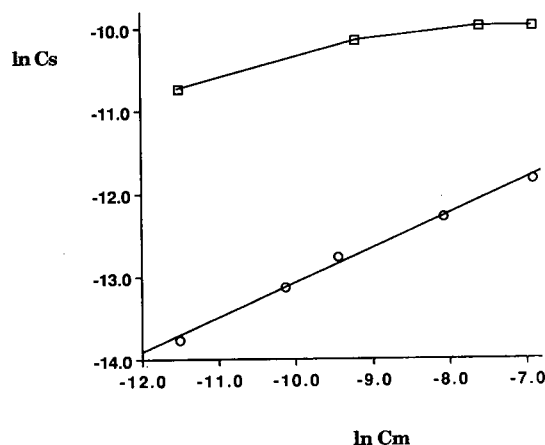


Fig. 6. Isotherms from Fig. 5 according to the retention model (eqn. 3). Symbols as in Fig. 5.

[*cf.*, the Eu(III) system] were observed for the tagatose–ribose, sorbitol–xylitol and arabitol–mannitol pairs and they were probably due to differences in ionic radius and electronic properties of the metal ions. Unexpectedly, glucuronic acid eluted with the front. As shown previously [10], few compounds were retained on the Fe(III) column and, tentatively, such a system may provide selective clean-up possibilities and subsequent separation of sugar alcohols and monosaccharides from complex matrices, *e.g.*, biological fluids.

Distribution isotherms

The isotherms for glucose and sorbitol using the Eu(III) and Fe(III) systems, respectively, were obtained from BT studies using 0.1 M NaOH as mobile phase and are shown in Fig. 5. C_s was calculated from eqn. 6. $\ln C_s$ versus $\ln C_m$ was plotted according to the retention model (eqn. 3) and the results are shown in Fig. 6. The non-linearity observed for the glucose–Eu(III) system was due to the very strong complex formation and, hence, solid-phase saturation, *i.e.*, the distribution became independent of the mobile phase concentration. Saturation effects have been previously obtained at $\ln C_s > -10.5$ [10]. The linear concentration range was probably at the low-to sub-micromolar level and because of the high capacity factors obtained (k'_{BT} for 10 μM glucose was *ca.* 3500), this was not studied further. Most of the other saccharides studied were retained to an even greater extent. The

magnitude of the complex formation constant for the sorbitol–Fe(III) system was, however, suitable and a linear relationship was obtained.

CONCLUSIONS

Saccharides were shown to form more stable complexes than the corresponding glycosides at alkaline pH with Eu(III) and Fe(III) metal ions electrostatically immobilized on a strong cation exchanger. All sugars were highly retained with the Eu(III) system whereas the Fe(III) system was selective for monosaccharides and sugar alcohols. The ligand-exchange reaction, studied by frontal analysis and being of second order, was metal ion, pH and concentration dependent. Rapid elution of the solutes was performed by introduction of an acidic mobile phase. Using this technique off- or on-line in a coupled column separation system, selective separation and isolation of saccharides from complex matrices is proposed.

ACKNOWLEDGEMENTS

Professor D. Westerlund is gratefully thanked for valuable discussions of the manuscript and Metric (Solna, Sweden) for providing the pulsed electrochemical detector.

REFERENCES

- 1 S. C. Churms, *J. Chromatogr.*, 500 (1990) 555.
- 2 J. S. Sawardeker, J. H. Sloneker and A. Jeanes, *Anal. Chem.*, 37 (1965) 1602.
- 3 C. C. Sweeley, R. Bentley, M. Makita and W. W. Wells, *J. Am. Chem. Soc.*, 85 (1963) 2497.
- 4 A. B. Blakeney, P. J. Harris, R. J. Henry and B. A. Stone, *Carbohydr. Res.*, 113 (1983) 291.
- 5 G. O. Aspinall, in G. O. Aspinall (Editor), *The Polysaccharides*, Vol. 1, Academic Press, New York, 1982, pp. 51–56 and 73–81.
- 6 F. M. Rabel, A. G. Caputo and E. T. Butts, *J. Chromatogr.*, 126 (1976) 731.
- 7 J. A. Rendleman, Jr., *Adv. Chem. Ser.*, 1 (1973) 17 and 51.
- 8 R. D. Rocklin and C. A. Pohl, *J. Liq. Chromatogr.*, 6 (1983) 1577.
- 9 R. W. Goulding, *J. Chromatogr.*, 103 (1975) 229.
- 10 M. Stefansson and D. Westerlund, *Chromatographia*, in press.
- 11 M. Stefansson and D. Westerlund, *J. Chromatogr. Sci.*, submitted for publication.
- 12 M. Stefansson and K.-J. Hoffman, *Chirality*, in press.
- 13 F. Helffrich, *Ion Exchange*, McGraw-Hill, New York, 1962, Ch. 6.

Separation of glucooligosaccharides and polysaccharide hydrolysates by gradient elution hydrophilic interaction chromatography with pulsed amperometric detection

Andrew S. Feste and Iftikhar Khan

US Department of Agriculture/Agricultural Research Service Children's Nutrition Research Center, Department of Pediatrics, Baylor College of Medicine, 1100 Bates Street, Houston, TX 77030 (USA)

(First received July 22nd, 1992; revised manuscript received October 23rd, 1992)

ABSTRACT

Commercial glucooligosaccharide mixtures (Polycose) and polysaccharide hydrolysates (acid and enzymatic) were fractionated by hydrophilic interaction chromatography and observed by pulsed amperometric detection. Seven peaks were observed when 625 ng of glucose oligomers in Polycose were fractionated. The between-run precision of retention times ($n = 10$, 100 μg , 15 peaks) ranged from a relative standard deviation (R.S.D.) of 0.09 to 0.40%; between-run precision of peak areas ($n = 10$) for the same separations had values that ranged from 2.66 to 14.4%. Injection-to-injection time was 48 min. When polysaccharide hydrolysates were fractionated using a gradient program capable of resolving all of the oligosaccharide species, dextran-derived α -(1 \rightarrow 6)-glucooligosaccharides were retained to a greater degree than amylose-derived α -(1 \rightarrow 4)-glucooligosaccharides, which were retained to a greater degree than β -(2 \rightarrow 1)-fructooligosaccharides derived from inulin. Excluding the peaks that eluted before glucose or fructose, 25 to 35 peaks were observed after fractionation of the hydrolysates. Differences in elution profiles were observed between acid and enzymatic hydrolysis products of the same polysaccharide as well as between hydrolysis products of different polysaccharides. In conjunction with high-performance size-exclusion chromatography, the method demonstrated the effect of preheating starch before hydrolysis with isoamylase.

INTRODUCTION

Hydrophilic interaction chromatography (HIL-IC) [1,2] describes the separation of polar molecules on a variety of hydrophilic bonded supports [3–12]. The mechanism by which carbohydrates are separated, as determined on silica bonded amine columns [7,11], appears to result from the partitioning of the carbohydrate between the amine-bound water layer and the mobile phase.

Glucose oligomers are used in medicine, biomedical research and the biotechnology industry. Consequently, a variety of chromatographic procedures have been devised for their separation and analysis. Size-exclusion chromatography has been used to

fractionate oligomers of amylose, cellulose, pullulan and dextran [13]; oligomers with a degree of polymerization (DP) between 1 and 20 have been resolved, and differences in the retention times of α -(1 \rightarrow 4)- and α -(1 \rightarrow 6)-glucosidic linkages have been observed. Cation-exchange supports loaded with either Ag^+ or H^+ counterions have been used to fractionate degradation products in biomass hydrolysates [14], enzymatic starch digests [15], and malto-, cello-, galacturonic- and chitooligosaccharides [16] (oligomers \leq DP 14 were resolved). Glucooligomers have been separated on a C_{18} -bonded vinyl alcohol copolymers support using alkaline eluents, and oligomers up to DP 23 were resolved [17]. Chromatography of cellooligosaccharides on a silica-bonded C_{18} column resulted in the resolution of oligosaccharides up to DP 30, and 10 pmol of cellotetraose were detected electrochemically after

Correspondence to: Dr. Andrew S. Feste, Children's Nutrition Research Center, 1100 Bates Street, Houston, TX 77030, USA.

passage through a cellulase-based enzyme reactor [18]. Glucooligosaccharides (up to DP 35) were resolved on a 3- μm amine-bonded silica support [10], and a polyamine-bonded polymer support was used to separate dextran oligosaccharides up to DP 8 [19]. High-performance anion-exchange chromatography resolved glucooligosaccharides and polysaccharides (DP \geq 50) using alkaline eluents followed by pulsed amperometric detection [20]. The same methodology was used to analyze isoamylase digests of amylopectin from various sources, and plots of concentration *versus* DP served as chromatographic “fingerprints” [21].

In a previous study [22], 33 μg of a glucooligosaccharide mixture with added monosaccharide were fractionated by HILIC on a Protein-Pak 60 column and 19 peaks were resolved; fractionation and column reequilibration required 90 min. The objectives of the present study were (1) to decrease the fractionation time of glucooligosaccharides in Polycose and to submit to HILIC nanogram amounts of Polycose, (2) to determine the retention times of enzyme and acid hydrolysates of polysaccharides using identical gradient conditions, and (3) to demonstrate the potential of HILIC and high-performance size-exclusion chromatography (HPSEC) as chromatographic tools in the investigation of starch structure.

EXPERIMENTAL

Materials

The custom-packed Protein-Pak 60 column was from Waters (Milford, MA, USA). The Bio-Gel SEC-60 XL and guard columns were purchased from Bio-Rad (Richmond, CA, USA). Inulin (from chicory root), amylose (Type III, from potato), amylopectin (from corn), starch (soluble ACS reagent, from potato), dextran (clinical grade, produced by *Leuconostoc mesenteroides*), trifluoroacetic acid (TFA), dextranase (EC 3.2.1.11, from *Penicillium* sp.), and isoamylase (EC 3.2.1.68, from *Pseudomonas amyloclavata*) were purchased from Sigma (St. Louis, MO, USA). Acetonitrile (HPLC grade) and sodium hydroxide solution, 50% (w/w), were obtained from Fisher Scientific (Houston, TX, USA).

Hydrophilic interaction chromatography

Chromatography was performed on a Waters 860 system; the system configuration was described previously [22]. A Waters custom-packed Protein-Pak 60 column (150 mm \times 7.9 mm I.D., 10 μm) was used to separate a commercially available mixture of glucooligosaccharides (Polycose) and acid and enzymatic hydrolysates of polysaccharides. A temperature control unit (Waters) was used to

TABLE I
GRADIENT ELUTION CONDITIONS FOR THE FRACTIONATION OF OLIGOSACCHARIDES

Oligosaccharides	Time (min)	Acetonitrile (% v/v)	Water (% v/v)
Glucose polymers from Polycose	0	67	33
	1	67	33
	8	60	40
	10	60	40
	17	55	45
	19	55	45
	27	50	50
	37	50	50
	48	67	33
Oligosaccharides from acid and enzymatic hydrolysates of amylose, amylopectin, starch, dextran and inulin	0	67	33
	10	67	33
	65	50	50
	75	50	50
	86	67	33

maintain the column temperature at 25°C. Samples (10–25 μ l) were injected by a Waters Model 710 Wisp autoinjector and separated by gradient elution at 1.0 ml/min using two Waters Model 510 pumps; the gradient programs for the elution of the oligosaccharides are described in Table I. Solvents were sparged with helium and maintained in a helium atmosphere. Postcolumn eluate was delivered into a 3-way PTFE mixing tee and mixed with 0.5 *M* sodium hydroxide which was delivered at a flow-rate of 0.6 ml/min (helium, at 4.13 bar). After mixing, the peaks were detected with a Waters Model 464 pulsed electrochemical detector equipped with a gold working electrode. The potentials and time periods were set as follows: E1 was 0.1 V, E2 was 0.6 V, E3 was –0.6 V, T1 was 500 ms, T2 was 166 ms, and T3 was 83 ms. For all fractionations, the detector was set at 2.0 μ A except where otherwise specified.

High-performance size-exclusion chromatography

Starch and isoamylase digests of starch were chromatographed on a Bio-Gel SEC-60 XL column (300 mm \times 7.5 mm I.D., 13 μ m) equipped with a guard column. Samples (10 μ l) were injected and eluted isocratically at 1.0 ml/min; Milli-Q water was the mobile phase. Polysaccharides were detected with the Model 464 detector, and with the exception of the detector setting (5.0 μ A), all other detector parameters were identical to those described for HILIC.

Partial acid hydrolysis

Amylose, amylopectin and starch (20 mg each) were mixed separately with 10 ml of 0.1 *M* TFA and hydrolyzed for 15.0 min at 100°C [10]; after hydrolysis, the solutions were centrifuged at 3600 *g* for 3.0 min to remove insoluble polysaccharide. The supernatant was lyophilized, and the dry material was weighed and redissolved in Milli-Q water to a final concentration of 10.0 mg/ml. Dextran (20 mg) was hydrolyzed with 10.0 ml of 0.3 *M* TFA for 30 min at 100°C [10]; after centrifugation and lyophilization of the supernatant as described above, the dry material was weighed and redissolved in Milli-Q water to a final concentration of 10.0 mg/ml. Inulin (20 mg) was mixed with 10.0 ml of 0.1 *M* TFA and hydrolyzed for 15 min at 30°C. This solution was centrifuged and the supernatant lyophilized as

above; the material was weighed and redissolved in Milli-Q water to a final concentration of 10.0 mg/ml.

Enzymatic hydrolysis

Amylose, amylopectin and starch (100 mg each) were digested with isoamylase, with modifications, as previously described [21]. Briefly, the polysaccharides were suspended separately in 0.025 *M* sodium acetate buffer, pH 4.5, to a final concentration of 10.0 mg/ml. Isoamylase (35 000 U, 5.54 μ g) was added and the mixtures were hydrolyzed for 16 h at 45°C. After hydrolysis, the mixtures were heated at 100°C for 5.0 min, then cooled to ambient temperature. The mixtures were centrifuged for 3.0 min at 3600 *g*, the supernatants were lyophilized, and the hydrolysates were resuspended in Milli-Q water to a final concentration of 10.0 mg/ml. In a separate experiment, starch was digested with isoamylase as stated above, except that before the addition of enzyme, the substrate was heated at 100°C for 5.0 min and then allowed to cool. The mixture was centrifuged for 3.0 min at 3600 *g*, lyophilized, and was resuspended in Milli-Q water to a final concentration of 10.0 mg/ml. In one set of substrate controls, one sample was heated for 5.0 min at 100°C while the other was not; both samples were then centrifuged (3.0 min, 3600 *g*), lyophilized, and resuspended to a final concentration of 10.0 mg/ml. In the second set, one sample was heated at 100°C for 5.0 min while the other was not; both samples were then incubated, without enzyme, for 16 h at 45°C. After centrifugation (3.0 min, 3600 *g*) and lyophilization of the supernatant, the dried material was resuspended in Milli-Q water to a final concentration of 10.0 mg/ml. Dextran (100 mg) was dissolved in 10.0 ml of 0.1 *M* potassium phosphate buffer, pH 6.0 and 50 μ l of dextranase (50 μ g, 10 U) was added. The mixture was heated for 15.0 min at 37°C [23], and the enzyme was deactivated by heating at 100°C for 5.0 min. After the mixture cooled, it was centrifuged (3.0 min, 3600 *g*), lyophilized, and resuspended to a final concentration of 10.0 mg/ml. After each aforementioned treatment, 10 μ l of sample were submitted to HPSEC, 25 μ l to HILIC.

Separation of a commercial glucose polymer mixture

Polycose was added to Milli-Q water to a concentration of 10.0 mg/ml then diluted to concentrations

of 2.5, 1.25, 0.625 and 0.0625 mg/ml. The solutions were injected separately onto the Protein-Pak 60 column and fractionated by the gradient program described in Table I. The detector sensitivity was set between 0.2 μA and 10.0 μA .

Precision studies

To determine reproducibility of the fractionation of glucooligosaccharides, five samples of the Polycose mixture were separated by HILIC on two consecutive days; the within-run ($n = 5$) and between-run ($n = 10$) precision of the retention times and peak areas were determined. A 10- μl volume containing 100 μg of the Polycose mixture was injected

and fractionated using the gradient program described in Table I. The detector sensitivity was set at 10.0 μA .

Determination of retention times of oligosaccharides from polysaccharide hydrolysates

A 25- μl volume of the amylose ($n = 3$), dextran ($n = 3$), and inulin acid hydrolysates (3 hydrolysates, 1 injection) were fractionated by HILIC using the gradient program described in Table I. The detector sensitivity was set at 2.0 μA .

Statistical methods

Analysis of variance for repeated measures and

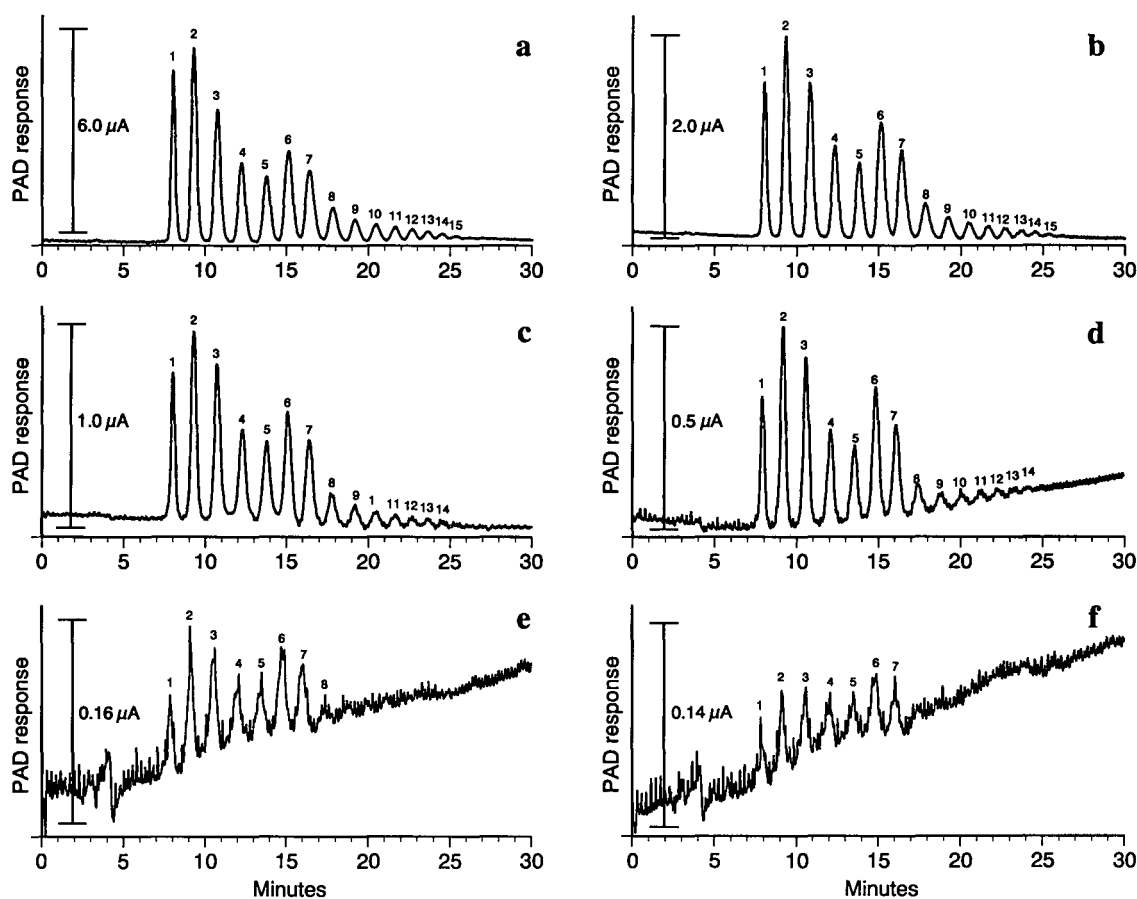


Fig. 1. The gradient elution HILIC fractionation of nanogram to microgram amounts of Polycose. The tracings depict the fractionation of Polycose in the following amounts: 100 μg (a), 25 μg (b), 12.5 μg (c), 6.25 μg (d), 1.25 μg (e) and 0.625 μg (f). The detector settings were 10.0 μA (a), 2.0 μA (b), 1.0 μA (c), 0.5 μA (d) and 0.2 μA (e and f). The gradient elution conditions are described in Table I, and the retention times of the peaks are listed in Table II. PAD = Pulsed amperometric detection.

trend analysis (BMDP2V statistical software package) were used to compare species (dextran, amylose, and inulin hydrolysates) across peaks. A multiple comparison procedure [24] was then used to isolate differences between species at specific peaks.

RESULTS AND DISCUSSION

Precision studies and chromatography of ng to μg amounts of glucose polymers

After separation of 100 μg (Fig. 1a) and 25 μg (Fig. 1b) of Polycose by HILIC, 15 peaks were observed; injection of 12.5 μg (Fig. 1c) and 6.25 μg (Fig. 1d) of material resulted in the detection of 14 peaks. Fractionation of smaller amounts of Polycose resulted in the detection of fewer peaks: 8 peaks for 1.25 μg (Fig. 1e), and 7 peaks for 625 ng (Fig. 1f). The within-run precision values of the retention times (Table II, $n = 10$, 100 μg , 15 peaks) were from 0.05 to 0.37% relative standard deviation (R.S.D.); the values for the between-run precision of the retention times were 0.09 to 0.40% R.S.D. (Table II). Values for the within-run precision for peak areas were from 1.14 to 6.19% R.S.D.; thir-

teen of the peaks had values less than 5.0% R.S.D. The between-run precision values of peak areas were from 2.66 to 14.4% R.S.D.; nine peaks had values less than 4.10% R.S.D. A previous report described the separation of glucose polymers on aqueous size-exclusion columns by HILIC [22]; of those columns, the Protein-Pak 60 (diol-bonded silica) resolved 19 peaks when 33 μg of a glucooligosaccharide mixture (Polycose) with added monosaccharides were fractionated by gradient elution; 90 min were required to separate the glucose polymers and reequilibrate the column (300 mm \times 7.9 mm I.D.). In addition, the α factors (ratio of capacity factors) for the separation of DP 1 through DP 7 were larger than were required for baseline resolution. In the present study, a custom-packed Protein-Pak 60 column (150 mm \times 7.9 mm I.D.) was used to shorten the analysis time, and an altered gradient program was used to decrease the α factors for the separation of DP 1 through DP 7. The initial starting condition was reduced from 70% aqueous acetonitrile [22] to 67% aqueous acetonitrile; the gradient slope was not significantly altered. The reduction in column length enabled the resolution of 15

TABLE II

WITHIN-RUN AND BETWEEN-RUN PRECISION OF RETENTION TIMES (t_R) AND PEAK AREAS FOR THE GRADIENT ELUTION SEPARATION OF GLUCOSE POLYMERS ON THE PROTEIN-PAK 60 COLUMN

Peak no. ^a	Within-run ($n = 5$)				Between-run ($n = 10$)			
	t_R (min)		Area ($\mu\text{V/s}$)		t_R (min)		Area ($\mu\text{V/s}$)	
	Mean	R.S.D. (%)	Mean	R.S.D. (%)	Mean	R.S.D. (%)	Mean	R.S.D. (%)
1	7.83	0.05	11 229 981	6.19	7.82	0.09	9 712 271	14.4
2	9.07	0.24	16 357 890	3.42	9.04	0.21	14 975 394	8.91
3	10.4	0.23	11 749 878	1.33	10.4	0.30	11 265 174	4.08
4	11.9	0.37	7 276 845	1.41	11.9	0.26	7 090 427	3.62
5	13.4	0.33	5 935 130	1.20	13.4	0.40	5 773 448	3.06
6	14.7	0.30	8 164 714	3.50	14.7	0.21	8 549 155	4.02
7	15.9	0.28	6 401 022	3.32	15.9	0.20	6 582 857	2.69
8	17.2	0.24	3 055 016	1.22	17.2	0.28	2 945 452	4.09
9	18.6	0.22	1 968 951	1.14	18.6	0.38	1 854 749	2.66
10	19.7	0.22	1 419 840	1.32	19.8	0.21	1 311 617	8.23
11	21.0	0.21	1 053 027	2.85	21.0	0.24	986 847	5.88
12	22.0	0.20	765 165	1.96	22.0	0.19	745 510	3.99
13	23.1	0.19	508 647	1.95	23.0	0.14	491 572	3.41
14	24.0	0.19	292 153	5.32	23.9	0.18	300 886	6.00
15	24.7	0.18	150 921	4.95	24.7	0.17	157 175	6.81

^a For peaks see Fig. 1a.

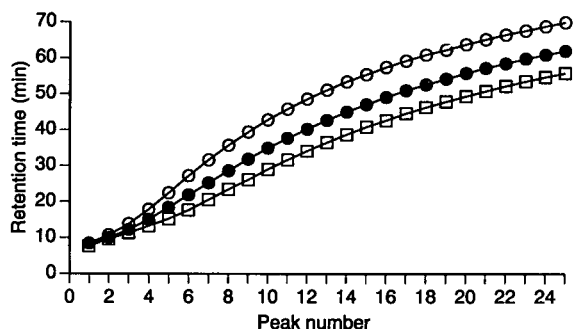


Fig. 2. Retention times of polysaccharide-derived oligosaccharides after HILIC. Oligosaccharides from dextran (○), amylose (●) and inulin (□) were prepared as described in the Experimental section and fractionated by gradient elution as described in Table I.

peaks within 26 min and an injection-to-injection time of 48 min. The lower starting concentration of acetonitrile reduced the α factors for the separation of DP 1 through DP 7 without sacrificing baseline resolution (Fig. 1). The gradient used for fractionation of glucooligosaccharides in Polycose (Table I) was also used to fractionate glucooligosaccharides and glucose polymers in hydrolysates of amylose, amylopectin, starch, and dextran (data not shown). Fructooligosaccharides fractionated with the same gradient, however, were not completely resolved (data not shown).

Retention times of polysaccharide hydrolysates

The retention times observed for the oligosaccharides and polysaccharides derived from polysaccharide hydrolysates are depicted in Fig. 2. The composition, bond type, and linkage position of the oligosaccharides studied are listed in Table III. The objective of this experiment was to determine the effect of composition and linkage position on the reten-

tion times of the different oligosaccharide and polysaccharide species. These retention times were determined using the same gradient elution program rather than an isocratic mobile phase, which requires inordinately long fractionation times for oligosaccharides of DP 10 to DP 30. The gradient depicted in Table I was chosen because it enabled resolution of the fructooligosaccharides obtained from acid hydrolysis of inulin; the gradient used for the fractionation of glucooligosaccharides in Polycose was not able to resolve the fructooligosaccharides in the inulin hydrolysate. For the oligosaccharides obtained from hydrolysates of amylose and dextran, the numbering of peaks was initiated with glucose (peak 1); for the oligosaccharides obtained from the hydrolysis of inulin, the numbering of the peaks was initiated with fructose (peak 1). The retention times of the oligosaccharides derived from the acid- and enzymatic hydrolysis of amylose, amylopectin and starch were identical; consequently, only the retention times of the amylose-derived oligosaccharides are depicted in Fig. 2. The R.S.D. of the retention times of the oligosaccharides derived from dextran, amylose, and inulin had values that ranged from 0 to 0.56% (80% < 0.36), 0 to 0.82% (88% < 0.30), and 0 to 0.60 (72% < 0.38), respectively. Although peak number cannot unequivocally be equated with DP (except for DP 1 to DP 10 for α -(1 → 4)-glucooligosaccharides, data not shown), it is likely that they correspond. Even so, each species of oligosaccharide (all peaks within a series) clearly exhibited different retention times ($p < 0.001$) when fractionated using identical gradient elution conditions. Glucose (peak 1, Fig. 2) produced by hydrolysis of amylose and dextran had a retention time of 8.42 min, and fructose (peak 1, Fig. 2) produced by hydrolysis of inulin had a retention time of 7.65 min. Subsequent comparisons at

TABLE III

GLYCOSIDIC BOND TYPE, LINKAGE POSITION, AND COMPOSITION OF THE POLYSACCHARIDES STUDIED

Polysaccharide	Glycosidic bond type, linkage position and composition
Amylose	Linear α -(1→4)-glucopyranosyl units with few α -(1→6)-glucopyranosyl units
Amylopectin	Linear α -(1→4)-glucopyranosyl and branched α -(1→6)-glucopyranosyl units
Dextran	Linear α -(1→6)-glucopyranosyl units
Starch	Amylopectin-amylose (80:20)
Inulin	Linear β -(2→1)-fructofuranosyl units with terminal α -(1→1)-glucopyranosyl

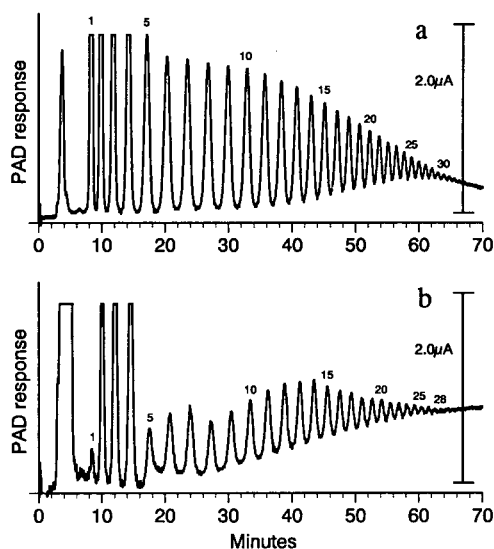


Fig. 3. HILIC of amylose hydrolysates. Elution profiles of the products of acid hydrolysis (a) and isoamylase hydrolysis (b). Hydrolysates were prepared as described in the Experimental section and chromatographed using the gradient elution program depicted in Table I.

specific peaks (for peaks 2–25) indicated differences between all three species ($p < 0.001$; p represents the probability value based on analysis of variance) at all peaks, *i.e.*, the retention time of any peak (2–25) was significantly different for all three species. The data clearly demonstrate that α -(1→6)-glucooligosaccharides (dextran) were retained to a greater degree than the α -(1→4)-glucooligosaccharides (amylose, amylopectin, and starch), which in turn were retained to a greater degree than β -(2→1)-fructooligosaccharides (inulin). When α -(1→4)- and α -(1→6)-glucooligosaccharides were separated on an amine-bonded silica column using an isocratic mobile phase composition of 57% (v/v) acetonitrile in water, similar results were obtained [10], *i.e.*, α -(1→6)-glucooligosaccharides were retained to a greater degree than were the α -(1→4)-glucooligosaccharides.

HILIC of the hydrolysates of amylose, amylopectin, dextran, and inulin

HILIC of the glucooligosaccharides obtained by partial acid hydrolysis of amylose (Fig. 3a) revealed 30 glucooligosaccharide peaks, whereas HILIC of the glucooligosaccharides obtained by isoamylase

hydrolysis of amylose (Fig. 3b) revealed 28 glucooligosaccharide peaks. The chromatogram depicted in Fig. 3b was not expected; amylose is comprised of a mixture of linear, α -(1→4) linked molecules and molecules with a limited number of long-chain branches involving $-(1 \rightarrow 6)$ linkages [25]. Enzymatic hydrolysis with isoamylase should not, therefore, have resulted in the profile observed (Fig. 3b). When amylose was digested under similar conditions without enzyme (0.025 M sodium acetate, pH 4.5, 45°C, 16 h, data not shown), peaks 1–4 were produced to the degree observed in Fig. 3b; however, peaks 5–20 were present in minor amounts and did not resemble the profile in Fig. 3b. Although the amylose preparation was supposed to be essentially free of amylopectin, a comparison of peaks 5–28 in Fig. 3b with peaks 5–33 in Fig. 4b (isoamylase digest of amylopectin) reveals a similarity in the elution profiles. It is likely, therefore, that the amylose preparation contained amylopectin. In a previous study that used a silica-bonded amine column to fractionate partial acid hydrolysates of amylose, 32 peaks were resolved [10]. When anion-exchange chromatography was used to fractionate a mixture of short-chain amylose, approximately 46 peaks were resolved; maltodextrins pre-

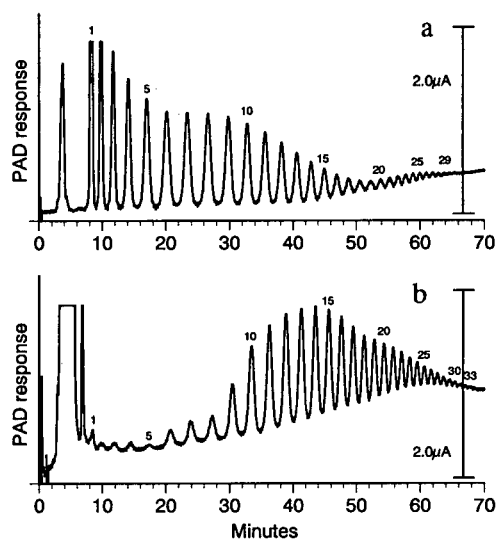


Fig. 4. HILIC of amylopectin hydrolysates. Elution profiles of the products of acid hydrolysis (a) and isoamylase hydrolysis (b). Hydrolysates were prepared as described in the Experimental section and chromatographed using the gradient elution program depicted in Table I.

pared from Amylo-Waxy maize were resolved into approximately 85 peaks [20]. The fractionation of amylose hydrolysates in this communication and on the silica-bonded amine column [10] used acetonitrile–water eluents, while the fractionation of the glucose polymers on the anion exchange column used alkaline eluents [20]. The greater solubility of glucose polymers in alkaline solution was responsible for the observation of the greater number of peaks observed after anion exchange analysis [20].

Fractionation of the partial acid hydrolysis products of amylopectin resulted in the separation of 29 peaks (Fig. 4a). Equal amounts of amylose and amylopectin were acid-hydrolyzed and fractionated using identical conditions; although the peaks were not quantitated, the amylopectin peak areas were smaller than the amylose peak areas, which indicated that the amylopectin was hydrolyzed less completely than the amylose. In addition, the relative intensity of peak areas for peaks 2–30 (Figs. 3a, 4a) was different for both hydrolysates. The elution profile of the fractionated enzymatic hydrolysates of amylopectin (Fig. 4b) was substantially different from the profile of the fractionated acid hydrolysates; a total number of 33 peaks were separated and the relative intensity of the peak areas of peaks

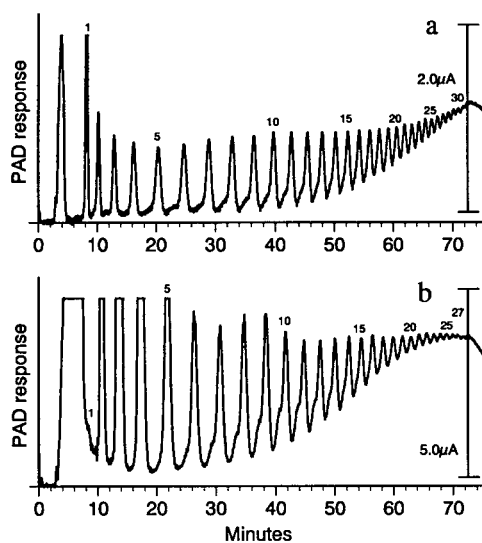


Fig. 5. HILIC of dextran hydrolysates. Elution profiles of the products of acid hydrolysis (a) and dextranase hydrolysis (b). Hydrolysates were prepared as described in the Experimental section and chromatographed using the gradient elution program depicted in Table I.

1–33 was different from that of the peak areas of peaks 1–30 observed after acid hydrolysis. Anion-exchange chromatography with alkaline eluents was used to estimate the chain-length distribution of amylopectin obtained from various sources [21]. Fifty-five to sixty peaks were resolved; as was the case with glucose polymers derived from amylose [20], the enhanced solubility of the higher-molecular-mass polymers in the alkaline mobile phase resulted in the greater number of peaks [21]. Although only 33 peaks were observed after HILIC (Fig. 4b), the elution pattern (peaks 1–33) closely resembled the patterns obtained after anion-exchange analysis [21].

Fractionation of the partial acid hydrolysis products of dextran resulted in the resolution of 30 peaks. When compared to the elution profiles of acid hydrolysates from amylose (Fig. 3a) and amylopectin (Fig. 4a), the profile of the dextran acid hydrolysates (Fig. 5a) was quite different; in general, smaller amounts (that is, lower relative intensity of peak areas) of the products represented by peaks 1–9 were produced by acid hydrolysis of dextran. In addition, the differences in the relative intensity of peak areas for peaks 2–30 (Fig. 5a) were less pronounced than for the acid hydrolysates of amylose (Fig. 3a) and amylopectin (Fig. 4a). Twenty-seven peaks were resolved after fractionation of the dextranase hydrolysis products (Fig. 5b). In contrast to the results from acid hydrolysis, much less of peak 1 (glucose) was produced by enzymatic hydrolysis with dextranase. Chromatography of partial acid hydrolysates of dextran on silica-bonded amine [10] and anion-exchange [20] columns resulted in the resolution of approximately 28 and 40 peaks, respectively.

Inulin represents a group of polymers called “fructans”; they are polymers comprised of β -(2→1)-D-fructofuranosyl units which contain terminal D-glucosyl residues [26]. The conditions for the partial acid hydrolysis of inulin were much milder than for the other polysaccharides. After fractionation of the hydrolysis products, 35 peaks were resolved; peak 1 was fructose. Including the three peaks that eluted before fructose, the total number of peaks observed was 38 (Fig. 6).

HILIC of starch hydrolysis products

The elution profile obtained after fractionation of the acid hydrolysates of starch (Fig. 7a) closely

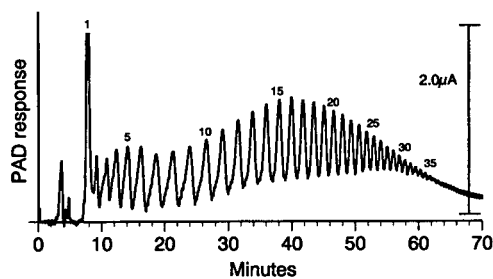


Fig. 6. HILIC of inulin acid hydrolysis products. Inulin was hydrolyzed as described in the Experimental section and the oligosaccharides were fractionated using the gradient elution program depicted in Table I.

resembled the elution profile of the amylose acid hydrolysates (Fig. 3a); a total of 30 peaks were resolved. Very little hydrolysis occurred when starch was digested with isoamylase for 16 h at 45°C (Fig.

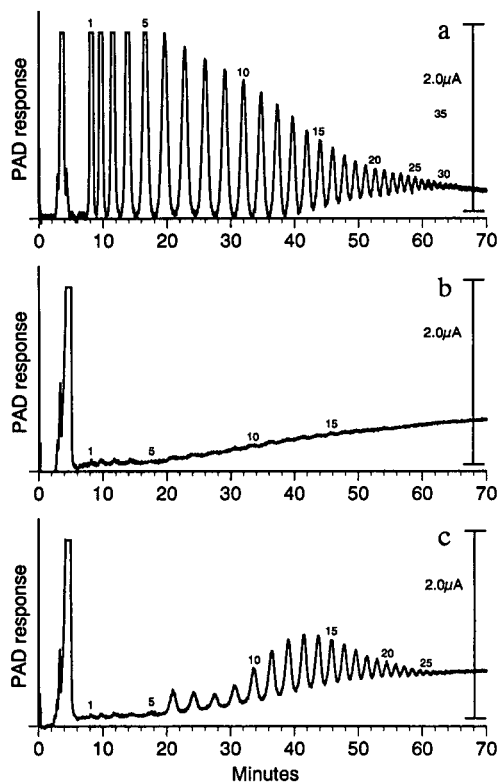


Fig. 7. HILIC of starch hydrolysates. Elution profiles of acid hydrolysate (a), isoamylase digest without preheating (b) and isoamylase digest with preheating (c). Hydrolysates were prepared as described in the Experimental section and chromatographed by the gradient elution program depicted in Table I.

7b). However, when starch was heated for 5.0 min at 100°C, cooled to ambient temperature, and then reacted with isoamylase, hydrolysis occurred (Fig. 7c). Potato starch contains approximately 80% amylopectin and 20% amylose [25], and the elution profile of the isoamylase digest of starch (Fig. 7c) resembled the elution profile obtained after fractionation of the isoamylase digest of amylopectin (Fig. 4b). Twenty-six peaks were observed (Fig. 7c). Starch granules are comprised of amorphous regions that are susceptible to hydrolysis and crystalline regions that are resistant to hydrolysis [27]. The crystalline regions may exist as a consequence of the presence of double helical chains formed between adjacent amylose molecules or adjacent clusters of chains in either the same or neighboring amylopectin molecules [27]. In addition, an amylopectin-rich zone may be located near the surface of the granule [27]. When potato starch in warm water was heated to approximately 70°C, amylose of relatively low DP was released and a high-molecular-mass β -amylolysis limit fraction could be extracted [28]; heating the starch enabled isoamylase hydrolysis, which might have occurred as a result of (1) hydrolysis of released species, or (2) hydrolysis of a newly exposed region of the heat-ruptured granule that contained amylopectin.

HPSEC of starch and starch hydrolysis products

The Bio-Gel SEC-60 XL column reportedly exhibits a fractionation range of M_r 40 000 to 8 000 000 for polyethylene glycols, and its range was estimated at $M_r \leq 200\,000\,000$ daltons for globular proteins [29]; the support is made up of a hydrophilic, hydroxylated polyether. When starch was left at ambient temperature for 5.0 min, then fractionated by HPSEC, one peak at 12.2 min was observed (Fig. 8a). However, after starch was exposed to 100°C for 5.0 min, the HPSEC elution profile revealed the presence of species that eluted at 4.34, 5.60, 6.77 and 12.1 min. (Fig. 8d). These products could represent the low-DP and high-DP species that were released when potato starch was heated at 70°C [28]. Fig. 8b represents the elution profile of starch after 16 h at 45°C, while Fig. 8e represents the elution profile of starch after it was heated at 100°C for 5.0 min, then at 45°C for 16 h. The elution profiles are identical. Heating (16 h, 45°C) caused the solubilization of the species depicted in Fig. 8b;

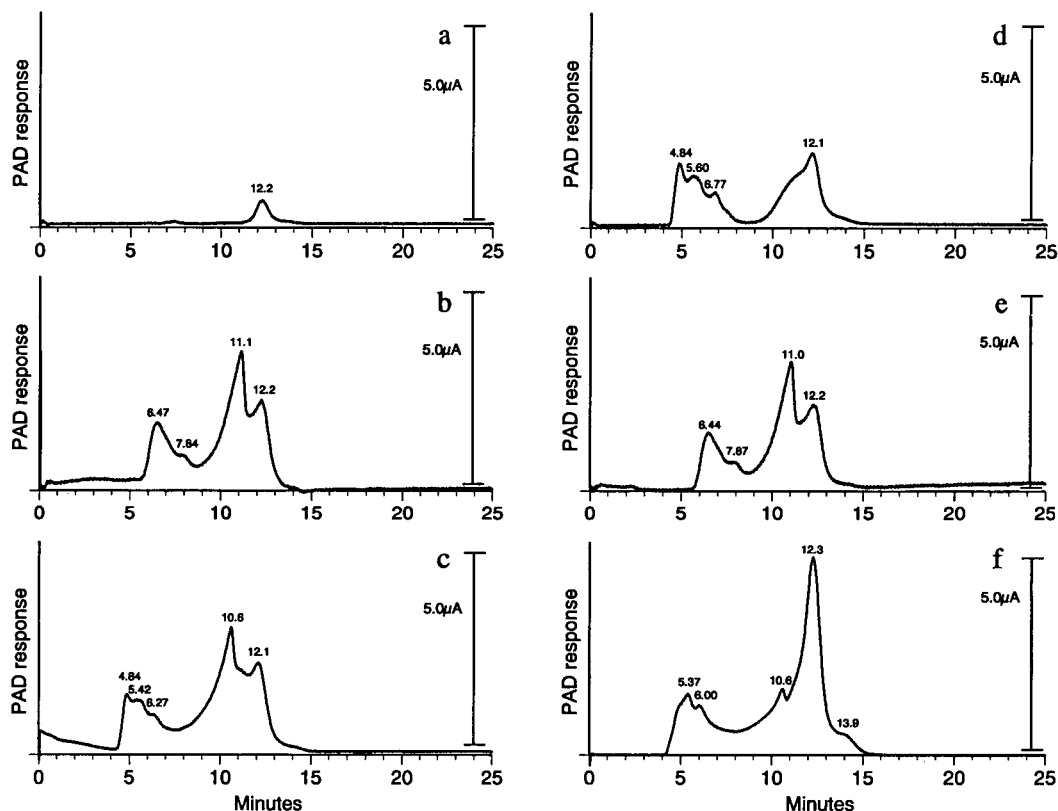


Fig. 8. HPSEC of starch and hydrolysis products. Fractionation of starch that was not preheated (a), starch that was not preheated, but was then heated at 45°C for 16 h (b), isoamylase digest of starch that was not preheated (c), starch that was preheated (d), starch that was preheated, then further heated at 45°C for 16 h (e) and isoamylase digest of starch that was preheated (f). Samples were prepared and chromatographed as described in the Experimental section.

these species do not, however, serve as substrates for isoamylase (Fig. 7b). Because the preheated starch produced the same elution profile after 16 h at 45°C (Fig. 8e) as did the starch that was not preheated (Fig. 8b), it is possible that the products released by heat rupture of the granule (Fig. 8d) are aggregates and that heating for 16 h at 45°C may cause dissociation and thereby result in the elution profile depicted in Fig. 8e. If so, then the products observed after heat pretreatment (Fig. 8d and e) are probably not substrates for isoamylase. When isoamylase was added to starch that was not preheated, and the mixture was then incubated, the elution profile changed (Fig. 8c), and species were observed whose molecular masses were apparently higher (4.84, 5.42 and 6.27 min). Although significant isoamylase hydrolysis did not occur (Fig. 7b), limited hydrolysis could have yielded the products ob-

served (Fig. 8c). Addition of isoamylase to starch after the heat pretreatment (Fig. 8f), resulted in an elution profile that was different from those depicted in Fig. 8a and e. Aside from the alteration in retention times, the peak at 12.3 min had a much larger peak area than the peak with the same retention time in any of the other chromatograms (Fig. 8a and e). The peaks at 12.3 and 13.9 min could represent species that were formed by hydrolysis of accessible regions of the starch granule that contained amylopectin; other products included the oligosaccharides depicted in Fig. 7c. Although the interpretations of the data depicted in the elution profiles in Figs. 7 and 8 are not conclusive, this communication demonstrates the utility of HILIC and HPSEC as tools for investigating starch structure.

CONCLUSIONS

Nanogram to microgram amounts of glucooligosaccharides were fractionated within 26 min. The method and the conditions described for the fractionation of Polycose have potential use for the manufacturers of infant formulas. When the gradient program was altered to enable the resolution of oligo- and polysaccharides from different polysaccharide hydrolysates, the retention behavior of the column was significantly different for the different polysaccharide hydrolysates that were fractionated. Although the lower solubility of higher-molecular-mass glucose polymers in acetonitrile–water eluents may not allow the fractionation of polymers of DP \geq 35–40, retention time precision and chromatographic resolution using different gradient programs demonstrate the utility of HILIC. Furthermore, these two chromatographic techniques, HILIC and HPSEC (with pulsed amperometric detection), will be powerful tools for the investigation of polysaccharide structure.

ACKNOWLEDGEMENTS

We thank Jerry Eastman for his editorial assistance, Adam Gillum for producing the figures, O'Brian Smith for the statistical analysis, and Daryl Friday of Waters, a division of Millipore, Inc., for his many helpful discussions.

This work is a publication of the US Department of Agriculture/Agricultural Research Service Children's Nutrition Research Center, Department of Pediatrics, Baylor College of Medicine and Texas Children's Hospital, Houston, TX, USA. This project has been funded in part with federal funds from the US Department of Agriculture, Agricultural Research Service under Cooperative Agreement number 58-6250-1-003. The contents of this publication do not necessarily reflect the views or policies of the US Department of Agriculture, nor does mention of trade names, commercial products, or organizations imply endorsement by the US Government.

REFERENCES

- 1 A. Alpert, *J. Chromatogr.*, 499 (1990) 177.
- 2 B.-Y. Zhu, C. T. Mant and R. S. Hodges, *J. Chromatogr.*, 594 (1992) 75.
- 3 M. Verzele and F. Van Damme, *J. Chromatogr.*, 362 (1986) 23.
- 4 V. Carunchio, A. M. Girelle and A. Messina, *Chromatographia*, 23 (1987) 731.
- 5 J. C. Linden and C. L. Lawhead, *J. Chromatogr.*, 105 (1979) 125.
- 6 F. C. Rabel, A. G. Caputo and E. T. Butts, *J. Chromatogr.*, 126 (1976) 731.
- 7 L. A. Th. Verhaar and B. F. M. Kuster, *J. Chromatogr.*, 234 (1982) 57.
- 8 M. D'Amboise, D. Noel and T. Hanai, *Carbohydr. Res.*, 79 (1980) 1.
- 9 K. Koizumi, Y. Okada, T. Utamura, M. Hisamatsu and M. Amemura, *J. Chromatogr.*, 299 (1984) 215.
- 10 K. Koizumi, T. Utamura and Y. Okada, *J. Chromatogr.*, 321 (1985) 145.
- 11 Z. L. Nikolav and P. J. Reilly, *J. Chromatogr.*, 325 (1985) 287.
- 12 C. Brons and C. Olieman, *J. Chromatogr.*, 259 (1983) 79.
- 13 V. M. B. Cabalda, J. F. Kennedy and K. Jumel, in R. B. Friedman (Editor), *Biotechnology of Amylodextrin Oligosaccharides* (ACS Symposium Series, No. 458), American Chemical Society, Washington, DC, 1991, p. 146.
- 14 G. Bonn, *J. Chromatogr.*, 387 (1987) 393.
- 15 H. Derler, H. F. Hormeyer and G. Bonn, *J. Chromatogr.*, 440 (1988) 281.
- 16 K. B. Hicks and A. T. Hotchkiss, Jr., *J. Chromatogr.*, 441 (1988) 382.
- 17 K. Koizumi and T. Utamura, *J. Chromatogr.*, 436 (1988) 328.
- 18 P. C. Maes, L. J. Nagels, C. Dewaele and F. C. Alderweireldt, *J. Chromatogr.*, 558 (1991) 343.
- 19 N. Hirata, Y. Tamura, M. Kasai, Y. Yanagihara and K. Noguchi, *J. Chromatogr.*, 592 (1992) 93.
- 20 K. Koizumi, Y. Kubota, T. Tanimoto and Y. Okada, *J. Chromatogr.*, 464 (1989) 365.
- 21 K. Koizumi, M. Fukuda and S. Hizukuri, *J. Chromatogr.*, 585 (1991) 233.
- 22 A. S. Feste and I. Khan, *J. Chromatogr.*, 607 (1992) 7.
- 23 J.-C. Janson and J. Porath, *Methods Enzymol.*, 8 (1966) 615.
- 24 G. A. Milliken and D. E. Johnson, *Analysis of Messy Data*, Vol. 1, Van Nostrand Reinhold, New York, 1987, p. 327.
- 25 L. F. Hood, in D. R. Lineback and G. E. Inglett (Editors), *Food Carbohydrates*, AVI Publishing, Westport, CT, 1982, p. 218 and 243.
- 26 H. G. Pontis and E. Del Campillo, in P. M. Dey and R. A. Dixon (Editors), *Biochemistry of Storage Carbohydrates in Green Plants*, Academic Press, San Diego, 1985, p. 209.
- 27 D. J. Manners, in P. M. Dey and R. A. Dixon (Editors), *Biochemistry of Storage Carbohydrates in Green Plants*, Academic Press, San Diego, CA, 1985, p. 160.
- 28 J. M. G. Cowie and C. T. Greenwood, *J. Chem. Soc.*, (1957) 2862.
- 29 *Bio-Rad Product Catalog*, Bio-Rad, Richmond, CA, 1990, p. 88.

Determination of hyaluronic acid by high-performance liquid chromatography of the oligosaccharides derived therefrom as 1-(4-methoxy)phenyl-3-methyl-5-pyrazolone derivatives

Kazuaki Kakehi, Minako Ueda, Shigeo Suzuki and Susumu Honda

Faculty of Pharmaceutical Sciences, Kinki University, 3-4-1 Kowakae, Higashi-Osaka 577 (Japan)

(Received September 23rd, 1992)

ABSTRACT

Hyaluronic acid (HA) was digested with various kinds of depolymerizing enzymes and the products were analysed by high-performance liquid chromatography (HPLC) after derivatization with 1-(4-methoxy)phenyl-3-methyl-5-pyrazolone (PMPMP). As hyaluronate 4-glycanohydrolase (EC 3.2.1.35) from sheep testis showed a high efficiency for depolymerization, giving the tetra- and hexasaccharides abundantly, and is inexpensive, a method for the specific determination of HA was established, based on digestion by this enzyme followed by determination of the tetra- or hexasaccharide derived therefrom as the PMPMP derivatives by HPLC with UV detection. This method allowed the determination of HA in the range 0.5-50 μg with high reproducibility.

INTRODUCTION

Hyaluronic acid (HA) is widely distributed among connective tissues of mammalian bodies and microorganisms, and is important for the treatment of geriatric arthritis and as an additive in cosmetics. HA is a macromolecular compound having a relative molecular mass of more than 10^6 . It is composed of glucuronic acid and N-acetylglucosamine linked alternatively through the $\beta 1 \rightarrow 3$ and the $\beta 1 \rightarrow 4$ linkages, respectively, as shown in Fig. 1.

In clinical analysis, HA is determined exclusively by electrophoresis on a cellulose acetate membrane. It can be also determined by size-exclusion chromatography with UV photometric detection at a low wavelength [1], but sensitivity and selectivity are not high. HA can be depolymerized by hydrolases to

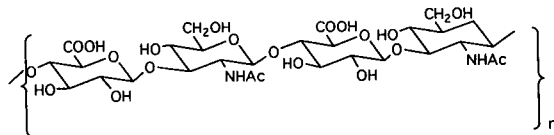


Fig. 1. Structure of hyaluronic acid.

give oligosaccharides having various degrees of polymerization (DP). Hyaluronate 4-glycanohydrolase (hyaluronoglucosaminidase, EC 3.2.1.35) from animal testes [2] and hyaluronate 3-glycanohydrolase (hyaluronoglucuronidase, EC 3.2.1.26) from leech [3] cleave the glucosaminide and glucuronide linkages, respectively. The resultant oligosaccharides can be measured by high-performance liquid chromatography (HPLC) after derivatization with 2-aminopyridine [4]. There is another type of depolymerizing enzyme, hyaluronate lyase (EC 4.2.2.1), which cleaves specifically the hexosaminide linkage, giving oligosaccharides having one double

Correspondence to: S. Honda, Faculty of Pharmaceutical Sciences, Kinki University, 3-4-1 Kowakae, Higashi-Osaka 577, Japan.

bond each on the glucuronic acid residue at the non-reducing ends. The resultant oligosaccharides show weak absorption at 232 nm due to the double bond [5]. Modification of the reducing ends of the resultant oligosaccharides with 2-aminopyridine enhances UV absorption and allows fluorescence detection with high sensitivity [4]. The accurate HPLC determination of individual oligosaccharides derived with these enzymes will make it possible to elucidate the mechanisms of enzymic reactions and also determine the content of HA.

In a previous study, we developed a method for the determination of urinary chondroitin sulphates based on the capillary electrophoresis of unsaturated disaccharides derived therefrom by digestion with chondroitinase ABC, as 1-phenyl-3-methyl-5-pyrazolone (PMP) derivatives [6]. This method allows the simultaneous sensitive determination of chondroitin, chondroitin sulphate A and C and related glycosaminoglycans with UV absorption, and is suitable for clinical analysis because of the simplicity of the procedure. In continuation of this work, we compared the capabilities of PMP analogues, and found that 1-(4-methoxy)phenyl-3-methyl-5-pyrazolone (PMPMP) derivatives of oligosaccharides showed a higher molar absorptivity than PMP derivatives.

In this paper, we propose a method for the determination of HA, based on HPLC of the oligosaccharides derived therefrom as PMPMP derivatives.

EXPERIMENTAL

Materials

A sample of HA from pig skin, obtained from Sigma (St. Louis, MO, USA) was used throughout. Hyaluronate 4-glycanohydrolase (sheep testis, Type V) was also obtained from Sigma. Samples of hyaluronate 3-glycanohydrolase (*Hirudo medicinalis*) and hyaluronate lyase (*Streptomyces hyalurolyticus*) were purchased from Seikagaku Kogyo (Tokyo, Japan). PMPMP reagent was prepared according to the method described previously [7]. All other chemicals were of the highest grade commercially available.

Instruments

The HPLC system consisted of a Hitachi 655A-12 liquid chromatographic pump, a Shimadzu

SPD-6A UV detector and a Shimadzu C-R6A chromato-recorder for measurements of peak area and elution time. A column (150 mm × 6 mm I.D.) packed with Cosmosil 5C18-AR (average particle diameter 5 μm) (Nacalai Tesque, Kyoto, Japan) was used as the stationary phase. Elution was performed with acetonitrile–100 mM phosphate buffer (pH 7.0) (15:85, v/v) at a flow-rate of 0.8 ml/min, and PMPMP derivatives of HA-derived oligosaccharides were monitored at 249 nm.

Fast atom bombardment mass spectrometry (FAB-MS) of HA-derived oligosaccharides was performed on a JEOL SX102 apparatus in the negative-ion mode (glycerol as matrix) using JEOL standard software.

Enzymic digestion

HA (50 mg) was dissolved in 60 mM citrate buffer (pH 5.2, 5.0 ml), hyaluronate 4-glycanohydrolase from sheep testis (0.5 mg) was added and the mixture was incubated for 24 h at 37°C. The enzymic reaction was terminated by keeping the mixture on a boiling water-bath for 3 min and the mixture was centrifuged at 10 000 g for 10 min. The supernatant solution was applied to a column of Sephadex G-15 (70 cm × 2.5 cm I.D.) equilibrated with 0.1% acetic acid, and the column was eluted with the same solvent. Fractions of 7 ml were collected, with UV monitoring at 220 nm. A 300-μl portion of each fraction was subjected to carbazole–sulphuric acid assay for glucuronic acid [8]. Each of the fractions that showed a positive reaction to the assay was lyophilized and a 100-μg portion was examined by FAB-MS. Another portion was derivatized with PMPMP and the elution volume of the product was compared with those of the peaks from the derivatized digestion mixture obtained on an analytical scale (see Fig. 3a).

Comparative study of depolymerizing enzymes

In the comparative study of various depolymerizing enzymes, HA (50 μg) was dissolved in water (10 μl) and an aqueous solution (1 U, 10 μl) of hyaluronidase and 100 mM citrate–phosphate buffer (pH 5.0 for hyaluronate 3-glycanohydrolase from *Hirudo medicinalis*, pH 5.2 for hyaluronate 4-glycanohydrolase from sheep testis and pH 6.0 for hyaluronate lysase from *Streptomyces hyalurolyticus*) (40 μl) were added. Each mixture was incubated for 24

h at 37°C. After terminating the enzymic reaction by heating the mixture on a boiling water-bath for 3 min, the mixture was evaporated to dryness in a centrifugal concentrator (CC-10; Tomy, Tokyo, Japan), derivatized with PMPMP and the product analysed by HPLC.

Time course study

HA (1 mg) was dissolved in 2 ml of water. An aqueous solution (20 U, 200 μ l) of hyaluronate 4-glycanohydrolase (sheep testis) and 100 mM citrate–phosphate buffer (pH 5.2) (800 μ l) were added and the solution was incubated at 37°C. After specified periods, aliquots (150 μ l each) were removed and evaporated to dryness in a centrifugal evaporator. The residues were derivatized with PMPMP and the products analysed by HPLC.

Determination of HA

An aqueous solution (100 μ l) containing HA (0.1–50 μ g) was added to citrate–phosphate buffer (pH 5.2) (40 μ l). Hyaluronate 4-glycanohydrolase from sheep testis (5 U per 10 μ l in water) was added to the mixture, which was incubated for 5 h at 37°C. The enzymic reaction was terminated by heating the mixture on a boiling water-bath for 3 min and the mixture was evaporated to dryness in a centrifugal evaporator. The residue was directly subjected to derivatization with PMPMP (see below).

Derivatization with PMPMP

The procedure was essentially the same as that reported for the derivatization of oligosaccharides from glycoproteins [7]. An 0.3 M solution of sodium hydroxide (20 μ l) was added to a lyophilized sample of HA-derived oligosaccharides or the residue obtained by the enzymic digestion described above. To the mixture was added a methanolic 0.5 M solution of PMPMP (20 μ l) was added and the solution was kept at 70°C for 20 min. After addition of 0.3 M HCl (20 μ l) for neutralization, water (200 μ l) and ethyl acetate (200 μ l) saturated with water were added. The mixture was shaken vigorously and the organic phase was carefully removed. Ethyl acetate (200 μ l) was added and the procedure was repeated twice more. The aqueous phase finally obtained was evaporated to dryness in a centrifugal evaporator, the residue was dissolved in 15% aqueous acetonitrile (200 μ l) and an aliquot (20 μ l) of the solution was injected onto the HPLC column.

RESULTS AND DISCUSSION

The reducing ends of reducing oligosaccharides are modified with PMPMP in such a manner that the hemiacetal bond is cleaved and two molecules of PMPMP are attached to C-1' of the sugar moiety through C-4 of the pyrazolone ring (Fig. 2).

The derivatization is quantitative under weakly alkaline conditions and the remaining reagent can be easily removed by extraction with ethyl acetate. The derivatives have a high molar absorptivity around 249 nm, and a negative charge due to enolization of the keto group at the C-3 position.

The PMPMP derivatives of HA-derived oligosaccharides were efficiently separated in the reversed-phase partition mode using an ODS column and a neutral phosphate buffer containing acetonitrile.

Fig. 3 compares the elution profiles of the PMPMP-derivatized products of HA digestion by (a) hyaluronate 4-glycanohydrolase from sheep testis, (b) hyaluronate 3-glycanohydrolase from *Hirudo medicinalis* and (c) hyaluronate lyase from *Streptomyces hyalurolyticus*. All of the enzymic reactions were carried out under conditions ensuring completion.

The product of digestion by hyaluronate 4-glycanohydrolase was derivatized with PMPMP. The chromatographic profile (Fig. 3a) shows a relatively simple pattern composed of a few peaks of PMPMP oligosaccharides. It also shows a peak of the remaining reagent (peak 3) and a few minor peaks. The digestion product similarly obtained was fractionated on a column of Sephadex G-50. Each fraction was monitored for uronic acid, and each uronic acid-containing fraction was examined by FAB-MS. The fraction giving the most intense colour in the carbazole–sulphuric acid assay gave a peak of

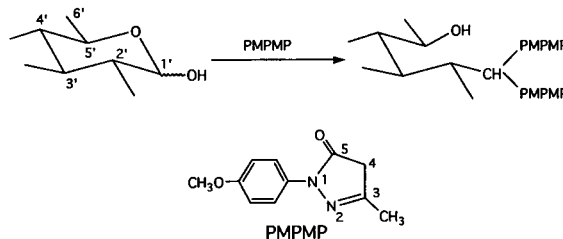


Fig. 2. Reaction of carbohydrates with PMPMP reagent.

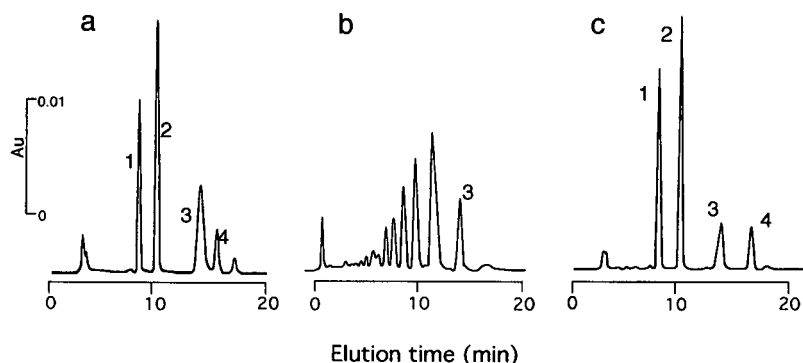


Fig. 3. Comparison of the elution profiles of the PMPMP-derivatized digestion mixture of HA. The digestion by all these enzymes was almost complete under the conditions employed. Digestion with (a) hyaluronate 4-glycanohydrolase from sheep testis, (b) hyaluronate 3-glycanohydrolase from *Hirudo medicinalis* and (c) hyaluronate lyase from *Streptomyces hyalurolyticus*. The procedures for enzymic digestion and derivatization with PMPMP are described under Experimental. Column, Cosmosil 5C18-AR (150 mm × 6 mm I.D.); column temperature, ambient; eluent, 100 mM phosphate buffer (pH 7.0)–acetonitrile (15:85, v/v); flow-rate, 0.8 ml/min; detection UV absorption at 249 nm. Peaks: 1 = hexasaccharide; 2 = tetrasaccharide; 3 = reagent (PMPMP); 4 = disaccharide.

m/z 797 (Fig. 4), which corresponds to $[M - 1]^-$ ion from the HA tetrasaccharide. Another portion of this fraction was derivatized with PMPMP and examined by HPLC under the conditions as in Fig. 3. The derivative from this fraction gave a peak identical with peak 2 in Fig. 3a. Hence peak 2 was identified as the tetrasaccharide $\text{GlcUA}\beta 1 \rightarrow 3\text{GlcNAc}\beta 1$

$\rightarrow 4\text{GlcUA}\beta 1 \rightarrow 3\text{GlcNAc}$. In a similar manner, peaks 1 and 4 were assigned to the hexa- and disaccharides, respectively. The PMPMP derivatives of this series of oligosaccharides were eluted in order of decreasing DP in this separation mode.

The digestion product with hyaluronate 3-glycanohydrolase (Fig. 3b) gave multiple peaks of oligo-

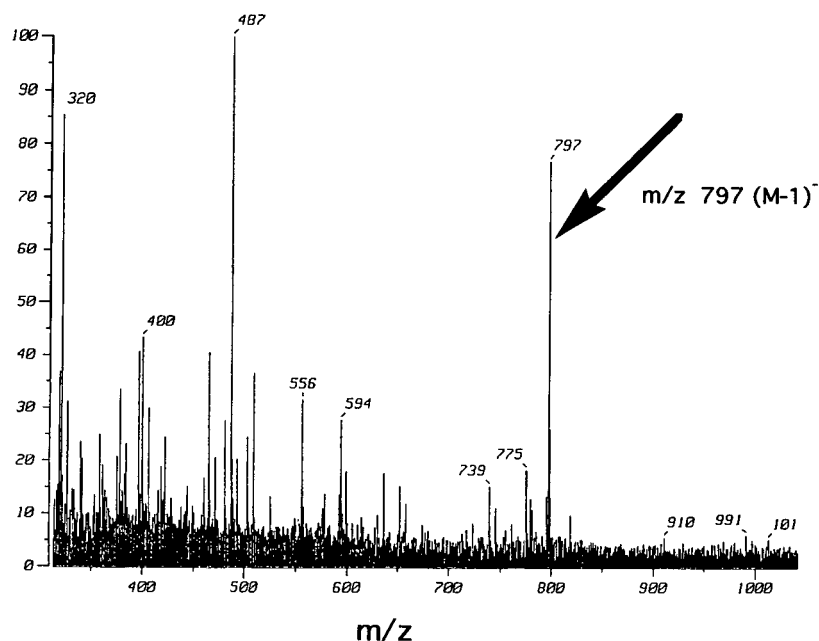


Fig. 4. Negative-ion FAB mass spectrum of the hyaluronate 4-glycanohydrolase-derived tetrasaccharide.

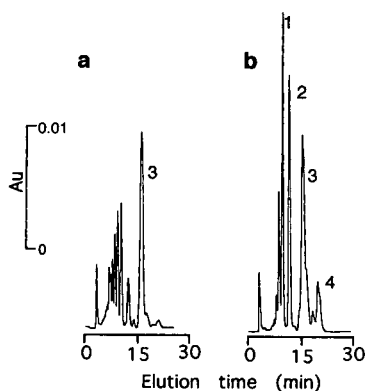


Fig. 5. Elution profiles of the PMPMP-derivatized incomplete digestion mixture of HA. HA (50 μ g) was digested by hyaluronate 4-glycanohydrolase from sheep testis. Digestion period: (a) 20 min; (b) 5 h. Peak assignment and analytical conditions as in Fig. 3.

saccharides having various DP values. Although HA was digested for an ample period using a large amount of the enzyme, oligosaccharides having high DP values were resistant to further hydrolysis.

The digestion of HA with hyaluronate lyase from *Streptomyces hyalurolyticus* (Fig. 3c) gave a similar pattern as that in Fig. 3a, although the structures of the resultant oligosaccharides are slightly different from those of the corresponding oligosaccharides in Fig. 3a in that they have a double bond per molecule.

Comparison of these three profiles led to the conclusion that the use of either hyaluronate 3-glycanohydrolase or hyaluronate lyase is advantageous for the determination of HA because of the higher depolymerizing efficiencies. Of these two enzymes, hyaluronate 3-glycanohydrolase is to be preferred because it is cheaper.

Fig. 5 shows the chromatographic patterns obtained with a smaller amount of hyaluronate 3-glycanohydrolase to establish the time course of digestion. The profile for a 20-min digestion (Fig. 5a) shows weak multiple peaks of higher oligosaccharides, whereas that for a 5-h digestion (Fig. 5b) shows large peaks of lower oligosaccharides (mainly the tetra- and hexasaccharides). However, oligosaccharides having DP values higher than 8 still remained with 5-h digestion. These observations suggest that this enzyme randomly cleaves interglycosidic linkages.

We optimized the conditions for the production of the tetra- and hexasaccharides from HA by digestion with hyaluronate 3-glycanohydrolase from sheep testis. Fig. 6a shows the pH dependence of the production of these saccharides. At *ca.* pH 5 the yields of both oligosaccharides became maximum.

Fig. 6b shows the effect of incubation period on the yields of both oligosaccharides. Under the conditions employed, the yields of both oligosaccharides became almost constant after 5 h of incubation. The production of the hexasaccharide was

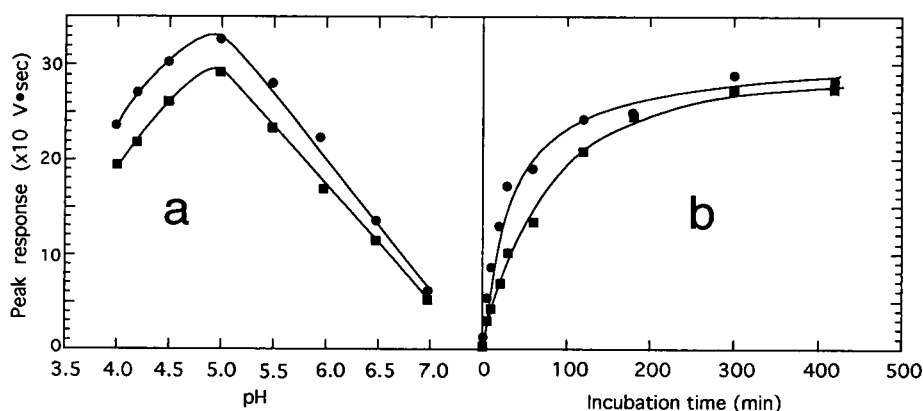


Fig. 6. Optimization of the enzyme digestion of HA by hyaluronate 4-glycanohydrolase from sheep testis. (a) pH dependence; (b) effect of incubation period. The conditions for the enzymic digestion are described under Experimental. Analytical conditions as in Fig. 3. ■ = PMPMP derivative of the tetrasaccharide; ● = PMPMP derivative of the hexasaccharide.

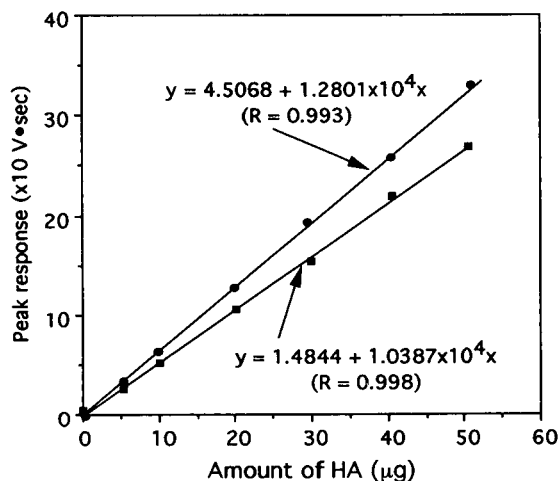


Fig. 7. Calibration graphs for HA, as observed from the yields of the tetra- or hexasaccharide derived therefrom. The conditions for the enzymic digestion are described under Experimental. Analytical conditions as in Fig. 3. ■ = Observed from the yield of the PMPMP derivative of the tetrasaccharide; ● = observed from the yield of the PMPMP derivative of the hexasaccharide.

much greater than that of the tetrasaccharide in the initial stages, but it was almost the same as the latter when the incubation time was longer than 7 h. It seems that large molecules of HA and HA-derived oligosaccharides are easily cleaved by hyaluronate 3-glycanohydrolase but the smaller oligosaccharides below hexasaccharides are resistant to this enzyme. This enzyme might require at least two binding sites to exert its enzymic affect. One of the binding sites is obviously the point of scission, and the other(s) are at point(s) sufficiently apart from the point of scission. HA-derived oligosaccharides smaller than the hexasaccharides cannot have these additional binding sites, and therefore cannot be cleaved. Hence hyaluronate 4-glycanohydrolase

randomly cleaves the glucuronide bond, provided that the DP is larger than 8, but it does not work on smaller oligosaccharides.

Under the conditions established above (incubation for 5 h at 37°C at pH 5.2), various amounts of HA were digested and the PMPMP derivatives of the tetra- and hexasaccharides were analysed by HPLC. The calibration graphs based on the peak response were linear from 0.5 to 50 μg of HA (Fig. 7), and the relative standard deviations of peak response at the 1.0-, 10.0- and 50-μg levels of HA were 2.3, 1.5 and 1.8%, respectively, for the derivative of the hexasaccharide. The detection limit was 0.1 μg as HA (10 ng as amount injected). Use of the calibration graph for the tetrasaccharide gave similar results.

The established method is sensitive. The specificity depends on that of hyaluronate 4-glycanohydrolase. The process of derivatization also excluded substances that could possibly interfere in the determination. Therefore, it may be useful for the determination of HA in drugs and cosmetics in addition to clinical samples. The results of its application to such samples will appear elsewhere.

REFERENCES

- 1 T. Irimura, M. Nakajima, N. DiFerrante and G. L. Nicolson, *Anal. Biochem.*, 130 (1983) 461.
- 2 A. Dorfman, *Methods Enzymol.*, 1 (1955) 166.
- 3 H. Yuki, and W. H. Fishman, *J. Biol. Chem.*, 238 (1963) 1877.
- 4 T. Takagaki, T. Nakamura, K. Kawasaki, A. Kon, S. Ohishi and M. Endo, *J. Biochem. Biophys. Methods*, 21 (1990) 209.
- 5 Y. Kaneko, T. Ohya, H. Ohiwa and S. Kubota, *J. Agric. Chem. Soc. Jpn.*, 42 (1968) 613.
- 6 S. Honda, T. Ueno and K. Kakehi, *J. Chromatogr.*, 608 (1992) 289.
- 7 K. Kakehi, S. Suzuki, S. Honda and Y. C. Lee, *Anal. Biochem.*, 199 (1991) 256.
- 8 Z. Dische, *J. Biol. Chem.*, 167 (1947) 189.

Separation and isolation of trace impurities in L-tryptophan by high-performance liquid chromatography[☆]

Mary W. Trucksess

Division of Contaminants Chemistry, Center for Food Safety and Applied Nutrition, Food and Drug Administration, Washington, DC 20204 (USA)

(First received January 24th, 1992; revised manuscript received October 10th, 1992)

ABSTRACT

A high-performance liquid chromatographic (HPLC) profiling method was developed to separate trace impurities in L-tryptophan products associated with the eosinophilia–myalgia syndrome (EMS) epidemic. The test portion was dissolved in water, and the solution was filtered and chromatographed on a silica-based C₁₈ reversed-phase HPLC column by using linear gradient elution with water and acetonitrile–water (80:20); both solvents contained 0.1% trifluoroacetic acid for ion-pairing. The method was used to profile 200 test samples from six manufacturers of L-tryptophan. The method was modified to include the use of a C₁₈ disposable cartridge to retain the 1,1'-ethylidenebis(L-tryptophan) (peak E, peak 97 or EBT), the impurity most strongly associated with EMS, and to remove the L-tryptophan before HPLC separation and quantitation. Recoveries of EBT added to test portions (2 µg/g and above) averaged 80%.

INTRODUCTION

In the fall of 1989, physicians in New Mexico, USA, noted that several patients had developed a peculiar illness marked by eosinophilia and severe myalgia [1]. Epidemiologic investigations by these physicians and researchers at the Mayo Clinic and the Centers for Disease Control (CDC) [2–6] associated this illness with the consumption of L-tryptophan (L-Trp). The CDC case definition of the syndrome has been (1) an eosinophil count $> 1 \cdot 10^9/l$, (2) generalized debilitating myalgia and (3) no evidence of infection or neoplasm that would explain the eosinophilia or the myalgia [7]. To date, more

than 1600 cases of eosinophilia–myalgia syndrome (EMS) have been reported, with 38 deaths [8]. Warnings and recalls of L-Trp by the Food and Drug Administration (FDA) in November 1989 [9] promptly ended the epidemic. Research was immediately initiated to determine the cause of EMS. Since L-Trp had been used previously without any reported toxicity, this research focused on the search for a contaminant or contaminants.

L-Trp was produced in Japan by six manufacturers. The bulk was made into capsules, powder or tablets by many distributors in the USA. It was used to treat insomnia, premenstrual syndrome, obesity and drug withdrawal.

In early February 1990, we developed a high-performance liquid chromatographic (HPLC) procedure to screen L-Trp products for minor impurities. Studies by the CDC and other researchers in Oregon and Minnesota found a strong association between EMS and L-Trp produced by Showa Denko K.K. between October 1988 and June 1989 [10]. A method for isolating and quantifying one of the impurities, 1,1'-ethylidenebis(L-tryptophan) (EBT, peak E or peak 97), was developed.

Correspondence to: M. W. Trucksess, Division of Contaminants Chemistry (HFS-346), Center for Food Safety and Applied Nutrition, Food and Drug Administration, Washington, DC 20204, USA.

[☆] Presented at the *11th International Symposium on High-Performance Liquid Chromatography of Proteins, Peptides and Polynucleotides*, Washington, DC, October 20–23, 1991. The majority of the papers presented at this symposium were published in *J. Chromatogr.*, Vol. 599 (1992).

EXPERIMENTAL

HPLC profiling of *L*-tryptophan

The laboratory sample was ground, 0.5 g of the powder was placed into a 15-ml polypropylene centrifuge tube and 5 ml of water were added. The mixture was vortexed for 2 min, centrifuged and filtered, and 50–100 μ l of the filtrate were injected into the HPLC system. The system consisted of a Waters U6K injector, a 15-cm Delta-Pak C₁₈, 300-Å (pore size), 3- μ m (particle size) column, two pumps, a UV detector set at 220 and 280 nm and a Digital Professional 350 computer equipped with Waters software. The linear gradient elution used consisted of solvent A: 0.1% trifluoroacetic acid (TFA) in water, and solvent B: 0.1% TFA in acetonitrile–water (80:20). The mobile phase started with 100% solvent A for 2 min followed by a linear gradient to 80% solvent B at 37 min.

Isolation of EBT

A saturated solution of *L*-Trp (10 ml) was passed through a Waters C₁₈ Sep-Pak cartridge that had been conditioned with 6 ml of methanol and 6 ml of water. The cartridge was washed with 30 ml of water, followed by 6 ml of acetonitrile–water (6:94) to eliminate most of the *L*-Trp. The contaminants were then eluted with 6 ml of acetonitrile–water (70:30). The solvent was evaporated by using a Speed Vac (Savant) vacuum evaporator, the residue was dissolved in 2 ml of water, the solution was filtered and 500 μ l of the filtrate were chromatographed on a 30-cm NovaPak C₁₈, 3- μ m (particle size) column by using a linear gradient from 20% solvent B to 60% solvent B over 23 min. The HPLC system and solvents A and B were the same as previously described.

Quantitation of EBT

EBT standard solution was prepared in 0.1 *M* triethylammonium acetate (pH 9.2) buffer. The *L*-Trp manufactured by Tanabe Seiyaku Co. contained no EBT and, therefore, was used as the control in the recovery studies. Various amounts of EBT were added to a 0.5-g test portion (from ground *L*-Trp tablets or contents of *L*-Trp capsules) in a 250-ml Erlenmeyer flask. The test portion was extracted with 100 ml of 0.1% TFA solution by shaking the mixture for 3 min, the extract was fil-

tered and 50 ml of the filtrate was passed through a C₁₈ Sep-Pak cartridge that had been conditioned with methanol and water. A vacuum manifold was used to adjust the flow-rate to about 10 ml/min. The cartridge was washed with 30 ml of water and 6 ml of acetonitrile–water (6:94). After most of the solvent had been eliminated by applying vacuum for an additional 2 min, a polyethylene 15-ml centrifuge tube was placed under each cartridge. A small amount of *L*-Trp and the impurities were then eluted with 6 ml of methanol–acetonitrile (1:1). The eluate was concentrated in a Speed Vac vacuum evaporator to about 0.2 ml. The final extract was diluted to 2 ml with water, centrifuged at high speed and injected onto a 30-cm Delta Pak C₁₈, 5- μ m (particle size) column. Solvents A and B were the same as previously described. The UV detector was set at 280 nm. A combination of gradient, isocratic and step gradient elution was used, starting with a linear gradient from 20% solvent B to 30% solvent B in 10 min, followed by isocratic elution for 15 min and then immediate step gradient elution to 80% solvent B for 10 min. The retention time of EBT was about 19.5 min.

RESULTS AND DISCUSSION

The HPLC fingerprint profiles (200 samples from different manufacturers) are relatively consistent from lot to lot of the individual manufacturers. HPLC profiling can be used to determine the source of an unknown lot. The variation in chromatographic patterns is probably related to differences in the manufacturing processes. The chromatograms from patient-related materials showed many more small peaks. More than 200 test samples of *L*-Trp were analyzed. Most of the patient-related materials were produced by Showa Denko K.K. Figs. 1 and 2 show typical chromatograms of *L*-Trp from two different manufacturers. Fig. 2 is that of a Showa Denko K.K. product.

Using similar HPLC profiling procedures, researchers at the CDC and at the Mayo Clinic have attempted to correlate the impurities found by HPLC with the incidence of EMS. They concluded that EBT (Fig. 2) may be associated with the illness [2,11]. Our effort has been centered on the isolation of EBT and some of the later-eluting components.

In the EBT isolation procedure, the disposable

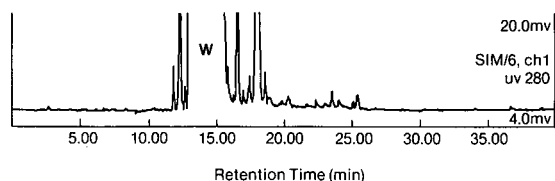


Fig. 1. Chromatogram of L-tryptophan (w) from manufacturer 1. Chromatographic conditions: 15-cm C_{18} column; linear gradient from 0 to 80% B over 35 min; detection at 280 nm. Mobile phase components: solvent A, 0.1% TFA in water; solvent B, 0.1% TFA in acetonitrile-water (80:20).

C_{18} cartridge was used to separate the bulk of the L-Trp from the contaminants. Components representing five of the HPLC peaks shown in Fig. 3 were collected and then analyzed separately by using various mass spectrometric (MS) techniques. In preliminary results obtained in collaboration with the University of Virginia, we found all five components to have molecular masses of less than 500, using a Fourier transform MS procedure. The exact molecular mass (M_r) of EBT (one of the five components, M_r 766) was determined in collaboration with PE Sciex, Canada. The MS data suggested several structures. High-resolution secondary ion MS performed at the FDA with a VG instrument gave the exact elemental composition, limiting the structure to an L-Trp dimer joined by an ethylidene bridge. However, it was not certain whether the two L-Trp molecules were joined with a bridge at the amino nitrogens or the indole nitrogens. By using a procedure developed by Showa Denko K.K., the component corresponding to peak E was synthesized and the structure was determined to be 1,1'-ethylidenebis(L-tryptophan), now known as EBT (Fig. 4) [12]. Researchers at the Mayo Clinic inde-

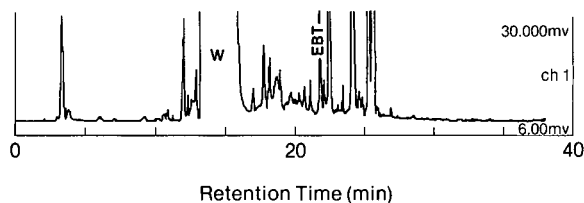


Fig. 2. Chromatogram of L-tryptophan (w) from manufacturer 2. Chromatographic conditions and mobile phase components as in Fig. 1.

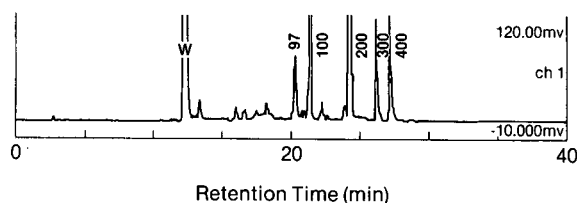


Fig. 3. Chromatogram of concentrated minor components in L-tryptophan (w). Chromatographic conditions: 30 cm C_{18} column; linear gradient from 20 to 60% B over 23 min; detection at 280 nm. Mobile phase components as in Fig. 1.

pendently determined the structure of this compound, which was isolated from the contaminated L-Trp [13]. EBT is an aminal, an L-Trp dimer joined by an ethylidene linkage at the indole nitrogens.

With the availability of EBT as a reference standard (purity >95%), it became possible to develop a quantitative method for EBT in L-Trp tablets or capsules. (MS showed that the M_r of 766 and the fragmentation pattern for the standard and the isolated EBT were the same.) The solubility and stability of EBT were determined. Although EBT is readily soluble in either acidic or basic solution, it is more stable in basic solution. EBT in 0.1% TFA solution kept at 5°C decomposed completely within 1 week (no HPLC peak at the retention time of the peak produced by the original solution before storage). A solution of 10 mg EBT/100 ml of 0.1 M triethylammonium acetate (pH 9.2) buffer kept at 5°C for 1 month gave an HPLC peak that was the same height as the peak produced by the original solution before storage for the same injection volume. L-Trp is more soluble in 0.1% TFA solution

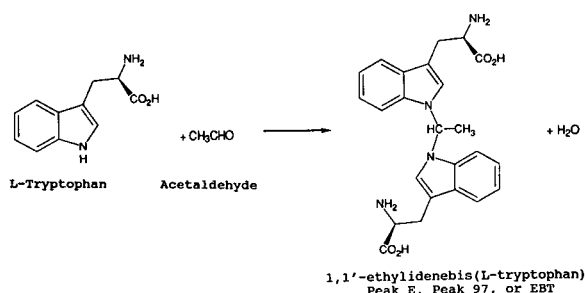


Fig. 4. Synthesis of 1,1'-ethylidenebis(L-tryptophan).

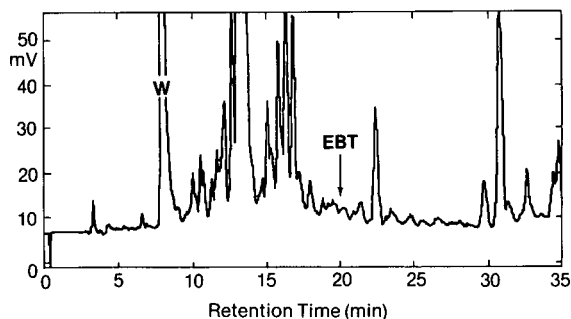


Fig. 5. Chromatogram of non-patient-related material. Chromatographic conditions: 30-cm C_{18} column; linear gradient from 20 to 3% B over 10 min, isocratic elution for 15 min, step-gradient elution to 80% B, hold for 8 min. Mobile phase components as in Fig. 1. W = L-Trp.

than in water (pK_a values for L-Trp are 2.43 and 9.44); therefore, spiked test portions were dissolved in TFA solution. It is not advisable to dissolve the compound in basic solution because most silica gel bonded-phase C_{18} cartridge packings will be destroyed at a $pH > 7$. Recoveries of EBT added at levels of 0.6, 1, 2 and 4 $\mu\text{g/g}$ of L-Trp were 117, 113, 84 and 82%, respectively. The high recoveries for the lower levels were due to slight background interferences.

This method was used to analyze some of the patient-related and non-patient-related materials. All of the patient-related materials were found to contain EBT at $> 70 \mu\text{g/g}$ of tablet, whereas the non-patient-related materials either did not contain EBT or contained significantly less EBT, as shown by the absence of a peak at the approximate retention time of EBT (Figs. 5 and 6).

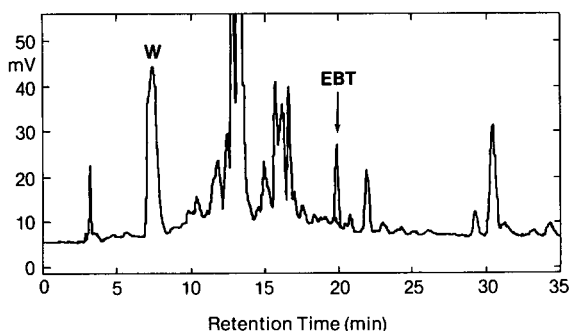


Fig. 6. Chromatogram of patient-related material. Chromatographic conditions and mobile phase components as in Fig. 5.

CONCLUSIONS

All L-Trp preparations contain various minor impurities. These vary with the manufacturing processes. One of the impurities, EBT (peak E or peak 97), from Showa Denko K.K. products was isolated. The structure was elucidated and a quantitative method of analysis was developed. Although preliminary testing in an animal model indicates that EBT may have some role in EMS, other factors may be involved [14].

ACKNOWLEDGEMENT

I wish to express my appreciation to Frederick S. Thomas and Mitchell J. Smith for preparing the EBT standard; to James A. Sphon for the MS data; and to Samuel W. Page for his support, advice and guidance.

REFERENCES

- 1 P. A. Hertzman, W. L. Blevins, J. Mayer, B. Greenfield, M. Ting and G. J. Gleich, *N. Engl. J. Med.*, 322 (1990) 869.
- 2 E. A. Belongia, C. W. Hedberg, G. J. Gleich, K. E. White, K. L. MacDonald and M. T. Osterholm, *N. Engl. J. Med.*, 323 (1990) 357.
- 3 Centers for Disease Control, *Morbid. Mortal. Weekly Rep.*, 38 (1989) 785.
- 4 Centers for Disease Control, *Morbid. Mortal. Weekly Rep.*, 38 (1989) 842.
- 5 Centers for Disease Control, *Morbid. Mortal. Weekly Rep.*, 39 (1990) 14.
- 6 Centers for Disease Control, *Morbid. Mortal. Weekly Rep.*, 39 (1990) 89.
- 7 E. M. Kilbourne, L. A. Swygert, R. M. Philen, R. K. Sun, S. B. Auerbach, L. Miller, D. E. Nelson and H. Falk, *Ann. Intern. Med.*, 112 (1990) 85.
- 8 R. Philen, Centers for Disease Control, personal communication, 1991.
- 9 *Food Chem. News*, Nov. 27 (1989) 49.
- 10 L. Slutsker, F. C. Hoesly, L. Miller, L. P. Williams, J. C. Watson and D. W. Fleming, *J. Am. Med. Assoc.*, 264 (1990) 213.
- 11 Centers for Disease Control, *Morbid. Mortal. Weekly Rep.*, 39 (1990) 589.
- 12 M. J. Smith, E. P. Mazzola, T. J. Farrell, J. A. Sphon, S. W. Page, D. Ashley, S. R. Sirimanne, R. H. Hill, Jr. and L. L. Needham, *Tetrahedron Lett.*, 32 (1991) 991.
- 13 A. N. Mayeno, F. Lin, C. S. Foote, D. A. Loegering, M. M. Ames, C. W. Hedberg and G. J. Gleich, *Science*, 250 (1990) 1707.
- 14 L. J. Crofford, J. I. Rader, M. C. Dalakas, R. H. Hill, S. W. Page, L. L. Needham, L. S. Brady, M. P. Heyes, R. L. Wilder, P. W. Gold, I. Illa, C. Smith and E. M. Sternberg, *J. Clin. Invest.*, 86 (1990) 1757.

Sequence-specific DNA affinity chromatography: application of a group-specific adsorbent for the isolation of restriction endonucleases

C. Pozidis and G. Vlatakis

Institute of Molecular Biology and Biotechnology, Enzyme Technology Division, P.O. Box 1515, Heraklion 711 10, Crete (Greece)

V. Bouriotis

Institute of Molecular Biology and Biotechnology, Enzyme Technology Division, P.O. Box, 1515, and Department of Biology, Division of Applied Biology and Biotechnology, University of Crete, P.O. Box 1470, Heraklion 711 10, Crete (Greece)

(First received July 27th, 1992; revised manuscript received October 9th, 1992)

ABSTRACT

The use of sequence-specific DNA affinity adsorbents for the isolation of restriction endonucleases *EcoRI* and *SphI* to near homogeneity has been reported. However, the high cost of these adsorbents is a limiting factor for their wider application. This paper reports the application of sequence-specific DNA affinity ligands containing recognition sequences for 34 restriction endonucleases as group-specific ligands in the isolation of restriction endonucleases. Crude samples of six restriction endonucleases, namely *BshFI*, *BamHI*, *SmaI*, *SacII*, *PvuII* and *SalI*, were shown to bind to these adsorbents and could be eluted at different KCl concentrations. High purification factors and recoveries were obtained. Restriction endonuclease *BshFI*, an isoschizomer of *HaeIII*, from the microorganism *Bacillus sphaericus* was purified to near homogeneity employing a two-step procedure which involves DNA-cellulose chromatography and oligonucleotide–ligand affinity chromatography. The enzyme exists as a monomer with an apparent relative molecular mass of 34 000 as determined by both sodium dodecyl sulphate–polyacrylamide gel electrophoresis and size-exclusion chromatography.

INTRODUCTION

Sequence-specific DNA affinity chromatography has been successfully applied to the isolation of proteins that interact with specific DNA sequences [1–6]. The use of this technique for the isolation of restriction endonucleases to homogeneity has also been reported [7,8]. Although several procedures have been published regarding the purification of restriction endonucleases, most of them involve lengthy and laborious protocols [9,10]. However,

rapid two-step chromatographic procedures involving triazine dye adsorbents, HPLC and affinity partitioning have been reported, resulting in partially purified restriction endonucleases free from contaminating nuclease activities [11–13]. Although sequence-specific DNA affinity chromatography compares favourably with other adsorbents used for the isolation of restriction endonucleases to homogeneity, the high cost of this technique, resulting from the different synthesis of the ligand for each restriction endonuclease, is a limiting factor for its wider application.

Affinity chromatography using specific ligands requires a different and elaborate synthesis for each purification problem. Further, as the choice of the ideal ligand is still largely empirical, extensive ex-

Correspondence to: V. Bouriotis, Institute of Molecular Biology and Biotechnology, Enzyme Technology Division, P.O. Box 1515, Heraklion 711 10, Crete, Greece.

perimentation is needed to achieve satisfactory separations [14,15].

Group-specific adsorbents exhibit affinity for whole groups of enzymes and therefore display great versatility in application. The development of oligonucleotide affinity adsorbents containing sites for a number of restriction enzymes which can therefore be used as group-specific adsorbents could potentially solve this problem.

This paper describes the synthesis of two group-specific DNA affinity adsorbents and their potential application in the isolation of a number of restriction endonucleases recognizing sequences within this oligonucleotide ligand. The purification of restriction endonuclease *BshFI*, an isoschizomer of *HaeIII*, [16] to homogeneity employing a two-step procedure is also presented.

EXPERIMENTAL

Materials

Restriction endonucleases (*BshFI*, *BamHI*, *PvuII*, *SmaI*, *SacII*, *SalI*), λ DNA, λ DNA–HindIII digest and T₄ DNA ligase were kindly supplied by Minotech (Heraklion, Greece), T₄ polynucleotide kinase was obtained from New England Biolabs (Beverly, MA, USA), DNA cellulose from Sigma (St. Louis, MO, USA), cyanogen bromide-activated Sepharose 4B from Pharmacia (Uppsala, Sweden) and a Sep-Pak C₁₈ column from Waters (Milford, MA, USA).

Yeast extract, tryptone and other chemicals were purchased from Merck (Darmstadt, Germany) and agarose for gel electrophoresis from Bethesda Research Labs. (Bethesda, MD, USA).

Growth of cells

Bacillus sphaericus (*BshFI*) was grown at 30°C until late logarithmic phase on a medium containing yeast extract 5 g/l, tryptone 10 µg/l and NaCl 5 g/l with a yield of 4 g of cell paste per litre of growth medium. Cells were harvested at 4°C by centrifugation and stored frozen at –70°C.

Enzyme assays

Routine assays for locating *BshFI*, *BamHI*, *PvuII*, *SmaI*, *SacII* and *SalI* endonuclease activity during the chromatographic runs were performed as described previously [12]. One unit of enzyme

activity is defined as the amount of enzyme required to produce a complete digest of 1.0 µg of λ DNA at 37°C (25°C for *SmaI*) for 1 h in a total volume of 50 µl.

Preparation of oligodeoxynucleotide affinity adsorbents

Two complementary oligodeoxynucleotides of the sequence 5'-GATCGCATGCCGCGGATCCCGGGCCCAGGTGGCCAGCTGTCGAC-3' and 3'-CGTACGGCGCCTAGGGCCCCGGGTC-CACCGGTCGACAGCTGCTAG-5' were synthesized (1-µmol scale; Applied Biosystems) and kindly provided by the Microchemistry Department of IMBB, already deprotected in ammonia solution.

The crude oligodeoxynucleotides were evaporated to remove ammonia, dissolved in water, centrifuged to remove benzamides formed during protection, evaporated and resuspended in 50 mM triethylammonium acetate (TEA-Ac) (pH 7.0). An initial purification step was then performed with a size-exclusion G-25 Sephadex gel column, followed by a desalting step with a Sep-Pak C₁₈ column [7]. Annealing of strands was performed in 100 µl of buffer containing 50 mM NaCl, 1 mM EDTA and 10 mM Tris-HCl (pH 8.0) by heating at 90°C for 2 min, then at 65°C for 90 min and 55 °C for 30 min and cooling slowly to room temperature.

Preparation of oligodeoxynucleotide affinity adsorbent I

After annealing had been performed, 1.8 mg of the DNA was phosphorylated in a reaction mixture containing 1800 U/ml T₄ polynucleotide kinase, 5 mM ATP (containing 5 µCi of [γ -³²P]ATP), 70 mM Tris-HCl (pH 7.6), 10 mM MgCl₂ and 5 mM dithiothreitol (DTT) for 2 h at 37°C. The DNA was precipitated with ethanol and dried *in vacuo*. The oligonucleotide was dissolved in ligation buffer containing 66 mM Tris-HCl (pH 7.5), 10 mM MgCl₂, 15 mM DTT, 1 mM spermidine-HCl and 1 mM ATP and was polymerized with T₄ DNA ligase (50 Weiss units) for 18 h at 15°C. DNA was extracted with phenol-chloroform, precipitated with ethanol and resuspended in water, to be used for coupling to cyanogen bromide-activated Sepharose gel (3.5 g) according to the method of Kadonaga and Tjian [4]. By measuring the radioactivity that remained in the washings after the coupling, the concentration

of bound DNA was calculated to be *ca.* 60 μg DNA/ml gel (10 ml total gel).

Preparation of oligodeoxynucleotide affinity adsorbent II

A 1.8-mg amount of the annealed DNA was phosphorylated as above and then coupled to 3.5 g of cyanogen bromide-activated Sepharose gel [4]. After coupling the concentration of bound DNA was *ca.* 70 μg DNA/ml gel (10 ml total gel).

Protein assay and electrophoresis techniques

Protein determination was performed according to Bradford using bovine serum albumin as protein standard [17]. Polyacrylamide gel electrophoresis (PAGE) of proteins in the presence of sodium dodecyl sulphate (SDS) was performed according to the method of Laemmli [18]. Agarose gel electrophoresis of DNA fragments was performed as described previously [12].

Comparison of properties of oligonucleotide affinity adsorbents I and II

The same sample of a partially purified preparation of *BshFI* (20 ml; 4 mg; 900 000 U/mg; 3 600 000 U) was applied to the same size of column of both affinity adsorbents I and II (2×1.6 cm I.D.; 4 ml). The columns were washed with 25 mM 4-(2-hydroxyethyl)-1-piperazineethanesulphonic acid (HEPES) (pH 7.8), containing 7 mM β -mercaptoethanol, 1 mM EDTA and 10% (v/v) glycerol until no absorption at 280 nm was evident in the effluents, and then developed with a 0.3 M step gradient of KCl.

Fractions with *BshFI* activity eluted with the 0.3 M KCl step gradient from adsorbent I (0.32 mg; 6 400 000 U/mg; 2 050 000 U) and adsorbent II (0.168 mg; 11 309 520 U/mg; 1 900 000 U) were pooled and stored at 4°C.

Enzyme purification procedures

For purification of *BshFI*, frozen cell paste (8 g) was thawed with 80 ml of 20 mM potassium phosphate buffer (pH 7.0) containing 7 mM β -mercaptoethanol, 1 mM EDTA and 5% (v/v) glycerol (buffer A), sonicated in an ice-bath for a total of 7 min (14×30 s) and centrifuged at 4°C for 1 h at 100.000 g. The supernatant (80 ml; 2 mg/ml; 160 mg) was loaded onto a dsDNA cellulose column (4

$\times 4.4$ cm I.D.; 60 ml) previously equilibrated in buffer A. The column was washed with buffer until no adsorption at 280 nm was evident in the effluents and then developed with a linear gradient of NaCl (600 ml total volume, 0–0.8 M) in buffer A at a flow-rate of 40 ml/h. Fractions (5 ml) with *BshFI* activity corresponding to *ca.* 0.15 M NaCl in the gradient were pooled (80 ml), concentrated with PEG (M_r 30 000) treatment and dialysed against 25 mM HEPES (pH 7.8) containing 7 mM β -mercaptoethanol, 1 mM EDTA, 10% (v/v) glycerol (buffer B) and 0.1 M KCl.

A sample (20 ml; 1 mg; 1 920 000 U) from the latter preparation was applied to an adsorbent bearing immobilized ligand II (adsorbent II, 5×1.6 cm I.D.; 10 ml) which had previously been equilibrated in buffer B containing 0.1 M KCl. The column was washed with buffer B containing 0.1 M KCl (56 ml) and subsequently with buffer B containing 0.2 M KCl (78 ml) and then developed with a linear gradient of KCl (114 ml; 0.2–0.4 M) in buffer B at a flow-rate of 9 ml/h. Fractions (2.8 ml) with *BshFI* activity corresponding to *ca.* 0.25 M KCl in the gradient were pooled (36.4 ml; 1.35 μg ; 40 U/ μl ; 1 456 000 units) and stored at 4°C.

Purification of restriction endonucleases BshFI, BamHI, SmaI, SacII, PvuII and SalI

Partially purified preparations of restriction endonucleases *BshFI* (1.26 mg; $3.96 \cdot 10^6$ U), *BamHI* (0.2 mg; 20 000 U), *SmaI* (0.46 mg; 40 000 U), *SacII* (3.22 mg; 42 500 U), *PvuII* (0.5 mg; 196 000 U) and *SalI* (0.35 mg; 80 000 U) were separately applied to Affinity adsorbent II (5×1.6 cm I.D.; 10 ml) which had previously been equilibrated in buffer B. The column was washed with buffer B until no absorption at 280 nm was evident in the effluents and then three successive step gradients consisting of 0.1, 0.2 and 0.3 M KCl in buffer B were applied at a flow-rate of 9 ml/h. *BshFI* (22.5 μg ; $3.4 \cdot 10^6$ U) and *BamHI* (0.5 μg ; 15 000 U) were eluted with 0.3 M KCl, *SmaI* (9.2 μg ; 35 000 U) and *SacII* (25 μg ; 40 000 U) with 0.2 M KCl and *PvuII* (4 μg ; 168 000 U) and *SalI* (35 μg ; 64 000 U) with 0.1 M KCl. Fractions with *BshFI*, *BamHI*, *SmaI*, *SacII*, *PvuII* and *SalI* activities were pooled and stored at 4°C.

RESULTS AND DISCUSSION

Several purification procedures have been described for the isolation of restriction endonucleases free from contaminating nuclease activities. Among these, recent methods based on dye–ligand chromatography [11], HPLC [12] and affinity partitioning [13], although effective, required the use of two or three columns, resulting in partially purified restriction enzyme preparations.

Sequence-specific DNA affinity chromatography has been successfully applied for the isolation of several proteins to homogeneity [1–6]. This technique has also been employed in order to prepare restriction endonucleases of high purity [7,8]. A limiting factor in the application of this technology is the high cost involved, resulting from the expensive synthesis of the oligonucleotide ligands. The construction of two oligonucleotide affinity ligands containing recognition sequences for 34 restriction endonucleases is reported in this paper. The restriction enzymes, their recognition sequences and recognition sites (number of first base) within the oligonucleotide affinity ligand are illustrated in Table I. One of the two affinity ligands was constructed after annealing of two oligonucleotides and subsequent polymerization and the other after annealing of two oligonucleotides without any further polymerization (Fig. 1). Both affinity ligands were subsequently coupled to cyanogen bromide-activated Sepharose. The oligonucleotides were designed in such a way that the resulting DNA affinity ligands contained 5'-single-strand overlapping termini in order that primary amines of the free bases could be coupled to activated agarose.

The resulting affinity adsorbents having roughly the same ligand concentration were compared in terms of capacity and specificity using partially purified preparations of the restriction endonuclease *BshFI*. Although both adsorbents exhibited similar capacities (ca. 500 000 U/ml gel) the adsorbent that resulted from the unligated ligand (adsorbent II) exhibited higher specificity (42 µg of protein/ml of gel were bound) than that resulting from polymerization of the oligonucleotide (80 µg of protein/ml of gel were bound, adsorbent I). We therefore employed adsorbent II for all subsequent experiments.

In order to hydrolyse DNA, restriction enzymes require the presence of divalent metal ions, usually

TABLE I

RESTRICTION ENZYME RECOGNITION SITES CONTAINED IN SEQUENCE-SPECIFIC DNA AFFINITY LIGANDS I AND II

Enzyme	Recognition sequence ^a	Recognition site (number of first base)
<i>AccI</i>	GTMKAC	39
<i>AluI</i>	AGCT	35
<i>AlwI</i>	GGATC	14
<i>ApaI</i>	GGGCCC	21
<i>AvaI</i>	CYCGRG	18
<i>BalI</i>	TGGCCA	30
<i>BamHI</i>	GGATCC	14
<i>BanII</i>	GRGCYC	21
<i>BglII</i>	GCCNNNNNGGC	23
<i>Bsp1286I</i>	GDGCHC	21
<i>BstNI</i>	CCWGG	25
<i>BstUI</i>	CGCG	11
<i>BstYI</i>	RGATCY	14
<i>EaeI</i>	YGGCCR	30
<i>Fnu4HI</i>	GCNGC	9
<i>HaeIII</i>	GGCC	22, 31
<i>HincII</i>	GTYRAC	39
<i>HpaII</i>	CCGG	19
<i>MboI</i>	GATC	15
<i>NciI</i>	CCSGG	18, 19
<i>NlaIII</i>	CATG	6
<i>NlaIV</i>	GGNNCC	14, 21
<i>NspI</i>	RCATGY	5
<i>NspBII</i>	CMGCKG	10, 34
<i>PvuII</i>	CAGCTG	34
<i>SacII</i>	CCGCGG	10
<i>SalI</i>	GTCGAC	39
<i>ScrFI</i>	CCNGG	18, 19, 25
<i>SecI</i>	CCNNGG	10, 18, 24
<i>SfiI</i>	GGCCNNNNNGGCC	22
<i>SmaI</i>	CCCGGG	18
<i>SphI</i>	GCATGC	5
<i>TaqI</i>	TCGA	40
<i>XmaI</i>	CCCGGG	18

^a D = G or A or T; H = A or C or T; K = G or T; M = A or C; N = A or C or G or T; R = A or G; S = G or C; W = A or T; Y = T or C.

Mg²⁺. For this reason, the addition of EDTA in all buffers for chelating the metal ion is necessary. The same method is used for DNA–cellulose or DNA–agarose in order to avoid hydrolysis from non-specific nucleases [19].

In order to examine the potential application of affinity adsorbent II as a group-specific adsorbent for the isolation of restriction endonucleases, we used partially purified enzyme preparations of

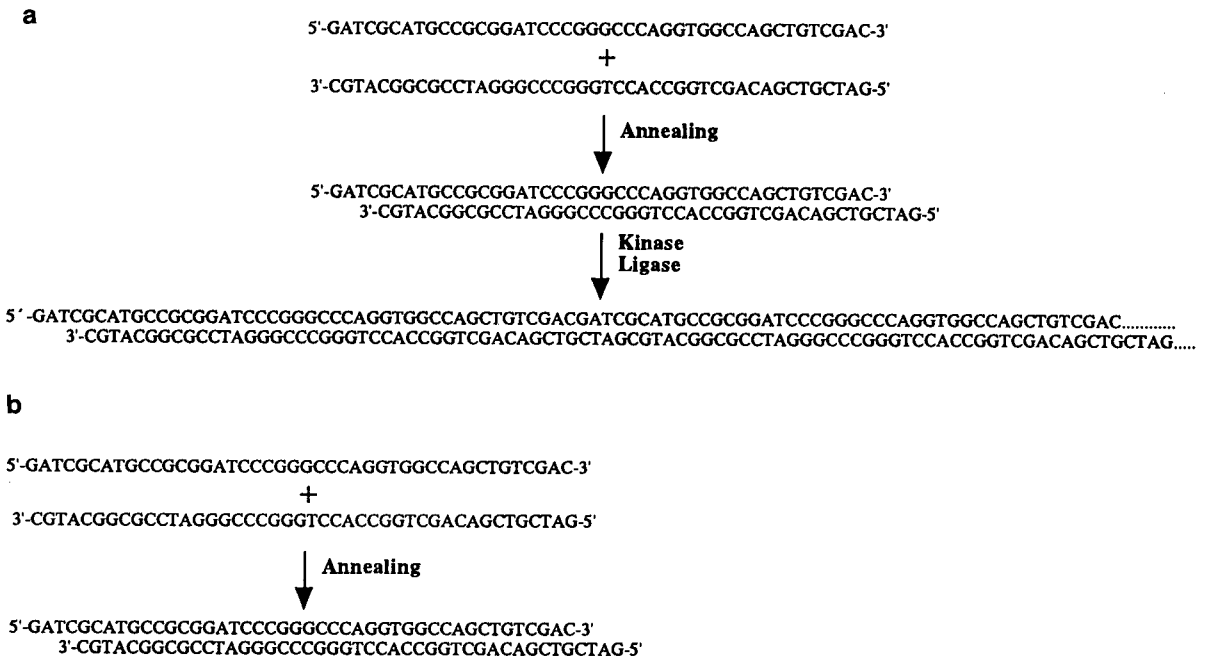


Fig. 1. Preparation of two sequence-specific DNA affinity ligands containing recognition sequences for 34 restriction endonucleases. (a) The two oligonucleotides were annealed, phosphorylated at the 5' protruding ends with T_4 polynucleotide kinase and ATP and complementary oligonucleotides were polymerized with T_4 DNA ligase and ATP (affinity ligand I). (b) The two oligonucleotides were annealed without subsequent polymerization (affinity ligand II).

BshFI, *BamHI*, *SmaI*, *SacII*, *PvuII* and *SalI*, which have recognition sequences within the oligonucleotide ligand. All enzyme preparations tested were bound to this adsorbent and were subsequently eluted at different salt concentrations by step gradients of KCl. The ability of adsorbent II, which was designed in order to interact specifically with

restriction enzymes, was evaluated on the basis of the KCl concentration that was necessary for the desorption of the enzymes. *BshFI* and *BamHI* were eluted with 0.3 M, *SmaI* and *SacII* with 0.2 M and *PvuII* and *SalI* with 0.1 M KCl, which is an indication of the different affinities of the enzymes for the ligand in the absence of Mg^{2+} (Table II). The purification factors obtained varied from 8- to greater than 300-fold and the recoveries varied from 75 to 94% (Table II). The estimated association constants of the interaction between the above restriction endonucleases and their recognition sites ($2.4 \mu M$ ligand concentration) varies from $1.2 \cdot 10^6$ to $6.5 \cdot 10^6 \text{ l mol}^{-1}$, under the buffer conditions described [20]. After each application the affinity column was regenerated with 2.5 M KCl in order to wash out traces of bound material. Despite the lability of the DNA ligand, the column showed very good stability and could be used more than ten times for the purification of the above enzymes.

Employing a two-step procedure including DNA-cellulose and affinity adsorbent II, we puri-

TABLE II
 ELUTION OF RESTRICTION ENDONUCLEASES FROM OLIGONUCLEOTIDE AFFINITY ADSORBENT II AT VARIOUS KCl CONCENTRATIONS

Enzyme	Elution [KCl (M)]	Purification (-fold)	Recovery (%)
<i>BshFI</i>	0.3	48	86
<i>BamHI</i>	0.3	> 300	75
<i>SmaI</i>	0.2	43	88
<i>SacII</i>	0.2	122	94
<i>PvuII</i>	0.1	108	86
<i>SalI</i>	0.1	8	80

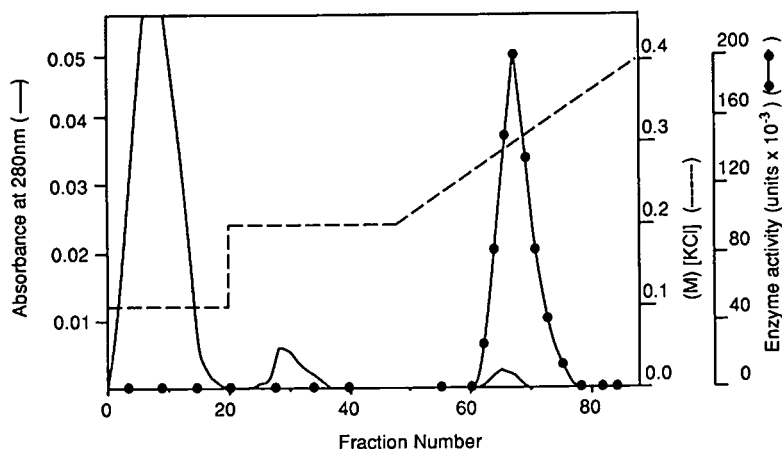


Fig. 2. Purification of *BshFI* by chromatography on oligonucleotide affinity adsorbent II. A sample (20 ml, 1 mg; $1.92 \cdot 10^6$ units) of partially purified *BshFI* on a dsDNA–cellulose column was applied to an oligonucleotide affinity adsorbent (5×1.6 cm; 10 ml) previously equilibrated in buffer B containing 0.1 M KCl. The affinity column was washed with buffer B containing 0.1 M KCl (56 ml) and subsequently with buffer B containing 0.2 M KCl (78 ml) and then developed with a linear gradient of KCl (114 ml total volume; 0.2–0.4 M) in buffer B at a flow-rate of 9 ml/h. Fractions (2.8 ml) with *BshFI* activity corresponded to ca. 0.25 M KCl. The protein content was followed with a UV monitor at 280 nm, 0.05 a.u.f.s. (solid line). Dashed line, KCl concentration. ● = Enzyme activity.

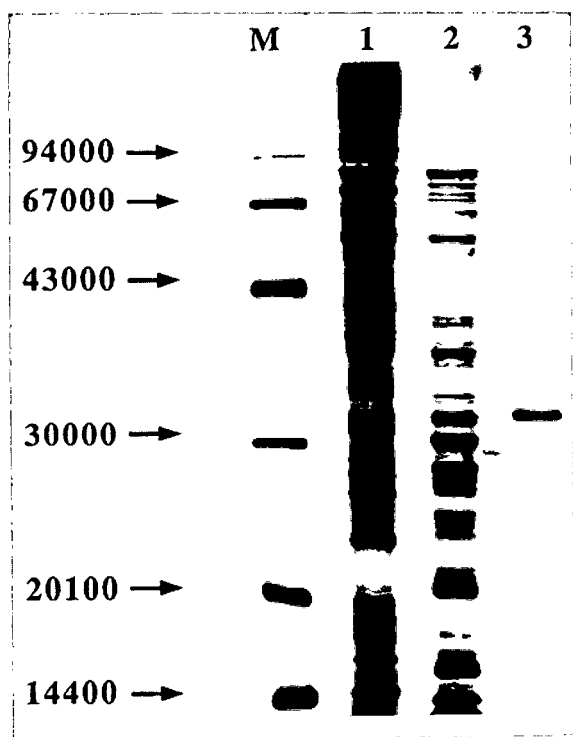


Fig. 3. Denaturing SDS-PAGE of the eluate containing *BshFI* activity and obtained from the oligodeoxynucleotide affinity adsorbent II. Lanes: 1 = crude protein mixture obtained from *Bacillus sphaericus* strain after cell lysis; 2 = fractions with *BshFI* activity eluted from the DNA–cellulose adsorbent; 3 = fractions with *BshFI* activity eluted from the oligonucleotide affinity adsorbent II; M = relative molecular mass markers, with the values shown on the left.

ried restriction endonuclease *BshFI* to homogeneity (Figs. 2 and 3, Table III). The successful isolation of the enzyme is mainly due to the effectiveness of the affinity chromatographic column. The enzyme preparation was enriched 562-fold and a 76% yield was obtained (Table II). The affinity column could be used repeatedly more than 20 times to isolate restriction endonuclease *BshFI* without any decrease in its performance. The enzyme exists in its native form as a monomer with an apparent relative molecular mass of 34 000 as determined by both SDS-PAGE and size-exclusion chromatography.

DNA–cellulose proved to be a very effective step in order to remove proteins that exhibited non-specific interaction with DNA from the crude extract, as reported previously [8].

A possible explanation for the weak interaction of *PvuII* and *SalI* with affinity adsorbent II is that the specific interaction of the enzymes with their recognition sequence might require the presence of Mg^{2+} ions. The only enzymes that have been studied and for which it has been demonstrated that the specific interaction with DNA is independent of the presence of Mg^{2+} ions are the enzymes *EcoRI* and *BglII* [19,21]. Further, it has been reported that in the absence of Mg^{2+} the binding affinities of *EcoRI* for specific and non-specific DNA differ by a factor of $1 \cdot 10^5$ [21–23]. Similar results were obtained with

TABLE III
SUMMARY OF THE PURIFICATION PROTOCOL FOR BshFI

Step	Protein (mg)	Enzyme activity (U)	Specific activity (U/mg)	Purification (-fold)	Yield (%)
Crude extract	160	–	–	–	–
DNA-cellulose	1	1.92·10 ⁶	1.92·10 ⁶	1	100
Adsorbent II	1.35·10 ⁻³	1.46·10 ⁶	1.08·10 ⁹	562	76

RsrI, an isoschizomer of *EcoRI* [24], whereas with *EcoRV* the ratio of binding affinities is 1 [25].

This study has demonstrated the effectiveness of a group-specific oligonucleotide affinity adsorbent for the isolation of restriction endonucleases. It is expected that restriction endonucleases that exhibit higher affinity for specific rather than non-specific DNA sequences will be successful candidates for purification by sequence-specific DNA affinity chromatography.

REFERENCES

- G. Herrick, *Nucleic Acids Res.*, 8 (1980) 3721.
- M. Oren, E. Winocour and C. Prives, *Proc. Natl. Acad. Sci. U.S.A.*, 77 (1980) 220.
- P. J. Rosenfeld and T. J. Kelly, *J. Biol. Chem.*, 261 (1986) 1398.
- J. T. Kadonaga and R. Tjian, *Proc. Natl. Acad. Sci. U.S.A.*, 83 (1986) 5889.
- K. A. Jones, J. T. Kadonaga, P. J. Rosenfeld, T. J. Kelly and R. Tjian, *Cell*, 48 (1987) 79.
- W. Lee, P. Mitchell and R. Tjian, *Cell*, 49 (1987) 741.
- R. Blanks and L. W. McLaughlin, *Nucleic Acids Res.*, 16 (1988) 283.
- G. Vlatakis and V. Bouriotis, *Anal. Biochem.*, 195 (1991) 352.
- R. A. Rubin and P. Modrich, *Methods Enzymol.*, 65 (1980) 96.
- L. Y. Fuchs, L. Covarrubias, L. Escalante, S. Sanchez and F. Bolivar, *Gene*, 10 (1980) 39.
- G. Vlatakis, G. Skarpelis, I. Stratidaki, Y. D. Clonis and V. Bouriotis, *Appl. Biochem. Biotechnol.*, 15 (1987) 201.
- V. Bouriotis, A. Zafeiropoulos and Y. D. Clonis, *Anal. Biochem.*, 160 (1987) 127.
- G. Vlatakis and V. Bouriotis, *J. Chromatogr.*, 538 (1991) 311.
- C. R. Lowe and P. D. G. Dean, *Affinity Chromatography*, Wiley, Chichester, 1974.
- C. R. Lowe, *An Introduction to Affinity Chromatography* [T. S. Work and E. Work (Editors), *Laboratory Techniques in biochemistry and Molecular Biology*, Vol. 7, Part 2], Elsevier, Amsterdam, 1979.
- G. Vlatakis, D. Clark and V. Bouriotis, *Nucleic Acids Res.*, 17 (1989) 8882.
- M. Bradford, *Anal. Biochem.*, 72 (1976) 248.
- U. K. Laemmli, *Nature*, 227 (1970) 380.
- R. M. Litman, *J. Biol. Chem.*, 243 (1968) 6222.
- B. Mattiasson and T. G. I. Ling, *J. Chromatogr.*, 376 (1986) 235.
- B. J. Terry, E. W. Jack, R. A. Rubin and P. Modrich, *J. Biol. Chem.*, 258 (1983) 9820.
- G. M. Clore, A. M. Gronenborn and R. W. Davies, *J. Mol. Biol.*, 155 (1982) 447.
- D. R. Lesser, M. R. Kurpiewski and L. Jen-Jacobson, *Science*, 250 (1990) 776.
- C. R. Aiken, E. W. Fisher and R. I. Gumpert, *J. Biol. Chem.*, 266 (1991) 19063.
- D. J. Taylor, J. I. Badcoe, R. A. Clarke and E. S. Halford, *Biochemistry*, 30 (1991) 8743.

Quantitative analysis of tylosin by column liquid chromatography

E. Roets, P. Beirinckx, I. Quintens and J. Hoogmartens

Katholieke Universiteit Leuven, Laboratorium voor Farmaceutische Chemie, Instituut voor Farmaceutische Wetenschappen, Van Evenstraat 4, B-3000 Leuven (Belgium)

(First received July 28th, 1992; revised manuscript received September 29th, 1992)

ABSTRACT

A column liquid chromatographic method suitable for the quality control of tylosin A is described. The determination can be carried out on different C₈ or C₁₈ columns, using a mobile phase containing acetonitrile, 0.2 M tetrabutylammonium hydrogensulphate, 0.2 M phosphoric acid and water. The flow-rate is 1 ml/min and detection is performed at 280 nm. The method shows good selectivity towards the major components tylosin A, B, C and D and demycinosyltylosin. Minor degradation products, mainly observed in solutions, are also separated. The compositions of several standards are compared and results for a number of commercial samples are presented.

INTRODUCTION

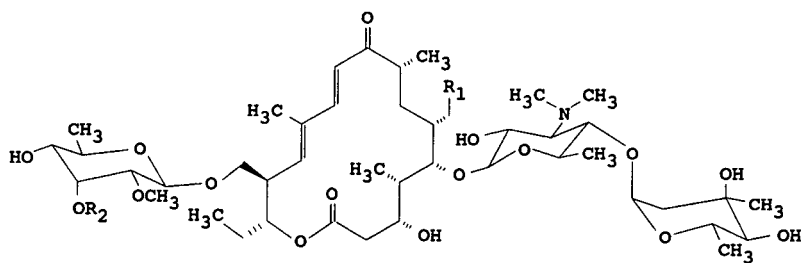
Tylosin, a macrolide antibiotic, is produced by fermentation of *Streptomyces* strains [1]. It consists of a substituted sixteen-membered lactone, an amino sugar (mycaminoses) and two neutral sugars, mycinose and mycarose [2,3]. Tylosin is used extensively as a feed additive and as a therapeutic substance in the treatment of mycoplasmosis in poultry and livestock [4]. In addition to the main compound, tylosin A (TA), several related structures are co-produced during the fermentation process. Desmycosin or tylosin B (TB) [2], macrocin (TC) [5], relomycin (TD) [6] and demycinosyltylosin (DMT) [7] have been isolated and their structures determined (see Fig. 1).

The first reversed-phase liquid chromatographic (LC) methods described did not allow the separation of the different tylosins [8,9]. It is necessary to separate these tylosins as it is known that they have

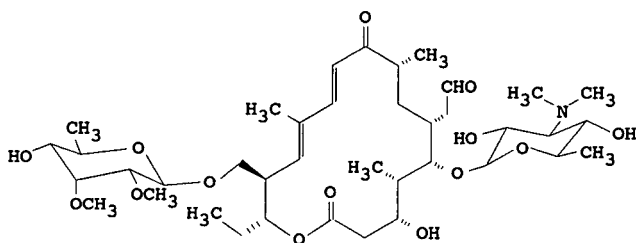
different antibiotic activities [4]. A method for the analysis of tylosin in fermentation broths has also been described [10]. The selectivity was poor and the pH of the mobile phase too basic (>11) for continuous use with reversed-phase columns. Later, an improved method at lower pH was published by the same author [11]. The separations were carried out on C₁₈ and C₈ columns. The mobile phase consisted of tetrahydrofuran (THF), acetonitrile (CH₃CN), sodium pentanesulphonate, acetic acid and water. The selectivity was further improved by increasing the temperature to 55°C [11,12]. The major disadvantage of this method was the poor selectivity towards impurities, eluted close to the main component.

This was much improved by the method described by Fish and Carr [13]. Three stationary phases were found suitable: Nucleosil ODS, Zorbax C₈ and Hypersil C₈. The mobile phase consisted of CH₃CN in 0.85 M sodium perchlorate adjusted to pH 2.5 with 1 M hydrochloric acid. The high salt concentration combined with the corrosive chloride ion is a drawback of the method. The variance in selectivity for different batches of the same stationary phase sometimes results in a decrease in resolu-

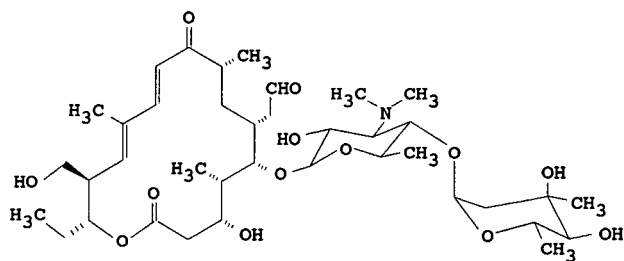
Correspondence to: J. Hoogmartens, Katholieke Universiteit Leuven, Laboratorium voor Farmaceutische Chemie, Instituut voor Farmaceutische Wetenschappen, Van Evenstraat 4, B-3000 Leuven, Belgium.



	R ₁	R ₂
Tylosin A	CHO	CH ₃
Tylosin D	CH ₂ OH	CH ₃
Tylosin C	CHO	H



Tylosin B



Demycinosyltylosin

Fig. 1. Structures of tylosins.

tion for minor components [13]. Using this method, it is necessary to adjust the composition of the mobile phase to provide sufficient resolution between the tylosin components. This method is now prescribed by the British Veterinary Pharmacopoeia (BP Vet) [14] and by the French Pharmacopoeia [15].

The LC method described here ensures a selectivity that is better than that obtained with the BP Vet method. The mobile phase is not corrosive and its composition needs less adjustment when the method is used on different stationary phases.

EXPERIMENTAL

Reagents and samples

Organic solvents were obtained from Janssen Chimica (Beerse, Belgium). Tetrahydrofuran (THF) was distilled after monitoring for the absence of peroxides. Tetrabutylammonium (TBA) hydrogensulphate was also obtained from Janssen Chimica. Other reagents were of analytical-reagent grade (Merck, Darmstadt, Germany). Water was freshly distilled from glass apparatus. Buffer solutions were prepared by mixing 0.2 M phosphoric acid with 0.2 M potassium dihydrogenphosphate until the desired pH was reached. The 0.2 M TBA solutions incorporated in the mobile phases were neutralized to the same pH as the mobile phase buffer with dilute sodium hydroxide.

The World Health Organization (WHO) international reference preparation of tylosin (WHO-IS, 1000 I.U./mg), the British Pharmacopoeia chemical reference substance (BP-CRS, batch 1226) and E. Lilly standards of tylosin A (lot 294-F14-180-1x) and of tylosin (lot 186TD 1, 1073 I.U./mg) were available. House standards were prepared of TA (89.2%), TB (93.9%), TC (93.0%) and TD (98.9%), this content (% w/w) being expressed on the substance "as is". Bulk samples of tylosin were of known origin (Bulgaria, Italy and USA). A small amount of demycinosyltylosin (DMT) was also prepared but the purity of this compound was not determined precisely as it is only a minor impurity.

Columns

The columns (250 × 4.6 mm I.D.) were packed in the laboratory following a published method [16]. The reversed-phase stationary phases were Zorbax

(DuPont, Wilmington, DE, USA), Nucleosil (Macherey–Nagel, Düren, Germany), Partisil (Whatman, Clifton, NJ, USA), RSil and RoSil (Bio-Rad, Eke, Belgium), Hypersil (Shandon, Runcorn, UK) and Spherisorb (Phase Separations, Queensferry, UK). The columns were always heated at 30°C.

LC apparatus and operating conditions

Isocratic elution was performed throughout the study. The apparatus consisted of a Milton Roy mini-pump (Laboratory Data Control, Riviera Beach, FL, USA), a Model CV-6-UHPa-N60 injector (Valco, Houston, TX, USA) equipped with a 20- μ l loop, a Model LC 3 UV variable-wavelength detector (Pye Unicam, Cambridge, UK) set at 280 nm and a Model 3390A integrator (Hewlett-Packard, Avondale, PA, USA). For the final analyses of standards and samples a RoSil C₈ (8 μ m) column was used with acetonitrile–0.2 M TBA–0.2 M phosphoric acid–water (20:8:5:67, v/v) as mobile phase. The mobile phase was degassed by sonication and the flow-rate was 1.0 ml/min. For all samples an amount equivalent to 50.0 mg of tylosin base was dissolved in water and diluted to 50.0 ml. The solutions were stored at 6°C in the dark.

RESULTS AND DISCUSSION

Development of the chromatographic method

The LC method was developed using a Zorbax C₈ column. A mobile phase containing CH₃CN, phosphoric acid and water was examined first. It was observed that the addition of quaternary ammonium ions improved both efficiency and symmetry. Tetrabutylammonium (TBA) gave better results than tetramethylammonium and therefore TBA was used in all further experiments. TBA masks the residual silanol activity and acts as a competing analyte [17,18]. This causes the tylosin components not only to be better separated but also eluted faster. The influence of the pH of the mobile phase was investigated by replacing the 0.2 M phosphoric acid with 0.2 M phosphate buffers of pH up to 4.0. Increasing the pH caused an increase in retention times and symmetry factors and a decrease in resolution. The use of 0.2 M sulphuric acid gave results similar to those obtained with 0.2 M phosphoric acid. The latter was chosen for further work.

The influence of the amount of TBA in the mo-

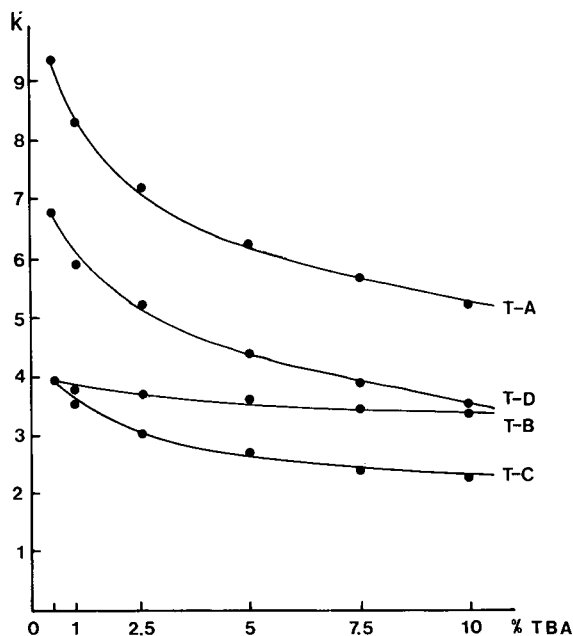


Fig. 2. Influence of the concentration (% v/v) of 0.2 M TBA in the mobile phase on the separation of tylosin A, B, C, D. Column, Zorbax C_8 (8 μ m); mobile phase, CH_3CN -0.2 M TBA-0.2 M phosphoric acid-water [23:x:5:(72 - x)].

mobile phase is shown in Fig. 2. The retention times decrease with increasing TBA concentration. The best resolution was obtained between 5 and 8% TBA. An amount of 5% TBA was chosen for further work. The influence of the organic modifier was also investigated. The capacity factors are reported in Table I. The amount of organic modifier was adjusted to obtain comparable retention times

or to improve the separation. The best selectivity and symmetry were obtained with CH_3CN , which was chosen for further work.

In order to examine the general applicability of the mobile phase thus developed, a sample containing tylosin A, B, C, D and some minor impurities was analysed on columns packed with different C_8 and C_{18} stationary phases. The capacity factors for tylosin A, B, C and D are given in Table II. The elution order was the same on all the columns examined. The selectivity towards minor impurities, eluted before TC and immediately before and after TA, was similar. It was also observed that the retention was weaker on the older Zorbax column, but the selectivity was similar. A more important influence of column age was reported previously for the LC of erythromycin [19]. In a series of separate experiments it was observed that the presence of TBA improves the reproducibility of the selectivity on the different columns. In the presence of TBA there is less difference between C_8 and C_{18} materials. The separation between major (TA, TB, TC, TD) and minor components can be improved also by variation of the 0.2 M TBA content in the mobile phase between 3 and 8% (v/v). Throughout the entire study a column temperature of 30°C was maintained to improve the uniformity of working conditions. Another temperature between 20 and 35°C may be chosen with no effect on the selectivity.

Fig. 3 shows the typical chromatogram accompanying the BP-CRS batch 1226 and obtained with the BP Vet method. TAD is an impurity called aldol impurity. Fig. 4 shows a typical chromatogram of the same substance obtained with the proposed

TABLE I

INFLUENCE OF THE ORGANIC MODIFIER ON THE CAPACITY FACTORS OF TYLOSIN A, B, C AND D

Column, Zorbax C_8 ; mobile phase, organic modifier-0.2 M TBA-0.2 M phosphoric acid-water [x:5:5:(90 - x), v/v].

Organic modifier	x (% v/v)	k'			
		TC	TB	TD	TA
Methanol	40	3.7	4.5	6.8	6.7
2-Propanol	17	4.8	6.1	9.1	9.4
2-Ethoxyethanol	27.5	4.2	5.0	6.6	7.5
Tetrahydrofuran	17.5	3.1	3.8	4.9	6.2
Tetrahydrofuran + acetonitrile	8.75 + 11.5	3.1	3.8	5.1	6.5
Acetonitrile	23	3.0	3.8	4.7	6.6

TABLE II

CAPACITY FACTORS OF TYLOSIN A, B, C AND D ON DIFFERENT COLUMNS

Mobile phase, CH₃CN–0.2 M TBA–0.2 M phosphoric acid–water [x:5:5:(90 – x), v/v].

Stationary phase	Particle size (μm)	<i>k'</i>				<i>x</i>
		TC	TB	TD	TA	
Zorbax BP-C ₈ (I) ^a	8	3.0	3.8	4.7	6.6	23
Zorbax BP-C ₈ (II) ^a	8	2.8	3.1	4.4	5.3	21
Partisil C ₈	10	2.2	2.4	3.3	4.0	20
RoSil C ₈	8	3.1	3.7	4.8	6.7	22
Partisil ODS	10	4.4	4.5	7.1	7.8	20
RSil C ₁₈ LL	10	2.9	3.4	4.6	5.9	23
RSil C ₁₈ HL	10	3.2	4.2	5.4	7.7	23
Spherisorb ODS 1	5	3.0	3.5	4.8	6.3	23
Spherisorb ODS 1	10	3.3	3.8	5.3	7.0	23
Spherisorb ODS 2	5	2.3	3.0	3.8	5.0	23
Spherisorb ODS 2	10	3.7	4.8	6.3	8.8	21
Nucleosil ODS	10	2.9	3.8	5.0	7.1	23
Hypersil ODS	5	2.5	3.1	4.2	6.1	23

^a I = New column; II = old column.

method. The general elution pattern obtained with both methods is very similar, but the selectivity towards minor impurities is better with the proposed method. The major advantage of the new method, however, is the better reproducibility of the selectivity on different stationary phases. To verify the selectivity a system suitability test was needed. It was observed that a resolution of at least 4.0 between TA and TB and a symmetry factor of less than 1.5 for TA guaranteed a sufficient separation on all the columns examined. TB was chosen for the resolution test because it can be prepared easily

from TA by acid degradation. TD and TAD are not commercially available, nor can they be obtained by easy to perform chemical reactions. Using purified TA it was checked that no TB was formed in the column during analysis.

Calibration graphs and repeatability

Quantitative work was carried out on a RoSil C₈ column. Calibration graphs were obtained with the house standards for TA, TB, TC and TD. The following relationships were found, where *y* = peak area, *x* = amount of base injected in micrograms,

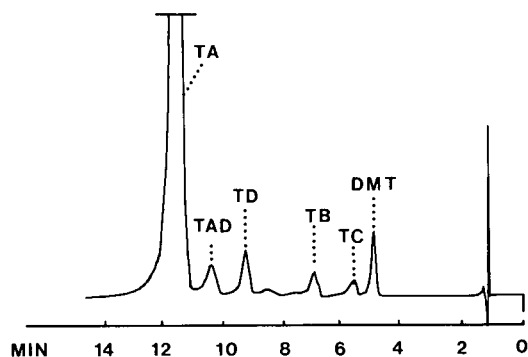
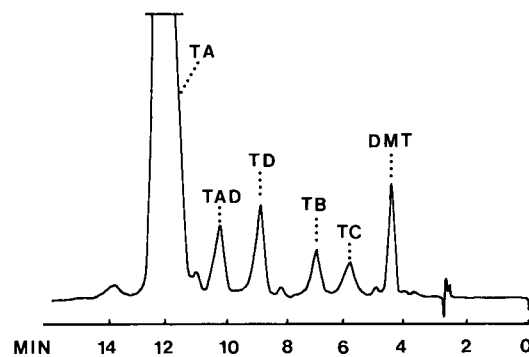


Fig. 3. Typical chromatogram accompanying the BP-CRS batch 1226 and obtained with the BP Vet method.

Fig. 4. Chromatogram of the BP-CRS batch 1226 obtained with the proposed method. Column, Hypersil C₁₈, mobile phase, CH₃CN–0.2 M TBA–0.2 M phosphoric acid–water (23:3:5:69).

n = number of analyses, r = correlation coefficient, $S_{y,x}$ = standard error of estimate and R = range of injected mass examined: TA, $y = 67 + 8913x$, $n = 10$, $r = 0.9989$, $S_{y,x} = 61$, $R = 12\text{--}24 \mu\text{g}$; TB, $y = 120 + 9009x$, $n = 10$, $r = 0.9996$, $S_{y,x} = 150$, $R = 0.1\text{--}0.35 \mu\text{g}$; TC, $y = 16 + 8698x$, $n = 10$, $r = 0.9999$, $S_{y,x} = 17$, $R = 0.1\text{--}3 \mu\text{g}$; TD, $y = 88 + 8961x$, $n = 10$, $r = 0.9998$, $S_{y,x} = 72$, $r = 0.1\text{--}2 \mu\text{g}$. The limit of quantification was 0.05%. When the house standard was analysed ten times over a period of 4 days, the relative standard deviation (R.S.D.) was 0.6%.

Comparison of tylosin standards

The composition of the tylosin A house standard was determined as follows. The total base content expressed as TA was determined by titration with perchloric acid in non-aqueous conditions, using acetic acid as the solvent. The mean result was 91.1% ($n = 4$, R.S.D. = 0.4%). The water content (9%) was determined by Karl Fischer titration ($n = 5$; R.S.D. = 2%). The total mass was therefore accepted to be explained by tylosin bases and water. The chromatographic purity was determined using the proposed method. As the values of the specific absorbance for the different tylosins must be very close, as can be concluded from the similarity of the

slopes of the calibration graphs and as only small amounts of impurities were present, their content was expressed as TA. The content of the TA house standard was therefore accepted to be $100 - (9.0 + 1.4 + 0.4) = 89.2\%$.

Using this TA house standard, the standards were compared by the proposed method and the results are reported in Table III. Titrations were not carried out on the standards, owing to the limited amount available. The deviation between the total mass explained and 100% may be due to the presence of solvents in the WHO and Lilly standards. The WHO standard was dried over phosphorus pentoxide before being sealed in ampoules and it is possible that the very hygroscopic sample took up some water during the packing procedure and/or after the opening of the ampoule. The BP CRS content is very low, probably because it is a tartrate salt. It should be emphasized that this CRS is not used for quantitative work. The content of the Lilly standard exceeds the theoretical amount of $1000 \mu\text{g}/\text{mg}$ because the micrograms concerned have to be interpreted as micrograms of activity, determined by microbiological assay against a standard, and not as micrograms of mass. This is confirmed by the deviation between declared content and that found by LC. This situation can be a source of confusion [20].

TABLE III
COMPOSITION OF TYLOSIN STANDARDS

Values in percent (w/w) in terms of the base; relative standard deviations (R.S.D., %) are given in parentheses.

Component	House standard TA ($n = 10$) ^a	WHO (1000 I.U./mg) ($n = 16$) ^a	BP-CRS ($n = 3$) ^a	E. Lilly house standard (1073 $\mu\text{g}/\text{mg}$) ($n = 7$) ^a	E. Lilly tylosin A ($n = 5$) ^a
DMT	1.4 (5.8)	0.3 (15)	2.6 (8.3)	0.3 (14)	0.1 (6.2)
TC	<0.05	0.2 (9.3)	1.4 (1.6)	5.8 (5.8)	0.1 (8.9)
TB	<0.05	0.2 (15)	1.6 (9.4)	0.2 (12)	0.3 (23)
TD	0.4 (31)	2.5 (3.0)	3.9 (3.8)	2.9 (1.4)	0.6 (13)
TAD	<0.05	<0.05	2.8 (3.6)	<0.05	<0.05
TA	89.2 (0.6)	93.0 (0.5)	73.4 (0.9)	86.0 (0.8)	96.6 (0.9)
Others	<0.05	1.0 (9.9)	0.1	<0.05	0.3 (3.6)
Subtotal	91.0	97.2	85.8	95.2	98.0
Water ^b	9.0 (2.0) ($n = 5$) ^a	0.0 ^c	ND ^d	ND	ND

^a Number of analyses.

^b Karl Fischer.

^c As mentioned on the label.

^d ND = Not determined owing to the limited amount of sample.

TABLE IV

COMPOSITION OF BULK SAMPLES OF TYLOSIN

Results are expressed in % (w/w). Tylosins and related substances are calculated as tylosin A. Water was determined by Karl Fischer titration.

Sample origin and number	n ^a	TA		DMT	TC	TB	TD	Others	Water			Total
		Mean	R.S.D. (%)						Mean	n	R.S.D. (%)	
A1	4	83.5	0.2	0.5	0.4	1.6	2.8	0.1	3.3	2	0.9	92.2
A2	4	81.8	0.4	1.0	0.7	1.0	4.2	0.4	4.6	2	3.3	93.7
A3	4	80.6	0.8	0.5	0.4	1.4	6.1	0.2	5.8	2	0.7	95.0
A4	4	88.0	0.4	0.5	0.7	0.9	3.7	0.4	5.4	4	4.3	99.6
A5	4	89.5	0.6	0.2	0.2	0.4	1.8	0.6	3.4	4	1.7	96.1
B1	5	90.7	0.7	0.2	1.5	0.3	4.6	0.1	2.0	5	0.6	99.4
B2	5	85.9	0.5	0.4	2.6	0.5	7.5	0.1	2.2	5	2.2	99.2
B3	8	81.2	1.4	1.0	3.4	0.3	3.2	0.4	2.3	3	3.8	91.8
B4	4	86.7	0.6	2.1	1.4	0.7	2.6	0.7	2.3	3	1.3	96.5
B5	5	86.5	0.6	1.8	1.2	0.9	2.9	<0.1	2.4	3	3.1	95.7

^a Number of analyses.

Analysis of commercial samples

Commercial samples were analysed as described above for the standards. Table IV gives the results for tylosin bulk samples. For simplicity, R.S.D. values are not mentioned for impurities. The repeatability for the TA assay is good. The major part of the impurities is explained by DMT, TC, TB and

TD, which is the major impurity. Most of the samples also contain small amounts of other related substances. The water content varied from 2.2% to 5.8%. The total mass explained ranges from 91.8% to 99.6%. It is probable that many of these samples contain salts which are not detected by LC.

Table V gives the results for tylosin tartrate sam-

TABLE V

COMPOSITION OF BULK SAMPLES OF TYLOSIN TARTRATE

Results are expressed in % (w/w). Tylosins and related substances are calculated as tylosin A base. Pure TA tartrate contains 92.4% of TA. Water was determined by Karl Fischer titration.

Sample origin and number	n ^a	TA		DMT	TC	TB	TD	Others	Total tylosins as tartrate	Water			Total
		Mean	R.S.D. (%)							Mean	n	R.S.D. (%)	
A4	3	67.9	0.6	2.2	0.5	8.0	2.3	<0.1	87.6	5.9	4	2.6	93.5
A5	4	78.1	0.8	0.2	0.2	2.0	2.5	0.1	89.9	3.5	4	4.0	93.4
A6	4	78.7	0.1	0.1	0.3	1.7	2.7	0.1	90.5	3.5	3	1.3	94.0
B4	6	69.1	0.6	0.4	1.2	3.4	3.7	<0.1	84.2	4.8	3	2.7	89.0
B5	5	68.9	0.4	0.9	1.2	3.5	3.4	<0.1	84.3	4.8	3	4.9	89.1
B6	4	70.3	0.4	0.2	0.7	4.5	3.3	<0.1	85.5	5.0	6	4.9	90.5
C1	3	68.9	0.1	0.2	2.1	1.2	9.5	0.2	88.9	1.6	4	4.4	90.5
C2	3	73.4	0.3	0.2	0.6	1.1	8.4	0.2	90.8	1.7	5	2.8	92.5
C3	3	69.8	0.9	0.2	3.8	0.9	7.7	0.5	89.7	1.5	6	3.8	91.2

^a Number of analyses.

ples. The same impurities are present, but the total amount is higher than for the base samples. The TB content is higher than in the base samples. TB can be formed from TA by acid hydrolysis. The sum of tylosins and related substances is calculated as the tartrate salt. The water content varies from 1.5% to 5.9%. The total mass explained ranges from 89.9% to 94.0%, which is much lower than for the base samples. The low content of these samples is due to impurities which are not detected by LC. This is reflected by the sulphated ash values, which are higher for the tartrate salts than for the base samples.

CONCLUSIONS

The results obtained have shown that the LC method described is suitable for the analysis of tylosin and its tartrate salt. Advantages over existing methods are the less corrosive chromatographic conditions, a better selectivity and, above all, a better reproducibility on different stationary phases.

ACKNOWLEDGEMENTS

The authors acknowledge the National Fund for Scientific Research (Belgium) for financial support, E. Lilly for the gift of standards and A. Decoux for secretarial assistance.

REFERENCES

- 1 J. M. McGuire, W. S. Boniece, C. E. Higgins, M. M. Hoehn, W. W. Stark, J. Westhead and R. N. Wolfe, *Antibiot. Chemother.*, 11 (1961) 320.
- 2 R. L. Hamill, M. E. Haney, Jr., M. Stamper and P. F. Wiley, *Antibiot. Chemother.*, 11 (1961) 327.
- 3 R. B. Morin, M. Gorman, R. L. Hamill and P. V. Demarco, *Tetrahedron Lett.*, (1970) 4737.
- 4 H. A. Kirst, G. M. Wild, R. H. Baltz, R. L. Hamill, J. L. Ott, F. T. Counter and E. E. Ose, *J. Antibiot.*, 35 (1982) 1675.
- 5 R. L. Hamill and W. M. Stark, *J. Antibiot.*, 17 (1964) 133.
- 6 H. A. Whaley, E. L. Patterson, A. C. Dornbush, E. J. Backus and N. Bohonos, *Antimicrob. Agents Chemother.*, (1963) 45.
- 7 H. A. Kirst, G. H. Wild, R. H. Baltz, E. T. Seno, R. L. Hamill, J. W. Paschal and D. E. Dorman, *J. Antibiot.*, 36 (1983) 376.
- 8 S. Omura, Y. Suzuki, A. Nakagawa and T. Hata, *J. Antibiot.*, 26 (1973) 794.
- 9 S. Bhupathapapun and P. Gray, *J. Antibiot.*, 30 (1977) 673.
- 10 J. H. Kennedy, *J. Chromatogr. Sci.*, 16 (1978) 492.
- 11 J. H. Kennedy, *J. Chromatogr.*, 281 (1983) 288.
- 12 W. K. Yeh, N. J. Bauer and J. E. Dotzlaw, *J. Chromatogr.*, 288 (1984) 157.
- 13 B. J. Fish and G. P. Carr, *J. Chromatogr.*, 353 (1986) 39.
- 14 *British Veterinary Pharmacopoeia 1985*, H.M. Stationery Office, London, 1985.
- 15 *Pharmacopée Française*, Maisonneuve, Sainte-Ruffine, 10th ed., 1990.
- 16 J. Hoogmartens, E. Roets, G. Janssen and H. Vanderhaeghe, *J. Chromatogr.*, 244 (1982) 299.
- 17 B. A. Bidlingmeyer, S. N. Deming, W. P. Price, Jr., B. Sachok and M. Petrusek, *J. Chromatogr.*, 186 (1979) 419.
- 18 B. A. Bidlingmeyer, *J. Chromatogr. Sci.*, 18 (1980) 525.
- 19 T. Cachet, I. O. Kibwage, E. Roets, J. Hoogmartens and H. Vanderhaeghe, *J. Chromatogr.*, 409 (1987) 91.
- 20 A. H. Thomas, *J. Pharm. Biomed. Anal.*, 5 (1987) 319.

Analysis of the explosive 2,4,6-trinitrophenylmethylnitramine (tetryl) in bush bean plants

S. D. Harvey, R. J. Fellows, D. A. Cataldo and R. M. Bean

Pacific Northwest Laboratory, P.O. Box 999, Richland, WA 99352 (USA)

(Received September 29th, 1992)

ABSTRACT

Previous attempts to delineate the metabolism of the explosive 2,4,6-trinitrophenylmethylnitramine (tetryl) in plants have been unsuccessful. Development of an appropriate analytical methodology has been thwarted due to the extreme thermal and base lability of tetryl as well as its propensity to undergo photodecomposition. This study presents a methodology based on solvent extraction of plant tissue followed by fractionation of the organic extract on silica gel with subsequent determination of tetryl by HPLC. This methodology allowed $82.70 \pm 5.54\%$ recovery of tetryl from fortified bush bean leaves. The developed methodology was applied to study tetryl uptake and metabolism in bush bean plants exposed to tetryl-amended hydroponic cultures.

INTRODUCTION

Munitions manufacturing, packing, and decommissioning activities result in large quantities of wastewaters. In the past, before the environmental impact of this practice was fully realized, the wastewaters were directed to holding lagoons for primary settling of solid material before being released to rivers and streams. Presently, munitions residues are removed from the wastewater streams by adsorption on carbon columns prior to discharge. However, the pollution legacy of lagooning practices remains because the holding lagoons have since evaporated, leaving heavily contaminated localized areas. Although 2,4,6-trinitrotoluene (TNT) and hexahydro-1,3,5-trinitro-1,3,5-triazine (RDX) are the principal pollutants of concern, significant quantities of tetryl were also released. It has been estimated that approximately 16 kg of tetryl was released from the daily operation of a single manufacturing plant [1]. The contaminated land is presently becoming revegetated, causing further con-

cerns based on the potential for plant uptake of munitions residues and their soil transformation products. The possibility exists that plant metabolism of these compounds may result in the formation of highly toxic metabolites that may propagate through the food chain.

The toxicity of tetryl is well documented. Early munitions workers often suffered dermatitis from exposure to this explosive [2,3]. Tetryl has also been shown to be mutagenic in several different bacterial assay systems [4].

Very little is known about the environmental fate of tetryl. It has recently been demonstrated that tetryl undergoes rapid transformation in the soil environment [5]. Two independent transformation pathways were implicated. The primary transformation pathway involved cleavage of the aniline nitro group resulting in the formation of N-methyl-2,4,6-trinitroaniline. The second, less prominent, pathway involved direct ring nitro reduction of tetryl, resulting in the formation of an aminodinitrophenylmethylnitramine isomer. Other, more polar transformation products were observed in Soxhlet extracts of tetryl-amended soil and were hypothesized to be nitro reduction products of N-meth-

Correspondence to: S. D. Harvey, Pacific Northwest Laboratory, P.O. Box 999, Richland, WA, 99352, USA.

yl-2,4,6-trinitroaniline and aminodinitrophenylmethylamine. Additionally, an unidentified tetryl transformation product was observed in room temperature methanol extracts of tetryl-amended soil that was absent from Soxhlet extracts. This thermally labile transformation product was quantitatively destroyed by conditions utilized for Soxhlet extraction (48 h at 65°C) [5].

Our past studies have shown extreme differences in the plant metabolism of the explosives TNT and RDX [6,7]. The hexahydrotriazine explosive RDX was found to be bioaccumulated in the aerial tissues of plants, whereas the nitroaromatic explosive TNT was rapidly metabolized to polar products which were localized primarily in the root tissue. Virtually nothing is known about the plant metabolism of tetryl. Slow progress in this area is primarily due to the lack of an appropriate analytical methodology to analyze for this explosive in plants. Undoubtedly these problems result from the extreme lability of tetryl. This explosive is photosensitive and known to undergo decomposition in the presence of base [8]. Additionally, tetryl is thermally labile. Decomposition of tetryl to N-methyl-2,4,6-trinitroaniline is known to occur upon gas chromatographic analysis, even when cold on-column injection is utilized [5,9]. Therefore, analysis by milder techniques, such as high-performance liquid chromatography (HPLC), is mandated.

The primary goal of this study was to develop an analytical procedure for the analysis of tetryl in plant tissues that gives both acceptable recoveries and precision. A secondary objective was to apply the developed methodology to study plant metabolism of tetryl in bush bean plants exposed hydroponically to this explosive for either 1 or 7 days. Central to our research approach was the use of uniformly ring-labeled ^{14}C -tetryl. Radiotracer studies allow for both unambiguous identification of metabolic products and a mass balance assessment.

EXPERIMENTAL

Radiolabeled and bulk tetryl

Uniformly ring-labeled ^{14}C -tetryl (specific activity of 14.64 mCi/mmol) was obtained from New England Nuclear (E.I. du Pont de Nemours, Boston, MA, USA). The purity of ^{14}C -tetryl was deter-

mined to be 98.70% by HPLC radiochromatography. This purity was judged adequate for plant uptake and metabolism studies and was used without purification. Bulk tetryl was obtained from US Army Biomedical Research and Development Laboratory (Fort Detrick, MD, USA). HPLC analysis of the bulk material indicated a purity in excess of 95%. The identities of both radiolabeled and bulk tetryl were verified by comparison of retention times with an authentic tetryl standard provided by the US Army Toxic and Hazardous Materials Agency (Aberdeen Proving Ground, MD, USA).

Analytical separations

The chromatographic system was manufactured by Waters Assoc. (Milford, MA, USA) and consisted of a Model 600E gradient controller and pump, a WISP Model 710 automatic injector, and a Model 490E variable wavelength detector. A Beckman Ultrasphere (San Ramon, CA, USA) octadecyl silica column (24 cm \times 4.6 mm I.D., d_p 5 μm) was utilized for separations. Injection volumes were 20 μl for all chromatographic runs. The column was developed with a water–acetonitrile mobile phase programmed from 35 to 100% acetonitrile over 30 min and held at the final composition for an additional 10 min. HPLC-grade solvents, obtained from J. T. Baker (Phillipsburgh, NJ, USA), were used throughout these studies. Detection was accomplished at 264 nm at a sensitivity of 0.008 AUFS. Integrated peak areas, provided by a Hewlett-Packard 3390A integrator, formed the basis for quantification.

Radiochromatographic detection was performed by collecting successive 0.5-ml fractions of the HPLC column eluate. After addition of 15.0 ml of Ready Solv EP scintillation cocktail (Beckman), the individual fractions were assayed for radiocarbon by liquid scintillation spectrometry.

In several instances, plant-produced tetryl metabolites were characterized by their alkylphenone retention indices [10,11]. These indices were determined by co-injection of a mixture of alkylphenones (Aldrich, Milwaukee, WI, USA) with the plant extract of interest. An authentic N-methyl-2,4,6-trinitroaniline standard was utilized during characterization of tetryl plant metabolites and was synthesized as described previously [5].

Plant cultivation and hydroponic exposures

Bush beans were chosen for these studies as a representative dicotyledon having a wide geographical distribution and agricultural significance. Bush bean (*Phaseolus vulgaris*, var., tendergreen) plants were grown from seed and maintained for 21 to 26 days in hydroponic nutrient solutions [12] prior to tetryl uptake exposures. Plant growth and hydroponic exposures were conducted in a growth chamber environment that simulated the luminous intensity and spectral dispersion of sunlight (180 W m^{-2} of photosynthetically active radiation) during the 16-h daily light cycle. The chamber temperature was regulated at a day/night temperature of 26/22°C and a relative humidity of 50%.

Tetryl-amended exposure solutions were prepared by adding 1.0 ml of methanol containing appropriate quantities of non-radiolabeled and radiolabeled tetryl to 500 ml of nutrient solution to give a final tetryl concentration of 10 ppm with a total of $5 \mu\text{Ci } ^{14}\text{C-tetryl}/500 \text{ ml}$. The solutions were filter-sterilized and placed in autoclaved 600-ml beakers to minimize microbial contamination that could promote tetryl transformation. Plant exposure beakers were equipped with aeration capillaries and sheathed with opaque covers to protect the roots from the growth chamber lights. Exposures were conducted in triplicate for either 1, 4, or 7 days. Controls were run concurrently with plant exposures and allowed assessment of tetryl loss due to volatilization and/or photodecomposition. Control solutions consisted of three hydroponic cultures; one of these solutions was aerated and exposed to the full intensity of the growth chamber lights, another was exposed to the lights and not aerated, and a third was aerated and maintained in the dark. Hydroponic exposure and control solutions were sampled for liquid scintillation spectrometry and HPLC analyses after amendment and at the conclusion of each exposure period. At harvest, plants were removed from the hydroponic cultures and the roots sequentially rinsed with 0.1 M calcium chloride and methanol–water (80:20, v/v). Both rinse solutions were assayed for radiocarbon content by liquid scintillation spectrometry. The plant was then segregated into leaf, stem, and root tissues; the individual tissues were minced and thoroughly mixed. Tissues were stored at -80°C until sampled for chemical analysis or oxidation.

Tissue fractionation and analysis of plant tissues

The quantity of radiolabel contained in the plant tissues was determined by total combustion on a Packard Model 306 oxidizer (Packard, Downers Grove, IL, USA). The $^{14}\text{CO}_2$ generated by oxidation of the tissues was subsequently assayed for radiocarbon by liquid scintillation spectrometry.

The tissue fractionation and extraction procedure is outlined in Fig. 1. Tissue samples (1.0 g fresh

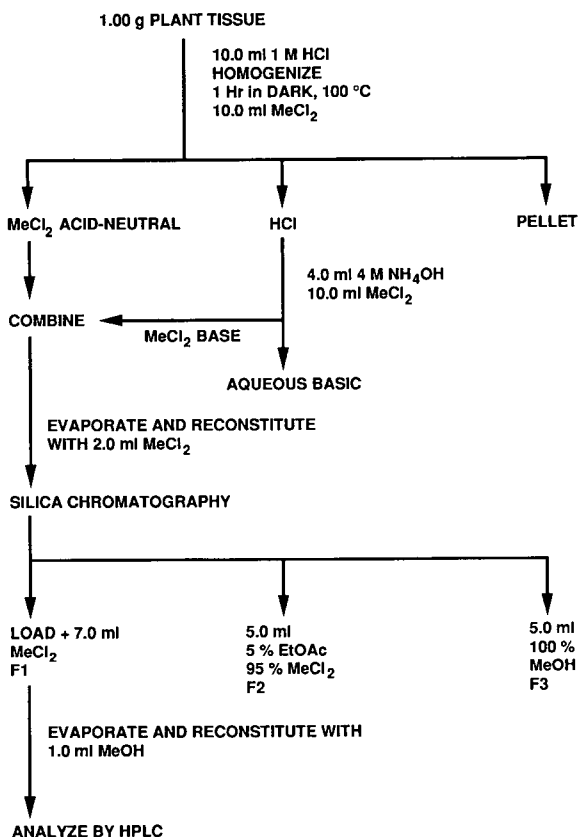


Fig. 1. Flowchart outlining the fractionation of tetryl from plant tissues. After homogenization and acid hydrolysis of tissue, the mixture was partitioned with methylene chloride, giving rise to the methylene chloride acid-neutral (MeCl_2 AN), aqueous hydrochloric acid (HCl), and pellet fractions. The HCl layer was made basic and again partitioned with methylene chloride. The resulting layers were designated the aqueous basic (Aqueous basic) and methylene chloride base (MeCl_2 base) fractions. The pooled methylene chloride layers were evaporated, reconstituted with 2.0 ml of methylene chloride (MeCl_2) and subjected to chromatography on silica with various mobile phases. The mobile phase compositions consisted of MeCl_2 , a mixture of MeCl_2 and ethyl acetate (EtOAc), or methanol (MeOH), as described above. Tetryl, which was contained in fraction F1, was further analyzed by reversed-phase HPLC, with detection at 246 nm.

weight) were homogenized for 2.5 min in 10.0 ml of 1 M HCl in a Sorval Omni-Mixer (Newton, CT, USA). The homogenized samples were transferred to 25-ml Corex centrifuge tubes and acid hydrolysis was performed by submerging the tubes in a boiling water bath for 1 h. The Corex tubes were wrapped in aluminum foil to exclude light during acid hydrolysis. After cooling to room temperature, the hydrolysis mixture was extracted with 10.0 ml of methylene chloride. The organic layer (MeCl₂ acid-neutral fraction) and pellet were separated from the aqueous hydrochloric acid layer (HCl fraction) after centrifugation for 10 min at 3000 g. Aliquots of each fraction (100 μl) were removed for liquid scintillation spectrometry. The tissue pellet was oxidized to determine the amount of sequestered radiolabel. The acidic aqueous layer was next made basic by the addition of 4.0 ml of 4 M NH₄OH and extracted with a second 10.0-ml portion of methylene chloride. After centrifugation the resulting organic (MeCl₂ base fraction) and the aqueous (aqueous basic fraction) phases were separated. Aliquots for liquid scintillation spectrometry were then removed, the organic fractions pooled, and the solvent evaporated to dryness with a gentle stream of nitrogen.

The residue remaining after evaporation of the pooled methylene chloride layers was reconstituted with 2.0 ml of methylene chloride prior to fractionation on silica gel. Silica Sep-Pak (Waters Assoc.) cartridges were preconditioned with 10.0 ml methylene chloride immediately before use. Three fractions were collected from silica gel chromatography of the plant extracts. The first fraction (fraction F1) resulted from application of the plant extract followed by 7.0 ml of methylene chloride mobile phase. Tetryl was contained within fraction F1. The second fraction (fraction F2) was eluted with 5.0 ml of methylene chloride–ethyl acetate (95:5, v/v). The final fraction (fraction F3) was eluted with 5.0 ml of methanol in an attempt to strip the silica of the maximal amount of adsorbed material. After removal of 100-μl aliquots from each fraction for scintillation spectrometry, fraction F1 was evaporated to dryness and reconstituted with 1.0-ml methanol in preparation for HPLC analysis. The spent silica sorbent was removed from the Sep-Pak cartridge and adsorbed radiolabel was determined by liquid scintillation spectrometry.

Determination of ¹⁴CO₂ and volatile organic plant emissions

Volatile organic and ¹⁴CO₂ emissions were measured by a previously described technique [13]. Briefly, a 28-day-old bush bean plant was placed in a specially designed split-chamber enclosure that isolated the roots from the aerial tissues. The plant was maintained on a hydroponic culture containing 7.5 ppm tetryl with a total of 22 μCi radiolabel. Air was pulled by vacuum through each chamber, then through a pair of sorbent traps, and finally through a series of bubbler traps at a flow-rate of 500 ml/min. Two tandem sorbent columns (10 × 1.0 cm) packed with XAD-II resin were located immediately after the chambers to sorb volatile organic emissions. This was followed by four sequential bubbler traps filled with 3 M NaOH designed to remove ¹⁴CO₂. Radiocarbon present in the sampling train was analyzed every 24 h for 3 consecutive days. Radiolabel contained in the NaOH traps and the methanol eluted from the XAD resin was determined by liquid scintillation spectrometry.

RESULTS AND DISCUSSION

Plant hydroponic exposures

Analysis of hydroponic control solutions indicated rapid tetryl photodecomposition. The control solution that was aerated and exposed to the growth chamber lights maintained a constant quantity of radiolabel throughout the 7-day exposure period; however, tetryl progressively decomposed from an initial 4.73 mg/beaker to 3.64 and 0.83 mg/beaker after 1 and 7 days of exposure, respectively. Similar results were obtained for the control solution exposed to the growth chamber lights but not aerated. HPLC analysis of the light-exposed control solutions revealed the formation of a photodecomposition product that increased in concentration throughout the 7-day exposure period. This photodecomposition product (alkylphenone retention index of 920) was subsequently identified by co-injection experiments as N-methyl-2,4,6-trinitroaniline. Formation of this colored product accounted, at least in part, for the bright yellow hue acquired by tetryl solutions upon exposure to light. The control solution that was maintained in the dark remained colorless and displayed only a small loss of tetryl throughout the exposure period. For this so-

lution, the quantity of radiolabel remained constant at 5.51 $\mu\text{Ci}/\text{beaker}$, while the tetryl content decreased from an initial 4.71 mg/beaker to 4.33 and 4.06 mg/beaker after 1 and 7 days of exposure, respectively. HPLC analysis of this control solution did not reveal the presence of transformation products absorbing at 264 nm.

Hydroponic exposure solutions that supported bush beans (solutions were aerated and shielded from light) displayed loss of radiolabel due to plant uptake and root-catalyzed transformation of tetryl. Initial exposure solutions contained $5.56 \pm 0.09 \mu\text{Ci}$ radiolabel with a total tetryl content of $5.03 \pm 0.07 \text{ mg}/\text{beaker}$. Analysis of solutions after supporting bush beans for 1 day indicated that practically all the tetryl had been transformed. Although these solutions contained 55% of the initial radiolabel, tetryl accounted for only 3% of the mass originally amended. Polar products that eluted coincident with the column dead volume were the principal transformation products observed in the plant exposure solutions. Analysis of solutions from the 7-day exposure period indicated that $1.23 \pm 0.07 \mu\text{Ci}$ radiolabel remained in solution and tetryl concentrations were below the detection limit of 0.10 ppm.

The quantity of radiolabel assimilated by the plant was calculated by subtracting the sum of the radiolabel remaining in the post-exposure hydroponic solution, the 0.1 M calcium chloride rinse, and the methanol-water (80:20, v/v) rinse solutions from the amount initially amended to the hydroponic solution. Total radiolabel uptake calculated in this manner was 1.89 ± 0.25 , 3.04 ± 0.34 , and $3.60 \pm 0.19 \mu\text{Ci}$ for the 1-, 4-, and 7-day exposures, respectively. The actual amount of radiolabel contained within the tissues was determined by oxidation. Plants contained 1.53 ± 0.31 , 2.04 ± 0.51 , and $2.27 \pm 0.20 \mu\text{Ci}$ for the 1-, 4-, and 7-day exposures, respectively, as based on oxidation. Values calculated from the oxidation data were consistently lower than values based on analysis of the hydroponic and rinse solutions. This discrepancy between plant uptake and tissue content of radiolabel may reflect tetryl metabolism to volatile organic products or $^{14}\text{CO}_2$.

Analytical methodology for analysis of tetryl in plant tissue

Previous studies conducted in this laboratory

have developed analytical methods for the analysis of TNT [5] and RDX [6] in plant tissues. Methodologies developed for these explosives were similar to the scheme outlined in Fig. 1, with the exceptions that diethyl ether rather than methylene chloride was utilized for solvent extraction and chromatographic fractionation was performed on Florisil (Sep-Pak cartridges, Waters, Milford, MA, USA) rather than silica adsorbent. The method previously developed for RDX [6] was evaluated for the analysis of tetryl-fortified bush bean leaf tissue as an entry point for studies described here. Application of the RDX method resulted in both low recoveries and decomposition of tetryl. A suitable analytical method for tetryl (shown in Fig. 1) was developed by investigating each step of the entire RDX fractionation scheme (starting from the last step and working backward) and incorporating changes that maximized tetryl recovery. RDX analysis steps that were not appropriate for tetryl analysis were traced to a combination of the following: (1) fractionation on Florisil adsorbent, (2) the use of diethyl ether as an extraction solvent, and (3) the acid hydrolysis procedure. These areas are individually discussed below.

Florisil adsorbent was evaluated by fractionating a methylene chloride extract of acid-hydrolyzed bush bean leaf tissue that was spiked with tetryl. It was found that Florisil chromatography of the tetryl-containing plant extract led to decomposition of this explosive. The composition of Florisil includes 18% magnesium oxide which confers basic properties to this adsorbent. It is likely that Florisil promotes tetryl decomposition due to the lability of this explosive toward basic conditions. This observation is consistent with previous studies describing irreversible alteration of tetryl resulting from chromatography on Florisil [14]. For this reason, silica gel was evaluated as an alternative chromatographic sorbent. Tetryl was not strongly adsorbed by silica and was eluted from silica with methylene chloride mobile phase. Methylene chloride was of sufficient solvent strength to elute some plant carotenoid pigments from silica within the same fraction that contained tetryl; however, these pigments did not interfere with the subsequent HPLC determination of tetryl. Liquid scintillation and HPLC analyses of fraction F1 revealed nearly quantitative recovery of tetryl from the silica gel. The majority of the plant

pigments were eluted within the second fraction by methylene chloride-ethyl acetate (95:5, v/v) mobile phase. Methanol was used to elute the final fraction, which contained a moderate quantity of plant pigment.

Problems associated with the solvent extraction portion of the analytical scheme were traced to the use of diethyl ether. Diethyl ether, a relatively high-polarity solvent, was used in the past studies of TNT and RDX due to its ability to extract fairly polar plant metabolites. However, for tetryl, use of this solvent led to poor recoveries. For example, diethyl ether extraction combined with silica gel fractionation of bush bean leaves spiked with tetryl gave a $73.85 \pm 1.31\%$ recovery based on radiocarbon analysis and a $68.26 \pm 6.26\%$ chromatographic recovery of tetryl within fraction F1. Higher recoveries of tetryl were obtained from tetryl-spiked acid-hydrolyzed tissues when methylene chloride was substituted for diethyl ether. An explanation of this result again emphasizes the lability of tetryl toward base. Diethyl ether allows a relatively large quantity of base to partition into the organic phase during extraction of the ammonium hydroxide-containing aqueous phase. Residual base is then concentrated during evaporation of the pooled organic extract which, in turn, leads to the decomposition of tetryl. By virtue of the low solubility of water in methylene chloride, extraction with this solvent minimizes transfer of base into the pooled organic extract and, consequently, tetryl decomposition is minimized.

The acid hydrolysis procedure was also found to contribute to tetryl decomposition. Tetryl decomposition was not felt to be due to the acidic conditions, but rather to sensitization of tetryl to photodecomposition at the elevated hydrolysis temperature. This concern was readily addressed by wrapping the hydrolysis tube in aluminum foil to exclude illumination from the laboratory fluorescent lights. Further alterations of the hydrolysis variables (*i.e.*, temperature and duration) were not pursued, as exclusion of light during this step resulted in reasonable tetryl recoveries. As a precaution against photodecomposition of tetryl, all extraction and fractionation steps were performed either under subdued light or, when possible, in the dark (*i.e.*, during evaporation of solvents).

Consolidation of the RDX methodology modifi-

TABLE I

RADIOLABEL DISTRIBUTION AMONG VARIOUS CHEMICAL FRACTIONS OF BUSH BEAN LEAVES SPIKED IN TRIPPLICATE WITH 4.58 PPM TETRYL

Chemical fraction	Percentage of total radiolabel \pm S.D. ($n = 3$)
HCl	2.60 ± 0.14
MeCl ₂ acid-neutral	84.33 ± 0.73
Aqueous basic	0.36 ± 0.34
MeCl ₂ base	0.04 ± 0.06
F1 ^a	80.49 ± 0.59
F2	3.87 ± 0.89
F3	0.68 ± 0.18
Silica sorbent	0.68 ± 0.18
Pellet	1.49 ± 0.45

^a Chromatographic recovery of tetryl in fraction F1 was $82.70 \pm 5.54\%$.

cations summarized above resulted in the analysis scheme for tetryl outlined in Fig. 1. Triplicate samples of bush bean leaf tissue were spiked with 4.58 ppm tetryl containing a total of 63 953 dpm radiolabeled tetryl and analyzed in accordance with Fig. 1 to evaluate the recovery and precision of this method. The distribution of radiolabel among the various chemical fractions is summarized in Table I. Radiolabel recovery of tetryl in fraction F1 was $80.49 \pm 0.59\%$. HPLC analysis of fraction F1 gave an $82.70 \pm 5.54\%$ chromatographic recovery of tetryl. A representative chromatogram of the F1 fraction resulting from this triplicate spike experiment is presented in the top of Fig. 2. The peak eluting with a retention time of 17.00 min in this chromatogram is due to tetryl. For comparison, a chromatogram of the F1 fraction of a bush bean leaf blank is shown in the bottom of Fig. 2. Several peaks that elute well after tetryl (retention times from 25 to 32 min) are due to the presence of carotenoid pigments within fraction F1. Examination of the tissue blank indicates that these pigments do not interfere with tetryl quantification. Application of the analytical scheme summarized in Fig. 1 allows both high recovery and precision for the analysis of tetryl in plant tissues.

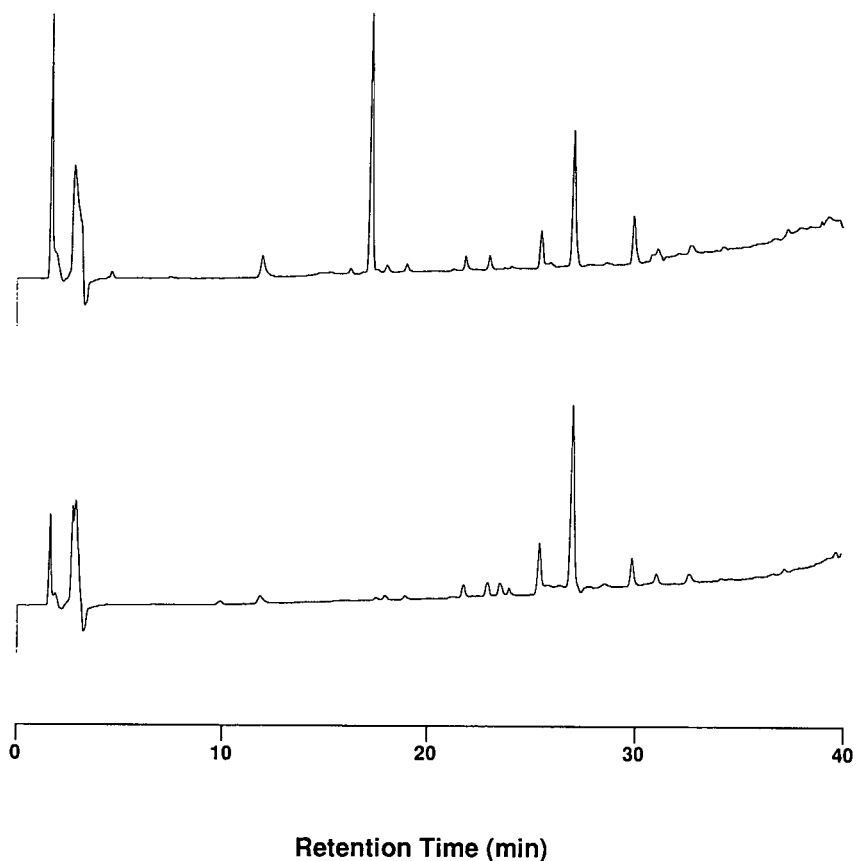


Fig. 2. Chromatograms of fraction F1 from leaf tissue spiked with tetryl (top) and a leaf blank tissue (bottom).

Fate of tetryl in plants

Tissue fractionation. Acid hydrolysis was included as an initial step in the analysis scheme to cleave polar conjugates formed during plant metabolism of tetryl. Insight regarding the formation of acid-hydrolyzable conjugates during tetryl metabolism was provided by comparing tissue hydrolyses performed in acid or water. This experiment was conducted with bush bean leaf tissue from a plant exposed to a tetryl-amended hydroponic culture for 7 days. Triplicate samples of tissue were homogenized either in water or 1 M HCl. Hydrolyses proceeded in the dark at 100°C for 1 h, at which time the preparations were extracted with methylene chloride. For the water hydrolysis treatment the aqueous layer contained $47.4 \pm 0.4\%$, the methylene chloride layer $2.9 \pm 2.2\%$, and the pellet 42.0

$\pm 0.7\%$ of the total radiolabel. The acid hydrolysis treatment resulted in a 62.1 ± 1.2 , 7.1 ± 0.7 , and $31.7 \pm 8.5\%$ distribution of radiolabel in the HCl layer, the methylene chloride phase, and the pellet, respectively. This experiment demonstrates that the acid hydrolysis treatment caused both the release of more radiolabel from the plant matrix (reflected in the higher percentage of extractable radiolabel) as well as the cleavage of some polar conjugates (reflected in the higher percentage of solubilized radiolabel that partitions into the methylene chloride layer).

The quantity of radiolabel contained in the bush bean tissues from plants exposed to tetryl hydroponic solutions for either 1 or 7 days is summarized in the top row of Table II. Assimilation of radiolabel occurred throughout the study, as evidenced by

TABLE II

TOTAL RADIOACTIVITY (BASED ON OXIDATION), PERCENTAGES OF TOTAL RADIOACTIVITY IN CHEMICAL FRACTIONS, AND MATERIAL BALANCE FOR THE ANALYSIS OF BUSH BEAN TISSUES

Values are the average \pm standard deviation from the analysis of 3 plants.

	Day 1			Day 7		
	Leaves	Stem	Roots	Leaves	Stem	Roots
<i>Activity (dpm/g)</i>	$(5 \pm 2)10^3$	$(21 \pm 5)10^3$	$(7 \pm 2)10^5$	$(17 \pm 4)10^3$	$(3 \pm 1)10^4$	$(37 \pm 6)10^4$
<i>Fraction (% total activity)</i>						
HCl	54 \pm 16	24 \pm 5	37 \pm 9	62 \pm 1	36 \pm 6	19 \pm 1
Aqueous basic	41 \pm 14	16 \pm 3	27 \pm 6	45 \pm 5	29 \pm 8	14 \pm 1
MeCl ₂ acid-neutral	6 \pm 5	11 \pm 6	14 \pm 3	7 \pm 1	12 \pm 2	7 \pm 2
MeCl ₂ base	1 \pm 1	4 \pm 1	4 \pm 1	5 \pm 1	6 \pm 1	2.8 \pm 0.2
F1	0.3 \pm 0.6	0.6 \pm 0.7	3.1 \pm 0.8	0.8 \pm 0.7	0.3 \pm 0.5	0.9 \pm 0.5
F2	0 \pm 0	1.4 \pm 1.4	1.5 \pm 0.2	1.2 \pm 1.2	1.6 \pm 1.0	1.0 \pm 0.2
F3	7 \pm 3	9 \pm 3	11 \pm 3	12 \pm 7	10 \pm 1	6 \pm 1
Silica sorbent	2.1 \pm 0.6	1.0 \pm 0.3	1.4 \pm 0.3	1.1 \pm 0.1	0.8 \pm 0.3	0.7 \pm 0.1
Pellet	37 \pm 5	37 \pm 15	46 \pm 11	32 \pm 8	62 \pm 10	64 \pm 19
<i>Tetryl equivalents in fraction F1</i>						
ng equivalents ^a	9 \pm 15	60 \pm 78	$(8.3 \pm 2.6)10^3$	53 \pm 46	25 \pm 44	$(1.3 \pm 0.9)10^3$
<i>Material balance</i>						
HCl + MeCl ₂ acid-neutral + pellet	97	72	97	101	110	90

^a Calculated from specific activity of hydroponic solutions.

the larger quantities of radiolabel in stem and leaf tissues from 7-day as compared to 1-day exposures. For both exposure periods the majority of radiolabel was localized within the root tissue. Stem tissue contained intermediate amounts of radiolabel, whereas the smallest quantity of radiocarbon was localized in the leaf tissue.

The distribution of radiolabel among the various chemical fractions for plants exposed to tetryl hydroponic solutions for either 1 or 7 days is also summarized in Table II. The resulting distributions are indicative of very rapid metabolism of tetryl toward more polar products. Metabolism was so extensive that less than 3.1% of the radiolabel contained in the tissues was associated with fraction F1. A significant quantity of radiolabel, an average of 9% over all analyses, was associated with fraction F3. This fraction contains methylene chloride extractable metabolites that are considerably more polar than tetryl. Large quantities of radiolabel were contained in the aqueous basic fraction. This fraction contains

highly polar compounds resulting from extensive metabolism of the parent munition. Over all analyses, the aqueous basic fraction was found to contain an average of 29% of the radiolabel. The largest percentage of radiolabel was found to be sequestered within the tissue pellets. This fraction contained an overall average of 46% of the radiolabel. Incorporation of radiolabel within the non-soluble biopolymeric pellet matrix is believed to represent an end point for metabolism of xenobiotics. Once the plant has compartmentalized xenobiotic metabolites within the lignin and cellulose pools, these metabolites are effectively removed from interfering with normal plant metabolic processes. A variety of aromatic xenobiotic residues, including chlorinated anilines, pentachlorophenol, 2,4-dichlorophenoxyacetic acid, and benzo[a]pyrene quinones, have been demonstrated to be incorporated within the lignin fraction [15]. It is interesting that all pellets from the 1-day-exposure tissues contained approximately the same proportion of sequestered radiola-

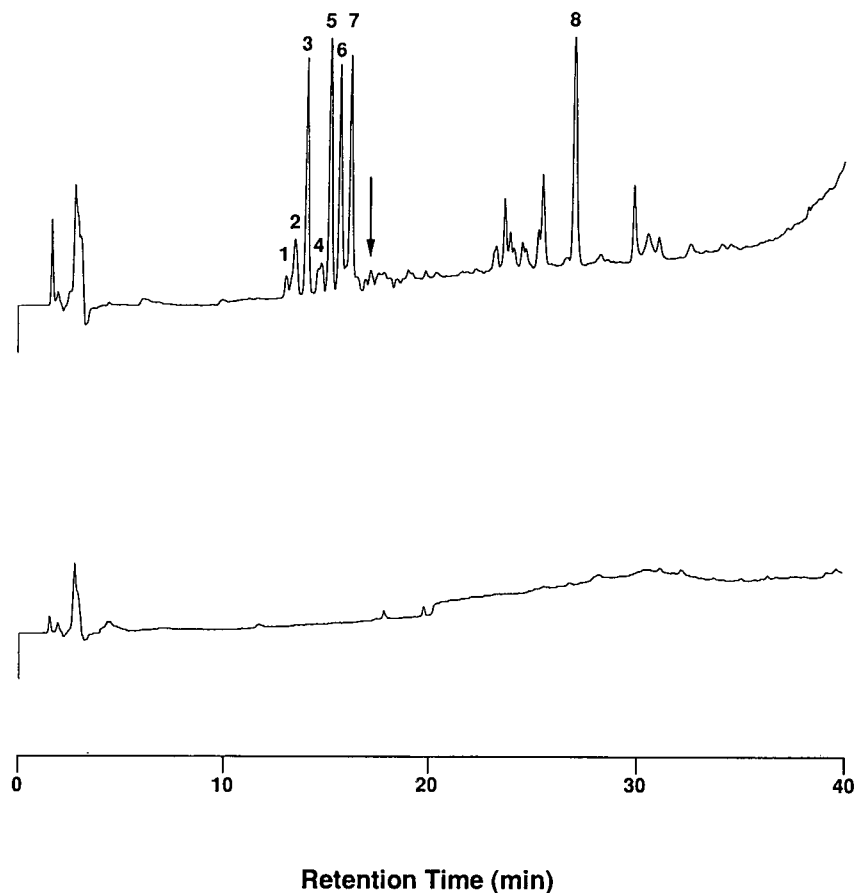


Fig. 3. Chromatographic profile of the F1 fraction of tetryl-exposed bush bean root tissue (top) compared to a control root extract (bottom). Metabolites of tetryl are numbered in the top chromatogram.

bel; whereas stem and root pellets from 7-day-exposure plants contained higher percentages of radiolabel than the corresponding leaf pellets. This result suggests that initial detoxification of tetryl involved sequestration of tetryl-derived radiolabel within the root and stem tissues. The mass balance for the fractionation scheme is included in the bottom row of Table III. These values represent the sum of the hydrochloric acid, the methylene chloride acid-neutral, and the pellet fractions. The material balance ranged from 72 to 110% with an overall average of 95%.

HPLC analysis. HPLC analysis was conducted on the F1 fractions; however, only the root tissues contained a sufficient amount of radiolabel to allow detection of tetryl metabolites. The top of Fig. 3

shows a representative chromatogram of fraction F1 from a bush bean root tissue that had been exposed to a tetryl-amended hydroponic culture for 4 days. The bottom of Fig. 3 shows a chromatogram of the corresponding fraction from a control bush bean root. The arrow in Fig. 3 indicates the retention time of tetryl. The parent explosive is present in this tissue at approximately the detection limit of 0.10 ppm. The most striking feature of this chromatogram is the series of tetryl metabolites appearing within the retention window of 12.85–15.93 min (compounds labeled 1 through 7 in Fig. 3). These compounds are slightly more polar than the parent munition and likely represent the very initial metabolic alterations of tetryl. Additionally, a compound eluting with a retention time of 26.79 min (labeled 8

TABLE III

ALKYLPHENONE RETENTION INDICES OF TETRYL AND PLANT METABOLITES OF TETRYL

Compound	Retention index
Aminodinitrophenylmethylnitramine ^a	872
N-methyl-2,4,6-trinitroaniline standard	922
Tetryl standard	946
Metabolite 1	852
Metabolite 2	861
Metabolite 3	873
Metabolite 4	889
Metabolite 5	coelutes with propiophenone
Metabolite 6	908
Metabolite 7	923

^a Tentative identification based on mass spectral data [5].

in Figure 3) is present in the tetryl-exposed root and absent from the corresponding control tissue. HPLC radiochromatography served to verify incorporation of radiolabel in each of these metabolites. Of the metabolites implicated in Fig. 3, one compound was identified by co-injection experiments. An authentic N-methyl-2,4,6-trinitroaniline standard was found to co-elute with metabolite number 7. Additionally, the alkylphenone retention index of metabolite number 3 matched that of an aminodinitrophenylmethylnitramine isomer that was tentatively identified during previous studies of tetryl in soils [5]. To aid future investigations focusing on the identification of tetryl plant metabolites, compounds 1 through 7 were characterized by their alkylphenone retention indices. These indices are presented Table III.

Monitoring of ¹⁴CO₂ and volatile organic emissions. Experiments designed to monitor ¹⁴CO₂ and volatile organic emissions indicated that a small amount of the radiolabel was oxidized to ¹⁴CO₂. No volatile organics evolved from the shoot during the 72-h exposure. Reliable data for emission of volatiles organics from plant roots could not be obtained due to aerosolization of small amounts of ¹⁴C-tetryl from the hydroponic solution. The ¹⁴CO₂ respiration amounted to 0.07 and 1.0% of the plant-accumulated radiolabel for the shoot and root, respectively. The amount of respired ¹⁴CO₂ was not sufficient to account for the discrepancy noted earlier between the amount of radiolabel as-

simulated from hydroponic cultures and the amount actually contained within the plant tissues. Possible explanations for this discrepancy include inefficient trapping of small volatile organic compounds on the XAD resin due to the large volumes and high flow-rates required to maintain plant turgor or stress-related metabolic differences induced by maintenance of the plant in the volatile emissions experimental chamber.

Comparison to plant metabolism of TNT and RDX. The plant metabolism of tetryl described in this study closely parallels results previously obtained for TNT [6]. Radiolabel from both nitroaromatic explosives was found to be localized primarily in the root tissue. Interestingly, plants exposed to dinitroaniline herbicides also display localization of radiolabel within the root tissue [16]. The presence of the nitroaromatic nucleus of these compounds seems to be associated with the tendency for root tissue accumulation. Chemical fractionation of TNT-exposed plants indicated extensive metabolism toward more polar metabolites; a result that again parallels the present studies with tetryl. Additionally, exposures of plants to either TNT or tetryl resulted in significant quantities of radiolabel being sequestered within the tissue pellets. Results from plant metabolism studies performed with the hexahydrotriazine explosive RDX [7] contrast sharply with those for TNT and tetryl. RDX-exposed plants were found to bioaccumulate the parent munition within the aerial tissues. Metabolism toward

polar products was also observed for RDX; however, the quantity of parent munition far exceeded the level of polar metabolites in leaf tissues. Additionally, the tissue pellets from RDX-exposed plants contained lower percentages of radiolabel than pellets from either TNT- or tetryl-exposed plants.

CONCLUSIONS

Studies described here allow, for the first time, analysis of the explosive tetryl in plant tissues with high recovery and precision. Analytical methodology is based on acid hydrolysis of the tissue to free polar conjugates followed by solvent extraction. The organic extract is then fractionated by silica gel chromatography to remove interfering indigenous plant components prior to HPLC determination of tetryl. Chromatographic recovery of tetryl from fortified bush bean leaves was $82.70 \pm 5.54\%$, whereas radiolabel recovery was $80.49 \pm 0.59\%$. The methodology was applied to study plant uptake and metabolism of tetryl in bush bean plants maintained on tetryl-amended hydroponic cultures for either 1 or 7 days. Importantly, the use of ^{14}C -tetryl combined with HPLC analysis of fraction F1 allowed assessment of the proportion of plant-sequestered radiolabel that was present as the parent munition. Analysis of plants exposed to tetryl-amended hydroponic solutions indicated very rapid metabolism of this explosive to polar metabolites, with less than 3.1% of the radiolabel found associated with the tetryl-containing silica gel fraction. Tetryl was at or below the chromatographic detection limit in the root tissues. As with previous studies on TNT plant metabolism [6], the majority of tetryl-derived radiolabel was found associated with the root tissue. Sequestration of radiolabel in the tissue pellet fraction was found to represent a major route for tetryl detoxification in the bush bean plants.

HPLC analysis of fraction F1 from root tissue indicated the presence of a variety of a tetryl metabolites that likely represent the initial metabolic transformation products of the parent munition. These tetryl metabolites were characterized by their alkylphenone retention indices. One of these components was identified by chromatographic co-elution experiments as N-methyl-2,4,6-trinitroaniline. This compound was also present in light-exposed hydroponic control solutions and was previously

implicated as being a principal soil transformation product of tetryl [5]. A match in the retention indices between metabolite 3 and an aminodinitrophenylmethyl nitramine isomer, that was characterized during previous studies [5], suggests that one metabolic route involves ring nitro reduction of the parent munition. Chemical identification of these tetryl-derived plant metabolites should be the focus of further studies.

ACKNOWLEDGEMENTS

This research was supported by the US Army Biomedical Research and Development Laboratory under a Related Services Agreement with the US Department of Energy under Contract DE-AC06-76RLO 1830. Pacific Northwest Laboratory is operated for the US Department of Energy by Battelle Memorial Institute. The views, opinions, and/or findings contained in this report are those of the authors and should not be construed as an official Department of the Army position, policy, or decision, unless so designated by other documentation.

REFERENCES

- 1 M. J. Small and D. H. Rosenblatt, *Munitions Production Products of Potential Concern as Waterborne Pollutants, Phase II, Technical Report No. 7404 (AD-919031)*, US Army Medical Bioengineering Research and Development Laboratory, Aberdeen Proving Ground, MD, 1974.
- 2 L. J. Whitkowski, C. N. Fisher and H. D. Murdock, *J. Am. Med. Assoc.*, 119 (1942) 1406.
- 3 H. B. Troup, *Br. J. Ind. Med.*, 3 (1946) 20.
- 4 W.-Z. Whong, N. D. Speciner and G. S. Edwards, *Toxicol. Lett.*, 5 (1980) 11.
- 5 S. D. Harvey, R. J. Fellows, J. A. Campbell and D. A. Cataldo, *J. Chromatogr.*, 605 (1992) 227.
- 6 S. D. Harvey, R. J. Fellows, D. A. Cataldo and R. M. Bean, *J. Chromatogr.*, 518 (1990) 361.
- 7 S. D. Harvey, R. J. Fellows, D. A. Cataldo and R. M. Bean, *Environ. Toxicol. Chem.*, 10 (1991) 845.
- 8 J. Yinon, *Toxicity and Metabolism of Explosives*, CRC Press, Boca Raton, FL, 1990, pp. 69–80.
- 9 T. Tamiri and S. Zitrin, *J. Energ. Mater.*, 4 (1986) 215.
- 10 R. M. Smith, *J. Chromatogr.*, 236 (1982) 313.
- 11 D. W. Hill, T. R. Kelley, K. J. Langner and K. W. Miller, *Anal. Chem.*, 56 (1984) 2576.
- 12 D. A. Cataldo, T. R. Garland and R. E. Wildung, *Plant Physiol.*, 62 (1978) 563.
- 13 R. J. Fellows, R. M. Bean and D. A. Cataldo, *J. Agric. Food Chem.*, 37 (1989) 1444.
- 14 F. I. Dubovitskii, G. B. Manelis and L. P. Smirnov, *Russ. J. Phys. Chem.*, 35 (1961) 225.
- 15 D. Scheel, W. Schafer and H. Sandermann, Jr., *J. Agric. Food Chem.*, 32 (1984) 1237.
- 16 S. J. Parka and D. Pramer, *Weed Science*, 25 (1977) 79.

Liquid–gel partitioning using Lipidex in the determination of polychlorinated biphenyls in cod liver oil

Cecilia Weistrand and Koidu Norén

Department of Physiological Chemistry, Karolinska Institutet, Box 60 400, S-104 01 Stockholm (Sweden)

(First received July 14th, 1992; revised manuscript received October 19th, 1992)

ABSTRACT

A technique was developed for transfer of fat and polychlorinated biphenyls from cod liver oil into the lipophilic gel Lipidex 5000. Subsequent elution of the gel separated about 60% of the fat from the sample. Following further purification on aluminium oxide and silica gel, toxic non-*ortho*- and mono-*ortho*-PCB congeners were isolated in two separate fractions on charcoal. Recoveries were studied by addition of twelve different PCB congeners to 0.2 g of fat. The non-*ortho*-PCBs were labelled with ^{13}C . The recoveries of 5–50 ng of the unlabelled compounds were 80–100% and those of 50–100 pg of the labelled compounds were 76–106%.

INTRODUCTION

In recent years, attention has been focused on the toxicity of polychlorinated biphenyls (PCBs), particularly on the congeners that elicit toxic responses similar to those of 2,3,7,8-tetrachlorodibenzo-*p*-dioxin (TCDD). These compounds induce aryl hydrocarbon hydroxylase (AHH) and ethoxyresorufin-O-deethylase (EROD) enzyme activities. The potency to induce such activities *in vitro* has been used to evaluate the toxicological significance of PCB congeners and their activities in relation to TCDD [1,2]. According to these investigations, the non-*ortho*-congeners, IUPAC Nos. 77, 126 and 169 (for structures, see Table I), are the most toxic. Among the mono-*ortho*-congeners, IUPAC Nos. 105, 118 and 156 are considered to be the most potent.

The determination of PCBs in biological samples is complicated by their presence at trace levels in highly complex matrices. The first step in the analysis of biological samples is to extract the organo-

chlorine compounds from the material. This is usually done by liquid–liquid partitioning, Soxhlet extraction or the sample is mixed with sodium sulphate and eluted with an organic solvent [3]. The co-extracted lipids can be removed by treatment with sulphuric acid or alkali (saponification). However, strong alkali decomposes certain polychlorinated dibenzofurans (PCDFs), polychlorinated dibenzo-*p*-dioxins (PCDDs) [4,5] and DDT [6] and concentrated sulphuric acid destroys dieldrin [7]. Complementary purification and separation from lipids and other interfering compounds have been achieved by column chromatography using aluminium oxide, silica gel and Florisil [3]. Gel permeation chromatography (GPC) with Bio-Beads is more efficient in removing lipids than these adsorbents [3]. However, this method requires special equipment for a forced liquid flow.

In studies of toxic non-*ortho*- and mono-*ortho*-PCBs, chromatography on activated charcoal has frequently been used for the separation of the non-*ortho*-congeners from the bulk of PCBs [8–10]. Only a few methods have been reported concerning the isolation of the toxic non-*ortho*- and mono-*ortho*-PCBs in separate fractions. Athanasiadou *et al.* [11] used multiple charcoal columns to isolate non- and

Correspondence to: K. Norén, Department of Physiological Chemistry, Karolinska Institutet, Box 60 400, S-104 01 Stockholm, Sweden.

TABLE I
IUPAC NUMBERS AND CHLORINE ATOM POSITIONS OF PCBs

IUPAC No.	Structure	IUPAC No.	Structure
15	<i>Dichlorobiphenyl</i> 4,4'-	132	<i>Hexachlorobiphenyls</i> 2,2',3,3',4,6'-
		138	2,2',3,4,4',5'-
28	<i>Trichlorobiphenyl</i> 2,4,4'-	149	2,2',3,4',5',6'-
		153	2,2',4,4',5,5'-
52	<i>Tetrachlorobiphenyls</i> 2,2',5,5'-	156	2,3,3',4,4',5'-
77	3,3',4,4'-	169	3,3',4,4',5,5'-
			<i>Heptachlorobiphenyls</i>
101	<i>Pentachlorobiphenyls</i> 2,2',4,5,5'-	171	2,2',3,3',4,4',6'-
105	2,3,3',4,4'-	180	2,2',3,4,4',5,5'-
118	2,3',4,4',5'-		<i>Docedachlorobiphenyl</i>
126	3,3',4,4',5'-	209	2,2',3,3',4,4',5,5',6,6'-

mono-*ortho*-PCBs in a technical PCB product, and Wilson-Yang *et al.* [12] employed charcoal for isolation of non- and mono-*ortho*-congeners in a biological sample. Recently, Haglund *et al.* [13] separated PCBs into similar groups by high-performance liquid chromatography (HPLC) on 2-(1-pyrenyl)ethyltrimethylsilylated silica. Depending on the concentrations, final determination of PCBs has been performed by gas chromatography with electron-capture detection (GC-ECD) or gas chromatography-mass spectrometry (GC-MS).

The aim of this study was to develop a simple and non-destructive method for the extraction and purification of organochlorine compounds from materials rich in lipids (*e.g.*, solution of lipids). Extraction with Lipidex was chosen as this gel has been shown to have a high capacity for lipids and lipid-soluble compounds [14] and it has been used successfully for the enrichment of organochlorine compounds from aqueous samples, *e.g.*, water [15], urine [15] and human milk [16]. In attempts to adapt the method for fatty samples, cod liver oil was chosen as a model matrix. This product is used as a vitamin supplement, and as organochlorine contaminants, such as PCBs, accumulate in cod liver, the investigation of this oil was of interest. A technique was developed to transfer lipids and lipid-soluble compounds from an organic solvent into the gel. The subsequent elution of the gel with solvents of different polarity permits the isolation of the compounds

and partial purification of the sample. No special equipment is required for the sample preparation. The separation of toxic non-*ortho*- and mono-*ortho*-PCBs from the bulk of PCBs was achieved by chromatography on a charcoal column, which was eluted with a modified solvent system.

EXPERIMENTAL

Sample

The cod liver oil (Apoteksbolaget, Solna, Sweden) was a common pharmacy product used as a vitamin A and D supplement. A 10-g amount of oil was weighed into a volumetric flask (100 ml), dissolved in hexane and diluted to the mark with hexane.

Solvents

All solvents were of analytical-reagent grade. Methanol was treated with sodium hydroxide and redistilled twice [15]. Acetonitrile, toluene and 2-propanol were redistilled once. Hexane, chloroform and methylene chloride were redistilled twice. Hexane used for the elution of silica gel was dried with sodium sulphate. Water was deionized and purified with a Milli-Q cartridge system (Millipore, Bedford, MA, USA).

Standards

Clophen A50 (Bayer, Leverkusen, Germany) was

used as a standard for the determination of total PCBs. ^{13}C -labelled PCBs Nos. 77, 126 and 169 (Cambridge Isotope Laboratories, Woburn, MA, USA) were used for the determination of non-*ortho*-PCBs. Standards for determination of PCBs Nos. 28, 52, 101, 105, 118, 138, 153, 156 and 180 were obtained from Ehrenstorfer (Augsburg, Germany), or were received as gifts from Dr. Åke Bergman, Wallenberg Laboratory, Stockholm University. Standards used for volume correction, PCBs Nos. 15 and No. 209, were obtained from Ehrenstorfer.

Column chromatography

Glass chromatographic columns were of 0.4, 1 and 2 cm I.D. [9,15]. Lipidex 5000 (Packard Instruments, Downers Grove, IL, USA) was washed and stored in methanol at 4°C [17]. Immediately before use, it was rinsed with 2-propanol (2 × 25 ml per 20 g of Lipidex) in a separating funnel, equipped with a sintered-glass disc and a PTFE stopcock at the end. A gentle stream of purified nitrogen was used to remove most of the remaining 2-propanol. Aluminium oxide 90 (activity grade II–III) (Merck, Darmstadt, Germany), silica gel 60 (70–230 mesh) (Merck) and activated charcoal (SP-1) (Serva, Heidelberg, Germany) were prepared as described elsewhere [9,10].

Gas chromatography

The GC analyses of di-*ortho*- and mono-*ortho*-substituted PCBs were performed using a Pye Unicam gas chromatograph equipped with an all-glass falling-needle injector with the heater at 220°C, a fused-silica capillary column coated with SE-54 (25 m × 0.32 mm I.D., 0.25 μm film thickness) (Quadrex, New Haven, CT, USA) and a ^{63}Ni electron-capture detector. Nitrogen was used as the carrier gas. The column temperature was kept at 190°C for 15 min, programmed to 260°C at 5°C/min and then kept isothermal at 260°C for 30 min. An on-column injector maintained at 220°C was used for the GC determination of the total amount of PCBs. The glass column (2 m × 2 mm I.D.) was packed with a mixture of 3% SF-96 and 6% QF-1 (32:68, w/w) on Chromosorb W HP (100–120 mesh) [18]. The column temperature was 185°C.

Gas chromatography–mass spectrometry

GC–MS analyses were performed with a VG 7070 E mass spectrometer equipped with a DANI gas chromatograph and a VG 11–250 data system (VG Analytical, Manchester, UK). A fused-silica capillary column coated with SE-30 (25 m × 0.32 mm I.D., 0.25 μm film thickness) (Quadrex) was directly connected to the ion source. The oven temperature was 190°C for 15 min, programmed to 270°C at 8°C/min and kept at this temperature for 8 min. An all-glass falling-needle injector was used with an injector heater at 270°C. The carrier gas was helium. Electron impact (EI) ionization was performed in an EI-only ion source at 48 eV. The acceleration voltage was 6 kV and the resolution was 8000–9000. Compounds were monitored in groups determined by the number of chlorine atoms in the molecule. Two ions of each molecular ion cluster were monitored. For each group, one ion from the column bleeding was selected as the reference mass for correction of mass spectrometer drift (lock mass). For each m/z value the dwell time was 80 ms and the delay time 20 ms.

Method

A flow scheme of the analytical procedure is shown in Fig. 1.

Extraction and preliminary purification. An aliquot of 2 ml of the oil solution (0.1 g/ml) was transferred into a 100 ml erlenmeyer flask. All samples were fortified with ^{13}C -labelled PCBs Nos. 77, 126, and 169. A number of samples were also fortified with unlabelled PCBs Nos. 28, 52, 101, 105, 118, 138, 153, 156 and 180 for recovery studies. One blank sample (2 ml of hexane) was run in parallel with each set of samples. A 15-ml volume of 2-propanol was mixed with the sample solution and 5.0 g of washed Lipidex were added. A dropping funnel equipped with a pressure equalizer was attached to the top of the flask. A 40-ml volume of water was added to the funnel, which was closed with a glass stopper at the top. The subsequent procedure was performed while shaking the flask at 35°C in a water-bath for a total of 2.5 h. After 5 min, water was added from the funnel (Teflon stopcock) with continuous shaking at a rate of about 0.5 ml/min. When all the water had been added, shaking was continued with the stopcock closed. The mixture was then transferred into a glass column (2 cm I.D.)

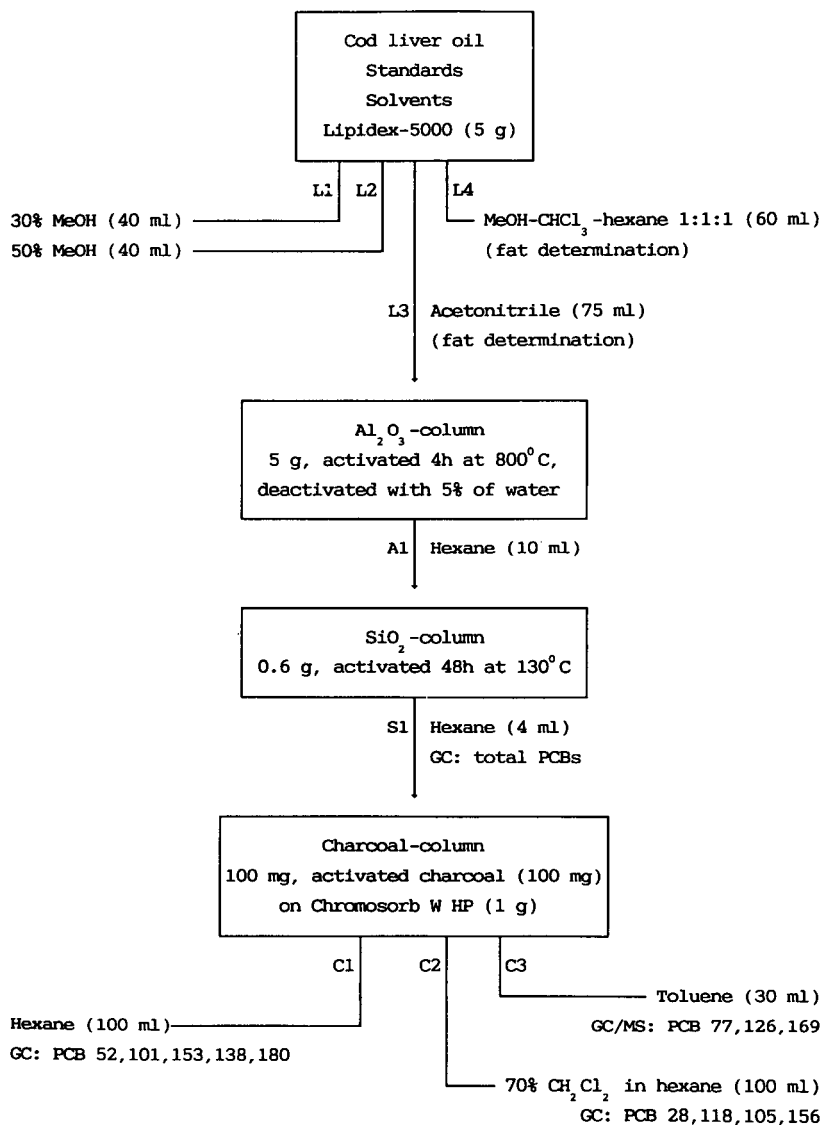


Fig. 1. Flow scheme of the method.

and the solvent was drained. The gel was washed with 40 ml of methanol–water (30:70, v/v) (fraction L1) and 40 ml of methanol–water (50:50, v/v) (fraction L2). The chlorinated compounds and some lipids were eluted with 75 ml of acetonitrile (fraction L3). Remaining lipids were eluted with 60 ml of methanol–chloroform–hexane, (1:1:1, v/v/v) (fraction L4).

Fat determination. Fractions L3 and L4 were tak-

en nearly to dryness in a rotary evaporator at 35°C and the residues were dried to constant mass in a desiccator at room temperature. The sum of the masses of fractions L3 and L4 defined the total amount of fat in the sample.

Purification and group separation. Partly deactivated aluminium oxide and activated silica gel were used for further purification and separation of the sample, according to ref. 16 and Fig. 1. The silica

gel fraction (S1) contained the PCBs. A standard (40 ng of PCB No. 15) was added for volume correction and the total amount of PCBs was determined by GC-ECD.

A column (0.4 cm I.D.) was packed with 100 mg of a mixture of activated charcoal and Chromosorb W HP [9,10] and washed with 30 ml of toluene, 20 ml of methylene chloride–hexane (10:90, v/v) and 20 ml of hexane. Fraction S1 from the silica gel was evaporated with a gentle stream of nitrogen to ca. 100 μ l and quantitatively transferred into the column with hexane. The column was then eluted with 100 ml of hexane (fraction C1). This fraction contained the PCBs, except for certain mono-*ortho*-PCBs and the non-*ortho*-PCBs. Mono-*ortho*-PCBs (IUPAC Nos. 28, 105, 118, 156) were eluted with 100 ml of methylene chloride–hexane (70:30, v/v) (fraction C2) and the non-*ortho*-PCBs with the following 30 ml of toluene (fraction C3). Fractions C1 and C2 were concentrated to 1–2 ml. After addition of internal standard (40 or 80 ng of PCB No. 15), the fractions were analysed by GC-ECD. Fraction C3, was evaporated to ca. 50 μ l. Internal standard (100 pg of PCB No. 209) was added and after further concentration the fraction was analysed by GC-MS.

RESULTS AND DISCUSSION

Lipidex proved to be an effective sorbent for fat and fat-soluble compounds in cod liver oil. The transfer of lipids from a hexane–2-propanol extract of testicular tissue into Lipidex has been demonstrated by Anderson and Sjövall [19] in the determination of steroids. They mixed the extract with Lipidex 1000 and evaporated the solvent with a rotary evaporator. The steroids were eluted from the dried gel with aqueous methanol leaving the lipids in the gel. We utilized the same approach for the determination of organochlorine compounds in cod liver oil. However, the method of evaporation was not suitable, as the material spread on the surface of the glassware and the resulting recoveries were low. Other methods were therefore tested for the transfer of fat and PCBs into the gel. Water was added in 10-ml portions to the hexane–2-propanol extract during shaking. This provided better results than the evaporation method, but the recoveries were still not acceptable. The continuous addition of wa-

ter during shaking proved to be essential for complete transfer into the gel.

About 60% of the lipids were removed from the sample by the elution system used for Lipidex (Table II). The average amount of fat in nine samples was 0.206 g (range 0.203–0.211 g). Further removal of lipids and separation from most of the pesticides were achieved with column chromatography on aluminium oxide and silica gel. The total amount of PCBs was determined in two samples (fraction S1). These determinations were made by GC-ECD using a packed column and Clophen A50 as a standard as described previously [18]. Congener-specific analyses were made for twelve compounds (IUPAC Nos. 28, 52, 77, 101, 105, 118, 126, 138, 153, 156, 169 and 180). Fig. 2 shows high-resolution gas chromatograms of an unspiked oil sample. From the complex mixture of PCBs in fraction S1 (Fig. 2a) the mono-*ortho*-PCBs were separated on charcoal and recovered in fraction C2 (Fig. 2c), leaving the bulk of PCBs in fraction C1 (Fig. 2b). By this procedure the mono-*ortho*-PCBs Nos. 105, 118 and 156 could be separated from the interfering compounds Nos. 132, 149 and 171, respectively. The selected-ion chromatograms of non-*ortho*-PCBs (fraction C3) obtained in the GC-MS analyses are shown in Fig. 3. The recoveries of di- and mono-*ortho*-PCBs added to 0.2 g of oil ranged from 80 to 100%, and the recoveries of added ^{13}C -labelled non-*ortho*-PCBs ranged from 76 to 106% (Table III).

The cod liver oil was intended as a vitamin A and D supplement and was purified from PCDDs according to the supplier. The total PCB concentration in this oil was 1 $\mu\text{g/g}$ fat and it contained toxic non- and mono-*ortho*-congeners of PCBs (Table III). Safe [1] and Ahlborg *et al.* [20] have proposed

TABLE II
DISTRIBUTION OF FAT IN THE FRACTIONS ELUTED FROM LIPIDEX ($n = 9$)

Fraction	Distribution (%)		
	Mean	Range	R.S.D.
L1	0	—	—
L2	0	—	—
L3	38	32–44	11
L4	62	56–67	7

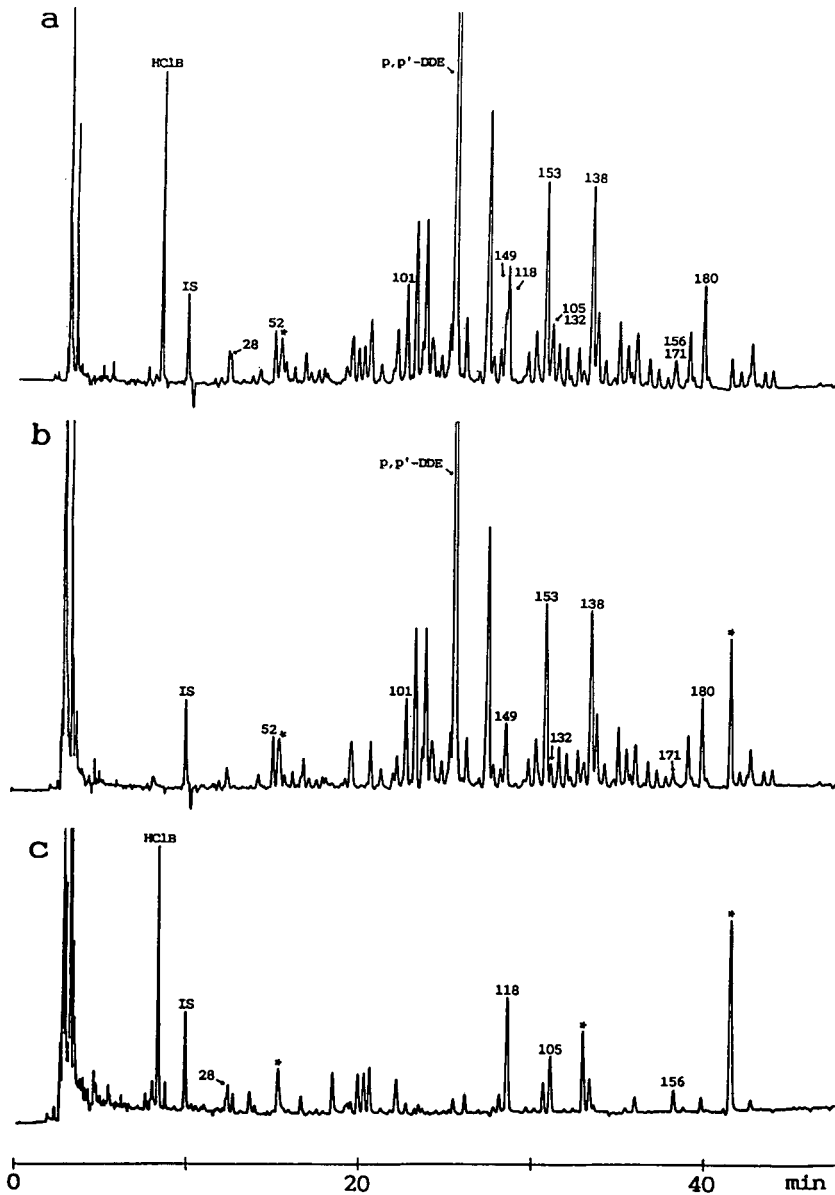


Fig. 2. High-resolution gas chromatograms of (a) cod liver oil before separation on charcoal (fraction S1); (b) the PCB pattern after group separation on charcoal with certain *mono-ortho*-PCBs and *non-ortho*-PCBs removed (fraction C1); and (c) *mono-ortho*-PCBs (fraction C2). The peaks marked with asterisks represent impurities. HClB = Hexachlorobenzene.

toxic equivalency factors (TEFs) for different PCB congeners. These factors express the toxicity of a compound relative to that of TCDD. Using these factors for *non-ortho*- and *mono-ortho*-PCBs in the cod liver oil, the toxic equivalents (TEQs) were calculat-

ed as 69 and 20 pg/g, respectively (Table IV). According to the Nordic risk assessment [21], a tolerable intake would be 0–35 pg TCDD per kg body-mass per week.

The proposed method for liquid–gel partitioning

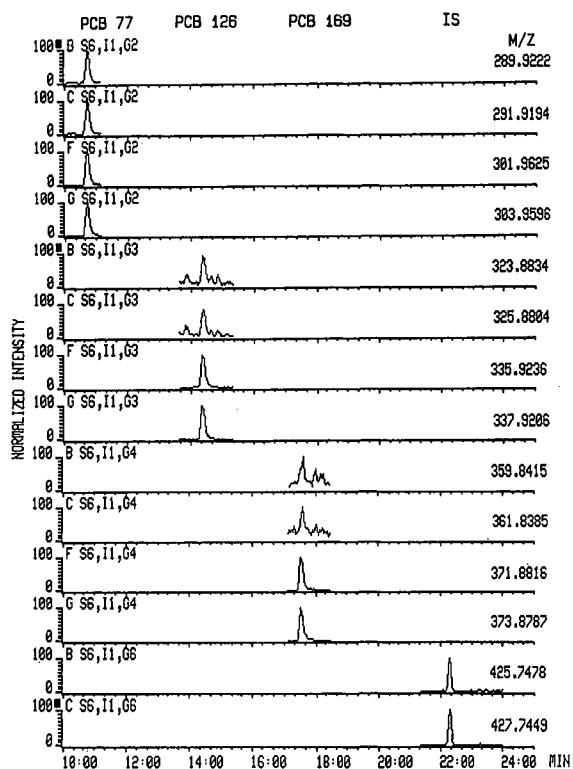


Fig. 3. Selected ion chromatograms of non-*ortho*-PCB congeners (fraction C3) obtained in the GC-MS analyses. The peaks with the two highest *m/z* values for each non-*ortho*-PCB represent ^{13}C -labelled compounds.

of lipids and lipid-soluble organochlorine compounds is advantageous compared with liquid-liquid partitioning as no emulsions are formed and repeated extractions and centrifugations are avoided. In recent years, GPC has been applied successfully for the purification of fatty extracts. However, although the lipids are efficiently removed, further purification is required for determinations of low levels of organochlorine compounds. In contrast to the present method, GPC requires special equipment and the throughput is limited unless multiple HPLC systems and columns are available. Lipidex has a high capacity to incorporate lipids and lipid-soluble compounds. In the proposed method 0.2 g of oil was used for analysis. However, the same distribution of fat in fractions L3 and L4 was obtained using up to 0.5 g of fat. The subsequent elution of the gel with solvents of different polarity facilitates partial purification of the sample. Only simple laboratory equipment is needed for the extraction procedure and the elution of the gel. The relatively long extraction time is compensated for by the fact that many extractions can be performed simultaneously. The technique adopted is partly based on a non-destructive method for the determination of organochlorine pesticides, PCDDs, PCDFs and PCBs in human milk [9,16]. Such compounds can also be included and analysed by the proposed method.

TABLE III

LEVELS OF CERTAIN PCB CONGENERS IN COD LIVER OIL AND RECOVERIES OF ADDED PCBs

PCB IUPAC No.	Level (ng/g fat)		Amount added (ng) ^a	Recovery (%)		
	Mean ^a	Range		Mean	Range	R.S.D.
<i>Di-ortho-</i>						
52	28 (2)	27–28	10–50 (7)	91	83–89	5
101	40 (2)	40–41	10–50 (7)	93	85–99	5
138	73 (2)	70–76	10–50 (7)	88	81–94	6
153	84 (2)	81–88	10–50 (7)	94	86–99	6
180	30 (2)	28–31	10–50 (7)	91	84–98	5
<i>Mono-ortho-</i>						
28	10 (2)	9–10	10–50 (7)	90	81–98	7
105	14 (2)	14–15	5–25 (7)	91	88–98	4
118	36 (2)	34–39	5–25 (7)	88	80–100	8
156	5 (2)	5–5	5–25 (7)	90	80–97	7
<i>Non-ortho-</i>						
77	0.26 (5)	0.23–0.27	0.05–0.10 (5)	89	70–106	12
126	0.10 (5)	0.09–0.11	0.05–0.10 (5)	90	79–102	11
169	0.02 (5)	0.02–0.03	0.05–0.10 (5)	88	83–97	11

^a Number of samples analysed is given in parentheses.

TABLE IV

TEF VALUES PROPOSED BY SAFE [1] AND AHLBORG ET AL. [20] AND TEQ VALUES FOR PCBs IN COD LIVER OIL

PCB IUPAC No.	TEF		TEQ (pg/g)	
	Ref. 1	Ref. 20	Ref. 1	Ref. 20
<i>Non-ortho-</i>				
77	0.01	0.0005	2.6	0.1
126	0.1	0.1	10.0	10.0
169	0.05	0.01	1.0	0.2
<i>Mono-ortho-</i>				
105	0.001	0.0001	14.0	1.4
118	0.001	0.0001	36.0	3.6
156	0.001	0.001	5.0	5.0
Total			68.6	20.3

The method can also be applied to the analysis of organic solvent extracts of other biological samples. The method was developed for small amount of samples, using small column systems and solvent volumes. Consequently, the risks of contamination from solvents and adsorbents are reduced, and the costs of the analyses are decreased.

ACKNOWLEDGEMENTS

This study was financially supported by the Swedish Environmental Protection Agency, contract No. 5323191-6, the Swedish Medical Research Council (03X-219), Stiftelsen Lars Hiertas Minne and Karolinska Institutet.

REFERENCES

- 1 S. Safe, *CRC Crit. Rev. Toxicol.*, 21 (1990) 51.
- 2 A. Hanberg, F. Wearn, L. Asplund, E. Haglund and S. Safe, *Chemosphere*, 20 (1990) 1161.
- 3 M. D. Erickson, *Analytical Chemistry of PCBs*, Butterworths, Stoneham, MA, 1986.
- 4 P. W. Albro, J. S. Schroeder, D. J. Harvan and B. J. Corbett, *J. Chromatogr.*, 312 (1984) 165.
- 5 J. J. Ryan, R. Lizotte, L. G. Panopio and B. P.-Y. Lau, *Chemosphere*, 18 (1989) 149.
- 6 R. Benecke, J. Brotka, J. Wijsbeek and R. A. Zeeuw, *J. High Resolut. Chromatogr. Chromatogr. Commun.*, 8 (1985) 30.
- 7 D. E. Wells, *Pure Appl. Chem.*, 9 (1988) 1437.
- 8 S. Tanabe, N. Kannan, T. Wakimoto and R. Tatsukawa, *J. Environ. Anal. Chem.*, 29 (1987) 199.
- 9 K. Norén, Å. Lundén, J. Sjövall and Å. Bergman, *Chemosphere*, 20 (1990) 935.
- 10 B. Jansson, R. Andersson, L. Asplund, Å. Bergman, K. Litzen, K. Nylund, L. Reutergård, U. Sellström, U-B. Uvemo, C. Wahlberg and U. Wideqvist, *Fresenius' Z. Anal. Chem.*, 340 (1991) 439.
- 11 M. Athanasiadou, S. Jensen and E. Wehler, *Chemosphere*, 23 (1991) 957.
- 12 K. M. Wilson-Yang, J. P. Power, E. A. Chrisholm and D. J. Hallett, *Chemosphere*, 23 (1991) 1139.
- 13 P. Haglund, L. Asplund, U. Järnberg and B. Jansson, *Chemosphere*, 20 (1990) 887.
- 14 B. Egestad, T. Curstedt and J. Sjövall, *Anal. Lett.*, 15 (1982) 293.
- 15 K. Norén and J. Sjövall, *J. Chromatogr.*, 414 (1987) 55.
- 16 K. Norén and J. Sjövall, *J. Chromatogr.*, 422 (1987) 103.
- 17 M. Axelsson and J. Sjövall, *J. Chromatogr.*, 126 (1976) 705.
- 18 K. Noren, *Arch. Environ. Contam. Toxicol.*, 12 (1983) 277.
- 19 S. H. G. Andersson and J. Sjövall, *Anal. Biochem.*, 134 (1983) 309.
- 20 U. G. Ahlberg, A. Hanberg and K. Kenne, *Risk Assessment of Polychlorinated Biphenyls (PCBs)*, Nordic Council of Ministers, Copenhagen, 1992.
- 21 U. G. Ahlberg, H. Håkansson, F. Waern and A. Hanberg, *Nordisk Dioxinriskbedömning*, Nordic Council of Ministers, Copenhagen, 1988.

High-performance liquid chromatographic determination of methanesulphinic acid as a method for the determination of hydroxyl radicals

Shozo Fukui, Yukiko Hanasaki and Shunjiro Ogawa

Kyoto Pharmaceutical University, Yamashina-ku, Kyoto 607 (Japan)

(First received June 9th, 1992; revised manuscript received September 24th, 1992)

ABSTRACT

For the determination of hydroxyl radicals, dimethyl sulphoxide was used as a molecular probe and the methanesulphinic acid produced was determined by high-performance liquid chromatography of its Fast Yellow GC salt derivative. The results for hydroxyl radicals formed using the Fenton and hypoxanthine-xanthine oxidase systems agreed well with the theoretical values. Interferences from phenols, aromatic amines and amino acids, which give coloured substances by reaction with the diazonium salt, could be avoided. The recovery of methanesulphinic acid added to liver homogenates and incubated for 1 h at 37°C was $70.2 \pm 2.1\%$. The detection limit for methanesulphinic acid in a sample solution was *ca.* 8 ng/ml.

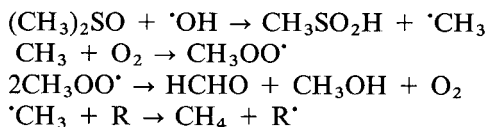
INTRODUCTION

Oxygen-derived free radicals are thought to be involved in the pathogenesis of many toxicological and disease states [1-3]. Further, the free radicals are involved in both the initiation and promotion of multi-stage carcinogenesis [4-6]. Among the various radicals, the hydroxyl radical ($\cdot\text{OH}$) is presumed to play a central role owing to its strong activity [7].

A number of methods have been developed for the determination of $\cdot\text{OH}$, *e.g.*, spin-trapping electron paramagnetic resonance spectroscopy [8-10], gas chromatography (GC) of ethylene produced from methional by the reaction of $\cdot\text{OH}$ [11] and GC or high-performance liquid chromatography (HPLC) of hydroxylated substances obtained by the reactions of $\cdot\text{OH}$ with aromatic compounds such as phenol, benzoic acid or salicylic acid [12,13].

Dimethyl sulphoxide (DMSO) has become of in-

terest as a probe for $\cdot\text{OH}$ formation in recent years. As pointed out by Babbs and Griffin [14], DMSO must be an ideal molecular probe for $\cdot\text{OH}$ owing to its unique chemical and biological properties such as its benign biological effects and the product of its reaction with $\cdot\text{OH}$, methanesulphinic acid (MSA), is stable and non-metabolized. DMSO interacts readily with $\cdot\text{OH}$ to produce MSA and a methyl radical ($\cdot\text{CH}_3$) [14]. Subsequently, $\cdot\text{CH}_3$ is converted into methane [15] and formaldehyde [16], but the reactions of formation of formaldehyde will occur very sparingly in biological system, because of alternative radical scavengers [14].



Among the above products, MSA, a stable non-radical compound and normally absent in biological samples, was successfully adopted for spectrophotometric measurement of $\cdot\text{OH}$ by Babbs and co-workers [14,17,18] by a method based on azo dye

Correspondence to: S. Fukui, Kyoto Pharmaceutical University, Yamashina-ku, Kyoto 607, Japan.

formation through the reaction of MSA and a diazonium salt (Fast Blue BB salt). In this paper, we describe HPLC for the determination of MSA formed by the reaction of $\cdot\text{OH}$ and DMSO. MSA was allowed to react with Fast Yellow GC salt and the resulting *o*-chlorobenzene diazomethyl sulphone was determined by HPLC. This procedure offered a quantitative determination of $\cdot\text{OH}$ generated by the Fenton reaction system and the hypoxanthine–xanthine oxidase system. Interferences due to coloured samples or the production of coloured substances by the reaction with diazonium salts (e.g., phenols or aromatic amines) were successfully avoided.

EXPERIMENTAL

Reagents

Fast Yellow GC salt (FY-GC, salt content 25%) was obtained from Sigma. FY-GC reagent was freshly prepared by dissolving 1.0 g of the salt in 100 ml of water and filtering.

Hypoxanthine, bovine milk xanthine oxidase, horse heart superoxide dismutase and catalase were obtained from Sigma and were used as received. Sodium methanesulphinate (MSA) was obtained from Fairfield Chemical. Other reagents were of special grade from Nacalai Tesque.

Equipment

A Shimadzu Model HLC-10AS high-performance liquid chromatograph equipped with an SPD-10AV UV-Vis spectrophotometric detector and a C-R6A Chromatopac integrator was used. A Capcell-Pak NH_2 column, (150 mm \times 4.6 mm I.D.) was obtained from Shiseido.

Chromatographic conditions

The stationary phase was Capcell-Pak NH_2 packed in a stainless-steel column (150 mm \times 4.6 mm I.D.) (Shiseido) and the column temperature was ambient. The mobile phase was an isocratic mixture of ethanol (specific gravity adjusted to 0.800 with water) and *n*-hexane (3:100, v/v) maintained at a flow-rate of 1 ml/min. A Shimadzu SPD-10AV UV-Vis detector was used at a wavelength of 285 nm. A 20- μl portion of sample was injected each time.

Determination of methanesulphinic acid (MSA)

To 5 ml of sample solution, 1 ml of 0.5 M phosphate buffer (pH 4.0) and 1 ml of FY-GC reagent were added and the mixture was shaken and allowed to stand for 10 min, then 2 ml of ethyl acetate were added and the mixture was shaken well for 5 min. The ethyl acetate layer was separated by centrifugation at 1000 g for 5 min and filtered through a Millipore filter (pore size 5 μm), then analysed under the above chromatographic conditions.

Fenton system

The procedure described by Steiner and Babbs [19] was used. To 2.5 ml of freshly prepared 1 mM FeSO_4 in 50 mM DMSO solution, 0–2.5 ml of 200 μM H_2O_2 were added dropwise. The volumes of the mixtures were made up to 5.0 ml with 50 mM DMSO solution and allowed to stand for 10 min. MSA in the mixtures was determined as described above.

Hypoxanthine–xanthine oxidase system

The procedure described by Babbs and Griffin [14] was used with a slight modification. To a solution of 2.0 ml of 250 μM hypoxanthine in 150 mM phosphate buffer (pH 7.4), 1.0 ml of 50 mM DMSO solution, 0.3 ml of 2 mM FeSO_4 solution, 0.3 ml of 2 mM EDTA solution, 1 ml of water or $\cdot\text{OH}$ scavenger solution and 0.4 ml of 0.60 U/ml xanthine oxidase solution were added. The mixtures were allowed to stand for 12 min at 37°C. The total volume of the mixture was 5.0 ml, hence the final concentrations were 100 μM hypoxanthine and 48 mU/ml xanthine oxidase. MSA in the mixtures was determined as described above.

Recovery of MSA from liver homogenate

A bovine liver was collected on ice immediately after killing the animal and was minced with scissors. A 1.0-g amount of the minced liver was blended for 1 min in a blender with 1.0 ml of ice-cold water and then homogenized in a motor-driven PTFE glass homogenizer with six downward strokes. The homogenate was centrifuged at 1000 g for 5 min, 2.5 ml of MSA standard solution were added to the supernatant and the volume was made up to 5.0 ml with water. The mixture was incubated at 37°C for 1 h, then extracted with 10 ml of *n*-hexane for defatting, and the aqueous layer was

passed through a Sep-Pak C₁₈ cartridge (Waters Assoc.). MSA in the eluate was determined as described above.

RESULTS AND DISCUSSION

Normal-phase HPLC using Capcell-pak NH₂ was used for the determination of the diazosulphone derived from MSA. The mobile phase was *n*-hexane–ethanol (100:3, v/v). It was necessary with this solvent system to add a trace amount of water to either solvent in order to obtain better resolution. Therefore, ethanol of specific gravity adjusted to 0.800 with water at 20°C was used.

Fast Blue BB salt was recommended by Babbs and Gale [17] as a satisfactory diazonium salt for the spectro-photometric determination of MSA. We examined several diazonium salts from the viewpoint of applicability to HPLC and the results are given in Table I. Fast Yellow GC salt gave a diazosulphone showing a single sharp peak on reaction with MSA, as shown in Fig. 1. Fast Red TR salt also gave a single sharp peak, but the peak height was lowered owing to the presence of Fe²⁺ ion, which did not occur with Fast Yellow GC. Fast Yellow GC was therefore selected as a satisfactory diazonium salt for the HPLC detection of MSA.

The dependence of the formation of the diazosulphone on the concentration of FY-GC reagent is shown in Fig. 2. When the concentration of FY-GC was higher than 1.0%, the peak height of the diazosulphone remained constant.

TABLE I

REACTIONS OF DIAZONIUM SALTS WITH METHANESULPHINIC ACID

Reaction conditions: to 3.0 ml of 1.0 mM methanesulphinic acid 1.0 ml of 1.0% diazonium salt was added and the product was extracted into 2.0 ml of ethyl acetate.

Diazonium salt	λ_{\max} (nm)	Peak height (cm)
Fast Yellow GC salt	285	8.97
Fast Red TR salt	310	10.51
Fast Blue BB salt	430	5.00
Fast Red AL salt	330	3.34
Fast Black K salt	— ^a	—
Fast Blue RR salt	—	—
Fast Red ITR salt	—	—

^a Visible reaction did not occur.

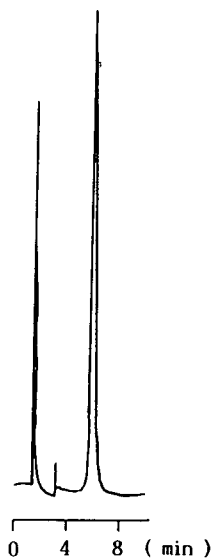


Fig. 1. High-performance liquid chromatogram of the diazosulphone derivative. For HPLC conditions, see Experimental.

For the extraction of the diazosulphone from the aqueous phase, ethyl acetate was successfully used. Table II presents the results of single extractions of the diazosulphone into several solvents.

Fig. 3 illustrates the relationship between pH during the MSA–FY-GC reaction and the peak height of the resulting diazosulphone. Under acidic conditions (pH 2–6) a constant peak height was obtained.

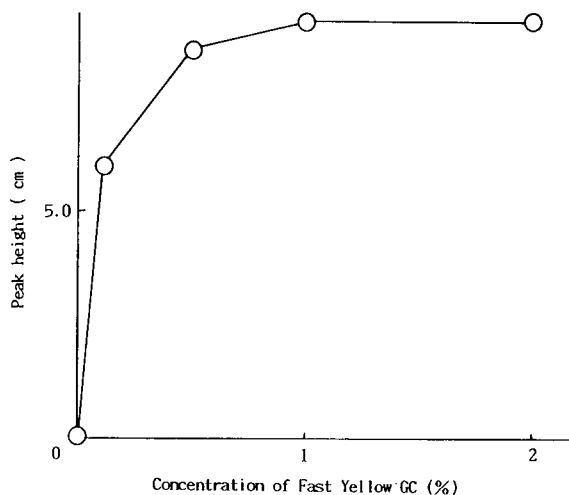


Fig. 2. Relationship between formation of the diazosulphone derivative and concentration of Fast Yellow GC.

TABLE II

EXTRACTION OF THE DIAZOSULPHONE DERIVATIVE INTO ORGANIC SOLVENTS

Reaction conditions: to 3.0 ml of 0.1 mM methanesulphinic acid 1.0 ml of 1.0% Fast Yellow GC salt and 0.5 ml of phosphate buffer (pH 4.4) were added and the product was extracted into 2.0 ml of organic solvent.

Solvent	Peak height (cm)
Ethyl acetate	8.35
Methyl isobutyl ketone	4.22
Hexane-butanol (2:1)	3.46
Hexane-ethanol (2:1)	2.46
Dichloromethane	0.92

The reaction of DMSO and $\cdot\text{OH}$ generated by the Fenton system may occur via the following reactions:

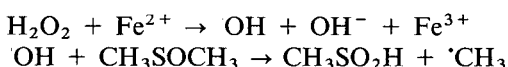


Fig. 4 shows that the two calibration graphs prepared from equimolar amounts of H_2O_2 and MSA were in good agreement with each other. This indicates that the formation of MSA from DMSO in the Fenton reaction is quantitative. A linear calibration graph was obtained in the range 0.1–100.0 μM $\cdot\text{OH}$ radical generated by the Fenton reaction.

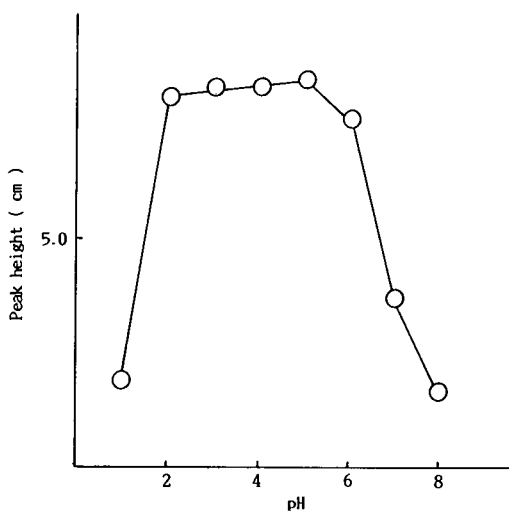


Fig. 3. Relationship between formation of the diazosulphone derivative and pH.

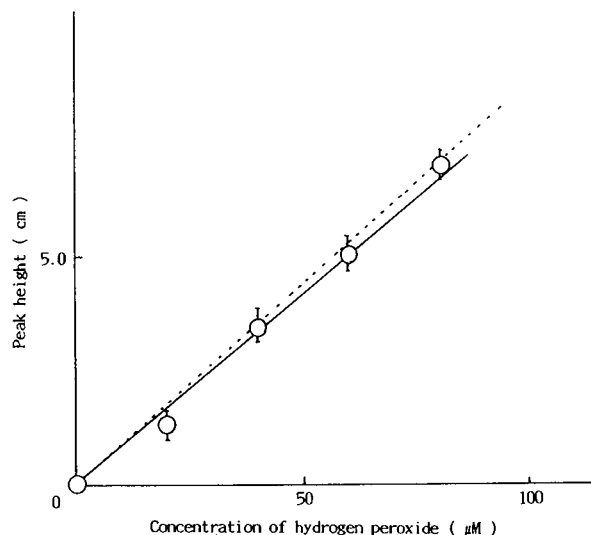


Fig. 4. Relationship between formation of the diazosulphone derivative and concentration of hydrogen peroxide in the Fenton system. Calibration graphs obtained from (solid line) H_2O_2 and (dashed line) methanesulphinic acid.

The detection limit was 0.1 μM $\cdot\text{OH}$ at 0.005 a.u.f.s. in a simple reagent system.

Babbs and Griffin [14] calculated the MSA production in the hypoxanthine–xanthine oxidase oxidation of DMSO by the use of a kinetic model of 50 relevant enzymatic and free radical reactions. They concluded that the concentration of MSA produced with the enzymatic system given under Experimental should be *ca.* 35 μM . The present method indicated that the MSA formed in this system was close to 35 μM , as shown in Fig. 5. The xanthine–xanthine oxidase enzyme system is known to generate several reactive oxygen compounds, including superoxide (O_2^-), hydrogen peroxide (H_2O_2) and hydroxyl radical ($\cdot\text{OH}$). The formation of MSA by the oxidation of DMSO is dependent on both O_2^- and H_2O_2 (Haber–Weiss reaction), as indicated by the inhibitory effects of both superoxide dismutase (SOD) and catalase (Table III). In addition, the formation of MSA was inhibited by known scavengers of $\cdot\text{OH}$, *e.g.*, ethanol, mannitol, benzoate and formate.

Diazonium salts can couple with diverse compounds, especially phenols and aromatic amines, to give coloured azo compounds. The reactions are fa-

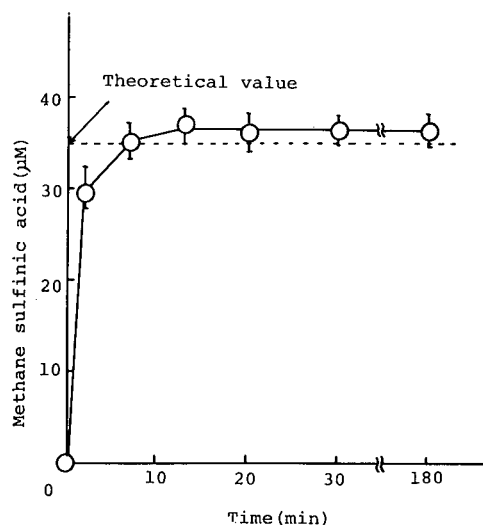


Fig. 5. Production of methanesulphinic acid from DMSO in the hypoxanthine-xanthine oxidase system: 2.0 ml of 250 μM hypoxanthine, 1.0 ml of 50 mM DMSO, 0.3 ml of 2 mM FeSO_4 , 0.3 ml of 2 mM EDTA and 0.4 ml of 0.6 U/ml xanthine oxidase.

TABLE III

EFFECT OF SCAVENGERS OF HYDROXYL RADICALS AND SUPEROXIDE ANIONS ON FORMATION OF METHANESULPHINIC ACID BY THE REACTION OF DMSO AND HYDROXYL RADICAL IN THE HYPOXANTHINE-XANTHINE OXIDASE SYSTEM

Reaction conditions: 1.0 ml of 50 mM DMSO, 2.0 ml of 250 μM hypoxanthine, 0.3 ml of 2 mM FeSO_4 , 0.3 ml of 2 mM EDTA and 1.0 ml of scavenger solution were mixed, 0.4 ml of xanthine oxidase (0.6 U/ml) was added and the mixture was allowed to stand for 12 min at 37°C.

Scavenger	Concentration		MSA detected (nmol/ml) ^a	Formation ratio of MSA (%) ^b
	U/ml	mM		
None			34.4	100.0
Superoxide dismutase	20		16.0 \pm 0.9	46.5
	2		23.1 \pm 0.4	67.1
	0.5		28.6 \pm 0.9	83.0
Catalase	20		18.9 \pm 0.8	54.9
	2		28.0 \pm 2.0	81.5
	0.5		31.2 \pm 1.2	90.7
Mannitol		20	14.0 \pm 0.01	40.7
		10	18.2 \pm 0.1	53.0
		2	31.3 \pm 1.8	90.3
Ethanol		20	23.3 \pm 0.7	67.8
		10	24.6 \pm 3.1	71.4
		2	32.5 \pm 0.8	94.5
Formate		5	17.3 \pm 1.7	50.2
		3	24.4 \pm 0.9	71.0
		1	32.7 \pm 2.3	95.1
Benzoate		5	18.4 \pm 0.1	53.4
		3	26.2 \pm 0.1	76.3
		1	34.2 \pm 2.3	99.4

^a Mean \pm S.D. ($n = 3$).

^b (With scavenger/without scavenger) \times 100.

voured at neutral and alkaline pH, while the reaction of diazonium salts with MSA is favoured at acidic pH, as shown in Fig. 3. Table IV illustrates the colour reaction of diverse compounds, including phenol, aniline, aromatic amino acids, methylsulphonate, Fe^{3+} or EDTA with FY-GC reagent, and the influence of chromatographic peaks of the reactants on that of the diazosulphone. Phenol and aromatic amino-acids yielded coloured substances, but the chromatographic peaks were well resolved from that of the diazosulphone. Among the substances tested, only aniline gave a broad peak partially overlapping that of the diazosulphone, but the influence on the determination of MSA was negligible when the concentration of aniline was up to 100 μM .

Bovine liver homogenate spiked with MSA was incubated for 1 h at 37°C and MSA was determined by the proposed procedure. The results are given in Table V. The mean recovery for 3 runs was 70.2 \pm

TABLE IV

COLOUR REACTIONS OF DIVERSE COMPOUNDS WITH FAST YELLOW GC SALT AND INFLUENCE OF THE REACTANTS ON HPLC OF THE DIAZOSULPHONE

Compound	Concentration (mM)	Absorbance at 285 nm	Interference in HPLC
Methanesulphonate	10	0.259	None
Phenol	10	0.604	None
Phenylalanine	10	0.263	None
Tryptophan	10	0.670	None
Tyrosine	10	0.258	None
Aniline	10	$\gg 2.000$	Partial ^a
	0.1	0.708	None
Fe ³⁺	10	0.453	None
EDTA	10	0.259	None

^a Showed a broad peak partially overlapping with the peak of the diazosulphone.

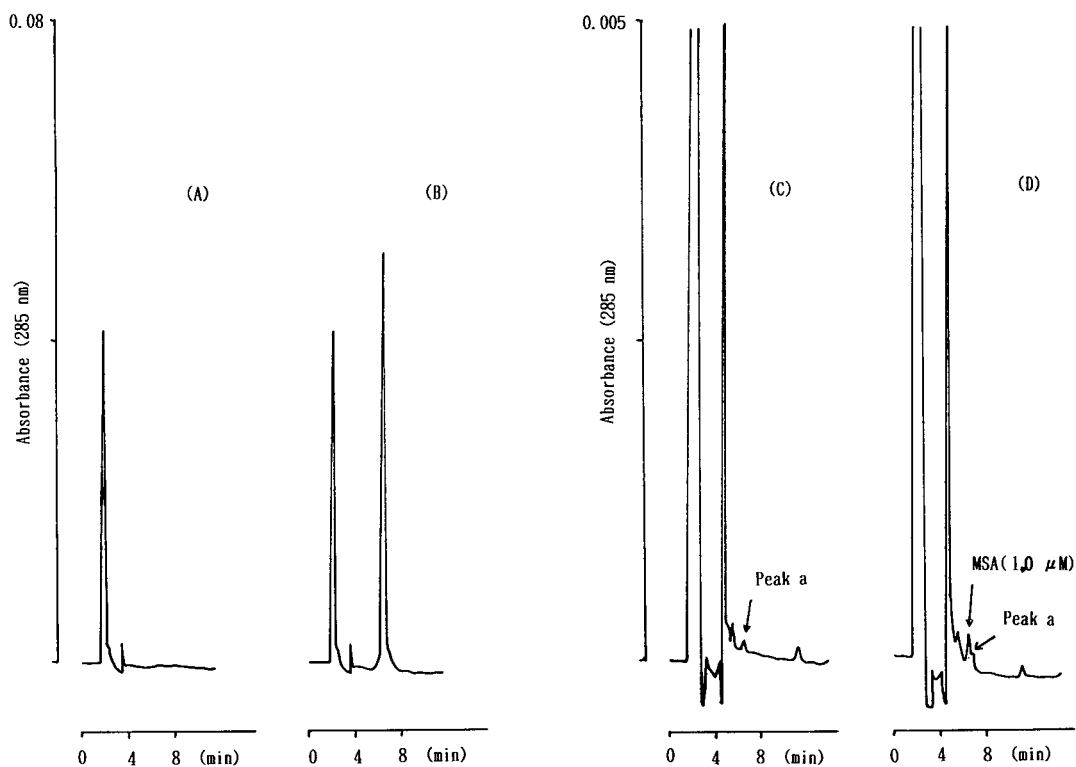


Fig. 6. High-performance liquid chromatogram of the diazosulphone derivative extracted from bovine liver homogenate. (A) Liver blank (0.08 a.u.f.s.); (B) 100 μM MSA-spiked homogenate (0.08 a.u.f.s.); (C) liver blank (0.005 a.u.f.s.); (D) 1.0 μM MSA-spiked liver homogenate (0.005 a.u.f.s.).

TABLE V
RECOVERY OF METHANESULPHINIC ACID FROM BOVINE LIVER HOMOGENATE

Methanesulphinic acid added ($\mu\text{mol/g}$)	Determined ($\mu\text{mol/g}$) ^a	Recovery (%) ^b
1.0	0.83 \pm 0.03	82.9 \pm 2.7
0.6	0.47 \pm 0.03	78.4 \pm 1.6
0.4	0.31 \pm 0.003	76.7 \pm 1.9
0.2	0.14 \pm 0.02	70.2 \pm 2.1

^a Mean \pm S.D. ($n = 3$).

^b Recovery (%) + C.V. (%).

2.1%, indicating that MSA is fairly resistant to enzymatic degradation in liver.

When the concentration of MSA in liver was at the $\mu\text{mol/g}$ level, MSA could be determined without any interference from other peaks, as shown in Fig. 6A and B. When the instrumental sensitivity was set to the highest possible range (0.005 a.u.f.s.), the liver blank showed a small peak (peak a) having a retention time close by that of MSA, as shown in Fig. 6C and D. The peak-height ratio of peak a to MSA was about 1:1 when the concentration of MSA in liver was 5 nmol/g (1 μM in the homogenate). Hence the practical detection limit is considered to be 1–2 μM MSA in liver homogenate.

ACKNOWLEDGEMENTS

Kazutoshi Inami, Akemi Okatake, Ritsuo Abe, Mariko Yamao, Youichiro Kawano, Satoshi Na-

kao and Kiyo Nagao are thanked for skilful technical assistance.

REFERENCES

- 1 D. A. Parks, G. B. Bulkey and D. N. Granger, *Surgery*, 94 (1983) 428.
- 2 U. Hagen, *Experientia*, 45 (1989) 7.
- 3 R. Bolli, M. O. Jeroudi, B. Patel, B. S. DuBose, E. K. Lai, R. Roberts and P. B. MaCay, *Proc. Natl. Acad. Sci. U.S.A.*, 86 (1989) 4695.
- 4 P. A. Cerutti, *Science*, 277 (1985) 375.
- 5 E. S. Copeland, *Cancer Res.*, 43 (1983) 5631.
- 6 S. M. Fisher, R. A. Floyd and E. S. Copeland, *Cancer Res.*, 48 (1988) 3882.
- 7 J. M. McCord, *N. Engl. J. Med.*, 312 (1985) 159.
- 8 C. M. Arroyo, J. H. Kramer, B. F. Dickens, W. B. Weglicki, *FEBS Lett.*, 221 (1987) 101.
- 9 J. E. Baker, C. C. Felix, G. N. Olenger and B. Kalyanaraman, *Proc. Natl. Acad. Sci. U.S.A.*, 85 (1988) 2786.
- 10 J. L. Zweer and M. L. Weisfeldt, *Proc. Natl. Acad. Sci. U.S.A.*, 84 (1987) 1404.
- 11 C. Beauchamp and I. Fridovich, *J. Biol. Chem.*, 25 (1970) 4641.
- 12 B. Halliwell, *Biochem. J.*, 167 (1977) 317.
- 13 S. R. Powell and H. Donna, *Free Radical Biol. Med.*, 9 (1990) 133.
- 14 C. F. Babbs and D. W. Griffin, *Free Radical Biol. Med.*, 6 (1989) 493.
- 15 G. Cohen and A. I. Cederbaum, *Arch. Biochem. Biophys.*, 199 (1980) 438.
- 16 S. M. Klein, G. Cohen and A. I. Cederbaum, *Biochemistry*, 20 (1981) 6006.
- 17 C. F. Babbs and M. J. Gale, *Anal. Biochem.*, 163 (1987) 67.
- 18 M. G. Steiner and C. F. Babbs, *Free Radical Biol. Med.*, 9 (1990) 67.
- 19 M. G. Steiner and C. F. Babbs, *Arch. Biochem. Biophys.*, 278 (1990) 478.

Ion chromatography of nitrite and carbonate in inorganic matrices on an octadecyl–poly(vinyl alcohol) gel column using acidic eluents

Souji Rokushika and Fumiko M. Yamamoto

Department of Chemistry, Faculty of Science, Kyoto University, Sakyo-ku, Kyoto 606-01 (Japan)

Kazuko Kihara

Notre Dame Women's College, Sakyo-ku, Kyoto 606 (Japan)

(First received July 7th, 1992; revised manuscript received October 13th, 1992)

ABSTRACT

Low levels of carbonate and nitrite contained in inorganic matrices were determined by ion chromatography on an Asahipak ODP-50 poly(vinyl alcohol) gel-based reversed-phase column. With an acidic mobile phase, inorganic matrix anions and cations eluted near the void volume of the column, whereas carbonate and nitrite were retained and separated completely from the matrix ions. After the separation column, the peak response was enhanced using a cation-exchange hollow fibre and 25 mM sodium sulphate or alkaline enhancers. Sea-water samples can be applied directly for the determination of carbonate and added nitrite at ppm levels. The maximum sample volume that can be loaded on the column without peak deformation depended on the pH of the sample solution and the sulphuric acid concentration in the eluent. A 50 μ l sea-water sample was applicable with a 2.5 mM acid eluent.

INTRODUCTION

The determination of low levels of ions in water samples is very important, especially when the analytes co-exist with highly concentrated matrix ions.

Various suggestions for the determination of trace concentrations of inorganic ions in the matrix have been presented. Chloride matrix ion in an aqueous sample was selectively separated from chloride on an anion-exchange column and μ g/ml levels of bromide, nitrate and nitrite ions were retained and completely separated [1,2]. The sensitive determination of carbonate by ion-exclusion chromatography using a conductivity detector and a pair of enhancement columns has been reported [3].

Carbonate was ionized during passage through the first enhancement column and in the second column the carbonate was converted into more sensitive hydroxide ion. Sample solutions including concentrated matrix ions, however, cannot be loaded over the capacity of the enhancement columns.

As an alternative method, an ion-exchange hollow-fibre suppressor system with an enhancer was applied to the determination of carboxylic acids and carbonate [4]. The ion-exchange hollow-fibre system is continuously regenerated by the outer flow of the enhancer. This system made it possible to inject samples consecutively.

Nitrite determination in sea-water samples has been achieved by a heart-cutting and recycling technique using ion chromatography on an anion-exchange resin column [5]. Kuchinicki *et al.* [6] reported the retention of nitrite on a reversed-phase column using acidified water as the eluent.

Correspondence to: S. Rokushika, Department of Chemistry, Faculty of Science, Kyoto University, Sakyo-ku, Kyoto, 606-01, Japan.

In previous papers we reported the retention behaviour of four UV-absorbing common anions using poly(vinyl alcohol) (PVA) gel-based columns with dilute sulphuric acid as the eluent [7,8]. At pH 2.3, bromate, bromide and nitrate eluted near the void volume of the column, whereas nitrite was retained, with a relatively large elution volume. It is of great importance in aquaculture and marine research to develop a sensitive and simple method for the determination of low levels of nitrite and carbonate in brine samples by direct injection. This paper reports the elution behaviour of nitrite and carbonate in ionic matrices on an octadecyl modified PVA gel column and its applicability to the analysis of brine sample.

EXPERIMENTAL

A Model IC 100 ion chromatographic analyser (Yokogawa Electric, Tokyo, Japan) equipped with an alkaline-compatible cation-exchange hollow-fibre suppressor system and a conductivity detector was employed [9]. A Model 638 variable-wavelength UV detector (Hitachi, Tokyo, Japan) was connected after the conductivity detector. The peak area was determined with a Chromatopak C-R1A integrator (Shimadzu, Kyoto, Japan). The wavelength of the UV detector was set at 210 nm and the column oven temperature was controlled at $40 \pm 0.1^\circ\text{C}$. An Asahipak ODP-50 octadecyl-modified PVA gel column (150 mm \times 4.6 mm I.D., particle diameter 5 μm) (Asahi Chemical Industry, Tokyo, Japan) was used as an analytical column. The ODP gel was prepared by reacting stearyl chloride with the hydroxy groups on the PVA gel [10,11]. A Model UV-3000 UV spectrophotometer (Shimadzu) was used for the measurement of the spectrum of nitrite solutions.

Sulphuric acid of concentrations from 0.05 to 5 mM as the eluent was prepared by dilution with water freshly deionized with a Nanopure water purification system (Barnstead, Newton, MA, USA). For the determination of carbonate, the eluent was degassed by bubbling helium through it followed by a degasser system to minimize the background level of carbonate. A laboratory-made degasser system composed of a thin-walled PTFE tube (2.5 m \times 2.4 mm I.D.) installed in a vacuum bottle was connected between the eluent reservoir and a pump. The

mobile phase flow-rate was maintained at 0.53 ml/min.

The suppressor system for anion determinations is constructed from a perfluorosulphonic acid cation-exchange hollow-fibre membrane inserted coaxially in a PTFE tube [9]. In this study, the column eluate flowed through the inside of the hollow-fibre tube, and on the outside 25 mM sodium sulphate or an alkaline solution was pumped as a peak enhancer in the opposite direction to the eluate at a flow-rate of 2 ml/min [4].

Sodium hydrogencarbonate and sodium nitrite of analytical-reagent grade were purchased from Nacalai Tesque (Kyoto, Japan) and sodium chloride, sodium nitrate and potassium sulphate of Suprapur grade for the matrices were obtained from Merck (Darmstadt, Germany). All other chemicals were of analytical-reagent from Nacalai Tesque.

Stock solutions of 1 mg/ml carbonate (as CO_3^{2-}) and nitrite (as NO_2^-) were made using freshly deionized water. Aliquots of these stock solutions were diluted to the appropriate concentration with deionized water or concentrated matrix solutions.

Sea-water samples were filtered through a 0.2- μm nylon membrane filter (Corning, Corning, NY, USA) before injection.

RESULTS AND DISCUSSION

Chromatography of nitrite and carbonate in matrix ions

Authentic sample mixtures of 20 $\mu\text{g/ml}$ nitrite and 200 $\mu\text{g/ml}$ carbonate containing various different matrix ions were injected on to the Asahipak ODP-50 column and eluted with 1 mM sulphuric acid. Inorganic anions and cations such as F^- , Cl^- , SO_4^{2-} , NO_3^- , HPO_3^- , Br^- , Li^+ , Na^+ , K^+ and NH_4^+ eluted around the void volume of the column, whereas nitrite and carbonate were retained and separated from each other, as shown in Fig 1. Both carbonate and nitrite can be detected with the conductivity detector after conversion into ionized form by increasing the eluate pH through the enhancer system. More sensitive detection of nitrite was performed with a UV detector connected after the conductivity detector.

The upper traces in Fig. 1 were obtained with the UV detector. The nitrite peak was clearly separated from all anion matrix peaks. As chloride ions do

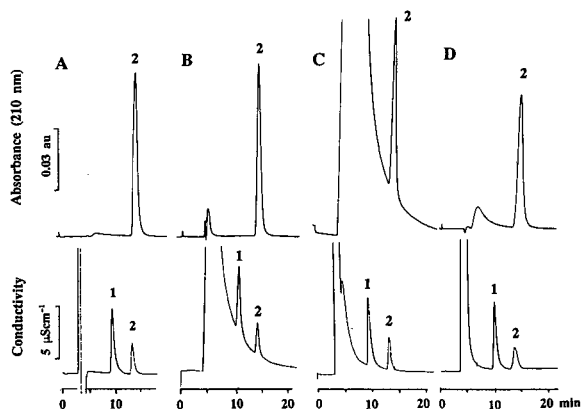


Fig. 1. Chromatograms of carbonate and nitrite in various matrix ions. Detection: upper traces, UV detector set at 210 nm; lower traces, conductivity detector. Peaks: 1 = carbonate (200 $\mu\text{g/ml}$); 2 = nitrite (20 $\mu\text{g/ml}$). Matrix ions: (A) none; (B) NaCl (30 mg/ml as Cl^-); (C) NaNO_3 (10 mg/ml as NO_3^-); (D) K_2SO_4 (10 mg/ml as SO_4^{2-}). Eluent: 1 mM H_2SO_4 . Sample volume: 20 μl . Enhancer: 25 mM Na_2SO_4 .

not absorb UV light at 210 nm, no effect of the matrix ion on the nitrite peak was observed. When the matrix was 10 mg/ml nitrate, a sharp nitrite peak appeared on the tail of a large matrix ion peak. The lower traces were obtained with the conductivity detector. The tail part of the chloride and the nitrate matrix ion peaks overlap the carbonate peak, but the retention time of carbonate was not affected by the presence of the matrix ions.

When the matrix was 10 mg/ml sulphate ion, the matrix ion eluted in a narrow band but the nitrite peak was broadened and the retention was reduced slightly. The shape and retention of the carbonate peak was not affected by the matrix ions.

Effects of the concentration of sulphuric acid in the eluent

In Fig. 2 the retention of nitrite and carbonate are plotted as a function of the concentration of sulphuric acid in the eluent. The retention of nitrite increased rapidly with increasing concentration of sulphuric acid and approached a constant value asymptotically. As the $\text{p}K_a$ value of nitrite is 3.15 [12], the fraction of the neutral molecule increases with increasing eluent concentration or decreasing pH. Hence the neutral nitrite molecules are retained on the column.

The retention time of carbonate was not affected

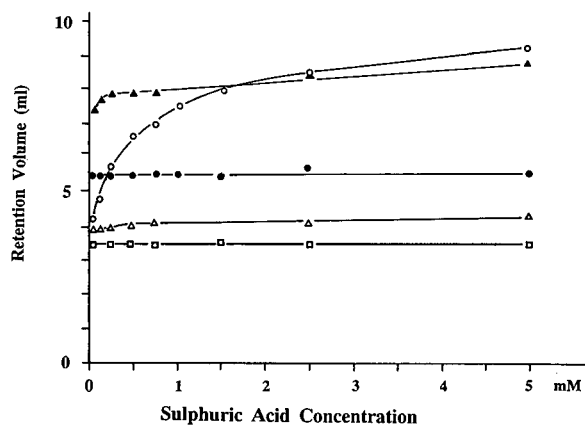


Fig. 2. Relationship between sulphuric acid concentration in the eluent and the retention volumes of nitrite, carbonate and three carboxylic acids. \circ = Nitrite; \bullet = carbonate; \blacktriangle = propionic acid; \triangle = acetic acid; \square = formic acid. Nitrite and carboxylic acids were monitored by UV detection, and carbonate by conductivity detection.

by the eluent concentration throughout the range examined. Considering the $\text{p}K_{a1}$ value of 6.33 [12], carbonate molecules in an aqueous acidic solution are in the equilibrium: $\text{CO}_2 + \text{H}_2\text{O} \rightleftharpoons \text{H}_2\text{CO}_3$. This equilibrium lies largely to the left [13], and therefore most of the carbonate molecules are present in the CO_2 form and adsorbed on the gel. Carbonate was not retained with a pure water eluent.

The retention behaviour of three carboxylic acids is also shown in Fig. 2 for comparison. Under the present conditions, these carboxylic acids are present in the neutral form, because the $\text{p}K_a$ values of these acids are higher than the eluent pH. The acids are retained on the column through hydrophobic interactions [14]. Therefore carboxylic acids eluted in order of increasing carbon number. The shorter retention time of these acids at lower eluent concentrations can be explained as the progress of the ionization of carboxylic groups at relatively higher pH. Formic acid eluted very close to the negative peak originating from water in the sample throughout the sulphuric acid eluent concentration.

Effects of the eluent concentration and the enhancer pH on the peak response

As the conductivity detector responds only to the ionized eluate components, the sensitivity for

carbonate was very low in the acidic eluate. Therefore, the peak enhancement system is essential for the detection of carbonate. When 25 mM sodium sulphate was employed as an enhancer, the response of the carbonate peak depended largely on the eluent concentration. The response of the carbonate peak decreased rapidly with increasing acid concentration in the eluent. Three causes can be considered to explain the relationship between the response and the eluent concentration. First, at higher eluent concentrations, a neutral enhancer does not have sufficient alkalinity to ionize carbonate molecules. Second, a higher concentration of the acid in the mobile phase resulted in a higher salt concentration in the eluate after neutralization by passage through the enhancement system and the ionization of the carbonate was suppressed, giving a lower detector response. Finally, as carbonate is present as carbon dioxide in the acidic eluent, these molecules are easy to release from the flow line to the outside through the wall of the cation-exchange hollow-fibre tube before conversion into the ionized form by the enhancer.

With the UV detector, the nitrite peak can be monitored before the enhancer, but the peak area decreases rapidly with increasing sulphuric acid concentration owing to the spectral change brought about by the neutralization of the nitrite molecules in the lower pH eluents. The effect of sulphuric acid concentration on the spectrum of nitrite is shown in Fig. 3. Below 0.5 mM sulphuric acid, where the pH of the solution is near the pK_a value of nitrite, ionization of nitrite progresses with strong absorption of UV radiation around 210 nm, whereas above 0.5 mM ionization of the molecules is suppressed and the UV absorption decreases with increase in acid concentration. Peak enhancement is also a useful technique for the determination of nitrite with UV detection.

Calibration graphs for carbonate and nitrite

Samples of 20 μ l containing various concentrations of carbonate were injected. The eluent used was 1 mM sulphuric acid. In addition to a neutral salt enhancer, alkaline enhancers, ranging from 0.2 to 0.6 M in concentration, were examined to solve the previously mentioned shortcomings of the enhancement system.

When 25 mM sodium sulphate solution was used

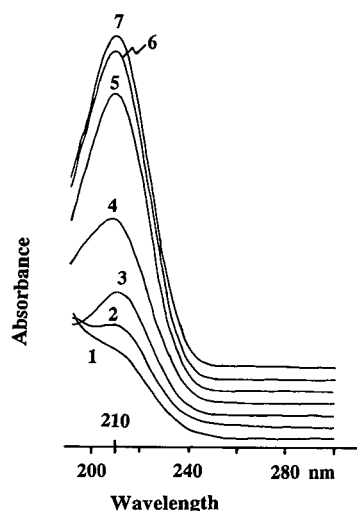


Fig. 3. Effect of the sulphuric acid concentration on the UV absorption spectrum of nitrite. Sample: 10 μ g/ml nitrite solution. Sulphuric acid concentration in the solvent: 1 = 5; 2 = 2.5; 3 = 1; 4 = 0.5; 5 = 0.05; 6 = 0.005; 7 = 0 mM.

as an enhancer, in the detector cell carbonate is present as HCO_3^- ion and the peak appears in the direction of increasing conductivity. In contrast, with concentrated alkaline enhancers, carbonate shows a large negative peak from a very high background level [4,15]. The carbonate peak area increased with increasing concentration of the alkaline enhancer. For example, the peak area with 0.6 M NaOH was 1.5 times larger than that with 0.4 M NaOH as enhancer. With the addition of 1 M sodium sulphate to 0.4 M NaOH solution, the carbonate peak area was enhanced to become equivalent to that obtained with 0.6 M NaOH enhancer. With both enhancers, the eluate pH was increased to *ca.* 11.5, which is sufficiently high to ionize the carbonate to CO_3^{2-} , considering the carbonate pK_{a2} value of 10.0 [12]. With 0.4 M NaOH and 1 M sodium sulphate enhancer, the peak area was three times larger than that obtained using a neutral salt enhancer. A relatively high concentration of sodium sulphate in the alkaline enhancer increases the penetration of the hydroxy ion into the inside of the cation-exchange hollow-fibre membrane to elevate the pH of the eluate. This salt effect is explained as suppression of the ionization of the sulphuric acid groups on the ion-exchange membrane tube, which reduces the ionic repulsion force of the Donnan potential against the hydroxy ions in the enhancer [16].

With both neutral and alkaline enhancers, a non-linear relationship between the peak area and the injected sample amount or concentration is observed. However, by plotting the logarithm of peak area against the logarithm of sample concentration, a linear relationship is obtained over the carbonate concentration range 5 $\mu\text{g/ml}$ –1 mg/ml (0.1–20 μg as CO_3^{2-}) with both neutral and alkaline enhancers, as shown in Fig. 4. The linear relationship in Fig. 4 can be expressed as $A = BC^{0.95}$, where A represents the peak area, C the carbonate concentration and B is a constant. Below 5 $\mu\text{g/ml}$, the plots deviated from linearity. Alkaline enhancers yielded a larger peak area than a neutral enhancer, but the higher background with alkaline enhancers resulted in high noise levels, which impeded the improvement in the sensitivity for carbonate. Consequently, a very close dynamic range in the linear relationship between peak area and carbonate concentration is obtained with both alkaline and neutral enhancers.

A linear calibration graph for nitrite ranging from 0.2 to 100 $\mu\text{g/ml}$ (from 2 ng to 2 μg as NO_2) is attained with the UV detector by applying a 20- μl aliquot of various concentrations of nitrite solutions.

Effects of sample volume on peak shape and retention

Sea water taken from the Pacific Ocean and spiked with 3.8 $\mu\text{g/ml}$ of nitrite was injected. The sea water contained 20 mg/ml of chloride and 110 $\mu\text{g/ml}$ of carbonate. When 0.75 mM sulphuric acid

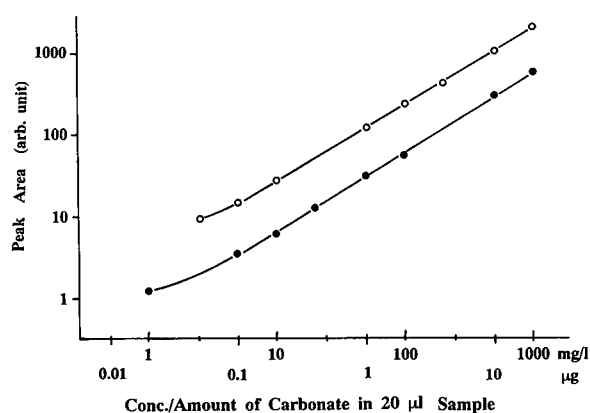


Fig. 4. Comparison of calibration graphs for carbonate obtained with neutral and alkaline enhancers. Eluent: 1 mM H_2SO_4 . Enhancer: ● = 25 mM Na_2SO_4 ; ○ = 0.4 M NaOH + 1 M Na_2SO_4 . Sample volume: 20 μl . Other conditions as in Fig. 1.

was used as the eluent, a symmetrical nitrite peak was obtained with up to 40- μl injections.

Significant band broadening, and even peak splitting, occurred when the sample was injected in a strong eluent, such as a neutral or basic salt solution, or when using large injection volumes. The explanation is that, in the column, the ionized solute moves faster than the neutral molecule in the band, the peak spreads toward the peak front and, in extreme cases, peak splitting takes place.

On the other hand, the shape and the retention volume of the carbonate peak at the conductivity detector were not affected by the sample volume with, up to 100- μl injections.

Effects of eluent concentration on peak shape and response

Higher eluent concentrations make it possible to inject larger volumes of sample for nitrite determination with UV detection but with a sacrifice of sensitivity to some extent. With higher sulphuric acid concentrations in the eluent a symmetrical peak shape is obtained with larger sample volumes. For example, when a 2.5 mM eluent was used, 50 μl of sea-water sample can be applied without peak deformation, as shown in Fig. 5.

With increasing eluent concentration, the sensitivity for carbonate with conductivity detection de-

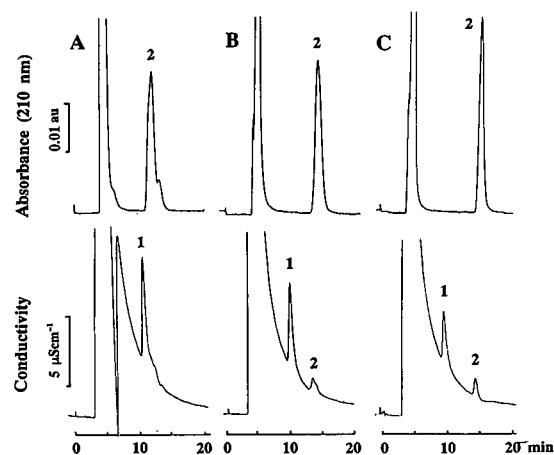


Fig. 5. Effect of the concentration of sulphuric acid in the eluent on the peak shape of carbonate and nitrite. Sample: sea water spiked with 3.8 $\mu\text{g/ml}$ of nitrite. Sample volume: 50 μl . Sulphuric acid concentration in the eluent: (A) 0.5; (B) 1; (C) 2.5 mM . Peaks and other conditions as in Fig. 1.

creased whereas the background noise level increased. Therefore, sulphuric acid with concentrations over 2.5 mM is not applicable as an eluent with conductivity detection. As the pK_{a1} value of carbonate is enough high for primary ionization in the present eluent, a 100- μ l sea-water sample can be applied using dilute acid eluents such as 0.75 mM H_2SO_4 without any deformation of the peak shape.

The octadecyl-modified PVA gel column coupled with an acidic eluent provides a simple and sensitive method for the determination of nitrite and carbonate in inorganic matrix solutions. However, the retention mechanism of these ions cannot be explained clearly.

Carbonate can be separated from inorganic anion matrices also by ion-exclusion chromatography, where completely ionized inorganic anions are excluded from a strong cation-exchange resin column with an acidic eluent. Carbonate, being in the CO_2 form, behaves as a small inert molecule eluted at a retention volume $V_0 + V_i$, where V_0 is the interstitial volume and V_i is the internal volume of the column [3,14,17,18]. However, the present results with the ODP gel column showed that the retention volumes of carbonate and nitrite with an acidic eluent are much larger than the column volume of 2.5 ml. This means that the retention of these solutes is controlled not by the penetration into the pore of the gel beads as observed in ion-exclusion chromatography, and that some other interaction force between the solute and the gel plays an important role in the retention of the solutes.

Considering the very low dipole moment of carbon dioxide, the interaction between carbon dioxide and the stationary phase may be attributed to the hydrophobic interactions. Whereas the neutral nitrite, HONO, is a more polar compound, it is dif-

ficult to ascribe the large retention volume of nitrite to hydrophobic interactions. It can be considered that in sulphuric acid solutions, some interaction may take place between HONO molecules and alcoholic OH groups on the surface of the PVA gel beads.

REFERENCES

- 1 P. Pastore, I. Lavagnini, A. Boaretto and F. Magno, *J. Chromatogr.*, 475 (1989) 331.
- 2 S. Rokushika, K. Kihara, P. F. Subosa and W.-X. Leng, *J. Chromatogr.*, 514 (1990) 355.
- 3 K. Tanaka and J. S. Fritz, *Anal. Chem.*, 59 (1987) 708.
- 4 T. Murayama, T. Kubota, Y. Hanaoka, S. Rokushika, K. Kihara and H. Hatano, *J. Chromatogr.*, 435 (1988) 417.
- 5 P. F. Subosa, K. Kihara, S. Rokushika, H. Hatano, T. Murayama, T. Kubota and Y. Hanaoka, *J. Chromatogr. Sci.*, 27 (1989) 680.
- 6 T. C. Kuchnicki, L. P. Sarna and G. R. B. Webster, *J. Liq. Chromatogr.*, 8 (1985) 1593.
- 7 F. M. Yamamoto and S. Rokushika, *Chromatographia*, 31 (1991) 80.
- 8 S. Rokushika, K. Kihara, F. M. Yamamoto and P. F. Subosa, *J. High Resolut. Chromatogr.*, 14 (1991) 68.
- 9 Y. Hanaoka, T. Murayama, S. Muramoto, T. Matsuura and A. Nanba, *J. Chromatogr.*, 239 (1982) 537.
- 10 Y. Yanagihara, K. Yasukawa, U. Tamura, T. Uchida and K. Noguchi, *Chromatographia*, 24 (1987) 701.
- 11 K. Yasukawa, U. Tamura, T. Uchida, Y. Yanagihara and K. Noguchi, *J. Chromatogr.*, 410 (1987) 129.
- 12 R. M. Smith and A. E. Martell, *Critical Stability Constants, Vol. 4, Inorganic complexes*, Plenum Press, New York, 1976.
- 13 G. Nilsson, T. Rengemo and L. G. Sillén, *Acta Chem. Scand.*, 12 (1958) 868.
- 14 K. Kihara, S. Rokushika and H. Hatano, *J. Chromatogr.*, 410 (1987) 103.
- 15 J. Haginaka, J. Wakai, H. Yasuda and T. Nomura, *J. Chromatogr.*, 447 (1988) 373.
- 16 P. K. Dasgupta, R. Q. Bligh, J. Lee and V. D'Agostino, *Anal. Chem.*, 57 (1985) 253.
- 17 H. Waki and Y. Tokunaga, *J. Chromatogr.*, 201 (1980) 259.
- 18 K. Tanaka and T. Ishizuka, *J. Chromatogr.*, 174 (1979) 153.

Use of an open-tubular trapping column as phase-switching interface in on-line coupled reversed-phase liquid chromatography–capillary gas chromatography[☆]

Hans G. J. Mol, Jacek Staniewski, Hans-Gerd Janssen and Carel A. Cramers

Faculty of Chemical Engineering, Laboratory of Instrumental Analysis, Eindhoven University of Technology, P.O. Box 513, 5600 MB Eindhoven (Netherlands)

Rudy T. Ghijsen and Udo A. Th. Brinkman

Department of Analytical Chemistry, Free University, De Boelelaan 1083, 1081 HV Amsterdam (Netherlands)

(First received September 8th, 1992; revised manuscript received October 12th, 1992)

ABSTRACT

The applicability of open-tubular traps for phase switching in coupled RPLC–GC was studied. The phase-switching process involves sorption of the analytes of interest from a methanol–water mobile phase into the stationary phase of an open-tubular column, removal of the aqueous phase by purging the trap with nitrogen and desorption of the analytes with hexane. Water elimination carried out in this manner appears to be highly efficient. In the sorption step the sampling flow-rate and the capacity factors of the analytes in the trap are critical parameters. Using a 2 m × 0.32 mm I.D. trap with a swollen 5- μ m stationary phase at flow-rates not exceeding 100 μ l/min, polycyclic aromatic hydrocarbons are trapped quantitatively from 300 μ l of aqueous phases containing up to 65% (v/v) of methanol. For desorption 70–125 μ l of hexane are needed. These volumes are easy to handle in solvent elimination carried out using a PTV injector prior to transfer of the analytes to a GC column.

INTRODUCTION

The main issue in on-line coupled LC–GC currently is the coupling of reversed-phase LC (RPLC) with capillary GC, *i.e.*, the introduction of aqueous eluents into the GC system. The most straightforward solution is direct transfer of the eluent fraction of interest into the GC system as is done in normal-phase LC–GC [1]. This involves refocusing of the analytes by means of a retention gap or by

using a PTV injector with a modified liner [2,3]. Both techniques rely on the formation of a solvent film, which in turn presupposes wettability. As water does not form a uniform solvent film on deactivated surfaces, it is not a suitable solvent for the above-mentioned techniques [4]. Moreover, water has a high boiling point, requiring high solvent evaporation temperatures, and it produces a very large volume of vapour per unit volume of liquid, which seriously limits the speed of introduction into the GC system. Also, it is chemically aggressive at higher temperatures, destroying the chemically deactivated surface of precolumns. So far, there is no fully water-resistant deactivation procedure [5]. As a consequence, for direct injections of aqueous samples into the GC system, problems with adsorption of analytes in the precolumn will arise sooner or

Correspondence to: H. Mol, Faculty of Chemical Engineering, Laboratory of Instrumental Analysis, Eindhoven University of Technology, P.O. Box 513, 5600 MB Eindhoven, Netherlands.

[☆] Paper based on a poster presented at the *14th International Symposium on Capillary Chromatography, Baltimore, MD, May 25–29, 1992.*

later. Nevertheless, the direct transfer of aqueous solvents has been used in a limited number of studies, *i.e.*, when only small volumes are involved (packed capillary LC–GC) [6,7] and when applying concurrent solvent evaporation [8]. Furthermore, introduction of mobile phases containing water can be successful if water evaporates before the other solvent(s) as in co-solvent trapping [9] and with solvent mixtures containing an amount of water not exceeding the azeotropic composition [10].

Eliminating the aqueous solvent prior to introduction into the GC system enhances the applicability of coupled RPLC–GC. Removal of water can be done by sorption–thermal desorption and phase-switching techniques. Pankow *et al.* [11] described a sorption–thermal desorption system in which water was sampled through a Tenax tube. The adsorbed analytes were thermally desorbed and introduced into the GC system after refocusing. Schomburg *et al.* [12] used a similar approach based on a two-oven system. More recently, the use of a PTV injector with packed liners was studied for the same purpose [13], thereby eliminating the need for two ovens. For trace analysis of organics in water, also non-coated [14,15] or coated capillaries [16–18] or entire GC columns [19–21] were used for trapping analytes from water. After thermal desorption and subsequent (cryogenic) refocusing the analytes were analysed.

In phase-switching techniques the analytes are transferred from the aqueous phase to an organic phase which is introduced into the GC system. Inspired by the promising results obtained in the field of automated sample preparation of water samples [22,23], Van Zoonen *et al.* [24] studied the use of on-line liquid–liquid extraction in a segmented flow system as a means of transferring the analytes from a methanol–water LC phase to an organic phase. Phase switching can also be carried out by the use of small packed trapping columns [25,26]. After trapping the analytes from the aqueous phase, the residual water has to be removed by drying with a flow of nitrogen. Incomplete elimination of water leads to reduced desorption efficiencies as part of the pores of the packing material are blocked by residual water. The need for a drying step can be avoided by using a desorption solvent which is (slightly) miscible with water, *e.g.*, ethyl acetate [27], but then again small amounts of water are

transferred to the GC system. Grob and Schilling [28] proposed the use of open-tubular trapping columns as an alternative to the use of packed adsorption tubes. The main advantage of the use of open-tubular traps is that complete removal of the remaining reversed-phase eluent can be obtained by simply purging a short plug of gas through the capillary. Grob and Schilling's attempts to trap analytes on a 2-m GC column were not very successful. According to the authors this was due to the low diffusion speeds in the liquid and insufficient retention power of the open-tubular trap.

The aim of this paper is to present a thorough study on the applicability of open-tubular traps as phase-switching devices for coupled RPLC–GC. A number of selected test compounds from a volume of methanol–water, which represents an average RPLC eluent, is trapped in a coated capillary. The eluent is then removed by emptying the trap by means of nitrogen prior to desorption of the analytes with hexane, which is next introduced directly into the GC system. Refocusing of the analytes is achieved by using a PTV injector. The phase-switching process was studied in two steps. First the sorption step was studied by determining the breakthrough volumes of polycyclic aromatic hydrocarbons (PAHs) in the LC elution mode. The effects of column dimensions, flow-rate, modifier concentrations and temperature are discussed. Second, starting from 100% sorption conditions, experiments on liquid desorption were carried out. Here the effect of desorption flow-rate and length of the trapping column on the desorption volume are discussed. The applicability of the system is demonstrated by the analysis of a PAH mixture.

EXPERIMENTAL

Instrumentation

Sorption experiments were carried out using an LC system which consisted of an LC pump (LKB 2150; Pharmacia, Woerden, Netherlands), a pulse damper (Free University, Amsterdam, Netherlands), a six-port valve with an 11- μ l loop, an open-tubular trapping column, a fluorescence detector (LS-4; Perkin-Elmer, Norwalk, CT, USA) and a recorder (BD40; Kipp & Zonen, Delft, Netherlands). The trapping capillaries were cut from new 0.32 mm I.D. GC columns with either a 1.1- or a 5.1- μ m film

of CP-Sil-5-CB (Chrompack, Bergen op Zoom, Netherlands). The valve and the trapping capillary were positioned in a thermostated water-bath. The fluorescence excitation/emission wavelength for naphthalene, phenanthrene and pyrene were 262/330, 243/365 and 236/392 nm, respectively.

The phase-switching device was built around two ten-port valves (Valco, Houston, TX, USA), depicted schematically in Fig. 1. The system consisted of a sampling pump (P1) (syringe pump, type MF-2 from Azumadenki Kogyo, Japan) and a pump used for desorption (P2). This pump was a microprocessor-controlled syringe pump (Digisampler, Gerstel, Mülheim a/d Ruhr, Germany) which allowed the introduction of defined volumes of up to 1 ml with a speed of 1–2000 $\mu\text{l}/\text{min}$. A fraction loop of 300 μl was connected between two ports of valve 1. The open-tubular coated traps were connected between two ports of valve 2. The nitrogen flow applied to valve 1 was controlled by a pressure regulator (adjusted to 1 bar) and a flow controller adjusted to 0.6 ml/min.

A gas chromatograph (Model 5890; Hewlett-Packard, Avondale, PA, USA) with flame ionization detection (FID) and thermal conductivity detection (TCD), and provided with an automated cold temperature-programmed injection system (PTV injector) (KAS 502; Gerstel) was used. For data collection a Nelson integration system (Perkin-Elmer) was used. The PTV injector was equipped with a liner containing a porous glass bed and a modified split vent as described elsewhere [2,3]. With this configuration low outlet pressures could be obtained, allowing high purge gas flow-rates (up to 620 ml/min). By means of a splitter, about 1% of the purge gas is transferred to the TCD instrument for monitoring the solvent elimination.

Operating conditions

Large-volume injections. Large-volume injections were carried out using the microprocessor-controlled syringe pump. A sample of PAHs dissolved in hexane was introduced into the PTV injector (initial temperature between -30 and 30°C) at a predefined rate. The sample was introduced in the solvent split mode, applying a purge gas flow-rate of 620 ml/min. When almost no solvent was left in the liner, as could be seen from the TCD signal, the GC run was started. The start of the GC run involves closing of

the split valve (splitless time, 1.0 min), starting the temperature programming of the column and heating the PTV injector to 275°C at $12^\circ\text{C}/\text{s}$. The PTV injector was kept at this temperature for 1 min.

For the GC separations a $12.5 \text{ m} \times 0.32 \text{ mm}$ I.D. column coated with $0.12\text{-}\mu\text{m}$ CP-Sil-5-CB was used with helium as the carrier gas at an inlet pressure of 45 kPa. The GC temperature programme was as follows: initial temperature, 40°C for 1 min, then increased at $15^\circ\text{C}/\text{min}$ to 250°C , the final temperature being held for 5 min.

On-line phase-switching GC. The position of the valves at the start of a phase-switching cycle is shown in Fig. 1. The LC fraction loop of valve 1 is filled manually with a PAH solution in water-methanol, simulating an LC fraction. When valve 1 is switched the sample is transferred to the open-tubular trap by pump 1 (containing methanol-water) and the trap is flushed with an additional 150 μl of solvent. Then valve 1 is switched back again. The nitrogen flow now slowly pushes the remaining aqueous solvent out of the trap (2 min for the 2-m trap and 4 min for the 5-m trap). Meanwhile pump 2 (containing hexane) is started and the transfer capillary is inserted into the PTV injector. When valve 2 is switched the analytes are desorbed from the trap and directly introduced into the PTV injector as described above for large-volume injections. Two minutes before the next sampling step valve 2 is switched back again to remove hexane remaining in the trap after desorption by the nitrogen flow. Meanwhile the sample loop is filled again, after which the next phase switching can take place.

Desorption experiments. For desorption experiments the trap was sampled using an aqueous phase containing 20% (v/v) of methanol at a low sampling flow-rate (28 $\mu\text{l}/\text{min}$). For this purpose 50-ng/ml PAH solutions were used. After sorption the aqueous solvent was removed as described above. De-

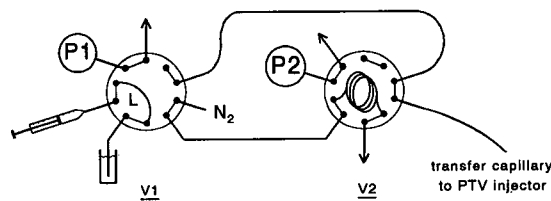


Fig. 1. Phase-switching system. V1 and V2 = valves; P1 and P2 = syringe pumps; L = 300- μl loop.

sorption was then carried out applying a variety of conditions to be discussed below. Desorption profiles were obtained by repeated sampling and subsequent desorption with a stepwise increased volume of hexane. Compounds remaining in the trap were flushed to waste before the next experiment was started.

THEORETICAL

The maximum volume of sample that can be passed through an adsorption column is determined by the breakthrough volume of the solute (V_b) defined as $V_r - 3\sigma_v$, where V_r is the retention volume and σ_v the standard deviation of the Gaussian peak eluting from the trapping column. The breakthrough volume of a component in a trapping column is given by the equation [29]

$$V_b = V_0 (1 + k) \left(1 - \frac{3}{\sqrt{N}} \right) \quad (1)$$

where V_0 is the void volume of the trapping column, k the capacity factor of the solute in the trap and N the plate number of the trapping column (with $N > 9$).

The process of trapping analytes in an open-tubular capillary is very similar to that in open-tubular LC with extremely wide-bore columns. Band broadening in an open-tubular trap can therefore be described by the Golay equation:

$$H = \frac{2D_m}{u} + \frac{1 + 6k + 11k^2}{96(k+1)^2} \cdot \frac{d_c^2}{D_m} \cdot u + \frac{2}{3} \cdot \frac{k}{(k+1)^2} \cdot \frac{d_f^2}{D_s} u \quad (2)$$

where D_m is the diffusion coefficient of the solute in the mobile phase, u the linear velocity, d_c the column diameter, d_f the stationary phase thickness and D_s the diffusion coefficient of the solute in the stationary phase. The diffusion coefficients of the PAHs selected as test solutes were calculated using the modified Wilke–Chang equation [30]; the values are about $0.40 \cdot 10^{-5} \text{ cm}^2/\text{s}$ [25% (v/v) methanol in water at 20°C]. The diffusion coefficients of the PAHs in a polysiloxane stationary phase are *ca.* $10^{-7} \text{ cm}^2/\text{s}$ [31], *i.e.*, almost two orders of magnitude lower than those in the mobile phase. As the linear velocity is far above the optimum and d_f is 5 μm or

less, the first and the last terms on the right-hand side of eqn. 2 can be neglected. When the capacity factor is very large, eqn. 2 reduces to

$$H = \frac{11}{96} \cdot \frac{d_c^2}{D_m} \cdot u \quad (3)$$

or, expressed in terms of the volumetric flow-rate, F , through the column,

$$H = \frac{44}{96 \pi} \cdot \frac{F}{D_m} \quad (4)$$

As can be seen from eqn. 4, band broadening at a constant flow-rate depends on D_m only and is independent of the column diameter. Substitution of eqn. 4 into eqn. 1 yields

$$V_b = V_0 (1 + k) \left(1 - \sqrt{\frac{396 F}{96 \pi D_m L}} \right) \quad (5)$$

After substitution of V_0 and k , with $k = K\beta$, where K is the distribution constant of the analyte and β the phase ratio given by the equation

$$\beta = \frac{V_m}{V_s} = \frac{(d_c - 2 d_f)^2}{4 d_f (d_c - d_f)} \quad (6)$$

eqn. 5 can be rewritten as

$$V_b = \frac{1}{4} \pi d_c^2 L \left(1 + \frac{K}{\beta} \right) \left(1 - \sqrt{\frac{396 F}{96 \pi D_m L}} \right) \quad (7)$$

Eqn. 7 shows that in order to obtain V_b values larger than zero, F should meet the following requirement:

$$F < \frac{96 \pi}{396} \cdot D_m L \quad (8)$$

In the situation described so far, the breakthrough volume was defined as $V_r - 3\sigma_v$. Under these conditions there is a one-sided loss of only 0.15% of a Gaussian-shaped band when the sampled volume equals the breakthrough volume. For practical applications this can be considered as quantitative trapping. When higher losses are tolerated, the breakthrough volume can be redefined, which will result in higher maximum allowable flow-rates. Table I shows that when losses of 1.0 or 2.5% are accepted, the maximum sampling flow-rates can be increased by a factor 1.7 or 2.3, respectively. For trapping analytes in a 2-m trap and with the earlier D_m value of $0.40 \cdot 10^{-5} \text{ cm}^2/\text{s}$, the maximum allow-

TABLE I
MAXIMUM ALLOWABLE SAMPLING FLOW-RATES FOR DIFFERENT DEFINITIONS OF BREAKTHROUGH VOLUME

Breakthrough volume	Loss (%) ^a	F_{\max} ($\mu\text{l/s}$) ^b
$V_b = V_r - 3 \sigma$	0.15	$0.762 D_m L$
$V_b = V_r - 2.326 \sigma$	1.0	$1.267 D_m L$
$V_b = V_r - 1.960 \sigma$	2.5	$1.784 D_m L$
$V_b = V_r - 1.645 \sigma$	5.0	$2.533 D_m L$
$V_b = V_r - 1.28 \sigma$	10.0	$4.184 D_m L$

^a One-sided loss for a Gaussian-shaped band.

^b Maximum allowable sampling flow-rate assuming $k = \infty$.

able sampling flow-rates corresponding to trapping efficiencies of 99.85, 99.0 and 97.5% are 37, 61 and 88 $\mu\text{l/min}$, respectively. Here, the retention power and capacity of the open-tubular trap are assumed to be sufficient. The capacity of the trap is expected to be sufficient for the relatively clean LC fractions. With direct sampling of real water samples however, overloading of the trap by other analytes or matrix components cannot be excluded.

From eqn. 7, one readily sees that larger breakthrough volumes are obtained when either d_c , L , K or D_m is increased or β is decreased. Further, reducing the sampling flow-rate is an alternative means of increasing the breakthrough volume. Although it is evident that large trapping column dimensions (d_c , L) are favourable for sorption, desorption puts limitations on the dimensions of the trapping column as the volume of organic solvent needed for desorption should not be too large. Too large desorption volumes will lead to a time-consuming introduction of the desorption liquid into the GC system. The effect of the other parameters on the breakthrough volume will be discussed in the next section.

RESULTS AND DISCUSSION

Sorption

Maximum allowable sampling flow-rates. The plate number of the open-tubular trap was determined to assess whether the trap meets the requirement of $N > 9$ (see above). Table II shows that the experimental values are 20–40% higher than the theoretical values. Apparently the D_m values are higher than

TABLE II
PLATE NUMBERS FOR NAPHTHALENE AND PHENANTHRENE IN A 2 m \times 0.32 mm I.D. TRAP

Conditions: 2 m \times 0.32 mm I.D. column, 1- μm CP-Sil-5-CB, methanol–water (25:75, v/v), 25°C.

F ($\mu\text{l/min}$)	u (cm/s)	Naphthalene ($k = 4$)		Phenanthrene ($k = 15$)	
		N_{th}^a	N_{exp}^b	N_{th}^a	N_{exp}^b
10	0.21	61	—	41	52
25	0.52	24	33	17	21
50	1.04	12	15	8	10

^a Calculated plate numbers in methanol–water (26:74, v/v) at 25°C. D_m for naphthalene and phenanthrene = $0.52 \cdot 10^{-5}$ and $0.44 \cdot 10^{-5}$ cm^2/s , respectively.

^b Plate numbers determined from elution chromatograms (injection: 11 μl of 1–2 ppm PAH dissolved in the mobile phase).

calculated. In order to have $N > 9$, flow-rates should not exceed 50 $\mu\text{l/min}$ for a 2-m trap with the mobile phase used. Analyte losses due to sampling at much higher flow-rates cannot be calculated by the theory described in the previous section because the compounds then no longer elute as Gaussian-shaped bands (see Fig. 2).

Retention on the open-tubular trap. As can be seen from eqn. 1 and by comparing Fig. 2A and B, an increase in capacity factor causes a distinct increase in the breakthrough volume. The capacity factor needed for quantitative (>99%) trapping depends on the sampling flow-rate and the volume that has to be sampled, *i.e.*, the volume of the LC fraction should not exceed the breakthrough volume of the trap. The LC fraction volume depends on the inside diameter of the LC column used. In this study volumes of 300 μl were used, which are typical for 1–2 mm I.D. LC columns. Calculating the breakthrough volume, with $V_0 = 0.15$ ml, $F = 45$ $\mu\text{l/min}$, $L = 2$ m and $D_m = 0.52 \cdot 10^{-5}$ cm^2/s [naphthalene in methanol–water (26:74, v/v) at 25°C], breakthrough volumes exceeding 300 μl are already obtained for a k value of 7. This means that naphthalene (Fig. 2A, at 45 $\mu\text{l/min}$) will be trapped quantitatively under the conditions mentioned. For the example in Fig. 2B (at 45 $\mu\text{l/min}$), a breakthrough volume of 800 μl is achieved with $k = 16$.

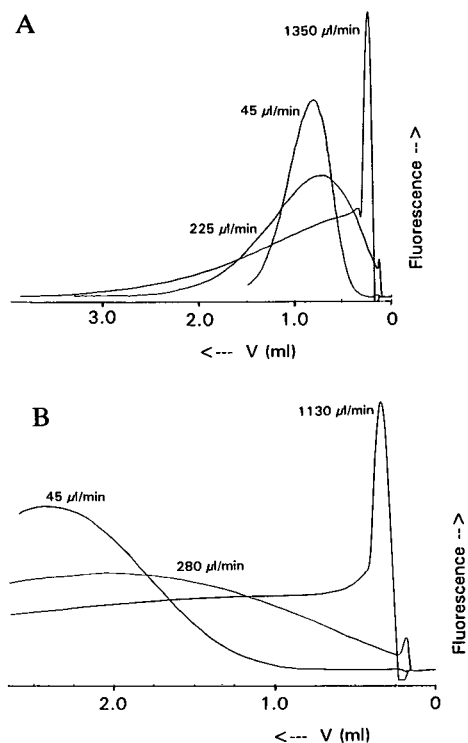


Fig. 2. Chromatograms of PAHs in an open-tubular trap. Conditions: 2 m × 0.32 mm I.D. column, 5- μ m CP-Sil-5-CB at 25°C applying different flow-rates. (A) Naphthalene ($k = 7.3$), methanol–water (30:70, v/v); (B) phenanthrene ($k = 15.7$), acetonitrile–water (20:80, v/v).

If the capacity factors are too low, the retention power can be increased by working at lower organic modifier percentages. To study the influence of methanol on the sorption process, the capacity factors of the PAHs on the open-tubular trap were determined for several methanol percentages. Fig. 3 shows plots of $\log k$ vs. percentage of methanol for the PAHs on 2 m × 0.32 mm I.D. traps coated with a 1- and a 5- μ m film. Although these plots are not really linear over a large range of methanol percentages [32], estimated capacity factors obtained by extrapolation can be safely used to calculate breakthrough volumes. The values obtained with the 1- μ m film trap are low [for naphthalene $k = 5$ at methanol–water (20:80, v/v)]. Therefore, a second trap was examined with a thicker film of stationary phase (5 μ m). The phase ratio of the 5- μ m trap is 14.5, which is almost five times lower than that of the 1- μ m trap. It was therefore expected that the capac-

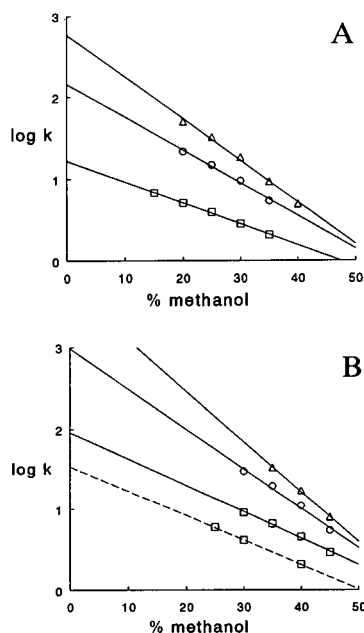


Fig. 3. Capacity factors of PAHs as a function of percentage of methanol in water at 25°C. (A) 2 m × 0.32 mm I.D. column, 1- μ m CP-Sil-5-CB; (B) 2 m × 0.32 mm I.D. column, 5- μ m CP-Sil-5-CB. \square = Naphthalene (dashed line, temperature 60°C); \circ = phenanthrene; \triangle = pyrene.

ity factors would increase by a factor of five. The experimental capacity factors, however, increased only 3.5-fold. With the 5- μ m film trap phenanthrene and pyrene can be trapped from up to 35–40% methanol in water mobile phases ($k > 16$).

A higher retention power can be achieved by using traps with still lower phase ratios, *i.e.*, with very thick films such as are used for trapping analytes from headspace samples [33,34]. With hexane as the desorption liquid, uptake of the desorption liquid into the stationary phase can cause a significant swelling, which results in an increased film thickness. As the hexane remaining in the trap after desorption is not removed until just before the next sorption, a swollen phase will be created in each cycle. A tremendous phase swelling was observed for the 5- μ m film: the internal volume of the trap decreased from 154 to 104 μ l after flushing with hexane. If the retained 50 μ l of hexane form a uniform film in the trap, this means that the film thickness increases from 5 to about 30 μ m, and the phase ratio now is a mere 1.2. The nature of the

stationary phase also changes, and capacity factors were found to increase strongly. In the swollen phase they were 15–20-fold higher than in the original 5- μm film trap. It should now be possible to trap phenanthrene and pyrene from 65% (v/v) and naphthalene from 55% (v/v) methanol in water ($k > 16$).

As hexane is slightly soluble in methanol–water mixtures, the mobile phase will strip the hexane from the stationary phase. Fig. 4 shows the decrease in retention power of the trap after the passage of various methanol–water mixtures. For methanol–water (60:40, v/v), there is essentially no decrease. For sample volumes not exceeding 1 ml, even 70–75% (v/v) methanol in water mixtures can be used without severe effects on k caused by stripping of the hexane, as the swollen film will be restored prior to the next run, *viz.*, during desorption.

Effect of temperature on sorption. The breakthrough volume is affected by the temperature via the diffusion coefficient of the analytes in the mobile phase and via the capacity factor. Theoretically, D_m values will increase with a factor of about 2.5 on increasing the temperature from 25 to 60°C, thereby allowing for higher sampling flow-rates (eqn. 8). The capacity factors of the PAHs were found to decrease by a factor of 2.2–3.4 (for an example, see the dashed line in Fig. 3). As in most instances retention power is expected to be more critical than sampling flow-rates, trapping of the analytes at room temperature

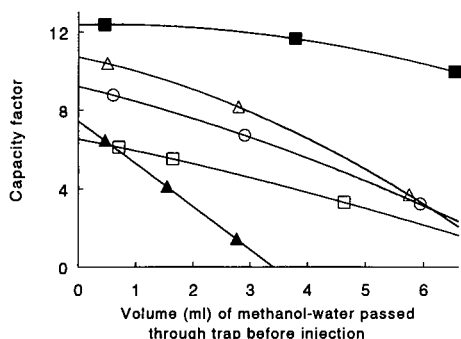


Fig. 4. Decrease in capacity factors due to stripping of hexane from a swollen stationary phase by methanol–water mixtures. Conditions: 2 m \times 0.32 mm I.D. column, 5- μm CP-Sil-5-CB swollen by rinsing with hexane; flow-rate, 45 $\mu\text{l}/\text{min}$; temperature, 25°C. ■ = Naphthalene [methanol–water (60:40, v/v)]; □ = naphthalene; ○ = phenanthrene; Δ = pyrene [all three in methanol–water (70:30, v/v)]; ▲ = pyrene [methanol–water (80:20, v/v)].

is generally preferable over trapping at elevated temperatures.

Stability of trap. An important practical aspect of the use of open-tubular traps for phase-switching is the stability of the stationary phase on flushing with large volumes of water–methanol and hexane. To this end, capacity factors were again determined after 5 months of continuous usage (*ca.* 600 ml of methanol–water passed through the trap). The decreases in the capacity factors were found to vary between 20% (naphthalene) and 33% (pyrene) and are no doubt merely due to degradation and dissolution of the stationary phase. From this it can be concluded that the solvent resistance of the trap is sufficient to ensure trouble-free use for many hundreds of phase-switchings.

Elimination of the aqueous phase

The aqueous phase was removed from the trap with a nitrogen flow-rate of 0.6 ml/min. Removal was carried out slowly (during 2 min) to prevent possible breaking up of the aqueous plug. No additional drying with nitrogen was performed, *i.e.*, introduction of hexane was started immediately after completion of the solvent removal. Hexane leaving the trap was transferred directly to the GC system. Elimination of the aqueous phase appears to be satisfactory as there was no indication (irregular solvent peak, peak shape of the solutes) that water entered the GC system. Chromatograms obtained after phase-switching were not different from those obtained on splitless injection of a hexane solution. A more detailed study using (more polar) analytes sensitive to adsorption or decomposition on active surfaces in the PTV liner or column is, however, necessary to evaluate whether water is really completely removed.

Desorption and introduction into the GC system

After sorption and elimination of water the analytes are desorbed with hexane, which is introduced directly into the GC system. As the desorption volume is relatively large, refocusing of the solutes is necessary. This is done by selective solvent elimination in a PTV injector. Both liquid desorption from the trap and solvent elimination in the PTV injector can affect the recovery of the analytes. The occurrence of losses during solvent elimination in the PTV injector was studied by performing large-volume

injections of PAHs dissolved in hexane. Next the combined desorption–solvent elimination process was examined. Low sorption flow-rates and low concentrations of modifier were used to ensure quantitative trapping of the PAHs during sorption.

Large-volume injections using a PTV injector. The PTV injector is equipped with a liner containing a deactivated porous glass bed. The PTV injector can be cooled for retaining volatile components more efficiently. The solvent introduction rate depends on the initial PTV temperature. Data on optimum introduction speeds have been published previously [2,3]. The initial PTV temperature and the volume injected can both affect the recovery of the solutes after solvent elimination. The effects of initial PTV temperature and injected volume on recovery of three PAHs are shown in Fig. 5. With the volatile naphthalene, even on cooling the PTV to -28°C (introduction rate applied at this temperature $25\ \mu\text{l}/\text{min}$) significant losses were observed when more than $50\ \mu\text{l}$ of the hexane solution were introduced. For the other PAHs solvent elimination was not so critical. Phenanthrene is still quantitatively recovered at an initial PTV temperature of 30°C (introduction rate $250\ \mu\text{l}/\text{min}$), provided that the volumes are not too large. An initial temperature of -10°C (introduction rate $50\ \mu\text{l}/\text{min}$) would offer a good compromise with regard to introduction time and recovery for naphthalene.

Desorption of PAHs with hexane. Two aspects are of major interest where desorption is concerned: desorption speed and desorption volume needed for

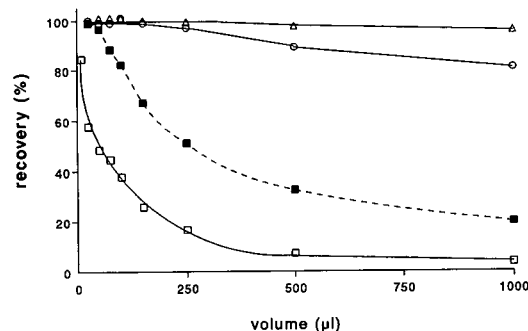


Fig. 5. Effect of initial PTV temperature and volume introduced on recovery for large-volume injections of PAHs in hexane. ■ = Naphthalene (PTV temperature -28°C , introduction speed $25\ \mu\text{l}/\text{min}$); □ = naphthalene; ○ = phenanthrene; △ = pyrene (PTV temperature 30°C , introduction speed $250\ \mu\text{l}/\text{min}$).

quantitative recovery of the analytes from the trap. These two aspects are interrelated. Desorption of the analytes with hexane is a chromatographic process. The volume needed for desorption depends on the chromatographic band broadening during desorption, which can be described similarly to broadening during sorption. Instead of a breakthrough volume which corresponds to the start of an eluting peak, a desorption volume (V_d) corresponding to the end of an eluting peak now has to be used. Here $V_d = V_r + 3\sigma_v$ or (cf., eqn. 1),

$$V_d = V_0 (k + 1) \left(1 + \frac{3}{\sqrt{N}} \right) \quad (9)$$

Because the trap is empty when desorption starts, the volume of liquid leaving the trap will be $V'_d = V_d - V_0$. Small desorption volumes are obtained if the void volume and the capacity factor are small and the plate number is large. The need for a small void volume in order to obtain small desorption volumes is in contradiction with the demand for a large void volume in order to create efficient sorption. This means that, especially with regard to the column diameter, a compromise has to be made in order to keep the desorption volume at an acceptable level.

The contribution of chromatographic band broadening to V_d cannot be determined reliably because accurate values for the diffusion coefficients of the analytes in the swollen stationary phase are not available. However, once the values for k and V_d for the desorption of an analyte from a trap (length L_1) have been experimentally determined (see below), it is possible to calculate the volume needed for desorption of that component from a similar trap of different length (L_2). The following equation for the unknown desorption volume V_{d_2} can be derived:

$$V_{d_2} = V_{d_1} (1 + k) \left(\frac{L_2}{L_1} - \sqrt{\frac{L_2}{L_1}} \right) + \sqrt{\frac{L_2}{L_1}} \cdot V_{d_1} \quad (10)$$

As regards the capacity factors, their values are determined by the distribution constant (K) and the phase ratio. During desorption the analytes partition between two very similar phases, a silicone phase strongly swollen by hexane (stationary phase) and hexane (mobile phase). It can therefore be expected that K will have a value of *ca.* 1. With the known phase ratio of 1.2, the expected capacity

factor of the PAHs during desorption is then about 0.8. Experimental values of capacity factors can be estimated from the desorption curves in Fig. 6. The desorption volume corresponding to 50% recovery is the adjusted retention volume (V'_r) of the PAHs. Introduction of the known void volume yields experimental capacity factors of about 0.45. Apparently the PAHs have a slight preference for the pure hexane phase; $K = 0.54$.

The desorption volumes are dependent on the desorption speed (see above). This was experimentally verified by desorbing the analytes at different flow-rates. The initial band width was assumed to be relatively small because a low flow-rate was used for sorption. The desorption profiles for two traps obtained at different desorption flow-rates are shown in Fig. 6. The higher the desorption flow-rate, the stronger is the band broadening and the larger the volume needed for complete desorption. Using the 2-m trap and applying desorption flow-rates of 10, 50 and 250 $\mu\text{l}/\text{min}$, the desorption volumes (V'_d) (>99% recovery) were 70, 80 and 125 μl , respectively. Knowing the capacity factors and the desorption volumes for the PAHs in the 2-m trap, the desorption volumes for longer traps can be calculated. The results are given in Table III. Calculated and measured V'_d values for the 5-m trap are seen to match well.

As far as desorption is concerned, the maximum length of trapping column that can be used depends on the application. For volatile analytes short

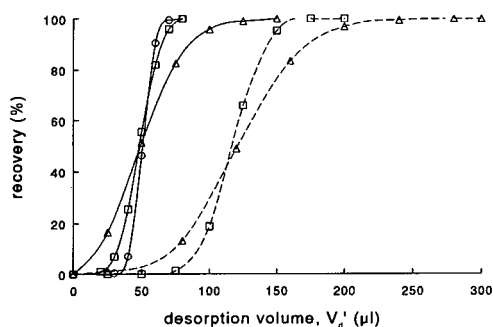


Fig. 6. Effect of desorption flow-rate (hexane) on the desorption profile. Flow-rate: $\circ = 10$; $\square = 50$; $\triangle = 250$ $\mu\text{l}/\text{min}$. Trap: 0.32 mm I.D., 5- μm film; solid line, 2 m; dashed line, 5 m. Sample: 300 μl of 50 ppb pyrene in methanol-water (20:80, v/v); sorption flow-rate, 28 $\mu\text{l}/\text{min}$.

TABLE III

EFFECT OF DESORPTION FLOW-RATE AND TRAP LENGTH ON DESORPTION VOLUMES

F ($\mu\text{l}/\text{min}$)	Desorption volume ^a , V'_d (μl)				
	Experimental ^b		Calculated ^c		
	2 m	5 m	5 m	10 m	25 m
10	60	—	140	260	625
50	70	150	150	280	650
250	95	190	195	340	750

^a Volume of hexane needed for 95% desorption of PAHs from 0.32 mm I.D. 5- μm CP-Sil-5-CB trap.

^b Experimental desorption volume.

^c Calculated desorption volume using data for 2-m trap.

trapping columns are preferable, for two reasons. First, the desorption volume should be small in order to obtain high recoveries in the solvent elimination step (Fig. 5). Second, short trapping columns yield acceptable desorption time. Volatile analytes require a low PTV temperature, which in turn necessitates a low introduction speed. The volume of desorption liquid needed to transfer the analytes from the trap to the PTV is equal to $V_d = V_0 + V'_d$ (the actual volume introduced is V'_d). For example, with a PTV temperature of -30°C corresponding to a desorption speed of 25 $\mu\text{l}/\text{min}$, desorption from a 10-m trap (swollen phase) would take about 32 min. For less volatile analytes, on the other hand, the use of a 10-m trap is fully acceptable. For a high-boiling analyte, such as pyrene, even a 25-m trapping column can be used with quantitative desorption and analyte recovery after solvent elimination within 8.5 min. Such long trapping columns are, of course, very favourable from the sorption point of view.

Quantitative aspects of on-line phase-switching GC

After completion of the sorption experiments in the LC mode and the desorption experiments, the effect of sampling flow-rate and modifier concentration on the overall recovery in on-line phase-switching GC was studied. Here the 2 m \times 0.32 mm I.D. trapping column coated with a 5- μm film was used. The volume of aqueous sample with which phase switching was carried out was 300 μl , which is a typical value for LC peak volumes eluting from

1–2 mm I.D. columns. Phase switching of larger volumes should be possible by taking longer trapping capillaries. Sampling was followed by flushing the trap with 150 μl of methanol–water, which may be necessary in future applications to remove buffer salts.

The effect of the sampling flow-rate on the recovery is shown in Table IV. In this example losses can be caused only by too high sampling rates, because the conditions were such that breakthrough caused by insufficient analyte retention and losses during desorption and solvent elimination in the PTV injector were excluded. In accordance with the predictions of Lövkvist *et al.* [35], the experimental recoveries were higher than those expected assuming Gaussian elution profiles. In other words, with a 2 m \times 0.32 mm I.D. trap at room temperature, a flow-rate of 100 $\mu\text{l}/\text{min}$ can be used without loss of analytes due to incomplete trapping. This flow-rate results in an acceptable sorption time of 4.5 min for the sample described.

The effect of the methanol percentage on recovery (applying a relatively high sorption flow-rate of 111 $\mu\text{l}/\text{min}$) is given in Table V. Under the applied PTV and desorption conditions naphthalene is partially lost during solvent elimination in the PTV. At a methanol concentration of 80% (v/v), losses due to insufficient retention power of the trap are

TABLE IV
RECOVERY OF PYRENE AT DIFFERENT SORPTION FLOW-RATES

F ($\mu\text{l}/\text{min}$)	Recovery (%)	
	Theoretical ^a	Experimental ^b
14	100	100
28	100	100
42	100	100
111	95	99
333	83	91
1000	71	81
2000	65	71

^a Based on Gaussian elution profile; D_m of pyrene = $0.37 \cdot 10^{-5} \text{ cm}^2/\text{s}$.

^b Conditions: trap, 2 m \times 0.32 mm I.D., 5- μm CP-Sil-5-CB; mobile phase, methanol–water (20:80, v/v); temperature, 20°C. Sample, 300 μl of 37 ppb pyrene. Desorption with 80 μl of hexane at 50 $\mu\text{l}/\text{min}$; PTV initial temperature, -10°C .

TABLE V

EFFECT OF METHANOL CONCENTRATION IN WATER ON RECOVERY IN ON-LINE PHASE-SWITCHING GC

Trap, 2 m \times 0.32 mm I.D., 5- μm film. Sample, 300 μl of 40–50 ppb PAH solution sampled at 111 $\mu\text{l}/\text{min}$. Desorption, 85 μl of hexane at 50 $\mu\text{l}/\text{min}$. PTV initial temperature, -10°C .

Methanol in water (%, v/v)	Recovery (%)		
	Naphthalene	Phenanthrene	Pyrene
20	69	101	102
50	66	100	99
65	61	100	97
80	34	82	90

observed for all analytes. The repeatability of the total phase-switching–solvent elimination process was found to be very good. The relative standard deviation (R.S.D.) was 2.5% ($n = 3$) or less both when the analyte recovery was quantitative and when losses occurred.

As an example, Fig. 7 shows the separation of

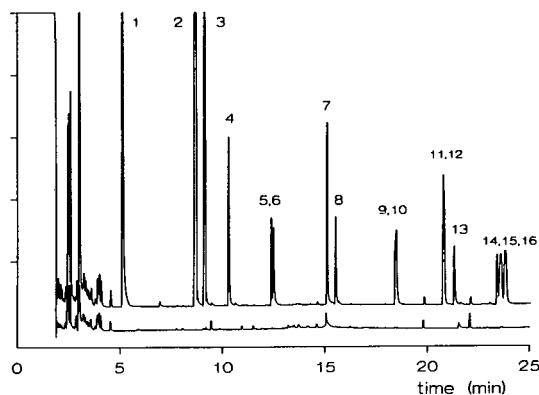


Fig. 7. On-line phase-switching GC of sixteen PAHs and a system blank (methanol–water). Sample, 300 μl of a solution of sixteen PAHs in methanol–water (50:50, v/v); concentrations, 200–400 ppb (1–3) and 20–40 ppb (4–16). Sampling flow-rate, 111 $\mu\text{l}/\text{min}$. Trap: 2 m \times 0.32 mm I.D., 5- μm film (swollen with hexane). Desorption, 80 μl of hexane at 25 $\mu\text{l}/\text{min}$. PTV initial temperature, -30°C . GC temperature programme, 40°C (2 min) $\rightarrow 10^\circ\text{C}/\text{min} \rightarrow 275^\circ\text{C}$. Recoveries: (1) naphthalene, 80%; (2) acenaphthylene, 98%; (3) acenaphthene, 97%; (4) fluorene, 99%; (5) phenanthrene, 100%; (6) anthracene, 97%; (7) fluoranthene, 102%; (8) pyrene, 99%; (9, 10) benzo[a]anthracene + chrysene (97%); (11, 12) benzo[b]fluoranthene + benzo[k]fluoranthene, 93%; (13) benzo[a]pyrene, 92%; (14) indeno[1,2,3-cd]pyrene, 88%; (15) dibenzo[a,h]anthracene, 85%; (16) benzo[ghi]perylene, 86%.

sixteen PAHs after phase switching from methanol–water (50:50, v/v) to hexane. Data on recoveries (80–102%) are given in the caption.

CONCLUSIONS

Theory allows the influence of various operating conditions, such as flow-rate, column dimensions and diffusion coefficients, on the phase-switching process to be described. In order to trap analytes quantitatively the sampling flow-rates should not exceed a certain maximum value which depends only on the diffusion coefficient of the analyte in the aqueous phase and the length of the trapping column. For a 2 m × 0.32 mm I.D. trap, the maximum sampling flow-rate was found to be ca. 100 µl/min. For trapping analytes from conventional LC eluents, *i.e.*, eluents containing high percentages of modifier, the phase ratio of the trap should be very low, *i.e.*, thick films have to be used. Stationary phase swelling due to the uptake of large amounts of desorption fluid (hexane) into the stationary phase leads to a substantial increase in the film thickness and hence the retentive strength of the trap. The retention power in a thick-film trap with a swollen stationary phase is found to be sufficient to trap PAHs from 300-µl LC fractions containing up to 65% (v/v) methanol. Elimination of the aqueous phase from the trap is easily performed by briefly purging with nitrogen. The volume of hexane needed for desorption of the trapped analytes can easily be handled by PTV injection devices. Using these devices solvent elimination is rapid and loss of analytes can be avoided.

It can be concluded that open-tubular traps are highly promising for phase-switching in coupled RPLC–GC. The system described here also holds promise for automated pretreatment of aqueous samples.

ACKNOWLEDGEMENT

The Foundation for Chemical Research in the Netherlands (SON) is gratefully acknowledged for their financial support.

REFERENCES

- 1 K. Grob (Editor), *On-Line Coupled LC–GC*, Hüthig, Heidelberg, 1991.
- 2 J. Staniewski and J. A. Rijks, *J. Chromatogr.*, 623 (1992) 105–113.
- 3 J. Staniewski and J. A. Rijks, in P. Sandra (Editor), *Proceedings of the 13th Symposium on Capillary Chromatography, Riva del Garda, Italy, 1991*, Hüthig, Heidelberg, 1991, pp. 1334–1347.
- 4 K. Grob, *J. Chromatogr.*, 473 (1989) 381–390.
- 5 K. Grob and A. Artho, *J. High Resolut. Chromatogr.*, 14 (1991) 212–214.
- 6 H. J. Cortes, C. D. Pfeiffer, G. J. Jewett and B. E. Richter, *J. Microcol. Sep.*, 1 (1989) 28–34.
- 7 D. Duquet, C. Dewaele, M. Verzele and S. McKinley, *J. High Resolut. Chromatogr.*, 11 (1988) 824–829.
- 8 K. Grob and Z. Li, *J. Chromatogr.*, 473 (1989) 423–430.
- 9 K. Grob, *J. Chromatogr.*, 477 (1989) 73–86.
- 10 E. C. Goosens, D. de Jong, J. H. M. van den Berg, G. J. de Jong and U. A. Th. Brinkman, *J. Chromatogr.*, 552 (1991) 489–500.
- 11 J. F. Pankow, L. M. Isabelle and T. J. Kristensen, *Anal. Chem.*, 54 (1982) 1815–1819.
- 12 G. Schomburg, E. Bastian, H. Behlau, H. Husmann, F. Weeke, M. Oreans and F. Müller, *J. High Resolut. Chromatogr. Chromatogr. Commun.*, 7 (1984) 4–12.
- 13 J. J. Vreuls, U. A. Th. Brinkman, G. J. de Jong, K. Grob and A. Artho, *J. High Resolut. Chromatogr.*, 14 (1991) 455–459.
- 14 A. Zlatkis, R. P. J. Ranatunga and B. S. Middleditch, *Anal. Chem.*, 62 (1990) 2471–2478.
- 15 A. Zlatkis, R. P. J. Ranatunga and B. S. Middleditch, *Chromatographia*, 29 (1990) 523–529.
- 16 D. A. M. MacKay and M. M. Hussein, *J. Chromatogr.*, 176 (1979) 291–303.
- 17 M. M. Hussein and D. A. M. MacKay, *J. Chromatogr.*, 243 (1982) 43–50.
- 18 S. Blomberg and J. Roeraade, *J. High Resolut. Chromatogr.*, 13 (1990) 509–512.
- 19 A. Zlatkis, F.-S. Wang and H. Shanfield, *Anal. Chem.*, 55 (1983) 1848–1852.
- 20 R. E. Kaiser and R. Rieder, *J. Chromatogr.*, 477 (1989) 49–52.
- 21 G. Goretta, M. V. Russo and E. Veschetti, *J. High Resolut. Chromatogr.*, 15 (1992) 51–54.
- 22 J. Roeraade, *J. Chromatogr.*, 330 (1985) 263–274.
- 23 E. Fogelquist, M. Krysell and L. G. Danielson, *Anal. Chem.*, 58 (1986) 1516–1520.
- 24 P. van Zoonen, G. R. van der Hoff and E. A. Hogendoorn, *J. High Resolut. Chromatogr.*, 13 (1990) 483–488.
- 25 E. Noroozian, F. A. Maris, M. W. F. Nielen, R. W. Frei, G. J. de Jong and U. A. Th. Brinkman, *J. High Resolut. Chromatogr. Chromatogr. Commun.*, 10 (1987) 17–20.
- 26 Th. Noy, E. Weiss, T. Herps, H. van Cruchten and J. Rijks, *J. High Resolut. Chromatogr. Chromatogr. Commun.*, 11 (1988) 181–186.
- 27 J. J. Vreuls, V. P. Goudriaan, U. A. Th. Brinkman and G. J. de Jong, *J. High Resolut. Chromatogr.*, 14 (1991) 475–480.
- 28 K. Grob and B. Schilling, *J. High Resolut. Chromatogr. Chromatogr. Commun.*, 8 (1985) 726–733.

- 29 C. E. Werkhoven-Goewie, U. A. Th. Brinkman and R. W. Frei, *Anal. Chem.*, 53 (1981) 2072–2080.
- 30 R. C. Reid, J. M. Prausnitz and T. K. Sherwood (Editors), *The Properties of Gases and Liquids*, McGraw-Hill, London, 1977.
- 31 O. van Berkel, H. Poppe and J. C. Kraak, *Chromatographia*, 24 (1987) 739–744.
- 32 P. J. Schoenmakers, H. A. H. Billiet and L. de Galan, *J. Chromatogr.*, 185 (1979) 179–195.
- 33 S. Blomberg and J. Roeraade, *J. High Resolut. Chromatogr.*, 13 (1990) 509–512.
- 34 B. V. Burger, M. le Roux, Z. M. Munro and M. E. Wilka, *J. Chromatogr.*, 52 (1991) 137–151.
- 35 P. Lövkvist and J. Å. Jönsson, *Anal. Chem.*, 59 (1987) 818–821.

Comparative study of the determination of triacylglycerol in vegetable oils using chromatographic techniques

Amalia A. Carelli and Arturo Cert

Instituto de la Grasa y sus Derivados, CSIC, Avda. Padre García Tejero 4, Apdo. 1078, 41012 Seville (Spain)

(First received July 17th, 1992; revised manuscript received October 20th, 1992)

ABSTRACT

The triacylglycerols of some vegetable oil samples were determined using isocratic HPLC with refractive index (RI) detection, gradient solvent HPLC with evaporative light scattering detection (ELSD), capillary GC and theoretical calculations from FAME analysis in order to establish the suitability of these techniques. The response factors and the repeatability were investigated. Generally, the HPLC–RI detection technique can be used without application of response factors. HPLC–ELSD yields inaccurate results for low concentrations. Calculations assuming a 1,3-random 2-random distribution of fatty acids gave good results for olive oil and acceptable results for sunflower oil. The GC analysis requires the use of response factors.

INTRODUCTION

Vegetable oils possess a characteristic and more or less unique pattern of triacylglycerols (TAGs) that can be used to determine origin and to detect adulteration. Thus in olive oil, a criterion of purity is based on the trilinolein content [1].

The triacylglycerol composition of oils is usually obtained by means of the IUPAC method, which uses isocratic non-aqueous reversed-phase high-performance liquid chromatography (HPLC) with refractive index (RI) detection [2], rendering separations based on the equivalent carbon number (ECN) of triacylglycerols.

While the poor solubility and long retention times of the higher saturated TAGs makes gradient elution desirable, this is not possible with RI detection. Therefore, a number of other detection methods have been tried. Of these, evaporative light scattering or “mass” detection (ELSD), is not affected by changes in mobile phase composition or small

variations in room temperature, provides a better signal-to-noise ratio and is easy to use [3,4]. However, the detector response depends on the physical properties and concentration of each eluting material, giving sigmoidal response curves, only a small portion of which is linear [4–6].

On the other hand, capillary gas chromatography (GC) offers high efficiency and high speed for the analysis of complex mixtures of acylglycerols with a broad range of relative molecular masses. On phenylmethylsilicone stationary phases the triacylglycerols are separated by carbon number (CN), and each carbon number peak is split up giving a fine structure governed by the number of unsaturations in order of increasing retention time [7]. Several applications to the analysis of fats and oils using a laboratory-made movable cold on-column injector and flame ionization detection (FID) have been described [7,8], but information is scarce about other injection systems and relative response factors [9].

Otherwise, the triacylglycerol composition can be calculated utilizing fatty acid methyl ester (FAME) determinations and computer programs, by applying the 1,3-random 2-random distribution theory either to the results of total and 2-glycerol fatty acid

Correspondence to: A. Cert, Instituto de la Grasa y sus Derivados, CSIC, Avda. Padre García Tejero 4, Apdo. 1078, 41012 Seville, Spain.

analysis [10] or only to the total fatty acid composition [11].

The purpose of this work was to establish the suitability of methods other than the IUPAC standard method to determine the triacylglycerol composition in vegetable oils, comparing the results obtained using the following techniques: isocratic HPLC with RI detection, gradient solvent HPLC with ELSD, capillary GC on a phenylmethylsilicone phase using a standard split injector and theoretical computer calculations from FAME analysis. For this, relative response factors were calculated from triacylglycerol standards and analyses of some vegetable oils were accomplished.

The following abbreviations for fatty acids are used: A = arachidic acid, eicosanoic acid, C20:0; B = behenic acid, docosanoic acid, C22:0; G = gadoleic acid, *cis*-11-eicosenoic acid, C20:1; L = linoleic acid, *cis,cis*-9,12-octadecadienoic acid, C18:2; Ln = linolenic acid, *cis,cis,cis*-9,12,15-octadecatrienoic acid, C18:3; M = myristic acid, tetradecanoic acid, C14:0; N = nonadecanoic acid, C19:0; O = oleic acid, *cis*-9-octadecenoic acid, C18:1; P = palmitic acid, hexadecanoic acid, C16:0; Po = palmitoleic acid, *cis*-9-hexadecenoic acid, C16:1; S = stearic acid, octadecanoic acid, C18:0.

EXPERIMENTAL

Materials

All reagents were of analytical-reagent grade, except acetone and acetonitrile, which were of HPLC grade from Merck.

The triacylglycerols trilinolein (LLL), trimyristin (MMM), trionadecanoin (NNN), triolein (OOO), 1,2-dioleoyl-3-palmitoyl-*rac*-glycerol (POO), 1,3-dipalmitoyl-2-oleoylglycerol (POP), tripalmitin (PPP), tripalmitolein (PoPoPo) and tristearin (SSS), of purity greater than 98% (GC), were obtained from Fluka (Buchs, Switzerland). Standard solutions for HPLC analysis were prepared mixing 20–300 mg of each triacylglycerol in 20 ml of chloroform. For GC analysis the solutions were diluted tenfold with hexane.

For the assays, virgin olive oil and refined sunflower oil were chosen because both contain the same fatty acids but in different proportions. On the other hand, the genetic variety of sunflower oil with

a high oleic acid content was used, as it shows a fatty acid composition similar to that of olive oil.

Solutions of oils of 5% in acetone and 0.5% in hexane were used for HPLC and GC analysis, respectively.

HPLC analysis

The HPLC separations were done on a LiChrospher 100 RP-18 (5 μ m) column (25 cm \times 4 mm I.D.) using an HP 1050 gradient pumping unit (Hewlett-Packard, Avondale, PA, USA). Using RI detection, an HP 1047A detector and a mobile phase of acetone–acetonitrile (1:1) at a flow-rate of 1.15 ml/min were used. Using ELSD, a Model 750/14 detector (ACS, Macclesfield, UK) was used with the following chromatographic conditions: flow-rate, 1 ml/min; elution using a two-step linear binary gradient from acetone–acetonitrile (30:70) to acetone–acetonitrile (65:35) at 20 min and then increasing to 100% acetone at 40 min; evaporator temperature, 45°C; air pressure, 2 bar; and photomultiplier sensitivity, 3. Between 5 and 10 μ l of a solution of oil in acetone (500 mg in 10 ml) were injected.

For the analysis with RI detection, response factors relative to OOO were used. For LLL, POO and POP the factors were experimentally determined using standards, and for the remaining mixed TAGs the factors (F_{xyz}) were calculated from the values for homogeneous TAGs through the equation

$$\frac{1}{F_{xyz}} = \frac{1}{3F_{xxx}} + \frac{1}{3F_{yyy}} + \frac{1}{3F_{zzz}} \quad (1)$$

This expression is deduced from the following two equations:

$$F_{xyz} = \frac{n_{ooo} - n_s}{n_{xyz} - n_s} \quad (2)$$

gives the factor as a function of refractive indices of the TAG (n_{xyz}), OOO (n_{ooo}) and the chromatographic solvent (n_s);

$$n_{xyz} = \frac{1}{3} n_{xxx} + \frac{1}{3} n_{yyy} + \frac{1}{3} n_{zzz} \quad (3)$$

assumes [12] that the refractive index of a mixed TAG can be calculated from those of the homogeneous TAGs.

GC analysis

Chromatographic analysis of triacylglycerols was performed using a Chrompack (Middelburg, Neth-

erlands) CP9000 gas chromatograph fitted with a flame ionization detector and a split injection system (splitting ratio 1:30). Separations were carried out on a high-temperature aluminium-clad fused-silica capillary column (25 m × 0.25 mm I.D.) coated with methyl-65% phenylsilicone of thickness 0.1 μm (Quadrex, New Haven CT, USA). The operating conditions were oven temperature 350°C for 1 min, then increased at 0.5°C/min to 360°C and remaining at 360°C for 8 min, injector temperature 360°C, detector temperature 365°C and carrier gas helium at 130 kPa.

FAMES from triacylglycerols

Standard solutions of triacylglycerols and oil samples were transmethylated by alkaline methanolysis followed by esterification of the fatty acids in acidic medium according to the IUPAC method [13]. GC analysis was carried out on a Supelcowax-10 fused-silica capillary column (30 m × 0.32 mm I.D.) of film thickness 0.25 μm, maintained at a temperature of 220°C for 3 min and then increased at 3°C/min to 255°C (held for 5 min), using helium as the carrier gas.

Fatty acids in the 2-position in the triacylglycerols of oils

The triacylglycerols of oils were partially hydrolysed by pancreatic lipase and then separated by silica gel thin-layer chromatography [14]. The monoacylglycerol band was scraped off and treated as indicated for FAME analysis.

Theoretical calculation of TAGs from FAME analysis

As a prior step for the TAG calculation from the fatty acid composition, the efficiency of the transmethylation method was tested by processing a standard of homogeneous TAGs. The calculations for the determination of the TAG composition from the total and 2-glycerol fatty acids were carried out with the mean values from five FAME analyses.

For comparison of the results with those from HPLC experiments, the TAGs were arranged by their ECN, calculated from the equation

$$\text{ECN} = \text{CN} - 2.52 b_{\text{O}} - 2.43 b_{\text{Po}} - 2.27 b_{\text{L}} - 2.09 b_{\text{Ln}} \quad (4)$$

where CN is the carbon number and b_{O} , b_{Po} , b_{L} and b_{Ln} are the number of double bonds attributable to oleic, palmitoleic, linoleic and linolenic acid, respectively. The coefficients were calculated by means of the reference triacylglycerols, taking into account that the logarithm of the relative retention time shows a linear relationship with ECN.

When comparison with GC data was required, the TAGs were put in order according to their CN and unsaturation number.

RESULTS AND DISCUSSION

A standard solution of TAGs analysed by HPLC with RI detection, using isocratic conditions, gave the relative response factors indicated in Table I. The factor for SSS could not be calculated as this compound gave a broad chromatographic peak at very long retention time. The experimental factors for homogeneous and mixed TAG were in agreement with those reported in the literature [12] and calculated from eqn. 1, respectively.

The TAG compositions found for olive, sunflower and high oleic sunflower oil samples applying the HPLC-RI method are given in Tables II, III and IV, respectively, the identities of the chromatographic peaks being established assuming the 1,3-random 2-random fatty acid distribution and discarding the TAGs with a level lower than 0.1%. It

TABLE I
RESPONSE FACTORS RELATIVE TO TRIOLEYLGLYCEROL USING HPLC WITH RI DETECTION

Results are means of five determinations with confidence interval at a significance level $\alpha = 5\%$.

TAG	Concentration (mg/ml)	Response factor	
		Experimental	Literature [12]
MMM	5.21	1.08 ± 0.06	1.106
PPP	5.33	1.05 ± 0.09	1.080
PoPoPo	5.82	1.02 ± 0.06	—
SSS	5.10	—	1.050
OOO	5.57	1	1
LLL	5.51	0.89 ± 0.05	0.924
POO	2.06	0.99 ± 0.05	1.025 ^a
POP	4.21	1.02 ± 0.06	1.052 ^a

^a Calculated by eqn. 1 from literature data [12].

TABLE II

TAG COMPOSITIONS (%) OF AN OLIVE OIL DETERMINED BY HPLC-RI AND HPLC-ELSD AND BY CALCULATION FROM TOTAL FAME ANALYSIS

The values are given as means of five determinations with confidence interval at a significance level $\alpha = 5\%$.

TAG	RI detection		From total FAME analysis	ELSD (uncorrected)
	Uncorrected	Corrected		
OLnL	0.24 ± 0.06	0.22 ± 0.05	0.18 ± 0.01	ND ^a
OLL + PoLO	0.95 ± 0.24	0.89 ± 0.22	0.91 ± 0.03	0.39 ± 0.05
LnOO + PLL	1.76 ± 0.05	1.63 ± 0.05	1.40 ± 0.03	0.89 ± 0.06
POLn	0.64 ± 0.06	0.60 ± 0.06	0.42 ± 0.01	0.22 ± 0.09
OLO + PoOO	10.01 ± 0.16	9.78 ± 0.16	11.18 ± 0.15	10.92 ± 0.72
PLO + PPOO	4.30 ± 0.25	4.33 ± 0.26	3.65 ± 0.05	4.20 ± 0.20
PLP	ND	ND	0.22 ± 0.01	ND
OOO	44.93 ± 0.50	44.82 ± 0.49	44.29 ± 0.17	49.19 ± 0.57
POO + SOL	22.76 ± 0.21	23.16 ± 0.22	22.99 ± 0.18	21.79 ± 0.56
POP + PLS	2.63 ± 0.09	2.70 ± 0.09	2.84 ± 0.05	2.06 ± 0.29
GOO	0.53 ± 0.22	0.53 ± 0.22	0.41 ± 0.05	0.11 ± 0.02
SOO + AOL	8.18 ± 0.16	8.24 ± 0.16	8.22 ± 0.07	8.65 ± 0.55
POS	1.75 ± 0.09	1.76 ± 0.09	2.00 ± 0.02	1.14 ± 0.12
AOO	0.70 ± 0.08	0.71 ± 0.08	0.73 ± 0.03	0.27 ± 0.03
SOS + AOP	0.62 ± 0.07	0.62 ± 0.07	0.55 ± 0.01	0.21 ± 0.03

^a ND = Not detected.

can be seen that the precision (R.S.D.) is good (less than 5%) for TAG concentrations higher than 8%, average (less than 15%) for TAG concentrations between 2 and 8% and bad (up to 43%) for concentrations lower than 2%. The introduction of the re-

sponse factors calculated as indicated under Experimental results in slightly different compositions, most of which lie within the confidence intervals. LLL is the compound most affected by the correction owing to its low response factor (0.89). There-

TABLE III

TAG COMPOSITION (%) OF A SUNFLOWER OIL DETERMINED BY HPLC-RI AND HPLC-ELSD AND BY CALCULATION FROM TOTAL FAME ANALYSIS

The values are given as means of five determinations with confidence interval at a significance level $\alpha = 5\%$.

TAG	RI detection		From total FAME analysis	ELSD (uncorrected)
	Uncorrected	Corrected		
LLL + PoLL	20.06 ± 0.53	19.01 ± 0.52	18.12 ± 0.16	18.91 ± 1.62
OLL + PoLO	28.57 ± 0.66	27.99 ± 0.68	29.91 ± 0.07	28.96 ± 3.38
PLL	9.05 ± 0.16	9.06 ± 0.18	7.83 ± 0.05	9.53 ± 0.33
OLO + GLL	15.30 ± 0.42	15.64 ± 0.45	16.55 ± 0.07	15.44 ± 1.05
PLO + SLL	12.68 ± 0.15	12.96 ± 0.17	12.76 ± 0.06	14.00 ± 0.54
PLP	0.83 ± 0.23	0.87 ± 0.24	0.86 ± 0.01	0.45 ± 0.02
OOO + GOL	4.79 ± 0.62	5.10 ± 0.65	3.19 ± 0.04	5.34 ± 0.22
SOL + POO + ALL	5.91 ± 0.91	6.42 ± 0.98	7.19 ± 0.05	5.58 ± 0.23
PLS + POP	1.03 ± 0.46	1.10 ± 0.49	1.37 ± 0.02	0.66 ± 0.11
BLL	0.59 ± 0.31	0.58 ± 0.30	0.69 ± 0.02	0.33 ± 0.14
SOO + AOL	1.18 ± 0.54	1.26 ± 0.58	1.55 ± 0.01	0.80 ± 0.12

TABLE IV

TAG COMPOSITION (%) OF A HIGH OLEIC SUNFLOWER OIL DETERMINED BY HPLC–RI AND HPLC–ELSD AND BY CALCULATION FROM TOTAL FAME ANALYSIS

The values are given as means of five determinations with confidence interval at a significance level $\alpha = 5\%$.

TAG	RI detection		From total FAME analysis	ELSD (uncorrected)
	Uncorrected	Corrected		
LLL	1.63 ± 0.06	1.45 ± 0.05	<0.1	0.92 ± 0.17
OLL	2.44 ± 0.25	2.25 ± 0.24	1.53 ± 0.02	1.80 ± 0.17
PLL	1.10 ± 0.28	1.04 ± 0.26	<0.1	0.49 ± 0.06
OLO + PoOO	6.99 ± 0.59	6.74 ± 0.57	16.04 ± 0.12	7.93 ± 0.26
PLO	1.61 ± 0.69	1.58 ± 0.68	1.86 ± 0.02	1.32 ± 0.12
OOO	61.93 ± 1.56	62.21 ± 1.56	54.28 ± 0.08	65.07 ± 2.00
POO + SOL	9.63 ± 0.45	9.87 ± 0.45	11.38 ± 0.14	9.72 ± 0.58
POP	0.23 ± 0.13	0.23 ± 0.13	0.42 ± 0.01	0.10 ± 0.03
GOO	0.57 ± 0.15	0.57 ± 0.15	0.61 ± 0.01	0.14 ± 0.04
SOO + AOL	10.91 ± 0.50	11.07 ± 0.51	9.34 ± 0.19	10.34 ± 0.50
POS	0.45 ± 0.17	0.46 ± 0.18	0.81 ± 0.02	0.15 ± 0.04
AOO + BLO	0.70 ± 0.22	0.70 ± 0.22	1.16 ± 0.04	0.37 ± 0.08
SOS	ND ^a	ND	0.39 ± 0.02	ND
BOO + BOP	1.82 ± 0.41	1.82 ± 0.41	2.17 ± 0.13	1.65 ± 0.16

^a ND = Not detected.

fore, the application of correction factors is unnecessary if they are very close to unity. In this work, the HPLC–RI method is taken as the reference method, as the oils analysed do not contain TAGs with long retention times and the response factors are known.

HPLC analysis using elution gradient and ELSD gives a sharp SSS peak, in contrast to the HPLC–RI method where this peak is very broad. For the calculation of the response factors a standard solution with a high content of reference TAG (OOO) was used, as the detector response might be expected to be non-linear at a low concentration range [4–6]. The results in Table V indicate that there is a rapid increase in the response factors for amounts of TAGs less than 10 μg , in agreement with the decrease in detector response cited in the literature [4,5]. Consequently, the results of the oil analysis (Tables II–IV) show very low values for the low-concentration (less than 2%) TAGs, in comparison with those obtained by HPLC–RI. The values for the remaining TAGs differ by up to 15% from the corresponding results obtained by the HPLC–RI method. On the other hand, the precision of the measurements is average (R.S.D. 5–10%) for medium and low concentrations and bad (R.S.D. up to

40%) for concentrations less than 1%. Although the time of analysis is short and the precision is acceptable, the use of HPLC–ELSD does not seem advisable for TAG analysis because of the wide range of TAG concentrations in the samples.

The TAG compositions of the oils calculated from the total FAME analysis assuming a 1,3-random 2-random distribution (Tables II–IV) show a very good precision (R.S.D. 2 and 10% for concentrations higher and lower than 2%, respectively), in accordance with the very good precision of the

TABLE V

RESPONSE FACTORS RELATIVE TO TRIOLEYLGLYCEROL USING HPLC–ELSD

TAG	Concentration (mg/ml)	Injection volume (μl)			
		2.5	5	10	15 ^a
LLL	3.285	2.68	1.5	1.38	1.39 ± 0.03
OOO	13.75	1	1	1	1
PPP	3.105	1.69	1.14	1.13	1.16 ± 0.02
SSS	2.175	2.08	1.30	1.24	1.17 ± 0.06

^a Means of five determinations with confidence interval at a significance level $\alpha = 5\%$.

FAME analysis method. In addition, these results are very close to those obtained by calculation from the total and 2-glycerol fatty acid compositions (difference less than 5%), except for POO in olive and high oleic sunflower oils (difference 10%), and are nearer to the HPLC–RI data than those obtained by calculation from the total and 2-glycerol fatty acid compositions. Therefore, the 2-glycerol fatty acid data seem unnecessary for calculation of the theoretical TAG composition.

Comparing the computer and HPLC–RI data, similar values are obtained for olive and sunflower oils, except OLO, PLO and POS in the former (difference 7–14%) and OLL, PLL and OOO in the latter (difference 7–38%). This corroborates the 1,3-random 2-random distribution for the olive oil and indicates an acceptable approximation for the sunflower oil. In contrast, the values for the high oleic sunflower oil are very discordant, indicating that the theoretical distribution is not applicable to this oil. This is in accord with the drastic changes in TAG composition observed throughout the development of this mutant seed [15]. Results from olive and sunflower oils confirm the TAG assignment for the chromatographic peaks of these oils, although the attribution of some minor TAGs might be uncertain.

Analysis of a standard solution by GC with FID, using split injection, gave very diverse relative response factors (Table VI), in accordance with the results reported using a movable cold on-column

TABLE VI

RESPONSE FACTORS (F) AND RETENTION TIMES (t_{RR}), BOTH RELATIVE TO OOO, USING GC–FID AND SPLIT INJECTION

The values are means of five determinations with confidence interval at a significance level $\alpha = 5\%$.

TAG	Concentration ($\mu\text{g/ml}$)	t_{RR}	F
PPP	533	0.41	0.53 ± 0.02
PoPoPo	582	0.49	0.64 ± 0.02
POP	421	0.56	0.59 ± 0.02
POO	206	0.75	0.77 ± 0.04
SSS	510	0.89	0.87 ± 0.02
OOO	557	1	1
LLL	551	1.17	1.34 ± 0.07
NNN	495	1.27	1.27 ± 0.09

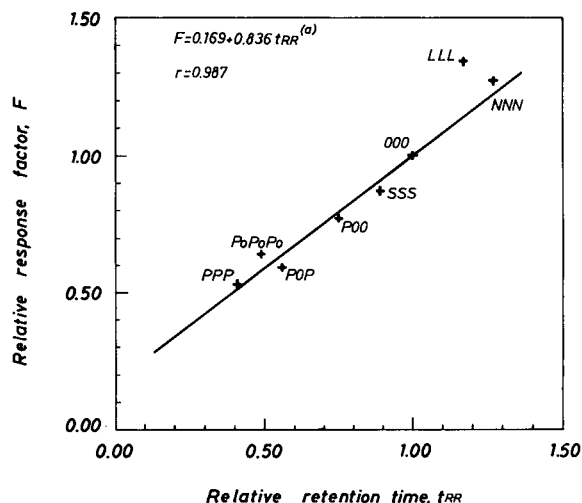


Fig. 1. Response factors versus retention times, both relative to OOO, for GC analysis using FID and split injection. ^a The data for LLL were not taken into account in the calculation.

injector and a phenylmethylsilicone stationary phase [9]. Except for LLL, the factors exhibited a linear relationship with the retention times of the TAGs (see Fig. 1), with a correlation coefficient of 0.987. This decrease in response with elution time has been attributed to quenching by the bleeding level of the methylphenylsilicone stationary phase [9], but in our experiments a contribution of the mass discrimination effect due to the split injection mode could be possible. The low response of LLL is in agreement with the losses of highly unsaturated TAGs reported in the literature [7] and suggests an alteration of the compound during analysis. The compositions of the vegetable oils, obtained applying the experimental factor for the LLL and those calculated by means of the regression curve for the remaining TAGs, are given in Tables VII, VIII and IX, where the peak identities (as in HPLC) were established assuming the 1,3-random 2-random fatty acid distribution. With respect to precision, the R.S.D. is less than 3% for peaks greater than 2%, rises to 15% for small peaks of short retention times and reaches up to 30% for small peaks with long retention times.

The differences between the GC data and the compositions calculated from FAME analysis are, in olive oil (Table VII) and sunflower oil (Table VIII), greater than with the HPLC–RI technique,

TABLE VII

COMPARISON OF TAG COMPOSITIONS (%) OF AN OLIVE OIL DETERMINED BY GC-FID ANALYSIS WITH THOSE OBTAINED BY HPLC-RI AND TOTAL FAME ANALYSIS

The values are means of five determinations with confidence interval at a significance level $\alpha = 5\%$.

TAG	GC-FID		From total FAME analysis	HPLC-RI
	F	%		
POP	0.64	2.37 ± 0.04	2.69 ± 0.06	2.60
PPoO + PLP	0.66	0.65 ± 0.05	0.82 ± 0.02	0.94
POS	0.76	1.59 ± 0.03	2.00 ± 0.02	1.76 ± 0.04
POO + PLS	0.80	23.11 ± 0.04	21.97 ± 0.20	21.94
PLO + PoOO	0.83	4.36 ± 0.13	4.96 ± 0.05	5.28
POLn + PoOL + PLL	0.86	0.47 ± 0.05	0.80 ± 0.01	1.02
SOS + AOP	0.92	0.60 ± 0.02	0.55 ± 0.01	0.62 ± 0.07
SOO	0.95	8.42 ± 0.07	8.11 ± 0.08	8.14
OOO + SOL	1.00	49.35 ± 0.35	45.35 ± 0.17	45.93
OLO + LnOS	1.04	6.85 ± 0.29	9.41 ± 0.16	8.21
OOLn + OLL	1.09	1.22 ± 0.32	1.93 ± 0.04	2.11
OLnL	1.13	0.21 ± 0.08	0.18 ± 0.01	0.22 ± 0.05
AOO	1.16	0.56 ± 0.11	0.73 ± 0.03	0.71 ± 0.08
GOO + AOL	1.20	0.26 ± 0.06	0.52 ± 0.03	0.53 ± 0.22

indicating a greater deviation of the GC results, but for the high oleic sunflower oil (Table IX) considerable deviations, such as those found between HPLC-RI results and theoretical calculations, are observed.

In the comparison between GC and HPLC-RI measurements, only a few chromatographic peaks have the same identity. In order to extend the number of comparable data, theoretical compositions deduced from FAME analysis were applied to the

TABLE VIII

COMPARISON OF TAG COMPOSITION (%) OF A SUNFLOWER OIL DETERMINED BY GC-FID ANALYSIS WITH THOSE OBTAINED BY HPLC-RI AND TOTAL FAME ANALYSIS

The values are means of five determinations with confidence intervals at a significance level $\alpha = 5\%$.

TAG	GC-FID		From total FAME analysis	HPLC-RI
	F	%		
POP	0.64	0.28 ± 0.02	0.48 ± 0.09	0.39
PLP	0.66	0.86 ± 0.04	0.86 ± 0.01	0.87 ± 0.24
POS	0.76	0.29 ± 0.03	0.50 ± 0.01	—
POO + PLS	0.80	3.80 ± 0.14	3.31 ± 0.04	2.77
PLO	0.83	7.83 ± 0.07	8.71 ± 0.07	8.50
PLL + PoOL	0.86	8.28 ± 0.13	8.10 ± 0.04	9.25
PoLL		ND ^a	0.19 ± 0.01	0.20
SOS	0.92	ND	0.13 ± 0.00	—
SOO + SLS	0.95	1.61 ± 0.12	1.50 ± 0.02	0.98
OOO + SOL	1	9.58 ± 0.50	7.61 ± 0.05	9.19
OLO + SLL	1.04	21.03 ± 0.13	20.65 ± 0.07	19.8
OLL	1.09	27.10 ± 0.23	29.91 ± 0.08	27.97
LLL	1.34	19.32 ± 0.33	18.06 ± 0.16	18.81

^a ND = Not detected.

TABLE IX

COMPARISON OF TAG COMPOSITION (%) OF HIGH OLEIC SUNFLOWER OIL DETERMINED BY GC-FID ANALYSIS WITH THOSE OBTAINED BY HPLC-RI AND TOTAL FAME ANALYSIS

The values are means of five determinations with confidence interval at a significance level $\alpha = 5\%$.

TAG	GC-FID		From total FAME analysis	HPLC-RI
	F	%		
POP	0.64	0.31 ± 0.02	0.42 ± 0.01	0.23 ± 0.13
PLP	0.66	0.16 ± 0.01	<0.1	ND ^a
POS	0.76	0.51 ± 0.04	0.82 ± 0.02	0.46 ± 0.18
POO	0.80	8.58 ± 0.09	9.66 ± 0.14	—
PLO + PoOO	0.83	1.36 ± 0.11	2.14 ± 0.03	—
PLL + PoOL	0.86	0.70 ± 0.06	<0.1	—
SOS	0.92	0.35 ± 0.06	0.39 ± 0.01	ND
SOO	0.95	10.99 ± 0.39	9.26 ± 0.20	—
OOO + SOL	1	64.68 ± 0.53	56.48 ± 0.07	—
OLO	1.04	5.79 ± 0.20	15.90 ± 0.12	—
OLL	1.09	1.90 ± 0.08	1.55 ± 0.02	2.25 ± 0.24
LLL	1.34	1.43 ± 0.07	<0.1	1.45 ± 0.05
AOO	1.16	0.82 ± 0.11	0.78 ± 0.02	—
GOO	1.20	0.54 ± 0.07	0.61 ± 0.01	0.57 ± 0.15
BOO	1.41	1.88 ± 0.24	2.00 ± 0.12	—
SOO + AOL		10.99 ± 0.39		11.07 ± 0.51
OOO + SOL + POO		73.26		72.09
OLO + PoOO + PLO		7.15		8.32
AOO + BLO		0.82 ± 0.11		0.70 ± 0.22
BOO + BOP		1.88 ± 0.24		1.82 ± 0.41

^a ND = Not detected.

HPLC-RI peaks of olive and sunflower oils, giving approximate values whose errors were not evaluated. In olive oil (Table VII), great variations (25–50%) occur for the minor peaks PPoO + PLP, POL_n + PoOL + PLL, OOL_n + OLL, AOO and GOO + AOL, and considerable variations (10–20%) for the medium peaks POP, PLO + PoOO and OLO + LnOS. In sunflower oil (Table VIII), better results are obtained; variations from 25 to 50% are found for the small peaks POP, POO + PLS and SOO + SLS and less than 10% for the remainder. Consequently, HPLC-RI seems a more appropriate technique than GC for TAG determination, in spite of its lower precision. For high oleic sunflower oil (Table IX), comparisons were made between the sums of several peaks, as the percentages derived from theoretical calculations are not applicable. The results show a variability similar to those for the other oils. The similarity of results for olive and sunflower oils reinforces the applicability

of the theoretical calculations for the identification of the main components of the chromatographic peaks in oils complying with a 1,3-random 2-random distribution. For high oleic sunflower oil, the proposed peak identities are a tentative approach that renders acceptable results.

As an example, Figs. 2, 3 and 4 show the chromatograms of high oleic sunflower oil obtained by HPLC-RI, HPLC-ELSD and GC-FID, respectively. These illustrate the different elution orders of triacylglycerol species according to the method used and the long time of analysis required when the isocratic HPLC method with RI detection is employed.

In summary, the TAG composition of vegetable oils can be determined by the isocratic HPLC-RI technique. Correction factors have to be applied if the differences between response factors of major peaks are greater than 10%. Calculation of the composition from FAME analysis is suitable only if

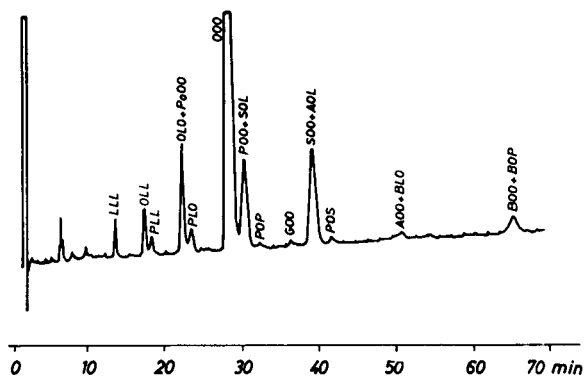


Fig. 2. TAG analysis of high oleic sunflower oil using the isocratic HPLC-RI technique.

it is known for certain that the fatty acids in the sample follow the 1,3-random 2-random distribution. In that event, the theoretical composition is useful to establish the main components of the chromatographic peaks resulting from analysis by other techniques. The determination of the fatty acid composition at the 2-position of the glycerol

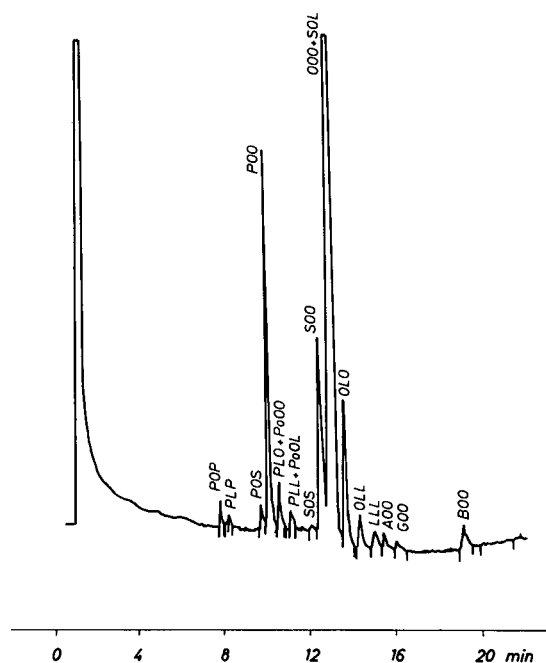


Fig. 4. TAG analysis of high oleic sunflower oil using capillary GC-FID on a phenylmethylsilicone stationary phase.

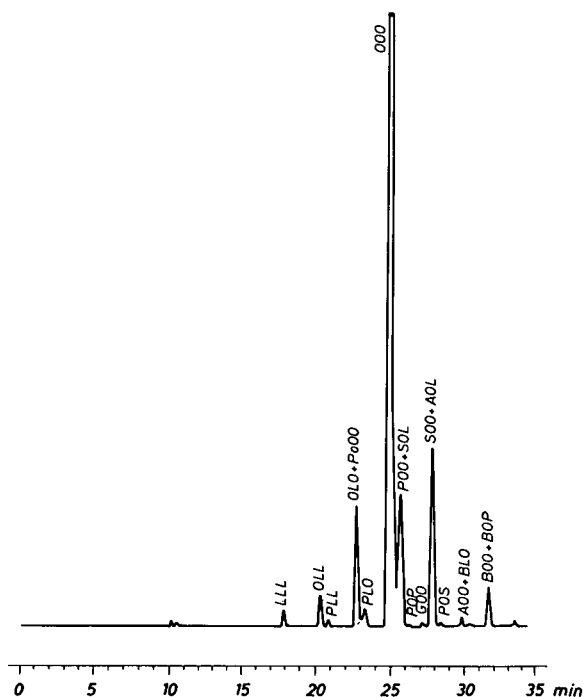


Fig. 3. TAG analysis of high oleic sunflower oil using the gradient solvent HPLC-ELSD technique.

seems unnecessary for calculation of theoretical TAG composition.

HPLC using a solvent gradient and ELSD is an appropriate technique for the separation of oils containing TAGs with a wide range of ECN, but the quantification of small peaks is very inaccurate.

Finally, capillary GC on a phenylmethylsilicone stationary phase shows great sensitivity and yields a distribution of the chromatographic peaks that, together with that obtained by the HPLC-RI technique, permits, in some instances, determination of the individual TAGs. Nevertheless, the application of response factors is necessary and special care has to be taken in the analysis of oils containing polyunsaturated TAGs.

ACKNOWLEDGEMENTS

We thank the Spanish Ministry of Education and Science for the award of a scholarship to A. A. C. and financial support. We also thank R. Garcés, F. Millán and J. Serrano for providing the computer programs.

REFERENCES

- 1 Commission Regulation (EEC) No. 2568/91 of 11 July 1991 on the Characteristics of Olive and Olive Pomace Oils and on Their Analytical Methods, *Off. J. Eur. Commun.*, L 248, 5 September (1991) 1–5.
- 2 Commission Regulation (EEC) No. 2568/91 of 11 Juli 1991 on the Characteristics of Olive and Olive Pomace Oils and on their Analytical Methods, *Off. J. Eur. Commun.*, L 248, 5 September (1991), Annex VIII, 29–32.
- 3 P. B. Stockwell and B. W. King, *Int. Chromatogr. Lab.*, 7 (1991) 4.
- 4 W. W. Christie, *Rev. Fr. Corps Gras*, 38 (1991) 155.
- 5 B. Herslöf and G. Kindmark, *Lipids*, 20 (1985) 783.
- 6 E. W. Hammond and J. W. Irvin, in R. Macrae (Editor), *HPLC in Food Analysis*, Academic Press, London, 1988, Ch. 4, p. 95.
- 7 E. Geeraert, in A. Kuksis (Editor), *Chromatography of Lipids in Biomedical Research and Clinical Diagnosis*, Elsevier, Amsterdam, 1987, Ch. 2, p. 48.
- 8 E. Geeraert and P. Sandra, *J. Am. Oil Chem. Soc.*, 64 (1987) 100.
- 9 M. Termonia, F. Munari, P. Sandra, *J. High Resolut. Chromatogr. Chromatogr. Commun.*, 10 (1987) 263.
- 10 R. J. Vander Wal, *J. Am. Oil Chem. Soc.*, 37 (1960) 18.
- 11 N. Cortesi, P. Rovellini and E. Fedeli, *Riv. Ital. Sostanze Grasse*, 67 (1990) 69.
- 12 J. L. Perrin et M. Naudet, *Rev. Fr. Corps Gras*, 30 (1983) 279.
- 13 *IUPAC Standard Methods for the Analysis of Oils, Fats and Derivatives*, Blackwell, Oxford, 7th ed., 1987, Method No. 2301, p. 123.
- 14 *IUPAC Standard Methods for the Analysis of Oils, Fats and Derivatives*, Blackwell, Oxford, 7th ed., 1987, Method No. 2210, p. 111.
- 15 R. Garcès, J. M. Garcia and M. Mancha, *Phytochemistry*, 28 (1989) 2600.

Structure–gas chromatographic retention time models of tetra-*n*-alkylsilanes and tetra-*n*-alkylgermanes using topological indexes

Eugene J. Kupchik

Department of Chemistry, St. John's University, Grand Central and Utopia Parkways, Jamaica, NY 11439 (USA)

(First received August 4th, 1992; revised manuscript received October 27th, 1992)

ABSTRACT

Structure–gas chromatographic retention time models were developed for 26 tetra-*n*-alkylsilanes, 26 tetra-*n*-alkylgermanes, and the mixed set of silanes and germanes using topological indexes. The topological indexes used were molecular connectivity indexes, the new Kier–Hall total topological indexes, and the new Kier–Hall electrotopological state atom index, *S*, for the silicon and germanium atoms. For the mixed data set, a model based on ${}^1\chi$, ${}^3\chi_c$ and *S* gave $r = 0.999$ and $s = 0.033$. In two cases the residual was more than twice the standard error. Replacement of ${}^1\chi$ by TTV, the new Kier–Hall total topological index using δ^v values for the silicon and germanium atoms, also gave $r = 0.999$ and $s = 0.033$ but in no case was there a residual greater than twice the standard error. A two-variable model based on ${}^0\chi^r$, which uses δ^r values for the metal atoms, and ${}^4\chi_{pc}^v$, which uses δ^v values for the metal atoms gave $r = 0.999$ and $s = 0.035$. The results demonstrate the adequacy of the Kier–Hall electrotopological state atom index for encoding the atomic characteristics of silicon and germanium in a mixed data set. The results show that the Kier–Hall total topological indexes can be used in place of ${}^1\chi$ to encode the size and skeletal branching of silanes and germanes.

INTRODUCTION

Topological indexes are numerical descriptors of molecules that are based on certain topological features of their hydrogen-suppressed graphs [1–6]. Topological indexes are used to correlate the structures of molecules with their physical, chemical, or biological properties. Probably the most widely used topological indexes are the molecular connectivity indexes. Molecular connectivity was extensively developed by Kier and Hall [7–11] from the alkane branching index of Randić [12]. The method describes the structure of a molecule by a set of molecular connectivity indexes, χ , which are calculated from a hydrogen-suppressed structural for-

mula or graph of the molecule. The simplest index, ${}^0\chi$, is given by:

$${}^0\chi = \sum \delta_i^{-1/2} \quad (1)$$

where the sum is over all non-hydrogen bonded atoms in the molecule and δ_i is a number assigned to each atom, which equals the number of atoms connected to it. The first order molecular connectivity index, ${}^1\chi$, which is often called the Randić branching index, is given by:

$${}^1\chi = \sum (\delta_i \delta_j)^{-1/2} \quad (2)$$

where the sum is over all of the edges of the graph whose two atoms have the δ values shown. The second order molecular connectivity index, ${}^2\chi$, is given by:

$${}^2\chi = \sum (\delta_i \delta_j \delta_k)^{-1/2} \quad (3)$$

where the sum is over all paths of length two whose three atoms have the δ values shown. Higher order

Correspondence to: E. J. Kupchik, Department of Chemistry, St. John's University, Grand Central and Utopia Parkways, Jamaica, NY 11439, USA.

path connectivity indexes, ${}^m\chi_p$, where p denotes path and m denotes path length, can also be calculated. In addition to paths, a molecule can be dissected into cluster and path-cluster fragments. ${}^3\chi_c$ is a third order cluster fragment given by:

$${}^3\chi_c = \sum (\delta_i \delta_j \delta_k \delta_l)^{-1/2} \quad (4)$$

where c denotes cluster and the sum is over all isobutane fragments whose four atoms have the δ values shown. ${}^4\chi_{pc}$ is a fourth order path-cluster index given by:

$${}^4\chi_{pc} = \sum (\delta_i \delta_j \delta_k \delta_l \delta_m)^{-1/2} \quad (5)$$

where pc denotes path-cluster and the sum is over all isopentane fragments whose five atoms have the δ values shown.

For non- sp^3 carbon atoms and heteroatoms, Kier and Hall [13–16] have suggested the use of δ^v (valence δ) values, instead of δ values. The use of δ^v gives a valence molecular connectivity index, ${}^m\chi_t^v$, where m is the order of the index and t is the type of index, namely path, cluster or path-cluster. δ^v is obtained from the following equation:

$$\delta^v = \frac{Z^v - h}{Z - Z^v - 1} \quad (6)$$

where Z^v is the number of valence electrons of the

atom, h is the number of attached hydrogen atoms, and Z is the atomic number of the atom. For an sp^3 carbon, $\delta^v = \delta$. As an alternate approach for encoding information about the heteroatom in heteroalkanes, Kupchik [17–19] has suggested that the heteroatom be assigned a radius δ (δ^r) value obtained from the following equation:

$$\delta^r = \frac{r_c}{r_{het}} \delta \quad (7)$$

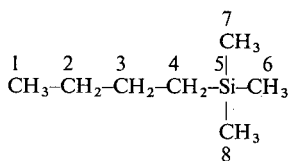
where r_c is the covalent radius of carbon, r_{het} is the covalent radius of the heteroatom and δ is the number of sp^3 carbon atoms attached to the heteroatom. The use of eqn. 7 gives a radius molecular connectivity index, ${}^m\chi_t^r$. Because it is based on experimentally determined covalent radii, δ^r is empirical and probably less attractive than δ^v which is essentially non-empirical. In this paper both δ^v and δ^r are employed and the results compared.

Recently Hall and Kier [20] introduced a new highly discriminating index called the total topological index. This index is obtained by adding the entries that appear in their novel topological state matrix of a molecule. Each entry in the matrix can be calculated using the formula

$$t_{ij} = \frac{GM_{ij}}{d_{ij}^2} \quad (8)$$

TABLE I

TOPOLOGICAL STATE MATRIX OF BUTYLTRIMETHYLSILANE ($\delta_{Si}^v = 0.44$)



	1	2	3	4	5	6	7	8	Topological state index T_i
1	1.000	0.354	0.176	0.105	0.051	0.034	0.034	0.034	1.788
2		2.000	0.500	0.222	0.086	0.051	0.051	0.051	3.315
3			2.000	0.500	0.134	0.072	0.072	0.072	3.526
4				2.000	0.235	0.106	0.106	0.106	3.380
5					0.440	0.166	0.166	0.166	1.444
6						1.000	0.085	0.085	1.599
7							1.000	0.085	1.599
8								1.000	1.599

Total topological index (TTV) = 14.345

where GM_{ij} is the geometric mean of the δ values of the atoms in the path of atoms of length d_{ij} atoms between atoms i and j ; t_{ij} gives the topological information for the vertex sequence beginning with atom i and ending with vertex j . Alternatively, other algorithms based on GM_{ij} and d_{ij} may be used to give alternate values of t_{ij} . The topological state matrix of butyltrimethylsilane is given in Table I. All entries were calculated using a hand-held calculator. To illustrate the use of eqn. 8 the value of 0.222 for $t_{2,4}$ is calculated as follows:

$$t_{2,4} = \frac{(2 \cdot 2 \cdot 2)^{1/3}}{3^2}$$

The sum of all of the entries in the matrix gives the total topological index value of 14.345. In this paper this index is given the symbol TTV, the V indicating that the δ values used were obtained using eqn. 6; the index is denoted by TTS if only simple δ values were used; the index is denoted by TTR if the δ values used were obtained from eqn. 7. Although total topological indexes can be obtained using a hand-held calculator, they are more easily obtained using the MOLCONN-X computer program^a. The topological state index T_i for atom i is obtained by adding the entries in column i and row i of the topological state matrix. Atoms having the same topological state index are topologically equivalent.

Hall *et al.* [21,22] recently introduced a new atom index called the electrotopological state index. In this method each atom in the hydrogen-suppressed graph is assigned an intrinsic state value, I_i , obtained from the following equation:

$$I_i = [(2/N)^2 \delta^v + 1]/\delta \quad (9)$$

where N is the principal quantum number of atom i , δ^v is the valence δ value of atom i , and δ is the simple δ value of atom i . The electrotopological state index for an atom i , S_i , is defined as follows:

$$S_i = I_i + \Delta I_i \quad (10)$$

where ΔI_i is a perturbation term arising from the electronic interaction between each atom in the molecule. The perturbations are summed over the entire molecule:

$$\Delta I_i = \frac{\sum (I_i - I_j)}{r_{ij}^2} \quad (11)$$

where r_{ij} is the graph separation between atoms i and j , counted as numbers of atoms, including i and j . Electrotopological state calculations for butyltrimethylsilane using a hand-held calculator are given in Table II. The electrotopological index value of -0.6792 for the silicon atom is obtained by adding the I value for silicon (0.694) to the ΔI value for silicon (-1.3732). Electrotopological state values for atoms are easily obtained with the MOLCONN-X program.

Only a few studies employing organometallic compounds and topological indexes have been reported [16–18,23]. Further studies of organometallic compounds and other organoelement compounds using topological indexes are needed to test the adequacy of the valence δ formalism and to test the new total topological indexes and the new electrotopological state atom index. The purpose of the present study was to determine if satisfactory structure–gas chromatographic retention time models could be found for some organosilicon and organogermanium compounds using molecular connectivity indexes, total topological indexes and electrotopological state indexes.

MATERIALS AND METHODS

Meaningful structure–property relationship studies require high-quality property data. This study uses the high-quality gas chromatographic retention time data of Semlyen *et al.* [24]. These workers obtained gas chromatographic retention time data for 26 tetra-*n*-alkylsilanes and 26 tetra-*n*-alkylgermanes. Analysis on columns of 2–13% squalene on Embacel at 100°C gave essentially similar results. Retention data were expressed as logarithms of retention times relative to mesitylene = 100, and agreement to within ± 0.01 was obtained between chromatograms.

All of the topological indexes used in this study were obtained using the MOLCONN-X program. The statistical analyses were performed using the SYSTAT statistical program [25]. The multiple regression equations presented in this paper appear to be free of the problem of multicollinearity, or near-linear dependence among the regression vari-

^a From L. H. Hall, Hall Associates Consulting, 2 Davis Street, Quincy, MA 02170, USA.

ables [26,27]. Regression models fit to data by the method of least squares when strong multicollinearity is present are very poor predictor equations. Intercorrelation data is presented with each multiple regression equation to demonstrate a non-multicollinearity problem. Other diagnostic tests employed to demonstrate non-multicollinearity were an inspection of the condition indices of the correlation matrix and an inspection of the tolerance of each variable. A condition index greater than 15 indicates a possible problem and one greater than 30 suggests a serious problem with multicollinearity [25,27]. Values of tolerance near zero indicate that some of the predictors are highly intercorrelated [25]. The multiple regression equations presented in this paper passed these tests.

RESULTS AND DISCUSSION

The 26 silanes in Table III were used in the stepwise regression procedure of the SYSTAT statistical program [25]. The following topological

indexes were included as final candidates in the regression equation: ${}^0\chi$, ${}^1\chi$, ${}^2\chi$, ${}^3\chi$, ${}^4\chi$, ${}^3\chi_c$, ${}^4\chi_c$, ${}^4\chi_{pc}$, the corresponding set of valence indexes, TTS, TTV, TTR and S for the silicon atom for a total of 20 indexes. No compound had a zero value for any index. Higher order path indexes were not used to avoid zero values for compounds. The following one-variable equation was obtained:

$$\text{Log } T = -0.426(0.055) + 0.507(0.010)^1\chi \quad (12)$$

$$n = 26 \quad r = 0.996 \quad s = 0.062 \quad F = 2822$$

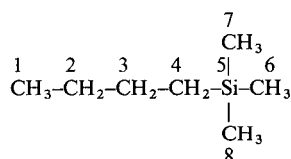
T is the retention time; the numbers in parentheses are the standard errors of the coefficients; n is the number of compounds, r is the correlation coefficient, s is the standard error of estimate, and F is the variance ratio. In only one case was there a residual greater than twice the standard error. Also the following two-variable equation was obtained:

$$\text{Log } T = -0.067(0.059) + 0.483(0.006)^1\chi - 0.251(0.035)^3\chi_c \quad (13)$$

$$n = 26 \quad r = 0.999 \quad s = 0.035 \quad F = 4441$$

TABLE II

ELECTROTOPOLOGICAL STATE CALCULATIONS FOR BUTYLTRIMETHYLSILANE



Intrinsic values: $I(1) = 2.000$, $I(2) = 1.500$, $I(3) = 1.500$, $I(4) = 1.500$, $I(5) = 0.694$, $I(6) = 2.000$, $I(7) = 2.000$, $I(8) = 2.000$.

$i \quad (I_i - I_j)/r_{ij}^2$ Matrix

i	1	2	3	4	5	6	7	8	$\Delta I_i = \text{row sum}$
1	0.0	0.1250	0.0556	0.0313	0.0522	0.0000	0.0000	0.0000	0.2641
2	-0.1250	0.0	0.0000	0.0000	0.0504	-0.0200	-0.0200	-0.0200	-0.1346
3	-0.0556	0.0000	0.0	0.0000	0.0896	-0.0313	-0.0313	-0.0313	-0.0599
4	-0.0313	0.0000	0.0000	0.0	0.2015	-0.0556	-0.0556	-0.0556	0.0034
5	-0.0522	-0.0504	-0.0896	-0.2015	0.0	-0.3265	-0.3265	-0.3265	-1.3732
6	0.0000	0.0200	0.0313	0.0556	0.3265	0.0	0.0000	0.0000	0.4334
7	0.0000	0.0200	0.0313	0.0556	0.3265	0.0000	0.0	0.0000	0.4334
8	0.0000	0.0200	0.0313	0.0556	0.3265	0.0000	0.0000	0.0	0.4334
									0.0000

$$\begin{array}{ccccccc}
 & & & & & 2.4334 & \\
 & & & & & \text{CH}_3 & \\
 2.2641 & 1.3654 & 1.4401 & 1.5034 & | & -0.6792 & \\
 S_i = I_i + \Delta I_i & & & & \text{CH}_3 - \text{CH}_2 - \text{CH}_2 - \text{CH}_2 - \text{Si} - \text{CH}_3 & 2.4334 & \\
 & & & & & | & \\
 & & & & & \text{CH}_3 & 2.4334 &
 \end{array}$$

TABLE III

LOGARITHMS OF RETENTION TIMES OF TETRA-*n*-ALKYLSILANES AND TETRA-*n*-ALKYLGERMANES AND TOPOLOGICAL INDEXES

No.	Compound ^a	$^1\chi$	$^3\chi_c$	S	TTV	Log T^b	Calc. ^c	Res. ^d
1	Me ₃ BuSi	3.5607	1.5607	-0.6782	14.3584	1.29	1.29	0.00
2	MeEt ₂ Si	3.6820	0.9286	-0.6713	14.1734	1.43	1.49	-0.06
3	Me ₂ Pr ₂ Si	4.1213	1.2071	-0.7033	17.2755	1.60	1.64	-0.04
4	Me ₂ EtBuSi	4.1213	1.2071	-0.6982	17.2958	1.61	1.64	-0.03
5	MeEt ₂ PrSi	4.1820	0.9268	-0.6973	17.2185	1.70	1.73	-0.03
6	Et ₄ Si	4.2426	0.7071	-0.6914	17.1717	1.80	1.80	0.00
7	Me ₂ PrBuSi	4.6213	1.2071	-0.7243	20.3554	1.90	1.88	0.02
8	MeEtPr ₂ Si	4.6820	0.9268	-0.7234	20.2999	1.95	1.97	-0.02
9	Et ₃ PrSi	4.7426	0.7071	-0.7174	20.2666	2.05	2.05	0.00
10	Me ₂ Bu ₂ Si	5.1213	1.2071	-0.7453	23.4573	2.15	2.12	0.03
11	MePr ₃ Si	5.1820	0.9268	-0.7494	23.4178	2.20	2.21	-0.01
12	Et ₂ Pr ₂ Si	5.2426	0.7071	-0.7434	23.3979	2.29	2.29	0.00
13	Et ₃ BuSi	5.2426	0.7071	-0.7384	23.3913	2.32	2.29	0.03
14	MePr ₂ BuSi	5.6820	0.9268	-0.7704	26.5620	2.47	2.45	0.02
15	MeEtBu ₂ Si	5.9067	1.1309	-0.7098	27.9648	2.49	2.49	0.00
16	EtPr ₃ Si	5.7426	0.7071	-0.7695	26.5656	2.52	2.53	-0.01
17	Pr ₄ Si	6.2426	0.7071	-0.7955	29.7698	2.74	2.77	-0.03
18	EtPr ₂ BuSi	6.2426	0.7071	-0.7905	29.7462	2.77	2.77	0.00
19	Et ₂ Bu ₂ Si	6.2426	0.7071	-0.7854	29.7254	2.82	2.77	0.05
20	MeBu ₃ Si	6.6820	0.9268	-0.8123	32.9167	2.99	2.93	0.06
21	Pr ₃ BuSi	7.0985	1.1154	-0.7609	33.9562	2.99	3.07	-0.08
22	EtPrBu ₂ Si	6.7426	0.7071	-0.8114	32.9489	3.03	3.01	0.02
23	Pr ₂ Bu ₂ Si	7.2426	0.7071	-0.8375	36.2088	3.24	3.25	-0.01
24	EtBu ₃ Si	7.2426	0.7071	-0.8324	36.1737	3.30	3.25	0.05
25	PrBu ₃ Si	7.7426	0.7071	-0.8584	39.4616	3.49	3.49	0.00
26	Bu ₄ Si	8.2426	0.7071	-0.8794	42.7365	3.72	3.73	-0.01
27	Me ₃ BuGe	3.5607	1.5607	-1.1086	13.4109	1.42	1.41	0.01
28	MeEt ₂ Ge	3.6820	0.9268	-1.1250	13.0229	1.57	1.61	-0.04
29	Me ₂ Pr ₂ Ge	4.1213	1.2071	-1.1597	16.1384	1.77	1.77	0.00
30	Me ₂ EtBuGe	4.1213	1.2071	-1.1503	16.1933	1.77	1.76	0.01
31	MeEt ₂ PrGe	4.1820	0.9286	-1.1632	15.9902	1.84	1.86	-0.02
32	Et ₄ Ge	4.2426	0.7071	-1.1667	15.8485	1.94	1.94	0.00
33	Me ₂ PrBuGe	4.6213	1.2071	-1.1885	19.1749	2.04	2.01	0.03
34	MeEtPr ₂ Ge	4.6820	0.9268	-1.2014	18.9886	2.09	2.10	-0.01
35	Et ₃ PrGe	4.7426	0.7071	-1.2049	18.8569	2.18	2.18	0.00
36	Me ₂ Bu ₂ Ge	5.1213	1.2071	-1.2172	22.2309	2.31	2.25	0.06
37	MePr ₃ Ge	5.1820	0.9268	-1.2396	22.0178	2.35	2.35	0.00
38	Et ₂ Pr ₂ Ge	5.2426	0.7071	-1.2431	21.8963	2.42	2.43	-0.01
39	Et ₃ BuGe	5.2426	0.7071	-1.2336	21.9310	2.45	2.42	0.03
40	MePr ₂ BuGe	5.6820	0.9268	-1.2683	25.1095	2.61	2.59	0.02
41	MeEtBu ₂ Ge	5.9067	1.1309	-1.2033	26.4804	2.64	2.63	0.01
42	EtPr ₃ Ge	5.7426	0.7071	-1.2813	24.9666	2.66	2.67	-0.01
43	Pr ₄ Ge	6.2426	0.7071	-1.3194	28.0678	2.89	2.92	-0.03
44	EtPr ₂ BuGe	6.2426	0.7071	-1.3100	28.0891	2.91	2.91	0.00
45	Et ₂ Bu ₂ Ge	6.2426	0.7071	-1.3006	28.1125	2.95	2.91	0.04
46	MeBu ₃ Ge	6.6820	0.9268	-1.3258	31.3514	3.14	3.07	0.07
47	Pr ₃ BuGe	7.0985	1.1154	-1.2926	32.1469	3.13	3.22	-0.09
48	EtPrBu ₂ Ge	6.7426	0.7071	-1.3388	31.2313	3.16	3.16	0.00
49	Pr ₂ Bu ₂ Ge	7.2426	0.7071	-1.3769	34.3810	3.38	3.40	-0.02
50	EtBu ₃ Ge	7.2426	0.7071	-1.3675	34.3930	3.40	3.40	0.00
51	PrBu ₃ Ge	7.7426	0.7071	-1.4057	37.5670	3.61	3.64	-0.03
52	Bu ₄ Ge	8.2426	0.7071	-1.4344	40.7725	3.85	3.89	-0.04

^a Me = Methyl, Et = ethyl, Pr = *n*-propyl, Bu = *n*-butyl.^b Logarithm of retention time taken from ref. 24.^c Calculated from eqn. 20.^d Residual = Log T - calc.

The intercorrelation of ${}^1\chi$ and ${}^3\chi_c$ in this equation is: $r = 0.521$, which is quite small, indicating that these variables are generally independent. In only one case was there a residual greater than twice the standard error. Eqn. 13 is a significant improvement over eqn. 12. The ${}^1\chi$ index in eqns. 12 and 13 encodes the size of the molecule and the skeletal branching. In the case of each silane molecule there are four four-atom fragments contributing to the ${}^3\chi_c$ index, each of which includes the silicon atom. The improvement obtained by adding ${}^3\chi_c$ to eqn. 12 demonstrates that the environment around the silicon atom is important in determining the retention time. Substitution of either TTV or TTR for ${}^1\chi$ in eqn. 13 gave improved results in that in no case was there a residual greater than twice the standard error. With TTV, $r = 0.999$ and $s = 0.032$, while with TTR, $r = 0.999$ and $s = 0.035$. TTV, which uses a δ value for silicon obtained from eqn. 6, and TTR, which uses a δ value for silicon obtained from eqn. 7, encode the silicon atom as well as the size and skeletal branching in the molecule. Substitution of TTS, which uses a simple δ value for silicon, for ${}^1\chi$ in eqn. 13 did not improve eqn. 13 ($r = 0.997$, $s = 0.050$).

When only the valence connectivity indexes were allowed to be candidates in the regression equation, stepwise regression gave the following two-variable equation:

$$\text{Log } T = -0.979(0.056) + 0.349(0.004){}^0\chi^v - 0.391(0.040){}^4\chi_c^v \quad (14)$$

$n = 26 \quad r = 0.999 \quad s = 0.029 \quad F = 6610$

In no case was there a residual greater than twice the standard error. The intercorrelation between ${}^0\chi^v$ and ${}^4\chi_c^v$ is: $r = 0.594$. When only the radius connectivity indexes were allowed to be candidates in the regression equation, a two-variable equation of equal quality was obtained:

$$\text{Log } T = -0.670(0.053) + 0.349(0.004){}^0\chi^r - 0.954(0.098){}^4\chi_c^r \quad (15)$$

$n = 26 \quad r = 0.999 \quad s = 0.029 \quad F = 6610$

In no case was there a residual greater than twice the standard error. The intercorrelation between ${}^0\chi^r$ and ${}^4\chi_c^r$ is: $r = 0.594$. In eqns. 14 and 15, ${}^0\chi^v$ and ${}^0\chi^r$ mostly encode atom identity and are only moder-

ately sensitive to skeletal branching; ${}^4\chi_c^v$ and ${}^4\chi_c^r$, which consist of one five-atom fragment containing the silicon atom, encode both atom identity and the environment around the silicon atom. These results further demonstrate that the structural and electronic environment around the silicon atom is important in determining the retention time.

The 26 germanes in Table III were also used in the stepwise regression procedure of the SYSTAT program. The same 20 topological indexes were used as in the case of the silanes. No compound had a zero value for any index. The following two-variable equation was obtained:

$$\text{Log } T = 0.067(0.057) + 0.481(0.006){}^1\chi - 0.230(0.034){}^3\chi_c \quad (16)$$

$n = 26 \quad r = 0.999 \quad s = 0.034 \quad F = 4633$

In two cases the residual was twice the standard error. The intercorrelation between ${}^1\chi$ and ${}^3\chi_c$ is: $r = 0.522$. Substitution of TTV or TTR for ${}^1\chi$ in eqn. 16 gave equations of higher quality. With TTV ($r = 0.999$, $s = 0.034$) in no case was there a residual greater than twice the standard error, while with TTR ($r = 0.999$, $s = 0.034$) in only one case was there a residual greater than twice the standard error.

As in the case of the silanes, when only the valence connectivity indexes were allowed to be candidates in the regression equation, an excellent two-variable equation was obtained:

$$\text{Log } T = -1.210(0.055) + 0.348(0.004){}^0\chi^v - 0.214(0.021){}^4\chi_c^v \quad (17)$$

$n = 26 \quad r = 0.999 \quad s = 0.026 \quad F = 7772$

In no case was there a residual greater than twice the standard error. The intercorrelation between ${}^0\chi^v$ and ${}^4\chi_c^v$ is: $r = 0.594$. An equation of equal quality was obtained when only the radius connectivity indexes were allowed to be candidates in the regression equation:

$$\text{Log } T = -0.529(0.049) + 0.347(0.004){}^0\chi^r - 0.880(0.089){}^4\chi_c^r \quad (18)$$

$n = 26 \quad r = 0.999 \quad s = 0.027 \quad F = 7615$

In no case was there a residual greater than twice the standard error. The intercorrelation between ${}^0\chi^r$ and ${}^4\chi_c^r$ is: $r = 0.594$. Eqns. 17 and 18 are analogous

to eqns. 14 and 15 obtained for the silanes, which is not surprising, since the silanes and germanes differ only in the nature of the metal atom.

It was of special interest to study a mixed set of the 26 silanes and 26 germanes. A mixed data set always provides a more stringent test for the adequacy of topological indexes. As in the cases of the silanes and germanes, the mixed set of 26 silanes and 26 germanes in Table III were used in the stepwise regression procedure of the SYSTAT program. The same topological indexes were included as final candidates in the regression equation, namely ${}^0\chi$, ${}^1\chi$, ${}^2\chi$, ${}^3\chi$, ${}^4\chi$, ${}^3\chi_c$, ${}^4\chi_c$, ${}^4\chi_{pc}$, the corresponding set of valence indexes, TTS, TTV, TTR and S for the metal atom for a total of 20 indexes. The following two-variable equation was obtained:

$$\text{Log } T = -0.434(0.036) + 0.478(0.007){}^1\chi + 0.022(0.002){}^3\chi^v \quad (19)$$

$n = 52 \quad r = 0.997 \quad s = 0.052 \quad F = 3521$

In two cases the residual was more than twice the standard error. The intercorrelation between ${}^1\chi$ and ${}^3\chi^v$ is: $r = -0.429$. The addition of ${}^0\chi$ to eqn. 19 lowered s to 0.035 but intercorrelation between ${}^1\chi$ and ${}^0\chi$ was unsatisfactory ($r = -0.996$).

It was desirable to obtain an equation involving the electrotopological atom index, S , to see if it could adequately encode the silicon and germanium atoms in the mixed data set. Accordingly, only the simple connectivity indexes, namely ${}^0\chi$, ${}^1\chi$, ${}^2\chi$, ${}^3\chi$, ${}^4\chi$, ${}^3\chi_c$, ${}^4\chi_c$, and ${}^4\chi_{pc}$, and the electrotopological state atom index, S , for the metal atom were allowed to be final candidates in the regression equation. The following excellent three-variable equation was obtained:

$$\text{Log } T = -0.215(0.041) + 0.468(0.004){}^1\chi - 0.228(0.023){}^3\chi_c - 0.281(0.018)S \quad (20)$$

$n = 52 \quad r = 0.999 \quad s = 0.033 \quad F = 6749$

The results of this analysis are given in Table III. In two cases the residual was more than twice the standard error. Multicollinearity is not a problem as is evidenced by the following intercorrelation results: $r = 0.212$ for S and ${}^1\chi$, $r = -0.034$ for S and ${}^3\chi_c$, and $r = 0.502$ for ${}^1\chi$ and ${}^3\chi_c$. In eqn. 20, S encodes the metal atom, ${}^1\chi$ encodes size and skeletal branching, and ${}^3\chi_c$ encodes the structural environ-

ment around the silicon atom. The replacement of ${}^1\chi$ in eqn. 20 by TTV ($r = 0.999$, $s = 0.033$) or TTR ($r = 0.999$, $s = 0.035$) gave improved results in that in no case was there a residual greater than twice the standard error. The replacement of ${}^1\chi$ in eqn. 20 by TTS gave a poorer result ($s = 0.046$).

Finally, the following excellent two-variable equation was obtained when only the valence connectivity indexes and the radius connectivity indexes were allowed to be candidates in the regression equation:

$$\text{Log } T = -1.255(0.031) + 0.371(0.003){}^0\chi^r + 0.039(0.002){}^4\chi_{pc}^v \quad (21)$$

$n = 52 \quad r = 0.999 \quad s = 0.035 \quad F = 8820$

In only one case was there a residual greater than twice the standard error. The intercorrelation between ${}^0\chi^r$ and ${}^4\chi_{pc}^v$ is: $r = -0.008$. Eqn. 21 is excellent because the two connectivity indexes are essentially orthogonal, which is an ideal result in a multivariate analysis. The problem of the non-orthogonality of descriptors has been addressed by Randić [28–31]. In eqn. 21, ${}^0\chi^r$ encodes mostly atom identity; ${}^4\chi_{pc}^v$ has several five-atom fragments contributing to it each of which contains the metal atom; it encodes the structural and electronic environment around the metal atom, further demonstrating that this environment is important in determining the retention time.

The results reported in this paper further demonstrate that molecular connectivity indexes can be successfully used to develop structure–property models for organosilicon and organogermanium compounds. The results especially demonstrate the adequacy of the new Kier–Hall electrotopological state atom index for encoding the atomic characteristics of silicon and germanium in a mixed data set. It has also been shown that the new Kier–Hall highly discriminating total topological index can be used in place of the less discriminating ${}^1\chi$ index to encode both size and skeletal branching in molecules. The adequacy of the δ^v values and δ^r values for the silicon and germanium atoms has also been demonstrated.

REFERENCES

- 1 D. H. Rouvray, *Sci. Am.*, 255 (1986) 40.
- 2 D. Bonchev, *Information Theoretic Indices for Characterization of Chemical Structures*, Wiley, New York, 1983.

- 3 N. Trinajstić, *Chemical Graph Theory*, Vol. II, CRC Press, Boca Raton, FL, 1983, pp. 105–140.
- 4 P. J. Hansen and P. C. Jurs, *J. Chem. Educ.*, 65 (1988) 574.
- 5 P. G. Seybold, M. May and U. A. Bagal, *J. Chem. Educ.*, 64 (1987) 575.
- 6 A. Sabljčić, in W. Karcher and J. Devillers (Editors), *Practical Applications of Quantitative Structure–Activity Relationships (QSAR) in Environmental Chemistry and Toxicology*, ECSC, EEC, EAEC, Brussels and Luxembourg, 1990, pp. 61–82.
- 7 L. B. Kier and L. H. Hall, *Molecular Connectivity in Chemistry and Drug Research*, Academic Press, New York, 1976.
- 8 L. B. Kier and L. H. Hall, *Molecular Connectivity in Structure–Activity Analysis*, Wiley, New York, 1986.
- 9 L. B. Kier, in S. H. Yalkowsky, A. A. Sinkula and S. C. Valvani (Editors), *Physical Chemical Properties of Drugs*, Marcel Dekker, New York, 1980, Ch. 9.
- 10 L. B. Kier, W. J. Murray, M. Randić and L. H. Hall, *J. Pharm. Sci.*, 65 (1976) 1226.
- 11 L. B. Kier and L. H. Hall, *Quant. Struct.–Act. Relat.*, 10 (1991) 134.
- 12 M. Randić, *J. Am. Chem. Soc.*, 97 (1975) 6609.
- 13 L. B. Kier and L. H. Hall, *J. Pharm. Sci.*, 70 (1981) 583.
- 14 L. B. Kier and L. H. Hall, *J. Pharm. Sci.*, 72 (1983) 1170.
- 15 L. B. Kier and L. H. Hall, *Molecular Connectivity in Structure–Activity Analysis*, Wiley, New York, 1986, pp. 15–20.
- 16 L. H. Hall and D. Aaserud, *Quant. Struct.–Act. Relat.*, 8 (1989) 296.
- 17 E. J. Kupchik, *Quant. Struct.–Act. Relat.*, 5 (1986) 95.
- 18 E. J. Kupchik, *Quant. Struct.–Act. Relat.*, 7 (1988) 57.
- 19 E. J. Kupchik, *Quant. Struct.–Act. Relat.*, 8 (1989) 98.
- 20 L. H. Hall and L. B. Kier, *Quant. Struct.–Act. Relat.*, 9 (1990) 115.
- 21 L. H. Hall, B. Mohnhey and L. B. Kier, *Quant. Struct.–Act. Relat.*, 10 (1991) 43.
- 22 L. H. Hall, B. Mohnhey and L. B. Kier, *J. Chem. Inf. Comput. Sci.*, 31 (1991) 76.
- 23 E. J. Kupchik, *Quant. Struct.–Act. Relat.*, 4 (1985) 123.
- 24 J. A. Semlyen, G. R. Walker, R. E. Blofeld and C. S. G. Phillips, *J. Chem. Soc.*, (1964) 4948.
- 25 L. Wilkinson, *SYSTAT: The System for Statistics*, SYSTAT, Evanston, IL, 1988.
- 26 D. C. Montgomery and E. A. Peck, *Introduction to Linear Regression Analysis*, Wiley, New York, 2nd ed., 1992.
- 27 S. Chatterjee and B. Price, *Regression Analysis by Example*, Wiley, New York, 2nd ed., 1991.
- 28 M. Randić, *J. Chem. Inf. Comput. Sci.*, 31 (1991) 311.
- 29 M. Randić, *New J. Chem.*, 15 (1991) 517.
- 30 M. Randić, *J. Comput. Chem.*, 12 (1991) 970.
- 31 M. Randić, *J. Chem. Educ.*, 69 (1992) 713.

Effect of variations in gas chromatographic conditions on the linear retention indices of selected chemical warfare agents

Mariitta Kokko

Department of Chemistry, University of Helsinki, Vuorikatu 20, SF-00100 Helsinki (Finland)

(First received June 18th, 1992; revised manuscript received September 23rd, 1992)

ABSTRACT

Temperature-programmed gas chromatographic retention indices, relative to *n*-alkane and *n*-alkylbis(trifluoromethyl)phosphine sulphide (M-standard) homologous series, were determined for nine chemical warfare agents using SE-54 fused-silica capillary columns. The influence of changes in the chromatographic conditions on the absolute values and on the reproducibility of the indices was evaluated. Nineteen parameters were investigated, with the purpose of discovering those most critical for the retention index monitoring of chemical warfare agents. The parameters most affecting the absolute value of the indices were the carrier gas flow-rate, the temperature programming rate and the properties of the column. Changes in conditions most strongly affected the indices of the low-volatility compounds O-ethyl S-2-(diisopropylamino)ethyl methylphosphonothioate (VX) and dibenz[*b,f*]-1,4-oxazepin (CR). The reproducibility of the indices was good in every case, even when the absolute values of the indices changed. Retention index monitoring is thus a reliable method for preliminary identification of compounds in mixtures, provided that the chromatographic system is regularly tested with a test mixture and corrections to the chromatographic conditions or the retention index library data are made where necessary.

INTRODUCTION

A reliable analytical system is needed for the international verification of chemical weapons disarmament. The Finnish Research Project on the Verification of Chemical Disarmament has been developing screening and identification methods for chemical warfare (CW) agents, their precursors and transformation or degradation products for the past 20 years. High-resolution gas chromatography with retention index monitoring (HRGC–RIM) has been selected as a primary screening technique, for several reasons: it offers separation of the sample components, location of suspected agents in a chromatogram, detection of agents containing specific heteroatoms, testing of agent purity, quantification

and an introduction method to mass (MS) and Fourier transform IR (FTIR) spectrometry for ultimate identification. The RIM method is especially valuable when hundreds of samples must be analysed, since then investigation by MS or FTIR is required only for positive samples or samples whose chromatograms are too complex to be resolved with selective detectors. The retention index window depends on the sample background; in most instances ± 2 index units is sufficient.

Linear retention indices calculated according to Van den Dool and Kratz [1] are preferred to Kováts isothermal retention indices [2] for the preliminary identification of compounds in complex sample mixtures because they allow the indices of highly volatile and less volatile compounds to be determined during a single analytical run.

Although straight-chain alkanes (C-standards) are the most widely used retention index standards, it is always preferable to employ retention index

Correspondence to: Mariitta Kokko, Department of Organic Chemistry, University of Helsinki, Vuorikatu 20, SF-00100 Helsinki, Finland.

standards that are structurally similar to the compounds of interest. Alkanes, moreover, cannot be detected with the selective detectors needed for CW agents and related compounds. For these reasons, several phosphorus-containing standard series were synthesized in the Finnish Project [3–5]. The series we have been using since 1985 is the multi-detector M-series of alkylbis(trifluoromethyl)phosphine sulphides [6], compounds that are sufficiently volatile for GC and detectable both with selective detectors [alkali thermoionization (ATD), electron capture (ECD), flame photometric (FPD) and photoionization (PID) instruments] and with the universal flame ionization detection (FID) [7]. The M-standards have proved useful in trace analysis and when the matrix is complex.

In theory, a retention index system can meet the requirements of a universal data-generating system if the indices are sufficiently reproducible. The Sadtler retention index library for capillary columns is nowadays commercially available [8]. The database, which is based on the C-standards, consists of both isothermal and linear temperature-programmed indices. The retention indices are highly reproducible so long as similar conditions are employed.

As our M-standards are not used elsewhere in the identification of CW agents, we were obliged to create our own database from the retention indices of authentic CW agents and related compounds [3,9,10]. The retention indices were determined by two-channel GC making use of two similar columns or two columns of different polarity. Columns were connected to the same injector and to two similar or two different detectors. Monitored compounds are identified using a computer program, which searches for the retention index pattern, calculates the retention indices of all peaks in the chromatogram and compares these with the indices in the database. RIM provides preliminary identification without the need for authentic compounds and it allows quantitative results from the same run.

Although retention indices have been extensively investigated, as three reviews show [11–13], few studies have dealt with the retention indices of CW agents. Moreover, in these studies, indices were determined using the on-column injection mode and relative to homologous *n*-alkanes [14–18]. An essential question for any interlaboratory screening system is whether reproducible temperature-pro-

grammed retention indices can be achieved under variable chromatographic conditions. Some aspects have been investigated [19–21], but not for CW agents and related compounds.

In this study we investigated those most critical parameters of GC conditions and laboratory setups that could be expected to affect the absolute values and reproducibility of linear HRGC retention indices of selected CW agents. The effects of the following factors were evaluated: (1) carrier gas flow-rate; (2) temperature programming rate; (3) starting point of the temperature programme; (4) multi-step temperature programming; (5) injection volume; (6) injection mode; (7) sample solvent; (8) background; (9) column length; (10) inside diameter of the column; (11) film thickness; (12) repeated use of the same column; (13) individual columns; (14) columns from different manufacturers; (15) make of instrument; (16) different operators; (17) different laboratories; (18) one or two retention index standard series in the same run; and (19) reduced number of retention index standards.

The C-series was included in the study along with the M-series not only because it is widely used but also because we wished to know of any important differences in the behaviour of the two sets of indices (I_C and I_M) under identical chromatographic conditions. The experiments in this work show that the two sets of indices can be derived from one another when the same column is used. Further, they demonstrate the essential reproducibility of retention indices and the reliability of the Project's approach to screening for CW agents.

EXPERIMENTAL

Instrumentation and chromatographic conditions

Our instruments were four Micromat HRGC 412 microcomputer-controlled gas chromatographs (HNU-Nordion) with two-channel integration and printing software, one Carlo Erba Fractovap 2900 capillary column gas chromatograph with HP 3390 A integrator and one Hewlett-Packard 5890 A gas chromatograph with HP 3392 A integrator. The accuracy of the temperature programmes of the chromatographs was checked with a Technoterm type 9500 digital instant-action thermometer.

Several different fused-silica capillary columns were employed: three 15 m × 0.32 mm I.D. cross-

linked SE-54 (5% phenyl methyl polysiloxane with 1% vinyl groups) columns with 0.25- μm film, from Orion Analytica (OA); an SE-54 column, 15 m \times 0.20 mm I.D. with 0.25- μm film, also from Orion Analytica; a DB-5 column, 30 m \times 0.32 mm I.D. with 0.25- μm film, from J & W Scientific (SE-54 type); and a cross-linked SE-54 type column, 25 m \times 0.31 mm I.D. with 0.17- μm film, from Hewlett-Packard (HP).

Standard chromatographic conditions with the 15 m \times 0.32 mm I.D. columns were as follows: injector and detector temperature (FID or ATD) 250°C; carrier gas flow-rate 2 ml/min; splitting ratio, 1:10; septum purge, 10 ml/min; starting point of the temperature programme, 40°C; temperature programming rate, 5 or 10°C/min, and end temperature of the programme, 260, 270 or 300°C, depending on the programming rate.

Chemicals

The M- and C-series provided the retention index

standard compounds for the investigation. Alkyl-bis(trifluoromethyl)phosphine sulphides, $(\text{CF}_3)_2\text{P}(\text{S})(\text{CH}_2)_n\text{CH}_3$, $n = 2-19$ (M-standards), were diluted in ethyl acetate and *n*-alkanes (C-standards) in hexane. The M-series is commercially available from HNU-Nordion. The test compounds were isopropyl methylphosphonofluoridate (sarin), 1,2,2-trimethylpropyl methylphosphonofluoridate (soman), ethyl N,N-dimethylphosphoramidocyanidate (tabun), O-ethyl S-2-(diisopropylamino)ethyl methylphosphonothioate (VX), bis(2-chloroethyl) sulphide (mustard), 2-chlorobenzalmalononitrile (CS), α -chloroacetophenone (CN) and dibenz[*b,f*]-1,4-oxazepin (CR), all obtained from the Research Centre of the Defence Forces of Finland. Not all test compounds were used in all experiments. The stock solutions of test compounds were diluted with ethyl acetate. Fresh solutions were prepared from time to time because of the slowly occurring decomposition (especially of VX). The concentration of each compound was about 50 ng/ μl .

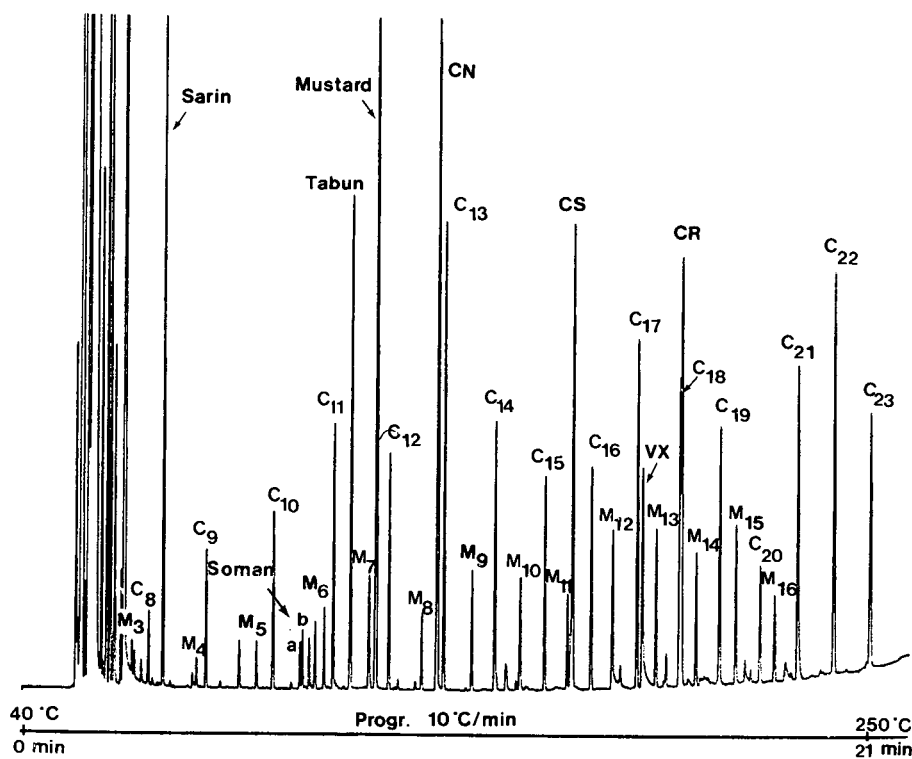


Fig. 1. Typical gas chromatogram of test compounds together with the C- and M-standards recorded under the standard chromatographic conditions: cross-linked fused-silica SE-54, 15 m \times 0.32 mm I.D., 0.25 μm ; FID, attenuation 32; split.

TABLE I
EFFECT OF CARRIER GAS FLOW-RATE ON RETENTION INDICES

Columns: cross-linked SE-54 (2), 15 m × 0.32 mm I.D., 0.25 μm; cross-linked SE-54 (3), 15 m × 0.32 mm I.D., 0.25 μm. Other conditions as in Table III.

Compound	Parameter	10°C/min									
		0.5 ml/min ^a		1.0 ml/min ^a		1.5 ml/min		2 ml/min		2.5 ml/min	
		<i>I</i>	S.D. (3 runs)	<i>I</i>	S.D. (3 runs)	<i>I</i>	S.D. (3 runs)	<i>I</i>	S.D. (3 runs)	<i>I</i>	S.D. (3 runs)
Sarin	<i>I</i> _C	823.5	0.3	823.7	0.1	—	—	—	—	—	—
	<i>I</i> _M	344.5	1.4	344.0	0.1	326.9	0.1	326.7	0.2	326.2	0.1
Tabun	<i>I</i> _C	1132.9	0.8	1132.5	0.4	1129.2	0.0	1129.9	0.3	1129.2	0.1
	<i>I</i> _M	667.9	0.7	666.9	0.4	662.3	0.1	662.0	0.4	660.9	0.1
Mustard	<i>I</i> _C	1179.0	0.6	1176.2	0.2	1172.9	0.2	1171.8	0.3	1170.6	0.1
	<i>I</i> _M	716.4	0.6	712.5	0.4	708.4	0.2	706.2	0.3	704.6	0.1
CN	<i>I</i> _C	1291.4	0.5	1287.4	0.4	1283.6	1.0	1281.4	0.1	1279.8	0.1
	<i>I</i> _M	834.6	0.9	829.2	0.4	823.7	0.4	821.0	0.0	818.8	0.2
CS	<i>I</i> _C	1564.2	0.8	1559.6	0.5	1554.4	0.2	1552.2	0.1	1550.7	0.2
	<i>I</i> _M	1116.6	0.8	1110.6	0.6	1103.8	0.2	1103.2	0.1	1100 ^c	—
VX	<i>I</i> _C	1716.3	1.0	1712.2	0.6	1705.6	0.4	1703.3	0.4	1700.0 ^d	—
	<i>I</i> _M	1272.6	1.1	1267.7	0.7	1260.5	0.4	1257.2	0.2	1255.0	1.1
CR	<i>I</i> _C	1814.8	1.4	1804.8	0.7	1793.2	0.2	1787.6	0.1	1783.7	0.5
	<i>I</i> _M	1373.9	1.3	1361.0	1.2	1350.0	0.2	1343.5	0.3	1338.7	1.3

^a Column SE-54 (3).

^b M₇ and mustard eluted together.

^c M₁₁ and CS eluted together.

^d C₁₇ and VX eluted together.

Calculations

The retention data were processed with the Project's LABOS program [22] using on-line or off-line data transfer from the chromatograph to a PDP 11/23+ computer.

Linear retention indices were calculated according to Van den Dool and Kratz's [1] equation:

$$I_{C(\text{or } M)} = 100C_n + 100(C_{n+i} - C_n) \frac{t_{R(x)} - t_{R(n)}}{t_{R(n+i)} - t_{R(n)}}$$

where C_n and C_{n+i} are carbon numbers of the C-standards (or carbon numbers of the alkyl chain of M-standards) eluted on either side of the unknown compound, $t_{R(x)}$ is the retention time of the unknown, and $t_{R(n)}$ and $t_{R(n+i)}$ are the retention times of C_n (or M_n) and C_{n+i} alkanes (or M_{n+i}), respectively.

We use linear retention indices because they are easier to calculate than the cubic spline indices [23]. They are also just as reproducible as the cubic spline indices, even though the absolute values may differ slightly.

RESULTS AND DISCUSSION

Carrier gas flow-rate

Although hydrogen is the best carrier gas from a purely chromatographic standpoint, helium was chosen as the carrier gas for safety reasons. Fig. 1 shows a typical gas chromatogram for a test mixture containing the C- and M-standards.

Flow-rates of 0.5, 1.0, 1.5, 2.0 and 2.5 ml/min were studied on 15 m × 0.32 mm I.D. columns; the exact flow-rate was measured with a soap-bubble flow meter at the starting conditions of the temper-

5°C/min					
1.5 ml/min		2 ml/min		2.5 ml/min	
<i>I</i>	S.D. (3 runs)	<i>I</i>	S.D. (5 runs)	<i>I</i>	S.D. (4 runs)
–	–	–	–	820.2	0.1
326.2	0.3	–	–	340.8	1.1
1130.3	0.7	1129.2	0.2	1129.0	0.1
661.2	0.6	658.9	0.3	657.8	0.1
1170.1	0.6	1168.5	0.3	1167.3	0.0
703.1	0.4	700.2	0.2	700.0 ^b	–
1278.8	0.2	1278.0	0.8	1274.5	0.2
816.5	0.6	814.5	0.3	811.5	0.1
1548.3	0.7	1547.7	0.5	1543.9	0.1
1096.0	0.6	1095.7	0.3	1090.3	0.2
1700.0 ^d	–	1699.4	0.4	1695.2	0.3
1251.9	0.1	1250.3	0.1	1246.8	0.2
1777.5	0.4	1774.1	0.1	1767.1	0.1
1330.8	0.4	1328.4	0.1	1319.6	0.1

ature programme. The column inlet pressure was kept constant, so that when the temperature increased in the column oven the viscosity of the carrier gas increased and the carrier gas flow-rate decreased. When the carrier gas flow-rate was increased from 1.5 to 2.5 ml/min and the temperature programming rate was 10°C/min, the retention indices of low-volatility compounds decreased more than those of high-volatility compounds [*e.g.*, CR by about 10 retention index unit (i.u.) and tabun by only 1 i.u.]. The trend was the same when the carrier gas flow-rate was increased from 0.5 to 1.0 ml/min. Although the results of the two experiments cannot properly be combined as the column was different, it is indicative that the I_M of CR was as much as 35 i.u. smaller at a flow-rate 2.5 ml/min than at 0.5 ml/min. With both programming rates the reproducibility in successive runs was good (S.D. usually 0.1–0.5 i.u.) (Table I).

Temperature programming rate

The Finnish Project uses a temperature programming rate of 10°C/min for rapid screening and characterization of samples and 5°C/min for more detailed studies. We investigated these two rates and, in addition, 2 and 8°C/min, which were used for the Sadtler capillary GC standard retention index library [8].

The retention indices increased with increase in the programming rate. The effect was only a few index units for the highly volatile compounds sarin and tabun. The effects for mustard, CN, CS and VX were all of the same magnitude and slightly greater than the effect for sarin. In contrast, the retention index of CR increased by as much as 40 i.u. when the programming rate was increased from 2 to 10°C/min (Table II). However, the reproducibility was good in every case. The influence of the programming rate on the retention indices was of the same magnitude when a small-bore column was used (Table III).

Golovnya and Uralez [24] found the effect of temperature programming rate (3, 5 and 8°C/min) on *n*-alkyl methyl ketones separated on a packed polar column to be more complicated: whereas the retention indices of low-volatility compounds increased with increase in the temperature programming rate, those of high-volatility compounds decreased.

Starting point of the temperature programme

With *n*-alkyl methyl ketones and a polar packed column, Golovnya and Uralez [24] found the values of retention indices to increase when the starting point of the temperature programme was raised from 75 to 100 and 125°C. We studied the effect on retention indices of initial oven temperatures between 30 and 45°C, the range we normally use. Sample components were dissolved in ethyl acetate so that the solvent trapping would work over the whole range. In these experiments mustard sometimes eluted together with M₇, CS with M₁₁ and VX with C₁₇.

In a first set of measurements carried out at 35, 40 and 45°C, the differences in retention index (ΔI) values due to different initial temperatures were in most instances less than 0.7 i.u. A second set of measurements (Table IV) was carried out with 30 and 40°C as the starting temperatures. The solvent

TABLE II

EFFECT OF TEMPERATURE PROGRAMMING RATE ON THE REPRODUCIBILITY OF THE RETENTION INDICES

Column: cross-linked SE-54, 25 × 0.32 mm I.D., 0.25 μm. Temperature programmes: I, 40 to 260°C at 10°C/min; II, 40 to 260°C at 8°C/min; III, 40 to 260°C at 5°C/min; IV, 40 to 260°C at 2°C/min. Other conditions as in Table III.

Compound	Parameter	I		II		III		IV		ΔI
		I	S.D. (4 runs)	I	S.D. (4 runs)	I	S.D. (3 runs)	I	S.D. (3 runs)	
Sarin	I_C	821.5	0.3	822.0	0.2	821.0	0.0	820.8	0.1	0.7
	I_M	342.9	0.2	342.7	0.1	341.5	0.0	338.7	0.1	3.1
Tabun	I_C	1130.3	0.9	1131.5	0.4	1129.3	0.1	1130.0	0.1	1.3
	I_M	664.8	0.8	665.2	0.3	661.8	0.1	658.5	0.1	6.7
Mustard	I_C	1176.2	0.7	1175.8	0.3	1171.4	0.1	1167.6	0.0	8.6
	I_M	713.2	0.5	711.8	0.1	706.2	0.1	700.0 ^a	–	13.2
CN	I_C	1287.2	0.6	1285.7	0.6	1280.5	0.1	1275.0	0.2	12.3
	I_M	829.9	0.6	827.8	0.5	820.7	0.1	811.9	0.2	18.0
CS	I_C	1559.9	0.6	1558.0	0.5	1551.4	0.1	1544.4	0.3	15.4
	I_M	1111.6	0.6	1109.0	0.4	1100.0 ^b	–	1091.1	0.4	20.5
VX	I_C	1710.2	0.2	1708.2	0.2	1702.4	0.2	1695.0	0.2	15.2
	I_M	1266.7	0.3	1264.1	0.2	1257.0	0.1	1246.7	0.2	19.9
CR	I_C	1805.7	0.4	1800.0 ^c	–	1786.8	0.1	1766.5	0.2	39.2
	I_M	1364.4	0.4	1358.0	0.2	1342.9	0.1	1319.2	0.2	45.2

^a M₇ and mustard eluted together.

^b M₁₁ and CS eluted together.

^c C₁₈ and CR eluted together.

effect more effectively retarded the elution of sarin and soman than the elution of the standards, and the retention indices of sarin and soman were higher at the 30°C starting temperature. VX eluted as a broad peak when the temperature programme was started at 40°C.

Multi-step temperature programme

Retention indices in these experiments were calculated using Van den Dool and Kratz's equation, even though the temperature programme was not linear. The effect of different multi-step temperature programmes on the test mixture is shown in Table V. M₃ eluted as a distinct peak after the solvent, and the I_M of sarin could be calculated reliably when an initial isothermal part was included in the temperature programme or the programming rate was

very slow. The results indicate the usefulness of multi-step temperature programmes in RIM analysis. Peak shapes of low-volatility compounds are improved, allowing more accurate integration, and the analysis time can be shorter. The reproducibility was as good as with a linear temperature programme.

Injection volume

Typical injection volumes in our work are 0.5–2 μl and the amounts of the test compounds are 25–50 ng. When the injection volume was increased from 0.5 to 2 μl, the ΔI values were less than 1 i.u. An injection volume of 2 μl caused a practical problem, however: M₃ and C₈ were not separated from the solvent peak and the retention indices of sarin could not be determined.

TABLE III

EFFECT OF THE PROGRAMMING RATE ON THE REPRODUCIBILITY OF THE RETENTION INDICES USING COLUMNS OF I.D. 0.32 and 0.20 mm

Instrument: Micromat HRGC 412. Columns: cross-linked SE-54 (2), 15 m × 0.32 mm I.D., 0.25 μm; cross-linked SE-54, 15 m × 0.20 mm I.D., 0.25 μm. Temperature programmes: 40 to 280°C at 10 and 5°C/min. Injector temperature, 250°C; detector temperature, 250°C; Splitting ratio, 1:10; carrier gas, helium at 2 ml/min.

Compound	Parameter	I.D. 0.32 mm					I.D. 0.20 mm				
		10°C/min		5°C/min		<i>ΔI</i>	10°C/min		5°C/min		<i>ΔI</i>
		<i>I</i>	S.D. (5 runs)	<i>I</i>	S.D. (5 runs)		<i>I</i>	S.D. (5 runs)	<i>I</i>	S.D. (5 runs)	
Tabun	<i>I_C</i>	1130.0	0.4	1129.2	0.2	0.8	1129.9	0.3	1129.3	0.7	0.5
	<i>I_M</i>	662.3	0.2	658.9	0.3	3.5	663.9	0.3	661.3	0.6	2.6
Mustard	<i>I_C</i>	1173.1	0.9	1168.5	0.3	4.6	1174.8	0.2	1170.4	0.5	4.4
	<i>I_M</i>	707.2	0.1	700.2	0.2	7.1	711.1	0.2	704.6	0.4	6.5
CN	<i>I_C</i>	1283.1	1.5	1277.9	0.8	5.2	1285.8	0.6	1279.5	0.3	6.3
	<i>I_M</i>	822.4	0.2	814.5	0.3	7.9	827.8	0.6	818.7	0.4	9.1
CS	<i>I_C</i>	1553.3	0.5	1547.7	0.5	5.6	1557.9	0.7	1550.2	0.5	7.7
	<i>I_M</i>	1104.5	0.3	1095.7	0.3	8.9	1109.0	0.6	1100.7	0.6	8.4
VX	<i>I_C</i>	1704.9	1.3	1699.4	0.4	5.5	1712.4	0.5	1703.6	0.5	8.9
	<i>I_M</i>	1258.9	0.2	1250.3	0.1	8.7	1264.2	0.3	1255.5	0.6	8.7
CR	<i>I_C</i>	1789.7	0.3	1774.1	0.1	15.7	1803.6	0.7	1783.6	0.4	19.9
	<i>I_M</i>	1346.8	0.2	1328.4	0.1	18.4	1359.2	0.7	1339.1	0.8	20.1

Injection mode

Retention indices measured with split, splitless and on-column injection modes were compared. We normally use the splitless injection mode for retention index monitoring in trace analysis; split injection is used when the sample is more concentrated. Instruments for these experiments were a Micromat HRGC 412 and Carlo Erba 2900. The Micromat is fully automated, but there is no on-column injector. In the old Carlo Erba 2900, the integrator and temperature programme are started up separately, the splitless time is measured with a stop-watch and the split valve is opened manually. The results obtained with the two instruments are not therefore fully comparable.

More solvent goes into the column in the splitless than in the split injection mode and the phase ratio of the column is temporarily changed. Whether or not the solvent has a similar effect on the sample

compounds and the retention index standards depends on the solvent and the structure of the compounds. According to Grob [25], the longer the time needed to evaporate the solvent, the greater are the retention times of compounds. Measured on the Micromat, retention indices of the test compounds were slightly greater (about 0.1–2.0 i.u.) in the splitless than in the split injection mode.

The flow-rate was slightly lower in measurements done on the Carlo Erba 2900 instrument and the indices were therefore higher than those measured on the Micromat. The retention indices were highest when measured on the Carlo Erba 2900 with the split injection mode and the 10°C/min temperature programme. With the 5°C/min temperature programme the retention indices were nearly the same with the split and splitless injection modes. At both programming rates the retention indices were smallest with on-column injection.

TABLE IV

EFFECT OF THE INITIAL TEMPERATURE (30 AND 40°C) OF THE TEMPERATURE PROGRAMME ON THE RETENTION INDICES USING DIFFERENT PROGRAMMING RATES

Column: cross-linked SE-54 (1), 15 m × 0.32 mm I.D., 0.25 μm. Temperature programmes: 30 to 300°C at 5 and 10°C/min; 40 to 300°C at 5 and 10°C/min. Other conditions as in Table III.

Compound	Parameter	5°C/min					10°C/min				
		30°C		40°C		ΔI	30°C		40°C		ΔI
		<i>I</i>	S.D. (5 runs)	<i>I</i>	S.D. (5 runs)		<i>I</i>	S.D. (5 runs)	<i>I</i>	S.D. (5 runs)	
Sarin	<i>I_C</i>	823.9	0.3	821.4	0.1	2.5	823.1	0.1	821.6	0.3	1.5
	<i>I_M</i>	351.0	0.3	341.9	0.1	9.1	345.1	0.1	—	—	—
Soman a	<i>I_C</i>	1042.8	0.6	1040.5	0.2	2.0	1041.6	0.1	1040.7	0.1	0.9
	<i>I_M</i>	568.0	0.6	566.2	0.2	1.8	568.9	0.1	568.2	0.1	0.7
Soman b	<i>I_C</i>	1047.3	0.6	1045.0	0.2	2.3	1046.0	0.1	1045.1	0.1	0.9
	<i>I_M</i>	572.8	0.6	571.1	0.2	1.7	573.7	0.1	573.0	0.1	0.7
Tabun	<i>I_C</i>	1130.5	0.5	1133.3	0.2	-2.7	1130.3	0.1	1132.6	0.4	-2.3
	<i>I_M</i>	660.1	0.4	662.7	0.2	-2.6	662.4	0.1	664.6	0.3	-2.2
Mustard	<i>I_C</i>	1168.0	0.1	1170.5	0.1	-1.5	1171.9	0.1	1173.7	0.3	-1.8
	<i>I_M</i>	700 ^a	—	702.7	0.1	—	706.4	0.1	707.9	0.2	-1.6
CN	<i>I_C</i>	1276.7	0.4	1279.4	0.1	-2.7	1281.6	0.2	1283.8	0.3	-2.1
	<i>I_M</i>	813.9	0.3	816.7	0.1	-2.8	821.4	0.1	823.7	0.3	-2.3
CS	<i>I_C</i>	1546.8	0.4	1548.8	0.2	-2.0	1553.1	0.2	1554.8	0.5	-1.7
	<i>I_M</i>	1093.9	0.5	1095.7	0.1	-1.8	1100 ^c	—	1103.6	0.5	—
VX	<i>I_C</i>	1700 ^b	—	1708.6 ^d	2.2	—	1704.0	0.8	1722.7 ^d	3.6	—
	<i>I_M</i>	1250.6	0.9	1260.2 ^d	2.2	—	1258.0	0.8	1276.4 ^d	3.7	—
CR	<i>I_C</i>	1773.2	0.4	1774.4	0.1	-1.2	1788.4	0.2	1789.8	0.2	-1.4
	<i>I_M</i>	1325.9	0.3	1327.1	0.2	-1.3	1344.3	0.2	1345.5	0.2	-1.2

^a M₇ and mustard eluted together.^b C₁₇ and VX eluted together.^c M₁₁ and CS eluted together.^d Broad peak.

Sample solvent

Solvents ethyl acetate, diethyl ether and acetone were chosen for the investigation, bearing in mind the preferred solvents for sample preparation procedures in GC analysis. Measurements with ethyl acetate and diethyl ether were done using a 35 or 40°C initial oven temperature and 10 and 5°C/min temperature programmes (Table VI), and measurements with diethyl ether and acetone using a 30°C initial temperature and 10°C/min temperature programme. The reproducibility was better for the 10°C/min temperature programme: the ΔI values

for different solvents were within the standard deviation. With the 5°C/min temperature programme the ΔI values were occasionally over 3 i.u. CR was most affected.

Background

In complex matrices, the amount of some component may be so great that it behaves like a solvent plug and temporarily alters the stationary phase. In this way it could have a reverse or normal solvent effect, respectively, on compounds that elute just before or after it [26]. Peak shifting between two

TABLE V

EFFECT OF THE MULTI-STEP TEMPERATURE PROGRAMME ON THE RETENTION INDICES

Columns: cross-linked SE-54 (I), 15 m × 0.32 mm I.D., 0.25 μm; cross-linked DB-5, 30 m × 0.3 mm I.D., 0.25 μm (DB-5 is a bonded phase from J & W Scientific corresponding to SE-54).

Temperature programmes:

I = 30°C $\xrightarrow{20^\circ\text{C}/\text{min}}$ 150°C $\xrightarrow{10^\circ\text{C}/\text{min}}$ 300°C;

II = 30°C (2 min) $\xrightarrow{10^\circ\text{C}/\text{min}}$ 150°C $\xrightarrow{5^\circ\text{C}/\text{min}}$ 250°C (5 min);

III = 30°C $\xrightarrow{1^\circ\text{C}/\text{min}}$ 32°C $\xrightarrow{2^\circ\text{C}/\text{min}}$ 35°C $\xrightarrow{5^\circ\text{C}/\text{min}}$ 40°C $\xrightarrow{10^\circ\text{C}/\text{min}}$ 100°C $\xrightarrow{15^\circ\text{C}/\text{min}}$ 200°C $\xrightarrow{20^\circ\text{C}/\text{min}}$ 250°C (10 min);

IV = 30°C $\xrightarrow{1^\circ\text{C}/\text{min}}$ 32°C $\xrightarrow{2^\circ\text{C}/\text{min}}$ 35°C $\xrightarrow{5^\circ\text{C}/\text{min}}$ 40°C $\xrightarrow{8^\circ\text{C}/\text{min}}$ 60°C $\xrightarrow{10^\circ\text{C}/\text{min}}$ 100°C $\xrightarrow{15^\circ\text{C}/\text{min}}$ 200°C $\xrightarrow{20^\circ\text{C}/\text{min}}$ 280°C (5 min).
Other conditions as in Table III.

Compound	Parameter	I ^a		II		III		IV	
		<i>I</i>	S.D. (5 runs)	<i>I</i>	S.D. (5 runs)	<i>I</i>	S.D. (5 runs)	<i>I</i>	S.D. (5 runs)
Sarin	<i>I_C</i>	823.4	0.2	823.2	0.1	824.8	0.1	824.2	0.1
	<i>I_M</i>	346.6	0.0	359.9	0.1	361.5	0.2	359.9	0.2
Soman a	<i>I_C</i>	1042.3	0.1	1041.9	0.1	1044.1	0.2	1044.1	0.1
	<i>I_M</i>	571.7	0.2	570.7	0.1	571.7	0.1	571.3	0.2
Soman b	<i>I_C</i>	1046.8	0.1	1046.4	0.1	1048.7	0.1	1048.7	0.1
	<i>I_M</i>	576.4	0.2	575.4	0.2	576.3	0.1	575.9	0.2
Tabun	<i>I_C</i>	1132.5	0.6	1131.9	0.1	1133.3	0.3	1133.6	0.2
	<i>I_M</i>	666.7	0.5	666.5	0.1	667.8	0.2	667.8	0.2
Mustard	<i>I_C</i>	1177.4	0.4	1179.2	0.1	1180.1	0.2	1179.9	0.2
	<i>I_M</i>	713.9	0.3	716.4	0.2	717.1	0.3	716.5	0.3
CN	<i>I_C</i>	1288.7	0.4	1291.3	0.1	1292.9	0.2	1292.6	0.2
	<i>I_M</i>	831.3	0.3	833.9	0.1	837.2	0.2	836.8	0.2
CS	<i>I_C</i>	1558.5	0.3	1561.4	0.2	1569.7	0.3	1569.9	0.2
	<i>I_M</i>	1110.4	0.2	1114.3	0.3	1123.5	0.3	1123.6	0.2
VX	<i>I_C</i>	1711.7	0.4	1708.6	0.3	1718.3	0.1	1718.2	0.1
	<i>I_M</i>	1266.3	0.3	1264.2	0.3	1276.3	0.2	1276.2	0.2
CR	<i>I_C</i>	1796.8	0.5	1803.6	0.5	1827.3	0.5	1828.7	0.3
	<i>I_M</i>	1353.9	0.4	1361.1	0.4	1388.2	0.4	1388.8	0.4

^a SE-54 column.

components not fully separated from each other might also occur. The retention behaviour of sarin, soman, tabun, CS and CR was studied in an air background.

An air sample extract was concentrated so that 1 μl corresponded to 0.8 m³ of air, and then diluted so that the air background was present in a ratio of 1:2:4 in three different samples. Each sample was

spiked with 500 ng each of sarin and tabun, 1.5 ng of soman and 2.5 ng of CS. The retention indices of sarin and soman were affected more ($\Delta I_M = 5.2$ and 0.9 i.u.) than those of tabun and CS (Fig. 2). Soman eluted partly together with a compound in the background. As expected, the reproducibility in successive runs was better when the amount of the air sample extract was low.

TABLE VI

EFFECT OF SOLVENT ON THE RETENTION INDICES WITH ETHYL ACETATE AND DIETHYL ETHER AS SOLVENTS

Column: cross-linked SE-54 (2), 15 m × 0.32 I.D., 0.25 μm. Temperature programmes: 35 to 280°C at 10 and 5°C/min; 40 to 280°C at 10 and 5°C/min. Other conditions as in Table III.

Compound	Parameter	35 to 280°C at 10°C/min					40 to 280°C at 10°C/min				
		Ethyl acetate		Diethyl ether		ΔI	Ethyl acetate		Diethyl ether		ΔI
		I	S.D. (3 runs)	I	S.D. (5 runs)		I	S.D. (3 runs)	I	S.D. (5 runs)	
Sarin	I_C	824.6	0.1	824.3	0.1	0.2	823.1	0.3	822.9	0.3	0.2
	I_M	—	—	—	—	—	—	—	—	—	—
Soman a	I_C	1043.3	0.1	1043.1	0.0	0.2	1042.7	0.1	1042.5	0.1	0.2
	I_M	570.3	0.1	570.1	0.1	0.3	570.1	0.1	570.0	0.1	0.2
Soman b	I_C	1047.6	0.1	1047.5	0.1	0.1	1047.1	0.1	1046.9	0.1	0.2
	I_M	575.0	0.1	574.8	0.1	0.3	574.9	0.1	574.7	0.1	0.2
Tabun	I_C	1130.4	0.2	1130.5	0.1	0.1	1130.5	0.3	1130.2	0.3	0.3
	I_M	662.5	0.2	662.6	0.1	0.1	662.8	0.3	662.4	0.3	0.4
Mustard	I_C	1171.7	0.2	1171.9	0.1	0.1	1172.0	0.2	1171.9	0.1	0.1
	I_M	706.1	0.1	706.2	0.1	0.1	706.5	0.2	706.5	0.1	0.0
CN	I_C	1281.3	0.1	1281.4	0.1	0.2	1281.5	0.2	1281.4	0.2	0.1
	I_M	821.0	0.2	821.1	0.2	0.1	821.2	0.3	1281.4	0.2	0.0
CS	I_C	1552.6	0.3	1552.8	0.2	0.2	1552.9	0.3	1552.6	0.2	0.3
	I_M	1100 ^b	—	1100 ^b	—	—	1100 ^b	—	1100 ^b	—	—
VX	I_C	1704.2	0.0	1703.9	0.3	0.2	1703.9	0.2	1700 ^c	—	—
	I_M	1258.2	0.0	1258.2	0.3	0.02	1258.0	0.2	1258.0	0.2	0.0
CR	I_C	1788.1	0.0	1788.5	0.4	0.4	1788.1	0.2	1788.2	0.3	0.1
	I_M	1343.8	0.1	1344.4	0.3	0.5	1344.0	0.2	1344.2	0.4	0.2

^a M₇ and mustard eluted together.

^b M₁₁ and CS eluted together.

^c C₁₇ and VX eluted together.

Column length

The experiments were done using a 25-m column, which was shortened by 5 m after each series of measurements, the column lengths thus studied being 25, 20 and 15 m. The absolute values of the retention indices decreased as the columns become shorter (Table VII). The decrease was small for sarin and tabun and greater for compounds with long retention times. Table VII shows that when the compound elutes near the retention index standard (VX and C₁₇ at a temperature programming rate of 5°C/min), the retention index does not change with column length. The retention index standard always interfered with the elution of a CW agent eluting

nearby, even when the concentration of the compounds was low.

Inside diameter of the column

In general, as the diameter of the column decreases the resolution increases and columns can be shorter. The capacity of the column also decreases, however. Two columns differing only in diameter (0.32 and 0.20 mm) were investigated. The average linear velocity (in cm/s) of the carrier gas was adjusted so as to be the same in the two columns. This meant that the flow-rate at the outlet was only 0.72 ml/min for the 0.20 mm I.D. column. Because such a small value is difficult to measure, we used the

35 to 280°C at 5°C/min					40 to 280°C at 5°C/min				
Ethyl acetate		Diethyl ether		ΔI	Ethyl acetate		Diethyl ether		ΔI
<i>I</i>	S.D. (5 runs)	<i>I</i>	S.D. (5 runs)		<i>I</i>	S.D. (5 runs)	<i>I</i>	S.D. (5 runs)	
—	—	823.6	0.4	—	821.2	0.1	822.2	0.4	1.0
—	—	—	—	—	—	—	—	—	—
—	—	1042.7	0.5	—	1042.8	0.1	1042.1	0.2	0.7
—	—	567.8	0.4	—	566.9	0.1	567.8	0.2	0.9
—	—	1047.2	0.5	—	1045.1	0.1	1046.5	0.2	1.4
—	—	572.7	0.4	—	571.6	0.1	572.7	0.2	1.0
1129.6	0.5	1130.1	0.2	0.6	1130.0	0.1	1129.8	0.2	0.2
659.5	0.5	659.0	0.2	0.5	660.0	0.1	658.7	0.2	1.3
1168.3	0.3	1167.7	0.1	0.6	1168.8	0.1	1167.7	0.1	1.1
700 ^a	—	700 ^a	—	—	700 ^a	—	700 ^a	—	—
1277.3	0.7	1275.6	0.2	1.7	1276.7	0.2	1275.8	0.2	0.8
814.3	0.3	812.4	0.2	1.8	814.3	0.2	812.9	0.2	1.3
1547.0	0.6	1545.3	0.6	1.7	1546.3	0.0	1545.5	0.2	0.8
1095.7	0.3	1092.0	0.7	3.7	1093.5	0.1	1092.3	0.2	1.2
1700 ^c	—	1700 ^c	—	—	1702.8	0.1	1700 ^c	—	—
1250.7	0.4	1249.3	0.6	1.4	1252.4	0.1	1249.2	0.4	3.3
1774.3	0.3	1772.3	0.6	1.9	1773.2	0.1	1771.7	0.2	1.5
1328.6	0.2	1324.6	0.6	4.0	1326.0	0.2	1324.3	0.4	1.7

retention time of propane to ensure that the velocity through the columns was the same.

The peak shapes of test compounds were slightly better with the 0.20 mm I.D. column. The reproducibility of successive runs was not as good for the small-bore column as for the 0.32 mm I.D. column. The retention indices of the test compounds were larger in the column with smaller inside diameter (see Table III).

Film thickness

Film thickness affects the column capacity. With a thinner film the indices are more susceptible to the

amount of solute. The column capacity is lower for compounds with high retention indices than for compounds with low retention indices [27,28].

On the SE-52 column, the reproducibility of retention indices for non-phosphorus CW agents is better with a thicker film. The retention indices are lower with the thinner film [29]. In our experiment, the columns of different film thickness were of the same type but from different manufacturers. The retention indices of all compounds except sarin and tabun were lower on the thinner film (0.17 μm) HP column than on the OA SE-54 (0.25 μm) column (see Table VIII).

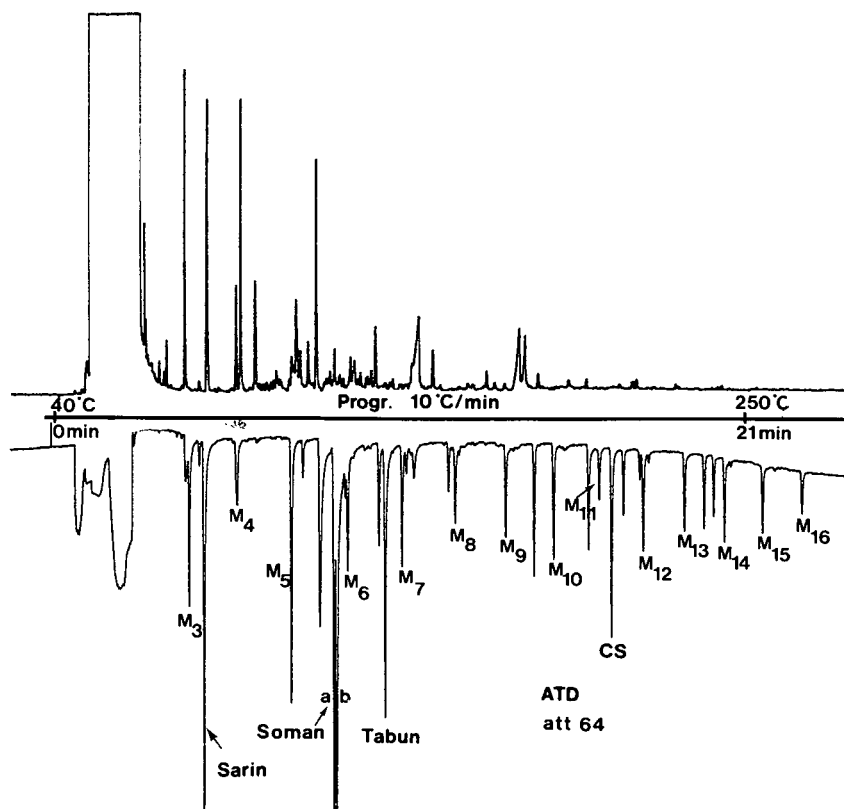


Fig. 2. Chromatogram of test mixture and M-standards with air background. Cross-linked fused-silica SE-54, 30 m \times 0.32 mm I.D., 1.0 μ m; effluent splitter; FID, attenuation 128.

Repeated use of the same column

Measurements were done over 5 months using the same individual SE-54 column and the same gas chromatograph. The column was in use most of the time for other experiments and from time to time was taken for reproducibility tests.

The properties of the column did not change much with time. However, the peak shape of VX, which is most sensitive to changes in the stationary phase, was poor in the third series of experiments. The ΔI values for different experiment series were less than 1.8 i.u., except for VX and CR, where the ΔI value was sometimes about 4 i.u. The stability of the cross-linked SE-54 column was better than that of the SE-52 and OV-1 columns used earlier. On these columns, retention indices decreased during long-term use as the film became thinner [30].

Individual columns

Our standard method for RIM analysis requires two similar or different columns attached in parallel to a common injector and two different or similar detectors. Even though two columns are attached to the same injector, the carrier gas flow-rate may be slightly different. Also, even though columns should be similar, the actual lengths, phase thicknesses or inside diameters may deviate slightly, resulting in non-identical flow.

The first experiments were made with one column installed into different detectors in different runs. In other experiments two similar individual columns were used in parallel in the same run. Retention indices for the same individual column when it was used alone and together with another similar column were within 0.8 i.u., except for tabun, where the difference was within 1.2 i.u.

TABLE VII
EFFECT OF COLUMN LENGTH ON RETENTION INDICES

Column: cross-linked SE-54, 25, 20 and 15 m \times 0.32 mm I.D., 0.25 μ m. Other conditions as in Table III.

Compound	25 m			20 m			15 m				
	10°C/min		5°C/min	10°C/min		5°C/min	10°C/min		5°C/min		
	I	S.D.	I	S.D.	I	S.D.	I	S.D.	I	S.D.	
Sarin	I_c	821.5	0.3	821.0	0.0	821.4	0.1	822.0	0.2	821.2	0.1
	I_M	342.9	0.2	341.5	0.0	342.4	0.2	342.1	0.2	340.4	0.1
Soman a	I_c	1042.4	—	—	—	1042.1	0.1	1041.4	0.1	1040.8	0.1
	I_M	572.5	—	—	—	570.8	0.1	567.9	0.1	566.9	0.1
Soman b	I_c	1046.8	—	—	—	1046.4	0.1	1046.5	0.1	1045.1	0.1
	I_M	575.9	—	—	—	575.4	0.1	572.7	0.1	571.6	0.1
Tabun	I_c	1130.3	0.9	1129.3	0.1	1130.1	0.2	1129.5	0.3	1130.0	0.1
	I_M	664.8	0.8	661.8	0.1	663.8	0.2	661.2	0.2	660.0	0.1
Mustard	I_c	1176.2	0.7	1171.4	0.1	1174.7	0.2	1170.6	0.2	1168.8	0.1
	I_M	713.2	0.5	706.2	0.1	710.8	0.2	704.7	0.2	700.0 ^a	—
CN	I_c	1287.2	0.6	1280.5	0.1	1285.0	0.1	1279.3	0.1	1276.7	0.2
	I_M	829.9	0.6	820.7	0.1	826.7	0.2	819.8	0.2	814.3	0.2
CS	I_c	1559.9	0.6	1551.4	0.1	1556.9	0.1	1549.9	0.2	1546.3	0.0
	I_M	1111.6	0.6	1100.0 ^b	—	1107.7	0.2	1100.0 ^b	—	1093.5	0.1
VX	I_c	1710.2	0.2	1702.4	0.2	1708.2	0.3	1702.7	0.1	1702.8	0.1
	I_M	1266.7	0.3	1256.9	0.1	1263.6	0.3	1254.1	0.2	1252.4	0.1
CR	I_c	1805.7	0.4	1786.8	0.1	1800.0 ^c	—	1782.6	0.3	1773.2	0.1
	I_M	1364.4	0.4	1342.9	0.1	1357.2	0.2	1337.4	0.3	1326.0	0.2

^a M₇ and mustard eluted together.

^b M₁₁ and CS eluted together.

^c C₁₈ and CR eluted together.

TABLE VIII
EFFECT ON RETENTION INDICES OF COLUMNS FROM DIFFERENT MANUFACTURERS

Column: cross-linked SE-54, 25 m × 0.32 mm I.D., 0.25 μm (Orion Analytica; OA); cross-linked 5% phenyl-methyl silicone, 25 m × 0.31 mm I.D., 0.17 μm (Hewlett-Packard; HP); DB-5, 30 m × 0.33 mm I.D., 0.25 μm (J & W Scientific; J & W). Other conditions as in Table III.

Compound	J & W			OA			HP						
	10°C/min	5°C/min	S.D.	10°C/min	5°C/min	S.D.	10°C/min	5°C/min	S.D.				
Sarin	I_C	819.5	0.8	819.5	819.5	0.4	821.5	821.0	0.0	829.0	1.8	829.0	3.3
	I_M	—	—	—	—	—	342.9	341.5	0.0	—	—	—	—
Tabun	I_C	1131.0	0.2	1130.2	1130.2	0.6	1130.3	1129.3	0.1	1132.4	0.3	1132.4	0.1
	I_M	666.4	0.2	663.2	663.2	0.5	664.8	661.8	0.1	666.1	0.4	666.1	0.2
Mustard	I_C	1178.7	0.1	1174.0	1174.0	0.3	1176.2	1171.4	0.1	1174.7	0.3	1174.7	0.2
	I_M	716.7	0.2	709.4	709.4	0.3	713.2	706.2	0.1	710.8	0.3	710.8	0.2
CN	I_C	1290.6	0.2	1284.0	1284.0	0.5	1287.2	1280.5	0.1	1285.5	0.4	1285.5	0.4
	I_M	834.2	0.2	824.8	824.8	0.5	829.9	820.7	0.1	827.1	0.5	827.1	0.3
CS	I_C	1563.5	0.2	1555.5	1555.5	0.5	1559.9	1551.4	0.1	1557.2	0.3	1557.2	0.3
	I_M	1116.3	0.2	1105.7	1105.7	0.5	1111.6	1100 ^a	—	1108.1	0.4	1108.1	—
VX	I_C	1712.6	0.1	1704.4	1704.4	0.3	1710.2	1700 ^b	—	1708.2	0.4	1708.2	—
	I_M	1269.7	0.2	1259.6	1259.6	0.3	1266.7	1256.9	0.1	1263.7	0.3	1263.7	0.7
CR	I_C	1814.3	0.4	1794.6	1794.6	0.6	1805.7	1786.8	0.1	1800 ^c	—	1800 ^c	0.2
	I_M	1373.6	0.3	1351.6	1351.6	0.6	1364.4	1342.9	0.1	1357.1	0.4	1357.1	0.7

^a M₁₁ and CS eluted together.

^b C₁₇ and VX eluted together.

^c C₁₈ and CR eluted together.

Make of column

Stationary phases and columns marketed under the same product name may have different properties. Columns of the SE-54 type with bonded phenyl methyl polysiloxane phases, purchased from J & W, HP and OA (see Experimental), were compared.

All test compounds were separated with good resolution from retention index standards at a 10 °C/min programming rate on the J & W (30 m) and OA (25 m) columns and at 5 °C/min on the J & W column. On the HP (25 m) column the peak of sarin was badly tailed and the peaks of tabun and VX were slightly tailed at both rates. Perhaps the thinner film causes wall effects to appear. The peak of VX was slightly tailed on the OA column at a programming rate of 5 °C/min.

There were no great differences in the reproducibility of successive runs on the different columns, even on the column from HP which had a thinner film (Table VIII). The absolute values of the retention indices were lower when measured on the HP column, except for sarin and tabun, which eluted slightly slower from the HP than from the OA column. This effect may be due to adsorption or different polarity of the columns. Values of retention indices obtained for the J & W column were higher than values obtained for the HP and OA columns, except for the retention indices of sarin and tabun. In part this may be because the J & W column was longer than the others.

The two sets of retention indices, I_M and I_C , showed a linear dependence on different columns. The correlation coefficients were high in each instance, however, and when I_M is known, I_C can be calculated, and *vice versa*. The linear regression equations were calculated from the results in Table VIII for the 10 °C/min temperature programme, as follows:

$$\text{OA column (25 m):} \\ I_C = 0.9656I_M + 487.2 \quad r = 0.99999$$

$$\text{J & W column (30 m):} \\ I_C = 0.9663I_M + 485.9 \quad r = 0.99999$$

$$\text{HP column (25 m):} \\ I_C = 0.9660I_M + 487.8 \quad r = 0.99999$$

Retention indices (I_C) calculated with these equations differed by 0.2–1.3 i.u. from the measured values, except for sarin, with a difference of 3.2 i.u.

Make of instrument

This study was done using two Micromat HRGC 412 instruments, a Hewlett-Packard (HP) 5890 A and a Carlo Erba Fractovap 2900. Peak shapes were good in the chromatograms obtained with all the instruments.

As all screening for CW agents involves temperature programming, it was also of interest to know exactly how the oven of the gas chromatograph used follows the temperature programme. The oven temperature of the Micromat 412 rose more slowly and that of the Carlo Erba 2900 faster than the programmed rate. The oven temperature of the HP 5890 A followed the programmed rate (10 °C/min) within $\pm 1^\circ\text{C}$, measured at the centre of the column coil. When the actual programming rate was calculated at a set value of 10 °C/min it was 9.25 °C/min for the Micromat HRGC 412 and 11 °C/min for the Carlo Erba 2900; at a set value of 5 °C/min the actual rate was 4.65 °C/min for the Micromat and 5.33 °C/min for the Carlo Erba instrument. As noted above, the retention indices of the test compounds increased when the rate of the temperature programme increased, and this may be one reason why the retention indices determined on the Hewlett-Packard and Carlo Erba instruments were slightly higher than those determined on the Micromat HRGC 412. The reproducibility, however, was good on all instruments.

Different operators

The retention indices measured by three operators on one instrument and on one individual column in most instances differed by less than 1 i.u. The slightly larger variations in the indices for CS and VX were due to the peaks not being fully separated from those of retention index standards in all runs.

Different laboratories

The reproducibility of the retention indices of the test compounds was good in three different laboratories using the same individual column (Table IX). The reproducibility was slightly better with the 10 °C/min temperature programme. ΔI values were usually less than 1 i.u. With the 5 °C/min temperature programme the ΔI value for soman was nearly 3 i.u.

TABLE IX
DIFFERENCES IN RETENTION INDICES RECORDED IN DIFFERENT LABORATORIES

Column: cross-linked SE-54 (2), 15 × 0.32 mm I.D., 0.25 μm. Other conditions as in Table III.

Compound	Parameter	10°C/min							
		Laboratory 1		Laboratory 2		Laboratory 3		Different laboratories	
		<i>I</i>	S.D. (6 runs)	<i>I</i>	S.D. (3 runs)	<i>I</i>	S.D. (6 runs)	ΔI	ΔI
Sarin	<i>I</i> _C	822.4	0.2	823.10	0.3	—	—	—	1.4
	<i>I</i> _M	—	—	—	—	—	—	—	—
Soman a	<i>I</i> _C	1042.0	0.2	1042.7	0.1	1042.4	0.3	0.7	0.7
	<i>I</i> _M	569.7	0.2	570.1	0.1	570.6	0.2	0.7	0.9
Soman b	<i>I</i> _C	1046.3	0.2	1047.1	0.1	1047.2	0.3	0.8	0.9
	<i>I</i> _M	574.4	0.2	574.9	0.1	575.3	0.3	0.7	0.9
Tabun	<i>I</i> _C	1129.6	0.1	1130.5	0.3	1130.8	0.5	1.3	1.2
	<i>I</i> _M	662.1	0.1	662.8	0.3	663.1	0.4	1.2	1.0
Mustard	<i>I</i> _C	1171.6	0.1	1172.0	0.2	1172.2	0.4	0.9	0.6
	<i>I</i> _M	706.5	0.1	706.5	0.2	706.8	0.3	0.7	0.3
CN	<i>I</i> _C	1281.0	0.1	1281.5	0.2	1281.5	0.3	0.7	0.5
	<i>I</i> _M	821.0	0.1	821.2	0.3	821.4	0.3	0.6	—
CS	<i>I</i> _C	1551.3	0.6	1552.9	0.3	1551.0	—	—	—
	<i>I</i> _M	1102.6	0.2	1104.0	0.4	1100 ^b	—	—	—
VX	<i>I</i> _C	1702.8	0.4	1703.9	0.2	1707.0	0.4	1.1	4.2
	<i>I</i> _M	1258.1	0.6	1258.0	0.2	1258.8	0.4	1.0	0.8
CR	<i>I</i> _C	1787.3	0.2	1788.1	0.2	1788.9	0.4	1.2	1.6
	<i>I</i> _M	1343.8	0.7	1344.0	0.2	1344.5	0.4	1.2	0.7

^a M₇ and mustard eluted together.

^b M₁₁ and CS eluted together.

One or two retention index standard series in the same run

The C- and M-series behaved very similarly and they did not seem to interfere with each other, with the consequence that the reproducibility of retention indices was the same whether one or both series were present in the run. The absolute values of the retention indices were nearly the same in the two instances.

Reduced number of retention index standards

The Project usually employs the internal standard method for RIM, where the retention index standards and sample compounds are present in the same mixture. In screening for a certain compound,

known to elute partially or totally overlapped with a retention index standard, it may be useful to omit this standard away. In the extreme case, the relative retention times of other compounds can be determined relative to only a single retention index standard [31].

One method for determining the relative retention times or retention indices of early eluting compounds is the calibration detector method [10,32]. A single column with effluent splitter and FID/ATD or FID/ECD detection may be used. FID is employed for detection of C-standards and ATD or ECD for detection of compounds of analytical interest. The ATD instrument is also used as a selective calibration detector for detecting M-standards,

5°C/min							
Laboratory 1		Laboratory 2		Laboratory 3		Different laboratories	
<i>I</i>	S.D. (5 runs)	<i>I</i>	S.D. (3 runs)	<i>I</i>	S.D. (5 runs)	ΔI	ΔI
821.0	0.6	821.2	0.1	—	—	—	0.2
—	—	—	—	—	—	—	—
1040.9	0.3	1042.8	0.1	1042.8	0.4	1.0	1.9
567.2	0.1	566.9	0.1	569.6	0.4	0.5	2.7
1045.2	0.3	1045.1	0.1	1047.1	0.4	1.0	2.0
572.0	0.1	571.6	0.1	574.4	0.4	1.0	2.8
1129.0	0.3	1130.0	0.1	1130.4	0.1	0.2	0.4
658.4	0.3	660.0	0.1	660.0	0.0	0.4	1.6
1167.0	0.2	1168.8	0.1	1167.8	0.4	0.8	1.0
698.4	0.1	700 ^a	—	700 ^a	—	—	—
1275.6	0.2	1276.7	0.2	1276.3	0.1	0.3	0.4
813.4	0.2	814.3	0.2	813.8	0.1	0.3	0.5
1545.0	0.3	1546.3	0.0	1545.4	0.1	0.4	1.3
1092.6	0.2	1093.5	0.1	1092.5	0.2	0.5	1.0
1703.8	0.5	1702.8	0.1	1701.8	0.7	0.3	2.0
1253.2	0.5	1252.4	0.1	1251.6	0.7	1.1	1.6
1771.9	0.3	1773.2	0.1	1773.1	0.2	0.3	1.3
1324.6	0.2	1326.0	0.2	1325.6	0.4	0.4	1.3

and FID or ECD provides analytical detection.

The absolute value of the retention index of a compound differed according to the number of standards used, but the reproducibility of retention indices was equally good whether every, every second, every third or every fourth member of the standard series was used. If the retention index library for RIM is created using every member of the standard series, wider index windows will be necessary for RIM with every second or third member of the series.

Table X presents a summary of the mean values of the retention indices of CW agents as these are affected by factors 1–3, 5, 7, 9, 10, 12, 13 and 16–18 (see Introduction). Only values recorded for the

flow-rate of 2 ml/min and programming rates of 10 and 5°C/min are included in the calculation. As can be seen, except for sarin the ΔI values were consistently less than ± 2 i.u.. Standards M₃ and C₈, which elute near sarin, also elute very near to the solvent peak.

CONCLUSIONS

The results of this work indicate that, in retention index monitoring (RIM) of the selected CW agents, the determination of retention indices is only slightly affected by the operator, different instruments from the same manufacturer with the same column in one or several laboratories, individual columns

TABLE X

THE MEAN VALUES OF RETENTION INDICES MEASURED UNDER SELECTED GAS CHROMATOGRAPHIC CONDITIONS

Instrument: Micromat HRGC 412. Column: cross-linked SE-54, 15 m × 0.32 mm I.D., 0.25 μm. For other conditions, see text.

Compound	Parameter	10°C/min		5°C/min	
		<i>I</i>	S.D.	<i>I</i>	S.D.
Sarin	<i>I_C</i>	823.5	3.9	821.6	1.1
	<i>I_M</i>	337.1	6.8	342.5	4.2
Soman a	<i>I_C</i>	1043.3	2.1	1042.2	1.0
	<i>I_M</i>	569.8	0.8	567.6	1.0
Soman b	<i>I_C</i>	1046.7	0.8	1046.1	1.1
	<i>I_M</i>	574.5	0.8	572.4	1.0
Tabun	<i>I_C</i>	1130.5	0.7	1130.0	0.9
	<i>I_M</i>	662.9	1.0	659.8	1.2
Mustard	<i>I_C</i>	1172.6	0.8	1168.7	1.0
	<i>I_M</i>	707.2	1.1	701.2	1.9
CN	<i>I_C</i>	1282.3	1.1	1277.4	1.2
	<i>I_M</i>	822.4	1.7	815.0	1.8
CS	<i>I_C</i>	1553.5	1.4	1547.4	1.4
	<i>I_M</i>	1104.2	1.8	1095.4	2.0
VX	<i>I_C</i>	1704.5	1.3	1701.9	1.5
	<i>I_M</i>	1258.7	1.0	1251.1	1.3
CR	<i>I_C</i>	1789.3	1.4	1773.7	1.1
	<i>I_M</i>	1345.4	1.9	1327.2	1.8

from the same manufacturer, different solvents (diethyl ether, acetone and ethyl acetate), use of M- and C-standards alone or together, use of a multi-step temperature programme and use of a Micromat 412 HRGC or HP 5890 A instrument. The same column could be used for 5 months without any serious deterioration in performance, except for sarin, which elutes at the beginning of the chromatogram near the solvent peak. Changes in the retention properties of the column may be due to deposition of non-volatile impurities at the column inlet. There was no significant difference in the reproducibility of one- and two-channel RIM.

The most critical parameters affecting the retention indices were the carrier gas flow-rate, the temperature programming rate and the properties of the column. The absolute values of the retention indices changed in response to these parameters anywhere from a few index units to 20–40 i.u., but

the reproducibility remained good. CR and VX were most affected in the case of nearly every parameter. Both are low-volatility compounds; CR contains aromatic rings, which means high sensitivity to temperature changes, and VX is a very large molecule. Where a compound eluted together with or very near a retention index standard, peak shifting tended to occur and the exact retention index was difficult to determine without omitting this standard.

The standard column used in this study was so short that the injection volume and the starting point of the temperature programme were important for the separation of M₃ and C₈ from the solvent peak and hence for the determination of the retention index of sarin. The background in the air sample extract strongly affected the detection of sarin and soman and longer columns are recommended for the screening of highly volatile agents.

There was no significant difference in the reproducibility of retention indices determined with the two index standard series. M-standards are relatively non-polar and on non-polar SE-54 phase behaved little differently from C-standards. Particularly the higher homologues of the M-standards behaved similarly to the C-standards. The most important property of the M-standards is that they are detectable by selective detectors at trace levels.

Overall we have found that RIM is a reliable and rapid method for the preliminary identification of CW agents, not requiring the use of authentic reference compounds provided that the chromatographic method is regularly tested with a test mixture and the chromatographic conditions or the retention index library are corrected if the deviations are too large. The retention index window ± 2 i.u. is suitable for all test compounds except VX and CR, for which a larger window of ± 5 i.u. may be necessary. The ultimate identification must, of course, be confirmed by another independent technique such as MS or FTIR.

ACKNOWLEDGEMENTS

The author thanks Maarit Enqvist for skilful technical assistance and Jouni Enqvist for valuable discussions. Thanks are due to Anneli Hesso and Merja Heinonen for their cooperation in the inter-laboratory comparison experiments.

REFERENCES

- H. van den Dool and P. D. Kratz, *J. Chromatogr.*, 11 (1963) 463.
- E. Kováts, *Helv. Chim. Acta*, 41 (1958) 1915.
- J. Enqvist, A. Hesso and H. Piispanen, in J. Enqvist (Editor), *Identification of Potential Organophosphorus Warfare Agents, B.1, An Approach for the Standardization of Techniques and Reference Data*, Ministry for Foreign Affairs of Finland, Helsinki, 1979, p. 28.
- A. Hesso, A. Manninen, in J. Enqvist (Editor), *Trace Analysis of Chemical Warfare Agents. C.1. An Approach to the Environmental Monitoring of Nerve Agents*, Ministry for Foreign Affairs of Finland, Helsinki, 1981, p. 67.
- A. Manninen, in M. Rautio (Editor), *Technical Evaluation of Selected Scientific Methods for the Verification of Chemical Disarmament*, Ministry for Foreign Affairs of Finland, Helsinki, 1984, p. 42.
- M. Kokko, M. Pajarinen and J. Enqvist, in M. Rautio (Editor), *Air Monitoring as a Means for Verification of Chemical Disarmament. C.2. Development and Evaluation of Basic Techniques, Part I*, Ministry for Foreign Affairs of Finland, Helsinki, 1985, p. 207.
- A. Manninen, M.-L. Kuitunen and L. Julin, *J. Chromatogr.*, 394 (1987) 465.
- J. F. Sprouse and A. Varano, *Int. Lab.*, 14 (1984) 54.
- J. Enqvist and A. Hesso, *Kem. Kemi*, 9 (1982) 176.
- J. Enqvist, P. Sunila and U.-M. Lakkisto, *J. Chromatogr.*, 279 (1983) 667.
- M. V. Budahegyi, E. R. Lombosi, T. S. Lombosi, G. Tarjan, I. Timar and J. M. Takacs, *J. Chromatogr.*, 271 (1983) 213.
- M. B. Evans and J. K. Haken, *J. Chromatogr.*, 472 (1989) 93.
- L. G. Blomberg, *Adv. Chromatogr.*, 26 (1987) 229.
- P. A. D'Agostino and L. R. Provost, *J. Chromatogr.*, 331 (1985) 47.
- P. A. D'Agostino, A. S. Hansen, P. A. Lockwood and L. R. Provost, *J. Chromatogr.*, 347 (1985) 257.
- P. A. D'Agostino, L. R. Provost and J. Visenti, *J. Chromatogr.*, 402 (1987) 221.
- P. A. D'Agostino and L. R. Provost, *J. Chromatogr.*, 436 (1988) 399.
- J. R. Hancock and G. R. Peters, *J. Chromatogr.*, 538 (1991) 249.
- H. Knöppel, M. De Bortoli, A. Peil and H. Vissers, *J. Chromatogr.*, 279 (1983) 483.
- T. Wang and Y. Sun, *J. Chromatogr.*, 407 (1987) 79.
- H. F. Yin and Y. L. Sun, *Chromatographia*, 29 (1990) 39.
- L. Koskinen and P. Sunila, in J. Enqvist (Editor), *Systematic Identification of Chemical Warfare Agents. B.3. Identification of Non-Phosphorus Warfare Agents*, Ministry for Foreign Affairs of Finland, Helsinki, 1982, p. 100.
- W. A. Halang, R. Langlais and E. Kugler, *Anal. Chem.*, 50 (1978) 1829.
- R. V. Golovnya and V. P. Uralez, *J. Chromatogr.*, 36 (1968) 276.
- K. Grob, Jr., *J. Chromatogr.*, 253 (1982) 17.
- W. Jennings, *Gas Chromatography with Glass Capillary Columns*, Academic Press, New York, 2nd ed., 1980, p. 58.
- T. Wang and Y. Sun, *J. High Resolut. Chromatogr. Chromatogr. Commun.*, 10 (1987) 603.
- H. F. Yin, Y. Zhu and Y. L. Sun, *Chromatographia*, 28 (1989) 502.
- T. Juutilainen, in J. Enqvist (Editor), *Systematic Identification of Chemical Warfare Agents. B.3. Identification of Non-Phosphorus Warfare Agents*, Ministry for Foreign Affairs of Finland, Helsinki, 1982, p.35.
- M. Kokko, in J. Enqvist (Editor), *Systematic Identification of Precursors of Warfare Agents, Degradation Products of Non-Phosphorus Agents, and Some Potential Agents*, Ministry for Foreign Affairs of Finland, Helsinki, 1983, p.38.
- J. Enqvist, A. Hesso and H. Piispanen, in J. Enqvist (Editor), *Identification of Potential Organophosphorus Warfare Agents, B.1, An Approach for the Standardization of Techniques and Reference Data*, Ministry for Foreign Affairs of Finland, Helsinki, 1979, p. 99.
- M. Kokko, in J. Enqvist (Editor), *Systematic Identification of precursors of Warfare Agents, Degradation Products of Non-Phosphorus Agents, and Some Potential Agents*, Ministry for Foreign Affairs of Finland, Helsinki, 1983, p. 43.

Relationship between Kováts retention indices and molecular connectivity indices of tetralones, coumarins and structurally related compounds

Ana C. Arruda, Vilma E. F. Heinzen and Rosendo A. Yunes

Departamento de Química, Universidade Federal de Santa Catarina, 88040-900 Florianópolis, Santa Catarina (Brazil)

(First received June 2nd, 1992; revised manuscript received August 18th, 1992)

ABSTRACT

A study was undertaken to test the ability of several molecular connectivity indices to predict the retention indices (I) of tetralones, coumarins and structurally related compounds determined on OV-17 and Apiezon L as stationary phases. The regression analyses with I_{OV-17} showed that a two-variable linear regression equation with ${}^2\chi$ and ${}^4\chi'_{pc}$ gives the best correlation coefficient, suggesting that retention depends basically on branching and the presence and number of adjacent atoms, and secondarily on unsaturations and the number and orientation of substituents. I_{ApL} gives the best correlation with a two-variable linear regression equation with ${}^1\chi$ and ${}^3\chi'_p$ indicating that on this stationary phase retention depends basically on the presence and number of adjacent atoms, and secondarily on unsaturation, branching of adjacent atoms and the presence of heteroaroms. ΔI ($\Delta I = I_{OV-17} - I_{ApL}$), according to the different polarities of both phases, considered to be a measure of the polar forces in retention, does not give a good correlation.

INTRODUCTION

Over the last few years, many workers have observed a good correlation between experimental retention indices and topological indices, such as the molecular connectivity index, first introduced by Randić [1] and later developed and extensively used by Kier [2].

With the discovery of topological indices, the capacity for the prediction of the chemical properties of substances is now becoming a reality. Although still in its early stages, it can already claim substantial success in a broad range of applications.

Thus, the topological method can be used to predict physico-chemical properties [2], chromatographic retention indices [3–8] and the extent to which various pollutants might spread in the environment and the harm they might do once they

have spread [9–11]. It can also be used to develop new anaesthetics and psychoactive drugs [12].

Kier [2] has shown good correlations between connectivity indices and psycho-chemical properties, such as density, boiling point and water solubility, and also molecular surface area for a series of alkanes.

Szász *et al.* [13] demonstrated the relationship between the partition data obtained by gas-liquid chromatography and molecular connectivity indices of derivatives of pyrido [1,2-*a*]pyrimidin-4-one. Szász *et al.* [14] also verified that the molecular connectivity indices can be used quantitatively to describe the gas chromatographic retention indices of a series of derivatives of pyrido[2,1-*a*]pyrimidine and pyrido[2,1-*b*]quinazoline. Sabljic [15] has shown that high correlation coefficients and a correct elution sequence are necessary for predicting retention indices.

This work was carried out to test the ability of the molecular connectivity method in predicting the Kováts retention indices (I) of tetralones and sub-

Correspondence to: R. A. Yunes, Departamento de Química, Universidade Federal de Santa Catarina, 88040-900 Florianópolis, Santa Catarina, Brazil.

stituted coumarins, using both correlation coefficients and correctly predicted elution sequence as criteria of fit, and also to determine the structural factors that are important in the chromatographic behaviour of the compounds studied.

EXPERIMENTAL

Samples

The tetralones, coumarins, tetrahydronaphthalene and monocyclic compounds studied are indicated in Table I. Most of them were obtained commercially and the others were synthesized.

TABLE I

EXPERIMENTAL RETENTION INDICES AND ΔI VALUES AT 170°C FOR TETRALONES, COUMARINS AND STRUCTURALLY RELATED COMPOUNDS ON NON-POLAR (APIEZON L) AND POLAR (OV-17) STATIONARY PHASES

No. Compound	Retention index (<i>I</i>)		ΔI
	OV-17	Apiezon L	
1 Cyclohexane	757	—	—
2 Methylcyclohexane	793	—	—
3 Benzene	774	—	—
4 Toluene	887	—	—
5 Cyclohexanone	1080	—	—
6 Methoxybenzene	1085	—	—
7 Tetrahydro-4 <i>H</i> -pyran-4-one	1088	—	—
8 δ -Valerolactone	1107	—	—
9 2-Methylcyclohexanone	1119	—	—
10 4-Methylcyclohexanone	1144	—	—
11 3-Methylcyclohexanone	1155	—	—
12 Tetrahydronaphthalene	1348	—	—
13 2-Coumarone	1501	1289	212
14 4-Chromanone	1621	1390	231
15 β -Tetralone	1625	1503	122
16 α -Tetralone	1645	1458	187
17 2-Methyl-1-tetralone	1667	1492	175
18 1-Methyl-2-tetralone	1669	1479	190
19 Dihydrocoumarin	1682	1434	248
20 4-Methyl-1-tetralone	1688	1514	174
21 Coumarin	1758	1521	237
22 6-Methylcoumarin	1863	1618	245
23 7-Methoxy-1-tetralone	1897	1666	232
24 7-Methoxy-2-tetralone	1903	1680	223
25 5-Methoxy-1-tetralone	1905	1690	219
26 6-Methoxy-2-tetralone	1910	1711	199
27 6-Methoxy-1-tetralone	1970	1820	162
28 7-Methoxycoumarin	2056	1798	258
29 4-Methoxycoumarin	2085	1844	241
30 7-Methoxy-4-methylcoumarin	2214	2021	193

The solutions were prepared with carbon tetrachloride at concentrations lower than 200 $\mu\text{g/ml}$, with the exception of δ -valerolactone, prepared with methyl ethyl ketone, and 7-methoxy-4-methylcoumarin, prepared with methanol. In the solutions of β -tetralone, 6-methoxy-2-tetralone and 7-methoxy-2-tetralone, ascorbic acid was utilized as an antioxidant and the solution was saturated with nitrogen.

Methods

Samples (1.0 μl) were injected into a gas chromatograph equipped with a flame ionization detector. A glass column (1.8 m \times 3.2 mm I.D.) packed with 3% OV-17 on Chromosorb W AW DMCS (80–100 mesh) and two nickel columns, one (1.8 m \times 3.2 mm I.D.) with 15% Apiezon L on Chromosorb W and the other (5.5 m \times 5.3 mm I.D.) with 3% OV-17 on Chromosorb W, were utilized. The samples (monocyclic compounds) that have low boiling points and consequently short retention times were studied with the longer nickel column. The carrier gas was nitrogen at a flow-rate of 30 ml/min in all instances.

Conditions that gave symmetrical chromatograms were selected. The temperature range using the OV-17 columns was 170–210°C for tetralones, 210–250°C for substituted coumarins, 170–200°C for tetrahydronaphthalene, 6-methylcoumarin and un-substituted aromatic lactones and 80–140°C for different monocyclic compounds. Using Apiezon L columns the ranges were 210–230°C for tetralones, 220–280°C for some methoxytetralones and substituted coumarins and 170–232°C for un-substituted aromatic lactones and 6-methylcoumarin. The measurements were made at four different temperatures in order to decrease the errors in extrapolations. For the same reason, 170°C was chosen for extrapolation of the *I* values on OV-17 because it is located between the ranges of temperatures utilized to determine the volatile (80–140°C) and slightly volatile compounds (210–280°C).

Calculation

The connectivity indices ${}^1\chi$, ${}^2\chi$, ${}^3\chi_p$, ${}^4\chi_p$, ${}^3\chi_{pc}$, ${}^4\chi_{pc}$, ${}^1\chi^v$, ${}^2\chi^v_p$, ${}^3\chi^v_c$ and ${}^4\chi^v_{pc}$ were calculated by the method of Kier [2] utilizing a Molconn-X computer program for molecular topology analysis. They are given in Table II.

TABLE II
CONNECTIVITY INDICES OF TETRALONES, COUMARINS AND STRUCTURALLY RELATED COMPOUNDS

No. ^a	Connectivity index										
	$^1\chi$	$^2\chi$	$^3\chi_p$	$^4\chi_p$	$^3\chi_{pc}$	$^4\chi_{pc}$	$^1\chi^v$	$^2\chi^v$	$^3\chi_p^v$	$^3\chi_c^v$	$^4\chi_{pc}^v$
1	3.0000	2.1213	1.5000	1.0607	—	—	3.0000	2.1213	2.1213	—	—
2	3.3938	2.7432	1.8938	1.3067	0.2887	0.4082	3.3938	2.7432	1.8938	0.2887	0.4082
3	3.0000	2.1213	1.5000	1.0607	—	—	2.0000	1.1547	0.6667	—	—
4	3.3938	2.7432	1.8938	1.3067	0.2887	0.4082	2.4107	1.6547	0.9405	0.1667	0.1924
5	3.3938	2.7432	1.8938	1.3067	0.2887	0.4082	2.9112	2.0993	1.4111	0.1020	0.1443
6	3.9319	2.9123	2.3021	1.5954	0.2041	0.4928	2.5231	1.5172	0.9789	0.0680	0.1466
7	3.3938	2.7432	1.8938	1.3067	0.2887	0.4082	2.4886	1.6510	1.0505	0.1020	0.1443
8	3.3938	2.7432	1.8938	1.3067	0.2887	0.4082	2.5505	1.6776	1.0383	0.0589	0.0833
9	3.8045	3.2388	2.5403	1.5017	0.4714	1.1381	3.3319	2.6131	1.8600	0.2875	0.5732
10	3.7877	3.3650	2.3045	1.4267	0.5773	0.8165	3.3048	2.7212	1.8320	0.3907	0.5526
11	3.7877	3.3764	2.1986	1.7374	0.5773	0.7416	3.3051	2.7402	1.7287	0.3907	0.4796
12	4.9663	4.0891	3.4663	2.8576	0.3333	0.9428	4.0345	2.9758	2.2606	0.2041	0.5244
13	4.4663	3.7355	3.2163	2.6868	0.3333	0.9428	2.8892	1.9584	1.3616	0.1423	0.3144
14	5.3770	4.6166	3.9332	3.2600	0.5384	1.4402	3.6278	2.5178	1.7742	0.2033	0.4612
15	5.3602	4.7228	3.8019	3.1081	0.6220	1.2920	3.9457	2.9842	2.1792	0.3062	0.6264
16	5.3770	4.6166	3.9332	3.2600	0.5384	1.4402	3.9886	2.9339	2.1677	0.2464	0.5847
17	5.7877	5.1214	4.5336	3.4488	0.7309	2.0673	4.4093	3.4611	2.5771	0.4373	0.9403
18	5.7877	5.1214	4.5336	3.4488	0.7309	2.0673	4.3933	3.3868	2.6453	0.4131	1.0295
19	5.3602	4.7228	3.8019	3.1081	0.6220	1.2920	3.6468	2.5818	1.7949	0.2199	0.4420
20	5.7877	5.1441	4.4140	3.5552	0.7436	1.9455	4.4093	3.4501	2.5965	0.4318	0.9787
21	5.3602	4.7228	3.8019	3.1081	0.6220	1.2920	3.3504	2.2923	1.5285	0.1904	0.3617
22	5.7540	5.3566	4.1374	3.3585	0.9107	1.6411	3.7605	2.7957	1.7748	0.3570	0.5348
23	6.3089	5.4189	4.6993	3.7013	0.7426	1.8888	4.5116	3.2998	2.4674	0.3144	0.7204
24	6.2920	5.5257	4.5612	3.5967	0.8261	1.7367	4.4687	3.3501	2.4742	0.3742	0.7599
25	6.3257	5.3351	4.7200	3.9462	0.6745	1.9348	4.5176	3.2631	2.4840	0.2917	0.7470
26	6.2920	5.5257	4.5612	3.5918	0.8261	1.7367	4.4687	3.3501	2.4742	0.3742	0.7599
27	6.3089	5.4184	4.6925	3.7526	0.7426	1.8849	4.5116	3.2996	2.4628	0.3144	0.7181
28	6.2920	5.5257	4.5612	3.5967	0.8261	1.7367	3.8735	2.6582	1.8303	0.2584	0.4985
29	6.3089	5.4526	4.5080	3.9237	0.7581	1.7496	3.8794	2.6300	1.8319	0.2381	0.5109
30	6.7027	6.0651	4.4374	4.1981	1.0313	2.1660	4.2901	3.1105	2.1585	0.3916	0.7662

^a See Table I.

To test the quality of the regression equation, the following statistical parameters were used: correlation coefficient (r), test of the null hypothesis (F -test) and Student's t -test. All calculations of single and multiple linear regression analyses were carried out on an IBM PC/XT computer.

The Ambrus [16] method was used to calculate the dead time for each column in order to obtain the adjusted retention indices that were used in all the correlations.

Experimental retention times are averages of three sample injections.

RESULTS AND DISCUSSION

It was observed that the relationship between the retention index of non-polar substances and temperature on a non-polar stationary phase is linear. However, on polar stationary phases and with different kinds of compounds, it is not linear. Thus Hoigné *et al.* [17] demonstrated that over large temperature ranges the retention index is a hyperbolic function. In this work, extrapolations were done in some instances assuming that the range of linearity will be large, considering the low polarity of the

compounds and of the stationary phases (OV-17, Apiezon L).

The adjusted retention indices obtained on the OV-17 column show excellent linearity with temperature, with correlation coefficients greater than 0.9700, over the range of experimental temperatures.

On the non-polar stationary phase (Apiezon L) the correlation coefficients are greater than 0.9800, with the exception of 4-methoxycoumarin ($r = 0.9686$), 4-chromanone ($r = 0.9666$) and 7-methoxy-4-methylcoumarin ($r = 0.9568$).

The values of the I adjusted or extrapolated to 170°C on the OV-17 and Apiezon L columns are given in Table I.

Application of the molecular connectivity method

Simple linear correlation. The best single linear regression equations between the I values on the polar OV-17 stationary phase for the 30 compounds studied and the connectivity indices were obtained with ${}^1\chi$ and ${}^2\chi$, as indicated by eqns. 1 and 2 and their statistical parameters:

$$I_{OV-17} = 341.1620 {}^1\chi - 188.8422$$

$$r = 0.9751, F = 541.92 (P > 0.0001), r^2 = 0.9509 \quad (1)$$

$$I_{OV-17} = 347.5188 {}^2\chi + 27.6842$$

$$r = 0.9769, F = 586.09 (P > 0.0001), r^2 = 0.9544 \quad (2)$$

It should be noted that ${}^1\chi$, which conveys more information about the number of atoms in a molecule, was not able to discriminate among 8 groups of compounds in a total of 23 compounds (3 groups of 2 compounds, 4 groups of 3 compounds and 1 group of 5 compounds) and ${}^2\chi$, which encodes more information about branching, among 7 groups of compounds in a total of 19 compounds (4 groups of 2 compounds, 2 groups of 3 compounds and 1 group of 5 compounds).

The inability of these indices to discriminate between such a number of compounds shows that they are not appropriate for the effective prediction of experimental retention indices considering Sabljic and Protic's criteria [11].

When the single linear regression equation is applied for the retention indices, I_{OV-17} of bicyclic compounds numbered from 12 to 30 (19 substanc-

es), the correlation coefficients with ${}^1\chi$ ($r = 0.8955$) and with ${}^2\chi$ ($r = 0.8999$) are lower than that corresponding to the 30 compounds.

On the non-polar phase Apiezon L, a single linear regression equation between the retention indices of bicyclic compounds numbered from 13 to 30 (18 substances) and the different connectivity indices studied gives low correlation coefficients, ${}^1\chi$ ($r = 0.9046$) and ${}^2\chi$ ($r = 0.8932$).

When the ΔI values ($I_{OV-17} - I_{ApL}$), for the compounds numbered from 13 to 30 are correlated with the above-indicated molecular connectivity indices, the correlation coefficients are very low. ΔI is considered to be a measure of the polar forces in chromatographic retention. ΔI does not measure the dispersion forces because these are considered to be the same on polar and non-polar phases. Hence the low correlation with ΔI suggests that the connectivity indices basically give information about the dispersion forces that act on the chromatographic retention. This has also been observed by other workers [11].

Multiple linear correlation. Despite the high values of the correlation coefficient obtained with ${}^1\chi$ and ${}^2\chi$ through a simple linear regression equation, the lack of discrimination among many compounds makes them incapable of determining the correct elution sequence. Consequently, two-variable regression equations, which give a more complete representation of the molecules, were tested to find the best equations able to discriminate all the compounds and predict their correct elution.

A correlation matrix was applied to select the connectivity indices, and the scatterplot method was used to define the type of function that relates the retention to the connectivity indices.

The best two-variable regression equation for I_{OV-17} of the 28 compounds and its statistical parameters was

$$I_{OV-17} = 425.0345 {}^2\chi - 422.5803 {}^4\chi_{pc}^v - 75.2959$$

$$r = 0.9882, F ({}^2\chi) = 633.63 (P > 0.0001)$$

$$r^2 = 0.9765, F ({}^4\chi_{pc}^v) = 36.46 (P > 0.0001) \quad (3)$$

The connectivity indices ${}^2\chi$ and ${}^4\chi_{pc}^v$ do not distinguish cyclohexanone from tetrahydro-4H-pyran-4-one because the connectivity index ${}^2\chi$ does not encode information about heteroatoms, and they do not distinguish 7-methoxy-2-tetralone from

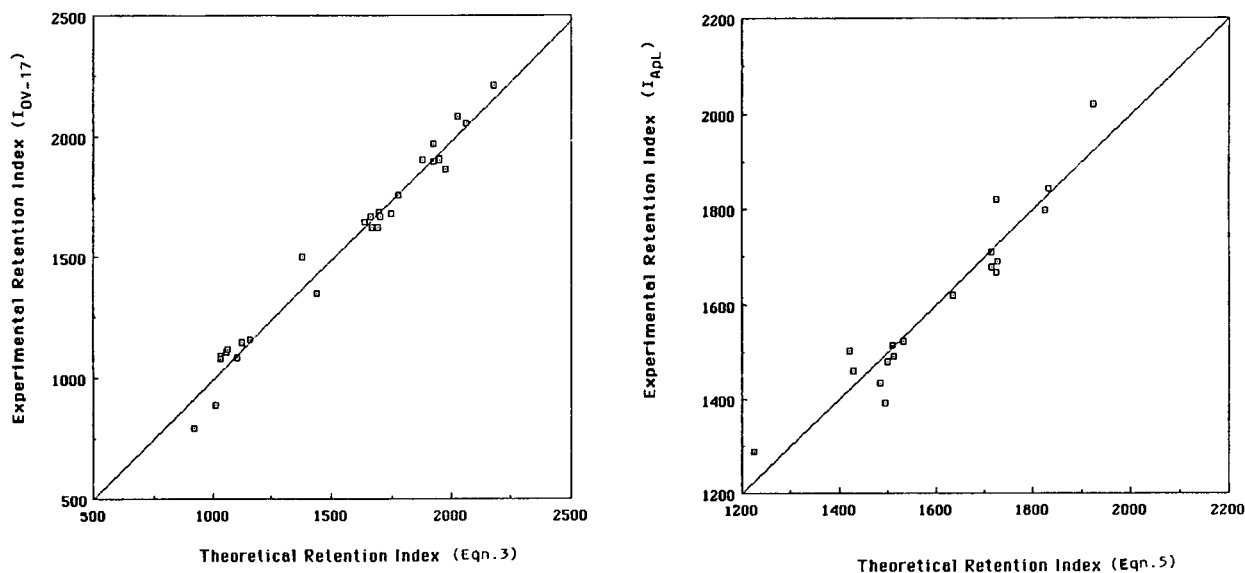


Fig. 1. Correlation between experimental I_{OV-17} and I_{ApL} values and calculated retention indices (eqns. 3 and 5) for tetralones, coumarins and structurally related compounds.

6-methoxy-2-tetralone owing to the inability of the connectivity index ${}^4\chi_{pc}^v$ to distinguish this kind of isomer.

For the bicyclic compounds (19 compounds) the two-variable regression equation for I_{OV-17} with ${}^2\chi$ and ${}^4\chi_{pc}^v$ is

$$I_{OV-17} = 425.6130 {}^2\chi - 431.2538 {}^4\chi_{pc}^v - 87.2267$$

$$r = 0.9651, F({}^2\chi) = 211.05 (P > 0.0001)$$

$$r^2 = 0.9315, F({}^4\chi_{pc}^v) = 28.36 (P > 0.0001)$$

(4)

As can be observed from eqns. 3 and 4 relative to eqns. 1 and 2, the chromatographic retention of the molecules studied depends basically on the presence and the number of adjacent atoms, and secondarily on the unsaturation and the number and orientation of substituents. The addition of these last factors gives a better differentiation of the compounds.

The best two-variable regression equation for I_{ApL} of 18 bicyclic compounds is with ${}^1\chi$ and ${}^3\chi_p^v$ (eqn. 5) considering the correlation coefficient and the discrimination of the compounds. It does not distinguish 7-methoxy-2-tetralone from 6-methoxy-2-tetralone.

$$I_{ApL} = 372.1000 {}^1\chi - 170.3856 {}^3\chi_p^v - 203.3994$$

$$r = 0.9548, F({}^1\chi) = 144.26 (P > 0.0001)$$

$$r^2 = 0.9263, F({}^3\chi_p^v) = 15.87 (P > 0.0012)$$

(5)

A graphical representation of the fit between the experimental I_{OV-17} and I_{ApL} values and those calculated by eqns. 3 and 5 is shown in Fig. 1.

The correlation between $\Delta I = (I_{OV-17} - I_{ApL})$ through the multiple linear regression equation, with two connectivity indices, did not show statistically acceptable correlation coefficients.

CONCLUSIONS

The retention indices showed good correlation coefficients through a simple linear correlation equation with some molecular connectivity indices (${}^1\chi$, ${}^2\chi$). However, the inability of these indices to discriminate among many compounds makes these correlations inadequate for predicting the correct elution sequence of the compounds.

In order to discriminate better between the compounds studied a two-variable linear regression equation that gives a more complete representation of the molecules was applied. The correlation coefficients and the capacity for discrimination were improved in all instances. The best correlation for I_{OV-17} was found with ${}^2\chi$ and ${}^4\chi_{pc}^v$, showing that branching, unsaturation and the presence and orientation of the substituents in the aromatic rings are important factors in differentiating the retention

indices of the compounds. ${}^2\chi$ and ${}^4\chi_{pc}^v$ fail to distinguish only two compounds among 30 compounds analyzed.

The best correlation for I_{ApL} was found with ${}^1\chi$ and ${}^3\chi_p^v$, showing in this instance that the presence and the number of adjacent atoms are the main factors in the retention and the unsaturation and the presence of heteroatoms are secondary factors.

The correlations of the ΔI values with the connectivity indices are not statistically acceptable with either simple or two-variable linear regression equations. As ΔI is a measure of the polar forces in the retention, it can be concluded that the connectivity indices basically give information about the dispersion forces in retention.

ACKNOWLEDGEMENTS

The authors thank CNPq (Brazil) for financial support and also Professors Pedro A. Barbetta and José Francisco Fletes of the Departamento de Ciências Estatísticas e da Computação (UFSC) for useful discussions of the statistical methods.

REFERENCES

- 1 M. Randić, *J. Am. Chem. Soc.*, 97 (1975) 6609.
- 2 L. B. Kier, in S. H. Yakowsky, A. Sinkula and S. C. Valvani (Editors), *Physical Chemical Properties of Drugs*, Marcel Dekker, New York, 1980, Ch. 9, p. 277.
- 3 A. Robbat, Jr., G. Xyrafas and D. Marshall, *Anal. Chem.*, 60 (1988) 982.
- 4 K. Heberger, *Chromatographia*, 25 (1988) 725.
- 5 V. A. Gerasimento and V. M. Nabivach, *J. Chromatogr.*, 498 (1990) 357.
- 6 M. Kuchar, H. Tomková, V. Rejholec and D. Slalicka, *J. Chromatogr.*, 333 (1985) 21.
- 7 O. Papp, Gy. Szász, M. Farkas, G. Simon and I. Hermecz, *J. Chromatogr.*, 403 (1987) 19.
- 8 M. N. Hasan and P. C. Jurs, *Anal. Chem.*, 62 (1990) 2318.
- 9 A. Sabljic, *Z. Gesamte Hyg. Ihre Grenzgeb.*, 33 (1987) 493.
- 10 R. Koch, *Toxicol. Environ. Chem.*, 6 (1983) 87.
- 11 A. Sabljic and M. Protic, *Chem. Biol. Interact.*, 42 (1982) 301.
- 12 L. B. Kier and R. L. Hall, *J. Med. Chem.*, 20 (1977) 1631.
- 13 G. Szász, K. Valkó, O. Papp and I. Hermecz, *J. Chromatogr.*, 243 (1982) 347.
- 14 G. Szász, O. Papp, J. Vámos, K. Hankó-Novák and L. B. Kier, *J. Chromatogr.*, 269 (1983) 91.
- 15 A. Sabljic, *J. Chromatogr.*, 314 (1984) 1.
- 16 L. Ambrus, *J. Chromatogr.*, 294 (1984) 328.
- 17 J. Hoigne, J. Widmer and T. Gaumann, *J. Chromatogr.*, 11 (1963) 459.

Ambient temperature gas purifier suitable for the trace analysis of carbon monoxide and hydrogen and the preparation of low-level carbon monoxide calibration standards in the field

B. E. Foulger and P. G. Simmonds

Defence Research Agency, Command and Maritime Systems Group, Holton Heath, Poole, Dorset BH16 6JU (UK)

(Received August 7th, 1992)

ABSTRACT

A novel gas purifier based upon Sofnocat 682, a catalyst containing platinum and palladium on a hydrophobic tin oxide support, is described for the quantitative removal at ambient temperatures of ppm (v/v) and sub-ppm (v/v) levels of carbon monoxide and hydrogen from air and nitrogen gas cylinders. This method provides a simple means of generating either a laboratory or field source of "zero grade" gas for both the trace analysis of carbon monoxide and hydrogen and the preparation of working calibration gas standards of carbon monoxide by using a simple one-step dilution of a higher concentration certified gas standard.

INTRODUCTION

Of particular interest to our laboratory and many other workers [1–9] is the analysis of carbon monoxide and hydrogen at ppm (v/v) and sub-ppm (v/v) levels, particularly since carbon monoxide and hydrogen are produced and released into the atmosphere from a variety of largely anthropogenic sources, including automobiles, domestic heating and biomass burning. Carbon monoxide also plays an important role in atmospheric chemistry through its reaction with hydroxyl radicals [4,10,11].

When the analysis of carbon monoxide and hydrogen involves gas chromatography with a sensitive detector, accurate quantitation can only be achieved when the carrier gas is free from the target analyte [12–14]. Similarly, where low-level calibra-

tion standards are made by successive dilution of a more concentrated certified standard, the diluent gas must also be free of the target analyte [14]. Commercial compressed gas supplies often contain levels of carbon monoxide and hydrogen in excess of their global mixing ratios. The purchase of commercial "zero grade" carrier gases is often an expensive option and, even then, is not always adequate for analyses at the sub-ppm (v/v) level [14]. Consequently, most laboratories purify their carrier gases by various methods including disposable [15] or thermally regenerable adsorbents [16], cryogenic traps [17] or catalytic removal at elevated temperatures [14,18,19]. However, because of the power constraints of heated catalysts and the logistics associated with cryogenic coolants a requirement exists in the field for a catalyst that can remove both carbon monoxide and hydrogen from either air or nitrogen carrier gas at ambient temperature and at varying levels of humidity.

The majority of catalysts used for the oxidation of carbon monoxide have been developed for high-

Correspondence to: Dr. B. Foulger, Defence Research Agency, Command and Maritime Systems Group, Holton Heath, Poole, Dorset BH16 6JU, UK.

temperature automobile catalytic converters. However, for conditions of ambient or moderate temperatures ($< 100^{\circ}\text{C}$) and varying levels of water, the choice of catalyst is severely restricted. Carbon monoxide can be removed by the passage of the gas over hopcalite [20], a proprietary mixture of oxides of copper and manganese, but although the hopcalite is resistant to poisoning, temperatures of $> 70^{\circ}\text{C}$ are required to avoid catalyst deactivation by adsorbed water [21]. Noble metal catalysts such as palladium and/or palladium on either alumina or charcoal will oxidise carbon monoxide at ambient temperatures but the catalysts are very sensitive to poisoning [22–24]. Furthermore, those on a hydrophilic alumina base are susceptible to deactivation by water, although it is claimed that methylsilation of hydrophobic supports alleviates this problem [25]. A further class of catalysts developed for ambient carbon monoxide oxidation is based upon copper salts, usually with smaller amounts of precious metal salts such as palladium chloride [26,27]. One such catalyst, LTC 987 from Teledyne Water Pik, is used in combination with activated charcoal for the removal under ambient conditions of carbon monoxide from buildings [28,29]. However its performance has been reported to be optimum only at 20–65% humidity levels [25]. Silver oxide has also been reported by Seiler *et al.* [10], to quantitatively remove carbon monoxide at room temperature but an additional high temperature hopcalite bed is required to remove hydrogen. Iodine pentoxide exhibits similar limitations [14].

In our own studies [30] on catalysts for the removal of carbon monoxide and hydrogen at ambient temperatures and humidities within enclosed environments, we have found Sofnocat 682 to be the most efficient catalyst, particularly in terms of hydrogen removal and resistance to poisoning. Sofnocat 682 contains both platinum and palladium and a promotor, such as nickel or manganese, on a hydrophobic tin oxide support [31]. With Sofnocat 682, residence times of < 0.1 s are required for the complete oxidation of carbon monoxide [32], this being less than the corresponding residence times for hopcalite (> 0.8 s) [24] and conventional precious metal catalysts (0.2–0.5 s) [23].

This paper describes the use of Sofnocat 682 catalyst operating at ambient temperature for the quantitative removal of both carbon monoxide and hy-

drogen from air and nitrogen gas cylinders so as to provide a field source of “zero grade” gas for both the trace analysis of carbon monoxide and hydrogen and the preparation of working calibration gas standards of carbon monoxide by using a simple one-step dilution of a higher-concentration certified gas standard.

EXPERIMENTAL

Catalyst material

Extrudates (1 mm) of Sofnocat 682 (Molecular Products, Thaxted, Essex, UK) were used as received. For laboratory studies the catalysts were contained in 316-grade stainless-steel tubes (12 in. \times 1 in. O.D. \times 0.040 in. wall; 1 in. = 2.54 cm) with welded 1/8-in. NPT(F) inserts into which were fitted Swagelok connectors incorporating 1/8 in. O.D. \times 1.8 in. thick coarse bronze sinters (“F” grade, 160–180 μm , Accumatic Engineering, Wrexham, UK). When packed, these tubes contained 238 g of Sofnocat 682 catalyst. For subsequent field tests, Sofnocat 682 catalyst (46.9 g) was contained in a 316-grade stainless-steel tube (6 in. \times 3/4 in. O.D. \times 1/16 in. wall) fitted with Swagelok 1/4-in. NPT(M) fittings containing integral bronze sinters.

Carbon monoxide and hydrogen analyses

Carbon monoxide and hydrogen were analysed using a RGA-2 reduction gas analyser (Trace Analytical, Menlo Park, CA, USA). This technique, pioneered by Seiler *et al.* [10], is based upon the reduction of hot mercuric oxide by carbon monoxide and hydrogen, and the photometric detection of the mercury vapour evolved. Air carrier gas (CP Grade, BOC, Wembley, UK) was supplied via a two-stage Model 11 regulator (Scott Environmental Technology, Plumsteadville, PA, USA). Using a 3 ft. \times 1/4 in. O.D. 5A molecular sieve column (1 ft. = 30.48 cm) maintained at 120°C and a nominal carrier gas flow of 40 ml/min, carbon monoxide and hydrogen were separated with baseline resolution at retention times of *ca.* 2.0 and *ca.* 0.4 min, respectively. The detector was operated at 270°C . Samples were introduced onto the column using a Valco 6-port 1/16-in. low-dead-volume valve (P/N 9105, Alltech Associates, Carnforth, UK) fitted with a Valco 1-ml sampling loop. The output from the detector was connected to a Hewlett-Packard 3396A

reporting integrator. Quantitation of carbon monoxide levels was determined by calibration with a single Scotty IV gas standard (Scott Environmental Technology) containing 1.02 ppm (v/v) (certified accuracy $\pm 2\%$) of carbon monoxide in air. Replicate analyses ($n = 5$) at this level gave a reproducibility of $\leq 0.5\%$. Using other Scotty IV standards, the detector response was shown to be linear up to at least the 2 ppm (v/v) level, thereby ensuring linearity of detection for all carbon monoxide levels used in our studies. Hydrogen levels were quantified using a single Scotty IV gas standard containing 12.2 ppm (v/v) (certified accuracy $\pm 2\%$) of hydrogen in nitrogen. This concentration gave a response within the linear range of the detector.

Long-term tests on catalysts

Long-term laboratory tests were performed to assess the ability of Sofnocat 682 to remove carbon monoxide and hydrogen from both air [0.327 ppm (v/v) CO, 3.00 ppm (v/v) H₂, CP grade, BOC] and nitrogen [0.196 ppm (v/v) CO, 0.040 ppm (v/v) H₂, 4.40 ppm (v/v) O₂, "White Spot" grade, BOC]. The test apparatus used to assess the catalytic efficiency is shown in Fig. 1. The flow through the catalyst

was controlled to 50 ml/min by a Brooks Model 8744 flow controller (Brooks Instruments, Stockport, UK). Periodic measurements of the input concentrations to the catalysts were made by operating the two Whitey OGS2 toggle valves (Bristol Valve and Fitting Company, Bristol, UK) to divert the gas flow. The diverted gas flow was set to 50 ml/min via a Nupro Model SS2 metering valve. For experiments at flows above 100 ml/min the Brooks flow controller was removed and the flow adjusted via the two stage regulator on the cylinder, a pressure of 13 p.s.i.g. (1 p.s.i.g. = 6894.76 Pa) being required to achieve a flow of *ca.* 100 ml/min through the Sofnocat 682 catalyst bed. In all cases the flows were measured with either 0–100 or 0–1000 ml/min Hastings mass flowmeters (Chell Instruments, Norfolk, UK).

Following the laboratory studies, a trap containing 46.9 gm of Sofnocat 682 was used for eighteen months as the "gas purifier" for air carrier gas cylinders used on a RGA-3 reduction gas analyser (Trace Analytical, Stanford Avenue, Menlo Park, California, USA) operated as a field monitor for tropospheric CO levels. The carrier gas flow-rate was nominally 20 ml/min. For all catalyst tests, ei-

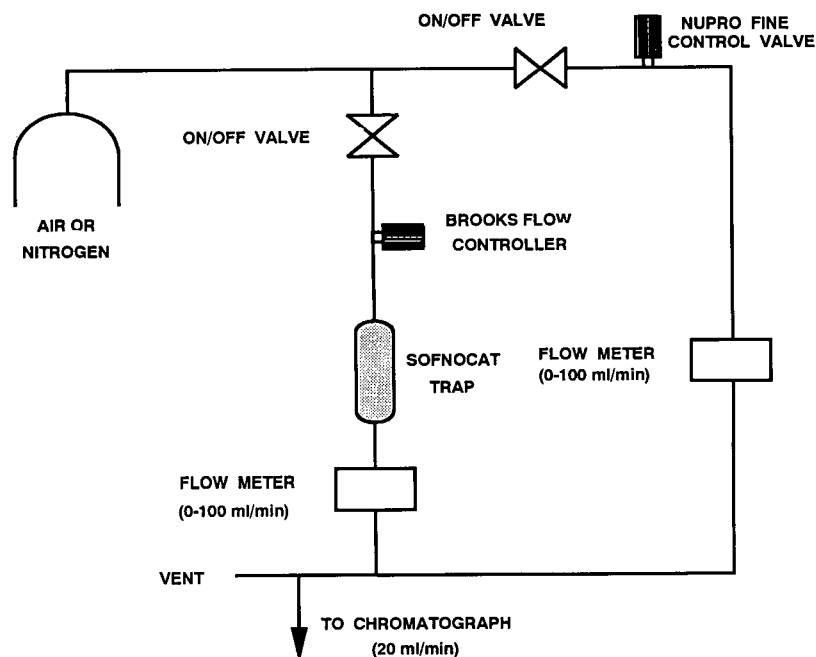


Fig. 1. Schematic diagram of the test system used to evaluate the catalyst efficiency.

ther in the laboratory or in the field, the ambient temperature was in the range 15–25°C.

Preparation of low-level carbon monoxide calibration standards using a one-stage dilution

Initially, a working CO standard was prepared by dilution of a 1000 ppm (v/v) CO standard (BOC) in air. This standard was analysed using the Scotty IV standards described earlier, and found to contain 1.82 ppm (v/v) of CO. Sub-ppm (v/v) standards of carbon monoxide were prepared by a single-step dilution of the 1.82 ppm (v/v) CO standard. The apparatus used was identical to that shown in Fig. 1, other than the addition of a 6 in. × 3/4 in. O.D. stainless-steel mixing volume where the two flows are combined. Prior to performing dilutions of the gas standard, it was confirmed that the Sofnocat 682 removed >99.5% of the carbon monoxide from the CO gas standard at flows of both 100 and 950 ml/min. Dilutions of up to 100-fold were made by simply blending the undiluted and “CO scrubbed” flows from the Sofnocat 682 to maintain a combined maximum flow of 100 ml/min. The flows were accurately measured using either 0–10 or 0–100 ml/min mass flow meters as appropriate. To avoid any memory effects the dilutions were performed using increasing concentrations. The diluted gas standard was split, part to the gas sampling valve, the balance being vented to avoid back pressuring the system. The quantitative removal efficiency of the Sofnocat 682 catalyst for carbon monoxide was confirmed at the end of each series of dilutions.

RESULTS AND DISCUSSION

The Sofnocat 682 trap containing 238 g of catalyst was tested in the laboratory for the purification of air at a flow-rate of 50 ml/min for a total of 2575 h (107 days). Of this time, 1920 hours were with air containing 0.327 ppm (v/v) CO and 3.00 ppm (v/v) H₂, and 655 h with the gas standard containing 1.82 ppm (v/v) CO and 1.08 ppm (v/v) H₂. At the end of these tests, the Sofnocat 682 was still removing >99% of both carbon monoxide and hydrogen from the air carrier gas. This quantitative removal efficiency was also observed during shorter duration tests at the higher flows of 100, 640 and 940 ml/min.

A similar Sofnocat 682 trap containing 246 g of

catalyst was evaluated at 50 ml/min for the purification of nitrogen for a total of 2136 h (89 days). At the end of these tests, the Sofnocat 682 was still removing >99% of carbon monoxide from an input concentration of 0.196 ppm (v/v). No hydrogen breakthrough was observed from the nitrogen test gas containing 0.040 ppm (v/v) of hydrogen. Since this level is not far above the system detection limit for hydrogen, the hydrogen removal efficiency was determined on completion using a nitrogen source containing 8.1 ppm (v/v) of hydrogen and 0.345 ppm (v/v) of carbon monoxide. Quantitative (*i.e.* >99%) removal of both species was observed. Since the mechanism for both carbon monoxide and hydrogen removal is oxidative [33], the quantitative removal of the gases in high-purity nitrogen of nominally 8 ppm (v/v) total impurities was somewhat unexpected. We therefore assume that sufficient residual oxygen is present in the system to facilitate oxidation.

The above results therefore demonstrate the suitability of Sofnocat 682 catalyst to purify the carrier gas on ambient carbon monoxide and hydrogen analysers in which either air or nitrogen are employed as carrier gases. Analysis of a random batch of ten, commercially supplied, air gas cylinders gave carbon monoxide levels in the range 0.044–0.800 ppm (v/v) [mean 0.354 ppm (v/v) S.D. ± 0.222 ppm (v/v)] and hydrogen levels of 0.87–2.76 ppm (v/v) [mean 1.43 ppm (v/v), S.D. ± 0.71 ppm (v/v)]. Analysis of four high-purity commercial nitrogen cylinders chosen at random gave carbon monoxide levels ranging from 0.078–0.345 ppm (v/v) [mean 0.178 ppm (v/v), S.D. ± 0.096 ppm (v/v)], the hydrogen levels varying over the range 0.049–8.1 ppm (v/v).

The results of our laboratory studies were confirmed in field experiments where a smaller trap containing 46.9 g of Sofnocat 682 was used to purify air carrier gas cylinders on a RGA-3 analyser continuously monitoring ambient carbon monoxide levels. After eighteen months of “scrubbing” air carrier gas at a flow-rate of 20 ml/min, the trap still removed ≥99% of both carbon monoxide and hydrogen from an air cylinder containing 1.71 ppm (v/v) carbon monoxide and 2.80 ppm (v/v) of hydrogen. This field Sofnocat 682 trap was also tested with high-purity nitrogen [0.198 ppm (v/v) CO, 0.018 ppm (v/v) H₂] whereupon a carbon monoxide

removal efficiency of *ca.* 91% was still present as compared to a >99% removal efficiency prior to the field trials. No hydrogen breakthrough was observed but the test input level of 0.018 ppm (v/v) hydrogen in nitrogen was approaching the detection limit of the analyser. No long term tests were performed in the field with nitrogen carrier gas, but since some degradation in performance was observed for nitrogen on the Sofnocat 682 trap that had been used for eighteen months with air, it is recommended that a larger trap changed at more frequent intervals be used if nitrogen carrier gas were to be used in the field. According to the manufacturers, "spent" Sofnocat 682 can be readily reactivated by heating in hydrogen diluted with dry nitrogen at *ca.* 50°C [34].

The results of the use of Sofnocat 682 as a simple scrubber for the provision of "zero grade" diluent gas in a simple one step dilution system for the provision of sub-ppm (v/v) calibration standards are shown in Fig. 2. A standard containing 1.82 ppm (v/v) of carbon monoxide can readily be diluted over two orders of magnitude down to *ca.* 0.020

ppm (v/v) with excellent linearity of detector response ($r^2 = 0.999$). The standard deviation from replicate dilutions is shown in Fig. 3, where it can be seen that the mean standard deviation for the dilution procedure is *ca.* 1.2%, of which *ca.* 0.5% is the observed reproducibility of the CO analyser itself. The greater standard deviations observed at 50 and 100-fold dilution are a consequence of the increased detector noise at those levels. Since atmospheric carbon monoxide mixing ratios in clean Northern hemispheric air are about 0.1 ppm (v/v) [7], this simple one-stage dilution system is ideal for the preparation, either in nitrogen or air, of field calibration standards at around ambient concentrations from low ppm (v/v) certified commercial standards. Since the Sofnocat 682 catalyst trap also quantitatively removes carbon monoxide (and hydrogen) at flow-rates of *ca.* 1000 ml/min, accurate dilutions over three orders of magnitude can be made thereby allowing higher-concentration certified standards to be used. Although, in principle our system using Sofnocat 682 is applicable to the preparation of sub-ppm (v/v) hydrogen standards, no attempt was

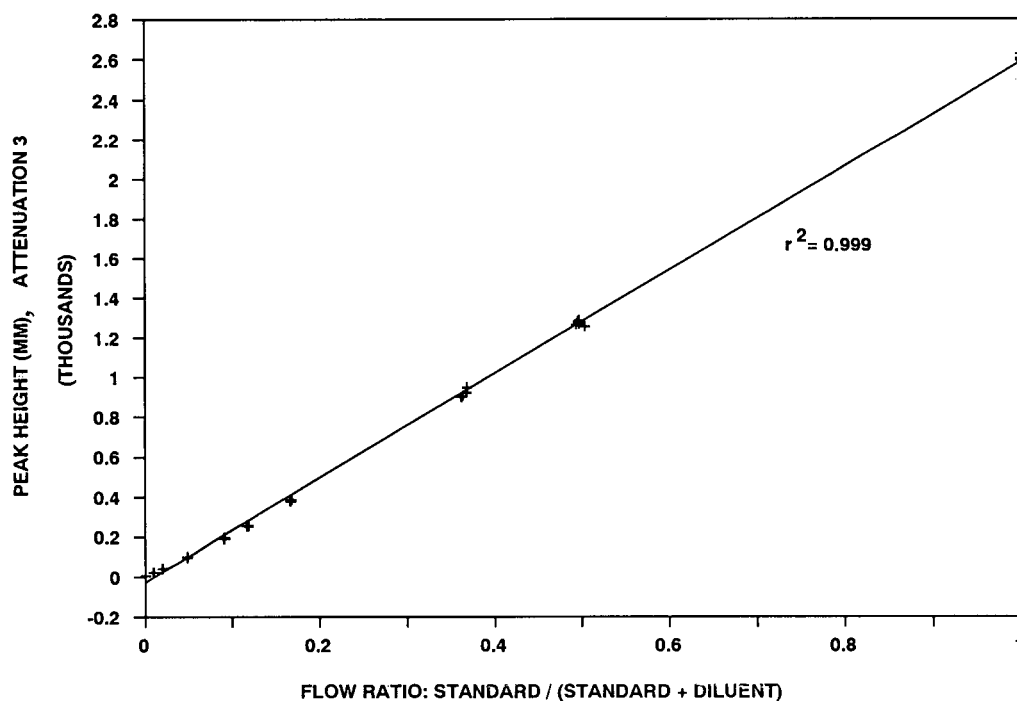


Fig. 2. Plot of the RGA-2 detector output *versus* dilution for the single stage dilution with "zero grade" air of a standard containing 1.82 ppm (v/v) carbon monoxide.

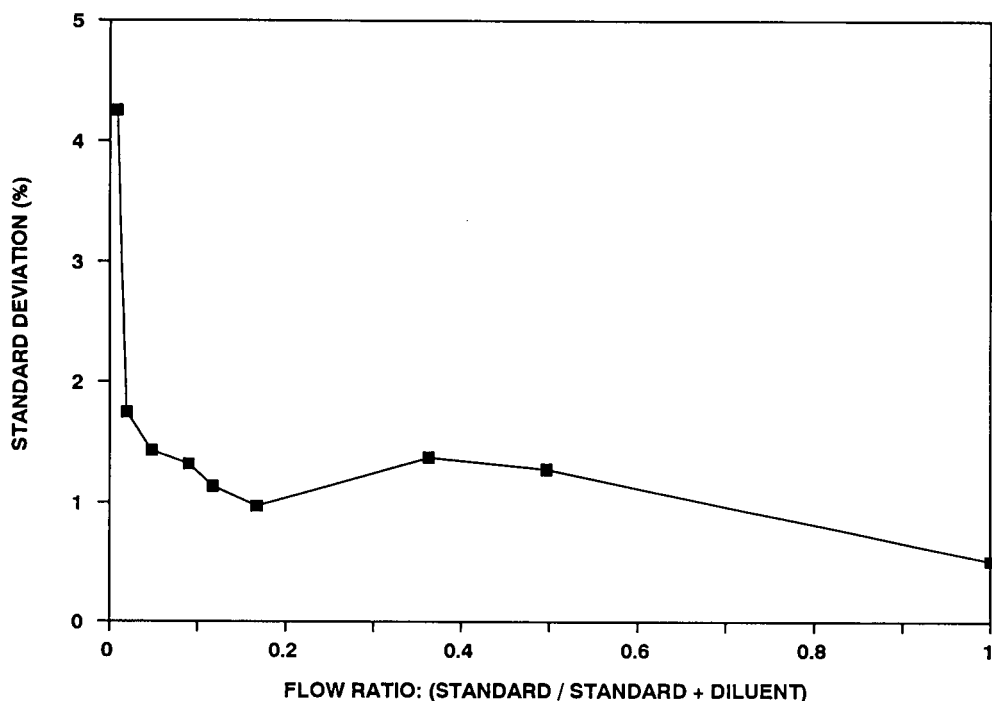


Fig. 3. Plot of the standard deviation (%) versus dilution for the single stage dilution with "zero grade" air of a standard containing 1.82 ppm (v/v) carbon monoxide.

made to prepare such standards of hydrogen using this method since the mixing ratio of hydrogen in clean air is an order of magnitude higher than carbon monoxide, at which level quantification can readily be achieved using low-ppm (v/v) hydrogen standards. However the system could be used for the generation of sub-ppm (v/v) calibration levels of hydrogen for other applications.

Although our studies have been restricted to carrier gases employed on a mercuric oxide detector, we consider the use of Sofnocat as a gas purifier is applicable to other inert gases such as helium and argon and alternative detection techniques (*viz.* electron-capture [12], non-dispersive infrared [35,36], flame ionisation [37] and helium ionisation [17]) used for measuring low levels, particularly ambient mixing ratios, of carbon monoxide and/or hydrogen.

ACKNOWLEDGEMENT

We are indebted to Mr. M. Law for performing the initial carbon monoxide and hydrogen analyses.

REFERENCES

- 1 W. Seiler, *Tellus*, 26 (1974) 116.
- 2 U. Schmidt, *Tellus*, 26 (1974) 79.
- 3 P. Fabian, R. Borchers, K. Weiler, U. Schmidt, A. Volz, D. Erhardt, W. Seiler and F. Muller, *J. Geophys. Res.*, 84 (1979) 4149.
- 4 A. Thompson and R. Cicerone, *Nature*, 321 (1986) 148.
- 5 P. Fraser, P. Hyson, R. Rasmussen, A. Crawford and M. Khahil, *J. Atmos. Chem.*, 4 (1986) 3.
- 6 V. Kirchhoff and E. Marinho, *Atmos. Environ.*, 23 (1989) 461.
- 7 M. Khahil and R. Rasmussen, *Chemosphere*, 20 (1990) 227.
- 8 E. Brunke, H. Scheel and W. Seiler, *Atmos. Environ.*, 24A (1990) 585.
- 9 M. Khahil and R. Rasmussen, *Nature*, 347 (1990) 743.
- 10 W. Seiler, H. Giehl and P. Roggendorf, *Atmos. Technol.*, 12 (1980) 40.
- 11 J. Logan, M. Prather, S. Wolfson and M. McElroy, *J. Geophys. Res.*, 95 (1981) 7210.
- 12 P. Goldan and F. Fehsenfeld, *J. Chromatogr.*, 239 (1982) 115.
- 13 A. Perretta, *Am. Lab.*, 8, No. 5 (1976) 35.
- 14 P. Novelli, J. Elkins and L. Steele, *J. Geophys. Res.*, [Atmos.], 96(D7) (1991) 13109.
- 15 G. Beskova, B. Nechaev and Z. Timokhina, *Khim. Prom-st. Axiom. Prom-st.*, 1 (1979) 56.
- 16 R. Bartram, W. Pinnick and R. Shirey, *J. Chromatogr.*, 338 (1987) 151.

- 17 P. Maroulis and C. Coe, *Anal. Chem.*, 61 (1989) 112.
- 18 J. Stetter and K. Burton, *Rev. Sci. Instrum.*, 47(6) (1976) 691.
- 19 F. Williams and H. Eaton, *Anal. Chem.*, 46 (1974) 179.
- 20 J. Musick and F. Williams, *Ind. Eng. Chem. Prod. Res. Dev.*, 14 (1975) 284.
- 21 J. Musick and F. Williams, *NRL Report 8397*, Naval Research Laboratory, Washington, DC, February 4, 1980.
- 22 D. Fine and C. Heller, *NWC Technical Publication 6179*, Naval Weapons Centre, China Lake, CA, May 1980.
- 23 R. Jagow, R. Lamparter, T. Katan and C. Ray, *Am. Soc. Mech. Eng.*, (Pap), 77-ENAS-28 (1977) 1.
- 24 L. Frevel and L. Kressley, *US Pat.*, 3 758 666, Sept. 11 (1973).
- 25 K. Chuang, J. McMonangle, R. Quaittini, W. Seddon and D. Clegg, *Eur. Pat. Appl.*, EP 246031 A2, Nov. 19, (1987).
- 26 W. Lloyd and D. Rowe, *US Pat.*, 4 521 530 (1985).
- 27 H. Hirai, K. Wada and M. Komiyama, *Chem. Lett.*, 6 (1986) 943.
- 28 M. Collins, *NASA Conference Publications*, 2456 (1987) 153.
- 29 M. Collins, *Chem. Eng. Monogr.*, 24 (1986) 859.
- 30 B. Foulger and A. Hedley (unpublished results).
- 31 A. Holt and D. White, *Eur. Pat. Appl.*, EP 107465, May 2 (1984).
- 32 I. McKernan, *Manuf. Chem.*, April (1988) 50.
- 33 C. Sampson and N. Judde, *NASA Conf. Pub. 2456*, (1987) 65.
- 34 I. McKernan, Molecular Products, Thaxted, UK, personal communication.
- 35 L. Chaney and W. McLenny, *Environ. Sci. Technol.*, 11 (1977) 1186.
- 36 D. Parrish, *J. Geophys. Res.*, 95 (1990) 1817.
- 37 M. Khahil and R. Rasmussen, *Nature*, 332 (1988) 242.

Evaluation of Carboxen carbon molecular sieves for trapping replacement chlorofluorocarbons

S. J. O'Doherty, P. G. Simmonds and G. Nickless

Biogeochemistry Centre, University of Bristol, Cantocks Close, Bristol BS8 1TS (UK)

W. R. Betz

Supelco Inc., Supelco Park, Bellefonte, PA 16823-0048 (USA)

(First received August 21st, 1992, revised manuscript received October 29th, 1992)

ABSTRACT

A method has been developed for trapping and preconcentrating the very volatile replacement chlorofluorocarbons (hydrofluorocarbons and hydrochlorofluorocarbons) using microtraps filled with Carboxen, a carbon molecular sieve type material, without the need for extensive cryotrapping using liquid nitrogen. We present here the adsorption characteristics of four Carboxen materials, Carboxen 569, 1000, 1001, and 1002, used to trap a range of replacement chlorofluorocarbons varying in boiling point from -48.4 to -9.8°C . The application of these traps for the automated analysis of trace gases in atmospheric and environmental chemistry could prove extremely useful.

INTRODUCTION

Since the signing of the Montreal Protocol (1987) agreeing to phase out the production and use of ozone depleting chlorofluorocarbons (CFCs), much emphasis has been directed towards the replacement of these compounds with environmentally more acceptable alternatives. A group of compounds currently being tested as alternatives are the hydrochlorofluorocarbons (HCFCs) and the hydrofluorocarbons (HFCs, the name which is adopted to describe all alternatives for this study). It is envisaged that these very volatile compounds will react more readily with tropospheric hydroxyl radicals thus reducing their atmospheric lifetimes and therefore their ozone depleting potential [1]. As a consequence it is anticipated that the atmospheric

mixing ratios for the HFCs will initially be in the ppt to sub-ppt (v/v) range. The accurate measurement and long-term monitoring of these compounds, as well as other trace organic contaminants in air, therefore requires a preconcentration step before analysis using gas chromatography (GC) or GC-mass spectrometry (MS).

The use of sampling tubes packed with adsorbent materials has proved a popular method for trapping organic pollutants present at trace levels in the atmosphere [2–6]. However, the commonly used adsorbents such as Tenax TA, Porapak Q, Porapak T, and Carbopak do not have the adsorptive capacity necessary to trap the very low boiling HFCs unless a cryogenic preconcentration step is used. The usual approach would be to use a fairly large primary trap and then thermally desorb into a small secondary trap or short length of capillary tubing (or column), which is cooled in liquid nitrogen [7–10]. This ensures that the sample is cryofocussed into a narrow band in order to optimise chromatographic res-

Correspondence to: S. J. O'Doherty, Biogeochemistry Centre, University of Bristol, Cantocks Close, Bristol BS8 1TS, UK.

TABLE I
PHYSICAL CHARACTERISTICS OF CARBOXEN ADSORBENTS

Carboxen adsorbent	Mesh size	BET surface area (m ² /g)	Porosity volume ^a		
			Micropore (3–20 Å)	Mesopore (20–500 Å)	Macropore (> 500 Å)
569	40–60	485	0.20	0.14	0.10
1000	60–80	1200	0.44	0.16	0.25
1001	60–80	500	0.22	0.13	0.11
1002	60–80	1100	0.36	0.28	0.3

^a Approximate values.

olution during a rapid final desorption step. In remote atmospheric monitoring stations there are considerable technical and logistical difficulties in routinely providing liquid nitrogen. Furthermore, the maintenance of automated cryogenic traps is equally difficult in remote field locations. It would therefore be desirable to use adsorbents which can be maintained at practical operating temperatures for both trapping and desorption steps.

Preliminary experiments with a number of the more commonly used adsorbents indicated that they had insufficient capacity to trap the trace HFCs from several litres of ambient air. It was found that the most suitable adsorbents for trapping the HFCs were carbon molecular sieve type materials called Carboxens [11] (Supelco). The adsorbent characteristics of these materials were evaluated for the HFCs using two different methods: (a) indirect sample introduction [12–14] and (b) direct sample introduction [14–16], a full description of

the two types of method is described later in the paper.

EXPERIMENTAL

Adsorbents and adsorbates

The physical characteristics of the Carboxen materials evaluated in this study are listed in Table I, and cover the range of HFCs being currently evaluated by industry as replacement compounds for existing CFCs. The physical characteristics of these compounds are described in Table II.

Indirect method of sample introduction

Sample preparation and chromatographic conditions. Gas samples were prepared by static dilution of individual pure gases (supplied by ICI, Cheshire, UK). A known volume of each HFC (200 µl) was transferred using a gas syringe to a glass flask (100 ml) equipped with a rubber septum cap. The flask had previously been purged with nitrogen to reduce possible sample contamination. A 20-µl portion of the sample gas was then injected into the gas chromatograph.

The instrument used was a Varian Model 3700 gas chromatograph (Varian, Palo Alto, CA, USA) equipped with a flame ionization detector. A variety of adsorbent traps were used and their dimensions are listed in Table III. Each trap was conditioned at 200°C for at least 12 h in a stream of nitrogen (20–30 ml/min). Nitrogen was used as the carrier gas at a flow-rate of 2–4 ml/min depending upon which trap was being evaluated.

Specific retention volume data for each adsor-

TABLE II
PHYSICAL CHARACTERISTICS OF HFCs

Compound	Structure	Boiling point (°C)	<i>M_r</i>
HFC 125	CF ₃ CF ₂ H	–48.4	120
HFC 143a	CF ₃ CH ₃	–47.6	84
HCFC 22	CHClF ₂	–40.8	86
HFC 134a	CF ₃ CH ₂ F	–25.9	102
HCFC 124	CF ₃ CFHCl	–11.8	136
HCFC 142b	CH ₃ CF ₂ Cl	–9.8	101

TABLE III
DIMENSIONS OF CARBOXEN TRAPS

Carboxen material	Trap dimensions (cm)	Adsorbent bed weight (mg)	Mesh size
569 ^a	27 × 0.08 O.D. × 0.05 I.D.	15	40–50
1000 ^b	57 × 0.63 O.D. × 0.51 I.D.	560	60–80
1000 ^c	30 × 0.16 O.D. × 0.05 I.D.	40	60–80
1001 ^b	60 × 0.63 O.D. × 0.51 I.D.	786	60–80
1001 ^c	30 × 0.16 O.D. × 0.05 I.D.	48	60–80
1002 ^a	30 × 0.08 O.D. × 0.05 I.D.	80	80–100

^a Trap used for indirect injection method.

^b Trap used for direct injection method.

^c Trap used for both injection methods.

bent–adsorbate interaction were obtained by injecting duplicate samples of each HFC standard at 3–5 different column/trap temperatures. These adsorbate retention volumes were used to construct a straight line plot of the specific retention volume ($\log V_g^1$) versus temperature ($1 \cdot 10^3/K$). This straight line was subsequently extrapolated via linear regression analysis to obtain V_g^1 values at ambient and sub-ambient temperatures.

Direct method of sample introduction

Sample preparation and chromatographic conditions. A 30-l electropolished stainless-steel canister containing a pressurised sample of HFC 125 (1.46 ppm) was prepared by injecting 1 ml of pure HFC 125 into the evacuated cylinder and pressurising to 325 p.s.i. (1 p.s.i. = 6894.76 Pa) with halocarbon-free nitrogen to give an approximate concentration

of 1.5 ppm. A laboratory-made system was constructed to enable direct injection of the HFCs into the microtraps. A diagram of the system is shown in Fig. 1. The HFC sample canister was connected to the microtrap via a pressure regulator (Porter Instruments Model 8286) and a flow controller (Brooks Instruments Model 8744A, Hatfield Co., Hatfield, PA, USA). Nitrogen and the HFC 125 standard was passed into a six port gas sampling valve (Rheodyne Model 7010, Cotati, CA, USA) and flowed either to vent or the microtrap depending upon the position of the valve. The flow rate of the gases were balanced using a flowmeter and a needle valve on the vent side and a mass flow transducer (Scott Speciality Gases, Plumsteadville, PA, USA) situated in line after the microtrap. A flame ionization detector, part of a Carlo Erba Model 490 gas chromatograph was connected in line with the microtrap via a short length of deactivated fused-silica tubing.

RESULTS AND DISCUSSION

Indirect method of sample introduction

A trap packed with Carboxen material can be regarded as a short chromatographic column, therefore, injection of a vaporized sample of each HFC will produce a chromatographic peak with a retention time dependent upon sample–adsorbent interactions and oven temperature.

Sample retention time data at a range of oven temperatures can be used to calculate the specific

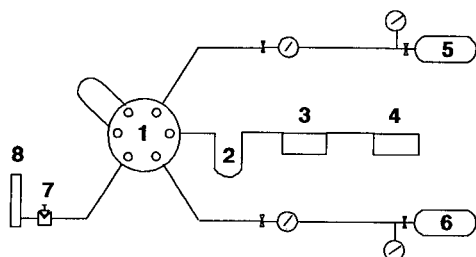


Fig. 1. Schematic diagram of the direct injection apparatus. 1 = Six-port valve; 2 = microtrap; 3 = flow transducer; 4 = flame ionization detector; 5 = carrier gas; 6 = HFC sample; 7 = needle valve; 8 = flow meter.

retention volume, V_g^t

$$V_g^t = \frac{3 \left(\frac{(Ip/Op)^2 - 1}{(Ip/Op)^3 - 1} \right) Fa \left(\frac{Tc}{Ta} \right) \left(\frac{(t_r - t_a)}{Wa} \right)}$$

where Ip and Op are the trap inlet and outlet pressures respectively, Fa is the carrier flow-rate through the trap at ambient temperature (ml/min), Tc is the trap operating temperature (K), Ta is the ambient temperature, t_r and t_a are retention times (min) of the sample and methane, respectively, and Wa is the weight of adsorbent (g).

The breakthrough volume (BTV) at any trapping temperature of interest can be obtained by linear extrapolation of the graph $\log V_g^t$ vs. $1/T$ determined at temperatures higher than the trapping temperature. This method is useful as a relatively quick means of estimating a particular trap capacity, and is typically more precise when using temperatures which approach the boiling points of the analytes.

Specific retention volumes *versus* $1/T$ values were plotted for each HFC on Carboxens 569, 1000, 1001 and 1002. The resulting straight line plots were extrapolated to give BTV data at temperatures as low as -50°C . It was assumed that the extrapolated lines would be linear at sub-ambient temperatures.

and correlation coefficient data was used to determine the variances associated with the plots. The results of the BTV calculations for the compounds of interest at temperatures between 20 and -50°C are presented in Tables IV–VII, and these results are illustrated graphically in Figs. 2–8. CFC 13B1 has been included in some of these experiments as it acts as a useful surrogate for the HFCs when using an electron capture detector, which is insensitive to most HFCs.

The results indicate that no single characteristic trend exists for the HFC group of compounds. The elution order for the HFCs on carboxen 569 and 1000 follow, however, an expected pattern taking into account the compounds boiling points, molecular sizes and possible surface interactions.

The order in terms of BTVs is: 143a < 125 < 134a < 22 < 142b < 124. It is interesting to note that this is also the elution order for these HFCs when chromatographed on a Poraplot Q column [17]. One unexpected observation is the exceptionally high BTV for HFC 125 on Carboxen 1001 (see Table VI). At this stage, we believe that HFC 125 has a very non-linear adsorption isotherm. Since the pore size of Carboxen 1001 has been expanded this could result in HFC 125 fitting perfectly into the pores of the adsorbent material and thus being

TABLE IV

BTVs FOR HFCs AT VARIOUS TEMPERATURES ON CARBOXEN 569

Temperature (°C)	BTV (ml/mg)						
	143a	125	134a	22	13B1	142B	124
20	1.3	4.8	7.3	28.0	3.1	44.8	204.9
15	1.7	6.5	10.0	37.1	4.0	61.9	303.5
10	2.1	9.0	13.8	49.8	5.2	86.6	456.0
5	2.7	12.6	19.2	67.4	6.8	122.4	694.9
0	3.5	17.9	27.0	92.4	9.1	175.3	1075
-5	4.6	25.7	38.6	128.1	12.2	254.4	1692
-10	6.1	37.3	56.0	179.8	16.5	374.8	2710
-15	8.2	55.0	82.3	255.8	22.6	560.2	4419
-20	11.1	82.4	122.8	368.9	31.5	850.7	7344
-25	15.2	125.4	186.1	539.8	44.3	1313	12452
-30	21.2	194.3	287.1	802.8	63.2	2065	21594
-35	29.7	306.5	451.1	1213	91.6	3309	38327
-40	42.4	493.0	722.32	1867	134.9	5410	69670
-45	61.5	810.1	1181.5	2930	202.1	9042	130137
-50	90.6	1360	1974.5	4687	308.1	15457	249783

TABLE V

BTVs FOR HFCs AT VARIOUS TEMPERATURES ON CARBOXEN 1000

Temperature (°C)	BTV (ml/mg)						
	143a	125	134a	22	13B1	142b	124
20	7.65	10.90	13.18	14.34	—	198.57	351.52
15	9.68	13.98	16.90	18.40	—	266.87	481.83
10	12.37	18.10	21.88	23.84	—	362.62	668.23
5	15.93	23.63	28.57	31.15	—	497.92	937.17
0	20.72	31.17	37.69	41.11	—	691.95	1331.2
–5	27.19	41.53	50.22	54.81	—	973.18	1915.4
–10	36.09	55.96	67.69	73.92	—	1387.3	2795.7
–15	48.40	76.26	92.26	100.82	—	2004.4	4139.9
–20	65.68	105.21	127.31	139.20	—	2938.4	6225.7
–25	90.18	146.98	177.89	194.64	—	4372.5	9513.1
–30	125.53	208.28	252.15	276.08	—	6618.0	14802
–35	177.17	299.53	362.71	397.42	—	10193	23465
–40	253.68	437.31	529.69	580.82	—	15984	37918
–45	369.20	649.55	786.99	863.63	—	25585	62626
–50	546.17	981.58	1189.6	1306.5	—	41799	105719

retained longer. Betz *et al.* [12] reported that the diameters of the micropores and the percentage of micropores present for a particular sieve are directly responsible for variances in specific retention vol-

umes for different sized adsorbents. Supelco also reports [11] that the adsorbent strength of the carboxens increases towards volatile materials as follows: 1001 > 1000 > 569. However, our research

TABLE VI

BTVs FOR HFCs AT VARIOUS TEMPERATURES ON CARBOXEN 1001

Temperature (°C)	BTV (ml/mg)						
	143a	125	134a	22	13B1	142b	124
20	1.59	65.34	3.61	6.34	3.07	31.76	50.40
15	2.10	106.46	4.91	7.93	3.98	43.28	69.96
10	2.82	176.64	6.75	10.01	5.20	59.68	98.30
5	3.81	298.22	9.37	12.74	6.86	83.19	139.74
0	5.22	513.52	13.19	16.36	9.15	117.43	201.31
–5	7.22	901.93	18.78	21.20	12.32	167.87	293.89
–10	10.12	1619.7	27.12	27.76	16.79	243.36	435.50
–15	14.38	2974.5	39.72	36.72	23.15	357.84	655.07
–20	20.70	5594.4	59.05	49.10	32.32	534.20	1001.3
–25	30.23	10785	89.16	66.41	45.73	810.09	1556.1
–30	44.86	21384	137.02	90.99	65.65	1250.5	2464.5
–35	67.69	43642	214.40	126.34	95.71	1966.0	3979.4
–40	103.91	91748	341.79	177.82	141.72	3149.7	6555.1
–45	162.65	199514	556.56	254.21	213.64	5155.5	11045
–50	259.6	448782	925.73	369.10	327.87	8621.4	19040

TABLE VII

BTVs FOR HFCs AT VARIOUS TEMPERATURES ON CARBOXEN 1002

Temperature (°C)	BTV (ml/mg)						
	143a	125	134a	22	13B1	142b	124
20	1.71	1.50	2.05	1.90	—	40.51	60.22
15	2.16	1.88	2.57	2.37	—	53.75	80.82
10	2.74	2.36	3.25	2.97	—	72.07	109.65
5	3.50	2.99	4.15	3.77	—	97.60	150.33
0	4.51	3.82	5.35	4.81	—	133.70	208.57
-5	5.88	4.92	6.95	6.20	—	185.26	292.84
-10	7.74	6.41	9.12	8.07	—	260.04	416.71
-15	10.29	8.43	12.10	10.61	—	369.74	600.99
-20	13.84	11.21	16.23	14.10	—	533.04	879.33
-25	18.83	15.07	22.02	18.94	—	779.56	1305.9
-30	25.95	20.52	30.28	25.78	—	1158.7	1972.4
-35	36.25	28.31	42.18	35.53	—	1751.4	3031.5
-40	51.36	39.58	59.58	49.64	—	2693.0	4743.2
-45	73.91	56.17	85.50	70.40	—	4222.9	7574.3
-50	108.08	80.95	124.62	101.39	—	6752.8	12343

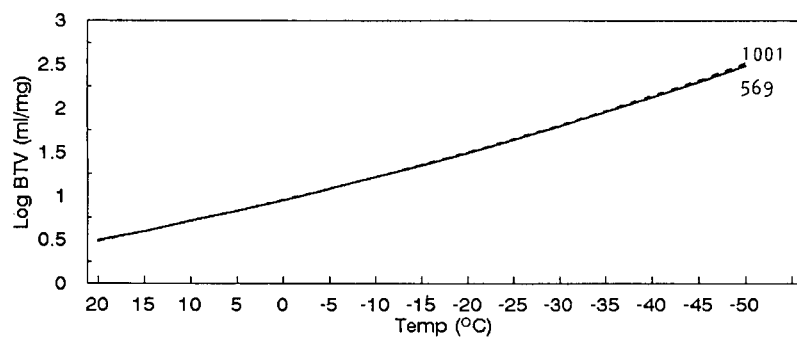


Fig. 2. Log BTV of CFC 13B1 versus temperature using Carboxen 569 and 1001.

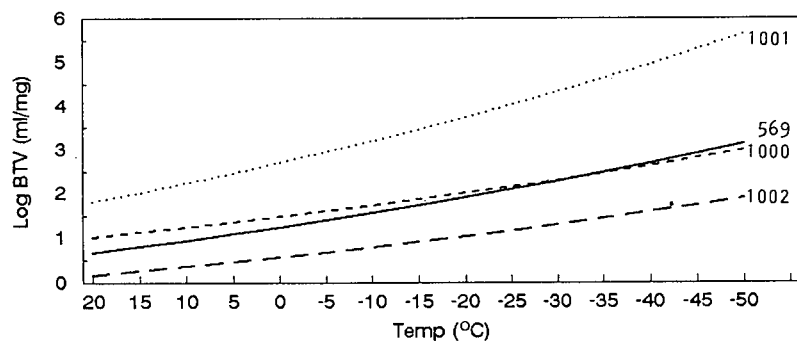


Fig. 3. Log BTV of HFC 125 versus temperature using Carboxen 569, 1000, 1001 and 1002.

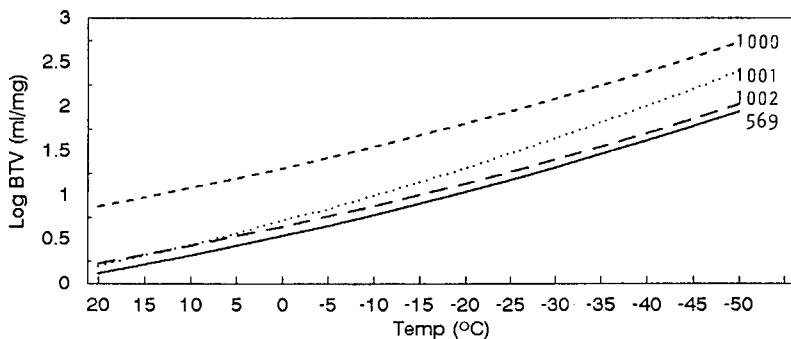


Fig. 4. Log BTV of HFC 143a versus temperature using Carboxen 569, 1000, 1001 and 1002.

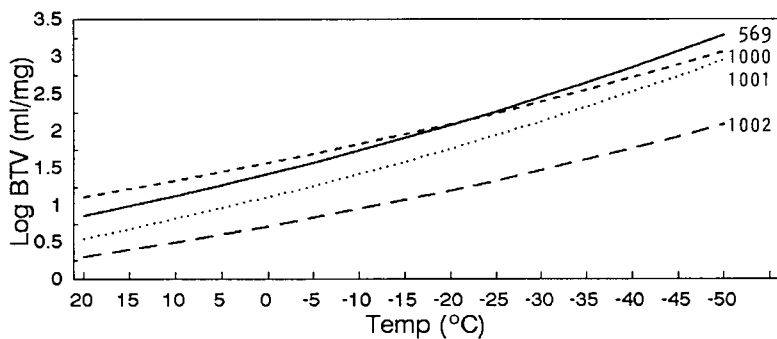


Fig. 5. Log BTV of HFC 134a versus temperature using Carboxen 569, 1000, 1001 and 1002.

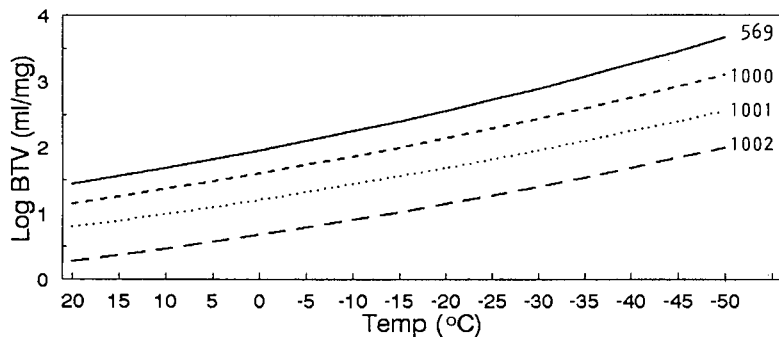


Fig. 6. Log BTV of HFC 22 versus temperature using Carboxen 569, 1000, 1001 and 1002.

indicates that for the HFCs at a sub-ambient temperature of -50°C the adsorbent strength of the different Carboxens is very compound dependent, as summarised in Table VIII. Clearly from these results either Carboxen 1000 or 569 would be the best general adsorbent for most HFCs. One other

important observation is that although HFC 125 (b.p. -48.4°C) has a slightly lower boiling point than HFC 143a (b.p. -47.6°C) it is more strongly retained on both Carboxen 569 and 1000. Similarly, HFC 22 (b.p. -40.8°C) is again more strongly retained than the higher boiling HFC 134a (b.p.

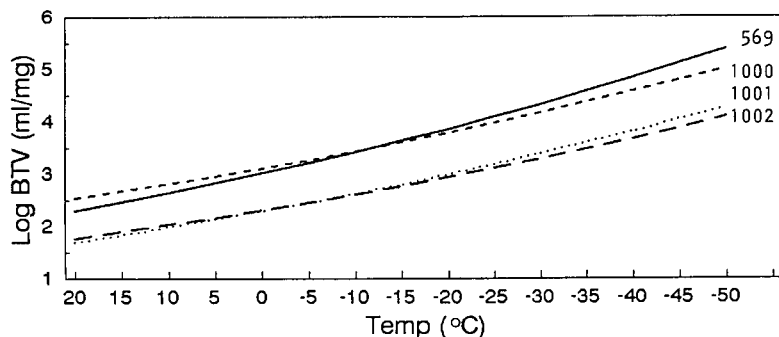


Fig. 7. Log BTV of HFC 124 versus temperature using Carboxen 569, 1000, 1001 and 1002.

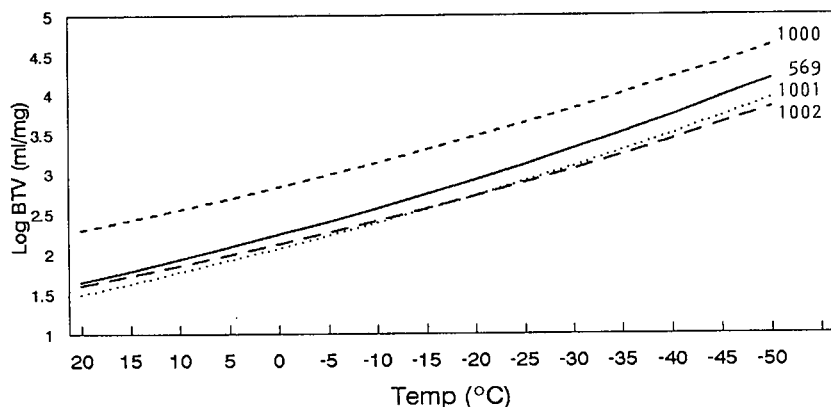


Fig. 8. Log BTV of HFC 142b versus temperature using Carboxen 569, 1000, 1001 and 1002.

-25.9°C). We attribute this to the presence of a single hydrogen atom in HFC 125, and HFC 22 which undergoes stronger interaction through hydrogen bonding with the adsorbent. The molecular

size and shape (*i.e.* surface area, volume) is also thought to be responsible for differences in adsorption in the micropores. Previous work [18] utilizing dichloromethane indicates the presence of larger (*i.e.* macro, meso) pores in the sieve structure which permits greater usage of the microporous region due to the more effective transfer within the porous regions. Micropore diameters also play an important role in the adsorption process.

Since the BTVs are reported in terms of ml per mg of adsorbent in all of our tables, we can quickly estimate the amount of adsorbent required to quantitatively trap each HFC for any size air sample. For all practical purposes, it is only necessary to determine the amount of adsorbent required for the least strongly retained HFC, since all other more strongly retained HFCs will also be trapped quantitatively. As an example, HFC 143a is one of the

TABLE VIII
ACTIVITY ORDER OF DIFFERENT CARBOXENS

Boiling point (°C)	HFC	Carboxen activity order
-48.4	125	1001 > 569 > 1000 > 1002 (indirect) 1000 > 569 > 1002 > 1001 (direct)
-47.6	143a	1000 > 1001 > 1002 > 569
-40.8	22	569 > 1000 > 1001 > 1002
-25.9	134a	569 > 1000 > 1001 > 1002
-11.8	124	569 > 1000 > 1001 > 1002
-9.8	142b	1000 > 569 > 1001 > 1002

TABLE IX

COMPARISON OF BTVs FOR HFC 125 ON VARIOUS CARBOXEN MATERIALS USING A DIRECT AND INDIRECT METHOD OF SAMPLE INTRODUCTION

Carboxen	Temperature (°C)	Direct injection		Indirect injection	
		BTV (l)	BTV (ml/mg)	BTV (l)	BTV (ml/mg)
569 (15 mg)	17.9	0.10	6.55	0.09	6.03
569 (15 mg)	18.2	0.10	6.77	0.09	5.98
1002 (80 mg)	17.5	0.36	4.50	0.14	1.79
1000 (560.5 mg)	18.4	>12.22	>21.80	7.25	12.94
1000 (40 mg)	21.3	1.03	25.84	0.41	10.24
1000 (40 mg)	-1.4	1.35	33.74	1.35	33.75
1001 (48 mg)	21.0	0.08	1.77	2.85	59.85

most difficult compounds to trap, and if we assume a trapping temperature of -40°C and a 2-l air sample, then the following amounts of each Carboxen would be needed: Carboxen 569, 47 mg; Carboxen 1001, 19 mg; Carboxen 1000, 8 mg; Carboxen 1002, 39 mg. The small amounts of adsorbent required, especially for Carboxen 1000, are consistent with the design of our microtraps where we expect to maintain good chromatographic resolution without the need for post desorption cryogenic focusing. Preliminary desorption studies carried out in our laboratory support this view. These results will be published as soon as trials have been completed.

Because of the large extrapolation needed to obtain retention volumes at ambient temperatures with the indirect method described above, the same carboxen traps were also evaluated by the direct (continuous flow) method of sample introduction.

TABLE X

COMPARISON OF BTVs FOR THE CFC 13B1 FOR INDIRECT METHOD OF INJECTION AND THE DIRECT INJECTION RESULTS USING 50 mg OF CARBOXENS IN ADSORPTION TUBES

Carboxen material	Temperature (°C)	Direct injection BTV (ml/mg)	Indirect injection BTV (ml/mg)
569	-21.6	14.35	31.47
1001	-22.1	38.90	32.33
1001	-22.0	39.66	32.33

Direct method of sample introduction

Carboxen microtraps were used under frontal analysis conditions, whereby a constant concentration of individual HFCs flowed continuously at a nominal flow-rate of 20 ml/min through a micro-trap maintained at a constant temperature. Initially the sample was completely retained by the adsorbent material, however, over time the gas volume flowing through the trap exceeds the retention volume of the sample, resulting in sample breaking through the adsorbent. Sample breakthrough was monitored by the flame ionization detector and the signal response displayed on a chart recorder. BTVs are normally quoted as the point at which 5% breakthrough occurs, however in order to directly compare the indirect and direct analysis results BTV was taken when the detector signal reached 50% of its maximum value.

It was not possible to determine BTVs for Carboxen 1000 and 1001 on the original columns used in the indirect method since they contained large amounts of adsorbent material (1000: 560.5 mg, and 1001: 786.1 mg), and their expected BTVs would be very large. Therefore, two new micro-columns were prepared containing substantially less of each adsorbent (1000: 40 mg, and 1001: 48 mg). A comparison of BTVs achieved using the two methods of analysis can be seen in Table IX. As a further check BTV results achieved at an earlier date using glass adsorption tubes and CFC 13B1 were also compared as is shown in Table X.

With the exception of HFC 125 on Carboxen

1001, the results indicate that the two methods of determining BTV correlate well, if anything the faster indirect method has underestimated the BTVs for the HFCs. The BTV for HFC 125 on Carboxen 1001 by the direct method is substantially lower than predicted using the indirect method of injection, where the steep slope of the regression line did appear anomalous. Therefore, as indicated in Table VIII, Carboxen 1000 would be the preferred adsorbent for all of the HFCs if we discount the unexpected and anomalous behaviour of HFC 125 by the indirect method.

CONCLUSIONS

The HFCs are only weakly adsorbed on most of the conventional adsorbents used in air pollution studies. To quantitatively trap these volatile compounds requires the much stronger adsorbents of the carbon molecular sieve type (Carboxens). Extrapolation of BTVs to ambient and sub-ambient temperatures from plots of the log of their retention volumes *versus* temperature provides a reasonable estimate of adsorbent capacity. However it is recommended that comparison of sample breakthrough also be checked by the more direct method of frontal chromatography, particularly where adsorbates have unusual adsorption isotherms.

Our detailed studies of the Carboxens indicate that several hundred milligrams of these adsorbents would be needed at ambient temperatures to ensure complete trapping of trace concentrations of the HFCs from a 1–2-l atmospheric sample. However, maintaining the strongest carbon molecular sieve, Carboxen 1000, at sub ambient temperatures (-40°C) during the trapping process, reduces the amount of adsorbent required to about 10–20 mg.

This small amount of adsorbent permits the design of a small microtrap with near capillary dimensions, thus reducing the dependency on liquid nitrogen for cryofocussing. Research is continuing in our laboratories to assess quantitative recoveries of various HFCs and CFCs from the Carboxen materials.

REFERENCES

- 1 J. S. Nimitz and S. R. Skaggs, *Environ. Sci. Technol.*, 26 (1992) 739–744.
- 2 J. Rudolph, F. Jochen, A. Khedim and G. Pilwat, *Int. J. Environ. Anal. Chem.*, 38 (1990) 143–155.
- 3 C. Vidal-Madjar, M. Gonnord, F. Benchah and G. Guiochon, *J. Chromatogr. Sci.*, 16 (1978) 190–196.
- 4 E. Atlas and S. Schaufli, *Environ. Sci. Technol.*, 25 (1991) 61–67.
- 5 R. H. Brown and C. J. Purnell, *J. Chromatogr.*, 178 (1979) 79–90.
- 6 F. Bruner, G. Crescentini and F. Mangani, *Chromatographia*, 30, (1990) 565–572.
- 7 T. Noy, P. Fabian, R. Borchers, F. Janssen, C. Crammers and J. Rijks, *J. Chromatogr.*, 393 (1987) 343–356.
- 8 S. R. Springston, *J. Chromatogr.*, 517 (1990) 67–75.
- 9 M. Fujita, W. T. Jung, H. Tatematu, D. H. Sohn and T. Maeda, *J. High Resolut. Chromatogr.*, 14 (1991) 83–90.
- 10 J. W. Cochran and J. M. Henson, *J. High Resolut. Chromatogr. Chromatogr. Commun.*, 11 (1988) 869–873.
- 11 S. A. Hazard, personal communication, 1991.
- 12 W. R. Betz, S. G. Maroldo, G. D. Wachob and M. C. Firth, *J. Am. Ind. Hyg. Assoc.* 50(4) (1989) 181–187.
- 13 T. Tanaka, *J. Chromatogr.*, 153 (1978) 7–13.
- 14 G. Bertoni, F. Bruner, A. Liberti and C. Perrino, *J. Chromatogr.*, 203 (1981) 263–270.
- 15 A. Raymond and G. Guiochon, *J. Chromatogr. Sci.*, 13 (1975) 173–177.
- 16 T. Noy, P. Fabian, R. Borchers, C. Crammers and J. Rijks, *Chromatographia*, 26 (1988) 149–156.
- 17 M. Choi, *M. Sc. Thesis*, University of Bristol, Bristol, 1991.
- 18 W. R. Betz and S. J. Lambiasi, *J. Chromatogr.*, 556 (1991) 433–440.

Application of dithiocarbamate resin–metal complexes as stationary phases in gas chromatography

Chia-Fu Yeh, Sun-Dsong Chyueh, Wei-Shi Chen, Jia-Der Fang and Chuen-Ying Liu

Department of Chemistry, National Taiwan University, Roosevelt Road, Section 4, Taipei (Taiwan)

(First received July 13th, 1992; revised manuscript received October 20th, 1992)

ABSTRACT

A chelating resin with dithiocarbamate functional groups to which silica gel was used as a matrix and silanes were used with diamino functional groups as a spacer was synthesized. The structure and the conversion of functional groups of the resin were confirmed by IR spectra and elemental analysis. The influence of pH on the adsorption of the resin for metal ions was also examined. The resin under optimum pH conditions formed a 1:1 metal complex with copper ion. The affinity of metal ions toward the synthesized resin decreased in the order $\text{Hg(II)} > \text{Cu(II)} > \text{Cd(II)} > \text{Zn(II)}$. The resin exhibited efficient complexation of transition metal cations. The cadmium, copper and zinc complexes were investigated for application as stationary phase for the gas chromatographic analysis of dialkyl sulphides. The material was packed in a 2.1 m \times 3.2 mm I.D. spiral glass column. Factors affecting the retention and sample selectivity were also studied. A shorter retention time and sharp peaks were obtained when ammonia was introduced into the mobile phase. At an oven temperature of 100°C, a flow-rate of 60 ml min⁻¹ and use of a flame ionization detector, the analysis of dialkyl sulphides showed that the copper resin complex as the stationary phase gave the best results. The stationary phase was also used for the separation of dialkyl sulphide from a hydrocarbon mixture.

INTRODUCTION

Dithiocarbamates and their derivatives are valuable reagents for the separation and photometric determination of heavy metals. Previous literature on their analytical applications is extensive [1]. The immobilization of such groups, either on a polymer or on a silica matrix, can convert them into useful metal-chelating sorbents. These can be used for the selective removal of heavy metal ions from aqueous solutions [2] and, in particular, for ligand-exchange chromatography (LEC). LEC is a process in which complex-forming compounds are separated through the formation and breaking up of labile coordinate bonds to a central metal atom, coupled with partitioning between a mobile and a stationary phase. It separates ligands by causing them to

change places around metal ions. The exchange can occur in either the stationary or the mobile phase.

LEC is one of the most powerful techniques among the variety of commonly used separation methods for resolving complex-forming substances. Much work has been done previously since its introduction in the early 1960s on the separation of isomers or homologues of amines, phenols, amino acids and other organic ligands containing nitrogen or oxygen atoms [3]. Some limitations in operating an LEC system through use of a liquid mobile phase exist, even though many types of samples or stationary phase can be selected and modification of the mobile phase is easy and effective. Additionally, detection is sometimes difficult if a UV–visible detector is being used. A stronger complexing group, dithiocarbamates, was introduced in this work into silica as the LEC sorbent, as a result of taking into account these disadvantages. So far, only a few workers have used the potential of dithiocarbamate resins as LEC sorbents [4,5]. The mobile

Correspondence to: C.-Y. Liu, Department of Chemistry, National Taiwan University, Roosevelt Road, Section 4, Taipei, Taiwan.

phase they used was, however, a liquid phase. Although the main principle of LEC is valid both for liquid chromatography in all its versions and for gas chromatography, the latter technique often cannot employ the same coordination systems. In liquid chromatography, solvent molecules or specially added components of the mobile phase actively compete with the solute species for vacant positions in the coordination sphere of the complexing metal ion. A real ligand exchange thus proceeds in the moving chromatographic zone of each solute. In contrast, nitrogen, helium or the other inert gases used in gas chromatography as mobile phases are not able to displace ligands from their sorption complexes. Only extremely labile complexes that easily dissociate at moderate temperatures can therefore be employed in gas chromatographic systems [6].

The complexing behaviour and the stability of the synthesized resin were studied in this investigation. The feasibility of using metal-loaded sorbents as stationary phases for the separation of dialkyl sulphides with a gaseous mobile phase, namely ligand-exchange gas chromatography, was also investigated.

EXPERIMENTAL

Apparatus

Infrared spectra of the synthesized resin and its metal complexes in KBr were recorded in the range 4000–200 cm^{-1} on an IR spectrophotometer (Perkin-Elmer 983). The electron paramagnetic resonance (EPR) spectra of the metal–resin complexes in the solid state were recorded at room temperature on an EPR spectrophotometer (Bruker ESP 300).

A gas chromatograph (Shimadzu Model GC-9A) equipped with a hydrogen flame ionization detector and integrator (Shimadzu Chromatopac C-R2AX) was used. Pure nitrogen and nitrogen containing 5 and 10% (v/v) of ammonia were used as carrier gases at flow-rates in the range 20–90 mL min^{-1} . The column temperature varied in the range 70–100°C.

Chemicals

Most chemicals were of analytical-reagent grade from Merck (Darmstadt, Germany). Dialkyl sulphides were supplied by Aldrich (Milwaukee, WI, USA).

Synthesis of sorbents

Silica gel (50 mesh) was ground, sieved and refluxed in 2-propanol for 2 h, then washed successively with water and acetone. A solution of N-[3-(trimethoxy silyl)propyl]ethylenediamine (5 ml) in toluene (100 ml) was added to this purified silica (4 g); after reaction at 75°C with acetic acid as catalyst for 3 h, the resulting modified silica was washed successively with 2-propanol, water and acetone and then dried overnight under vacuum at 60°C. A solution of carbon disulphide (10 ml) and potassium *tert.*-butoxide (6 g) in toluene (300 ml) was added to the above product. The mixture was stirred for 6 h at 60°C. The product was called S-DTC.

Preparation of metal-loaded sorbents

A 3-g amount of the synthesized resin was suspended in 0.1 M Cd(II), Cu(II), Hg(II) or Zn(II) solution (90 ml). Acetic acid–sodium acetate buffer (1 M, pH 5) (10 ml) was added and each mixture was mechanically shaken for 4 h. The metal-loaded phases were collected on glass filters and washed with pure water (> 16 M Ω , 100 ml) and dried for 2 h in a vacuum oven.

Analytical application

Gas chromatography was carried out on 2.1 m \times 3.2 mm I.D. spiral glass columns which were packed under ultrasonic conditions with the synthesized resin metal complexes. The columns were conditioned for 5 h before measurements were taken.

RESULTS AND DISCUSSION

Characterization

The composition and structures of the synthesized resin were characterized after each step of the synthesis by elemental analysis and IR spectrometry. The functionality of ethylenediamine to the silica gel was 1.55 mmol g^{-1} and that of dithiocarbamate to the above product was 1.41 mmol g^{-1} . The elemental analysis data are given in Table I.

The pK_a values of the synthesized resin were determined by potentiometric titration and calculated by a modification of Bjerrum's method. The pK_a values were 7.0 and 9.4 (Table II). By comparison with the pK_a values of some protonated amine [7] and dithiocarbamate compounds [8], the former

TABLE I

ELEMENTAL ANALYSIS DATA OF CHELATING RESINS WITH SILICA GEL AS MATRIX

Resin	C		H (%)	N		S		EN group (mmol g ⁻¹)	DTC group (mmol g ⁻¹)
	%	mmol g ⁻¹		%	mmol g ⁻¹	%	mmol g ⁻¹		
S-EN	10.35	9.03	2.37	4.35	3.10	—	—	1.55	—
S-DTC	13.41	11.17	3.30	4.46	3.18	9.03	2.82	1.59	1.41

valve can be concluded possibly to be the dissociation constant of the NH₂⁺ group and the latter the dissociation constant of the -NCS₂H group of S-DTC resin. The results are reasonable as the steric hindrance is larger in the resin, even though the pK_a values for the resin are higher than those for the monomeric compounds.

The adsorption capacities of the resin for Cd(II), Cu(II), Hg(II) and Zn(II) were measured at various pH values and the results are shown in Fig. 1. At the optimum pH, the adsorption capacities of S-DTC for Cd(II), Cu(II), Hg(II) and Zn(II) were 0.63, 1.12, 3.06 and 0.43 mmol g⁻¹, respectively. The resin presumably formed a 1:1 metal complex with copper ion and water molecules might be ligands for the unsaturated coordination site of the copper ion. The affinity of metal ions toward the synthesized resin decreased in the order Hg(II) > Cu(II) > Cd(II) > Zn(II) on the basis of the sorptive capacity. This order was coincident with that for the analogous complexes of the monomeric dithiocarbamate in aqueous solution [8]. Hence the fixation of the dithiocarbamate group on the silica surface does not lead to substantial changes in the complexing properties of its functional groups. The relatively high uptake of mercury by the resin might be attributed to the additional complexing power of the two nitrogen atoms of the spacer. The capacity of the resin for each metal ion nearly approached saturation in the medium in the pH range 4–5, ex-

TABLE II

pK_a VALUES OF SOME PROTONATED AMINE AND DITHIOCARBAMATE COMPOUNDS

Species	pK _a	Species	pK _a
NH ₄ ⁺	9.24 ^a	Me ₂ NCS ₂ H	3.66 ^b
<i>n</i> -BuNH ₃ ⁺	10.60 ^a	Et ₂ NCS ₂ H	4.04 ^b
Me ₂ NH ₂ ⁺	10.77 ^a	<i>n</i> -Pr ₂ NCS ₂ H	4.79 ^b
⁺ NH ₃ CH ₂ CH ₂ NH ₃ ⁺	pK ₁ 6.95 ^a pK ₂ 9.93 ^a	<i>n</i> -Bu ₂ NCS ₂ H	5.19 ^b
NH ₂ ⁺ of S-DTC	9.4	-NCS ₂ H of S-DTC	7.0

^a Ref. 7.^b Ref. 8.

periment in aqueous solution [8]. Hence the fixation of the dithiocarbamate group on the silica surface does not lead to substantial changes in the complexing properties of its functional groups. The relatively high uptake of mercury by the resin might be attributed to the additional complexing power of the two nitrogen atoms of the spacer. The capacity of the resin for each metal ion nearly approached saturation in the medium in the pH range 4–5, ex-

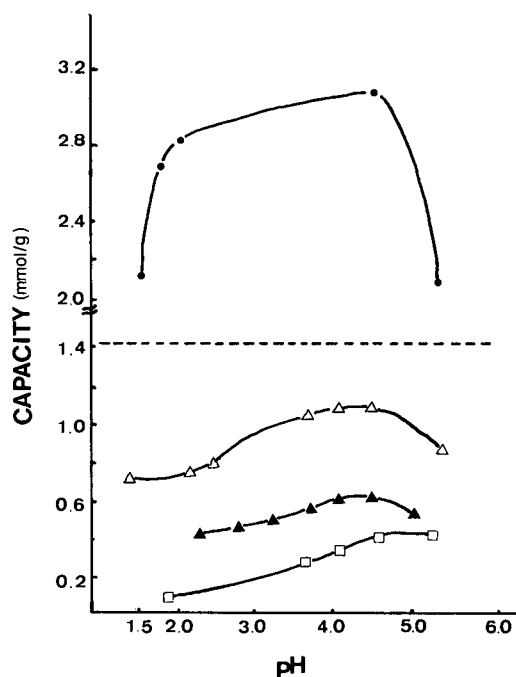
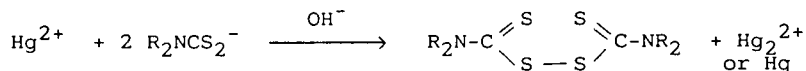


Fig. 1. Metal capacity as a function of pH for S-DTC resin. ● = Hg(II); △ = Cu(II); ▲ = Cd(II); □ = Zn(II). Dashed line: functionality of S-DTC.

TABLE III
PRINCIPAL IR ABSORPTION BANDS (cm⁻¹) OF THE SYNTHESIZED RESIN AND ITS METAL COMPLEXES

Material	$\nu(\text{OH})$	$\nu(\text{NH})$	$\nu(\text{CH})$	$\delta(\text{NH})$	$\nu(\text{N-CS}_2) + \delta(\text{CH}_2)$	$\nu[(\text{C})\text{CN}]$	$\nu(\text{CNC} + \text{CS}_2)$
S-DTC		3433	2937	1618	1467	1096	959
Cu-S DTC	3447	3425		1639	1510	1109	
Hg-S-DTC	3446	3415		1629	1511	1095	



cept that for mercury, which approached saturation in the medium in the pH range 2–5. The metal ion capacity at pH > 5 obviously decreases, and the yellow colour of the resin turns greyish black. These effects might be due to the reducing power of the resin, undergoing the following reaction as reported by Dwyer and Mellor [9] for the reaction of Et₂DTC and Cu(II) at pH > 5 shown above. All the phenomena stated above appeared to occur with the metal ions tested. However, the potential difference of the oxidation–reduction pair is not as large for Cu(II), Cd(II) and Zn(II) as that for Hg(II).

Peak positions and assignments of the IR spectra are given in Table III. Coordination of dithiocarbamate causes $\nu(\text{N-CS}_2)$ to move towards higher wavenumbers and the $\nu(\text{CNC} + \text{CS}_2)$ peak intensity decreases. This is evidence for the coordination of the dithiocarbamate groups of the resin for each metal ion.

TABLE IV
PARAMETERS OF THE EPR SPECTRA OF Cu-S-DTC COMPLEXES AT VARIOUS pH VALUES

Condition	g Values			
pH 1.5	–	2.167	2.080	–
pH 2.8	2.335	2.144	2.077	–
pH 4.5	2.335	–	2.061	–
pH 5.3	2.335	–	2.031	2.012
Start at pH 1.5 then complexation with Cu(II) at pH 4.5	2.335	–	2.031	–

All the EPR spectra of the copper-loaded S-DTC resin complexes in Table IV were measured at room temperature. In the EPR spectra the g value decreased with increasing pH of the solution. The g value at a higher pH of the solution was coincident with that for the monomeric Cu–diethyldithiocarbamate complex (2.035) [10]. The value at a lower pH of the solution approached that of the Cu–polyiminoethylenedithiocarbamate complex (2.089) [11]. The result is rational, even though the latter was a one-dimensional polymer and the resin studied here was a three-dimensional polymer. At pH < 3, one additional very broad signal results with an average g value of 2.14. This must be caused by a weak Cu–Cu interaction resulting in the disappearance of the hyperfine structure. At pH > 2.5, g_{\parallel} components with an average value of 2.335 and an A_{\parallel} value of 107 could be found in their EPR spectra. This indicated the presence of Cu–O coordination [12]. The oxygen came from a water molecule. The results indicated that the presence of an unsaturated coordination of copper in the resin complexes was suitable for application in LEC.

The basic principle of LEC is that a metal ion is fixed on a solid support via a chelating ligand. The interaction occurring between a transition metal and the solute occurs with the formation of coordination bonds inside the coordination sphere of the complex-forming ion, provided that the coordination sphere of this ion is unsaturated. This applies even though various mechanisms could also be responsible for the interaction between the solute to be determined and LEC sorbents, such as ion exchange and hydrophobicity, in addition to ligand exchange. The specific coordination properties are

TABLE V
RESULTS OF DETERMINING THE STABILITY CONSTANTS OF COPPER–RESIN COMPLEXES (25°C)

Parameter	Value
pK_a (EN)	9.4
pK_a (DTC)	7.0
pH for complexation	5.5
pH for decomplexation	3.5
$\text{Log } K_f$	10.8

expected to play the most important role. As the complexation properties and complex equilibria can be characterized by the formation constant, for the calculation of the stability constants of the copper–resin complexes the following equation was used [13]:

$$\log K_{MR} = \log B'_j - nD_{pH}$$

where B'_j is the apparent cumulative protonation constant of the ligand, n is the number of protons

bound to the ligand and D_{pH} is the pH for decomplexation. The protonation constant of the synthesized resin and the D_{pH} values of the copper–resin complex were investigated and are given in Table V. The stability constant of the copper–resin complex can then be calculated (Table V).

Analytical application of the synthesized resin in ligand-exchange chromatography

Thermal stability was studied with regard to the practical use of S-DTC metal complexes as stationary phases in gas chromatography. Thermogravimetric analysis (TGA) (Fig. 2) showed that S-DTC–Cu was very stable below 150°C. Mass loss occurred above 160°C, *i.e.*, at 164.15, 313.73 and 388.51°C, corresponding to N–CS₂ and Si–C bond cleavage and loss of surface silanol groups of silica gel, respectively [14]. The S-DTC–Cu phase was also found to be very stable for longer than 25 days with continuous heating at 90°C. These properties suggested the suitability of the resin for use as a stationary phase in gas chromatography for the separation of volatile compounds.

In LEC, a change in the concentration of ligands

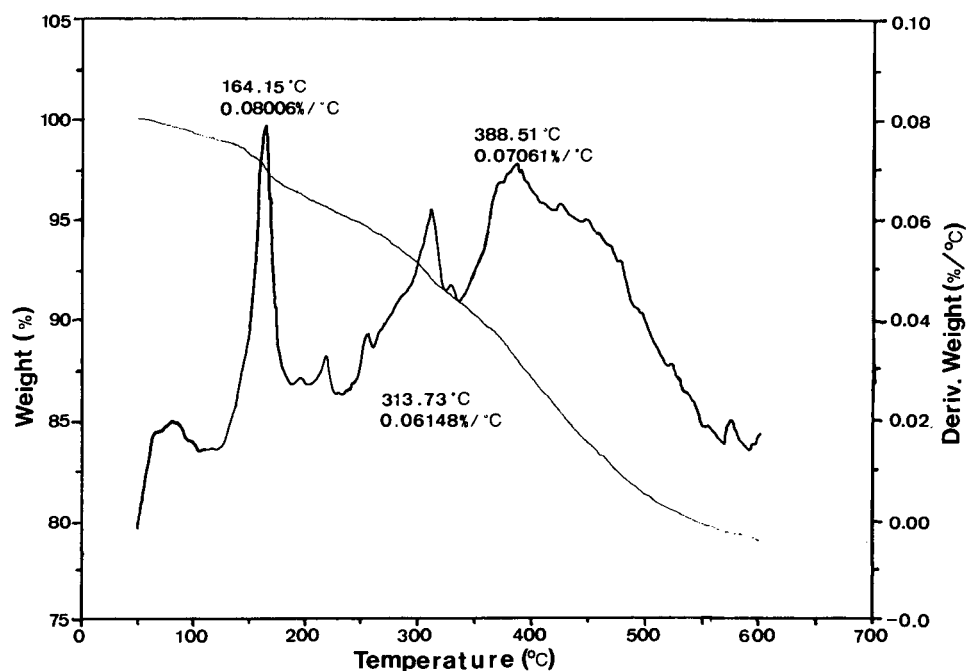


Fig. 2. TGA of S-DTC–Cu(II) complex.

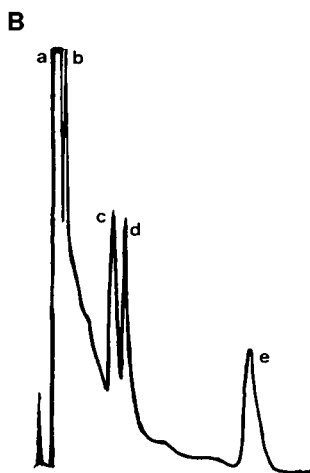
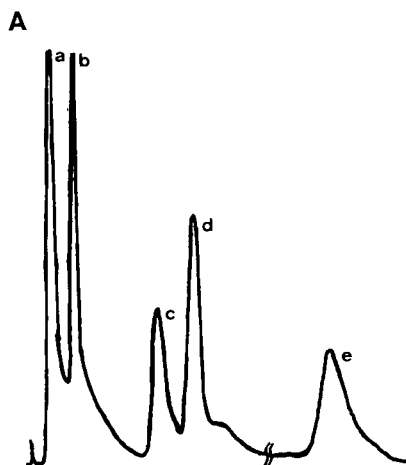


Fig. 3. Separation of mixtures. Stationary phase, S-DTC-Cu(II) complex; carrier gas, (A) nitrogen and (B) 10% (v/v) $\text{NH}_3\text{-N}_2$; flow-rate, 60 ml min^{-1} ; oven temperature, 100°C ; injection temperature, 155°C ; sample, $2 \mu\text{l}$, 1% in CS_2 . (A) Peaks: a = CS_2 ($t_R = 2.2 \text{ min}$); b = dimethyl sulphide ($t_R = 13.0 \text{ min}$); c = allyl methyl sulphide ($t_R = 49.4 \text{ min}$); d = diethyl sulphide ($t_R = 64.4 \text{ min}$); e = diisopropyl sulphide ($t_R = 186.3 \text{ min}$). (B) Peaks: a = CS_2 ($t_R = 2.2 \text{ min}$); b = dimethyl sulphide ($t_R = 8.8 \text{ min}$); c = allyl methyl sulphide ($t_R = 28.9 \text{ min}$); d = diethyl sulphide ($t_R = 33.4 \text{ min}$); e = diisopropyl sulphide ($t_R = 86.0 \text{ min}$).

in the mobile phase had a pronounced effect on the retention of sample components. The presence of ammonia in the mobile phase drastically reduced

the retention of samples. The concentration of ammonia tested was 5% and 10% (v/v) in nitrogen. The presence of ammonia in the mobile phase was found to affect not only the retention but also the peak shape (Fig. 3). A 10% concentration of ammonia in nitrogen was chosen as the mobile phase. The effects of flow-rate and column temperature on retention when 10% ammonia in nitrogen was used as the mobile phase are shown in Figs. 4 and 5. The theoretical plate numbers in the separation of dialkyl sulphides using S-DTC-Cu as the stationary phase under various conditions are shown in Tables VI and VII.

The concentration of ammonia, flow-rate and the column temperature are important factors for the separation of sulphides, as discussed above. The factors responsible for the retention order are con-

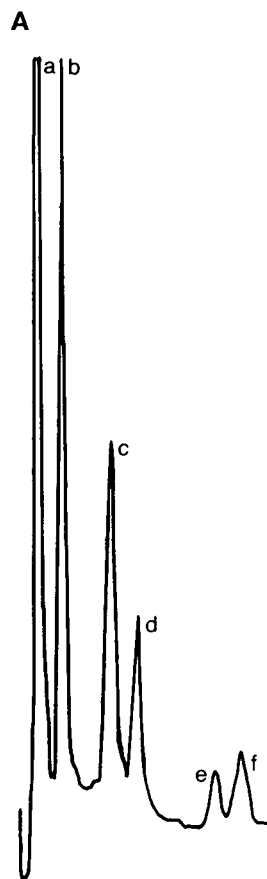


Fig. 4.

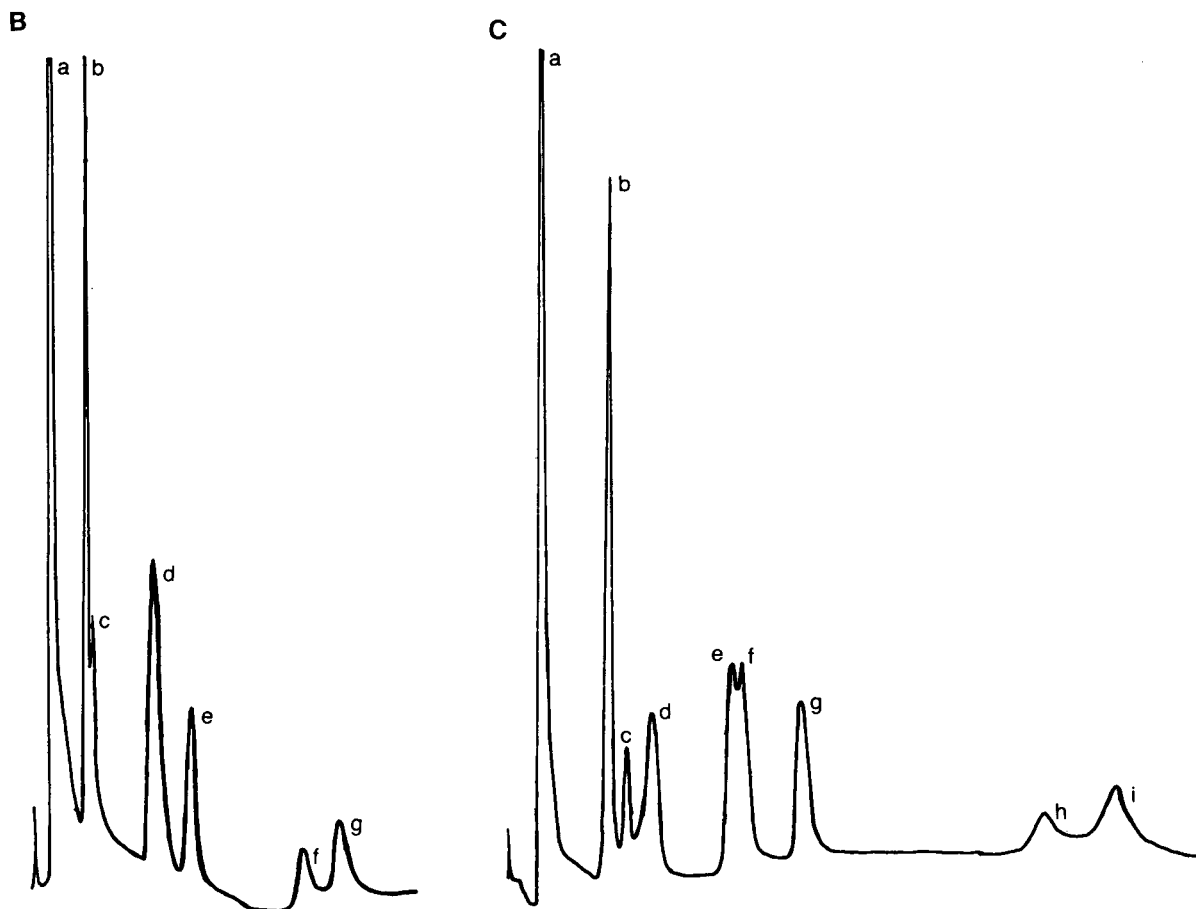


Fig. 4. Separation of hydrocarbons and dialkyl sulphides. Stationary phase, S-DTC–Cu(II) complex; carrier gas, 10% (v/v) $\text{NH}_3\text{--N}_2$; flow-rate, (A) 30, (B) 60 and (C) 90 ml min^{-1} ; oven temperature, 100°C ; injection temperature, 155°C ; samples, $2 \mu\text{l}$, 1% in CS_2 . (A) Peaks: a = CS_2 ($t_R = 3.0 \text{ min}$); b = cyclohexane and *n*-hexane ($t_R = 8.5 \text{ min}$); c = dimethyl sulphide ($t_R = 9.3 \text{ min}$); d = *n*-heptane and benzene ($t_R = 19.1 \text{ min}$); e = iso-octane ($t_R = 24.7 \text{ min}$); f = allyl methyl sulphide ($t_R = 41.4 \text{ min}$); g = diethyl sulphide ($t_R = 47.0 \text{ min}$). (B) Peaks: a = CS_2 ($t_R = 3.9 \text{ min}$); b = cyclohexane and *n*-hexane ($t_R = 11.2 \text{ min}$); c = dimethyl sulphide ($t_R = 12.7 \text{ min}$); d = *n*-heptane and benzene ($t_R = 26.0 \text{ min}$); e = iso-octane ($t_R = 33.3 \text{ min}$); f = allyl methyl sulphide ($t_R = 57.0 \text{ min}$); g = diethyl sulphide ($t_R = 64.6 \text{ min}$). (C) Peaks: a = CS_2 ($t_R = 6.6 \text{ min}$); b = cyclohexane ($t_R = 21.3 \text{ min}$); c = *n*-hexane ($t_R = 25.3 \text{ min}$); d = dimethyl sulphide ($t_R = 38.6 \text{ min}$); e = *n*-heptane ($t_R = 47.2 \text{ min}$); f = benzene ($t_R = 49.3 \text{ min}$); g = iso-octane ($t_R = 62.2 \text{ min}$); h = allyl methyl sulphide ($t_R = 105.9 \text{ min}$); i = diethyl sulphide ($t_R = 121.0 \text{ min}$).

TABLE VI

THEORETICAL PLATE NUMBERS OF DIALKYL SULPHIDES USING S-DTC–Cu(II) AS STATIONARY PHASE AT AN OVEN TEMPERATURE OF 100°C AND A FLOW-RATE OF 60 ml min^{-1} WITH DIFFERENT CARRIER GASES

Carrier gas	Dimethyl sulphide	Diethyl sulphide	Allyl methyl sulphide
10% $\text{NH}_3\text{--N}_2$	2344	763	233
Nitrogen	108	694	195

TABLE VII

THEORETICAL PLATE NUMBERS OF DIALKYL SULPHIDES USING S-DTC–Cu(II) AS STATIONARY PHASE WITH 10% NH₃–N₂ AS CARRIER GAS AT DIFFERENT OVEN TEMPERATURES AND FLOW-RATES

Oven temperature (°C)	Flow-rate (ml/min)								
	90			60			30		
	90	60	30	90	60	30	90	60	30
	Dimethyl sulphide			Diethyl sulphide			Allyl methyl sulphide		
100	670	2344	1826	667	763	1913	168	233	438
85	190	268	1293	501	948	2154	462	518	411
70	774	676	417	1413	1362	1368	1095	924	1246

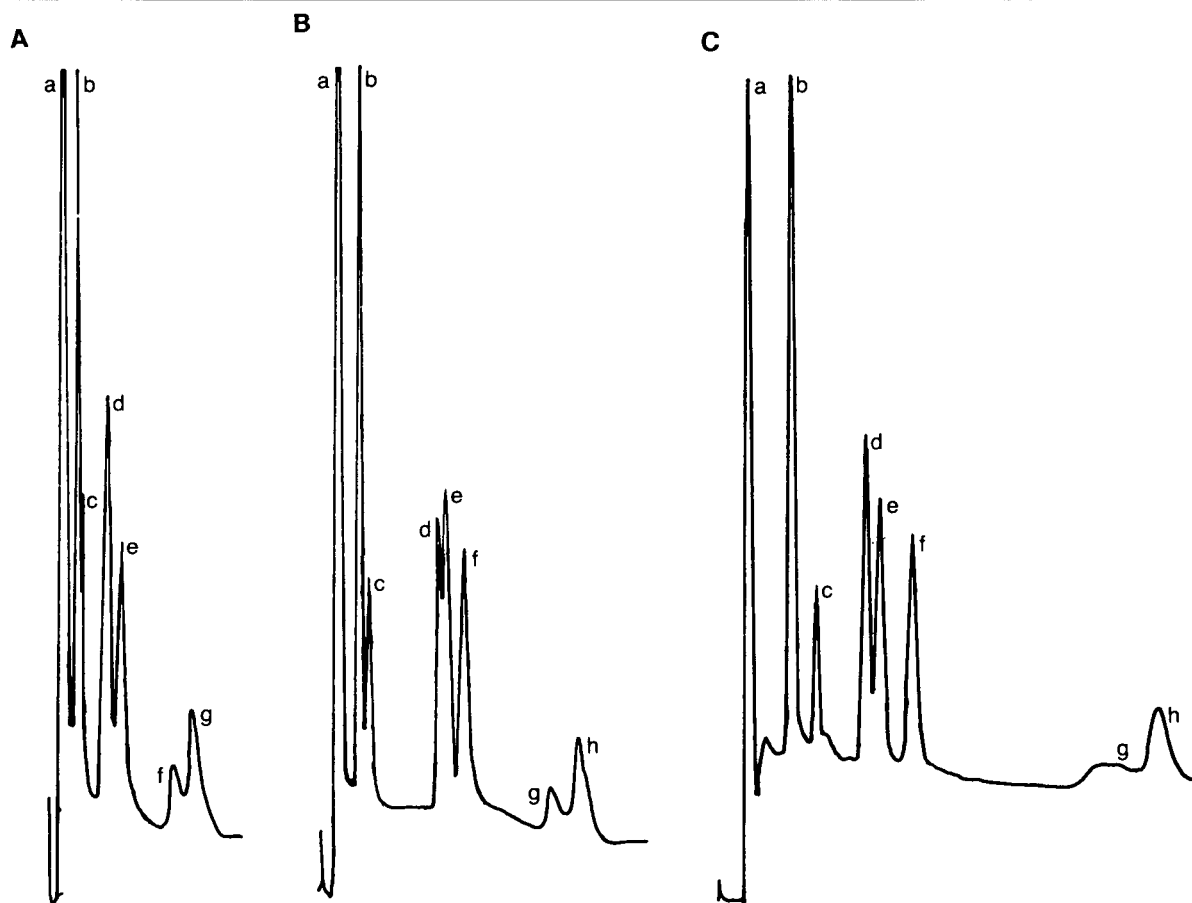


Fig. 5. Separation of hydrocarbons and dialkyl sulphides. Stationary phase, S-DTC–Cu(II) complex; carrier gas, 10% (v/v) NH₃–N₂; flow-rate, (A) 30, (B) 60 and (C) 90 ml min⁻¹; oven temperature, 85°C; injection temperature, 155°C; sample, 2 μl, 1% in CS₂. (A) Peaks: a = CS₂ (*t*_R = 2.2 min); b = cyclohexane and *n*-hexane (*t*_R = 5.6 min); c = dimethyl sulphide (*t*_R = 6.9 min); d = *n*-heptane and benzene (*t*_R = 12.3 min); e = iso-octane (*t*_R = 15.0 min); f = allyl methyl sulphide (*t*_R = 26.8 min); g = diethyl sulphide (*t*_R = 30.7 min). (B) Peaks: a = CS₂ (*t*_R = 3.0 min); b = cyclohexane and *n*-hexane (*t*_R = 8.02 min); c = dimethyl sulphide (*t*_R = 9.1 min); d = *n*-heptane (*t*_R = 16.4 min); e = benzene (*t*_R = 17.8 min); f = iso-octane (*t*_R = 21.6 min); g = allyl methyl sulphide (*t*_R = 39.8 min); h = diethyl sulphide (*t*_R = 46.2 min). (C) Peaks: a = CS₂ (*t*_R = 5.5 min); b = cyclohexane and *n*-hexane (*t*_R = 15.0 min); c = dimethyl sulphide (*t*_R = 20.2 min); d = *n*-heptane (*t*_R = 30.6 min); e = benzene (*t*_R = 33.5 min); f = iso-octane (*t*_R = 40.5 min); g = allyl methyl sulphide (*t*_R = 81.1 min); h = diethyl sulphide (*t*_R = 92.8 min).

sidered, on the basis of the chromatograms, to be as follows. In LEC, the ligand-exchange equilibrium and the basicity of the sulphur atom of a sulphide are thought to be responsible for the elution order. Other factors should exist that affect the elution order, as the basicities of dialkyl sulphides are not very different from one another. Branching of the alkyl group inhibits the copper–sulphur coordination and causes weak retention. Di-*sec.*-butyl sulphide (retention time > 180 min) and di-*tert.*-butyl sulphide (retention time > 130 min), for example, were eluted in this order (not shown in Fig. 6). For sulphides having the same carbon number and which possess two alkyl groups, that which has the longest alkyl chain was most strongly retained. Diethyl sulphide and methyl allyl sulphide, for example, were eluted in this order (Fig. 4). The differ-

ence in the vapour pressure of samples at a given column temperature was an important factor in determining the elution order, because the retention of a sample molecule was based on its gas–solid distribution. The boiling point of dimethyl sulphide is the lowest among the sulphides studied, hence in most separations dimethyl sulphide was eluted first.

The determination of dialkyl sulphides by the proposed ligand-exchange GC method was also studied (Fig. 6). The calibration graphs are shown in Fig. 7. As these compounds were highly volatile and difficult to handle accurately, the correlation coefficients were lower than expected, with values of 0.9983 (dimethyl sulphide), 0.9963 (allyl methyl sulphide), 0.9857 (diethyl sulphide) and 0.9970 (diisopropyl sulphide), based on the average of three measurements of the sample mixture.

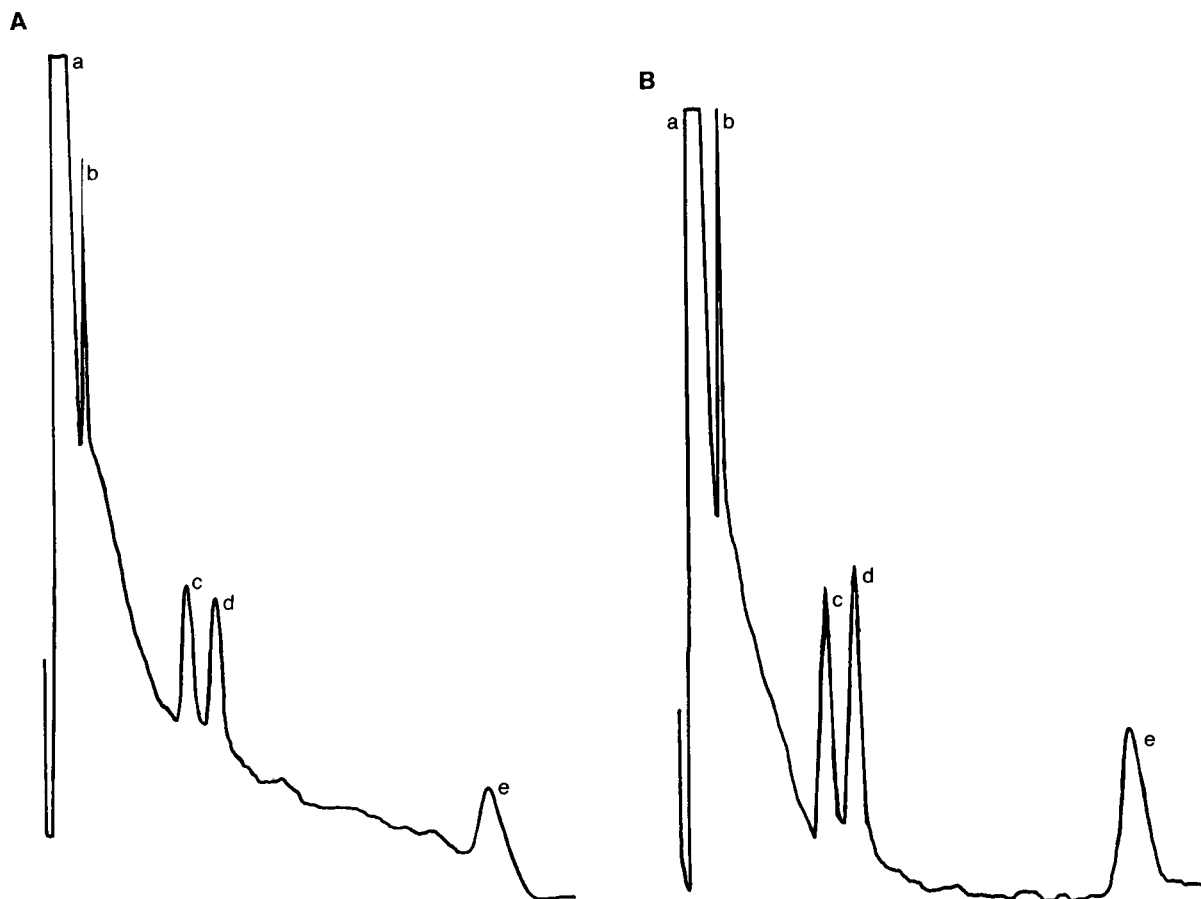


Fig. 6.

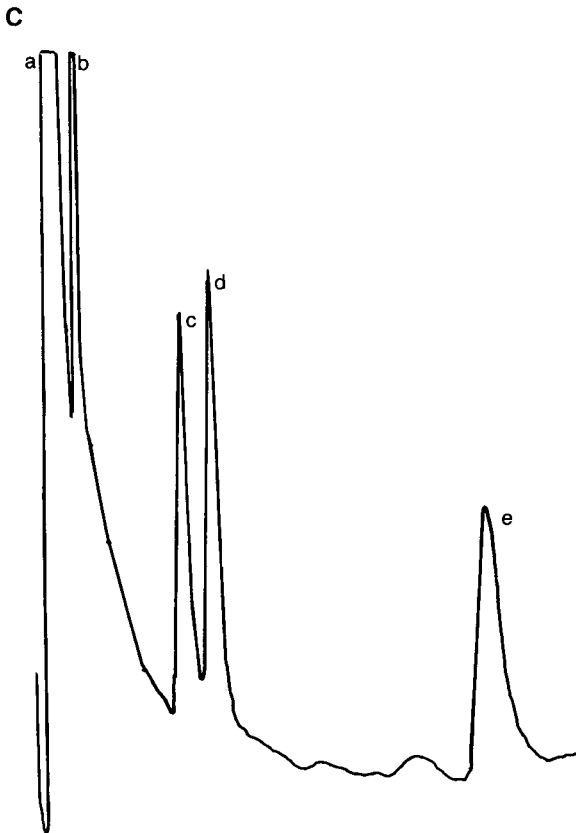


Fig. 6. Separation of mixtures. Stationary phase, S-DTC-Cu(II) complex; carrier gas, 10% (v/v) $\text{NH}_3\text{-N}_2$; flow-rate, 60 ml min^{-1} ; oven temperature, 100°C ; injection temperature, 155°C . (A) Peaks: a = CS_2 ($t_R = 2.4 \text{ min}$); b = dimethyl sulphide ($t_R = 9.3 \text{ min}$, $1.06 \mu\text{g}$); c = allyl methyl sulphide ($t_R = 32.3 \text{ min}$, $1.59 \mu\text{g}$); d = diethyl sulphide ($t_R = 38.7 \text{ min}$, $1.17 \mu\text{g}$); e = diisopropyl sulphide ($t_R = 110.5 \text{ min}$, $1.35 \mu\text{g}$). (B) Peaks: a = CS_2 ($t_R = 2.4 \text{ min}$); b = dimethyl sulphide ($t_R = 9.3 \text{ min}$, $1.99 \mu\text{g}$); c = allyl methyl sulphide ($t_R = 32.6 \text{ min}$, $2.63 \mu\text{g}$); d = diethyl sulphide ($t_R = 39.3 \text{ min}$, $2.67 \mu\text{g}$); e = diisopropyl sulphide ($t_R = 112.6 \text{ min}$, $2.71 \mu\text{g}$). (C) Peaks: a = CS_2 ($t_R = 2.4 \text{ min}$); b = dimethyl sulphide ($t_R = 9.3 \text{ min}$, $4.78 \mu\text{g}$); c = allyl methyl sulphide ($t_R = 32.8 \text{ min}$, $5.45 \mu\text{g}$); d = diethyl sulphide ($t_R = 39.6 \text{ min}$, $5.10 \mu\text{g}$); e = diisopropyl sulphide ($t_R = 111.6 \text{ min}$, $5.40 \mu\text{g}$).

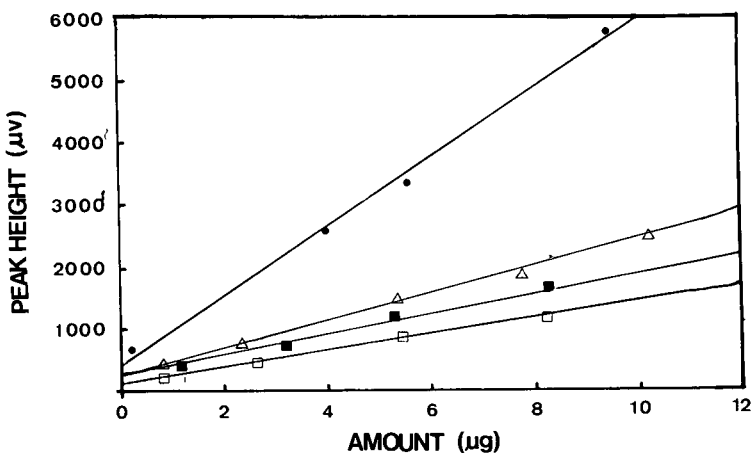


Fig. 7. Determination of dialkyl sulphides by ligand-exchange GC. Oven temperature, 100°C ; carrier gas, 10% (v/v) $\text{NH}_3\text{-N}_2$; flow-rate, 60 ml min^{-1} ; injection temperature, 155°C . ● = dimethyl sulphide ($r = 0.9983$); Δ = allyl methyl sulphide ($r = 0.9963$); ■ = diethyl sulphide ($r = 0.9857$); □ = diisopropyl sulphide ($r = 0.9970$).

CONCLUSIONS

The synthesized dithiocarbamate resin has been demonstrated to have a high affinity for the metal ions studied. The thermal stability of the resin–metal complexes made them very suitable for use as stationary phases for the ligand-exchange GC for the separation of dialkyl sulphides. The results showed that the elution order of samples was dependent on the surface structure of the matrices, the central metal ion, the complex-forming ability of the sample and the steric hindrance to complex formation.

ACKNOWLEDGEMENT

Financial support of this work by the National Science Council of Taiwan is gratefully acknowledged.

REFERENCES

- 1 Z. Marczenko, *Separation and Spectrophotometric Determination of Elements*, Ellis Horwood, Chichester, 1985.
- 2 G. V. Myasoedova and S. B. Savvin, *CRC Crit. Rev. Anal. Chem.*, 17 (1987) 1.
- 3 F. Helfferich, *Nature*, 189 (1961) 1001.
- 4 N. W. F. Nielen, H. E. van Ingen, A. J. Valk, R. W. Frei and U. A. Th. Brinkman, *J. Liq. Chromatogr.*, 10 (1987) 617.
- 5 H. Takayanagi, O. Hatano, K. Fujimura and T. Ando, *Anal. Chem.*, 57 (1985) 1840.
- 6 V. A. Davankov, J. D. Navratil and H. F. Walton, *Ligand Exchange Chromatography*, CRC Press, Boca Raton, FL, 1988.
- 7 D. A. Skoog and D. M. West, *Fundamentals of Analytical Chemistry*, Saunders College Publishing, New York, 5th ed., 1988.
- 8 G. D. Thorn and R. A. Ludwig, *The Dithiocarbamates and Related Compounds*, Elsevier, Amsterdam, 1962.
- 9 F. P. Dwyer and D. P. Mellor, *Chelating Agents and Metal Chelates*, Academic Press, New York, 1964.
- 10 H. R. Gersmann and J. D. Swalen, *J. Chem. Phys.*, 36 (1962) 3221.
- 11 P. C. H. Mitchell and M. G. Taylor, *Polyhedron*, 1 (1982) 225.
- 12 B. Prabhakar and P. Lingaiah, *Polyhedron*, 9 (1990) 805.
- 13 R. Hering, *Chelatbildende Ionenaustauscher*, Akademie Verlag, Berlin, 1967.
- 14 D. E. Leyden, *Silanes, Surfaces, and Interfaces*, Gordon and Breach, New York, 1986, p. 29.

Gas chromatographic analysis of high-molecular-mass polycyclic aromatic hydrocarbons

II. Polycyclic aromatic hydrocarbons with relative molecular masses exceeding 328

Agneta Bemgård, Anders Colmsjö and Bengt-Ove Lundmark

Department of Analytical Chemistry, National Institute of Occupational Health, S-171 84 Solna (Sweden)

(First received July 6th, 1992; revised manuscript received October 15th, 1992)

ABSTRACT

Three columns were used for the gas chromatographic analysis of polycyclic aromatic hydrocarbons (PAHs) with relative molecular masses (M_r) up to 450. Two of the columns were commercially available, coated with a 50% methyltrifluoropropyl-substituted polysiloxane and a 5% diphenyl-substituted methylpolysiloxane. The third column was laboratory made, coated with a biphenyl-substituted silarylene-siloxane copolymer. All three columns were utilized for the analysis of high- M_r PAHs as regards both thermal stability of the stationary phases, *i.e.*, low bleeding rate, and chromatographic efficiency. The column coated with a trifluoropropyl-substituted stationary phase showed, however, a low separation efficiency, possibly owing to low solute-stationary phase compatibility. The biphenyl-substituted stationary phase, on the other hand, showed a very high separation efficiency, but the retention of the PAHs was significantly higher on this column compared with the other two, leading to the demand for higher oven temperatures. Different retention mechanisms were observed on these columns, as shown by differences in the retention indices of the PAHs measured in a system using PAHs as retention index markers. A comparatively faster elution of non-planar PAHs was observed on the columns coated with the trifluoropropyl-substituted stationary phase and the biphenyl-substituted stationary phase compared with the column coated with the 5% diphenyl-substituted polymer. The usefulness of the columns for separations of high- M_r PAHs is demonstrated by gas chromatograms of carbon black extracts and a coal tar extract standard reference material.

INTRODUCTION

Interest in the analysis of polycyclic aromatic hydrocarbons (PAHs) is mainly due to their carcinogenicity and/or mutagenicity. PAHs can be formed from incomplete combustion of fossil fuels and hence they are widespread in the environment. The group is large, with a large number of isomers, and this requires efficient separation methods in order to identify and determine individual PAH isomers.

Focus has mostly been on analyses of PAHs having up to six aromatic rings. For this reason gas chromatography (GC) has become a useful method. For the analysis of higher relative molecular mass (M_r) compounds, high-performance liquid chromatography (HPLC) has mostly been used [1–7]. However, some drawbacks are associated with this method, *e.g.*, in ordinary HPLC the separation efficiency is often poor compared with GC and in micro-LC the analysis is often time consuming. A number of advantages can thus be gained if an efficient GC method for high- M_r PAHs existed. In 1974 Grob [8] chromatographed rubrene (M_r 532) on a 5.5-m capillary column. However, such short columns cannot

Correspondence to: A. Bemgård, Department of Analytical Chemistry, National Institute of Occupational Health, S-171 84 Solna, Sweden.

be used for the separation of complex mixtures. In other investigations, carbon black samples were chromatographed and PAHs with molecular masses exceeding 300 were found [5,9,10]. Recently, a retention index system for PAHs having $M_r = 328$ was presented [11]. The isomers could be separated on a number of selected commercially and specially manufactured capillary columns with high temperature stability. In this study, the same chromatographic technique was used for the separation of PAHs with M_r up to 450.

EXPERIMENTAL

Columns

Following a careful evaluation of more than ten different types of high-temperature-stable columns, three columns were chosen as suitable for GC of the high- M_r PAHs. One of these was a stainless-steel column coated with a thin layer of fused silica and a methyltrifluoropropyl-substituted polysiloxane stationary phase, Rtx-200 (15 m \times 0.28 mm I.D.; film thickness 0.10 μm). Second, a column coated with a methyl-5% diphenyl-substituted polysiloxane stationary phase was used. The tubing material, length, I.D. and film thickness were the same as for the Rtx-200 column. This column is denoted XTI-5. Those columns were obtained from Restek (Bellefonte, PA, USA). The third column (20 m \times 0.32 mm I.D.) was prepared from polyimide-covered fused silica from Chrompack (Middelburg, Netherlands). This was coated with a biphenyl-substituted silarylene-siloxane copolymer synthesized at the University of Neuchatel (Neuchatel, Switzerland). The film thickness was only 0.05 μm . The columns were of the same types as in ref. 11, but in that instance the Rtx-200 and the XTI-5 columns had stationary phase film thicknesses of 0.25 μm .

Apparatus

Chromatography was performed on a Carlo Erba (Milan, Italy) Mega gas chromatograph equipped with a flame ionization detector. A special high-temperature resistant detector tip made from polyimide was used. Hydrogen, passed through an oxygen trap, was used as the carrier gas. Signal recording and data handling were performed with an ELDS 900 laboratory data system (Chromatography Data System, Kungshög, Stenhamra, Sweden).

For the M_r assessments of unknown samples, the columns were connected to an INCOS 50 quadrupole mass spectrometer (Finnigan MAT, San Jose, CA, USA) run in the electron impact (EI) mode. The gas chromatograph in that set-up was a Varian (Walnut Creek, CA, USA) Model 3400 and helium was used as the carrier gas. The columns were connected directly to the ion source. The transfer line temperature was kept at its maximum temperature of 350°C.

Solutes

The structures of the compounds used for this evaluation are shown in Fig. 1a. The PAHs were all *peri*-condensed, with M_r ranging from 352 to 426. In Fig. 1b, the compounds used for retention index determinations are shown. Two standard series were evaluated: the picene standard series with picene, benzo[*c*]picene and dinaphtho[2,1-*a*:2,1-*h*]anthracene and the coronene standard series with coronene, benzo[*a*]coronene and dibenzo[*a,j*]coronene. All of the standard compounds were either purchased from Promchem (Wessel, Germany) or obtained from other laboratories (see Acknowledgements).

Apart from the pure standard compounds, two more complex samples were chromatographed. One of these was an HPLC fraction from standard reference material (SRM) 1597 (National Institute of Standards and Technology), a coal tar extract [12] containing PAHs with M_r exceeding 328. The other applications were two carbon black extracts: one dichloromethane extract and one chlorobenzene extract.

Chlorobenzene (BDH, Poole, UK) was used as the solvent for both the pure PAHs and the SRM and carbon black extracts.

Test conditions

Hydrogen was used as the carrier gas and the inlet pressure was maintained so as to result in gas velocities of *ca.* 1.3 m/s at 140°C. On-column injections were performed in all instances. The oven temperature was kept at 140°C during injection. After a 2-min isothermal period, the oven temperature was increased at 30°C/min to 200°C and 4 min from the injection time the temperature programme was started at a rate of 5°C/min to different upper temperature levels. The Rtx-200 column was used up to

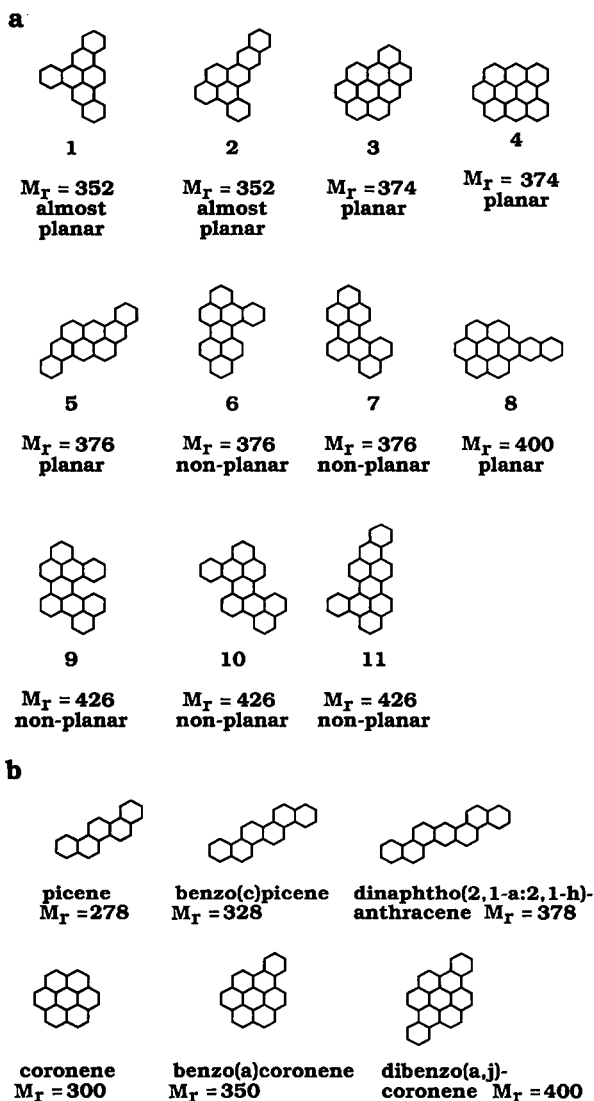


Fig. 1. Molecular structures of (a) *peri*-condensed PAHs and (b) retention index markers.

360°C, the XTI-5 column up to 380°C, and the silabiphenyl column up to 400°C. The upper temperature was dependent on the last-eluting compound, *i.e.*, all the standard compounds (Fig. 1) were forced to elute within the temperature programming ramp in order to obtain a temperature-programmed retention index for each compound.

The individual PAH components were diluted in chlorobenzene at concentrations resulting in constant retention times and symmetrical peaks inde-

pendent of sample sizes injected. The injection volume was kept as small as possible and ranged from 0.2 to 1.0 μl .

Retention index determinations

Temperature-programmed retention indices were measured according to Lee *et al.* [13], *i.e.*, by linear interpolation between two PAH index markers adjacent to the compound to be measured. In the picene standard series, picene was given the value of 500, benzo[*c*]picene 600 and dinaphtho[2,1-*a*:2,1-*h*]anthracene 700. In the coronene standard series, coronene was given a value of 100, benzo[*a*]coronene 200 and dibenzo[*a,j*]coronene 300. For all compounds eluting after the last retention index marker in each system, the retention index values were extrapolated. For comparison, in one example retention indices were calculated with *n*-alkane homologues ranging from C_{15} to C_{34} according to ref. 14.

RESULTS AND DISCUSSION

Columns

In a previous study, PAHs of M_r 328 were subjected to GC [11]. After careful evaluation of the available columns and stationary phases, four columns were found suitable in that work. However, for higher M_r , those columns were found not to be useful owing to high retention times. However, this could be overcome by using columns with decreased film thicknesses. In this work, the Rtx-200 and XTI-5 types of columns were used with film thicknesses of 0.10 μm . For the silabiphenyl column the elution temperature was decreased by means of an increased inlet pressure, *i.e.*, from 0.5 to 0.9 bar. As was observed previously [11], the trifluoropropyl-substituted stationary phase exhibited low retentions for the high- M_r PAHs. From the peak shapes it was concluded that the low retention mainly was due to low solubility of the high- M_r PAHs in the stationary phase. This was also experienced in this work. In Fig. 2, chromatograms of a mixture of the *peri*-condensed PAHs injected together with the retention index markers are shown. In Fig. 2a, the chromatogram obtained from the XTI-5 column shows that two of the highest- M_r compounds (M_r 426) were eluted at 360°C. On the Rtx-200 column in Fig. 2b, the elution temperature for these com-

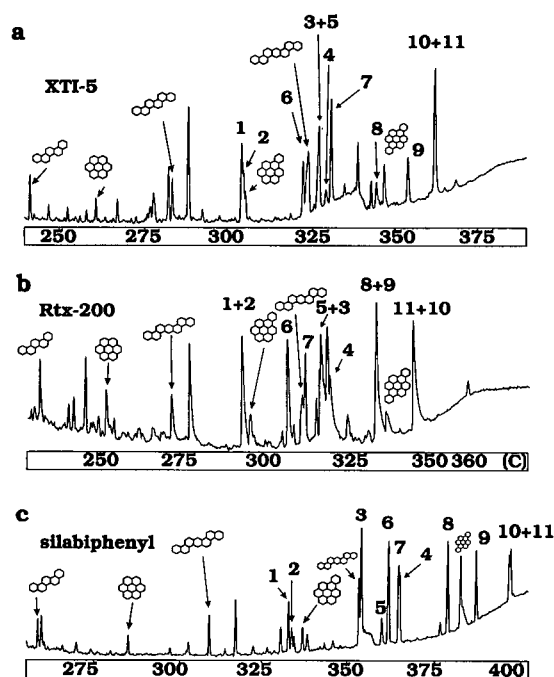


Fig. 2. Gas chromatograms with flame ionization detection (FID) of *peri*-condensed PAHs on (a) the XTI-5, (b) the Rtx-200 and (c) the silabiphenyl column. Conditions: on-column injection at 140°C, after a 2-min isothermal period heated at 30°C/min to 200°C and after 4 min from the injection programmed at 5°C/min to (a) 380°C, (b) 360°C and (c) 400°C. Peak numbers refer to Fig. 1a.

pounds was below 350°C. The column dimensions, film thicknesses, inlet pressures and temperature programming rate were identical for these two columns. In Fig. 2c, the chromatogram of the same

mixtures obtained on the silabiphenyl column shows that the elution temperature of the two last eluting compounds was almost 400°C. A valuable observation is that the silabiphenyl column was able to separate slightly the two last-eluting isomers of M_r 426.

Column efficiency can be measured in terms of Trennzahl numbers when temperature-programmed runs are considered. The Trennzahl numbers for coronene–benzo[*a*]coronene were 35, 58 and 76 for the Rtx-200, XTI-5 and silabiphenyl columns, respectively. For all columns, the separation numbers were slightly higher for the *peri*-condensed types of PAHs, *i.e.*, coronene–benzo[*a*]coronene, than for the linear (*cata*-condensed) types of PAHs (benzo[*c*]picene–dinaphtho[2,1-*a*:2,1-*h*]anthracene).

Retention indices

Commonly used markers for retention index assessments are a homologous series of *n*-alkanes. However, the advantage of employing retention index markers similar to the compounds to be measured has been pointed out earlier concerning both isothermal [15] and temperature-programmed runs [13,14]. Dissimilar markers and compounds to be measured will have different partition coefficients at different temperatures, which can result in temperature-dependent retention indices and even changes in elution order [16]. A consequence of this is that when using an *n*-alkane homologous series as retention index markers for PAHs, the retention indices will be dependent on elution temperature. Table I shows a comparison between retention indices obtained by use of an *n*-alkane standard series and the

TABLE I

COMPARISON OF INDICES IN THE PICENE STANDARD SERIES AND THE *n*-ALKANE SERIES OBTAINED ON THE SILABIPHENYL COLUMN OPERATED AT DIFFERENT INLET PRESSURES (12–15°C DIFFERENCE IN ELUTION TEMPERATURE)

Compound	<i>n</i> -Alkane standard			Picene standard		
	$P_i = 55$	$P_i = 90$	ΔA	$P_i = 55$	$P_i = 90$	ΔP
Chrysene	2836	2819	17	400	400	–
Benzo[<i>e</i>]pyrene	3314	3276	38	454.4	454.1	0.3
Picene	3765	3685	80	500	500	–
Coronene	4288	4183	105	553.2	554.3	–1.1
Benzo[<i>c</i>]picene	4747	4637	110	600	600	–
Benzo[<i>a</i>]coronene	5348	5213	135	662.5	663.1	–0.6

TABLE II

TEMPERATURE-PROGRAMMED AVERAGE RETENTION INDICES OF THE *PERI*-CONDENSED PAHs MEASURED WITH THE PICENE STANDARD SYSTEM

Compound ^a	$I \pm$ S.D		
	XTI-5	Rtx-200	Silabiphenyl
Picene	500	500	500
Coronene	546.41 \pm 0.07 ^c	549.57 \pm 0.43 ^d	552.69 \pm 0.06 ^e
Benzo[c]picene	600	600	600
1	651.93	653.20	653.01
2	653.44	656.15	655.00
Benzo[a]coronene	654.77 \pm 0.21 ^f	660.02 \pm 0.37 ^d	662.36 \pm 0.14 ^e
6	697.73	688.32	701.59
Dinaphtho[2,1- <i>a</i> :2,1- <i>h</i>]anthracene	700	700	700
3^b	708.80	715.48	719.50
5^b	709.55	715.19	714.86
4^b	714.66	721.18	727.01
7^b	718.81	703.50	726.15
8^b	752.57	756.85	758.99
Dibenzo[<i>a,j</i>]coronene ^b	758.47 \pm 1.00 ^c	765.36 \pm 1.46 ^d	767.32 \pm 0.34 ^e
9^b	775.90	756.26	777.56
10^b	795.35	785.48	799.54
11^b	796.35	784.97	800.78

^a Numbers refer to compounds in Fig. 1a.^b Extrapolated values from benzo[c]picene–dinaphtho[2,1-*a*:2,1-*h*]anthracene.^c Fourteen determinations.^d Eleven determinations.^e Twelve determinations.^f Thirteen determinations.

picene standard series. The column used was silabiphenyl at two different inlet pressures, 0.5 and 0.9 bar. This pressure difference resulted in a *ca.* 15°C lower elution temperature for the higher inlet pressure, 0.9 bar. Some lower- M_r PAHs were added to this mixture, *i.e.*, chrysene and benzo[*e*]pyrene. The temperature programming, at 7°C/min, was started 2 min from injection, which was performed at 70°C. Differences in the *n*-alkane system, denoted ΔA , show that the *n*-alkane retention index differences will increase during the temperature-programmed run. On the other hand, the retention indices measured with the picene standard system remain fairly constant (ΔP). The absolute figures also reflect the fact that the PAH retention index system is much more insensitive to changes in elution temperature. However, it should be kept in mind that 1 index unit in the PAH system is comparable to 10 units in the *n*-alkane system, although the accuracy of the PAH

retention index system is superior to the *n*-alkane system when applied to PAHs.

Based on the above discussion, it was of interest to compare retention indices observed on different columns. If the forces acting on the retention index markers and the solutes are similar, similar retention indices should be obtained independent of the stationary phase properties. The retention indices for the *peri*-condensed PAHs in the picene standard system are listed in Table II and in the coronene standard system in Table III. It can be seen that the retention indices for some compounds differ considerably between columns.

As shown in an earlier study [11], differences in the retention indices of PAHs were observed when comparing different columns. Deviations could be referred to differences in planarity. This was also found to be true for the higher- M_r PAHs (Tables II and III). A comparatively lower retention for the

TABLE III

TEMPERATURE-PROGRAMMED AVERAGE RETENTION INDICES OF THE *PERI*-CONDENSED PAHs MEASURED WITH THE CORONENE STANDARD SYSTEM

Compound ^a	<i>I</i> ± S.D		
	XTI-5	Rtx-200	Silabiphenyl
Picene ^b	55.83 ± 0.07 ^c	55.36 ± 0.96 ^d	48.32 ± 0.17 ^e
Coronene	100	100	100
Benzo[<i>c</i>]picene	150.97 ± 0.09 ^c	145.63 ± 0.56 ^e	146.41 ± 0.10 ^e
1	197.47	193.79	192.00
2	198.70	196.37	193.72
Benzo[<i>a</i>]coronene	200	200	200
6	241.37	226.75	237.48
Dinaphto[2,1- <i>a</i> :2,1- <i>h</i>]anthracene	243.54 ± 0.39 ^c	237.83 ± 0.94 ^e	235.82 ± 0.13 ^e
3	252.26	252.98	254.72
5	252.66	251.89	250.14
4	257.86	258.65	261.48
7	261.86	240.88	260.79
8	294.83	292.76	291.88
Dibenzo[<i>a,j</i>]coronene	300	300	300
9 ^f	315.99	290.66	309.96
10 ^f	335.40	318.14	330.94
11 ^f	335.90	317.54	331.90

^a Numbers refer to compounds in Fig. 1a.^b Extrapolated value from coronene–benzo[*a*]coronene.^c Thirteen determinations.^d Eleven determinations.^e Twelve determinations.^f Extrapolated values from benzo[*a*]coronene–dibenzo[*a,j*]coronene.

non-planar PAHs was observed on the Rtx-200 column (Fig. 2b), where, *e.g.*, compound **9** elutes prior to dibenzo[*a,j*]coronene. Further, both the non-planar compounds **6** and **7** elute before the planar compounds **3**, **4** and **5** on this column. The differences in retention indices (ΔI) between the Rtx-200 and the XTI-5 columns (expressed as $I_{\text{Rtx-200}} - I_{\text{XTI-5}}$) are shown in Fig. 3. The retention indices were measured with the coronene standard system. Large deviations were observed for the non-planar PAHs (black bars in Fig. 3). Retention differences with up to 25 index units were observed. For the planar and almost planar compounds, the difference in no case exceeded 5 index units. If the same comparison is made for the silabiphenyl column and the XTI-5 column (Fig. 4), the result is not so evident. The absolute differences in retention indices (ΔI) between the silabiphenyl and XTI-5 column never exceeded 8 index units. However, a decreased retention for the non-planar PAHs can also be ob-

served on this column. This can be seen from, *e.g.*, the last three compounds, **9**, **10** and **11**, having M_r 426, which are all non-planar. The increased retention of the planar PAHs is probably greater for this column, *e.g.* compounds **3** and **4**. An attempt to correlate the retention indices with polarizability and connectivity [17] could not easily explain the behaviour for the silabiphenyl column, but probably a complex charge-transfer interaction between the biphenyl units and the PAHs is involved, in addition to other shape parameters apart from planarity.

Applications

A fraction of SRM 1597, a coal tar extract, previously fractionated by HPLC was injected on to the XTI-5 and silabiphenyl columns together with the retention index markers. This fraction should contain PAHs of $M_r > 328$. In previous work [11], the fraction having M_r 328 was analysed in a similar

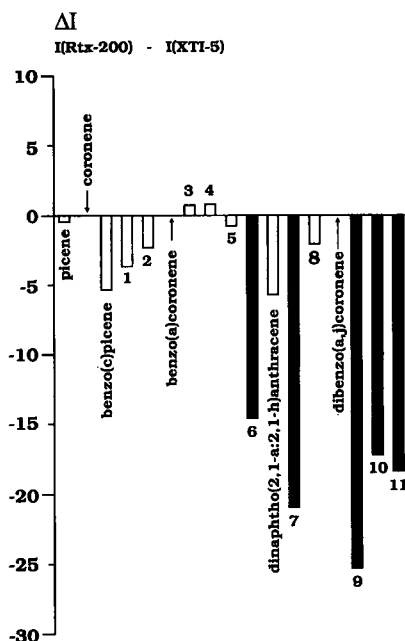


Fig. 3. Absolute differences in retention indices, ΔI , between the Rtx-200 and the XTI-5 columns, measured with the coronene standard system. Black bars indicate non-planar compounds. Numbers refer to the compounds in Fig. 1a.

manner and then found to be a mixture of PAHs having M_r 326 and 328. In Fig. 5, the chromatograms of the fraction having $M_r > 328$ obtained on (a) the XTI-5 and (b) the silabiphenyl columns are shown. From mass spectrometric measurements, it was concluded that this fraction mainly contained PAHs having M_r 352 and a few compounds with M_r 374 and 376.

As a second application, a dichloromethane and a chlorobenzene extract of a carbon black sample were chromatographed. In Fig. 6, the chromatograms obtained on the XTI-5 column are shown. The ability to resolve the higher- M_r compounds was limited for this column, but owing to the comparatively low elution temperature (380°C) it was possible to identify the individual masses in the different fractions by mass spectrometry. The group eluting after dibenzo[*a,j*]coronene consisted mainly of PAHs having M_r 424 and a few with M_r 426. The next group consisted mainly of PAHs having M_r 448 and a few compounds with M_r 450. The last-eluting group contained mainly PAHs with M_r 472.

In Fig. 7, the same fractions were chromato-

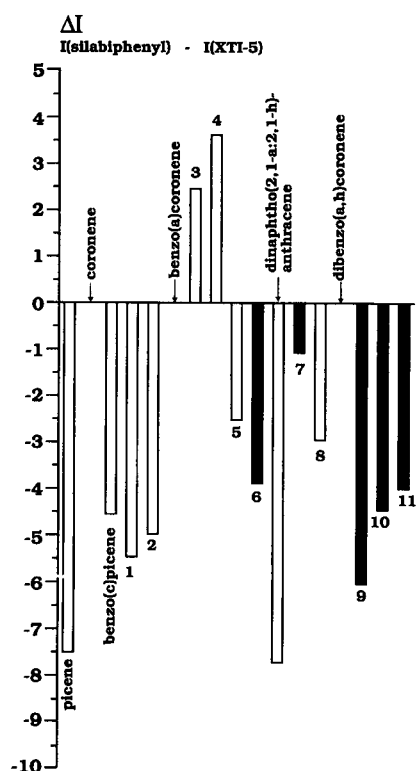


Fig. 4. Absolute differences in retention indices, ΔI , between the silabiphenyl and the XTI-5 columns, measured with the coronene standard system. Black bars indicate non-planar compounds. Numbers refer to the compounds in Fig. 1a.

graphed on the silabiphenyl column. The elution temperature for the last-eluting groups was 400°C. On connecting the column to the mass spectrometer, these compounds were trapped within the last section of the column in the transfer line, which was temperature limited to 350°C. The last compound identified by GC-MS was ovalene, having M_r 398. The masses indicated in the chromatogram in Fig. 7 were tentatively identified by guidance from the MS data obtained from the XTI-5 column (Fig. 6). However, the silabiphenyl column demonstrates a marked separation efficiency even at temperatures up to 400°C.

CONCLUSIONS

The results clearly demonstrate that comparably high- M_r PAHs can be separated and identified by using GC. A few commercial columns are already

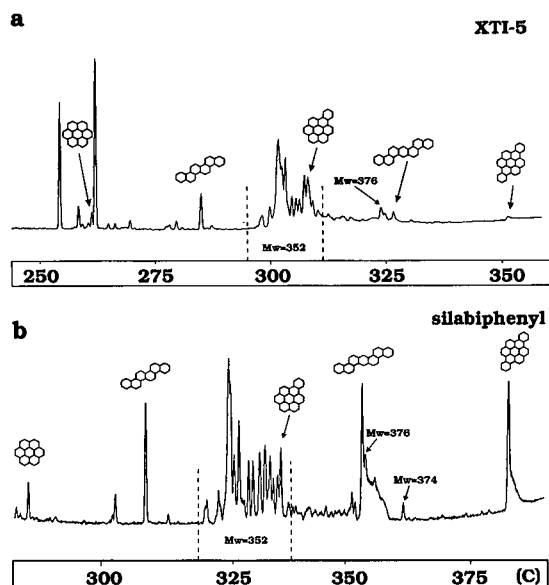


Fig. 5. Gas chromatograms (FID) of SRM 1597, an HPLC fraction having $M_r > 328$, injected together with the retention index markers on (a) the XTI-5 and (b) the silabiphenyl column. Temperature programming as in Fig. 2.

available that can be used successfully in the separation process. It is hoped that other high-temperature stable stationary phases such as the biphenyl-based material described here will become available.

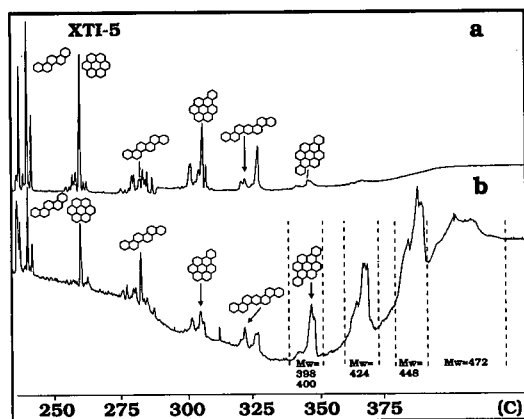


Fig. 6. Gas chromatograms (FID) of (a) a dichloromethane extract and (b) a chlorobenzene extract of carbon black on the XTI-5 column. Temperature programming as in Fig. 2. The indicated mass numbers were identified by GC-MS.

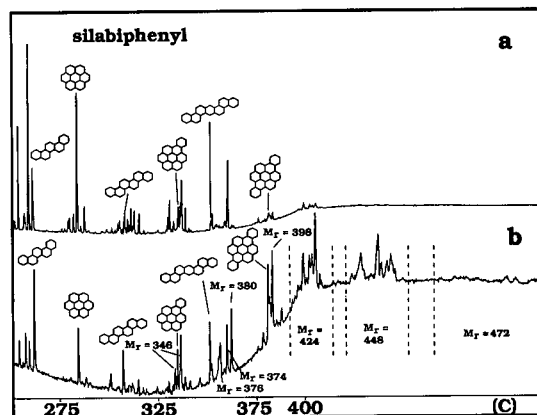


Fig. 7. Gas chromatograms (FID) of (a) a dichloromethane extract and (b) a chlorobenzene extract of carbon black on the silabiphenyl column. Temperature programming as in Fig. 2. The indicated mass numbers > 400 were tentatively identified by guidance from the GC-MS data obtained from the XTI-5 column.

ACKNOWLEDGEMENTS

Acknowledgements are due to various workers who contributed to the realization of this project. We gratefully thank Dr. A. Schuyler (Restek, Bellefonte, PA, USA) for providing Rtx-200 and XTI-5 columns. Dr. S. Claude (University of Neuchatel, Neuchatel, Switzerland) is thanked for synthesising the silabiphenyl stationary phase. Dr. J. Fetzer (Chevron Research, Richmond, CA, USA) and Dr. S. Wise (National Institute of Standards and Technology, Gaithersburgh, MD, USA) are acknowledged for supplying standard reference materials and Dr. S. Wise is further acknowledged for providing a sample of the HPLC fraction of SRM 1597. Dr. M. Lee is also thanked for the donation of the carbon black sample. The authors thank Mary Reuterdaahl for reviewing the manuscript.

REFERENCES

- 1 K. Jinno, J. C. Fetzer and W.R. Biggs, *Chromatographia*, 21 (1986) 274.
- 2 J. C. Fetzer, W. R. Biggs and K. Jinno, *Chromatographia*, 21 (1986) 439.
- 3 J. C. Fetzer and W. R. Biggs, *J. Chromatogr.*, 295 (1984) 161.
- 4 P. A. Peaden, M. L. Lee, Y. Hirata and M. Novotny, *Anal. Chem.*, 52 (1980) 2268.
- 5 Y. Hirata, M. Novotny, P. E. Peaden and M. L. Lee, *Anal. Chim. Acta*, 127 (1981) 55.

- 6 A. Hirose, D. Wiesler and M. Novotny, *Chromatographia*, 18 (1984) 239.
- 7 A. L. Colmsjö and C. E. Östman, *Anal. Chim. Acta*, 208 (1988) 183.
- 8 K. Grob, *Chromatographia*, 7 (1974) 94.
- 9 T. Romanowski, W. Funcke, J. Knig and E. Balfanz, *J. High Resolut. Chromatogr. Chromatogr. Commun.*, 4 (1981) 209.
- 10 W. J. Simonsick, Jr. and R. A. Hites, *Anal. Chem.*, 58 (1986) 2114.
- 11 A. Bemgård, A. Colmsjö and B. O. Lundmark, *J. Chromatogr.*, 595 (1992) 247.
- 12 *Certificate of Analysis, Standard Reference Material 1597, Complex Mixture of Polycyclic Aromatic Hydrocarbons from Coal Tar*, National Bureau of Standards, Gaithersburg, MD, 1987.
- 13 M. L. Lee, D. L. Vassilaros, C. M. White and M. Novotny, *Anal. Chem.*, 51 (1979) 768.
- 14 H. van den Dool and P. D. Kratz, *J. Chromatogr.*, 11 (1963) 463.
- 15 U. Heldt and H. J. K. Köser, *J. Chromatogr.*, 192 (1980) 107.
- 16 M. Mehran, W. J. Cooper, N. Golkar, M. G. Nickelsen, E. R. Mittlefehldt, E. Guthrie and W. Jennings, *J. High Resolut. Chromatogr.*, 14 (1991) 745.
- 17 K. J. Miller and J. A. Savchick, *J. Am. Chem. Soc.*, 101 (1979) 7206.

Simultaneous determination of planar chlorobiphenyls and polychlorinated dibenzo-*p*-dioxins and -furans in Dutch milk using isotope dilution and gas chromatography–high-resolution mass spectrometry

J. A. van Rhijn, W. A. Traag, P. F. van de Spreng and L. G. M. Th. Tuinstra

DLO–State Institute for Quality Control of Agricultural Products, Bornesteeg 45, 6708 PD Wageningen (Netherlands)

(Received August 19th, 1992)

ABSTRACT

A method is described for the simultaneous determination of planar chlorobiphenyls and dioxins in milk using isotope dilution and gas chromatography–high-resolution mass spectrometry (GC–MS). The method is based on gel permeation chromatography, alumina clean-up and carbon chromatography and is highly automated, making a high sample throughput possible. Data on recovery, accuracy and reproducibility of results obtained with quality control samples are presented. Data for both dioxins and planar chlorobiphenyls from the analysis of samples of Dutch milk from several areas in the Netherlands are also presented. Possible interference of the chlorobiphenyls in the determination of the dioxins in the GC–MS method is discussed.

INTRODUCTION

As the knowledge of the toxicological behaviour of organic contaminants increases, so does the need for more sensitive and more accurate methods of analysis. An example is the determination of planar chlorobiphenyls (CBs), *i.e.*, 3,4,3',4'-tetrachlorobiphenyl (CB 77), 3,4,5,3',4'-pentachlorobiphenyl (CB 126) and 3,4,5,3',4',5'-hexachlorobiphenyl (CB 169) [1]. The toxicities of individual CBs have been reviewed by McFarland and Clarke [2]. The planar (non-*ortho*-substituted) CBs seem to have much higher toxicity than the non-planar compounds [2–4]. However, naturally occurring levels of these planar compounds in biological samples are much lower than those of the non-planar compounds.

Therefore, an extensive clean-up of samples, including separation of planar and non-planar CBs, is necessary.

Methods for the determination of planar CBs in different types of matrices have been reported by several groups [5–8]. The clean-up procedures used are very similar to those used in the determination of dioxins, including the use of carbon chromatography to separate planar and non-planar compounds. The actual determination has been carried out using gas chromatography (GC) with either electron-capture or mass spectrometric (MS) detection [5–8]. The latter is also the method of choice for determining dioxins. Further, the concept of toxicity equivalence factors (TEF) has been developed [9]. However, the TEF values for dioxins [11] have been internationally accepted where as those for PCBs are still the subject of discussion. Therefore, we refer to TEF values for dioxins as I-TEF values. With such close similarities it is obvious to combine the determination of dioxins and planar CBs, which

Correspondence to: L. G. M. Th. Tuinstra, DLO–State Institute for Quality Control of Agricultural Products, Bornesteeg 45, 6708 PD Wageningen, Netherlands.

may result in more information at approximately the same expense.

In this paper we describe the simultaneous determination of dioxins and planar CBs in the same extract. As the analytical procedures for the separate determination of both planar CBs and dioxins have already been described [10], only relevant modifications are given. Emphasis is on the MS aspects of combining CBs and dioxins in the same MS procedure. Further, a survey study was carried out concerning the dioxin and planar PCB contents of Dutch milk originating from various areas in the Netherlands.

EXPERIMENTAL

The materials and methods used have been described previously [10]. To perform isotope dilution for the determination of the planar chlorobiphenyls, ^{13}C -labelled analogues of CB 77, CB 126 and CB 169 were purchased from Cambridge Isotope Laboratories (Woburn, MA, USA). All reagents used were of analytical-reagent grade.

Control samples

One quality control sample (QCS 1) was a batch of milk fat originating from an industrial area in the Netherlands. Repeated analysis revealed that this sample contained 2.62 pg of TEQ per gram of fat (2,3,7,8-TCDD toxicity equivalent) originating from the dioxins and *ca.* 4, 25 and 5 pg per gram of fat of CB 77, CB 126 and CB 169, respectively. Using the TEF factors proposed by Van Zorge [9], this corresponds to a total of 2.56 pg TEQ per gram of fat originating from the planar CBs.

The other quality control sample (QCS 2) was milk fat accurately spiked with PCDD/PCDF and planar CBs. Milk fat was first decontaminated using active carbon. Thereafter, amounts of 2 pg per gram per compound of native PCDD/PCDF were added. The octachlorinated compounds were added at a level of 4 pg per gram of fat. The native planar CBs were added at a level of 5 pg/g each for CB 77 and CB 169 and 10 pg/g for CB 126. This resulted in an artificially contaminated batch of milk fat theoretically containing 5.85 pg/g of I-TEQ originating from the dioxins and 1.08 pg/g of TEQ from the planar CBs.

Survey samples

Thirty-nine milk samples from various areas in the Netherlands were collected. Each sample consisted of 1 l of cows' milk taken from the pooled milk of the cooperating dairy farms. The samples were stored at -20°C until fat extraction was performed.

Of these samples, seventeen samples were taken from different agricultural areas, five originated from an industrial area, seven were taken from farms near two different municipal waste incinerators and ten from farms that kept their dairy cows on the outlying land of the main rivers of the Netherlands (see Table III).

Sample extraction and clean-up

The clean-up procedure has been described previously [10] and only minor adjustments were made here. To combine the elution of the planar CBs with the elution of the dioxins, the carbon column is eluted in the back-flush mode immediately after the solvent change from dichloromethane–cyclohexane (1:1, v/v) to toluene. To apply isotope dilution to both dioxins and chlorobiphenyls, the fat was not only fortified with 10 pg/g each of the ^{13}C -labelled PCDDs and PCDFs but also with 10 pg/g each of the ^{13}C -labelled planar CBs. As especially CB 77 is much more volatile than the dioxins and the other CBs, 50 μl of dodecane is used as a keeper throughout the clean-up procedure. However, after the carbon chromatography no keeper is used as complete evaporation of the solvent is required. Although the use of isotope dilution also permits automatic correction for evaporation losses, a low recovery causes a high limit of detection. Therefore, evaporation to dryness has to be performed very carefully in order to prevent unnecessary evaporation losses.

Gas chromatography–mass spectrometry

The conditions used have been described previously [10]. Mass spectrometric data acquisition for both dioxins and planar CBs is based on selected ion retrieval (SIR) at mass resolution 10 000. To determine the planar CBs, the number of ions to be monitored had to be extended, resulting in a slightly decreased sensitivity for the tetra- and pentachlorinated dioxin congeners compared with the separate determination of dioxins.

Table I gives an overview of the ions measured within each time window.

TABLE I

SOME ACQUISITION AND IDENTIFICATION PARAMETERS FOR POLYCHLORINATED DIOXINS AND DIBENZOFURANS AND CHLORINATED BIPHENYLS, INCLUDING THEIR ^{13}C -LABELLED ANALOGUES, ACCORDING TO EPA RECOMMENDATIONS FOR DIOXIN ANALYSIS

Compound ^a	Selected ion ratio, A/B ^b	<i>m/z</i> (A)	<i>m/z</i> (B)	Theoretical abundance (A/B)
PCB 77	M/M + 2	289.92	291.92	0.77
[^{13}C]PCB 77	M/M + 2	301.96	303.96	0.77
PCB-126	M/M + 2	323.88	325.88	0.62
TCDF	M/M + 2	303.90	305.90	0.77
TCDD	M/M + 2	319.90	321.89	0.77
[^{13}C]PCB 126	M/M + 2	335.92	337.92	0.62
[^{13}C]TCDF	M/M + 2	315.94	317.94	0.77
[^{13}C]TCDD	M/M + 2	331.94	333.93	0.77
PCB 169	M/M + 2	357.85	359.84	0.51
PeCDF	M + 2/M + 4	339.86	341.86	1.55
PeCDD	M + 2/M + 4	355.85	357.85	1.55
[^{13}C]PCB 169	M/M + 2	369.89	371.88	0.51
[^{13}C]PeCDF	M + 2/M + 4	351.90	353.90	1.55
[^{13}C]PeCDD	M + 2/M + 4	367.89	369.89	1.55
HxCDF	M + 2/M + 4	373.82	375.82	1.24
HxCDD	M + 2/M + 4	389.82	391.81	1.24
[^{13}C]HxCDF	M/M + 2	383.86	385.86	0.51
[^{13}C]HxCDD	M + 2/M + 4	401.86	403.85	1.24
HpCDF	M + 2/M + 4	407.78	409.78	1.03
HpCDD	M + 2/M + 4	423.78	425.77	1.03
[^{13}C]HpCDF	M/M + 2	417.83	419.82	0.44
[^{13}C]HpCDD	M + 2/M + 4	435.82	437.81	1.03
OCDF	M + 2/M + 4	441.74	443.74	0.89
OCDD	M + 2/M + 4	457.74	459.73	0.89
[^{13}C]OCDD	M + 2/M + 4	469.78	471.78	0.89

^a TCDF = Tetrachlorinated dibenzofuran; TCDD = tetrachlorinated dibenzodioxin; PeCDF = pentachlorinated dibenzofuran; PeCDD = pentachlorinated dibenzodioxin; HxCDF = hexachlorinated dibenzofuran; HxCDD = hexachlorinated dibenzodioxin; HpCDF = heptachlorinated dibenzofuran; HpCDD = heptachlorinated dibenzodioxin; OCDF = octachlorinated dibenzofuran; OCDD = octachlorinated dibenzodioxin.

^b M = molecular ion, containing ^{35}Cl exclusively.

Calibration was performed using seven calibration standards for the dioxins ranging from 100 fg/ μl to 10 pg/ μl . For the planar CBs only one calibration standard was used, containing 5 pg/ μl for CB 77 and CB 169 and 10 pg/ μl for CB 126.

RESULTS AND DISCUSSION

Mass spectrometric aspects

For the simultaneous determination of planar CBs and dioxins to be performed, some ions characteristic of the planar CBs have to be measured in

addition to the ions characteristic for the dioxins. Table I gives an overview of the ions measured within each time window. The diagnostic ions for the dioxins are in accordance with EPA recommendations. In comparison with the separate determination of dioxins, measuring a larger number of ions causes some decrease in sensitivity. This decrease, depending on the number of extra ions to be measured, is about 20% and is limited to the time windows in which tetra- and pentachlorinated dioxins elute together with CB 126 and CB 169, respectively. As the limit of determination for the dioxins

is sufficiently low, a small decrease in sensitivity can be tolerated.

From the data presented in Table I, possible MS interferences become clear. First, MS interferences only exist when compounds are unresolved by GC. Critical GC-separations, where MS interference also may occur, are the separation between 1,2,3,4-TCDD and 2,3,7,8-TCDD, CB 169 and 1,2,3,7,8-PeCDD, 1,2,3,4,7,8-HxCDF and 1,2,3,6,7,8-HxCDF and 1,2,3,4,7,8-HxCDD and 1,2,3,6,7,8-HxCDD. The differences in retention times are all *ca.* 10 s, which is the absolute minimum for GC resolution (Fig. 1A-D).

Most of these critical separations already existed in the determination of dioxins without incorporating the planar CBs, as three of the four critical separations concern two dioxin or furan congeners. Incorporating the planar CBs in the method adds only

one critical separation, *i.e.*, that of CB 169 and 1,2,3,7,8-PeCDD.

The M^+ and $[M + 2]^+$ ions of hexachlorobiphenyl (a.o. CB 169) and the $[M + 4]^+$ and $[M + 6]^+$ ions of pentachlorodioxin with their respective m/z values of 357.8517, 359.8415, 357.8517 and 359.8490 are unresolved by MS at mass resolution 10 000. It is worth noting that the $[M + 6]^+$ ion of pentachlorodioxin is not a diagnostic ion and is therefore not mentioned in Table I. Nevertheless, it is present and selecting the $[M + 2]^+$ ion of hexachlorobiphenyl will give rise to a signal due to the $[M + 6]^+$ ion of PeCDD.

As CB 169 is a hexachlorobiphenyl, interference may therefore occur. It is obvious that incomplete removal of other non-planar hexachlorobiphenyls that co-elute with either CB 169 or 1,2,3,7,8-PeCDD will give rise to interference, indicating the

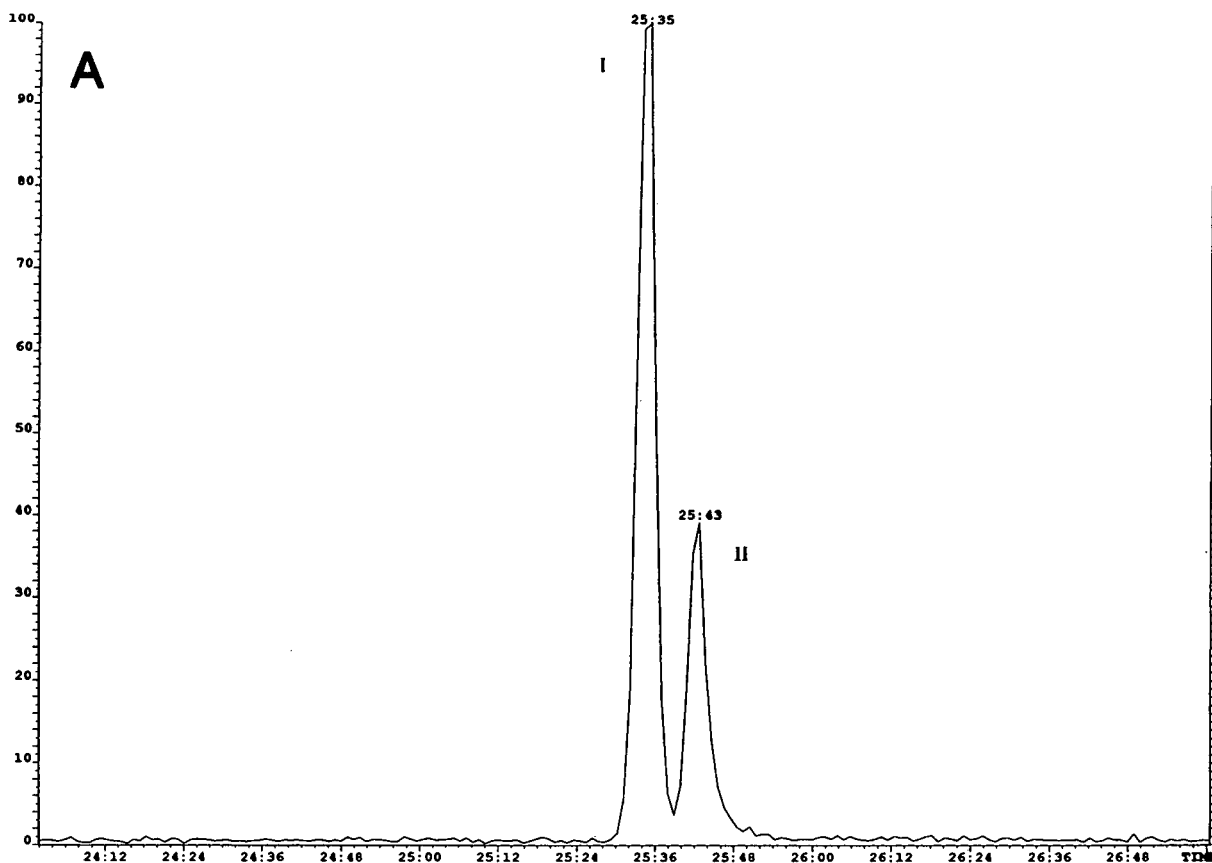


Fig. 1.

necessity to separate non-planar from planar compounds. Especially when there is a large difference in concentration between the two compounds, which may easily occur in some types of biological samples, interference can be expected to result in a faulty isotope ratio and high results for the compound subject to interference.

The $[M + 2]^+$ ion of PeCDD (m/z 355.8546), which is one of the diagnostic ions, and the M^+ ion (m/z 353.8576), are unaffected by the presence of hexachlorobiphenyl. In fact, choosing the M^+ ion of PeCDD instead of $[M + 4]^+$ as the diagnostic ion offers the possibility of avoiding any MS interference due to hexachlorobiphenyls on the PeCDD. There will still be interference of the PeCDD on the hexachlorobiphenyl but, considering the small TEF value of CB 169 (0.005), the effect of slightly higher results for CB 169 is negligible when expressed as the TEQ value of the sample. On the other hand,

1,2,3,7,8-PeCDD has a TEF value of 0.5 and high results for this compound will give rise to a significantly higher I-TEQ value for the sample compared with the non-interfered with result of analysis and should therefore be avoided.

It is worth noting that even when CB 169 is not a target compound, interference of CB 169 on 1,2,3,7,8-PeCDD may still occur when a cleaning procedure is used that is not capable of separating the planar CBs from the dioxins.

Another possible MS interference is caused by the tetrachlorinated dioxins. The ions $[M + 4]^+$ and $[M + 6]^+$ of TCDD interfere with the M^+ and $[M + 2]^+$ ions, respectively, of pentachlorobiphenyl. No interferences of the CB on the TCDD occurs.

However, GC resolution of CB 126 and 2,3,7,8-TCDD is readily achieved. Especially in environmental analysis, other TCDD congeners may be

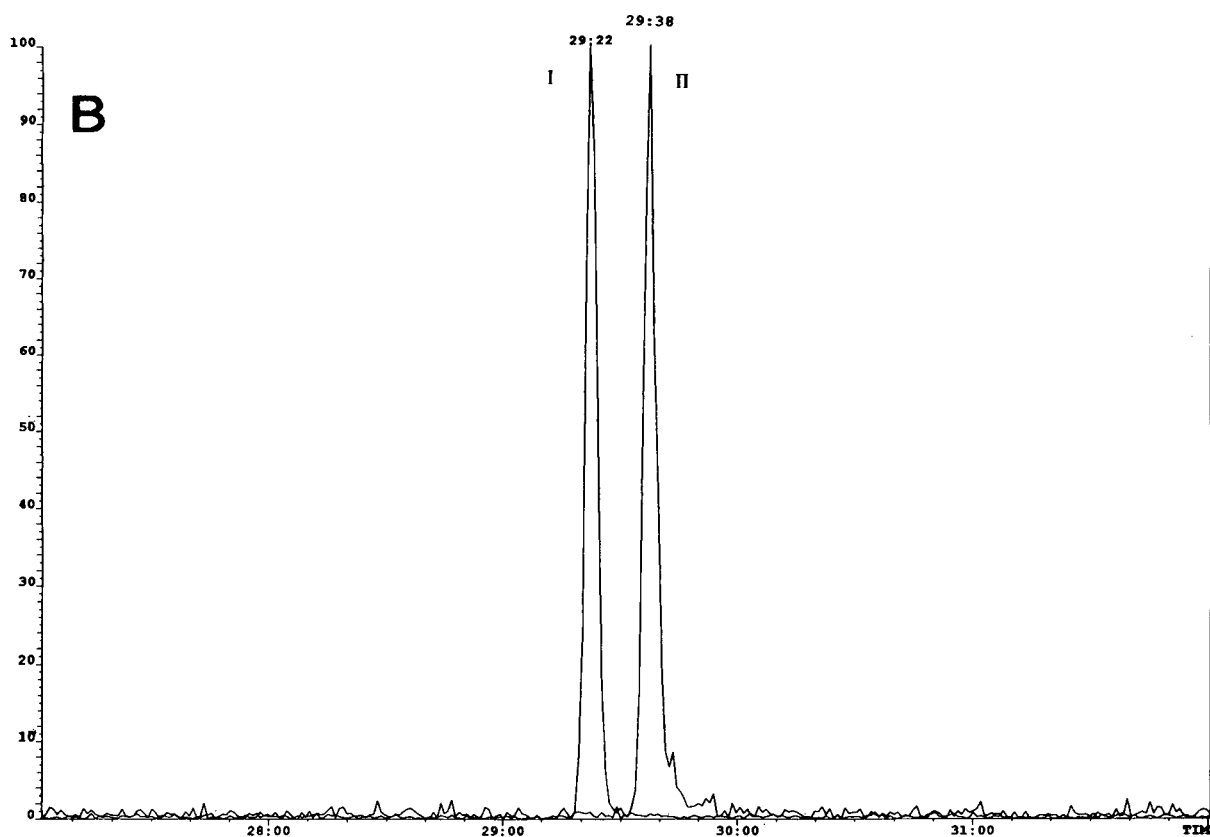


Fig. 1.

(Continued on p. 302)

present that may co-elute with CB 126. In that event interference may occur.

The last planar CB, *i.e.*, CB 77, elutes earlier than the tetrachlorinated dioxins and therefore no interference is expected. In our opinion, it is therefore advantageous to combine the determination of the planar CBs and dioxins. As mentioned before, calibration for the determination of dioxins is performed using as calibration graph consisting of seven different concentration levels whereas calibration for the determination of planar CBs only uses one calibration level. We found that linearity of the calibration graph for the planar CBs is better than or at least equal to that for the dioxins. This is probably due to the better GC properties of the CBs. Hence, when linearity of the dioxins is checked daily, as is common practice in our laboratory, and found to be satisfactory, there is no need to check for calibration linearity for the CBs and single point-calibration can be used without any problems.

Clean-up aspects

To combine the dioxins and the planar CBs in the same extract, the porous graphitized carbon (PGC) column has to be eluted in the back-flush mode immediately after the solvent change from dichloromethane–cyclohexane to toluene. This may alter the elution profile of the CBs and therefore this aspect was investigated. The elution profile shows a shoulder peak for all planar CBs, probably due to switching to the back-flush mode at a relatively high flow-rate. However, carbon chromatography is used for preparative purposes and therefore these shoulder peaks can be tolerated. More serious is the fact that the planar CBs show severe tailing on the PGC column. Collection of the eluate was therefore extended from 15 to 30 min. The total elution time of the column with toluene in the back-flush mode was also extended to 60 min. The planar CBs show much greater tailing than the dioxins, indicating a stronger adherence of these solutes to the sorbent.

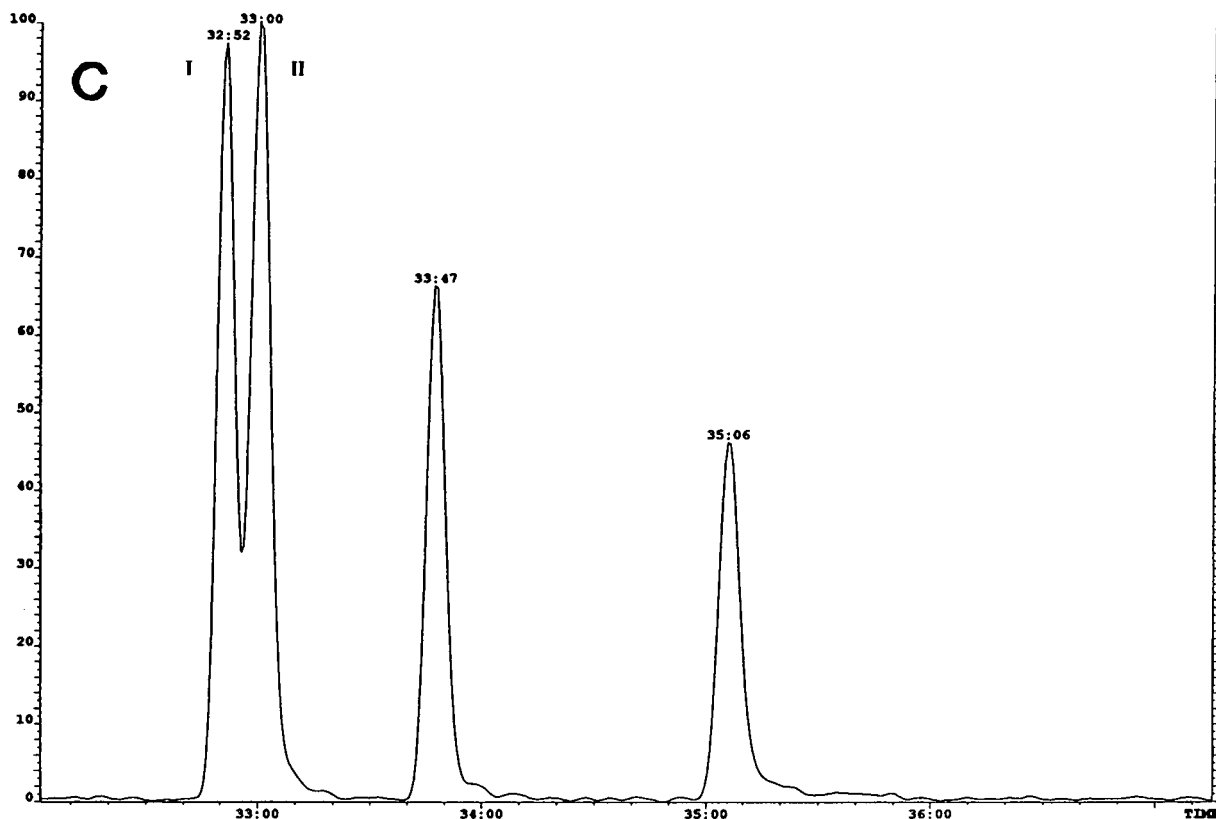


Fig. 1.

A stronger interaction of the planar CBs than the dioxins with the carbon sorbent is unexpected, as the dioxins are perfectly planar compounds whereas CBs are only planar or approximately planar owing to steric hindrance of the attached chlorine atoms.

In order to improve the peak shape of the planar CBs on the PGC column we used several eluents, including benzene and tetrahydrofuran–toluene mixtures, but tailing was not removed or decreased. This tailing may also be the cause of the contaminated blanks that were encountered. Blanks do not contain significant amounts of dioxins but they may contain planar CBs. Especially CB 77 is present in appreciable and widely varying amounts up to about 1 pg/ μ l. CB 126 and CB 169 are present in much lower concentrations. In terms of TEQ value, the influence of the presence of CB 77 is almost negligible as the proposed TEF value for this com-

ponent and its natural occurrence are only small. Further, CB 126, with its high occurrence and proposed TEF value, contributes more than 90% of the PCB TEQ value of a sample. For this reason and because the actual contamination of sample extracts with CB 77 not originating from the sample cannot be estimated properly, results of analysis are not corrected for blank values.

Quality control samples

The quality control procedure and the performance of the method for the determination of dioxins has been described previously [10]. Therefore, attention is focused on the quality control (QC) aspects for the determination of planar CBs. As described under Experimental, two QC samples are used; QCS1 is a naturally contaminated milk fat and QCS2 is a decontaminated and subsequently

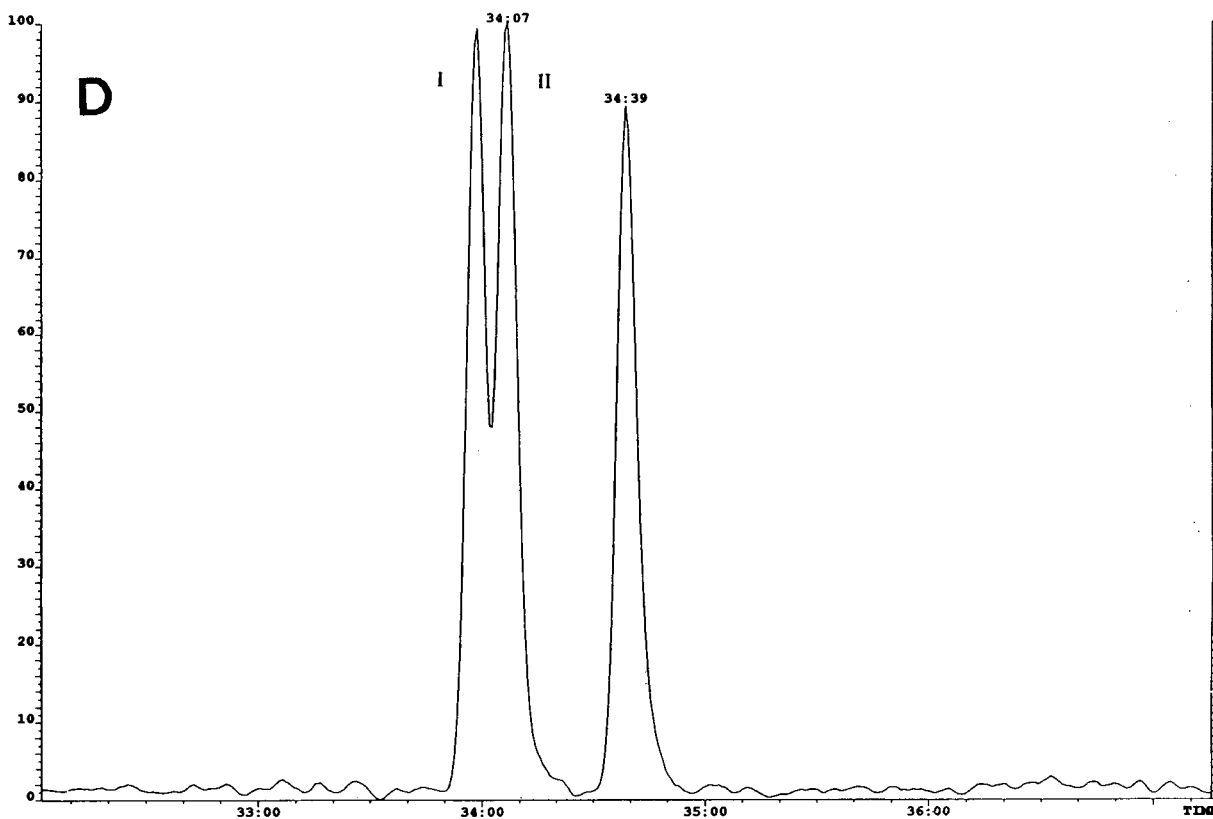


Fig. 1. Parts of chromatograms showing critical separations in the determination of planar CBs and dioxins. (A) (I) 1,2,3,4-TCDD and (II) 2,3,7,8-TCDD; (B) (I) PCB 169 and (II) 1,2,3,7,8-PeCDD; (C) (I) 1,2,3,4,7,8-HxCDF and (II) 1,2,3,6,7,8-HxCDF; (D) (I) 1,2,3,4,7,8-HxCDD and (II) 1,2,3,6,7,8-HxCDD.

TABLE II

MEAN RESULTS OF ANALYSIS OF PLANAR CHLORINATED BIPHENYLS FROM REPEATED ANALYSIS OF QC SAMPLES

	QCS1			QCS2			
	Recovery (%)	Mean ^a (pg/g)	C.V. (%)	Recovery (%)	Mean ^b (pg/g)	C.V. (%)	Accuracy (%)
CB 77	48	4.4	13.1	43	6.5	6.4	131
CB 126	50	25.9	10.3	46	10.6	5.9	110
CB 169	39	5.3	28.9	43	4.7	6.9	95
TEQ		2.56	5.2		1.24	2.8	111

^a *n* = 8.^b *n* = 11.

spiked sample of milk fat of exactly known content. In Table II data from repeated analysis of both QC samples are presented. Fig. 2 gives the QC charts for the determination of the TEQ value due to planar CBs.

The accuracy for QCS1 cannot be estimated be-

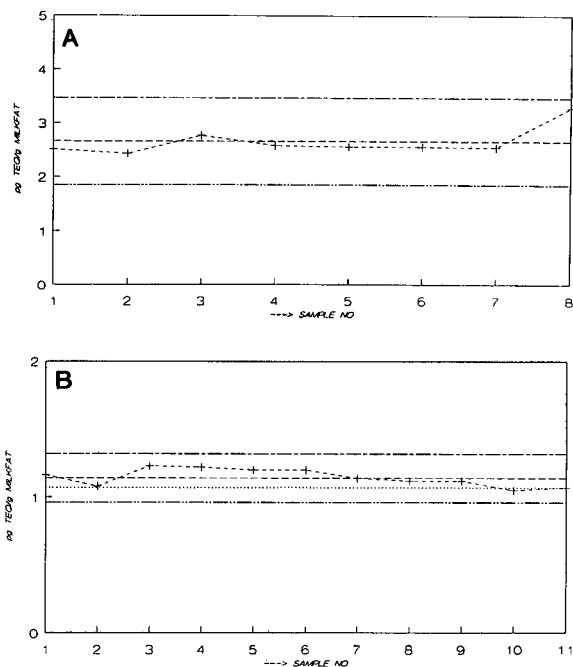


Fig. 2. Quality control charts based on data resulting from the determination of planar CBs in (A) quality control sample 1 and (B) quality control sample 2 (see text). + (---) = Sample; --- = mean; - - - = +3 S.D.; ····· = -3 S.D.; = theoretical.

cause, being a naturally contaminated and not a spiked sample, its true value is unknown. Nevertheless, the results are reproducible with relative standard deviations (R.S.D.) of 5–10%. The amount of CB 77 may be high owing to high blanks. For true samples, CB 126 seems to make by far the largest contribution to the TEQ value. Not only is its proposed TEF the largest of the planar CBs, but the levels of occurrence are also the highest. In QCS1 about 95% of the PCB TEQ value is due to CB 126.

QCS2 was spiked with 5 pg/g each of CB 77 and CB 169 and 10 pg/g of CB 126. It is clear from Table III that the results for CB 77 are systematically high. The results for CB 126 and CB 169 are, in our opinion, fairly good concerning both accuracy and reproducibility. Results for the QC samples concerning the determination of dioxins are comparable to the previously presented data [10].

Table II is based on only 8–11 determinations of the QC samples. As with the QC programme for the determination of dioxins, the number of QC data will increase as more samples are analysed. Nevertheless, the initial results are encouraging although the problems with contaminated blanks have still to be solved. The amount of the main component, CB 126, can be determined accurately and consequently so can the PCB TEQ value.

Survey samples

Table III gives the mean results of the analysis for milk samples collected from several areas in the Netherlands. The TEF values used for the PCBs are 0.01, 0.1 and 0.005 for CB 77, CB 126 and CB 169

TABLE III

ORIGIN OF THE SURVEY SAMPLES AND MEAN RESULTS OF ANALYSIS FOR DIOXINS AND PLANAR CHLORINATED BIPHENYLS

Origin	n	Dioxins I-TEQ (pg/g)	Amount (pg/g)			PCBs TEQ (pg/g)
			CB 77	CB 126	CB 169	
<i>Agricultural area</i>						
Friesland	4	0.8	3.3	11.6	2.0	1.1
Woerden	5	1.8	2.8	18.0	2.7	1.9
Achterhoek	3	1.6	3.2	18.8	2.8	1.9
Betuwe	5	1.5	6.1	17.7	2.7	1.9
<i>Industrial area</i>						
Rijnmond	5	2.7	3.3	20.5	4.0	2.1
<i>Near municipal waste incinerator</i>						
Duiven	2	3.6	2.8	17.9	3.8	1.8
Rijnmond	5	7.7	11.4	42.9	10.2	4.5
<i>Outlying land of main rivers</i>						
Roer/Meuse	5	1.5	11.9	29.7	4.0	3.1
Rhine/Yssel/Waal	5	3.0	4.9	30.8	4.3	3.2

respectively [9]. Fig. 3 gives a graphical representation of the 39 individual data. The samples are grouped together according to the type of area where they were collected.

It should be noted that the presented samples are not characteristic of the whole of the Netherlands. These samples were taken from selected areas to obtain impression of the order of magnitude and

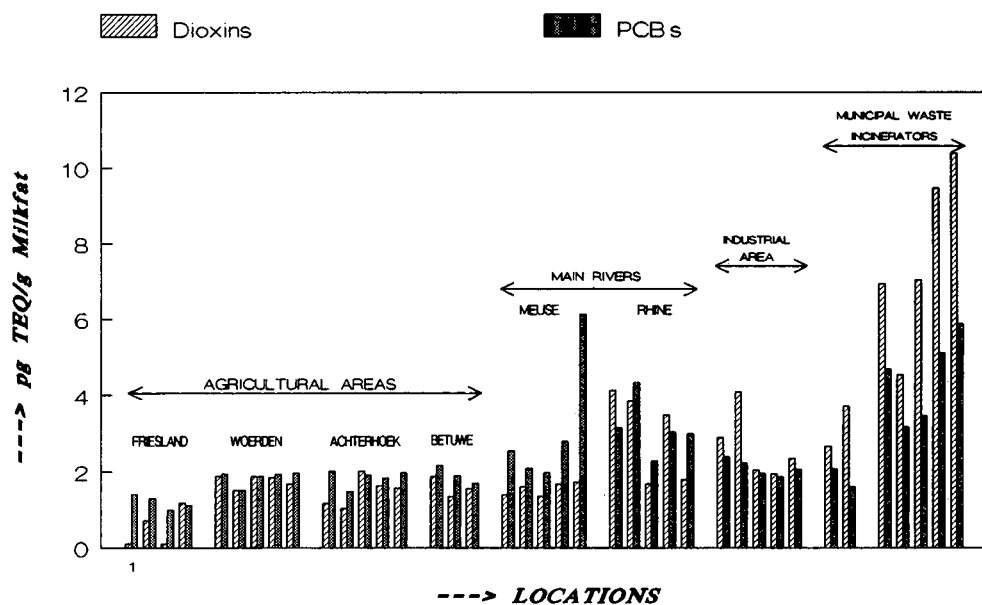


Fig. 3. Results of the determination of planar CBs and dioxins in Dutch cows' milk from several areas in the Netherlands, expressed as pg TEQ and pg I-TEQ, respectively, per gram of milk fat.

the relationship between CB and dioxin contamination in different types of areas.

As expected, the samples from agricultural areas are the least contaminated, with minimum contamination in Friesland, a relatively remote area, whereas samples from the surroundings of municipal waste incinerators are most contaminated. For the samples originating from agricultural areas the contamination with dioxins and CBs expressed as TEQ value generally seems to be of the same order of magnitude with slightly higher PCB TEQ values. The contamination with CBs in industrial areas is only slightly higher but significantly more dioxins were found. The reverse is true for the outlying land of the river Roer and Meuse; the dioxin levels are approximately the same as in agricultural areas but the CB levels are higher, probably because these rivers flow through a mining area where CBs might have been used as hydraulic fluids in the past. The river Rhine and its side rivers show both higher dioxin and higher CB levels.

The results for the samples taken near municipal waste incinerators need some extra comment. One of the incinerators is relatively old-fashioned and is located in an industrial area. Both CBs and dioxins show high levels of contamination compared with the agricultural areas. Especially the dioxin contamination is higher by a factor of about five; CB contamination is higher by a factor of about two. Compared with the industrial area these factors are about three and two, respectively. The other incinerator is located in an agricultural area and samples from the surroundings do not show higher CB contamination, the dioxin levels being higher by about a factor of two. This indicates, as expected, that CB contamination is a more general problem whereas dioxin contamination is mainly caused by local sources of pollution.

CONCLUSIONS

Combination of the determination of planar CBs with that of dioxins has been shown to be possible without introducing serious difficulties. One minor drawback is the small decrease in sensitivity for the tetra- and pentachlorinated dioxins. The clean-up procedure gives reproducible and accurate results for CB 126 and CB 169. Blanks contaminated with CB 77 are obtained, causing systematically high results for the determination of this compound. When expressed as a PCB TEQ value, the impact of this error is negligible. A survey study on 39 selected milk samples from several areas in the Netherlands gave good results, showing that dioxin contamination is mainly caused by local sources whereas CBs are thought to be evenly distributed throughout the environment.

REFERENCES

- 1 K. Ballschmitter and M. Zell, *Fresenius' Z. Anal. Chem.*, 302 (1980) 20–31.
- 2 V. A. McFarland and J. U. Clarke, *Environ. Health Perspect.*, 18 (1989) 225–239.
- 3 S. Tanabe, N. Kannan, A. Subramanian, S. Watanabe and R. Tatsukawa, *Environ. Pollut.*, 47 (1987) 147–163.
- 4 J. A. Goldstein, P. Hickman, H. Bergman, J. McKinsey and M. P. Walker, *Chem. Biol. Interact.*, 17 (1977) 69–87.
- 5 S. Tanabe, N. Kannan, T. Wakimoto and R. Tatsukawa, *Int. J. Environ. Anal. Chem.*, 29 (1987) 199–213.
- 6 J. Falandysz, N. Yamashita, S. Tanabe and R. Tatsukawa, *Z. Lebensm.-Unters.-Forsch.*, 194 (1992) 120–123.
- 7 C. S. Hong, B. Bush and J. Xiao, *Ecotoxicol. Environ. Saf.*, 23 (1992) 118–131.
- 8 L. G. M. Th. Tuinstra, J. A. van Rhijn, A. H. Roos, W. A. Traag, R. J. van Mazijk and P. J. W. Kolkman, *J. High Resolut. Chromatogr.*, 13 (1990) 797–801.
- 9 J. A. van Zorge, personal communication, 1990.
- 10 J. A. van Rhijn, W. A. Traag, W. Kulik and L. G. M. Th. Tuinstra, *J. Chromatogr.*, 595 (1992) 289–299.
- 11 J. A. van Zorge, J. H. van Wijnen, R. M. C. Theelen, K. Olie and M. van den Berg, *Chemosphere*, 19 (1989) 1881–1895.

Injection of large volumes of aqueous solutions in capillary supercritical fluid chromatography and sample preconcentration by multiple injections

S. Bouissel, F. Erni and R. Link

Sandoz Pharma Ltd., Basle (Switzerland)

(First received March 31st, 1992; revised manuscript received September 28th, 1992)

ABSTRACT

The possibility of using water or aqueous solutions as the solvent in capillary supercritical fluid chromatography was successfully demonstrated. Large volumes (up to 1 μ l) of aqueous sample solutions were injected. Sample preconcentration was performed by means of multiple injections of aqueous sample solutions. The solutes were trapped at the beginning of the column at low density (high temperature and low pressure) and eluted using a density programme. The method can be applied to trace analysis. It proved to be linear in the range examined. Flame ionization detection was used for the studies. As this technique is not sensitive to water, no solvent peak appears, which may be an advantage for certain applications. The influence of water injections on the column performance and the reproducibility of injection was investigated.

INTRODUCTION

The properties of the solvent are known to play an important role in supercritical fluid chromatography (SFC) [1,2]. Very complex solubility phenomena may occur during injection, as combinations of a supercritical fluid, neat or mixed with solvent, a subcritical liquefied gas, solvent and solutes may be present simultaneously in the injector and the column head. The band-broadening effect of solvents, which is well known in LC, has also been demonstrated in SFC. Split peaks result from the injection of excessive volumes.

Although peak splitting may be caused by various phenomena in the injector or the column inlet, an important mechanism in SFC seems to be incomplete mixing of the injection solvent with the fluid. Part of the sample is eluted with the solvent plug until complete mixing is obtained on the col-

umn, while the remainder is slightly retained by partitioning in the first part of the column [3]. Additionally, the column diameter in open-tubular column SFC is about five times smaller than in, *e.g.*, open-tubular gas chromatography (GC). With an allowable injection volume in SFC of approximately one tenth of that in GC, a five to ten times more concentrated sample must be introduced into the column in order to obtain comparable quantitative levels. Such a sample is then introduced into the column dissolved in a solvent that often has better solubilizing properties for the solute than does the mobile phase under the injection conditions. There is, nevertheless, sometimes a need for large injection volumes, *e.g.*, in trace analysis.

Various splitless methods that allow the injection of up to 1 μ l have been reported. Most of the methods are based on the separation of the solutes from the solvent. This includes the retention gap technique [4,5], solvent venting [5–8] and backflushing [9]. In contrast, Hirata and co-workers [10–12] developed a mixing method and indicated that solute focusing can be greatly facilitated by dilution of the

Correspondence to: Dr. R. Link, Sandoz Pharma AG, Lichtstrasse, Bau 360/1005, CH 4002 Basle, Switzerland.

solvent with carbon dioxide. By combination of solvent venting and dilution, injection of 100- μ l volumes on to a 100 μ m I.D. column became possible [13]. An advantage of the various venting techniques and solvent backflushing is the almost complete elimination of the solvent. With 10–15-m open-tubular columns, the solvent often takes more than 10 min to elute, which contributes significantly to the analysis time. Additionally, a broad solvent peak may interfere with the determination of early eluting peaks.

In this paper we describe the injection of large volumes (up to 1 μ l) of aqueous sample solutions. The influence of water injections on the column and detector performance and the reproducibility of injection were studied. Sample preconcentration was performed by means of multiple injections of the same sample solution. The solutes were trapped at the beginning of the column at low density (high temperature and low pressure) and eluted using a density programme [14]. The linearity of this accumulation procedure was investigated.

EXPERIMENTAL

Instrumentation

A Lee Scientific (Salt Lake City, UT, USA) Series 600 SFC instrument was used with flame ionization detection (FID). The detector was kept at 375°C. The pump was cooled by circulating a water–ethylene glycol mixture at 7°C using a Haake (Karlsruhe, Germany) refrigerating unit. Carbon dioxide (Carbagas, Basle, Switzerland) was used as the mobile phase. Sample was introduced using a Rheodyne (Cotati, CA, USA) Model 7520 injector. Commercially available sample rotors with 0.2- and 1.0- μ l loops were used. A 9 m \times 50 μ m I.D. SB Cyanopropyl-25 open-tubular capillary column (Lee Scientific) with a film thickness of 0.25 μ m was used as an analytical column. A frit restrictor (25 cm \times 50 μ m I.D. (Lee Scientific) was used to maintain the pressure. Data collection and reporting were performed on a Perkin Elmer Class 2000 system.

Operating conditions

Samples were introduced by direct injection on to the analytical column. The density was kept low (0.17 g/ml; oven temperature 200°C; pressure *ca.* 135 bar) during injection. Under these conditions

the solubility of the solutes is decreased and trapping with peak focusing is achieved on the top of the column [5,15].

After a 5-min hold (for the 1- μ l loop the hold time was increased to 20 min), the density was programmed to 0.49 g/ml at a rate of 0.04 g/ml-min (oven temperature 200°C). By increasing the density, the solutes are redissolved in the mobile phase and chromatographed through the column.

For sample accumulation several successive injections were performed (time interval *ca.* 3 min) at low density (0.17 g/ml) before the SFC density programme was started.

Sample solution

A 14.6-mg amount of PCO 400 (benzopyran derivative) was dissolved in 25 ml of water.

RESULTS AND DISCUSSION

The miscibility of the injection solvent with the mobile phase is very important in order to avoid split solute peaks [2]. For the injection of aqueous solutions of PCO 400 a high operating temperature was chosen (oven temperature 200°C) in order to promote the solubility of water in carbon dioxide.

Examples of chromatograms obtained by single and multiple injections of aqueous PCO 400 sample solutions are given in Figs. 1 and 2. Water does not influence the performance of the system, even if large amounts (*e.g.*, 1 μ l) are injected.

As the detector is not sensitive to water, no solvent peak is observed. This may be an advantage for certain applications, *e.g.*, if early eluting peaks are covered by the solvent peak.

The peak shape is influenced by the density and, more important, the polarity of the sample solvent [2,3]. Both properties affect the miscibility of the sample solvent with the mobile phase. Therefore, the peak shapes may vary if different solvents are used for the analysis of the same solute. PCO 400 samples (0.58 mg/ml) were injected with the 1- μ l loop using either pure ethanol or water as solvent (Fig. 3). Whereas slight fronting of the PCO 400 peak appears when ethanol is used as the solvent, slight tailing is observed with water under the same conditions. In both instances, however, the peak shape is acceptable. With water as solvent virtually no solvent peak is visible compared with ethanol.

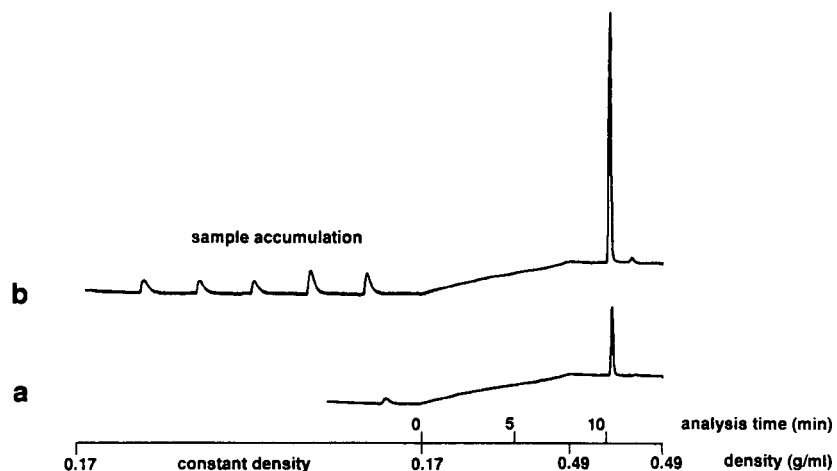


Fig. 1. Direct injection of aqueous PCO 400 solutions. (a) 116 ng of PCO 400 in water, obtained by one injection; (b) 580 ng of PCO 400 in water, obtained by five successive injections of the same sample solution. Conditions: $9 \text{ m} \times 50 \mu\text{m}$ I.D. SB-Cyanopropyl-25 fused silica column ($0.25\text{-}\mu\text{m}$ film thickness), $25 \text{ cm} \times 50 \mu\text{m}$ I.D. frit restrictor, $0.2\text{-}\mu\text{l}$ sample loop, injection time 1.8 s, CO_2 at 200°C , linear density programme from 0.17 to 0.49 g/ml at 0.04 g/ml-min after an initial isopycnic period of 5 min (solute trapping).

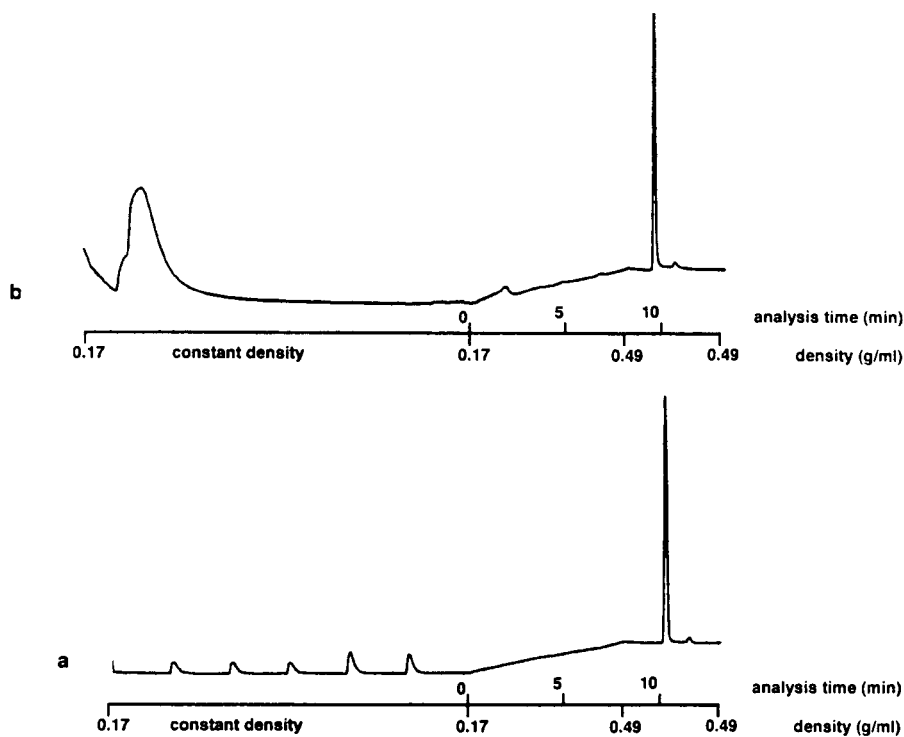


Fig. 2. Direct injection of aqueous PCO 400 solutions with different loops. (a) Sample accumulation with five successive injections with the $0.2\text{-}\mu\text{l}$ sample loop; (b) one injection with the $1.0\text{-}\mu\text{l}$ sample loop. Conditions as in Fig. 1b except for a slightly shorter restrictor for (b).

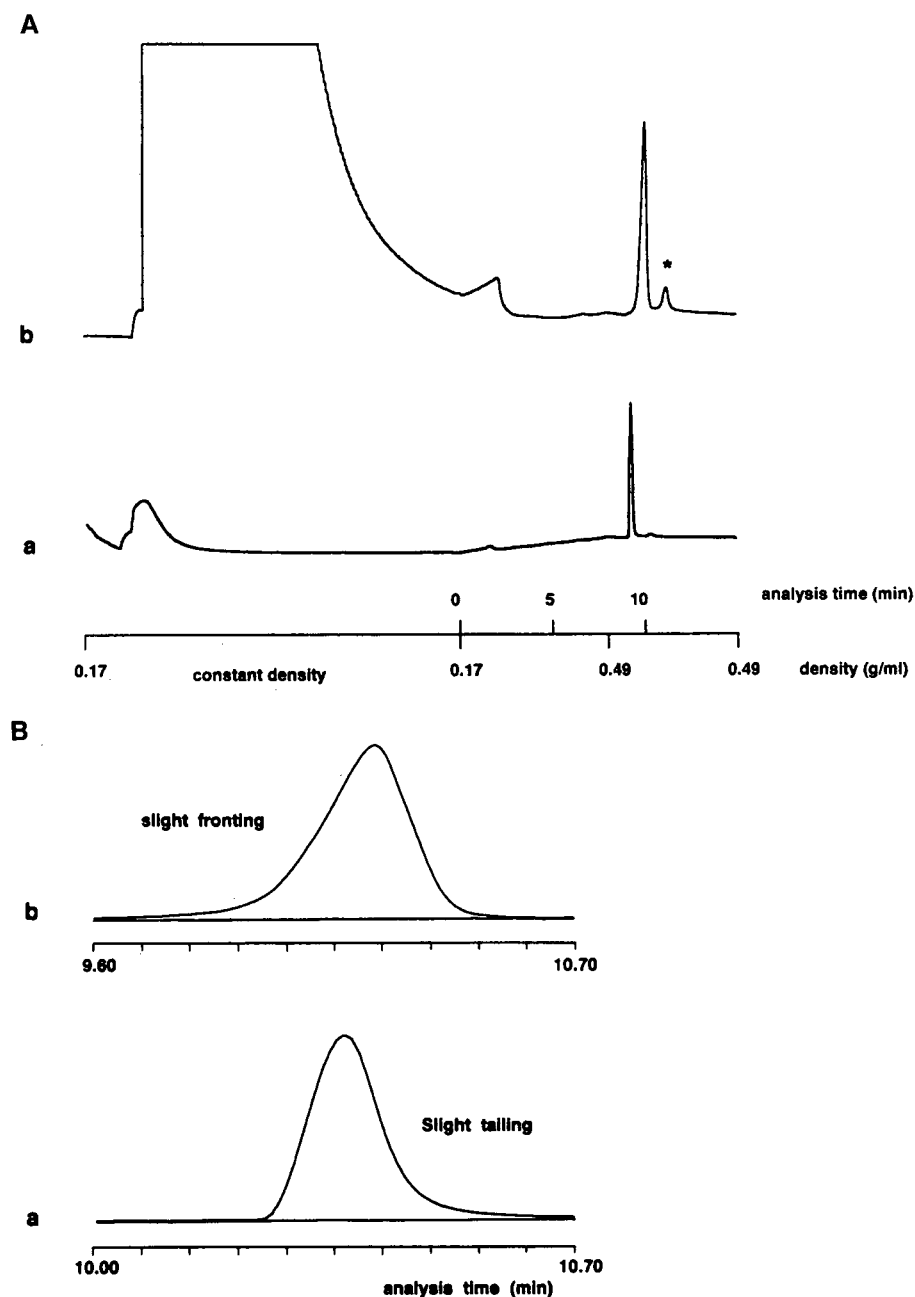


Fig. 3. (A) Direct injection of PCO 400 solutions with different solvents: (a) water and (b) ethanol. Conditions: $9\text{ m} \times 50\ \mu\text{m}$ I.D. SB-Cyanopropyl-25 fused silica column ($0.25\text{-}\mu\text{m}$ film thickness), $25\text{ cm} \times 50\ \mu\text{m}$ I.D. frit restrictor (slightly shorter for (a)), $1.0\text{-}\mu\text{l}$ sample loop, injection time 40 s, CO_2 at 200°C , linear density programme from 0.17 to 0.49 g/ml at $0.04\text{ g/ml}\cdot\text{min}$ after an initial isopycnic period of 20 min. The asterisk indicates a degradation product of PCO 400. (B) Influence of the solvent on the peak shape ($1.0\text{-}\mu\text{l}$ sample loop): (a) water; (b) ethanol. Conditions as in (A).

TABLE I

RELATIVE STANDARD DEVIATION OF THE ABSOLUTE PEAK AREA OF PCO 400 (0.58 mg/ml) IN DIFFERENT SOLVENTS AND WITH DIFFERENT LOOPS

Loop (μ l)	Solvent	R.S.D. of the absolute peak area (%)
1.0	Ethanol	3.1 ($n = 4$)
	Water	7.3 ($n = 9$)
0.2	Ethanol	6.7 ($n = 5$)
	Water	10.6 ($n = 6$)

The small peak that is observable with the aqueous solution is due to residual ethanol which was used to rinse the syringe. With ethanol the solvent peak is broad and may cover early eluting peaks.

The detector response is influenced by the solvent. For a 1- μ l injection of PCO 400 in ethanol (0.58 mg/ml) an average peak area ($n = 4$) of *ca.* 10^6 (arbitrary units) was found for the PCO 400 peak, whereas under the same conditions with water as solvent an area of only *ca.* $3.25 \cdot 10^5$ (average of nine injections) was observed. The decrease in sensitivity may be caused by quenching of the flame of the detector owing to the large amount of water injected. Detector parameters such as make-up gas flow must therefore be optimized in order to achieve optimum sensitivity.

The relative standard deviation (R.S.D.) of the absolute peak areas was determined for injections with the 1.0- and 0.2- μ l loops (Table I). The values obtained are, in our experience, representative for direct injection and well within the range reported in the literature for this injection technique [4]. For both solvents the R.S.D.'s are lower for the 1.0- than the 0.2- μ l loop.

No decrease in the performance of the system was observed even when water was used as the solvent over a long period of time. The peak shape and retention time did not change after *ca.* 340 injections of aqueous PCO 400 solutions (Fig. 4).

Sample preconcentration was performed by means of multiple injections of aqueous solutions of PCO 400. The solutes were trapped at the beginning of the column at low density (high temperature and low pressure) and eluted with a density programme. Up to $10 \times 0.2 \mu$ l and $12 \times 1.0 \mu$ l volumes of PCO 400 in water (0.58 mg/ml) were injected on to the

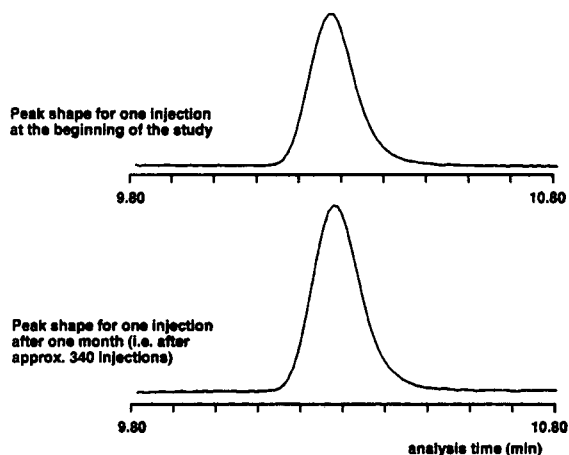


Fig. 4. Peak shape before and after the experiments with aqueous PCO 400 solutions (0.2- μ l sample loop).

column. The linearity of the accumulation procedure was studied for an aqueous PCO 400 solution in the range of 116 ng PCO 400 (corresponding to one individual injection) up to 928 ng (corresponding to eight successive injections).

A linear correlation (correlation coefficient $r = 0.995$) between the amount injected and the peak area detected was found in the range examined (Fig. 5). The column efficiency decreased slightly when the multiple injection technique was used. Whereas for a single injection with the 1.0- μ l loop *ca.* 38 000 theoretical plates per meter (based on the PCO 400 peak) were achieved, only *ca.* 30 000 theoretical plates per meter were obtained when the same amount of sample was analysed by injecting $5 \times 0.2 \mu$ l. Some peak broadening was observed with the multiple injection technique, probably because solute focusing was not optimum. Solute focusing might be improved by using the multiple injection technique in combination with an appropriate focusing device.

The multiple injection technique may be applied to trace analysis. The amount of sample to be analysed can be increased without increasing the injection volume or the concentration of the sample solution.

CONCLUSIONS

Water can be successfully used as a solvent in capillary SFC. Under appropriate operating condi-

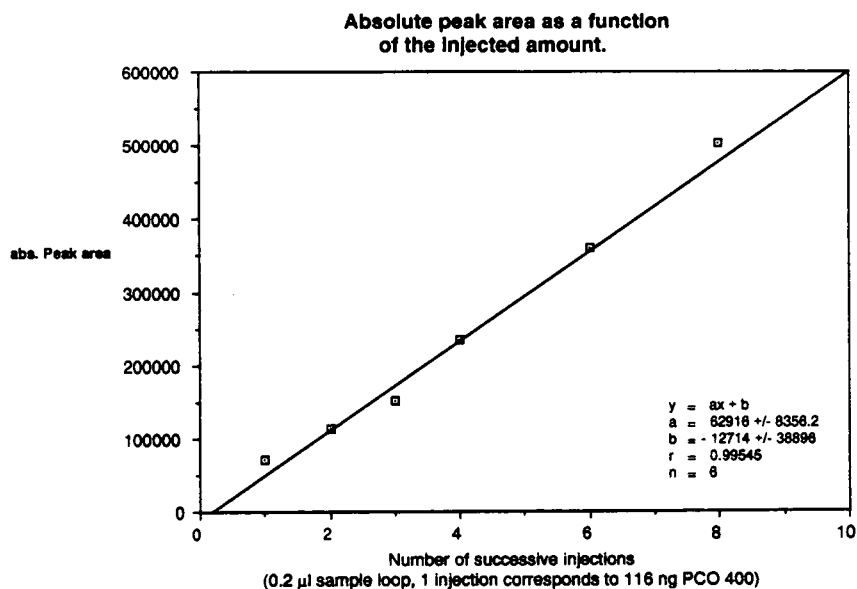


Fig. 5. Linearity of the accumulation procedure.

tions no miscibility problems between the solvent and mobile phase occur which might affect the performance of the system.

Sample preconcentration by means of multiple injections can be used to increase the amount of sample to be analysed. This technique may be very useful in trace analysis.

REFERENCES

- 1 T. L. Chester and D. P. Innis, *J. High Resolut. Chromatogr. Chromatogr. Commun.*, 8 (1985) 561.
- 2 J. P. Tuominen, K. E. Markides and M. L. Lee, *J. Microcol. Sep.*, 3 (1991) 229.
- 3 M. L. Lee and K. E. Markides (Editors), *Analytical Supercritical Fluid Chromatography and Extraction*, Chromatography Conferences, Provo, UT, 1990.
- 4 B. E. Richter, D. E. Knowles, M. R. Andersen, N. L. Porter, E. R. Campbell and D. W. Later, *J. High Resolut. Chromatogr. Chromatogr. Commun.*, 11 (1988) 29.
- 5 I. J. Koski and M. L. Lee, *J. Microcol. Sep.*, 3 (1991) 481.
- 6 A. F. Buskhe, B. E. Berg, O. Gyllenhaal and T. Greibrokk, *J. High Resolut. Chromatogr. Chromatogr. Commun.*, 11 (1988) 16.
- 7 I. J. Koski, K. E. Markides and M. L. Lee, *J. Microcol. Sep.*, 3 (1991) 521.
- 8 B. E. Berg and T. Greibrokk, *J. High Resolut. Chromatogr. Chromatogr. Commun.*, 12 (1989) 322.
- 9 M. L. Lee, B. Xu, E. C. Haung, N. M. Djordjevic, H-C. K. Chang and K. E. Markides, *J. Microcol. Sep.*, 1 (1989) 7.
- 10 Y. Hirata and K. Inomata, *J. Microcol. Sep.*, 1 (1989) 242.
- 11 Y. Hirata, F. Nakata and M. Kawasaki, *J. High Resolut. Chromatogr. Chromatogr. Commun.*, 9 (1986) 633.
- 12 Y. Hirata, H. Koshiba and T. Maeda, *J. High Resolut. Chromatogr.*, 13 (1990) 619.
- 13 Y. Hirata, Y. Kadota and T. Kondo, *J. Microcol. Sep.*, 3 (1991) 17.
- 14 L. Q. Xie, Z. Juvancz, K. E. Markides and M. L. Lee, *Chromatographia*, 31 (1991) 233.
- 15 G. Schomburg and W. Roeder, *J. High Resolut. Chromatogr.*, 12 (1989) 218.

pH gradient simulator for electrophoretic techniques in a Windows environment

Emilio Giuffreda, Carlo Tonani and Pier Giorgio Righetti

Chair of Biochemistry and Department of Biomedical Sciences and Technologies, University of Milan, Via Celoria 2, Milan 20133 (Italy)

(First received July 14th, 1992; revised manuscript received October 19th, 1992)

ABSTRACT

A new program is presented for optimizing mixtures of buffers and titrants for creating pH gradients for isoelectric focusing in immobilized pH gradients and in general for chromatographic processes. The program is written on a windows platform and it includes several novel features compared with previous simulators. First, the estimation of a pH gradient (a non-linear problem) has been transformed into a linear programming problem, thus allowing the use of the simplex as an optimization algorithm. Second, several types of pH gradients can be simulated and optimized, including linear, exponential, logarithmic and sigmoidal. Finally, an equation has been implemented in the program that accounts for the variation of the activity coefficients of ions as a function of the prevailing ionic strength in solution. This simulator was checked experimentally by eluting solutions from a two-vessel gradient mixer and verifying the shape of the various pH gradients. An excellent correlation was found between simulated and experimental data. The program allows the calculation and optimization of pH profiles (including the accompanying ionic strength and buffering power values) for mixtures of up to 50 different monoprotic or oligoprotic buffers and titrants. Calculations and optimizations are performed in a fraction of the time required by previous programs (often in less than 1 min, even for highly complex mixtures).

INTRODUCTION

In contrast to the approximate science represented by isoelectric focusing (IEF) in soluble amphoteric buffers (carrier ampholytes, CAs) (nothing is known on the several hundred chemicals composing wide-pH mixtures and the shape and range of the generated pH gradient is never reproducible) [1], the science dealing with immobilized pH gradients (IPGs) appears to be more precise: the chemicals are well defined and the pH gradient can be engineered as required [2]. This science has been exacting, however: the chemistry of the Immobiline chemicals (acrylamido buffers and titrants grafted to the polyacrylamide matrix) has taken years to develop (see ref. 3 for an update on these compounds) and

the calculation of wide-pH recipes has required the development of complex computer algorithms (see ref. 4 for a general survey).

The aim of this paper is to present a new, powerful IPG simulation program, based on the experience we have accumulated in the last 10 years in this field. We shall briefly summarize here what has been developed so far and give the reasons for this latest evolution. Our first simulation program (MGS, or monoprotic electrolyte gradient simulation) was operating by the end of 1982. A first approach to the formation of extended pH gradients was through the sequential elution of buffering species of increasing pK from a five-chamber mixer [5]. This procedure was soon abandoned in favour of standard two-vessel gradient mixing [6,7], for which we studied the conditions for gradient linearity, as a function of the pK distribution of the buffers and of the titrants [7]. We thus produced formulations for a series of wide immobilized pH gradients (spanning 2–6 pH units

Correspondence to: P. G. Righetti, Chair of Biochemistry and Department of Biomedical Sciences and Technologies, University of Milan, Via Celoria 2, Milan 20133, Italy.

within the pH range 4–10), optimized in terms of gradient linearity [8,9]. We compared [8] two approaches to the generation of extended pH gradients: in one case each buffering Immobiline had the same concentration in both vessels of the mixer; in the other, different concentrations of buffering ions could be present in each chamber.

In the case of two-dimensional (2D) maps, however, the best resolution in the focusing dimension would be obtained by non-linear pH gradients, following the relative abundance of isoelectric proteins along the pH scale. Hence we also calculated wide, non-linear IPG recipes for use in 2D maps and in cases requiring the analysis of highly heterogeneous samples [10].

During 1986, we started to expand the fractionation capability of IPGs: up to that time, the most extended pH interval described was 4–10. For this reason, we had not included the dissociation products of water (H^+ and OH^-) in our simulations, because in the pH 4–10 range their concentration is negligible. At that time, we started focusing dansylated amino acids (which exhibited pI values in the pH range 3–4) and we realized that there was a strong divergence between calculated and experimental pH gradients; therefore, our computer program was expanded to include the effects of H^+ and OH^- on the buffering power (β), ionic strength and pH profile [11]. In fact, simulations were not only limited to acidic but also included basic (pH 10–11) intervals [12]. As chemicals with more acidic and more basic pK values became available, extended formulations including pH extremes were recently computed; the widest pH range that could be formulated was a 2.5–11 interval [13].

During 1988, we started a long-range program on the characterization of existing Immobilines and on the synthesis of new species [3]. The family of Immobilines was thus considerably expanded and our former program (which was limited to mixtures of not more than ten species, including buffers and titrants) could no longer handle the new generation. These factors forced us to develop a new program, PGS (polyelectrolyte gradient simulation), for IEF in IPGs and for chromatography [14,15].

All these programs, however, had some shortcomings, as outlined below.

(a) The approach of minimizing the coefficient of variation of the buffering power [$CV(\beta)$], for pro-

ducing linear pH gradients, is a successful strategy only if the concentration of the Immobiline mixture is constant, *i.e.*, only when the two vessels of the gradient mixer contain the same solution titrated at the two extremes of the pH interval (equal concentration method) [8]; however, more flexibility in recipe calculation is obtained by the “unequal concentration” method, *i.e.*, by using different molarities of the same Immobilines in each vessel. With this latter approach, Righetti *et al.* [16] proposed minimizing $SD(pH)$ (the standard deviation along the pH course) by using the steepest descent principle in the search for buffer concentrations allowing for a better linearity of the pH course.

(b) Minimization of $CV(\beta)$, although working satisfactorily in the pH range 4–10, cannot perform properly outside these boundaries, where there is a strong contribution of water to the buffering power; as the latter is represented by two branches of a hyperbola, $CV(\beta)$ as a target function becomes almost meaningless.

(c) Both our previous programs (MGS and PGS, for mono- and polyelectrolytes, respectively) were meant for modelling only linear pH gradients, whereas there are many applications also for non-linear recipes.

Given the above limitations, we have recently expanded our previous programs so as to be able to calculate and optimize not only linear, but also logarithmic, exponential and sigmoidal gradients [17,18]. Another novelty of our latest development was that we abandoned the minimization of $CV(\beta)$ and adopted as a target function the minimization of the sum of squares of residuals (μ_2). The new simulator performed up to ten times better than our previous programs and could formulate recipes having deviations from linearity well below 1% of the given pH interval (a limit set with the previous MGS and PGS programs).

In this work, we delineate what could possibly be the ultimate step in “pH gradient engineering”. The following major improvements have been made: (a) the new program is written under a Windows environment, a most powerful and “user-friendly” program manager; (b) we have been able to adopt, in the optimization algorithm, the simplex method for linear programming (LP), which is much faster and accurate than Monte Carlo or steepest descent procedures; and (c) for the first time, a new algo-

rithm has been introduced that corrects the activity coefficients of ions according to the prevailing ionic strength in solution.

With the latter improvements, we feel that “pH gradient engineering” has now become a numerical science. The program is available from Hoefer Scientific Instruments (654 Minnesota Street, San Francisco, CA 94107, USA).

EXPERIMENTAL

The chemicals listed in Table I were purchased from Fluka (Buchs, Switzerland) and were of analytical-reagent grade.

pH gradient measurements

In order to check the quality of the simulated gradients and for the correction of activity coefficients introduced, we eluted from a two-vessel gradient mixer some simulated mixtures and measured the pH of the fractions. The following procedure was adopted: 60 ml of each limiting solution (corresponding to the “acidic” and “basic” extremes of the pH gradient, respectively) were prepared, degassed, equilibrated under argon and loaded in a two-vessel gradient mixer (the acid solution usually being in the mixing chamber). If the pH gradient extended above pH 7, the alkaline part of the gradient (usually placed in the reservoir) was protected from CO₂ adsorption by flushing with argon. Production of the correct pH gradient on elution was ensured by (a) using a stirrer in both chambers, (b) avoiding glycerol or other additives in the mixing chamber and (c) flushing with argon all eluted fractions above pH 7. Volumes of 2 ml were collected, for a total of 60 fractions. Prior to pH measurements, all fractions were equilibrated at 25°C.

As a gradient mixer, we used that designed by Svensson and Pettersson [19] for isoelectric focusing; stirring action was provided by placing the two electrically driven helices in both vessels simultaneously. The absence of back-flow was checked by visual inspection at the interface of the two solutions, one of them being strongly coloured with bromophenol blue. Linearity of the elution profile was also checked by readings at 600 nm of the blue fraction. Note that, in the absence of a density-forming agent in the mixing chamber (as is custom-

ary in gradient mixing), the two solutions are truly hydrostatically equilibrated.

THEORY

The problem of finding a solution to the creation of a linear (or non-linear) pH gradient on mixing two limiting solutions containing a mixture of buffering (and titrant) ions is not trivial. We have already given in previous papers [4–7] all the relevant equations needed for solving the problem (*i.e.*, the dissociation of weak acids and bases; the electroneutrality conditions; the total buffering power of the solution; the total ionic strength of the system; and the Peterson–Sober equation allowing the calculation of the actual concentrations dispensed in each liquid element eluted from the mixer). However, a difficult task is the choice of the target function to be extremized and the selection of the proper optimization algorithm working on such a target. In the past, we had chosen, as a target function, the minimization of the coefficient of variation of the buffering capacity [CV(β)], defined as the ratio between the standard deviation of the buffering capacity and its mean value: $CV(\beta) = SD(\beta)/\beta$. As an alternative method, we had also used, as a goal for maintenance of pH gradient linearity, the minimization of SD(pH). As optimization algorithms, we had already discarded stochastic (also known as Monte Carlo) methods, which utilize random extraction of the vector to be optimized and compute the target function. Unfortunately, stochastic methods usually converge too slowly, rendering their use on personal computers impractical.

We had then opted for the “steepest descent (Cauchy)” algorithm. In this method, the minimum of a function $f(k)$ is found by descending from a given starting point, defined by the parameter vector k^* , along the steepest slope, defined by the minimum value of $f'(k^*)$, found by exploring in all directions the space around k^* . After one descending step, the new steepest direction is searched and the process is then iterated until the attainment of the desired minima [20–22]. The most serious drawback of the steepest descent approach is that the search comes to an end when a minimum is reached, regardless of it being an absolute or relative minimum. In order to avoid this, we had provided in previous programs

the possibility of interrupting the routine calculations and allowing educated guesses to be entered by a machine–user interaction procedure. This method also was extremely slow and often computation of complex mixtures encompassing wide pH intervals required several days of calculations.

Ideally, one might want to use the simplex method, by reformulating the objective function, so that it is linear. Linear objective functions then lead automatically to linear programming (LP). In the following section, we shall show how it is possible to transform the problem of pH gradient optimization from a non-linear to a linear case, thus allowing the adoption of the simplex as an optimization algorithm.

Linearization of the problem and the simplex algorithm

We can express the problem as follows: given m polyprotic species, of known pK values, and a pH curve, represented by the function $pH(t)$, it is necessary to find an algorithm able to calculate the initial concentrations of the m species: c_{zA} , c_{zB} , $z = 1, \dots, m$, to be placed in each chamber of a two-vessel gradient mixer so that, upon linear mixing, the eluate will contain a variable pH (with time), approximating the desired function $pH(t)$. For a solution, the problem will be analysed first from a hydrodynamic point of view, then from its chemical side and finally from a numerical point of view.

Hydrodynamically, if equal volumes of two solutions, one in a mixing chamber (called “acidic”, as it contains the lowest pH value) and the other in a reservoir (“basic” solution) are linearly mixed, it can be demonstrated that, for each species $c_A(t)$ in the mixing chamber, the variation in concentration during elution can be expressed by the following differential equation:

$$S \left[\frac{d}{dt} \cdot c_A(t) \right] \left[l(0) - \frac{q}{2S} \cdot t \right] = \frac{q}{2} [-c_A(t) + c_B] \quad (1)$$

where $l(t)$ is the height of the solution in the two chambers, S is the section of each chamber, q is the liquid flux per time unit and c_B is the concentration of each species in the basic chamber. On integration, and remembering that the eluted volume V is given by $V = (Sl)$, one obtains the explicit form of $c_A(t)$:

$$c_A(t) = c_A \left(1 - \frac{q}{2V} \cdot t \right) + \frac{q}{2V} \cdot tc_B \quad (2)$$

Note that eqn. 2 is the equation of Peterson and Sober [23], simplified for a two-chamber gradient mixer. The same reasoning can be extended to the case of m non-interacting species, resulting in the following equation:

$$\sum_{i=1}^m c_{iA}(t) = \sum_{i \neq 1}^m c_{iA} - \frac{q}{2V} \cdot t \sum_{i=1}^m c_{iA} + \frac{q}{2V} \cdot t \sum_{i=1}^m c_{iB} \quad (3)$$

We have so far treated the hydrodynamic facet of the problem; we shall now proceed to the chemical aspects. We recall here the general equations for the dissociation degrees of polyprotic acids (\tilde{g}_a), bases (\tilde{g}_b) and zwitterions (\tilde{g}_z):

$$\tilde{g}_a(t) = \sum_{i=0}^n \alpha_{ai}(t)(n-i) \quad (4)$$

$$\tilde{g}_b(t) = \sum_{i=0}^n \alpha_{bi}(t)(n-i) \quad (5)$$

$$\tilde{g}_z(t) = \tilde{g}_a(t) - \tilde{g}_b(t) \quad (6)$$

where α_i is the dissociation degree of the i th species and n is the number of protolytic groups. The degree of dissociation, in turn, depends on the pK of each ionizable group, on the prevailing pH in solution and (in our particular solution) on time t . As we know the starting pH in the “acidic” chamber, we shall be able to calculate at each time t the electrolytic equilibrium in this chamber as elution progresses, *i.e.*, we can calculate the degree of dissociation of each species as the content of the “acidic” chamber is progressively titrated by the content of the “basic” chamber. By assuming that of the m input species l are acids, p bases and the remaining zwitterionic, according to the electroneutrality law, it will be

$$-\sum_{i=1}^l c_{iA}(t)\tilde{g}_{ia}(t) + \sum_{i=l+1}^{l+p} c_{iA}(t)\tilde{g}_{ib}(t) + \sum_{i=l+p+1}^m c_{iA}(t)\tilde{g}_{iz}(t) - [H^+](t) + \frac{K_w}{[H^+](t)} = 0 \quad (7)$$

The first member of eqn. 7 can be written as an implicit function, depending on time t and on $2m$ parameters, of the type

$$f(c_{1A}, c_{2A}, \dots, c_{mA}, c_{1B}, c_{2B}, \dots, c_{mB}, t) \quad (8)$$

which is linear in the parameters c_{iA} , c_{iB} . The original problem can thus be reduced to the search for the $2m$ parameters $c = (c_{1A}, c_{2A}, \dots, c_{mA}, c_{1B}, c_{2B}, \dots, c_{mB})$, such that

$$f(c, t) \approx 0 \forall t \in [t_0, t_n] \quad (9)$$

The problem now consists in selecting from a family of functions of the type $f(\mathbf{c}, t)$ a particular function $f(\mathbf{c}^*, t)$ satisfying the condition that, in the interval $[t_1, t_n]$, it will approximate zero. The search for such a function can take two pathways: either exact calculus, or methods of discrete calculus. As the latter seems more manageable, the family of functions $f(\mathbf{c}, t)$ is now considered as an assembly of discrete functions, defined over the points $\{t_1, \dots, t_n\}$ rather than over the continuous interval $[t_1, t_n]$. In addition, as f is linear in its $2m$ parameters, the function $f(\mathbf{c}, t)$ can be rewritten in a vectorial form of the type

$$A \cdot \mathbf{c} - \mathbf{b} \tag{10}$$

where A is an $n \times 2m$ matrix, \mathbf{c} is a $2m$ -dimensional vector and \mathbf{b} is a n -dimensional vector. Under this terminology, eqn. 9 can be rewritten as follows:

$$\min_{\mathbf{c}} \|A \cdot \mathbf{c} - \mathbf{b}\|_p \tag{11}$$

where $\|e\|_p$ indicates the L_p norm of the vector e [24]. When using the L_1 norm, the problem can be transformed into a problem of linear programming. In fact, for L_1 approximations, the problem can be reduced to

$$\min \sum_{i=1}^n |\mathbf{b}_i - \sum_{j=1}^{2m} a_{ij}c_j| \tag{12}$$

subject to no restrictions whatsoever. Even though eqn. 12 still does not represent a linear programming problem, it can be easily converted into one. Consider the problem

$$\min \sum_{i=1}^n e_i$$

subject to

$$\begin{aligned} e_i + \sum_{j=1}^{2m} a_{ij}c_j &\geq b_i & i = 1, 2, \dots, n \\ e_i - \sum_{j=1}^{2m} a_{ij}c_j &\geq -b_i & i = 1, 2, \dots, n \end{aligned} \tag{13}$$

It is not difficult to see that, in an optimum solution $e_1, e_2, \dots, e_n, c_1, c_2, \dots, c_{2m}$ of eqn. 13, e_i should be the smallest possible value in between the two bounds $b_i - a_{ij}c_j$ and $b_i + a_{ij}c_j$. Hence,

$$e_i^* = |\mathbf{b}_i - \sum_{j=1}^{2m} a_{ij}c_j^*| \tag{14}$$

and the objective function e_i takes the value

$$e_i = \sum_{i=1}^n |\mathbf{b}_i - \sum_{j=1}^{2m} a_{ij}c_j^*| \tag{15}$$

as desired. We conclude that c_1, c_2, \dots, c_n is the best L_1 approximation to a solution of eqn. 11. This solution is not the final one, however, as we need the following additional constraints to the program: (a) the sum of concentrations of the m species in the two chambers must be lower than a molarity predetermined by the user; (b) the average β power can also be predetermined by the user (in a linear form, as for the electroneutrality law); and (c) each concentration c_i must be greater than zero. The first condition can be met by adding to eqn. 13 the following constraint:

$$\sum_{i=1}^m c_{iA} \leq k \quad \sum_{i=1}^m c_{iB} \leq k \tag{16}$$

The second condition can also be satisfied by adding a constraint to eqn. 13 of the type

$$\sum_{i=1}^n \beta(t_i) = n\beta_M \tag{17}$$

where $\beta(t_i)$ is the buffering power of the solution in the acidic chamber at time t and β_M is the average β preselected by the user (note that summation of β is used in order to obtain a β average). The last condition is easily met by adding to eqn. 13 the constraint $c \geq 0$. At this point, it is clear that the simplex algorithm can be applied to the above problem, as it has now been converted into a linear programming problem.

The simplex, first proposed by Dantzig in 1948 (see ref. 25 for a review), is a powerful optimization algorithm consisting of (a) making a series of linear combinations at each step, so that the value of the target function diminishes, and (b) finding an optimum solution, after a number of iteration steps, which is always smaller than the larger of the two dimensions of the constraint matrix.

The calculus routine finally adopted is that implemented by Kuenzi *et al.* [26].

The problem of the activity coefficients of ions

This is a formidable problem, which has been avoided in all our previous computations [4–8]. Previously, we assumed that, provided that IPG gels were made to contain small total amounts of

buffering and titrant ions (not exceeding 10 mM), this problem could be neglected. However, in several recipes encompassing wide pH intervals (e.g., 4–8 pH units), and also in Immobiline membranes [27], the total ion molarity grafted in the gel often exceeds 30 mM, which calls for a correction to the activity coefficients of the ions, if an exact science is sought.

The original Debye–Hückel theory is still the basis for most calculations of activity coefficients. This theory assumes that ions in solution behave as point charges, distributed in a homogeneous dielectric (the solvent); by applying the electrostatic and thermodynamic laws, the Debye–Hückel relationship is derived, valid only for highly diluted solutions and for fully dissociated ions:

$$-\log \gamma = Az_+z_- \sqrt{I} \quad (18)$$

where γ is the average activity coefficient of a binary electrolyte, z_+ and z_- the respective charges, I the ionic strength and A a constant that depends on the absolute temperature and the dielectric constant of the solvent (for water at 25°C $A = 0.509$; in many textbooks, A is simply given as 0.5). The experimental results agree with the Debye–Hückel theory only for concentrations lower than 1 mM. Thus, a modified Debye–Hückel expression has been derived for higher molarities:

$$-\log \gamma = Az^2 \cdot \frac{\sqrt{I}}{1 + Ba\sqrt{I}} \quad (19)$$

where a is a parameter, measured in ångströms, which is roughly proportional to the diameter of a hydrated ion and B is a constant which again depends on the absolute temperature and the dielectric constant of the solvent (for water at 25°C $B = 0.328$). It should be noted that, if a is taken as 6 Å (which corresponds to the average diameter of a number of ions) the error in the estimation of γ is less than 1% in solutions having I values lower than 0.2 equiv. l^{-1} . In contrast, eqn. 18 does not represent experimental data properly: in solutions up to 0.1 equiv. l^{-1} the error is >10% (Fig. 1).

Over the years, a number of equations have been derived in an attempt to obtain better γ estimates (see ref. 28 for a review and for additional references to eqns. 20–22). Thus, Guggenheim proposed the following parametric equation:

$$-\log \gamma = Az^2 \cdot \frac{\sqrt{I}}{1 + \sqrt{I}} - bI \quad (20)$$

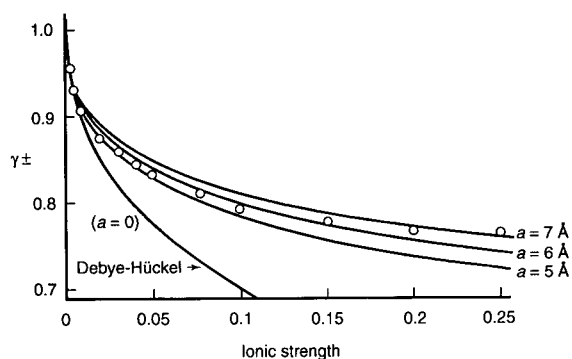


Fig. 1. Theoretical plot of the dependence of activity coefficients on prevailing ionic strength in solution for different ion diameters. Note that, according to the original Debye–Hückel theory, the diameter of an ion should be zero. In most calculations, however, an average diameter of 6 Å is adopted.

where the average ion diameter has been taken as $a = 3$ Å (note that, in this case, $Ba = 1$). A similar equation was proposed by Guntelberg:

$$-\log \gamma = Az_+z_- \frac{\sqrt{I}}{1 + \sqrt{I}} \quad (21)$$

based on the same assumption of $Ba = 1$. Finally, an empirical relationship was derived by Davies:

$$-\log \gamma = Az_+z_- \left(\frac{\sqrt{I}}{1 + \sqrt{I}} - 0.2I \right) \quad (22)$$

The dependence of the activity coefficient on the ionic strength, according to eqns. 18, 21 and 22, has been plotted in Fig. 2. It appears that the Davies equation (eqn. 22) follows the experimental data more closely: in solutions of ionic strength up to 0.1 the error is only 3%, and at I up to 0.5 the error is still <8%.

The situation is even more complex for oligoprotic ions, as shown in Fig. 3. It is seen that, whereas for a monoprotic ion the γ value tends asymptotically to 0.7, at high ionic strength for a divalent ion it decreases dramatically to a limit value of 0.3. For higher valency ions, the fall-off is even more pronounced: for a triprotic ion the asymptotic value is barely 0.05 and for a tetravalent ion the activity coefficient falls off rapidly to zero already at an ionic strength of 0.2.

As will be shown in the Results section, the Davies equation (eqn. 22) seems to fit our experimental data

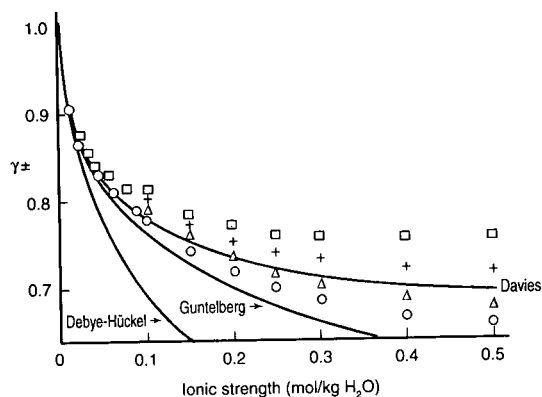


Fig. 2. Plot of the dependence of activity coefficients on prevailing ionic strength in solution according to different equations: Debye-Hückel (eqn. 18), Guntelberg (eqn. 21) and Davies (eqn. 22). Note that the Davies equation is empirical and is based on experimental data for (□) HCl, (+) HNO₃, (Δ) NaClO₄ and (○) KCl.

most satisfactorily, so this equation was incorporated in our computer program for automatic correction of the activity coefficients as a function of the prevailing ionic strength in solution. Since, in practice, when introducing into our computing routines the correction for the activity coefficients, only the stoichiometric constants are altered and the mathematical formulations of equilibria and the mass and charge balance equations are left unal-

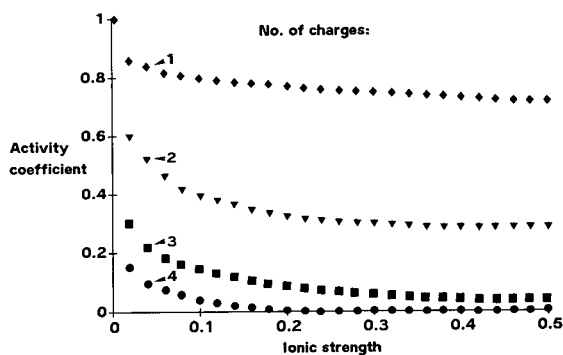


Fig. 3. Plot of the dependence of activity coefficients on prevailing ionic strength in solution for ions of different valency. Note the huge decrease in the coefficients in the transition from monoprotic to diprotic species. Note also how, for a tetravalent ion, the activity coefficient is essentially zero at an ionic strength of 0.2 equiv. l⁻¹.

tered, the following two-step computation procedure was adopted. Once a mixture of acids and bases is given, the problem is solved to a first approximation by using the concentrations instead of the activities. Once the final ionic strength of the solution has been derived, the activity coefficients of the various ions are calculated at the given *I* value. At this point, new values of p*K* and pH gradients are derived, corrected according to the activity coefficients.

Program architecture

The above algorithms were implemented in C language under the programming platform Windows 3.0. Windows is a most powerful operating program, which offers the following main innovations: (a) object-oriented programming, (b) message-driven architecture and (c) multitasking. The main “window” usually contains a “title bar”, a “menu”, a “sizing border”, a “system menu icon” and “maximize/minimize icons”. The inner area of the main window (or workspace) can be used to generate new “child windows”, each containing a document. In our case, we prepared three types of document windows: (a) a first type for handling the input data, *i.e.*, the different buffers and titrants with their physico-chemical characteristics (*e.g.*, p*K* values, type of substance, such as acid, base, zwitterion); (b) a second type for handling the input data, and precisely for calculating the molarities of each species to be placed in the “acidic” and “basic” chambers, respectively; this sheet is similar to the previous one, but in addition it will create archives for storage of the optimized recipes for the various pH intervals calculated; and (c) a third type used for the graphic display of simulated recipes and pH intervals.

Examples of the data obtained and experimental validation of the simulations are given below.

RESULTS

Program and simulations

Fig. 4 shows the main dialogue box in our computer program for creating a new mixture and inserting data. It is seen that, in contrast to our previous programs (except for refs. 18 and 19), the user has an option of up to four types of gradients: linear, logarithmic, exponential and sigmoidal. Once

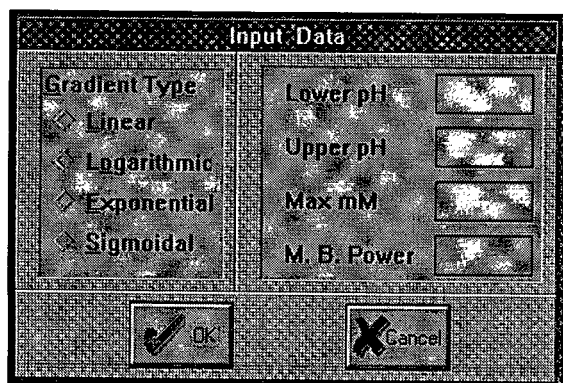


Fig. 4. Dialogue box for data insertion for creation of a new mixture. Note that options are given for the creation of four different types of pH gradients. The other required input data are the starting (lower) and ending (upper) pH values (*i.e.*, the bounds of the pH interval to be generated), the maximum total molarity of all species in solution and the average desired β power along the eluted pH gradient.

the type of gradients is selected, the program needs, as input data, the lower starting pH (*i.e.*, the desired pH of the solution that will be placed in the “acidic” or mixing chamber) and the upper pH (*i.e.*, the pH of the solution which will fill the “basic” chamber, or

TABLE I

LIST OF BUFFERS (WITH RESPECTIVE pK VALUES) USED IN MODELLING AND MEASURING pH GRADIENTS

No.	Name	Type	pK values
1	HCl ^a	Acid	0.4
2	Citric acid	Acid	3.128, 4.762, 6.4
3	Chloroacetic acid	Acid	2.92
4	Itaconic acid	Acid	3.85, 5.45
5	Acetic acid	Acid	4.75
6	Malonic acid	Acid	2.83, 5.69
7	Sulphanilic acid	Acid	3.23
8	Glutaric acid	Acid	4.31, 5.41
9	Tris base	Base	8.3
10	Imidazole	Base	6.9
11	NaOH ^a	Base	13
12	Diethylamine	Base	10.489
13	Piperazine	Base	9.83
14	Quinine	Base	8.52
15	Azetidine	Base	11.29
16	Pilocarpine	Base	6.87

^a For computational purposes HCl was assigned $pK=0.4$ and NaOH $pK=13$.

TABLE II

OPTIMIZED RECIPE FOR CREATION OF A LINEAR pH 3–11 GRADIENT, AS PLOTTED IN FIG. 5

No.	Name	Chamber A (mM)	Chamber B (mM)
1	HCl	30.134	0.000
2	Citric acid	2.822	9.685
3	Chloroacetic acid	0.000	0.000
4	Itaconic acid	4.253	0.000
5	Acetic acid	0.000	0.000
6	Malonic acid	0.000	0.000
7	Sulphanilic acid	1.021	5.143
8	Glutaric acid	0.000	0.000
9	Tris base	4.324	4.051
10	Imidazole	0.000	8.086
11	NaOH	0.000	33.308
12	Diethylamine	0.000	6.164
13	Piperazine	23.833	1.913
14	Quinine	0.000	1.650
15	Azetidine	0.000	0.000
16	Pilocarpine	3.613	0.000

reservoir). Important options given to the user are (a) the selection of maximum total molarity (as a sum of the partial molarity of each ion in solution) and (b) the selection of the mean β power along the pH gradient.

We shall now give some examples of different types of gradients that can be generated by our computer program. Table I gives a mixture of sixteen common acids and bases (weak and strong), some oligoprotic and most monoprotic (pK values as given in refs. 29 and 30). These tables can be prepared and stored by the user as databases. Table II gives the same kind of table, with already calculated and optimized molarities of all components for creation of a linear pH 3–11 gradient with the following preset requirements: maximum total molarity of all ions, 100 mM; and average β , 6 mequiv. $l^{-1} pH^{-1}$. It should be noted that everything is done automatically by the computing algorithms: thus, during the calculations and optimization, some components are automatically excluded by the mixture, since their pK values would hamper the generation of a linear gradient. In this particular case, components 3, 5, 6, 8 and 15 have been automatically excluded from the mixture. The resulting gradient is shown in Fig. 5; it is seen that,

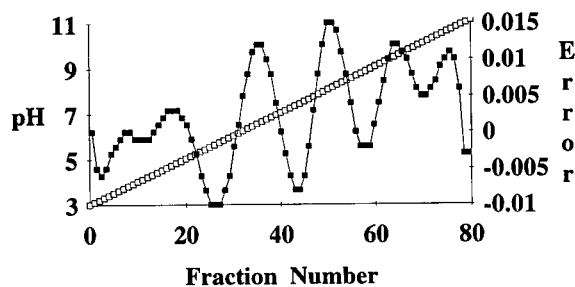


Fig. 5. Simulation of (□) the pH gradient profile and (■) deviation from linearity of the mixture in Table II. Parameters of the gradient: linear pH 3–11 gradient; maximum total molarity, 100 mM; average β , 6 mequiv. l^{-1} pH^{-1} . Note the minute deviations from linearity and their constant oscillations around zero.

by linear elution, from a two-vessel gradient mixer, of two equal volumes of the compositions as given in Table II for the “acidic” and “basic” chambers, a remarkably linear pH gradient is obtained. The deviations from linearity are extremely minute, and are well below 1% of the width of the generated pH interval, a limit given in previous calculations [4–8].

Table III gives the same mixture, but for the calculation of a logarithmic gradient spanning the pH range 4–10, with the following constraints:

TABLE III
OPTIMIZED RECIPE FOR CREATION OF A LOGARITHMIC pH 4–10 GRADIENT, AS PLOTTED IN FIG. 6

No.	Name	Chamber A (mM)	Chamber B (mM)
1	HCl	18.129	0.000
2	Citric acid	4.083	5.794
3	Chloroacetic acid	0.000	0.000
4	Itaconic acid	0.000	0.000
5	Acetic acid	0.000	0.000
6	Malonic acid	2.527	0.000
7	Sulphanilic acid	0.000	0.000
8	Glutaric acid	0.000	0.000
9	Tris base	9.363	0.000
10	Imidazole	0.000	11.203
11	NaOH	0.000	11.380
12	Diethylamine	0.000	0.000
13	Piperazine	10.181	11.816
14	Quinine	0.000	9.852
15	Azetidine	0.000	0.000
16	Pilocarpine	5.718	0.000

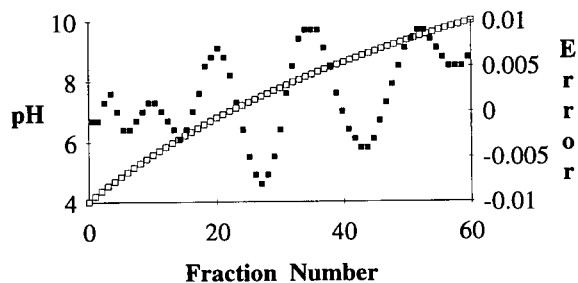


Fig. 6. Simulation of (□) the pH gradient profile and (■) deviation from the desired shape of the mixture in Table III. Parameters of the gradient: logarithmic pH 4–10 gradient; maximum total molarity, 50 mM; average β , 6 mequiv. l^{-1} pH^{-1} .

maximum total molarity of all ions, 50 mM; and average β power along the pH gradient, 6 mequiv. l^{-1} pH^{-1} . The gradient thus formed is shown in Fig. 6; it is seen that the pH profile has the desired shape and that again the deviation (this time from the desired logarithmic shape) is still minute. Note in Fig. 6, as in Fig. 5, how the deviations oscillate constantly around zero in an almost sinusoidal fashion, a prerequisite for minimizing this function [17,18].

TABLE IV
OPTIMIZED RECIPE FOR CREATION OF A CONCAVE EXPONENTIAL pH 4–10 GRADIENT, AS PLOTTED IN FIG. 7

No.	Name	Chamber A (mM)	Chamber B (mM)
1	HCl	14.360	0.000
2	Citric acid	0.000	14.958
3	Chloroacetic acid	0.000	0.000
4	Itaconic acid	0.000	2.780
5	Acetic acid	0.000	0.000
6	Malonic acid	0.000	3.338
7	Sulphanilic acid	30.632	3.797
8	Glutaric acid	9.029	0.000
9	Tris base	9.033	2.764
10	Imidazole	0.000	0.000
11	NaOH	0.000	57.530
12	Diethylamine	0.000	0.000
13	Piperazine	34.829	6.709
14	Quinine	0.000	0.939
15	Azetidine	0.000	0.000
16	Pilocarpine	2.117	7.135

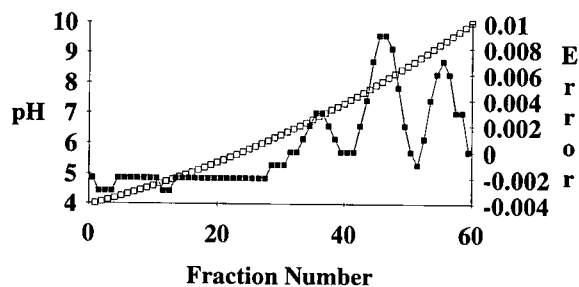


Fig. 7. Simulation of (□) the pH gradient profile and (■) deviation from the desired shape of the mixture in Table IV. Parameters of the gradient: exponential pH 4–10 gradient; maximum total molarity, 100 mM; average β , 6 mequiv. $l^{-1} pH^{-1}$.

Table IV gives again the same mixture, but for the calculation of a concave exponential pH 4–10 gradient with the following constraints: maximum total molarity of all ions, 100 mM; and average β power along the pH gradient, 6 mequiv. $l^{-1} pH^{-1}$. The gradient thus formed is shown in Fig. 7; here too the minute deviation from the desired shape should be appreciated. Such deviations (of barely a few thousandths of a pH unit) cannot be appreciated even by the most sensitive pH meters.

Experimental validation of the activity coefficient corrections

We have seen above that it is possible to select different shapes of pH gradients, and that such shapes are automatically calculated and optimized by our simulator in extremely short times (usually in less than 1 min). It remains to be seen whether the activity coefficient corrections we have implemented (the Davies equation) have any practical meaning and can be reproduced in routine work. We therefore explored how the Davies equation applies in different cases, such as conditions of low to very

TABLE V

OPTIMIZED RECIPE FOR A pH 3.3–6.6 GRADIENT (MAXIMUM MOLARITY 75 mM PER CHAMBER, MEAN BUFFERING POWER 14 mequiv. $l^{-1} pH^{-1}$)

Recipe used for modelling the pH gradient in Fig. 8.

Name	Chamber 1 (mM)	Chamber 2 (mM)
Chloroacetic acid	3.415	0.000
Itaconic acid	16.35	16.03
Acetic acid	10.28	9.81
Imidazole	4.17	46.69

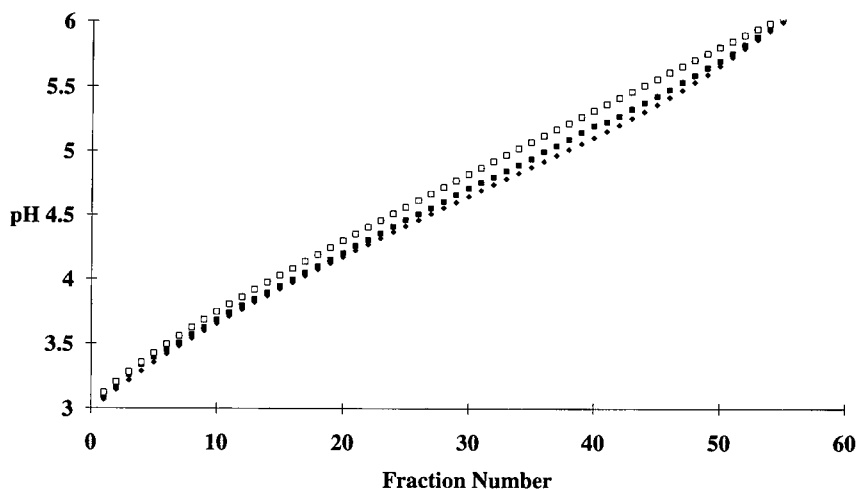


Fig. 8. Comparison between simulated and experimental pH profiles. A pH 3.3–6.3 gradient was generated according to the recipe in Table V. Constraints: maximum molarity (in each chamber), 75 mM; average β power, 14 mequiv. $l^{-1} pH^{-1}$. Sixty 2-ml fractions were eluted and the pH carefully measured at 25°C in a thermostated vessel (■ = pH-measured). The simulated pH profiles, with (◆ = pH-Davies) and without (□ = pH-NoCorr) Davies correction, are also plotted. Note the divergence between the two simulated profiles and the good agreement between experimental and Davies-corrected simulations.

TABLE VI

EXAMPLE OF THE CALCULATIONS PERFORMED ON ELUTED FRACTIONS FOR THE pH GRADIENT PLOTTED IN FIG. 8

Abbreviations: meas. = fraction number; pH-meas. = experimentally measured pH gradient; pH-NoCorr. = simulated pH gradient without any correction; pH-Huck. = pH gradient simulated with the Debye-Hückel correction; pH-Davies = pH gradient simulated with the Davies correction; I = ionic strength of each fraction (expressed in equiv. l^{-1}); β = buffering power (expressed in mequiv. l^{-1} pH^{-1}).

Meas.	pH-meas.	pH-NoCorr.	pH-Huck.	pH-Davies	I	β
1	3.098	3.121	3.068	3.065	0.00556	9.568
2	3.171	3.202	3.143	3.14	0.00611	9.898
3	3.258	3.279	3.216	3.213	0.00668	10.288
4	3.335	3.354	3.287	3.283	0.00726	10.715
5	3.395	3.425	3.354	3.35	0.00786	11.159
6	3.453	3.494	3.419	3.414	0.00847	11.601
7	3.504	3.56	3.481	3.476	0.00909	12.027
8	3.571	3.624	3.541	3.536	0.00973	12.426
9	3.622	3.685	3.6	3.594	0.01039	12.788
10	3.683	3.745	3.656	3.65	0.01105	13.11
11	3.74	3.804	3.712	3.705	0.01173	13.389
12	3.792	3.861	3.766	3.759	0.01242	13.623
13	3.842	3.918	3.819	3.812	0.01312	13.814
14	3.893	3.974	3.871	3.864	0.01384	13.965
15	3.946	4.029	3.923	3.915	0.01457	14.081
16	3.996	4.083	3.974	3.966	0.0153	14.167
17	4.049	4.138	4.025	4.016	0.01605	14.229
18	4.101	4.192	4.075	4.066	0.01681	14.272
19	4.152	4.246	4.125	4.115	0.01759	14.303
20	4.203	4.299	4.174	4.164	0.01837	14.326
21	4.259	4.353	4.224	4.213	0.01917	14.347
22	4.306	4.406	4.272	4.261	0.01999	14.369
23	4.357	4.459	4.321	4.309	0.02082	14.393
24	4.411	4.511	4.369	4.357	0.02166	14.423
25	4.464	4.564	4.417	4.404	0.02252	14.458
26	4.509	4.616	4.464	4.45	0.02341	14.497
27	4.555	4.668	4.511	4.497	0.02431	14.54
28	4.608	4.72	4.558	4.543	0.02523	14.585
29	4.66	4.771	4.604	4.589	0.02617	14.631
30	4.712	4.822	4.65	4.634	0.02713	14.677
31	4.758	4.872	4.696	4.679	0.02811	14.719
32	4.8	4.923	4.742	4.724	0.02911	14.757
33	4.847	4.973	4.787	4.769	0.03014	14.788
34	4.894	5.023	4.832	4.813	0.03118	14.81
35	4.942	5.072	4.878	4.858	0.03224	14.819
36	4.996	5.122	4.923	4.903	0.03332	14.814
37	5.043	5.171	4.969	4.948	0.03441	14.791
38	5.096	5.22	5.015	4.994	0.03551	14.746
39	5.148	5.269	5.062	5.04	0.03661	14.677
40	5.2	5.318	5.11	5.087	0.03772	14.581
41	5.23	5.367	5.158	5.135	0.03883	14.456
42	5.275	5.416	5.207	5.184	0.03993	14.302
43	5.329	5.465	5.258	5.234	0.04102	14.12
44	5.377	5.514	5.31	5.287	0.04208	13.913
45	5.429	5.563	5.364	5.34	0.04313	13.685
46	5.481	5.612	5.42	5.397	0.04415	13.444
47	5.539	5.661	5.478	5.455	0.04513	13.204

(Continued on p. 324)

TABLE VI (continued)

Meas.	pH-meas.	pH-NoCorr.	pH-Huck.	pH-Davies	<i>I</i>	β
48	5.591	5.71	5.538	5.516	0.04607	12.976
49	5.648	5.759	5.6	5.58	0.04697	12.78
50	5.699	5.807	5.665	5.647	0.04781	12.635
51	5.759	5.855	5.732	5.716	0.04861	12.56
52	5.826	5.901	5.8	5.787	0.04935	12.576
53	5.89	5.947	5.868	5.858	0.05003	12.696
54	5.964	5.992	5.936	5.93	0.05064	12.931
55	6.032	6.035	6.002	5.999	0.05119	13.282
56	6.094	6.077	6.066	6.066	0.05168	13.745
57	6.151	6.117	6.126	6.129	0.05209	14.31
58	6.208	6.156	6.183	6.188	0.05244	14.963
59	6.261	6.193	6.236	6.243	0.05271	15.69
60	6.308	6.228	6.285	6.294	0.05292	16.476

high ionic strength and narrow and wide pH gradients.

Fig. 8 gives the pH profiles generated by computer simulation without (open boxes) and with (diamonds) the Davies correction. The starting mixture spans the pH interval 3.3–6.3 and has the following constraints: maximum molarity (in each chamber),

75 mM; and average β power, 14 mequiv. l^{-1} pH^{-1} . This mixture was selected so as to avoid CO_2 adsorption and as a representative low ionic strength recipe (as given in Table V). In parallel to the simulation, 60 ml of each of the two solutions were prepared, loaded in a two-vessel gradient mixer and eluted, collecting 2 ml per fraction.

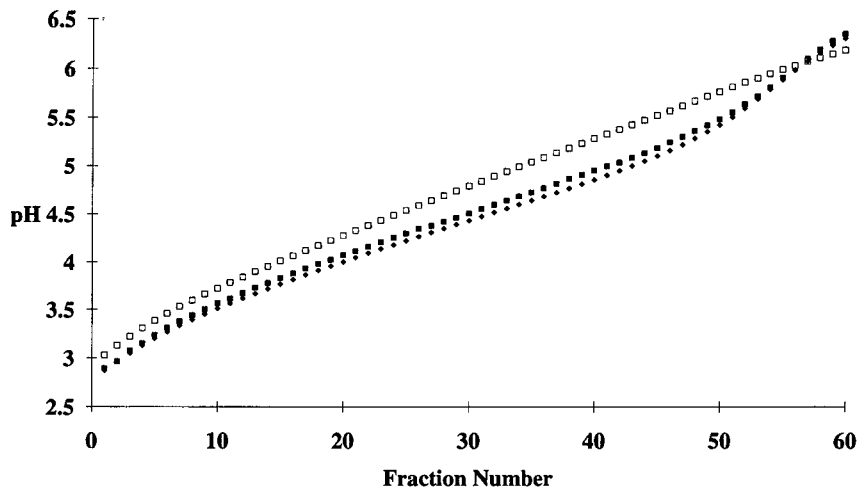


Fig. 9. Comparison between simulated and experimental pH profiles. A pH 3.3–6.3 gradient was generated according to the recipe in Table V (with a tenfold increase in molarity of each ion). Constraints: maximum molarity (in each chamber), 750 mM; average β power, 140 mequiv. l^{-1} pH^{-1} . Sixty 2-ml fractions were eluted and the pH carefully measured at 25°C in a thermostated vessel (■ = pH-measured). The simulated pH profiles, with (◆ = pH-Davies) and without (□ = pH-NoCorr) Davies correction, are also plotted.

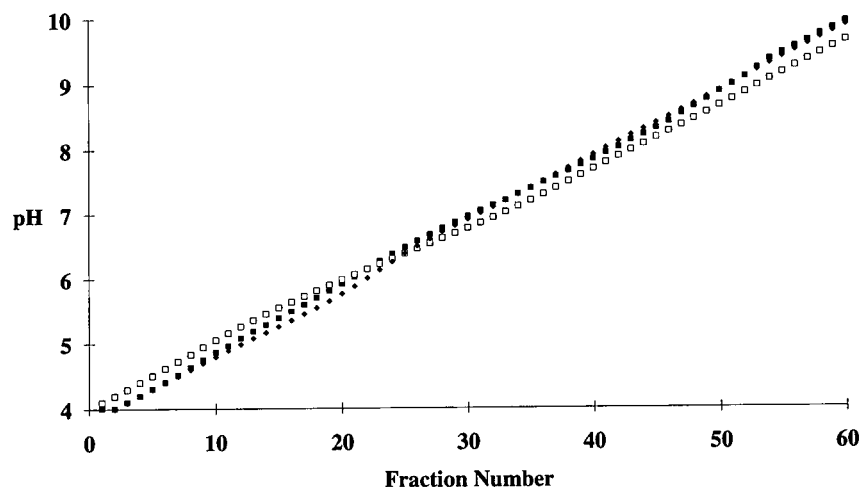


Fig. 10. Comparison between simulated and experimental pH profiles. A pH 4–10 gradient was generated according to the recipe in Table VII. Constraints: maximum molarity (in each chamber), 200 mM; average β power, 15 mequiv. $l^{-1} pH^{-1}$. Sixty 2-ml fractions were eluted and the pH carefully measured at 25°C in a thermostated vessel (■ = pH-measured). The simulated pH profiles, with (◆ = pH-Davies) and without (□ = pH-NoCorr) Davies correction, are also plotted.

Two phenomena are immediately apparent: there is a strong divergence between the two computed pH profiles in the absence and presence of the Davies correction, and the real pH gradient, as eluted from the gradient mixer, follows closely the simulated profile with the Davies correction. Note that the divergence between the two simulated profiles follows closely the prevailing ionic strength of the eluted fractions; thus, as the total ionic strength

increases (towards the basic end of the gradient, owing to progressive deprotonation of weak acids), the divergence increases from only 0.1 pH unit (between fractions 10 and 20) to as high as 0.2 pH unit (between fractions 40 and 50) (see also the corresponding Table VI, which gives the main parameters of each eluted fraction).

At this point, it is of interest to see what happens to the same mixture at a much increased ionic strength. We therefore took the mixture in Table V and multiplied all the molarity values by a factor of 10. In this new mixture (still encompassing the pH interval 3.3–6.3) the new parameters are therefore maximum total molarity (in each chamber) 750 mM and average β power 140 mequiv. $l^{-1} pH^{-1}$. Fig. 9 shows the new simulated pH profiles; now the divergence between the two profiles (with and without correction) is much more pronounced (up to 0.45 pH unit in the region of maximum ionic strength, *i.e.*, fractions 40–50). Here again it can be appreciated that the experimental, measured pH in the eluted fractions follows very closely the Davies-corrected profile.

We next explored whether the corrections adopted apply also in extended pH intervals and in alkaline pH ranges. A new recipe was prepared (see Table VII) encompassing the pH range 4–10, with the following

TABLE VII

OPTIMIZED RECIPE FOR A pH 4.0–10.0 GRADIENT (MAXIMUM MOLARITY 200 mM PER CHAMBER, MEAN BUFFERING POWER 15 mequiv. $l^{-1} pH^{-1}$)

Recipe used for modelling the pH gradient in Fig. 10.

Name	Chamber 1 (mM)	Chamber 2 (mM)
Chloroacetic acid	106.8	21.79
Itaconic acid	0.00	57.55
Acetic acid	15.04	0.00
Imidazole	30.06	0.00
Tris base	53.16	9.115
Diethanolamine	19.64	1.975
Ethanolamine	0.00	32.98
NaOH	0.00	126.6

constraints: maximum molarity (per chamber), 200 mM and average β power, 15 mequiv. l⁻¹ pH⁻¹. As shown in Fig. 10, the simulated patterns follow very closely those obtained previously (Figs. 8 and 9); in the acidic part of the gradient, the two simulated profiles (with and without Davies correction) diverge, the latter being higher than the former; around neutrality, there is a cross-over (as clearly hinted in the upper parts of the graphs depicted in Figs. 8 and 9) and at alkaline pH the Davies-corrected (and experimentally measured) pH courses run higher than the uncorrected ones. We can therefore conclude, from the experimental evidence presented here, that the correction algorithm proposed fulfils the expectations.

DISCUSSION

The simulator presented here has some unique features compared with previous programs [4–7] that are worth highlighting. First, we have been able to introduce, as an optimization algorithm, the simplex, one of the most powerful and fastest for this kind of task. We had discarded the simplex in all our previous simulations on the grounds that it cannot be applied to solving non-linear problems. We were therefore forced to adopt mathematical transformations of all the basic equations, so as to transform a non-linear into a linear programming problem. That we are on correct grounds was also checked by resimulating all our optimized mixtures with the other available programs and also by experimentally eluting the simulated gradients and checking the pH values of the collected fractions.

The advantages of the simplex are several. First, it finds the exact solution to the problem. Second, it is much quicker than other optimization methods we had adopted in the past. For example, in our early programs [5,8], based on Cauchy's steepest descent algorithm, the calculations were extremely slow; thus, for calculating and optimizing a pH 4–10 recipe (containing only six or seven species) often >24 h were required, and sometimes the ideal solution could not be found, so that the user had to stop the program and enter educated guesses (for varying the molarity of the different species). Enormous progress was already made with the recent work of Tonani and Righetti [17,18], the direct precursor of the present program, in which the

calculation routines were reduced to only 10–15 min.

Another unique feature of our program is the introduction of the Davies equation for correcting the activity coefficient of ions as a function of the prevailing ionic strength in solution. As the preparation of immobilized pH gradients has been claimed to be finally an exact science [2], able to overcome all the defects and imprecisions connected with conventional isoelectric focusing in soluble, amphoteric buffers [1], all sources of errors have to be removed, if "pH gradient engineering" is aimed for. In addition, in IPGs, it is customary to measure the isoelectric point of a protein by a simple interpolation procedure along a pH gradient with a well known profile. A precision of ± 0.01 pH unit is generally claimed.

All the above cannot be completely valid unless extra effort is made to eliminate the last source of uncertainty, *i.e.*, the variation of activity coefficients as a function of ionic strength. It is known that, as the ionic strength in solution is increased, the diffuse double layer around an ion "shrinks" and progressively moves close to the rigid layer. Among the effects of such a phenomenon is a small, but non-negligible, pK change of the weak anions and cations in solution. As the recipes we formulate assume "constant pK values", if the latter assumption is no longer valid one would expect a shift of the generated pH gradient. This shift is in general small (perhaps of the order of a few hundredths of a pH unit) at small values of ionic strength in solution. As in general our IPG recipes were made to contain not more than 10 mM buffering ion, we had in the past neglected such corrections. However, the deviation becomes appreciable at higher buffer and titrant molarities: we have seen (Fig. 8) that even with 75 mM total ions in solution the discrepancy between the simulated and experimental pH curves is as high as 0.2 pH unit. At molarities > 700 mM, this discrepancy is as high as 0.45 pH unit. In many recipes proposed today the total ion molarity often exceeds 50 mM, so it seems impossible to continue to ignore such corrections.

We therefore tested the various corrections proposed (see eqns. 18–22) and it seems safe to conclude, from our data, that the Davies correction more closely follows the experimental pH gradient obtained. We therefore feel that the present program

is a major step in rendering “pH gradient” engineering an exact science. Needless to say, although our knowledge has mostly been applied, in this decade, to the generation and optimization of immobilized pH gradients to be used under isoelectric focusing conditions, it is implicit that this know-how is valid in all other instances, e.g., for generating pH gradients in ion-exchange chromatography and in all problems of titration.

ACKNOWLEDGEMENTS

This work was supported in part by grants from the Agenzia Spaziale Italiana (ASI), Consiglio Nazionale delle Ricerche (CNR, Rome, Italy), Progetti Finalizzati Biotecnologie e Biostrumentazione, Chimica Fine II e FATMA. We thank Dr. Marco Fazio for help with pH gradient measurements.

REFERENCES

- 1 P. G. Righetti, *Isoelectric Focusing: Theory, Methodology and Applications*, Elsevier, Amsterdam, 1983.
- 2 P. G. Righetti, *Immobilized pH Gradients: Theory and Methodology*, Elsevier, Amsterdam, 1990.
- 3 M. Chiari and P. G. Righetti, *Electrophoresis*, 13 (1992) 187–191.
- 4 F. C. Celentano, E. Gianazza and P. G. Righetti, *Electrophoresis*, 12 (1991) 693–703.
- 5 G. Dossi, F. Celentano, E. Gianazza and P. G. Righetti, *J. Biochem. Biophys. Methods*, 7 (1983) 123–142.
- 6 E. Gianazza, G. Dossi, F. Celentano and P. G. Righetti, *J. Biochem. Biophys. Methods*, 8 (1983) 109–133.
- 7 F. C. Celentano, E. Gianazza, G. Dossi and P. G. Righetti, *Chemometr. Intell. Lab. Syst.*, 1 (1987) 349–358.
- 8 E. Gianazza, F. C. Celentano, G. Dossi, B. Bjellqvist and P. G. Righetti, *Electrophoresis*, 5 (1984) 88–97.
- 9 E. Gianazza, S. Astrua-Testori and P. G. Righetti, *Electrophoresis*, 6 (1985) 113–117.
- 10 E. Gianazza, P. Giacon, B. Sahlin and P. G. Righetti, *Electrophoresis*, 6 (1985) 53–56.
- 11 P. G. Righetti, E. Gianazza and F. C. Celentano, *J. Chromatogr.*, 356 (1986) 9–14.
- 12 R. A. Mosher, M. Bier and P. G. Righetti, *Electrophoresis*, 7 (1986) 59–66.
- 13 E. Gianazza, F. C. Celentano, S. Magenes, C. Ettori and P. G. Righetti, *Electrophoresis*, 10 (1989) 806–808.
- 14 F. C. Celentano, C. Tonani, M. Fazio, E. Gianazza and P. G. Righetti, *J. Biochem. Biophys. Methods*, 16 (1988) 109–128.
- 15 P. G. Righetti, M. Fazio, C. Tonani, E. Gianazza and F. C. Celentano, *J. Biochem. Biophys. Methods*, 16 (1988) 129–140.
- 16 P. G. Righetti, E. Gianazza and C. Gelfi, in V. Neuhoff (Editor), *Electrophoresis '84*, VCH, Weinheim, 1984, pp. 29–48.
- 17 C. Tonani and P. G. Righetti, *Electrophoresis*, 12 (1991) 1011–1021.
- 18 P. G. Righetti and C. Tonani, *Electrophoresis*, 12 (1991) 1021–1027.
- 19 H. Svensson and S. Pettersson, *Sep. Sci.*, 3 (1968) 209–215.
- 20 R. I. Jennrich and M. L. Ralston, *Annu. Rev. Biophys. Bioeng.*, 8 (1979) 195–238.
- 21 W. J. Kennedy and J. E. Gentle, *Statistical Computing*, Marcel Dekker, New York, 1980.
- 22 D. A. Ratkowsky, *Non-Linear Regression Modelling*, Marcel Dekker, New York, 1983.
- 23 E. A. Peterson and H. A. Sober, in P. Alexander and A. Block (Editors), *Analytical Methods of Protein Chemistry I*, Pergamon Press, New York, 1960, pp. 88–102.
- 24 P. G. Ciarlet and J. L. Lions, *Handbook of Numerical Analysis*, Elsevier, Amsterdam, 1990.
- 25 D. J. Leggett, *J. Chem. Educ.*, 60 (1983) 707–710.
- 26 A. Kuenzi, L. Tzschach and M. Zehnder, in W. H. Press, B. P. Flannery, S. A. Teukolsky and W. T. Vetterling (Editors), *Numerical Recipes in C. The Art of Scientific Computing*, Cambridge University Press, Cambridge, 1987, pp. 276 and 290.
- 27 P. G. Righetti, E. Wenisch and M. Faupel, *J. Chromatogr.*, 475 (1989) 293–309.
- 28 J. N. Butler, *Ionic Equilibrium*, Addison-Wesley, New York, 1964, pp. 457–479.
- 29 R. G. Bates, *Determination of pH: Theory and Practice*, Wiley, New York, 1973.
- 30 R. C. Weast (Editor), *CRC Handbook of Chemistry and Physics*, CRC Press, Boca Raton, FL, 67th ed., 1987, pp. D159–D164.

Protein and peptide mobility in capillary zone electrophoresis

A comparison of existing models and further analysis

Vincent J. Hilser, Jr.^{*} and Gregory D. Worosila

Physical and Analytical Chemistry Department, Ciba-Geigy Corporation, Suffern, NY 10901 (USA)

Suzanne E. Rudnick

Department of Chemistry, Manhattan College, Riverdale, NY 10471 (USA)

(First received March 3rd, 1992; revised manuscript received November 2nd, 1992)

ABSTRACT

Capillary zone electrophoresis of peptide fragments from the tryptic digest of human recombinant insulin-like growth factor I (rhIGF-I) has been carried out and the observed mobilities used to compare the relative applicability of existing mobility models. In addition, the physical forces affecting electromigration have been systematically analyzed in order to more accurately describe the physical chemistry involved. Such an approach should further improve the ability to predict electrophoretic mobility in capillary zone electrophoresis.

INTRODUCTION

Capillary zone electrophoresis (CZE) is rapidly becoming a major laboratory method for the separation, analysis, and characterization of biomolecules. Several recent studies have focused on deriving a correlation between certain physical attributes of proteins and peptides and the observed electrophoretic mobilities in CZE. Such correlations would facilitate the prediction of electrophoretic mobilities, and thus the design of optimum experimental conditions.

Several treatments have been the subject of recent studies [1–4]. Grossman *et al.* [1] have proposed a semi-empirical model which correlates charge and polymer number to electrophoretic mobility [1]. In another study, Rickard *et al.* [2] used charge and molecular mass to establish a similar correlation. We have applied these treatments to peptides obtained in our laboratory from the tryptic digestion of rhIGF-I (human recombinant insulin-like growth factor I), in order to determine which approach best predicts mobility in capillary electrophoresis. We have also investigated a more accurate description of the mobility using a systematic analysis of the physical forces affecting electromigration.

THEORY

Electrostatic attraction between the cathode and positively charged peptides is the primary driving

Correspondence to: G. D. Worosila, Physical and Analytical Chemistry Department, Ciba-Geigy Corporation, Suffern, NY 10901, USA.

^{*} Present address: Graduate Program in Biology, The Johns Hopkins University, Seeley Mudd Hall, Baltimore, MD 21218, USA.

force in CZE at low pH. While electrostatic attractions will be affected by changes in pH, ionic strength, temperature, and dielectric constant, experimental conditions have been developed to minimize changes in these solvent characteristics during CZE separations. The pH and ionic strength can be easily controlled through the choice of buffer and its concentration. Temperature is also controlled by modern CZE instrumentation.

In CZE, the net velocity of an individual peptide will vary as a direct function of charge and as an inverse function of size. This is demonstrated in Stokes' equation for frictional drag in an electric field.

$$\mu = \frac{q}{6 \pi r \eta} \quad (1)$$

where q is the net charge, η is the viscosity of the separation buffer, and r is the radius of spherical species. The Stokes radius is a parameter which defines size and is intended to describe the mobility of uniform spherical ions, thus making its application to peptide mobility correlations of limited use. Therefore, an analogous value must be derived which will describe peptide size in solution and which will mathematically define the physical impedance observed in CZE separations.

In their recent study, Grossman *et al.* [1] attempted to characterize the contribution of local dielectric to the electrophoretic mobility of a series of heptapeptides which contained one variable amino acid at the fourth position in the chain with lysine residues at positions three and five. This treatment accounted for the observed mobility differences between the peptides as a function of the degree of solvent perturbation by each substituted residue in the microenvironment of the lysine prosthetic groups. The resultant change in local dielectric was proposed to affect the degree of ionization and, ultimately, the charge of the lysines at pH 2.5. In order to significantly affect the local dielectric in the region surrounded by two charged lysine residues, a structure capable of solvent perturbation must be generated [5–9]. Since it has been demonstrated that small peptides are generally unable to form more than very limited secondary structure [10,11], it would seem highly unlikely that the mobility differences observed by Grossman *et al.* [1] can be attributed to charge differences caused by shifts in local dielectric.

We therefore proposed that a more discriminating treatment of the real size of each peptide should facilitate explanation of the observed mobility differences. Initial attention focused on an analysis of the means by which size is accounted for in existing peptide mobility correlations. In the model described by Grossman *et al.* [1], the size of each peptide is defined by the number of constituent amino acids. Every peptide is viewed as a homopolymer. From a physical perspective, this homopolymeric treatment of peptides represents a random coil model. It relies on a one-dimensional separation mechanism, with the root-mean-square end-to-end distance being the only size factor considered.

The use of molecular mass, as described by Rickard *et al.* [2] is, in principle, an improvement. Theoretically, a molecular mass model should account for volume because individual amino acids possess characteristic length-to-mass ratios and some discrimination would occur as a result. Separation according to this model involves a component of length, as the peptide backbone is considered identical for all amino acids. The mass will increase with the addition of each amino acid residue, and the average excess molecular mass remaining after subtraction of the backbone molecular mass would represent the width component. This approach assumes that the overall average shape of each peptide is disk-like.

Therefore, we wanted to identify a mechanism that would properly account for the size of each amino acid residue and also agree with existing solution models. Since CZE separations occur in the absence of inter-phase mass transfer, the nature of the "size phenomena" should be a function of the thermodynamic interactions between the solvent and the sample. If the effective size of a sample is a function of such solute-solvent interactions, then solvation should greatly affect the effective size of the solute. Since the water ordering is a function of surface area, this is extremely useful in defining the "effective size" in CZE separations. The greater the surface area, the greater the degree of water ordering that occurs, and, consequently, the larger the hydration sphere that surrounds the residue. Hence, it is the degree of hydration which would, theoretically, define "effective size".

Comparison between existing models should prove useful in describing the factors contributing

to the “effective size” of residues. In addition, some insight should be gained into the relative contributions of forces involved in CZE separations.

EXPERIMENTAL

Reagents and materials

rhIGF-I was obtained from Ciba-Geigy Pharmaceuticals Division. A single batch of rhIGF-I was used to generate peptide fragments, and was chromatographically determined to have a purity > 98% by protein mass. HPLC-grade acetonitrile (Fisher, Pittsburgh, PA, USA) was used for HPLC analysis of tryptic fragments, optima-grade acetonitrile (Fisher) was utilized for all amino acid analysis experiments, and certified trifluoroacetic acid (TFA) (Fisher) was used for all HPLC analysis. In addition reagent-grade iodoacetamide (Sigma, St. Louis, MO, USA), gold label triethylamine (Aldrich, Milwaukee, WI, USA), and sequanal-grade phenylisothiocyanate (PITC) and constant boiling HCl (Pierce, Rockford, IL, USA) were used. All other chemicals used were analytical grade and were not further purified. Distilled, deionized Milli-Q water (Millipore, Bedford, MA, USA) was utilized in all experimentation. Trypsin, in various treated forms, was obtained from three sources (Sigma, Pierce, and ICN, Cleveland, OH, USA) and was used without further purification.

Instrumentation

Reversed-phase HPLC. All chromatographic separations were performed with a system composed of a Waters (Milford, MA, USA) 600E gradient pump and WISP Model 712 autosampler with a refrigeration unit, a Kratos (Foster City, CA, USA) Spectroflow 783 UV detector at 214 nm, and a Dionex (Sunnyvale, CA, USA) Eluant Degas Module. Data collection was performed with a Nelson (Danbury, CT, USA) 760 Series interface and a modified version of Nelson Analytical Software.

Capillary electrophoresis. CZE was performed on an Applied Biosystems 270A Capillary Electrophoresis System with a fused silica capillary (122 cm × 100 μm I.D.). Ultraviolet detection at 200 nm was used for peak analysis. Data collection and peak processing were performed as described for the HPLC analysis.

Amino acid analysis. Peptides were identified by

amino acid analysis. The Waters Pico-Tag work station was utilized for the gas-phase hydrolysis of each peptide fragment and subsequent generation of phenylisothiocyanate (PITC)-derivatized amino acids. Separation of derivatized amino acids, data collection, and peak processing were performed as described for HPLC.

Methods

Trypsin digestion of rhIGF-I. The hydrolysis conditions utilized were a modification of those described by Worosila [12]. An aliquot of 10 μl of trypsin solution (10 mg/ml in 0.1 mM HCl) was added to the rhIGF-I solution (250 μl of a 10 mg/ml solution in water) initially and again after 3 h [trypsin–rhIGF-I (1:25)]. After an 18-h incubation at 37°C, the reaction was quenched with 100 μl of 10% (v/v) trifluoroacetic acid (TFA) in water.

Reversed-phase HPLC. Reversed-phase chromatographic analyses of rhIGF-I tryptic digests were performed using a Vydac Protein & Peptide C₁₈ column (15.0 cm × 4.6 mm I.D.) (Vydac, Hesperia, CA, USA) at ambient temperature. The flow-rate was 0.8 ml/min. Mobile phases consisted of (A) 0.1% TFA in water and (B) 0.08% TFA in acetonitrile–water (80:20). A gradient was employed which ran according to the following program: 100% A at 3 min, 65% A at 38 min, 0% A at 55 min. Final gradient conditions were kept for 5 min before being returned to the initial conditions. A 15-min equilibration time was utilized between each run. The injection volume utilized for optimum resolution was 20 μl, and the injection volume for fraction collection was 30 μl.

Peak identification of peptides. Peptides were identified by amino acid analysis. HPLC fractions were pooled from ten runs and lyophilized in acid washed vials. Peak purity was determined chromatographically using the gradient elution described for peak analysis. The lyophilisate was then redissolved in 200 μl of distilled water and 30 μl used for amino acid analysis using a modification of the Waters Pico-Tag PITC method.

Capillary zone electrophoresis. CZE was performed on all peptide peaks isolated from reversed-phase chromatography. Samples were dissolved in 10 mM sodium citrate, pH 2.5 to an approximate concentration of 0.5 mg/ml, as determined by calculation of recovery from the reversed-phase separa-

tions. The CZE mobile phase utilized was 20 mM sodium citrate, pH 2.5. CZE was performed at a temperature of 30°C, with a constant voltage of 30 kV. Samples were introduced by a 1-s vacuum injection onto a 122-cm capillary (99.7 cm to the detector). A proprietary mobility standard was utilized to facilitate the calculation of the peptide mobilities. Electrophoretic mobilities of samples were calculated according to the equation:

$$\mu = \left(\frac{L_D L_t}{V} \right) \left(\frac{1}{t} - \frac{1}{t_s} \right) + \mu_s \quad (2)$$

where:

L_D = length of capillary to detector, in cm

L_t = total length of capillary, in cm

V = system voltage

t = retention time of sample peak

t_s = retention time of standard peak

μ_s = mobility value for standard peak

Charge calculations. All peptide charges were calculated with the Henderson–Hasselbach equation using the pK_a values in ref. 2.

RESULTS AND DISCUSSION

Earlier work with peptides to determine a mobility model in CZE was performed using synthesized peptides [1]. As discussed previously, a model was derived which utilizes the polymer number of the sample peptides to define “size”. Mathematically, this was justified by combining the classic mobility (eqn. 1) with the root-mean-square end-to-end distance equation to yield the semi-empirical relationship

$$\mu \propto \frac{\ln(q + 1)}{N^{0.43}} \quad (3)$$

The charge term, $\ln(q + 1)$, in the equation was obtained from a systematic analysis of charge changes within a system of identically sized peptides. The deviation from the square root function for the polymer number (N) was empirically determined to give the most linear relationship. The mobility relationship which was derived from molecular mass (M_r) values [2] was determined entirely from empirical observations. The molecular mass-dependent equation was determined to be

$$\mu \propto \frac{q}{M_r^{2/3}} \quad (4)$$

One obvious difference between the two equation forms is the natural log dependence for the charge (q) in eqn. 3. Since this function was determined by systematic analysis, we predicted that the polymer-based equation would result in a more accurate treatment of charge effects. With respect to the “size” component of the samples, both equations represent a different approach to the physical impedance imposed on the samples. Ideally, linearity would be achieved with the polymer equation if (1) all amino acids were the same size, (2) the peptide backbone were fluid, and (3) there were no steric interactions between different parts of the peptide chain. The physical model for this equation assumes only minor contributions of the width dimension to the overall size of the amino acids. The molecular mass equation represents an attempt to account for the second dimension, width. Although this model does not take into account solvation properties and differences between chemical moieties, it does theoretically account for differences in mobility between peptides with identical polymer numbers.

A valid starting point for an analysis of mobility correlations is a comparison between the two published empirical models [1,2]. A comparison of the predictive ability of each equation can be used to assess the relative contribution of charge and size toward mobility. In addition, analysis of deviant peptides should also facilitate the recognition of contributing forces. In order to generate peptides for our use, trypsin was used to cleave rhIGF-I. In addition, some non-tryptic fragments of rhIGF-I were obtained and used in this work. The primary sequence of rhIGF-I is shown in Fig. 1, along with the predicted tryptic cleavage sites and the tryptic fragments obtained. The peptide fragments isolated from the tryptic digestion of rhIGF-I were identified by amino acid analysis and eqn. 2 was used to calculate the respective electrophoretic mobilities. To avoid variations due to drift, mobilities were calculated based on that of a proprietary standard ($\mu_s = 3.95 \cdot 10^{-4} \text{ cm}^2/\text{Vs}$). In addition, the charge of each fragment was calculated and the molecular mass and polymer number determined. However, as discussed by Rickard *et al.* [2], the assignment of pK_a values is critical in charge calculations. Rickard *et al.* [2] compared pK_a values of free amino acids with values obtained from non-electrophoretic

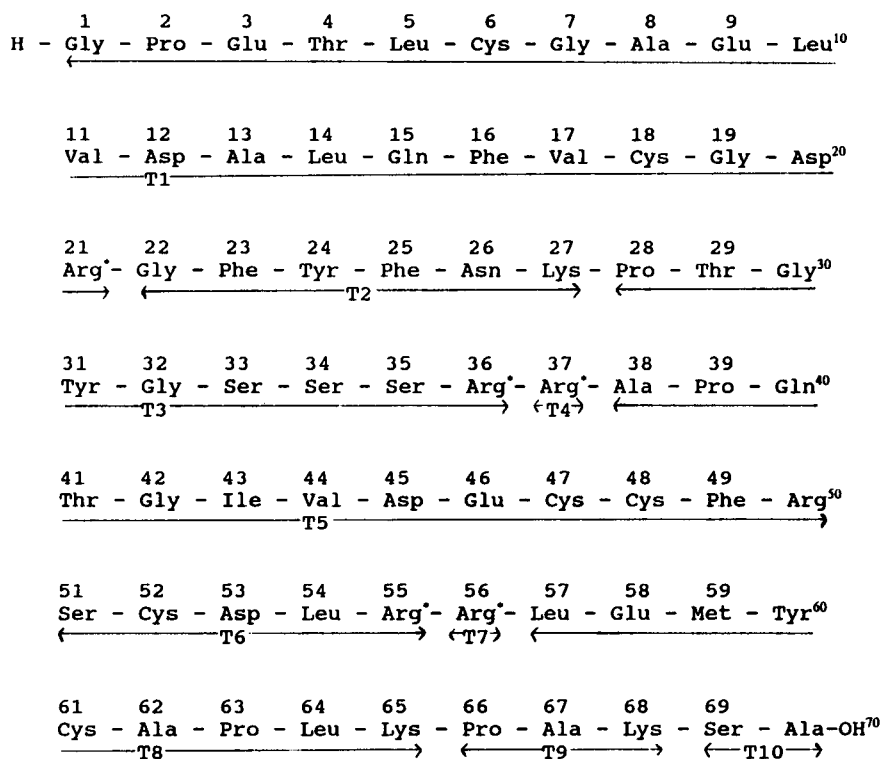


Fig. 1. The predicted tryptic cleavage sites of rhIGF-I. Arrows with (*) represent cleavage sites at the carboxyl terminals of Arg and Lys residues. Tryptic fragments are labeled according to their position within the rhIGF-I sequence.

measurements. These adjusted pK_a values improved their linearity and were used in their correlations. As our experiments were done at pH 2.5, ionization constants for the carboxyl terminal residues and for aspartic and glutamic acid must be accurately characterized to assure correct charge assignments. To determine the relative accuracy of the two mobility equations, we felt it necessary to use identical charge values for each. Therefore, linearities were developed for both functions using pK_a values obtained from the free amino acids (AApK values) and from the adjusted values (PpK values) of Rickard *et al.* [2]. Table I lists the data used to plot the mobilities of the individual peptide fragments in eqns. 3 and 4.

When the molecular mass function of eqn. 4, using both AApK- and PpK-derived charges, was plotted against the corresponding mobility for each peptide, a linear trend was established (Figs. 2A

and B). The correlation coefficients indicated marginally linear relationships ($r^2 = 0.870$ and 0.851 , respectively). When the same mobility values were plotted against the polymer function in eqn. 3, a linear trend was again established for functions using AApK- and PpK-derived charges (Figs. 3A and B). The correlation coefficients for these functions ($r^2 = 0.908$ and 0.878 , respectively) demonstrate an improvement over the molecular mass-derived functions.

Interestingly, when each function is examined separately, the correlations made with the AApK-derived charges differed very little from correlations made with the PpK charges. However, these small differences in the correlation coefficients were accompanied by large changes in the distribution of the data points from AApK- to PpK-derived functions, as seen by comparing Figs. 2A and B or Figs. 3A and B. This indicates that the degree of ion-

TABLE I
VALUES USED IN CZE MOBILITY CALCULATIONS

Peptide fragment	Designation	Charge (<i>q</i>) AApK	Charge (<i>q</i>) PpK	Polymer number (<i>N</i>)	Molecular mass	Mobility (μ) ($\times 10^4$)
Leu 57–Tyr 60	A	0.31	0.82	4	554.7	1.31
Gly 22–Tyr 24	B	0.33	0.83	3	385.4	1.58
Gly 1–Leu 14 ^a	C	0.31	0.71	14	1443.6	0.90
Gln 15–Phe 16	D	0.43	0.83	2	293.3	1.74
Gly 22–Phe 25	E	0.43	0.83	4	532.6	1.41
Gly 1–Arg 21 ^a	F	1.06	1.61	21	2305.6	1.18
Val 17–Arg 21 ^a	G	1.16	1.73	5	604.6	2.25
Ser 51–Arg 55 ^a	H	1.16	1.73	5	648.7	2.23
Leu 57–Lys 65 ^a	I	1.30	1.82	9	1123.4	1.91
Arg 56–Tyr 60	J	1.31	1.82	5	710.9	2.14
Pro 66–Lys 68	K	1.32	1.83	3	314.4	2.60
Cys 61–Lys 65 ^a	L	1.32	1.83	5	586.7	1.86
Phe 25–Tyr 31	M	1.33	1.83	7	825.9	1.97
Arg 37–Arg 50 ^a	N	2.13	2.73	14	1706.9	1.94
Arg 56–Lys 65 ^a	O	2.31	2.82	10	1279.6	2.31
Leu 57–Ala 70 ^a	P	2.39	2.82	14	1577.9	2.03
Phe 25–Arg 36	Q	2.20	2.83	12	1300.4	2.21
Arg 56–Lys 68 ^a	R	3.30	3.82	13	1576.0	2.46

^a These fragments contain a carboxymethylated cysteine. The molecular masses of the fragments reflect this.

^b These fragments resulted from the hydrolysis of rhIGF-I.

ization at pH 2.5 is not the primary contributing factor to the deviation from linearity for either function.

A further analysis of the charge and its contribution to both eqn. 2 and eqn. 3 was performed. Inspection of Table I reveals three distinct groups of

charge values; Group I (0 to + 1.0), Group II (+ 1.0 to + 2.0), and Group III (+ 2.0 to + 3.0). At pH 2.5, peptides in Group I contain one protonated amino terminal group contributing a charge of + 1.0, and one partially ionized carboxyl group. In addition to the amino and carboxyl terminal

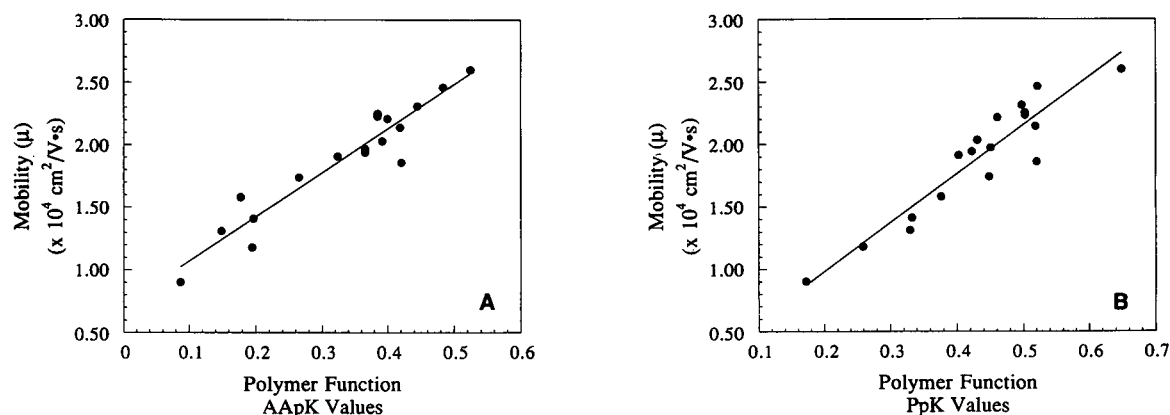


Fig. 2. Plots of the molecular mass function (eqn. 4) for the peptides in Table I versus the experimentally observed mobilities. (A) This plot was obtained using pK_a values of free amino acid residues (AApK), and (B) used the adjusted pK_a values (PpK) described in ref. 2.

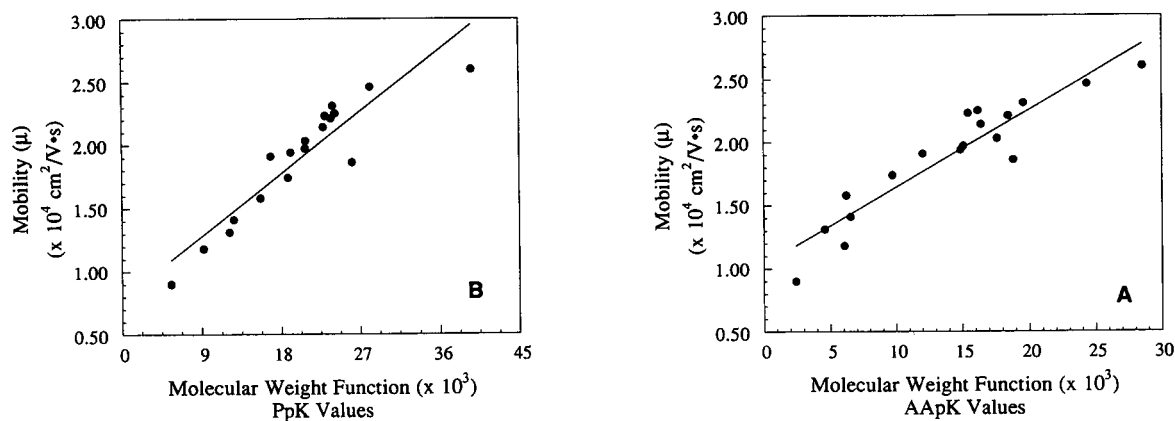


Fig. 3. Plots of the polymer function (eqn. 3) for the peptides in Table I versus the experimentally observed mobilities. (A) This plot was obtained using pK_a values of free amino acid residues (AApK), and (B) used the adjusted pK_a values (PpK) described in ref. 2.

groups, peptides in Groups II and III contain basic prosthetic groups, adding a charge of +1.0 for each group. By generating linearities for each respective charge group, the relative contributions were established. Table II lists the relative contributions for both functions.

As determined by the r^2 values, there was no charge related variability in any of the functions. Further inspection of the trends in Table II, however, reveals that in every instance the linearity is substantially improved when adjusted pK_a values (PpK) are used for the correlation.

In addition to charge-related trends in the mobility correlation, an analysis of size was performed using the eqn. 3. Unlike the trend seen with charge, there was no statistically significant distribution of

peptides based on any component of size in the polymer equation. Efforts were made to incorporate surface area data, volume, hydrophobicities, and partition coefficients into the equation to improve linearity. While minor improvements were seen in the r values obtained using these altered equations, the general distribution of points remained virtually identical to the original form.

CONCLUSIONS

Both the homopolymer function (eqn. 3) and the molecular mass function (eqn. 4) represent semi-empirical correlation models for mobility. By utilizing an experimental situation, mobility analysis of the tryptic fragments of rhIGF-I, the relative ap-

TABLE II
CORRELATION COEFFICIENTS (r^2) FOR COMPARISON OF MOBILITY EQUATIONS

Groups (charge values)	Molecular mass function		Polymer function	
	AApK (Fig. 2A)	ppK (Fig. 2B)	AApK (Fig. 3A)	ppK (Fig. 3B)
I (0 to +1.0)	0.883	0.991	0.875	0.979
II (+1.0 to +2.0)	0.729	0.765	0.824	0.864
III (+2.0 to +3.0)	0.869	0.949	0.862	0.942
Overall function	0.870	0.851	0.908	0.878

plicability of both treatments was assessed. In this treatment, all available experimental data were used. All data points were treated equally, and no data points were eliminated because we found no suitable criteria which would justify differential treatment. Using these data and this treatment, the homopolymer function [1] displays better linearity than the molecular mass function [2]. In addition, the adjusted pK_a values (PpK) appear to be the more accurate, and therefore some other factor or combination of factors must be the source of the deviations from linearity observed. We believe that a large percentage of that deviation is due to the inadequate treatment of size in both equations. For a size function to be ideal it must define the space a molecule occupies in solution, the ability of the solute to hydrogen bond with the solvent, the degree of ordering that the solute imposes on the solvent, and the effect of charge on these parameters. We therefore believe that size must ultimately be defined by a more complex thermodynamic function which involves entropic and enthalpic contributions of both polar and apolar groups. Such a treatment should further improve our ability to predict electrophoretic mobility in CZE.

NOTE ADDED IN PROOF

Another mobility model has been proposed and appears in refs. 3 and 4. The implications of the referenced model are not fully explored in this manuscript, since it appeared in print after the submission of this paper.

REFERENCES

- 1 P. D. Grossman, J. C. Colburn and H. Lauer, *Anal. Biochem.*, 179 (1989) 28.
- 2 E. C. Rickard, M. M. Strohl and R. G. Nielsen, *Anal. Biochem.*, 197 (1991) 197.
- 3 B. J. Compton, *J. Chromatogr.*, 559 (1991) 357.
- 4 B. J. Compton and E. A. O'Grady, *Anal. Chem.*, 63 (1991) 2597.
- 5 S. M. Parsons and M. A. Raftery, *Biochemistry*, 11 (1972) 1623.
- 6 D. E. Schmidt, Jr. and F. H. Westheimer, *Biochemistry*, 10 (1971) 1249.
- 7 J. G. Voet, J. Coe, J. Epstein, V. Matossian and T. Shipley, *Biochemistry*, 20 (1981) 7182.
- 8 S. Karplus, G. H. Snyder and B. D. Sykes, *Biochemistry*, 12 (1973) 1323.
- 9 F. A. Johnson, S. D. Lewis and J. A. Shafer, *Biochemistry*, 20 (1981) 44.
- 10 H. J. Dyson, M. Rance, R. A. Houghten, R. A. Lerner and P. E. Wright, *J. Mol. Biol.*, 201 (1988) 161.
- 11 H. J. Dyson, M. Rance, R. A. Houghten, P. E. Wright and R. A. Lerner, *J. Mol. Biol.*, 201 (1988) 201.
- 12 G. Worosila, *Ph. D. Thesis*, Rutgers University, New Brunswick, NJ, 1985, p. 45.

Capillary electrophoretic protein separations in polyacrylamide-coated silica capillaries and buffers containing ionic surfactants

Mark A. Strege and Avinash L. Lagu

Lilly Research Laboratories, Eli Lilly and Company, Indianapolis, IN 46285 (USA)

(First received January 4th, 1992; revised manuscript received October 30th, 1992)

ABSTRACT

Capillary electrophoretic protein separations of high efficiency and resolution were obtained using polyacrylamide-coated silica capillaries and buffers containing ionic surfactants. The presence of micellar concentrations of sodium dodecyl sulfate or cetyltrimethylammonium chloride minimized protein–capillary wall interactions, and facilitated concurrent separations of a mixture of both acidic and basic proteins, while the polyacrylamide coating provided increased resolution and migration time reproducibility via a reduction in electroosmotic flow. Attempts to obtain size-based protein separations via sieving through buffers containing the hydrophilic polymers methylcellulose and polyethylene glycol were unsuccessful.

INTRODUCTION

There exists a great demand for rapid, high-resolution bioanalytical techniques to monitor the isolation and purification of proteins. Capillary electrophoresis (CE) is one such method which potentially offers rapid and quantitative protein analyses of high resolution and efficiency.

Although there are several reports of the use of CE for the successful separation of proteins (see ref. 1 for a review), the inherent tendency of these macromolecules to adsorb to the walls of fused-silica capillaries has hindered the achievement of efficient and reproducible separations, and has prevented the adoption of CE as a routine qualitative or quantitative bioanalytical technique [2].

Among the strategies employed to facilitate successful separations of proteins via CE, the use of ionic surfactants may have significant applicability. Although evidence has suggested that ionic surfac-

tants denature proteins [3], for some applications a denaturing medium is acceptable and perhaps beneficial, since analyte solubility may be maximized under these conditions [4–6]. The ability of the anionic surfactant sodium dodecyl sulfate (SDS) to denature and impart a strong negative charge upon proteins has been successfully exploited for the facilitation of size-based separations of these molecules via sieving through cross-linked polyacrylamide in the slab gel format, using a technique known as SDS-polyacrylamide gel electrophoresis (PAGE) [7,8]. Recently, sieving separations of SDS–protein complexes have been demonstrated inside silica capillaries employed in conjunction with both cross-linked [9,10] and non-cross-linked polyacrylamide gel [11]. Non-ionic surfactant-coated octadecylsilane-derivatized capillaries have been reported to facilitate successful separations of native proteins in the presence of reduced electroosmotic flow [12]. Also, a polyacrylamide capillary coating was found to be beneficial in regard to the reduction of both protein–silica adsorption and electroosmotic flow in the presence of a zwitterionic surfactant [13]. Al-

Correspondence to: A. L. Lagu, Lilly Research Laboratories, Eli Lilly and Company, Indianapolis, IN 46285, USA.

though they offer significant potential for protein analyses, separations of protein-ionic surfactant complexes obtained in free solution inside polyacrylamide-coated capillaries, where the electroosmotic flow is minimal, have not been reported.

In this paper, the applicability of the use of ionic surfactants for the separation of proteins inside polyacrylamide-coated capillaries is demonstrated.

EXPERIMENTAL

Chemicals

The proteins used in this investigation were purchased from Sigma (St. Louis, MO, USA) and were used without further purification. SDS, cetyltrimethylammonium chloride (CTAC) (25% solution in water), and methylcellulose (high viscosity) were obtained from Fluka (Ronkonkoma, NJ, USA). Sodium acetate and mesityl oxide were purchased from Mallinckrodt (Paris, KY, USA) and Aldrich (Milwaukee, WI, USA), respectively. Polyethylene glycol ($M_r = 40\,000$) was obtained from Serva (New York, NY, USA).

Apparatus

Separations were performed in a commercial instrument (P/ACE System 2100, Beckman, Palo Alto, CA, USA) equipped with, unless otherwise noted, 67 cm (60 cm inlet-to-window) 50 μm I.D. capillaries. All capillaries were thermostated at 25°C. Injections of the protein mixtures were carried out hydrodynamically via application of a low positive pressure [0.5 p.s.i. (1 p.s.i. = 6894.76 Pa)] for 5 s, unless otherwise noted.

Procedures

The internal surfaces of the capillaries used in this investigation were coated with polyacrylamide in the manner described by Hjerten [14]. Sodium acetate buffers were adjusted to the desired pH by the addition of glacial acetic acid. Acidic buffers were employed to prolong the polyacrylamide coating lifetime, since silica derivatizations such as that described in ref. 14 are known to be unstable in an alkaline environment [15]. Buffer surfactant concentrations are reported in this study as % (w/v). Protein samples were made up as 1 mg/ml (each protein) solutions. The peaks corresponding to proteins in the mixtures were identified via analyses of

injections of the mixture spiked with 10-s injections of samples of the individual proteins. Buffers and samples were made using deionized water, and were filtered through 0.45- μm pore size filters (Millipore, Milford, MA, USA) and degassed prior to use. To substantiate reproducibility, all separations were performed at least in triplicate in three different capillaries. Separation efficiencies were calculated by an HP1000 minicomputer using an empirical equation developed for the characterization of either Gaussian or skewed chromatographic peaks [16].

RESULTS AND DISCUSSION

Permanent modification of silica capillary walls has proven to be an effective method, under certain conditions, for minimizing protein-silanol interactions as well as the electroosmotic flow [1,17]. The use of non-cross-linked polyacrylamide bonded to capillary walls through the use of an organosilane reagent has been reported to reduce protein adsorption and enhance separation efficiencies [14]. However, using a 67-cm capillary coated in this manner, together with a 50 mM sodium acetate pH 4.5 buffer, acceptable separation (30 kV, outlet = cathode) of a mixture, solubilized in running buffer, of bovine serum albumin (BSA) ($M_r = 68\,000$, $pI = 4.8$), β -lactoglobulin ($M_r = 18\,400$, $pI = 5.2$), myoglobin ($M_r = 17\,200$, $pI = 7.0$), ribonuclease A ($M_r = 13\,700$, $pI = 9.3$), and lysozyme ($M_r = 14\,300$, $pI = 11.0$) was not obtained (see Fig. 1). The electroosmotic flow inside this capillary was presumed negligible, since an injected neutral marker (0.5% mesityl oxide) did not pass the detector window during a 90-min separation (outlet = cathode). Under these conditions, where the pH of the buffer is below the pI of each of the five proteins, all of the analytes would be expected to migrate toward the cathode. However, β -lactoglobulin and BSA were not recovered, and the peaks corresponding to lysozyme, ribonuclease, and myoglobin were observed to tail significantly. These results indicated that adsorption of the proteins to either the silica surface or the wall-anchored polyacrylamide chains had occurred, probably via electrostatic and/or hydrogen bonding mechanisms [18,19].

A separation (30 kV, outlet = anode) of the same mixture of proteins solubilized in 0.5% SDS in wa-

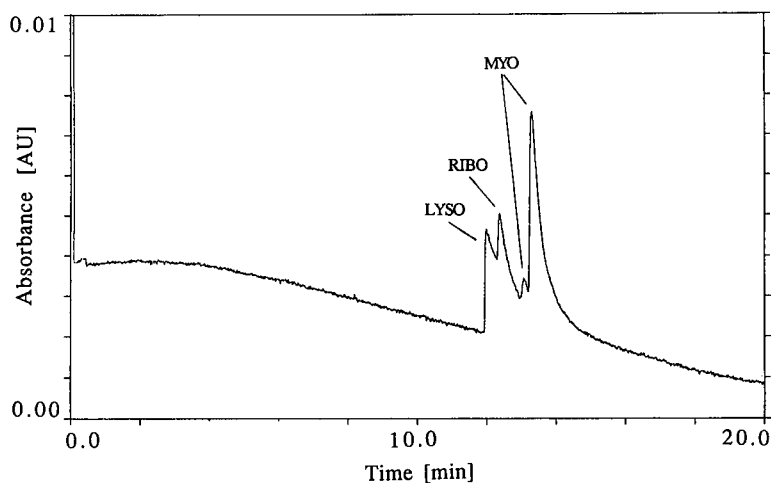


Fig. 1. Separation (outlet = cathode) of a 5-s injection of a mixture of myoglobin (MYO), β -lactoglobulin, lysozyme (LYSO), BSA, and ribonuclease (RIBO) in a polyacrylamide-coated capillary (60 cm inlet-to-window, 67 cm total length) using a 50 mM sodium acetate pH 4.5 buffer, 30 kV applied potential, and 214 nm UV detection.

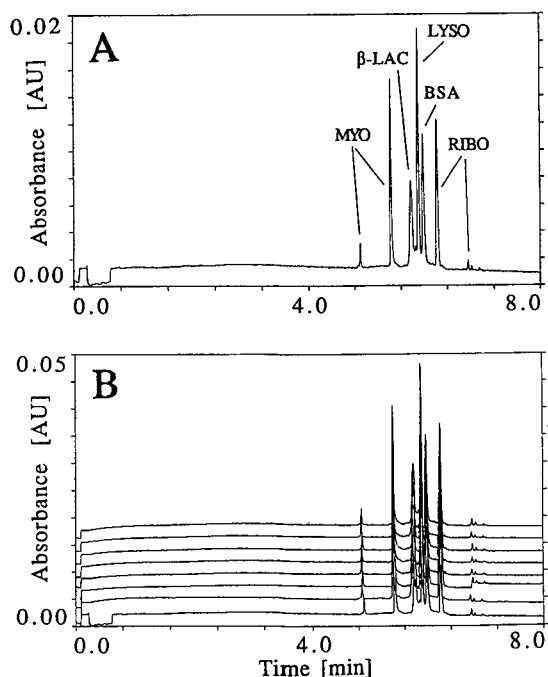


Fig. 2. (A) Separation (outlet = anode) of a 5-s injection of a mixture of myoglobin (MYO), β -lactoglobulin (β -LAC), lysozyme (LYSO), BSA, and ribonuclease (RIBO) in a polyacrylamide-coated capillary (60 cm inlet-to-window, 67 cm total length) using a 50 mM sodium acetate pH 4.5, 0.5% SDS buffer, 30 kV applied potential, and 214 nm UV detection; (B) Eight replicate injections obtained using the conditions listed in (A).

ter was obtained in a 67-cm polyacrylamide-coated capillary using 50 mM sodium acetate pH 4.5, 0.5% SDS as running buffer, and is displayed in Fig. 2A. The association of the anionic surfactant with the proteins promoted the anodic migration of all the analytes, and also appeared to minimize protein adsorption, since peaks corresponding to all five proteins were observed, and peak tailing was not evident. Under these conditions, all five proteins were well resolved. The reproducibility of this separation is demonstrated in Fig. 2B, where eight replicate electropherograms are overlaid. No buffer replenishment was performed between injections. Migration time and peak area precision data obtained from these separations are listed in Table I. Using myoglobin as a standard, the method was linear over the domain 25 to 6000 μ g/ml (correlation coefficient = 0.999) employing peak area for quantitation. The upper limit of the linear response using peak height was 2000 μ g/ml. The multiple minor peaks observed in the separations of the model protein mixture were believed to represent contaminants present in the commercially available protein standards.

To determine the effect of surfactant concentration upon the separation of the protein mixture, electropherograms were obtained at 30 kV (outlet =

TABLE I

RELATIVE STANDARD DEVIATIONS (%) OF MIGRATION TIME AND PEAK AREAS OBTAINED FOR PROTEINS SEPARATED IN 50 mM SODIUM ACETATE pH 4.5, 0.5% SDS

All data are mean values from eight replicate injections.

Protein	Migration time precision (R.S.D., %)	Peak area precision (R.S.D., %)
Myoglobin	0.3	4.9
β -Lactoglobulin	0.2	4.6
Lysozyme	0.2	4.7
Bovine serum albumin	0.2	4.8
Ribonuclease	0.2	4.6

anode) using a 67-cm polyacrylamide-coated capillary and 50 mM sodium acetate pH 4.5 buffer with SDS concentrations of 0.1, 0.2, 0.5, and 1.0%. The results displayed in Fig. 3 revealed significant changes in resolution between the components in the mixture, particularly lysozyme, β -lactoglobulin, and BSA, taking place as surfactant concentration was increased. These occurrences may be effects of the differential tendencies of the protein-SDS complexes to associate with SDS micelles (the critical micelle concentration of SDS in water is *ca.* 0.2%

[20,21]), the number of which grow as surfactant concentration increases. The strongly anionic micelles can be expected to migrate at a much faster rate than that of the protein-surfactant monomer complexes.

To investigate the effect of the polyacrylamide capillary coating upon protein separations, an electropherogram (30 kV, outlet = anode) of the protein mix solubilized in 0.5% SDS was obtained in a 67-cm bare silica capillary using 50 mM sodium acetate pH 4.5, 0.5% SDS as running buffer. Under

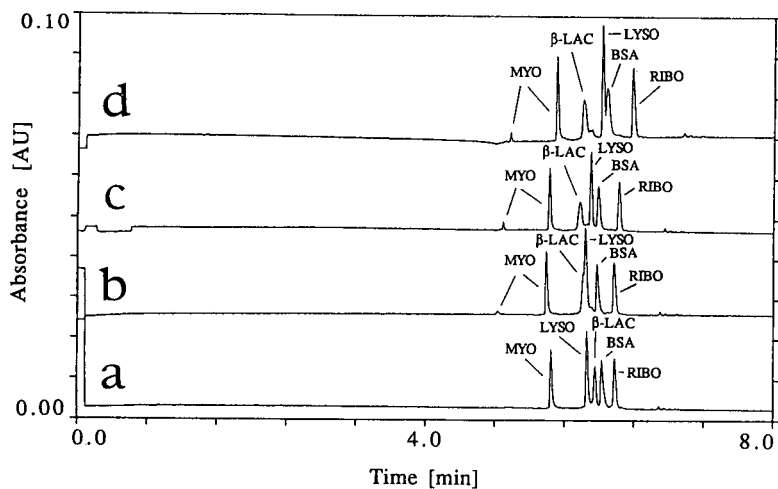


Fig. 3. Separations (outlet = anode) of a 5-s injection of a mixture of myoglobin (MYO), β -lactoglobulin (β -LAC), lysozyme (LYSO), BSA, and ribonuclease (RIBO) in a polyacrylamide-coated capillary (60 cm inlet-to-window, 67 cm total length) using 30 kV applied potential, 214 nm UV detection, and 50 mM sodium acetate pH 4.5 buffers containing (a) 0.1% SDS; (b) 0.2% SDS; (c) 0.5% SDS; (d) 1.0% SDS.

these conditions, the negatively charged protein–surfactant complexes appeared to be able to slowly electrophoretically migrate toward the anode, overcoming the weak cathodic electroosmotic flow. However, due to the slow net migration of the proteins, not all of the individual components of the injected mixture migrated past the detector window during the course of a 100-min separation, and the peaks that were observed during this timeframe were very broad (data not shown). Therefore, it appeared that the presence of a polyacrylamide capillary coating significantly improved protein separations performed in the presence of SDS at pH 4.5 by minimizing the electroosmotic flow inside the capillaries.

An investigation of the polyacrylamide capillary coating lifetime was performed by monitoring the efficiency (the algorithm employed for the determination of efficiency considers peak asymmetry [16]) and migration time of myoglobin in separations of the protein mixture obtained in a single coated capillary over time. Efficiency and sample migration times can be expected to decrease and increase, respectively, in response to degradation of the capillary coating. These changes may occur as the coating degrades due to an increase in both protein–silica interactions and a cathodic silanol-generated electroosmotic flow which opposes the anodic electrophoretic migration of the negatively charged protein–SDS complexes. Separations (30 kV, outlet = anode) of the protein mixture were obtained in a 67-cm polyacrylamide-coated capillary using 50 mM sodium acetate pH 4.5, 0.5% SDS buffer at 0, 1, 5, 11, 12, and 16 days following derivatization. The efficiencies and migration times of the major peak corresponding to myoglobin were measured during this time period. In the acidic environment (pH 4.5) employed in this investigation, the polyacrylamide coating appeared to be stable for *ca.* 11 days before the effects of coating degradation became evident, as demonstrated in the plots of migration time and efficiency vs. capillary coating lifetime in Fig. 4.

Cationic surfactants have also been utilized to minimize protein adsorption during CE separations in bare silica capillaries [22,23]. A separation (30 kV) of the protein mixture obtained in a 67-cm polyacrylamide-coated capillary using 50 mM sodium acetate pH 4.5, 0.5% CTAC buffer is displayed in

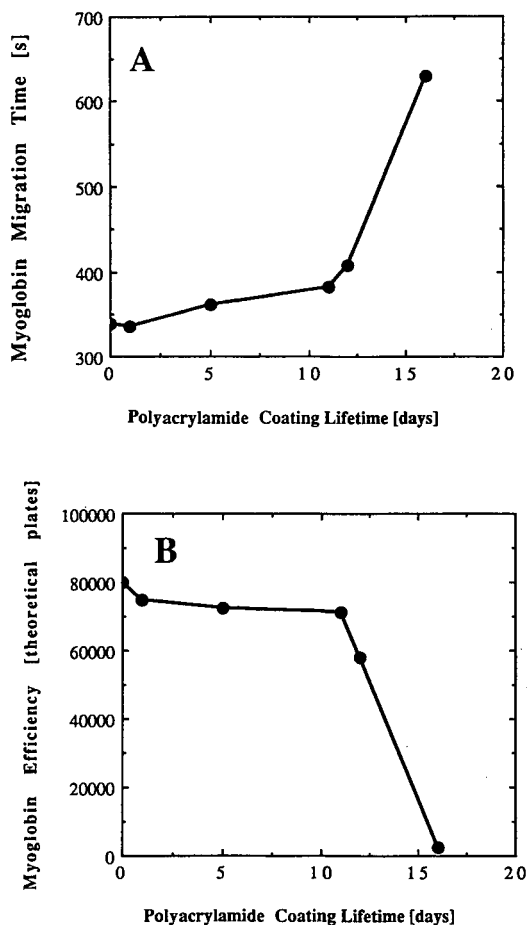


Fig. 4. (A) Plot of myoglobin peak migration time vs. capillary coating lifetime obtained following separations of the protein mixture in a polyacrylamide-coated capillary (60 cm inlet-to-window, 67 cm total length) using a 50 mM sodium acetate pH 4.5, 0.5% SDS buffer, 30 kV applied potential, and 214 nm UV detection; (B) Plot of myoglobin peak efficiency vs. capillary coating lifetime obtained from the same separations described in A.

Fig. 5. Since the proteins formed complexes of net positive charge in the presence of the cationic surfactant, the outlet reservoir was made cathodic for these separations. Both analyte resolution and migration order varied significantly from that of the separation obtained in SDS, probably reflecting differences in the magnitudes of the positive and negative zeta potentials of the migrating species in the presence of CTAC and SDS, respectively. Interestingly, while lysozyme generated only one peak

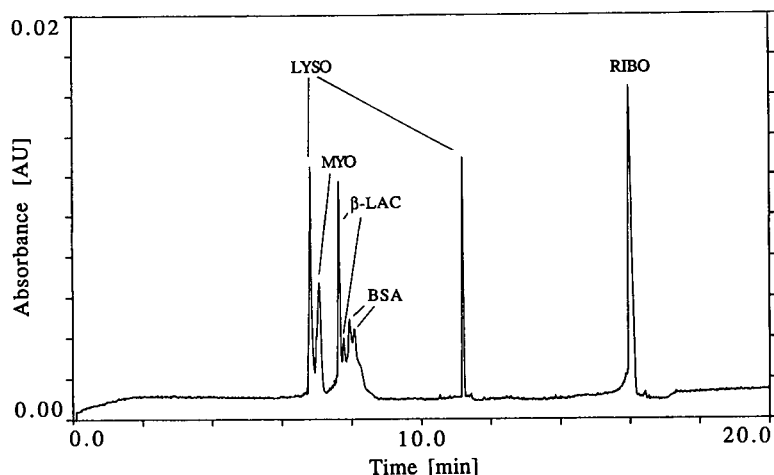


Fig. 5. Separation (outlet = cathode) of a 5-s injection of a mixture of myoglobin (MYO), β -lactoglobulin (β -LAC), lysozyme (LYSO), BSA, and ribonuclease (RIBO) in a polyacrylamide-coated capillary (60 cm inlet-to-window, 67 cm total length) using a 50 mM sodium acetate pH 4.5, 0.5% CTAC buffer, 30 kV applied potential, and 214 nm UV detection.

when analysed in SDS buffer, two major peaks were found to correspond to the lysozyme separated in CTAC buffer. These peaks may represent different conformations of the protein which appear to be present and separable in micellar solutions of CTAC. Lysozyme is known to unfold reversibly in solution, and has been reported to generate two peaks in reversed-phase liquid chromatographic separations [24,25].

To determine the effects of the presence of a hydrophilic linear polymer network upon protein analyses achieved inside the polyacrylamide-coated capillaries, separations (30 kV, outlet = cathode) of the protein mixture (solubilized in running buffer) obtained in 50 mM sodium acetate pH 4.5 and 0.1% methylcellulose or 5.0% polyethylene glycol (PEG) using a 47-cm polyacrylamide-coated capillary were performed. Methylcellulose is a material which has displayed the ability to sieve double-stranded DNA fragments [26,27], and it has been suggested that 5.0% PEG may provide sieving capacity sufficient to separate the monomer, dimer, and trimer of BSA [26]. As mentioned earlier, under these conditions in the absence of ionic surfactant, where the pH is below the isoelectric points of all five proteins, the analytes can be expected to possess a net positive charge, facilitating their migra-

tion toward the cathode. In the presence of both methylcellulose and PEG, the proteins appeared to migrate very slowly through the capillary (perhaps due to the high viscosity of the buffers), and only three very broad peaks appeared during the course of a 100-min separation (data not shown).

A more acceptable analysis was achieved by reversing the instrument polarity and separating (30 kV) a 1-s high-pressure (20 p.s.i.) injection (from the "outlet end" of the capillary), using the 7-cm short section of the capillary which lies between the detector window and the outlet reservoir for the analysis. The electropherogram obtained using this technique, with a 50 mM sodium acetate pH 4.5, 5.0% PEG buffer, is displayed in Fig. 6A. A separation obtained in a buffer containing 0.1% methylcellulose instead of 5.0% PEG was similar (see Fig. 6B). The order of migration correlated with protein pI , as the high positive zeta potential of the basic proteins apparently enables them to migrate more rapidly than myoglobin and the acidic proteins. The presence of the hydrophilic polymer also reduced peak tailing relative to that observed to occur in sodium acetate buffer alone (see Fig. 1). In both separations, β -lactoglobulin appeared to split into two components. These may be β -lactoglobulins A and B present in the commercially available

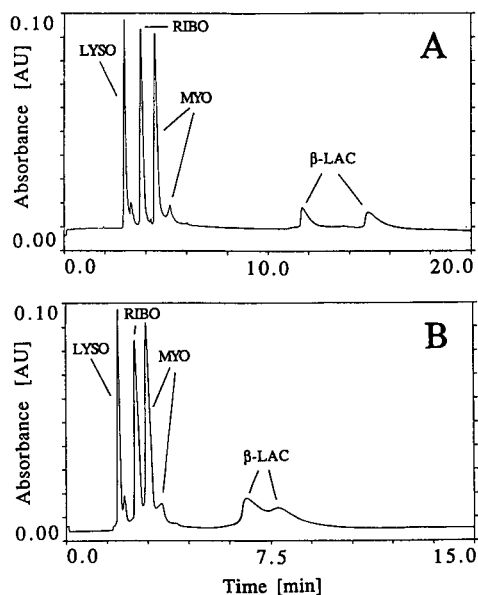


Fig. 6. (A) Separation (outlet = anode) of a 1-s high-pressure (20 p.s.i.) injection of a mixture of myoglobin (MYO), β -lactoglobulin (β -LAC), lysozyme (LYSO), BSA, and ribonuclease (RIBO) in a polyacrylamide-coated capillary (7 cm inlet-to-window, 47 cm total length) using 30 kV applied potential, 214 nm UV detection, and 50 mM sodium acetate pH 4.5, 0.5% SDS buffer also containing (A) 5.0% PEG; (B) 0.1% methylcellulose.

standard, an occurrence which has also been reported in other studies [12,28,29]. BSA, the protein with the greatest acidic character, was not identified in these separations, probably due to the very low electrophoretic mobility of the native species at a pH so close to its pI .

The incorporation of 0.5% SDS into both the sample of the protein mixture and the running buffer facilitated the separation (30 kV, outlet = anode) displayed in Fig. 7A and B, achieved using a 47-cm polyacrylamide-coated capillary in the normal manner (*i.e.* using 40-cm capillary section between the inlet and detector window for the separation). The buffers employed for the separations presented in Fig. 7A and B were 50 mM sodium acetate pH 4.5 solutions containing 0.1% methylcellulose and 5.0% PEG, respectively. The separation of the protein mix, including the order of protein elution, obtained in the presence of 5.0% PEG (Fig. 7A) was significantly different from that obtained in its absence (see Fig. 2). However, this phenomenon may

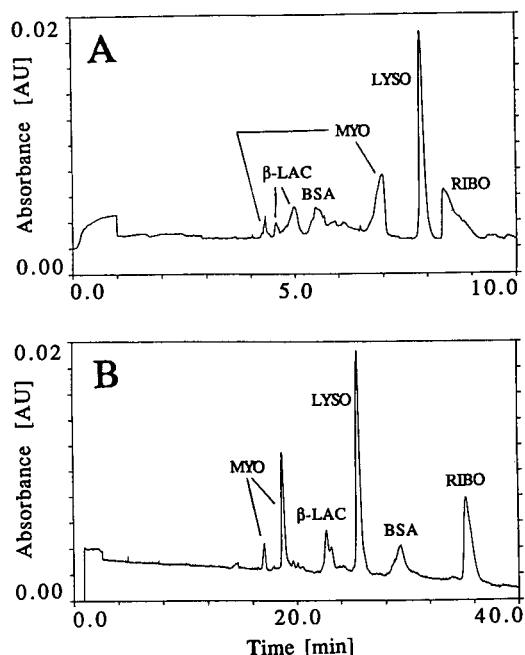


Fig. 7. (A) Separation (outlet = anode) of a 5-s injection of a mixture of myoglobin (MYO), β -lactoglobulin (β -LAC), lysozyme (LYSO), BSA, and ribonuclease (RIBO) in a polyacrylamide-coated capillary (40 cm inlet-to-window, 47 cm total length) using 30 kV applied potential, 214 nm UV detection, and 50 mM sodium acetate pH 4.5, 0.5% SDS buffer also containing (A) 5.0% PEG; (B) 0.1% methylcellulose.

be due to differential tendencies among proteins for interaction with the hydrophilic PEG network, and is probably not a result of sieving since BSA, by far the largest protein in the mixture, eluted earlier than three of the smaller proteins in the separation displayed in Fig. 7A. Also, no evidence for the occurrence of sieving was observed when the buffer containing 0.1% methylcellulose was employed to separate the protein mixture in the presence of 0.5% SDS (see Fig. 7B), since the migration order of the proteins observed in this separation was identical to that displayed in Fig. 2.

CONCLUSIONS

The results of this study suggest that protein separations of high efficiency and resolution may be obtained in free solution, in the absence of polymeric additives, through the use of both polyacrylamide-coated capillaries and buffers containing ion-

ic surfactants. Although attempts to obtain size-based protein separations using buffers containing hydrophilic polymer networks were unsuccessful, future work employing linear, non-cross-linked polyacrylamide gels in conjunction with polyacrylamide-coated capillaries may offer significant potential for the separation of proteins by CE. Also, the lifetimes of polyacrylamide capillary coatings may be significantly lengthened through the use of silica derivatizations of greater stability, such as that described by Cobb *et al.* [15].

ACKNOWLEDGEMENTS

We wish to thank Ms. S. L. Vanderstelt and Mr. D. F. Schmidt for their technical assistance.

REFERENCES

- 1 M. V. Novotny, K. A. Cobb and J. Liu, *Electrophoresis*, 11 (1990) 735.
- 2 W. D. Pickering, *LC-GC*, 7 (1989) 752.
- 3 F. W. Putnam, *Adv. Prot. Chem.*, 4 (1948) 79.
- 4 T. C. Furman, J. Epp, H. M. Hsiung, J. Hoskins, G. L. Long, L. G. Mendelsohn, B. E. Schoner, D. P. Smith and M. C. Smith, *Biotechnology*, 5 (1987) 1047.
- 5 P. T. Wingfield, P. Graber, G. Buell, K. Rose, M. G. Simona and B. D. Burleigh, *Biochem. J.*, 243 (1987) 1047.
- 6 R. J. Kirschner, N. T. Hatzenbuehler, M. W. Moseley and C. C. Tomich, *J. Biotechnol.*, 12 (1989) 247.
- 7 A. L. Shapiro, E. Vinuela and J. V. Maizel, *Biochem. Biophys. Res. Commun.*, 28 (1967) 815.
- 8 U. K. Laemmli, *Nature*, 227 (1970) 680.
- 9 S. Hjerten, *J. Chromatogr.*, 270 (1983) 1.
- 10 A. S. Cohen and B. L. Karger, *J. Chromatogr.*, 397 (1987) 409.
- 11 A. Widhalm, C. Schwer, D. Blaas and E. Kendler, *J. Chromatogr.*, 549 (1991) 446.
- 12 J. K. Towns and F. E. Regnier, *Anal. Chem.*, 63 (1991) 1126.
- 13 M. A. Strege and A. L. Lagu, *J. Liq. Chromatogr.*, 16 (1993) in press.
- 14 S. Hjerten, *J. Chromatogr.*, 347 (1985) 191.
- 15 K. A. Cobb, V. Dolnik and M. Novotny, *Anal. Chem.*, 62 (1990) 2478.
- 16 J. P. Foley and J. G. Dorsey, *Anal. Chem.*, 55 (1983) 730.
- 17 J. R. Mazzeo and I. S. Krull, *Biotechniques*, 10 (1991) 638.
- 18 P. Holt and J. Bowcott, *Biochem. J.*, 57 (1954) 471.
- 19 R. A. Messing, *J. Am. Chem. Soc.*, 91:9 (1969) 2370.
- 20 D. W. Armstrong, *Sep. Purif. Methods*, 14 (1985) 213.
- 21 J. G. Dorsey, *Adv. Chromatogr.*, 27 (1987) 167.
- 22 J. E. Wiktorowicz and J. C. Colburn, *Electrophoresis*, 11 (1990) 769.
- 23 A. Emmer, M. Jansson and J. Roeraade, *J. Chromatogr.*, 547 (1991) 544.
- 24 K. Benedek, S. Dong and B. L. Karger, *J. Chromatogr.*, 317 (1984) 227.
- 25 N. Nimura, H. Itoh, T. Kinoshita, N. Nagae and M. Nomura, *J. Chromatogr.*, 585 (1991) 207.
- 26 M. Zhu, D. L. Hansen, S. Burd and F. Gannon, *J. Chromatogr.*, 480 (1989) 311.
- 27 M. A. Strege and A. L. Lagu, *Anal. Chem.*, 63 (1991) 1233.
- 28 H. H. Lauer and D. McManigill, *Anal. Chem.*, 58 (1986) 166.
- 29 J. S. Green and J. W. Jorgenson, *J. Chromatogr.*, 478 (1989) 63.

Determination of the number and relative molecular mass of subunits in an oligomeric protein by two-dimensional electrophoresis

Application to the subunit structure analysis of rat liver amidophosphoribosyltransferase

Takashi Yamaoka and Kamejiro Yamashita

Division of Endocrinology and Metabolism, Institute of Clinical Medicine, University of Tsukuba, Tsukuba-City, Ibaraki 305 (Japan)

Mitsuo Itakura

Otsuka Department of Clinical and Molecular Nutrition, University of Tokushima, School of Medicine, Kuramoto-cho, Tokushima-City 770 (Japan)

(First received February 18th, 1992; revised manuscript received October 6th, 1992)

ABSTRACT

To determine simultaneously the relative molecular mass (M_r) of a native oligomeric protein, and the number and M_r of its subunits, a method using two-dimensional electrophoresis was developed. To determine the M_r of a native oligomeric protein, pore gradient gel electrophoresis was performed for the first dimension. Native proteins were dissociated into their subunits by sodium dodecyl sulphate (SDS) in a gel slice, then applied to SDS polyacrylamide gel electrophoresis for the second dimension to determine the M_r of subunits. The advantage, accuracy, limitations and application of the method are discussed.

INTRODUCTION

Most proteins are composed of subunits. The subunit structure plays an important role in exhibiting biological characteristics and in the functional regulation of various oligomeric proteins. The determination of the number and relative molecular mass (M_r) of subunits is therefore essential to understanding the biochemical regulation played by oligomeric proteins.

Although gel chromatography has been widely used to determine the M_r of native oligomeric proteins [1], as it is simple and inexpensive, the results are subject to unavoidable errors due to sample dilution and low resolution capacity. Pore gradient gel electrophoresis (PGGE) based on the concept of gel electrophoresis has been used to determine the M_r of native proteins with a high resolution capacity [2–8]. In PGGE, proteins migrate from the lower to the higher concentration of a polyacrylamide gradient in a slab gel. As the gel pores decrease in size, the migration rate of proteins also decreases. The proteins reach their respective “pore limits” determined by their molecular sizes irrespective of

Correspondence to: Takashi Yamaoka, Division of Endocrinology and Metabolism, Institute of Clinical Medicine, University of Tsukuba, Tsukuba-City, Ibaraki 305, Japan.

ionic charges of protein molecules, and form sharp bands. Although each protein in a band formed at the approximate pore limit continues to migrate very slowly, the relative mobility of each protein becomes constant relative to other proteins. Therefore, the M_r of a native protein of interest can be determined by comparing its migration with those of standard proteins. Sodium dodecyl sulphate-polyacrylamide gel electrophoresis (SDS-PAGE) with thiol reagents such as 2-mercaptoethanol (2-ME) or dithiothreitol using a discontinuous buffer system [9,10] has been widely used for the determination of subunit M_r . The mobility of subunits denatured by SDS on PAGE reflects their M_r irrespective of their original charges or conformation [11,12].

Two-dimensional (2D) electrophoresis with a combination of PGGE for the first dimension and SDS-PAGE for the second has been developed to determine simultaneously the M_r of native oligomeric proteins and the number and M_r of their subunits. Oligomeric proteins separated by PGGE were dissociated into subunits by SDS and 2-ME in a gel slice and applied to SDS-PAGE. The M_r of native proteins and the number and M_r of their subunits were established from the positions in the gel compared with those of molecular markers. The accuracy and limitations of this method were tested by using standard oligomeric proteins, the subunit structures of which are known. This method was used to determine the subunit structure of partially purified rat liver ATase (EC 2.1.2.14), which is considered a rate-limiting enzyme in the *de novo* purine synthetic pathway.

EXPERIMENTAL

Materials

Acrylamide-HG, N,N'-methylenebisacrylamide-HG (Bis), SDS, ammonium peroxodisulfate (APS), N,N,N',N'-tetramethylethylenediamine (TEMED), glycerol, 2-ME, glycine, boric acid and EDTA were purchased from Wako (Osaka, Japan) and Tris and 5-phosphoribosyl 1-pyrophosphate (PRPP) from Sigma (St. Louis, MO, USA). Radioactive [^{14}C]glutamine and anti-rabbit [^{125}I]immunoglobulin F(ab') fragment were purchased from Amersham International (Amersham, UK). High- M_r standard proteins for electrophoresis including

hog thyroid thyroglobulin ($M_r = 669\,000$, subunit $M_r = 330\,000$), horse spleen ferritin ($M_r = 440\,000$, subunit $M_r = 18.5$), beef liver catalase ($M_r = 232\,000$, subunit $M_r = 36\,000$), and bovine serum albumin, egg white ovalbumin ($M_r = 43\,000$), bovine carbonic anhydrase ($M_r = 232\,000$, subunit $M_r = 60\,000$), beef heart lactate dehydrogenase (LDH; $M_r = 140\,000$, subunit $M_r = 36\,000$), and bovine serum albumin ($M_r = 67\,000$, monomer), an M_r marker kit for electrophoresis, bromphenol blue, agarose, Sephadex G-25 and a gradient maker were purchased from Pharmacia-LKB Biotechnology (Uppsala, Sweden). A silver staining kit was purchased from Daiichi Pure Chemicals (Tokyo, Japan). A peristaltic pump was purchased from Taiyo Scientific Industrial (Tokyo, Japan). Seven-week-old male Wistar rats and female New Zealand White rabbits weighing 3 kg were purchased from Shizuoka Laboratory Animal Centre (Shizuoka, Japan). A hydroxyapatite column was purchased from Toa Nenryo Kogyo (Tokyo, Japan).

PGGE for the first dimension

Gels were made with a linear gradient from 3 to 20, 22.3, 25 and 30%T^a, respectively; to achieve complete gel transparency [7,8], Bis was added at 2.7%C. The abbreviations %T and %C indicate, respectively, the percentage concentration of acrylamide and Bis per total volume, and the percentage concentration of Bis per %T [13]. The acrylamide solutions at high and low concentrations containing 2.7%C Bis, 0.04% APS, 0.06% TEMED, 22.5 mM Tris-HCl (pH 8.4), 20 mM boric acid, and 0.6 mM EDTA were gradually mixed in a gradient maker and poured into the mould (140 × 140 × 1 mm) assembled with two glass plates and spacers at a constant flow-rate controlled by a peristaltic pump. After polymerization at room temperature, the slab gel was equilibrated with an electrode buffer (90 mM Tris-HCl-80 mM boric acid - 2.5 mM EDTA, pH 8.4) at 70 V for 20 min. Approximately 60 μg of a mixture of five standard proteins were dissolved in 60 μl of electrode buffer with 10% glycerol and applied to the top of the gel. Electrophoresis was performed with the vertical slab gel system at 150 V for 15 h in a cold room.

^a T = (g acrylamide + g Bis)/100 ml solution.

SDS-PAGE for the second dimension

According to Laemmli's method [9], the lower separating gel (12.5%T, 2.7%C) and the upper stacking gel (3.0%T, 2.7%C) were polymerized in the same mould as used for PGGE. After PGGE, the gel slice was longitudinally excised to a width of 3 mm, then incubated in a small amount of sample buffer containing 62.5 mM Tris-HCl (pH 6.8), 2.3% SDS, 5% 2-ME, 10% glycerol and 0.002% bromphenol blue for 1 h at room temperature. To attach the sliced pore gradient gel closely to the upper stacking gel, 0.7% hot agarose solution in the sample buffer was poured onto the top of the upper gel. The gel slice after the incubation with SDS was quickly submerged in this solution before it solidified. The slab gel was set in a vertical system and the electrode buffer containing 25 mM Tris-HCl, 192 mM glycine and 0.1% SDS was poured into the upper and lower electrode chambers. Proteins in the gel slice and M_r marker proteins were electrophoresed at 20 mA until the tracking dye front migrated to within 1 cm from the gel bottom.

Determination of protein mobility

The gels after electrophoresis were stained with a silver staining kit based on the method of Ohsawa and Ebata [14]. During PGGE, the same protein samples were applied to the individual wells at intervals of 1 h and the migration rate (mm/h) of the protein was calculated as the difference in migration distance between adjacent bands of the same protein. The relative mobility (R_F) on SDS-PAGE was calculated as the ratio of the distance from the top of the separating gel to the densest point in each protein spot relative to the dye front.

Partial purification of rat liver ATase

ATase was partially purified according to the method of Tsuda *et al.* [15] with the following modifications. In brief, purification procedures included ultracentrifugation at 55 000 g for 3 h, heat treatment at 56°C, acid precipitation at pH 5.1, ammonium sulphate fractionation from 30 to 55% and high-performance liquid chromatography through a hydroxyapatite column. ATase was eluted with a linear gradient from 25 to 350 mM potassium phosphate buffer with 70 mM 2-ME. Fractions containing enzyme activity were desalted through a Sephadex G-25 column equilibrated with the electrode buffer for the first electrophoresis.

Analysis of the subunit structure of rat liver ATase

The desalted rat liver ATase sample was applied to PGGE with 10% glycerol. After the electrophoresis, two gel slices were longitudinally excised to a width of 3 mm. One was cut into 3 × 8 mm sections and the ATase activity in each was assayed as described below. The other slice was applied to the second dimension SDS-PAGE and stained with silver.

Assay of ATase activity

The method for the assay of ATase enzyme activity was the same as reported previously [16]. In principle, PRPP-dependent glutaminase activity was regarded as ATase activity, which was determined by the PRPP-dependent hydrolysis of [^{14}C]glutamine to glutamate.

Preparation of antibodies against two ATase subunits

Partially purified ATase was separated by SDS-PAGE, stained with copper [17] and then M_r 62 000 and 57 000 protein bands were cut out. The gels including each ATase subunit were individually sheared through a 21-gauge needle and conjugated with Freund's adjuvant. The conjugates were injected subcutaneously into female New Zealand White rabbits five times at intervals of 2 weeks. After the fifth injection, blood was drawn and the serum containing antibodies for each ATase subunit was separated. Western blotting was performed by a standard method [18] using a radioactive second antibody.

RESULTS AND DISCUSSION

The standard proteins, including thyroglobulin, ferritin, catalase, LDH and albumin, were applied to PGGE. During the electrophoresis, the migration rate (per unit time) of the standard proteins decreased gradually and reached a constant value as their respective pore limits were approached (Fig. 1). The proteins with a larger M_r reached their pore limits relatively sooner. As even the smallest protein, albumin, reaches its pore limit after 10 h at 150 V and an electrophoretic time equivalent to about 2000 V h has been recommended previously [7], PGGE in this study was performed at 150 V for 15 h. After PGGE, each standard protein was concen-

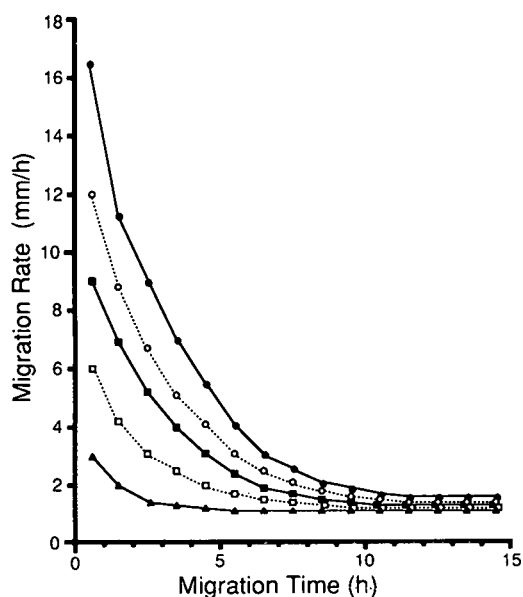


Fig. 1. Change of the migration rate of standard proteins during PGGE with a linear gradient from 3 to 30%T. ▲ = Thyroglobulin; □ = ferritin; ■ = catalase; ○ = LDH; ● = albumin.

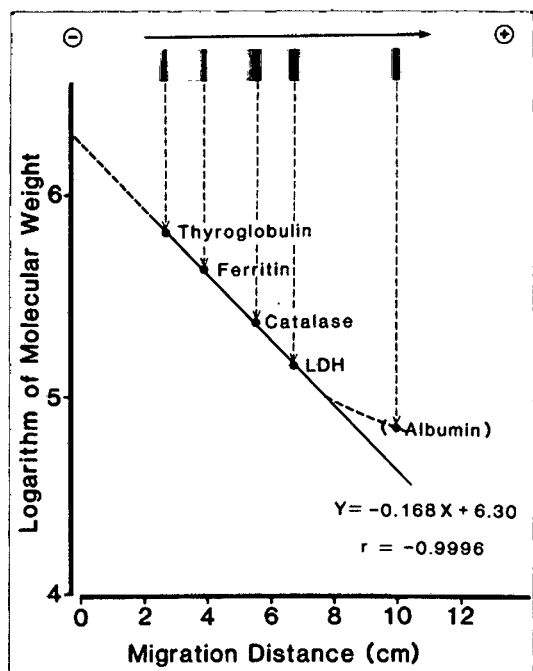


Fig. 2. Plots of the migration distance of the standard proteins against $\log M_r$ after PGGE with a linear gradient from 3 to 22.3%T.

trated in a sharp band in the gel as shown in Fig. 2. The calibration graph of migration distance versus $\log M_r$ was linear with a correlation coefficient of -0.9996 in the M_r range from 140 000 of LDH to 669 000 of thyroglobulin. However, the migration at 10 cm of albumin in the gradient gel from 3 to 22.3%T was 15% more than that expected at 8.7 cm. These results suggest that the calibration graph is actually sigmoidal and the range obeying a linear relationship on a semi-logarithmic scale can be used for accurate M_r determination by PGGE and gel filtration [1]. Indeed, the relationship between the migration distance and $\log M_r$ for all standard proteins including albumin is linear in the gradient gel from 3 to 30%T (data not shown). Thus, the linear range is dependent on the gel concentration. The migration distance of an oligomeric protein in PGGE is dependent on its molecular size and shape. Because all standard protein molecules used in this study were globular, as are the majority of oligomeric proteins, the relationship between migration distance and $\log M_r$ of standard proteins was linear.

Ferritin, catalase, LDH and albumin in a gel slice

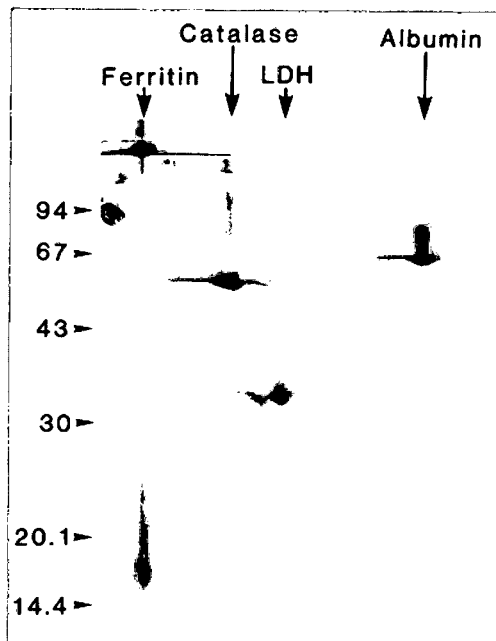


Fig. 3. Two-dimensional electrophoresis of four standard proteins with a combination of PGGE and SDS-PAGE. The positions of the M_r marker proteins are shown on the left (M_r values $\times 10^{-3}$).

TABLE I

COMPARISON BETWEEN CALCULATED AND ESTABLISHED VALUES: NATIVE PROTEIN M_r OBTAINED BY PGGE FROM 3 TO 23.3%T

Protein	Measured M_r	True M_r	Deviation (%)
Thyroglobulin	674 000	669 000	+0.7
Ferritin	442 000	440 000	+0.5
Catalase	226 000	232 000	-2.6
LDH	143 000	140 000	+2.1
Albumin	(65 000) ^a	67 000	-3.0

^a Data obtained by the gradient gel from 3 to 30%T.

after separation by PGGE were applied to SDS-PAGE. The silver-stained gel after 2D electrophoresis is shown in Fig. 3. Ferritin gave two protein spots at M_r 220 000 (a half unit) and 18 500 (a true subunit) because of incomplete dissociation. Catalase, LDH and albumin each migrated as one spot. Because the ferritin in the gel slice was completely separated into its subunits by boiling with SDS for 5 min before the second electrophoresis, the gel slice after PGGE should be boiled so long as the peptide bonds of proteins are not cleaved.

In addition to the M_r of native proteins, the number and M_r of their subunits were determined and are summarized in Tables I–III. The M_r values determined for either native proteins by PGGE or their subunits by SDS-PAGE deviated from the established M_r by less than 3 and 4%, respectively. Because the M_r of albumin is too small to be determined using a gradient gel from 3 to 22.3%T, it was

TABLE III

COMPARISON BETWEEN CALCULATED AND ESTABLISHED VALUES: NO. OF SUBUNITS

Protein	Calculated No. of subunits	True No. of subunits	Judgement
Thyroglobulin	2.1 (2)	2	Correct
Ferritin	24.6 (25)	24	Incorrect
Catalase	3.6 (4)	4	Correct
LDH	4.1 (4)	4	Correct
Albumin	1.0 (1)	1	Correct

obtained from migration in a gel containing 3–30%T. Also, because the subunit of thyroglobulin hardly entered the separating gel at 12.5%T, its M_r was determined as 317 000 by SDS-PAGE at 6%T. The calculated numbers of subunits for thyroglobulin, ferritin, catalase, LDH, and albumin were 2, 25, 4, 4 and 1, respectively. Because the true numbers of subunits are 2, 24, 4, 4 and 1, respectively, the calculated values were precise except for ferritin. Although the deviations in the M_r determination for both native ferritin and its subunit were less than 3%, the calculated number of its subunits was not correct. Therefore, the accuracy of the calculated number of subunits depends on the number of subunits itself, the number of different subunits and the experimental error. According to the calculation from the deviations of M_r determined by PGGE and SDS-PAGE, the proposed method can precisely determine the number of subunits in an oligomeric protein when it is ≤ 8 .

Fig. 4 shows the results of the analysis of the

TABLE II

COMPARISON BETWEEN CALCULATED AND ESTABLISHED VALUES: SUBUNIT M_r OBTAINED BY SDS-PAGE AT 12.5%T

Protein	R_f	Measured subunit M_r	True subunit M_r	Deviation (%)
Thyroglobulin	0	(317 000) ^a	333 000	-3.9
Ferritin	0.732	18 000	18 500	-2.7
Catalase	0.267	62 000	60 000	+3.3
LDH	0.484	35 000	36 000	-2.8
Albumin	0.232	68 000	67 000	+1.5

^b Data obtained by SDS-PAGE at 6%T.

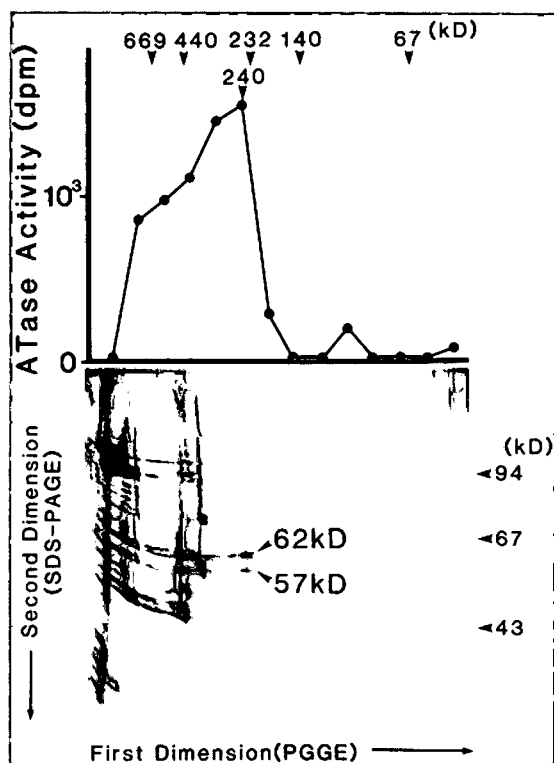


Fig. 4. Analysis of ATase subunit structure. After PGGE, the gel was sliced into two. One section was used to assay ATase activity (upper half). The other section was applied to 2D electrophoresis and silver stained (lower half). The arrowheads indicate M_r 62 000 and 57 000 subunits of ATase, respectively. The positions of standard proteins in the first-dimension PGGE those of M_r marker proteins in the second-dimension SDS-PAGE are shown at the top and on the right, respectively (M_r values $\times 10^{-3}$). The native M_r (240 000) of ATase obtained by PGGE was similar to the values given by gel chromatography and sucrose density gradient centrifugation (data not shown). There was a single protein band corresponding to M_r 240 000 on PGGE and this protein was dissociated into M_r 62 000 and 57 000 protein bands. Considering the sensitivity of silver staining, the amount of ATase protein and the enzyme activity are comparable. However, ATase activity is very labile, especially at its pore limit where molecular jamming, aggregation or shearing in the gel network and the subsequent heating due to increased electric resistance may occur. Therefore, the enzyme activity is not completely proportional to the staining intensity of the M_r 62 000 and 57 000 protein bands. The lower a gel concentration is, the more directly proportional is the relationship between the activity and the staining intensity. kD = kilo dalton.

ATase subunit structure. A peak of ATase activity was detected in the gel piece and its pore limit corresponded to the size of M_r 240 000 globular proteins.

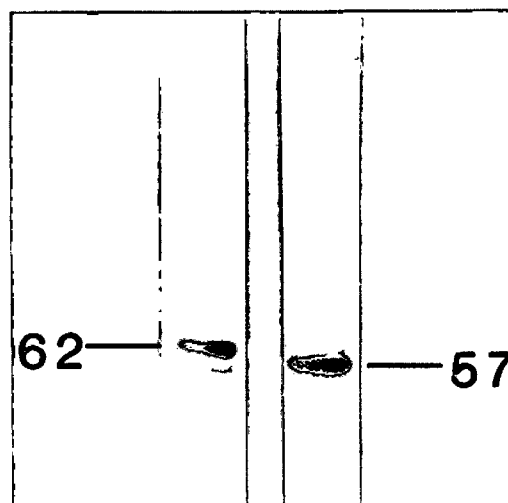


Fig. 5. Western blotting of M_r 62 000 and 57 000 subunits of ATase. Although both anti- M_r 62 000 (left) and 57 000 (right) subunit antibodies have a slight cross-reactivity with each other, the antigenicity of each is apparently different.

The protein at this point was shown by 2D electrophoresis to be composed of M_r 62 000 and 57 000 subunits. These results suggested that ATase is an M_r 240 000 heterotetrameric protein with two kinds of subunits. To ascertain whether or not the M_r 57 000 subunit of ATase was the degradation product of the M_r 62 000 subunit, the difference in antigenicity of the two subunits was examined by Western blotting (Fig. 5). Because the antigenicities of the M_r 62 000 and 57 000 subunits were different, it is suggested that the M_r 57 000 subunit is not the degradation product of the M_r 62 000 subunit and that ATase is a heterotetrameric protein. However, both anti- M_r 62 000 and anti- M_r 57 000 subunit antibodies had a little cross-reactivity to the other subunit, and 240 000 measured as the native M_r of ATase is nearly equal to 248 000, that is, the sum of four M_r 62 000 subunits, considering of the deviation of this technique. Therefore, a more detailed analysis of ATase subunits including N-terminal sequencing, HPLC mapping of cleavage fragments and cDNA cloning, etc., is necessary to obtain definitive evidence that the M_r 57 000 protein is not derived from the M_r 62 000 subunit.

Because PGGE was performed under non-denaturing condition, the biological activities of most proteins were conserved, as shown for ATase.

Moreover, because the proteins in the sample were concentrated both by PGGE and SDS-PAGE, a high degree of resolution was attained. This method is therefore useful even for very small amounts of the impure protein samples. In fact, 1 μg of rat liver ATase in an impure sample was determined by this 2D electrophoresis. The method is also applicable to basic proteins such as histone with a pI above the pH 8.4 of the electrode buffer in PGGE, by exchanging the anode for a cathode (data not shown).

In conclusion, the analysis of the subunit structure of an oligomeric protein by the present method is very useful as it has a high resolution capacity when its limit of accuracy is properly considered.

REFERENCES

- 1 P. Andrews, *Biochem. J.*, 96 (1965) 595–606.
- 2 J. Margolis and K.G. Kenrick, *Nature*, 214 (1967) 1334–1336.
- 3 J. Margolis and K. G. Kenrick, *Anal. Biochem.*, 25 (1968) 347–362.
- 4 G. G. Slater, *Anal. Chem.*, 41 (1969) 1039–1041.
- 5 D. Rodbard, G. Kapadia and A. Chrambach, *Anal. Biochem.*, 40 (1971) 135–157.
- 6 K. Felgenhauer, *Hoppe-Seyler's Z. Physiol. Chem.*, 335 (1974) 1281–1290.
- 7 J. Margolis and C. W. Wrigley, *J. Chromatogr.*, 106 (1975) 204–209.
- 8 W. P. Campbell, C. W. Wrigley and J. Margolis, *Anal. Biochem.*, 129 (1983) 31–36.
- 9 U. K. Leammli, *Nature*, 227 (1970) 680–685.
- 10 D. M. Neville, *J. Biol. Chem.*, 246 (1971) 6328–6334.
- 11 J. A. Reynolds and C. Tanford, *J. Biol. Chem.*, 245 (1970) 5161–5165.
- 12 K. Shirahama, K. Tsujii and T. Takagi, *J. Biochem.*, 75 (1974) 309–319.
- 13 A. Chrambach, T. M. Jovin, P. J. Svendsen and D. Rodbard in N. Catsimpooolas (Editor), *Methods of Protein Separation*, Vol. 2, Plenum Press, New York, 1976, pp. 27–144.
- 14 K. Ohsawa and N. Ebata, *Anal. Biochem.*, 135 (1983) 409–415.
- 15 M. Tsuda, N. Katunuma and G. Wever, *J. Biochem.*, 85 (1979) 1347–1354.
- 16 M. Itakura and E. W. Holmes, *J. Biol. Chem.*, 254 (1979) 333–338.
- 17 C. Lee, A. Levin and D. Branton, *Anal. Biochem.*, 166 (1987) 308–312.
- 18 E. Harlow and D. Lane, *Antibodies*, Cold Spring Harbor Laboratory, Cold Spring Harbor, NY, 1988, pp. 471–510.

Separation of drug stereoisomers by capillary electrophoresis with cyclodextrins

Teresa E. Peterson

Alcon Laboratories, Inc., 6201 South Freeway, Fort Worth, TX 76134-2099 (USA)

(First received July 20th, 1992; revised manuscript received October 21st, 1992)

ABSTRACT

Using capillary electrophoresis, the enantiomers and isomers of several chiral drug molecules were resolved with cyclodextrins. Parameters affecting the resolution between (+)- and (–)-epinephrine, such as pH, cyclodextrin concentration, buffer concentration, and capillary dimensions were investigated. In addition to this, the effect of cyclodextrin type (β and several derivatized β -cyclodextrins) on resolution between stereoisomers of several chiral drug was also investigated. This study showed that the structural features of the molecule, the derivative groups on the cyclodextrin, the buffer composition and the capillary dimensions influence resolution. The chiral drugs used in this study were propranolol, atenolol, betaxolol, dipivefrin, AL03152 (an aldose reductase inhibitor), AL03363 (an oxidation product of AL03152) and the *cis/trans* isomers of pilocarpine.

INTRODUCTION

Regulatory agencies are now demanding more stringent investigations to evaluate the safety and efficacy of chiral drug products [1]. In order to ensure the purity of these chiral drugs and monitor stability studies, stereoselective analytical methods are needed.

Cyclodextrins have been used in HPLC [2–6] to resolve chiral compounds and they are now being used in capillary electrophoretic techniques [7–18] with very promising results. The properties of cyclodextrins which make them unique chiral selectors have been discussed in detail [19,20]. Only a brief review of their properties will be given here.

Cyclodextrins are chiral, neutral, cyclic polysaccharides composed of 6 to 8 *d*-glucose units having the shape of a hollow truncated cone. The interior of the cavity is hydrophobic and the rim of the cavity, lined with hydroxyl groups, is hydrophilic. Al-

though there are still many fundamental questions on the chiral recognition process with cyclodextrins there are two generally accepted requirements for chiral recognition in aqueous solution [21]. First, the analyte must have a proper structural fit to the cyclodextrin. This fit is usually referred to as an inclusion complex and requires at least one aromatic ring structure in the molecule. Secondly, the groups on the rim of the cyclodextrin cavity must interact with a substituent group on or near the stereogenic center of the molecule. If this interaction is stronger for one of the two isomers they can be resolved from one another.

The stereoselectivity will change when some of the rim hydroxyl groups of β -cyclodextrin are replaced with other groups such as methyl, hydroxyethyl or hydroxypropyl. These derivatized cyclodextrins can provide unique selectivities for a separation.

In this work, cyclodextrins were added to the buffers used in capillary electrophoresis (CE) to resolve the stereoisomers of several chiral drug molecules. Parameters such as pH, buffer (Tris) concentration, cyclodextrin concentration, cyclodextrin type and

Correspondence to: Teresa E. Peterson, Ciba Vision Ophthalmics, 11460 John's Creek Parkway, Duluth, GA 30136-1518, USA (present address).

capillary dimensions were varied to optimize these separations. These studies show that the structural features of the molecule, as well as the type of cyclodextrin, plays an important role in resolution.

EXPERIMENTAL

Chemicals

Orthophosphoric acid, sodium phosphate dibasic (Na_2HPO_4), hydrochloric acid and sodium hydroxide were obtained from J. T. Baker (Phillipsburg, NJ USA). Tris(hydroxymethyl)amino methane (Tris), (+, -)-epinephrine, (-)-epinephrine, and heptakis (2,6-di-O-methyl) β -cyclodextrin (Me- β -CD) were obtained from Sigma (St. Louis, MO, USA). β -Cyclodextrin (β -CD), γ -cyclodextrin, (+)-atenolol, (-)-atenolol, (+, -)-propranolol, (+)-propranolol and pilcarpine were obtained from Aldrich (Milwaukee, WI, USA). A mixture of pilocarpine-isopilocarpine (50:50) was obtained from Inland Alkaloid (Pipton, IN, USA). Hydroxyethyl- β -cyclodextrin (HE- β -CD) and hydroxypropyl- β -cyclodextrin (HP- β -CD) were obtained from American Maize-Products Company (Hammond, IN, USA). Betaxolol was obtained from Laboratoires D'Etudes et de Recherches Synthelabo (Porcheville, France). Dipivefrin was obtained from Pharm-Eco (Simi Valley, CA, USA). AL03152 (2,7-difluoro-4-methoxy-spiro(9H-fluorene-9,4'-imidazolidine)-2',5'-dione) and AL03363 (2,7-difluoro-4-hydroxy-spiro(9H-fluorene-9,4'-imidazolidine)-2',5'-dione) enantiomers were synthesized in-house. The AL03152 enantiomers were available individually while the AL03363 enantiomers were only available as a racemic mixture.

Apparatus

The experiments were performed with a Dionex CES system (Sunnyvale, CA, USA) equipped with a UV detector. Separations were performed in unmodified fused-silica capillaries of varying lengths and internal diameters (Polymicro Technologies, Phoenix, AZ, USA). Samples were injected by gravity for 10 s at 50 mm. The injection end was the anode (+). The applied voltage was 10 or 15 kV, depending on the sample and the observed current was always less than 50 μA . Separations were achieved with cyclodextrin buffers of varying concentrations and pH values. Electropherograms were

recorded with a Spectra-Physics Chrom-Jet integrator (San Jose, CA, USA).

Procedure

At the beginning of each day, and whenever the buffer solution was changed, the capillary was pressure-rinsed two times for 180 s with 0.1 M H_3PO_4 and two times with 0.5 M NaOH. Then the entire system (capillary, source and destination vials) was rinsed four times with purified water and four times with the buffer solution. These rinse cycles were performed automatically by the instrument. Once this procedure was complete, it was only necessary to rinse the entire system one time with buffer after each injection. This one-time rinse cycle was performed automatically by the instrument.

Solutions

The basic compounds, epinephrine, atenolol, propranolol, betaxolol, dipivefrin and pilocarpine, were dissolved in 0.01 M HCl. The acidic compounds, AL03152 and AL03363, were dissolved in 0.01 M NaOH. High- and low-pH buffers were prepared containing varying amounts of the four cyclodextrins (β , Me- β -CD, HE- β -CD and HP- β -CD). The pH 11 buffers were composed of Tris and Na_2HPO_4 with the pH adjusted to 11 with NaOH. The pH 2.4–9 buffers were composed of Tris and the pH was adjusted with phosphoric acid and sodium hydroxide. All buffers were filtered through a 0.45- μm filter prior to use.

Calculations

The resolution (R) values were calculated by the following equation:

$$\text{Resolution } (R) = 2(d_2 - d_1)/(w_1 + w_2)$$

where d_1 and d_2 are the migration times, in cm, and w_1 and w_2 are the widths at the base, in cm, of the first and second peaks, respectively.

RESULTS AND DISCUSSIONS

Cyclodextrins have been used successfully in capillary isotachopheresis [7–9] and CE [10–17] to resolve chiral compounds. These reports have shown that pH [7], temperature [11], organic solvents [11], cellulose derivatives [16], cyclodextrin amount [7,8,11,12,15], and cyclodextrin type [12,15] can

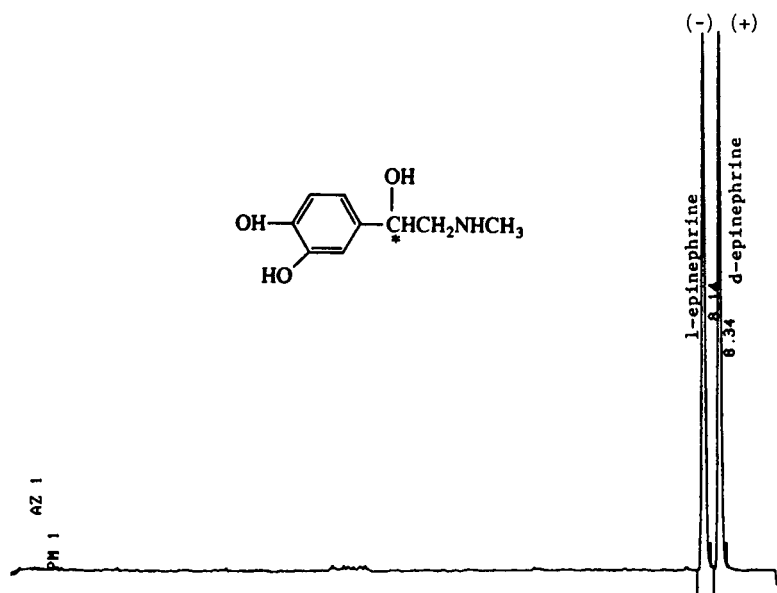


Fig. 1. Resolution of (+)- and (-)-epinephrine (25 ppm each isomer). Conditions: 20 mM Tris- H_3PO_4 -9 mM Me- β -CD; pH 2.4, fused-silica capillary, 50 cm \times 0.050 mm I.D. (45 cm to detector), 15 kV, 206 mm (0.1 AUFS), 10 s 50 mm gravity inject.

influence resolution between isomers. Thin-layer chromatography separations with cyclodextrin mobile phases have also shown similar effects [22–24].

The separation of (+)- and (-)-epinephrine by CE with Me- β -CD was shown by Fanali [12] with a coated capillary. In this investigation, the enantiomers of epinephrine were resolved with an unmodified fused-silica capillary. A typical electro-

pherogram is shown in Fig. 1. The effect of pH, buffer concentration, cyclodextrin concentration and capillary dimensions on the resolution between these enantiomers is illustrated in Table I and II.

Table I shows that resolution between the enantiomers of epinephrine improves as pH decreases and buffer (Tris) concentration and cyclodextrin (Me- β -CD) concentration increases. At the

TABLE I

EFFECT OF BUFFER pH, TRIS CONCENTRATION AND CYCLODEXTRIN CONCENTRATION ON THE RESOLUTION OF (+)- AND (-)-EPINEPHRINE

Conditions: fused-silica capillary, 50 cm \times 0.075 mm I.D. (45 cm to detector), 15 kV, 206 nm (0.1 AUFS), 10 s 50 mm gravity inject.

Buffer A: 20 mM Tris- H_3PO_4 -9 mM Me- β -CD; pH (variable)					
pH	2.4	5	7	9	11
Resolution	1.60	1.47	0.95	0	0
Buffer B: (variable) mM Tris- H_3PO_4 -9 mM Me- β -CD; pH 2.4					
Tris (mM)	1	10	20	40	60
Resolution	0.88	1.6	1.6	1.6	1.1
Buffer C: 20 mM Tris- H_3PO_4 -(variable) mM Me- β -CD; pH 2.4					
Me- β -CD (mM)	4	9	18	28	
Resolution	1.25	1.60	2.38	2.53	

TABLE II

EFFECT OF CHANGING CAPILLARY LENGTH AND INTERNAL DIAMETER (I.D.) ON THE RESOLUTION OF (+)- AND (-)-EPINEPHRINE

Conditions: buffer, 20 mM Tris- H_3PO_4 -9 mM Me- β -CD; pH 2.4; 15 kV; 206 nm (0.1 AUFS), 10 s 50 mm gravity inject.

Capillary length (cm) \times I.D. (mm) (to detector)	Resolu- tion	Migration time (min)	
		(+)	(-)
45 \times 0.025	3.2	12.54	12.95
45 \times 0.050	2.5	11.38	11.69
45 \times 0.075	1.6	9.23	9.41
55 \times 0.075	2.5	15.58	15.98
65 \times 0.075	2.8	21.88	22.45

TABLE III
EFFECT OF CYCLODEXTRIN TYPE ON CHIRAL RESOLUTION

See Figs. 2–5 for electropherograms and conditions.

Note: the basic enantiomers and isomers (propranolol, atenolol, pilocarpine) were only resolved with cyclodextrin buffers of pH 2.4 not pH 11. The acidic enantiomers (AL03152, AL03363) were only resolved with cyclodextrin buffers of pH 11 not pH 2.4.

Compounds	β -CD	Me- β -CD	HE- β -CD	HP- β -CD
Propranolol	× ^a	×	yes	yes
Atenolol	×	Partial	×	×
AL03152	yes ^a	yes	yes	yes
AL03363	yes	yes	yes	yes
Pilocarpine	yes	yes	×	×
Betaxolol	×	×	×	×
Dipivefrin	×	×	×	×

^a × = Isomers not resolved; yes = isomers resolved.

lower pH values epinephrine is positively charged and less likely to degrade. Increasing the amount of cyclodextrin improves resolution significantly while only minor improvements in resolution were obtained when the Tris concentration was increased. A point is eventually reached where increasing the Tris and cyclodextrin concentration does not improve resolution further.

Table II shows that decreasing the internal diameter (I.D.) of the capillary and increasing the length of the capillary will also improve resolution. Resolution improves because decreasing the column radius and increasing the column length enhances the capillaries ability to dissipate heat and minimizes thermally induced zone broadening [17]. These changes do not come without drawbacks. Increasing the length of the capillary will increase analysis time and decreasing the capillary I.D. will decrease the sensitivity. The sensitivity of the method decreases because detection is performed on-line and the absorbance is directly proportional to the path-length of the cell which in this case is the capillary. Improving resolution by manipulating capillary dimensions may be a less expensive alternative to increasing the amount of cyclodextrin if the cyclodextrin is expensive. However, capillaries less than or equal to 25 μ m I.D. tend to clog easily and can be troublesome to use.

Studies with propranolol, atenolol, pilocarpine,

AL03152, AL03363, betaxolol and dipivefrin show how resolution is influenced by the type of cyclodextrin (Table III). Table III shows that the enantiomers of propranolol, atenolol, AL03152, AL03363 and the *cis/trans* isomers of pilocarpine could be resolved with at least one of the cyclodextrin buffers used in this study. The enantiomers of betaxolol and dipivefrin, however, were not resolved with any of these buffers.

Four cyclodextrins were used in this study; β -cyclodextrin, Me- β -CD, HE- β -CD and HP- β -CD. The cyclodextrins were dissolved in pH 2.4 (20 or 40 mM Tris) and pH 11 (20 mM Tris–10 mM Na₂HPO₄) buffers. The basic enantiomers (propranolol and atenolol) and the basic *cis/trans* isomers (pilocarpine/isopilocarpine) were only resolved with cyclodextrin buffers of pH 2.4 not pH 11. The acidic enantiomers (AL03152 and AL03363) were only resolved with cyclodextrin buffers of pH 11 not pH 2.4. Apparently resolution only occurs when the molecules are charged. These separations, illustrated in Figs. 2–5 were optimized by adjusting the buffer composition and capillary dimensions.

Fig. 2 shows that the enantiomers of propranolol were equally resolved with a pH 2.4 HE- β -CD and HP- β -CD buffer. Racemic atenolol, however, was only partially resolved with a pH 2.4 Me- β -CD buffer (Fig. 3). Increasing the amount of Me- β -CD from 28 mM to 35 mM did not improve resolution further.

The *cis/trans* isomers, pilocarpine and isopilocarpine, were resolved with equal concentrations of β - and Me- β -CD in a pH 2.4 buffer (Fig. 4). The resolution with 9 mM Me- β -CD (Fig. 4B) is clearly superior to that with 9 mM β -cyclodextrin (Fig. 4A). The separation with β -cyclodextrin can not be improved by increasing the cyclodextrin concentration since β -cyclodextrin is not soluble above 9 mM in this electrolyte system. However, the resolution can be improved by decreasing the capillary I.D. from 75 to 50 μ m (Fig. 4C). Resolution with the 50 μ m I.D. capillary using a β -cyclodextrin buffer is now sufficient for quantitation. This is important to note because beta cyclodextrin is less expensive than Me- β -CD. Fig. 4D shows that decreasing the capillary I.D. also improves resolution with the Me- β -CD buffer.

The enantiomers of AL03152 and AL03363 were resolved with equal concentrations of all four cyclo-

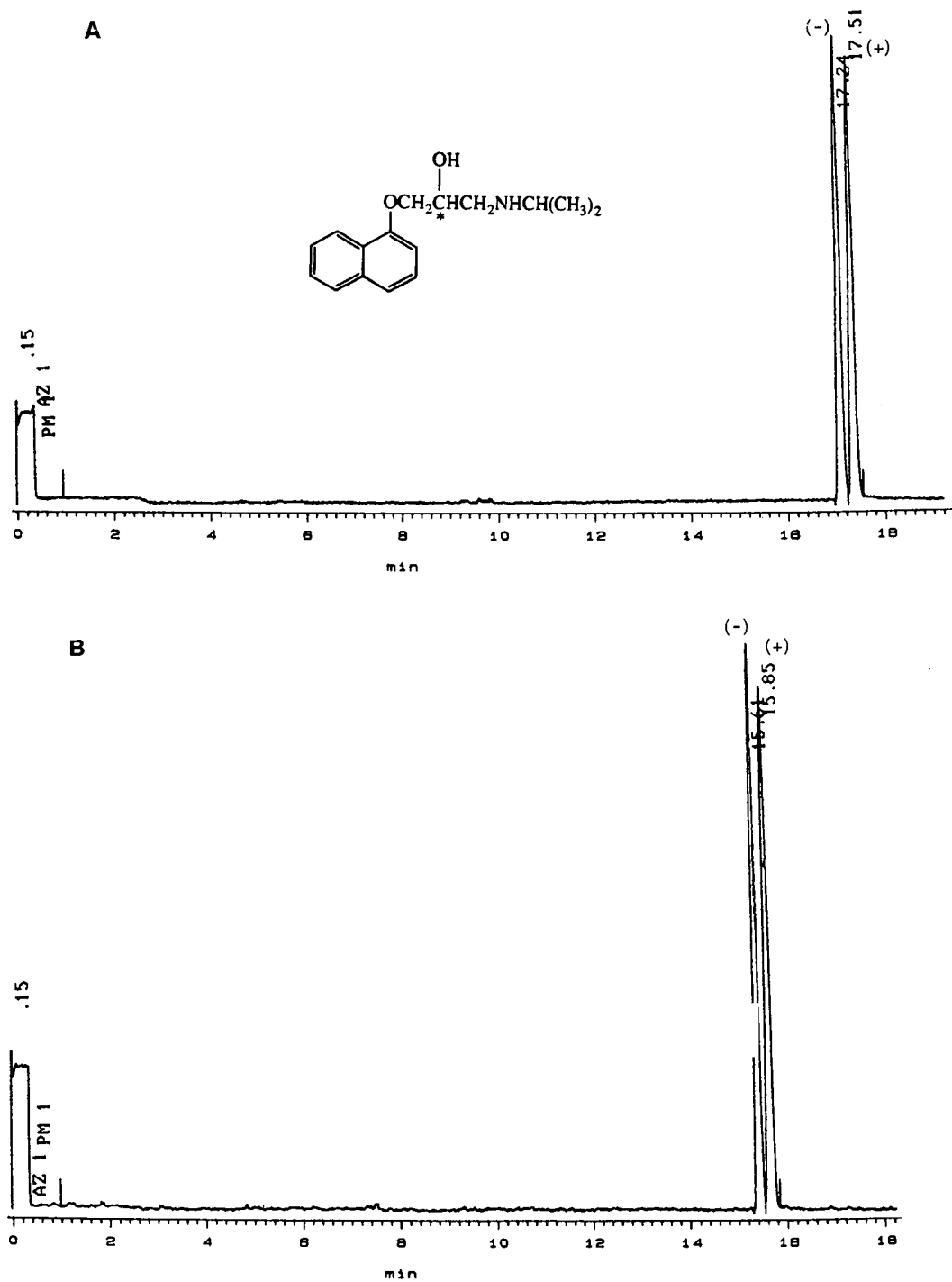


Fig. 2. Resolution of (+)- and (-)-propranolol (48 ppm each) with HE- β -CD and HP- β -CD. Conditions: fused-silica capillary, 50 cm \times 0.050 mm I.D. (45 cm to detector), 15 kV, 206 mm (0.05 AUFS), 10 s 50 mm gravity inject. (A) 20 mM Tris- H_3PO_4 -28 mM HE- β -CD; pH 2.4; (B) 20 mM Tris- H_3PO_4 -28 mM HP- β -CD; pH 2.4.

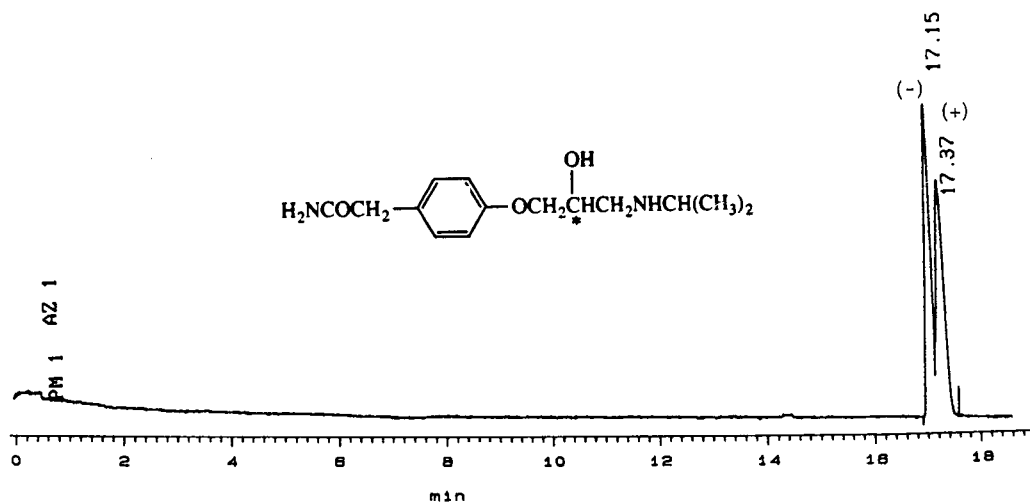


Fig. 3. Resolution of (+)- and (-)-atenolol (50 ppm each). Conditions: same as Fig. 5 except buffer, 20 mM Tris- H_3PO_4 -28 mM Me- β -CD; pH 2.4.

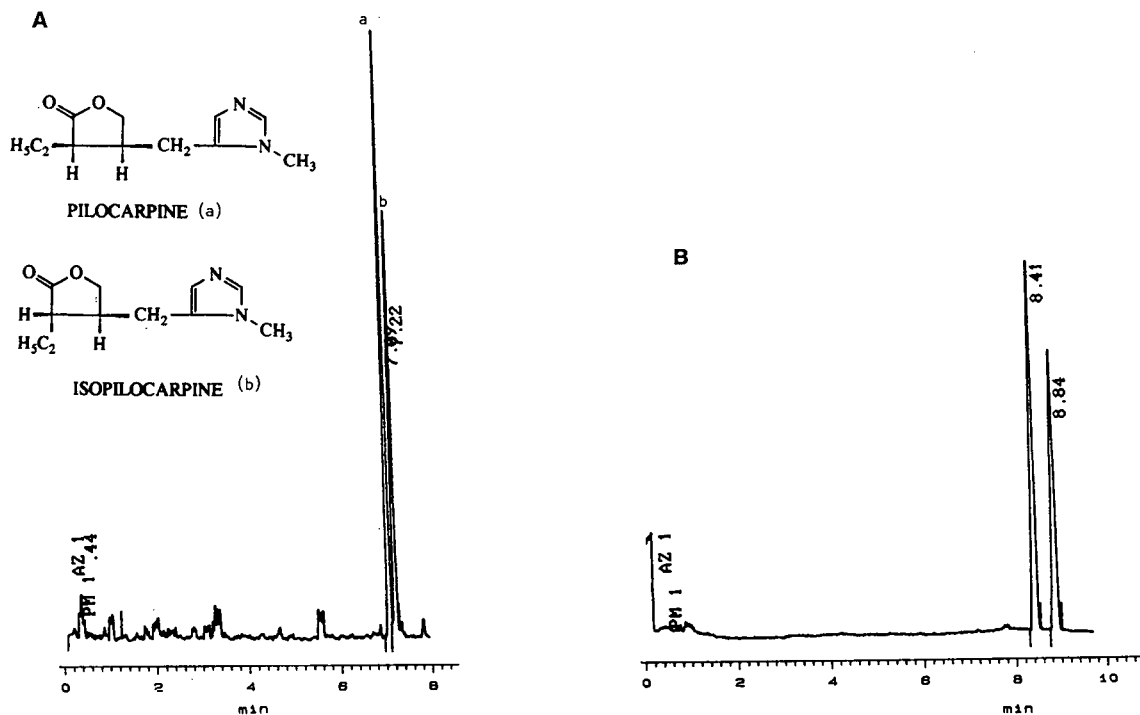


Fig. 4.

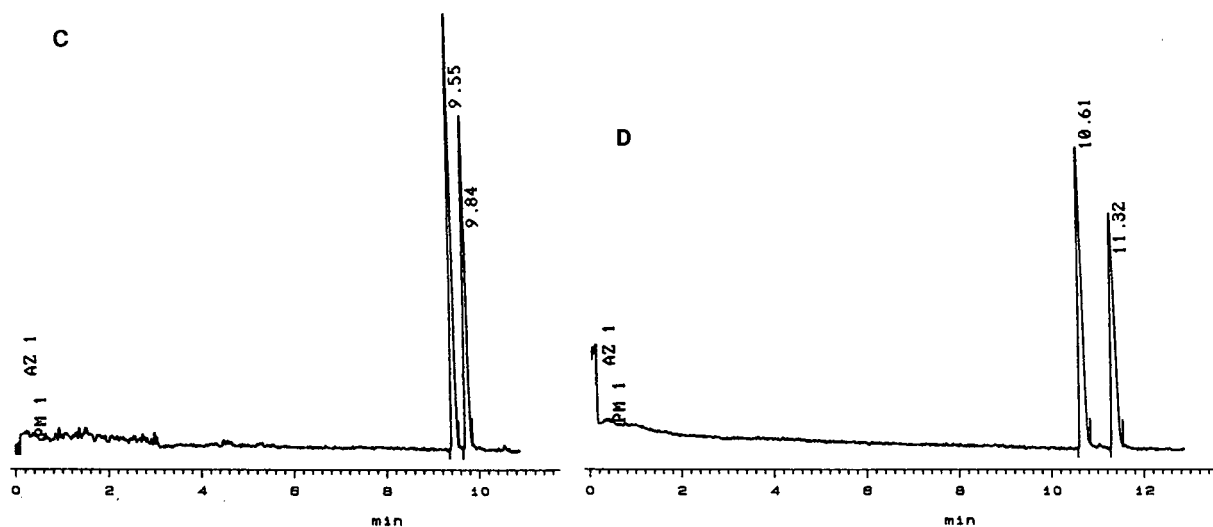


Fig. 4. (a) Separation of isopilocarpine-pilocarpine mixture (125 ppm each). Conditions: 40 mM Tris- H_3PO_4 -9 mM β -CD; pH 2.4, fused-silica capillary, 50 cm \times 0.075 mm I.D. (45 cm to detector), 15 kV, 206 nm (0.1 AUFS), 10 s 50 mm gravity inject; (B) same as A except buffer is 40 mM Tris- H_3PO_4 -9 mM Me- β -CD, pH 2.4; (C) same as A except 0.05 AUFS and fused-silica capillary is 0.050 mm I.D.; (D) same as B except 0.05 AUFS and fused-silica capillary is 0.050 mm I.D.

dextrins (β , Me- β -CD, HE- β -CD and HP- β -CD) in a pH 11 buffer (Table IV). Table IV shows that resolution between the enantiomers of these structurally similar compounds, with equal concentrations of the same cyclodextrin, can vary considerably (structures are shown in Fig. 5). The AL03152 enantiomers were best resolved with Me- β -CD (Fig. 5A) while the AL03363 enantiomers were best resolved with β -cyclodextrin (Fig. 5B). The AL03152 compound has an $-\text{OCH}_3$ group on the aromatic ring and AL03363 has a hydroxyl group in this position. Structurally, these compounds are very similar but resolution varies considerably with the same

cyclodextrin as shown in Table IV. Clearly, the structural features of the molecule as well as the type of cyclodextrin play a role in resolution.

Betaxolol and dipivefrin were not resolved with any of the cyclodextrin buffers used in this study. The structures of these molecules are shown in Fig. 6. γ -Cyclodextrin, which has a larger cavity than β -cyclodextrin, gave no resolution either. The bulky groups opposite the chiral center attached to the aromatic ring probably prevent inclusion inside the cyclodextrin cavity. It is quite possible that if an inclusion complex does not form the enantiomers can not be resolved from one another in aqueous solution.

The mechanism of these chiral separations is believed to be from inclusion complex formation between the analyte and the cyclodextrin. Some additional studies, however, are needed to confirm this. Binding studies between the drug and the cyclodextrin as well as additional experiments using the linear form of the cyclodextrin (if available) would be helpful.

TABLE IV

RESOLUTION VALUES FOR THE AL03152 AND AL03363 ENANTIOMERS WITH CYCLODEXTRINS

Conditions: buffer, 20 mM Tris-10 mM Na_2HPO_4 -9 mM cyclodextrin, pH 11, rest of conditions same as Fig. 5.

Cyclodextrin	AL03152	AL03363
β -CD	1.1	3.4
Me- β -CD	5.7	1.2
HE- β -CD	3.6	0.73
HP- β -CD	3.5	2.4

CONCLUSIONS

These experiments show that resolution between

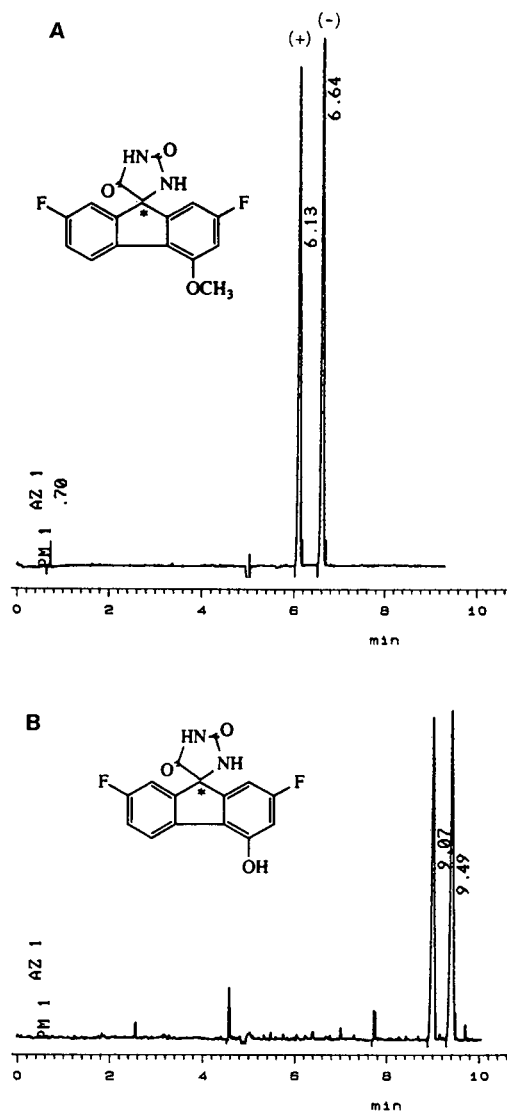


Fig. 5. (A) Resolution of (+)- and (-)-AL03152 (50 ppm each). Conditions: 20 mM Tris–10 mM Na_2HPO_4 –9 mM Me- β -CD, pH 11, fused-silica, 50 cm \times 0.075 mm I.D. (45 cm to detector), 10 kV, 225 nm (0.1 AUFS), 10 s 50 mm gravity inject; (B) AL03363 enantiomers (50 ppm each), same as A except buffer contains 9 mM β -CD.

stereoisomers of acidic and basic chiral drug molecules can be obtained rapidly with CE by adding to the buffer a chiral reagent such as cyclodextrin. The acidic enantiomers were best resolved in high pH buffers while the basic enantiomers and isomers

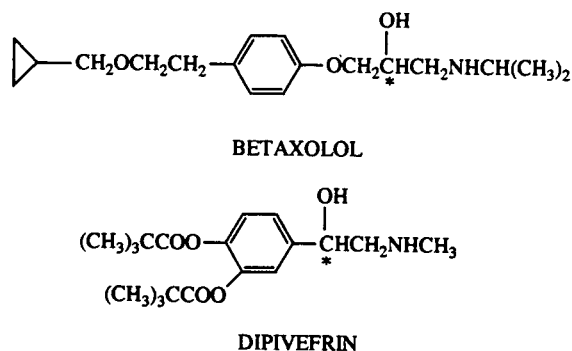


Fig. 6. Structures of betaxolol and dipivefrin.

were best resolved in low pH buffers. In addition to pH, decreasing the capillary I.D. and increasing the cyclodextrin concentration can improve resolution. Minor improvements in resolution can be obtained by increasing capillary length or increasing buffer (Tris) concentration. The cyclodextrin type as well as the structural features of the molecule play an important role in resolution. Structural features such as bulky groups opposite the chiral center can affect inclusion complex formation while derivative groups on the rim of the cyclodextrin cavity can affect stereoselectivity.

ACKNOWLEDGEMENTS

I thank Dr. Karen B. Sentell at the University of Vermont for her many helpful comments on this manuscript. I also thank Alcon for providing the time and facilities to complete this work.

REFERENCES

- 1 M. Gross, *Regulatory Affairs*, 3 (1991) 483–494.
- 2 A. Berthod, S. Chang and D. Armstrong, *Anal. Chem.*, 64 (1992) 395–404.
- 3 S. Han, Y. Han and D. Armstrong, *J. Chromatogr.*, 441 (1988) 376–381.
- 4 M. Gazdag, G. Szepesi and L. Huszar, *J. Chromatogr.*, 351 (1986) 128–135.
- 5 D. Armstrong, T. Ward, R. Armstrong and T. Beesley, *Science (Washington, D.C.)*, 232 (1986) 1132–1135.
- 6 D. Armstrong and W. DeMond, *J. Chromatogr. Sci.*, 22 (1984) 411–415.
- 7 J. Snopek, I. Jelinek and E. Smolková-Keulemansová, *J. Chromatogr.*, 438 (1988) 211–218.
- 8 S. Fanali, *J. Chromatogr.*, 470 (1989) 123–129.

- 9 I. Jelínek, J. Snopek and E. Smolková-Keulemansová, *J. Chromatogr.*, 557 (1991) 215–226.
- 10 S. Terabe, J. Ozaki, K. Otsuka and T. Ando, *J. Chromatogr.*, 332 (1985) 211–217.
- 11 A. Guttman, A. Paulus, A. Cohen, N. Grinberg and B. Karger, *J. Chromatogr.*, 448 (1988) 41–35.
- 12 S. Fanali, *J. Chromatogr.*, 474 (1989) 441–446.
- 13 A. Dobashi, T. One and S. Hara, *J. Chromatogr.*, 480 (1989) 413–420.
- 14 S. Fanali and P. Bocek, *Electrophoresis*, 11 (1990) 757–760.
- 15 S. Fanali, *J. Chromatogr.*, 545 (1991) 437–444.
- 16 J. Snopek, H. Soini, M. Novotny, E. Smolková-Keulemansová and I. Jelínek, *J. Chromatogr.*, 559 (1991) 215.
- 17 J. Jorgenson and K. Lukacs, *J. High. Resolut. Chromatogr. Chromatogr. Commun.*, 8 (1985) 407–411.
- 18 T. Peterson and D. Trowbridge, *J. Chromatogr.*, 603 (1992) 298–301.
- 19 W. Lough (Editor), *Chiral Liquid Chromatography*, Chapman & Hall, New York, 1989, pp. 148–164.
- 20 A. Krstulovic (Editor), *Chiral Separation by HPLC*, Halsted Press, New York, 1989, pp. 208–286.
- 21 *Cyclobond Handbook — A Guide to Using Cyclodextrin Bonded Phases*, Advanced Separation Technologies, Whippany, NJ, p. 8.
- 22 D. Armstong, F. He and S. Han, *J. Chromatogr.*, 448 (1992) 345–354.
- 23 W. Burkert, C. Owensby, W. Hinze, *J. Liq. Chromatogr.*, 4 (1992) 1065–1085.
- 24 D. Armstong, *J. Liq. Chromatogr.*, 3 (1992) 895–900.

Separation and simultaneous determination of the active ingredients in theophylline tablets by micellar electrokinetic capillary chromatography

Quan-xun Dang and Ling-xiao Yan

Shaanxi Institute for Drug Control, Zhu-que Street, Xian 710061 (China)

Zeng-pei Sun and Da-kui Ling

National Institute for the Control of Pharmaceutical and Biological Products, Temple of Heaven, Beijing 100050 (China)

(First received June 30th, 1992; revised manuscript received October 20th, 1992)

ABSTRACT

The separation and determination of seven active ingredients in theophylline tablets by micellar electrokinetic capillary chromatography is described. On a 35 cm × 50 μm I.D. capillary, baseline separation is possible with a carrier solution containing 0.05 M sodium dodecyl sulphate (SDS) in 0.02 M borate buffer (pH 9.2) solution. The migration time of solutes increased markedly with increasing SDS concentration and slightly with increasing pH. With consecutive injections of samples, slight decreases in the migration times of the solutes occurred, but they were in parallel, owing to the temperature rise of the capillary with time. The column efficiency was influenced by the micellar concentration and applied voltage, and optimum values at which the highest theoretical plate number was achieved were established. The determination of the active ingredients was performed using hydrochlorothiazide and levamisole hydrochloride (for ephedrine hydrochloride only) as internal standards, with good linearity with correlation coefficients from 0.9965 to 0.9999 and recoveries from 94.1% to 101.1%. For quantitative information, measurements of peak height were better than peak area.

INTRODUCTION

Micellar electrokinetic capillary chromatography (MECC) was first reported by Terabe *et al.* [1] nearly 10 years ago, since when there have been several studies on the theory and application of MECC [2–4] and separations of chlorinated phenols [5], aspicillin [6], β-lactam antibiotics [7], sulphonamides [8], etc., have been successfully achieved. MECC has also been applied to the determination of active ingredients in pharmaceutical preparations and body fluids [6,9,10]. Generally, these determinations were performed on single-ingredient preparations or a few components of the same kind.

In the paper, we describe the separation and determination of seven active ingredients in theophylline tablets, irrespective of whether these ingredients are the same kind of compound or not. Although the molecular structures of the ingredients are completely different from each other, except for three derivatives of xanthine, the separation was successfully achieved simply by adjusting and selecting the pH value and the concentration of surfactant. The simultaneous determination of the seven active ingredients was completed within 8 min employing hydrochlorothiazide and levamisole hydrochloride (for ephedrine hydrochloride only) as internal standards. The application of a second internal standard improved the precision of the determination of ephedrine hydrochloride.

Correspondence to: Q.-X. Dang, Shaanxi Institute for Drug Control, Zhu-que street, Xian 710061, China.

EXPERIMENTAL

Apparatus

A Bio-Rad (Richmond, CA, USA) HPE 100 apparatus equipped with a UV detector set at 210 nm, a power supply able to deliver up to 12 kV d.c. and a Bio-Rad 148-3014 HPE capillary cartridge (35 cm \times 50 μ m I.D., uncoated) were employed. A Chromatopac C-R3A (Shimadzu, Kyoto, Japan) was used for data processing. Electrokinetic sampling was used to introduce samples into the capillary.

Drug and chemicals

Three derivatives of xanthine and phenobarbital were purchased from the National Institute for the Control of Pharmaceutical and Biological Products (Beijing, China). Amidopyrine, phenacetin, ephedrine hydrochloride, hydrochlorothiazide and levamisole hydrochloride were authentic specimens, obtained from the Shaanxi Institute for Drug Control (Xian, Shaanxi, China). Theophylline tablets (three batches) were purchased from Xian Pharmaceutical Factory (Xian, Shaanxi, China).

Sodium dodecyl sulphate (SDS) was obtained from Nacalai Tesque (Kyoto, Japan). All other reagents and solvents, of analytical-reagent grade, were products of the Beijing Chemical Factory (Beijing, China). A carrier solution was obtained by dissolving a suitable amount of SDS in a buffer solution prepared by mixing 0.02 M sodium tetraborate solution with 0.2 M sodium dihydrogenphosphate solution to given pH 8.0, 8.5 and 9.0, or adding 0.1 M sodium hydroxide solution to sodium tetraborate solution to give pH 9.5 and 10.0. The solutions were filtered through a 0.45- μ m membrane filter and degassed by ultrasonication before use.

Procedure for the quantitative analysis

A test solution for separation studies was prepared by shaking the solutes with an appropriate amount of methanol first, owing to the low solubility of phenacetin in water, then with a mixture of methanol and pH 9.2 buffer solution that was added later, the final concentration of methanol in the solution being 20%. Five solutions were prepared as above to give a series of concentrations in the ranges 8–10 μ g/ml of phenobarbital and ephedrine hydrochloride, 12–60 μ g/ml of caffeine, 20–100 μ g/

ml of theophylline and theobromine and 80–400 μ g/ml of amidopyrine and phenacetin for the determination of the linear range and response factors. After preparation as described above, the concentrations of the solutions for the recovery test were about 20 μ g/ml of phenobarbital and ephedrine hydrochloride, 30 μ g/ml of caffeine, 50 μ g/ml of theophylline and theobromine and 200 μ g/ml of amidopyrine and phenacetin and two other concentration levels equivalent to 80% and 120% of these concentrations. An appropriate amount of finely ground powder of theophylline tablets was dissolved to give a solution at the same concentrations as above. The concentrations of internal standards in all the solutions were about 70 μ g/ml of hydrochlorothiazide and about 15 μ g/ml of levamisole hydrochloride.

Sample solutions were introduced into the capillary by the electrokinetic method at the positive end of the capillary using a constant voltage of 5 kV and a loading time of 5 s. All the experiments were completed at ambient temperature.

Procedure for capillary rinsing

In order to obtain good working conditions and reproducible data, it is helpful to wash the internal wall of the capillary between each individual injection. The capillary was washed with carrier solution after each analysis and, when the carrier solution was replaced, was washed first with water, then with 0.1 M sodium hydroxide solution, with water again and finally washed and filled with carrier solution to be used for the next run. These procedures were carried out by injecting the appropriate fluid into the capillary with a 100- μ l syringe (Hamilton, Reno, NV, USA) at the negative end.

RESULTS AND DISCUSSION

Migration characteristics

The seven active ingredients in theophylline tablets and the two internal standards were successfully separated by MECC. A typical electropherogram is shown in Fig. 1; each compound was baseline resolved.

Experimental conditions such as pH value, SDS concentration and the order of priority of consecutive runs could affect the migration behaviours of the solutes. When the concentration of SDS was 0.05 M and the applied voltage was 10 kV, the effect

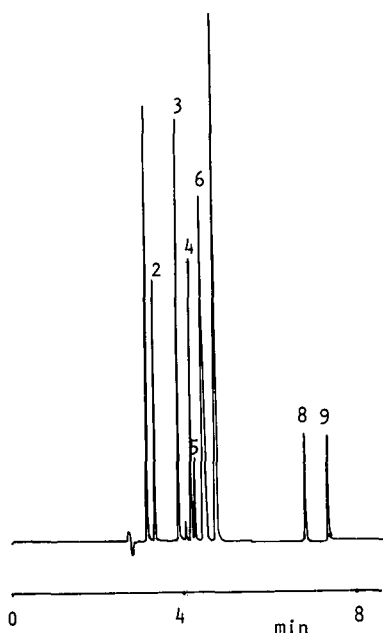


Fig. 1. Separation of seven ingredients by MECC. Carrier, 0.02 *M* borate-phosphate buffer (pH 9.2) containing 0.05 *M* SDS. Applied voltage, 10 kV. Peaks: 1 = theobromine; 2 = caffeine; 3 = hydrochlorothiazide (I.S. 1); 4 = theophylline; 5 = phenobarbital; 6 = amidopyrine; 7 = phenacetin; 8 = levamisole hydrochloride (I.S. 2); 9 = ephedrine hydrochloride.

of pH on migration time of solutes is as shown in Fig. 2. The migration times of all the solutes except theobromine and theophylline increased slightly with increasing pH from 8 to 10. In contrast, the migration times of theobromine and theophylline increased considerably. Xanthine molecules contain an acidic functional group owing to the tautomeric shift of hydrogen from nitrogen to keto oxygen (enolization), a weakly acidic H being formed on the resulting OH group [11]. Hence theobromine and theophylline gradually dissociated, having a negative charge within the above pH range, and migrated slowly towards the cathode owing to an opposite electrophoretic migration. Having no NH group to participate in enolization, caffeine is an exception. Because the acid dissociation constant ($pK_a = 8.77$) of theophylline is stronger than that of theobromine ($pK_a = 10.04$) [12], theophylline migrated more slowly than theobromine.

Phenobarbital is also an acidic compound, with

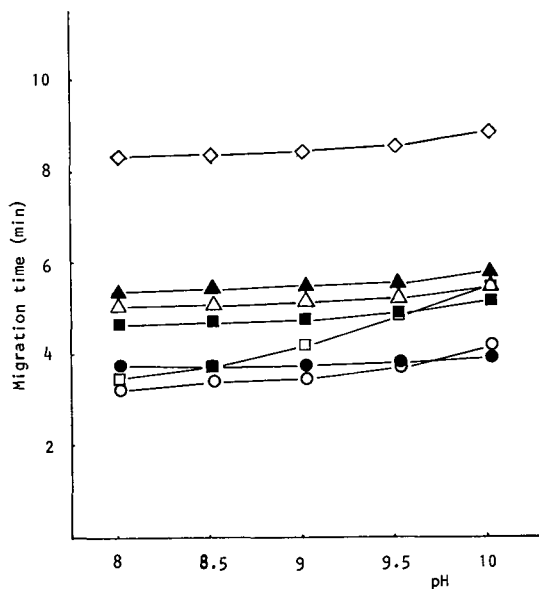


Fig. 2. Effect of pH on the migration times of (○) theobromine, (●) caffeine, (□) theophylline, (■) phenobarbital, (△) amidopyrine, (▲) phenacetin and (◇) ephedrine hydrochloride. Other conditions as in Fig. 1.

the strongest dissociation constant ($pK_1 = 7.3$, $pK_2 = 11.8$) [13] of these compounds, but its migration time did not change much. Possibly phenobarbital dissociated and achieved a sufficiently slow migration velocity prior to pH 8, also owing to its electrophoretic migration to the anode, and consequently the migration time of phenobarbital did not increase with increase in pH from 8 to 10. Also, we observed that for MECC separation a high pH is always better than a low pH.

The dependence of the migration times of the seven active ingredients on SDS concentration was examined at pH-9.2 with surfactant concentrations in the range 0–0.1 *M* (Fig. 3). Theobromine, caffeine, amidopyrine and phenacetin were not resolved by electrophoresis without SDS. The migration times of all the the ingredients increased gradually with increasing SDS concentration. The changes in the migration time of amidopyrine, phenacetin and ephedrine hydrochloride were larger, indicating that they were more readily solubilized in the surfactant, presumably owing to their higher hydrophobicity at pH 9.2.

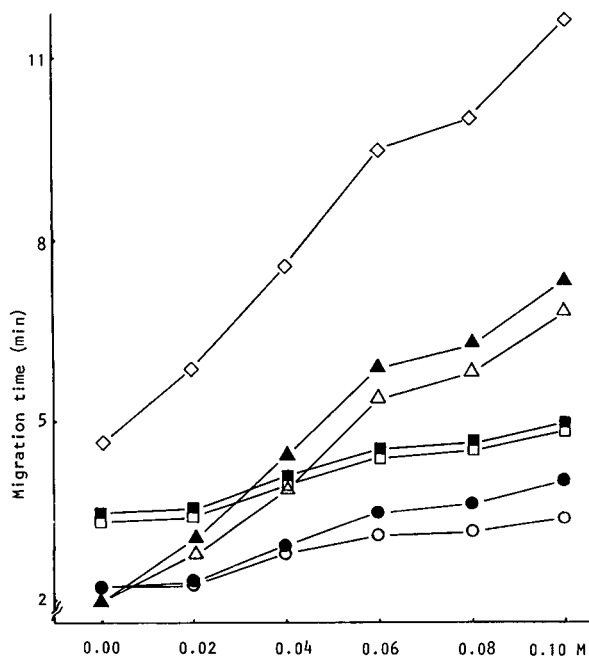


Fig. 3. Effect of SDS concentration on the migration times of solutes. Other conditions as in Fig. 1. Compound identifications as in Fig. 2.

When consecutive runs were made under constant chromatographic condition (pH 9.2, 0.05 M SDS), the migration times of the ingredients decreased with increasing number of injections. The

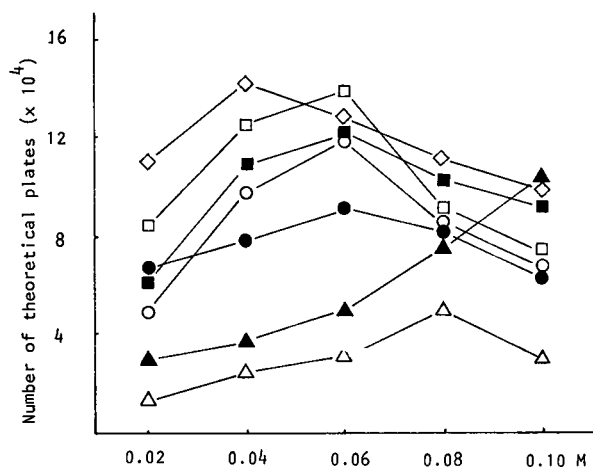


Fig. 4. Effect of SDS concentration on column efficiency. Other conditions as in Fig. 3. Compound identifications as in Fig. 2.

results indicated that the changes in the migration times of the solutes are parallel and tended gradually to become stable. This may be related to the temperature inside the capillary, which increased with the time during which the electrical field was applied, and accordingly, the migration times of the ingredients decreased slightly.

Efficiency of separation

The results of a study of the effect of surfactant concentration and applied voltage on the efficiency of separation are shown in Figs. 4 and 5. The plate number (N) was calculated according to the equation $N = 2\pi(t_R h/A)^2$, where t_R , h and A are retention time, peak height and peak area, respectively [14]. The results indicated that both of them influenced the column efficiency in MECC.

Fig. 4. shows that the separation efficiency, except for phenacetin, increased with increasing SDS concentration, but after solute-specific levels had been reached it decreased with increasing micellar concentration. The optimum surfactant concentration for the separation efficiency of most of the compounds was *ca.* 0.06 M; an SDS concentration of 0.05 M was selected for subsequent determinations.

Spaniak and Cole [3] studied the experimental factors that influence column efficiency and reported that there was an optimum applied voltage for the most efficient separation. Fig. 5 shows some

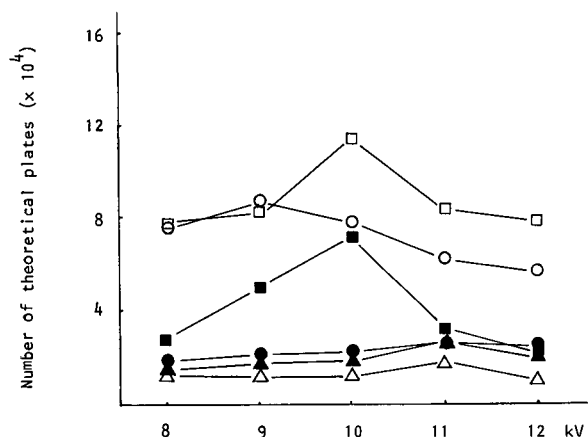


Fig. 5. Effect of applied voltage on column efficiency. Other conditions as in Fig. 1. Each point is the mean of six determinations and the R.S.D.s are between 3.7% and 6.2%. Compound identifications as in Fig. 2.

TABLE I

RESULTS OF THE DETERMINATION OF LINEAR RANGE AND RESPONSE FACTORS ($n = 6$)

Compound	Concentration range ($\mu\text{g/ml}$)	Correlation coefficient	Intercept	Slope	Response factor	R.S.D. (%)
Theobromine	20-100	0.9965	0.01483	0.6690	1.150	2.75
Caffeine	12-60	0.9998	0.01251	0.6958	1.026	3.30
Theophylline	20-100	0.9998	0.00694	0.5863	1.471	1.80
Phenobarbital	8-40	0.9999	0.00892	0.3076	1.690	4.28
Amidopyrine	80-400	0.9996	0.02781	0.2673	2.766	2.82
Phenacetin	80-400	0.9983	0.02708	0.3910	2.070	2.56
Ephedrine HCl	8-40	0.9990	0.00171	0.1408	6.838	3.24

plots of theoretical plate number vs. applied voltage, indicating that the optimum applied voltage for each of the ingredients was within the range 9-11 kV.

Quantitative analysis

Quantitative analyses were performed in three

steps, determination of linearity and response factor, test of recovery, and assay of a preparation, using 0.02 M borate-phosphate buffer solution (pH 9.2) containing 0.05 M SDS and an applied voltage of 10 kV in the constant-voltage mode, the results were calculated by the peak-height ratio method. The solutions for the determination of the linear

TABLE II

RESULTS OF RECOVERY STUDY

Six injection at each level

Compound	Amount added ($\mu\text{g/ml}$)	Amount found ($\mu\text{g/ml}$)	Recovery (%)	Average (%)	R.S.D. (%)
Theobromine	40.68	41.60	102.3	101.1	1.34
	48.78	49.48	101.4		
	59.70	59.47	99.6		
Caffeine	23.78	23.39	98.4	95.8	2.41
	30.80	28.96	94.0		
	36.75	34.87	94.9		
Theophylline	39.95	40.94	102.5	100.1	3.05
	49.90	50.48	101.2		
	63.15	61.04	96.7		
Phenobarbital	17.06	17.26	101.2	97.6	3.64
	22.36	21.80	97.5		
	23.88	22.46	94.1		
Amidopyrine	160.0	160.8	100.5	97.6	2.73
	200.6	191.2	95.3		
	240.2	233.0	97.0		
Phenacetin	162.0	156.6	96.7	95.2	1.65
	196.0	186.4	95.1		
	238.1	223.1	93.6		
Ephedrine · HCl	17.14	16.53	96.4	94.1	3.40
	19.98	18.07	90.4		
	25.22	24.04	95.3		

TABLE III
RESULTS OF THE DETERMINATION OF ACTIVE INGREDIENTS IN THEOPHYLLINE TABLETS ($n = 6$)

Compound	Label claim (mg)	Sample	Amount found (mg)	Percentage of label claim	R.S.D. (%)
Theobromine	25	A	26.7	106.6	1.64
		B	24.5	98.2	1.24
		C	24.8	99.2	2.47
Caffeine	15	A	14.4	95.7	2.18
		B	13.8	92.0	1.62
		C	14.0	93.0	2.17
Theophylline	25	A	25.0	99.9	3.05
		B	24.4	97.6	3.15
		C	25.9	103.4	1.30
Phenobarbital	10	A	10.1	101.1	4.46
		B	9.5	94.8	2.16
		C	9.8	97.8	4.07
Amidopyrine	100	A	96.8	96.8	1.20
		B	99.5	99.5	2.30
		C	98.8	98.8	2.50
Phenacetin	100	A	91.6	91.6	1.75
		B	97.7	97.7	2.88
		C	96.2	96.2	2.38
Ephedrine · HCl	10	A	9.2	92.3	3.98
		B	9.2	91.9	3.86
		C	9.9	99.2	3.83

range and relative response factor were chromatographed and the calibration graphs of h_s/h_i vs. M_s/M_i , where h_s and h_i are peak heights and M_s and M_i are the masses of the sample (s) and internal standard (i), showed good linearity over a suitable range. Response factors relative to internal stan-

TABLE IV
COMPARISON OF THE PRECISION [SHOWN BY R.S.D. ($n = 6$)] BETWEEN PEAK-HEIGHT RATIOS AND PEAK-AREA RATIOS

Compound	R.S.D. (%)	
	Peak-height ratio	Peak-area ratio
Theobromine	3.78	5.36
Caffeine	3.21	5.86
Theophylline	2.12	5.79
Phenobarbital	2.28	4.57
Amidopyrine	3.28	5.01
Phenacetin	2.86	4.78
Ephedrine · HCl	3.38	—

dards were calculated by a general method and all the results are given in Table I.

Under the chromatographic conditions described above, recoveries were checked at three concentration levels and six repeated injections per level. The results and their relative standard deviations are given in Table II and show that the average recoveries were fairly good.

The assay of theophylline tablets was performed according to the above procedure under the optimized conditions. The results are given in Table III and suggest that MECC is suitable for the analysis of multi-component preparations.

Reproducibility

The chromatographic results obtained by consecutive runs under the same experimental conditions indicated that peak-height ratios changed with increasing number of injections in addition to the change in migration time described above. The peak-height ratios of the ingredients that migrated rapidly tended to increase and those of the ingre-

dients that migrated slowly tended to decrease; the longer the migration time of an ingredient, the greater was its change. This is presumably due to different adsorption, relative to the internal standard, of the sample migrating at a different velocity on the internal wall of the capillary with increasing temperature inside the capillary.

In this work, the quantitative results were calculated using peak-height ratio method, as the precision of the results was better than that given by the peak-area ratio method (Table IV).

For the solutes that migrate slowly and are of low concentration in a pharmaceutical preparation, in addition to the unfavourable effects of the MECC technique itself, large differences in retention times and responses between a solute and internal standard may result in poor precision in quantitative analysis. In this work ephedrine hydrochloride, similarly to trimethoprim in a previous study [8], belonged to this category. The use of a second internal standard, levamisole hydrochloride, which was located near ephedrine hydrochloride on the chromatogram, improved the reproducibility for ephedrine hydrochloride.

REFERENCES

- 1 S. Terabe, K. Otsuka, K. Ichikawa, A. Tsuchiya and T. Ando, *Anal. Chem.*, 56 (1984) 111.
- 2 S. Terabe, K. Otsuka and T. Ando, *Anal. Chem.*, 57 (1985) 834.
- 3 M. J. Sepaniak and R. O. Cole, *Anal. Chem.*, 59 (1987) 472.
- 4 G. Werner, *Anal. Chem.*, 62 (1990) 403R.
- 5 K. Otsuka, S. Terabe and T. Ando, *J. Chromatogr.*, 348 (1985) 39.
- 6 H. Nishi, T. Fukuyama and M. Matsuo, *J. Chromatogr.*, 515 (1990) 245.
- 7 H. Nishi, N. Tsumagari, T. Kakimoto and S. Terabe, *J. Chromatogr.*, 479 (1989) 259.
- 8 Q. X. Dang, Z. P. Sun and D. K. Ling, *J. Chromatogr.*, 603 (1992) 259.
- 9 H. Nishi, T. Fukuyama, M. Matsuo and S. Terabe, *J. Chromatogr.*, 513 (1990) 279.
- 10 H. Nishi, T. Fukuyama, M. Matsuo and S. Terabe, *J. Chromatogr.*, 498 (1990) 313.
- 11 V. S. Venturella, in A. R. Gennaro, R. E. King, G. D. Chase, A. N. Martin, M. R. Gibson, T. Medwick, C. B. Granberg, E. A. Swinyard, S. C. Harvey and G. L. Zink (Editors), *Remington's Pharmaceutical Sciences*, Mack, Easton, PA, 17th ed., 1985, Ch. 25, p. 419.
- 12 S. Budavari, M. J. O'Neil, A. Smith and P. E. Heckelman, *The Merck Index*, Merck, Rahway, NY, 11th ed., 1989, pp. 1460–1461.
- 13 S. Budavari, M. J. O'Neil, A. Smith and P. E. Heckelman, *The Merck Index*, Merck, Rahway, NJ, 11th ed., 1989, p. 1149.
- 14 L. R. Snyder and J. J. Kirkland, *Introduction to Modern Liquid Chromatography*, Wiley, New York, 2nd ed., 1979, pp. 222–223.

Determination of alkylphosphonic acids by capillary zone electrophoresis using indirect UV detection

G. A. Pianetti

Laboratoire de Chimie Analytique, Faculté de Pharmacie, 5 Rue J. B. Clément, F-92290 Chatenay-Malabry (France) and Laboratório de Controle de Qualidade de Produtos Farmacêuticos e Cosméticos, Faculdade de Farmácia UFMG, Belo Horizonte, MG (Brazil)

M. Taverna, A. Baillet, G. Mahuzier and D. Baylocq-Ferrier

Laboratoire de Chimie Analytique, Faculté de Pharmacie, 5 Rue J. B. Clément, F-92290 Chatenay-Malabry (France)

(First received August 12th, 1992; revised manuscript received October 23rd, 1992)

ABSTRACT

Capillary zone electrophoresis with indirect UV detection was used for the determination of a series of alkylphosphonic acids. For this purpose, a few UV-absorbing background electrolytes were tested and phenylphosphonic acid, which has a mobility close to that of the analysed compounds, was shown to be the most suitable. The influence of several parameters such as concentration of the UV-absorbing background electrolyte and concentration of borate on both sensitivity and efficiency was investigated. An increase in the borate concentration produced an improvement of the signal-to-noise ratio. Conversely, the sensitivity decreased with increasing concentration of the phenylphosphonic acid. The reproducibility of the method was very satisfactory and limits of detection were less than 0.21 pmol injected.

INTRODUCTION

Alkylphosphonic acids represent a great variety of components which are widely used as herbicides, insecticides and antibiotics. The determination of these compounds is of relevance not only in the environmental field, owing their biocidal potency, but also in biological fluids for trace determinations of antibacterial (fosfomycin) or antiviral compounds (foscarnet). However, the alkylphosphonic acids do not absorb or fluoresce in the UV or visible spectral range, which is why many attempts have been made by different workers to convert these compounds into ester derivatives to allow their separation by GC [1–4] or to produce fluorescing [5] or UV-absorbing species [6] for their analysis by RP-HPLC.

Schiff *et al.* [7] described an ion chromatographic method for the analysis of phosphonic acids, but the technique is limited by the poor efficiency and the low sensitivity achieved using conductimetric detection. Other direct detection methods such as mass spectrometry [8] and dual flame photometry–phosphorus-selective detection [9] have also been mentioned.

Here we report the separation of linear alkylphosphonic acids using capillary zone electrophoresis (CZE). A series of homologous alkylphosphonic acids was selected to evaluate the applicability of the method to separate related compounds and to obtain more information on the selectivity of this technique. No derivatization was required as indirect UV detection was used to monitor these compounds. Parameters affecting both efficiency of separation and sensitivity, such as the nature of the UV-absorbing background electrolyte and its concentration, were investigated. Finally, the method

Correspondence to: A. Baillet, Laboratoire de Chimie Analytique, Faculté de Pharmacie, 5 Rue J.B. Clément, F-92290 Chatenay-Malabry, France.

was validated in terms of limits of detection, linearity of the response and reproducibility.

EXPERIMENTAL

Chemicals

The formulae of the alkylphosphonic acids used are shown in Fig. 1. Methylphosphonic acid (MPA), ethylphosphonic acid (EPA), propylphosphonic acid (PPA) and butylphosphonic acid (BPA) were obtained from Aldrich (St. Quentin Fallavier, France). Standard solutions of each alkylphosphonic acid were prepared in distilled water at a 0.5 mg ml⁻¹ concentration. The working solution consisted of a mixture of the four alkylphosphonic acids at a 0.1 mg ml⁻¹ concentration. Boric acid and phthalic acid were purchased from Sigma (St. Quentin Fallavier, France), benzoic acid from Pro-labo (Paris, France) and phenylphosphonic acid from Fluka (Mulhouse, France). A 2 M NaOH solution used to adjust the pH of the buffer was obtained from Merck (Nogent-sur-Marne, France). All other chemicals were of analytical-reagent grade.

Apparatus

CZE experiments were performed using a P/ACE 2000 system (Beckman, Gagny, France), at 30 kV. The temperature was set at 30°C. A fused-silica cap-

illary with an effective length of 50 cm (total length 57 cm) and 75 μm I.D. was used for the separation. Samples were introduced into the capillary by hydrodynamic injection for 3 s. Two wavelengths of UV detection were chosen according to the nature of the UV-absorbing background electrolyte in order to obtain the best sensitivity: 200 nm for indirect detection when phenylphosphonic acid was added to the buffer, otherwise 254 nm. Direct UV analyses, performed to calculate the electrophoretic mobilities of benzoic acid, phenylphosphonic acid, phthalic acid and sorbic acid, were carried out at 200 nm.

Procedures

A 200 mM sodium borate buffer (pH 6.0) was employed for direct UV analyses while various concentrations of the UV-absorbing background electrolyte were added to perform the indirect UV measurements. For comparison studies, 10 mM of either sorbic acid, phenylphosphonic acid or benzoic acid were added to 100 mM borate buffer (pH 6.0). All buffers were filtered through a 0.22-μm membrane (Millex-Millipore, St. Quentin-en-Yvelines, France) prior to use. Before each run, the capillary was rinsed with 0.1 M NaOH and then filled with the running buffer.

RESULTS AND DISCUSSION

As shown in Fig. 2, the four alkylphosphonic acids were separated in less than 9 min. The anionic species were transported to the cathode by the competition of the electroosmotic flow and the electrophoretic flow. The separation was carried out with the monoionic acid alkylphosphonic acids, which permitted a shorter analysis time than with dianionic species. At the chosen pH of 6.0, the monoionized form was predominant for all the investigated alkylphosphonic acids with respect to their pK_{a2} values (MPA = 7.10, EPA = 8.05, PPA = 8.18 and BPA = 8.19 at 25°C). Moreover, at this pH, the amplitude of electroosmotic flow was high enough to allow their migration towards the cathode. As expected, the order of migration is inversely related to the number of CH₂ groups as the electrophoretic mobility decreases with increasing relative molecular mass. As shown in Fig. 3, a linear relationship was observed between the charge/mass ratio of the com-

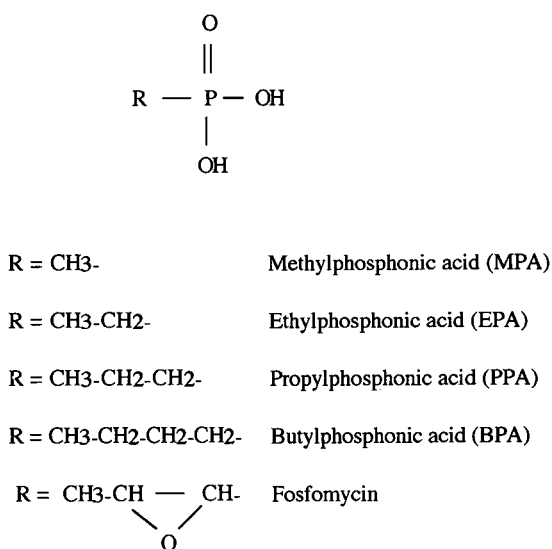


Fig. 1. Structural formulae of the alkylphosphonic acids used.

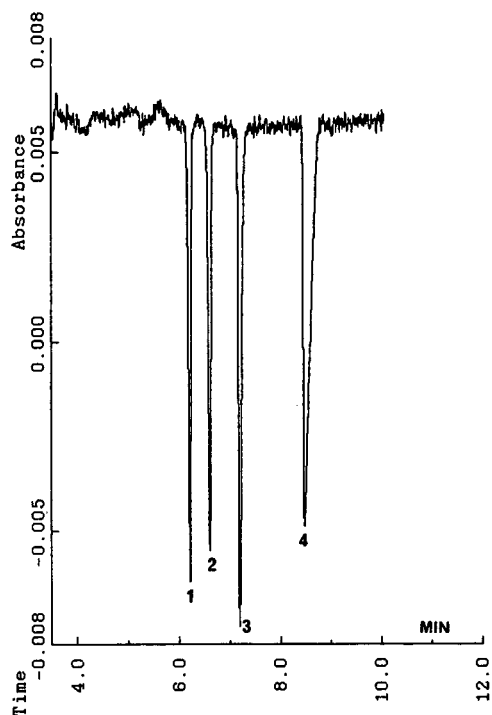


Fig. 2. Separation of alkylphosphonic acids by CZE. Conditions: 200 mM sodium borate buffer (pH 6.0)–10 mM phenylphosphonic acid; fused silica, 50 cm \times 75 μ m I.D.; applied voltage, 30 kV; temperature, 30°C. Peaks: 1 = BPA; 2 = PPA; 3 = EPA; 4 = MPA.

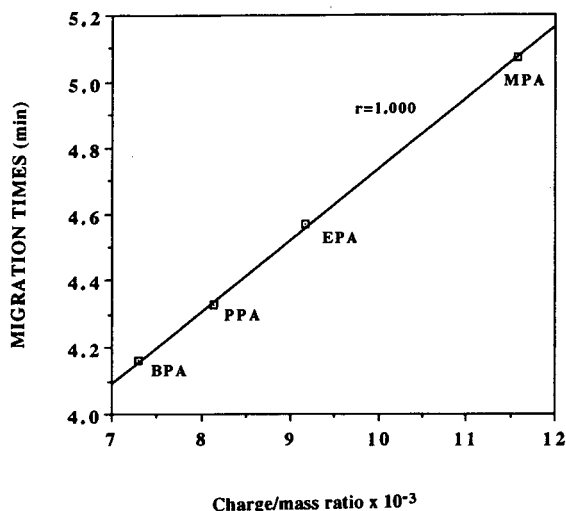


Fig. 3. Plot of the charge/mass ratios of alkylphosphonic acids versus their migration times.

pounds and their migration time for MPA, EPA, PPA and BPA ($r = 1.000$). The migration time of methanol used as the neutral marker was 2.35 min. At the temperature set for the analysis (30°C) the pK_{a2} value of MPA is 7.0 and is therefore the lowest of all the investigated alkylphosphonic acids. As the separation was carried out at pH 6.0, we assumed that the diionized form of MPA represents 10% of the total MPA. The presence of this diionized form leads to a shift of the monoionized MPA to a higher apparent mobility. This feature could be corrected by applying to MPA a charge of 1.1 (10% of diionized and 90% of monoionized) instead of 1.0.

Choice of the UV-absorbing background electrolyte

Selection of the most suitable UV-absorbing background electrolyte is conditioned by a few parameters that affect both the sensitivity of detection and the efficiency of separation. These two factors depend mostly on the electromigration dispersion. The highest sensitivity can be achieved for compounds having apparent mobilities close to the mobility of the UV-absorbing background electrolyte. The sensitivity of detection can be greatly increased by using a low-concentration but highly UV-absorbing background electrolyte [10]. Efficiencies are improved by using UV-absorbing background ions with a low mobility in order to diminish the dispersion phenomenon due to Joule heating [11]. The selection of a UV-absorbing background ion with an apparent mobility close to those of the analysed compounds will lead to symmetrical peaks and a negligible band-broadening, resulting in higher efficiency [10,12]. In fact, anionic compounds which exhibit, for example, a higher mobility than that of the UV-absorbing background ion will give rise to broad peaks with a diffuse front and sharp rear boundary. Consequently, the detection response will be lower for these compounds.

The electrophoretic mobilities of various electrolytes were determined at 30 kV using borate buffer (pH 6.0). Methanol was used as the marker of the electroosmotic flow. The calculated electrophoretic mobilities were $-33.25 \cdot 10^{-5}$, $-33.42 \cdot 10^{-5}$, $-30.87 \cdot 10^{-5}$ and $-30.50 \cdot 10^{-5}$ $\text{cm}^2 \text{V}^{-1} \text{s}^{-1}$ for benzoic acid, phthalic acid, sorbic acid and phenylphosphonic acid, respectively. As the electrophoretic mobilities of alkylphosphonic acids ranged from $-27.17 \cdot 10^{-5}$ (BPA) to $-34.33 \cdot 10^{-5}$ $\text{cm}^2 \text{V}^{-1} \text{s}^{-1}$

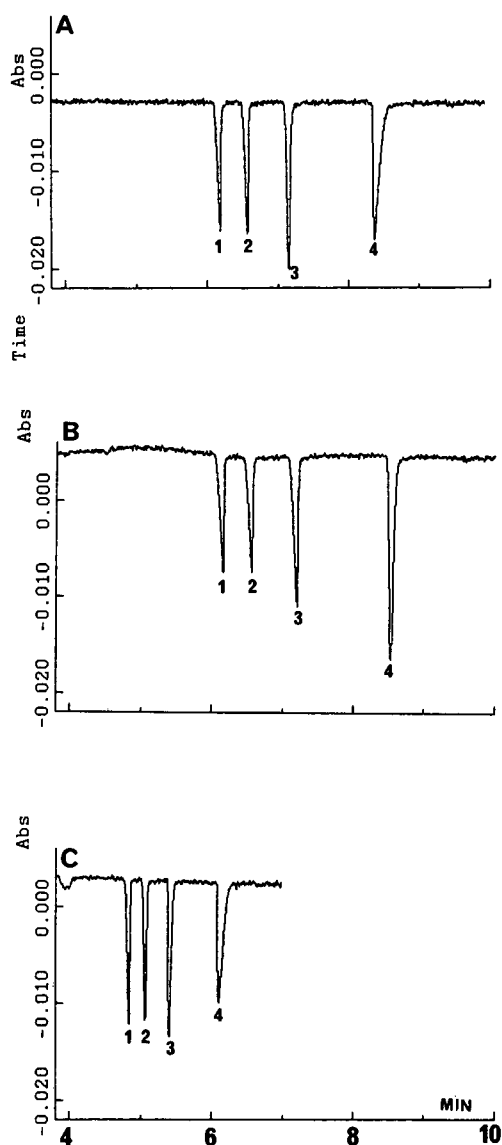


Fig. 4. Electrophoretic profiles obtained in three different buffer systems: 100 mM sodium borate buffer (pH 6.0) containing 10 mM of (A) sorbic acid, (B) benzoic acid and (C) phenylphosphonic acid. Other conditions as in Fig. 2.

(MPA), we selected three of them, benzoic acid, sorbic acid and phenylphosphonic acid, to investigate the sensitivity, efficiency and time of the separation. Fig. 4 shows the electrophoretic profiles obtained using 100 mM sodium borate buffer (pH 6.0) with the three UV-absorbing background electrolytes.

Fig. 5 compares the performances of the three

UV-absorbing background electrolytes in terms of resolution, migration time and sensitivity of detection. For the purpose of comparison, experimental conditions such as pH, concentration of borate and concentration of the UV-absorbing background ion were kept constant. The applied voltage was 30 kV and the temperature was set at $30 \pm 1^\circ\text{C}$. The sample consisted of a mixture of the four alkylphosphonic acids, each at 0.1 mg ml^{-1} . Resolution factors calculated for each adjacent peaks were above 2.5, indicating that the resolution was very satisfactory regardless of the nature of the UV-absorbing background electrolyte. In contrast to what is commonly observed using chromatographic methods, the resolution between adjacent peaks increases with the migration times and is therefore higher between EPA and MPA than between BPA and PPA. On the other hand, we achieved the best resolution with benzoic acid. The shortest analysis time was obtained when phenylphosphonic acid was added to the buffer. Accordingly, peaks were broader using the two other UV-absorbing ions.

A more important feature is the comparison between the sensitivity, expressed as the signal-to-noise ratio, achieved for the various alkylphosphonic acids with the three different systems. Three of the four compounds studied showed a much better sensitivity using phenylphosphonic acid, whereas for MPA the sensitivity was of the same order with benzoic acid and phenylphosphonic acid. When phenylphosphonic acid was employed, a slightly higher sensitivity of detection was observed for EPA, which could be attributed to its closer electrophoretic mobility to that of phenylphosphonic acid. As a consequence of the short eluting period (1.2 min), the EPA, PPA and BPA response coefficients are very similar. MPA, which is the slowest ion, produces an asymmetric peak with a sharp front and a diffuse rear boundary, giving rise to a poorer sensitivity. In contrast, using benzoic acid as the absorbing electrolyte, the sensitivity is higher for MPA than for the other alkylphosphonic acids investigated because it has roughly the same electrophoretic mobility as benzoic acid.

Apparently, the use of phenylphosphonic acid provides satisfactory results. With regard to both sensitivity and efficiency this UV-absorbing background ion seems to be the most suitable. As expected, the number of theoretical plates obtained

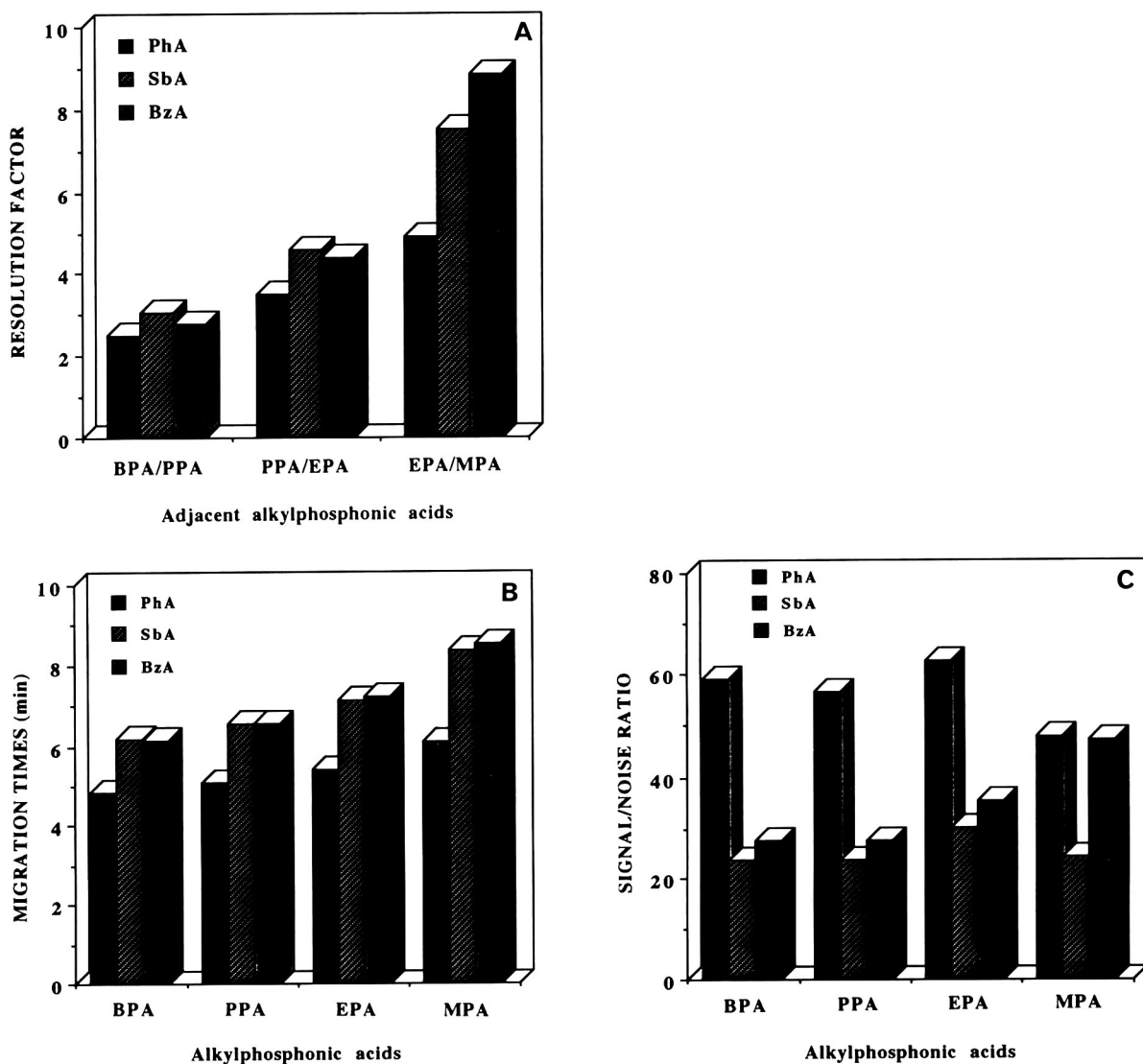


Fig. 5. Comparison of (A) resolution factors, (B) migration times and (C) signal-to-noise ratios determined with buffer systems containing either sorbic acid (SbA), benzoic acid (BzA) or phenylphosphonic acid (PhA) as the UV-absorbing background electrolyte. For conditions, see Experimental.

with this buffer is better for EPA ($N = 53\,500$), having an electrophoretic mobility close to that of phenylphosphonic acid. The number was lower for MPA ($N = 37\,300$), which exhibits a greater difference in the electrophoretic mobilities.

Optimization of the electrophoretic parameters

In an attempt to improve the separation, we sub-

sequently investigated the influence of the sodium borate and phenylphosphonic acid concentrations on the quality of the separation. Fig. 6 shows the influence of the concentrations of sodium borate and phenylphosphonic acid on the signal-to-noise ratio. A general trend was observed with the variation of the concentration of sodium borate from 50 to 200 mM, higher concentrations producing an ap-

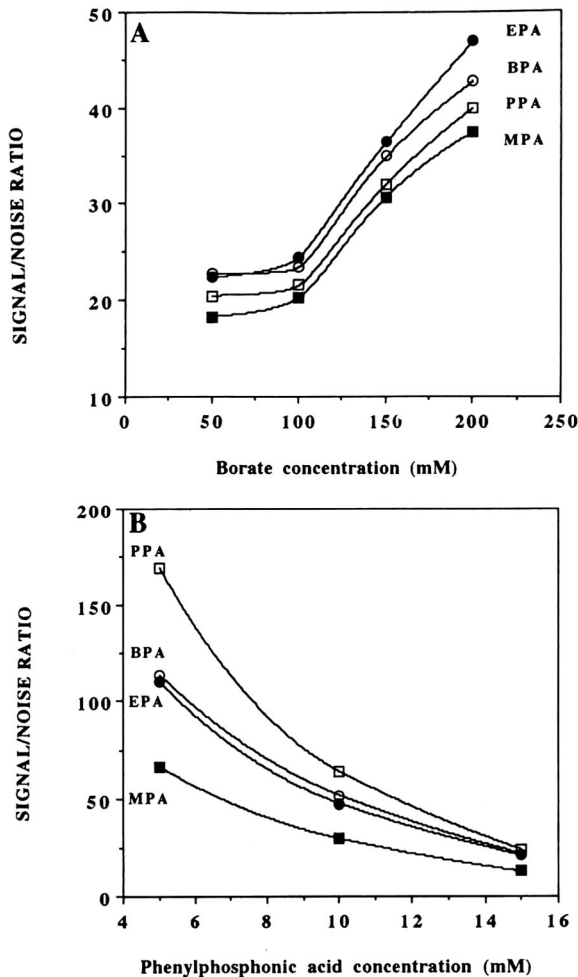


Fig. 6. Variation of the signal-to-noise ratio with increasing (A) sodium borate and (B) phenylphosphonic acid concentration. The concentration of phenylphosphonic acid was kept at 10 mM in (A) and that of sodium borate at 200 mM in (B). Other conditions as in Fig. 3.

TABLE I

REPEATABILITY AND REPRODUCIBILITY OF THE ELECTROPHORETIC MOBILITIES (μ_{ep} AND PEAK HEIGHTS EXPRESSED AS RELATIVE STANDARD DEVIATION

Factor	Parameter	BPA	PPA	EPA	MPA
Repeatability (%) ($n = 8$)	μ_{ep}	0.93	1.80	1.66	1.47
	Peak height	2.09	2.34	2.45	1.44
Reproducibility (%) ($n = 17$)	μ_{ep}	1.39	1.80	1.78	1.65
	Peak height	3.62	3.81	2.95	1.97

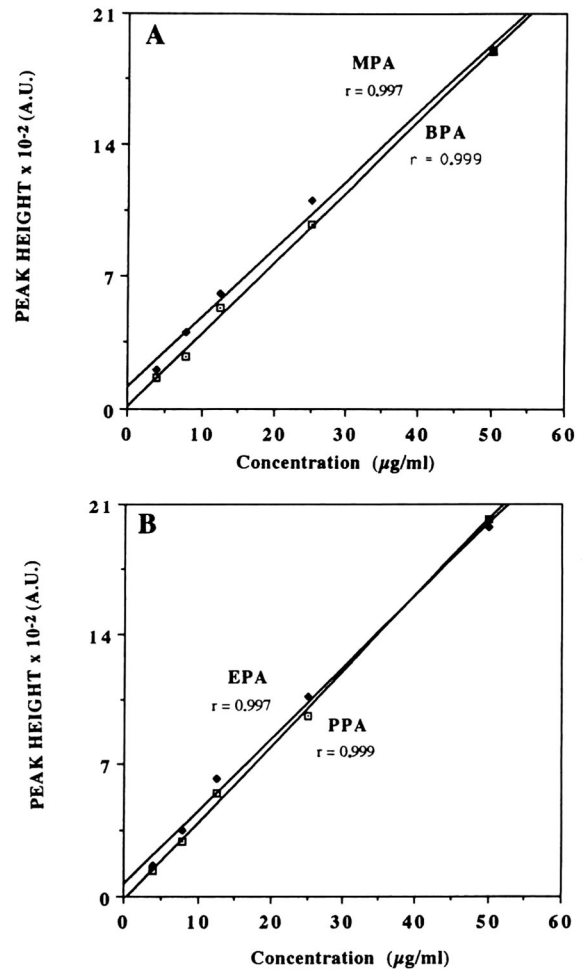


Fig. 7. Calibration graphs obtained for (A) MPA–BPA and (B) EPA–PPA.

preciable improvement in the signal-to-noise ratio. In contrast, the sensitivity increased with a decrease in the concentration of phenylphosphonic acid, which is in agreement with the results reported by Foret *et al.* [10] and Nielen [12]. In addition, a substantial increase in the migration times is observed with increasing concentration of phenylphosphonic acid. Lowering the concentration to 5 mM leads to baseline perturbations. Accordingly, a 10 mM concentration of phenylphosphoric acid was found to be the best compromise between high sensitivity and buffer stability and 200 mM sodium borate was chosen to produce the best signal-to-noise ratio.

Validation of the method

Detection limits, expressed as twice the baseline noise, ranged from 0.15 to 0.21 pmol injected, making this method more sensitive than some of those previously reported such as ion chromatography [7] or column liquid chromatography with detection of alkylphosphonic acids as their bromophenacyl esters [6]. The present technique is at least as sensitive as gas chromatography [3,4], while column liquid chromatography coupled with a laser fluorimetric detection allowed detection in the femtomole range [5]. Nevertheless, these techniques require a long esterification procedure and/or an extraction step with poor recoveries. However, even though the minimum amount of sample injected is very small using CZE, the small volumes injected (less than 10 nl) require solution concentrations as high as $2 \mu\text{g ml}^{-1}$.

Calibration graphs obtained for MPA, EPA, PPA and BPA showed a linear response of the detector in the concentration range studied ($5\text{--}50 \mu\text{g ml}^{-1}$) (Fig. 7). Values of peak heights represent the average of five experimental data. The slopes were similar for all the alkylphosphonic acids investigated.

The repeatability ($n = 8$) and between-day reproducibility ($n = 17$) of the method were evaluated and the results are summarized in Table I. With regard to the relative standard deviations (less than 1.8%), we concluded that the electrophoretic mobilities are very reproducible. The relative standard deviations for the peak heights are satisfactory (less than 3.8%), given that absolute peak heights are involved.

CONCLUSIONS

The proposed method was able to separate different alkylphosphonic acids according to their size. We stress the reliability of this technique, which is rapid and sensitive. The method can be applied to a wide range of alkylphosphonic acid derivatives and current studies are directed towards its application to the determination of fosfomycin and foscarnet in biological sera.

REFERENCES

- 1 M. L. Rueppel, L. A. Suba and J. T. Marvel, *Biomed. Mass Spectrom.*, 3 (1976) 28.
- 2 C. G. Daughton, A. M. Cook and M. Alexander, *Anal. Chem.*, 51 (1979) 1949.
- 3 J. Aa. Tørnes and B. A. Johnsen, *J. Chromatogr.*, 467 (1989) 129.
- 4 M. L. Shih, J. R. Smith, J. D. McMonagle, T. W. Dolzine and V. C. Gresham, *Biol. Mass Spectrom.*, 20 (1991) 717.
- 5 M. C. Roach, L. W. Ungar, R. N. Zare, L. M. Reimer, D. L. Pompliano and J. W. Frost, *Anal. Chem.*, 59 (1987) 1056.
- 6 P. C. Bossle, J. J. Martin, E. W. Sarver and H. Z. Sommer, *J. Chromatogr.*, 267 (1983) 209.
- 7 L. J. Schiff, S. G. Pleva and E. W. Sarver, in J. D. Mulick and E. Sawicki (Editors), *Ion Chromatographic Analysis of Environmental Pollutants*, Vol. 2, 1979, pp. 329–344.
- 8 E. R. J. Wils and A. G. Hulst, *J. Chromatogr.*, 454 (1988) 261.
- 9 T. L. Chester, *Anal. Chem.*, 52 (1980) 1621.
- 10 F. Foret, S. Fanali, L. Ossicini and P. Bocek, *J. Chromatogr.*, 470 (1989) 299.
- 11 H. T. Rasmussen and H. M. McNair, *J. Chromatogr.*, 516 (1990) 223.
- 12 M. W. F. Nielen, *J. Chromatogr.*, 588 (1991) 321.

Metal ion capillary zone electrophoresis with direct UV detection: determination of transition metals using an 8-hydroxyquinoline-5-sulphonic acid chelating system

A. R. Timerbaev[☆], W. Buchberger, O. P. Semenova and G. K. Bonn

Department of Analytical Chemistry, Johannes Kepler University Linz, Altenbergerstrasse 69, A-4040 Linz (Austria)

(Received August 11th, 1992)

ABSTRACT

The application of capillary zone electrophoresis to the separation and determination of metal ions after the precolumn formation of negatively charged chelates is described. Multi-component mixtures of transition metal complexes with 8-hydroxyquinoline-5-sulphonic acid (HQS) were separated in about 10 min in a fused-silica capillary column with a borate buffer of pH 9.2 at an applied voltage of 15 kV followed by direct UV detection. The capillary pretreatment with an electroosmotic flow modifier, namely a tetraalkylammonium salt, is necessary to achieve reasonable migration times of these metal complexes. Incorporating the chelating reagent in the electrophoretic buffer markedly improves the detectability of relatively unstable chelates, such as those of Co(II), Zn(II) and Cd(II), and allows the separation of metal ions that form unstable HQS chelates, such as Mn(II) and alkaline earth metals. The effects of electrophoretic buffer parameters affecting the complexation reaction and migration behaviour are discussed. Linearity of calibration graphs is observed for about three orders of magnitude with sub-ppm detection limits. The applicability of the method to the analysis of real samples is demonstrated.

INTRODUCTION

High-performance capillary zone electrophoresis (CE) is a highly efficient separation method capable of yielding excellent resolution of ionized compounds based on the combined effects of electrophoresis and electroosmosis. Although a multitude of CE applications have been reported in the past decade, this method has been introduced into inorganic analysis only in the last 3 years [1–4]. The determination of metal ions by CE, particularly transition metal ions as ionic species of nearly identical charge and dimensions, and hence very similar electrophoretic mobilities, is still a complicated

problem because the efficiency of CE might often be inadequate for the separation. Obviously, the enhancement of separation selectivity would be the only alternative to achieve a satisfactory resolution.

A fairly promising approach in this direction is based on the addition of complexing components to the electrophoretic buffer. These complexing agents can selectively moderate the mobility of metal cations owing to the formation of metal complexes of different stability within the capillary. This CE separation mode was first proposed by Foret *et al.* [5] in combination with indirect UV detection for the separation of lanthanides (using hydroxyisobutyric acid as a complexing counter ion) and then intensively developed by Weston *et al.* [6]. Swaile and Sepaniak [7] employed the formation of fluorescent complexes of 8-hydroxyquinoline-5-sulphonic acid (HQS) for the sensitive detection of metal ions separated by CE using laser-based fluorimetry.

Another promising possibility of complexation

Correspondence to: A. R. Timerbaev, Department of Analytical Chemistry, Johannes Kepler University Linz, Altenbergerstrasse 69, A-4040 Linz, Austria.

[☆] Permanent address: Mendeleev Moscow Institute of Chemical Technology, 125190 Moscow, Russian Federation.

CE is the complete conversion of metal ions into negatively charged chelates (instead of establishing only an equilibrium between free and complexed metal ions), which can move with different mobilities in the opposite cathode-to-anode direction. In addition, direct spectrophotometric detection of metal chelates can be performed, as has been used in ion chromatography [8,9].

This paper presents a detailed evaluation of HQS for the CE of transition and alkaline earth metals as precolumn-formed chelates. The migration behaviour and the optimization of the separation conditions for metal–HQS complexes by controlling the electrophoretic buffer parameters are discussed. Special attention is paid to consideration of the effects of the precolumn and on-column complexation conditions on mobility, separation efficiency and detectability.

EXPERIMENTAL

Reagents

8-Hydroxyquinoline-5-sulphonic acid was obtained from Aldrich Chemie (Steinheim, Germany). The reagent was dissolved in 0.01 M sodium tetraborate to give a $5 \cdot 10^{-3}$ M stock solution. Standard solutions of metal ions were prepared from the nitrates (Merck, Darmstadt, Germany) at a concentration $2 \cdot 10^{-3}$ M in 0.01 M nitric acid. Borate buffers prepared by dissolving appropriate amounts of sodium tetraborate (Merck) in doubly distilled water and containing $1 \cdot 10^{-4}$ M HQS were used as the main electrophoretic buffers. The pH of the electrophoretic buffer was adjusted with 0.1 M HCl or NaOH. All chemicals were of analytical-reagent grade.

Apparatus

A Waters Quanta 4000 CE system with a negative and a positive high-voltage power supply was used. Separations were carried out in a fused-silica capillary of 35 cm in effective length and 75 μ m I.D. obtained from Waters (AccuSep). The voltage applied was adjusted to 15 kV. Detection was performed by on-column UV measurements at 254 nm. Electropherograms were recorded and processed with a Hewlett-Packard Model 3359 data acquisition system.

Procedure

For conditioning of the capillary, it was flushed once a week with 5 mM tetradecyltrimethylammonium bromide (TTMAB) (Fluka, Buchs, Switzerland) for 15 min followed by water and the electrophoretic buffer for the same duration. All electrophoretic buffers were filtered through 0.45- μ m membrane filters before use. The sample solutions were injected with a siphonic injection technique for a specified time and were separated using the negative power supply. Electroosmotic flow velocity was determined from the migration time of acetophenone (Merck), which served as a neutral marker, using the positive power supply.

Sample preparation

Samples of tap water were acidified to pH \approx 2 with concentrated nitric acid and stored in a refrigerator in polyethylene bottles at 4°C prior to analysis.

RESULTS AND DISCUSSION

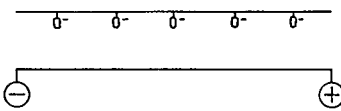
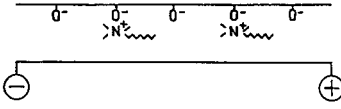
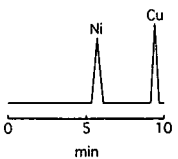
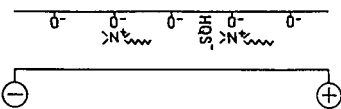
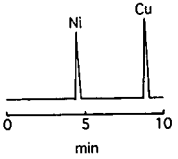
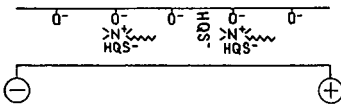
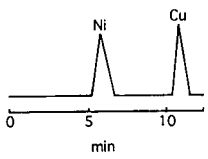
Capillary electrophoretic behaviour of metal–HQS complexes

In CE, separation is based on the differences in electrophoretic mobility (EPM) of solutes in the presence of an electric field, which is dependent on the charge and size of the solutes. In this investigation, the electroosmotic flow (EOF) was towards the cathode whereas the electrophoretic flow (EPF) was in the opposite direction, in contrast to ref. 7, where both EPF and EOF were towards the detector (the negative end of the capillary). Another distinguishing feature of the CE system studied by Swaile and Sepaniak [7] is that the metal analytes (zinc, magnesium and calcium) were separated in the HQS-complexes form, but of different composition and charge (due to the stepwise complexation equilibrium under CE conditions). Thus, for metal–HQS complexes as for the negatively charged solutes, the migration direction and velocity must be strongly influenced by the electrophoretic *versus* electroosmotic flow ratio and, consequently, by CE system parameters affecting the vectorial combination of EPM and electroosmotic mobility (EOM).

According to the above, we observed the following migration behaviour of the complexes depicted schematically in Table I. Using an untreated fused-

TABLE I

MIGRATION BEHAVIOUR OF METAL–HQS COMPLEXES IN CAPILLARY ZONE ELECTROPHORESIS

CE conditions	Electrophoresis versus electroosmosis and modification effects in the capillary	CE behaviour
(A) Untreated capillary–borate buffer	 $ \mu_{eo} \gg \mu_{ep} ; \mu_{ob} < 0$	No peaks
(B) Capillary pretreated with TTMAB–borate buffer	 $ \mu_{ep} > \mu_{eo} ; \mu_{ob} > 0$	
(C) Pretreated capillary–borate buffer + 0.1–0.2 mM HQS	 $ \mu_{ep} > \mu_{eo} ; \mu_{ob} > 0$	
(D) Pretreated capillary–borate buffer + 0.4 mM HQS	 $ \mu_{ep} \geq \mu_{eo} ; \mu_{ob} > 0$	

silica capillary and alkaline buffers, no peaks could be recorded in the electropherograms, because under these conditions the EOF ($-71.7 \cdot 10^{-5} \text{ cm}^{-2}/\text{V} \cdot \text{s}$ in 10 mM borate buffer) is much higher than the EPM (Table I, A) and metal complexes move to the cathode (reversed movement), their velocity decreasing with increasing EPM. A further reason for the non-appearance of peaks might be that the complexes undergo decomposition as a result of ligand-exchange reactions with surface silanol groups. This experimental fact is well described in reversed-phase chromatography [10].

The treatment of the capillary with a hydrophobic tetraalkylammonium salt, namely TTMAB, resulted in a marked decrease in EOF ($\mu_{eo} = -19.8 \cdot 10^{-5} \text{ cm}^2/\text{V} \cdot \text{s}$). As a result, the EPM becomes large enough to counteract the EOF (Table I, B) and the complexes migrate in the opposite direction (decel-

erated movement). With the treated capillary, the apparent mobilities correspond to the EPM.

It should be noted that the migration order of metal–HQS complexes is completely the reverse of the elution sequence of these chelates in ion-pair reversed-phase chromatography [11]. The CE separation may be explained (i) by some “chromatographic” effects (see below) and (ii) by the effective charge of the solute, which can be a factor controlling the migration ability (divalent metal 1:2 complexes are of approximately the same size). In confirmation, the overall stability constants, β_n , as a parameter closely connected with the electron-acceptor strength of metal ion, were found to be well correlated with normalized observed mobilities, μ'_{ob} (M) = $\mu_{ob}(M) / \mu_{ob}(Fe)$, where M = metal (Fig. 1; to obtain more reproducible results, the iron complex was used as an internal standard).

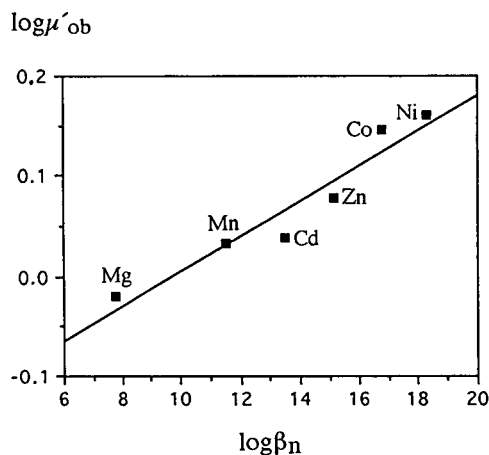


Fig. 1. Plot of $\log \mu'_{ob}$ vs. $\log \beta_n$ values for metal-HQS chelates.

When the free ligand is added to the electrophoretic buffer (see below), a decrease in the EOF occurs ($\mu_{eo} = -16.6 \cdot 10^{-5} \text{ cm}^2/\text{V} \cdot \text{s}$ at $1 \cdot 10^{-4} \text{ M}$ HQS in 10 mM borate buffer), resulting in an increase in the observed mobility of metal complexes. Obviously, HQS molecules can partially adsorb at the capillary walls, mainly by a hydrophobic mechanism (but electrostatic interaction are also probable), giving a decrease in the electroosmotic velocity (it will be shown below that the adsorption of HQS has an experimental manifestation). It is also possible that the EOF-modifying effect is not the only reason for reduced migration times. The long alkyl chains may also act as a pseudo-stationary phase, interacting by hydrophobic association with chelate molecules carried along with EPF. If this is so, HQS can prevent this "chromatographic" effect owing to its highly hydrophobic nature [12] and, as a consequence, increase the EPM. This effect of the free ligand in the buffer can be seen in Fig. 2.

However, if higher HQS concentrations are used (which are desirable to complete the complexation reaction for metals of low complex stability), a decrease in the mobilities followed by a decrease in efficiency will be observed (Table I, D). One of the presumable explanations for this effect is the formation of the next adsorption layer at the capillary-buffer interface via dynamic coating of the hydrophobically treated wall with an excess of HQS molecules. This secondary negatively charged layer can re-establish the initial charge separation between

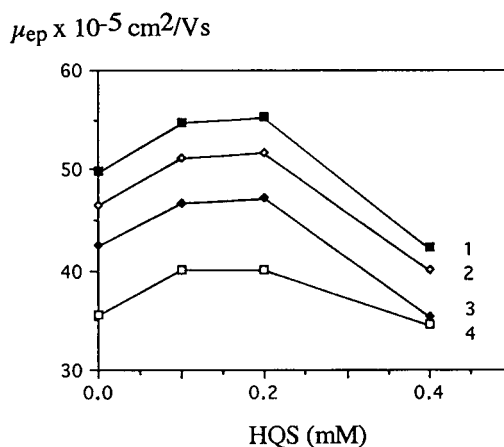


Fig. 2. Dependence of the electrophoretic mobilities of metal complexes on the HQS concentration in the electrophoretic buffer. 1 = Ni; 2 = Zn; 3 = Fe; 4 = Cu. Electrophoretic buffer: 10 mM borate buffer (pH 9.2).

the capillary walls and electrophoretic medium and hence increase the EOF velocity ($\mu_{eo} = -20.2 \cdot 10^{-5} \text{ cm}^2/\text{V} \cdot \text{s}$ at $4 \cdot 10^{-4} \text{ M}$ HQS).

Optimization of metal complexation conditions

The applicability of the proposed metal ion CE mode presupposes the completeness of the complex formation under the electrophoretic conditions, otherwise constancy of the complex composition cannot be ensured so that the observed mobility of the resulting peak will be determined by the equilibrium between the different possible forms of the metal ion (complexed and non-complexed). This observed mobility would be a combination of the individual mobilities of those forms. In addition, this problem could become complicated by the creation of multiple peaks. Finally, determination of metals becomes difficult and the separation is less efficient.

To overcome these problems, two approaches commonly adopted in the high-performance liquid chromatographic determination of metal ions may be used, namely the application of higher concentrations of chelating reagent in the injected samples or its incorporation in the electrophoretic buffer. We studied both of these complexation techniques.

Precolumn complexation. When using a stoichiometric HQS concentration, the complex formation

is complete only for metals of high complex stability, such as copper(II) and iron(III), and to a lesser extent nickel(II). Following the addition of an excess of HQS (up to a threefold excess) with resultant more complete complexation, the detectability is substantially improved, especially for metals such as Zn(II), Co(II), Cd(II) and Mn(II) (even less stable complexes of alkaline earth metals can be detected). However, beginning from a 3:1 molar ratio, an increase in HQS concentration is followed by increasing interference with the metal detectability. Large reagent excesses impair the signal-to-noise ratio (due to the increased background signal) and also cause overlapping peaks (HQS migrates with a mobility between those of the zinc and the iron chelate).

Further, the pH of the electrophoretic buffer must be controlled during complexation optimization, as it affects the conditional formation constant of the complexes. Increasing the pH above 9.5 or decreasing it below 7.5 decreases the complex formation (as is generally the case for metal complexes in solutions), resulting in smaller peak areas and zone spreading. Moreover, on further decreasing the pH (below 6.5), the peaks become very broad and even split (divalent metals can react with HQS to form both 1:1 and 1:2 complexes). Therefore, we considered that moderately alkaline buffers should be studied for optimum detectability of metal ions.

Electrophoretic buffer complexation. Incorporating the chelating reagent into the electrophoretic buffer will favour the complexation reaction and facilitate the establishment of the equilibrium after sample injection. Therefore, when the effect of HQS concentration in the buffer is considered, a general increase in detectability will be expected with increasing concentration. The corresponding electropherograms for precolumn-formed metal chelates at different concentrations of HQS are shown in Fig. 3. As can be seen, increased peak intensities can be observed only with sufficiently low concentrations of HQS (*cf.*, electropherograms a and b). At 0.2 mM and especially 0.4 mM HQS an increase in the absorbance background, a reduction in the observed mobilities and band broadening take place, all of which reduce detectability. As stated above, the last two effects are connected with the impact of HQS on the EOF velocity.

Complexation without addition of HQS to the

injected samples is far from completion, even with 0.4 mM HQS (the largest concentration investigated) and for the most stable complexes. This is probably a result of both comparatively small migration times (*i.e.*, insufficient reaction times) and a low flow mixing in the narrow-bore capillary. Because of slow kinetic effects one could not use simply the on-column complexation alone to maintain the equilibrium conditions in the capillary.

Therefore, the complete on-column formation of complexes requires a certain amount of HQS in the sample. The electropherograms shown in Fig. 4 will be used to illustrate the influence of varying HQS concentration on detectability.

As for the precolumn complexation, lower HQS to metal ion ratios (even if the most favourable 0.1 mM concentration of HQS in the buffer is used) resulted in peaks with small heights and poor efficiency for Ni, Co and Zn complexes (less stable manganese, magnesium and calcium chelates were detected as very broad and asymmetric zones). Further, a lack of chelating reagent in the sample not only led to incomplete complex formation, but also additional unfavourable detection effects (a slow positive baseline drift, a small rapidly migrating peak and a matrix dippeak) were observed. The main reason of these effects, which are typical of metal ion chromatography with HQS-containing eluents [12,13] (we came across them specifically in ion-pair reversed-phase chromatography [11]), is the large adsorption of HQS and the perturbation of the adsorption equilibrium between HQS and the stationary phase (here the hydrophobically treated capillary).

Increasing the HQS concentration will improve the complex-forming conditions and thereby increase detectability; the aforementioned “chromatographic” effects also disappear. The most probable reason for the latter improvements is that the sample matrix closely matches the electrophoretic buffer. On reaching an optimum concentration ratio, corresponding to a *ca.* threefold molar excess of reagent, a further increase in the HQS concentration has little effect on peak heights, but interferes with the detection of the iron(III) complex (Fig. 4c).

Summarizing, it should be stressed that the achievement of optimum metal detectability with this method requires the reasonable combination of pre- and on-column complexation techniques.

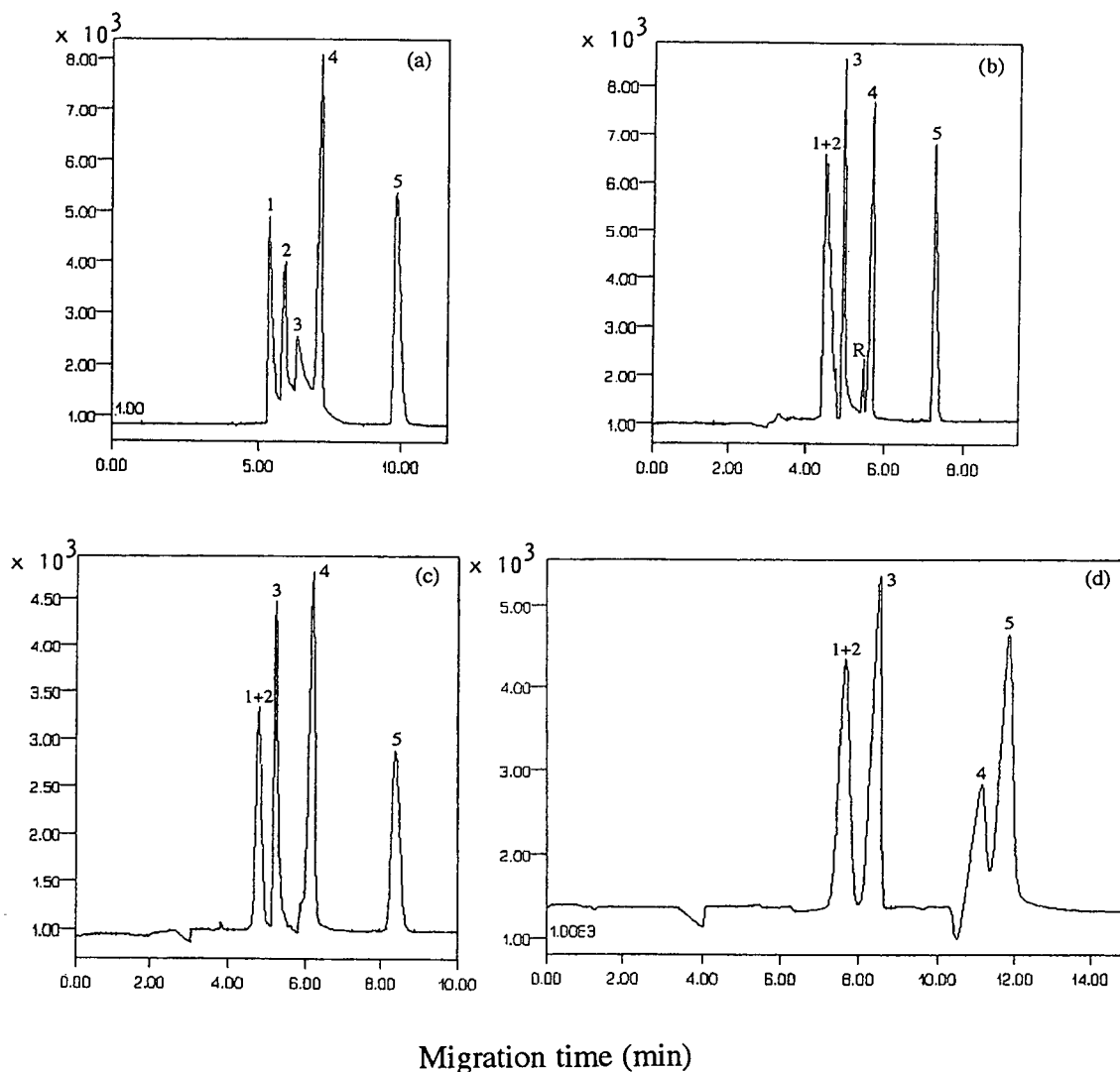


Fig. 3. CE of metal-HQS chelates at various concentrations of HQS in electrophoretic buffer. Peaks: 1 = Ni; 2 = Co; 3 = Zn; 4 = Fe; 5 = Cu; R = HQS. Electrophoretic buffer: 10 mM borate buffer containing HQS at (a) 0, (b) 0.1, (c) 0.2 and (d) 0.4 mM. Applied voltage: 15 kV. Complexation conditions: $[\text{metal ion}] = 1.8 \cdot 10^{-4} \text{ M}$; $[\text{HQS}] = 2.8 \cdot 10^{-3} \text{ M}$. Y-axis represents absorbance units.

Optimization of separation

Among the factors that affect the observed velocity of metal complexes and thereby the separations, we considered the nature, concentration, pH and content of HQS in electrophoretic buffer and the applied voltage.

Applied voltage. Increasing the applied voltage only slightly improves the resolution. Although a higher efficiency is obtained by applying higher

voltages, the smaller differences in migration time observed tend to level out this effect. Hence this CE parameter is insufficiently effective for the increase in resolution. In this work we used an applied voltage of 15 kV, which was chosen mainly with respect to decreasing the analysis time.

Nature of buffer. Borate buffers are more preferable for the separation owing to the more complete complexation, better detectability and resolution.

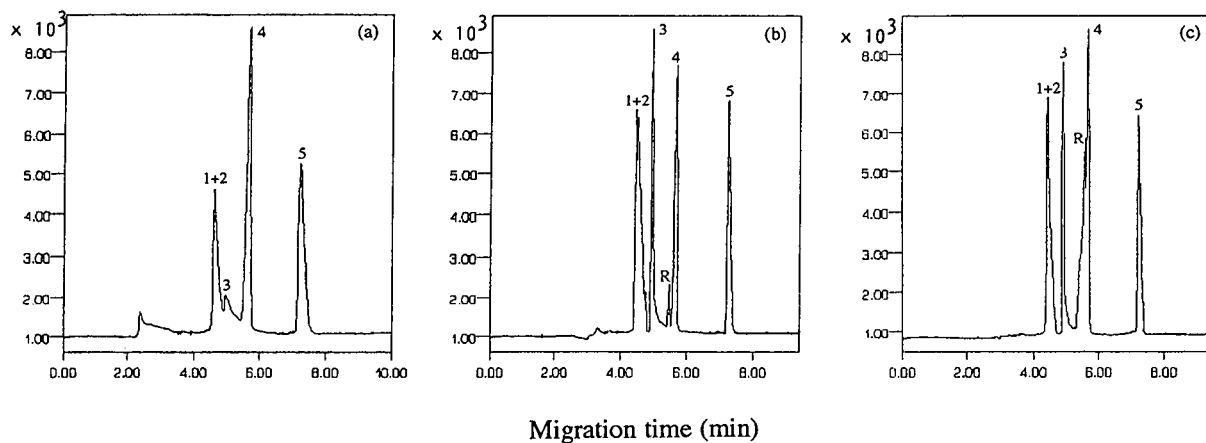


Fig. 4. Effect of HQS concentration in the samples on detectability. Electrophoretic buffer: 0.1 mM HQS. Complexation conditions: [HQS] = (a) 2.5, (b) 2.8 and (c) 3.0 mM. Other conditions as in Fig. 2. Y-axis represents absorbance units.

Using phosphate buffers with the same pH, larger peak broadening (especially for the less stable complexes) and lower mobility were observed. The poorer efficiency is probably a result of the counteraction from the phosphate ions (as a stronger complexing agent than the borate ions). Carbonate buffers provide very good selectivity, but with the drawback of a lower average mobility and a longer analysis time (migration times reach more than 20 min).

pH. The pH dependence of the resolution can be complicated by cooperative and counteractive effects of EPM and EOM changes [14]. For instance, when using pH adjustment to optimize mobility dif-

ferences, one should take into account that the changes in the buffer composition also affect the EOF (Fig. 5). We observed an unexpected decrease in the EOF with increasing the pH, although the deviations in ionic strength were negligibly small ($\pm 0.003 M$). This disagreement with literature data for fused-silica capillaries [15] can be assumed to be related to the partially hydrophobic nature of the capillary walls. Nevertheless, the “bell-shaped” Δt_M vs. pH plots shown in Fig. 6 indicate a certain optimum pH range, in which the highest resolution is obtained. However, this range is narrow, because at higher and lower pH values negative pH effects on the efficiency are strongly pronounced (see above).

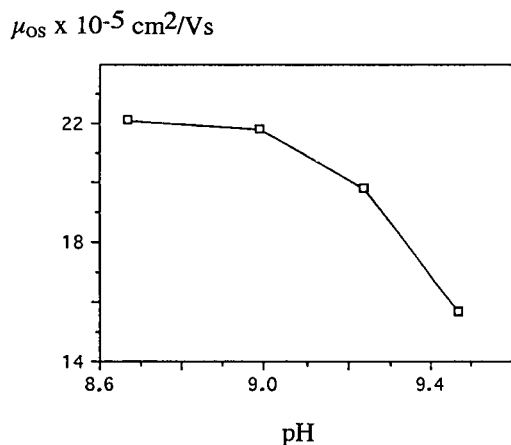


Fig. 5. Effect of borate buffer pH on electroosmotic flow.

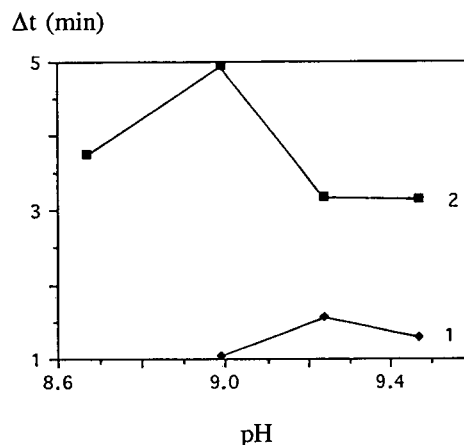


Fig. 6. Dependence of mobility differences of metal complexes on pH. 1 = Ni-Fe; 2 = Fe-Cu.

TABLE II

DEPENDENCE OF ELECTROOSMOTIC AND ELECTROPHORETIC MOBILITIES OF METAL COMPLEXES ON BORATE BUFFER CONCENTRATION

Concentration (mM)	$-\mu_{os}$ (10^{-5} cm ² /V · s)	μ_{ep} (10^{-5} cm ² /V · s)			
		Cu	Fe	Zn	Ni
5	23.6	40.8	48.2	52.1	55.7
10	19.8	37.1	43.8	46.8	50.8
15	16.5	37.5	44.8	48.5	51.2
20	16.7	38.0	45.3	48.8	52.2

The use of a pH scale with a fixed ionic strength (by adding a 0.1 M solution of different salts to 10 mM sodium tetraborate) revealed that the effect of ionic strength on migration times is much stronger than the “pure” pH effect. An increase in ionic strength of 15 mM reduces the migration time by 4–7 min, depending on the metal complex, whereas decreasing the pH by 1.5 units is accompanied by a decrease of only *ca.* 0.6 min. These results correspond well with the double-layer theory [14], according to which EOMs are influenced by changes in pH and ionic strength in the opposite way, the pH being less important than ionic strength.

Concentration. Table II shows the EPM of metal complexes at different borate buffer concentrations together with the corresponding EOM values. As the buffer concentration was increased, the EPM gradually decreased, reaching some constant level at a concentration of 10 mM. The EOM related to buffer concentration displays approximately the same dependence. Thus, varying the buffer concentration within the range 5–20 mM influenced the migration to only a minor extent.

The improvement in resolution that might be observed at higher borate concentrations as a result of the increase in efficiency with increasing current cannot be obtained, as shown in Fig. 7. Based on these data, a borate concentration of 10 mM was chosen because its use allowed not only the selectivity but also the detectability to be enhanced.

Content of HQS. As the effect of HQS in the electrophoretic buffer on the EOF is strongly pronounced (Table I), mobilities can also be manipulated by changing this buffer parameter. However, much shorter migration times observed with some

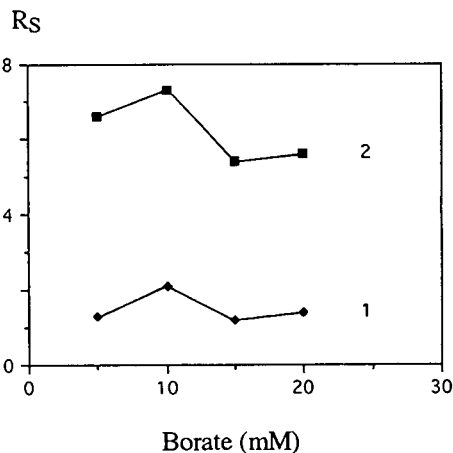


Fig. 7. Effect of borate concentration on resolution of metal complexes. 1 = Ni-Zn; 2 = Fe-Cu.

HQS-bearing buffers (*cf.*, electropherograms a and b in Fig. 2) can result in a decreased selectivity for metal complexes. Therefore, when choosing the electrophoretic buffers for metal determination, one should try to attain a good compromise between resolution and detectability.

An electropherogram showing the representative separation of a six-component metal ion mixture under optimum conditions is presented in Fig. 8

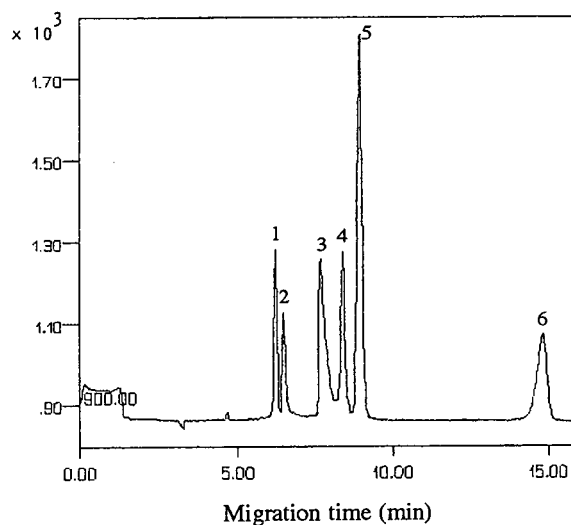


Fig. 8. CE separation of metal chelates of HQS. Electrophoretic buffer: 10 mM borate buffer containing 0.1 mM HQS. Applied voltage: 15 kV. Injection: 2 s. Peaks: 1 = Ni; 2 = Co; 3 = Zn; 4 = Cd; 5 = Fe; 6 = Cu. Metal ion concentration: $1 \cdot 10^{-4}$ M Ni, Zn, Fe, Cu and $2 \cdot 10^{-4}$ M Co, Cd. Y-axis represents absorbance units.

TABLE III
PARAMETERS OF CALIBRATION GRAPHS

CE conditions as in Fig. 3b. Injection: 25 s. $n = 4-6$.

Metal ion	Concentration range (M) ^a	Intercept	Slope $\times 10^6$	Correlation coefficient
Ca(II)	$2 \cdot 10^{-6}-9 \cdot 10^{-4}$	-43.6	47.1	0.9997
Cd(II)	$1 \cdot 10^{-5}-4.5 \cdot 10^{-4}$	11.5	8.5	0.9914
Co(II)	$5 \cdot 10^{-6}-4.5 \cdot 10^{-4}$	3.6	11.9	0.9928
Cu(II)	$4 \cdot 10^{-7}-1 \cdot 10^{-4}$	37.1	77.0	0.9991
Fe(III)	$4 \cdot 10^{-7}-2 \cdot 10^{-4}$	7.6	50.4	0.9997
Mg(II)	$4 \cdot 10^{-6}-9 \cdot 10^{-4}$	-26.8	44.1	0.9998
Mn(II)	$1 \cdot 10^{-6}-9 \cdot 10^{-4}$	60.9	24.5	0.9999
Ni(II)	$4 \cdot 10^{-7}-2 \cdot 10^{-4}$	7.0	44.2	0.9997
Zn(II)	$4 \cdot 10^{-7}-2 \cdot 10^{-4}$	27.5	59.2	0.9973

^a The upper limit corresponds to the maximum concentration studied.

(manganese, magnesium and calcium complexes migrate with close mobilities between those of the cadmium and iron chelates, whereas the aluminium-HQS complex co-migrates with the iron chelate).

Calibration and detection limits

The calibration graphs of peak area against metal concentration are given in Table III with the respective regression coefficients. The linear dynamic range was at least two orders of magnitude and reached about three orders of magnitude for metals that form more stable complexes and/or complexes

with a higher absorptivity, such as copper(II), zinc(II), iron(III), nickel(II) and cobalt(II). In the absence of HQS in the electrophoretic buffer, peak area gave a comparatively narrow dynamic range.

Table IV gives the detection limits of injected concentration and amount for metal ions as HQS chelates, defined as three times the signal-to-baseline noise ratio, for an electrophoretic buffer containing 0.1 mM HQS. Injected volumes were determined as described in ref. 14 for an elevation of 10 cm of the injection vial. It should be pointed out that the detection wavelength of 254 nm is an instrumental constraint, but not the optimal wavelength for the detection of HQS complexes. Also, a background signal detected for some metals, mainly zinc(II) and iron(III), originating from metal impurities in the electrophoretic buffer and water used, limits the detectability of these metals.

The relative standard deviations of the peak areas were found to be 1.5, 0.8, 0.6, 0.6 and 1.1% for Cu(II), Fe(III), Ni(II), Co(II) and Zn(II), respectively, for six replicate runs with $4 \cdot 10^{-5}$ M of each metal ion. As these values indicate reasonable reproducibility, there was no necessity to use an internal standard.

Analytical data

In order to evaluate the quantitative performance of the method, a sample of tap water was analysed. Fig. 9 gives a typical electropherogram in comparison with an electropherogram of the same sample spiked with a small amount of zinc. The second

TABLE IV
DETECTION LIMITS

Metal ion	Minimum detectable concentration ^a		Minimum detectable amount (pg)
	M	ppb	
Ca(II)	$2 \cdot 10^{-6}$	80	1.5
Cd(II)	$2 \cdot 10^{-6}$	225	26.0
Co(II)	$1 \cdot 10^{-6}$	58.9	1.6
Cu(II)	$5 \cdot 10^{-8}$	3.2	0.06
Fe(III)	$3 \cdot 10^{-7}$	16.7	1.0
Mg(II)	$4 \cdot 10^{-6}$	97	1.7
Mn(II)	$1 \cdot 10^{-6}$	55	2.5
Ni(II)	$4 \cdot 10^{-7}$	23.5	1.1
Zn(II)	$1 \cdot 10^{-7}$	6.5	0.6

^a Injection time 5 s.

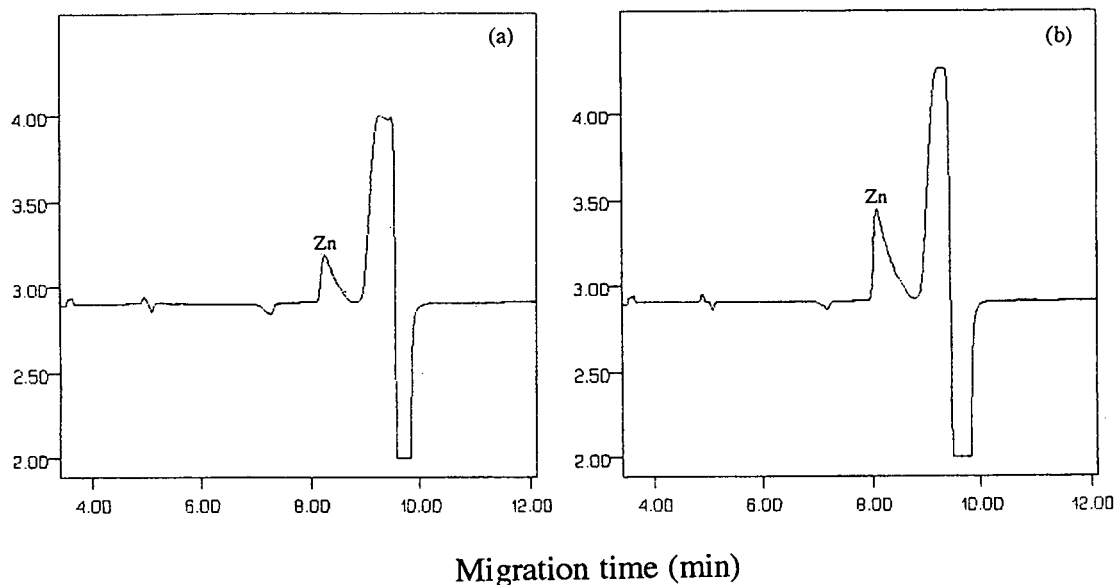


Fig. 9. Electropherograms of (a) a tap water sample and (b) the same sample spiked with 14.5 ppb of zinc. Injections: 25 s. Other conditions as in Fig. 8. Y-axis represents absorbance units.

peak migrating just after the Zn–HQS complex is attributed to iron– and alkaline earth metal–HQS complexes. Owing to the sufficiently high sensitivity, this method can be recommended for environmental samples without preconcentration techniques. However, the following relatively minor problem should be taken into account. The comparatively high background signal of metal impurities mentioned previously, mainly because of inadequate purity of the reagent, necessitates a “blank” analysis and subtraction of the “blank” electropherogram from the sample electropherogram (the dip peak observed in Fig. 9 is caused by this operation).

CONCLUSIONS

HQS is a promising reagent in metal ion CE. The application of this reagent to the CE separation and determination of transition metal ions after precolumn formation of negatively charged chelates appears to be a good alternative to traditional capillary methods for ion analysis. Complete chelation before the separation not only allows the direct spectrophotometric detection of metal ions in the mid-ppb range, but also imparts a negative charge

to the metal ion which makes its adsorption interactions with capillary walls negligible. In addition, as only one metal-containing species exists within each zone when using a sufficiently strong chelating reagent, small band broadening and small competing complexing effects of buffer components should be expected. Further, incorporating HQS in the electrophoretic buffer markedly improves the detectability and makes it possible additionally to regulate the separation.

Useful developments of the method, which are worthy of further investigation, might be connected with extending greatly the range of metals that can be determined (involving aluminium group metals, molybdenum, tungsten and vanadium or platinum metals), introducing new chelating agents (e.g., dithiocarbamic acids containing ionized groups) and the extension of practical applications.

ACKNOWLEDGEMENT

This work was supported by research grant No. 45.213/2–27b/91 from the Austrian Ministry of Science and Scientific Research.

REFERENCES

- 1 J. Romano, P. Jandik, W. R. Jones and P. E. Jackson, *J. Chromatogr.*, 546 (1991) 411.
- 2 L. Gross and E. S. Yeung, *Anal. Chem.*, 62 (1990) 427.
- 3 W. Beck and H. Engelhardt, *Chromatographia*, 33 (1992) 313.
- 4 W. Buchberger and P. Haddad, *J. Chromatogr.*, 608 (1992) 65.
- 5 F. Foret, S. Fanali, A. Nardi and P. Bocek, *Electrophoresis*, 11 (1990) 780.
- 6 A. Weston, P. R. Brown, P. Jandik, W. R. Jones and A. L. Heckenberg, *J. Chromatogr.*, 593 (1992) 289.
- 7 D. F. Swaile and M. J. Sepaniak, *Anal. Chem.*, 63 (1991) 179.
- 8 J. J. Toei, *Chromatographia*, 23 (1987) 355.
- 9 A. R. Timerbaev, O. M. Petrukhin, V. I. Orlov and A. A. Aratskova, *J. Liq. Chromatogr.*, 15 (1992) 1443.
- 10 K. Robards, P. Starr and E. Patsalides, *Analyst*, 116 (1991) 1247.
- 11 A. R. Timerbaev, O. P. Semenova, W. Buchberger and G. Bonn, *International Ion Chromatography Symposium 1992, Linz, September 1992*, abstract No. 66.
- 12 P. K. Dasgupta, K. Soroka and R. S. Vithanage, *J. Liq. Chromatogr.*, 10 (1987) 3287.
- 13 K. Soroka, R. S. Vithanage, D. A. Phillips, B. Walker and P. K. Dasgupta, *Anal. Chem.*, 59 (1987) 629.
- 14 J. Vindevogel and P. Sandra, *Introduction to Micellar Electrokinetic Chromatography*, Hüthig, Heidelberg, 1992.
- 15 K. D. Lukacs and J. W. Jorgenson, *J. High Resolut. Chromatogr. Chromatogr. Commun.*, 8 (1985) 407.

Short Communication

Glycosaminoglycans and proteins: different behaviours in high-performance size-exclusion chromatography

Nicola Volpi and Lorenzo Bolognani

Chair of Biological Chemistry, "Biologia Animale" Department, University of Modena, Via Berengario 14, 41100 Modena (Italy)

(First received September 11th, 1992; revised manuscript received October 28th, 1992)

ABSTRACT

The influence of the conformation of globular proteins and glycosaminoglycans in high-performance size-exclusion chromatography (HPSEC) was studied. Glycosaminoglycans (heparin, chondroitin sulphate and dermatan sulphate) with different primary structures, sulphate-to-carboxyl ratios and physico-chemical properties were extracted and purified. Their physico-chemical properties and purity were evaluated by several analytical techniques. Glycosaminoglycans with different relative molecular masses (M_r) were prepared by a chemical depolymerization process. These heteropolysaccharides were evaluated by HPSEC and compared with globular proteins of known relative molecular mass. The two third-degree polynomial regression curves for proteins and glycosaminoglycans have different coefficients and the columns present different exclusion limits. In particular, under the experimental conditions, the M_r exclusion limits for high M_r are 44 000 for glycosaminoglycans and 240 000 for globular proteins. In contrast, the behaviours of these two classes of macromolecules are similar for lower M_r . In fact, the two third-degree polynomial curves show the same regression below about $M_r = 1000$. The behaviour in HPSEC is discussed in relation to the different steric conformations for proteins and glycosaminoglycans with different relative molecular masses.

INTRODUCTION

Size-exclusion chromatography (SEC) (also termed gel filtration, gel permeation or molecular sieving) involves a simple principle of separation. Unlike other separation systems, such as ion-exchange, reversed-phase or affinity chromatography, SEC generally obviates chemical interactions between the sample and stationary phase. The elution order depends mainly on the molecular size dissolved in the eluent and also on hydrodynamic volume [1].

For linear polymers, which are present in solution as random coils, the size can be directly related to relative molecular mass (M_r). For molecules with an ordered structure the usual plot of the $\log M_r$ versus elution volume does not properly describe their behaviour in SEC properly [2].

Glycosaminoglycans (GAGs) are complex, polydisperse, sulphated polysaccharides. They are alternating copolymers of uronic acids and amino sugars; the structures are commonly represented by their prevalent disaccharide sequences obtained by enzymatic cleavage. They are very heterogeneous polysaccharides in terms of relative molecular mass, physico-chemical properties and biological activities [3].

Heparin (Hep) has a heterogeneous structure due

Correspondence to: N. Volpi, Chair of Biological Chemistry, "Biologia Animale" Department, University of Modena, Via Berengario 14, 41100 Modena, Italy.

to the presence of variously sulphated regions distributed along the chain. It is a polysaccharide composed of alternate sequences of differently sulphated residues of uronic acid (β -D-glucuronic acid and α -L-iduronic acid) and α -D-glucosamine linked by $\alpha(1\rightarrow4)$ bonds [4].

Polysaccharide chains of dermatan sulphate (DS) consist of a prevailing disaccharide unit [(1 \rightarrow 4)-O-(α -idopyranosyluronic acid)-(1 \rightarrow 3)-O-(2-acetamido-2-deoxy- β -D-galactopyranosyl 4-sulphate)] [5].

Chondroitin sulphate (CS) is a heteropolysaccharide composed of alternate sequences of differently sulphated residues of uronic acid (β -D-glucuronic) and α -D-N-acetylgalactosamine linked by $\beta(1\rightarrow3)$ bonds [6]. The regular disaccharide sequence of chondroitin sulphate A (CS-A), chondroitin-4-sulphate, is constituted by (1 \rightarrow 4)-O-(β -D-glucopyranosyluronic acid)-(1 \rightarrow 3)-O-(2-acetamido-2-deoxy- β -D-galactopyranosyl-4-sulphate). Chondroitin sulphate C (CS-C), chondroitin-6-sulphate, is mainly composed of a disaccharide unit [(1 \rightarrow 4)-O-(β -D-glucopyranosyluronic acid)-(1 \rightarrow 3)-O-(2-acetamido-2-deoxy- β -D-galactopyranosyl-6-sulphate)] [6].

In this paper we report the different chromatographic behaviours of GAGs and proteins in high-performance size-exclusion chromatography (HPSEC). The different chromatographic behaviours of these two classes of macromolecules depending on relative molecular mass, are discussed in relation to their different secondary and tertiary structure and different conformation. Moreover, these differences should be considered in those processes influenced by steric conformation.

EXPERIMENTAL

Materials

Proteins of different molecular mass were obtained from Sigma: catalase from bovine liver (C-10) ($M_r = 240\,000$); β -galactosidase from *Escherichia coli* (G-8511) ($M_r = 116\,000$); bovine serum albumin (A-6793) ($M_r = 66\,000$); egg albumin (A-7642) ($M_r = 45\,000$); carbonic anhydrase from bovine erythrocytes (C-2273) ($M_r = 29\,000$); trypsinogen from bovine pancreas (T-9011) ($M_r = 24\,000$); trypsin inhibitor from soybean (T-9767) ($M_r = 20\,100$); α -lactalbumin from bovine milk (L-6385) ($M_r = 14\,200$); insulin from bovine pan-

creas (I-5500) ($M_r = 6000$); and glutathione from cell culture (G-4251) ($M_r = 310$).

GAGs of different relative molecular mass were prepared by chemical depolymerization of native heteropolysaccharides, as reported below. An unsaturated disaccharide with known relative molecular mass (503) was from Sigma (C-4045).

All reagents and solutions were of analytical-reagent grade.

Extraction and purification of glycosaminoglycans: heparin, dermatan sulphate and chondroitin sulphate

Hep (from beef mucosa), DS (from pig skin) and CS (from bovine trachea) were isolated and purified according to Taniguchi [7]. CS was also purified from shark cartilage.

Preparation of glycosaminoglycans of different relative molecular mass

Native Hep, DS and CS from bovine trachea were depolymerized by a controlled chemical reaction, according to Volpi and co-workers [8–10].

GAGs of different relative molecular mass were obtained by a controlled chemical depolymerization process induced by free radicals. A 5-g amount of Hep or DS or CS and 0.2 g of copper acetate monohydrate (0.02 mol/l) were dissolved with 50 ml of water into a reaction vessel fitted with a thermostated bath, stirrer, calibrated dropping funnels and a thermometer. The temperature was kept constant at 60°C and the pH was adjusted to 7.5 by addition of 1 M NaOH solution. Hydrogen peroxide solution (9%) was added at a rate of 10 ml/h. The reactions for Hep, DS and CS were stopped at different times, and at the end of the reaction the chelating resin Chelex 100 (Bio-Rad) was utilized to remove copper contaminant from the product and a strong anion-exchange resin in the OH⁻ form was used to remove acidic contaminants. The pH of the percolate was adjusted to 5.5 with acetic acid, then two volumes of acetone were added. The precipitate, collected by filtration and washed with acetone, was dissolved in 100 ml of water. A 5-g amount of sodium acetate was added to this solution, and then low- M_r GAG sodium salt was precipitated with two volumes of acetone. The precipitate was collected and dried.

The relative molecular masses of the various GAGs obtained (Hep from 12 000 to 2000, DS

from 35 000 to 5000 and CS from 30 000 to 5000) were evaluated by ultracentrifugation according to Nieduszinski [11] and by HPSEC utilizing a calibration graph constructed using GAGs of known M_r .

High-performance size-exclusion chromatography (HPSEC)

The HPLC system from Jasco consisted of a Model 880 PU pump, a Model 801 SC system controller, a Model 880-02 ternary gradient unit, a Rheodyne injector equipped with a 100- μ l loop and a Model 875 UV detector. The mobile phase was 125 mM Na₂SO₄–2 mM NaH₂PO₄ adjusted to pH 6.0 with 0.1 M NaOH. The flow-rate was 0.9 ml/min with a back-pressure of 25 kg/cm². Proteins and GAGs of different relative molecular mass were dissolved in the mobile phase at a concentration of 5 mg/ml and volumes of 10 μ l (50 μ g) were injected into the HPLC system.

Protein Pak 125 and 300 columns (Waters) were assembled in series. The Protein Pak 125 column (30 cm \times 7.8 mm I.D.) had M_r ranges of native globular 2000–80 000 and random coil 1000–30 000 and the Protein Pak 300 column (30 cm \times 7.5 mm I.D.) had M_r ranges of native globular 10 000–400 000 and random coil 2000–150 000.

The retention times were plotted against log M_r for proteins and GAGs. The curve that fitted the experimental data was a third-degree polynomial $y = -ax^3 + bx^2 - cx + d$, performed with a Macintosh computer program.

Determination of the purity and physico-chemical properties of glycosaminoglycans

Sulfate and carboxyl groups were determined by potentiometric titration with 0.1 M NaOH [12] in water–dimethylformamide (Merck) (50:30) of heparinic, dermatanic and chondroitinic acids obtained by removing the cations using strong ion-exchange resins (Amberlite IRA-400, strongly basic polystyrene gel-type resin, and Amberlite IRA-120, strongly acidic polystyrene gel-type resin; Rohm & Haas). The sulphate-to-carboxyl ratio was also determined by enzymatic degradation (by heparinases for Hep and chondroitinases for DS and CSs) after HPLC separation of the constituent disaccharides [8–10]. The ratio was calculated by considering the percentage and the presence of carboxyl and sulphate groups for each disaccharide.

The presence of possible GAGs as contaminants in the preparations and the ratio of “slow-moving” component (constituted by the most highly sulphated and higher- M_r species) to “fast-moving” component (less sulphated and lower- M_r species) of heparin was determined by electrophoresis on agarose in barium acetate/1,2-diaminopropane according to Cassaro and Dietrich [13].

The specific optical rotation was determined at 25°C at a concentration of 5% (w/v) of GAGs in water using a polarimeter.

The different physico-chemical properties of purified native heparin, DS and CS (from bovine trachea and shark cartilage) are reported in Tables I and II.

The different M_r values and the log M_r versus retention time for GAGs obtained by chemical depolymerization are given in Table III, which also reports the standard errors. Table IV gives the values of M_r and log M_r versus retention time with standard errors for proteins.

RESULTS AND DISCUSSION

The extracted and purified GAGs had a purity of 100% as tested by agarose electrophoresis, specific optical rotation and HPSEC. Heparin has M_r 11 600, DS 32 110, bovine trachea CS 26 140 and shark cartilage CS 44 120.

TABLE I
PHYSICO-CHEMICAL CHARACTERISTICS OF PURIFIED BEEF MUCOSA HEPARIN

Parameter	Value	
Peak M_r	11 600	
Sulphate/carboxyl ratio (titrimetric)	2.19	
Sulphate/carboxyl ratio (enzymatic cleavage)	2.42	
Optical rotation	+ 50°	
Agarose electrophoresis:	Fast moving	Slow moving
Mobility (%)	48	18
Glycosaminoglycans (%)	80	20

TABLE II

PHYSICO-CHEMICAL CHARACTERISTICS OF PURIFIED PIG SKIN DERMATAN SULPHATE, AND BOVINE TRACHEA (BT) AND SHARK CARTILAGE (SC) CHONDROITIN SULPHATES

Parameter	DS	CS (BT)	CS (SC)
Peak M_r ($\times 1000$)	32.11	26.14	44.12
Sulphate/carboxyl ratio (titrimetric)	1.12	0.99	1.13
Sulphate/carboxyl ratio (enzymatic cleavage)	1.09	0.97	1.15
Optical rotation	-55°	-20°	-14°
Agarose electrophoresis:			
Mobility (%)	62	75	75
Glycosaminoglycans (%)	100	100	100

TABLE III

RELATIVE MOLECULAR MASSES, LOGARITHMS OF RELATIVE MOLECULAR MASSES, RETENTION TIMES AND STANDARD ERRORS FOR STANDARD PROTEINS

Protein standard	M_r ($\times 1000$)	Log M_r	Retention time (min)	Standard error
Catalase	240.0	5.38	16.82	0.21
β -Galactosidase	116.0	5.06	16.98	0.28
Bovine serum albumin	66.0	4.82	17.58	0.19
Egg albumin	45.0	4.65	18.86	0.25
Carbonic anhydrase	29.0	4.46	20.26	0.27
Trypsinogen	24.0	4.38	20.42	0.32
Trypsin inhibitor	20.1	4.30	20.92	0.29
α -Lactalbumin	14.2	4.15	21.02	0.34
Insulin	6.0	3.78	22.96	0.32
Glutathione	0.3	2.49	24.37	0.30

TABLE IV

RELATIVE MOLECULAR MASSES, LOGARITHMS OF RELATIVE MOLECULAR MASSES, RETENTION TIMES AND STANDARD ERRORS FOR STANDARD GLYCOSAMINOGLYCANS

GAG standard	M_r ($\times 1000$)	Log M_r	Retention time (min)	Standard error
CS 45	44.12	4.64	13.50	0.31
DS 32	32.11	4.51	13.89	0.38
CS 26	26.14	4.42	14.29	0.35
CS 17	17.02	4.23	15.13	0.35
DS 16	15.64	4.19	15.22	0.37
DS 13	12.78	4.11	16.11	0.32
Hep 9	8.70	3.94	16.92	0.38
CS 6	6.26	3.80	19.27	0.42
DS 6	5.83	3.77	19.76	0.42
Hep 4	3.70	3.57	21.52	0.45
Hep 2	2.13	3.33	22.90	0.47
4-Di-4s	0.50	2.70	23.85	0.43

GAGs of different and lower M_r than the native molecule can be produced by various processes, such as enrichment of low- M_r fractions of commercial heteropolysaccharides or their chemical depolymerization products. Recent methods involve controlled chemical depolymerization by nitrous acid, chemical β -elimination and utilization of peroxides and redox systems [14]. Chemical synthesis [15] and enzymatic depolymerization [16] represent other methods of preparation. The radical depolymerization process we used to produce GAGs of different M_r [8,9] was controlled by means of the reaction kinetics, calculated by withdrawing the specimens at different times and evaluating their relative molecular masses by HPSEC. The relative molecular mass decreases with time according to an exponential-like function, as shown in Fig. 1, which shows the reaction kinetics of beef lung heparin, pig skin DS and bovine trachea CS. The GAGs of different M_r produced by the chemical process were used to construct a calibration graph in HPSEC and to evaluate the differences compared with proteins.

The third-degree polynomial calibration graph was constructed using GAGs with different primary structure. The backbones of CS, DS and Hep pre-

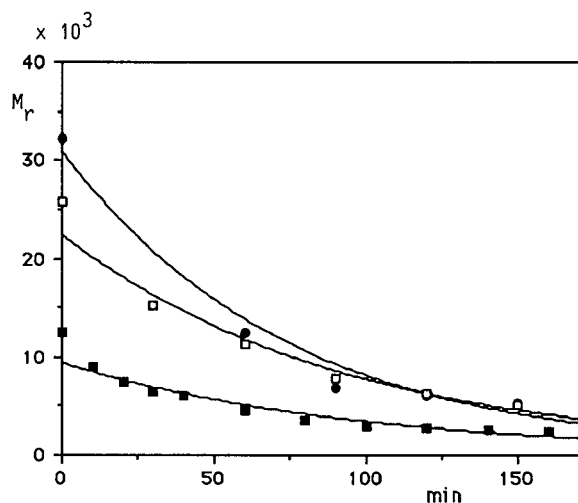


Fig. 1. Chemical process of depolymerization of glycosaminoglycans. Relative molecular mass versus time in min of chemical reaction is reported. Coefficients of exponential regression and correlation coefficients are as follows: for DS (●), $y = 30.8 \cdot 10^{-5.7} \cdot e^{-3x}$, $R = 0.930$; for CS (□), $y = 22.3 \cdot 10^{-4.5} \cdot e^{-3x}$, $R = 0.971$; and for heparin (■), $y = 9.4 \cdot 10^{-4.3} \cdot e^{-3x}$, $R = 0.935$.

sent different uronic acids, different hexosamines and O-sulphate groups in different amounts and O-linked in different positions. The prevailing monosaccharides identified in DS, CS and Hep are α -L-iduronic and β -D-glucuronic acids, N-acetyl- α -D-glucosamine, N-sulpho- α -D-glucosamine and N-acetyl- α -D-galactosamine. Sulphate groups can be O-linked in position 2 of uronic acids, in positions 4 and 6 of N-acetyl- α -D-galactosamine, in position 6 of N-acetyl- α -D-glucosamine and in positions 3 and 6 of N-sulpho- α -D-glucosamine [4, 5, 6]. However, the secondary and tertiary structures are relatively similar for GAGs with different monosaccharide units and charge density solubilized in the same aqueous medium [17,18]. In fact, these linear polyelectrolytes were assumed to be long cylinders in aqueous solutions with a continuous distribution of point charges upon them [19]. In these conditions, a difference in charge density, about 1–1.1 for CS and DS and about 2.2–2.4 for heparin, has a minimum influence on HPSEC. The calibration graph was constructed using different GAGs to check high and very low relative molecular masses. In fact, natural CS from shark cartilage has $M_r \approx 44\,000$, natural DS from pig skin *ca.* 32 000 and natural CS from bovine trachea *ca.* 26 000. On the other hand, the chemical depolymerization process of heparin is controlled easier than the degradation of CS or DS to obtain very-low- M_r fractions (Table IV).

HPSEC gives different upper limits of M_r for proteins and GAGs, as in Fig. 2. Under our experimental conditions, the M_r exclusion limits for higher M_r are 240 000 for globular proteins and 44 000 for GAGs. In contrast, the behaviour for these two classes of macromolecules are similar for low M_r . In fact, the two third-degree polynomial curves show the same regression below about $M_r = 1000$. This effect stems from the loss of globular conformation of lower- M_r proteins due to the decreased number of hydrogen bonds [20]. In this condition, the proteins in solution present a random coil, a conformational state which is similar to that of GAGs.

Proteins utilized to evaluate the behaviour in HPSEC have a generally globular conformation. The secondary structure is stabilized by hydrogen bonds between N–H and C = O groups involved in peptidic linkages [20]. The tertiary structure is stabilized by hydrogen bonds of amino acid side-chains, by hydrophobic interactions and by disulphur (co-

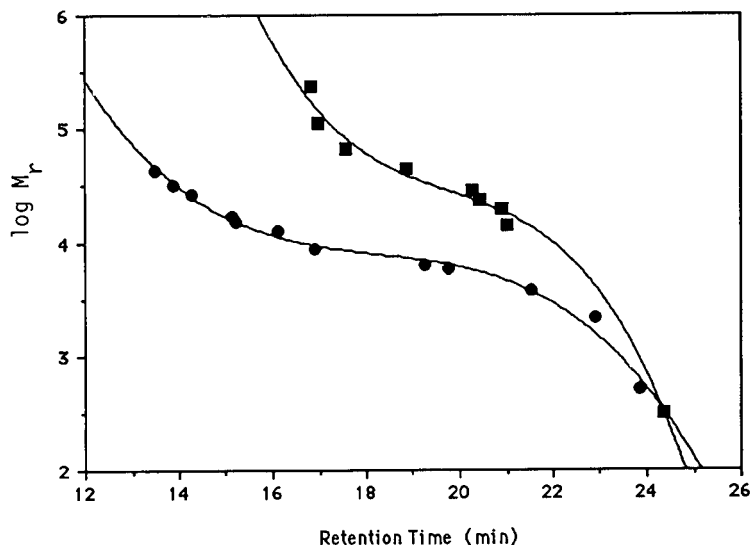


Fig. 2. Comparison of the different third-degree grade polynomial curves for standard (■) proteins and (●) glycosaminoglycans in HPSEC. For proteins, $J = -0.018x^3 + 1.07x^2 - 21.54x + 149.08$, $R = 0.993$; for glycosaminoglycans, $y = -0.0051x^3 + 0.29x^2 - 5.22x + 36.29$, $R = 0.993$.

valent) bridges [20]. The globular conformation is imposed to achieve a stable state with minimum energy and entropy. Thus, proteins in aqueous solution are generally closely packed, although some degree of flexibility is possible [20]. Therefore, high- M_r globular proteins have a very compact conformation.

Heteropoly acids, in contrast, do not present a well defined packed conformation. The absence of covalent bridges and the irregular location and direction of hydrogen bonds produce very deformable saccharidic chains. The presence of numerous negative groups extends the saccharidic frame, depending on the nature and concentration of the ions present in the solution. Although the flexibility of the chains is different for different GAGs owing to the presence of heterogeneous monosaccharides with various conformations [4, 21], the GAGs present extended chains in aqueous solution [22]. GAGs assume the form of a "small elongated stick" surrounded by water molecules [23], which gives these heteropoly acids a larger steric conformation than proteins with the same relative molecular mass.

In particular, this work confirms the importance of steric conformation in HPSEC experiments per-

formed to evaluate relative molecular masses and also in preparative processes to produce purified GAGs. Moreover, we should stress that GAGs, in addition to their polyanionic nature, behave as high- M_r proteins under conditions of steric hindrance, such as in gel filtration and dialysis.

ACKNOWLEDGEMENTS

The authors are grateful to Biofer (Biopharmaceutical Industry Research Laboratories) for the use of instrumentation.

REFERENCES

- 1 D. Johns, in R. W. A. Oliver (Editor), *HPLC of Macromolecules. A Practical Approach*, IRL Press, Oxford, 1989, pp. 1–42.
- 2 A. Henschen, K. P. Hupe, F. Lottspeich and W. Voelter (Editors), *High Performance Liquid Chromatography in Biochemistry*, VCH, Weinheim, 1985.
- 3 F. A. Ofofu, I. Danishefsky and J. Hirsh (Editors), *Ann. N. Y. Acad. Sci.*, 556 (1989).
- 4 B. Casu, *Adv. Carbohydr. Chem. Biochem.*, 43 (1985) 51.
- 5 H. E. Conrad, *Ann. N. Y. Acad. Sci.*, 556 (1989) 19.
- 6 K. Murata and Y. Yokoyama, *Anal. Biochem.*, 149 (1985) 261.
- 7 N. Taniguchi, in *Glycosaminoglycans and Proteoglycans in*

- Physiological and Pathological Processes of Body Systems*, Karger, Basle, 1982, pp. 20–40.
- 8 N. Volpi, G. Mascellani, P. Bianchini and L. Liverani, *Farmacologia*, 47 (1992) 841.
 - 9 N. Volpi, G. Mascellani and P. Bianchini, *Anal. Biochem.*, 200 (1992) 100.
 - 10 N. Volpi, P. Bianchini and L. Bolognani, *Biochem. Int.*, 24 (1991) 243.
 - 11 I. Nieduszynski, in D. A. Lane and U. Lindahl (Editors), *Heparin. Chemical and Biological Properties. Clinical Applications*, Edward Arnold, London, 1989, pp. 51–63.
 - 12 K. E. Kuettner and A. Lindenbaum, *Biochim. Biophys. Acta*, 101 (1965) 223.
 - 13 C. M. F. Cassaro and C. P. Dietrich, *J. Biol. Chem.*, 252 (1977) 2254.
 - 14 E. Holmer, in D. A. Lane and U. Lindahl (Editors), *Heparin. Chemical and Biological Properties. Clinical Applications*, Edward Arnold, London, 1989, pp. 575–595.
 - 15 M. Petitou, *Nouv. Rev. Fr. Hematol.*, 26 (1984) 221.
 - 16 C. P. Dietrich, Y. C. M. Michelacci and H. B. Nader, in *Mechanism of Saccharide Polymerization/Depolymerization*, Academic Press, New York, 1980, pp. 317–329.
 - 17 J. P. Duclos (Editor), in *L'héparine. Fabrication, Structure, Propriétés, Analyses*, Masson, Paris, 1984.
 - 18 J. E. Scott, *FASEB J.*, 6 (1992) 2639.
 - 19 G. S. Manning, in E. Selegny (Editor), *Polyelectrolytes*, Reidel, Dordrecht, 1974.
 - 20 A. Fersht, *Enzymes Structure and Mechanism*, Freeman, New York, 1985.
 - 21 G. Gatti, B. Casu, G. K. Hamer and A. S. Perlin, *Macromolecules*, 12 (1979) 1001.
 - 22 P. A. Liberti and S. S. Stivala, *Arch. Biochem. Biophys.*, 130 (1966) 361.
 - 23 S. Hirano, *Int. J. Biochem.*, 3 (1972) 677.

Short Communication

Adsorption losses during extraction and derivatization efficiency by benzylation of plant putrescine for high-performance liquid chromatographic analysis

Michael Z. Hauschild

Laboratory of Environmental Sciences and Ecology, Building 224, Technical University of Denmark, DK-2800 Lyngby (Denmark)

(First received September 4th, 1992; revised manuscript received November 2nd, 1992)

ABSTRACT

The method for the determination analysis of plant polyamines through the reversed-phase HPLC separation of the benzamide derivatives was investigated for putrescine (1,4-diaminobutane) with the purpose of increasing reproducibility without losing speed. Putrescine was found not to adsorb on differential vial materials, but a significant binding to plant material in the extraction step was found. The overall benzylation efficiency varied between 59 and 83%, and the use of 1,6-diaminohexane as an internal standard is suggested in order to obtain reproducible results.

INTRODUCTION

For the determination of aliphatic polyamines, Redmond and Tseng [1] introduced the reversed-phase HPLC separation of benzamide derivatives obtained through benzylation by the Schotten–Baumann technique. Flores and Galston [2] developed it into a rapid and sensitive method for use on crude plant extracts, with subsequent modifications [3].

An investigation of the possible application of the free form of one of the polyamines, putrescine (1,4-diaminobutane), as a biomarker of pollution-induced stress in a higher plant test [4,5] created the necessity for a highly quantitative and reproducible

determination of putrescine in plant material, to be used on large numbers of samples.

The method of Flores and Galston is a useful starting point, but it involves several steps with recoveries that vary and may be unsatisfactory. Furthermore, free polyamines are suspected to adsorb on glass surfaces [2,6], leading to possible losses of the amines before HPLC separation and detection. A thorough examination of the method of Flores and Galston was carried out for putrescine to optimize the different steps, to reveal operations leading to loss of this polyamine and, with this background, to improve the reproducibility of the benzylation method for the determination of free putrescine in plant material.

EXPERIMENTAL

Chemicals

Putrescine (98% free base), 1,6-diaminohexane

Correspondence to: M. Z. Hauschild, Laboratory of Environmental Sciences and Ecology, Building 224, Technical University of Denmark, DK-2800 Lyngby, Denmark.

(crystalline) and benzoyl chloride (99%) were obtained from Sigma (Deisenhofen, Germany), and [^{14}C]putrescine (98.8% pure dihydrochloride, specific activity 3.3 GBq/mmol), labelled at C-1 and C-4, from DuPont (Brøndby, Denmark).

Cultivation of plants

Plant material (barley or rape) was cultivated as described elsewhere [4].

Determination of polyamines

The harvest and benzylation procedure was adopted and modified from that of Flores and Galston [2].

Extraction of plant material. Approximately 200 mg (fresh mass) was macerated in 1 ml followed by washing in 1 ml of cold (4°C) protein denaturing acid extractant (a 5% solution of trichloroacetic acid or perchloric acid with 25 μM 1,6-diaminohexane added) in a blender (Ultra Turrax, 25 000 rpm for 60 s) and allowed to stand for 60 min on ice. The supernatant was isolated by centrifugation (45 000 g for 15 min), withdrawn and kept at -18°C .

Benzylation of plant extracts. To 500 μl of plant extract were added 1 ml of 2 M NaOH and 20 μl of benzoyl chloride. After 10 s of vortex mixing, 20 min at ambient temperature was allowed for reaction. A 2-ml volume of saturated NaCl was added followed by 2.0 ml of diethyl ether. The mixture was vortex mixed for exactly 10 s and allowed to separate for 10 min, then 1.0 ml of the ether phase was transferred to an HPLC autosampler vial, from which the ether was allowed to evaporate during 4–5 h at ambient temperature. After addition of 250 μl of the HPLC eluent and vortex mixing for 10 s, the sample was analysed by HPLC or stored at -18°C .

HPLC of benzyolated plant extracts. Separation of benzyolated amines was carried out by isocratic reversed-phase HPLC using a Waters Model 501 pump and a 200 \times 3 mm I.D. C_{18} column, particle size 5 μm (ChromSpher B; Chrompack) with ethanol–water (3:7) as the eluent at a flow-rate of 0.3 ml/min. The amines were detected spectrophotometrically at 254 nm with a Waters Model 455 LC spectrophotometer, corrected with the internal standard and quantified against external standards.

Investigations using [^{14}C]putrescine

Adsorption of [^{14}C]putrescine on vial materials.

The types of vials tested were (A) completely new 100 \times 16 mm I.D. glass tube with virgin glass surfaces; (B) completely new 100 \times 16 mm I.D. glass tube, surfaces exposed to contact with plant extract for 30 min; (C) old glass centrifugal tube, used and washed at least ten times; and (D) polycarbonate centrifuge tube. In the test, 1000 μl of $1 \cdot 10^{-3}$ M putrescine standard solution with a specific activity of 980 Bq/ml was vortex mixed in the vial and allowed to stand for 30 min before withdrawal of 500 μl for scintillation counting. Each type of tube was tested empty or containing 1 ml 2 M NaOH, and each test was replicated five times.

Benzylation of [^{14}C]putrescine. A 500- μl volume of [^{14}C]putrescine was benzyolated according to the procedure described above. After the diethyl ether extraction, the activities of the ether phase and the water phase were determined. The determination was replicated five times. The activity due to the content of [^{14}C]putrescine was determined by counting in a United Technologies Packard Model 2000 Tri-Carb liquid scintillation analyser. The counts obtained were corrected for background activity and quenching by the matrix.

Statistics

All statistical analysis was performed by using the PC-SAS statistics program pack, notably the procedures GLM (analysis of variance, Newman Keul range test) and CORR (correlation analysis) [7].

RESULTS AND DISCUSSION

The examination of the procedure for derivatization of free putrescine present in plant material suggested by Flores and Galston [2] was focused on the handling of plant extracts and the derivatization procedure.

Extraction of putrescine

Choice of extractant. Extraction of the plant material was carried out in 5% perchloric acid or 5% trichloroacetic acid, both of which are protein denaturing. No difference was found in the efficiency of these extractants (ANOVA, $p = 0.05$, $n = 16$).

Adsorption losses of polyamines. At physiological

TABLE I
RECOVERY OF [¹⁴C]PUTRESCINE AFTER 30 min OF CONTACT WITH VIAL

Vial	Recovery (%) ^a	
	Empty glass	1 ml of 2 M NaOH in glass
New glass vial, unused	99 ± 0.9	100 ± 7.0
New glass vial, saturated	99 ± 0.4	101 ± 4.5
Old glass vial	99 ± 0.5	100 ± 1.9
Polycarbonate vial	104 ± 6.8	103 ± 2.8

^a Each value is the mean of five replicates ± standard deviation. None of the recoveries is significantly different (ANOVA and Newman Keul range test $p = 0.05$).

pH, the amino groups of the free polyamines carry positive charges, making them amenable to binding to negatively charged groups on the surfaces that they encounter. Following the rupture of plant cells in the extraction step, free polyamines may adsorb on glass surfaces by binding to free silanol groups. Such adsorption losses have been reported by Liang *et al.* [6], and caused Flores and Galston [2] to suggest that plant extracts and polyamine standards be handled and stored in plastic vials. The adsorption of putrescine on different vial materials was investigated in a tracer experiment with [¹⁴C]putrescine. The vials were tested empty or containing 1 ml of 2 M NaOH (the benzylation procedure starts with alkalization of the acid plant extract in 1 ml of 2 M NaOH). The recoveries of the tracer are given in Table I.

The adsorption experiment revealed no significant difference between any of the vial materials tested (one-way ANOVA, $p = 0.05$, $n = 40$). Addition of plant extract to the putrescine standard produced similar results, and further studies comparing polyethylene and polycarbonate vials revealed no difference between the two plastic materials (data not shown). As no adsorption loss was observed for any of the materials tested, the investigation does not support the preference of plastic materials over glass materials for handling and storage of polyamine samples.

Although free putrescine does not adsorb on the

vials, it may bind to the solid phase of the plant tissue slurry in the extraction step. In order to investigate the loss of polyamines from the liquid phase during the extraction of plant material, 1,6-diaminohexane [a diamine that is chemically closely related to putrescine (1,4-diaminobutane) but does not occur in plants] was added to the extractant prior to maceration in the extraction step. Table II gives the results obtained from the analysis of chromatographic data from experiments reported elsewhere [4].

The diamino-hexane peak height shows a very strong negative correlation with the amount of plant material extracted, indicating a loss of diamino-hexane from the liquid phase of the plant tissue slurry through adsorption on the plant tissue present. Similar adsorption must be expected for the endogenous plant amines, and should be corrected for in the calculation of free polyamine concentration in the plants.

Benzylation of plant extract

Benzylation takes place through the addition of a large excess of benzoyl chloride to the alkalized acid extract. Contact between the hydrophobic benzoyl chloride and the hydrophilic amines is established by sonicating the mixture or shaking it with a vortex mixer. A comparison of different mixing methods and intensities (vortex mixing for 3, 10 or 30 s or sonication for 60 s) showed no significant difference in benzylation efficiency ($p = 0.18$), indicating that this step is not particularly critical.

TABLE II
CORRELATION COEFFICIENTS BETWEEN PEAK HEIGHT OF 1,6-DIAMINOHEXANE ADDED PRIOR TO EXTRACTION, AND AMOUNT OF PLANT MATERIAL EXTRACTED

Results from individual polyamine analyses of 292 barley plants and 238 rape plants [4]. The range of the amount of plant material extracted for barley was 19-358 mg and for rape 75-598 mg.

Plant material	Correlation coefficient ^a
Barley	-0.4977
Rape	-0.3219

^a In both instances the correlation was significant at a level of $p = 0.0001$.

Following a reaction period of 20 min (duration not critical), the benzamides are extracted from the mixture with diethyl ether. Intimate contact between the ether and water phases for the extraction is established through vortex mixing, the duration of which was found to be important. Equilibrium was not attained after 60 s of vortex mixing [ANOVA and the Newman Keul range test show significant differences ($p = 0.05$) between 10, 30 and 60 s of vortex mixing], and care should be taken to standardize this step of the benzylation procedure.

The low surface tension of diethyl ether makes the addition and withdrawal of exact volumes difficult. However, the operation is facilitated by wetting the inside of the pipette tip with diethyl ether just prior to aspiration of the ether sample.

The ether and water phases are allowed to separate for 10 min (centrifugation is superfluous) before a well defined and fixed fraction (e.g., 50%) is withdrawn from the ether phase and evaporated to dryness. Drying is rapid under a flow of nitrogen. However, for the concurrent benzylation of a large number of samples, passive ether evaporation at room temperature under a dust-preventing shelter for several hours may be preferable, and does not influence the final results (data not shown).

Overall benzylation efficiency. The overall efficiency of the benzylation procedure was investigated in a tracer experiment with [^{14}C]putrescine. An investigation of the distribution of [^{14}C]putrescine after a diethyl ether–water equilibration showed that only about 1% of the free putrescine is found in the ether phase (data not shown). Adsorption of putrescine on glass was found to be insignificant. The activity found in the ether phase following benzylation is therefore ascribed to benzyolated [^{14}C]putrescine alone. The overall benzylation efficiency, defined as activity of benzyolated putrescine in the ether phase after benzylation divided by total activity of putrescine in mixture after benzylation, can be calculated as activity of ether phase after benzylation divided by total activity in sample prior to benzylation.

The benzylation efficiency was found to be 75%, varying between 59 and 83% ($n = 5$) with a standard error of 5%. The overall recovery of the tracer after benzylation was 99%. Roberts *et al.* [8] found a benzylation efficiency of 94% with [^{14}C]putrescine added to tissue slurries before ben-

zylation, and Lauren *et al.* [9] found an efficiency of 79% with a range of 68–97%.

Internal standard

The variation in benzylation efficiency justifies the addition of an internal standard to the sample to ensure quantitative determination of the polyamines. Redmond and Tseng [1] suggested 1,6-diaminohexane. With no natural occurrence in plants, and close chemical similarity to putrescine, it is an obvious choice as an internal standard for the determination of putrescine.

By addition of the internal standard to the solvent used for extracting the plant material, the internal standard will experience exactly the same conditions as the polyamines from the plant during benzylation. Roberts *et al.* [8] found nearly identical recoveries of diaminohexane and putrescine after addition to plant extract and subsequent benzylation. Variations in benzylation efficiency can thus be corrected by the use of an internal standard. It is unclear, however, whether externally added diaminohexane and endogenous free plant polyamines will behave alike during the extraction of plant material, in which process diaminohexane starts outside the plant cells and the endogenous polyamines inside. Table III summarizes information obtained from analysis of chromatographic data from experiments reported elsewhere [4].

The plants were grown under identical conditions

TABLE III
CORRELATION COEFFICIENTS BETWEEN PEAK HEIGHT OF ADDED 1,6-DIAMINOHEXANE AND PEAK HEIGHTS OF PUTRESCINE AND SPERMIDINE AFTER HPLC ANALYSIS

Plants were grown under identical conditions: 53 barley plants for 2–4 weeks and 51 rape plants for 3–5 weeks (control plants from experiments reported elsewhere [4]). Peak heights of putrescine and spermidine were calculated for a fixed amount of plant material.

Compound	Correlation coefficient ^a	
	Barley	Rape
Putrescine	0.5192	0.7145
Spermidine	0.6921	0.7205

^a In all instances the correlation was significant at a level of $p = 0.0001$.

and were expected to show similar contents of putrescine and of spermidine. For a fixed amount of plant material extracted, the concentrations of each of the two polyamines would therefore be expected to be at the same level in all the samples, as is the case for the diamino-hexane that was added together with the extractant.

The positive correlation between the peak heights of diamino-hexane and putrescine or spermidine obtained after HPLC of the benzoylated plant extracts is very strong. This indicates that the overall behaviour of diamino-hexane, putrescine and spermidine is similar, not only during the derivatization procedure but also in the plant tissue slurry. The endogenous plant polyamines therefore seem to suffer adsorption losses similar to the externally added diamino-hexane during extraction of the plant material.

The addition of diamino-hexane as an internal standard at the start of the polyamine analysis through the extractant used for extracting polyamines from the plant material thus permits the correction of errors and variations in efficiencies of the entire procedure.

ACKNOWLEDGEMENTS

The author thanks the Director of Research, Dr. Hans Løkke, Department of Terrestrial Ecology, National Environmental Research Institute, and Professor Finn Bro-Rasmussen, Laboratory of Environmental Sciences and Ecology, Technical University of Denmark, for fruitful discussions and valuable advice. The skilled technical assistance of Birthe Ebert is gratefully acknowledged. This study was financed by the Danish Centre of Environmental Biotechnology, University of Copenhagen.

REFERENCES

- 1 J. W. Redmond and A. Tseng, *J. Chromatogr.*, 170 (1979) 479.
- 2 H. E. Flores and A. W. Galston, *Plant Physiol.*, 69 (1982) 701.
- 3 R. D. Slocum, H. E. Flores, A. W. Galston and L. H. Weinstein, *Plant Physiol.*, 89 (1989) 512.
- 4 M. Z. Hauschild, *Ecotoxicol. Environ. Saf.*, in press.
- 5 M. Z. Hauschild, *Sci. Total Environ.*, in press.
- 6 T. Liang, G. Mezzetti, C. Chen and S. Liao, *Biochim. Biophys. Acta*, 542 (1978) 430.
- 7 *SAS Release 6.03*, SAS Institute, Cary, NC, 1987.
- 8 D. R. Roberts, M. A. Walker and E. B. Dumbroff, *Phytochemistry*, 24 (1985) 1089.
- 9 D. R. Lauren, C. H. Parker, M. P. Agnew and G. S. Smith, *J. Liquid Chromatogr.*, 4 (1981) 1269.

Short Communication

High-performance liquid chromatographic determination of cardenolides in *Digitalis* leaves after solid-phase extraction

Hans Wiegrebé and Max Wichtl

Institut für Pharmazeutische Biologie, Philipps-Universität, Deutschhausstrasse 17 1/2, W-3550 Marburg/Lahn (Germany)

(First received July 7th, 1992; revised manuscript received October 27th, 1992)

ABSTRACT

For HPLC analysis of cardenolide glycosides of *Digitalis lanata* the separation of the main compounds from other constituents is useful. An improved method for doing this, based on solid-phase extraction on a C₁₈ modified poly(styrene–divinylbenzene) polymer, is described. The presented assay permits quantitative estimation of more than 50 cardenolides in about 2 mg of dried leaf powder of *Digitalis lanata* with high speed and accuracy.

INTRODUCTION

The analysis of cardenolides in *Digitalis* leaves has been the subject of a large number of publications during the last 25 years. By implementing more and more efficient chromatographic methods in order to separate the different cardenolides, the analysis has been simplified and sensitivity improved.

After the first successful determination of the whole cardenolide pattern, using a combined column and paper chromatographic method [1], high-performance liquid chromatography (HPLC) is today considered to be the standard method for analysis of cardenolides in *Digitalis* leaves [2–6]. For

HPLC analysis, the cardenolides are extracted with aqueous–alcoholic mixtures and preconcentrated by extraction with organic solvents. The extraction of cardenolides from the leaf extract with chloroform–isopropanol mixtures can be replaced by using Extrelut extraction columns for sample preparation [7]. Both methods are based on liquid–liquid extraction and lead to similar results. A disadvantage of the former methods is the loss of cardenolides of up to 10%, and a disadvantage of Extrelut extraction is a partial decomposition of gitaloxigenin glycosides to the corresponding gitoxigenin glycosides [8].

In this paper we present an improved method of cardenolide determination by HPLC, based on solid-phase extraction using an extraction column filled with RP-18 modified polystyrene (Adsorbex-Polyspher RP-18).

Correspondence to: M. Wichtl, Institut für Pharmazeutische Biologie, Philipps-Universität, Deutschhausstrasse 17 1/2, W-3550 Marburg/Lahn, Germany.

EXPERIMENTAL

Chemicals and solid-phase extraction columns

Methanol LiChrosolv was used for extraction and acetonitrile gradient-grade LiChrosolv was used for chromatography (both from Merck, Darmstadt, Germany). Most of the cardenolides are products of previous isolations [8–10]. The internal standard β -methylidigoxin (β -MDg) was donated by Dr. W. Kreis (Tübingen, Germany) and some of the cardenolides were gifts from Boehringer Mannheim (Germany). Adsorbex extraction columns filled with silica-based materials and Adsorbex-Polyspher RP-18 columns were obtained from Merck.

HPLC conditions and apparatus

Chromatography was carried out at a flow-rate of 1.2 ml/min and a column temperature of 40°C on a high-performance liquid chromatograph consisting of a Model 600 E solvent-delivery system, a Model U6K injector, a Model 481 variable-wavelength UV absorbance detector operating at 225 nm (analytical cell) and a Model 745 integrator (all from Millipore-Waters, Milford, MA, USA).

A LiChroCART 250-4 cartridge column was used in combination with a LiChroCART 4-4 guard cartridge, both filled with LiChrospher 100 RP-18 (5 μ m) packing material (all from Merck).

Cardenolides were eluted with an acetonitrile-water gradient as follows: initial = 20% acetonitrile (A), 35 min = 32% A, 45 min = 40% A, 55 min = 50% A, 59 min = 55% A, 61 min = 20% A. The composition of the mobile phase changes linearly.

Extraction procedures

About 300 mg of dried leaf powder were accurately weighed and treated with 20 ml of methanol (70%) containing 1 ml of a methanolic solution of β -methylidigoxin as internal standard at a concentration of 1.2 mg/ml. This solution was refluxed on a boiling water bath for 10 min and then rapidly cooled to room temperature. After addition of 5 ml of a solution of lead acetate (15%), the extract was mixed well, 5 ml of a solution of monosodium phosphate (4%) were added and the extract was mixed again. The extract was diluted with water to 50 ml and centrifuged for 5 min at 3300 g (solution A).

Before use, the Adsorbex-Polyspher RP-18 extraction columns were treated by washing with 2 \times 2 ml of methanol, followed by 2 \times 2 ml of water. A vacuum of 300 mbar was applied to the end of the column at each stage of the extraction procedure. An aliquot of 10 ml of solution A was passed through the column, followed by washing with 2 ml of water. The columns were eluted with 2 \times 1 ml of methanol and 20 μ l of this solution were used for HPLC.

For estimation of cardenolides in smaller quantities of drug powder, the method was modified as follows: 1.5–2 mg of leaf powder were treated with 4 ml of methanol (70%) containing 10 μ l of the internal standard solution and extracted as described above. Cleaning procedures were carried out with reduced volumes of the above-mentioned solutions of lead acetate and monosodium phosphate. The extract was diluted with water to a volume of 10 ml, and after centrifugation the whole supernatant was passed through the Adsorbex-Polyspher RP-18 column. The eluate was evaporated to dryness and the residue dissolved in 100 μ l of methanol. A 20- μ l aliquot of this solution was used for HPLC.

RESULTS AND DISCUSSION

Sample preparation by solid-phase extraction

Different materials were tested to determine the most suitable adsorbent for solid-phase extraction of cardenolides. While all modified silica-based adsorbents were unable to retain cardenolides from aqueous solutions, Adsorbex-Polyspher RP-18 extraction columns as adsorbent yielded a cardenolide-free aqueous eluate.

According to the information supplied by the manufacturer, these columns contain 100 mg of a macroporous, C₁₈ modified poly(styrene-divinylbenzene) polymer. The spherical polymer particles have a size of 35 \pm 5 μ m.

The optimum retention of cardenolides passing the extraction column is achieved at a methanol concentration of the leaf extract of about 30%. Lower concentrations of methanol lead to small losses of all cardenolides as a result of a poor surface contact of the hydrophobic adsorbent with the aqueous solution being extracted. Methanol concentrations greater than 40% lead to losses of polar cardenolides. To remove polar substances like sug-

TABLE I

RECOVERY OF SELECTED CARDENOLIDES AFTER SOLID-PHASE EXTRACTION

A 10-ml volume of a mixture of some cardenolides in methanol (30%) was passed through an Adsorbex-Polyspher RP-18 extraction column and eluted with 2×1 ml of methanol (sample B). As reference the same solution was injected without being passed through the column (sample A). The concentration of the cardenolides in the sample mixture was about 0.1–0.2 mg/10 ml, corresponding to the cardenolide concentration in a leaf extract obtained in the described way.

Glycoside (retention time)	Sample A		Sample B		Recovery (%)
	Area (mean of $n=3$)	R.S.D. (%)	Area (mean of $n=3$)	R.S.D. (%)	
Digitalinum verum (13.9 min)	3768	6.8	3590	2.7	95.3
Digoxigenin mono- digitoxoside (15.1 min)	3266	3.7	3193	2.9	97.8
Strospeside (23.2 min)	5589	2.7	5729	1.9	101.0
Lanatoside B (47.6 min)	867	2.7	871	1.8	100.5
Digitoxin (58.6 min)	2998	2.0	3000	2.3	100.1

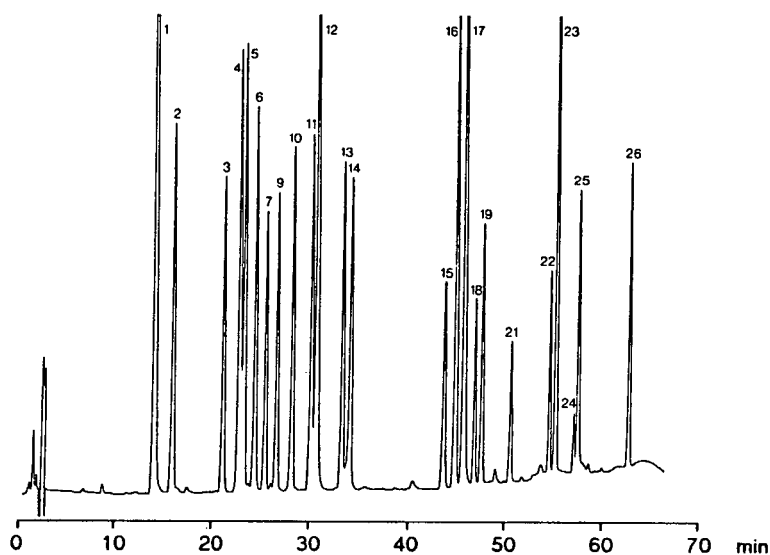


Fig. 1. Chromatogram of a mixture of different cardenolides. A 20- μ l aliquot of a sample solution containing 0.05–1.5 μ g of each cardenolide was injected. HPLC conditions were as described in the text. Peaks: 1 = digitalinum verum; 2 = Gl-Dx-Dx-C; 3 = glucoverodoxin; 4 = strospeside; 5 = glucogitoroside; 6 = desacetyllanatoside C; 7 = Glum-Dx-Dx-C; 8 = neo-glucodigifucoside; 9 = glucodigifucoside; 10 = neo-odorobioside G; 11 = odorobioside G; 12 = verodoxin; 13 = lanatoside C; 14 = glucoevatromononide; 15 = Gl-Dx-Dx-A; 16 = α -acetyldigoxin; 17 = β -methyldigoxin; 18 = lanatoside B; 19 = β -acetyldigoxin; 20 = purpurea glucoside A; 21 = lanatoside E; 22 = lanatoside A; 23 = α -acetylgitoxin; 24 = β -acetylgitoxin; 25 = digitoxin; 26 = α -acetyldigitoxin.

TABLE II

RETENTION TIME (t_R) OF DIFFERENT CARDENOLIDES FROM *DIGITALIS* LEAVES

Aglycones: A = digitoxigenin; B = gitoxigenin; C = digoxigenin; D = dignatigenin; E = gitaloxigenin; F = oleandrigenin. Sugars: AcDx = acetyldigitoxose; Didesgl = 2,6-dideoxyglucose; Dtl = digitalose; Dx = digitoxose; Fuc = fucose; Gl = glucose; Glum = glucumethylose.

Common name	Abbreviated form (according to ref. 11)	t_R (min)	Relative t_R (β -methyl digoxin = 1)
Digoxigenin	Dtl-D	4.57	0.099
	C	8.23	0.178
Digitalinum verum	Dtl-C	12.97	0.280
	Gl-Dtl-B	13.88	0.300
Subalpinoside	Gl-Dtl-F	14.49	0.313
	Dx-C	15.08	0.326
	Glum-Dx-C	15.45	0.334
	Gl-Dx-Dx-C	15.69	0.339
	Gl-A	19.09	0.412
	Xyl-Dx-Dx-C	20.26	0.437
	Glucoverodoxin	Gl-Dtl-E	21.06
Strosposide	Didesgl-Dx-C	21.38	0.462
	Dtl-B	22.62	0.488
Glucogitoroside	Gl-Dx-B	23.15	0.500
Gitoxigenin	B	23.77	0.513
Desacetyl lanatoside C	Gl-Dx-Dx-Dx-C	24.15	0.521
	Gl-AcDx-C	24.61	0.531
	Dx-Dx-C	24.90	0.538
Diginatin	Dx-Dx-Dx-D	24.92	0.538
	Glum-Dx-Dx-C	25.51	0.551
Neo-glucodigifucoside	N-Gl-Fuc-A	26.04	0.562
Lanatoside D	Gl-AcDx-Dx-Dx-D	26.06	0.563
	Gl-Glum-A	26.57	0.574
	Gl-Fuc-A	26.71	0.577
Glucolanadoxin	Gl-Dx-E	28.33	0.612
Neo-odorobioside G	N-Gl-Dtl-A	28.33	0.612
Odorobioside G	Gl-Dtl-A	30.28	0.654
Verodoxin	Dtl-E	30.80	0.665
	Didesgl-Dx-Dx-C	30.98	0.669
Glucodigoxoside	Gl-Dx-Dx-Dx-Dx-C	32.68	0.706
Lanatoside C	Gl-AcDx-Dx-Dx-C	33.43	0.722
Digoxin	Dx-Dx-Dx-C	33.51	0.724
Glucovatromonoside	Gl-Dx-A	34.31	0.741
	Glum-A	36.00	0.777
	AcDx-Dx-C	37.33	0.806
	Xyl-Dx-A	39.93	0.862
	Gl-Dx-Dx-Dx-B	40.69	0.879
Purpurea glycoside B	Dx-E	40.87	0.883
Lanadoxin	A	41.15	0.889
Digitoxigenin	Dx-Dx-Dx-Dx-C	41.53	0.897
	Gl-Dx-Dx-A	44.23	0.955
α -Acetyldigoxin	α -AcDx-Dx-Dx-C	45.48	0.982
β -Methyl digoxin	β -MethylDx-Dx-Dx-C	46.31	1.000
Glucogitaloxin	Gl-Dx-Dx-Dx-E	46.34	1.001
Lanatoside B	Gl-AcDx-Dx-Dx-B	47.62	1.028
Evatromonoside	Dx-A	48.45	1.046
β -Acetyldigoxin	β -AcDx-Dx-Dx-C	48.47	1.047
Gitoxin	Dx-Dx-Dx-B	49.80	1.075
Purpurea glycoside A	Gl-Dx-Dx-Dx-A	51.27	1.107
Lanatoside E	Gl-AcDx-Dx-Dx-E	51.48	1.112

TABLE II (continued)

Common name	Abbreviated form (according to ref. 11)	t_R (min)	Relative t_R (β -methylidigoxin = 1)
Lanatoside F	Gl-AcDx-Dx-Dx-F	52.49	1.133
	Dx-Dx-A	54.15	1.169
Gitaloxin	Dx-Dx-Dx-E	54.15	1.169
Lanatoside A	Gl-AcDx-Dx-Dx-A	55.62	1.201
α -Acetylgitoxin	α -AcDx-Dx-Dx-B	56.26	1.215
β -Acetylgitoxin	β -AcDx-Dx-Dx-B	58.31	1.259
Digitoxin	Dx-Dx-Dx-A	58.57	1.265
α -Acetylgitaloxin	α -AcDx-Dx-Dx-E	59.88	1.294
α -Acetyldigitoxin	α -AcDx-Dx-Dx-A	63.94	1.381
β -Acetyldigitoxin	β -AcDx-Dx-Dx-A	66.29	1.431

ars, the column was washed after adsorption of the cardenolides with 2 ml of water. The recoveries shown in Table I demonstrate the elution of the selected cardenolides using methanol as eluent. The methanolic eluate served as sample solution for HPLC analysis. If this sample solution is stored at low temperatures (4°C) no decomposition of cardenolides is detectable. For extraction and sample preparation only about 45 min are needed. Moreover, the Adsorbex-Polyspher RP-18 extraction columns can be used several times without loss of performance.

HPLC

Chromatograms of a mixture of cardenolides (Fig. 1) and of a *Digitalis lanata* leaf extract (Fig. 2) demonstrate the performance of the HPLC method described in this paper. Using β -methylidigoxin as internal standard the different cardenolides can be identified by their relative retention times (Table II).

The limit of detection for quantitative determination of cardenolides with this method is about 10 pmol (corresponding to approximately 11 ng of lanatoside C).

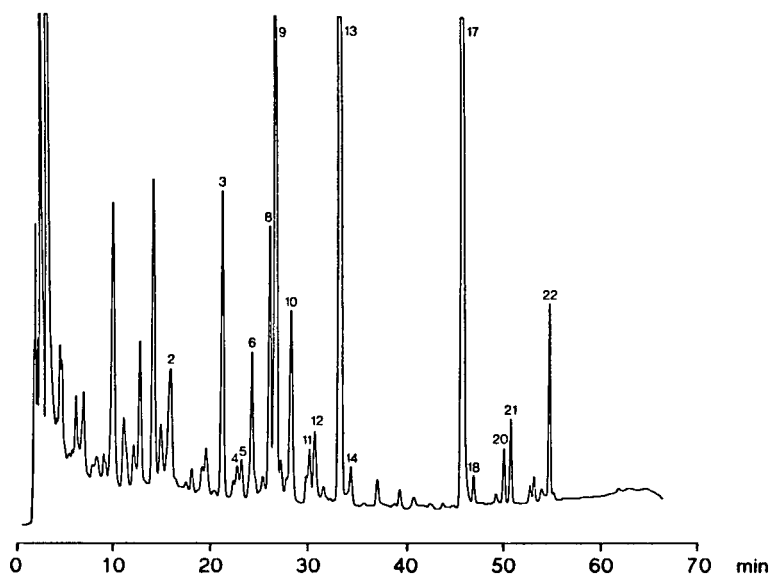


Fig. 2. Chromatogram of a *Digitalis lanata* leaf extract. For preparation of the leaf powder the leaves were collected and immediately frozen to -196°C in liquid nitrogen, then freeze-dried at a product temperature of -5°C . The dried leaves were powdered and analysed as described in the text. Acetyltridigitoxosides as products of fermentations could not be detected in the leaf extract. Peaks as in Fig. 1.

ACKNOWLEDGEMENT

Financial support of this work by Deutsche Forschungsgemeinschaft (DFG, Wi 584/6-1) is gratefully acknowledged.

REFERENCES

- 1 F. Kaiser, *Arch. Pharm. (Weinheim)*, 299 (1966) 263.
- 2 M. Wichtl, M. Mangkudidjojo and W. Wichtl-Bleier, *J. Chromatogr.*, 234 (1982) 503.
- 3 W. Kreis, U. May and E. Reinhard, *Plant Cell Rep.*, 5 (1989) 442.
- 4 J. J. Lichius and M. Wichtl, *Sci. Pharm.*, 57 (1989) 439.
- 5 Y. Fujii, Y. Ikeda and M. Yamazaki, *J. Chromatogr.*, 479 (1989) 319.
- 6 Y. Fujii, Y. Ikeda, I. Okamoto and M. Yamazaki, *J. Chromatogr.*, 508 (1990) 241.
- 7 G. Tittel, *Pharm. Ind.*, 48 (1986) 822.
- 8 Th. Fingerhut, *Doctoral Thesis*, Philipps-Universität, Marburg/Lahn, 1992.
- 9 D. Krüger, *Doctoral Thesis*, Philipps-Universität, Marburg/Lahn, 1984.
- 10 J. J. Lichius, D. El Khyari and M. Wichtl, *Planta Med.*, 57 (1991) 159.
- 11 M. Wichtl, *Pharm. Unserer Zeit*, 7 (1978) 33.

Short Communication

Determination of acidic saponins in crude drugs by high-performance liquid chromatography on octadecylsilyl porous glass

Hideko Kanazawa, Yoshiko Nagata, Yoshikazu Matsushima and Masashi Tomoda
Kyoritsu College of Pharmacy, Shibakoen 1–5–30, Minato-ku, Tokyo 105 (Japan)

Nobuharu Takai

Institute of Industrial Science, University of Tokyo, Roppongi 7–22–1, Minato-ku, Tokyo 106 (Japan)

(First received July 10th, 1992; revised manuscript received November 3rd, 1992)

ABSTRACT

High-performance liquid chromatographic (HPLC) analysis on octadecylsilyl porous glass was investigated for acidic saponins in ginseng, bupleurum root and senega. The acidic saponins, malonyl-ginsenosides, malonyl-saikosaponins and senegins, as well as neutral saponins in the crude drugs were separated rapidly by HPLC on this column with aqueous acetonitrile containing KH_2PO_4 as the mobile phase at room temperature.

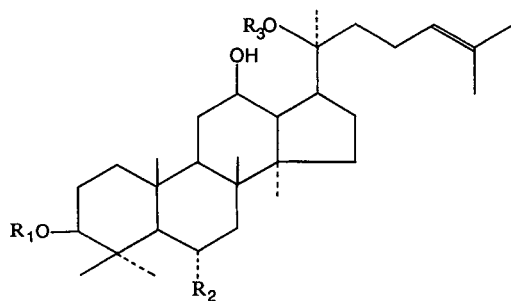
INTRODUCTION

In previous work, an octadecylsilyl porous glass (MPG-ODS) was prepared and it was found to be a useful packing material for reversed-phase high-performance liquid chromatography (HPLC) [1,2]. Saponins of ginseng, the root of *Panax ginseng*, and other crude drugs were determined by HPLC on MPG-ODS [3–5].

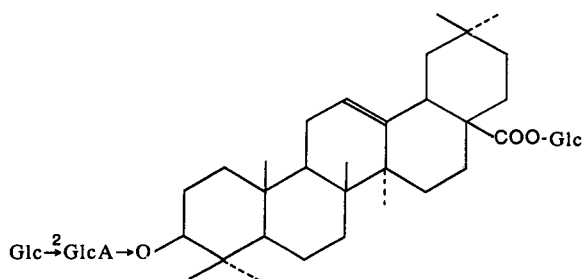
Neutral dammarane saponins (ginsenosides-Rb₁, -Rb₂, -Rc and -Rd) and an acidic saponin (ginsenoside-Ro, a glucuronide saponin of oleanolic acid) isolated from ginseng have been extensively studied from the chemical, pharmacognostic and pharma-

cological view points [6–8]. Kitagawa *et al.* [9] reported that white ginseng contains a considerable amount of acidic malonate of the dammarane saponins, malonyl-ginsenosides-Rb₁, -Rb₂, -Rc and -Rd. These malonyl-ginsenosides are unstable and readily demalonylated by heating. Recently, acidic malonate of saikosaponins, malonyl-saikosaponin a and d, were also isolated from bupleurum root [10]. Other well known acidic saponins are those contained in senega. Senega is the root of *Polygala senega* and has been used as an expectorant. Acidic saponins of Senega, senegins II, II', III and IV, are the glycosides of pentacyclic triterpenes and the sugar moieties contain glucose, fucose, rhamnose, xylose, galactose, etc. The structures of the acidic saponins and related neutral saponins are shown in Fig. 1.

Correspondence to: Y. Matsushima, Kyoritsu College of Pharmacy, Shibakoen 1–5–30, Minato-ku, Tokyo 105, Japan.

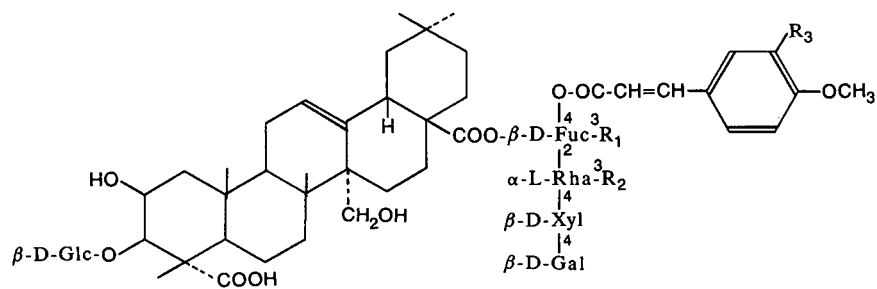


	R ₁	R ₂	R ₃
malonyl-ginsenoside Rb ₁	Ma ⁶ →Glc ² →Glc→	H	Glc ⁶ →Glc→
malonyl-ginsenoside Rb ₂	Ma ⁶ →Glc ² →Glc→	H	Ara _p ⁶ →Glc→
malonyl-ginsenoside Rc	Ma ⁶ →Glc ² →Glc→	H	Ara _f ⁶ →Glc→
malonyl-ginsenoside Rd	Ma ⁶ →Glc ² →Glc→	H	Glc→
ginsenoside Rb ₁	Glc ² →Glc→	H	Glc ⁶ →Glc→
ginsenoside Rb ₂	Glc ² →Glc→	H	Ara _p ⁶ →Glc→
ginsenoside Rc	Glc ² →Glc→	H	Ara _f ⁶ →Glc→
ginsenoside Rd	Glc ² →Glc→	H	Glc→
ginsenoside Re	H	Rha ² →Glc→O	Glc→
ginsenoside Rf	H	Glc ² →Glc→O	H
ginsenoside Rg ₁	H	Glc→O	Glc→
ginsenoside Rg ₂	H	Rha ² →Glc→O	H

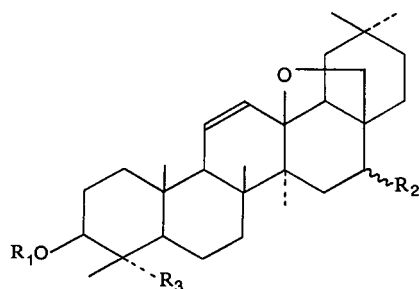


ginsenoside Ro (chikusetsusaponin-V)

Fig. 1.



	R_1	R_2	R_3
senegin II	H	H	OCH_3
senegin II'	H	H	H
senegin III	$\alpha\text{-L-Rha}$	H	H
senegin IV	$\alpha\text{-L-Rha}$	$\alpha\text{-L-Rha}$	H



	R_1	R_2	R_3
malonyl-saikosaponin a	$\text{Ma} \xrightarrow{6} \text{Glc} \xrightarrow{3} \text{Fuc} \rightarrow$	$\beta\text{-OH}$	CH_2OH
malonyl-saikosaponin d	$\text{Ma} \xrightarrow{6} \text{Glc} \xrightarrow{3} \text{Fuc} \rightarrow$	$\alpha\text{-OH}$	CH_2OH
saikosaponin a	$\text{Glc} \xrightarrow{3} \text{Fuc} \rightarrow$	$\beta\text{-OH}$	CH_2OH
saikosaponin c	$\text{Rha} \xrightarrow{4} \text{Glc} \rightarrow$ $\text{Glc} \xrightarrow{6}$	$\beta\text{-OH}$	CH_3
saikosaponin d	$\text{Glc} \xrightarrow{3} \text{Fuc} \rightarrow$	$\alpha\text{-OH}$	CH_2OH

Fig. 1. Structures of saponins. Ma = malonyl; Glc, β -D-glucopyranosyl; Rha = α -L-rhamnopyranosyl; Ara_p = α -L-arabinopyranosyl; Ara_f = α -L-arabinofuranosyl; GlcA = β -D-glucopyranosyl; Xyl = xylopyranosyl; Gal = galactopyranosyl; Fuc = β -D-fucopyranosyl.

In traditional oriental medicine, several crude drugs are generally prescribed in a single formula. Ginseng is one of the most important crude drugs in such medicine. Bupleurum root is often prescribed with ginseng.

In this paper, we report the HPLC analysis on an MPG-ODS column of the acidic saponins in the crude drugs. Simultaneous determinations of the acidic and neutral saponins were successful at room temperature.

EXPERIMENTAL

Materials

Acetonitrile was of HPLC grade (Wako, Tokyo, Japan). Water for use as a mobile phase constituent was prepared by passage through a Milli-Q water purification unit (Millipore, Bedford, MA, USA). Other chemicals were of analytical-reagent grade. A Sep-Pak C₁₈ cartridge (Waters, Milford, MA, USA) was used for pretreatment of samples.

The standard samples of ginsenosides-Rb₁, -Rb₂, -Rc, -Rd, -Rf, -Rg₂ and -Ro, and senegins II, II', III and IV were kindly supplied by Professor J. Shoji (Showa University, Tokyo), those of malonyl-ginsenosides-Rb₁, -Rb₂, -Rc and -Rd by Professor I. Kitagawa (Osaka University, Osaka) and those of malonyl-saikosaponins a and d by Dr. H. Taguchi (Tsumura, Ibaragi, Japan). Saikosaponins a, c and d were purchased from Wako.

HPLC conditions

Octadecylsilyl porous glass (MPG-ODS) was supplied by Ise Chemical Industrial (Tokyo, Japan). Its pore size was 550 Å and its particle size distribution was 8–10 μm. MPG-ODS was packed into stainless-steel columns (150 × 4.0 mm I.D. and 250 × 4.0 mm I.D.) by the high-pressure slurry technique. The effective theoretical plate numbers were 6100 and 7070, respectively. The HPLC system used consisted of a Tosoh Model CCPM multi-pump, a Rheodyne Model 7125 valve, a Tosoh Model UV-8000 monitor and a Hitachi Model 833A data processor. The system was operated at room temperature.

Sample preparation from crude drugs

A 1.0-g mass of crude drugs was pulverized and extracted with 20 ml of 70% methanol at room tem-

perature (20°C) for 30 min and the extract was filtered. After the procedure had been repeated five times, the extracts were combined and evaporated. The residue was dissolved in water and applied to a Sep-Pak C₁₈ cartridge pretreated with 5 ml of water and 2 ml of methanol. After washing the cartridge with 10 ml of water and 15 ml of 30% methanol, the sample was eluted with 5 ml of methanol and the eluate was evaporated to dryness under reduced pressure. The residue was dissolved in 2 ml of the eluent and a 1–10-μl portion was injected into the HPLC system.

RESULTS

For the HPLC of neutral saponins on the MPG-ODS columns, a mixture of acetonitrile and water was used as the mobile phase [3–5]. A mobile phase containing 15–50% of acetonitrile in water did not give satisfactory results for the separation of the acidic saponins.

With aqueous acetonitrile containing KH₂PO₄, excellent HPLC separation of the acidic saponins and also the neutral saponins was achieved. Fig. 2 shows the correlation of the concentration of KH₂PO₄ with the *k'* values of the saponins.

Isocratic elution was examined for quantitative analysis. As shown in Fig. 3, ginsenosides-Rb₁,

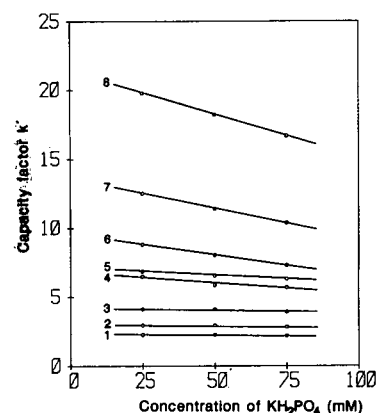


Fig. 2. Effect of concentration of KH₂PO₄ on the capacity factors (*k'*) of the saponins: 1 = malonyl-ginsenoside-Rb₁; 2 = malonyl-ginsenoside-Rc; 3 = malonyl-ginsenoside-Rb₂; 4 = ginsenoside-Rb₁; 5 = malonyl-ginsenoside-Rd; 6 = ginsenoside-Rc; 7 = ginsenoside-Rb₂; 8 = ginsenoside-Rd. Concentration of acetonitrile, 25%.

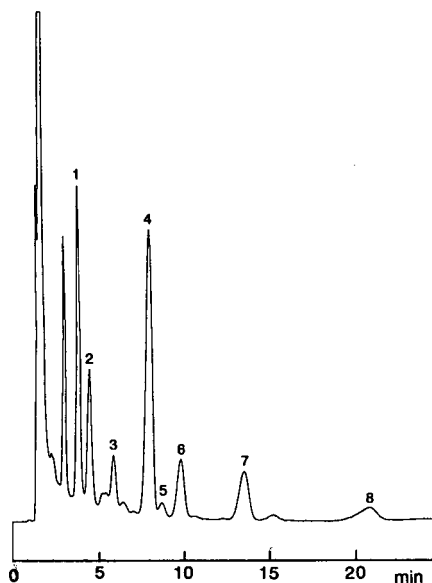


Fig. 3. Chromatogram of ginsenosides and malonyl-ginsenosides in an extract of ginseng (sample 1). Saponins as in Fig. 2. Column, MPG-ODS (150 × 4 mm I.D.); eluent, acetonitrile–50 mM KH_2PO_4 (25.5:74.5); flow-rate, 1.0 ml/min; detection at 203 nm.

-Rb₂, -Rc and -Rd and malonyl-ginsenosides-Rb₁, -Rb₂, -Rc and -Rd in an extract of ginseng were well separated on the 150 mm × 4 mm I.D. MPG-ODS column with acetonitrile–50 mM KH_2PO_4 (25.5:74.5). The flow-rate was 1.0 ml/min and the peaks were monitored at 203 nm. With this eluent, linear responses between peak areas and amounts injected were obtained from five replicate injections of standard solutions of malonyl-ginsenosides-Rb₁, -Rc and -Rb₂ in the range of 0–5 μg , as indicated by following equations:

$$y = 1.70x - 0.01; r = 0.999 \text{ (malonyl-ginsenoside-Rb}_1\text{)}$$

$$y = 1.17x - 0.01; r = 0.999 \text{ (malonyl-ginsenoside-Rc)}$$

$$y = 0.83x - 0.02; r = 0.997 \text{ (malonyl-ginsenoside-Rb}_2\text{)}$$

where y is the peak area and x the amount injected (μg). For the least-squares regression the correlation coefficients were very close to 1.

The mean recovery of known amounts of malo-

nyl-ginsenosides-Rb₁, -Rc and -Rb₂ in ginseng extracts was 96% (R.S.D. = 2.1%; $n = 5$).

From the results of quantitative analysis ($n = 4$), the contents of malonyl-ginsenosides-Rb₁, -Rc and -Rb₂ were 0.40% (S.D. = 0.003%), 0.23% (S.D. = 0.04%) and 0.13% (S.D. = 0.006%), respectively, in the extract of ginseng in Fig. 3.

For the separation of other ginsenosides such as ginsenosides-Rf, -Rg₂ and -Ro, the 250 × 4.0 mm I.D. MPG-ODS column was used. Simultaneous analysis of eleven acidic and neutral saponins was achieved in 25 min with acetonitrile–50 mM KH_2PO_4 (25.5:74.5), as shown in Fig. 4. The eleven saponins simultaneously analysed were malonyl-ginsenosides-Rb₁, -Rb₂, -Rc and -Rd and ginsenosides-Ro, -Rf, -Rg₂, -Rb₁, -Rb₂, -Rc and -Rd. The flow-rate was 2.0 ml/min.

The HPLC of malonyl-saikosaponins a and d, acidic saponins in bupleurum root, was also possible by addition of 50 mM KH_2PO_4 to the mobile

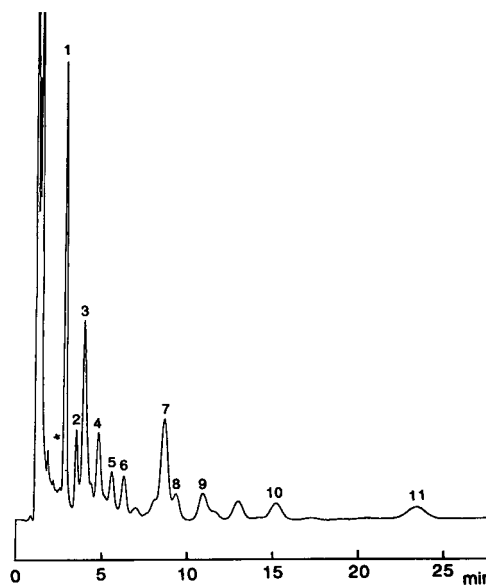


Fig. 4. Chromatogram of ginsenosides and malonyl-ginsenosides in an extract of ginseng (sample 2). Saponins: 1 = ginsenoside-Ro; 2 = ginsenoside-Rf; 3 = malonyl-ginsenoside-Rb₁; 4 = malonyl-ginsenoside-Rc; 5 = ginsenoside-Rg₂; 6 = malonyl-ginsenoside-Rb₂; 7 = ginsenoside-Rb₁; 8 = malonyl-ginsenoside-Rd; 9 = ginsenoside-Rc; 10 = ginsenoside-Rb₂; 11 = ginsenoside-Rd. Column, MPG-ODS (250 × 4 mm I.D.); eluent, acetonitrile–50 mM KH_2PO_4 (25.5:74.5); flow-rate, 2.0 ml/min; detection at 203 nm.

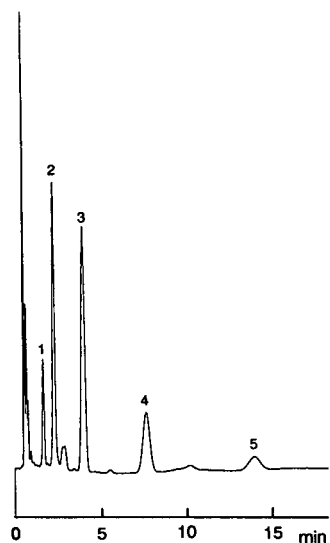


Fig. 5. Chromatogram of saikosaponins and malonyl-saikosaponins in an extract of bupleurum root. Saponins: 1 = saikosaponin c; 2 = malonyl-saikosaponin a; 3 = saikosaponin a; 4 = malonyl-saikosaponin d; 5 = saikosaponin d. Column, MPG-ODS (150 × 4 mm I.D.); eluent, acetonitrile–50 mM KH_2PO_4 (27.5:72.5); flow-rate, 2.0 ml/min; detection at 203 nm.

phase. Malonyl-saikosaponins a and d and saikosaponins a, c and d were separated on the MPG-ODS column (150 mm × 4.0 mm I.D.) in 20 min with acetonitrile–50 mM KH_2PO_4 (27.5:72.5), as shown in Fig. 5. The flow-rate was 2.0 ml/min and the peaks were monitored at 203 nm.

Separation of senegins II' and III by HPLC was found to be difficult with aqueous acetonitrile containing KH_2PO_4 . For their rapid separation, a mixture of acetonitrile and phosphate buffer (containing 25 mM KH_2PO_4 and 25 mM K_2HPO_4 ; pH 6.8) was used as the mobile phase. On the 150 mm × 4 mm I.D. MPG-ODS column, an excellent separation of senegins II, II', III and IV was obtained in 15 min with 30% acetonitrile in phosphate buffer as the mobile phase, as shown in Fig. 6. The flow-rate was 1.0 ml/min and the peaks were monitored at 315 nm.

DISCUSSION

HPLC of acidic saponins of ginseng and other crude drugs has been reported by Yamaguchi and

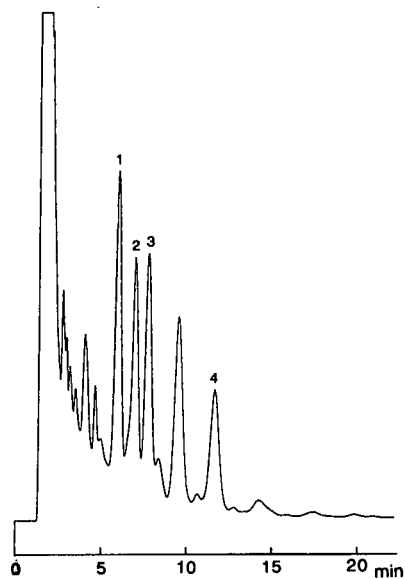


Fig. 6. Chromatogram of senegins in an extract of senega. Saponins: 1 = senegin IV; 2 = senegin III; 3 = senegin II'; 4 = senegin II. Column, MPG-ODS (150 × 4 mm I.D.); eluent, 30% acetonitrile in phosphate buffer (pH 6.8); flow-rate, 1.0 ml/min; detection at 315 nm.

co-workers [11,12]. The reported method took about 40 min for the separation of a mixture of ginsenosides and the column temperature was 40°C. The present method was more rapid: the eleven ginsenosides were separated within 25 min at room temperature. Rapid and excellent separation of acidic saikosaponins was also achieved with this method. The method was suitable for separation of these acidic saponins, which are unstable towards heat.

Nakajima *et al.* [13] reported the separation of senegins II, II', III and IV by HPLC on a TSK gel LS-410K (ODS silica gel) column using acetonitrile–water–acetic acid–triethylamine as the mobile phase. Much more rapid separation of the saponins was possible by using the MPG-ODS columns described here.

It is concluded that the rapid separation of the acidic saponins and also neutral saponins of ginseng, bupleurum root and senega is possible by HPLC on the MPG-ODS column. The column was found to be suitable for preparative purposes. We have previously reported a preparative separation

of the saponins from the root of *Panax ginseng* using this column [14,15]. Preparative applications to other saponins are in progress.

ACKNOWLEDGEMENTS

This work was supported in part by the Science Research Promotion Fund of the Japan Private School Promotion Foundation. We thank Professor J. Shoji of Showa University, Professor I. Kitagawa of Osaka University and Dr. H. Taguchi of Tsumura for gifts of the standard samples.

REFERENCES

- 1 N. Takai, H. Kanazawa, Y. Matsushima, Y. Nagata and M. Tomoda, *Seisan Kenkyu*, 41 (1989) 773.
- 2 Y. Matsushima, Y. Nagata, K. Takakusagi, M. Niyomura and N. Takai, *J. Chromatogr.*, 332 (1985) 265.
- 3 H. Kanazawa, Y. Nagata, Y. Matsushima, M. Tomoda and N. Takai, *Chromatographia*, 24 (1987) 517.
- 4 H. Kanazawa, Y. Nagata, Y. Matsushima, M. Tomoda and N. Takai, *Shoyakugaku Zasshi*, 43 (1989) 121.
- 5 H. Kanazawa, Y. Nagata, Y. Matsushima, M. Tomoda and N. Takai, *J. Chromatogr.*, 507 (1990) 327.
- 6 K. Takagi, H. Saito and M. Tsuchiya, *Jpn. J. Pharmacol.*, 22 (1972) 339.
- 7 H. Oura, A. Kumagai, S. Shibata and K. Takagi (Editors), *Yakuyo Ninjin*, Kyoritsu, Tokyo, 1981.
- 8 K. Gommori, F. Miyamoto, Y. Shibata, T. Higashi, S. Sanada and J. Shoji, *Chem. Pharm. Bull.*, 24 (1976) 2985, and references cited therein.
- 9 I. Kitagawa, T. Taniyama, T. Hayashi and M. Yoshikawa, *Chem. Pharm. Bull.*, 31 (1983) 3353.
- 10 N. Ebata, K. Nakajima, H. Taguchi and H. Mitsuhashi, *Chem. Pharm. Bull.*, 38 (1990) 1432.
- 11 H. Yamaguchi, R. Kasai, H. Matsuura, O. Tanaka and T. Fuwa, *Chem. Pharm. Bull.*, 36 (1988) 3468.
- 12 H. Yamaguchi, H. Matsuura, R. Kasai, O. Tanaka, M. Satake, H. Kohda, H. Izumi, M. Nuno, S. Katsuki, S. Isoda, J. Shoji and K. Goto, *Chem. Pharm. Bull.*, 36 (1988) 4177.
- 13 A. Nakajima, S. Sakuma, J. Shoji, O. Ishikawa and H. Watanabe, *100th Annual Meeting of the Japanese Society of Pharmacology, Tokyo, 1980*, Abstracts, p. 258.
- 14 H. Kanazawa, Y. Nagata, Y. Matsushima, M. Tomoda and N. Takai, *Chem. Pharm. Bull.*, 38 (1990) 1630.
- 15 H. Kanazawa, Y. Nagata, Y. Matsushima, M. Tomoda and N. Takai, *J. Chromatogr.*, 537 (1991) 469.

Short Communication

Determination of Lovastatin (mevinolin) and mevinolinic acid in fermentation liquids

Roman Kysilka

Watřex Institut, Hořtálkova 117, 169 00 Prague 6 (Czechoslovakia)

Vladimír Křen

Institute of Microbiology, Czech Academy of Sciences, Videňská 1083, 142 20 Prague 4 (Czechoslovakia)

(First received August 26th, 1992; revised manuscript received October 23rd, 1992)

ABSTRACT

A rapid and simple HPLC method for the determination of Lovastatin (mevinolin) and mevinolinic acid in fermentation fluids of *Aspergillus terreus* using a Separon SGX C₁₈ column and methanol–18 mM orthophosphoric acid (77.5:22.5, v/v) as mobile phase with detection at 238 nm is described. The detection limit of Lovastatin and mevinolinic acid was 20–30 ng/ml.

INTRODUCTION

Lovastatin (1',2',6',7',8',8a'-hexahydro-3,5-dihydroxy-2',6'-dimethyl-8'-(2"-methyl-1"-oxobutyl)-1-naphthaleneheptanoic acid 5-lactone) (Fig. 1) is a very potent hypocholesterolaemic drug (mevinolin, Mevacor). It is produced by fungi of the genera *Monascus*, *Aspergillus* and *Penicillium* [1]. The biologically active substance is mevinolinic acid, into which Lovastatin is converted *in vivo* [2].

Lovastatin and mevinolinic acid have been separated as trimethylsilyl derivatives by gas chromatography and identified by mass spectrometry [3]. Reversed-phase HPLC has been used for ethyl acetate extracts of fermentation liquids, blood plasma

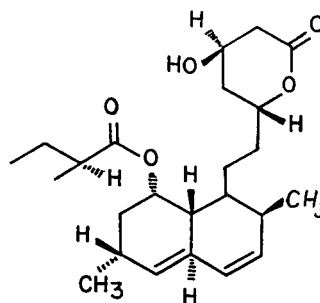


Fig. 1. Structure of Lovastatin.

and bile analysis. The substances were separated as their 4-nitrobenzoyl derivatives isocratically [4] or without derivatization by gradient elution (for bile samples) [5].

In this paper, a rapid method for the determination of Lovastatin and mevinolinic acid under iso-

Correspondence to: V. Křen, Institute of Microbiology, Czech Academy of Sciences, Videňská 1083, 142 20 Prague 4, Czechoslovakia.

cratic conditions and without preliminary sample treatment and derivatization is described.

EXPERIMENTAL

Chemicals

Lovastatin (mevinolin) was obtained from Sigma (St. Louis, MO, USA). Mevinolinic acid was prepared by alkaline hydrolysis of Lovastatin according to Endo *et al.* [6]. Methanol was of HPLC purity (Pierce, Rockford, IL, USA). All other chemicals were of at least analytical-reagent grade from Lachema (Brno, Czechoslovakia).

Sample treatment

The samples of fermentation broth were centrifuged at 4500 g for 5 min and the clear supernatant (10 μ l) was injected directly into the HPLC column.

Cultivation

Aspergillus terreus ATCC 20542 [1] for Lovastatin production was cultivated at 28°C on a rotary shaker in conical flasks with 40 ml of medium. Inoculum (24 h) was prepared on the following medium: corn steep 5, tomato paste 40, oat meal 10, glucose 10 g/l, and trace elements [1], (pH 6.8), and 5–10% of the inoculum was transferred into the production medium: glucose 45, milk peptone 24, yeast extract 2.5 and polyethylene glycol P2000 2.5 g/l, (pH 7.4) and cultivated for 5 days (maximum production) [1]. This cultivation liquid was used directly for Lovastatin and mevinolinic acid analyses.

Instruments

The HPLC system was composed of and LC-3B high-pressure pump (Perkin-Elmer, Norwalk, CT, USA) combined with a Rheodyne Model 7125 injection valve with a 10- μ l sample loop and a Model 990+ diode-array detector (Waters, Milford, MA, USA), set at 238 nm. A glass column (150 \times 3 mm I.D.) packed with Separon SGX C₁₈, 5 μ m (Tessek, Prague, Czechoslovakia) was used. The compounds were eluted isocratically with methanol–18 mM orthophosphoric acid (77.5:22.5, v/v) at a flow-rate of 0.5 ml/min. Spectral scanning from 200 to 350 nm was used during method development.

RESULTS AND DISCUSSION

The aim of this work was to develop a rapid method for the determination of Lovastatin and mevinolinic acid in fermentation broths from *Aspergillus terreus* cultivation on complex cultivation media. Previously described methods involve extraction with acidified ethyl acetate, which is time consuming and might be a source of analytical errors. As the concentrations of both substances in the medium usually range from tens to hundreds of μ g/ml, extraction as a preconcentration step is not necessary.

Using a chromatographic optimization function (COF) and the computer program COST [7], we determined the volumetric fraction of methanol in 18 mM orthophosphoric acid solution to be 77.5% for the optimum separation of Lovastatin and mevinolinic acid (resolution > 1.5). Under these conditions no interference from the components of the media with the analyte metabolites was observed (Fig. 2). The duration of one analysis is less than 10 min.

The effluent from the chromatographic column was monitored with a diode-array spectrophotom-

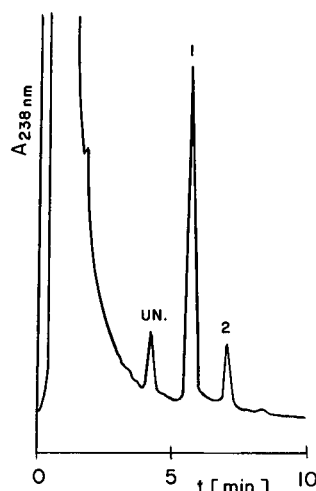


Fig. 2. Chromatogram of fermentation liquid of *Aspergillus terreus* containing (1) mevinolinic acid (424 mg/ml) and (2) Lovastatin (83 mg/ml). UN = unidentified peak. Column, Separon SGX C₁₈; mobile phase, methanol–18 mM orthophosphoric acid (77.5:22.5, v/v); flow-rate, 0.5 ml/min; UV detection at 238 nm

TABLE I
CALIBRATION DATA FOR MEVINOLINIC ACID AND
LOVASTATIN AT 238 nm

Parameter ^a	Mevinolic acid	Lovastatin
<i>b</i>	$1.18 \cdot 10^{-3}$	$1.26 \cdot 10^{-3}$
<i>a</i>	$1.28 \cdot 10^{-2}$	$1.49 \cdot 10^{-2}$
<i>r</i>	0.9896	0.9973
D.L.	0.022	0.020

^a *b*, *a* = Slope and intercept of the calibration line, respectively; *r* = correlation coefficient; D.L. = detection limit ($\mu\text{g/ml}$) for signal-to-noise ratio = 2.

eter. Continuous measurement enables the identity of the peaks to be checked not only according to correspondence of retention times but also by comparison of their UV absorption spectra. Multi-channel recording can be also used for checking the peak homogeneity.

Lovastatin and mevinolinic acid display coincidence in their spectra with absorption maxima at 231, 238 and 245 nm, which fit well with published data (231, 238 and 247 nm) [8]. Calibration data for 238 nm are presented in Table I. The detection limits of Lovastatin and mevinolinic acid (signal-to-noise ratio = 2) under the given conditions are 20–30 ng/ml. The relative deviation for five parallel de-

terminations in fermentation fluid does not exceed 3%. The range of linearity for the determination of Lovastatin and mevinolinic acid was 1–500 $\mu\text{g/ml}$. The day-to-day reproducibility of Lovastatin determination (difference of the average result for the same sample) did not exceed 2% relative.

The proposed method is suitable for the efficient screening of strains for Lovastatin production and possibly also for the determination of Lovastatin and mevinolinic acid in complex biological fluids.

REFERENCES

- 1 A. W. Alberts, J. Chen, G. Kuron, V. Hunt, J. Huff, C. Hoffman, J. Rothrock, M. Lopez, H. Joshua, E. Harris, A. Patchett, R. Monaghan, S. Currie, E. Stapley, G. Albers-Schonberg, O. Hensons, J. Hirshfield, K. Hoogsteen, J. Liesch and J. Springer, *Proc. Natl. Acad. Sci. U.S.A.*, 77 (1980) 3957.
- 2 A. Endo, D. Komagata and H. Shimada, *J. Antibiot.*, 39 (1986) 1670.
- 3 G. Albers-Schonberg, H. Joshua, M. B. Lopez, O. D. Hensons, J. P. Springer, J. Chen, S. Ostrove, C. H. Hoffman, A. W. Alberts and A. A. Patchett, *J. Antibiot.*, 34 (1981) 507.
- 4 V. P. Gullo, R. T. Goegelman, I. Putter and Y.-K. Lam, *J. Chromatogr.*, 212 (1981) 234.
- 5 R. J. Stubbs, M. Schwartz and W. T. Bayne, *J. Chromatogr.*, 383 (1986) 438.
- 6 A. Endo, K. Hasumi and S. Negishi, *J. Antibiot.*, 38 (1985) 420.
- 7 R. Kysilka and M. Wurst, *J. Chromatogr.*, 446 (1988) 315.
- 8 M. Windholz (Editor), *The Merck Index*, Merck, Rahway, NJ, 10th ed., 1983.

Short Communication

Simultaneous high-performance liquid chromatographic determination of altersolanol A, B, C, D, E and F

Nobuyuki Okamura and Akira Yagi

Faculty of Pharmacy and Pharmaceutical Sciences, Fukuyama University, Hiroshima 729-02 (Japan)

Hiroyuki Haraguchi and Kensuke Hashimoto

Faculty of Engineering, Fukuyama University, Hiroshima 729-02 (Japan)

(First received August 4th, 1992; revised manuscript received November 10th, 1992)

ABSTRACT

A high-performance liquid chromatographic model for the simultaneous determination of altersolanol A–F by using a reversed-phase column with an acetonitrile–water gradient elution system is described. The analysis can be completed within 13 min, the detection limits are 0.2–0.5 pmol per injection (5 μ l) and the relative standard deviations are 0.90–1.34%. The method was applied satisfactorily to the determination of altersolanols in culture media of a strain of *Alternaria solani* without any prepurification.

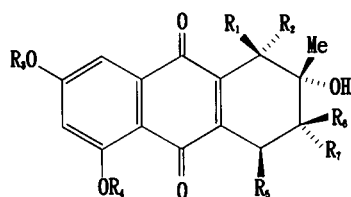
INTRODUCTION

The fungus *Alternaria solani*, a pathogen of early blight disease of tomato and potato [1], has been known to produce altersolanol A, B and C as metabolic pigments [2], which are rare but not unique examples of naturally occurring tetrahydroanthraquinones. These compounds have also been found as a phytotoxin from *Alternaria porri* [3] and *Dactylaria lutea* [4] and they exhibit phytotoxic activities in the seeds of lettuce and stone-leek [5]. Altersolanol A is a precursor [6] of altersolanol B, which is strongly cytotoxic to HeLa [7] and Ehrlich ascites carcinoma cells [8]. In a previous study we

found that altersolanol A exhibited antimicrobial activity against Gram-positive and -negative bacteria and this activity was closely related with the interference of the respiratory chain in the bacterial membrane of *Pseudomonas aeruginosa* as an electron acceptor [9].

In a previous paper we reported the identification of the related tetrahydroanthraquinones altersolanol D, E and F, together with altersolanol A, B and C, and discussed the antimicrobial activities of altersolanol A–F against *Pseudomonas aeruginosa* [10] (Fig. 1). Suemitsu and co-workers [11,12] reported the presence of altersolanol A–C and related anthraquinones in *Alternaria porri* using reversed-phase high-performance liquid chromatographic (HPLC) methods. However, these methods are not applicable to the simultaneous determination of altersolanol A–F. We therefore initiated the present

Correspondence to: N. Okamura, Faculty of Pharmacy and Pharmaceutical Sciences, Fukuyama University, Hiroshima 729-02, Japan.



Altersolanol	R ₁	R ₂	R ₃	R ₄	R ₅	R ₆	R ₇
A	OH	H	Me	H	OH	H	OH
B	H	H	Me	H	H	H	OH
C	OH	H	Me	H	H	H	OH
D	OH	H	H	Me	OH	H	OH
E	OH	H	Me	H	OH	OH	H
F	H	OH	H	Me	OH	H	OH

Fig. 1. Structures of altersolanols.

studies on the development of a simple and rapid method for the determination of altersolanol A–F in culture media of the strain of *Alternaria solani*. In this paper we describe the simultaneous HPLC determination of altersolanol A–F and the culture conditions for producing altersolanol A–F. With this method it was possible to study the production of altersolanol A–F in culture media.

EXPERIMENTAL

Materials

Altersolanol A–F were isolated from the culture liquid of the strain of *Alternaria solani* as metabolic pigments [10].

The water used for chromatography was deionized with a Milli-Q system (Millipore, Bedford, MA, USA). Acetonitrile was of HPLC grade and other solvents and chemicals were of analytical-reagent grade, all of which were obtained from Wako (Osaka, Japan).

Sample preparation

A stock standard solution was made by diluting with methanol to give concentrations of 9.35 (altersolanol A), 8.74 (altersolanol B), 2.50 (altersolanol C), 8.06 (altersolanol D), 1.87 (altersolanol E) and 4.24 $\mu\text{mol/ml}$ (altersolanol F).

The strain of *Alternaria solani* was isolated from a diseased tomato leaf in the greenhouse of the university. *Alternaria solani* (IFO 7516) was obtained from Institute for Fermentation, Osaka, and *Alternaria porri* (IFO 9762) was also obtained from the

same Institute was a standard strain. The morphological characteristics suggest that this strain was a synonym of *Alternaria solani*. The fungus was maintained on malt agar and cultured in the medium (20 ml per 100-ml flask) [10]. To assess the influence of detergent, dimethyl sulphoxide (DMSO) and N,N-dimethylformamide (DMF) were added at final concentrations of 2% and 1%, respectively. Cultivation was carried out at 25°C under continuous fluorescent lighting (43 $\mu\text{E/m}^2$, 3000 lux; 1 E = 6.02 $\cdot 10^{23}$ photons) or in the dark for 10 days. The culture liquid was filtered through a Millipore syringe filter unit (0.45 μm) and then a portion was injected into the HPLC column. For the calibration graph for altersolanols, standard solutions were diluted with methanol and the filtration was omitted.

Apparatus

HPLC was performed using a gradient system from Tosoh (Tokyo, Japan) with two CCPD pumps and a dynamic mixer, a Rheodyne Model 7125 syringe-loading sample injector equipped with a 5- μl sample loop and Tosoh UV-8000 UV-Vis detector set at 270 nm. The data were processed by means of a SIC Chromatocorder-II integrator to evaluate the peak areas. The purity of the chromatographic peaks was estimated using a Waters (Milford, MA, USA) M990J photodiode-array detector.

Chromatographic conditions

The reversed-phase column was made of stainless steel (150 \times 4.6 mm I.D.) and packed with Wako Wakosil-II 5C18 HG (5 μm). The separation was carried out using a linear gradient programme with the following eluents: 0–3 min, acetonitrile–water (18:82); 3–20 min, linear change to acetonitrile–water (90:10); 20–23 min, acetonitrile–water (90:10). A re-equilibration period of 12 min was used between individual runs. The flow-rate was maintained at 1.0 ml/min and the temperature at 20–25°C.

RESULTS AND DISCUSSION

HPLC was carried out on a Wako Wakosil-II 5C18 HG reversed-phase column, which was selected because of its large number of theoretical plates, its specific characteristics towards polyketides and the avoidance of poor peak shapes of altersolanols. Fig. 2A shows the separation of a standard mixture

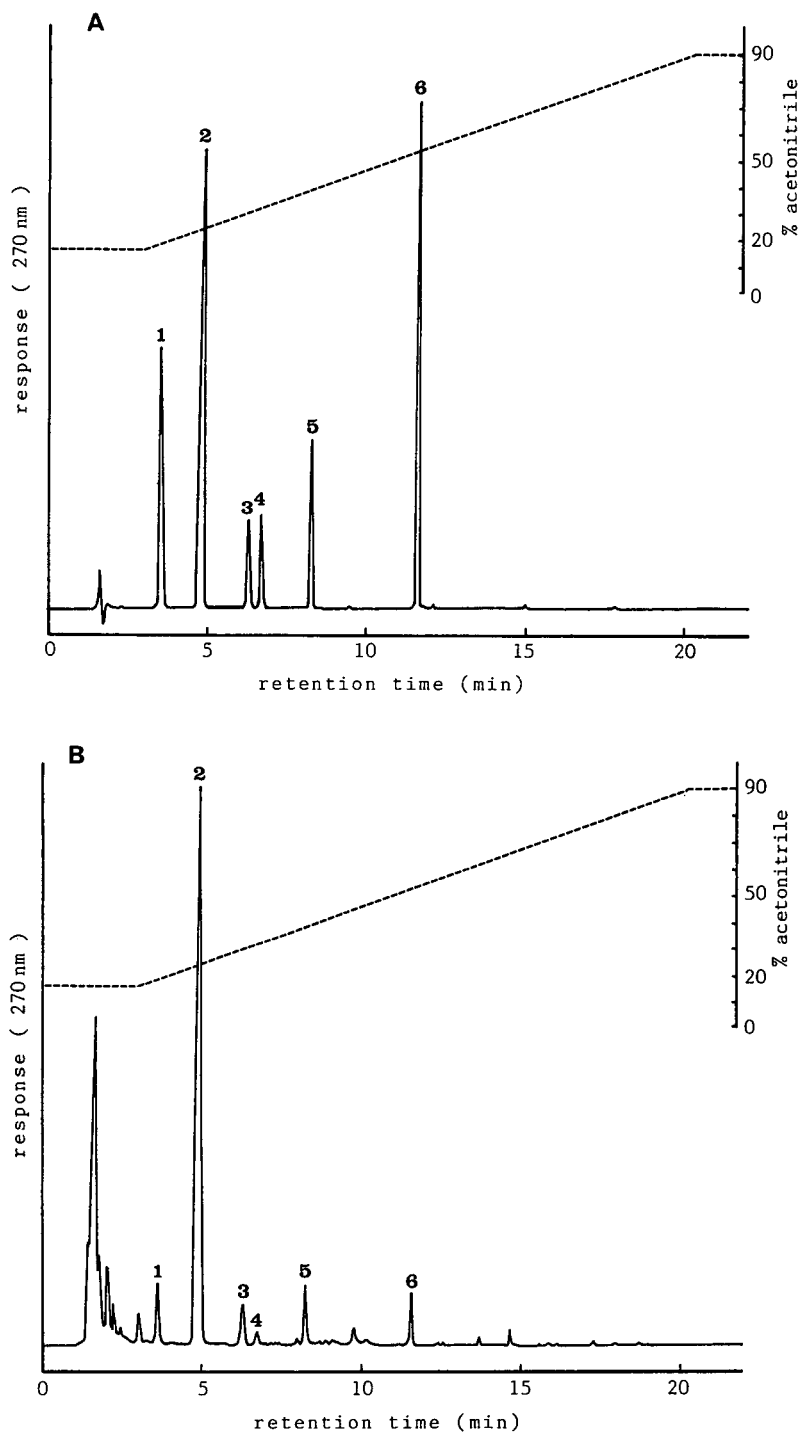


Fig. 2. Separations of altersolanols in (A) standard mixture and (B) the strain of *Alternaria solani*. Concentrations: (A) 1 = 80.6, 2 = 93.5, 3 = 42.4, 4 = 18.7, 5 = 25.0, 6 = 87.4 μM ; (B) 1 = 69.8, 2 = 467.0, 3 = 72.5, 4 = 7.5, 5 = 43.5, 6 = 47.2 μM . Peaks: 1 = altersolanol D; 2 = altersolanol A; 3 = altersolanol F; 4 = altersolanol E; 5 = altersolanol C; 6 = altersolanol B.

TABLE I
RETENTION TIMES AND CAPACITY FACTORS FOR
ALTERSOLANOLS

Compound	t_R (min)	k'
Altersolanol D	3.60	1.31
Altersolanol A	4.75	2.04
Altersolanol F	6.19	2.97
Altersolanol E	6.61	3.24
Altersolanol C	8.18	4.24
Altersolanol B	11.54	6.40

of altersolanols and Table I lists retention times (t_R) and capacity factors (k') of these compounds. The chromatogram of these compounds from a culture medium is shown in Fig. 2B. HPLC can be accomplished by applying a culture liquid without any prepurification and the determination of altersolanols can be achieved within 13 min. The detection limits (signal-to-noise ratio = 3) of altersolanols were 0.2–0.5 pmol per injection. There was good linearity from 0.4 to 1 μM of altersolanol A–F with correlation coefficients of 0.999–1.000. The relative standard deviations ($n = 10$) were 1.34 (altersolanol A), 1.24 (altersolanol B), 1.10 (altersolanol C), 1.20 (altersolanol D) and 0.90% (altersolanol E and F) using a standard mixture as shown in Fig. 2A.

Recovery tests were performed by adding known

TABLE II
RECOVERY AND PRECISION FOR ALTERSOLANOLS

Altersolanol	Initial amount (μg)	Added (μg)	Recovery (%) ^a
A	36.96	10.84	103.6 \pm 2.0
		21.68	104.1 \pm 1.2
B	6.78	9.92	91.6 \pm 1.4
		19.85	95.5 \pm 1.5
C	4.93	7.58	98.2 \pm 0.7
		15.17	93.0 \pm 0.9
D	9.04	10.16	103.7 \pm 0.8
		20.32	102.2 \pm 1.3
E	2.79	4.35	95.9 \pm 2.6
		8.70	96.3 \pm 1.1
F	7.46	8.02	100.4 \pm 0.5
		16.03	98.1 \pm 1.7

^a Results are means \pm standard deviations from three independent experiments.

amounts of altersolanols to culture liquid (1 ml). The mixture was filtered and assayed according to the above procedure. Table II summarizes the recoveries of the altersolanols, which were $\geq 91.6\%$.

Altersolanols in culture media were determined using the proposed method. Usually, light exposure during the growth phase inhibits the accumulation of polyketides in *Alternaria alternata* [13]. However, the results in Table III demonstrate that light is nec-

TABLE III
CONTENT OF ALTERSOLANOLS IN CULTURE MEDIA OF *ALTERNARIA* SPECIES

<i>Alternaria</i> species	DMSO (%)	Altersolanol (μmol per flask)											
		Light						Dark					
		A	B	C	D	E	F	A	B	C	D	E	F
Strain of <i>A. Solani</i>	0	nd ^a	tr ^b	nd	nd	nd	tr	nd	nd	nd	nd	nd	nd
	2	36.40	2.50	1.84	3.12	0.58	2.96	0.72	0.06	0.10	0.01	0.02	0.01
<i>A. solani</i>	0	0.08	0.26	0.08	nd	0.02	0.02	0.01	nd	tr	nd	nd	nd
	2	0.2	0.14	0.04	nd	0.02	0.04	0.18	nd	tr	nd	nd	nd
<i>A. porri</i>	0	28.74	nd	0.02	1.58	0.18	1.72	19.36	0.02	0.06	0.36	0.12	0.40
	2	0.38	nd	tr	nd	nd	nd	1.00	nd	tr	nd	nd	nd

^a Not detected.

^b Trace.

essary for a high productivity of altersolanols in a culture medium of the strain. Photosporogenesis is one of the most important in the morphological differentiation in fungi [14], which is closely related to the production of secondary metabolites. The secondary metabolites produced are often stored within the fungal cells. Application of an agent that releases the metabolites into the surrounding medium results in increased productivity. Table III shows that the production of altersolanols by *Alternaria porri* was completely inhibited by light exposure and addition of 2% DMSO, whereas *Alternaria solani* produced altersolanols under the same conditions. In the present experiment, however, the culture medium of the strain of *Alternaria solani* contained 4–14 times more altersolanols than the other on addition of either 2% DMSO or 1% DMF under light exposure. Comparison of altersolanols between *Alternaria porri*, *Alternaria solani* and the strain of *Alternaria solani* showed that a higher amount of altersolanols in the strain of *Alternaria solani* was induced by light exposure and detergent than the others in both mycelia and culture liquid. Hence this treatment presents a useful means for the production of altersolanols.

CONCLUSION

A reliable method for the simultaneous determination of altersolanol A–F in the strain of *Alternaria solani* has been developed. This method is excel-

lent for identifying altersolanols in culture media of *Alternaria* species without any prepurification.

ACKNOWLEDGEMENTS

We thank Miss Keiko Nozaki and Mr. Takahiro Abo for excellent technical assistance.

REFERENCES

- 1 P. W. Brian, G. W. Elson, H. G. Hemming and J. M. Wright, *Ann. Appl. Biol.*, 9 (1952) 308.
- 2 A. Stoessl, *Can. J. Chem.*, 47 (1969) 767.
- 3 R. Suemitsu, A. Nakamura, F. Isono and T. Sano, *Agric. Biol. Chem.*, 46 (1982) 1693.
- 4 A. M. Becker, R. W. Rickards, K. J. Schmalzl and H. C. Yick, *J. Antibiot.*, 31 (1978) 324.
- 5 R. Suemitsu, Y. Yamada, T. Sano and K. Yamashita, *Agric. Biol. Chem.*, 48 (1984) 2383.
- 6 A. Stoessl, C. H. Unwin and J. B. Stothers, *Can. J. Chem.*, 61 (1983) 372.
- 7 K. Horakova, J. Navarova, P. Nemeč and M. Kettner, *J. Antibiot.*, 27 (1974) 408.
- 8 M. Miko, L. Drobnica and B. Chane, *Cancer Res.*, 39 (1979) 4242.
- 9 H. Haraguchi, T. Abo, K. Hashimoto and A. Yagi, *Biosci. Biotechnol. Biochem.*, 56 (1992) 1221.
- 10 A. Yagi, N. Okamura, H. Haraguchi, T. Abo and K. Hashimoto, *Phytochemistry*, in press.
- 11 R. Suemitsu, Y. Tamada, T. Sano and M. Kitayama, *J. Chromatogr.*, 318 (1985) 139.
- 12 R. Suemitsu, K. Horiuchi, K. Ohnishi and S. Yanagawase, *J. Chromatogr.*, 454 (1988) 406.
- 13 P. Haggblom and T. Unestam, *Appl. Environ. Microbiol.*, 38 (1979) 1074.
- 14 T. Kumagai, *Physiol. Plant.*, 57 (1983) 468.

Short Communication

Isolation and determination of alizarin in cell cultures of *Rubia tinctorum* and emodin in *Dermocybe sanguinea* using solid-phase extraction and high-performance liquid chromatography

Zoltán A. Tóth

Department of Plant Anatomy, Eötvös Lorand University, Puskin u. 11-13, Budapest 1088 (Hungary)

Olavi Raatikainen, Toivo Naaranlahti and Seppo Auriola

Department of Pharmaceutical Chemistry, University of Kuopio, P.O. Box 1627, SF-70211 Kuopio (Finland)

(First received June 24th, 1992; revised manuscript received October 28th, 1992)

ABSTRACT

A high-performance liquid chromatographic method was developed for the determination of the non-glycosidic anthraquinones alizarin (1,2-dihydroxy-9,10-anthracenedione), emodin (1,3,8-trihydroxy-6-methyl-9,10-anthracenedione) and anthraquinone (9,10-anthracenedione). The anthraquinones were separated by isocratic elution on a 125 × 4.6 mm I.D. column containing ODS Hypersil 5 reversed-phase material using methanol-5% acetic acid (pH 3.0) (70:30) as the mobile phase. Free alizarin was determined in plant cell suspension cultures of *Rubia tinctorum* and free emodin in mushrooms (*Dermocybe sanguinea*). The effective extraction of anthraquinones from plant cells was achieved with 80% (v/v) ethanol after incubation for 10 h at 80°C. Prepurification and concentration of anthraquinones in the plant cell and mushroom extracts were effected by a solid-phase technique using C₈ cartridges.

INTRODUCTION

Rubia tinctorum, the source of a natural dye, produces anthraquinone pigments in the roots and also in the cultured cells, one of them being alizarin [1]. The herbal drugs consisting of crude *Rubia* extracts have the activity of dissolving bladder and kidney stones. It has been shown that *R. tinctorum* pro-

duces lucidin, in addition to alizarin, and that these hydroxyanthraquinones are present as glycosides which decompose in rat to the genotoxic hydroxyanthraquinones lucidin and 1-hydroxyanthraquinone [2]. Alizarin, produced in cell cultures, can be used as an indicator for the production of the anthraquinone metabolites in cultured *Rubia* cells.

Dermocybe sanguinea, a wild mushroom also used as a natural dye, contains several anthraquinone pigments, the most important being emodin [3]. It was shown previously that *D. sanguinea* extracts are genotoxic, which is only partially ex-

Correspondence to: Olavi Raatikainen, Department of Pharmaceutical Chemistry, University of Kuopio, P.O. Box 1627, SF-70211 Kuopio, Finland.

plained by emodin [4]. Further research on other anthraquinones and genotoxic compounds of *D. sanguinea*, as mushrooms or cultured cells, needs more sophisticated HPLC methods for isolation, identification and determination.

Many methods have been reported for the separation of the naturally occurring free anthraquinone aglycones. These have been based on paper chromatography [5], thin-layer chromatography (see, for example, refs. 6 and 7), low-pressure column chromatography [8] and high-performance liquid chromatography (HPLC) (see, for example, refs. 4 and 9–15). The adsorption of anthraquinone pigments on Amberlite XAD-2 resin was described previously, but the method was not suitable for routine use with cell and tissue culture extracts [14]. Column purification, however, was practical and C₁₈ cartridges proved to be effective in the HPLC determination of anthraquinone in pulping liquors [12].

In this paper we describe an isocratic HPLC method for the extraction and purification of alizarin from *R. tinctorum* plant cells and emodin from *D. sanguinea* mushroom cells. Isolation and subsequent purification using solid-phase extraction (SPE) with C₈ cartridges, following HPLC analysis and UV detection, provided a fast, sensitive and easy method for the determination of free alizarin and emodin.

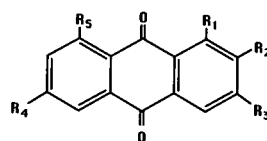
EXPERIMENTAL

Chemicals

Alizarin (1,2-dihydroxy-9,10-anthracenedione) and anthraquinone (9,10-anthracenedione) were purchased from Reanal (Budapest, Hungary), emodin (1,3,8-trihydroxy-6-methyl-9,10-anthracenedione) from Aldrich Chemie (Steinheim, Germany), ethanol from ALKO (Helsinki, Finland), methanol of HPLC grade from Rathburn (Walkerburn, UK) and acetic acid of analytical-reagent grade from Merck (Darmstadt, Germany). Water was purified with Millipore Milli-Q UF Plus equipment. The structures of the anthraquinones studied are shown in Fig. 1.

Plant and mushroom material

Rubia tinctorum L. cell suspension cultures, grown in a basic Murashige and Skoog medium



	R ₁	R ₂	R ₃	R ₄	R ₅
Anthraquinone:	H	H	H	H	H
Alizarin:	OH	OH	H	H	H
Emodin:	OH	H	OH	CH ₃	OH

Fig. 1. Structures of alizarin, anthraquinone and emodin.

containing indoleacetic acid (IAA) (1.0 mg/l), naphthaleneacetic acid (NAA) (0.1 mg/l) and kinetin (0.2 mg/l) (cultivated by Dr. J. Kretovics, ELTE University, Budapest, Hungary), were used for the analysis. Specimens of *Dermocybe sanguinea* (identified by H. Heikkilä, Department of Natural History, Museum of Kuopio, Kuopio, Finland) were collected from the Kuopio area in Eastern Finland. The mushrooms were extracted as fresh or dried samples or they were frozen within 8 h of collection and stored at –20°C until extraction.

Sample preparation

Dried and powdered material (10 mg) obtained from *R. tinctorum* cell culture was suspended in 2.5 ml of 80% (v/v) ethanol [16], sonicated for 5 min (Branson 2200 sonicator) and soaked at 80°C for 0–10 h. The extract was separated by centrifugation, the residue was mixed with 1.5 ml of 80% (v/v) ethanol, incubated for 4 h at 80°C and centrifuged again. The combined supernatants were evaporated to dryness and the residue was dissolved in 1 ml of 80% (v/v) ethanol and used as the crude extract in further HPLC studies.

D. sanguinea was extracted with 94% (v/v) ethanol for 48 h at room temperature, the filtered extract was concentrated with a rotary evaporator and the residue was acidified [4]. The precipitate which was formed after acidification was used, in addition to the ethanol extract, as the crude extract of *D. sanguinea* for this study.

Purification of the crude extracts

The crude extract (1 ml) was diluted tenfold with

water and passed dropwise through preactivated SPE cartridges (Bond Elut LRC C₈ 1 cc; Analytichem, Harbor City, CA, USA), which were then washed with 2 ml of water followed by 1 ml of methanol–water (30:70, v/v). After drying the cartridges with air, the fraction containing the three anthraquinones was eluted from the tube with 1 ml of methanol–water (80:20, v/v).

HPLC of the extracts

Chromatography was performed using a Beckman 342 HPLC system, equipped with a Beckman 114 M solvent-delivery module, a Beckman 420 controller, a Beckman 165 variable-wavelength detector and an Altex 210 loop injector (20- μ l loop volume). The ratiograms (254/280 nm) were recorded with a BBC Goertz Metrawatt SE-120 two-channel recorder (BBC) and chromatograms (254 nm, quantitation signal) with a Merck–Hitachi D-2000 chromato-integrator. The ratio threshold was set at 2%. The components were separated on an ODS Hypersil (5- μ m particle size) reversed-phase column (125 mm \times 4.0 mm I.D.) (Bischoff Chromatography, Leonberg, Germany). The isocratic elution of components was accomplished using methanol–5% acetic acid (pH 3.0) (70:30) at a flow-rate of 1.0 ml/min. Peaks were identified by comparing their retention times, ratiogram plots and on-line detection of the UV spectra with those of standards.

RESULTS AND DISCUSSION

The results from the extraction extraction of al-

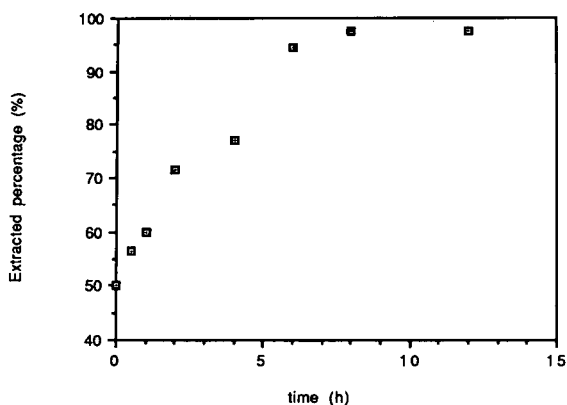


Fig. 2. Effect of incubation time on the extraction of alizarin from *Rubia tinctorum* L. cells at 80°C with ethanol–water (80:20, v/v).

izarin with ethanol at 80°C at different times indicate that incubation for 10 h was needed to achieve the maximum recovery for cultured plant cell suspension material (Fig. 2). The typical free alizarin content was 2 mg/g in dry *R. tinctorum* ma-

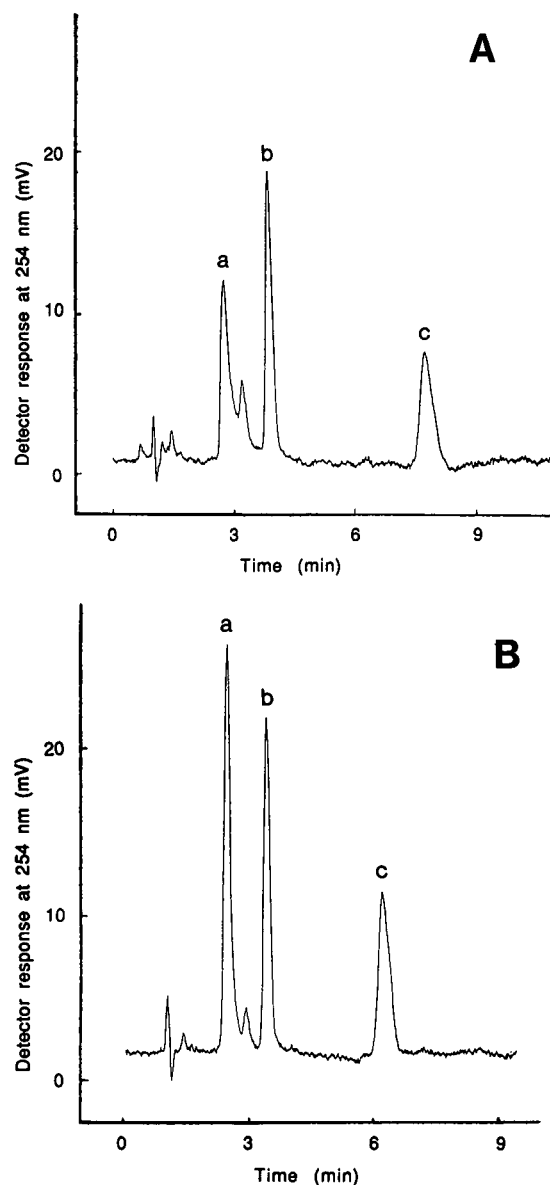


Fig. 3. Isocratic HPLC separation of a standard solution containing 3.3 μ g/ml each of (a) alizarin, (b) anthraquinone and (c) emodin on a Hypersil ODS column. The mobile phase was (A) methanol–water (70:30) (pH 7.0) or (B) methanol–5% acetic acid (70:30) pH 3.0.

terial, with a range of 0.4–4 mg/g depending on the culture. *D. sanguinea* contained emodin at about 1.4 mg/g dry mass and 0.3 mg/g fresh mass, with the content depending on the location and age of the mushroom.

Linear calibration graphs (based on the peak heights in mm) with good correlation ($r^2 > 0.999$) were obtained for alizarin (range 78–10 000 ng/ml), anthraquinone (156–20 000 ng/ml) and emodin (312–10 000 ng/ml), the first value of the range showing the detection limit at a signal-to-noise ratio of 3. The precision of the whole assay was 1.5% (from six identical plant cell culture samples) and the recovery from the SPE step was estimated to be more than 99% ($n = 3$) for alizarin; however the recovery of emodin was about 78%. When methanol–5% acetic acid (90:10, v/v) was used for elution, the recovery was increased to 95%, including emodin. This was more effective than elution with 100% methanol (data not shown).

Acetic acid in the mobile phase affected the peak shape of the anthraquinones, the strongest effect being with alizarin (Fig. 3). The use of acetic acid also shortened the retention time of emodin, but only a slight effect was seen with the other compounds (Fig. 3). In the standard alizarin a small peak due to some degradation product, an isomer or impurity, was seen, the relative amount of which seemed to decrease when acetic acid was used (Fig. 3).

The washing and elution process with SPE removed most of the impurities having short or long retention times, lowering the detection limit in the HPLC analysis (Figs. 4 and 5). It is possible that some of the impurities removed by SPE and unknown components in the purified eluate are other anthraquinones (free or glycosidic), as they are known to be synthesized in both *R. tinctorum* and *D. sanguinea* [1,3]. A higher concentration of methanol (60%, v/v) in water was needed to remove the impurities with short retention times found in the

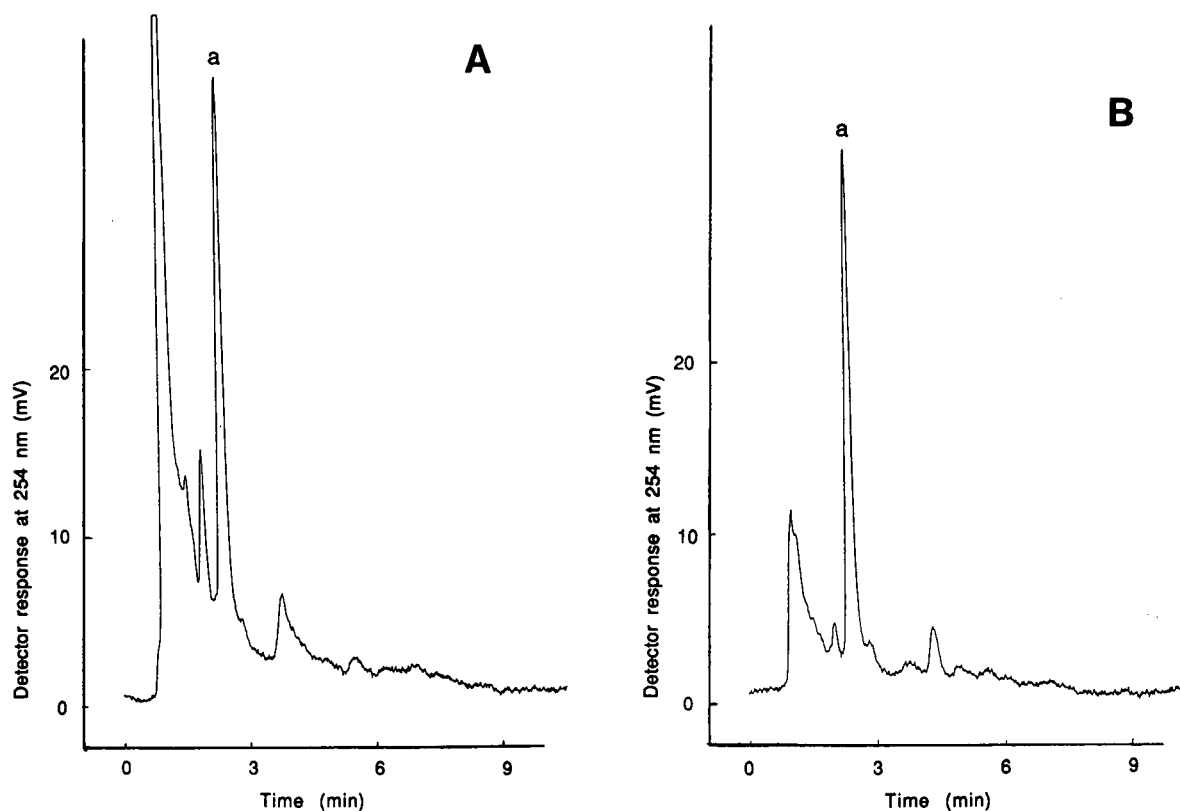


Fig. 4. HPLC of (a) alizarin (A) in a crude extract of *R. tinctorum* L. cell suspension culture and (B) after C_8 SPE purification. Alizarin concentration, 4.0 $\mu\text{g/ml}$.

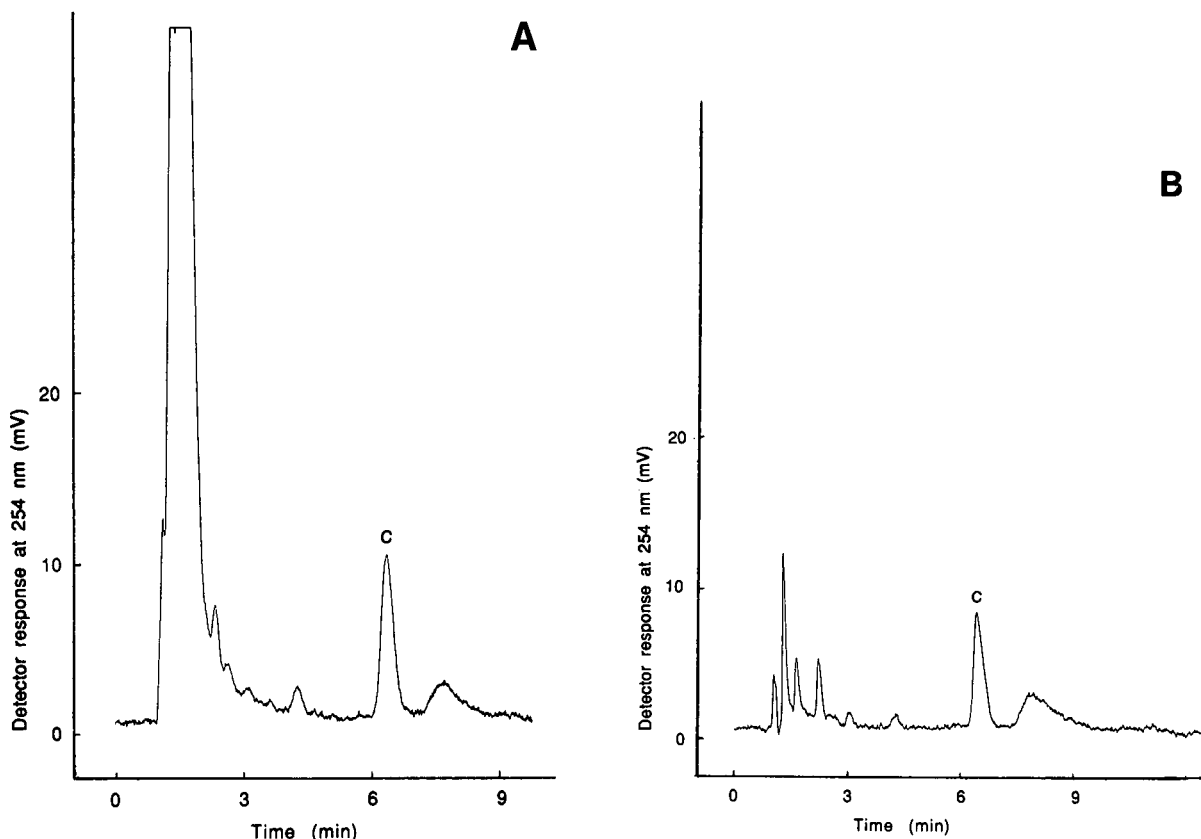


Fig. 5. HPLC of (c) emodin, (A) in a crude extract of *D. sanguinea* and (B) after C_8 SPE purification. Emodin concentration, $3.0 \mu\text{g/ml}$.

ethanol extracts of dried mushrooms. Stepwise development of the SPE cartridges seems to be useful for the purification of other anthraquinones in mushrooms, but if the cartridge size or sample type is changed then the SPE process should be optimized again.

This isocratic HPLC technique method is useful for studies with alizarin and other anthraquinones produced by *R. tinctorum*, and should also facilitate the further isolation, identification and determination of emodin and other anthraquinone components of cultured *D. sanguinea* mushrooms. Further studies are needed to identify the glycosidic and other anthraquinones of *Dermocybe* species. The combination of SPE, HPLC assay and hydrolysis of the glycosides makes it possible to separate the two forms of anthraquinones present in plant or mushroom material.

Non-glycosidic forms of alizarin and emodin can

be used as marker molecules in further studies of anthraquinone biosynthesis in cultured *R. tinctorum* and *D. sanguinea*, respectively.

ACKNOWLEDGEMENTS

This work was financially supported by the University of Kuopio and by a personal grant (to Z. A. T.) from the ELTE Peregrinatio II (Budapest, Hungary). We thank Mr. J. Callaway for language assistance.

REFERENCES

- 1 A. R. Burnett and R. H. Thomson, *J. Chem. Soc. C*, (1968) 2437.
- 2 B. Blömeke, B. Poginsky, C. Schmutte, H. Marquardt and J. Westendorf, *Mutat. Res.*, 265 (1992) 263.
- 3 W. Steglich, W. Lösel and V. Austel, *Chem. Ber.*, 102 (1969) 4104.

- 4 A. von Wright, O. Raatikainen, H. Taipale, S. Kärenlampi and J. Mäki-Paakkanen, *Mutat. Res.*, 269 (1992) 27.
- 5 S. Chao Yung Su and N. M. Ferguson, *J. Pharm. Sci.*, 62 (1973) 899.
- 6 P. P. Rai, T. D. Turner and S. L. Greensmith, *J. Pharm. Pharmacol.*, 26 (1974) 722.
- 7 P. P. Rai and M. Shok, *Chromatographia*, 14 (1981) 599.
- 8 K. Savonius, *Farm. Aikak.*, 81 (1972) 85.
- 9 P. P. Rai, T. D. Turner and S. A. Matlin, *J. Chromatogr.*, 110 (1975) 401.
- 10 B. Rittich and M. Krska, *J. Chromatogr.*, 130 (1977) 189.
- 11 P. P. Rai, M. Shok and R. G. Stevens, *J. High Resolut. Chromatogr. Chromatogr. Commun.*, 6 (1983) 212.
- 12 K. H. Nelson and D. J. Cietek, *J. Chromatogr.*, 281 (1983) 237.
- 13 D. E. Wurster and S. M. Upadrashta, *J. Chromatogr.*, 362 (1986) 71.
- 14 R. Wijnsma, T. B. van Vliet, P. A. A. Harkes, H. J. van Groningen, R. van der Heijden, R. Verpoorte and A. B. Svendsen, *Planta Med.*, 53 (1987) 80.
- 15 K. Sato, T. Yamazaki, E. Okuyama, K. Yoshihara and K. Shimomura, *Phytochemistry*, 30 (1991) 1507.
- 16 P. Prodelius, B. Deus, K. Mosbach and M. H. Zenk, *FEBS Lett.*, 103 (1979) 93.

Short Communication

Improved procedure for the derivatization and gas chromatographic determination of hydroxycarboxylic acids treated with chloroformates

P. Hušek

Institute of Endocrinology, Narodni trida 8, 116 94 Prague 1 (Czechoslovakia)

(First received May 19th, 1992; revised manuscript received October 9th, 1992)

ABSTRACT

Hydroxymonocarboxylic acids with a hydroxyl group adjacent to the carboxylic group can easily be converted with alkyl chloroformates into derivatives amenable to gas chromatography. However, the main reaction product, the O-alkoxycarbonylalkyl ester, is always accompanied by a certain amount of reaction side-products, by altering the sequence of addition of the organic base and the reagent. Under optimum conditions, $\geq 94\%$ of the mass of the analyte can be converted into the desired main product.

INTRODUCTION

Considering chloroformates as possible reagents for organic acid profiling of biological fluids, we were especially interested in the determination of hydroxycarboxylic acids (HA), as these compounds are of prime analytical importance mainly in diabetes [1–3]. A rapid and reliable method for serum lactic acid is still required [4,5].

According to a previous study [6], HA can easily be converted into O-alkoxycarbonylalkyl esters [$R'OCOO-(R)CH-COOR'$] by reaction with alkyl chloroformates. However, the main reaction product was always accompanied with a certain amount of at least two side-products, one with a lower and the other with a higher retention time than the main

product. The conclusion was drawn that the side-product with the higher retention time was the non-decarboxylated product, the alkoxycarbonyl ester [mixed anhydride, $R'OCOO-(R)CH-COOR'$], which was prepared preferentially under altered reaction conditions.

However, the preceding statement had to be corrected as a subsequent GC-MS study [7] revealed that more than one peak emerged on the chromatogram after the main reaction product. Moreover, none of them had a retention time identical with that of the mixed anhydride prepared alternatively. In addition, in the previous paper [6] a mistake in the procedure was made in that the addition of chloroform should be accompanied by addition of sodium hydrogencarbonate solution to perform the extraction. In that connection, it was observed that the mixed anhydride decomposed progressively by action of the hydrogencarbonate whereas the side-products did not.

Correspondence to: P. Hušek, Institute of Endocrinology, Narodni trida 8, 116 94 Prague 1, Czechoslovakia.

In this work, paper the reaction conditions were re-examined in order to minimize the side-product formation and a new approach to achieving of this goal is presented.

EXPERIMENTAL

Apparatus

A Carlo Erba MEGA Series 5000 gas chromatograph with a flame ionization detector and a Hewlett-Packard Model 3396A integrator were employed. The injector and detector temperatures were 240 and 270°C, respectively. The analysis was carried out on a 25 m × 0.25 mm I.D. FS-OV-1701-DF-0.25 fused-silica capillary column (Macherey–Nagel, Düren, Germany) in the temperature range

60–200°C or 80 (3-min hold)–240°C, programmed at 10 or 15°C/min. Helium was used as the carrier gas with a head pressure of 100 kPa and sample size 2 µl with a splitting ratio of 1:20.

Chemicals

Methyl and ethyl chloroformate (MCF, ECF), pyridine, acetonitrile, methanol, 96% ethanol and chloroform (stabilized with amylenes) were obtained from Aldrich (Steinheim, Germany) and Merck (Darmstadt, Germany). The HA, *i.e.*, 2-hydroxyacetic (glycolic), D-2-hydroxypropionic lithium salt (D-lactic), 2-hydroxybutyric sodium salt (HB), 2-hydroxyisovaleric (HIV), 2-hydroxyvaleric (HV), 2-hydroxyisocaproic (HIC), 3-hydroxybutyric (3HB) and 4-hydroxybutyric (4HB) acid, were

TABLE I

INFLUENCE OF REACTION CONDITIONS ON THE SIDE-PRODUCT FORMATION OF LACTIC ACID DERIVATIZED WITH MCF (I) OR ECF (II)

The values are means of five derivatization carried out at the particular composition of the medium; the relative standard deviation was below 5% on average.

(I) Reaction medium for MCF treatment (% v/v)			Peak abundance (%)							
A	W	M	0	1	2	3	4	5	6	
a	99	1	0	(<1)	80	3.4	11.1	2.2	<1	1.7
b	80	20	0	(2)	62	4.8	16.2	8.0	2.5	4.5
c	95	1	4	(4)	81	4.4	7.2	<1	<1	2.4
d	94	5	1	(2)	77	5.1	11.2	2.1	<1	1.7
e	90	5	5	(5)	81	4.5	7.0	1.0	<1	1.5
f	70	25	5	(6)	68	7.3	11.5	1.4	2	3.7
g	70	25 ^a	5	(8)	74	4.3	9.9	<1	<1	1.8
h	46	46	8	(10)	65	8.0	8.5	1.5	2.5	4.5

(II) Reaction medium for MCF treatment (% v/v)			Peak abundance (%)					
A	W	E	0	1	2	3	∑ (minor peaks)	
a	99	1	0 ^b	1	93	1.5	3	2
b	80	20	0 ^b	1	68	4	15	12
c	95	1	4	1	91	2	3.5	2
d	80	10	10	2	84	5	7	2
e	0	2	98	17	70	6	5	2
f	33	33	33	6	64	13	14	3
g	50	25	25	5	72	9	11	3
h	17	50	33	8	74	6	7	5

^a Acidified water (0.5 M HCl).

^b Incomplete derivatization.

obtained from Aldrich. An equimolar mixture (without 4HB) of HA was prepared in water (100 μmol of each HA in 1 ml); individual HA were dissolved in water at the same concentration.

Procedures

General approach. A 2- μl volume of the aqueous solution of HA was covered with 200 μl of the corresponding medium (see Table I) composed of acetonitrile (A), methanol (M) or ethanol (E) and water (W, replaced with 0.5 M HCl in some instances), and pyridine in an amount of 10% (v/v) (7.5–15% in some instances) was added. Subsequently, MCF or ECF in half the amount of pyridine was added, followed by 100 μl of chloroform and 200 μl of 1 M HCl. By briefly shaking the tube for about 10 s, the pyridine was transferred into the upper aqueous phase, which was removed by means of a push-button pipette. The chloroform phase was subsequently shaken with 200 μl of 1 M aqueous hydrogencarbonate solution and an aliquot was injected into the column. In some instances or for special purposes the wash of the organic phase with aqueous HCl or hydrogencarbonate solution was omitted; the results were not influenced by this change.

Special approach. The reaction medium for the highest yields of the main product consisted of acetonitrile containing 10% of water and 1% of methanol or .5% of ethanol for treatment with MCF or

ECF, respectively (A and C in the figures). A parallel medium consisted of acetonitrile with containing 25% of water and 2.5% of methanol or 25% of ethanol, respectively (B and D in the figures).

Then, 200 μl of the corresponding medium were mixed with either (i) 20 μl of pyridine and 10 μl of MCF or ECF were added (= normal mode: reagent after base, C and D); or (ii) 10 μl of MCF or ECF and 15 μl of pyridine were added (= reversed mode: base after reagent, A and B).

Following addition of 100 μl of chloroform the extraction was carried out as in the preceding section.

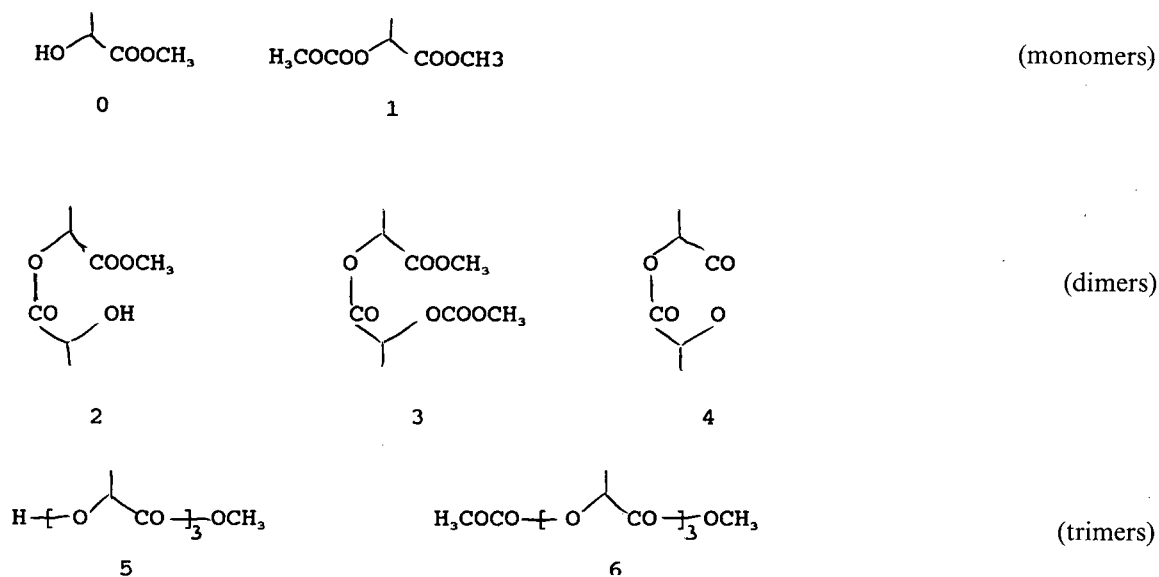
RESULTS AND DISCUSSION

General approach

The derivatization yields of HA treated with chloroformates were studied previously [6] using an equimolar mixture of the analytes. Under optimum reaction conditions the side-product formation was minimized but could not be fully eliminated.

With the individual HA at higher concentrations the occurrence of side-products was augmented. The most problematic HA proved to be lactic acid, affording largest amount of accompanying side-products, as is apparent from Fig. 1C and D.

The structures of the peaks were identified in the preceding study as follows:



Apart from the main reaction product, the O-methoxycarbonyl methyl ester (1), the activated molecules conjugate to form lactides or interester oligomers with alkoxy-carbonyl-treated and with untreated hydroxyl groups.

Regarding the distinct side-products, the influ-

ence of the composition of the reaction medium on the reaction yield was re-examined. The results are summarized in Fig. 2 and Tables I and II, where the pre-peak, main peak and post-peaks are represented by 0, 1 and 2–6, respectively.

First, the previous findings were confirmed,

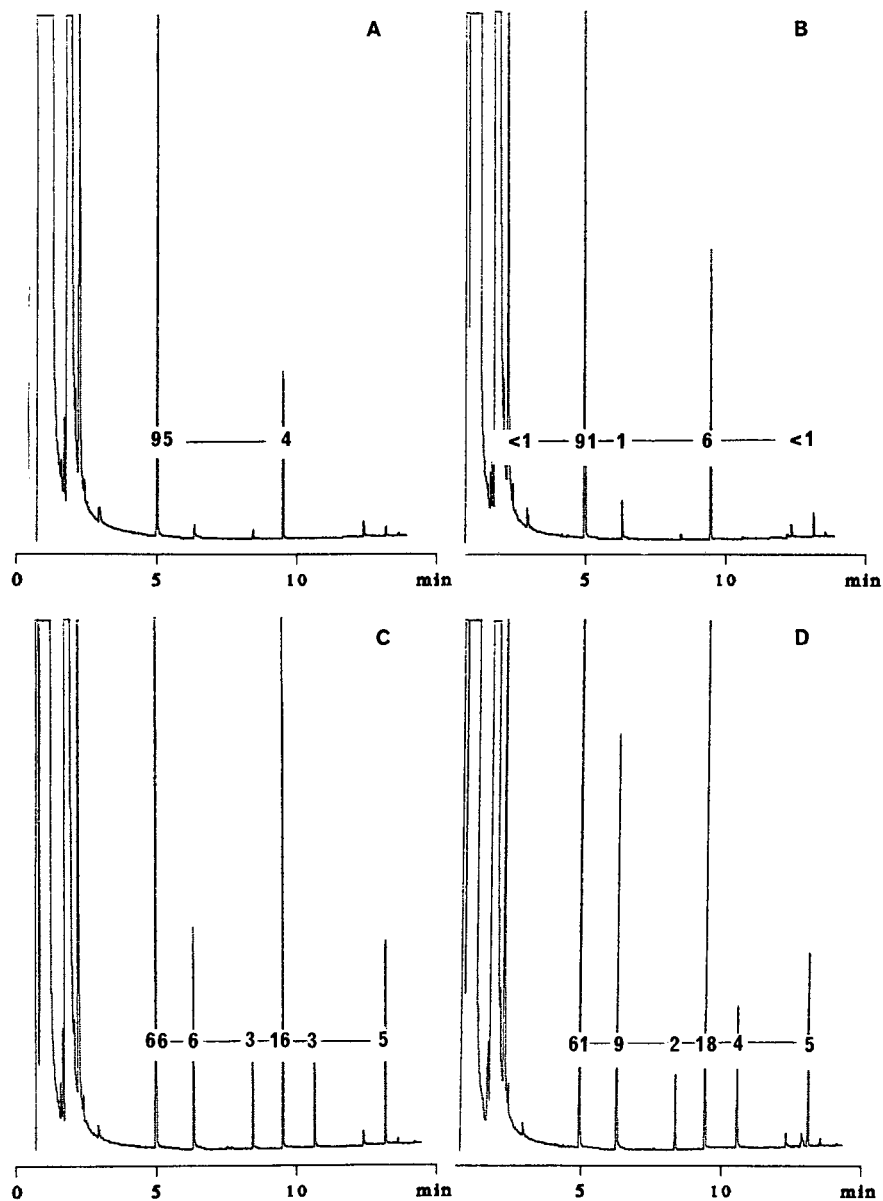


Fig. 1. GC profile of the reaction products of D-lactic acid treated with MCF according to the "normal mode" (C,D) and the "reversed mode" (A,B) in two different reaction media (A,C and B,D; see Experimental). The percentage peak abundance are given on the on the abscissa.

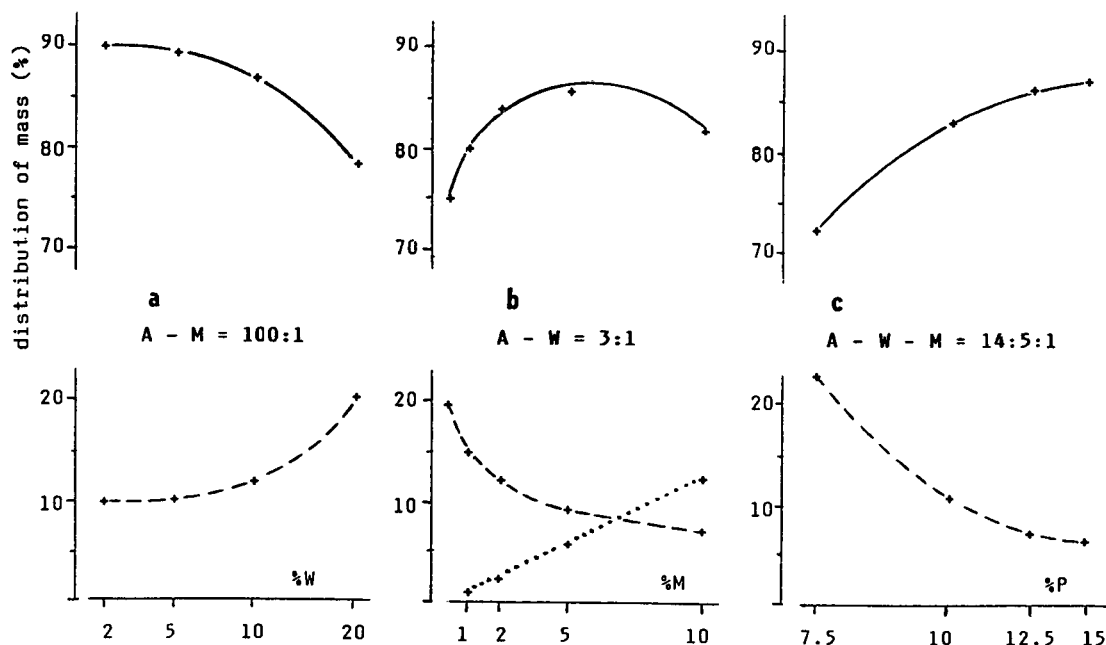


Fig. 2. Influence of water, methanol and pyridine concentration changes in the corresponding reaction media (a,b,c) on the distribution of mass of the MCF-derivatized HA (seven in total) between the main product (full line) and the side-products (dashed line = post-peaks, dotted line = pre-peak).

namely that acetonitrile should predominate in the reaction medium for the highest yields of the main product. When partially replaced with acetone, a small amount of mixed anhydride was always present on the chromatogram, confirming the results of

the previous study [6]. Addition of water to acetonitrile causes a rapid decrease in the yield with a concomitant increase in the rear side-products. Moreover, the reaction with ECF does not proceed to completeness in acetonitrile–water or acetonitrile

TABLE II

DISTRIBUTION OF MASS OF THE DERIVATIVES OF THE PARTICULAR HYDROXYCARBOXYLIC ACID TREATED WITH MCF IN A–W–M (14:5:1) AND WITH ECF IN A–W–E (2:1:1), RESPECTIVELY

The values are means of five identically derivatized samples; the relative standard deviations were less than 5% on average.

Hydroxycarboxylic Acid	Peak abundance (%)					
	MCF			ECF		
	Pre-peak	Main peak	Post-peaks	Pre-peak	Main peak	Post-peaks
Glycolic	6	87	6	5	82	12
Lactic	8	74	17	5	72	22
Butyric	8	75	16	12	77	10
Isovaleric	1	95	4	2	95	2
Valeric	6	89	5	6	87	6
Isocaproic	9	79	12	9	83	7
All (on average)	6	84	10	7	83	10

alone. Addition of ethanol is necessary, in general. Optimum yields with both MCF and ECF were achieved when the amount of alcohol added to acetonitrile was about 4–5%, and this is just the same reaction medium as for the treatment of fatty acids [8]. When water is added to replace acetonitrile partially in the medium, the yield of the main product declines, provided that alcohol is not co-added (Fig. 2a). From Fig. 2b it follows that even 25% of water is tolerable when the amount of methanol is increased from 1 to about 5%. However, an increase in methanol concentration causes a rise of peak 0 (the values are in parentheses for MCF-treated lactic acid in Table I, as this peak more than less co-elutes with the front peaks and its amount is difficult to estimate), so that for an optimum yield of the main product a compromise between pre-peak and post-peak sizes, in relation to the content of alcohol, has to be found.

With ECF the best yields are achieved with 4–5% of ethanol in acetonitrile, and an increase in water content should be accompanied by the addition of an approximately equal amount of alcohol. It is interesting that even with 50% of water in the medium the third best results with lactic acid can be obtained (IIIh, Table I). In contrast, the lowest yield of the main product was noted with equal amounts of the three solvents in the medium.

The preceding experiments were done with 10% of pyridine in the medium. However, the yields were improved by increasing the pyridine concentration to 15%, as shown in Fig. 2c and Table I (Ig). The same applies for treatment with ECF.

In Table II, individual differences in HA with regard to side-product formation are presented. As is apparent, lactic and HB acids are the most problematic, affording the highest abundance of the side-products. HIV and HV acids, on the other hand, give only small amounts of side-products. Hence the derivatization yield proved to be compound dependent to a certain extent.

The main reaction products of 3HB and 4HB acids have the hydroxyl group underivatized, as found previously [6]. However, about 5–8% are also alkylated on the hydroxyl group. This is true for MCF treatment; with ECF only 3HB acid behaves as described. When 4HB acid was subjected to treatment with ECF, the product formed was found to be the internal ester:



Special approach

The distribution of mass between the main and side reaction products can be positively influenced in favour of the main product by reversing the order of addition of the organic base and the reagent. With this “reversed mode”, *i.e.*, when reagent is added to the reaction medium first followed by addition of pyridine, the formation of side-products is substantially reduced. This concerns especially lactic acid treated with MCF (Fig. 1), where the yield of the main product is 30% higher. With the ECF-treated lactic acid the difference is about 20% (Fig. 3), which means that the effect of reversing the order of addition is not so marked here. With the MCF-treated 2HB the yield of the main reaction product is relatively high even with the “normal mode”; the improvement after the reversal is about 10%. Moreover, the occurrence of double peaks points to the formation of diastereomeric interesters and lactides due to the racemic reference substance used.

Considering to the baseline at the rear of the chromatogram in Fig. 4, where an equimolar mixture of 7HA was analysed after treatment with MCF, the improvement with the reversed mode is also clearly apparent. Another phenomenon is the number of rear peaks, which are eluted almost continuously one after the other. With a high probability it can be concluded that interesters are formed not only by conjunction of two molecules of the same HA but even by conjunction of various members in the mixture. Hence the difficulty of minimizing the formation of side-products increases with increasing number of analytes in a mixture of HA, and this is of prime importance when a quantitative analysis is taken in account.

Under the optimum reaction conditions (main-product yields of 94–98%), the reproducibility was high enough to make the procedure suitable for quantitative analysis. The relative standard deviations were below 3% and a linear relationship was observed between the peak height and the amount of the lactic acid in the range 1–1000 nmol. Moreover, the same accuracy and linearity were maintained even under the less favourable conditions

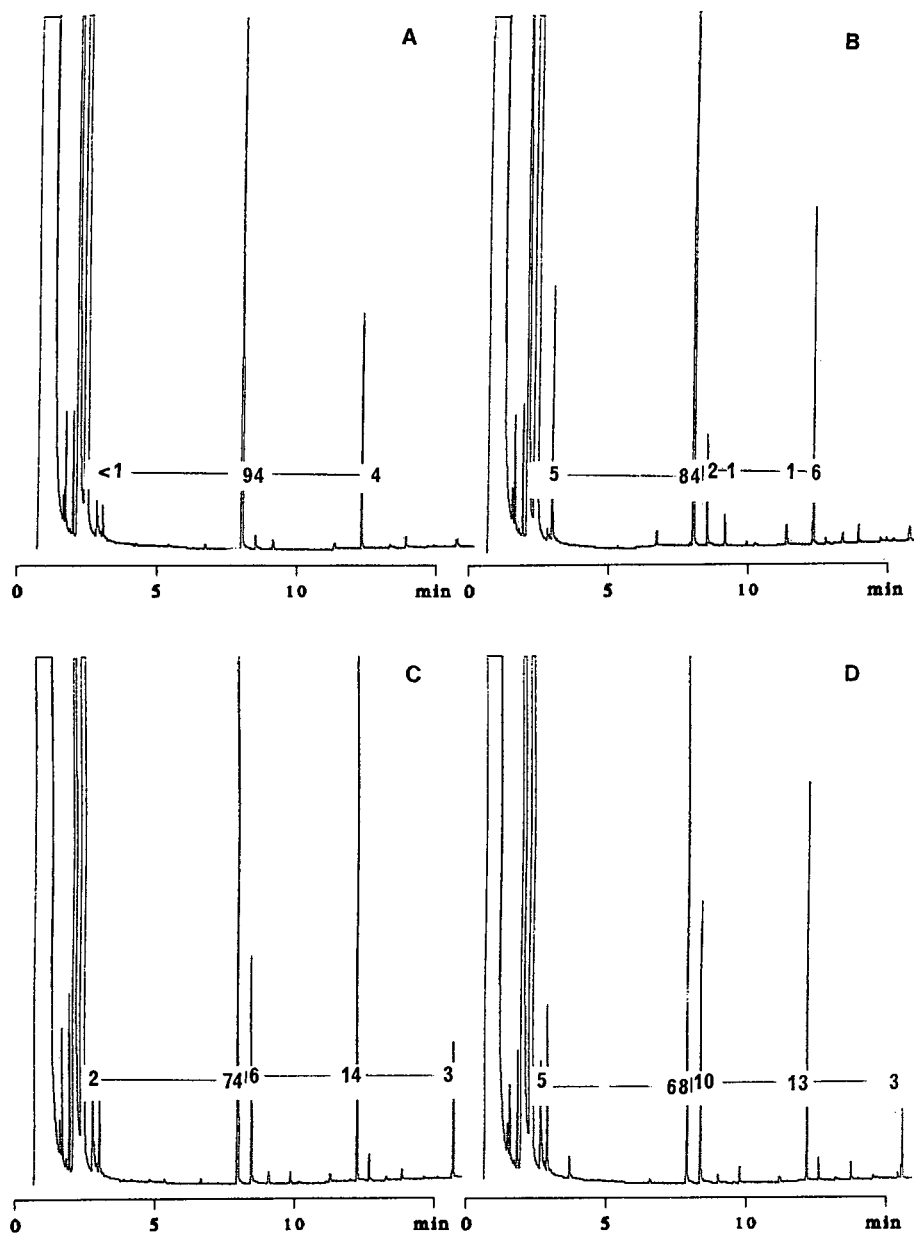


Fig. 3. GC profile of the reaction products of D-lactic acid treated with ECF in the same manner as with MCF in Fig. 1.

with a higher water content in the medium, which are, however, convenient for practical work up of biological fluids.

CONCLUSIONS

In previous papers concerning the derivatization of carboxylic acids with chloroformates, it was

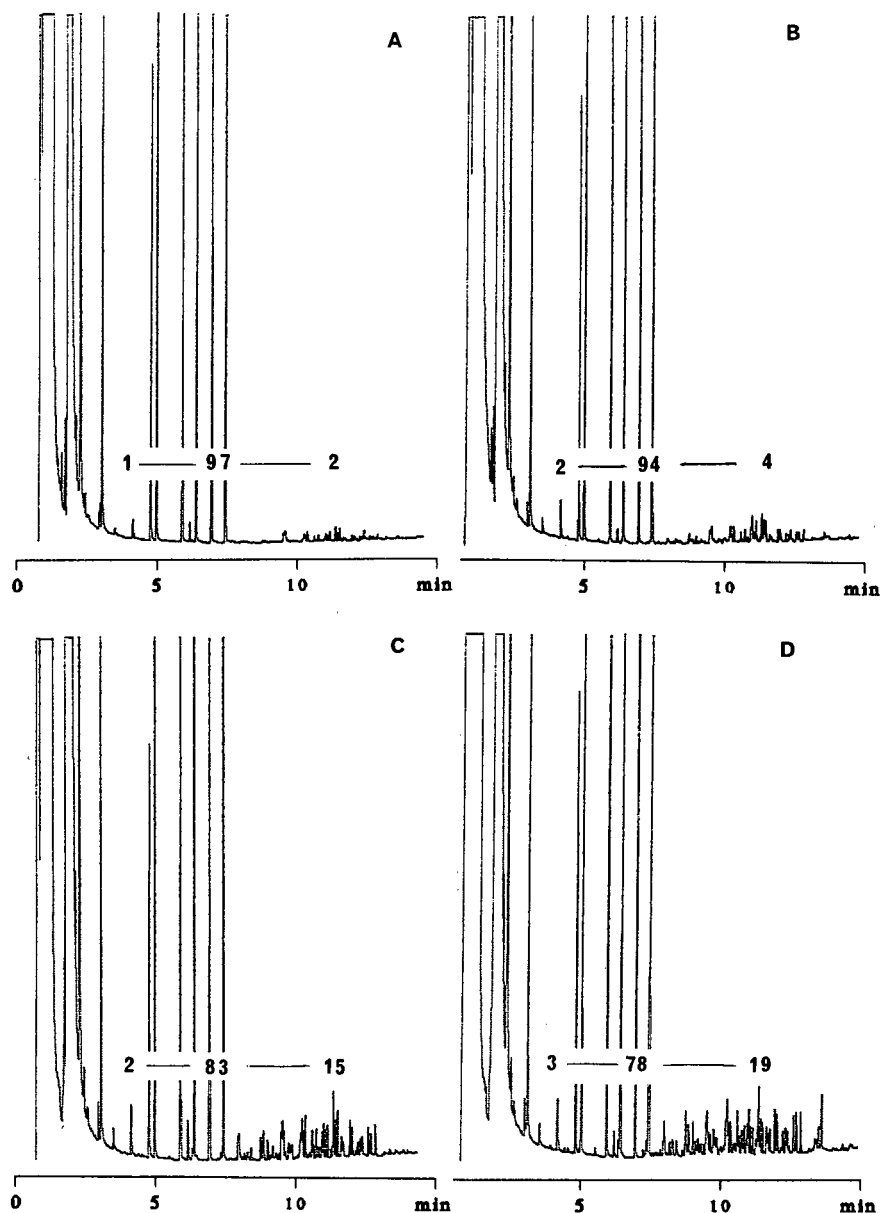


Fig. 4. GC analysis of an equimolar mixture of six 2-hydroxycarboxylic acids plus 3-hydroxybutyric acid (the first large peak after the solvent peak) after treatment with MCF as in Fig. 1.

demonstrated that with hydroxymonocarboxylic acids the optima of reaction conditions are especially important. Evidence is presented here that addition of the reagent to the reaction medium prior to the organic base, being the catalyst of the reaction, improves the yield of the main reaction product

substantially and makes this procedure suitable even for quantitative analysis. The formation of oligomers by interesterification is greatly suppressed by this way, especially when methyl chloroformate is used.

ACKNOWLEDGEMENT

Financial support of the University of Tübingen, Medical Clinic, Laboratory for Gas Chromatography and Mass Spectrometry (Head: Professor H.M. Liebich) is highly acknowledged.

REFERENCES

- 1 H. M. Liebich, *J. Chromatogr.*, 379 (1986) 347.
- 2 W. Yu, T. Kuhara, Y. Inoue, I. Matsumoto, R. Iwasaki and S. Morimoto, *Clin. Chim. Acta*, 188 (1990) 161.
- 3 A. Avogaro and D. M. Bier, *J. Lipid Res.*, 30 (1989) 1811.
- 4 K. Koike, Y. Urata and N. Hiraoka, *J. Clin. Biochem. Nutr.*, 9 (1990) 151.
- 5 B. Bleiberg, J. J. Steinberg, S. D. Katz, J. Wexler and T. LeJemtel, *J. Chromatogr.*, 568 (1991) 301.
- 6 P. Hušek, *J. Chromatogr.*, 547 (1991) 307.
- 7 H. M. Liebich, E. Gesele, H. G. Wahl, C. Wirth, J. Woll and P. Hušek, *J. Chromatogr.*, submitted for publication.
- 8 P. Hušek, J. A. Rijks, P. A. Leclercq and C. A. Cramers, *J. High Resolut. Chromatogr.*, 13 (1990) 633.

Short Communication

Preparation of methyl esters of fatty acids with trimethylsulphonium hydroxide —an appraisal

A. H. El-Hamdy[☆] and W. W. Christie

Hannah Research Institute, Ayr, Scotland KA6 5HL (UK)

(First received October 6th, 1992; revised manuscript received November 12th, 1992)

ABSTRACT

The rates of reaction of the new basic transesterification catalyst, trimethylsulphonium hydroxide (TMSH), have been compared with an established sodium methoxide-catalysed procedure. Although the latter is more rapid, the difference is only of practical importance when cholesterol esters are transesterified. Some losses of polyunsaturated components from fish oils were observed when methods were employed in which TMSH was injected directly into the heated injection port of the gas chromatograph, as had been recommended.

INTRODUCTION

Preparation of methyl ester derivatives of fatty acids for gas chromatographic (GC) analysis is one of the fundamental reactions in lipid chemistry [1–5]. Trimethylsulphonium hydroxide (TMSH) was introduced in 1979 as a mild methylating agent for acidic organic molecules [6]. It can be used in two ways, *i.e.* to methylate free acids by pyrolysis of the salt in the heated injection port of a gas chromatograph [6,7], or to effect base-catalysed transesterification of lipids [8–12]. As the only by-products of these reactions are dimethylsulphide and methanol, the excess reagent itself decomposing to these compounds, methyl esters can be prepared for chromatographic analysis in simple one-pot procedures with little or no work-up.

TMSH has been used to methylate bacterial fatty acids [11,12], which include monoenoic, branched-chain and cyclopropane components, and a limited range of animal and vegetable fats and oils [8–11]. It is evident from the published papers that the reagent gives as clean GC traces with stable baselines as any other procedure. However, there is no information on the rate of the reaction with different lipid classes. Nor has there been any quantitative comparison with data obtained by alternative procedures for polyunsaturated fatty acid components, which might be most sensitive to alteration. We have now addressed these problems.

EXPERIMENTAL

Reagents

Trimethylsulphonium iodide was obtained from Aldrich (Gillingham, UK). It was converted to an 0.2 M solution of the hydroxide by two different methods, *i.e.* by reaction with silver oxide in methanol [7,8], and by reaction with an ion-exchange resin [10,12].

Correspondence to: W. W. Christie, The Scottish Crop Research Institute, Invergowrie, Dundee, Scotland DD2 5DA, UK (present address).

[☆] Present address: Al-Fateh University, Tripoli, Libya.

All other solvents and reagents were “reagent” or “HPLC” grade and were from FSA Scientific Apparatus (Loughborough, UK). Synthetic lipid standards were from Sigma (Poole, UK). Cod liver oil was from a local pharmacy.

Methylation

Timed reaction studies were carried out at room temperature by dissolving the lipid (0.1 to 3 mg), with methyl nonadecanoate (0.1 to 0.5 mg) added as internal standard, in sodium-dried diethyl ether (0.5 ml) and methyl acetate (20 μ l), before 0.2 M TMSH in methanol (100 μ l) was added. The reaction was stopped at specified time intervals by adding acetic acid (5 μ l); the solvent was removed on a rotary evaporator, and the sample was re-dissolved in hexane for GC analysis. In some experiments, the reaction was not stopped by the addition of acid.

For comparison purposes, an established base-catalysed transesterification procedure was used with conditions as above except for 1 M sodium methoxide in dry methanol as catalyst (20 μ l) [13].

Free fatty acids, prepared by hydrolysis of cod-liver oil [5], were converted to methyl esters with TMSH in a pyrolysis–methylation reaction. TMSH solution (0.1 ml) was added to the free acids (1 mg) in methyl-*tert.*-butyl ether (0.5 ml) and an aliquot (1 μ l) was injected directly into the heated injection port of the gas chromatograph. For comparison purposes, 1% sulphuric acid in methanol was used for methylation prior to injection [5].

Gas chromatography

GC analyses of fatty acid methyl esters were performed on a Carlo Erba Model 4130 capillary gas chromatograph (Erba Science, Swindon, UK), equipped with a split/splitless injector maintained at 260°C. A fused-silica capillary column (25 m \times 0.22 mm I.D., film thickness 0.2 μ m) coated with Carbowax 20M (Chrompack UK, London, UK) was used. The oven temperature was programmed for three min isothermally at 175°C, then to 205°C at a rate of 4°C/min and held at the final temperature for 20 min more. Hydrogen was the carrier gas. Fatty acids methyl esters were identified by reference to standards and were quantified by electronic integration.

RESULTS AND DISCUSSION

Two methods have been described for preparation of the TMSH reagent. One involving the use of an ion-exchange resin [10,12] was tried first and gave excellent preliminary results. However, in attempting to do timed experiments to measure the rate of reaction, it was observed that the products were free fatty acids which were only converted to methyl esters when injected into the gas chromatograph, *i.e.* reaction proceeded entirely via the pyrolytic mechanism, since the reagent was effecting hydrolysis rather than transesterification. This is presumed to be because water was retained by the ion-exchange resin during conversion to the correct salt form, and this passed into the reagent. When the reagent was prepared under anhydrous conditions with dry methanol and silver oxide [7,8], methyl esters were prepared directly by transesterification. The latter procedure was adopted in all the experiments described below. The reagent prepared in this way is an equimolar mixture of the hydroxide and methoxide.

The rates of reaction of TMSH and sodium methoxide with cod liver oil triacylglycerols, dipalmitoylphosphatidylcholine and cholesteryl palmitate were determined by stopping the reaction at timed intervals by the addition of acetic acid, and measuring the amounts of methyl esters relative to the internal standard by GC. The results are shown in Fig. 1. It is evident that reaction was somewhat more rapid with sodium methoxide as catalyst in each instance, but with triacylglycerols and phospholipids the reaction was essentially complete in about 5 min. The difference would not be of practical importance with these lipids.

It is well established that cholesterol esters are transesterified only slowly by most reagents (note the difference of time scale in Fig. 1) [5,13]. Cholesterol esters were transesterified completely in 1 to 2 h with the sodium methoxide method, but the reaction was still far from complete after 5 h with TMSH. In practice, complete esterification should be possible with the latter and cholesterol esters if a higher concentration of reagent and higher temperatures were to be employed.

The analysis of a fish oil, because of its high content of polyunsaturated fatty acids, is a more rigorous test of a method than is application to depot

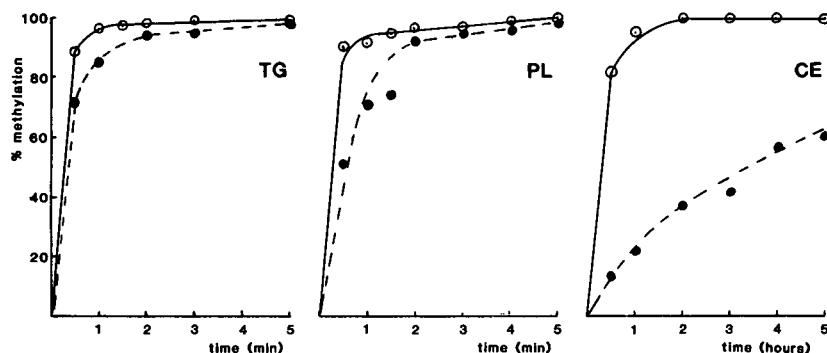


Fig. 1. Rates of transesterification of lipid classes with sodium methoxide (O) and trimethylsulphonium hydroxide (TMSH) (●). TG = Triacylglycerols (cod liver oil); PL = phospholipids (dipalmitoylphosphatidylcholine); CE = cholesterol esters (cholesteryl palmitate).

fats or vegetable oils. Fatty acid compositions of cod liver oil, determined by GC after various methylation procedures were applied, are shown in Table I. To simplify matters, only the data for 20:5(*n*-3) and 22:6(*n*-3) fatty acids are listed, since these are the components at greatest risk from an over-vigorous reaction. Sodium methoxide-catalysed transesterification [5] is a well-established and safe method against which others can be judged. TMSH used under similar conditions, *i.e.* in which the reaction was stopped with acetic acid so no TMSH was injected into the GC column, gave re-

sults that were not significantly different. However, when the medium was not acidified and an aliquot of the reaction mixture was injected directly onto the column, as has been recommended [8-12], a loss of approximately 5% of the polyunsaturated components was observed. Somewhat greater losses were obtained when free acids were methylated with TMSH in a pyrolysis-methylation procedure [6,7] or with methanolic sulphuric acid [5], although part of these losses may be because of the more extensive manipulations involved because of the initial hydrolysis step.

TABLE I

CONTENT OF 20:5(*n*-3) AND 22:6(*n*-3) IN COD LIVER OIL AS DETERMINED BY GC FOLLOWING TRANSESTERIFICATION WITH TMSH, OR BY ALTERNATIVE METHODS

Results are means and standard deviations of three analyses.

No.	Method	Fatty acid (% w/w)	
		20:5(<i>n</i> -3)	22:6(<i>n</i> -3)
1	Sodium methoxide transesterification [13]	10.58 ± 0.059	9.75 ± 0.197
2	TMSH; same conditions as in 1	10.36 ± 0.078	9.48 ± 0.108
3	As 2 but acetic acid not added to stop reaction (and solvents not evaporated) [8-12]	10.05 ± 0.035	9.04 ± 0.116
4	Pyrolysis-methylation of free acids with TMSH [6,7]	9.07 ± 0.047	7.70 ± 0.425
5	Methanol-1% sulphuric acid [5]	8.42 ± 0.215	7.13 ± 0.309

In practice with TMSH, it may not always be necessary to stop the reaction by adding acid, especially for samples that do not contain significant amounts of polyunsaturated fatty acids. TMSH should pyrolyse to give volatile products only, and no deleterious effects on the column were observed in this study. However, there remains a possibility that column life might be shortened over a period of several months if any unchanged reagent survived the pyrolysis. It seems to be a sensible precaution (when long-chain fatty acids only are present) to employ the simple expedient of stopping the reaction with acetic acid, evaporating excess solvents and re-dissolving in hexane for analysis, when TMSH is used. Minimal losses of polyunsaturated fatty acids should then occur, even on prolonged storage, and column life may be lengthened. Under these conditions, the reaction is still a simple one-pot one. TMSH is easy to prepare under safe conditions in small quantities, and can be recommended for more general use.

ACKNOWLEDGEMENT

This paper is published as part of a programme funded by the Scottish Office Agriculture and Fisheries Department.

REFERENCES

- 1 W. W. Christie, in F. D. Gunstone (Editor), *Topics in Lipid Chemistry*, Vol. 3, Paul Elek, London, 1972, pp. 171–197.
- 2 A. J. Sheppard and J. L. Iverson, *J. Chromatogr. Sci.*, 13 (1975) 448.
- 3 A. Darbre, in K. Blau and G. S. King (Editors), *Handbook of Derivatives for Chromatography*, Heyden, London, 1978, pp. 36–103.
- 4 C. D. Bannon, G. J. Breen, J. D. Craske, N. T. Hai, N. L. Harper and K. L. O'Rourke, *J. Chromatogr.*, 247 (1982) 71.
- 5 W. W. Christie, *Gas Chromatography and Lipids*, Oily Press, Ayr, 1989.
- 6 K. Yamauchi, T. Tanabe and M. Kinoshita, *J. Org. Chem.*, 44 (1979) 638.
- 7 W. Butte, J. Eilers and M. Kirsch, *Anal. Lett.*, 15 (1982) 841.
- 8 W. Butte, *J. Chromatogr.*, 261 (1983) 142.
- 9 L. Matter, D. Schenker, H. Husmann and G. Schomburg, *Chromatographia*, 27 (1989) 31.
- 10 E. Schulte and K. Weber, *Fat Sci. Technol.*, 91 (1989) 181.
- 11 K.-D. Muller, H. Husmann, H. P. Nalik and G. Schomburg, *Chromatographia*, 30 (1990) 245.
- 12 K.-D. Muller, H. Husmann and H. P. Nalik, *Zentralbl. Bakteriolog.*, 274 (1990) 174.
- 13 W. W. Christie, *J. Lipid Res.*, 23 (1982) 1072.

Short Communication

Capillary electrophoretic separation of recombinant granulocyte-colony-stimulating factor glycoforms

E. Watson and F. Yao

Amgen Inc., Amgen Center, 1900 Oak Terrace Lane, Thousand Oaks, CA 91320 (USA)

(First received September 30th, 1992; revised manuscript received November 23rd, 1992)

ABSTRACT

Free zone capillary electrophoresis separated recombinant human granulocyte-colony-stimulating factor, expressed in Chinese hamster ovary cells, into two well-resolved species. Following incubation with neuraminidase, these species comigrated, eluting earlier than either of the original two species. This indicated that the observed heterogeneity was caused by different amounts of sialic acid present on the carbohydrate portion of the protein. It was determined that optimum separation occurred in the buffer pH range 7–9. Evidence is also presented to show that these glycoforms migrate in order of increasing numbers of sialic acids present.

INTRODUCTION

Determination of glycoprotein heterogeneity has become increasingly important in analytical biotechnology since many of the recombinant proteins with commercial value are highly glycosylated. Traditionally, the separation has been performed using gel isoelectric focusing (IEF). Glycoforms can contain different numbers of sialic acid residues and as a result show differences in their isoelectric points. Separation by IEF is based on the establishment of a stable pH gradient. Under the influence of an electric field the differently charged glycoforms migrate to the point where their pI values are equivalent to the pH and, hence, no further migration takes place. While the separations obtained with this technique are excellent, it is slow, labor intensive and the results are semi-quantitative. To over-

come some of these problems, Pharmacia has introduced their PhastGel system that permits automation of staining but still requires a separate step for quantitation. Recently, the separations obtained by Phast IEF Gel and IEF in coated capillary columns have been compared for monoclonal antibody Her-2 4D5. Capillary IEF showed a superior degree of species resolution [1].

High-performance capillary zone electrophoresis (CZE) has shown great success in separating peptides and proteins. While these separations can typically be carried out with no more than pH and ionic strength manipulations, the application of CZE for the separation of proteins based on their isoelectric points or pI values is not such a simple procedure. Several publications have described the separation of glycoforms by isoelectric focusing using capillary electrophoresis instrumentation [2–5]. In all of these instances separations were achieved using coated capillary columns. When uncoated columns were used, electroosmotic flow

Correspondence to: E. Watson, Amgen Inc., Amgen Center, 1900 Oak Terrace Lane, Thousand Oaks, CA 91320, USA.

was a limiting factor that precluded the possibility of attaining stable focused zones necessary for IEF to occur. Very recently, automated IEF has been reported on two commercial capillary electrophoresis systems, one using chemical mobilization [6] and the other using vacuum mobilization [7].

We have evaluated the utility of free zone electrophoresis as an alternative technique for the separation of glycoforms. Recombinant human granulocyte-colony-stimulating factor (rhGCSF) produced in CHO cells was selected because it is a well-characterized protein present in a highly purified state, containing two O-linked carbohydrate moieties that differ only in having one and two sialic acid residues. This glycoprotein represents one of the simplest, yet well defined carbohydrate structures for the evaluation of experimental conditions that can control the separations of proteins differing in sialic acid content.

METHODS

hGCSF produced in mammalian cell lines was manufactured at Amgen, Thousand Oaks, CA, USA. All capillary zone electrophoresis was performed using a Beckman PACE 2000 high-performance capillary electrophoresis system. Capillaries of 50 cm \times 75 μ m were supplied by Beckman, those of 100 cm \times 75 μ m were assembled in our laboratory and were obtained from Polymicro Technologies (Phoenix, AZ, USA).

Separations were carried out with cathode placed at the detector end of the capillary. Before analysis was carried out, capillary electrophoresis system was set to maintain a constant temperature at 25°C. For each run, the capillary was rinsed with running buffer for 3 min. Sample was then introduced by low pressure for 5 s. After sample loading, voltages of 5–20 kV were applied and maintained constant throughout the run. Separated species were then monitored with UV detection set at 214 nm and detector signal was transmitted to a Chromjet integrator (Spectra-Physics, San Jose, CA, USA). Post-separation rinses with 0.1 M NaOH, followed by water were carried out for 3 min each to ensure removal of residual protein from the previous run. Experimental conditions are as described in the figure captions.

Sialic acid residues were removed from rhGCSF

by digestion at 37°C with neuraminidase (*Vibrio Cholerae* Type II) in sodium acetate, pH 5.0.

RESULTS AND DISCUSSION

There are several major advantages in using recombinant derived proteins for developing new analytical separation methods. Since these proteins are intended for human therapeutic use, they are extremely well-characterized and highly purified. Carbohydrate structures on rhGCSF have been identified as NeuAc α 2 \rightarrow 3Gal β 1 \rightarrow 3(\pm NeuAc α 2 \rightarrow 6)GalNAcol [NeuAc = N-acetylneuraminic

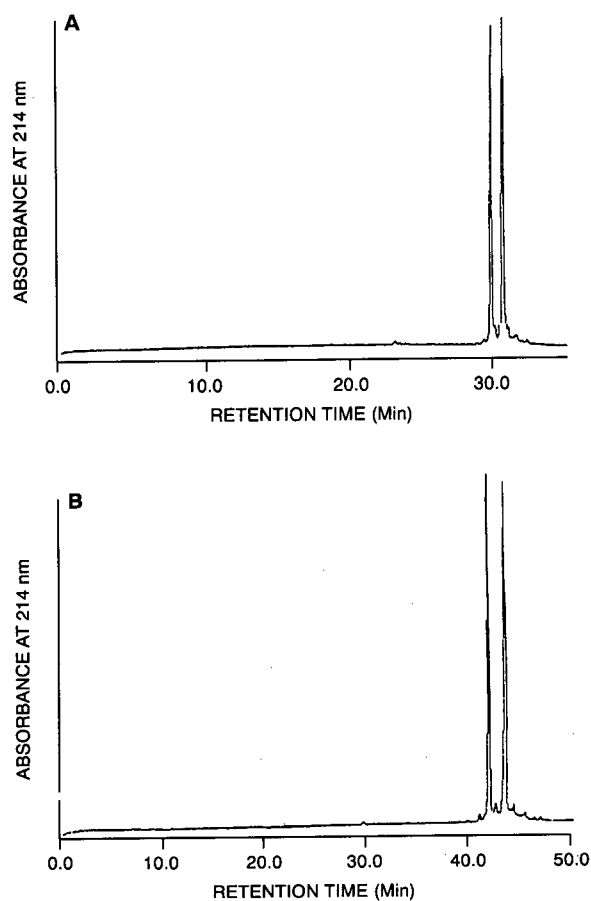


Fig. 1. Capillary electrophoretic separations of rhGCSF at 1 mg/ml in (A) pH 8.0, 50 mM phosphate–50 mM borate buffer and (B) pH 8.0, 50 mM phosphate–50 mM borate buffer with 2.5 mM diaminobutane. Separations were obtained under 30 kV using a 100 cm \times 75 μ m capillary.

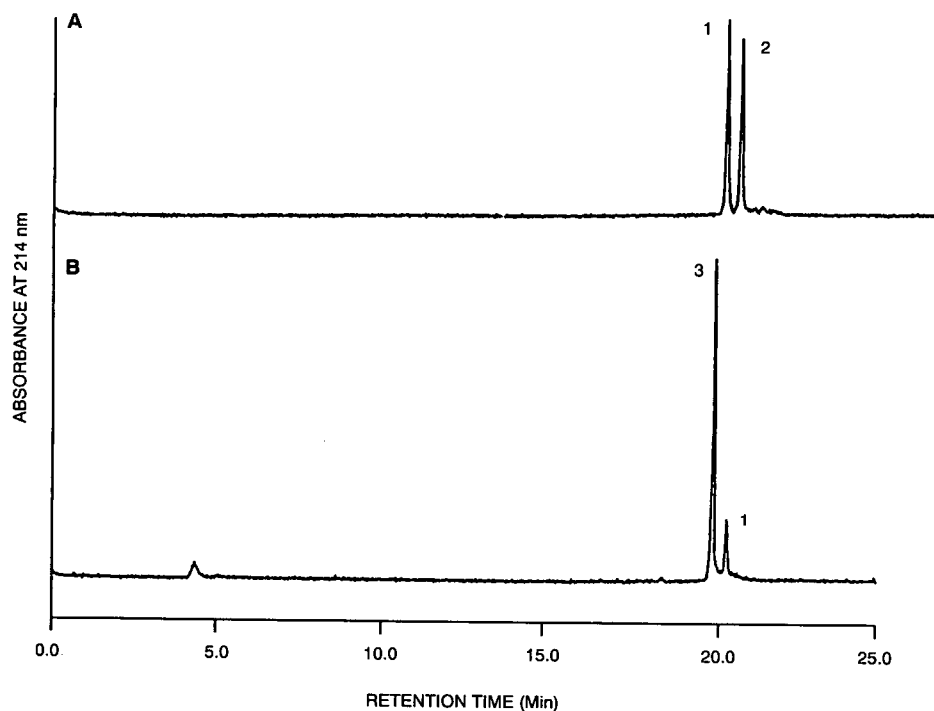


Fig. 2. Capillary electrophoretic separations in pH 9.0, 100 mM borate buffer. (A) rhGCSF and (B) rhGCSF after 10 h of incubation with neuraminidase. Separations were obtained under 20 kV using a 100 cm \times 75 μ m capillary. See text for peak identification.

acid, Gal = galactose, GalNAc = N-acetylglucosamine (reduced)] and are present in equal amounts differing only in the number and linkage of the sialic acid residues present [8].

The separation of rhGCSF glycoforms was evaluated in buffers with pH values ranging from 2.5–9. At pH 5 or less, no rhGCSF migrated past the detector. rhGCSF may have precipitated on the column or its mobility was so slow that it did not migrate sufficiently in the time allotted for analysis (<60 min). When pH 6 was used, rhGCSF migrated as two overlapping peaks. At pH values of 7–9, these separated into two equally sized peaks showing baseline resolution with little quantitative difference among the separations obtained at each pH.

The experimental conditions that can affect separations and resolution have been the subject of many studies [9–12]. From these reports it has been shown that column length, buffer type, ionic strength, pH, voltage and a variety of additives can all have a major impact. These were systematically evaluated on an individual basis for their effects on

analysis time and peak resolution. Fig. 1A shows the optimum electrophoretic separation obtained for the two glycoforms present in rhGCSF. Enhancement of the resolution was next evaluated by incorporating organic additives such as methanol, ethanol, tetrahydrofuran, urea and 1,4-diaminobutane. All of these are known to reduce electroosmotic flow to different extents. Of these, 1,4-diaminobutane showed the most effectiveness in improving resolution at a final concentration of 2.5 mM. The results is shown in Fig. 1B.

At pH values of 6–9, sialic acids present on rhGCSF are negatively charged and migrate in the opposite direction from the detector. The electroosmotic flow dominates the overall migration carrying the negatively charged rhGCSF species toward the detector. Since the migration velocity of a charged species is the vector sum of the electroosmotic flow and that of the species, the presence of negatively charged sialic acid causes the glycoforms to migrate at a slower rate than the electroosmotic flow, with a net flow which is differ-

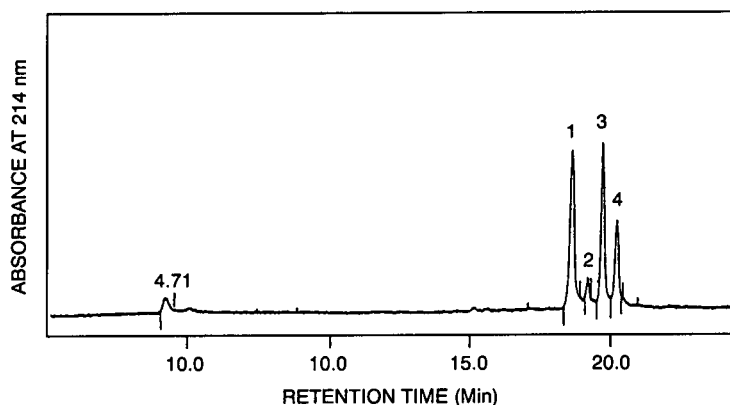


Fig. 3. Capillary electrophoretic separations in pH 9.0, 100 mM borate buffer. Sample of rhGCSF was incubated with neuraminidase for 30 min and spiked with non-glycosylated rhG-CSF. Peaks: 1 = non-glycosylated rhGCSF; 2 = desialylated rhG-CSF; 3, 4 = glycosylated rhG-CSF.

ent for charged glycoforms containing one and two sialic acids. Glycoforms containing one sialic acid will migrate faster than those with two sialic acids. As a result, it can be expected that these glycoforms will migrate in order of increasing numbers of sialic acids. Peak 1 is assigned to the glycoform with one sialic acid and peak 2 to that containing two sialic acids (Fig. 2a).

To verify peak assignments, rhGCSF was incubated with neuraminidase which selectively removes sialic acid from the carbohydrate moiety. These incubation studies were conducted over 24 h with samples removed at various time points for CZE analysis. The results showed the peak 2 decreased more rapidly than peak 1. A new peak, identified as peak 3, emerged migrating faster than peak 1 and gradually increased in response as peak 1 and peak 2 decreased. Fig. 2b shows the rhGCSF separation profile after 10 h of incubation with neuraminidase.

It was of interest to compare the electrophoretic behavior of non-glycosylated rhGCSF produced in *Escherichia coli* cells and desialylated rhGCSF. These could be baseline resolved with *E. coli* produced rhGCSF migrating faster than desialylated rhGCSF (Fig. 3). These results indicate that the carbohydrate structures remaining on rhGCSF at pH 9 affect to a significant extent the mobility of the protein under the experimental conditions used.

In addition to developing a capillary electropho-

retic separation of isoforms, we investigated the feasibility of obtaining quantitative separation data. A series of concentrations from 0.10, 0.25, 0.50, 0.75 and 1.0 mg/ml were used and the areas of the separated isoforms determined. The results indicated that the amounts determined are consistent over the concentration range with a relative standard deviation of <2%. Retention time reproducibility was evaluated by injecting rhGCSF six times and determining consistency of retention times. The relative standard deviation was determined to be $\pm 0.1\%$.

CONCLUSIONS

The use of free zone capillary electrophoresis is shown to be a highly efficient and fast technique capable of separating glycoforms based on the number of sialic acids present. The glycoforms are eluted in order of increasing number of sialic acids and with this information the results can be directly compared to gel IEF. rhGCSF has a *pI* value of 4.5 and is negatively charged under the pH conditions in the range 7-9 used to separate the glycoforms. As a consequence, protein adsorption onto the capillary walls which are negatively charged at these pH values is minimized by charge repulsion. The effect of various additives was evaluated to further enhance separation but results indicated that pH control in itself was sufficient to obtain satisfactory baseline resolution. In contrast to gel IEF electro-

phoresis, the separation of the glycoforms is fast with total analysis times of < 30 min, simple to perform, provides for automation and the results are quantitative in terms of reproducibility and linearity.

REFERENCES

- 1 K. W. Yim, *J. Chromatogr.*, 559 (1991) 401.
- 2 S. Hjertén, K. Elenbring, F. Kilar and J. Laiao, *J. Chromatogr.*, 403 (1987) 47.
- 3 F. Kilar and S. Hjertén, *Electrophoresis*, 10 (1989) 23.
- 4 T. Wehr, M. Zhu, R. Rodriguez, D. Burke and K. Duncan, *Am. Biotech. Lab.*, 8 (1990) 22.
- 5 K. Shields and C. Silveran, presented at *NCI-FCRDC Conference on Capillary Electrophoresis, 1990*.
- 6 M. Oheda, S. Hase, M. Ono and T. Ikenaka, *J. Biochem.*, 103 (1988) 544.
- 7 H. Lauer and D. McManigill, *Anal. Chem.*, 58 (1986) 166.
- 8 R. McCormick, *Anal. Chem.*, 60 (1988) 2322.
- 9 P. Grossman, J. Colburn and H. Lauer, *Anal. Chem.*, 61 (1989) 1186.
- 10 S. Fujiwara and S. Honda, *Anal. Chem.*, 59 (1987) 487.
- 11 M. J. Sepaniak and R. O. Cole, *Anal. Chem.*, 59 (1987) 472.
- 12 Y. Walbroehl and J. W. Jorgenson, *Anal. Chem.*, 58 (1986) 479.

Book Review

Advances in lipid methodology 1, edited by W. W. Christie, Oily Press, Ayr, 1992, IX + 360 pp., price £ 54.00, ISBN 0-9514171-8.

This is the first volume in what the editor proposes as an occasional series of new volumes dealing with selected aspects of lipid methodology. The aspects covered in this multi-author book represent eight areas of active current applications and development covered only partially or not at all in previous books by the Oily Press. Chapter 1 by William Christie contains a short review on the uses of solid-phase extraction columns in lipid analyses, which save solvents and time by miniaturizing the operation. However, the author fails to point out that these routines are presently carried out blindly, since on-line detectors are not used to monitor the column effluents. Chapter 2 by David Harvey reviews mass spectrometry techniques for structure determination of fatty acids as the picolinyl and other nitrogen-containing derivatives. This is a detailed and comprehensive coverage of a field which the author has pioneered along with a discussion of parallel developments proposed by others. Chapter 3 by Paivi Laakso reviews the application of supercritical fluid chromatography for lipid analyses and compares it to alternative methodologies. A short introduction to the principles of SFC indicates that it lies somewhere between GLC and HPLC. The chapter cautions against the hyperbole of instrument makers, and points out that technical deficiencies related to injection methods, flow restriction and detector interfacing have yet to be corrected. In Chapter 4 William Christie reviews the advances recently made in the chromatographic resolution of chiral lipids and the potential that these methods hold for stereospecific analysis of triacylglycerols, which, however, is not discussed. In Chapter 5 Peter Kaufmann reviews chemometric approaches to method development for lipid analyses, and includes a brief description of the principles involved. Although chemometrics can be used in all stages of

experimentation, not all possible applications are likely to yield practical improvements in experimental efficiency. The chapter concludes with guidelines for beginners. In Chapter 6, Boryana Nikolova-Damyanova discusses silver ion chromatography of lipids. It is an old subject, which has received new lease on life due to recent applications in HPLC. This is an authoritative account of the practical aspects of the subject and of the remaining uncertainties about the technique. The author emphasizes that this is the only method that provides effective chromatographic resolution of the reverse isomers of neutral glycerolipids (e.g. SOO and OSO), which constitutes one of the last unresolved problems in glycerolipid separations. In Chapter 7 William Christie discusses detectors for HPLC with special emphasis on the evaporative light-scattering detector, which at present comes closest to a practical universal lipid detector. However, the transport flame ionization detector still remains a desirable goal for lipid monitoring in HPLC column effluents in the future. In Chapter 8 David Firestone and Alan Sheppard discuss the determination of *trans*-fatty acids, which remains a problem in fatty acid analyses. The authors review a wide variety of the techniques, which have been used to distinguish between *cis*- and *trans*-fatty acids, but a completely satisfactory solution is not provided by any one or a combination of two or more methods. Clearly, additional separation of positional isomers is necessary before the geometric isomerism can be adequately determined.

Each chapter contains a list of pertinent references, which constitute reliable sources of primary information. Some of these references are repeated in an Appendix, which lists the more important papers in lipid methodology for 1989 and 1990, but not for 1991. Many of the latter can be found in the

bibliography of individual chapters. The book contains a modest Index, which could have been expanded to cover both text and Appendix. The major strength of the book lies in the expertise and personal experience of the authors, which has resulted in a competent coverage and a guarantee that the readers employ correct tools in each instance. Although several of the chapters lack conclusions (which the reviewer has attempted to provide),

overall the book is well written, essentially free of typographical errors, and neatly printed. It is equally well suited for lipid experts and beginners. I highly recommend the book to anyone seriously interested in the separation and identification of lipids from natural sources.

Toronto (Canada)

A. Kuksis

Author Index

- Alvarez-Zepeda, A., see Fóti, G. 630(1993)1
- Arruda, A. C., Heinzen, V. E. F. and Yunes, R. A.
Relationship between Kováts retention indices and molecular connectivity indices of tetralones, coumarins and structurally related compounds 630(1993)251
- Auriola, S., see Tóth, Z. A. 630(1993)423
- Baillet, A., see Pianetti, G. A. 630(1993)371
- Bayloqç-Ferrier, D., see Pianetti, G. A. 630(1993)371
- Bean, R. M., see Harvey, S. D. 630(1993)167
- Beirinckx, P., see Roets, E. 630(1993)159
- Belvito, M. L., see Fóti, G. 630(1993)1
- Bemgård, A., Colmsjö, A. and Lundmark, B.-O.
Gas chromatographic analysis of high-molecular-mass polycyclic aromatic hydrocarbons. II. Polycyclic aromatic hydrocarbons with relative molecular masses exceeding 328 630(1993)287
- Betz, W. R., see O'Doherty, S. J. 630(1993)265
- Bolognani, L., see Volpi, N. 630(1993)390
- Bonn, G. K., see Timerbaev, A. R. 630(1993)379
- Bouissel, S., Erni, F. and Link, R.
Injection of large volumes of aqueous solutions in capillary supercritical fluid chromatography and sample preconcentration by multiple injections 630(1993)307
- Bouriotis, V., see Pozidis, C. 630(1993)151
- Boyajian, J. M., see Yau, W. W. 630(1993)69
- Brinkman, U. A. T., see Mol, H. G. J. 630(1993)201
- Buchberger, W., see Timerbaev, A. R. 630(1993)379
- Carelli, A. A. and Cert, A.
Comparative study of the determination of triacylglycerol in vegetable oils using chromatographic techniques 630(1993)213
- Cataldo, D. A., see Harvey, S. D. 630(1993)167
- Cert, A., see Carelli, A. A. 630(1993)213
- Charton, F., Jacobson, S. C. and Guiochon, G.
Modeling of the adsorption behavior and the chromatographic band profiles of enantiomers. Behavior of methyl mandelate on immobilized cellulose 630(1993)21
- Chen, W.-S., see Yeh, C.-F. 630(1993)275
- Christie, W. W., see El-Hamdy, A. H. 630(1993)438
- Chyueh, S.-D., see Yeh, C.-F. 630(1993)275
- Claeys, P., see Paesen, J. 630(1993)117
- Colmsjö, A., see Bemgård, A. 630(1993)287
- Cramer, S. M., see Gadam, S. D. 630(1993)37
- Cramer, S. M., see Jayaraman, G. 630(1993)53
- Cramers, C. A., see Mol, H. G. J. 630(1993)201
- Dang, Q., Yan, L., Sun, Z. and Ling, D.
Separation and simultaneous determination of the active ingredients in theophylline tablets by micellar electrokinetic capillary chromatography 630(1993)363
- DeStefano, J. J., see Yau, W. W. 630(1993)69
- El-Hamdy, A. H. and Christie, W. W.
Preparation of methyl esters of fatty acids with trimethylsulphonium hydroxide — an appraisal 630(1993)438
- Erni, F., see Bouissel, S. 630(1993)307
- Fang, J.-D., see Yeh, C.-F. 630(1993)275
- Feld, T., see Nowotnik, D. P. 630(1993)105
- Fellows, R. J., see Harvey, S. D. 630(1993)167
- Feste, A. S. and Khan, I.
Separation of glucooligosaccharides and polysaccharide hydrolysates by gradient elution hydrophilic interaction chromatography with pulsed amperometric detection 630(1993)129
- Fóti, G., Belvito, M. L., Alvarez-Zepeda, A. and Kováts, E.
Retention on non-polar adsorbents in liquid–solid chromatography. Effect of grafted alkyl chains 630(1993)1
- Foulger, B. E. and Simmonds, P. G.
Ambient temperature gas purifier suitable for the trace analysis of carbon monoxide and hydrogen and the preparation of low-level carbon monoxide calibration standards in the field 630(1993)257
- Fukui, S., Hanasaki, Y. and Ogawa, S.
High-performance liquid chromatographic determination of methanesulphonic acid as a method for the determination of hydroxyl radicals 630(1993)187
- Gadam, S. D., see Jayaraman, G. 630(1993)53
- Gadam, S. D., Jayaraman, G. and Cramer, S. M.
Characterization of non-linear adsorption properties of dextran-based polyelectrolyte displacers in ion-exchange systems 630(1993)37
- Ghijsen, R. T., see Mol, H. G. J. 630(1993)201
- Giaffreda, E., Tonani, C. and Righetti, P. G.
pH gradient simulator for electrophoretic techniques in a Windows environment 630(1993)313
- Graff, J. F., see Yau, W. W. 630(1993)69
- Guiochon, G., see Charton, F. 630(1993)21
- Hanasaki, Y., see Fukui, S. 630(1993)187
- Haraguchi, H., see Okamura, N. 630(1993)418
- Hargitai, T., Reinholdsson, P., Törnell, B. and Isaksson, R.
Functionalized polymer particles for chiral separation 630(1993)79
- Harvey, S. D., Fellows, R. J., Cataldo, D. A. and Bean, R. M.
Analysis of the explosive 2,4,6-trinitrophenylmethylnitramine (tetryl) in bush bean plants 630(1993)167
- Hashimoto, K., see Okamura, N. 630(1993)418
- Hauschild, M. Z.
Adsorption losses during extraction and derivatization efficiency by benzylation of plant putrescine for high-performance liquid chromatographic analysis 630(1993)397
- Heinzen, V. E. F., see Arruda, A. C. 630(1993)251
- Hilser, Jr., V. J., Worosila, G. D. and Rudnick, S. E.
Protein and peptide mobility in capillary zone electrophoresis. A comparison of existing models and further analysis 630(1993)329
- Honda, S., see Kakehi, K. 630(1993)141
- Hoogmartens, J., see Paesen, J. 630(1993)117
- Hoogmartens, J., see Roets, E. 630(1993)159
- Hušek, P.
Improved procedure for the derivatization and gas chromatographic determination of hydroxycarboxylic acids treated with chloroformates 630(1993)429

- Isaksson, R., see Hargitai, T. 630(1993)79
- Itakura, M., see Yamaoka, T. 630(1993)345
- Jacobson, S. C., see Charton, F. 630(1993)21
- Janssen, H.-G., see Mol, H. G. J. 630(1993)201
- Jayaraman, G., see Gadam, S. D. 630(1993)37
- Jayaraman, G., Gadam, S. D. and Cramer, S. M.
Ion-exchange displacement chromatography of proteins.
Dextran-based polyelectrolytes as high affinity displacers
630(1993)53
- Takehi, K., Ueda, M., Suzuki, S. and Honda, S.
Determination of hyaluronic acid by high-performance
liquid chromatography of the oligosaccharides derived
therefrom as 1-(4-methoxy)phenyl-3-methyl-5-pyrazolone
derivatives 630(1993)141
- Kanazawa, H., Nagata, Y., Matsushima, Y., Tomoda, M. and
Takai, N.
Determination of acidic saponins in crude drugs by
high-performance liquid chromatography on
octadecylsilyl porous glass 630(1993)408
- Khan, I., see Feste, A. S. 630(1993)129
- Kihara, K., see Rokushika, S. 630(1993)195
- Kirkland, J. J., see Yau, W. W. 630(1993)69
- Kokko, M.
Effect of variations in gas chromatographic conditions on
the linear retention indices of selected chemical warfare
agents 630(1993)231
- Kováts, E., see Föti, G. 630(1993)1
- Křen, V., see Kysilka, R. 630(1993)415
- Kuksis, A.
Advances in lipid methodology (edited by W. W.
Christie) (Book Review) 630(1993)447
- Kupchik, E. J.
Structure-gas chromatographic retention time models of
tetra-*n*-alkylsilanes and tetra-*n*-alkylgermanes using
topological indexes 630(1993)223
- Kysilka, R. and Křen, V.
Determination of Lovastatin (mevinolin) and mevinolinic
acid in fermentation liquids 630(1993)415
- Lagu, A. L., see Strege, M. A. 630(1993)337
- Lim, K. B., see Yau, W. W. 630(1993)69
- Ling, D., see Dang, Q. 630(1993)363
- Link, R., see Bouissel, S. 630(1993)307
- Liu, C.-Y., see Yeh, C.-F. 630(1993)275
- Lundmark, B.-O., see Bengård, A. 630(1993)287
- Mahuzier, G., see Pianetti, G. A. 630(1993)371
- Matsushima, Y., see Kanazawa, H. 630(1993)408
- Mol, H. G. J., Staniewski, J., Janssen, H.-G., Cramers, C. A.,
Ghijsen, R. T. and Brinkman, U. A. T.
Use of an open-tubular trapping column as phase-
switching interface in on-line coupled reversed-phase
liquid chromatography-capillary gas chromatography
630(1993)201
- Naaranlahti, T., see Tóth, Z. A. 630(1993)423
- Nagata, Y., see Kanazawa, H. 630(1993)408
- Nickless, G., see O'Doherty, S. J. 630(1993)265
- Norén, K., see Weistrand, C. 630(1993)179
- Nowotnik, D. P., Feld, T. and Nunn, A. D.
Examination of some reversed-phase high-performance
liquid chromatography systems for the determination of
lipophilicity 630(1993)105
- Nunn, A. D., see Nowotnik, D. P. 630(1993)105
- O'Doherty, S. J., Simmonds, P. G., Nickless, G. and Betz, W.
R.
Evaluation of Carboxen carbon molecular sieves for
trapping replacement chlorofluorocarbons 630(1993)265
- Ogawa, S., see Fukui, S. 630(1993)187
- Okamura, N., Yagi, A., Haraguchi, H. and Hashimoto, K.
Simultaneous high-performance liquid chromatographic
determination of altersolanol A, B, C, D, E and F
630(1993)418
- Paesen, J., Claeys, P., Roets, E. and Hoogmartens, J.
Evaluation of silanol-deactivated silica-based reversed
phases for liquid chromatography of erythromycin
630(1993)117
- Pesek, J. J., Sandoval, J. E. and Su, M.
New alumina-based stationary phases for high-
performance liquid chromatography. Synthesis by olefin
hydrosilation on a silicon hydride-modified alumina
intermediate 630(1993)95
- Peterson, T. E.
Separation of drug stereoisomers by capillary
electrophoresis with cyclodextrins 630(1993)353
- Pianetti, G. A., Taverna, M., Baillet, A., Mahuzier, G. and
Bayloq-Ferrier, D.
Determination of alkylphosphonic acids by capillary zone
electrophoresis using indirect UV detection 630(1993)371
- Pozidis, C., Vlatakis, G. and Bouriotis, V.
Sequence-specific DNA affinity chromatography:
application of a group-specific adsorbent for the isolation
of restriction endonucleases 630(1993)151
- Quintens, I., see Roets, E. 630(1993)159
- Raatikainen, O., see Tóth, Z. A. 630(1993)423
- Reinholdsson, P., see Hargitai, T. 630(1993)79
- Rementer, S. W., see Yau, W. W. 630(1993)69
- Righetti, P. G., see Giuffrè, E. 630(1993)313
- Roets, E., Beirinckx, P., Quintens, I. and Hoogmartens, J.
Quantitative analysis of tylosin by column liquid
chromatography 630(1993)159
- Roets, E., see Paesen, J. 630(1993)117
- Rokushika, S., Yamamoto, F. M. and Kihara, K.
Ion chromatography of nitrite and carbonate in inorganic
matrices on an octadecyl-poly(vinyl alcohol) gel column
using acidic eluents 630(1993)195
- Rudnick, S. E., see Hilser, Jr., V. J. 630(1993)329
- Sandoval, J. E., see Pesek, J. J. 630(1993)95
- Semenova, O. P., see Timerbaev, A. R. 630(1993)379
- Simmonds, P. G., see Foulger, B. E. 630(1993)257
- Simmonds, P. G., see O'Doherty, S. J. 630(1993)265
- Staniewski, J., see Mol, H. G. J. 630(1993)201
- Stefansson, M.
Selective complex formation of saccharides with
europium(III) and iron(III) ions at alkaline pH studied by
ligand-exchange chromatography 630(1993)123
- Strege, M. A. and Lagu, A. L.
Capillary electrophoretic protein separations in
polyacrylamide-coated silica capillaries and buffers
containing ionic surfactants 630(1993)337
- Su, M., see Pesek, J. J. 630(1993)95
- Sun, Z., see Dang, Q. 630(1993)363
- Suzuki, S., see Takehi, K. 630(1993)141

- Takai, N., see Kanazawa, H. 630(1993)408
- Taverna, M., see Pianetti, G. A. 630(1993)371
- Timerbaev, A. R., Buchberger, W., Semenova, O. P. and Bonn, G. K.
Metal ion capillary zone electrophoresis with direct UV detection: determination of transition metals using an 8-hydroxyquinoline-5-sulphonic acid chelating system 630(1993)379
- Tomoda, M., see Kanazawa, H. 630(1993)408
- Tonani, C., see Giaffreda, E. 630(1993)313
- Törnell, B., see Hargitai, T. 630(1993)79
- Toth, Z. A., Raatikainen, O., Naaranlahti, T. and Auriola, S.
Isolation and determination of alizarin in cell cultures of *Rubia tinctorum* and emodin in *Dermocybe sanguinea* using solid-phase extraction and high-performance liquid chromatography 630(1993)423
- Traag, W. A., see Van Rhijn, J. A. 630(1993)297
- Trucksess, M. W.
Separation and isolation of trace impurities in L-tryptophan by high-performance liquid chromatography 630(1993)147
- Tuinstra, L. G. M. T., see Van Rhijn, J. A. 630(1993)297
- Ueda, M., see Kakehi, K. 630(1993)141
- Van de Spreng, P. F., see Van Rhijn, J. A. 630(1993)297
- Van Rhijn, J. A., Traag, W. A., Van de Spreng, P. F. and Tuinstra, L. G. M. T.
Simultaneous determination of planar chlorobiphenyls and polychlorinated dibenzo-*p*-dioxins and -furans in Dutch milk using isotope dilution and gas chromatography-high-resolution mass spectrometry 630(1993)297
- Vlatakis, G., see Pozidis, C. 630(1993)151
- Volpi, N. and Bolognani, L.
Glycosaminoglycans and proteins: different behaviours in high-performance size-exclusion chromatography 630(1993)390
- Watson, E. and Yao, F.
Capillary electrophoretic separation of recombinant granulocyte-colony-stimulating factor glycoforms 630(1993)442
- Weistrand, C. and Norén, K.
Liquid-gel partitioning using Lipidex in the determination of polychlorinated biphenyls in cod liver oil 630(1993)179
- Wichtl, M., see Wiegrebe, H. 630(1993)402
- Wiegrebe, H. and Wichtl, M.
High-performance liquid chromatographic determination of cardenolides in *Digitalis* leaves after solid-phase extraction 630(1993)402
- Worosila, G. D., see Hilser, Jr., V. J. 630(1993)329
- Yagi, A., see Okamura, N. 630(1993)418
- Yamamoto, F. M., see Rokushika, S. 630(1993)195
- Yamaoka, T., Yamashita, K. and Itakura, M.
Determination of the number and relative molecular mass of subunits in an oligomeric protein by two-dimensional electrophoresis. Application to the subunit structure analysis of rat liver amidophosphoribosyltransferase 630(1993)345
- Yamashita, K., see Yamaoka, T. 630(1993)345
- Yan, L., see Dang, Q. 630(1993)363
- Yao, F., see Watson, E. 630(1993)442
- Yau, W. W., Rementer, S. W., Boyajian, J. M., DeStefano, J. J., Graff, J. F., Lim, K. B. and Kirkland, J. J.
Improved computer algorithm for characterizing skewed chromatographic band broadening. II. Results and comparisons 630(1993)69
- Yeh, C.-F., Chyueh, S.-D., Chen, W.-S., Fang, J.-D. and Liu, C.-Y.
Application of dithiocarbamate resin-metal complexes as stationary phases in gas chromatography 630(1993)275
- Yunes, R. A., see Arruda, A. C. 630(1993)251

PUBLICATION SCHEDULE FOR THE 1993 SUBSCRIPTION

Journal of Chromatography and Journal of Chromatography, Biomedical Applications

MONTH	O 1992	N 1992	D 1992	J	F	M	
Journal of Chromatography	623/1 623/2 624/1 + 2	625/1 625/2	626/1 626/2 627/1 + 2	628/1 628/2 629/1 629/2	630/1 + 2 631/1 + 2 632/1 + 2 633/1 + 2	634/1 634/2	The publication schedule for further issues will be published later.
Cumulative Indexes, Vols. 601-650							
Bibliography Section						649/1	
Biomedical Applications				612/1	612/2	613/1	

INFORMATION FOR AUTHORS

(Detailed *Instructions to Authors* were published in Vol. 609, pp. 439-445. A free reprint can be obtained by application to the publisher, Elsevier Science Publishers B.V., P.O. Box 330, 1000 AH Amsterdam, The Netherlands.)

Types of Contributions. The following types of papers are published in the *Journal of Chromatography* and the section on *Biomedical Applications*: Regular research papers (Full-length papers), Review articles, Short Communications and Discussions. Short Communications are usually descriptions of short investigations, or they can report minor technical improvements of previously published procedures; they reflect the same quality of research as Full-length papers, but should preferably not exceed five printed pages. Discussions (one or two pages) should explain, amplify, correct or otherwise comment substantively upon an article recently published in the journal. For Review articles, see inside front cover under Submission of Papers.

Submission. Every paper must be accompanied by a letter from the senior author, stating that he/she is submitting the paper for publication in the *Journal of Chromatography*.

Manuscripts. Manuscripts should be typed in **double spacing** on consecutively numbered pages of uniform size. The manuscript should be preceded by a sheet of manuscript paper carrying the title of the paper and the name and full postal address of the person to whom the proofs are to be sent. As a rule, papers should be divided into sections, headed by a caption (*e.g.*, Abstract, Introduction, Experimental, Results, Discussion, etc.). All illustrations, photographs, tables, etc., should be on separate sheets.

Abstract. All articles should have an abstract of 50-100 words which clearly and briefly indicates what is new, different and significant. No references should be given.

Introduction. Every paper must have a concise introduction mentioning what has been done before on the topic described, and stating clearly what is new in the paper now submitted.

Illustrations. The figures should be submitted in a form suitable for reproduction, drawn in Indian ink on drawing or tracing paper. Each illustration should have a legend, all the *legends* being typed (with double spacing) together on a *separate sheet*. If structures are given in the text, the original drawings should be supplied. Coloured illustrations are reproduced at the author's expense, the cost being determined by the number of pages and by the number of colours needed. The written permission of the author and publisher must be obtained for the use of any figure already published. Its source must be indicated in the legend.

References. References should be numbered in the order in which they are cited in the text, and listed in numerical sequence on a separate sheet at the end of the article. Please check a recent issue for the layout of the reference list. Abbreviations for the titles of journals should follow the system used by *Chemical Abstracts*. Articles not yet published should be given as "in press" (journal should be specified), "submitted for publication" (journal should be specified), "in preparation" or "personal communication".

Dispatch. Before sending the manuscript to the Editor please check that the envelope contains four copies of the paper complete with references, legends and figures. One of the sets of figures must be the originals suitable for direct reproduction. Please also ensure that permission to publish has been obtained from your institute.

Proofs. One set of proofs will be sent to the author to be carefully checked for printer's errors. Corrections must be restricted to instances in which the proof is at variance with the manuscript. "Extra corrections" will be inserted at the author's expense.

Reprints. Fifty reprints will be supplied free of charge. Additional reprints can be ordered by the authors. An order form containing price quotations will be sent to the authors together with the proofs of their article.

Advertisements. The Editors of the journal accept no responsibility for the contents of the advertisements. Advertisement rates are available on request. Advertising orders and enquiries can be sent to the Advertising Manager, Elsevier Science Publishers B.V., Advertising Department, P.O. Box 211, 1000 AE Amsterdam, Netherlands; courier shipments to: Van de Sande Bakhuizenstraat 4, 1061 AG Amsterdam, Netherlands; Tel. (+31-20) 515 3220/515 3222, Telefax (+31-20) 6833 041, Telex 16479 els vi nl. *UK:* T. G. Scott & Son Ltd., Tim Blake, Portland House, 21 Narborough Road, Cosby, Leics. LE9 5TA, UK; Tel. (+44-533) 753 333, Telefax (+44-533) 750 522. *USA and Canada:* Weston Media Associates, Daniel S. Lipner, P.O. Box 1110, Greens Farms, CT 06436-1110, USA; Tel. (+1-203) 261 2500, Telefax (+1-203) 261 0101.

Hyphenated Techniques in Supercritical Fluid Chromatography and Extraction

edited by K. Jinno, Toyohashi University of Technology, Toyohashi, Japan

Journal of Chromatography Library Volume 53

This is the first book to focus on the latest developments in hyphenated techniques using supercritical fluids. The advantages of SFC in hyphenation with various detection modes, such as, FTIR, MS, MPD and ICP and others are clearly featured throughout the book. Special attention is paid to coupling of SFE with GC or SFC.

In this edited volume, chapters are written by leading experts in the field. The book will be of interest to professionals in academia, as well as to those researchers working in an industrial environment, such as analytical instrumentation, pharmaceuticals, agriculture, food, petrochemicals and environmental.

Contents:

1. General Detection Problems in SFC
(*H.H. Hill, D.A. Atkinson*).
2. Fourier Transform Ion Mobility Spectrometry for Detection after SFC
(*H.H. Hill, E.E. Tarver*).
3. Advances in Capillary SFC-MS
(*J.D. Pinkston, D.J. Bowling*).
4. Advances in Semi Micro Packed Column SFC and its Hyphenation
(*M. Takeuchi, T. Saito*).
5. Flow Cell SFC-FT-IR
(*L.T. Taylor, E.M. Calvey*).
6. SFC-FT-IR Measurements Involving Elimination of the Mobile Phase
(*P.R. Griffiths et al.*).
7. Practical Applications of SFC-FTIR
(*K.D. Bartle et al.*).
8. Recycle Supercritical Fluid Chromatography - On-line Photodiode-Array Multiwavelength UV/VIS Spectrometry/IR Spectrometry/Gas Chromatography
(*M. Saito, Y. Yamauchi*).
9. Inductively Coupled Plasma Atomic Emission Spectrometric Detection in Supercritical Fluid Chromatography
(*K. Jinno*).
10. Microwave Plasma Detection SFC
(*D.R. Luffer, M.V. Novotny*).
11. Multidimensional SFE and SFC
(*J.M. Levy, M. Ashraf-Khorassani*).
12. Advances in Supercritical Fluid Extraction (SFE)
(*S.B. Hawthorne et al.*).
13. Introduction of Directly Coupled SFE/GC Analysis
(*T. Maeda, T. Hobo*).
14. SFE, SFE/GC and SFE/SFC: Instrumentation and Applications
(*M.-L. Riekkola et al.*).
15. Computer Enhanced Hyphenation in Chromatography - Present and Future
(*E.R. Baumeister, C.L. Wilkins*).

Subject Index.

1992 x + 334 pages

Price: US \$ 157.00/ Dfl. 275.00

ISBN 0-444-88794-6

ORDER INFORMATION

For USA and Canada

ELSEVIER SCIENCE

PUBLISHERS

Judy Weislogel

P.O. Box 945

Madison Square Station,

New York, NY 10160-0757

Tel: (212) 989 5800

Fax: (212) 633 3880

In all other countries

ELSEVIER SCIENCE

PUBLISHERS

P.O. Box 211

1000 AE Amsterdam

The Netherlands

Tel: (+31-20) 5803 753

Fax: (+31-20) 5803 705

US\$ prices are valid only for the USA & Canada and are subject to exchange fluctuations; in all other countries the Dutch guilder price (Dfl.), is definitive. Books are sent postfree if prepaid.



ELSEVIER
SCIENCE PUBLISHERS